Individual R&D Contribution Review IRCR

Individual R&D Contribution Review
Issue (1) 2023
Malaysian Nuclear Agency

Publishing Office
Research Management Centre
Malaysian Nuclear Agency, Bangi,
43000 Kajang, Selangor Darul Ehsan,
MALAYSIA
Tel : +6 03 8911 2000
Fax : +6 03 8911 2154

Website
http://www.nuclearmalaysia.gov.my

FOREWARD

Within the pages of this compilation, we embark on a journey into the dynamic world of research and applications in nuclear technology. The research presented in this issue showcases the remarkable strides contributed by individual Nuklear Malaysia's researchers, pushing the boundaries of what is possible in medical, agriculture, materials science, environment, agriculture and other related fields including energy.

Nuclear science and technology holds the key to transformative breakthroughs, and the diverse contributions in this collection exemplify the collaborative efforts required to unlock its potential. From cleaner environment solutions to ground breaking medical advancements, each study represents a crucial step forward in our understanding and application of nuclear phenomena.

The collaborative efforts of individual which is contributed to the main projects as presented here reflect the dedication of the researchers in navigating the challenges of nuclear research and their applications. May this compilation inspire a continuous excellence in this field of research, contributing to Malaysia's sustainable development and serving as a catalyst for future breakthroughs to the nation and people.

Rosli Bin Darmawan, PhD
Director General,
Malaysian Nuclear Agency,
Ministry of Science, Technology and Innovation

This publication is issued by Nuclear Malaysia on a yearly basis. Inquiries about availability and/or copyright of the contents in this publication should be address to Research Management Center, Malaysian Nuclear Agency.

Contents

Research Articles

Radiation Processing

Industrial Technology

Agrotechnology and Biosciences

Engineering

Radiation Health and Safety

Medical Technology

Individual Research Contribution Review, 2023, 1(1): 1–2

IRCR

Thermal Stability of Irradiated Empty Fruit Bunch and Recovery of Biochar via Microwave Pyrolysis

Ahmad Zuhdi Mohd On
Radiation Processing Technology Division
Malaysian Nuclear Agency
43000 Kajang, Selangor
zuhdi@nm.gov.my

Abstract

Natural bio waste which is empty fruit bunch (EFB) fibre has been produced tonnes per day in daily palm oil productions and mostly used to generate electricity for the palm oil mill. Thus, in this study, EFB was used to investigate the thermal stability and level of degradation when bombarded with electron irradiation and biochar recovery by using microwave assisted technique. The long strands of EFB fibre was mechanically pulverized in fined 300 μm mesh sized powder. The long strands and powder form of EFB was irradiated under electron beam accelerator with the intensity of 100 to 400kGy with increment of 100kGy. The thermal stability of irradiated EFB depicted that the 400kGy exposed to the sample induced to early and rapid loss of weight for both strands and powder. The recovery of biochar using microwave pyrolysis was also analyzed in this study.

1 Introduction

Biomass is mainly composed of cellulose, hemicellulose and lignin, it has been identified as one of the most significant sources of renewable energy on earth that can be converted into liquid fuel and has recently received considerable attention in the pursuit for a fossil fuel supplement (Rocha et al., 1996; Tang et al., 2009; Isahak et al., 2012). The US renewable energy supply by sources disclosed that the woody biomass plays a key role in the renewable energy. A stable supply for the woody biomass that could be converted to biofuels was observed in the United States in the past ten years.

Microwave heating has been employed in many applications such as food drying and heating, chemical synthesis and so on. The rapid, uniform and selective irradiation of the microwaves provides indirect contact between microwave and heating materials. However, microwave heating has not received sufficient attention in the area of high-temperature biomass refining (Sobhy and Chaouki, 2010). Recent studies on pyrolysis have started to demonstrate microwaves as heating resource to produce biomass pyrolysis oil, such as coffee hulls and sewage sludge, rice straw, Douglas fir pellet, and lignin. Microwave pyrolysis is a process that tests the decomposition of biomass at different microwave powers (temperatures), which yields both gaseous and liquid products which can be used in various combinations. Heating rate was optimized as it related to the maximum oil yield as well as the best oil quality which can be obtained through the analysis of different components of decomposition products (Bilali et al., 2005). However in this preliminary research, microwave pyrolysis was introduce to decompose the lignocellulosic structure of irradiated empty fruit bunch to investigate the composition of bio oil produced.

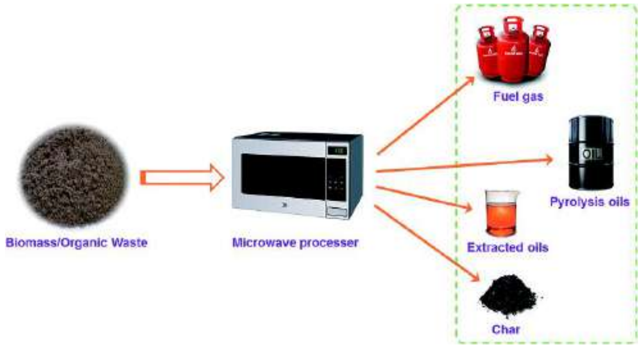

Figure 1: Potential application on microwave pyrolysis of biomass & organic waste

2 Methods

The long stranded EFB has been pulverised in a 200µm mesh with an average moisture content reading between 6 – 10%. The pulverised EFB then was irradiated at 3MeV, 2A electron accelerator at the elevated interval dose of 5kGy from 0kGy – 20kGy. 5gram of irradiated EFB was then undergo the microwave pyrolysis using the modified domestic microwave with microwave power from 100W to 400W. The various power is to determine the residence time for the irradiated fibre converted to biochar.

3 Characterisation

The irradiated EFB samples was undergo the thermal stability test via thermogravimetric analaysis(TGA). It was tested from the temperature from room temperature until 700°C under nitrogen condition at 5°C/min.

4 Results and Discussion

Figure 2 shows the thermal stability of irradiated samples where the decomposition of cellulose occurred at the range of 200°C - 350°C. The cellulose is a soft segment in a lignocellulosic structure where low thermal stability occur in that range of temperature. As the increment of radiation dose, the scission and rupture rupture of cellulosic bond leads to the aggravation of thermal stability. In the time residence obsera-vation Table 1, the higher dose of irradiated samples depicted a faster conversion to biochar due to the bond scissioning of cellulosic structure.

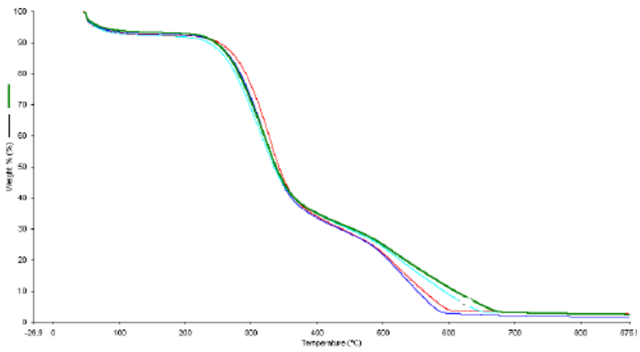

Figure 2: Thermal stability of irradiated EFB

Table 1: Residence time – microwave power of the EFB samples conversion to biochar

DOSE IRRADIATED SAMPLES (kGy)	MICROWAVE POWER (W)	RESIDENCE TIME (S)
0		140
5		128
10	100	88
15		80
20		80
0		30
5		25
10	400	20
15		20
20		20

5 Conclusions

This study shows that the microwave pyrolysis could lead the vital and rapid biochar and biofuel recovery from agricultural lignocellulosic fibre. The increment of irradiated EFB samples showed the low thermal stability due the scissioning of cellulosic bond. The expose of higher radiation dose leads to the low residence time to convert into biochar. The increment of microwave power obviously declining the residence time of the biochar conversion. This research will be proceed with the composition of biochar and biofuel characterization.

References

L. Bilali, M. Benchanaa, K. El harfi, A. Mokhlisse, and A. Outzourhit. 2005. A detailed study of the microwave pyrolysis of the moroccan (Youssoufia) rock phosphate. *Journal of Analytical and Applied Pyrolysis*, 73:1–15.

W.N.R.W. Isahak, M.W.W. Hisham, M.A. Yarmo, and T.Y. Hin. 2012. A review on bio-oil production from biomass by using pyrolysis method. *Renewable and Sustainable Energy Reviews*, 16:5910–5923.

J.D. Rocha, C.A. Luengo, and C.E. Snape. 1996. Hydrodeoxygenation of oils from cellulose in single and two-stage hydropyrolysis. *Renewable Energy*, 9:950–953.

A. Sobhy and J. Chaouki. 2010. Microwave-assisted biorefinery. *Chemical Engineering Transactions*, 19:25–30.

Z. Tang, Q. Lu, Y. Zhang, X.F. Zhu, and Q.X. Guo. 2009. One step bio-oil upgrading through hydrotreatment, esterification, and cracking. *Industrial and Engineering Chemistry Research*, 48:6923–6929.

Individual Research Contribution Review, 2023, 1(1): 3–4

Antimicrobial Properties of Polyvinyl Alcohol/Sago Starch as Antimicrobial Active Food Packaging

Farah Fadzehah Hilmi
Radiation Processing Technology Division, Malaysian Nuclear Agency
43000 Kajang, Selangor
farah@nm.gov.my

Abstract

Cinnamaldehyde (CN) is incorporated into polyvinyl alcohol/sago starch (PVA/SS) film to serve as antimicrobial active packaging. PVA/SS film was irradiated with electron beam irradiation at an optimum dose of 110 kGy and grafted with cinnamaldehyde in vapor phase to produce grafted film. The grafted film (PVA/SS)-g-CN was used to packaged strawberries to evaluate the effectiveness of the grafted film on antimicrobial property. Visual observation shows that strawberries packaged in control film, PVA/SS deteriorate faster than strawberries packaged in grafted film, (PVA/SS)-g-CN. To further quantitatively analyse the antimicrobial property, the strawberries total plate count and yeast mould count were conducted. The result revealed that both total plate count and yeast mould count of strawberries in grafted film is lower as compared to strawberries in packaged in control film. This concludes that the grafted film has the potential to be used as an antimicrobial active packaging film for food.

Keywords: Radiation induced grafting, active packaging, antimicrobial active packaging, essential oil.

1 Introduction

As described by Labuza and Breene (Labuza and Breene, 1989), active packaging has been shown to be an effective method for satisfying demand from the consumer for fresh, safe, and high-quality processed foods while also extending their shelf life. In order to increase the shelf life of the packaged food, antimicrobial (AM) agents were added to the surface of the starch-based film materials to control food spoilage and pathogenic bacteria on the food. One common method is the direct incorporation of antimicrobial agents into the polymer matrix during the film formulation process (Atarés and Chiralt, 2016; Norcino et al., 2020). This can be done using techniques such as melt mixing or solution casting, which involves dissolving the antimicrobial agent in a suitable solvent before adding it to the polymer matrix. One of the primary concerns with this approach is the possible migration of the antimicrobial agent from the packaging material to the food itself (Abreu et al., 2015). To overcome these drawbacks, alternative methods, radiation-induced grafting (RIG) in solution has been used. This method offers surface immobilization antimicrobial agent by covalent bonds where free radicals are created on the surface of the substrate polymer (Othman, 2016; Shukri et al., 2014). In this novel study, a biodegradable antimicrobial active packaging film was developed using the irradiation method. Polyvinyl alcohol (PVA)/sago starch (SS) were irradiated with electron beam system, EPS-3000 before grafting process was carried out in vapour. Cinnamaldehyde (CN) was used as an antimicrobial agent in this work and the effectiveness of CN towards microbes were analysed. Objectives of this study is to evaluate the effects of cinnamaldehyde on the PVA/SS film in real foods. The effectiveness of the (PVA/SS)-g-CN as AM active packaging was analysed on strawberry for five days.

2 Methods

PVA/SS film was prepared according to a method described by Azahari et al. (Azahari et al., 2011) where PVA and SS at 70:30 weight percent ratio and the amount of plasticizer, glycerol, is 1 % of the total solution. The casted films then undergo an irradiation process using an electron beam accelerator (EPS 3000, Malaysian Nuclear Agency). The electron beam was operated at two (2) MeV at 30 kGy with 10 kGy per pass for cross-linking. The grafting reaction was taken place in the modified grafting chamber made from pyrex glass with an inner diameter of 10 cm and a length of 25 cm. The grafting reaction is carried out by vapourizing the antimicrobial agent, CN, into the modified reaction chamber supplied from the round flask bottom. The round flask was attached at the bottom of the modified glass chamber. It is heated using an oil bath at 165 °C for 10 minutes to produce vapour. Once the grafting had taken place, the grafted film (PVA/SS)-g-CN was carefully removed from the modified grafting chamber using a tweezer, wiped using tissue, and blow-dried with a small pump to remove ungrafted CN. The grafted film (PVA/SS)-g-CN was kept in a zipper bag before proceeding with further characterisations.

3 Results

Figure 1 shows the visual observation of strawberries after storage at 25°C for day 0 and day 3. As can be seen in the picture, the strawberries are packaged in two types of packaging, which are (1) PVA/SS film and (2) (PVA/SS)-g-CN film. On day 3, strawberries in PVA/SS packaging started to show circular brownish spots in several places, as shown in yellow circles. This spot could be due to anthracnose fruit rot caused by fungi of the genus *Colletotrichum* (Mertely and Peres, 2012).This type of fruit rot commonly occurs during periods of warm wet weather. On the other hand, strawberries in (PVA/SS)-g-CN show no sign of deterioration on day 3 of storage. The strawberries appear to retain their original condition and are free from any spot and lesion.

Figure 1: Comparison of strawberries in PVA/SS and (PVA/SS)-g-CN on day 0 and day 3

To further quantitatively analyse the antimicrobial property, the total plate count (TPC) was counted. The TPC of strawberries packaged in control (PVA/SS) film and grafted (PVA/SS)-g-CN packaging film during storage for five (5) days interval. The TPC had a range of 3.8×10^3 to 8.0×10^4 during the storage period. Strawberries in PVA/SS packaging show TPC values of 3.8×10^3, 2.2×10^4, 3.9×10^4, and 8.0×10^4 CFU/g on the 0^{th}, 1^{st}, 3^{rd}, and 5^{th} day respectively. For strawberries in (PVA/SS)-g-CN packaging, the TPC shows lower values starting from the 1^{st} to the 5^{th} day. The values are 3.8×10^3, 1.3×10^4, 2.5×10^4 and 6.1×10^4 for 0^{th}, 1^{st}, 3^{rd} and 5^{th} day respectively.

4 Conclusions

The findings of the present study revealed that cinnamaldehyde can suppress the growth of a broad spectrum of food pathogenic and spoilage microorganisms in the fruit. Based on the visual observation, (PVA/SS)-g-CN film can delay the growth of the microbes. The microbiological analyses show that strawberries packed in (PVA/SS)-g-CN exhibit lower value of total plate and yeast mould count with value of 6.1×10^4 cfu/g and 2×10^5 cfu/g, respectively.

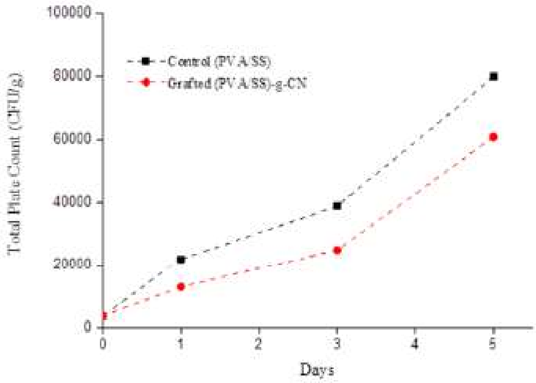

Figure 2: Total plate count in strawberries stored at 25°C for five days in both PVA/SS

References

A. S. Abreu, M. Oliveira, A. de Sa, R. M. Rodrigues, M. A. Cerqueira, A. A. Vicente, and A. V. Machado. 2015. Antimicrobial nanostructured starch based films for packaging. *Carbohydr Polym*, 129:127–134, doi:10.1016/j.carbpol.2015.04.021.

L. Atarés and A. Chiralt. 2016. Essential oils as additives in biodegradable films and coatings for active food packaging. *Trends in Food Science Technology*, 48:51–62, doi:10.1016/j.tifs.2015.12.001.

N. A. Azahari, N. Othman, and H. Ismail. 2011. Bidodegradable studies of PVA - corn starch. *Journal of Physical Science*, 22(2):15–31.

T. P. Labuza and W. Breene. 1989. Applications of "active packaging" for improvement of shelf-life and nutritional quality of fresh and extended shelf-life foods. *Journal of food processing and preservation*, 13(1):1–69.

J. C. Mertely and N. A. Peres. 2012. Anthracnose fruit rot of strawberry. *EDIS*, 9.

L. Norcino, J. Mendes, C. Natarelli, A. Manrich, J. Oliveira, and L. Mattoso. 2020. Pectin films loaded with copaiba oil nanoemulsions for potential use as bio-based active packaging. *Food Hydrocolloids*, 106(105862).

N. A. F. Othman. 2016. Preparation of radiation grafted kenaf absorbent for aluminium removal via chemical vapour deposition. *Universiti Teknologi Malaysia*.

N. A. Shukri, Z. Ghazali, N. A. Fatimah, S. F. Mohamad, and M. U Wahit. 2014. Physical, mechanical and oxygen barrier properties of antimicrobial active packaging based on LDPE film incorporated with sorbic acid. *Advances in Environmental Biology*, pages 2748–2753.

Individual Research Contribution Review, 2023, 1(1): 5–6

FLOODCOM: Floating Flood Disaster Command Center

Khairil Nor Kamal Umar
Radiation Processing Technology Division
Malaysian Nuclear Agency
43000 Kajang, Selangor
kn_kamal@nm.gov.my

Abstract

FLOODCOM: Floating Flood Disaster Command Center is a floating structure built from biocomposite material and RX-HDPE floating module and will be functioning as a flood disaster command center. This floating structure are placed in a strategic area at Kampung Bantal, Ulu Tembeling, Jerantut, Pahang and will be used by Civil Defense Emergency response Team (CDERT) under Malaysian Civil Defense Force (Angkatan Pertahanan Awam Malaysia) to assist rescue operation, evacuation and humanitarian aid to flood victim. Malaysian Nuclear Agency has the technology and expertise in the construction of floating disaster command center from biocomposite material. The expertise of Malaysian Nuclear Agency in the field of biocomposite material, polymer material and composite processing equipment has been proven in previous projects, mostly community projects such as aquacultural floating biocomposite cage, biocomposite floating jetty and anchovy catching floating biocomposite barge (bagang terapung biokomposit). The successfulness of the project was a proof that the technology was well accepted by the community.

1 Introduction

Mukim Ulu Tembeling is located at the head of Sungai Tembeling, in Jerantut district, Pahang. Ulu Tembeling is located at the entrance of the National Park in Pahang. This area consisting 5 main villages namely Kampung Bantal, Kampung Pagi, Kampung Kuala Sat, Kampung Gusai and Kampung Bukit Mat Daling. The five villages are inhabited by about 2595 people who mostly were self employed. The location of these villages is isolated, where it involves a long distance and takes a long time to reach. Furthermore, Kampung Bantal, which is inhabited by the largest population, is separated by the Tembeling River and a boat service must be used to cross the river to the village.

All of these villages are located in areas that are very vulnerable to flood and every time a flood occurs, the village will be cut off from any communication road resulting in the aid delivery process being blocked as well as rescue operations and the evacuation of victims being delayed or taking a long time to arrive. Furthermore, the operation of delivering aid through the river route are very costly and endangers the Malaysian Civil Defense Force (APM) personnel and there have been several incidents of overturned boats.

Figure 1: Kampung Bantal's condition during flood season

Figure 2: Capsized boat

The Malaysian Nuclear Agency has the technology and expertise in the field of manufacturing floating structures from biocomposite materials. In this project, a floating structure consisting of biocomposite material and RX-HDPE modules will be built which will serve as a floating disaster command center. This floating command center will be placed in a strategic location for use by the Malaysian Civil Defense Force (APM) of the State of Pahang for rescue operations, evacuation and delivery of humanitarian aid to flood victims. In addition, this command center will act as a first responder preparedness center for search and rescue operations in the event of an accident along the river. In a normal situation, this floating center will be a standby station that will be used by the APM CDERT.

This floating biocomposite technology has already been used and applied in previous projects, namely as a biocomposite floating jetty for the MSI project in Semporna, Sabah and as a floating anchovy fishing station for the MySI project in Kota Belud, Sabah. The same technology has been used by the Malaysian Armed Forces through the Joint Forces Headquarters in Sabah as a jetty for the movement and operation of the quick response force in the responsibility of safeguarding the security of the country's waters from foreign invasion.

2 Methods

a) Preparation of biocomposite compound with the addition of additive using compounding machine at Malaysian Nuclear Agency.

b) Production of biocomposite structure [1] component through compression molding method.

c) Production of floating module [2] from radiation modified polymeric material RX-HDPE by extrusion blow molding technique.

d) Pre-assembly of framing structure, biocomposite decking and floating module.

e) Installation of FLOODCOM structure [3,4].

3 Result and Discussion

Figure 3: RX-HDPE floating module

Figure 4: Biocomposite decking

Figure 5: Aluminum framing material

Figure 6: Stainless steel long bolt complete with nut and washer

Figure 7: Rust proof decking screw

Figure 8: Drilled holes on framing material

Figure 9: Pre-assembly of framing material, floating module and stainless steel bolt.

4 Conclusion

The use of a floating flood disaster operation center is very important in helping the Malaysian Civil Defense Force carry out rescue operations, the evacuation of flood victims and the delivery of humanitarian aid during a flood disaster. The usage of biocomposite materials and RX-HDPE floating modules in the FLOODCOM structure has given good performance and its durability has been proven in previous floating structure projects.

References

Modular For Aquaculture Farming and Method Thereof, MY-183424-A, Malaysian Patent.

[1] 'Composition of an Armor Unit and Method of Fabrication Thereof', MY-173338-A, Malaysian Patent

[2] 'Marine Floating Module Unit', MY 20-E0735-0101, Malaysian Industrial Design

[3] 'Maritime Works – Part 2: Code of Practice for the Design of Quay Walls, Jetties and Dolphins', BS 6349-2: 2019.British Standard

[4] 'Maritime Works – Part 4: Code of Practice for Design of Fendering And Mooring System', BS 6349-4: 2014. British Standard

Individual Research Contribution Review, 2023, 1(1): 7–8

Potential of Palm oil-based Polyol as Water-based Radiation Curable Resin

Khairul Azhar bin Abdul Halim
Radiation Processing Technology Division, Malaysian Nuclear Agency
43000 Kajang, Selangor
azharhalim@nm.gov.my

Abstract

This study investigates the viability of water-borne polyurethane acrylate (WPUA) coatings derived from palm oil, aiming to mitigate environmental concerns linked to traditional solvent-based coatings. Leveraging radiation curing techniques, this research explores the synthesis process involving palm oil polyol and isocyanate, dispersed in water to yield distinctive properties compared to petrochemical-based counterparts. The WPUA dispersions derived from palm oil exhibit higher viscosity and particle size, influencing film characteristics with enhanced mechanical properties, including increased hardness and crosslinking. However, these coatings demonstrate reduced glossiness and increased haziness due to compositional differences affecting light scattering. This study explores the potential of palm oil-derived WPUA coatings produced via radiation curing, which offers eco-friendly, rapid curable coatings with distinct attributes for potential industrial applications.

Keywords: water-based, radiation curable, polyurethane coating

1 Introduction

Conventional solvent-borne polyurethane (PU) coatings pose environmental and health risks due to VOC emissions and carcinogenic solvents. Water-borne PU coatings, while addressing these concerns, rely on time-consuming thermal curing. Recent advancements leverage radiation curing technology for water-borne PU coatings, providing rapid curing, lower energy consumption, environmental friendliness, chemical stability, and cost-efficiency. This study focuses on enhancing sustainability by incorporating palm oil into waterborne polyurethane acrylate (WPUA) coatings. The palm oil polyol, synthesized by AOTD MPOB, aims to reduce curing time through radiation curing. Collaboration between AOTD MPOB and Nuklear Malaysia will develop an eco-friendly, rapid-curing water-borne coating using palm oil-derived materials. The process involves synthesizing a polyurethane prepolymer, dispersing it in water, stabilizing it, and exposing the resulting PUA dispersion to UV for film formation and evaluation of properties.

2 Methods

2.1 Synthesis of WPUA dispersion

In the controlled setup shown in Figure 1, the synthesis of the polyurethane acrylate (PUA) prepolymer involves reacting palm oil polyol (Pioneer 135 (PE135) supplied by AOTD MPOB) with isophorone diisocyanate (IPDI) and dimethylol propionic acid (DMPA), maintaining an NCO:OH ratio of 2.0. N-Methyl-2-pyrrolidone is utilized as a co-solvent during the reaction process. The mixture was heated at 80°C until homogeneous. Tin based catalyst was introduced, and the reaction monitored hourly by titration following ASTMD2572 until the NCO content reached the theoretical value. 2-Hydroxyethyl acrylate (HEA) was then added and reacted at 60°C until all NCO was consumed. DMPA's carboxylic acid group was neutralized with triethylamine (TEA) for 30 minutes. The resulting PUA prepolymer was dispersed in deionized water through gradual addition and vigorous stirring over 30 minutes, creating a 40% solid content WPUA dispersion, as shown in Figure 2. For the control sample, the synthesis step is repeated, utilizing petrochemical polyol, namely polypropylene glycol (PPG).

2.2 Preparation PUA film

The WPUA dispersion were vacuum treated to remove trapped air. 5% w/w of Irgacure 500 photoinitiator was added to the dispersion and it was allowed to settle for 24 hours. To form PUA coating film, the dispersion was applied on glass substrate using a 4-sided bar coater at 100 μm wet films thickness. It was then irradiated under UV curing at 365 nm with a conveyor speed of 10 m/min using a UV-IST machine. Quality check involved a thumbprint test for complete film curing. The properties of the PUA film were studied.

2.3 Characterisation of PUA

The WPUA dispersions was analysed with Brookefield viscometer, Sartorius pH meter and Microtrac/ X100 particle size analyzer. Meanwhile, PUA films were analysed with BYK Gardner pendulum hardness, BYK Gardner Hazeguard Plus hazemeter and BYK Gardner micro-tri-gloss three angle glossmeter. The gel content of PUA film was analysed according to method by Tan & Yusof (Tan and Yusof, 2003).

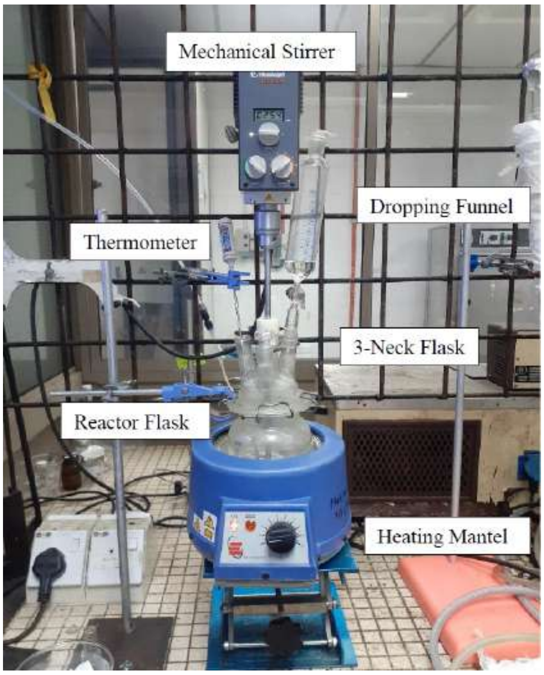

Figure 1: WPUA synthesis setup

3 Results & Discussion

3.1 WPUA dispersion properties

The WPUA dispersion properties in Table 1 revealed similar pH levels around 7 for both PPG and PE135 dispersions caused by neutralization reaction of carboxylic acid groups by TEA. Notably, PE135 displayed significantly higher viscosity and particle size compared to PPG. This may be due to the larger molecular structures and multiple functional groups present in PE135 derived from palm oil (Ismail et al., 2018), causing increased entanglement and friction with water molecules.

Table 1: WPUA dispersion properties.

Sample	PPG	PE135
pH	7.79	7.27
Viscosity (mPa.s)	37	152
Particle size (nm)	108	264

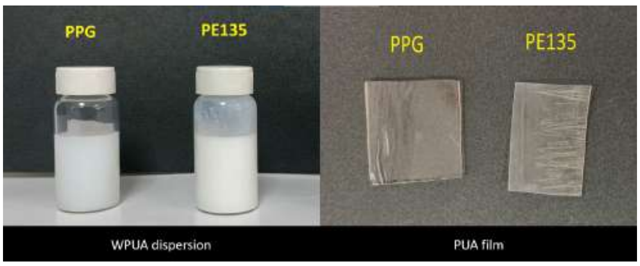

Figure 2: PUA dispersion and film

3.2 PUA film properties

Table 2 shows that both PPG and PE135 dispersions require about 11 passes for curing, possibly due to water hindering UV light penetration. PE135 has higher film hardness and crosslinking degree than PPG, likely because of its higher molecular weights and increased rigidity from vegetablebased polyol. PPE135 film has lower glossiness and higher haziness compared to PPG, attributed to chemical structure differences between vegetable-based and petrochemical-based polyol. Unsaturated bonds in natural oil-based coatings scatter light, resulting in lower gloss and higher haziness, while petrochemical-based coatings tend to have higher gloss and lower haziness due to more uniform molecular structures.

Table 2: PUA film properties.

Sample	PPG	PE135
Curing (Number of passes)	11	10
Film hardness (Oscillation)	40	90
Gel content (%)	33.3	47
Gloss at 20° (GU)	171	100
Haze	2.45	8.13

4 Conclusions

This study explores the development of water-borne polyurethane acrylate (WPUA) coatings derived from palm oil, addressing environmental concerns associated with conventional solvent-based coatings. The palm oil-based WPUA dispersions exhibit higher viscosity and particle size, impacting their film characteristics, including mechanical properties such as increased hardness and crosslinking. However, these coatings display lower glossiness and higher haziness due to differences in molecular structures affecting light scattering behavior. This research highlights the potential of palm oil derived WPUA coatings synthesized through radiation curing, offering eco-friendly, rapidly curable coatings with unique attributes for potential industry applications.

References

Tuan Noor Maznee Tuan Ismail, Nor Azowa Ibrahim, Mohd Azmil Mohd Noor, Seng Soi Hoong, Kosheela Devi Poo Palam, Shoot Kian Yeong, Zainab Idris, Christi M Schiffman Ibrahim Sendijarevic, Emilia Abd Malek, and et al. Norhazlin Zainuddin. 2018. Oligomeric composition of palm olein-based polyols: The effect of nucleophiles. *European Journal of Lipid Science and Technology*, 120(4):1700354.

KS Tan and A Yusof. 2003. Some studies on the effect of solvents in ENR 60 gel content measurements. *Journal of Rubber Research.*

Individual Research Contribution Review, 2023, 1(1): 9–10

Removal of Diclofenac and Gliclazide in Sewage Treatment Plant Effluent by Electron Beam Irradiation

Khomsaton Abu Bakar
Radiation Processing Technology Division, Malaysian Nuclear Agency
43000 Kajang, Selangor
khomsaton@nm.gov.my

Abstract

A study examined the degradation of pharmaceutical chemicals in sewage treatment plant (STP) effluents using electron beam irradiation (EBI). Using EBI at 200 keV, 1 mA current, and irradiation doses from 10 to 100 kGy, the degradation of diclofenac (DFC), gliclazide (GLZ), and a combination of the two drugs was studied. The COD, TOC, NH_3-N, and pH of Sewage Treatment Plant (STP) effluent samples were measured before and after irradiation. The STP effluent samples were tested for toxicity using the mung bean germination screening approach. Targeted pharmaceutical molecules degraded significantly at irradiation dosages from 10 to 100 kGy, starting at 50 mg/L. At a dose of 10 kGy, the COD levels in STP effluent samples with DFC, GLZ, and DFC/GLZ drop by up to 51.82, 38.44, and 38.38%, respectively. STP effluent samples with DFC and GLZ showed nearly 100% TOC reduction at 10 kGy. At 10 kGy of irradiation, DFC/GLZ in STP effluent samples reduced TOC levels by 87.90%. The results suggest that ammonia nitrogen conversion to nitrogen nitrate may negatively impact the degradation rate of targeted medicinal compounds at doses from 50 to 100 kGy. Electron beam irradiation consider- ably increases the toxicity of STP effluent samples with DFC/GLZ.

Keywords: STP effluent, Diclofenac, Gliclazide, Irradiation

1 Introduction

Malaysia's wastewater treatment plants are releasing pharmaceutical residues into the environment, causing harm to humans and aquatic life. Ionizing radiation, a greener remediation technique, could potentially address this issue. This study investigates the degradation of DCF, GLZ, and DCF/GLZ mixture in STP effluent samples using the EBI technique, detecting degradation using HPLC and monitoring COD and TOC values.

2 Methods

The study used effluent samples from residential STPs, spiked with DCF, GLZ, and a mixture at 50mg/l, irradiated with low-energy electron accelerators, quantified using high-performance liquid chromatography, and conducted a toxicity screening test using mung bean germination.

3 Results

3.1 Degradation of DCF, GLZ and Mixture of DCF/GLZ in STP Effluent by Irradiation

Figure 1(a) and Figure 1(b) exhibit the degradation of DCF, GLZ, and a mixture of DFC and GLZ, respectively. The degradation percentage for DCF at irradiation doses of 50 kGy and 100 kGy was approximately 53% and 87%, respectively. The lowest concentrations of DCF attained at an irradiation dose of 50 kGy. Meanwhile, GLZ had shown a reduction of around 18% at 100 kGy. The result obtained clearly indicates that the degradation of DCF is relatively faster in comparison to GCZ. On the other hand, the degradation of both DFC and GLZ increases with irradiation doses in the mixture of DFC and GLZ. However, GCZ shows rapid degradation compared to DFC at an irradiation dose ranging from 10 kGy to 50 kGy. Meantime, both displayed a slower degradation trend at doses ranging from 50 kGy to 100 kGy.

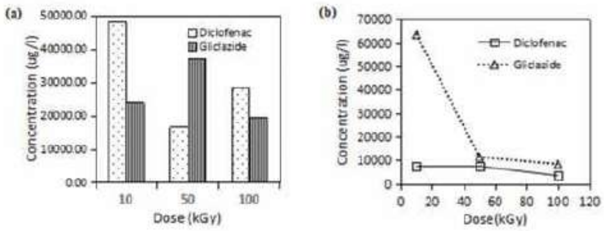

Figure 1: Degradation of single analyte (a) and mixtures of analyte by EBI in STP effluent

3.2 COD and TOC Removal

The study investigates the degradation of DFC and GLZ in STP effluent in terms of COD and TOC levels. The results (Figure 2) show a rapid reduction of these pollutants upon electron beam irradiation (EBI) at 10 kGy dose, slowed at 50 kGy, and almost insignificant at 100 kGy. The COD level for the mixture of DFC and GLZ was slightly higher at 50 kGy and 100 kGy compared to 10 kGy. The COD reduction percentage attained at 10 kGy was approximately 51.82, 38.44, and 38.38% for GLZ, DCF, and DCF/GLZ samples, respectively. However, at 50 and 100 kGy, the COD reduction percentage showed insignificant changes. The degradation of

GLZ and DFC is relatively rapid at 10 kGy due to the reaction of reactive species formed via the water radiolysis process. At higher doses, the degradation decreases due to competition between reactive species with the initial analyte, analyte by-products, and other matrices.

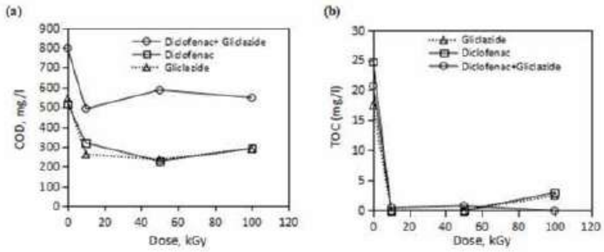

Figure 2: Effect of absorbed dose on (a) COD and (b) TOC in sample DCF, GLZ and DCF/GLZ

3.3 Effect of irradiation on NH_3-N, NO_2-N, NO_3-N

Ammonia-nitrate content decreases, and meanwhile, nitrite and nitrate content increase after EBI for all DFC, GCZ, and DFC/GCZ samples. The recorded ammonia-nitrogen reduction percentage were 89.5% and 83.9% for the GCZ and DCF samples, respectively, in comparison to 6.7% only for the DCF/GCZ at 10 kGy of irradiation dose.

3.4 Toxicity screening test

Figure 3 shows mung bean germination on the 5th day of irrigation with STP effluent (a), non-irradiated STP effluent containing a DCF/GLZ mixtures (b) and irradiated STP effluent having a mixtures of DCF/GLZ (c-e). The length of bean sprout in (a) and (b) were almost similar indicate that DCF/GLZ mixtures in STP effluent was not toxic on the mung bean germination. Irradiated STP effluent containing DCF/GLZ at 10 kGy and 50 kGy decreased mung bean germination, as demonstrated in 3(c) and 3(d), respectively; nevertheless, 3(d) demonstrated improved germination.

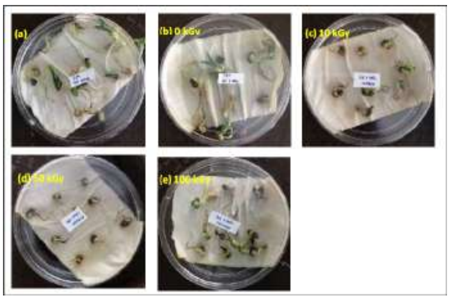

Figure 3: Changes in germination of Mung Bean after watering with STP effluent (a), non-irradiated STP effluent containing a DCF/GLZ mixtures (b), and irradiated STP effluent having a mixture of DCF/GLZ (c-e).

4 Discussion

Exposure to EBI causes the formation of reactive radical intermediates such hydroxyl radicals, hydrated electrons, and hydrogen atoms during water radiolysis (J.Wang and L.Chu, 2016). Radicals primarily degrade DFC and GLZ, which surged in STP effluent samples. Various solutes and organic compounds compete with reactive radical intermediates in wastewater. Real wastewater often contains large levels of chloride, carbonate, bicarbonate ions, and other organic compounds. Hydroxyl radicals combine with Cl^-, HCO_3^-, and CO_3- ions, forming dichloride radicals Cl_2- and carbonate radicals CO_3-, which oxidize contaminants. These radicals react intermediates interact with organic compounds via electron transfer, double bond addition, and H-atom abstraction, resulting in compound degradation. (S and Pal, 2015).

The degradation of GLZ and DFC in term of COD and TOC is relatively rapid at 10 kGy due to the reaction of reactive species formed via the water radiolysis process. At higher doses, the degradation decreases due to competition between reactive species with the initial analyte, analyte by-products, and other matrices.

Ammonia nitrogen reacts with OH radicals in order to form NH_2 radicals. Subsequently, NH_2 radicals react with H_2O_2 and OH. Thereafter, the oxidation of radical ammonia will rapidly occur • NHOH and NH_2O-$_2$. The unstable NH_2O-$_2$ will split into NO_2-, which can be oxidized to NO_3- by OH or H_2O_2. This explains the reduction in ammonia nitrate and the increase in nitrite and nitrate content upon irradiation.

It is possible that the more hazardous by-product of DCF/GCZ breakdown in STP effluent is the reason why germination is inhibited. Mung bean germination under 100 kGy irradiated STP effluent with DCF/GCZ resulted in superior growth, nonetheless, as demonstrated in. Possible explanation: increased NO_3-N levels brought on by greater doses of irradiation, which provide nutrients that promote better germination.

5 Conclusions

The EBI technique effectively degrades 50 mg/L of DCF, GCZ, and DCF/GLZ in STP effluent, but complete degradation cannot be achieved at doses ranging from 10 kGy to 100 kGy. Generally, reduction of DFC, GLZ, and DCF/GCZ concentrations, COD, and TOC level significantly slows down at irradiation doses ranging from 50 kGy to 100 kGy. This is most likely due to the increase in NO_2-N and NO_3-N concentrations. Irradiated STP effluent containing DCF/GLZ indicates are likely to be more toxic and significant germination inhibition were observed at a dose ranging from 10 kGy to 100 kGy.

References

J.Wang and L.Chu. 2016. Irradiation treatment of pharmaceutical and personal care products (PPCPs) in water and wastewater: an overview. *Radiation Physics and Chemistry*, 125:56–64.

B.Nimse S and D. Pal. 2015. Free radicals, natural antioxidants, and their reaction mechanisms. *Rsc Advances*, 5(35):27986–28006.

Individual Research Contribution Review, 2023, 1(1): 11–12

Study on Full Factorial Design of Epoxidized Natural Rubber/ Acrylonitrile-Butadiene-Styrene (ENR/ABS) Membrane by Electrospinning

Mahathir Mohamed
Radiation Processing Technology Division, Malaysian Nuclear Agency
43000 Kajang, Selangor
mahathir@nm.gov.my

Abstract

This study created membrane nanofibres using the electrospinning method and newly studied a mixture of ENR and ABS. The two-level complete factorial designs with centre points were used to characterise the functionality of the constructed membrane. The variables considered for experimental design were the polymer concentration, materials ratio (ENR concentration), applied voltage and distance between the needle tip and collector. According to the analysis of variance (ANOVA), the concentration of solution and distance were statistically significant parameters that affected the tensile properties of the ENR/ABS electrospun membrane. A mathematical model of the tensile property of polymer fibres was created using Response Surface Methodology (RSM). This model was built based on essential process factors.

1 Introduction

Electrospinning is a simple and versatile techniques to produce ultrafine fiber in a variety of materials, such as polymers, inorganic materials, and hybrid materials production. This technique can easily fabricate highly functional nanofibrous mats with high surface area to volume ratio, high porosity and uniform morphology (Tarus et al., 2016). Electrospinning involves a high voltage being applied on a contained polymer solution to create electrically charged jets of solution that get accelerated through a spinneret toward a grounded target that acts as a collector (Kim and Kim, 2017). There are two possibility to happen during jet travel which is fiber forming or spray forming. The production of ultrafine fibers from nanometer to sub micrometer range has being used in numerous applications, including food packaging, tissue engineering, wound dressing, protective clothing, high efficiency filtration, and many more (Chiu et al., 2016).

In this work, a copolymer of Acrylonitrile-butadiene-styrene (ABS) were prepared by using electrospinning technique. This polymer widely used in industry because of its good physical and mechanical properties, such as impact resistance and toughness. These properties are related to the composition blends of polymer. Polymer blend commonly will increase the mechanical and physical properties by adding Liquid Epoxidised Natural Rubber (LENR). Addition of LENR would further improve some special characteristics such as hydrophilicity and enhanced oil resistance and thermal stability. Further, it also would reduce surface tension, promote compatibility and improve the properties of the material (Saramolee et al., 2014).

In order to determine the relationship between factors that affecting electrospinning process so design of experiment (DOE) being applied. This DOE were based on the two level (2^k) with full factorial design. The 2-levels full factorial design particularly useful in the early stages of experimental work and the number of factors is less than or equal to 4. Combination of ABS and low molecular weight ENR would give essential impact on tensile properties of electrospun nonwoven membrane.

2 Methods

2.1 Materials

In this research, industrial grade Toyolac ABS (Acrylonitrile Butadiene Styrene) was used as the host polymer due to its high thermal and mechanical properties. Epoxidized natural rubber (ENR, 50 mol % conversion) was used as the modifier supply by Guthrie Malaysia. Degradation of ENR via UV irradiation to form low molecular weight liquid epoxidized natural Rubber (LENR). Acetone as solvent was purchased from Sigma Aldrich Chemical Co.

2.2 Preparation of the Electrospun Fiber Samples

ABS and LENR were dissolved in acetone at room temperature. The solutions were mixed and stirred thoroughly for 5 hours. The solutions were loaded into 20mL syringe and the inner diameter of needle was 1.2 mm.

Monitoring structural properties and morphological changes of electrospun membrane can be done using FTIR spectroscopy, thermal gravimetric analysis (TGA), contact angle and scanning electron microscopy (SEM). Physical properties can be investigated by universal tensile. The tensile tests were performed according to the ASTM 882 standard on INSTRON Universal Tester 4381L with 20N load. Five samples were tested per material at a 0.5 mm/min cross-head velocity. The length and width of the samples were 35 mm and 5 mm respectively.

2.3 Full factorial design of experiment method

Full factorials can be used to estimate the effects of all interactions. Analysis of variance (ANOVA) is reliable method of analysis and statistically significant in determine hypothesis on sample testing. ANOVA was utilized to gain those parameters which are significant furthermore affecting the quality of electrospun fibers and attain the optimum condition (Said et al., 2018).

The tensile properties of electrospun membrane fiber was carried out using 2-levels full factorial design. Total of 19 experimental runs including 3 replicates of center points were performed. The parameters conditions are shown in Table 1. These parameter settings considered based on preliminary study. Design Expert software version 10 (US, Stat-Ease Inc.) was used as tool for data statistical analysis.

Table 1: List of Parameters and their levels

Parameter (unit)	Symbol	Level 1	Level 2	Level 3
Concentration (%)	A	15	20	25
Ratio ENR:ABS (%)	B	10	30	50
Voltage (kV)	C	15	22.5	30
Distance (cm)	D	5	10	15

3 Result and Discussion

The parameters used in this study were evaluated by analysis of variance (ANOVA). Table 2 shows the influence of control variables on the measured responses.

Table 2: ANOVA results for tensile strength.

Source	Sum of Squares	df	Mean Square	F Value	p-value Prob > F
Model	0.58	7	0.083	4.26	0.0163
A-Concentration	0.18	1	0.18	9.24	0.0113
B-Ratio	9.950E-003	1	9.950E-003	0.51	0.4888
C-voltage	0.014	1	0.014	0.71	0.4159
D-distance	0.17	1	0.17	8.51	0.0140
BD	0.064	1	0.064	3.32	0.0957
CD	0.097	1	0.097	4.98	0.0474
BCD	0.050	1	0.050	2.57	0.1373
Residual	0.21	11	0.019		
Lack of Fit	0.21	9	0.023	6.29	0.1447
Pure Error	7.283E-003	2	3.641E-003		
Cor Total	0.79	18			
R-Squared	0.7306				
Adj R-Squared	0.5592				
Pred R-Squared	0.4967				
Adeq Precision	8.948				

Design expert software give analysis for the experiment datasheet of the response surface design. The p-values (significance) of the models are<0.0163 for tensile strength. Meanwhile other significant model terms are A (concentration), D (distance) and CD (interaction of voltage and distance). The R-squared (R^2) value for tensile strength is 0.7306 or 73% variability in response. The predicted R^2 of 0.4967 is in reasonable agreement with the adjusted R^2 of 0.5592 (the difference is less than 0.2). Lack of fit calculation ($p > 0.05$) suggested that the model still fits the data. Adequate precision is measurement of signal to noise ratio and the value 8.948 is adequate signal (greater than 4 is desirable).

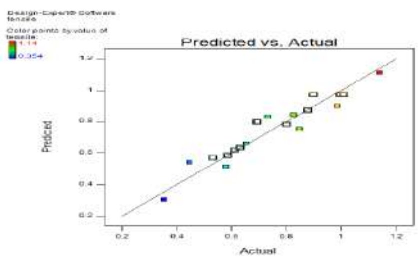

Figure 1: Predicted versus actual data for tensile strength

Figure 1 shows a graphical examination on the predicted versus actual plot. Actual tensile value is distributed relatively near to the predicted straight line. This reveal that parameters chosen gives some effect to the response thus the model can be considered reliable and repeatable.

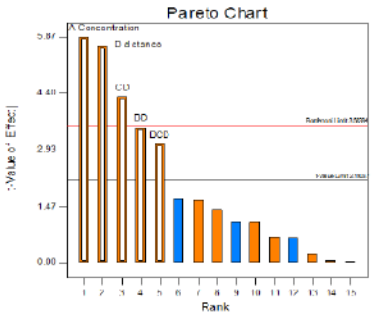

Figure 2: Pareto chart of standardized effects

Figure 2 shows the pareto graph for each parameter that influences the tensile strength. There are two parameters have a significant effect on the response of tensile which are concentration (A) and distance (D). These two parameters give positive effect which is tensile value was increased with increased the concentration or distance. The interaction parameters that can be considered give some effect to the response are CD, BD and BCD.

4 Conclusion

In this study, the electrospun ENR/ABS membrane were successfully prepared by electrospinning technique. The interaction of low molecular weight LENR and ABS in spinning solutions affects the solution viscosity and spinning ability. From the two-level (2^4) full factorial showed factor A, D and CD gives statistically significant compared another factor. Factor B, C, BD and BCD showed statistically insignificant, nevertheless it does not mean these factors are unimportant but it implies a little influence on fiber formation and response.

References

Yu-Jing Chiu, Mu-Huan Chi, Ying-Hsuan Liu, and Jiun-Tai Chen. 2016. Fabrication, morphology control, and electroless metal deposition of electrospun ABS fibers. *Macromol. Mater. Eng.*

Joo Ran Kim and Jung J. Kim. 2017. Epoxy resins toughened with surface modified epoxidized natural rubber fibers by one-step electrospinning. *Materials*, 10(464; doi:10.3390).

Jamal Abbas Ibtisam Said, Manaf Mohamed, Suhad Yasin, Zeravan Ali, and Idrees H Ahmed. 2018. Electrospinning of polyethylene terephthalate (PET) nanofibers: optimization study using taguchi design of experiment. *Materials Science and Engineering*, 454.

Prachid Saramolee, Natinee Lopattananon, and Kannika Sahakaro. 2014. Preparation and some properties of modified natural rubber bearing grafted poly(methyl methacrylate) and epoxide. *groups Montgomery: Design and Analysis of Experiments.*, 7th Edition. John Wiley Sons, Inc.

Bethwel Tarus, Nermin Fadel, Affaf Al-Oufy, and Magdi El-Messiry. 2016. Effect of polymer concentration on the morphology and mechanical characteristics of electrospun cellulose acetate and poly (vinyl chloride) nanofiber mats. 55:2975–2984.

Physical and Chemical Characteristics of EPOLA/PEGDA as a 3D Scaffold for Tissue Engineering Application

Marina Talib
Radiation Processing Technology Division
Malaysian Nuclear Agency
43000 Kajang, Selangor
marina@nm.gov.my

Abstract

In this study, EPOLA is incorporated into PEGDA resin as a natural based polymer resin to enhance properties of the scaffold. Characterization of the newly developed EPOLA/PEGDA scaffold is crucial before the full potential of the scaffold can be studied. Therefore, this paper reports the analysis from the characterizations conducted to confirm a successful crosslinking between EPOLA and PEGDA bioresin through UV crosslinking process. All the characterizations support the successful crosslinking of EPOLA and PEGDA bioresin, thus, can be further used to study the biofunctionality of the newly developed scaffold.

1 Introduction

Stereolithography (SLA) 3D printing that uses ultraviolet (UV) radiation as the curing source to build tissue scaffold has becoming more popular since UV offers a fast, efficient, requires less energy, and uses fewer chemicals (Ibrahim et al., 2022). In this study, Polyethylene Glycol Diacrylate (PEGDA) is chosen to be the control scaffold material since acrylates monomers are known for their high reactivity, polymerize rapidly in the present of photogenerated free radicals (Chen et al., 2018). To enhance the biological functionality of PEGDA scaffold, Epoxidized Palm Oil Acrylate (EPOLA) is introduced into a new bioresin for tissue scaffold development. It is expected that there will be an increase in the crosslinking percentage of the scaffold which further increases its porosity.

2 Methods

2.1 Design and Fabrication

A 3D scaffold of EPOLA/PEGDA was fabricated using stereolithography (SLA) 3D printer under The scaffold model was fabricated using a mixture of 54.584% PEGDA, 44.413% EPOLA, with 1.0% IR369 photoinitiator; UV crosslinked in SLA 3D Printer (ANYCUBIC LCD based SLA 3D Printer, UV integrated light - wavelength 405nm). The resin was stirred for 24 hr at 700 rpm using a magnetic stirrer after mixing to ensure smooth printing process. SLA 3D printer consists of a build platform, a resin tank, and an ultraviolet (UV) laser or light source. The build platform is positioned at the bottom of the resin tank, and the resin is poured into the tank. When the UV light hits the liquid resin, it causes a chemical reaction known as photopolymerization. The UV light triggers the resin to solidify and harden, layer by layer,based on the pattern of the specific slice from the chosen scaffold model.

2.2 Characterization

After the fabrication, characterizations were done to analyze the effects on the addition of EPOLA onto PEGDA resin after going through UV crosslinking process. These analyses are focused to study the successful crosslinking by chemical, morphological, and mechanical properties. Thus, degree of crosslinking was calculated using Gel Fraction Test, before were further analyzed using FTIR, AFM, and Universal Testing Machine to confirm the successful crosslinking.

3 Result and Discussion

3.1 Gel Fraction Test

Determination of EPOLA/PEGDA scaffold gel fraction percentage after UV crosslinking is the basis of the successful crosslinking of the new bioresin formulation. Figure 1 shows the comparison of gel fraction percentage of PEGDA and EPOLA/PEGDA.

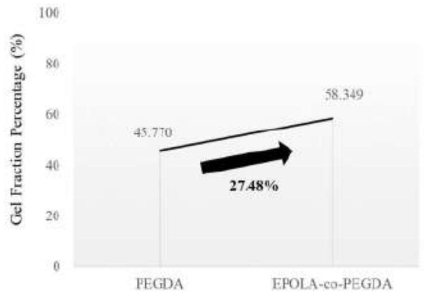

Figure 1: Gel Fraction Percentage (%) of PEGDA and EPOLA/PEGDA

From the gel fraction test conducted, gel fraction percentage of EPOLA/PEGDA is recorded at 58.349%, an increment of 27.48% from PEGDA, which recorded at 45.770%. A higher gel fraction percentage suggests a higher degree of crosslinking in the polymer network as more polymer chains were bonded with covalent bonds during the UV crosslinking process.

3.2 Fourier Transform Infrared Spectroscopy (FTIR) Analysis

IR spectra provides valuable information about molecular structure and functional groups. Figure 2 compares the FTIR spectral of PEGDA and EPOLA before crosslinking, with EPOLA/PEGDA after the UV crosslinking process.

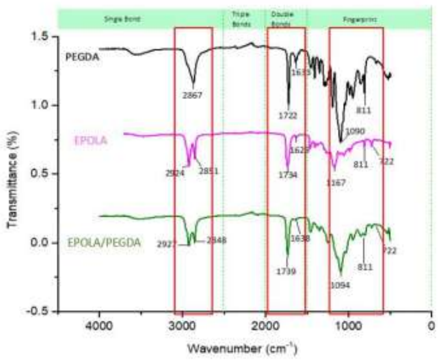

Figure 2: FTIR spectral of (a) PEGDA (b) EPOLA and (c) EPOLA/PEGDA

Based on the FTIR results as in Figure 2, the two peaks of EPOLA at 2924cm^{-1} and 2851cm^{-1} appeared in the crosslinked 3D Scaffold. It is also observed that there is shifting of peaks from 2924cm^{-1} to 2927cm^{-1} and 2851cm^{-1} to 2848cm^{-1}. The intensity of the peaks at the area of 1638cm^{-1} and 1739cm^{-1} are also reduced most probably due to the elimination of double bonds of C-H from PEGDA. Most peaks in the fingerprint region are also seen to shift and reduce in intensities in the area from 1500cm^{-1} - 500cm^{-1}. Obvious reductions can be seen at peak 1094cm^{-1}, 811cm^{-1}, and 722cm^{-1}. The shifting and reduction in intensities could suggest that there are changes in the molecular structure of EPOLA/PEGDA after UV crosslinking process.

3.3 Atomic Force Microscopy (AFM) Analysis

Topography changes can be observed after the crosslinking process. Figure 3 shows the 3D surface topography image of (a) PEGDA and (b) EPOLA/PEGDA Scaffold

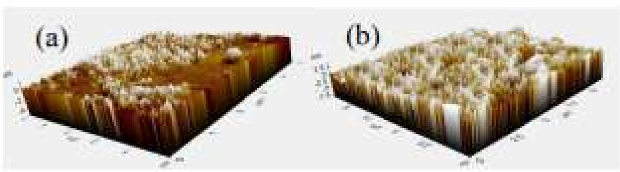

Figure 3: 3D Surface topography image of (a) PEGDA Scaffold and (b) EPOLA/PEGDA Scaffold

It can be observed that the surface of PEGDA scaffold appeared as a smooth, uniform surface with occasional bumps or ridges, while the surface of EPOLA/PEGDA scaffold displays a slightly undulating texture caused by the random orientation or the chance arrangement of its polymer chains.

3.4 Compressive Strength Analysis

The compressive strength of PEGDA and EPOLA/PEGDA scaffolds determined how much load the samples can bear under compressive forces. Figure 4 shows the comparison in compressive strength between both scaffolds.

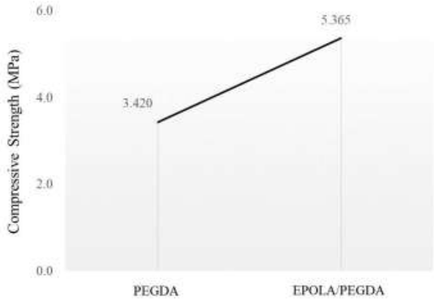

Figure 4: Compressive Strength of PEGDA and EPOLA/PEGDA

The compressive strength is recorded at 536.352 kPa for EPOLA/PEGDA, an increase of 56.82% as compared to PEGDA at 342.022 kPa. The compressive modulus is expected to be able to be tuned by varying the degree of crosslinking, which affects the density and stiffness of the polymer network.

4 Conclusion

The experimental data from the study proved a successful crosslinking between EPOLA and PEGDA, hence supporting the improvement of existing PEGDA resin served as resin for 3D scaffold development using UV crosslinking. Further research can be conducted to study the suitability of the new bioresin in terms of its biofunctionality to serve as a good tissue scaffold.

References

JY Chen, Hwang JV, Ao-Ieong WS, Lin YC, Hsieh YK, Cheng YL, and Wang J. 2018. Study of physical and degradation properties of 3D-printed biodegradable, photocurable copolymers, PGSA co-PEGDA and PGSA-co-PCLDA. *Polymers (Basel)*.

SNSS Ibrahim, Wahit MU, Talib M, Othman N, Shukri NA, Hilmi FF, Arshad MA, and editors. 2022. UV radiation crosslinking of Acrylated Palm Olein (APO) copolymer resins for 3D printing. *Key Engineering Materials*, Trans Tech Publ.

Individual Research Contribution Review, 2023, 1(1): 15–16

Performance Improvements in Graphene Nanoplatelet Modified Nylon 66 with Regard to Both Mechanical and Electrical Properties

Mohammed Iqbal Shueb
Radiation Processing Technology Division
Malaysian Nuclear Agency
43000 Kajang, Selangor
iqbal@nm.gov.my

Abstract

This research investigates the mechanical and electrical properties of nylon 66 containing a little quantity of graphene nanoplatelets (GNP). Nylon 66/GNP nanocomposites were created by dry mixing and then melted. The addition of 0.3 weight percent GNP increased nylon 66's tensile strength The increased electrical conductivity indicates how the improved dispersion of GNP at 0.3 weight percent can form an effective network for electron channel transmittance.

1 Introduction

Electromagnetic interference (EMI) arises when an electronic device emits disruptive electromagnetic radiation conducted or radiated channels (Tong, 2016). Shielding materials are crucial for safeguarding electronic and electrical equipment from EMI. One possible method for accomplishing this aim is to employ conductive metal in the form of filaments or particles by dissemination or spreading in the polymer (Geetha et al., 2009). The conductivity of electricity is an important factor in the operation of conductive polymer composites, CPC. Adding gold, silver, and copper particles to insulating polymers boosts their electrical conductivity (Al-Saleh and Sundararaj, 2012). Pure graphite is an excellent material for increasing the conductivity of polymer composites. Because of its high aspect ratio and conductivity, graphene nanoplatelet (GNP) increases polymer electrical conductivity at low concentrations (Eswaraiah et al., 2011). Graphene nanoplatelets (GNP) outperform carbon nanotubes (CNT) as EMI shielding inlays (Liang et al., 2009) because they are two-dimensional.

In this work, the introduction of GNP into nylon 66 as an infill material increases electrical conductivity. Sonication is the exfoliation of GNPs. The conductivity and physical-mechanical properties are examined to assess the effect of GNP enrichment.investigated in order to determine the influence of GNP enrichment.

2 Methodology and Materials

Nanocomposites were made using GNP and pure Nylon 66. Ultrasonic separation coupled nylon 66 with GNP. ASTM standard test sections were made using a Sino PSM 30 co-rotating twin screw extruder and HM 80 Battenfeld injection moulding machine. Nanocomposites were tested for tensile strength, and surface structure. FTIR examined the polymer nanoparticle's surface structure, while XRD studies the crystalline structure and interlayer spacing. At 1000x magnification, Leica Cambridge S-360 SEMs showed the nanocomposite's morphology.

3 Results and Discussion

3.1 Tensile Properties

Figures 1(a) and 1(b) show pure nylon 66 has the highest tensile strength at 55.17 MPa. Each 0.3 weight percent of GNP increases value by 15.2%, or 63.56 MPa. At 0.5 and 1.0 weight percent GNP, ultimate tensile strength is 44.19 and 41.34 MPa, respectively. Composites containing more than 0.3 wt% GNP may lose tensile strength. Because of improved interfacial stress transfer, dispersion, and aspect ratio, 0.3% GNP outperforms 0.5 and 1.0 wt%. Stress transmission and dispersion across interfaces contribute to reduced stress concentrations and better stress distribution as shown in Figure 1(b). Nylon 66 is soft due to its high tensile modulus (0.92 GPa) and low elongation at break (39.68%). GNP reduces elongation at break, which has an inverse relationship with Young's modulus. Modulus decreases by 9% when GNP is 1% of weight. Break elongation increases by 94% at a 1.0 wt% GNP intensity. GNP somewhat improved the composite's strength and ductility.

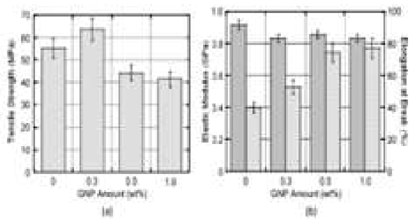

Figure 1: The values of (a) ultimate tensile strength and (b) Young's elastic modulus (left bar) and elongation at break (right bar) of nylon 66/GNP nanocomposites at various GNP amount

3.2 Crystallization

Figure 2(a) depicts the XRD patterns of pure GNP, pure nylon 66 (control), and nylon 66/GNP nanocomposite. The usual diffraction peak of GNP is 26.3° to 26.4°. The XRD pattern of the nylon 66/GNP nanocomposite reveals a crystal reflection of α-form polyamide 6. The presence of GNP in nylon 66 caused the 26.4° diffraction peak to disappear. The nylon 66/GNP composites with GNP concentrations of 0.5 and

1.0 wt% show different peaks at 45° and 51° angles. However, nylon 66 with a GNP concentration of 0.3 wt% lacks a diffraction peak. The presence of 0.3 wt% GNP in the nylon 66 matrix is evenly distributed and does not cluster inside the graphene layers. Figure 2(b) demonstrates that 0.3 wt% GNP concentration significantly affects the crystallization, aggregation, and assembly of nylon 66 chains.

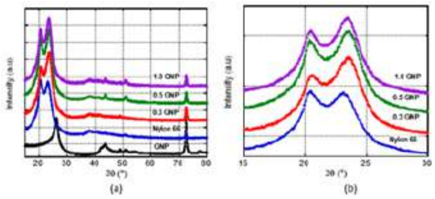

Figure 2: XRD spectra for (a) ($15° \leq 2\theta \leq 80°$) range, and (b) ($19° \leq 2\theta \leq 25°$) range of GNP, neat nylon 66 and nylon 66/GNP nanocomposited

3.3 Conductivity of electricity

Figure 3 shows the electrical conductivity values for the nylon 66/GNP nanocomposites. At 0.3 wt% GNP, electrical conductivity increased by seven-fold, from 10-14 to 10-07. The excellent electrical conductivity of high-dispersion graphene nanocomposites can be attributed to the electron-route transmittance network produced by GNP (0.3 wt%).

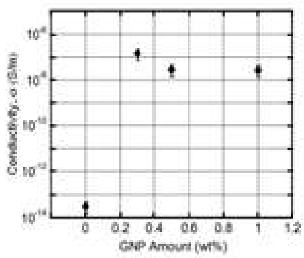

Figure 3: Electrical conductivity of nylon 66/GNP nanocomposites at various GNP amounts

3.4 Morphological Analysis

Figure 4(a)-(d) depicts SEM images of GNP nanocomposites and fragmented nylon 66. Shear-yielding lines on the fracture surfaces of nylon 66/GNP nanocomposites suggest the presence of graphene nanoplatelets, which assist to reinforce the matrix. Layered nylon 66/GNP nanocomposites have a rougher surface and are more malleable (see Figure 4b-d). Shear yielding causes nylon 66 nanocomposites containing GNPs to produce a fibrillar structure devoid of holes. GNP improves nylon 66 ductility (Figure 1(b). As a reinforcing material, 0.3% GNP transfers external stress to the reinforcement phase, lowering the matrix phase's load capacity. GNP induces brittleness in nylon 66.

4 Conclusions

In conclusion, our work reveals that a tiny amount of GNP can improve the mechanical and electrical properties of nylon 66.

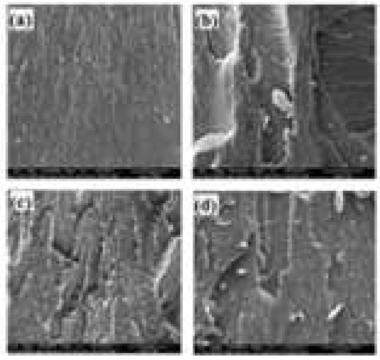

Figure 4: SEM images of nylon 66 filled with (a) 0 wt%; (b) 0.3 wt%; (c) 0.5 wt% and (d) 1.0 wt% of GNP at 500x magnification

It also highlights the significance of establishing great GNP dispersion in order for the addition to have the intended effect.

References

Mohammed H. Al-Saleh and Uttandaraman Sundararaj. 2012. Microstructure, electrical, and electromagneticinterference shielding properties of carbon nanotube/acrylonitrile–butadiene–styrene nanocomposites. *Journal of Polymer Science Part B: Polymer Physics*, 50(19):1356–1362.

Varrla Eswaraiah, Venkataraman Sankaranarayanan, and Sundara Ramaprabhu. 2011. Functionalized graphene–PVDF foam composites for EMI shielding. *Macromolecular Materials and Engineering*, 296(10):894–898.

S. Geetha, K. K. Satheesh Kumar, Chepuri RK Rao, M. Vijayan, and D. C. Trivedi. 2009. EMI shielding: Methods and materials—A review. *Journal of Applied Polymer Science*, 112(4):2073–2086.

Jiajie Liang, Yan Wang, Yi Huang, Yanfeng Ma, Zunfeng Liu, Jinming Cai, Chendong Zhang, Hongjun Gao, and Yongsheng Chen. 2009. Electromagnetic interference shielding of graphene/epoxy composites. *Carbon*, 47(3):922–925.

Xingcun Colin Tong. 2016. Advanced materials and design for electromagnetic interference shielding. *New York: CRC Press*.

Individual Research Contribution Review, 2023, 1(1): 17–18

Structural Hydrodynamic Behaviour and Wave Resistance Evaluation of Biocomposite Floating Jetty

Mohd Faizal Bin Abd Rahman
Radiation Processing Technology Division
Malaysian Nuclear Agency
43000 Kajang, Selangor
faizal@nm.gov.my

Abstract

This study focuses on the structural hydrodynamic behaviour and wave resistance evaluation of biocomposite floating jetty. The tests require all developed components for the floating biocomposite jetty including RX-HDPE floaters and biocomposite decking planks were produced and assembled to a 6500 x 1500 x 600mm pontoon. Hydrodynamic evaluation was conducted in a 50,000 x 30,000 mm coastal hydraulic basin facility in the National Hydraulic Research Institute of Malaysia, NAHRIM with maximum basin depth of 1,200 mm. No deflection and damage on the pontoon were observed during and after the test. Total loading capacity has been measured to be at 2,358.00 kg at 241.85kg/m^2 which is three times higher than application load per square meter for Malaysian Armed Forces personnel. Minimum mooring line strength requirement for jetty and pontoon boat application has been identified to be 2,784kg and 89.88kg respectively.

1 Introduction

Biocomposite floating jetty developments involves works from material formulations to product application evaluation. Structural hydrodynamics and wave resistance properties evaluation were essential to ensure application limits and workability of the floating jetty structures being installed in the field to suitably being used by Malaysian Armed Forces in their operations and logistics support.

To fulfil this application requirements, hydrodynamics evaluation was conducted to evaluate structural resilience and application limitations to simulate actual field environment. The evaluation was conducted using 1:1 scale prototype of biocomposite floating jetty module in a 50,000 x 30,000 x 1,200mm coastal basin capable of storing 1,200m^3 of water. The simulated oceanic wave was generated using multiple planar servo actuation.

The wave controls include wave intervals from 1.0-5.0 seconds and wave heights between 20mm to 400mm pre-setting. A wave scale was used to measure wave heights and wave lengths. This setup is capable to simulate rapid wave during windy or stormy weather and also simulating large wave lengths up to 10,000mm.

2 Methods

Figures 1 shows the experimental setup for hydrodynamic evaluation of biocomposite floating jetty module in the coastal basin in four point and single point mooring system.

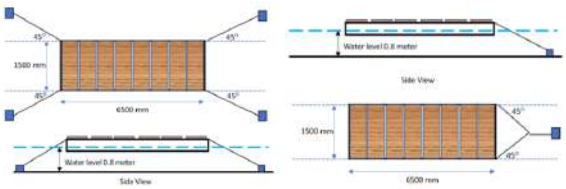

Figure 1: (Left) 4 point mooring setup and (Right) Single point mooring setup

Figure 2: Experimental setup of 6500 x 1500mm pontoon in 50,000 x 30,000mm Coastal basin

Prior to the hydrodynamic evaluation, static load data was measured to evaluate maximum loading capacity and total buoyancy of the pontoon module. Parameters and testing ranges are Wave Interval (sec),1.50/2.50/5.00; Wave Heights (mm),100/200/300/400; and Mooring type, 1-point / 4-point.

Table 1: Test Parameters

Controlled Variables	
Parameters	**Test Setting Range**
Wave Interval (sec)	1.50/2.50/5.00
Wave Heights (mm)	100/200/300/400
Mooring type	1-point / 4-point

A 700kg fixed load placed on top of the pontoon decks represents an approximate nine fully geared armed forces personnel as per one square meter per personnel area occupancy of the module. This setup simulates full operational load of pontoon in actual application. A wave force sensor is installed at both bow end of the pontoon.

3 Data Collection

3.1 Static load data

Figure 3: Static load data collection

Table 2: Pontoon Static Load Test Data

No. of Tank (x100kg)	Forward Draft (mm)	IBC Tank (kg)	Stern Draft (mm)	Total Load (kg)
400	26	700	34	1,100
500	27	700	35	1,200
600	30	700	35	1,300
700	34	700	34	1,400
700	34	800	36	1,500
700	35	900	40	1,600
700	32	1,000	40	1,700
Measured structure weight:			658 kg	

3.2 Hydrodynamic data collection

Figure 4: Hydrodynamic evaluation of pontoon

Table 3: Hydrodynamic Data Collection

Test Condition	Max. Wave Height (mm)	Wave Intervals (sec)	Max. Wave Force (kg/m^2)	Minimum Required Mooring Capacity (kg)	Max. Drag Force (kg)
No Load 4 mooring point	691.30	1.50/2.50/ 5.00	69.08	2,234.00	2,892.00
700kg load 4 mooring point	590.10	1.50/2.50/ 5.00	55.92	2,784.00	5,521.00
700kg load 1 mooring point	534.10	2.50	26.31	89.88	2,032.80

3.3 Post Test Structural Observation

It was observed that no damage had been implied to any components of the biocomposite floating jetty module during hydrodynamic tests conducted. No leaks have been found in all RX-HDPE floater units and no cracks found on biocomposite decking planks.

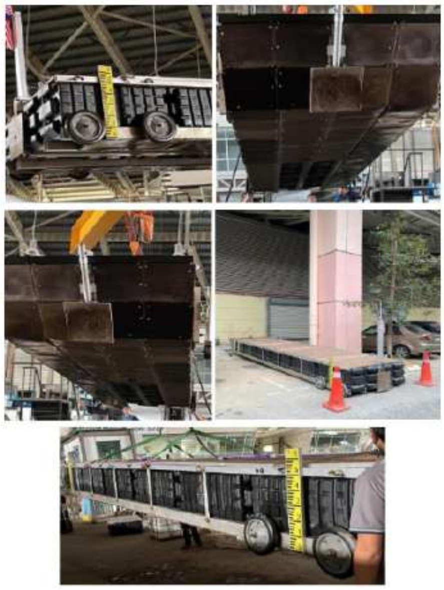

Figure 5: Structural integrity inspection post hydrodynamic test

4 Discussions

Throughout the hydrodynamic test conducted, maximum wave heights and wave lengths measured was 691.3mm and 10,000mm respectively. Wave force was recorded up to 69.80kg/m^2. A good structural resilience was seen on the pontoon structures and components throughout the tests against dynamic forces generated from waves and loads implied on the pontoon. Even when some extreme waves over topping the structures, no sign of failure were seen on the pontoon components as well as no load shifts happen.

The pontoon structure has a flat bottom design creating high stability. Use of modular floaters in the structural assembly permits high buoyancy and stable load carrying capacity of 1400kg maximum not including 658kg of overall structure weight.

The pontoon drafts at maximum 2,358.00kg static load were 420mm equivalent to 70 percent immersion of total pontoon body. Therefore, the jetty structure has a total carrying capacity of 241.85kg/m^2 with 30 percent load safety factor. 700kg fixed load placed on top of the pontoon decks represents an approximate nine fully geared Malaysian Armed Forces personnel as per one square meter per personnel area occupancy of the module. From hydrodynamic test, it is seen that the assembly of floaters creating a flat bottom hull design has high stability even at maximum 619.30mm wave heights and rapid waves of below 2.5 seconds interval simulating high wind or storm weathe

Individual Research Contribution Review, 2023, 1(1): 19–20

Gamma Degraded κ-Carrageenan as Plant Growth Promoter

Maznah Mahmud
Radiation Processing Technology Division
Malaysian Nuclear Agency
43000 Kajang, Selangor
maznah@nm.gov.my

Abstract

The κ-carrageenan powder was exposed to gamma ray at 75kGy to prepare low molecular weight carrageenan (LMCarra), 10kDa. The LMCarra was then tested on kale and mustard to observe its growth promoting activity on seed germination and plants.

Keywords: carrageenan; growth promoter; gamma ray

1 Introduction

Sabah is the main red seaweed producer from *Kappaphycus sp*. and *Eucheuma sp*. in Malaysia (Salleh et al., 2013). The seaweed is processed through alkaline treatment to produce carrageenan. Generally, carrageenan exists as long chain polymer, exhibits low solubility property and has high viscosity solution that limits its application. Carrageenan indicates better performance as plant growth promoter and plant elicitor at low molecular weight (García et al., 2015). Carrageenan can be degraded to lower molecular weight by chemical (acidolysis), biological (enzymatic) and physical techniques (sonication, microwave, gamma radiation and electron beam radiation) (Naeem et al., 2015a). The irradiation of carrageenan powder by gamma induces glycosidic chain scission. Study by San et al. in 2021 the LMCarra below 10 kDa indicated promising results on chloropyll content and bean yield of coffee plants. Meanwhile Naeem and friend (Naeem et al., 2015b) reported irradiated carrageenan with Mw, 20kDa induces tremendous growth promotion and alkaloid content of *Catharanthus roseus*.

2 Methods

2.1 Preparation of CarraPGP & Investigation of its growth promotion activity

The 10000 Da CarraPGP was prepared by gamma irradiation at 75kGy in powder form. The CarraPGP powder was dissolved in water at 4 different concentrations which were 20, 40, 60, 80, and 100 ppm. The solutions were applied on plants by spraying 2 times a week. The soil was supplied with fertilizer according to the farmer's practice. The growth promotion was observed on yield, leaf area and root length. The untreated plants were labelled as Water. The pot test was carried out for 33 days for both mustard and kale under greenhouse.

3 Results

3.1 Growth activity on mustard

Figure 1. illustrates the growth rate of plant height of mustard after treated with CarraPGP at various concentrations. Treatment of 80 ppm showed the highest shoot growth. Meanwhile for roots, the growth rate is similar for all treatments and untreated plants as shown in Figure 2. The Figure 3, the CarraPGP also indicates an insignificant effect on leaf width (area) compared to untreated mustard. However, 80 ppm indicated highest biomass and yield, as shown in Figure 4.

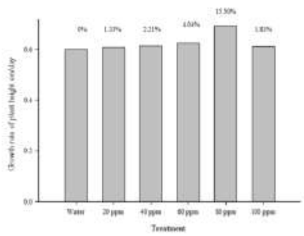

Figure 1: The plant height growth rate of mustard treated with various concentrations of CarraPGP.

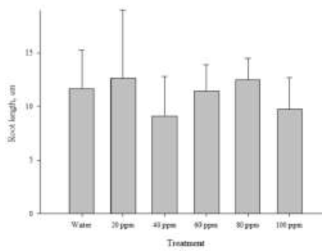

Figure 2: The effect of CarraPGP on root length of mustard.

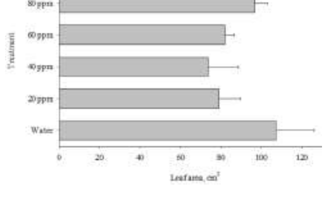

Figure 3: The effect of CarraPGP on the mustard leaf size.

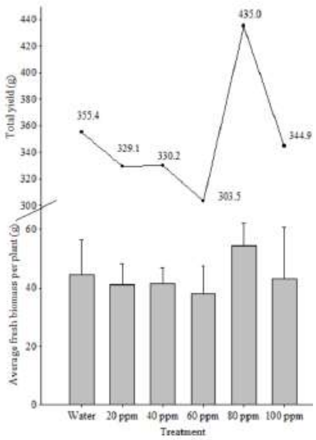

Figure 4: The average fresh biomass (g) per plant and yield after treated with CarraPGP at various concentrations.

3.2 Growth activity on kale

The different effects of CarraPGP observed on kale. In Figure 5, the growth rate of kale significantly improved for all CarraPGP treatments compared to untreated kale. The treatment of 60 ppm gives the highest growth rate. Figure 6, the CarraPGP shows an insignificant effect on kale root. However, the CarraPGP still gives better effect on root length of kale root compared to untreated kale. The kale leaf size also improved as treated with CarraPGP as in Figure 7, the 80 ppm contributes to great leaf development. Figure 10, the 80 ppm also gave promising results on fresh biomass and yield of kale.

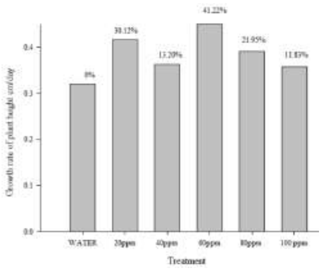

Figure 5: The growth rate of kale height after treated with CarraPGP at various concentrations.

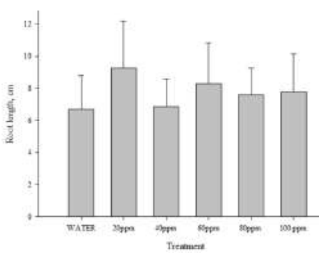

Figure 6: The effect of CarraPGP on root of kale

4 Conclusion

The CarraPGP prepared through radiation induced degradation reaction on carrageenan. The CarraPGP shows growth

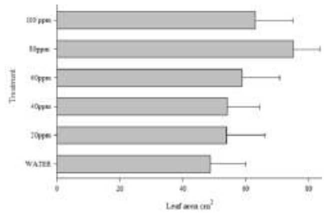

Figure 7: The effect of CarraPGP on the kale leaf size

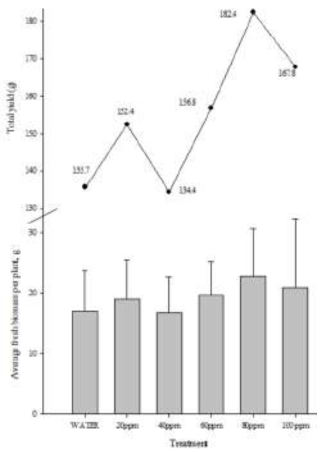

Figure 8: The average fresh biomass (g) and yield after CarraPGP treatments.

promoting effects on mustard and kale at all concentration (20–100 ppm). However, the 60–80 ppm indicated the highest growth promoting activity on mustard and kale.

References

M. A. García, N. de la Paz, C. Castro, J. L. Rodríguez, M. Rapado, R. Zuluaga, and A. Casariego. 2015. Effect of molecular weight reduction by gamma irradiation on the antioxidant capacity of chitosan from lobster shells. *Journal of Radiation Research and Applied Sciences*, 8(2):190–200.

M. Naeem, M. Idrees, T. Aftab, M. M. Alam, M. M. A. Khan, M. Uddin, and L. Varshney. 2015a. Radiation processed carrageenan improves plant growth, physiological activities, and alkaloids production in Catharanthus roseus L. *Advances in Botany*, 2015:1–11.

M. Naeem, M. Idrees, T. Aftab, M. M. Alam, M. M. A. Khan, M. Uddin, and L. Varshney. 2015b. Radiation processed carrageenan improves plant growth, physiological activities, and alkaloids production in Catharanthus roseus L. *Advances in Botany*, 2015.

Norhuda Salleh, Aisah Hosin, and Budi Anto Tamring. 2013. Estet mini rumpai laut: Program ke arah peningkatan taraf hidup isi rumah berpendapatan rendah , Semporna Sabah. *Prosiding Perkem Viii*, 3:1167–1176.

P. T. San, C. M. Khanh, H. H. N. Khanh, T. A. Khoa, N. Hoang, P. D. Thinh, and T. D. Nguyen. 2021. Impacts of - oligocarrageenan application on photosynthesis, nutrient uptake and bean yield of coffee (Coffea robusta). *Sains Malaysiana,*, 50(11):3171–3179.

Individual Research Contribution Review, 2023, 1(1): 21–22

Characterization of Recycled Electron Beam Irradiated Polyethylene terephthalate (PET) flakes for Potential Synthesis of Carbon Nanomaterials as Functional Fillers for Radiation Curable Radon Mitigation Coating and Antiviral Coating

Mohd Hamzah Harun
Radiation Processing Technology Division, Malaysian Nuclear Agency
43000 Kajang, Selangor
hamzah@nm.gov.my

Abstract

Research is underway to identify novel uses for recycled plastic, with polyethylene terephthalate (PET) emerging as the most promising option for recycling. One strategy is to upcycle recycled plastic to create a better material by using electron beam irradiation. In this study, PET was irradiated with five different doses of electron beam irradiation and the purpose is to investigate the physicochemical changes occurring in PET flakes in comparation with virgin recycled plastic (PET) flakes. This was accomplished by the use of characterization technique, such as the structural and chemical composition analysis (XPS – X-ray photoelectron spectroscopy). The results of the comparative study between the virgin and the irradiated PET flakes concluded that electron beam irradiation can be used to improve the properties of PET. However, the effects of the irradiation are complex and depend on the dose of irradiation.

Keywords: recycled PET, microplastics, electron beam irradiation

1 Introduction

The abundance of waste disposal in the plastics industry is a major environmental problem. Polyethylene terephthalate being one of the most widely used plastics, and it can take hundreds of years to decompose in a landfill. Electron beam irradiation is a promising technology for upcycling PET waste, which can be used to sterilize PET and improve its mechanical properties.

In this study, we will evaluate the effects of electron beam irradiation on PET used as an upcycling material in comparison with the virgin recycled PET flakes. PET flakes are produced by sorting, washing, grinding, drying, and other processes from PET bottle wastes (Telli and Özdil, 2015). The findings of this research will aid in our understanding of the possibilities of electron beam irradiation to be a useful tool for lowering the environmental impact of the plastics industry.

2 Methods

The PET bottles were crushed into flaky fragments using a crusher machine as part of a mechanical recycling process. The crushed PET size ranges between 1-10 mm. The PET is prepared in 6 plastic bags, with approximately a teaspoon of PET flakes in each packet. 1 of the packets will be the control virgin PET and 5 packets for the electron beam irradiated PET flakes. The Alurtron Malaysian Nuclear Agency's EPS 3000 electron beam equipment is used for the sample preparation of electron beam irradiation. The five samples were irradiated at five different dosages (20, 40, 60, 80, and 100 kGy), respectively.

2.1 Materials

Polyethylene terephthalate (PET) flakes used in this study was sourced from recycled water bottles. Before utilization, recycled PET microplastic flakes were recovered and crushed by a crusher machine. The crushed PET flakes' size ranges between 1-5 mm.

2.2 Characterization

The X-ray photoelectron spectroscopy (XPS) method was used to investigate the modifications in composition on the surface of PET after irradiation. Monochromatic X-ray source from Al-Kα (hni = 1486.7 eV) with Nexsa G2 Thermo Fisher Scientific were used. The survey spectra, deconvoluted C1s and O1s core lines, valence band spectra, and atomic concentration with C/O ratio were acquired.

3 Data/Results

3.1 X-ray Photoelectron Spectroscopy (XPS)

Because of the shallow depth of penetration (a few nanometers), X-ray photoelectron spectroscopy highlights potential surface modifications. The C1s XPS spectra demonstrate that the identical bonds, originating from the structure of PET, are present in all materials at 284.8 eV, 286.7 eV, 288.6 eV, and 290.9 eV, which are characteristic for C-C, C-O, C=O, and O=C-O, respectively, as shown in Figure 1. Table 1 shows the quantitative variations in the chemical composed of the materials investigated. Predominantly, the C/O ratio varies in relation to irradiation dose. An atomic concentration per specific carbon bonds in the PET flakes suggests that the quantity of C-C bonds falls a little after 60 kGy irradiation and fluctuates at higher irradiation doses. Predominantly, the C/O ratio varies in relation to irradiation dose. After 20 kGy electron beam irradiation, the C/O ratio increases slightly from 2.89 to 3.13, and after 40 kGy irradiation, it climbs to 4.18. At 60 kGy, the ratio falls to the value of 3.05. After 80 kGy irradiation the value increases to 3.53 and decreases again to 3.19 after 100 kGy electron beam irradiation. However,

Table 1: Atomic concentrations of carbon, oxygen, and specific carbon bonds on the PET surface following radiation at various radiation doses, determined with XPS

Sample (PET flakes)	Atomic Concentration (%)			C/O ratio	Atomic concentration per carbon bonds (%)			
	C1s	O1s	Si		C-C	C-O	C=O	O=C-O
0 kGy	74.3	25.7	-	2.89	32.60	48.19	14.32	4.89
20 kGy	75.79	24.21	-	3.13	71.81	10.53	8.29	9.37
40 kGy	80.71	19.29	-	4.18	58.52	24.77	7.32	9.39
60 kGy	75.3	24.7	-	3.05	55.86	20.44	15.20	8.50
80 kGy	77.91	22.09	-	3.53	63.88	20.10	7.47	8.55
100 kGy	75.69	23.7	0.61	3.19	43.87	39.47	13.98	2.69

silicon (Si) element is detected at 100 kGy electron beam irradiation, possibly due to silicon contamination from the PET flakes themselves. These impurities may come from the raw materials used to make the PET, or they may be introduced during the PET manufacturing process. Tapes, lubricants, and silicone adhesives are all potential sources of silicone contamination. Physical contact with materials or apparatus can spread silicone contamination. Silicones are found in a wide range of lotions, personal care products, hair products, deodorants, and glasses cleaning tissues (Petrie, 2013).

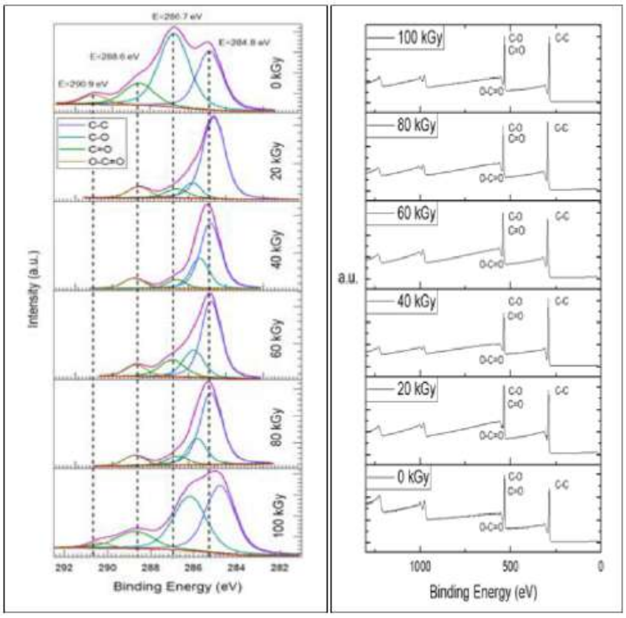

Figure 1: C1s XPS spectra with fitting for PET – unirradiated and irradiated at different doses and XPS spectra of valence band (VB) of PET – control and irradiated at different doses

4 Discussion/Conclusions

Electron beam irradiated polyethylene PET with 5 different doses were successfully developed. The results of the X-ray photoelectron spectroscopy demonstrate that following electron beam irradiation, the PET flakes' chemical composition has changed. The PET irradiated properties effect is very minor due to the stable pristine structure of the PET although after being irradiated by high ionization energy. The irradiation enhanced and damaged the properties of materials, leading to a complex interplay between beneficial modifications and subtle detrimental structural changes.

References

E. M. Petrie. 2013. Addressing silicone contamination issues. *Metal Finishing*, 111(4):27–29, https://doi.org/10.1016/S0026–0576(13)70253–8.

E. Sarioğlu and H. K. Kaynak. 2018. PET bottle recycling for sustainable textiles. *In Polyester - Production, Characterization and Innovative Applications. InTech.*, (https://doi.org/10.5772/intechopen.72589).

A. Telli and N. Özdil. 2015. Effect of recycled PET fibers on the performance properties of knitted fabrics. *Journal of Engineered Fibers and Fabrics.*

A. Torlakoğlu and G. Güçlü. 2009. Alkyd–amino resins based on waste PET for coating applications. *Waste Management*, 29(1):350–354, https://doi.org/10.1016/j.wasman.2008.02.018.

Individual Research Contribution Review, 2023, 1(1): 23–24

Development of Filtration Membrane from CNT-reinforced Carbon Fibers based Radiation-Assisted Nanocomposite for Water Purification and Desalination

Mohd Roslie Ali
Radiation Processing Technology Division, Malaysian Nuclear Agency
43000 Kajang, Selangor
roslie@nm.gov.my

Abstract

The paper is discussing on development of membrane technology as one of critical solution in prevention of clean water scarcity. Recent advances in nanotechnology provide effective approaches to enhance the performance of membrane with their synergistic effects for water purification and desalination. Carbon Nanotubes (CNT), combined with Carbon Fibers (CF) as reinforcement duo, can offer promising advanced composites as smart materials to adapt in membrane for enhancing the performance of permeability and rejection, simultaneously. By combination of Electrophoretic deposition (EPD) technique as coating method with assisted radiation in composite formation, new top barrier layer of CNT-reinforced CF based nanocomposite can be obtained as smart membrane to satisfy both the need of a high-performance membrane and the fouling-resistant ability. This review will cover the development aims, from the preparation of CNT suspension, the reinforcement of CNT-reinforced CF in nanocomposite matrix as a layer of membrane and the evaluation of membrane properties as significance performance improvement in water purification and desalination.

Keywords: Filtration; Membrane; CNT-reinforced CF; Nanocomposite; Electrophoretic Deposition; Radiation-Assisted; Purification; Desalination

1 Introduction and Methods

In the following sections, the development on water purification and desalination of mixed matrix membrane, based in polymer matrix, improved with nanocomposite layers which consist of Carbon Fibers Reinforced with CNT via electrodeposition (EPD) method, assisted with radiation (UV or EB) will be mainly focused and aimed. The functions and factors which affecting the properties of the membrane, the optimization in filtration membrane efficiency as well the improvement in resistance and antifouling, are comprehensively discussed.

2 Discussion and Conclusion

This membrane will grow demand for treated and purified water in emerging economies and also will solving the problem of clean water scarcity especially in major city and the dependency of untreated natural water sources in rural areas. The free-scarcity of water sources will be the factor in development and acceleration of socioeconomic driver (WATER & FOOD) and will provide a good life for people.

This membrane filtration with improved properties of antifouling, biocides resistant and more durable, will helps

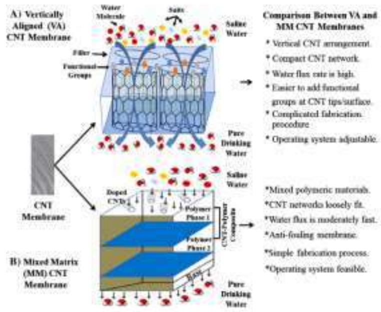

Figure 1: A prototype of CNT membrane. Shown are trapping of salts and movement of water molecules from salinated water through (A) SWCNT and (B) Mixed Matrix CNT-based membranes

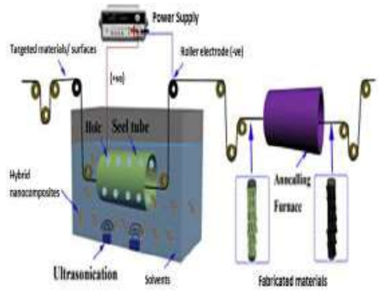

Figure 2: A pilot scale or E-coat of CNTs on CF surface by EPD

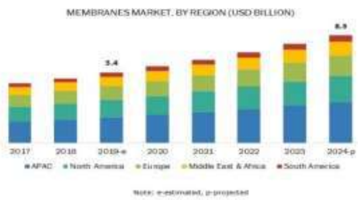

Figure 3: Global membranes market in 5 years projection (2019-2024)

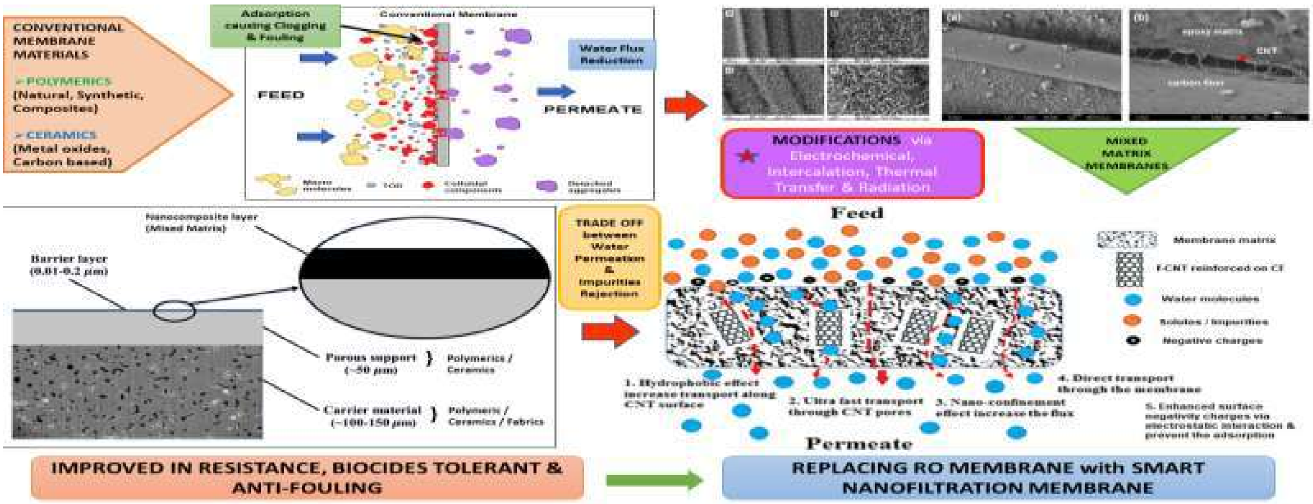

prevent the consumption of energy which already remains top problems. This will help in consolidate various water-treatment associations and societies, and to gain profit for local filtration product maker, which reduce dependable on imported filtration technology.

References

Mohammed Hossein Davood Abadi Farahani and Vahid Vatanpour. 2019. Polymer/carbon nanotubes mixed matrix membranes for water purification. *Nanoscale Materials in Water Purification*, 4.

Lining Ma, Xinfa Dong, Mingliang Chen, Li Zhu, Chaoxian Wang, Fenglin Yang, and Yingchao Dong. 2017. Fabrication and water treatment application of carbon nanotubes (CNTs)-based composite membranes: A review. *Membranes*, 16(7).

Individual Research Contribution Review, 2023, 1(1): 25–26

The Optimisation of Mechanical Properties of Fish Gelatin as Biodegradable Films

Mohd Shahrulnizam Ahmad
Radiation Processing Technology Division
Malaysian Nuclear Agency
43000 Kajang, Selangor
m_shahrulnizam@nm.gov.my

Abstract

The mechanical properties of the biodegradable polymer are crucial to determine the application of the materials. The gelatin from the skin of tilapia fish is dissolved in 100 millilitres (ml) of distilled water and mixed with glycerol as a hydrophilic plasticiser, then cast and dried to produce films. The range contents of fish gelatin and glycerol used are 5.0 to 9.0 grams (g) and 10 to 20 % (w/w), respectively for 200 bloom and 8.0 to 12.0 g with glycerol 30 to 40 % (w/w) for 250 bloom of gelatin. The maximised formulation for 200 bloom is 9 g with 10% glycerol (Ts) and 9 g with 20% glycerol (EB). For 250 bloom, the maximised formulation is 8 g with 30% glycerol and 10 g with 40% glycerol.

Keywords: biodegradable, gelatin, casting, glycerol, plasticiser

1 Introduction

Biodegradable materials break down through the enzymatic action of bacteria, fungi, and algae when placed in bioactive environments (Folino et al., 2020). A group of proteins known as gelatin has been carefully studied and has the ability to form films (N. et al., 2018). Plasticisers can reduce gelatin's brittle and easy crack properties (A. et al., 2011). A plasticiser's function minimises gelatin's natural brittleness by lowering intermolecular pressures. RSM is a group of mathematical and statistical methods beneficial for issue modelling and analysis where the objective is to maximise a response that is of interest and is affected by several variables (Noordin et al., 2004).

2 Methods

Using a mechanical stirrer at room temperature, quantities of fish gelatin powder weighing 5.0, 7.0, and 9.0 grams (g) for 200 bloom were mixed with 100 ml of distilled water for each. Respective portions of glycerol from 10, 15, and 20% (w/w) were then added to the solution of fish gelatin. For 250 bloom, gelatin powder weighed 8.0, 10.0 and 12.0 grams with glycerol of 30 to 40% (w/w). All mixtures were heated at 50°C for 10 minutes under continuous stirring to obtain homogenous solutions. Each filmogenic solution was added to a clean Petri dish in a quantity of around 25 ml, and the plates were then dried in a drying oven for 48 hours at 45°C. Then, dried films were peeled off to undergo tensile strength and elongation at break testing.

Tensile strength (Ts) and elongation at break (EB) values were determined using a Universal Tensile Machine 20 kilonewton (kN) (Shimadzu AG-Xplus) from Kyoto, Japan, with the ASTM D882 method. Filmstrips measuring 60 mm × 15 mm were prepared with a cutting blade. The gauge length was 40 mm, and filmstrips were stretched 10 millimeters (mm)/min until rupture. Ts (MPa) was calculated as equation (1) below:

$$\text{Tensile Strength} = \frac{F_{max}(N)}{A(m^2)} \tag{1}$$

where F_{max} is the maximum load (N) required for rupture and (A) is the cross-sectional area (m^2) of the film.

The percentage of EB was calculated as equation (2) below:

$$\text{Elongation at Break} = \frac{I_{max}}{I_0} \times 100 \tag{2}$$

3 Results and Discussion

Tables 1 and 2 showed that EB increased while tensile strength declined with increasing glycerol concentrations. The plasticising effect of glycerol, which reduces connections between neighbouring chains in the biopolymer and increases mobility and film flexibility, is most likely the cause of this activity. However, the bloom of 250 fish gelatin in Table 2 gives a higher value of EB than 200 bloom. This is attributed to the fish films exhibiting plastic flow during the tensile test. As proof, Hanani et al. (2012) reported that 8 g of 240 bloom fish gelatin showed the highest EB (100.91%) with an incorporation of 40% glycerol.

Figures 1(a) and 2(a) showed that the Ts decreased, and Figures 1(b) and 2(b) showed that EB increased significantly, especially for 200 bloom with glycerol. This can be proved by the study on the impact of the physical characteristics of gelatin plasticised with glycerol and sorbitol mixtures (Thomazine et al., 2005). However, the EB of 250 bloom of fish gelatin at 12 grams (g) gelatin is dropped with glycerol. This might be because this plasticised film has already achieved antiplasticisation at this formulation stage. Other than that, these plasticiser contents (30-40% w/w) also exceed the compatibility limit, as Bakry et al. (2017) reported.

4 Conclusion

In summary, by using the response surface methodology (RSM) method or Design-Expert Software, it can be concluded that the maximised formulation for 200 bloom is 9 g

Table 1: Coded values of fish gelatin films (200 bloom) condition and responses of 13 experimental runs

Run	Factors		Responses	
	Fish Gelatin Contents (g)	Glycerol Contents (% w/w)	Tensile Strength (N/mm^2)	Elongation at Break (%)
1	7	20	6.51	38.70
2	7	15	8.63	21.95
3	5	20	10.23	24.56
4	9	10	29.04	2.83
5	7	15	11.78	28.83
6	7	15	12.19	32.54
7	5	10	21.57	11.43
8	9	15	13.66	31.98
9	7	15	15.23	39.29
10	7	15	9.08	22.72
11	5	15	14.24	25.27
12	9	20	10.60	44.31
13	7	10	19.68	7.07

Table 2: Coded values of fish gelatin films (250 bloom) condition and responses of 13 experimental runs.

Run	Factors		Responses	
	Fish Gelatin Contents (g)	Glycerol Contents (% w/w)	Tensile Strength (N/mm^2)	Elongation at Break (%)
1	8	35	4.77	67.21
2	10	35	2.96	118.42
3	10	35	2.84	117.94
4	10	35	3.03	113.39
5	10	35	3.29	109.00
6	10	40	3.05	123.55
7	10	35	3.13	117.61
8	10	30	3.75	105.02
9	12	30	3.63	78.72
10	8	30	5.42	63.16
11	8	40	4.15	72.30
12	12	35	3.05	88.32
13	12	40	3.04	77.36

with 10% glycerol (Ts) and 9 g with 20% glycerol (EB). For 250 bloom, the maximised formulation is 8 g with 30% glycerol and 10 g with 40% glycerol. The maximised formulation of 250 bloom gelatin will be used for the next modification, which is crosslinking incorporation.

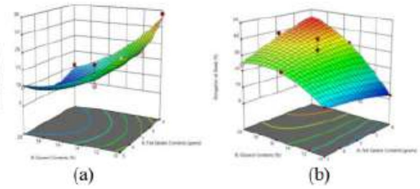

Figure 1: The Effect of Fish Gelatin and Glycerol Contents in 3D Surface Plots (200 bloom) for (a) Tensile Strength; (b) Elongation at Break

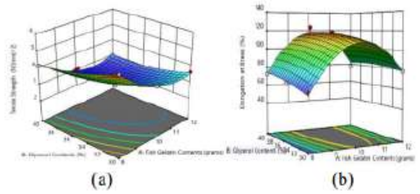

Figure 2: The Effect of Fish Gelatin and Glycerol Contents in 3D Surface Plots (250 bloom) for (a) Tensile Strength; (b) Elongation at Break

References

Vieira M. G. A., Silva M. A., Santos L. O., and Beppu M. M. 2011. Natural-based plasticizers and biopolymer films: A review. *European Polymer Journal*, 47(3):254–263.

Bakry N. F., Isa M. I. N., and Sarbon N. M. 2017. Effect of sorbitol at different concentrations on the functional properties of gelatin/carboxymethyl cellulose (CMC)/chitosan composite films. *International Food Research Journal*, 24(4):1753–1762.

A. Folino, A. Karageorgiou, P. S. Calabrò, and D. Komilis. 2020. Biodegradation of wasted bioplastics in natural and industrial environments: A review. *Sustainability*, 12(15):6030.

Hanani Z. N., Roos Y. H., and Kerry J. P. 2012. Use of beef, pork and fish gelatin sources in the manufacture of films and assessment of their composition and mechanical properties. *Food Hydrocolloids*, 29(1):144–151.

Suderman N., Isa M. I. N., and Sarbon N. M. 2018. The effect of plasticizers on the functional properties of biodegradable gelatin-based film: A review. *Food Bioscience*, 24:111–119.

M. Y. Noordin, V. C. Venkatesh, S. Sharif, S. Elting, and A. Abdullah. 2004. Application of response surface methodology in describing the performance of coated carbide tools when turning AISI 1045 steel. *Journal of Materials Processing Technology*, 145(1):46–58.

M. Thomazine, Carvalho R. A., and Sobral P. J. 2005. Physical properties of gelatin films plasticized by blends of glycerol and sorbitol. *Journal of Food Science*, 70(3):E172–E176.

Individual Research Contribution Review, 2023, 1(1): 27–28

Electro Impedance Spectroscopy (EIS) Analysis for Graphene Oxide as Corrosion Agent Preventive in POBUA

Mohd Sofian Alias
Radiation Processing Technology Division, Malaysian Nuclear Agency
43000 Kajang, Selangor
sofian@nm.gov.my

Abstract

Metal oxide layer produced via electrochemical cell assisted by corrodent agent on metal surface is known as corrosion. The mechanism involved oxidation of metal at the anode and the reduction of oxygen at the cathode. In this article the responsible of Graphene oxide (GO) to retard corrodent agent pathway in POBUA curable coating were studied by using Electrochemical Impedance Spectroscopy (EIS).

Keywords: corrosion, graphene oxide, EIS

1 Introduction

Corrodent agent is an element that causes the rusting on metal surface. Therefore it is very important to control the presence and movement of corrosion agents. Polymer protective layer application is one of the practical method to prevent corrosion process on metal surface. However, this layer can still be penetrated by corrosive agents due to the voids in the polymer layer (Alias et al., 2022). Therefore, the addition of GO is very effective to extend the period of corrosion agent penetration rate and at the same time protect the metal surface from corrosion. EIS is a very useful method to investigate the properties of coatings against the corrosion process. This technique indicates the movement of the electron charge in the polymer layer which can be used as a guide in understanding the behaviour of the polymer layer as well as studying the influence of the composition of the polymer layer in inhibiting the corrosion process.

1.1 Methodology

Electrochemical Impedance Spectroscopy (EIS) was used to study the corrosion behaviour of the coatings. All samples POBUA + GO (0.1 wt.%, 0.5 wt.%, 0.8 wt.%) were evaluated in 3.5% NaCl.

The three-electrode assembly included the coated specimen as the working electrode, a graphite rod as the counter electrode, and SCE as the reference electrode. The exposed coated steel surface area was 1 cm^2. The EIS measurements were performed at the open circuit potential with a 10 mV RMS sinusoidal amplitude and 10 points per decade, covering a frequency range from 0.01 Hz to 100 kHz. For the Tafel polarization curves, they were plotted with a scanning rate of 0.125 mV/s and an initial potential of 250 mV below Eoc to a final potential of 250 mV above Eoc. To interpret all the collected data, the Gamry Echem Analyst software was employed.

2 Results

The EIS data were analyzed by fitting them with circuit models depicted in Figure 1. The obtained results include the following parameters: solution resistance (Rs), resistance of the POBUA-GO rich coating (Rcoat), charge transfer (corrosion) resistance (Rct), capacitance of the POBUA-graphite coating (Qc), and electric double layer capacitance (Qdl).

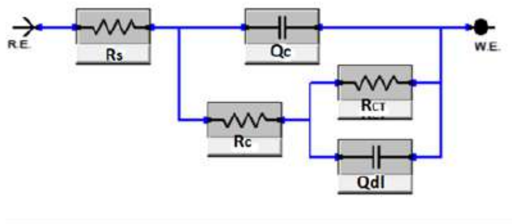

Figure 1: Equivalent circuits (EC) for the one-time constant system

Nyquist fitted plots, elucidate the corrosion resistance performance of mild steel coated with blank POBUA and POBUA coatings containing 0.1 wt.%, 0.5 wt.%, and 0.8 wt.% of GO. The percentage of corrosion protection calculated using Equation 1 as follows:

$$\text{Percentage of protection} = \frac{Rct - Rct^0}{Rct} \times 100 \quad (1)$$

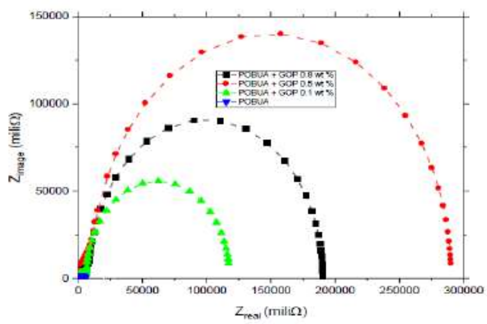

Figure 2: Nyquist fitted plots of POBUA and POBUA/GO coatings with different percentages of GO

3 Discussion

Each fitted plot consists of two-time constants, indicating the occurrence of corrosion beneath the coating. The plots suggest that the electrolyte penetrated through pores or cracks, while the second time constant at low frequencies corresponds to the corrosion process (Suleiman et al., 2020). The presence of a second loop in the Nyquist curve explains the corrosion process that occurs after the formation of a passive layer due to the reaction between the mild steel surface and the electrolyte beneath the coating. It was observed that the increasing percentage of GO led to larger semicircles in the Nyquist plots, indicating improved corrosion protection compared to the blank POBUA coatings. The Rct value exhibited a similar trend, reaching its highest value for the POBUA coatings with 0.5 wt.% and 0.8 wt.% GO. The Rct value explains the contribution of GO in protecting mild steel from corrosion.

The increase in GO content in the POBUA matrix hinders the penetration of corrosive agents from the electrolyte to the mild steel surface and increases the diffusion path length. Furthermore, the presence of well-distributed GO in the POBUA matrix is believed to contribute to filling the fine pores within the coating. This reduces the penetration of water through the coating layer, thereby improving its corrosion resistance properties, this phenomenon is well described by Kumar et al 2021 (Kumar et al., 2021). in this study the highest percentage for corrosion protection is from POBUA with 0.5 wt. % which gives 99.64% protection compared to neat POBUA which only gives a protection of 63.6%.

4 Conclusion

Regarding EIS analysis, the coating's performance can be measured by corrosion protection percentage via Rct value. Nyquist plot which extract from EC value also give good explanation for polymer coating performance behaviour in protecting metal surface from corrosion.

References

M.S. Alias, N.K. Othman, S.R.M. Kamarudin, M.H. Harun, M. Mohamed, N.U. Saidin, S.F. Mohamad, and Z. Samsu. 2022. Influence of graphite particles in uvcurable corrosion protection coating from palm oil based urethane acrylate (POBUA). *Ind Crops Prod.*, 187(115436, https://doi.org/https://doi.org/10.1016/j.indcrop.2022.115436.).

S.S.A. Kumar, S. Bashir, K. Ramesh, and S. Ramesh. 2021. New perspectives on graphene/graphene oxide based polymer nanocomposites for corrosion applications: The relevance of the graphene/polymer barrier coatings. *Prog Org Coat*, 154(106215,https://doi.org/https://doi.org/10.1016/j.porgcoat.2021.106215).

R.K. Suleiman, A.M. Kumar, A.Y. Adesina, F.A. Al-Badour, M.H. Meliani, and T.A. Saleh. 2020. Hybrid organosilicon-metal oxide composites and their corrosion protection performance for mild steel in 3.5 *Corros Sci.*, 169, https://doi.org/10.1016/j.corsci.2020.108637.

Individual Research Contribution Review, 2023, 1(1): 29–30

Gamma-Induced Modification of LCST Value for Thermosensitive Nanogels

Mohd Yusof Hamzah
Radiation Processing Technology Division
Malaysian Nuclear Agency
43000 Kajang, Selangor
m_yusof@nm.gov.my

Abstract

A promising cancer-targeting strategy employing a heat-responsive delivery system was explored. This system undergoes reversible physical or chemical changes in response to changes in temperature depending on its lower critical solution temperature (LCST), which is near to that of a tumour (~40°C). However, an extensive literature review shows that most synthesized heat-responsive materials have LCSTs below 37°C, risking a premature trigger condition outside a tumour site. The ideal LCST value is ~40°C, so a triggered tumour release can be achieved. A single-step, carcinogenic-free, and green technique to synthesize nanogels with tunable LCST using the gamma radiation-induced copolymerization method has been demonstrated herein. Nanogels with LCST values up to ~40°C were successfully produced.

Keywords: gamma radiation; nanogels; LCST; thermosensitive material

1 Introduction

Cancer has been one of the top killers in Malaysia; in 2018 alone, there were 26,365 deaths from cancer, with 43,837 new cases (WHO and others, 2010). It has not only presented a substantial burden on the government finances for drug costs but also the quality of lives of the patients. One possible way of addressing the government's high spending on imported drugs and treatment costs is by developing local drug delivery materials of high efficiency. Among many delivery materials, temperature-responsive nanogels have gained the most interest due to their reversible structural changes in response to temperature depending on their lower critical solution temperature (LCST).

On the other hand, tumour tissues that undergo high growth rate, as well as rapid metabolism, differ from normal tissues in that the former has lower pH (5.3), higher temperature (~40°C) and large irregular cellular gaps (>50 nm) (Koay et al., 2004), these discrepancies can be exploited. A high-efficiency drug delivery system can be designed by modifying its LCST value up to ~40°C.

Herein, a single-step, carcinogenic-free, and green technique to synthesize nanogels with tunable LCST value using gamma radiation-induced copolymerization was proposed. The amplification of the LCST is done by chemically grafting amine moieties from DMAEMA to the main polymeric chains.

2 Methodology

2.1 Materials

NIPAAM, 99%, PVP, 99%, PEGDA, and 98% DMAEMA were purchased from Sigma-Aldrich and used without prior purification. Ultrapure water (UPW) was used throughout this work for all solution preparations.

2.2 Synthesis of Thermosensitive Nanogels

NIPAAM, PVP, PEGDA and DMAEMA were dissolved in water at specific molar ratios (Shafie et al., 2021). The mixture was aliquoted into several vessels and purged with N_2 30m before irradiation. Each vessel was irradiated at 5, 10, 15 and 20 kGy. Then, the nanogels were dialyzed against UPW using a 12kDa MCO membrane (48h). They were then lyophilized and resuspended in UPW for subsequent characterization and testing.

Changes in chemical structures were monitored using a Brucker FTIR, and the particle size was monitored using a Sympatec particle size analyzer.

3 Result

3.1 Formation of Thermosensitive Nanogels

Figure 1 illustrates the FTIR spectra of the nanogels. Strong peaks at 800–1,000 cm^{-1} corresponding to the stretching mode of vinyl double bonds were diminished, indicating complete polymerization and corresponding monomer depletion. The peaks at 2,913–2,971 cm^{-1} represent -CH stretching vibration of the backbone polymers. Two additional peaks at 1,635 and 1,557 cm^{-1} can be attributed to the amide carbonyl group and the bending of the amide N–H group, respectively, while absorption bands at 1,443– 1,457 cm^{-1} were expected due to the bending vibration from the CH_3 group.

4 Discussion

In the dilute solution regime, upon absorption of the ionizing energy, the aqueous media absorbed the energy from the irradiation source, which then led to the formation of several species of radicals (1):

$$H_2O \rightarrow \text{e-aq}, .OH, H., H_2O_2, H_2, H+, OH- \qquad (1)$$

Out of these radicals, the hydroxyl radicals (.OH) are known to react with the macromolecules due to their much higher rate

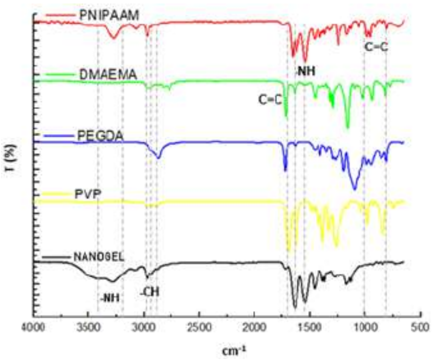

Figure 1: FTIR spectrums of unirradiated monomers and nanogels irradiated at 20 kGy.

of reaction and concentration compared to the other species (Shimanovich et al., 2015).

The .OH radicals reacted with the polymeric reactants via hydrogen abstraction of the vinyl group from the polymers (Wang et al., 2008), hence creating macroradicals with active sites on polymeric backbones. It has been established that the reaction paths of these unstable macroradicals are molecular recombination, forming grafted polymeric structures.

The decline in size of the nanogels from 25 to 40°C (Figure 2) corroborated the suggested mechanism and FTIR spectra.

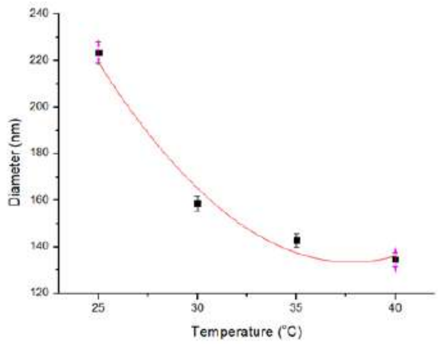

Figure 2: The changes in the nanogels size as a function of temperature demonstrate the increase in LCST values.

The sample with the highest concentration of DMAEMA formed the smallest nanogels, measuring from 134 nm to 223 nm, within the ideal size range for drug delivery applications, which was 70-200 nm. This observation suggests a compaction that may be due to the steric effect of the amine moieties on the main polymeric backbones.

The concept of the LCST modification is based on the addition of the amine moieties from the DMAEMA oligomers. The more amine group grafted on the backbone polymers, the more stable the nanogels are at a higher temperature due to the stronger hydrogen bonds between the moieties and the nanogels backbone and the adjacent solvating water molecules. Therefore, instead of losing their solubility at 37°C, they were able to resist the higher temperature. As the nanogels become insoluble, they collapse and release their payload (Figure 3). This observation was consistent with other works (Klouda, 2015).

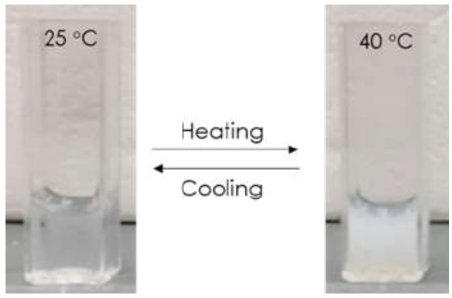

Figure 3: The nanogels lose their solubility, collapse and release their payload at 40°C.

5 Conclusions

A single-step, carcinogenic-free, and green technique to synthesize nanogels with tunable LCST using gamma radiation-induced copolymerization method has been demonstrated. Nanogels with LCST value up to ~40°C were successfully produced.

References

L. Klouda. 2015. Thermoresponsive hydrogels in biomedical applications: A seven-year update. *Eur J Pharm Biopharm*, 97(Pt B):338–49.

J. Koay, C. Herry, and M. Frize. 2004. Analysis of breast thermography with an artificial neural network. *The 26th Annual International Conference of the IEEE Engineering in Medicine and Biology Societyc*, pages 1159–1162.

Wolfbeis. O.S. 2015. An overview of nanoparticles commonly used in fluorescent bioimaging. *Chemical Society Reviews*, 44(14):4743–4768.

N. F. A. Shafie, M. Y. Hamzah, and R. R. Ali. 2021. Nanogels obtained by gamma radiation-induced polymerization. *Polimery*, 66(9):451–458.

U. Shimanovich, Y. Song, J. Brujic, H.C. Shum, and T.P. Knowles. 2015. Multiphase protein microgels. *Macromolecular bioscience*, 15(4):501–508.

B. Wang, X. D. Xu, Z. C. Wang, S. X. Cheng, X. Z. Zhang, and R. X. Zhuo. 2008. Synthesis and properties of Ph and temperature sensitive P(Nipaam-Co-Dmaema) hydrogels. *Colloids Surf B Biointerfaces*, 64(1):34–41.

WHO et al. 2010. Pharmaceuticals: restrictions in use and availability.

Individual Research Contribution Review, 2023, 1(1): 31–32

Bio-Enhanced Geopolymer using Fly Ash and Biocomposite

Muhammad Aidell Amir
Radiation Processing Technology Division
Malaysian Nuclear Agency
43000 Kajang, Selangor
aidell@nm.gov.my

Abstract

This research explores the synthesis of sustainable geopolymer materials by incorporating fly ash and biocomposite elements, aiming to create environmentally friendly alternatives to conventional cement-based structures. Compressive strength results after 28 days of curing reveal intriguing findings. The compressive strength of the conventional Ordinary Portland Cement (OPC) mortar stands at 10.6 MPa. In comparison, the geopolymer derived solely from fly ash exhibits a strength of 4 MPa, underscoring its potential as a sustainable alternative but revealing a need for improvement. However, the introduction of biocomposite materials into the geopolymer mixture results in a compressive strength of 8.32 MPa, signifying a promising enhancement over the geopolymer without biocomposite. This novel combination demonstrates not only the viability of geopolymerization using fly ash but also the potential for biocomposite materials to contribute to the mechanical robustness of the resulting geopolymer. The findings highlight a path toward sustainable construction materials with improved compressive strength, offering a greener alternative for the building industry.

Keywords: Geopolymer, Fly Ash, Biocomposite

1 Introduction

Fly ash is a by-product of coal combustion generated by energy production company. It has become a significant environment issue as their production of coal waste (slug and fly ash) has increased year over year with fly ash constituting about 500 milion tones at 75-80% of the total ash produced (Joshi and Lothia, 1997). The large-scale storage of wet fly ash in ponds, which consumes a great deal of precious land, is still used to dispose of sizable amount of ash. In the near future, it could also lead to serious environmental devastation.

Although it is considered as waste, fly ash is a resource that has not yet been fully utilized from the standpoint of coal utilization. Fly ash can be considered as the world's fifth largest raw material resource (Mukherjee et al., 2008). Therefore, there is a dire need to develop a sustainable cement technology. It is also being studied as a use in recycling materials for agriculture (Kikuchi, 1999) and engineering (Iyer and Scott, 2001). With reduced carbon footprint, geopolymer has been found to possess superior edge. However, the optimum formulation which yields superlative performance of geopolymer has yet to be determined.

This project focuses on developing a formulation for fly ash based geopolymer, by comparing with a standard Portland Cement as a based line, and with addition of biocomposite kenaf based. The product was compared according to the compressive tested at 7, 14 and 28 days.

2 Methods

Briefly, formulation begin with producing fly ash geopolymer concrete with different concentration and ratio. Then continue with compatibility of other material while testing its strength and compare it with the commercial product. If the product does not achieve its designated strength, formulation will start over as per flow chart Figure 1. Succeeded product undergoes characterization using multiple kind of instrument and machine to compare with the literature.

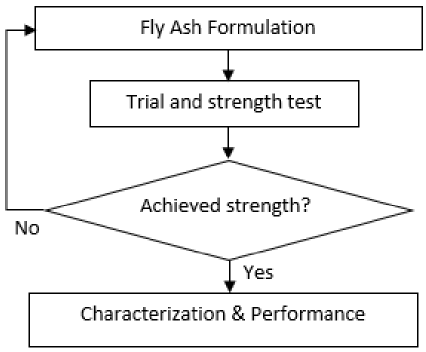

Figure 1: Flow chart of formulation and characterization of fly ash geopolymer concrete

3 Data/Results

Compressive strength results after 28 days of curing shows interesting findings as per Table 1.

3.1 Compressive strength over time

The compressive strength of the Normal OPC Mortar shows a steady increase over time. At 3 days, it starts at 3.2 MPa and progresses to 10.6 MPa at 28 days. This aligns with the expected trend of cement-based materials. In contrast, the biocomposite fly ash geopolymer demonstrates a slower but

Table 1: Compressive strength test between OPC vs with vs without bio composite fly ash geopolymer

Age (days)	Normal OPC mortar		Biocomposite fly ash geopolymer		Without biocomposite fly ash geopolymer	
	Reading	Compressive Strength (Mpa)	Reading	Compressive Strength (Mpa)	Reading	Compressive Strength (Mpa)
3	72	3.2	24	1.1	11	0.5
7	112	5	97	4.32	22.5	1
14	221	9.8	160	7.12	65	2.9
28	239	10.6	187	8.32	89.9	4

continuous improvement in compressive strength. It begins at 1.1 MPa at 3 days and reaches 8.32 MPa at 28 days. This suggests a unique strength development pattern compared to the OPC mortar. Similarly, the geopolymer without biocomposite exhibits an increase in strength over time. Starting at 0.5 MPa at 3 days, it reaches 4 MPa at 28 days. The trend is similar to the biocomposite geopolymer but with lower final strength.

4 Discussion

Comparing the compressive strengths at 28 days, the Normal OPC Mortar has the highest strength at 10.6 MPa. The biocomposite fly ash geopolymer follows at 8.32 MPa, and the without biocomposite fly ash geopolymer is at 4 MPa. While the geopolymer variants have lower strengths than OPC mortar, they demonstrate potential as environmentally friendly alternatives.

4.1 Influence of Biocomposite

Notably, at all measured ages, the geopolymer with biocomposite consistently outperforms the geopolymer without biocomposite in compressive strength. This suggests a positive impact of the biocomposite on the overall strength of the geopolymer. In terms of rate of strength gain, it is interesting to observe that the biocomposite geopolymer shows a more gradual strength gain compared to the geopolymer without biocomposite. This gradual increase may indicate a sustained and progressive development of strength over time in the presence of biocomposite materials.

The presence of biocomposite materials significantly contributes to the compressive strength of the geopolymer. This highlights the potential of using biocomposites in geopolymerization for sustainable construction practices. Understanding the time-dependent nature of strength development is crucial for predicting the material's behavior in real-world applications. The slower, more sustained strength gain observed in the geopolymer with biocomposite materials may have implications for construction timelines.

4.2 Implications and future directions

The project's emphasis on geopolymerization, especially with the integration of biocomposite materials, aligns with sustainability goals in construction. Despite slightly lower strengths, the environmental benefits of these materials may outweigh the reduction in strength. Further optimization of the biocomposite geopolymer mixture could potentially enhance its strength without compromising its sustainability. This might involve adjusting the ratio of components or exploring additional strengthening agents. The study could benefit from an exploration of other mechanical and durability properties of the materials. This would provide a more comprehensive understanding of their performance in practical applications.

5 Conclusions

In conclusion, the project underscores a nuanced balance between sustainability and compressive strength. While the geopolymer with biocomposite materials exhibits lower strength compared to OPC mortar, it emerges as a promising sustainable alternative. This lays the groundwork for future improvements and applications in the construction industry.

References

M. Ahmaruzzaman. 2010. A review on the utilization of fly ash. *Progress in Energy and Combustion Science*, pages 327–363.

R. Iyer and J. Scott. 2001. Power station fly ash - a review of value-added utilizaton outside of the construction industry. *Resour Conserv Recycl*, 31:217–228.

R. Joshi and R. Lothia. 1997. Fly ash in concrete: production, properties and uses. In: Advances in concrete technology.

R. Kikuchi. 1999. Application of coal ash to environmental improvement - transformation into zeolite, potassium fertilizer, and FGD absorbent. *Resour Conserv Recycl*, 27:333–346.

A. Mukherjee, R. Zevenhoven, P. Bhattacharya, K. Sajwan, and R. Kikuchi. 2008. Mercury flow via coal and coal utilization by-products: a global perspective. *Resour Conserv Recycl*, 52(4):571–591.

Individual Research Contribution Review, 2023, 1(1): 33–34

Determination of Factor Influence on Irradiated Waste Polyethylene Terephthalate (PET) as a Filler for Construction Material

Muhammad Hazim Muhammad Sayuti
Radiation Processing Technology Division
Malaysian Nuclear Agency
43000 Kajang, Selangor
hazim@nm.gov.my

Abstract

The recycle PET which is acquired from bottle preform manufacturing waste is subjected to 3.0 MeV EB to produce RC-PET. Absorbed radiation dose of recycle PET ranging from 0 – 200 kGy being investigate for their crystallization phase, molecular weight. Characterization of irradiated PET performed in order to achieve the optimum dose for recycle PET before being use as filler in construction material. The irradiated samples undergo mechanical, thermal and morphological testing. The specialty material from recycle PET will be further used in concrete reinforcement. Concrete mixer machine will be employed to produce the concrete of nano silica and RC-PET. The mixing parameters such as filler percentage and absorbed radiation dose will be optimized in order to obtain better compressive strength and cost effectiveness. The changes in compressive strength, impact strength, modulus of rupture, elastic modulus, water absorption, density, mechanical and physical properties of the concrete will be evaluated.

1 Introduction

Recycle PET used for the concrete reinforcement was already widely being used as a concrete reinforcement such as in Malaysia, Bangladesh, Mexico, China and India. This is due to the environmental pollution caused by PET that has been extensively discussed and the best solution proposed is recycling. Therefore, one of the potential means to the problem is to recycle polyethylene terephthalate (PET) in the construction industry as fiber concrete (FC). Based on literature review and global citations, no yet studies on PET crystallization phase using Electron Beam technique and being used as in concrete reinforcement.

This project aims to study the Electron Beam Radiation Crystallization, RC techniques on recycle PET for recycling purpose. PET was widely used in plastic bottles industry as its promising properties as a recyclable material. PET Plastics are some of the more commonly discussed plastics when searching for solutions for drinking water. Unlike other types of plastics, PET considered safe and is represented on water bottles with the number "1", indicating it is a safe option. These plastics are a type of thermoplastic, useful in various applications.

As in this project, the study of recycle PET on its crystallization phase using irradiation technique by using Electron Beam irradiation will be studied. Various doses will be bombarded on PET in order to achieved optimum dose for crystallization of PET. The optimum RC-PET will be used in the preparation of concrete with nano silica, before undergo the characterization on physical and mechanical properties.

2 Methods

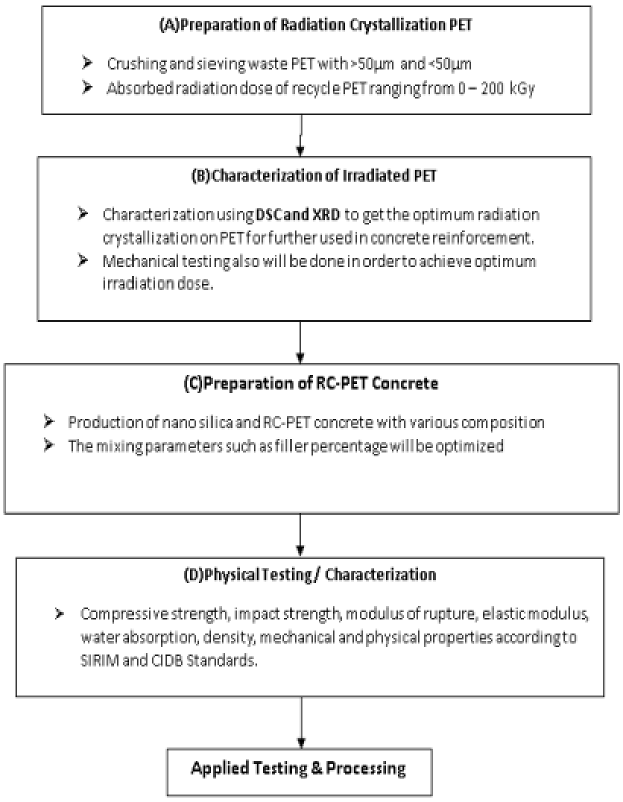

3 Results and Discussion

The irradiated samples showed some increment in their mechanical properties after being bombarded with electron beam. Tensile strength with different dose was summarized in Figure 1. Tensile strength of the PET increased with increasing of irradiation dose. Tensile strength of pure PET was 30.1 MPa. When undergo the irradiation dose from 50 up to 200kGy, the tensile strength increasing to 30.3, 31.3, 32.2 and 32.1 MPa respectively. This occurred due to the cross linking of the

PET. The highest tensile strength recorded is 32.2 MPa with irradiation dose of 150 kGy.

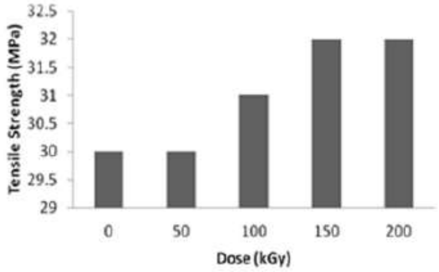

Figure 1: Tensile Strength

The hardness test was carried out and the results shown in the Figure 2 below. From the figure, the hardness of cross-linked PET showed at 150 kGy achieved the highest value and decreasing when being radiated with 200 kGy.

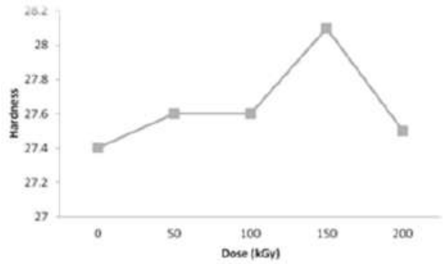

Figure 2: Hardness

From the graph shown, the degree of crosslinking was increased with increasing of irradiation dose. From 0% of gel content degree, it is increased up to 42% when being irradiated with electron beam with dose of 50, 100, 150 and 200kGy respectively. This showed PET undergoes the crosslinking process throughout the irradiation using electron beam.

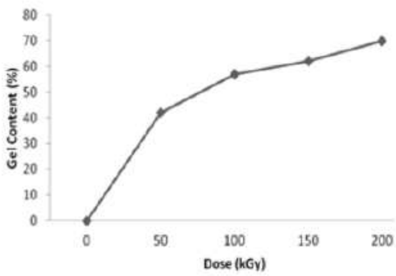

Figure 3: Gel Content

The thermal properties of samples were determined by DSC analysis. The value of melting temperature, Tm, glass transition temperature, Tg and degree of crystallinity, %Xc of each samples were summarized in Table 1.

The Tm value of the PET pure is increase in increasing of the irradiation dose but decreasing when being bombarded with 200kGy. For the Tg, the Tg for the PET pure is decreased when bombarded with electron beam. The reduction of Tg could be attributed to chain branching due to a crosslinking reaction between PET backbones. Researcher also reviewed that the endothermic peaks at Tg could be attributed to the enthalpy relaxation effects coming from the thermal history of the samples. The Xc showed in table were increasing when the PET is being irradiate with electron beam. It is seeming that, by exposed to electron beam, PET had increase it Tm and but decreasing their Tg.

Table 1: Thermal Properties

Sample Description	Tm (°C)	Tg (°C)	Xc (%)
PET pure	131.38	67.34	54.41
PET 50	131.98	66.70	55.62
PET 100	131.98	66.28	55.51
PET 150	132.41	66.45	56.78
PET 200	131.82	65.67	55.97

4 Conclusions

In summary, it can be concluded that the optimum irradiation dose for PET irradiation is at 150kGy with promisingly increase the mechanical and thermal properties of the recycle PET. The optimum dose will be used further in concrete reinforcement.

References

Meza A, Pujadas P, Meza LM, Pardo-Bosch F, and López-Carreño RD. 2021. Mechanical optimization of concrete with recycled PET fibres based on a statistical-experimental study. *Materials (Basel)*, Jan 6;14(2):240. doi: 10.3390/ma14020240. PMID: 33418955; PMCID: PMC7825144.

Piatek-Hnat M, Bomba K, Peksiński J, Koz lowska A, Sośnicki JG, and Idzik TJ. 2020 May 2. Effect of e-beam irradiation on thermal and mechanical properties of ester elastomers containing multifunctional alcohols. *Polymers (Basel)*, 12(5):1043. doi: 10.3390/polym12051043. PMID: 32370247; PMCID: PMC7284812.

Nkosilathi Nkomo, LM Masu, and PK. Nziu. 2022. Effects of polyethylene terephthalate fibre reinforcement on mechanical properties of concrete. *Advances in Materials Science and Engineering*, 6, 100147, ISSN 2772-3976.:1–9. 10.1155/2022/4899298.

Vimal Panara, Vedang Bhonde, Shivam Patel, Shivang Jayswal, Kannan K. R Iyer, and Mahesh Mungule. 2022. Effect of waste PET strips as reinforcement in concrete under cyclic loading. *Cleaner Materials*, 6, 100147, ISSN 2772-3976.

Individual Research Contribution Review, 2023, 1(1): 35–36

Replast Kenaf Poles: Pembangunan Ekonomi B40 Holistik

Muhammad Hazim Muhammad Sayuti
Radiation Processing Technology Division
Malaysian Nuclear Agency
43000 Kajang, Selangor
hazim@nm.gov.my

Abstract

Re-Plast Kenaf Poles is a new initiative for the production of multipurpose poles produced from recycled plastic sources with kenaf fiber. The production of this product can help the economic development of the B40 target group economically in the collection of plastic waste, kenaf plantation and the production of the product itself. The expertise of the Malaysian Nuclear Agency in the field of biocomposites and composite processing equipment allows the Re-Plast Kenaf Pole production facility to be adapted to the capabilities of the community that will receive the technology. NM's experience in successful project MSI17108: Building the manufacturing capability of biocomposite floating jetty components for use in the fishing and eco-tourism sectors and also MSI 2016, proved that the technology's ability to be accepted by the community

1 Introduction

This Replast project is planned to develop the capacity of the community around Kampung Karanaan, Tambunan, Sabah in the production of Re-Plast Kenaf Poles from kenaf fiber and recycled plastic by using advanced processing techniques. Through this program, the National Kenaf and Tobacco Board (LKTN) agreed to act as a collaborator in assisting the Malaysian Nuclear Agency in implementing this project and will benefit the Sabah Mamasok Welfare Association.

The National Kenaf and Tobacco Board (LKTN) plays a role in helping:

- Be the secretary for the management of the kenaf tree plantation in Tambunan, Sabah
- Plantation management and kenaf fiber processing at Kampung Karanaan, Tambunan, Sabah as shown in Figure 1

Figure 1: Kenaf tree plantation proposal site

Sabah Mamasok Welfare Association (MWS) plays a role in helping:

- Be the secretary for the management of Re-Plast Kenaf Pole by MWS
- Workforce management and income distribution to beneficiaries, especially the 100 members of the B40 group
- Management of product processing operations and tool maintenance
- Product marketing by MWS Sabah to local retail markets around Sabah.

2 Methods

a) Preparation of equipment and processing facilities for kenaf fiber using radiation technology as a biocomposite raw material at the Malaysian Nuclear Agency.

b) Development of the process of collecting, cleaning, processing and recycling plastic molds with kenaf fiber/additives.

c) Transfer of Re-Plast Kenaf Pole manufacturing technology to the Tambunan community:

   i. Installation of plastic waste processing equipment and facilities
   ii. Training and development of plastic waste processing skills and Re-Plast Kenaf Pole products
   iii. Production of Re-Plast Kenaf Pole

3 Results and Discussion

Preparation of Equipment and processing facilities for Kenaf Poles Re-Plast Products.




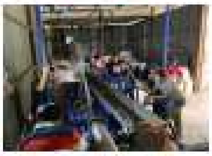




4 Conclusion

The benefit of this project is the implementation of environmentally friendly technology or green technology by reducing environmental pollution in addition to being able to produce multi-purpose biocomposite poles based on kenaf fiber where they can be used as plant support poles or as fence poles for plants/fields. In relation to this, planting and farming activities can be further intensified with the presence of this multi-purpose biocomposite pole.

References

O. Ezekiel Babatunde, J. Mohamad Yatim, M. Y. Ishak, R. Masoud, and R. Meisam. 2015. Potentials of kenaf fibre in bio-composite production: A review. *Jurnal Teknologi*, 77(12):https://doi.org/10.11113/jt.v77.6304.

Junghoon Kim and Donghwan Cho. 2020. Effects of waste expanded polypropylene as recycled matrix on the flexural, impact, and heat deflection temperature properties of kenaf fiber/polypropylene composites. *Polymers*, 12:2578.10.3390/polym12112578.

Borneo Waste Industries Sdn Bhd Report. 2018. Waste composition at Kayu Madang Sanitary Landfill.

Vineta Srebrenkoska, Gordana Bogoeva-Gaceva, Maurizio Avella, Maria Errico, and Gennaro Gentile. 2008. Recycling of polypropylene-based eco-composites. *Polymer International*, 57:1252 – 1257. 10.1002/pi.2470.

Individual Research Contribution Review, 2023, 1(1): 37–38

Determining the Effective Conjugation Length of Polydiacetylene and Its Blends for Optical Shift upon Ionizing Radiation

Naurah Mat Isa
Radiation Processing Technology Division, Malaysian Nuclear Agency
43000 Kajang, Selangor
naurah@nm.gov.my

Abstract

Polydiacetylene (PDA) prepared into three supramolecules known as vesicles, planar and rod-like, has been investigated for its effective conjugation length for indicating ionizing radiation. The supramolecules were chosen based on the PDA's packing ability for polymerization. A BBD method was used to find an optimum parameter for the supramolecules preparation. Samples prepared were characterized and tested for its response against gamma radiation. Results obtained from this study suggest that the effective conjugation length of PDA was around 20nm, as demonstrated by PDA_{THF} vesicles. However, the result must be coupled with the absorbance value obtained from the radiation-induced topochemical reaction for an effective indication.

Keywords: conjugate length, absorbance, radiation, polydiacetylene

1 Introduction

Polydiacetylene (PDA) polymer composed of repeating units of carbon-carbon triple bonds. The unique optical and electronic properties of PDAs have made them a promising material for various applications, including sensors, optoelectronics, and energy storage. In particular, the extended conjugation and narrow band gap of PDAs result in their characteristic blue or purple color, and their nonlinear optical properties make them useful in photonics. PDA is a well-known radiation indicator label used for monitoring irradiation treatment in food and industrial goods. However, the inconsistent color shift exhibited by PDA has led to uncertain among radiation operators and product owners, resulting in unnecessary re-treatment or release of insufficiently treated products. The effective conjugation length of PCDA for radiation indication was not well understood in the literature, leaving a gap in our understanding of the relationship between conjugation length and optical shift upon gamma ray radiation. In this study, the role of PDA's conjugation length in defining its optical shift upon gamma ray radiation was investigated.

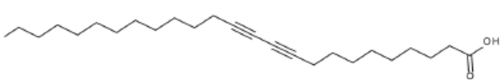

Figure 1: Chemical structure of pentacosa-10,12-diynoic acid monomer for PDA assembly.

2 Methodology

2.1 Material

Pentacosa-10,12-diacetylene for the polydiacetylene monomer (PDA) was purchased from Sigma-Aldrich and used without further purification. Solvents were of high-grade tetrahydrofuran (THF) and chloroform (Ch) purchased from Merck. Ultrapure water (UPW) was used throughout this work for dispersions.

2.2 Synthesis and preparation of Polydiacetylene (PDA)

PDA was synthesized into three supramolecular shapes known as vesicle, rod-like and planar formation. Vesicles and rod-like PDA were in water dispersion, while planar shape PDA was on a dried surface. PDA vesicle was synthesized using two different solvents, chloroform (PDA-Ch) and tetrahydrofuran (PDA-THF). The vesicles formed from two solvents were characterized and optimized. PDA rod-like was synthesized by altering the hydrophobic head with PDA 4.

2.3 Response Surface Methodology (RSM)

Box-Behnken Design (BBD) was used for the optimization of parameters such as temperature, concentration, and types of solvent for the formation of PDA vesicles, rod-like structures, and planar shapes.

2.4 PDA Characterization

The changes in the physicochemical and optical properties of the materials were characterized using Fourier Transform Infrared Spectroscopy (FTIR), Dynamic Light Scattering (DLS), Field Emission Scanning Electron Microscopy (FESEM), Proton Nuclear Magnetic Resonance (^{1}HNMR), Atomic Force Microscopy (AFM), Raman Spectroscopy, UV-vis Spectroscopy, and zeta potential before and after radiation of gamma ray. The average conjugation length of each PDA supramolecular at different radiation doses were identified and a dose response curve for gamma radiation was established.

3 Result

PDA vesicles' diameter dispersed in aqueous was recorded at 200 nm upon preparation and maintained at 300nm during storage at 4°C. The roughness value, R_a of 1-layer planar PDA and 5-layer PDA were initially measured as 30.6 nm and 26.2 nm. The value decreased to 10.9 nm and 10.7 nm, subsequently after the exposure to gamma ray. Rod-like PDA particle was approximately 7:2 (L/D).

The optical density of each supramolecules were measured between 400-700 nm of spectrometer wavelength. Based on the RSM study, PDA prepared at 2mM concentration, using THF solvent and processed at 60°C, has the maximum absorbance value upon radiation (Figure 2). PDA planar has a lower radiation indication compared to the vesicle sample, while PDA rod-like turned yellowish, signaling unsuccessful topochemical reaction (Figure 4).

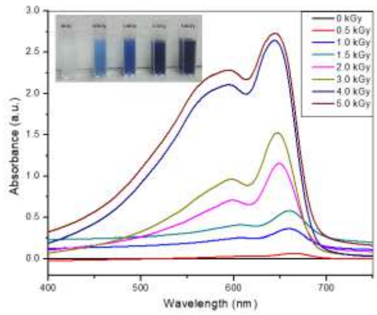

Figure 2: Colourless PDA vesicles turned blue upon exposure to the radiation.

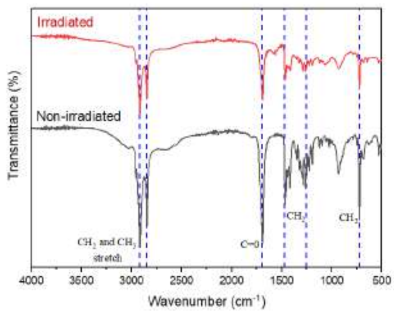

Figure 3: FTIR spectrums of PDA with and without exposure to gamma irradiation (5 kGy).

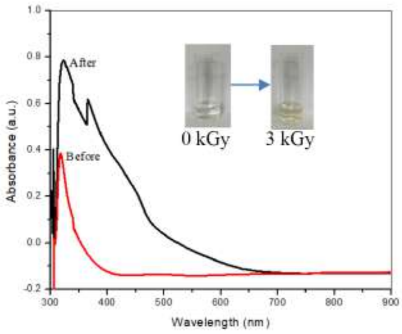

Figure 4: Optical density of PDA rod-like turned from colourless solution to a slight yellowish solution upon radiation.

4 Discussion

PDA monomers that were assembled into three supramolecules have different optical result upon polymerization by radiation. Among the three shapes, PDA vesicles has the highest optical difference against gamma radiation. Vesicle shape allows PDA monomers to assembled at a closed proximity for topochemical polymerization.

Successful polymerization resulted from radiation exposure was presented in the form of optical change that were recorded using visible peaks between 550 nm to 700 nm (Figure 2). The intensity of the peaks increased with the increasing radiation dose, indicating that more PDA molecules were undergoing the structural change (Huang et al., 2020). An ultimate response to radiation was noted after the samples were exposed to 5kGy of radiation dose. Despite the highest degree of absorbance recorded by PDA_{THF}, the longest conjugation was recorded by PDA_{Ch} for similar radiation exposure (Table 1). These were attributed to solvent's polarity that caused for different monomer packings.

Table 1: Length of conjugation, λ for each PDA samples.

Sample Type	$\triangle\lambda$	$\triangle$ **Abs**
PDA_{THF} (yes)	20.0	2.664
PDA_{Ch} (ves)	25.0	1.695
PDA (planar 1L, 2mM)	22.0	0.001
PDA (planar 5L, 3mM)	16.5	0.388
PDA (rod-like)	13.0	0.166

Large aromatic and hydrophobic head group in the PDA rod-like system resulted to an irregular shaped of particles and unorganized clusters (Khanantong et al., 2019). These eventually led to a decrease in packing parameter which caused to unsuccessful topochemical polymerization that was required for an optical shift (Abdel-Fattah and Soliman, 2017).

Chemical structures of PDA before and after radiation did change but similar functional groups remained for both conditions Figure 3. Decrement of peaks were noted, and it was attributed to the radiation-induced polymerization reaction, which leads to an increase in hydrogen bonding throughout the system (Mittal et al., 2020; Phonchai et al., 2019).

5 Conclusions

The solo shift in the conjugation length for the indication of radiation is not sufficient as it should be accompanied with the sufficient degree of optical densities to tell a difference. More work shall be done to find the contributing factors to the polymer response against radiation.

References

A.A. Abdel-Fattah and Y.S. Soliman. 2017. Performance improvement of pentacosa-diynoic acid label dosimeter for radiation processing tech. *Radiation Physics and Chemistry*, 141:66–72.

Q. Huang, W. Wu, K. Ai, and Liu J. 2020. Highly sensitive polydiacetylene ensembles for biosensing and bioimaging. *Front Chem*, 8(565782).

C. Khanantong, Charoenthai N., Kielar F., and R Traiphol. 2019. Influences of bulky aromatic head group on morphology, structure, and color-transition behaviors of polydiacetylene assemblies upon exposure to thermal and chemical stimuli. *Colloids and Surfaces A: Physicochemical and Engineering Aspects*, 561:226–235.

A. Mittal, N. Gopishankar, J. Koleda, A.K. Verma, and P. Kumar. 2020. Dev. and char. of urethane substituted diacetylene based radiochromic films for medical radiation dosimetry. *Radiation Physics and Chemistry*, 93:177.

N. Phonchai, C. Khanantong, F. Kielar, R. Traiphol, and N. . Traiphol. 2019. Low-temp reversible thermochromic polydiacetylene/zinc (ii)/zinc oxide nanocomposites for colorimetric sensing. *ACS Applied Nano Materials*, 2(7):4489–4498.

Preparation and Characterization of Polyvinyl Chloride (PVC)/Irradiated Polytetrafluoroethylene (i-PTFE) Composite via In- Situ Polymerization

Noora'tiqah Mohamad Fauzi
Radiation Processing Technology Division, Malaysian Nuclear Agency
43000 Kajang, Selangor
nooratiqah@nm.gov.my

Abstract

In general, polyvinyl chloride (PVC) is a versatile polymer with a wide range of applications. However, it exhibits very poor heat resistance or flame retardancy. Polytetrafluoroethylene (PTFE), on the other hand, is a heat-resistant, non-flammable, and chemically inert polymer. In this study, in-situ polymerization was used to embed trimethylolpropane triacrylate (TMPTA)-crosslinked PVC in irradiated PTFE (i-PTFE) to produce novel polymer composites.

Keywords: Polyvinyl chloride, Irradiated polytetrafluoroethylene, In-situ polymerization, Thermal stability

1 Introduction

Polymers have been well-known for their versatility which enables them to be used widely in advanced applications. Typically, high-performance polymers used in sophisticated technologies require distinctive characteristics such as enhanced mechanical strength, durability, flexibility, and resistance to degradation (Hsissou et al., 2021). However, essentially a single polymer is unlikely to meet the requirements for commercially significant polymers for advanced applications. Thus, the development of polymer composites attracted global attention. Polymer composites are composed primarily of reinforcement and matrix. As a matrix and reinforcement, the composite may contain metals, ceramics, and other polymers as well (Nawab et al., 2021). The most common polymeric matrices used in composites are polypropylene (PE), polyethylene (PP), acrylonitrile butadiene styrene (ABS), and polyvinyl chloride (PVC). PVC used widely in industrial, technical, and daily applications, including building, transport, packaging, electrical/electronic, and healthcare sectors. Moreover, PVC is often combined with other substances such as metals, salts, and nanoparticles to improve its toughness and impact properties (Lewandowski and Skórczewska, 2022). Nevertheless, one of the major disadvantages of PVC is its low heat distortion temperature, which limits its applications across multiple disciplines (Shi et al., 2012). However, blending PVC with other polymers significantly increases the heat distortion temperature of the latter. As a result, PVC and polytetrafluoroethylene powder (i-PTFE) composites were prepared via in-situ polymerization, and their properties were assessed in this study. PVC and i-PTFE in situ polymerization represents a promising avenue for thermally efficient polymer composites. In this study, i-PTFE blended with PVC in order to improve the thermal properties. Previosly, Qi et al. (Qi et al., 2020) reported that silicone rubber composites with excellent mechanical properties, little temperaturedependent friction change, and exceptional high-temperature abrasion resistance were produced with the addition of PTFE and the use of fluoro-silicone rubber as a compatibilizers (Qi et al., 2020). Another study performed by Vásquez-Rendón & Álvarez-Láinez (Vásquez-Rendón and Álvarez-Láinez, 2021) proved the toughness and processability of polyethyleneimine/polybutylene terephthalate blends were enhanced by the addition of PTFE, due to the mechanical performance was influenced by dualphase and spore-like morphology with PTFE acting as an impact modifier (Vásquez-Rendón and Álvarez-Láinez, 2021). Prior to polymerization with PVC, PTFE was irradiated with cobalt-60. PTFE is irradiated to reduce its molecular weight, which improves interfacial bonding with PVC during polymerization (Lunkwitz et al., 2000). Therefore, this study aims to determine the optimal conditions and parameters for in-situ polymerization, including a thorough exploration of i-PTFE compositions. In addition, comprehensive characterization was performed to analyze the mechanical and thermal properties of the novel composites produced in order to identify the best composition to achieve the desired characteristics.

2 Methods

In the present study, a method has been developed for evaluating polymer blends containing PVC and PTFE powder, cross-linked with TMPTA. Gamma irradiation was used with a cobalt-60 source to provide controllable radiation treatment to enhance the compatibility of PTFE powder with PVC. Blending was conducted using an internal mixer, specifically the Thermo Scientific Haake Polylab, operated at 160°C and 50 rpm. In order to ensure controlled dispersion within the PVC matrix, PTFE powder was introduced at the 2-minute mark during the mixing process. In order to create test specimens for subsequent analysis, the resulting blend was subjected to hot press treatment. This method aims to explore the impact of PTFE powder modification through gamma irradiation and the incorporation of TMPTA cross-linking on the mechanical properties, morphology, and crystalline structure of the PVC/i-PTFE blend.

3 Results

It observes that when the percentage or content of i-PTFE rises, there is a noticeable decrease in the tensile strength of

PVC. Figure 1 clearly illustrates this trend, showing a noticeable and steady decline in tensile strength as the i- PTFE content increases. This pattern implies that the addition of i-PTFE to PVC has an adverse effect on the material's tensile strength, either as a result of changed material characteristics or interactions between the two parts.

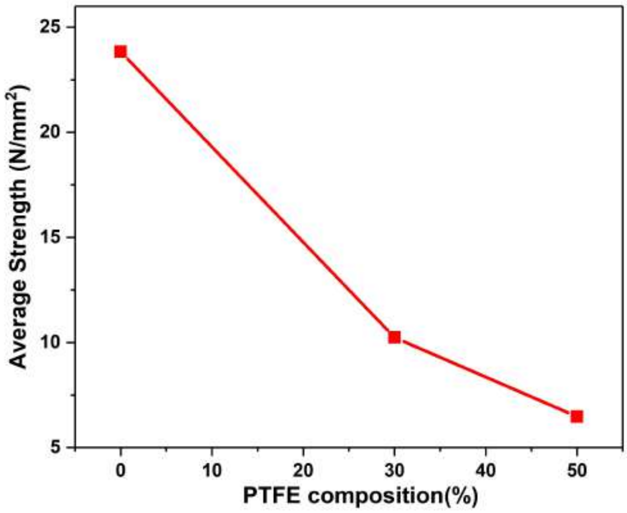

Figure 1: Tensile strength of PVC/i-PTFE

The thermogravimetric analysis (TGA) revealed different behaviors for three different material compositions containing varying amounts of i-PTFE.

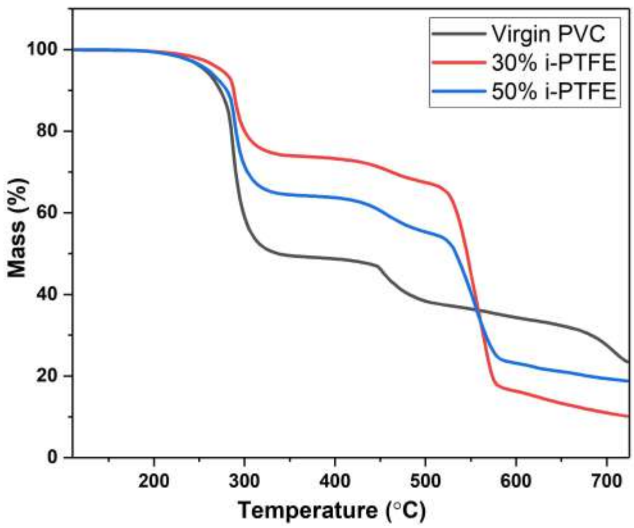

Figure 2: TGA of PVC/i-PTFE

Virgin PVC (0% i-PTFE) degradation started at 282.5°C and peaked at 335°C, amounting to 50% degradation by weight. The material showed stronger resilience to thermal degradation upon the addition of 30% of i-PTFE to the PVC, which starts to degrade at 287.5°C and reaches 50% disintegration at a much higher temperature of 532.5°C.

Moreover, degradation began at 292.5°C and occurred in equal parts at 545°C upon the addition of 50% i-PTFE to PVC.

4 Discussion

A number of factors contribute to the decline in tensile strength. In addition, i-PTFE has characteristics such as a low coefficient of friction and a high chemical resistance that make it relatively non-reactive and non-adhesive when mixed with PVC. Thus, PVC and i-PTFE have fewer intermolecular contacts, resulting in weaker bonds between them, reducing the overall strength of the composite. In addition, the incorporation of i-PTFE particles may result in a less homogeneous dispersion inside the PVC matrix, which may lead to local weak points or defects in the material, further compromising its tensile strength. Moreover, i-PTFE's low modulus of elasticity may also contribute to its apparent loss of tensile strength. Meanwhile for TGA results, PTFE content is a key factor in the thermal stability of a material, with higher PTFE levels being associated with better resistance to high-temperature degradation. The thermal stability of PTFE is well known. Incorporating i-PTFE with PVC provides enhanced resistance to high temperatures without degrading significantly.

5 Conclusions

In conclusion, the thermal properties show the reverse trend whereas the tensile strength decreases as the i-PTFE concentration increases. The thermal performance of PVC composites improves as the i-PTFE content improves.

References

R. Hsissou, R. Seghiri, Z. Benzekri, M. Hilali, M. Rafik, and A. Elharfi. 2021. Polymer composite materials: A comprehensive review. *Composite structures*, 262:113640.

K. Lewandowski and K. Skórczewska. 2022. A brief review of poly (vinyl chloride)(PVC) recycling. *Polymers*, 14(15):3035.

K. Lunkwitz, U. Lappan, and D. Lehmann. 2000. Modification of fluoropolymers by means of electron beam irradiation. *Radiation Physics and Chemistry*, 57(3-6):373–376.

Y. Nawab, S. Sapuan, and K. Shaker. 2021. Composite solutions for ballistics. *Woodhead Publishing*.

M. Qi, X. Jia, G. Wang, Z. Xu, Y. Zhang, and Q. He. 2020. Research on high temperature friction properties of PTFE/fluorosilicone rubber/silicone rubber. *Polymer Testing*, 91:106817.

A. Shi, G. Zhang, and C. Zhao. 2012. Study of rigid crosslinked PVC foams with heat resistance. *Molecules*, 17(12):14858–14869.

M. Vásquez-Rendón and M. L. Álvarez-Láinez. 2021. PTFE as a toughness modifier of high-performance PEI/PBT blends: Morphology control during melt processing. *Polymers for Advanced Technologies*, 32(2):714–724.

Individual Research Contribution Review, 2023, 1(1): 41–42

Poly(ethylene) Furanoate (PEF) Bioplastic Synthesized From Biowaste For Packaging Application

Nor Azwin Shukri
Radiation Processing Technology Division, Malaysian Nuclear Agency
43000 Kajang, Selangor
azwin@nm.gov.my

Abstract

Malaysia has always attempted to promote sustainable development by balancing economic growth and environmental conservation in accordance with the Sustainable Development Goals of the United Nations. Specifically, the Ministry of Science, Technology, and Innovation (MOSTI) has launched a Roadmap Towards Zero Single-use Plastics to address singleuse plastics by encouraging the plastic industry to transition to eco-friendly products. This is because Malaysia has abundant biomass resources that have the potential to be utilized to replace petrolbased packaging materials. For instance, bamboo waste is generated yearly in landfills due to the massive industrial consumption of bamboo, creating large quantities of biomass resources in Malaysia. However, investigations on producing PEF and monomer production from bamboo waste biomass in Malaysia have been rarely reported. Thus, this work proposes to synthesize polyethylene 2,5-furandicarboxylate (PEF) from bamboo biomass as an alternative to polyethylene terephthalate (PET), one of the commonly used single-use plastics today.

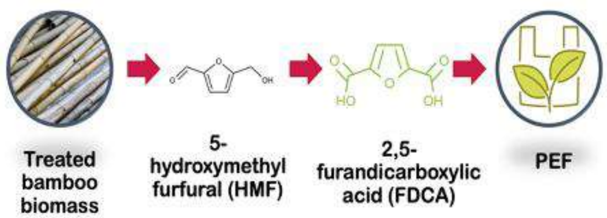

Keywords: Poly(ethylene) Furanoate, Bioplastic, Biomass materials

1 Introduction

One of the most significant current situations in the world is environmental pollution which is becoming worse each day. Pollution from plastics can alter habitats and natural processes, reducing ecosystems' capacity to adapt to climate change, and negatively impacting millions of people's livelihoods, food production capabilities, and general well-being (Kumar et al., 2021). According to the United Nations Environment Programme (UNEP) (Li et al., 2018), single-use plastics, which include grocery bags, containers and bottles, disposal cutlery, water bottles, disposal cups, and straws, constitute the majority of plastic packaging that contributes about 400 million tonnes of plastic waste every year, globally. A study estimated that Malaysia produced 0.94 million tons of mismanaged plastic waste, especially from single-use plastic (Janaswamy et al., 2022). Moreover, based on statistics only 9% of plastic waste materials are recycled and 12% are incinerated, while 79% are disposed of in landfills, oceans, or the environment (Geyer et al., 2017).

Bamboo biomass is mainly composed of cellulose (37–47%), hemicellulose (15–30%), and lignin (18–31%), although this composition varies from species to species (Li, Remón et al. 2018). With the ideal technology in deconstructing lignocellulosic biomass, it can be converted into several worthwhile bio-products. Among various chemicals that can be synthesized from biomass, 5-hydroxymethylfurfural (HMF) is one most promising and flexible platform compounds. HMF has been identified as a bridge between biomass resources and petrochemical refining. It can be used to prepare biobased fuels via hydrogenation and etherification reactions, to synthesize compounds such as 2,5-furan dicarb acid (FDCA) or to replace petroleum to produce esters. In addition, FDCA has gained significant interest in recent years for the development of poly(ethylene) furanoate (PEF) that could replace PET. The PEF primary chain structure is similar to that of PET, except that benzene in PET is replaced by furan in PEF. Therefore, this study proposed a PEF production method based on bamboo waste as an alternative to PET, which is one of the most common single-use plastics in use today.

2 Methods

The purpose of this research is to investigate the feasibility of synthesizing PEF from bamboo waste biomass as an alternative to PET and evaluate their performance as packaging. Initially, the bamboo biomass will undergo electron beam irradiation pretreatment. The operating conditions of electron beam irradiation were determined based on glucose conversion and the physicochemical properties of lignocellulose after the pre-treatment. Following the pyrolysis of bamboo biomass that has been pretreated with electron beam irradiation, a new type of biodegradable plastic, polyethylene furandicarboxylate (PEF), will be synthesized using FDCA. However, PEF is not biodegradable or compostable similar to PET. Thus, end-of-life measures must be considered to prevent adding to the buildup of plastic waste. For this reason, upon successful conversion of bamboo waste into PEF, it is proposed to copolymerize PEF with PHA to combine the biodegradable character of PHA with good gas barrier and mechanical properties of PEF. Last but not least, biochar absorbent derived from the by-product of pyrolysis for carbon dioxide capture will be prepared to fully utilize the biomass product. The overall research process is illustrated in Figure 1.

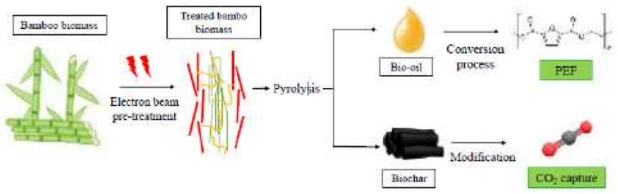

Figure 1: Overall research process

3 Expected Results

It is expected that at the end of the research, the following will be achieved:

i) Irradiating bamboo biomass with an electron beam should improve the sugar yield.

ii) Improvement in reaction conversion of PEF produced by polymerization of FDCA from bamboo biomass.

iii) Improvement in physicochemical properties including biodegradability of PEF as food packaging.

iv) Improvement in CO_2 uptake by biochar absorbent derived from the by-product of pyrolysis.

References

R. Geyer, J. R. Jambeck, and K. L. Law. 2017. Production, use, and fate of all plastics ever made. *Sci Adv*, 3(7):e1700782.

S. Janaswamy, M. P. Yadav, M. Hoque, S. Bhattarai, and S. Ahmed. 2022. Cellulosic fraction from agricultural biomass as a viable alternative for plastics and plastic products. *Industrial Crops and Products*, 179:114692.

R. Kumar, A. Verma, A. Shome, R. Sinha, S. Sinha, P. K. Jha, R. Kumar, P. Kumar, Shubham, S. Das, P. Sharma, and P. V. Vara Prasad. 2021. Impacts of plastic pollution on ecosystem services, sustainable development goals, and need to focus on circular economy and policy interventions. *Sustainability*, 13(17):9963.

T. Li, J. Remón, Z. Jiang, V. L. Budarin, and J. H. Clark. 2018. Towards the development of a novel "bamboo-refinery" concept: Selective bamboo fractionation by means of a microwave-assisted, acid-catalysed, organosolv process. *Energy Conversion and Management*, 155:147–160.

Individual Research Contribution Review, 2023, 1(1): 43–44

Radiation Cross-linked Low- Smoke Halogen-Free Flame- Retardant Cable for Automotive and Construction Industry

Nor Azwin Shukri
Radiation Processing Technology Division, Malaysian Nuclear Agency
43000 Kajang, Selangor
azwin@nm.gov.my

Abstract

The fire resistance performance of cables in automotive and buildings is currently in demand to improve fire safety for public users. This is because electrical cables are frequently implicated as the culprits of a fire. Consequently, there is a compelling need to develop a cable that is flame-retardant, low in smoke emission, and halogen-free to address these critical concerns. However, the application of current FR cable is limited because of its low mechanical properties due to poor compatibility. Radiation-induced crosslinking offers an improvement to this limitation through the three-dimensional network without the need for heat or pressure that can impede the physical properties of the polymer. Thus, the potential of radiation-induced crosslinking of flame-retardant (FR) cable that is both low in smoke production and free of halogen content will be studied through electron beam irradiation.

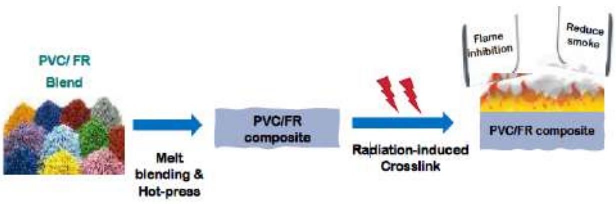

Keywords: PVC, Cable insulation, flame-retardant, low-smoke, halogen-free, radiation-crosslinking

1 Introduction

Radiation technology related to polymer modification was successfully implemented in industrial applications over 50 years ago. The crosslinking of polymer can be performed efficiently in an electron beam facility during a continuous irradiation process. Electron beam (EB) radiation processing of electric wire and cable insulations is one of the successful applications in radiation technology industries, especially for building and automotive applications.

The quality of electrical cables used in industrial plants, power stations, multi-story buildings, hotels, subway tunnels, road tunnels, vehicle construction, etc. must comply with the electrical and mechanical standards corresponding to the characteristics of the material. Prevention of fire, lowering smoke and fire spread, extinguishing a fire, and the possibility of safe escape are all crucial aspects of fire safety (Cvetković et al., 2022). Therefore, the demand for flame retardant (FR) and halogen-free (HF) solutions and their use, especially for cross-linked polymers is becoming more relevant.

This was due to electrical, thermal, and thermomechanical degradation of the insulation layer is a major factor that can cause failure of non-crosslink cable such as electrical breakdown. Electrical breakdown of the insulation material often promoted by the void, chemical impurities, or physical defect in the insulation leads to cavities that propagate through the insulation in the form of a branched tree. This process ultimately leads to the complete breakdown of the insulation and thus, destroying the cable.

Cross-linked polymer such as polyvinyl chloride (PVC) and polyethylene (PE) is the most widely used insulation material for electrical cables with enhanced stability against electrical breakdown (Meng et al., 2020; Liu et al., 2021). Crosslinking not only prevents the polyolefin insulations of wires and cables from extreme deformation for over current and high temperatures but also makes them possible to be used at temperatures above the inherent softening point for a long period of time.

2 Methods

The PVC blends will be prepared by blending the PVC resin with the additives using an internal mixer at a constant temperature of 160°C for 10 minutes. At first, the PVC is melted and the additives mixture is added. Then, these blends were subsequently pressed into sheets using a hot press machine using a 1 mm thickness mould at 160°C for 10 minutes. Next, the sheets will be cooled between two plates of cold press at a temperature of 25°C. All samples were exposed to electron beam irradiation for crosslinking purposes. The irradiation parameters used were 2 MeV energy and 10 mA current. The samples will be irradiated at 0, 60, 80, 100, and 150 kGy doses. Then, to preserve the samples from moisture, all samples will be packed in plastic zipper bags immediately after the irradiation process. In summary, Figure 1 depicts the research flow chart for this work.

3 Expected Results

It is expected that at the end of the research, the following will be achieved:

i) The addition of polyfunctional monomer in the PVC blend can result in a higher degree of crosslinking (>40%) at a low irradiation dose.

ii) Improvement in tensile properties of irradiated PVC blend with ATH (≥19MPa) compared to non-irradiated PVC blends.

iii) Improvement in the flammability properties of the irradiated ATH-added in PVC blends (LOI ≥25%). In addition, the smoke density is expected to be less than 60% to meet the low smoke requirement.

iv) Irradiating ATH-added in PVC blends with an electron beam should result in improved electrical characteristics (≥30 Kv cm^{-1}), which reflect better insulator reliability.

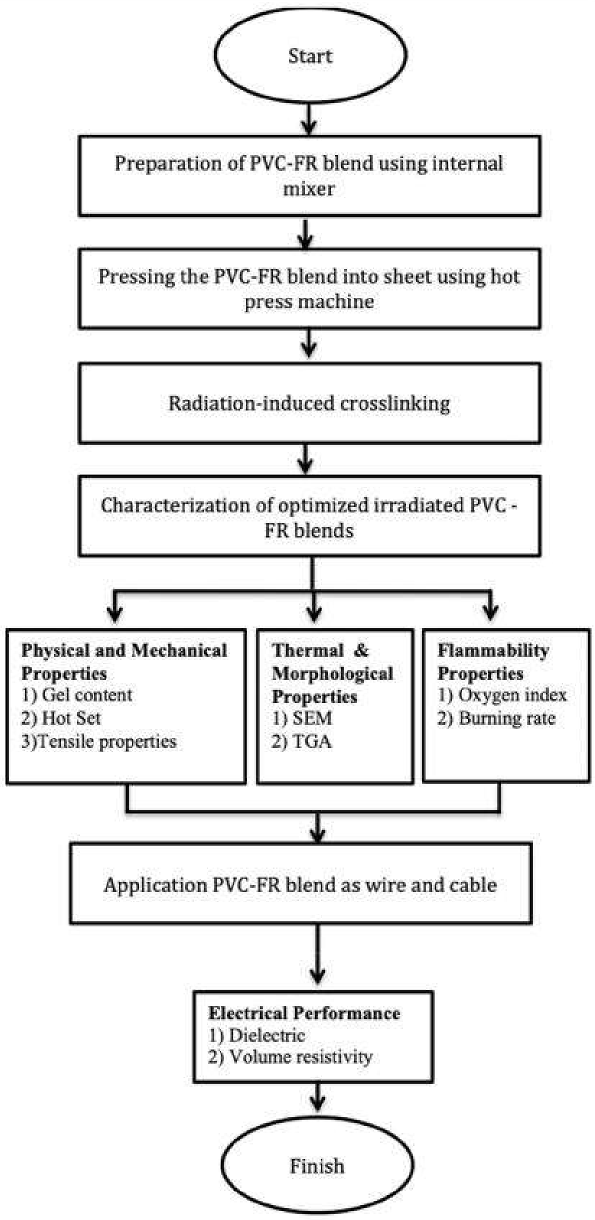

Figure 1: Overall research flowchart

References

V.M. Cvetković, A. Dragašević, D. Protić, B. Janković, N. Nikolić, and P. Milošević. 2022. Fire safety behavior model for residential buildings: Implications for disaster risk reduction. *International Journal of Disaster Risk Reduction*, 76:102981.

S. Liu, L.S. Fifield, and N. Bowler. 2021. Aging mechanisms of filled cross-linked polyethylene (XLPE) cable insulation material exposed to simultaneous thermal and gamma radiation. *Radiation Physics and Chemistry*, 185:1094.

W. Meng, Y. Dong, J. Li, L. Cheng, H. Zhang, C. Wang, Y. Jiao, J. Xu, J. Hao, and H. Qu. 2020. Bio-based phytic acid and tannic acid chelate-mediated interfacial assembly of Mg(OH)2 for simultaneously improved flame retardancy, smoke suppression and mechanical properties of PVC. *Composites Part B: Engineering*, 188:107854.

Individual Research Contribution Review, 2023, 1(1): 45–46

Effect of Gamma Irradiated Super Water Absorbent from Sago Waste on Mustard Plant

Norhashidah Talip
Radiation Processing Technology Division
Malaysian Nuclear Agency
43000 Kajang, Selangor
norhashidah@nm.gov.my

Abstract

Super water absorbent (SWA) can be used as water retainer in agriculture as it can absorb water and release to the plants. In this study, SWA from sago waste has been successfully prepared using gamma radiation technique and properties of SWA have been carried out. SWA was mixed with soil at three different compositions (0.1, 0.3 and 0.5%) to study the capability of SWA as water retainer on mustard. Generally, the height and weight of the plants were at the highest at 0.1% of SWA content in the soil.

Keywords: Super Water Absorbent, Sago waste, Radiation

1 Introduction

Sago waste or residue from sago production was usually discharged into the river, which contributed to water pollution (Ngaini et al., 2014). Sago waste is mostly made out of starch and lignocellulosic components, which can be transformed into useful products such as biosorbents, biogas and biodegradable composite material (Rasyid et al., 2020). Thus, in this study sago waste was mixed with other polymers and introduced to gamma radiation for crosslink or grafting to take place to produce super water absorbent (SWA). SWA produced is potentially to be used in agriculture as water retainer and might be useful during drought season.

Rather than synthesizing new materials using chemical or enzymatic techniques, radiation processing has been widely used due to its simple processing, effective, environmental-friendly and more convenient compared to other conventional method.

2 Methods

2.1 Preparation of super water absorbent

CMC was prepared by dissolving in water. Acrylic acid was then added into the solution and continued stirring for 30 minutes. This solution was poured into the basin containing sago waste and mixed for 45 minutes. KOH later was added and mixed again. The mixture was then packed into plastic bags and sealed prior to irradiation. These mixtures were irradiated at 15 to 35 kGy from Co-60 source facility at Sinagama, Malaysian Nuclear Agency. Upon completion of irradiation process, the mixtures, which now became SWA were dried in oven at 70°C until reach constant weight. The dried SWA were grind to have smaller size of SWA.

2.2 Characterization of super water absorbent

2.2.1 Gel fraction

The SWA samples were put into tea bag and weight accurately. The tea bags were soaked in distilled water and autoclave for 15 minutes at 121°C. The samples were then dried in oven at 60°C until it reached constant weight (Idris, 2008). The estimation of gel fraction was measured by the insoluble part after immersion in water. A minimum of five specimens was tested for each sample and average were calculated. Gel fraction was calculated using Equation 1.

$$\%\text{Gel fraction} = \frac{W_2}{W_1} \times 100 \qquad (1)$$

where W_1 is the initial weight of sample and W_2 is the weight of insoluble part after immersion.

2.2.2 Degree of swelling

Swelling performance of SWA when exposed to irradiation was done by immersing known weight of the sample in distilled water at room temperature for 24 h. Swelling degree of samples was calculated using Equation 2.

$$\text{Swelling}(\%) = \frac{W_s - W_D}{W_D} \times 100 \qquad (2)$$

where W_S and W_D represent the weight of swollen and dried sample, respectively.

2.2.3 Scanning electron microscopy

The morphology of the samples was investigated by scanning electron microscopy (SEM), FEI Quanta 400. Prior to scanning process, the samples were freeze-dried (Epsilon 1.8) at -75°C. The freeze-dried method on the samples is considered as the best method to observe the pore morphology or interpolymer network (IPN) of hydrogel. The dried samples were gold sputter-coated before analyzing by SEM. SEM images was obtained from the fractured surface of dried samples.

2.3 Pot experiment with mustard

One kilogram of soil was used in each pot (poly bag). 600 g of soil were first poured into the pot. Then SWA after swell was added (0.1%, 0.3% and 0.5%) and later pot were filled with another 400 g of soil and ready for plant transferred. Mustard which have been germinated for 2 weeks have been chosen by similar height and transferred into each pot. Each pot will have one plant. Pot experiments were to study the effect of SWA on the growth of mustard and were conducted under control environment.

3 Results and Discussion

Cross sectional images of sago waste SWA after irradiation are shown in Figure 1. From these images, can be seen that sago waste mixture that exposed to irradiation will form three dimensional (3D) network (Yacob et al., 2014) to form SWA. This 3D network porous structure was form due to crosslinking process that took place under irradiation (Talip and Mahmud, 2017). This porous structure in the irradiated SWA will help to absorb and retain water. The bigger the pore size, more water can be absorbed.

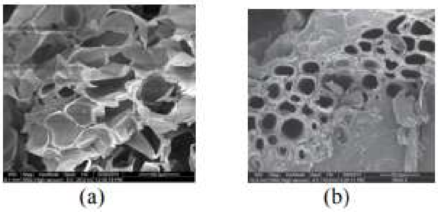

Figure 1: SEM images of (a) sago waste and (b) SWA

Super water absorbent has the ability to absorb water hundreds times more than its original weight. The water will be absorb and retain in the 3D network form in the SWA structure. Swelling characterization on the SWA will give information on how much water has been absorb by the SWA. Figure 2 and Figure 3 show the gel fraction and swelling of the SWA when irradiated at different gamma irradiation dose. SWA when further exposed to gamma irradiation particularly at dose of 25 kGy, the gel fraction gives the highest reading at around 145% and at higher doses the gel fraction was decreased. It shows that at 25 kGy, the crosslinking to form 3D network has formed at the highest and at that particular irradiation dose, the density of the network became higher (Suwanmala et al., 2014).

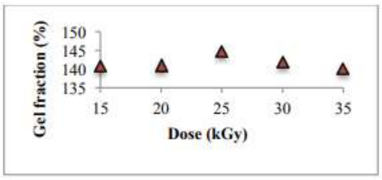

Figure 2: Gel fraction of SWA irradiated at various dose

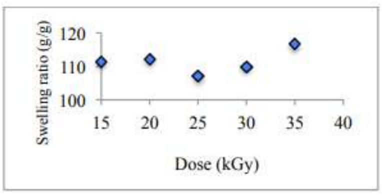

Figure 3: Swelling degree of SWA irradiated at various dose

As can be seen in Figure 2 and Figure 3 at dose of 25 kGy, SWA gives highest value of gel fraction but lowest value of swelling. This is due to the density of the crosslink network in the SWA. When crosslink is too much it will affect the pore sizes in the SWA. More pores will occur but in smaller size. Therefore, less water can be absorbed by the SWA.

To choose optimum irradiation dose for preparing SWA is by choosing the highest value of swelling. Therefore there will be more water that can be absorbed, retained and later to be released to the soil for the uptake of the plants.

Presence of SWA in the soil did improve the growth of mustard as can be seen in Figure 4. With SWA concentration of 0.1%, gave the highest value in the weight of mustard. The increasing weight of mustard at SWA concentration of 0.1% compared to the control (no SWA) is about 35%. It shows that having SWA in the soil will improve the growth of the plant. From this data, it can be concluded that SWA not only can absorb water but, at the same time can release water to the soil to be taken by the plant for their growth. Other researcher obtained similar result where, SWA has the ability to absorb water and can improved irrigation system (Ghobashy et al., 2020). As SWA concentration increased, the weight of the plant reduced. SWA at only 0.1% content in the soil is the optimum concentration and can improved the plant growth significantly.

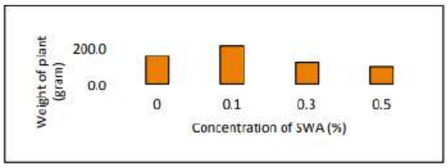

Figure 4: Weight of mustard with different concentration of SWA in the soil

References

M.M. Ghobashy, H. Abd El-Wahab, M.A. Ismail, A.M. Naser, F. Abdelhai, B.K. El-Damhougy, and S.A. Alkhursani. 2020. Characterization of starch-based three components of gamma-ray cross-linked hydrogels to be used as a soil conditioner. *Materials Science and Engineering: B*, 260, 114645. doi:10.1016/j.mseb.2020.114645.

S. Idris. 2008. Charcterization of electron beam-irradiated sago starch-polyvinyl alcohol blend films. (Master Degree), University Putra Malaysia.

Z. Ngaini, R. Wahi, D. Halimatulzahara, and N.A.-N.M. Yusoff. 2014. Chemically modified sago waste for oil absorption. *Pertanika Journal Science and Technology*, 22(1):153–161.

T.H. Rasyid, Y. Kusumawaty, and S. Hadi. 2020. The utilization of sago waste: prospect and challenges. *IOP Conference Series: Earth and Environmental Science*, 415(1)012023. doi:10.1088/1755- 1315/415/1/012023.

P. Suwanmala, T. Tangthong, and K. Hemvichian. 2014. Superabsorbent prepared by radiation induced graft copolymerization of acrylic acid onto cassava starch. *Radiation Processed Materials in Products from Polymers for Agricultural Applications*, Vienna: International Atomic Energy Agency.

N. Talip and M. Mahmud. 2017. Polisakarida sebagai penyerap air super dan penggalak pertumbuhan. In R. Tajau, K. Hashim, J. Sharif and C.T. Ratnam (Eds.), Teknologi Pemprosesan Sinaran Mengion: DBP.

N. Yacob, K. Hashim, N. Talip, and M. Mahmud. 2014. Preparation and characterization of modified sago waste for superabsorbent. presented at the RD Seminar. Selangor, Malaysia: Malaysian Nuclear Agency.

Individual Research Contribution Review, 2023, 1(1): 47–48

Optical Contact Angle Measurement with Topography: Principle and Application

Norliza Ishak
Radiation Processing Technology Division, Malaysian Nuclear Agency
43000 Kajang, Selangor
norliza@nm.gov.my

Abstract

Optical Contact Angle (OCA) measurements serve multiple purposes and provide valuable information in a wide range of disciplines. The contact angle analysis performs a number of key functions, such as the assessment of wettability, the calculation of surface free energy, the control of surface quality, and the optimization of surface treatments. In most cases, the angle at which liquid droplets encounter solid surfaces is used to determine whether a material is hydrophilic or hydrophobic. Factors such as roughness and heterogeneity of the surface may affect wetting behavior accuracy. Thus, the advanced mode of OCA with topography measurement will improve data interpretation reliability by providing a corrected contact angle. The information is vital to understanding the interaction between liquids and solids, as well as its application to material science, coating development, and surface modification.

Keywords: Optical contact angle, Topography, Wetting behaviour, Surface quality, Advanced mode

1 Introduction

Surface characterization is crucial in material science. The integration of optical contact angle measurement with topographical analysis has emerged as a novel approach to enhance this process. This technique involves combining contact angle analysis with surface topography measurements to assess the wetting behavior of a liquid droplet on a solid surface. Optical contact angle measurements are used to quantify the contact angle, which helps understand wetting properties (Tianyi and Lei, 2018). Researchers can examine the effect of surface characteristics like bumps, ridges, or roughness on the contact angle by incorporating topography measurements. This provides insights into the interaction between liquid droplets and micro- or nano-scale structures on the surface. The wettability properties description of materials conducted via contact angle measurement can provide valuable information about the nature of hydrophobicity and hydrophilicity. Generally, a solid surface with a contact angle of < 90° considered hydrophilic, while a surface with >90° is hydrophobic and a superhydrophobic surface if the contact angle is > 150° (Junchou et al., 2020; Wang et al., 2015). In real life, wettability and contact angle depend on the surface chemistry of the studied material. They also depend on the topography, which is the feature distribution of the material itself. This paper explores the utility of optical contact angle measurement with topography and its impact on surface characterization. It provides a comprehensive understanding of the potential of optical contact angle measurement and insight into wettability evaluation with topography in surface characterization.

2 Methods

The purpose of this study is to explores the utility of optical contact angle measurement with topography and its impact on surface characterization.

2.1 Measuring Principle of Contact Angle wıth Topography

It is most common to measure contact angle at room temperature and in an open atmosphere. The sample is placed directly on the sample stage during the measurement. As a rule of thumb, the tip that contains deionized water will squeeze water at a constant drop volume of 7μL on the surface of the sample. As illustrated in Figure 1, the sample surface will undergo topography for surface roughness calculation before the liquid drops on the surface material. The contact angle will be measured at the same spot in which the surface image was captured.

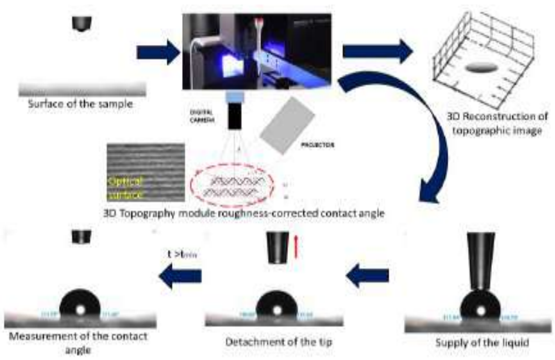

Figure 1: The measurement step for roughness corrected contact angle

3 Data/Results

3.1 Data Analysis Based On Nature Application: PEPP Fibers

The PEPP fibers morphology and roughness were measured on a flat fracture surface for practical measurement. An area of 1.4 mm x 1.1 mm was measured for the sample surface area. Each surface was scanned five times and used as an evaluation index to analyze differences in surface morphology and roughness. The optical image, 2D, and 3D topography of fractured surfaces of PEPP fiber were reconstructed as shown in Figure 2. Some data for topography reconstruction was missing due to reflections, and the missing area was displayed as blank.

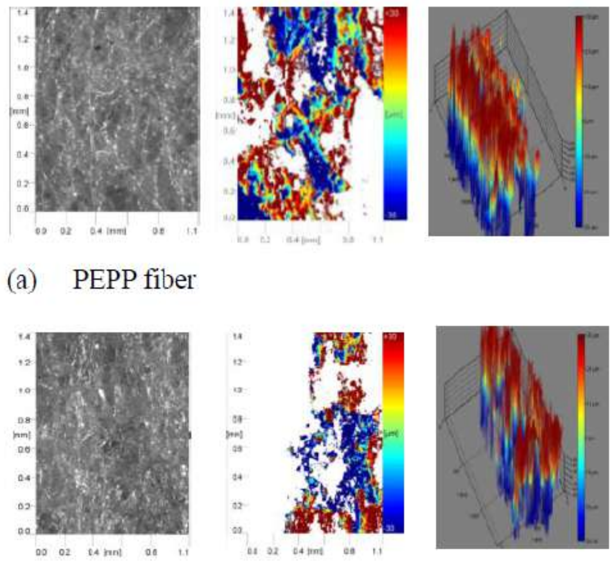

(a) PEPP fiber

(b) Radiation induced surface modification of PEPP fiber

Figure 2: The Optical images, 2D and 3D reconstructed topography of non-irradiated and irradiated PEPP fibers

According to Young's theory of 1805 (Young, 1805), the sample's surface is hydrophobic, despite decreasing contact angle. The corrected contact angle analysis measures contact angle based on surface roughness, which increases the hydrophilic component. The actual contact angle is determined by the relationship between surface roughness and wettability. This relationship was defined by Wenzel in 1936 (Wenzel, 1936), with increased roughness enhancing wettability due to hydrophilic substances' surface composition. The roughness ratio is used to measure actual contact angle values.

4 Conclusions

Optical contact angle measurement and topographical analysis revealed the material affected by surface roughness based on real surfaces providing a comprehensive understanding of surface properties. However, limitations include the need for specialized equipment and potential biases from sample preparation and measurement techniques. Future research should explore the technique's application to different materials and applications. Combining these techniques could enhance surface characterization and contribute to advancements in various fields, including polymer surface modification.

Table 1: Representative advanced contact angles with topography Corrected Contact Angle of PEPP fibers

Material	**Contact Angle (°)**	**Corrected Contact Angle (°)**
PEPP fiber	128.15	92.75
Radiation induced surface modification of PEPP fiber	116.66	91.44

References

W. Junchou, C. Yankun, W. nd Yijun, L. Guosheng, and L. Yinfei. 2020. Influence of surface roughness on contact angle hysterisis and spreading work. *J. Coll. Poly Sci*, 298:1107–1112.

Z. Tianyi and J. Lei. 2018. Contact angle measurement of natural materials. *J. colloids and Surface B: Biointerfaces*, 161:324–330.

S. Wang, K. Liu, Y. Xi, and J. Lei. 2015. Bioinspired surfaces with superwettability: new insight on theory, design, and applications. *Chem. Rev.*, 115:705–709.

R.N. Wenzel. 1936. Resistance of solid surfaces to wetting by water. *Ind.Eng.Chem.*, 28:988.

T. Young. 1805. An essay on the cohesion of fluids. *philos.Trans. R. Soc. Lond.*, 95:65–87.

Individual Research Contribution Review, 2023, 1(1): 49–50

Preparation of Radiation-Grafted Polyethylene Filter Cartridges for Heavy Metal Removal and Industrial Applications

Norliza Ishak
Radiation Processing Technology Division, Malaysian Nuclear Agency
43000 Kajang, Selangor
norliza@nm.gov.my

Abstract

The increasing concentration of heavy metals in water resources is a significant concern. Economic wastewater treatment efficiency is essential for industries to adopt cost-effective adsorbents for heavy metal removal. Radiation-induced grafting technique is one of the most popular methods for polymeric materials surface modification. Therefore, the main objective of this study is to prepare, characterize and evaluate the modified polyethylene (PE) filter cartridge via a simultaneous radiation-induced grafting (SRIG) process with Glycidyl Methacrylate (GMA) by employing gamma irradiation and followed by subsequent chemical functionalization with an amine functional group. This modification technique to enhance the surface properties of the material as an adsorbent.

Keywords: Simultaneous radiation-induced grafting, PE filter cartridge, gamma irradiation

1 Introduction

Industrialization and economic growth in developing countries have led to pollution, particularly the release of toxic metal ions into water bodies. Researchers are exploring ways to remove these ions, focusing on cellulosic biofibers and biopolymers due to their abundance, biodegradability, and hydrophilicity (Kolya and Kang, 2023). However, these biofibers have limitations such as poor mechanical properties and moisture sensitivity. The development and cost-effectiveness of polymeric materials as adsorbents are significant due to their flexibility and ability to be chemically modified to suit specific applications (Chalykh et al., 2023). Adsorption is known as the most effective method for the removal of metal ions from aqueous solution due to its ease of applicability both industrially and laboratory scale, and also its high efficiency (Hong et al., 2019). The flexibility of synthetic polymers makes them an ideal choice for water treatment adsorbents. The synthetic polymers are available in different physical forms and are subject to chemical modification to attach different functional groups based on the intended use.

In general, there are several surface modification techniques to enhance polymeric materials' surface properties, including surface coating, surface functionalization, and surface grafting. The main aim of the modification is to improve and introduce a specific characteristic that acts as a precursor for metal removal from water. Radiation-induced grafting (RIG) is a widely used method for modifying polymers with GMA. It offers advantages such as simplicity, homogeneous reaction, control, and lack of initiators (Shin et al., 2017). Two main approaches are simultaneous irradiation and pre-irradiation. RIG techniques have been used to produce polymeric selective materials with tailored functionalities for metal ion separation. However, the choice of monomer for the chemical modification onto the polymer substrate depends on the targeted application of the polymeric materials. Glycidyl methacrylate (GMA) is a common remarkable chemical and widely used in coating, grafting, adhesives, textile, and ion exchange resins because of its dual functionality (Tahir et al., 2021). With the presence of epoxide rings, GMA can be modified with a variety of other functional groups easily. Studies have shown that RIG can improve polymer properties and adsorption capacity by adding monomers to their surface.

This research focuses on the preparation of a grafted PE filter cartridge by the RIGP technique using gamma. The effect of absorbed dose, dose rate, and GMA concentration on grafting yield will be investigated. Furthermore, the grafted PE will be examined for chemical composition, surface morphology, thermal properties, and surface topology. Batch adsorption tests will be performed to evaluate the suitability of the modified PE filter cartridge as an adsorbent for the removal of metal ions from actual industrial effluents.

2 Methods

The research aims to prepare the PE filter cartridge using simultaneous radiation induced grafting via gamma irradiation for metal ions removal.

2.1 Grafting of GMA onto PE Filter Cartridge

The simultaneous grafting process of glycidyl methacrylate (GMA) onto PE filter cartridge with different concentrations (5,7 and 10% volume/volume) at room temperature to performed graft polymerization. The samples were irradiated by ^{60}Co gamma rays provided by with different doses (10, 15 and 25 kGy) at room temperature condition.

2.2 Functionalization of Grafted PE Filter Cartridge

The grafted PE filter cartridge was chemically functionalized using 3 types of amine groups (Ethylene diamine (EDA) and Dimethyl Amine (DMA) and Triethylenetetramine (TETA)) with a solvent. The functionalization processes will be at temperature of 70°C for 1 hour.

2.3 Batch Adsorption Experiment

A batch adsorption experiment will be carried out to determine the adsorption capacity of the modified PE filter cartridge. A known mass of functionalized PE filter cartridge-g-GMA will be immersed in the metal ions solution under acidic conditions. for 24 hours at room temperature. Inductively Coupled Plasma Mass Spectrometry (ICPMS) will be used to measure the remaining metal ions in the solution after it has been filtered from the adsorbent.

3 Data/Results

3.1 Preparation of modified PE Filter Cartridge

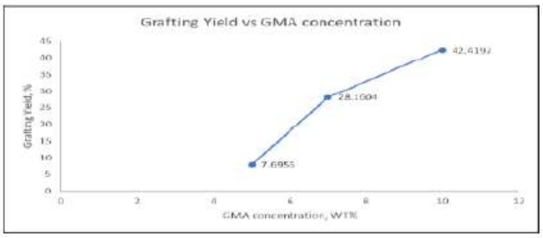

(a) Different GMA concentration at 25kGy

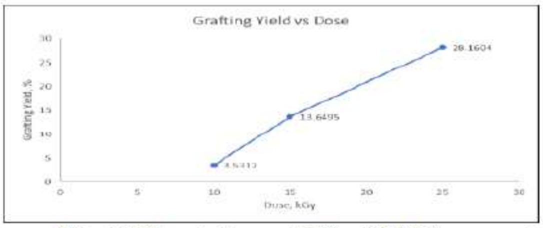

(b) Different dose at 7% of GMA concentration

Figure 1: The grafting yield obtained as (a) a function of GMA concentration and (b) different dose irradiated PE filter cartridge

The effect of GMA concentrations of 5%, 7%, and 10% and dose of 10, 15 and 25 kGy with a reaction time of 24 hours on the grafting yield of the industrial filter cartridge was examined as obtained in Figure 1(a) and (b). The grafting yield increased as the concentration increased to about 10%. However, at monomer concentrations greater than 7%, the formation of homopolymers may also contribute to increased grafting yield due to exposure of gamma irradiation. The concentration of GMA above 10% lead to the decreasing in grafting yield thereafter because of the fast-initial reaction rate. Thus, the determination of chemical functionalities of industrial polyethylene (PE) filter cartridge was determined with optimum yield of 28.1601% at 7% of glycidyl methacrylate (GMA) concentration and irradiation dose of 25 kGy.

FTIR analysis was performed on GMA-grafted material and its chemical functionalization with the amines functional group to improve its surface properties as an adsorbent. The surface composition of PE filter cartridges was characterized before and after modification as in Figure 2. The spectra showed distinct grafting interactions, including carbonyl group (C=O) at 1729 cm^{-1}, ester group C–O, and C-O-C vibration which originates from –COO– ester group of GMA

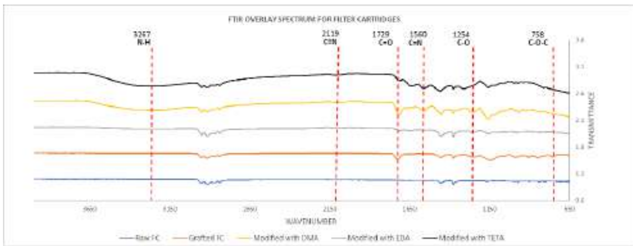

Figure 2: FTIR Spectra of raw, grafted at 7% of GMA concertation and amines functionalized

at 1254 cm^{-1} and 1242 cm^{-1}, respectively. In addition, the characteristics of transmittance peaks arising from aliphatic amine groups are also identified. Specifically, the peaks at 3267 cm^{-1} correspond to N-H stretching, whereas the peaks at 2119 cm^{-1} and 1560 cm^{-1} represent the C=N group and N-H bending respectively. These peaks further confirmed the success of the RIG technique used to modify the material as adsorbent.

4 Conclusions

The modification of an industrial PE filter cartridge as an adsorbent by simultaneous radiation-induced grafting using gamma radiation was successfully prepared for enhancement of surface properties. Herein, a significant correlation between contact angle measurement and the attachment of functional groups (C=O and NH_2) to the surface material is established. In future of this discovery, the adsorbent's performance and functionality may be improved through simultaneous radiation-induced grafting. For future work, the metal ion removal could be further evaluated with adsorption studies using ICPMS.

References

A. E. Chalykh, R. R. Khasbiullin, A. D. Aliev, V. V. Matveev, V. K. Gerasimov, N. A. Slesarenko, I. A. Avilove, V. i. Volkov, and V. A. Tverskoy. 2023. The effect of divinylbenzene on the structure and properties of polyethylene films with related radiation chemical grafted polystyrene and sulfocationite membranes. *J. membranes*, 13(6):287.

T.T. Hong, H. Okabe, Y. Idaka, B.A. Omoldi, and K. Hara. 2019. Radiation induced modified cmc-based hydrogel with enhanced reusability of heavy metal ions adsorption. *J.Polymer*, 181:121772.

H. Kolya and C. H. Kang. 2023. Next-generation water treatment: Exploring the potential of biopolymer-based nanocomposites in adsorption and membrane filtration. *J. Polymers*, 15(16):3421.

I. H. Shin, S. Hong, S. J. Lim, Y. S. Son, and T. H. Kim. 2017. Surface modification of PVDF membrane by radiation-induced graft polymerization for novel membrane bioreactor. *J. Ind. Eng. Chem.*, 46:103–110.

M. Tahir, A. Raza, A. Nasir, and T. Yasin. 2021. Radiation induced graft polymerization of glycidyl methacrylate onto sepiolite. *J. Radiation Physics Chemistry*, 179:109259.

Individual Research Contribution Review, 2023, 1(1): 51–52

Development of Recycled Carbon Fiber Reinforced Polyethylene Composite by Using Electron Beam Irradiation

Norshafarina Ismail
Radiation Processing Technology Division, Malaysian Nuclear Agency
43000 Kajang, Selangor
norshafarina@nm.gov.my

Abstract

This paper deals with recycled carbon fiber (rCF) as a reinforcement in high-density polyethylene. rCF was compounded with high-density polyethylene at 5, 10, 20, and 30 wt.% using an internal mixer. The compound was pressed into specimen shape at 1mm thickness and subjected to electron beam irradiation for polymer composite crosslinking at 50, 100, 150, and 200kGy using 2MeV electron beam irradiator. The effect of rCF weight percent in the composite and the effect of electron beam irradiation on the polymer composite crosslinking is presented specifically on thermal properties, tensile strength, and morphology observation.

Keywords: electron irradiation, polymer composite crosslinking, recycled carbon fiber

1 Introduction

The interface between fiber and matrix is an important aspect in controlling the overall properties of the composites. A strong interface increases the structural stability of the composites and transfers stress efficiently from matrix to fiber. However, carbon fiber's smooth surface and chemical inertness usually result in poor adhesion with the resin and hence less enhancement in the performance properties of the composite (Tiwari et al., 2011).

Hassan (Hassan et al., 2005) demonstrated the role of irradiation as a compatibilizer in carbon fiber-reinforced polypropylene waste. Tiwari 2011 reported the contributing factors for interfacial adhesion in irradiated fibers are surface roughening and polar functionality. Crosslinking and modifying polymers via high-energy irradiation gamma and electron beams are established techniques. Numerous attempts have been carried out on polyethylene polymer blends. Ronkay (Ronkay et al., 2010) employed electron beam irradiation in HDPE/PET blends to improve the compatibility of these materials.

From the material perspective, the surface of a carbon fiber exhibits a smooth morphology and inter-chemical properties, which influence the fiber-matrix adhesion. Therefore, the carbon fibers' surfaces need to be treated to improve the interfacial interaction that influences the mechanical properties of the prepared composites. Various research works have reported on improving the interfacial adhesion of carbon fibers with matrices such as polypropylene, polyamide, and polycarbonate using surface treatment techniques including plasma, electrochemical oxidation, wet chemical, and thermal treatment.

Although PE is low cost and abundant, no study on PE as a polymer matric of carbon fiber reinforced composite is reported. Despite the efforts to improve the interfacial adhesion and mechanical properties, preparing the carbon fiber-reinforced composite required a complex procedure. Therefore, there is a need to design a low-cost composition using recycled carbon fibers and polyethylene matric with a straightforward procedure of using electron beam irradiation. Ionizing radiation provides an effective and convenient technique to improve the adhesion between the fiber and matrix. It can create chemical interaction resulting from radicals produced within the matrix and surface of carbon fibers. In this work, an attempt to use electron beam irradiation on the carbon fiber and the resultant composites is reported.

2 Methods

2.1 Materials

The high-density polyethylene is a blow molding grade HD 5403AA supplied by Etilinas Sdn. Bhd is a medium molecular weight density polyethylene copolymer. It has a density of 0.952 g/cm^3 and a melt flow index of 25 dg/min (ASTM D1238, 190°C 21.6kg). The recycled carbon fiber used in this work was purchased from ELG Carbon Fiber with a length and diameter of 6 mm and 6μm, respectively. The rCF was reclaimed by an established pyrolysis process and meant for thermoplastic processing.

2.2 Preparation of rCF/HDPE compounding

rCF/HDPE compounds were prepared in a Haake Rheomix laboratory internal mixer fitted with a rotor that operates at 50 rpm with the chamber wall maintained at 160°C. Batch mass was selected to fill 60% of the processing chamber volume during the molten state. HDPE as received with and without rCF was dry mix before loaded into the chamber. rCF was added by weight percent (5, 10, 20, and 30). The melt-mixed compound was pressed into the sheet for tensile properties test and thermal test.

2.3 Thermal properties

Thermogravimetric analysis (TGA) was performed on Netzsch TG. Samples with approximately 5 mg were heated in an alumina pan from 30°C to 700°C using a heating rate of 10°C/min, under a nitrogen flow of 50 mL/min. Differential thermogravimetry (DTG) scans were also computed.

2.4 Polymer composite crosslinking by electron beam

The prepared samples were subjected to electron beam irradiation using a 2 MeV electron beam facility for polymer composite crosslinking. The samples were exposed to 50, 100, 150 and 200kGy.

2.5 Determination of mechanical properties

Mechanical properties in tension were measured according to ASTM D638 using specimens type IV. The mechanical properties of the rCF/HDPE were measured Tests were performed in a Shimadzu Universal Testing Machine operating at 50mm/min with a load cell of 50kN. Elastic modulus, tensile strength, and elongation at break results were automatically obtained from the equipment software. Mechanical tests were conducted at room temperature and the presented results were an average of 5 test specimens.

2.6 Scanning Electron Microscope

Morphology of irradiated samples was performed using a Scanning Electron Microscope (SEM). Samples were gold-coated before being subjected to a high-energy beam.

3 Discussion/Conclusions

3.1 Thermogravimetric Analysis

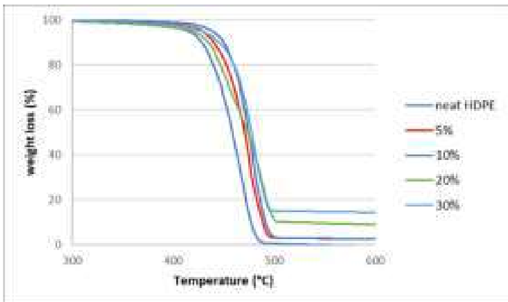

Figure 1: TGA graph of rCF/HDPE composite

Figure 1 shows the TGA graph for the rCF/HDPE composite without crosslinking. The onset temperatures ($T_{20\%}$ and $T_{50\%}$) of 20% and 50% weight loss, respectively, were used as the indicator of the sample's thermal stability. rCF content showed higher thermal stability compared to neat HDPE. At 20 wt.% of rCF, the onset temperature reduced slightly for T20% while for T50% it did not change.

Table 1: TGA data

Sample	Weight Loss T_{20}(°C)	Weight Loss T_{50}(°C)
Neat HDPE	439.70	457.20
5%	452.47	469.97
10%	459.99	472.49
20%	447.50	472.50
30%	460.02	477.52

3.2 Morphology observation

Figure 2 shows the morphology of the composite comprised of 5% rCF (a) without electron beam irradiation and (b) with electron beam irradiation. Tensile behavior such as elongation and necking before failure is exhibited in crosslinked samples. Pull-out fibers are obvious in all samples suggesting adhesion failure that is accountable for insignificant changes in composite strength (30-36MPa) specifically for non-irradiated composite.

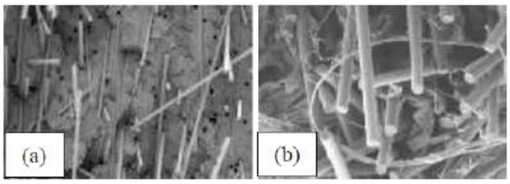

Figure 2: SEM of 5%rCF/HDPE (a) non-crosslinked and (b) crosslinked

3.3 Mechanical properties

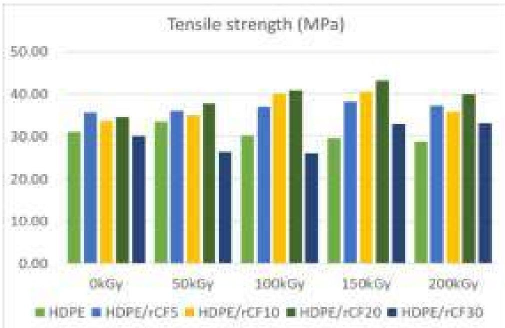

Figure 3: Tensile strength of developed composites

The tensile strength of crosslinked polymer composite developed from carbon fiber as reinforcement and polyethylene as a matrix is shown in Figure 3. rCF content plays a role in improving the strength. However, the strength is only distinguished upon crosslinking by electron radiation, in which beyond 150kGy the composite strength starts to decrease.

References

M.M. Hassan, A. El-Hag Ali, G.A. Mahoud, and E.S.A. Hegazy. 2005. Synergistic effect of short reinforced fibers and gamma rays on the thermal and mechanical properties of waste poly (propylene) composites. *Journal of Applied Polymer Science*, 96(5):1741–1747.

F. Ronkay, L. Mészáros, G. Jánoki, and T. Czvikovszky. 2010. The effect of pre-electron beam irradiation of HDPE on the thermal and mechanical properties of HDPE/PET blends. *Materials Science Forum, Trans Tech Publications Ltd.*, 659:85–90.

S. Tiwari, J. Bijwe, and S. Panier. 2011. Gamma radiation treatment of carbon fabric to improve the fiber–matrix adhesion and tribo-performance of composites. *Wear*, 271(9-10):2184–2192.

Individual Research Contribution Review, 2023, 1(1): 53–54

Melt Flow Index of Irradiated Ground Tire Rubber

Norshafarina Ismail
Radiation Processing Technology Division, Malaysian Nuclear Agency
43000 Kajang, Selangor
norshafarina@nm.gov.my

Abstract

MFI is an instrument used to measure the ease of flow of the melted thermoplastic polymer. The result indicates whether the material is viscous or non-viscous in the molten state under a known applied pressure and temperature. The MFI value provides information about the flowability of the polymer. Ground tire rubber has the potential to be incorporated into the polymer to produce thermoplastic elastomer. However, the 3D network formed during vulcanization hinders the movement of this material affecting flowability. Electron beam irradiation is applied to degrade and modify the GTR by breaking down the 3D network. Irradiation doses from 50 to 750kGy are subjected to the GTR before being compounded with HDPE by melt mixing method. MFI for these compounds is measured and reported as a function of irradiation dose to assess how the flow characteristics of the material change with varying levels of irradiation, which can provide valuable insights into the modified GTR's suitability for thermoplastic elastomers.

Keywords: Fluidity, melt flow index, polymer processing, rheology, thermoplastic polymer, viscosity

1 Introduction

The melt Flow Index (MFI) of any thermoplastic material is defined as a deposition per 10 minutes through the melt flow tester at a certain standard temperature and load condition, for example, 190°C and 5.0kg for HDPE in this study. The MFI is an indicator of the flowability of thermoplastic materials. This property is essential for quality control as well as subsequent processes. MFI is also related to molecular weight.

Ground tire rubber (GTR) produced by mechanical grinding of waste tire rubber contains a high amount of high-quality natural and synthetic rubber. These combinations are potential sources for filler in polymers. Thermoplastic polymers may be from polypropylene (PP), polyethylene (PE), and ethylene vinyl acetate (EVA). Polymer blends based on recycled rubbers and thermoplastic resins lead to thermoplastic elastomer (TPE) production, exhibiting flexibility from the rubber phase and processability from the thermoplastic resin. These blends can be economical alternatives for virgin TPE with applications ranging from household to automotive seals and interiors.

Energy sources for polymer degradation such as ionizing radiation, excite active species such as free radicals, ions, and molecules and can significantly modify the molecular structures of irradiated polymer. The mechanism includes molecular chain branching that increases the molecular weight of the polymer and chain scissoring that leads to main chains of molecule breakage. The external energy breaks down the three-dimensional crosslinked rubber network into lower molecular weight fragments, producing a physical recovery of rubber waste fragments for non-reinforcing filler (Manaila et al., 2021). A melt flow indexer measures the mass (weight) of melt polymer extruded through a specified die under constant temperature and constant pressure during a fixed time. It is an indirect measure of molecular weight, with a high melt flow rate corresponding to low molecular weight thus is inversely proportional to the melt's viscosity at the measurement condition. This study aims to determine the melt flow index of a high-density polyethylene compound filled with irradiated ground tire rubber.

2 Methods

2.1 Materials

High-density polyethylene (HDPE) with melt flow index 1.3 g/10 min at 190°C, 5.0kg was purchased from Etilinas HD 5403AA. The ground tire rubber (GTR) was from Sin Rubtech Consultancy Sdn. Bhd. with particle sizes ranging from 500 to 700μm.

2.2 Beta Irradiation

Beta irradiation of GTR was performed by EPS-3000 electron beam accelerator, utilizing a 2 MeV. The GTR were exposed to 50, 200, 500, and 750kGy with 50kGy/pass, under air atmosphere. Ground tire rubber was packed in an aluminum foil.

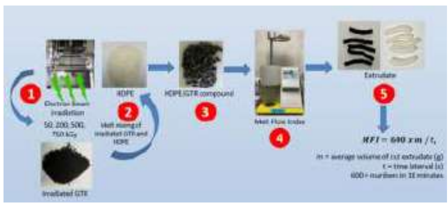

2.3 Compound Preparation

The irradiated GTR later were compounded with high-density polyethylene (HDPE) polymer according to the defined GTR weight ratio using melt mixer HAAKE for 10 minutes at 60 rpm rotor speed (Table 1). The resultant TPE was prepared for melt flow index measurement.

Table 1: The MFI measurement for HDPE and GTR/HDPE blends.

GTR content (%)	HDPE content (%)	TOTAL weight (%)	Melt Flow Index (MFI)				
			0kGy	50kGy	200kGy	500kGy	750kGy
0	100	100	1.08	n/a	n/a	n/a	n/a
5	9	100	0.96	1.00	0.96	1.04	1.02
10	90	100	0.92	0.90	0.82	0.90	0.92
20	80	100	0.76	0.82	0.78	0.83	0.78
30	70	100	0.60	0.68	0.66	0.70	0.62

2.4 Determination of Melt Flow Index

The melt flow index was measured by Thermo Haake Meltfixer at 190°C and 5.0 kg load for 10 minutes according to ASTM D1238. About 3.00 grams of HDPE/GTR compound was loaded into the barrel. For comparison purposes, the MFI of the virgin HDPE was also measured.

A plunger was used to pack the compound to eliminate any air gap. The average values were reported after two repetitions for each sample. The equation for melt flow index (MFI) in grams per 10 min is as follows;

$$\mathrm{MFI} = 600 \times \frac{m}{t} \tag{1}$$

Where,
m = average volume of cut extrudate (g)
t = time interval (s)
600 = numbers in 10 minutes

3 Data/Results

3.1 Melt Flow Index

Figure 1 shows extrudate from the MFI instrument in which HDPE extrudate has a smooth surface while GTR/HDPE extrudate has a rough surface. Both were subjected to the same temperature (190°C) and load (5.0kg).

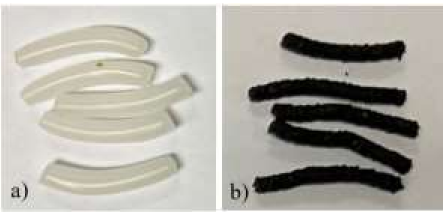

Figure 1: Typical extrudate of a) HDPE and b) GTR/HDPE compound

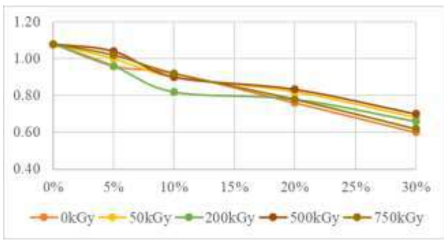

Figure 2: MFI declining trends with high content of GTR and high irradiation doses

Figure 2 illustrates the declining MFI trend with the addition of GTR into the HDPE resin. The fluidity of the HDPE drops by about 44% when incorporating 30% of GTR into HDPE. The MFI measurement is expected to keep declining with higher content of GTR as reported (Fazli and Rodrigue, 2021). Lower MFI measurement shows higher viscosity, suggesting crosslinked GTR does not flow and agglomerates in the matrix.

The idea of irradiating the GTR before compounding with HDPE is to break down the crosslinks between the rubber chains so the number and nature of double bonds change and decrease the molecular weights. Molecular weights influence the MFI measurement. MFI measurements incline for HDPE compound melt-mixed with high irradiation doses. For example, HDPE melt-mixed with non-irradiated GTR of 30 wt.% is 0.60 g/10mins while HDPE with 500kGy irradiated GTR shows 0.70 g/10mins. The same trend applies to GTR of 20 wt.%. It indirectly shows an indication of the fluidity of an irradiated GTR/HDPE compound. This suggests chain scissoring may have taken place and lowered the molecular weight that directly influences MFI measurement.

4 Conclusions

This preliminary study shows that a high dose of irradiation by electron beam can break down the rubber crosslinked network and change the melt flow index compared to non-irradiated rubber, simultaneously affecting the compound fluidity. The control MFI reading is 1.08 g/10 mins. The addition of 30 wt.% irradiated GTR (500kGy) and non-irradiated GTR has an MFI measurement of 0.70 g/10 mins and 0.60 g/10 mins, respectively. Further tests and analyses such as FTIR, CHNS elemental analysis, and gel content are recommended to comprehensively conclude the irradiation dose's effect on ground tire rubber.

References

Kelly C. de Lira Lixandrão and Fabio F. Ferreira. 2019. Polypropylene and tire powder composite for use in the automotive industry. *Heliyon, ISSN 2405-8440*, 5(9):e02405, https://doi.org/10.1016/j.heliyon.2019.e02405.

A. Fazli and D. Rodrigue. 2021. Effect of ground tire rubber (GTR) particle size and content on the morphological and mechanical properties of recycled high-density polyethylene (rHDPE)/GTR blends. *Recycling*, 6(3):44, http://dx.doi.org/10.3390/recycling6030044.

E. Manaila, G. Craciun, D. Ighigeanu, I. B. Lungu, M. Dumitru, and M. D. Stelescu. 2021. Electron beam irradiation: A method for degradation of composites based on natural rubber and plasticized starch. *Polymers, MDPI AG*, 13(12):1950, http://dx.doi.org/10.3390/polym13121950.

M.J. Spear, A. Eder, and M. Carus. 2015. 10 - wood polymer composites, editor(s): Martin p. ansell. *Wood Composites, Woodhead Publishing, ISBN 9781782424543*, pages 195–249, https://doi.org/10.1016/B978–1–78242–454–3.00010–X.

Jiayi Zhu, Chamil Abeykoon, and Nazmul Karim. 2021. Investigation into the effects of fillers in polymer processing. *International Journal of Lightweight Materials and Manufacture, ISSN 2588-8404*, 4(3):370–382, https://doi.org/10.1016/j.ijlmm.2021.04.003.

Individual Research Contribution Review, 2023, 1(1): 55–56

Biopolymer Coating on Paper Packaging

Norzita Yacob
Radiation Processing Technology Division
Malaysian Nuclear Agency
43000 Kajang, Selangor
norzita@nm.gov.my

Abstract

Chitosan is a biopolymer that may be employed as a film or coating to replace synthetic polymers. However, the use of chitosan has been limited because of its poor mechanical and barrier properties. This study was conducted to investigate the effect of nanocellulose on hydrophilicity and water absorption of chitosan-based film. The results demonstrated that the addition of nanocellulose as a filler enhanced the properties of this biofilm.

Keywords: Chitosan film, nanocellulose, swelling, wettability

1 Introduction

Petroleum-based plastic has been widely used in many applications due to its superior properties. However, the increase of using synthetic packaging has led to waste disposal problems. Therefore, biopolymers such as chitosan, have been the focus of much research in recent years because of interest in their potential use as edible and biodegradable films and coatings for food packaging.

The use of chitosan and other biopolymers has been limited because of their usually poor mechanical and barrier properties as compared to synthetic polymers. The addition of reinforcing fillers to biopolymers has proven to be effective in enhancing their thermal, mechanical, and barrier properties. The use of the nanocomposite concept was made to improve the properties of the biopolymers. The smaller size of the filler causes better interaction between the filler and matrix (Abdollahi et al., 2012; Arfat et al., 2014). A uniform dispersion of nanocellulose leads to a very large matrix/filler interfacial area, which changes the molecular mobility, the relaxation behavior, and the consequent thermal and mechanical properties of the material.

With the recent development of nanotechnology, nanocellulose is getting more attention due to its availability, large surface area, high mechanical properties, biodegradability and biocompatibility. Hence, lignocellulose waste should be considered as a source of nanocellulose. The preparation of nanocellulose from agricultural waste has been studied by many researchers from several sources such as oil empty fruit bunch (Hastuti et al., 2018). Moreover, cellulose nanofibrils in agricultural waste are less tightly attached to the primary cell wall. As a consequence, lower energy consumption is needed to prepare nanofibrils.

Thus, this research will study the preparation and properties of chitosan-based film with the addition of nanocellulose to maximize the function of the film. The study reports the influence of nanocellulose on wettability properties of the film.

2 Methodology

Nanocellulose was isolated from sago pith waste by chemical and ultrasonic treatment. Subsequently, the nanocellulose (1% v/w) was dispersed in distilled water before being added to the film solution. The films were prepared by dissolving PVA and chitosan solution and mixed until a clear and homogenous solution was achieved. Nanocellulose (1% v/v) was added to the solution and mixed continuously for 1 h. The solutions were cast onto a plastic mould (100 x 100 mm) and dried at room temperature. The films were kept at 23 ± 2°C and 50 ± 5% relative humidity (RH) until tested. Samples were tested for water contact angle and water absorption.

3 Results and Discussion

Extraction of cellulose from sago pith waste was done by chemical treatment. Afterward, the cellulose was exposed to high intensity ultrasonic to isolate the nanocellulose. Atomic force microscopy (AFM) was used to analyze the size of nanocellulose obtained from this study. The diameter of the nanocellulose was calculated and their distribution is illustrated in Figure 1. The histogram shows a wide distribution pattern with various ranges of size. It displays nanocellulose with a size greater than 100 nm and 78% of the nanocellulose have a size between 30 nm to 80 nm.

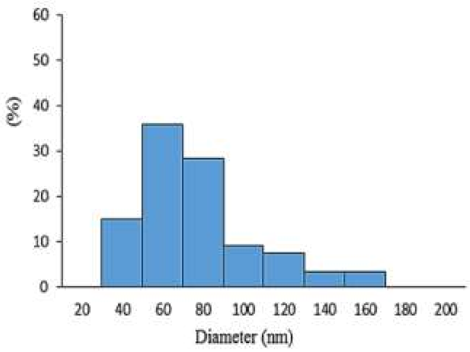

Figure 1: The average size of nanocellulose after exposing to high intensity ultrasonication at 40% amplitude.

Figure 2 explains the effect of nanocellulose on the water uptake of the film in distilled water. Nanocellulose remarkably decreased the swelling percentage from 180% to 90% after 24 h. Nanocellulose restricted the flexibility of the chitosan chain and acted as an interpenetrated network with the matrix (Talebi et al., 2022).

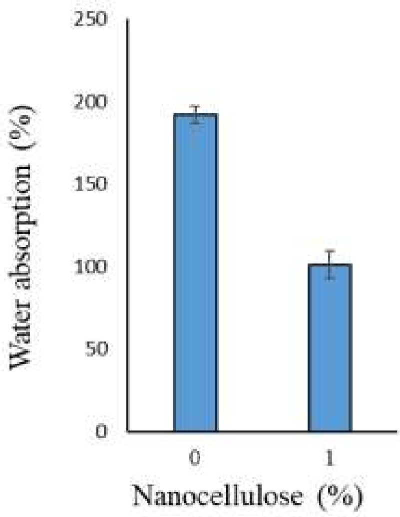

Figure 2: The effect of nanocellulose (1% v/v) on water absorption of chitosan film.

The results are supported by the wettability test as shown in Figure 3. Wettability shows the hydrophilicity of the film surface as studied by contact angle. The contact angle of the film without nanocellulose was 65.1°. The addition of nanocellulose increased the contact angle up to 110.7°. Thus, it was found that the incorporation of nanocellulose decreased the hydrophilicity of the films. The reduction of these properties is probably because of intermolecular and intramolecular hydrogen interactions between nanocellulose and chitosan matrix which resulted in a stiffer and more compact film. As a result, the mobility of the matrix chain was restricted, thus lowering the ability of water molecules to absorb into the films.

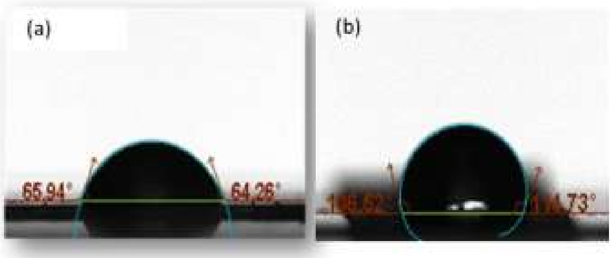

Figure 3: The water contact angle of chitosan-based film (a) without nanocellulose and (b) with the addition of 1% v/v of nanocellulose.

4 Conclusion

This study investigated the effect of nanocellulose as fillers on the swelling and wettability of chitosan-based film. The nanocellulose was successfully isolated from sago pith waste using alkaline followed by ultrasonic treatment. The results revealed that the incorporation of nanocellulose reduced the swelling and hydrophilicity of the film. These films could be potentially used for food packaging or as a coating layer on packaging paper.

References

M. Abdollahi, M. Rezaei, and G. Farzi. 2012. A novel active bionanocomposite film incorporating rosemary essential oil and nanoclay into chitosan. *Journal of Food Engineering*, 111:343–350.

Y.A. Arfat, S. Benjakul, T. Prodpran, P. Sumpavapol, and P. Songtipya. 2014. Properties and antimicrobial activity of fish protein isolate/fish skin gelatin film containing basil leaf essential oil and zinc oxide nanoparticles. *Food Hydrocolloids*, 41:265–273.

N. Hastuti, K. Kanomata, and T. Kitaoka. 2018. Hydrochloric acid hydrolysis of pulps from oil palm empty fruit bunches to produce cellulose nanocrystals. *J Polym Environ*, 26(9):3698–3709.

Hamidreza Talebi, Faramarz Ashenai Ghasemi, and Alireza Ashori. 2022. The effect of nanocellulose on mechanical and physical properties of chitosan-based biocomposites. *Journal of Elastomers & Plastics*, 54(1):22–41.

Individual Research Contribution Review, 2023, 1(1): 57–58

Encapsulation of Jatropha Oil-Based Resin for Self-Healing Coating Application

Nurul Huda Mudri
Radiation Processing Technology Division, Malaysian Nuclear Agency
43000 Kajang, Selangor
nurul_huda@nm.gov.my

Abstract

Microcapsule system is one of the popular approaches in producing self-healing coating. By applying specific conditions like moisture, sunlight, and pH, the reservoir of healing agents in the microcapsule will flows out and polymerize to seal the cracked areas. Jatropha oil (JO) is one of the natural abundance oils that has been planted in Malaysia. JO is classified as a non-edible oil with a high iodine value (94 to 120 mg/g). This paper aims to study the effect of agitation rate during the preparation of the microcapsule containing JO and evaluate the physicochemical properties. In this experiment, JO was encapsulated into a polyurea formaldehyde (PUF)-based microcapsule. The stirring rate was varied at 200 rpm, 400 rpm and 800 rpm during the encapsulation procedure for 3 hours. The PUF shell encapsulating the JO was verified by Fourier Transform Infrared (FTIR) analysis. In both microcapsule of neat PUF and PUF-JO, the peak of the amide group (C=O) was found at 1625 cm^{-1}, and the wagging (-NH) was detected at the band of 767 cm^{-1} . At a speed of 400 rpm, the microcapsules obtained the highest yield of core content (71.6 ± 2.7 %). Based on the physical and chemical analysis, JO 400 was selected in the preparation of coating formulation for self-healing coating application in future work.

Keywords: jatropha, self-healing, microcapsule, polyurea formaldehyde, stirring rate

1 Introduction

Self-healing coatings are categorized as smart materials that can detect damage such as tear, scratch, and crack and subsequently initiate the repair response based on the specific mode of action. This invention gave a significant advantage, particularly regarding less maintenance service, especially in remote areas, and extended the lifetime of the coating (Zhao et al., 2015). The microcapsule-based approach is favourable and nearly ready for commercialisation among the self-healing coating system. Jatropha oil (JO) is one of the sources of non-edible in Malaysia (Amri et al., 2021). This oil is collected from the seed of the Jatropha curcas fruit via extraction process. Jatropha is a subtropical shrub tree under the Euphorbiaceous family (Mandy et al., 2017). JO contain a phorbic ester compound that make it poisonous for oral intake that leads to vomiting and nausea, which similar to insecticide poisoning symptoms (Primandari et al., 2017; Taib et al., 2017). Among local sources of vegetable oils in Malaysia, JO (78% to 84%) has higher unsaturated fatty acids content than palm oil (40% to 50%) (Abdullah et al., 2013; Khalil et al., 2013). Moreover, the IV of JO is around 94 to 120 mg/g and is therefore doubled compared to palm oil (44 to 58 mg/g) which make it more favorable in the selection of healing agent materials. As far as it is known, no study has reported on using jatropha oil resin as a selfhealing coating material. This paper aims to investigate the influence of agitation rate when preparing microcapsules containing JO. The properties of the JO-based microcapsules were analysed physically and chemically using FTIR, particle size analysis, core content analysis and FESEM.

2 Methods

2.1 Preparation of polyurea-formaldehyde (PUF) microcapsule

This involved two steps: (i) preparation of hydroxymethyl urea pre-polymer known as UF prepolymer and (ii) encapsulation process via oil in water emulsion technique. The second step involved adding surfactant and JO to the aqueous solution with controlled of agitation speed. In 200 ml beaker, SDBS, resorcinol and ammonium chloride were added into 70 ml of ultra-pure water. Then, 10 g of pure JO was added to the solution and mixed until it was uniform. Next, the aqueous mixture was transferred into a 250 ml four-neck flask and mixed with the hydroxymethyl urea prepolymer produced in the first step and stirred at 25°C, 200 rpm for 1 hour. The temperature was raised to 60°C and diluted HCl was used to adjust the pH to 3 to introduce acidic condition in the mixture. The speed of reaction was set to 200 rpm, 400 rpm, and 800 rpm for each encapsulation process.

2.2 Characterization of PUF microcapsule

Fourier Transform Infra-Red (FTIR) Spectroscopy was conducted to verify the encapsulation process of JO. The average diameter size (d_{50}) of the microcapsule particles was determined using Particle Sizer Analysis (Microtrac, USA). The morphology of the microcapsules at variation speed of reaction was examined using Field Emission Scanning Electron Microscopy (JOEL, USA). The amount of encapsulated JO was determined using an ultrasonic (Vobra Cell, USA) extraction method.

3 Data/Results

3.1 FTIR analysis

The success of the encapsulation process of JO-based resins was studied using FTIR analysis as displayed in Figure 1.

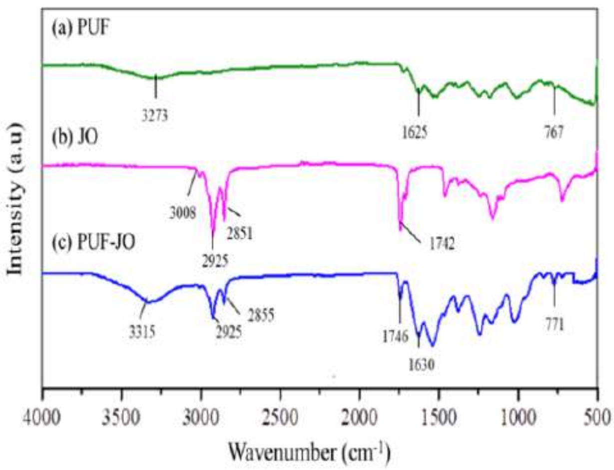

Figure 1: FTIR spectra of a PUF microcapsule, JO and PUFJO

4 Discussion/Conclusions

From Figure 1, the PUF microcapsule showed broad absorption bands of (-OH) and (-NH) in the wavenumber's region of 3100 to 3500 cm^{-1} . The characteristic band of stretching of the amide group (C=O) was detected at 1625 cm^{-1} whilst the wagging (–NH) appeared at the band of 767 cm^{-1} . The findings directly aligned with previous results on neat the PUF microcapsule characterisation (Zhang et al., 2018).

For the JO sample, the absorption peak of 3008 cm^{-1} confirmed the significant carbon double bond that exists in the oil. In addition, PUF-JO adopted similar absorption peaks between the PUF microcapsules and the JO, respectively. Therefore, it can be concluded that the JO was being encapsulated by PUF resin. These conclusions are aligned with previous findings to verify the encapsulation process (Alizadegan et al., 2018; Miguel et al., 2016; Zhang et al., 2018).

The average particle size of the synthesized microcapsules was in the range of 37.9 μm to 56.7 μm. Under the FESEM micrograph, all microcapsules maintained the spherical shape at reaction speeds of 200 rpm and 400 rpm but showed agglomeration at 800 rpm, respectively. At the agitation rate of 400 rpm, the JO 400 (71.6 ± 2.7%) had the highest core content and will be used for self-healing coating application for future work.

References

B. M. Abdullah, R. M. Yusop, J. Salimon, E. Yousif, and N. Salih. 2013. Physical and chemical properties analysis of jatropha curcas seed oil for industrial applications. *International Journal of Chemical, Molecular, Nuclear, Materials and Metallurgical Engineering*, 7(12):893–896.

F. Alizadegan, S. M. Mirabedini, S. Pazokifard, S. Goharshenas Moghadam, and R. Farnood. 2018. Improving self-healing performance of polyurethane coatings using PU microcapsules containing bulky-ipdi-ba and nano-clay. *Progress in Organic Coatings*, 123:350–361, https://doi.org/10.1016/j.porgcoat.2018.07.024.

M. R. Amri, S. S. O. Al-Edrus, C. T. Guan, F. M. Yasin, and L. S. Hua. 2021. Jatropha oil as a substituent for palm oil in biobased polyurethane. *International Journal of Polymer Science*, 3:1–12, https://doi.org/10.1155/2021/6655936.

H. P. S. A. Khalil, N. A. S. Aprilia, A. H. Bhat, M. Jawaid, M. T. Paridah, and D. Rudi. 2013. A jatropha biomass as renewable materials for biocomposites and its applications. *Renewable and Sustainable Energy Reviews*, 22.

M. Mandy, W. P. Hock, H. H. Kai, J. Kodoh, and L. K. Chiang. 2017. Growth responses of varieties of jatropha curcas seedlings to varying NPK fertilizer rates. *International Journal of Agriculture, Forestry and Plantation*, 5:104–109.

M. de la P. Miguel, R. Ollier, V. Alvarez, and C Vallo. 2016. Effect of the preparation method on the structure of linseed oil-filled poly (urea-formaldehyde) microcapsules. *Progress in Organic Coatings*, 97:194–202, https://doi.org/10.1016/j.porgcoat.2016.04.026.

S. R. P. Primandari, A. K. M. A. Islam, Z. Yaakob, and S. chakrabarty. 2017. Jatropha Curcas L. biomass waste and its utilization. *In Advances in Biofuels and Bioenergy*, pages 273–282, IntechOpen. https://doi.org/http://dx.doi.org/10.5772/intechopen.72803.

E. R. J. Taib, L. C. Abdullah, M. M. Aung, M. Basri, M. Z. Salleh, , S. Saalah, S. Mamat, C. Y. Chee, and J. L. Wong. 2017. Physico-chemical characterisation of epoxy acrylate resin from jatropha seed oil. *Pigment and Resin Technology*, 46(6):485–495, https://doi.org/10.1108/PRT11–2016–0116.

C. Zhang, H. Wang, and Q. Zhou. 2018). Preparation and characterization of microcapsules based self-healing coatings containing epoxy ester as healing agent. *Progress in Organic Coatings*, 125(May):403–410, https://doi.org/10.1016/j.porgcoat.2018.09.028.

J. Zhao, W. Millians, S. Tang, T. Wu, L. Zhu, and W. Ming. 2015. Self-stratified antimicrobial acrylic coatings via one-step UV curing. *ACS Applied Materials and Interfaces*, 7:18467–18472, https://doi.org/10.1021/acsami.5b04633.

Individual Research Contribution Review, 2023, 1(1): 59–60

Preparation of TPE Filled Irradiation Modified Silica for Thermal Application

Pairu bin Ibrahim
Radiation Processing Technology Division, Malaysian Nuclear Agency
43000 Kajang, Selangor
pairu@nm.gov.my

Abstract

This research aimed to change the hydro nature and to modulate the porosity of nano-SiO_2 by surface modification using radiation-induced graft polymerization GMA by electron beam accelerator utilizing the pre-irradiation-peroxidation method. The effect of irradiation dose (10 to 50 kGg) was studied using BET, FTIR and TGA analysis. BET analysis, it can be concluded that the irradiation process enhanced the pore's size due to the less agglomeration of the particles inhibited by a certain amount of grafting chains formed on the surface of SiO_2. Meanwhile, the hydrophobicity of prepared materials is strongly confirmed by the contact angle test which shows that a high dosage of irradiation produced strong hydrophobic properties. The results of FTIR analysis manifested a new peak at 770cm^{-1} assigned to Si-O whose presence after irradiation clearly indicated that this group was actively involved in the grafting reaction. The shifting of degradation point to the higher temperature in the DTGA test confirmed that SiO_2 contains grafting chains of SiO_2- poly GMA.

Keywords: hydro, nanosilica, grafting

1 Introduction

Surface modification of filler is a very significant technique in increasing the functionality of filler's surface which is known has directly affect the chemical interaction between filler and rubber. In this case, some filler need to be modified in order to match the surface chemistry to a specific rubber. Silica, for example, is one of the active fillers which require a surface modification as will be described later. Recent research has been focusing on radiation induced polymer grafting on silica for the surface modified of filler material. Polymerization reaction was carried out on pre-irradiated silica with the hope to afford polymers of better defined compositions, since it avoids tampering of electron beam with the "ideal" polymer structure (Acunzo et al., 2013). The formation of free radicals was initiated by the reaction of gamma irradiation during the exposure onto the silica's surface and can be considered as an active compound which has the tendency to interact with monomers via a grafting reaction to form either chemical bond, hydrogen bond or physical adsorption (Xu et al., 2013). Formation of grafting chains provide advantages not only aids the dispersion of fillers through organic modification, but also provides better interfacial connections through interdiffusion or entanglement between the grafted chains and the matrix polymer chains (Yuan et al., 2018; Watanabe et al., 2020).

2 Methods

There are three steps involved in this method :

i Irradiation nanosilica suspension

The purpose of irradiation was to initiate the formation of free radicals.

ii Graft polymerization

Reactive nanosilica was reacted with GMA solution to perform graft polymerization

iii Purification

The purification was done to obtain high yield of grafted polyGMA-nanosilica.

3 Data/Results

3.1 FTIR

Refer Figure 1 below:

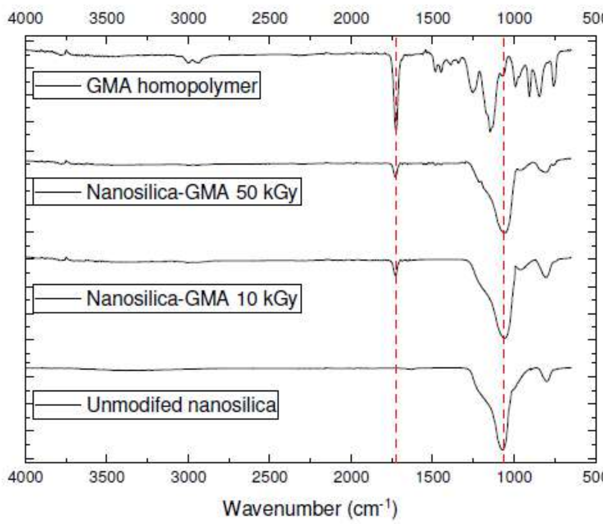

Figure 1: FTIR

3.2 Optical Contact Angle

Refer Figure 2 (a) Control and (b) polyGMA-nanosilica 50kGy below:

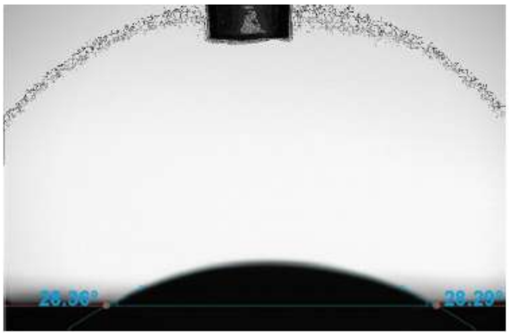

(a) Control

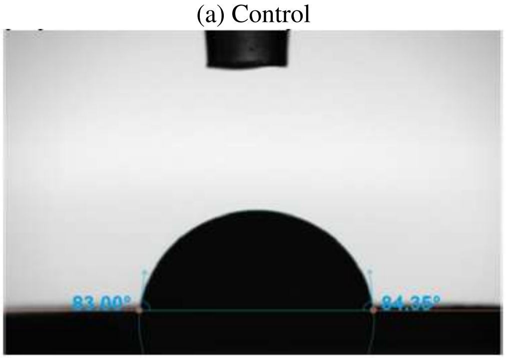

(b) polyGMA-nanosilica 50kGy

Figure 2: (a) Control and (b) polyGMA-nanosilica 50kGy

3.3 Particle Size Analyzer

Refer Figure 3 below:

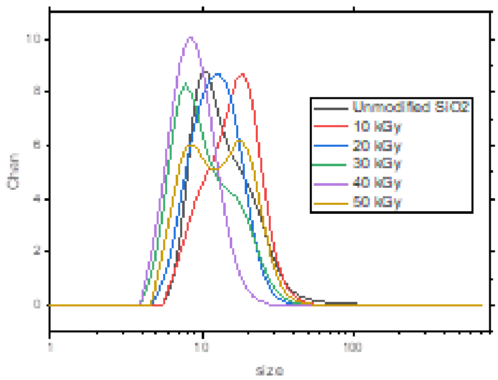

Figure 3: Particle Size Analyzer

3.4 BET Surface Area

	surface area (m^2/g)	pore volume (cm^3/g)	pore size (nm)
Unmodified	167.14	0.5667	13.56
nanosil- GMA 10kGy	172.37	0.9012	20.91
nanosil- GMA 20kGy	171.59	0.9147	21.32
nanosil- GMA 30kGy	169.86	0.9790	23.05
nanosil- GMA 40kGy	164.63	0.8819	21.42
nanosil- GMA 50kGy	145.56	1.0407	28.59

Refer Figure 4 below:

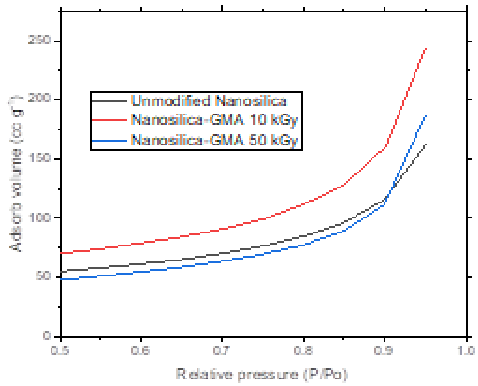

Figure 4: BET Surface Area

4 Discussion/Conclusions

In this study, we successfully prepared surface modified of SiO_2 using irradiation technique via the reaction of free radicals with the establishment of strong hydrophobicity nature. Irradiation onto SiO_2 surface has significant effect on the porosity where the increasing of irradiation enhanced the size of the pore. Meanwhile, hydrophobicity nature was enhanced by the presence of poly GMA attached onto SiO_2 surface. Formation of grafting chains was confirmed by both FTIR and TGA where FTIR test manifested new peak at $770cm^{-1}$ assigned to SiO which presence after irradiation and DTGA test shows the shifting of degradation point to higher temperature. To summarize, irradiation effect could improve the modification process of silica's surface by interaction with GMA monomer.

References

F.D. Acunzo, D. Capitani, G. Masci, and C Cherubini. 2013. Polymerization , grafting and adsorption in the presence of inorganic substrates: Thermal polymerization of styrene with untreated and g -irradiated silica gel as a case study. *Polymer*, 54(25):6695–6701.

R. Watanabe, A. Sugahara, H. Hagihara, H. Sato, J. Mizukado, and H. Shinzawa. 2020. Study of matrix-filler interaction of polypropylene/silica composite by combined infrared (IR) spectroscopic imaging and disrelation mapping. *Composites Part A: Applied Science and Manufacturing*, Elsevier Ltd.

Q. Xu, J. Ma, J. Zhou, and J. Wang, Y. and Zhang. 2013. Bio-based core-shell casein-based silica nano-composite latex by double-in situ polymerization: Synthesis, characterization and mechanism. *Chemical Engineering Journal*, 228:281 – 289.

W. Yuan, F. Wang, Z. Chen, C. Gao, P. Liu, Y. Ding, S. Zhang, and M. Yang. 2018. Efficient grafting of polypropylene onto silica nanoparticles and the properties of PP/PP-g-SiO_2 nanocomposites. *Polymer (United Kingdom)*, 151:242–249.

Individual Research Contribution Review, 2023, 1(1): 61–62

Emerging Palm Oil Materials Processed using Radiation Technology as Targeted Drug Delivery Systems for Cancer Therapy

Rida Tajau
Radiation Processing Technology Division, Malaysian Nuclear Agency
43000 Kajang, Selangor
rida@nm.gov.my

Abstract

This study attempts to synthesise poly (APO-*b*-polyol ester) nanoparticles (NPs) utilizing emerging palm oil materials such as APO and polyol ester via low-dose gamma radiation-induced RAFT polymerisation and cross-linking processes on the synthesis of core–shell NPs. These properties were particularly crucial in designing a nano-structured drug delivery system, including peptide functionalisation for the targeted delivery of paclitaxel in breast cancer therapy.

Keywords: cancer therapy, drug delivery system, emerging technology, gamma radiation, palm oil

1 Introduction

Several industries, including surface finishing, packaging, automotive, and biomaterials, have demonstrated significant interest in palm oil derivatives such as polyol and epoxidized palm oil acrylate (EPOLA®), also known as Acrylated Palm Olein (APO) (Tajau et al., 2020a; Tajau et al., 2021a; Tajau et al., 2021b). The molecular weights and functional groups of polyol ester and APO are essential in developing novel products. They have a low molecular weight of less than 5500 Daltons and hydrocarbon chains containing ester compounds, which might play a significant role in the hydrolytic breakdown. This essential characteristic could enhance the biodegradability of APO and polyol ester compared to petrochemical-based or synthetic polymers. Furthermore, their chemical structures, such as carbon double bonds (-C=C-) and hydroxyl groups (-OH), are valuable in fine-tuning and generating novel products with distinct features.

APO has been used in the preliminary development of drug delivery systems by radiation of materials such as polymeric micelles and nanoparticles (Tajau et al., 2021a). Gamma-induced cross-linking has been successfully performed on different APO microemulsions to develop micro/nanoparticles. A recent announcement identified the combination of microemulsion and radiation processing methods as a viable strategy for developing a new drug carrier. The three-dimensional (3D) network structure and nanoparticles from palm oil-based products such as APO and polyol ester were developed using these integrated processes (Tajau et al., 2022).

Gamma irradiation-induced RAFT was employed to develop targeted copolymer nanoparticles utilizing APO and polyol ester as reactants of started polymer matrices. The poly(APO-*b*-polyol ester) nanoparticles are synthesised from palm oil using the RAFT process induced by gamma radiation (Figure 1). These copolymer nanoparticles are potent and used in drug-delivery systems for breast cancer (Figure 2).

The RAFT polymerisation technique is reported to be employed in the production of well-defined intelligent surfaces as well as complex molecular structures for the construction of nanostructures such as micelles, vesicles, and NPs. In RAFT polymerisation, gamma radiation was considered one of the most powerful methods for generating radicals. This technology offers several advantages, including ease of setup, cheap cost, less hazardous, and an environmentally friendly process. As a result, several investigations have employed RAFT polymerisation to synthesize polymeric nanomaterials using gamma radiation (Tajau et al., 2022).

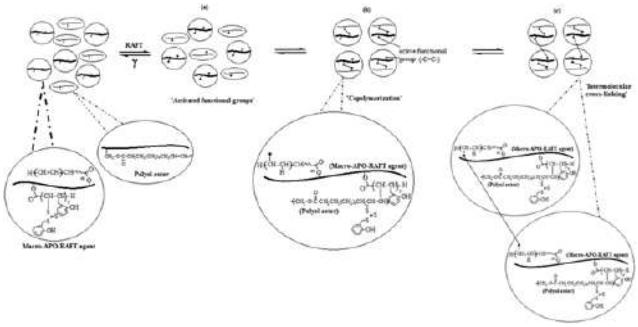

Figure 1: Schematic diagram of the RAFT polymerisation and cross-linking process of poly(APO-*b*-polyol ester) nanoparticles throughout the application for radiation using a gamma source

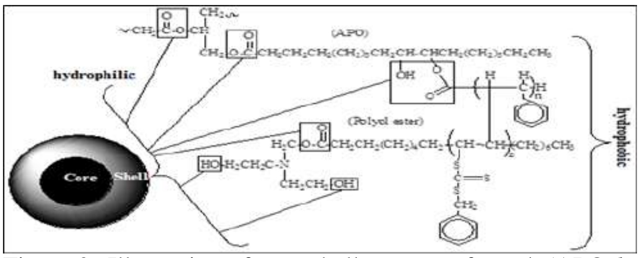

Figure 2: Illustration of core-shell structure for poly(APO-*b*-polyol ester) nanoparticle

2 Methods

2.1 Radiation synthesis of poly (APO-*b*-polyol ester) nanoparticles

The pre-formed polymer or macro-APO-RAFT agent was first prepared by exposing the microemulsion system to 500 Gy of gamma irradiation, followed by the gamma radiation energy absorption of the water molecules under the pulse radiolysis technique with the presence of S,S-dibenzyl trithiocarbonate (DBTTC). The polyol ester (second monomer) was introduced to the macro-APO-RAFT agent system to generate cross-linked-blocked-copolymers with a thiocarbonyl thio end-group, known as poly(APO-*b*-polyol ester) NPs.

2.2 Surface functionalisation of nanoparticles

The carboxylic (-COOH) group was functionalised to the poly(APO-*b*-polyol ester) NPs using the succinylation technique in the presence of succinyl anhydride, 4-Dimethylaminopyridine (DMAP), triethylamine and 1,4-dioxane to form the carboxylate NPs. The NHS-activated NPs were subsequently produced by activating the NHS with the carboxylic-functionalized NPs utilizing the EDC and dichloromethane. The NHS-activated-nanoparticle solution was mixed with a peptide solution. The sample was redissolved in ethyl acetate and precipitated with diethyl ether before being centrifuged and dried under vacuum to form peptide-functionalized nanoparticles.

2.3 Paclitaxel encapsulation of nanoparticle

Peptide-functionalised-nanoparticles were added in 50 nM of paclitaxel in the DMSO solution for entrapment. Diethyl ether was used to precipitate the sample, which was then centrifuged, and the supernatant was collected. The sample was purified by dialysis against deionised water. The excess fluid in the dialysis tubing was vacuum-dried at room temperature to produce solid NPs.

3 Results and Discussion

The production of poly(APO-*b*-polyol ester) nanoparticles utilising gamma radiation-induced RAFT polymerisation technique is promising, well-suited, and environmentally sustainable due to the absence of initiators and catalysts (Figure 3). Apart from having a hydrodynamic particle diameter of less than 200 nm after a very short gamma irradiation exposure (i.e. 700 Gy), the hydrolysed ester bond of these poly(APO-*b*-polyol ester) nanoparticles was discovered to have excellent biodegradable properties: an average MW of 24 kDa, a controlled MW distribution, and a narrow PDI of 1.01 (Tajau et al., 2022).

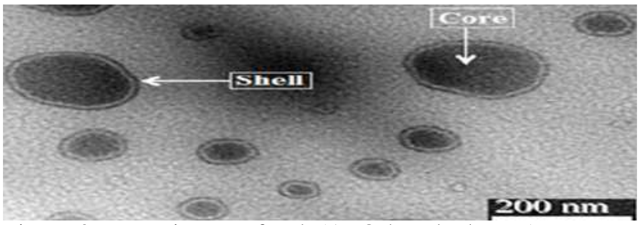

Figure 3: TEM image of Poly(APO-b-polyol ester) nanoparticles

The findings reveal that poly(APO-*b*-polyol ester) nanoparticles can be modified with peptides and loaded with paclitaxel to develop active-targeting NPs (NPfTX) (Figure 4). The localisation of these MCF-7 cell lines into the cytoplasm of the activated-targeted poly(APO-*b*-polyol ester) nanoparticles revealed the efficacy of these NPs at 1000 and 2000 μg/ml concentrations across specific deliveries. In this study, the percentage of cell viability for MCF-7 inhibition could be at 5–20% over 24, 48, and 72 hours of incubation (Figure 5) (Tajau et al., 2020b).

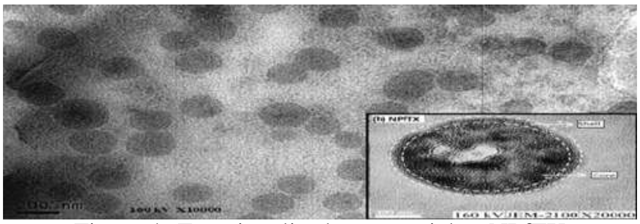
Figure 4: Functionalised nanoparticles, NPfTX

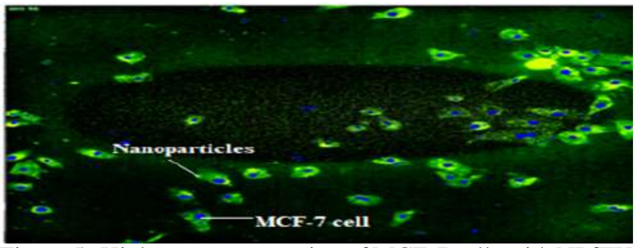

Figure 5: High-content screening of MCF-7 cells with NPfTX nanoparticles after 2 h of incubation.

4 Conclusion

The NPfTX nanoparticles tended to act as the active targeting NPs. They demonstrated potential cancer cell binding and destroying features.

References

R. Tajau, R. Rohani, and M.Z. Salleh. 2020a. Synthesis, characterization, and properties of low molecular weight acrylated palm olein as a promising biopolymer. *Journal of Polymers and the Environment*, 28(10):2734–2748.

R. Tajau, R. Rohani, S.S. Abdul Hamid, Z. Adam, Mohd Janib S.N., and M.Z. Salleh. 2020b. Surface functionalisation of poly-APO-b-polyol ester cross-linked copolymer as a core-shell of nanoparticles for targeted breast cancer therapy. *Sci Rep.*, 10(1):21704.

R. Tajau, K.Z. Mohd Dahlan, M.H. Mahmood, and M.Z. Salleh. 2021a. A composition susceptible to irradiation for use as a compound carrier. *Malaysia Patent No. MY-182996-A*.

R. Tajau, R. Rohani, M.S. Alias, N.H. Mudri, K.A. Abdul Halim, M.H. Harun, N. Mat Isa, R. Che Ismail, S. Muhammad Faisal, M. Talib, M. Rawi Mohamed Zin, N. Izni Yusoff, I. and; Khairul Zaman, and I. Asyila Ilias. 2021b. Emergence of polymeric material utilising sustainable radiation curable palm oil-based products for advanced technology applications. *Polymers*, 13(11):1865.

R. Tajau, R. Rohani, WNR Wan Isahak, and M.Z. Salleh. 2022. Radiation-induced RAFT copolymerization and crosslinking of palm oil-based block copolymers nanoparticles. *e-Jurnal Sains Nuklear Malaysia*, 34:37–49, (eISSN: 2232–0946).

Individual Research Contribution Review, 2023, 1(1): 63–64

Characteristics of Irradiated Chitosan Use in Aquaponics

Sarada Idris
Radiation Processing Technology Division
Malaysian Nuclear Agency
43000 Kajang, Selangor
sarada@nm.gov.my

Abstract

Oligochitosan added to aquaponics systems serves as food supplement for fishes and promote plant growth. Oligochitosan in the form of liquid solution was obtained from irradiated chitosan. Chitosan was irradiated with gamma irradiation at 25 kGy to produced low molecular weights chitosan (oligochitosan). This study was conducted to examine the characteristics of oligochitosan derived from irradiated chitosan. The parameters of shelf life (viscosity, turbidity and pH), protein digestion, visual inspection, morphology, antimicrobial study and toxicity were evaluated. The low molecular weight chitosan (Mw = 5 kDa), was further used as dietary supplement for tilapia. Nitrogen, one of the most important macro-nutrients for plant growth and crop productivity was supplied by fish feces and food waste containing oligochitosan in fish tank, as well as phosphorus and potassium. Results obtained in this study showed the potential use of oligochitosan as food supplement for tilapia and plant growth promoter in aquaponics system.

Keywords: Oligochitosan, gamma irradiation, growth promoter

1 Introduction

The inclusion of irradiated chitosan in aquaponics systems functions as a nutritional supplement for fish and facilitates the enhancement of plant development. Oligochitosan in the form of aqueous solution obtained from irradiation of chitosan at 25 kGy was characterized using suitable methods and equipment. The parameters such as molecular weight, chemical structural, nutrient analysis, protein digestion test, microbial and toxicity test were evaluated in this study.

2 Methods

The chitosan powder was mixed with distilled water and irradiated under gamma irradiation (SINAGAMA) at 0 to 100 kGy to produced low molecular weight chitosan. The molecular weight of chitosan before and after irradiated by gamma ray was measured by Size Exclusion Chromatoghraphy (SEC) equipped with MALLS (multi angle laser light scattering) detector brand Wyatt. The chemical bonding of chitosan was analysed by Fourier-Transformed Infrared Spectroscopy (Bruker -Tensor II).

3 Results and Discussion

Irradiation of chitosan at 25 kGy reduced its molecular weight from 37 kDa to 5 kDa (Figure 1).The FTIR spectrum (Figure 2) showed slight decrease in the band between 865 and 1124 cm^{-1} is probably due to decay of C-O-C groups indicated chitosan degradation caused by splitting of 1-4 glycosidic bonds. Figure 2 indicated that only the change in relative intensity could be seen due to the overlapping of the bands corresponding to the tensions of the carboxyl groups with other bands. The intensity of the absorption peak at 1600 cm^{-1} assigned to the N–H bend vibration of $–NH_2$ was slightly increases after chitosan was irradiated. This may be due to the decreasing of inter or intra molecular hydrogen bonding between the –OH and $–NH_2$ groups (El-Rahim et al., 2015). During exposure to the γ-irradiation source, random polymer chains scission occurs (Faisant et al., 2002), and the average macromolecular weight decreases (Choi et al., 2002). This leads to a decrease in the extent of polymer chain entanglement and to an increased mobility of the macromolecules.

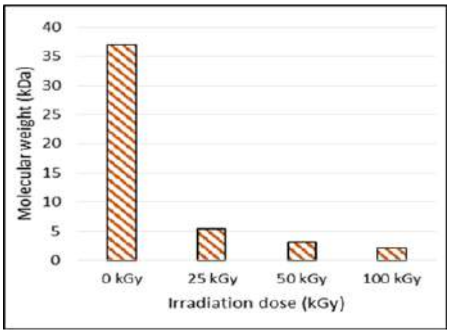

Figure 1: Molecular weight of irradiated and non irradiated chitosan

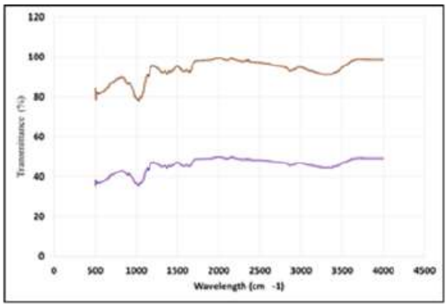

Figure 2: FTIR of chitosan before and after irradiated (25 kGy) by gamma ray

Irradiated chitosan has antimicrobial activity against *e.Coli* bacteria (Figure 3), which is indicated as a good supplement to protect fish against this bacteria. Brine shrimp toxicity study (Figure 4) proposed that oligochitosan is safe to use at 3.14 percent of its original concentration. It is important to mention that protein digestion test (Figure 5) of fish feed pallet revealed the performance of oligochitosan is as good as protease enzyme in digesting protein molecule to amino acid, hence promoting growth rate and improving feed conversion ratio of tilapia. Dietary of oligochitosan present at low concentrations increases nitrogen consumption and amino acid digestibility. Nitrogen, phosphorus and potassium which are important macro-nutrients for plant growth and crop productivity, supply by irradiated chitosan as well as fish feces and food waste (Table 1).

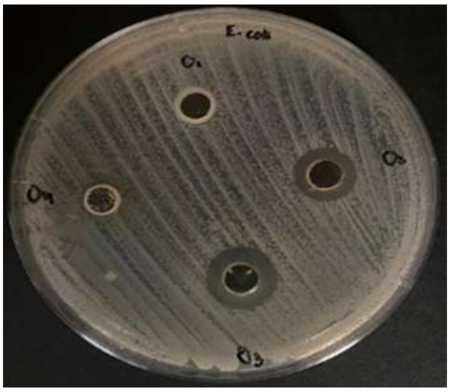

Figure 3: Antimicrobial activity of irradiated chitosan

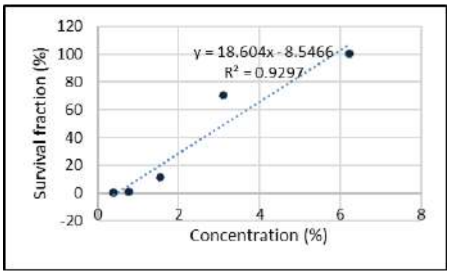

Figure 4: Survival fraction vs oligochitosan concentration (Brine shrimp toxicity study IC_{50})

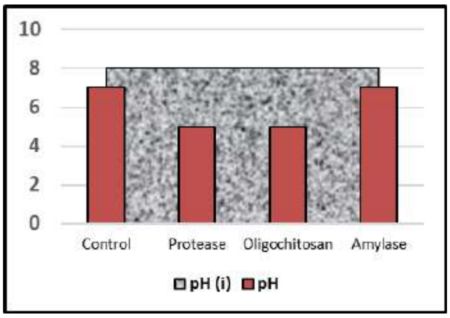

Figure 5: Digestibility of fish feed pallet by oligochitosan, protease and amylase enzyme

Table 1: Nutrients in oligochitosan, hydroponic and aquaponic systems

	N (ppm)	P (ppm)	K (ppm)	EC (mS/cm)
Oligochitosan	408	598	1295	
Hydroponic	142	260	479	1.8
Aquaponics	224	329	502	2.23

4 Conclusions

Irradiation of chitosan causes the chain to scission into smaller fragments and improving its molecular mobility due to its shorter chain and size, suitable for use in production of oligochitosan for aquaponics. Irradiated chitosan, or oligochitosan, has valuable characteristic such as great nutritional resources for plants and improved protein digestion and absorbtion in fish gut. It is concluded that irradiated chitosan is a biocompatible material having potential use as food supplement for tilapia and plant growth promoter in aquaponics systems.

References

W. S. Choi, K. J. Ahn, D. W. Lee, M. W. Byun, and H. J. Park. 2002. Preparation of chitosan oligomers by irradiation. *Polym. Deg. Stab.*, 78:533– 538.

Hassan A. Abd El-Rahim, Dalia A. Zahran, Naeem M. El-Sawy, El-Sayed A. Hegazy, and Ahmed M. Elbarbary. 2015. Gamma irradiated chitosan and its derivatives as antioxidants for minced chicken. *Biotechnology, and Biochemistry*, 79(6):997–1004.

N. Faisant, J. Siepmann, P. Oury, V. Laffineur, E. Bruna, J. Haffner, and J. P. Benoit. 2002. The effect of gamma-irradiation on drug release from bioerodible microparticles: A quantitative treatment. *Int. J. Pharm*, 242:281– 284.

Individual Research Contribution Review, 2023, 1(1): 65–66

Oligochitosan for Mutual Paddy and Tilapia Growth Performance in Aquaponics System

Sarada Idris
Radiation Processing Technology Division
Malaysian Nuclear Agency
43000 Kajang, Selangor
sarada@nm.gov.my

Abstract

This study was conducted to evaluate the influence of oligochitosan added to the fish tank to benefit both tilapia and paddy in aquaponics system. Chitosan was irradiated at 25 kGy to produced low molecular weigt chitosan (oligochitosan). The characteristic of chitosan such as molecular weight, solubility, viscosity and color were investigated. The low molecular weight chitosan (Mw = 5 kDa), obtained from the radiation degradation by gamma ray was further used as dietary supplement for tilapia. Nitrogen, one of the most important macro-nutrients for plant growth and crop productivity was supplied by fish feces and food waste containing oligochitosan in fish tank. Therefore, in this study we aimed to evaluate the effects of oligochitosan on growth performance of tilapia and paddy.

Keywords: Oligochitosan, gamma irradiation, growth promoter

1 Introduction

Oligochitosan or low molecular weight chitosan are the hydrolytic products of chitosan, which possess, high water solubility and reduced viscosity, thus making these polymers suitable for various applications (Y-Z et al., 2010). Oligochitosan obtained from gamma irradiated chitosan is a potential product to enhanced growth of plant such as chili, mulberry, banana tissue culture and pineapple. Recent study (Idris et al., 2020) showed that, it also has potential for growth performance and feed digestibility of tilapia. Addition of oligochitosan in dietary supplement of tilapia show the best result on final weight, growth rate, feed conversion ratio, protein efficiency ratio and survival rate. The performance of oligochitosan as plant growth promoter and in aquaculture can be explore in combination system of aquaculture and hydroponic (aquaponics). Aquaponics will produce fish and plants in the one system with a large reduction in water use. Microorganisms converting fish waste and feces into nitrogen for plant growth the while plant root purify water for fish.

2 Methods

The chitosan powder was mixed with distilled water and irradiated under gamma irradiation (SINAGAMA) at 25 kGy to produced low molecular weight chitosan.

Paddy seedlings (MR 219) were first prepared in nursery and then transplanting in the combination of film nutrient and media bed aquaponic system after about 35 days. In aquaculture tank, tilapia was fed with food pellet with addition of irradiated chitosan (oligochitosan). The fish was fed at the rate of 5% of their body weight thrice per day. The paddy taking up the nutrients from fish tank containing fish excrete, food waste and oligo chitosan which was added into the tank earlier.

3 Results and Discussion

3.1 Growth performance of tilapia

The addition of irradiated chitosan (oligo chitosan) into the fish tank has influenced the weight gain performance of tilapia (Figure 1). In this study, oligo chitosan has improved the growth performance of tilapia compared to the fish in control tank. Oligo chitosan cannot be decomposed by endogenous digestive enzymes due to their intermolecular binding positions and binding types, but it can be hydrolyzed by glycosidase secreted by beneficial bacteria such as Lactobacillus and Bifidobacterium. These bacteria generates monosaccharides, volatile fatty acids, etc., and then be used by the body or microorganisms to indirectly achieve the growth-promoting effect.

Further more, addition of oligo chitosan also help to improve the distribution of tilapia intestinal microbes. It is considered to be an important intestinal function regulator, which can improve the microflora in the digestive tract of animals. A large number of scientific studies have confirmed that oligo chitosan can effectively reduce the number of harmful bacteria such as Escherichia coli in fish intestines and increase the number of bifidobacteria and lactobacilli (Oligo, 2019).

The effect of chitosan on growth performance of fish has been reported by Niu et al. (2011), which concluded that chitosan is an active growth promoter and can be considered as an essential element for the growth of aquatic animals. Improvement in the morphological structure of small intestine can be the main effect of chitosan, which may improve nutrients absorption and growth performance as revealed by Zaki et al. (2015).

3.2 Performance of paddy

The paddy seedling grow exponentially from 13 cm height (Figure 2) until the rice were ready for harvested at about 140 days. The pH was maintained at 6.8 – 7.4, ammonia and nitrit at 2.0 ppm. Nitrate, one of the most important element was

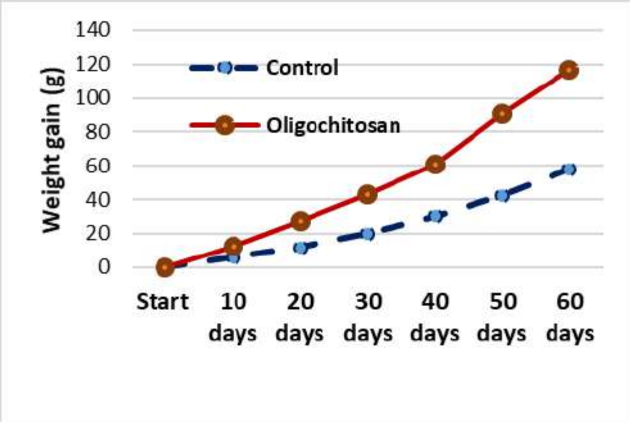

Figure 1: Weight gain of the tilapia fed with oligochitosan

increased from 10 ppm to 80 ppm in two weeks and further increased to 160 ppm. It is initially indicated that the ammonia and nitrite have been decomposed by nitrifying bacteria to nitrate. The nitrifying bacteria (Pilinszky et al., 2015) assisted with oligochitosan detoxify ammonium (excreted by the fish) by converting it to the much less toxic nitrate in which the demand of nitrogen was fulfilled. Nitrogen is largely responsible for the growth of leaves on the plant. Phosphorus is largely responsible for root growth, and flower and fruit development. Phosphorus supply naturally found in protein-rich foods such as meats, poultry, fish, nuts, beans and dairy products which are ingredients composed in tilapia pallet (32% protein). On the other hand, Potassium (K) as a nutrient that helps the overall functions of the plant perform correctly was also supplied by fish pallet which is abundant in whole foods including fish ingredients.

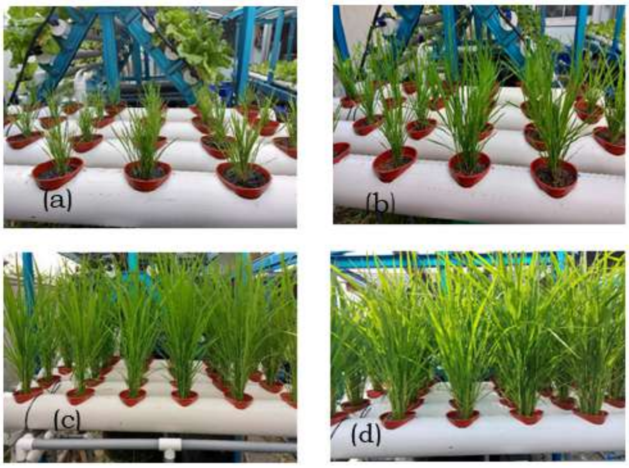

Figure 2: Growth performance of paddy (MR 219) (a) 1, (b) 5 (c) 19 and (d) 24 days in aquaponics system

After 140 days, the rice grains growed in aquaponics system were harvested (Figure 3). There are many factors could be taking into account on producing the quality of the rice. For normal paddy plantation on fields, level of water is to be maintained according to the growth and the fields are drained dry before the crop is harvested. Although this study proven that paddy plantation in aquaponic system with oligochitosan in tilapia tank served as fertilizer has successfully gave good result in term of paddy yields, the water management and oligokitosan inputs must be properly timed to obtain optimum stands, tillering, and panicle and grain formation.

Figure 3: Paddy yield in aquaponics system

4 Conclusions

Tilapia performed well with oligochitosan in aquaponics system. In fish tank, nitrifying bacteria converts ammonia to nitrite, and nitrite to nitrate further supply N macronutrient for paddy. Future research will determine the production capacity of paddy and variety of vegetables and evaluate less expensive construction materials and methods for different plants crops.

References

S. Idris, M. Mahmud, K.A. Bakar, N. Talip, M. Talib, Z. Abdullah, Sani N.A., N.A. Fabillah, and M.N. Shukri. 2020. Study of gamma irradiated chitosan as a dietary supplement for tilapia. *International Journal of Agriculture, Forestry and Plantation*, 10 (Sept) ISSN 2462-1757.

Niu J, Liu YJ, Lin HZ, Mai KS, Yang HJ, and Liang GY. 2011. Effect of dietary chitosan on growth and stress tolerance of postlarval (Litopenaeus vannamei). *Aquaculture Nutrition*, 17:406–412.

Zaki MA, Salem M El-S, Gaber MM, and Nour AM. 2015. Effect of chitosan supplemented diet on survival, growth, feed utilization, body composition and histology of sea bass (Dicentrarchus labrax). *World Journal of Engineering and Technology*, 3:38 – 47.

Marine Oligo. 2019. The function of COS in agricultural applications. Rep. Series 2019-09-04, Qindao, China.

K. Pilinszky, A. Bittsanszky, G. Gyulai, and T. Komives. 2015. Plant protection in aquaponic systems - Comment on “A novel report of phytopathogenic fungi Gilbertella persicaria infection on Penaeus monodon. *Aquaculture*, 435:275–276.

Du Y-Z, Ying X-Y, Wang L, Zhai Y, Yuan H, Yu R-S, and et al. 2010. Sustained release of ATP encapsulated in chitosan oligosaccharide nanoparticles. *International Journal of Pharmaceutics*, 392(1):164.

Individual Research Contribution Review, 2023, 1(1): 67–68

Assessing the Fate, and Environmental Impact of Plastics in Soil and Crop Ecosystems Using Isotopic Techniques

Sarala Selambakkannu
Radiation Processing Technology Division, Malaysian Nuclear Agency
43000 Kajang, Selangor
sarala@nm.gov.my

Abstract

The consumption of plastics (P) has increased from 1.7 million metric tons in 1950 to 359 million metric tons in 2018. Despite the remarkable benefits of plastics to society, there are increasing concerns associated with the vast amount of plastic entering our environment, where it is degraded into microplastics (MP), particles less than 5 mm in diameter. Most plastics produced each year end up in the environment. The soil acts as a long-term sink for plastic debris before some find its way to the aquatic ecosystem. According to a recent report by the United Nations Food and Agriculture Organization, the earth's soil may be more saturated with plastic pollution than the oceans. An estimated 80% of plastics found in marine environments are first disposed of on land. Therefore, it is critical to ensure that we understand the turnover, fate, and the latest methodologies developed for sampling and analysis of P and MP, as well as their environmental impact on soil and crop ecosystems.

1 Introduction

Soils are a nonrenewable resource that contributes to the production of agricultural crops, grazing lands, diversity of wildlife habitats, and ecosystem services. Despise this, the soil is being degraded and lost at an unprecedented rate due to intensive land use changes, agricultural practices, climate change, and variability. Plastics have become one of the most significant urban wastes and are one of the most common polymers in everyday life. On the top ten mishandled plastic waste list, Malaysia ranked eighth. Under varying environmental conditions, plastic waste can disintegrate and fragment into small particles with a size of less than 5 millimeters which are considered microplastics. A global threat to the agriculture sector is plastic pollution, which easily accumulates in soil and is difficult to reverse. Soil properties and ecological functions are potentially affected by microplastics accumulated in agricultural soils. There are higher possibilities for microplastics to alter soil structure or lead to direct toxicity, which impairs nutrient availability in the soil. Furthermore, contaminants are likely to be transported or absorbed into the soil, which may negatively affect the microbial community and root symbionts. Furthermore, exposure to microplastics may alter the collembolan gut microbiota, altering isotopic and elemental incorporation, growth, and reproduction. Therefore, plant growth and performance are adversely affected by any disturbance to the gut microbiota, which plays a crucial role in nutrient absorption. The identification and distribution of microplastics in the soil allow assessment of the hazards and risks microplastics pose to the ecosystem. Nevertheless, limited studies have been conducted on microplastics effects on soil ecosystems and plant performance. The purpose of this study is to examine the impacts of microplastics on plants and their fate in soils, as well as the interactions between microplastics and soil quality. A reference point will be provided by the findings of this study on the origin of microplastics, the mechanism of microplastics degradation, and the potential risks associated with microplastics in soil.

2 Methods

The research aims to assess the fate, dynamics and impact of microplastics in agricultural soils and ecosystem services using compound-specific stable isotopes (CSSI) and stable isotope Raman micro-spectroscopy (SIRM). The project also aims to assess the rate and identify the environmental drivers of microplastics degradation.

2.1 Assessment of microplastics pollution in soil

In order to investigate the effects of microplastics weathering in natural environments, samples of microplastics will be collected from lowland agriculture soil in Sabak Bernam, Selangor, and highland agriculture soil in Cameron Highland, Pahang, systematically. After extraction and separation of microplastic from the soil, the microplastic will be subjected to analysis. Physical characterization including visual and microscopy analysis will be done to determine the particle size, color, shape, and morphology of the samples. Chemical characterization using Fourier transform infrared spectroscopy and Raman spectroscopy will be conducted for the chemical composition identification of microplastics. Identifying the types of microplastics is essential for determining the treatment methods and traceability analysis of microplastics.

2.2 Degradation study of non-biodegradable and biodegradable plastic in soil by laboratory incubation via stable carbon isotope labeling assessment

Following the identification of the major types of microplastics contributors, measurements of both non-biodegradable and biodegradable plastic mineralization to $13CO_2$ will be conducted in soil incubation and the demineralize residual 13C remaining in the soil will be determined by using the stable carbon isotope (13C) labeled method to study the degradation of both plastics, respectively. In order to provide a remediation plan for contaminated soils, a thorough understanding of the degradation pathway of the plastic is crucial.

2.3 Assessment of plant performance responses in the soil contaminated with microplastics

The experiments will be performed in laboratory environments. Oryza Sativa L. (commonly known as rice plant) seeds will be sterilized with 1% sodium hypochlorite solution for 15 min then rinsed with deionized water before the germination process. The rice seeds will be kept in the dark and incubated in a controlled atmosphere at 30°C for germination. After 15 days, the seedlings of uniform height will be transplanted into planting boxes containing soils with different treatments. 2 types of plastic (non-biodegradable plastic and biodegradable plastic) sieved at < 5 mm will be mixed with the dry soil at application rates of 0, 0.01, 0.03, and 0.05 kg^{-1}. Thus, a total of seven treatments are prepared. Sequential variations in plant growth will be monitored and microplastics, plants, and soil combinations will be analyzed at the end of the 125 days experiment.

3 Data/Results

3.1 Biodegradability Test of dual-layer polyhydroxyalkanoate (PHA)/polycaprolactone (PCL) mulch film

As for preliminary study, the biodegradability of PHA/PCL film with different ratios, PHA and PCL films were investigated via a soil burial test. The result obtained on the soil burial degradation test is displayed in Figure 1. The appearance of the PHA/PCL film with the mixed ratio of 90/10, 70/30 and 50/50 remains almost intact. The mulch film with 100% of PHA and PCL had shown some visual defects in terms of appearance. Align with this observation, the mulch film with 100% of PHA and PCL exhibited the highest degradation degree, approximately 48.43%. According to Standard for Biodegradable Mulch Films (EN17033), conversion of more than 90% of the mulch carbon to CO_2 at ambient soil conditions within time frame of two years is considered as biodegradable. The dual layered PHA/PCL had achieved degradation of almost around 50% in just five weeks. This signifies the efficient biodegradability of the prepared mulch film. The rest of the mulch film with 100% PHA with the mixed ratio of PHA/PCL had shown quite a low degradation rate. It can be concluded that the decomposition of virgin PHA and PCL is relatively faster than the mixture of both PHA and PCL.

3.2 Thermal properties of dual-layer polyhydroxyalkanoate (PHA)/polycaprolactone (PCL) mulch film

The thermogravimetric curves for single-layered PHA, single-layered PCL, and double-layered PHA/PCL (100%) are shown in Figure 2. Single-layered PHA film exhibits only single-step thermal degradation with good thermal stability. PHA represented a massive weight loss of approximately, 95% which

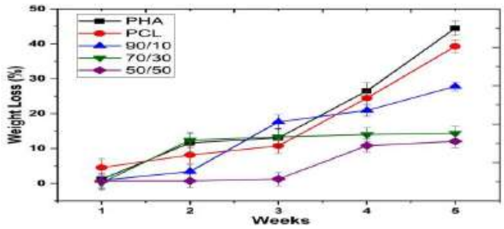

Figure 1: Weight loss values (%) vs. degradation time for polyhydroxyalkanoate (PHA)/polycaprolactone (PCL) double layered mulch film

took place at the temperature range from 300°C to 390°C. The heavyweight loss in PHA corresponds to the removal of hydrocarbons from the polymeric chain. The single-layered PCL had shown a two-step thermal degradation with good thermal stability, too. The first stage of degradation in PCL occurs at a temperature between 250°C to 330°C with a weight loss of almost 30%. The second stage of degradation was detected from 330°C to 440°C with a weight loss of 69%. The weight loss is ascribed to the polymeric material carbonization. On the other hand, the initial stage of degradation corresponds to PCL, from 250°C to 330°C with a weight loss of almost 20%. The second stage of degradation was observed in dual-layered film from 330°C to 360°C with a weight loss of 25%. The third stage of degradation ascribes PHA, with a weight loss of 64% at the temperature range from 360°C to 460°C.

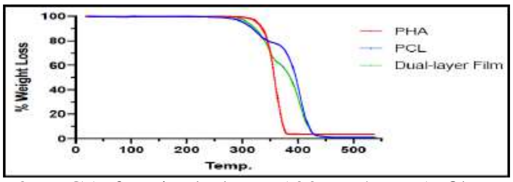

Figure 2: TGA for single-layer 100 wt% PHA film, single-layer 100 wt% PCL film and dual-layered film consisting PHA/PLA (100%)

4 Conclusions

FAO and UNEP consider soil pollution with microplastics an emerging environmental issue with serious consequences for soil carbon turnover and greenhouse gas fluxes. Isotopic methods, proposed in the project, can determine the final products of microplastics decomposition in soil and the environmental conditions optimal for reducing microplastics debris in soil. This project will also provide tools and recommendations that will benefit and help to stiplulate microplastics policies and management strategies and contribute to FAO's action plan on plastics in agriculture.

References

R. Adhikari, K. L. Bristow, P. S. Casey, J. W. Freischmidt, G. andHornbuckle, and B. Adhikari. 2016. Preformed and sprayable polymeric mulch film to improve agricultural water use efficiency. *Agricultural Water Management*, 169:1–13.

Individual Research Contribution Review, 2023, 1(1): 69–70

Exfoliation of Hexagonal Boron Nitride Nanosheet (BNNS) for Water Purification: Method and Performance

Sarala Selambakkannu
Radiation Processing Technology Division, Malaysian Nuclear Agency
43000 Kajang, Selangor
sarala@nm.gov.my

Abstract

The purpose of this study is to investigate the potential removal of arsenic (As) by polyvinylidene fluoride (PVDF) deposited with radiation exfoliated bulk hexagonal boron nitride (h-BN). The main objective of this study is to prepare, characterize and test the h-BN deposited onto PVDF membrane for the removal of arsenic from water by using electron beam irradiation technique for exfoliation of h-BN and subsequent functionalization with phosphoric acid 2-hydroxyethyl methacrylate ester (PA). Thereafter, grafting of PA-functionalized exfoliated BN (PA-BN) on PEG was performed. Subsequently, the PEG-g-PA-BN melt-blended with PVDF using internal mixer and casted into thin membrane using phase inversion membrane. The performance of prepared membranes was evaluated in terms of arsenic removal via ultrafiltration.

1 Introduction

This study aim to incorporate modified hexagonal boron nitride nanosheets (BNNS) boron nitride with specific functional moieties into polymeric membrane matrix for the removal of arsenic via melt blending process. BNNPs have demonstrated unique interactions with a variety of elements in recent studies, making them one of the most promising and popular inorganic nanomaterials. The performance of PEG-g-BN cast with PVDF membrane (PVDF-PA/BN) in the removal of arsenic from an aqueous solution was investigated thoroughly. The water permeability, anti-fouling resistance, and solute rejection efficiency of PVDF-PA/BN with different PEG-g-BN compositions were also evaluated.

2 Methods

The research objectives of this study was achieved by executing six main steps, namely, electron beam irradiation, functionalization, grafting, melt blending and phase inversion casting and arsenic removal performance.

2.1 Pre-treatment and Irradiation

Pre-treatment of h-BN nanosheets by liquid-phase sonication intercalation in the present of sodium hydroxide (NaOH) at different concentration (10% - 30%) in different solvent (water, methanol, ethanol, propanol) at different volume and weight percentage (vol/wt%) of at probe sonication amplitude, 80% and at room temperature. Electron beam irradiation treatment onto pre-treated h-BN nanosheets at different irradiation dose (20-100 kGy) and different irradiation energy (1-3 MeV) for exfoliation of the nanosheet.

2.2 Functionalization

Performed chemical functionalization onto exfoliated h-BN nanosheets with phosphoric acid 2-hydroxyethyl methacrylate ester (PA) in methanol solution in order to associate ionic character under different reaction parameter such as concentration of PA (7% - 10%), reaction temperature (60°C - 80°C), reaction time (60min -300 min) and mass (0.1g - 0.5g) of exfoliated h-BN used.

2.3 Grafting

Grafting of polyethylene glycol (PEG) onto functionalized h-BN nanosheets (PEG-g-PA/BN) via conventional chemical grafting process in the present of benzoyl peroxide as an radical initiator.

2.4 Melt-blending and membrane casting

Blending of polyvinylidene fluoride (PVDF) with PEG-g-PA/BN (different mass percentage) by using internal mixer and casting of thin membrane with thickness of 500 μm via phase inversion technique.

2.5 Metal removal

Study the performance of fabricated PVDF deposited with different mass percentage of PEG-g-PA/BN on removal of arsenic (III) tested in dead end filtration system at different arsenic concentration. The removal of arsenic was tested using Inductively Coupled Plasma Mass Spectrometry (ICP-MS).

3 Data/Results

3.1 Exfoliation

Figure 1 illustrates a schematic diagram of electron beam irradiation-assisted BNNS exfoliation. Staged exfoliation is expected to take place in two steps. Primarily, the dispersion of bulk h-BN in sodium hydroxide solution prepared with water is followed by the insertion of small ions of Na^+ and OH^- into the interlayer spacing of BN sheets via a mild ultrasonic process. Secondly, the intercalation of OH^- between the layers leads to rapid hydroxylation which is facilitated by electron beam irradiation. Rapid hydroxylation leads to the formation of B-OH, which expands the interlayer spacing of h-BN resulting in the peeling off of BNNS from the bulk h-BN.

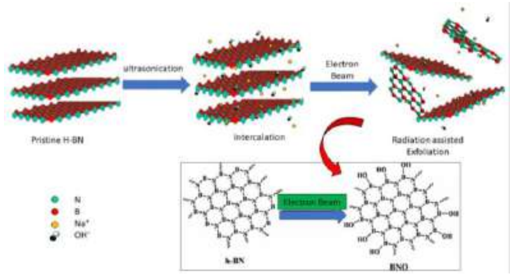

Figure 1: Mechanism for irradiation-assisted exfoliation of BNNS

3.2 Functionalization of exfoliated h-BN

The functionalization of PA with exfoliated BN nanosheets is expected to be straightforward via protonation of $^-$OH bonds which leaves oxygen as active radicals through a thermo-kinetic process in the presence of methanol in acidic medium by esterification process. Additionally, PA monomers will act as a precursor to radicals that react with oxygen. The functionalization of exfoliated BN nanosheets with PA results in the formation of new functional groups suitable for ion exchange or chelate formation. The schematic diagram for functionalization of exfoliated BN with PA is shown in Figure 2.

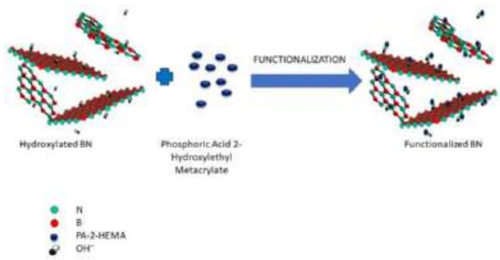

Figure 2: Mechanism for functionalization of exfoliated BN nanosheets with PA

3.3 Grafting of PEG onto PA/BN

The chemical grafting of PEG on PA/BN was carried out with the present initiator, dibenzoyl peroxide to enhance the hydrophilicity which improves the anti-fouling performance of the PVDF composite membrane. The long hydrophilic chains of PEG tend to form aqueous layers on PA/BN surfaces due to their non-ionic water-soluble nature. The functionalized BN (PA/BN) contains phosphoric acid monomer and diethyl methacrylate that facilitates PEG grafting by extraction of the hydroxyl group in phosphoric acid via polymerase chain reaction. The schematic course for grafting polyethylene glycol with phosphoric acid 2-hydroxyethyl methacrylate (PA) is shown in Figure 3.

3.4 Preparation of PVDF/BN-based composite membranes

PVDF resin was loaded into the mixing chamber of an internal mixer set at 130°C, and after 8 minutes of melting, PEG-g-PA/BN was added. Figure 4 illustrates the torque versus

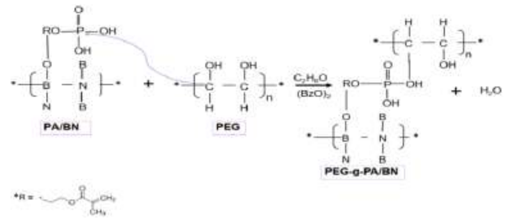

Figure 3: Schematic diagram for grafting of PEG onto PA/BN

time graph from the combination of PVDF resin and PEG-g-PA/BN. Upon the addition of PEG-g-PA/BN a slight decrease in torque was observed attributed to the initial low viscosity and high density. PVDF is completely melted in 8 minutes, and the addition of PEG-g-PA/BN requires relatively lower energy to fuse both materials, explaining the reduction in torque.

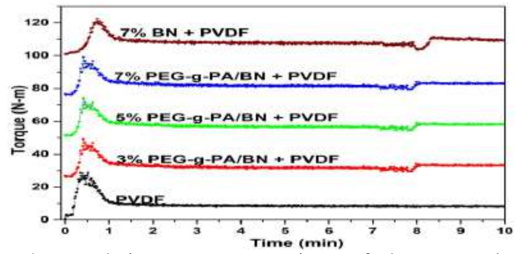

Figure 4: Real-time torque vs time of the PVDF/PEG-g-PA/BN blends

3.5 Removal of arsenic

The arsenic removal efficiency of pristine PVDF, 97:3 BN, 95:5 BN, 93:7 BN, and 93:7 BNNS with arsenic solution at concentrations 3, 5, and 10 ppm is shown in Figure 3. The permeance of the membranes reduces as the concentration of arsenic solution increases and the similar trend observed for pristine PVDF, 97:3 BN, 95:5 BN, 93:7 BN, and 93:7 BNNS, too.

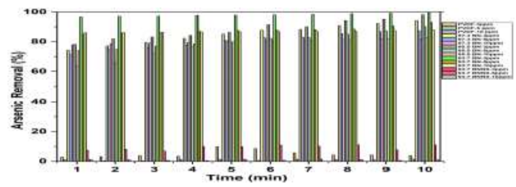

Figure 5: Arsenic removal efficiency of arsenic by PVDF/PEG-g-PA/BN

4 Conclusions

It was concluded that the arsenic ion is capable of forming complexation with PA/BN in the PVDF matrix which results in the removal of arsenic. In the future, the metal ion removal mechanism could be further evaluated with kinetics studies.

References

N. Abdullah, N. Yusof, W.J. Lau, J. Jaafar, and A.F. Ismail. 2019. Recent trends of heavy metal removal from water/wastewater by membrane technologies. *Journal of Industrial and Engineering Chemistry*, 76:17–38.

Individual Research Contribution Review, 2023, 1(1): 71–72

Physicochemical Properties of PVDF Membranes in the Presence of cellulose nanocrystals

Siti Fatahiyah Mohamad
Radiation Processing Technology Division
Malaysian Nuclear Agency
43000 Kajang, Selangor
fatahiyah@nm.gov.my

Abstract

In this work, 1- 4 wt% of CNC from its original suspension was pour in to the mixture of 18-wt of PVDF in NMP (as solvent). The dope solution were characterized using a Rheometer to obtain the change in its viscosity. After casting via the inversed phase, the membrane were characterization using AFM, SEM and water contact angle to determine the effect of CNCs loading on its surface properties. The relationship of pore size and its water flux was also performed discussed.

1 Introduction

A nanopore membrane, also known as a nanoscale pore membrane. These membranes are often fabricated from materials like silicon nitride, graphene, or other nanoscale materials. However, the choice of materials for nanopore membranes is critical, and finding materials that are durable, stable, and suitable for various applications was an ongoing challenge. This includes identifying new materials or optimizing existing ones.

2 Preparation of membrane

PVDF-CNCs films prepared by phase-inversion method. The dope solution was prepared according to the Table 1.

Table 1: Weight (%) of materials used

Films	NMP (wt-%)	PVDF (wt-%)	CNCs (wt-%)*
Neat PVDF	82	18	0
PVDF-CNCs-1wt-%	81	18	1
PVDF-CNCs22wt-%	80	18	2
PVDF-CNCs-3wt-%	79	18	3
PVDF-CNCs-4wt-%	78	18	4

*from 1wt% CNCs Suspension

The viscosity of dope solutions with different CNCs loading was used for the rheological measurements. The surface morphology was studied by JKF AFM instrument. The Wettability of the membranes was assessed from contact-angle measurement of pure water using the static sessile drop method. At least five stabilized contact angles from different directions of each sample were obtained to calculate the average value and standard deviation. The pore size distribution for each membrane was also obtained by intrusion mercury porosimetry. The measurement of the intrusion volume of a non-wetting liquid to calculate data related to the pore structure of the sample.

3 Result and Discussion

3.1 Effect of CNC Concentration on Shear Viscosity

The viscosity increment is due to the self-assembly of CNCs induced by thermal during the reaction, leading to gelation and higher viscosity as shown in Figure 1. Higher viscosity is important for suppressing microvoids (Lessan et al., 2019). The study compared the viscosity of neat PVDF dope solution as a control and demonstrated a trend of increasing viscosity with CNC loading from 1-3 wt%, followed by a decrease at 4 wt%. The arrangement of individual polymer chains in CNC-containing solutions was more compact, forming a denser and larger polymer-rich phase (Yang et al., 2007).

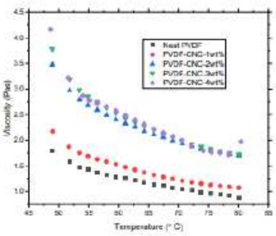

Figure 1: Viscosity of PVDF/CNC at range temperature 50 – 80°C .

3.2 Morphology properties by FESEM

The study involved observing the morphology changes in dope solutions with varying amounts (1-4 wt%) of cellulose nanocrystals (CNCs) as shown in Figure 2.

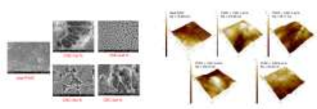

Figure 2: Morphology and topography of Neat PVDF and PVDF with different CNCs loading with its Average surface area (Ra)

The neat PVDF exhibited a smooth surface, while PVDF with CNCs displayed spherical surfaces. The presence of CNCs induced self-assembly during dope preparation, forming spherical structures due to electrostatic interactions between cellulose and PVDF. Increasing CNCs led to higher viscoelastic properties, impacting the membrane fabrication process (NIPS). This caused slower nonsolvent diffusion and a delayed front migration, resulting in a longer time for the polymer lean phase to grow, leading to more porous surfaces and longer cavities in the membrane sub-layer.

3.3 Effect of Nanoparticles concentration on surface roughness (R_a)

As shown in Figure 2, the neat PVDF demonstrated the smoothest with average R_a of 73.6 nm which similar to previous studies (Mahdavi et al., 2022). Then, the R_a is decreased as the CNCs loading increased. The decrease can be explained by the rapid phase separation in the membrane surface during the membrane preparation process, in which the nano-particles acted as nucleation agents and elevated the polymer crystallization rate. (Fosi-Kofal et al., 2016; Hou et al., 2014)

3.4 Water Contact angles and surface

Figure 3 (left) shows the water contact angle of neat PVDF membrane, PVDF+CNC with different loading (1 wt% to 4 wt%). The neat PVDF demonstrated contact angle at 77.25 possesses the highest contact angle. The contact angle is reduced once 1wt% of CNCs loading. However, the increment of CNC loading shows an increment contact angle up to 80.1 for membrane with 4 wt% CNC loading.

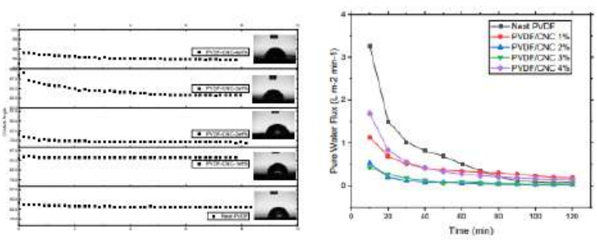

Figure 3: (left) Effect of CNCs loading on water contact angle. (right) Pure water flux of PVDF/CNC membrane

This result confirms that the wettability of the membrane surface is improved, which is attributed to the introduction of hydroxyl groups of CNC that can interact with water molecules (Lessan et al., 2019). The reasons may be that the hydrophilic CNC could spontaneously migrate to the membrane surface during the phase inversion process, and in this case, their oxygen-bearing functional groups and the sulfate ester groups introduced during H_2SO_4 hydrolysis would interact with non-solvent, leading to the enhanced water adsorption and membrane hydrophilicity (Lv et al., 2018a).

3.5 Water Flux

The results of pure water flux for PVDF/CNCs at 1-4 wt% are presented in Figure 3 (right). It is observed that when blending of CNCs within PVDF nanofiber, membrane exhibited higher pure water flux than pristine PVDF nanofiber membrane. This increment can be related with network structure permits more pathways for water transport through the membrane which water molecules simplify their transmission from side to side the membrane (Mousa et al., 2022; Lv et al., 2018b).

3.6 Porosity by Mercury porosity

The correlation between the pore diameter and the Distribition of differential Intrusion (mL g^{-1}) as the effect of CNCs loading did not shown any trend. However, the pore sized range between 175 to 341 nm as given in Figure 4.

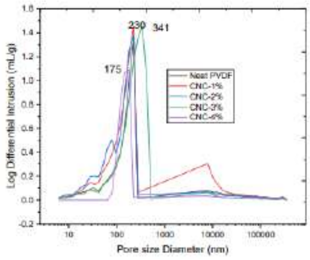

Figure 4: Pore size diameter of PVDF/CNCs membrane

4 Conclusion

The presence of CNCs increased the viscosity of the dope solution. An increment of viscosity creates a dense surface creating hydrophobic surface behaviour. The pore size also reduces hence lower membrane water flux behavior.

References

M. Fosi-Kofal, A. Mustafa, A.F. Ismail, M. Rezaei-DashtArzhandi, and T. Matsuura. 2016. PVDF/CaCO3 composite hollow fiber membrane for CO2 absorption in gas-liquid membrane contactor. *Journal of Natural Gas Science and Engineering*, 31:428 – 436.

D. Hou, G. Dai, H. Fan, J. Wang, C. Zhao, and H. Huang. 2014. Effects of calcium carbonate nano-particles on the properties of PVDF/nonwoven fabric flat-sheet composite membranes for direct contact membrane distillation. *Desalination*, 347:25 – 33.

F. Lessan, M. Karimi, J.L. Bañuelos, and R. Foudazi. 2019. Phase separation and performance of polyethersulfone/cellulose nanocrystals membranes. *Polymer*, 121969.

J. Lv, G. Zhang, H. Zhang, and F. Yang. 2018a. Graphene oxide-cellulose nanocrystal (GO-CNC) composite functionalized PVDF membrane with improved antifouling performance in MBR: Behavior and mechanism. *Chemical Engineering Journal*, 352:765–773.

J. Lv, G. Zhang, H. Zhang, C. Zhao, and F. Yang. 2018b. Improvement of antifouling performances for modified PVDF ultrafiltration membrane with hydrophilic cellulose nanocrystal. *Applied Surface Science*, 440:1091–1100.

H. Mahdavi, M.A. Kerachian, and M. Abazari. 2022. Synergistic effect of GO@SiO2 and GO@ZnO nano-hybrid particles with PVDF-g-PMMA copolymer in high-flux ultrafiltration membrane for oily wastewater treatment and antifouling properties. *Journal of Industrial and Engineering Chemistry*, 108:374–388.

H.M. Mousa, H.S. Fahmy, R. Abouzeid, G.T. Abdel-Jaber, and W.Y. Ali. 2022. Polyvinylidene fluoride-cellulose nanocrystals hybrid nanofiber membrane for energy harvesting and oil-water separation applications. *Materials Letters*, 306.

Y. Yang, H. Zhang, P. Wang, Q. Zheng, and J. Li. 2007. The influence of nano-sized TiO2 fillers on the morphologies and properties of PSF UF membrane. *Journal of Membrane Scienc*, 288(1):231–238.

Individual Research Contribution Review, 2023, 1(1): 73–74

Sustainable Eco-Remediation via Aquatic Plastic Waste Recovery

Siti Salwa Mohammad Shirajuddin
Radiation Processing Technology Division
Malaysian Nuclear Agency
43000 Kajang, Selangor
sitisalwa@nm.gov.my

Abstract

Every year, million tons of plastic waste leaks into aquatic ecosystems, polluting lakes, rivers and seas, accounting for 85 percent of all marine litter. The recovery and utilization of this plastic waste as a sustainable and low-cost raw material for new products is one of the alternatives of cleaning up 'the waste' in the ecosystem. The goal of this community project was to develop a fully functional system for processing land and aquatic plastic waste into a new multipurpose plank. This was accomplished by utilizing the rover (a mode of transportation for collecting aquatic plastic waste) built for this project to collect aquatic plastic waste and process it at the SEAPlast facility. The facility was constructed and equipped with machines and instruments to process plastic waste from shredding, drying, and molding into a new multipurpose plank. The plank can be used for outdoor application such as jetty planks, pavement blocks, furniture as well as for decoration. The community (Persatuan Nelayan Kawasan Kuala Perlis) involves will earn extra income by selling products made from recycled plastic while utilizing the complete facility provided by this project. This project also was also overseen by Jabatan Pengairan dan Saliran Negeri Perlis and Lembaga Kemajuan Ikan Malaysia Negeri Perlis authority.

1 Introduction

Sustainable Eco-Remediation via Aquatic Plastic Waste Recovery (SEAPlast) is a new initiative for the production of multipurpose planks produced from recycled plastic waste. The production of this product can help the economic development of the B40 target group economically in the collection of plastic waste and the production of the product itself. The expertise of the Malaysian Nuclear Agency in the field of plastic recycling and composite processing equipment allows the SEAPlast production facility to be adapted to the capabilities of the community that will receive the technology. NM's experience in successful project MSI17108: Building the manufacturing capability of biocomposite floating jetty components for use in the fishing and eco-tourism sectors and also MSI 2016, proved that the technology's ability to be accepted by the community.

This SEAPlast project is planned to develop the capacity of the community around Kampung Tandiap, Kuala Perlis, Perlis in the production of SEAPlast's product from recycled plastic by using advanced processing techniques. Through this program, Jabatan Pengairan dan Saliran Negeri Perlis (JPS NP) and Lembaga Kemajuan Ikan Malaysia Negeri Perlis (LKIM NP) agreed to act as a collaborator in assisting the Malaysian Nuclear Agency in implementing this project and will benefit the Persatuan Nelayan Kawasan Kuala Perlis.

2 Methods

a) Procurement of raw materials, equipment and processing facilities for recycled plastic waste at the Malaysian Nuclear Agency.

b) Preparation of rover for SEAPlast equipped with engine drive which used for collection of aquatic plastic waste for the recycling process.

c) Preparation of SEAPlast facility using the floating platform system developed by researchers in Malaysian Nuclear Agency.

d) Installation of SEAPlast floating structure and placement of plastic processing equipment in the facility.

e) Development of the process of collecting, cleaning, processing and recycling plastic molds into multipurpose planks.

f) Training and development of recycled plastic waste processing skills and multipurpose planks production capabilities.

g) Transfer of SEAPlast manufacturing technology to the PNK Kuala Perlis community.

3 Results and Discussion

Refer Figure 1 and Figure 2.

4 Conclusion

The benefit of this project is the implementation of environmentally friendly technology or green technology by reducing plastic waste pollution in addition to being able to produce multipurpose planks in the provided facility given. The products developed from the SEAPlast facility can be used as jetty plank, outdoor furniture and decorative fence. In relation to this, environmental pollution and economical activities are improved for the community in Kampung Tandiap, Kuala Perlis through the implementation of the SEAPlast project.

Figure 1: The recycled plastic processing facility and equipment for SEAPlast project provided to the community.

Figure 2: The training provided to the community for the SEAPlast project.

References

Marine Floating Module Unit, MY 20-E0735-0101, Malaysian Industrial Design.

Maritime Works – Part 4: Code of Practice for Design of Fendering And Mooring System, BS 6349-4: 2014. British Standard.

Modular For Aquaculture Farming and Method Thereof, MY-183424-A, Malaysian Patent.

Individual Research Contribution Review, 2023, 1(1): 75–76

Effects of Electron Beam Irradiation at High Doses on The Thermal Properties of Polytetrafluoroethylene

Sivanesan Appadu
Radiation Processing Technology Division, Malaysian Nuclear Agency
43000 Kajang, Selangor
siva@nm.gov.my

Abstract

This study is focused on analyzing the effects of electron beam (EB) irradiation at high doses and normal atmospheric conditions on the thermal properties of polytetrafluoroethylene (PTFE) to facilitate the recycling process of the material by grinding it into micro-powder additives for various applications. In this work PTFE scrap with thickness not exceeding 1 mm was irradiated in doses between 0 - 1500 kGy using an electron beam accelerator machine (EBM) with a voltage energy of 3 MeV and current of 10 mA. The changes in thermal properties of PTFE with increasing irradiation dose was studied by using thermogravimetric analysis (TGA) and differential scanning calorimetry (DSC). DSC analysis showed that the crystallization temperature (T_c) and melting temperature (T_m) decreased with increasing irradiation doses as a result of lower molecular weight. TGA results showed that initial decomposition temperature (T_{onset}) is distinctly lower at 1500 kGy dose compared to the other irradiated samples due to an increase in degradation of the sample at that particular dose.

Keywords: Polytetrafluoroethylene, Electron beam, Irradiation, Degradation, Thermal properties

1 Introduction

Polytetrafluoroethylene (PTFE) is a fluoropolymer with a long chain $(CF_2–CF_2)_n$ molecular structure with some interesting properties such as its hydrophobicity, resistance to high temperatures, non-stick characteristics, chemical stability and low friction coefficient (Vijay et al., 2020; Barylski et al., 2020; Goel et al., 2011; Liu et al., 2015). PTFE still retains the intrinsic properties of the material even after irradiation and thus can be modified to be used in composite materials or as additives in rubber and synthetic elastomers where it functions as an internal solid lubricant that improves the friction and wear properties of the base material.

2 Materials and Methods

PTFE scrap material with thickness not exceeding 1 mm was irradiated at doses from 0 to 1500 kGy. Irradiation of the PTFE scraps was done with an EPS-3000 electron beam accelerator machine (EBM) with a voltage processing parameter of 3 MeV, 10 mA electric current and dose rate of 50 kGy per pass. Differential scanning calorimetric (DSC) analysis of the samples was performed using the Mettler Toledo STAR^e to obtain a thermogram in the temperature range from 30°C to 400°C with a heating rate of 10°C per minute. Thermogravimetric analysis (TGA) tests were performed using the Netzsch TG209 equipment in the temperature range from 35°C to 700°C.

3 Results and Discussion

DSC 1st heating and cooling scans of the PTFE samples were used to determine the T_m and T_c peaks respectively and to calculate the percentage of crystallinity (X_c) based on the value of the enthalpy of fusion of the polymer sample in J/g. The DSC exothermic and endothermic curves are shown in Figure 1 and Figure 2 respectively. From the heating exothermic peaks in Figure 1, it can be observed that Tm decreases only slightly at 250 kGy, indicating that cross-linking of the molecular chain is the dominant process and decreases in value rapidly from 500 kGy onwards where chain-scission dominates with the peaks shifting further left where the lowest T_m is observed at 1500 kGy dose. From the endothermic scan in Figure 2, with increasing doses of irradiation, the crystallization peak Tc decreased with the peaks shifting further to the left of the thermogram where the crystallization process happens at much lower temperatures in comparison to the unirradiated PTFE sample.

The heating and cooling scans from the DSC thermogram provides information about the effect of irradiation on the molecular chain crystallization process and the final crystallinity (Frick et al., 2013). When the molecular weight of PTFE decreases, it results in thermally less stable semi-crystalline structure which melts at a lower temperature due to the disentanglement of polymer chains leading to the formation of a more disordered structure.

TGA weight loss curves are shown in Figure 3, where the unirradiated PTFE sample shows a single-step degradation pattern, with no weight loss up to 570 °C beyond which thermal decomposition of molecular chains of PTFE occurs in the range of 570–628 °C. The initial decomposition temperature (T_{onset}) decreased from 570 °C for the unirradiated sample to 518 °C at 1500 kGy. It can also be observed from the weight loss curves that Tonset is distinctly lower at 1500 kGy dose compared to the other irradiated samples due to an increase in degradation of the sample at that particular dose. This result is consistent with our observation for the PTFE scrap

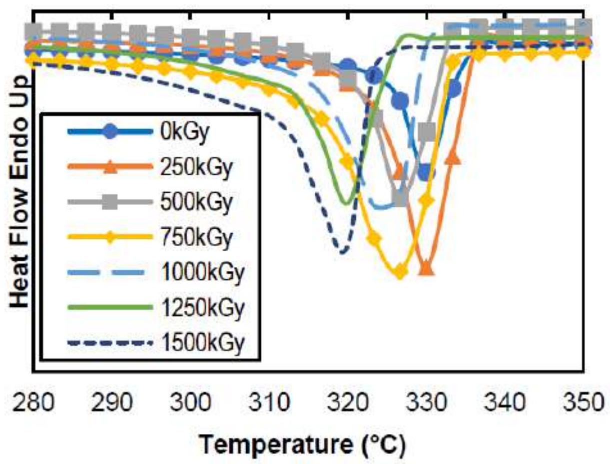

Figure 1: DSC heating thermogram of PTFE at irradiation doses of 0 -1500 kGy.

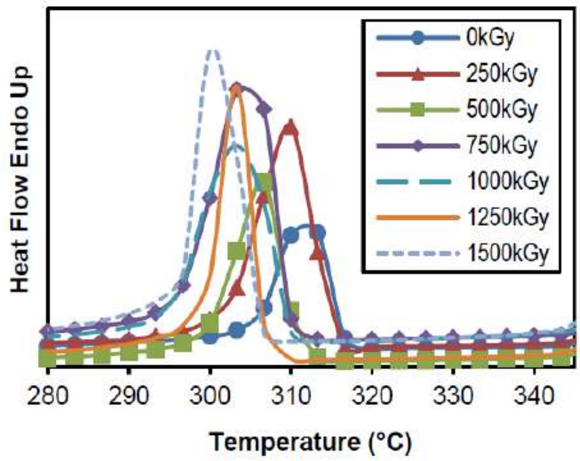

Figure 2: DSC cooling thermogram of PTFE at irradiation doses of 0 -1500 kGy.

sample irradiated at 1500 kGy where the material breaks in to pieces when removed from the irradiation tray due to a steep reduction in mechanical properties caused by degradation.

4 Conclusion

It can be concluded that EB irradiation dose of up to 1500 kGy in normal atmospheric conditions reduces the thermal stability of PTFE material where T_m, T_c and T_{onset} decreases with increasing dose. T_{onset} is distinctly lower at 1500 kGy dose compared to the other irradiated samples due to an increase in degradation of the sample at that particular dose. This result is consistent with our observation for the PTFE scrap sample irradiated at 1500 kGy where the material had become very brittle and breaks when removed from the irradiation tray.

References

A. Barylski, K. Anio lek, A.S. Swinarew, S. Kaptacz, J. Gabor, Z. Waśkiewicz, and A. Stanula. 2020. Novel organic

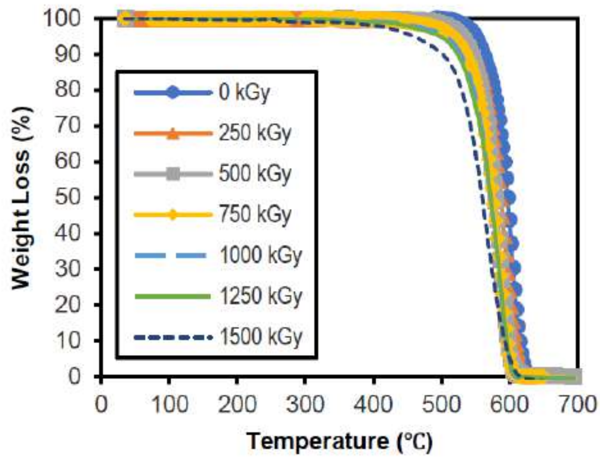

Figure 3: TGA weight loss curves of PTFE at irradiation doses of 0 -1500 kGy

material induced by electron beam irradiation for medical application. *Polymers*, 12(2):1–11.

A. Frick, D. Sich, G. Heinrich, D. Lehmann, U. Gohs, and C. Stern. 2013. Properties of melt processable PTFE/PEEK blends: The effect of reactive compatibilization using electron beam irradiated melt processable PTFE. *Journal of Applied Polymer Science*, 128(3):1815–1827.

N.K. Goel, V. Kumar, S. Pahan, Y.K. Bhardwaj, and S. Sabharwal. 2011. Development of adsorbent from Teflon waste by radiation induced grafting: Equilibrium and kinetic adsorption of dyes. *Journal of Hazardous Materials*, 193:17–26.

S. Liu, C. Fu, A. Gu, and Z. Yu. 2015. Structural changes of polytetrafluoroethylene during irradiation in oxygen. *Radiation Physics and Chemistry*, 109:1–5.

A.R.M. Vijay, C.T. Ratnam, M. Khalid, S. Appadu, and T.C.S.M. Gupta. 2020. Effect of radiation on the mechanical, morphological and thermal properties of HDPE/rPTFE blends. *Radiation Physics and Chemistry*, 177(April):109190.

Individual Research Contribution Review, 2023, 1(1): 77–78

Recycling of Polymer Waste for Structural and Non-structural Materials by Using Ionizing Radiation: Recycling of PTFE Wastes by Ionizing Radiation

Teo Ming Ting
Radiation Processing Technology Division, Malaysian Nuclear Agency
43000 Kajang, Selangor
tmting@nm.gov.my

Abstract

This research project is utilizing ionizing radiation to convert PTFE waste into micro-powder additives through controlled irradiation, with the overarching goal of optimizing the recycling process. The laboratory prototype, operating with irradiation, consistently produces 1 kg of PTFE micro powder per cycle. The intrinsic properties of PTFE remain essentially intact after irradiation, enhancing the recyclability of PTFE waste. The study compares the particle size distribution of laboratory-produced PTFE with commercial PTFE, acknowledging variations influenced by the grinding machine's limitations. The incorporation of PTFE micro-powder into FKM polymer yields promising results, enhancing friction coefficient, wear resistance, and mechanical properties. This research contributes valuable insights into the efficient recycling of PTFE waste, showcasing its potential for sustainable and enhanced material applications.

Keywords: Recycling, PTFE waste, Micro Powder

1 Introduction

The increasing demand for polymeric materials has led to a significant concern regarding the management of polymeric waste at the end of its life cycle. This predicament is particularly pronounced in the case of polymers like polytetrafluoroethylene (PTFE), polyolefin and other plastic wastes. Recycling these materials presents a viable strategy to foster a sustainable supply chain and promote environmentally friendly processes.

Polytetrafluoroethylene (PTFE), a fluoropolymer characterized by its elongated molecular structure (CF2–CF2)n, boasts remarkable properties such as hydrophobicity, resistance to high temperatures, non-stick characteristics, chemical stability, and a low friction coefficient. These unique attributes, attributed to the presence of electronegative fluorine atoms in its chemical composition, render PTFE an extensively utilized material in diverse industries, including aerospace, electronics, and household equipment.

Numerous studies have previously explored the impact of irradiation on the chemical structure of PTFE under varying conditions and parameters. Factors such as dose rate, range, temperature, and atmospheric conditions, including the presence of oxygen, play a pivotal role in altering the morphology, mechanical, and chemical structures of PTFE during irradiation processes. The literature highlights that irradiation in different environments, such as air, vacuum, or inert gases, leads to distinct changes in the chemical structure, manifesting as either cross-linking or chain-scission of the long-chain polymer. The dominance of these processes is contingent upon specific irradiation parameters and conditions.

Chain-scission predominantly occurs in PTFE when irradiated in air at room temperature, while cross-linking and branching become dominant in a molten state or under oxygen-free vacuum conditions or inert gases. Irradiation-induced radicals react with oxygen, leading to the formation of acid fluoride groups (COF) within the polymer. In the presence of atmospheric humidity, these COF groups hydrolyze to form carboxylic acid groups (COOH). Although degradation occurs after irradiation at room temperature, PTFE retains its intrinsic properties, making it suitable for modification and incorporation into composite materials or as additives in rubber and synthetic elastomers.

Despite undergoing irradiation, PTFE maintains its essential properties, making it amendable for recycling. The reduction of molecular weight through irradiation processing facilitates the conversion of scrap PTFE into micro-powder through mechanical processing. This micro-powder can serve as a dry lubricant, enhancing the properties of industrial products such as inks, plastics, and coatings. The degradation of PTFE molecular chains typically initiates at doses exceeding 100 kGy under normal conditions.

The focus of this study is on the recycling of PTFE waste through radiation. The objective is to transform PTFE scrap into polymeric additives or reinforcing fillers for polymers. The PTFE waste was processed into micron-sized powder. The resulting micro powder was melt-blended into elastomers, and the blended polymer's property was also discussed.

2 Methods

The PTFE waste samples were irradiated using gamma and electron beam machine, 3.0 MeV. The dose rate of gamma was 1.5 kGy / hour. The electron beam accelerator machine (EBM), with a voltage of 3 MeV, current of 10 mA and dose rate of 1 kGy/pass to 25 kGy / pass were applied. The total dose studied was in the range of 0 to 700 kGy. Subsequently, it was ground into micro-powder using an laboratory mill, employing a cutting speed in the range of 15,000 - 20,000 rpm.

The particle size analyzer was analyzed using Horiba Scientific, LA-960. The micro powder was filled into the FKM rubber compound, it was blended during the polymer preparation phase, ensuring a homogeneous distribution for subsequent testing and analysis. After the compound was prepared the characterization of sample was performed to obtain the mechanical and tribological properties.

3 Results and Discussion

3.1 Particle Size Distribution

The D10 value for the laboratory-produced PTFE is higher than that of commercial PTFE, indicating that 10% of the particles are larger. The D50 value for the laboratory-produced PTFE is also larger compared to commercial PTFE, indicating that the median particle size is higher (Table 1). The D90 value for the laboratory-produced PTFE is significantly higher than that of commercial PTFE, suggesting that 90% of the particles are larger. Overall, the data indicates differences in the particle size distribution between commercial PTFE and the laboratory-produced PTFE.

In evaluating the particle size results of the laboratory-produced PTFE in comparison to commercial PTFE, it's important to acknowledge the observed variations. The discrepancies are influenced by the inherent limitations of the grinding machine employed in the laboratory setting.

Table 1: Particle size distribution of irradiated recycled PTFE

Micro Powder Particle Size		
Product Name / Label	PTFE used by Industry	PTFE produced by this project
D10 (μm)	0.852	6.64
D50 (μm)	17.1	28.6
D90 (μm)	34.8	97.3

3.2 Polymer Compound

The introduction of PTFE micro-powder significantly reduces the friction coefficient, enhancing the material's lubricity and potentially improving its performance in applications where low friction is critical.

The addition of PTFE micro-powder contributes to a reduction in wear resistance, and this phenomenon can be attributed to the inherent strength of FKM rubber in exhibiting effective wear resistance. The FKM rubber, even without additional particles, already possesses commendable wear resistance characteristics. However, with the introduction of PTFE micro-powder, there is a natural influence on the wear and tear behavior, leading to an increase in the value of wear resistance. This change is not indicative of a deterioration in performance but rather a modification in the wear resistance profile. The FKM rubber, reinforced with PTFE micro-powder, may exhibit different wear characteristics that align with specific application requirements. While the numerical value of wear resistance may increase, it is essential to interpret this within the context of achieving tailored material properties to suit particular operational conditions.

The addition of PTFE micro-powder enhances the mechanical properties of the FKM, resulting in increased tensile strength and modulus, with a minor reduction in elongation (Table 2). This suggests improved structural integrity and strength, making it suitable for applications requiring higher mechanical performance.

In summary, the incorporation of PTFE micro-powder into FKM leads to notable improvements in friction coefficient and mechanical properties, making it a potentially favorable choice for applications demanding enhanced performance in these aspects.

Table 2: Property of micro powder filled polymer

FKM polymer loaded with 30% wt PTFE micro-powder		
Product property	Non filled PTFE FKM	PTFE filled FKM
Friction of coefficient	Mean CoF: 1.69	Mean CoF: 1.10
Wear resistance	0.00018 mm^3/Nm	0.0015 mm^3/Nm
Mechanical properties	Tensile strength: 1.18 MPa Modulus 100%: 0.55 MPa Elongation: 228.81%	Tensile strength: 2.12 Mpa Modulus 100%: 1.51 MPa Elongation: 219.67%

4 Conclusion

This research explores the impact of ionizing radiation, conducted under normal atmospheric conditions, on the thermal stability of discarded polytetrafluoroethylene (PTFE) material. The primary aim is to optimize the recycling process by converting PTFE waste into micro-powder additives suitable for diverse applications. PTFE waste underwent irradiation with doses ranging from 0 to 700 kGy, employing both an electron beam accelerator machine (EBM) with a voltage energy of 3 MeV and a current of 10 mA, and gamma irradiation. Subsequently, the irradiated material underwent grinding into powder using a laboratory mill. The integration of PTFE micro-powder into polymer demonstrates significant enhancements in both friction coefficient and mechanical properties. The addition of the micro-powder contributes to an overall improvement in the material's characteristics, making it well-suited for demanding applications where enhanced friction control and robust mechanical performance are paramount.

References

S. Ata, S. Tomonoh, T. Yamda, and K. Hata. 2017. Improvement of thermal durability of fluorinated rubber by the addition of single-walled carbon nanotubes as a thermally stable radical scavenger. *Polymer (Guildf)*, 119:112–117.

I. Banik, A.K. Bhowmick, S.V. Raghavan, A.B. Majali, and V.K. Tikku. 1999. Thermal degradation studies of electron beam cured terpolymeric fluororocarbon rubber. *Polym. Degrad. Stab.*, 63:413–421.

D.S. Ogunniyi and C Hepburn. 2003. Compounding studies of a fluoroelastomer. *Iran. Polym. J.*, 12(5):367–371.

Y. Wang, L. Liu, Y. Luo, and D. Jia. 2009. Aging behavior and thermal degradation of fluoro elastomer reactive blends with poly-phenol hydroxy EPDM. *Polym. Degrad. Stab.*, 94:443–449.

Q.L. Wang, J.K. Pei, G. Li, X. He, Y.H. Niu, and G.X. Li. 2020. Accelerated aging behaviors and mechanism of fluoroelastomer in lubricating oil medium. *Chinese J.Polym. Sci.*, 38:853–866.

Individual Research Contribution Review, 2023, 1(1): 79–80

Preparation Of DSRS Inventory For The Borehole Disposal Facility

Ahmad Hasnulhadi bin Che Kamaruddin
Waste Technology and Environmental Division
Malaysian Nuclear Agency
43000 Kajang, Selangor
hadi@nm.gov.my

Abstract

Disused Sealed Radioactive Sources or DSRS were categorized in five classes due to the risk and security aspects. In the Borehole Disposal Facility (BDF) project, only DSRS category 3 to 5 to be included in the disposal system and the BDF has been designed to disposed the lower risk sources that have been analysed and evaluated in the safety assessment and safety case. For the higher category of the sources, which involve category 1 and 2, the recovery of the souces will be more safe using Mobile Hot Cell (MHC) compared to the normal recovery operation for category 3 to 5 that using Mobile Tool Kit Facility (MTKF) or Conditioning Room Facility for dismantling devices and recovery of the sealed sources in the control environment. The records of the DSRS must be kept and maintained from cradle to grave. It should be sustained and documented in the control manner by the waste operator to make sure traceability of the information when there are needed to retrieve or track back detail of the sources in the waste management cycle or processes. Furthermore, all the waste information regarding our inventory records need to be declared to AELB annually to fulfill the compliance of Class G licensing from Atomic Energy Licensing Board (AELB).

1 Methodology

1.1 Collection or the DSRS data

The acquisition of the DSRS data or records can be retrieved by waste operator from an organized and controlled filing system in Waste Technology Development Centre (WasTeC). Information of the DSRS from the year of 1985 until 2016 has been considered in the BDF project. Data acquisition of the DSRS can be found based on the unique waste identification created for the sources. The waste identification (Waste ID) is the key for looking other details or information for all types of the radioactive waste including DSRS. However, not all the DSRS can be found with the identification number because it may be lost or missing due to package transfer and repacking during operation, corrosion and other related reason. Then, the investigation from the inventory records can be done if there are some details (such as device or source model and serial number, activity, radionuclides etc.) that can be matched from the devices to track back the original identification. If the process is still failure, the DSRS need to be characterized and a new waste identification will be created and updated in the inventory system accordingly.

1.2 Sorting information of the DSRS

The radioactive waste needs to be classified according to its physical and chemical characteristics. The DSRS can be classified into different radionuclides, radioactivity, and its category. Different radionuclide means the activity of the sources will decay depends on its half-life. There are sources with the long-lived radionuclides such as Ra-226 with the half-life of 1600 years, Am-241 with the half-life of 432 years and Cs-137 with the half-life of 30 years that will bring significant impact to the safety assessment. The DSRS with the short-lived radionuclides such as Sr-90 with the half-life of 29.1 years and Co-60 with the half-life of 5.3 years also being considered in the safety assessment and safety case for the BDF.

The DSRS were categorized into 5 different categories based on their risk and security consideration. It can be determined by the ratio of the actual activity (A) to the specific D value for the radioactive source (IAEA, 2003).

1.3 Check and review records periodically

After dismantling activities were carried out in a conditioning room facility, all the records related to the activities should be prepared, verified, and recorded properly. The DSRS Conditioning Form (WasTeC-F10) is a standard form that has been used for dismantling and conditioning activities. An operator must ensure the information recorded properly and hand over the records to a designated inventory officer or RWMO. The form must be verified and reviewed periodically to ensure all the DSRS information is reliable and well recorded.

1.4 Visual inspection for the waste (physical observation)

The DSRS can be identified by operator based on its physical observation. The information such as types of sources, activity, dose rate or Waste ID can be found whether from its device or sources. If there is lack of information, source characterization must be carried out to ensure more detail about the sources.

2 Analysis and Results

2.1 BDF Inventory (Year 1985 until 2016)

There are 58 capsules with 12 215 units DSRS in total with the total activity of 26.2 Curie containing various types of radionuclides were planned to be disposed into BDF. Capsule ID of MAL-07, MAL-08 and MAL-09 contributes to the highest number of sources which consists of 9248 unit of Am-241 from smoke detectors. However, the total activity of 8.86E-06 Curie for smoke detectors is still low and not too significant. These seven capsules of MAL-01, MAL-03, MAL-06, MAL-18, MAL-19, MAL-49 and MAL-50 have the activity more than 1 curie with the activity of 2.08 Ci, 2.96 Ci, 2.99 Ci, 2.87 Ci, 1.12 Ci, 7.79 Ci, and 1.67 Ci per capsule respectively.

2.2 Current inventory (Year 2017 - Jun 2022) for Ra-226

The 96 units of Ra-226 in total were collected from the year of 2017 until Jun 2022. 86 units of them were mainly check or cup sources which came from educational sector. In year 2019, they contributes the largest amount of the quantity for a year with the total of 41 units cup sources. There were also planning to optimize all of the DSRS from Previous Conditioning Capsule (PCC) into Source Conditioning Capsule (SCC). In addition, Nuclear Malaysia top management agree to withdraw Ra-226 from the total inventory as decided earlier in the safety assessment. The Ra-266 sources will be sent to other countries such as Canada or US who interested to have them for their benefit.

A Radioactive Waste Managment Officer (RWMO) will be responsible to submit the radioactive waste inventory records in their storage facility to the Atomic Energy Licensing Board (AELB) every year as stipulated in the Radioactive Waste Management Regulation 2011. This is to make sure the compliance from operator with Class G license prior to dispose the DSRS into BDF.

3 Discussion

Classification of the radioactive waste including DSRS by considering the physical, chemical and radiological characteristics is very crusial in planning a disposal option for the waste. By considering current activity of the DSRS, some of the sources were not significant in term of their risk because they will be fully decayed for some period of time. The waste also can be exempted or cleared from the regulatory control if the activity limit is below the exemption value as gazetted by federal government under Atomic Energy Licensing for Low Activity Radioactive Material (Exemption) Order 2020. Output from the structured inventory data can be used to choose a disposal option for Malaysia such as borehole disposal facility (BDF) and Low-Level Radioactive Waste Repository.

4 Conclusion

Sorting and organizing the radioactive waste inventory is an initial step before upgrading the structured data into an inventory database system. Dealing with many records will need consistency in checking, reviewing, tracking and fixing the missing records, managing uncertainties with the best practise and optimizing the current records to make sure data or records that we have is convincing and reliable. Inventory data could be structured into a database system by using an intelligent software to organize the records in the efficient and effective way. The records can be accessed, retrieved and easily updated in a good tracking system which also can be controlled securely in the quality management system. It can minimize the uncertainties and human error in the efficient way as we are going to the Fourth Industrial Revolution (IR 4.0) that need the intelligent approach or skills in data science and software development.

References

AELB. 2011. Atomic Energy Licensing (Radioactive Waste Management) Regulations 2011. Federal Government Gazette. PU(A)274. 16 August 2011, Malaysia.

IAEA. 2003. Categorization of radioactive sources, IAEA-TECDOC-1344. Vienna, Austria.

IAEA. 2004. Code of conduct on the safety and security of radioactive sources. Vienna, Austria.

IAEA. 2005. Categorization of radioactive sources, IAEA safety standards, safety guide no. RS-G-1.9. Vienna, Austria.

Individual Research Contribution Review, 2023, 1(1): 81–82

Radioactive Dose Mapping of Interim Storage Facility using Geographical Information System (GIS)

Ahmad Hasnulhadi bin Che Kamaruddin
Waste Technology and Environmental Division
Malaysian Nuclear Agency
43000 Kajang, Selangor
hadi@nm.gov.my

1 Introduction

Radioactive dose mapping is were used among researchers or scientists to analyse, represent and visualize radiation dose rate or contaminated radioactive materials in order to have better understanding of radiation exposure patterns or potential risks in specific locations.

Instead of local interpolation methods such as natural neighbour, spline, kriging and the others, Inverse Distance Weighting or IDW is an interpolation technique that commonly used to estimate values at unknown locations based on observations from nearby known locations (Jongkwan Kim, 2022). It can be done by assigning more weight to nearby known points and less to those farther away, resulting in a smooth interpolated surface. So, the equation of Inverse Distance Weighting can be written as below (Chong, 2022).

Instead of complying with licensing purpose for the storage facility which also related to the radiological monitoring program, the information from radiation dose interpolation can be beneficial for the operator to visualize the dose based on its risk pattern from low to high dose rate This study is only limited to the interim storage facility at Block 33 Nuclear Malaysia where the most of radioactive wastes collected throughout peninsular Malaysia including Sabah and Sarawak are stored.

2 Methods

The fishnet sampling method was used for sampling grid of the Nuclear Malaysia Interim Storage Facility Building Block 33. The fishnet sampling involves creating a grid in a systematic way to collect data of spaced sampling points across study area. This technique is efficient and commonly used in environmental monitoring where it allows for unbiased sampling.

Two types of survey meters were used to measure dose rate of gamma emitters from the radioactive materials inside the interim storage facility. As defined by the fishnet grid, twenty (20) sampling points were determined to better understand the radiation dose inside the building. The dose rate measurements at the sampling points were taken 1 meter above the ground or floor. These active monitoring were carried out on 31 May 2023.

Then all the details about dose rate were analyzed and presented in GIS to produce IDW mapping of the interim storage facility. The IDW mapping using Ludlum and RedEye survey meter are presented in the map as shown in Figure 1(a) and Figure 1(b).

An passive dose monitoring was carried out using Thermoluminescent Dosimeter (TLD) at 18 stations around the interim storage building. These TLD records were obtained from Secondary Standard Dosimetry Laboratory (SSDL) and IDW interpolation mapping was performed using GIS software based on accumulated dose from January until April 2023.

3 Results and Discussion

The background radiation recorded using Ludlum and RedEye survey meter were 0.53 μSvh^{-1} and 0.27 μSvh^{-1} respectively. Interpolation of the dose rate per year by using IDW method with different types of survey meter were shown as below.

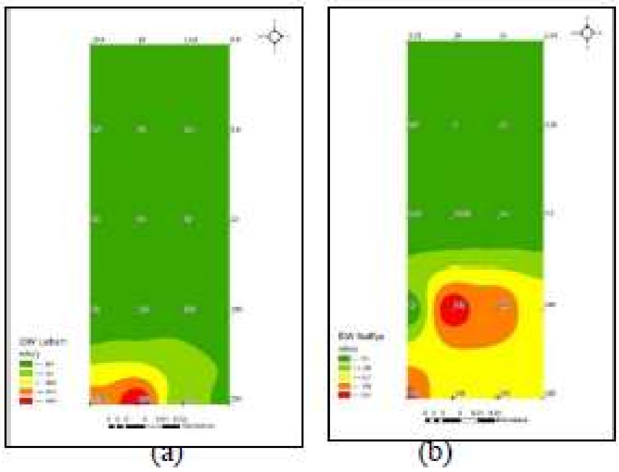

Figure 1: (a, b) The dose rate interpolation mapping using Ludlum and RedEye survey meter

4 Conclusion

The fishnet sampling method was used to avoid unbiased sampling from the study area. The Inverse Distance Weighting (IDW) interpolation using GIS software had showed us the variation of the dose rate at the interim storage facility from active and passive monitoring conducted at the study area. The risk area of the building Block 33 could be defined and classified effectively from the GIS mapping conducted in this study. These classification area from this study will fulfil and verify Class G license requirement from the Atomic Energy Department (JTA).

References

AELB. 2021a. Panduan pengelasan kawasan kerja menurut peraturan-peraturan Perlesenan Tenaga Atom (Perlindungan Sinaran Keselamatan Asas) 2010 [P.U. (A) 46] LEM/TEK/65 Sem.2.

AELB. 2021b. Technical guidance code of practice on radiation protection in industrial radiography (LEM/TEK/33 Rev.2). Atomic Energy Licensing Board (AELB).

K. C. Chong. 2022. Modified inverse distance weighting interpolation for particulate matter estimation and mapping. *MDPI Journal*.

J. H. Jongkwan Kim. 2022. Improved IDW interpolation application using 3D search neighborhoods: Borehole data-based seismic liquefaction hazard assessment and mapping. *MDPI Journal Applied Science*.

Z. Nur Khairunisa and F. A. 2023. Dose mapping using Thermoluminenscene Dosimeter (TLD) and Geographical Information System (GIS) Tool for Long Term Storage Facility (LTSF), Bukit Kledang, Perak, Malaysia. *e-Jurnal Sains Nuklear Malaysia*, 35(1):22 – 28.

Individual Research Contribution Review, 2023, 1(1): 83–84

Statistical Analysis for Disused Sealed Radioactive Sources (DSRS) in Waste Technology Development Centre (WasTeC)

Ahmad Hasnulhadi bin Che Kamaruddin
Waste Technology and Environmental Division
Malaysian Nuclear Agency
43000 Kajang, Selangor
hadi@nm.gov.my

1 Introduction

The preparation of inventory data for Disused Sealed Radioactive Sources or DSRS is very important for developing a safety assessment and determining the borehole design. Detailed information of the devices and radioactive sources is usually required not only in the early stages of purchase, but also applied when it is time for disposal activities to be carried out.

Radioactive waste was generated by waste generators in a few sectors such as industrial, public, education, medical and research and in the form of disused sealed radioactive sources (DSRS), liquid, solid and gas. However, this study only limited to DSRS which had been collected and received by Waste Technology Development Center (WasTeC) from 2019 until 2022 prior to final disposal. These data will be analyzed with descriptive analysis and the results will be discussed.

2 Methods

All the DSRS data need to be sorted in yearly basis from 2019 until 2022 according to different sectors, purpose and applications, quantities, types of radionuclides, half-life, radioactivity and categories.

2.1 Collection or the DSRS data

The acquisition of the DSRS data or records can be retrieved by waste operator from an organized and controlled filing system in Waste Technology Development Centre (WasTeC). Data acquisition of the DSRS can be found based on the unique waste identification created for the sources.

2.2 Sorting information of the DSRS

The radioactive waste needs to be classified according to its physical and chemical characteristics. The DSRS can be classified into different radionuclides, radioactivity, and its category. The DSRS were categorized into 5 different categories based on their risk and security consideration. It can be determined by the ratio of the actual activity (A) to the specific D value for the radioactive source (IAEA, 2003).

3 Results and Discussion

In 2019, 274 DSRS were collected throughout the year. From the total, 268 radionuclides had been verified and identified and the other 6 units need to be identified and characterized from physical observation. The current total activity of DSRS from all radionuclides is 202 GBq. Most of the sources (192 units) came from educational sectors like schools and they were used in experiments in their science laboratory. The other units mostly came from different types of gauges, followed by smoke detectors and only one unit of lightning arrestor collected in this particular year.

In 2020, 109 DSRS were collected throughout the year. The current total activity of DSRS from all radionuclides is 144 GBq. In this year, there were 48 units DSRS collected from medical sectors which had the highest quantity compared to the other sectors. Then, it was followed by 36 units of gauges from industries, 16 units of cup sources from educational sector, and only 6 units from the total DSRS are smoke detector devices.

In 2021, 247 DSRS were collected throughout the year. The current total activity of DSRS from all radionuclides is 63.8 GBq.

In 2022, 343 DSRS were collected throughout the year which arising from different sectors and application. 173 units of the DSRS are cup sources which distributes the highest number of sources in this year. In total, the current activity is 194 GBq.

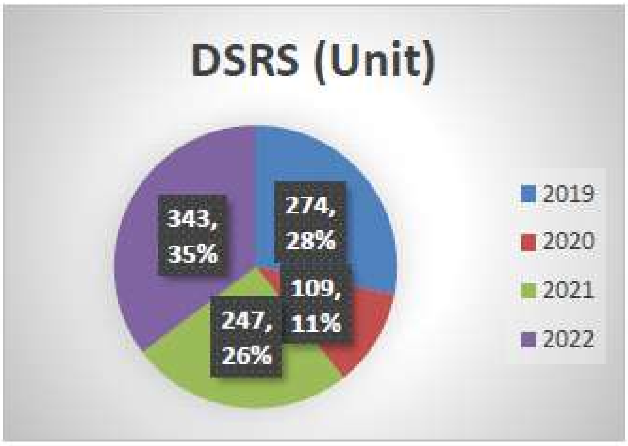

Figure 1: The fraction or percentage of DSRS from year 2019 until 2022

In total, from the year of 2019 until 2022, there were 973 units of DSRS collected and received by Nuclear Malaysia. The fraction or percentage of DSRS can be shown in Figure 1 as above. The highest collections were carried out in 2022 (343 units or 35%) followed by 2019 (274 units or 28%) and 2021 (247 units or 26%). The lowest collections were carried-out in the year of 2020 (109 units) which only involved 11%

from the total DSRS collected.

4 Conclusion

By considering current activity of the DSRS, some of the sources were not significant in term of their risk because they will be fully decayed for some period of time. The waste also can be exempted or cleared from the regulatory control if the activity limit is below the exemption value as gazetted by federal government under Atomic Energy Licensing for Low Activity Radioactive Material (Exemption) Order 2020. Output from the structured inventory data can be used to choose a disposal option for Malaysia such as borehole disposal facility (BDF) and Low-Level Radioactive Waste Repository.

References

AELB. 2011. Atomic Energy Licensing (Radioactive Waste Management) Regulations 2011. Federal Government Gazette. PU(A)274. 16 August 2011, Malaysia.

IAEA. 2003. Categorization of radioactive sources, IAEA-TECDOC-1344. Vienna, Austria.

IAEA. 2004. Code of conduct on the safety and security of radioactive sources. Vienna, Austria.

IAEA. 2005. Categorization of radioactive sources, IAEA safety standards, safety guide no. RS-G-1.9. Vienna, Austria.

Individual Research Contribution Review, 2023, 1(1): 85–86

Study on Air Monitoring in Klang Valley using Acacia Tree Leaves with Neutron Activation Analysis (NAA)

Azian Hashim
Waste Technology and Environmental Division,
Malaysian Nuclear Agency
43000 Kajang, Selangor
azian@nm.gov.my

Abstract

Klang Valley is one of the rapidly growing areas with heavy and medium industry and has a high population density. Acacia auriculiformis was selected in this study as bioindicator plant, as this plant is widely planted around industrial areas as an ornamental plant. Elemental measurement in this study is using Neutron Activation Analysis (NAA) technique. From the data obtained, each industrial area gives a different value of data in the study area depending on the type of industry in the area.

Keywords: Air pollution, acasia tree, neutron activation analysis (NAA)

1 Introduction

Malaysia with a tropical climate suitable for the growth of acacia trees that shows in Figure 1. This tree has been identified as one of the ornamental plants or shade plants in heavy industrial areas by local authorities. In botanical science, acacia tree is cluster as an evergreen tree that grows up to 15-30 m and has a high resistance to disease/pollution. According to (Salih and Aziz, 2019), plants can take a large amount of pollutants and translocate them into vegetative tissues and other tissues that can show the level of quality of the environment they occupy. Thus characteristics, acacia tree leaves have been chosen in this study.

Figure 1: Acacia trees in the heavy industrial areas.

2 Methods

The sampling area in the Klang Valley has been divided into 3 regions to carry out the sampling of acacia tree leaves as shown in Figure 2. Region 1 - The Western Region of the Klang Valley covers the industrial area from Shah Alam to Kapar, Klang, Region 2 covers the Central Valley area Klang which is the industrial area of Puchong up to Shah Alam whilst Region 3, the industrial area in the East of the Klang Valley part, which is area included Serdang and Balakong, Cheras.

Figure 2: Sampling area of acacia trees in the Klang Valley.

Leaves sample from acacia trees were collected, dried and finely grind for sample preparation for the NAA technique. The samples that have been processed will be sent to the TRIGA MARK II Reactor, Malaysian Nuclear Agency to be irradiated. All samples and reference material (CRM) were irradiated with a thermal neutron flux of 4.0x10^{12} ncm^{-2}s^{-1} using a TRIGA Mark II research reactor operating at 500 kW using a pneumatic transfer system (PTS) for short half-life elements. While 6-hours irradiation process in a rotary rack (RR) is done for element with a long half-life. Sample for RR will start counting after 3 days, while followed with the 2^{nd} counting after 21 days of the sample decay (Elias et al., 2018). Gamma ray with specific energy for each radionuclide were detected by using HPGe detector system supplied by ORTEC. Procedure was shown in Figure 3 below.

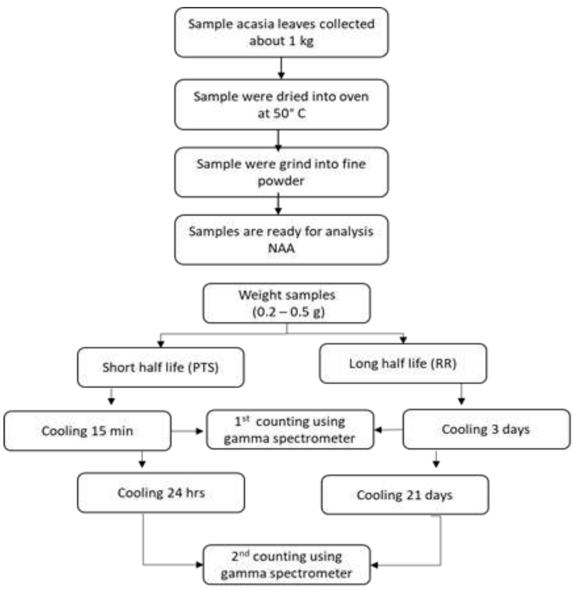

Figure 3: Summary of samples preparation for NAA

Table 1: Results for major and trace element in acacia leaves samples for Regions 1, 2 and 3

Element (ppm)	Region 1				Region 2			Region 3			
	R1F07	R1F10	R1F12	R1F14	R2 F2	R2 F4	R2 F7	R3F1	R3F2	R3F3	R3F5
Fe	148	84.0	388	68.0	151	134	74.5	184	82.0	141	88.5
Zn	16.7	15.4	28.4	10.4	17.5	18.5	23.2	16.6	22.3	31.2	24.0
Al	131	105	339	88.2	156	116	16.7	43.9	57.7	< 0.05	< 0.05
Mg	2,136	1,691	2,549	1,473	2,284	1,826	1,488	1,439	1,279	< 0.05	< 0.05
Na	513	3,440	3,492	1,680	1,232	1,168	425	1,857	7,767	3,865	456
K	14,151	6,298	8,887	10,662	8,592	7,893	11,839	10,042	4,252	9,905	9,113
Cl	6,758	8,034	10,919	7,362	8,774	8,980	6,786	7,157	6,098	10,938	5,540
As	0.53	0.15	0.54	1.15	< 0.05	0.74	< 0.05	0.23	< 0.05	< 0.05	0.72
Cs	0.69	0.92	0.38	0.10	0.65	0.63	0.16	0.76	1.82	0.53	1.53
Mn	72.4	37.8	90.9	55.9	120	122	171	285	145	< 0.05	62.7
Co	< 0.05	0.05	0.08	< 0.05	0.06	0.07	< 0.05	0.06	0.05	0.07	0.05
Br	18.2	26.1	41.8	53.5	536	101	3.30	6.28	8.30	32.0	4.72
Cr	0.70	0.49	5.36	0.44	0.59	0.49	0.24	0.93	0.93	0.82	0.79
Sb	0.20	0.08	0.24	0.098	0.59	0.81	0.12	0.32	0.38	0.59	0.62

3 Results

The results of the analysis obtained are shown in Table 1. The results are divided into 3 regions, namely Region 1 - the Western Klang Valley area, Region 2 - the Central Klang Valley area and Region 3 - the Eastern Klang Valley area. From the results, data values are significant difference for major element, and this difference is may course by dependent on the type of industries that carries out activities in the area involved. However, the concentration range for this acacia tree leaves sample is lower compared to the element sampled from the polluted area in Pasir Gudang (Rahman et al., 2021). With reference to (Abbas et al., 2018; Ma et al., 1997), the results obtained of each concentration element are within the normal range for plants.

4 Conclusion

The data obtained from several sampling locations of acacia tree leaves in the Klang Valley industrial area found that the values for the concentration of each element were in normal conditions for the plant. If there is pollution in the study area, the data can be used as a guideline for measuring the level of pollution.

Although basically Malaysia has several stations for air monitoring sampler, but in an emergency case the sampling will be carried out randomly with various type of plants around the location. Therefore, this study can be used as a reference for a data guideline.

References

G. Abbas, Murtaza B, Bibi I., and et al. 2018. Arsenic uptake, toxicity, detoxification, and speciation in plants: Physiological, biochemical, and molecular aspects. *Int J Environ Res Public Health*, 15(1):59. Published 2018 Jan 2. doi:10.3390/ijerph15010059.

M. S. Elias, Ibrahim S., Samuding K., Rahman A. R., and Hashim A. 2018. The sources and ecological risk assessment of elemental pollution in sediment of Linggi Estuary, Malaysia. *Marine Pollution Bulletin*, 137:646 – 655.

J. F. Ma, S. Hiradate, K. Nomoto, T. Iwashita, and H. Matsumoto. 1997. Internal detoxification mechanism of Al in Hydrangea. Identification of Al form in the leaves. *Plant Physiol*, 113.

Y. Rahman, L. Zalina, M. Lakam, H. Azian, M. Mohamad Syahiran, M. H. Mohd Muzamil, O. Siti Aminah, and A. S. Muhammad Azfar, A. dan Shakirah. 2021. Pencirian kimia bahan buangan keluaran kilang (Chemical fingerprint) dan pemetaan taburan kehadirannya dalam alam sekitar di Sungai Selangkah dan Sungai Kim kim, Pasir Gudang, Johor. NUKLEARMALAYSIA/L/2021/33(S).

Zhian Salih and Farhad Aziz. 2019. Heavy metals accumulation in leaves of five plant species as a bioindicator of steel factory pollution and their effects on pigment content. *Pol. J. Environ. Stud.*, 28(6):4351 – 4358.

Individual Research Contribution Review, 2023, 1(1): 87–88

On-site Radiometric Mapping System for Natural Radioactive Sediment Transport Monitoring and Efficient Coastal Erosion Monitoring

Engku Mohd Fahmi Engku Chik
Waste Technology and Environmental Division
Malaysian Nuclear Agency
43000 Kajang, Selangor
mohdfahmi@nm.gov.my

Abstract

On-site radiometric mapping system for natural radioactive sediment transport monitoring and efficient coastal erosion monitoring was performed in this study. The radiometric survey was conducted to quantify and map the natural radioactivity levels within Langkawi black sand, focusing on the radionuclides Ra-226 and Ra-228. The activity concentrations of Ra-226 and Ra-228 in black sand from Pasir Hitam beach were 955 ± 115 Bq/kg and 530 ± 85 Bq/kg, respectively. The concentration of K-40 was 150 ± 41.5 Bq/kg. It was also reported that about 22 elements were detected in Langkawi black sand. The black sand consists of 4% ilmenite, 5.1% magnetite, 6.1% monazite, 14.1% albite, 41.4% anorthite, and 28.3% tourmaline.

Keywords: Langkawi black sand, natural tracer, radiometric mapping

1 Introduction

In recent years, many countries face some issues with erosion in the coastal areas. Current technology used for shoreline coastal erosion management now use airborne, satellite and un-manned aerial vehicle (UAV) drone. However, those methods have an accuracy issue because of a limited supporting data by on-land remote sensing equipment for validation. Latest nuclear technology focus on mapping the sediment movement by collecting natural gamma radioisotope sample and costing long time for spectrometry counting in the laboratory. By using MUDSkipper scan system, it can be used to collect total count data along 2-3 kilometres shoreline during low tides. The system will be move along the beach, doing several profiles from the seawater line, till the dunes with 3-4 parallel profiles. Therefore, this study aims to utilize radiometric mapping techniques to identify and evaluate its potential as a natural tracer for studying sediment transport dynamics.

2 Methods

2.1 Radiometric mapping

The study employed a NaI detector (Sodium Iodide Scintillation Detector) for radiometric mapping. The detector was mounted on a custom-designed trolley to facilitate movement and positioning. Additionally, the detector could be carried by hand to traverse challenging terrains or navigate around boulders on the beach. At each location, three readings were taken for a duration of 60 seconds each. All readings were recorded and stored for subsequent mapping and distribution analysis.

Figure 1: MUDSkipper scan system.

2.2 Sample analysis

Black sand samples were collected along the shoreline of Black Sand Beach in Langkawi. The samples were collected from 32 locations along a straight line spanning 3 km along the beach. At each sampling point, approximately 3 kg of sand were collected from a depth of 5 cm below the surface. The samples were air-dried and subsequently analysed using Neutron Activation Analysis (NAA) for U/Th, gamma spectrometry for Ra-226, Ra-228, and K-40.

Figure 2: Black sand samples at Black Sand Beach in Langkawi.

3 Result and Discussion

Figure 3 presents a GIS (geographic information system) map of Black Sand Beach in Langkawi. The distribution of black sand was determined using in-situ analysis with a NaI detector. The collected data was analysed using GIS software and plotted in units of counts per second (CPS). The map shows several red spots, indicating high CPS values. These spots represent areas where black sand is abundantly distributed. Consequently, GIS maps provide a clear visual representation of black sand distribution patterns, allowing for easy identification of concentrated areas.

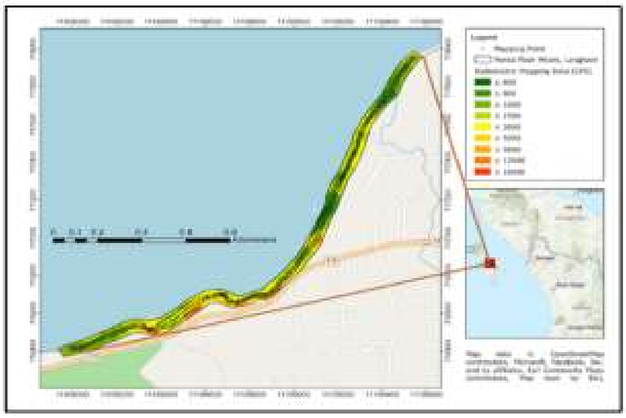

Figure 3: GIS mapping for Black Sand Beach, Langkawi.

Table 1 presents the results of radionuclide concentrations in Langkawi black sand. The activity concentrations of Ra-226, Ra-228, and K-40 were 955 ± 115 Bq/kg, 530 ± 85 Bq/kg, and 150 ± 41.5 Bq/kg, respectively. Compared to the activity concentration of Ra-226 in sand from Batu Ferringhi, which was 34 ± 2 Bq/kg (Shuaibu et al., 2017), the black sand in Langkawi exhibited significantly higher Ra-226 levels. This is attributed to its higher heavy mineral content (Khandaker et al., 2018).

Table 1: Radionuclides concentration in Langkawi Black Sand.

Radionuclides	**Activity Concentration (Bq/Kg)**
Ra-226	955±115
Ra-228	530±84
K-40	150±41.5
U	896.71
Th	623.21

4 Conclusion and Attention

In conclusion, this study provides a comprehensive assessment of Langkawi Black Sand as a natural tracer for sediment transport studies. The combination of mineralogical characterization and radiometric mapping highlights the potential of Langkawi Black Sand as a valuable tool for tracking sediment movement and understanding coastal processes.

References

Noorzahan Begum, Adilah Maisyarah, Fazlul Bari, Khairel Rafezi Ahmad, and Nur Hidayah. 2012. Leaching behaviour of Langkawi black sand for the recovery of titanium. *Procedia APCBEE*, 3:1 – 5. Elsevier.

Mayeen Uddin Khandaker, Khandoker Asaduzzaman, Abdullah Fadil Bin Sulaiman, D.A Bradley, and Matthew Omoniyi Isinkaye. 2018. Elevated concentration of naturally occurring radionuclides in heavy mineral-rich beach sand of Langkawi Island, Malaysia. *Marine Pollution Bulletin*, 127:654–663. Elsevier.

Hauwau Kulu Shuaibu, Mayen Uddin Khandaker, Tareq Alrefae, and D.A. Bradley. 2017. Assessment of natural radioactivity and gamma-ray dose in monazite rich black sand beach of Penang Island, Malaysia. *Marine Pollution Bulletin*, Elsevier.

Borehole Disposal Project: Post-closure Safety Assessment

Esther Phillip
Waste Technology and Environmental Division
Malaysian Nuclear Agency
43000 Kajang, Selangor
esther@nm.gov.my

Abstract

Post-closure safety assessment of Malaysian borehole disposal facility for disused sealed radioactive sources (DSRS) was performed using the IAEA BDC Scoping Tool and AMBER Model. The safety assessment evaluates the reliability and safety of the borehole disposal concept to a point of licensability. The safety assessment needs to be updated with every change to the borehole disposal system such as changes in the inventory of the DSRS and dimensions of the borehole. With active construction going on in 2023, the safety assessment has been updated accordingly.

Keywords: DSRS, Borehole, Disposal

1 Introduction

In 2018, Nuklear Malaysia completed a safety assessment and safety case for the disposal of its DSRS using the borehole disposal concept (IAEA, 2009). The safety assessment included modelling of the disposal system using the IAEA BDC Scoping Tool and AMBER to assess safety. Experience gained from attempts to drill a disposal borehole in 2023 resulted in some changes to the previously assumed inventory, site characteristics and design upon which the 2018 safety assessment was based. It is necessary to consider the impact of these changes on the safety assessment.

2 Findings/Discussion

2.1 Inventory

Table 1 shows the changes in the assumed inventory for disposal for the 2018 Safety Case and the current Safety Case (Nuklear Malaysia, 2023). The most significant change is the removal of Ra 226 sources from the inventory to be disposed.

A total of 42 waste packages manufactured from 316L stainless steel are now assumed to be disposed, as opposed to the 60 waste packages considered in the 2018 Safety Case.

2.2 Site characteristics

The 2018 Safety Case assumed that, although there was a zone of breccia from 97 m to 99 m, there were no cavities encountered when drilling the disposal borehole. However, a cavity was encountered when drilling the disposal borehole between 120 m to 130 m.

Table 1: 2018 and 2023 inventories.

Radionuclides	**Total activity for 2008 Safety Case (GBq)**	**Total activity for 2023 Safety Case (GBq)**
Ra-226	$1.05 \times 10^{+2}$	0
Am-241	$1.61 \times 10^{+2}$	$7.36 \times 10^{+1}$
Cs-137	$5.125 \times 10^{+2}$	$3.3 \times 10^{+2}$
Sr-90	$6.51 \times 10^{+1}$	$5.1 \times 10^{+1}$
Co-60	$4.3 \times 10^{+1}$	$7.54 \times 10^{+0}$
Kr-85	$2.78 \times 10^{+2}$	$4.45 \times 10^{+2}$
Fe-55	$1 \times 10^{+0}$	$3.82 \times 10^{+1}$
Cd-109	3.7×10^{-1}	7.84×10^{-2}
Ni-63	$7.92 \times 10^{+0}$	$4.22 \times 10^{+0}$
Tl-204	5.14×10^{-4}	4.14×10^{-5}
Po-210	9.08×10^{-3}	1.64×10^{-22}
Se-75	-	1.81×10^{-3}
Na-22	-	7.77×10^{-4}
Bi-207	-	2.73×10^{-4}
Pm-147	$3.54 \times 10^{+0}$	1.37×10^{-3}
Total	**$1.18 \times 10^{+3}$**	**$9.49 \times 10^{+2}$**

2.3 Dimension

Consistent with the 2018 Safety Case, the capsules and disposal containers have weld thickness of 3 and 6 mm, respectively. Updated waste package and casing dimensions are provided in Table 2.

Table 2: Updated dimensions.

Component	**Dimension**	**2018 value (mm)**	**2023 value (mm)**
Capsule	Length	195	*185/195
	Outer Diameter	65	65
	Inner Diameter	55	55
Containment barrier	Length	238	244
	Outer Diameter	102	102
	Inner Diameter	66	66
Disposal container	Length	300	300
	Outer Diameter	115	115
	Inner Diameter	102	102
HDPE casing	Outer Diameter	160	160
	Inner Diameter	No data	140

2.4 Design

The other actual/potential changes are summarised in Table 3.

Table 3: Further deviations from the 2018 Safety Case design assumptions.

No.	2018 Safety Case Design Assumption	Assumed As-built Condition
1	Steel casing is temporary.	Steel casing left in borehole. 16" mild steel casing is embedded to the depth of 20 m from the ground surface. 12" mild steel casing is embedded to the depth of 111 m from the ground surface.
2	Annulus between borehole wall and HDPE casing is filled with cement grout.	The annulus between borehole wall and HDPE casing is filled with rock rubble and water rather than OPC.
3	Same cement grout formulation, Ordinary Portland Cement (OPC), is used in the entire borehole.	OPC is used for the containment barrier in the disposal container but a 1 part OPC and 3 parts Ground Granulated Blast furnace Slag (GGBS) mix is used for the borehole backfill. The annulus between borehole wall and HDPE casing is filled with rock rubble and water rather than cement.
4	Disposal containers are emplaced in the borehole in dry conditions.	Disposal containers are emplaced in the borehole in saturated conditions.
5	There is a 0.75 m spacing between the top of a disposal container and the base of the disposal container placed above it in the disposal borehole.	There is a 0.25 m spacing between the top of a disposal container and the base of the disposal container placed above it in the disposal borehole.
6	Only 1 disposal borehole drilled.	Up to 4 potential disposal boreholes are drilled within 2-5 m of each other but only one is used for disposal. At least one borehole is drilled to the same depth of the actual disposal borehole. The unused boreholes are filled with soil.

3 Conclusion

The outcome of this Project has been documented and reported in the Safety Assessment Report as well as the Safety Case Synthesis Report for Borehole Disposal Facility Project (NUKLEARMALAYSIA/L/2023/58(S)2023).

References

IAEA. 2009. Borehole disposal facilities for radioactive waste. Specific Safety Guide No. SSG-1.

IAEA. December 2012. Generic post-closure safety assessment for borehole disposal of disused sealed sources, IAEA-TECDOC(draft).

Nuklear Malaysia. 2023. Safety assessment report. (NUKLEARMALAYSIA/L/2023/58(S)2023).

NECSA. 2004. Site specific safety assessment for the borehole disposal concept. GEA 1625, NECSA, Pretoria (October 2004).

Borehole Disposal Project: Sustainable Management of DSRS

Esther Phillip
Waste Technology and Environmental Division
Malaysian Nuclear Agency
43000 Kajang, Selangor
esther@nm.gov.my

Abstract

Effective and safe management of disused sealed radioactive sources (DSRS) is essential in ensuring sustainability in radioactive waste management particularly in countries without extensive nuclear power program like Malaysia. Malaysia is adopting borehole disposal as an approach to wisely and safely manage its Category 3-5 DSRS and at the same time promoting sustainability of the environment and economy. The final disposal of the DSRS managed to remarkably resolve most of the back-end issues associated with the accumulation and storage of DSRS that the country had been facing for the past 40 years. Longer-lived and higher radioactivity sources such as Am-241, Cs-137, Sr-90, Kr-85 and Co-60 were the main inventories disposed into the borehole. Post-closure safety assessment indicated that the borehole disposal facility is effective in providing safe solution for the disposal of the DSRS, with a maximum dose rate of 10 magnitudes lower than public dose limit of 1 mSv/y received by human 450,000 years after the disposal. With its small footprint of approximately 300 mm, the borehole disposal resulted in low land usage and impact. During its construction, very minimal environmental intrusion and damage were involved. The borehole disposal system implemented contributes to circular economy not only in terms of reducing radioactive waste and its associated risks to human and the environment but also promoting other economic activities for example recycling of uncontaminated shielding parts for other applications. Additionally, the implementation of borehole disposal is more cost-effective than other disposal options for Malaysia that has limited amount of radioactive waste. Expertise and experience as well as resources such as the mobile tool kit facility (MTKF) acquired serve as invaluable long-term sustainable assets to be shared with other countries interested in the same purpose.

Keywords: DSRS, Borehole, Disposal

1 Introduction

Like in any other disposal options, safety and security are prioritized in borehole disposal of DSRS and are demonstrated in its concept and design. The safety and security of the borehole disposal system are further assessed to provide confidence to the performance of the disposal system to ensure continuous safety and security to the future generations. While providing safety and security, the implementation of the borehole disposal at the same time enables the sustainable management of DSRSs. Sustainable management ensures that balance in safety and wellbeing of human, environmental protection, economic growth and social development can be achieved and is reflected in various aspects of the borehole disposal planning and implementation such as the system itself, technology and innovation involved, safety assessment, circular economy and its social contribution in terms of lesson learned and partnership forged.

2 Findings/Discussion

Sustainable management ensures that balance in safety and wellbeing of human, environmental protection, economic growth and social development can be achieved. In borehole disposal of DSRS, sustainability is reflected in various aspects of the borehole disposal planning and implementation such as the system itself, technology and innovation involved, safety assessment, circular economy and its social contribution in terms of lesson learned and partnership forged.

2.1 Borehole disposal system

Safety and security of the borehole disposal system is supported by its design. For example, the borehole has a deep closure zone of approximately 115 m from the ground surface equipped with a deflector plate to make intrusion impossible. Additionally, the closure zone is grouted almost to the ground surface and is topped with local soil and vegetation to conceal the area. The borehole itself has a very small footprint about 300 mm and therefore co-locating it with existing waste management facilities is possible.

Environmental protection is also supported by the design of the borehole. In comparison to other disposal options that frequently require massive construction using material such as cement, the small diameter borehole prevents the excessive use of cement. Other than that, the borehole is constructed on a smaller piece of land and therefore land use is minimized with less disturbance and destruction to the nature.

2.2 Technology and innovation

The sustainable management of DSRS by borehole disposal is also demonstrated in technology and innovation involved. One such technology and innovation is the successful implementation of the mobile tool kit facility (MTKF) for waste package preparation and disposal operation. The MTKF is regarded as a valuable long-term sustainable asset that is meant to be shared with other Member States interested in the same purpose. The technology it delivers is easily adopted, improvised and improved by any interested party.

2.3 Safety assessment

Sustainable management of DSRS by borehole disposal is also proven by safety assessment of the disposal facility that provides proof of safety and approval from regulatory body. Post-closure radiological safety assessment for the Malaysian borehole is prepared using Tier 3 IAEA BDC Scoping Tool and Tier 5 AMBER Model. For the purpose of the assessment, critical groups considered as receiver of the resulting doses are site dweller and farmer residing near a river 1.3 km from the borehole. In scenario where the facility is implemented as designed and functioned as expected, the maximum annual dose exposure received by farmer and site dweller residing at a river 1.3 km from the borehole is 10 orders of magnitudes lower than the public limit of 1 mSv/yr 450,000 years after disposal.

2.4 Circular economy

Circular economy shares the same vision as sustainability in the sense that it also places importance on economic growth, environmental protection and social development. In borehole disposal for DSRS, the circular economy approaches and their resulting contributions in achieving the SDGs are noticeable in various areas since the beginning in the design phase to the current construction phase. For example, in terms of reduction of DSRS inventory. The borehole project in Malaysia potentially allows the disposal of approximately 80% of its DSRS inventory from 1984 until 2022.

Another example is on the secondary waste generated from the removal of sources from their original housing. This secondary waste of uncontaminated parts is more manageable and can be treated as normal waste without any complex procedures. Those without foreseen future purpose are discarded as non-hazardous waste. Meanwhile, those with potential for reuse, repurpose and recycling are kept.

The implementation of borehole disposal is more economical than other disposal options for Malaysia that has limited amount of DSRS. The materials used are common construction materials such as cement and HDPE pipe. Other than that, the construction of the borehole itself also involve common drilling technology which Malaysia is familiar with looking at the fact that Malaysia has a long and established oil and gas exploration industry.

The implementation of borehole disposal is also relatively more economical as limited land and infrastructures are required. Furthermore, in Malaysia, the borehole facility is co-located with the existing interim storage facility that is already equipped with infrastructures such as road access, electricity, water supply and robust security thus requires less additional infrastructural cost. The construction, operation and closure periods are also relatively brief therefore the cost incurred in activities involved is generally lower. Unlike other disposal options, subsequent maintenance of the facility during post-closure is unneeded.

3 Lesson learnt and partnership

Lesson learnt from Malaysia's experience is important to many especially for countries having the intention to go for borehole disposal. As the borehole disposal for DSRS emphasizes strongly on radiation safety, it is therefore different from borehole commonly used for water abstraction or mining of oil and gas. Borehole for disposal prioritizes on verticality to ensure smooth emplacement of casing and eventually waste packages. The construction requirements are therefore unique to borehole disposal and may differ from the conventional and usual specifications. Partnerships fostered among Member States enable improvement and advancement in the current borehole disposal technology and thus open a wider opportunity for economic gain and social acceptance.

4 Conclusion

Borehole disposal offers promising long-term safe and secure solution for back-end issues associated with accumulation and storage of DSRS. Not only that future generations will be protected against the harmful effect of radiation, borehole disposal also opens the door for economic gain and partnership among countries around the world. The environment will also be preserved due to the small foot print nature of the borehole that requires responsible consumption of resources and safety features of the facility.

Therefore, it is justifiable to say that sustainable management of DSRS can be achieved through the implementation of borehole disposal.

References

E.T. Glover and P. Essel. 2020. Implementation of the borehole disposal system for safe and secure management of disused sealed radioactive sources in Ghana.

IAEA. 2006. Safety standards series no. 1, fundamental safety principles, safety fundamentals.

IAEA. 2011. BOSS: Borehole disposal of disused sealed sources: A technical manual. IAEA-TECDOC-1644.

IAEA. 2014. Management of disused sealed radioactive sources. IAEA Nuclear Energy Series No. NW-T-1.3,.

IAEA. 2016. Generic post-closure safety assessment for disused sealed radioactive sources in narrow diameter borehole, draft safety report. IAEA Safety Report Series.

IAEA. 2020. Underground disposal concepts for small inventories of intermediate and high level radioactive waste. IAEA-TECDOC-1934.

IAEA. 2021. Borehole disposal facilities for DSRS, draft safety guide DS512.

H.A. Sucipta, Pratama. 2020. Planning and concept of borehole disposal technology for disposal of disused sealed radiation sources from using in health and industry. *IOP Conf. Series: Journal of Physics: Conf. Series 1436*, 012033.

Individual Research Contribution Review, 2023, 1(1): 93–94

Isodose Mapping of the Terrestrial Gamma Radiation Dose Rate in Sarawak, Malaysia

Hairul Nizam Idris
Waste Technology and Environmental Division
Malaysian Nuclear Agency
43000 Kajang, Selangor
hairul_nizam@nm.gov.my

Abstract

A study of terrestrial gamma radiation (TGR) dose rate was conducted in Sarawak to construct baseline data of TGR dose rate level for the whole state area. The in-situ measurements of TGR dose rate were taken using NaI(Tl) scintillation detector at 1 meter above ground level. With the aid of the Sarawak reference and thematic maps, a total of 1044 measurement survey points were identified based on the stratified sampling method. The average TGR dose rate is found to be 100 nGy h^{-1}. The minimum and maximum values are 7 nGy h^{-1} and 320 nGy h^{-1}, respectively. The findings indicate that the average TGR dose rate of Sarawak is above the global average of 59 nGy h^{-1}, as prescribed by UNSCEAR. Using Geographical Information System (GIS) software, an isodose map was also generated to display the spatial distribution of the TGR dose rate for the entire state of Sarawak.

Keywords: Terrestrial Gamma Radiation, TGR Dose Rate, Isodose, Sarawak

1 Introduction

Natural radioactivity can be found almost everywhere; in soil, water, air, and the universe (Kurnaz, 2013). Over 80 per cent of our exposure to radiation is from natural sources (Environment, 2016). The radioactivity in nature are mainly contributed by primordial radionuclides such as ^{40}K (Potassium) and also from ^{238}U (Uranium) and ^{232}Th (Thorium) decay series. The terrestrial gamma radiation emitted from primordial radionuclides is one of the main external sources of radiation on earth (UNSCEAR, 2000).

Radiological mapping has been done in Peninsular Malaysia, but no details natural environment radiological studies have been carried out in Sarawak. Therefore, this study aimed to establish the baseline data of terrestrial gamma radiation (TGR) dose rates for the entire state area of Sarawak. It can later be used as a beneficial reference if new nuclear facilities are being developed or transboundary nuclear events occur in the future.

2 Methods

Type of geological background, soil distribution, and ease of access to the study area are the main factors taken into consideration for determining the location of measurement survey points. By utilising reference maps (Sarawak physical and topographic maps) and thematic maps (Sarawak geology and soil maps), a total of 1044 measurement survey points were identified using the stratified sample method. The Garmin MONTERRA NAVI, a global positioning system (GPS) device, is used for navigating to survey point locations. The TGR dose rate was measured with a NaI(Tl) scintillation detector (Ludlum-19 Micro R survey meter). The in-situ measurements were taken at approximately 1 meter above the ground. Then, using the Kriging spatial analysis technique, the ArcGIS 10.5 software was used to generate an isodose map of the entire state of Sarawak.

3 Results

Figure 1 shows the location of the identified measurement survey points, and a total of 1044 TGR dose rates were measured from this study. The mean dose rate of the measured TGR data is 100 nGy h^{-1}, with a range of 7–320 nGy h^{-1}. Table 1 tabulates the descriptive statistics results of the collected dose rate data, whereas Figure 2 displays the histogram graft. Meanwhile, Figure 3 shows the isodose map of TGR dose rate distribution for the entire state of Sarawak.

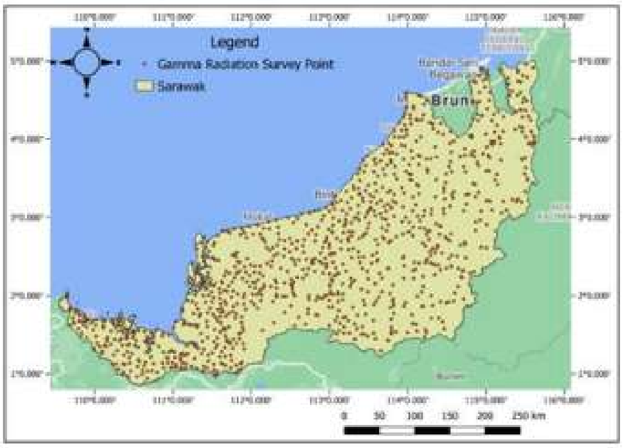

Figure 1: TGR measurement survey point locations.

4 Discussion

In this study, the TGR dose rate data was collected using the in-situ direct measurement method. The average dose rate of the measured TGR data is found to be 100 nGy h^{-1}. The

Table 1: Descriptive statistics of all measured TGR dose rate.

Descriptive statistics	TGR dose rate (nGy/hr)
n	1044
Mean ± standard error	100 ± 1
Confidence level of mean (95 %)	98 – 103
Minimum – maximum	7 – 320
Standard deviation	38
Kurtosis	1
Skewness	0

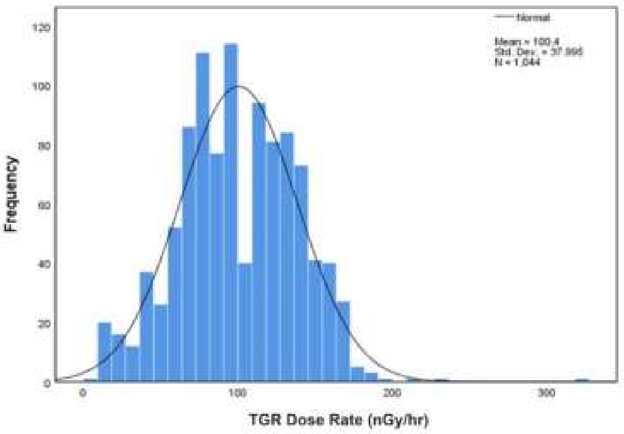

Figure 2: Histogram of all measured TGR dose rate.

lowest and highest recorded dose rate values are 7 nGy h^{-1} and 320 nGy h^{-1}, respectively.

In relative comparison, the TGR dose rate measured in Sarawak is lower than the dose rate observed in Peninsular Malaysia, with an average of 190 nGy h^{-1} and a range of 9–1349 nGY h^{-1} (Sanusi et al., 2014; Sanusi et al., 2016). However, the average dose rate values in Sarawak exceed the global average (59 nGy h^{-1}) prescribed by the United Nations Scientific Committee on the Effects of Atomic Radiation (UNSCEAR, 2008).

The Kriging spatial analysis technique successfully develops the spatial distribution of the TGR dose rate for the entire state of Sarawak. The isodose map of Sarawak indicates that most of the areas having a dose level below 104 nGy h^{-1} are situated in the coastal area. Conversely, the areas with dose levels ranging from 104 to 320 nGy h^{-1} are primarily located in the higher elevation regions.

5 Conclusion

This study has established the baseline data and isodose map of terrestrial gamma radiation (TGR) dose rates for the state of Sarawak. The mean dose rate of TGR is found to be 100 nGy h^{-1}. The findings indicate that the average TGR dose rate in Sarawak is above the global average of 59 nGy h^{-1}, as prescribed by UNSCEAR. However, the level of this gamma radiation dose is merely low and falls within the normal range for ionising radiation emitted by the environment. The baseline data and isodose maps established by this study provide

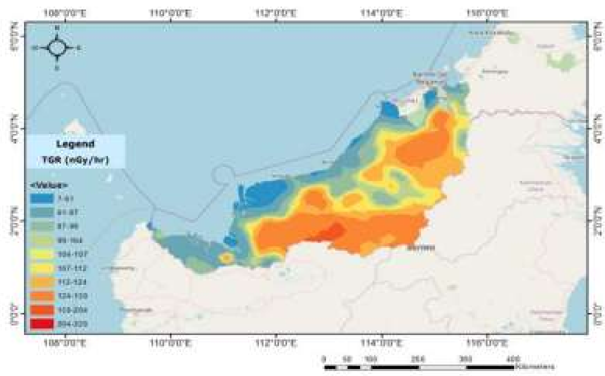

Figure 3: Isodose map of Sarawak.

beneficial references for future nuclear facility development or in the case of transboundary nuclear incidents.

References

UN Environment. 2016. Radiation effects and sources: What is radiation? What does radiation do to us? Where does radiation come from? *United Nations, New York.*

A. Kurnaz. 2013. Background radiation measurement and cancer risk estimates for Sebinkarashisare, Turkey. *Radiation Protection Dosimetry*, 199(13):e1 – e10.

M.S.M. Sanusi, A.T. Ramli, H.T. Gabdo, N.N. Garba, A. Heryanshah, H. Wagiran, and M.N. Said. 2014. Isodose mapping of terrestrial gamma radiation dose rate of Selangor State, Kuala Lumpur and Putrajaya, Malaysia. *Journal of Environmental Radioactivity*, 135:67 – 74.

M.S.M. Sanusi, A.T. Ramli, H. Wagiran, and et al. 2016. Investigation of geological and soil influence on natural gamma radiation exposure and assessment of radiation hazards in Western Region, Peninsular Malaysia. *Environ. Earth Sci.*, 75:485.

UNSCEAR. 2000. United Nations Scientific Committee on the Effect Atomic Radiation 2000. Effects of ionizing radiationa. *UNSCEAR 2000 Report to the General Assembly with Scientific Annexes*, United Nations, New York.

UNSCEAR. 2008. United Nations Scientific Committee on the Effect Atomic Radiation 2008. Sources and Effects of ionizing radiational. *UNSCEAR 2008 Report on the General Assembly with Scientific Annexes*, United Nations, New York.

Individual Research Contribution Review, 2023, 1(1): 95–96

A Study of Soil Erosion and Sedimentation in Sembrong Catchment Using Cesium-137

Jalal Bin Sharib@Sarip
Waste Technology and Environmental Division
Malaysian Nuclear Agency
43000 Kajang, Selangor
jalal@nm.gov.my

Abstract

This research paper aims to determine the rate of soil erosion and sedimentation by using Cesium-137, ^{137}Cs as a medium-term tracer in the Sembrong catchment, Malaysia, over two different study seasons. The dry season had rates of soil erosion between 5.09 t/ha/y to 51.03 t/ha/y. Meanwhile, the wet season had soil erosion and sedimentation rates between 8.02 t/ha/y to 39.78 t/ha/y and -4.81 t/ha/y to -50.81 t/ha/y, each respectively. As a conclusion, ^{137}Cs as a medium-term tracer was successfully used to determine rates of soil erosion and sedimentation.

Keywords: Soil erosion, Sedimentation, Cesium-137, Catchment Management

1 Introduction

Soil erosion is one of the most significant effects of global climate change and it has provided a global threat that can negatively affect ecosystem function and its ability to provide ecosystem services (Lal, 2010). In addition, human activities that are increasingly becoming the main contributors in recent times such as logging activities for the opening of new land such as the increase in agricultural activities, plantations, animal husbandry, industry, mining, settlement and release of CO_2 gas and others. Thus, it involves various aspects such as nutrient cycling, water retention and habitat provision (Blum, 1995). The use of Fallout Radionuclides (FRNs) is gaining ground among local researchers, especially in support of soil erosion and sedimentation studies.

Some local and international studies have also reported to determine the rate of erosion and deposition by using FRNs as tracers mainly for short and medium term, ^{7}Be and ^{137}Cs mainly between two different seasons in Timah Tasoh, Perlis and other world research sites (Blake et al., 2002; Jalal et al., 2019; Jalal et al., 2020; Jalal et al., 2021). This research paper aims to determine the rate of soil erosion and sedimentation by using FRNs, Cesium-137,^{137}Cs as medium-term tracers in the Sembrong catchment area, Kluang, Johor, Malaysia during two different seasons.

2 Materials and methods

The Sembrong catchment area was selected based on various factors that have been identified for this study. The Sembrong catchment is one of an important ecosystems in Peninsular Malaysia. Since 1960's, this reservoir has evolved from natural ecosystem to human-dominated ecosystem. The Sembrong catchment is located in Kluang, Johor between latitudes 3°26'42" to 3°26'42" N and longitudes 102°54'18" to 102°55'54" E as presented in Figure 1.

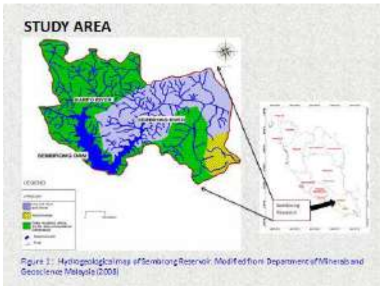

Figure 1: The Sembrong catchment area.

All soil and sediment samples were collected using metal corers and integrated suspended trap samplers. These samples were then taken to the Radiochemistry and Environment Laboratory (RAS), Nuclear Malaysia for the process of drying, sieving and counting. Finally, all samples before being counted using gamma spectrometry should be dried first by using an oven at a temperature of 45 - 60°C for several days until the weight becomes constant or stable. Measurements of ^{137}Cs will be carried-out by using gamma spectrometry utilizing high-purity Germanium (HPGe) detector with relative efficiency of 28%. The proportional model used to estimate soil erosion rate in tonnes/hectare/year. The model can be represented as follows:

$$Y = 10\frac{Bdx}{100TP}$$

where
Y = mean annual soil loss (t/ha/yr);
d = depth of the plough or cultivation layer (m);
B = bulk density of soil (kg/m^3);
X = percentage reduction in total ^{137}Cs inventory (defined as (Aref-A)/Aref×100);
T = time elapsed since the initiation of ^{137}Cs accumulation or the commencement of cultivation, whichever is later (w/yr);
A ref = local ^{137}Cs reference inventory (Bq/m^2);
A = measured total ^{137}Cs inventory at the sampling point (Bq/m^2);
P = particle size correction factor for erosion (P=1).

3 Results and discussion

Table 1 shows the overall results of the analysis of soil erosion and sedimentation rates from twenty (20) stations throughout the study period. The dry season has given the result of soil erosion rate only at each station when compared to the wet season which is more mixed with the rate of sedimentation and soil erosion itself. Soil erosion rates have given values between 5.09 t/ha/y to 65.2 t/ha/y throughout for both seasons. Meanwhile, the value of soil erosion and sedimentation in the rainy season is between 8.02 t/ha/y to 39.78 t/ha/y and -4.81 t/ha/y to -50.81 t/ha/y, respectively. Station 10 and station 11 have recorded the highest erosion rate values when compared to station 14 which were only able to record the lowest rate. However, the soil erosion rate values for all study seasons did not show any significant differences.

Table 1: Soil erosion and sedimentation rate during two seasons at different land use estimated using ^{137}Cs

Sample location	Land Use	Erosion/sedimentation rate (t/ha/yr)	
		Dry season	Wet season
Station 1-3	Settlement	41.4	-4.81
Station 4 and 6	Oil Palm Plantation	28.39	-50.81
Station 5	Animal farm	6.33	-8.16
Station 7	Modern agriculture	35.6	23.8
Station 8 and 9	Oil palm plantation	11.06	-7.88
Station 10 and 11	Mixed crop	65.2	29.78
Station 12	Banana plantation	15.39	28.11
Station 13	UK's Farm	28.66	8.0
Station 14	Modern agriculture	5.09	8.02
Station 15	Mixed crop	21.63	28.42
Station 16	Oil palm plantation	11.08	19.44
Station 17	Rubber tree plantation	51.03	39.78
Station 18	Fruit orchard	36.26	9.38
Station 19	Forest	18.11	23.9

Note: (-) values indicate sedimentation

The dry season has provided overall erosion values and no sedimentation values were recorded for all study stations. However, the wet season has provided both erosion and sedimentation values. The sedimentation value given is in the range of -4.81 t/ha/y to -50.81 t/ha/y, respectively. It was also reported by (Jalal et al., 2019; Jalal et al., 2020; Jalal et al., 2021) in the same area giving erosion and sedimentation rate values that are not very different by using the short and medium term FRNs approach as ^{7}Be and ^{137}Cs. Meanwhile, the rate of soil erosion and sedimentation from this study is not much different when compared to the previous study in Timah Tasoh, Perlis. In addition, the value of this study is also still considered small when compared to the contribution of erosion and sedimentation from large agricultural areas in the United States and the production of silt or soil brought into production in the last century in Northeast China, 6 Mg/ha/yr and 15 Mg/ha/yr, respectively (Mark et al., 2017).

4 Conclusion

The results presented in this paper are evaluated to confirm the potential to use ^{137}Cs as a tracer in the investigation of soil erosion and sedimentation. Moreover, the value of the analysis results from this study is not much different from the previous study that has been reported in the Timah Tasoh, Perlis and other studies around the world. As a conclusion, ^{137}Cs as a medium-term tracer was successfully used to determine rates of soil erosion and sedimentation in two different seasons for the Sembrong catchment area.

References

W.H. Blake, D.E. Walling, and Q. He. 2002. Using cosmogenic beryllium-7 as a tracer in sediment budget investigations. *Geografiska Annaler*, 84A:89 – 102.

Blum. 1995. Soil protection concept of the council of Europe Soil and Groundwater Pollution. *Springer, Netherlands, Dordrecht*, pages 72 – 73.

S. Jalal, O. Zainudin, and N.F.A.T. Dainee. 2019. Determination of medium-term soil erosion and sedimentation rates in two seasons. *International Journal of Agriculture, Forestry and Plantation*, 8(June):120 – 127, ISSN 2462–1757.

S. Jalal, O. Zainudin, N.F.A.T. Dainee, Y. Noor Fadzilah, T.I . Mohd, and I.A.A. Mohd. 2020. The short-term erosion rates in different land use study. *International Journal of Agriculture, Forestry and Plantation*, 9(Feb):19 – 27, ISSN 2462–1757.

S. Jalal, O. Zainudin, and N.F.A.T. Dainee. 2021. Quantifying the relative amounts of soil erosion and sedimentation in different land use. *ASM Sc.J.*, 16(Special Issue 1, 2021 for SCIEMATHIC 2019):172 – 179.

R. Lal. 2010. Managing soils and ecosystems for mitigating anthropogenic carbon emissions and advancing global food security. *BioScience*, 60(9):708 – 721.

A. Nearing Mark, Yun Xie, Baoyuan Liu, and Yu Ye. 2017. Natural and anthropogenic rates of soil erosion. *International Soil and Water Conservation Research*, 5(Issue 2):77 – 84.

Individual Research Contribution Review, 2023, 1(1): 97–98

Development of Direct CO_2 Absorption Line for Environmental ^{14}C Concentration Measurement

Jeremy Andy Anak Dominic
Waste Technology and Environmental Division
Malaysian Nuclear Agency
43000 Kajang, Selangor
jeremy@nm.gov.my

Abstract

The direct CO_2 absorption line for carbon dating analysis in hydrogeological investigation was developed.

Keywords: Radiocarbon, ^{14}C dating, direct CO_2 absorption

1 Introduction

The rapid increase of atmospheric carbon dioxide (CO_2) and its significant effects on the global climate and environment have created great awareness on the importance of radiocarbon analysis. The current analytical protocols for ^{14}C determination are the Accelerator Mass Spectrometry (AMS), benzene synthesis and CO_2 absorption method. The first method is highly accurate but very expensive.

The second method produces better accuracy of results compared to the third method although the accuracy of results exceeds the requirements for most hydrogeological. The sample preparation for the second method is rather complex and more expensive. The third method involves the extracted CO_2 gas from the sample is directly absorbed into a mixture of an absorbent Carbo-Sorb® E (Perkin-Elmer) and a scintillator Permafluor® E+ (Perkin-Elmer) prior LSC (liquid scintillation counting) counting (Bronic´ et al., 2009; Leaney et al., 1994; Qureshi et al., 1989).

Therefore, the third method which is more simple, safe, economical and time-saving compared to other methods is preferable for hydrogeological study. The objective of this study is to develop a direct CO_2 gas absorption line for carbon dating analysis in hydrogeological investigation.

2 Methods

The direct CO_2 gas absorption line setup comprises of two main sections, the CO_2 extraction and absorption unit. The setup component for the extraction unit comprises of a magnetic stirrer, glass funnel, conical flask, stainless steel storage cylinder and vacuum pump, whereas the absorption unit comprises of a U-tube glass and carbosorb-scintillator mixture (Figure 1).

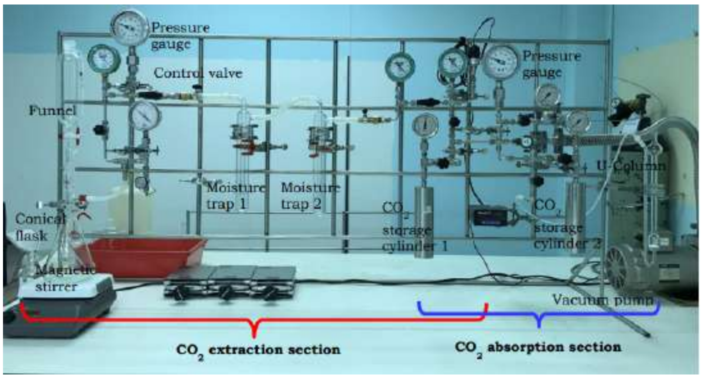

Figure 1: Direct CO_2 absorption line setup

The components were interconnected using stainless steel and silicon tubes. The flow control valves and vacuum pressure gauges were installed to monitor the pressure and flow condition in the system. The CO_2 gas produced from the acidification of carbonate mineral samples flows through two inline glass moisture traps before it is collected in a storage cylinder. The close system must be initially vacuumed in order to reduce mixtures between the atmospheric and extracted CO_2 gas.

The setup line was repeatedly tested under the lowest possible vacuum pressure to identify any potential leakage at the tubing connectors and storage cylinder. The standard vacuum condition required for each process were then identified. The absorption unit were tested repeatedly for CO_2 gas absorption efficiency.

3 Data/Results

Refer Figure 1.

4 Discussion/Conclusions

The direct CO_2 absorption line for carbon dating analysis was developed. The CO_2 absorption and carbon dating analysis using the new line setup needs further improvement on efficiency and standard procedures.

References

K. I. Bronic´, N. Horvatincˇic´, J. Baresˇic´, and B Obelic. 2009. Measurement of 14C activity by liquid scintillation counting. *Applied Radiation and Isotopes*, 67:800 – 804.

FW Leaney, AL Herczeg, and JC Dighton. 1994. New developments for the direct CO2 absorption method for radiocarbon analysis. *Quaternary Geochronology (Quaternary Science Review)*, 13:171 – 178.

RM Qureshi, R Aravena, F Peter, and R Drimmie. 1989. The CO_2 absorption method as an alternative to benzene synthesis method for ^{14}C dating. *Applied Geochemistry*, 4:625 – 633.

Individual Research Contribution Review, 2023, 1(1): 99–100

Assessment of Surface and Groundwater Quality and Quantity for Managed Aquifer (MAR) in the Melaka River Basin using Isotope and Related Techniques

Lakam Anak Mejus
Waste Technology and Environmental Division
Malaysian Nuclear Agency
43000 Kajang, Selangor
lakam@nm.gov.my

Abstract

Climate change is a general problem in the Asia–Pacific region (APR) which is increasingly experiencing extreme events such as tropical storms, floods/droughts, and sea level rise. Isotope techniques are excellent tools for interpreting climate patterns and projecting future climate variability. Water isotope data can be used for atmospheric circulation model development, calibration, and validation. The analysis of water and environmental isotope variabilities offers fundamental information for hydrological and environmental investigations.

Keywords: Hydrological, Water isotope

1 Introduction

In the APR, the exponential growth of the human population and the development of agricultural and industrial sectors in recent decades have caused a sharp increase in nitrogen, sulphur, and carbon loadings to the surface water bodies and associated groundwater resources. Contributions of untreated chemical effluents from industry, agriculture (pesticides and fertilizers), and domestic sewage are deteriorating surface water and subsequently groundwater quality. In addition to the direct input of contaminants to water, climate change is also adding to the water problems. The problem in the region now is shrinking of good quality water resources. There is a need to monitor the variability of water quality and water resources in the region for better adaptation and protection. Such variability should be interpreted as a reflection of anthropogenic activities and/or climate change impacts. Managed aquifer recharge (MAR) is commonly used to replenish depleted aquifers. The quality of water from these sources is usually high and is anticipated to improve groundwater quality after recharge. However, few studies investigate the impacts of MAR on regional scale groundwater quality, especially deep aquifers, and at the time scales of decades to centuries (Guo et al., 2023).

2 Methods

A total of 32 surface water samples have been collected during a field campaign from 13 to 18 June 2022 and have been analyzed for their isotopic composition at the Malaysian Nuclear Agency laboratory using Liquid Water Isotope Analyser (LWIA). Physical parameters of the surface water (i.e. pH, temperature, conductivity, resolved oxygen, turbidity and alkalinity) have been recorded on-site during the sampling activity using water quality monitoring system (YSI and Hanna instrument). However, the elemental analyses have not being conducted yet because currently the instrument (ICP-MS) is under maintenance. According to the person in-charge of the ICP-MS, the elemental analyses only can be resumed in early 2023. Second batch sampling activity has been conducted in mid-December 2022.

A total of 18 boreholes have been established in the area of interest (courtesy of NAHRIM). The construction of boreholes started in July 2022 and completed in October 2022 with the depth ranging from 10 m to 40 m. Groundwater samples will be collected during the second batch sampling activity. The age of the groundwater will be determined based on tritium and carbon-14 analyses (as well as other isotopic composition, physical parameters and elemental analyses). Figure 1 displaying the location sampling points.

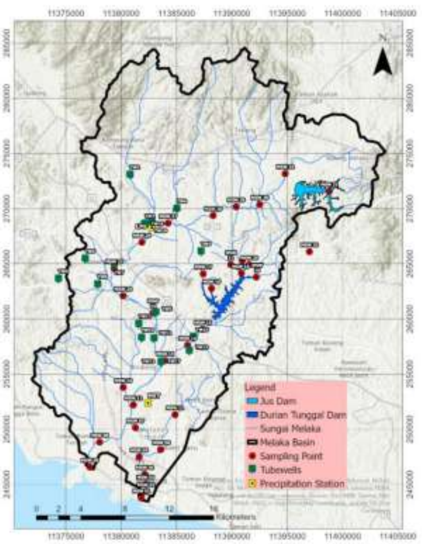

Figure 1: Map showing the Melaka Basin and sampling locations.

3 Results and discussion

Rainfall data has been obtained for a period of 2010 to 2021 as shown in Figure 2. The rainfall average is approximately 2000 mm. Extreme rainfall events are increasing though their occurrence in time and space is highly variable. In 2013 there is low rainfall but increasing gradually for 5 years. Mean annual temperature fluctuate approximately 1°C.

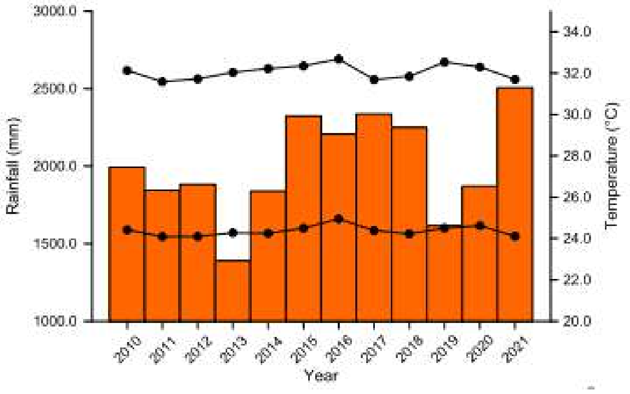

Figure 2: Rainfall (mm) and temperature (max and min, °C) for a period of 2010 to 2021.

The Malaysian Meteoric Water Line (MMWL; δ^2H = 8δ^{18}O+13.255; (Ayub, 2006)) and the Global Meteoric Water Line (GMWL; δ^2H = 8δ^{18}O +10; (Craig, 1961)) served as reference lines. A large range of δ^{18}O and δ^2H signatures and plotted below GMWL and MMWL can be observed along the river transect showing that evaporation occurred toward the estuary (Figure 3). Additionally, the river water tend to have more depleted δ^{18}O and δ^2H signatures at the center part of the river (SW5, SW4) and enrichment at the southern part of the Melacca River.

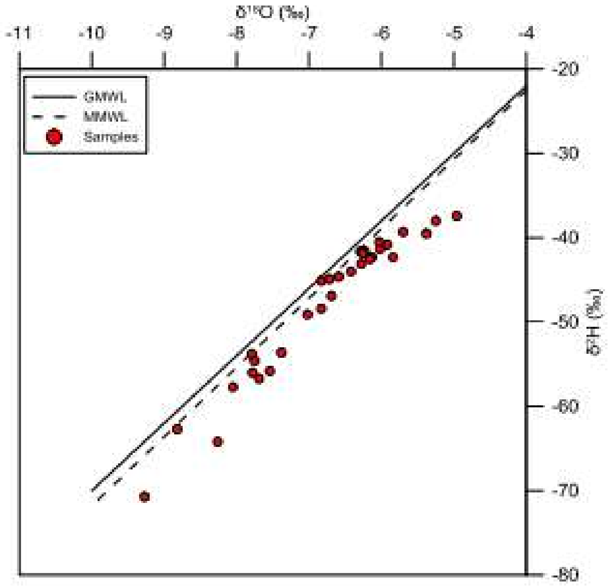

Figure 3: Plot of δ^2H versus δ^{18}O for river water.

In Figure 4, d-excess is plotted versus temperature, indicating that the river water is subjected to high rainwater evaporation (d-excess<10‰). The d-excess was negatively correlated with temperature. However, this trend should be monitor for the seasonal changes between wet and dry seasons as well as the influence of wind direction.

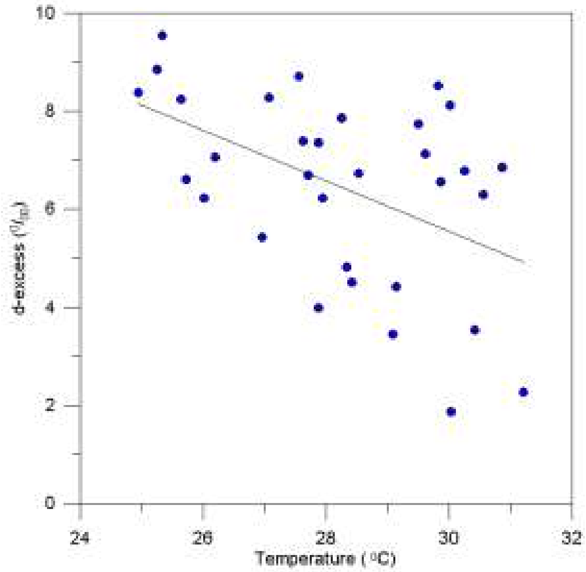

Figure 4: Plot of d-excess (‰) versus temperature (°C) for the river water.

4 Conclusions

In order to assess the surface and groundwater quality and quantity for MAR, we have presented preliminary finding of isotopic composition during transition from dry to wet seasons. Large amount of rainfall in shorter duration results in higher quantity of runoff and lesser natural recharge. This is supported by the wide isotopic variation indicated that the river water samples came from variable discharge area or water regime, but mainly from rainfall. In brevity, one can conclude that seasonal rainfall significantly affects the Melacca River Basin recharge. These preliminary results is useful information in gaining a better understanding of the hydrogeological processes taking place at the river aquifer interface.

References

M.S. Ayub. 2006. Malaysian meteoric water line: An input to isotopes hydrological studies. *Malaysia Institute for Nuclear Technology Research (MINT) R&D Seminar, Selangor, Bangi, Malaysia.*

H. Craig. 1961. Isotopic variations in meteoric waters. *Science*, 133(3465):1702 – 1703.

Z. Guo, G.E. Fogg, K. Chen, R. Pauloo, and C. Zheng. 2023. Sustainability of regional groundwater quality in response to managed aquifer recharge. *Water Resources Research*, 59, e2021WR031459:https://doi.org/10.1029/2021WR031459.

Individual Research Contribution Review, 2023, 1(1): 101–102

Assessment of Air Quality Pollution in Kuala Lumpur, Malaysia

Md Suhaimi Elias
Waste Technology and Environmental Division
Malaysian Nuclear Agency
43000 Kajang, Selangor
mdsuhaimi@nm.gov.my

Abstract

Nowadays, in Malaysia, the air quality status has been referred to the Malaysian Ambient Air Quality Standard 2020 (MAAQS- 2020). The air quality in Kuala Lumpur city centre showed that the average mass concentration for three years (2021 – 2023) of $PM_{2.5}$ exceeded the MAAQS, whilst the average mass concentration of PM_{10} was below the MAAQS value.

Keywords: air quality, $PM_{2.5}$, PM_{10}, Kuala Lumpur

1 Introduction

Air quality is one of the major issues in many countries in the Asian region including Malaysia. Haze episodes, open burning, release of smoke/dust from industries, land use and motor vehicles are possible major contributions to the air quality index in Malaysia (Abdul Rahman et al., 2011; Rahman et al., 2015). Many efforts have been made to increase air quality by encouraging the public to use public transport, car-pooling and enforcement of a new air quality standard guideline. In Malaysia, a new ambient air quality standard was established in order to replace the older Malaysian Ambient Air Quality Guideline that has been used since 1989. The new ambient air quality standard adopts 6 air pollutants criteria that include 5 existing air pollutants which are particulate matter with the size of less than 10 microns (PM_{10}), sulphur dioxide (SO_2), carbon monoxide (CO), nitrogen dioxide (NO_2), and ground-level ozone (O_3) as well as one additional parameter which is air particulate matter (APM) with the size of less than 2.5 microns (P_2M_5). The target set values of standard in 2020 for PM_{10} are 40 μg/m^3 (yearly) and 100 μg/m^3 (24 hours) whilst the target set values for $PM_{2.5}$ are 15 μg/m^3 (yearly) and 35 μg/m^3 (24 hours) (Department of Environment Malaysia 2020). However, there are still lack of information related to the elemental content in airborne particulate matter (APM) and to identify the sources of air pollution. In this study, the research activities will involve sampling of airborne particulate matters (PM_{10} and $PM_{2.5}$) at Kuala Lumpur city centre, in Klang Valley in order to assess the extent of pollution in the air due to industrial and developmental activities. The objective of this study is to identify the air quality pollution in Kuala Lumpur. This study will be focused on monitoring and analysis of PM_{10} and $PM_{2.5}$ in APM samples and to assist the DOE, Malaysia, in the capability for the development of new MAAQS.

2 Methods

2.1 Method for sampling of air particulate matter (APM)

The sampling of APM using a Gent stack sampler was located at the Department of Museum Malaysia, Kuala Lumpur, representing the urban area of Kuala Lumpur. The sampler was placed approximately more than 10 meters high from the ground level. The sampler was programmed to run automatically at an airflow rate of 15L/min to collect two fractions (< 2.5 μm and 2.5 -10 μm particles) of 24 hours duration.

2.2 Measurement of mass concentration of APM samples

The total mass of air filter samples was determined by weighing the filter using a microbalance (Mettler, Model MT5). The balance was equipped with a Po–212 (alpha emitter) electrostatic charge eliminator (Staticmaster) to eliminate the static charge accumulated on the filters before each weighing.

3 Results and Discussion

The Malaysian Ambient Air Quality Standard 2020 (MAAQS – 2020) for $PM_{2.5}$ are 15 μg/m^3 (yearly) and 35 μg/m^3 (24 hours), whilst standard values for PM10 are 40 μg/m^3 (yearly) and 100 μg/m^3 (24 hours). Analysis results of mass concentration of $PM_{2.5}$ and PM_{10} in the air filter were depicted in Figure 1 and 2, respectively. Analysis results indicate, that higher mass concentrations of $PM_{2.5}$ were observed from February to May 2021 and November to February 2022, which is most of the daily mass concentration of $PM_{2.5}$ higher than the standard. In general, from March 2022 until Sept 2023 the mass concentration of $PM_{2.5}$ within 10 – 35ug/m^3 (Figure 1). Nine days were recorded the mass concentration of $PM_{2.5}$ was higher than 40ug/m^3, which was three times higher than the MAAQS-2020 standard. The mass concentration of PM_{10} was two times higher than MAAQS on 30 Nov. 2021 (97.1 ug/m^3) and 16 Aug. 2023 (86.7 ug/m^3) as shown in Figure 2. The obtained result indicates that the daily mass concentration of $PM_{2.5}$ and PM_{10} levels recorded from February 2021 to September 2023 were in the range of 4.0 – 54.6 μg/m^3 and 5.0 – 97.14μg/m^3, respectively. The average concentration of $PM_{2.5}$ and PM_{10} were 21.1 μg/m^3 and 34.5 μg/m^3 as shown in Figure 1 and 2, respectively.

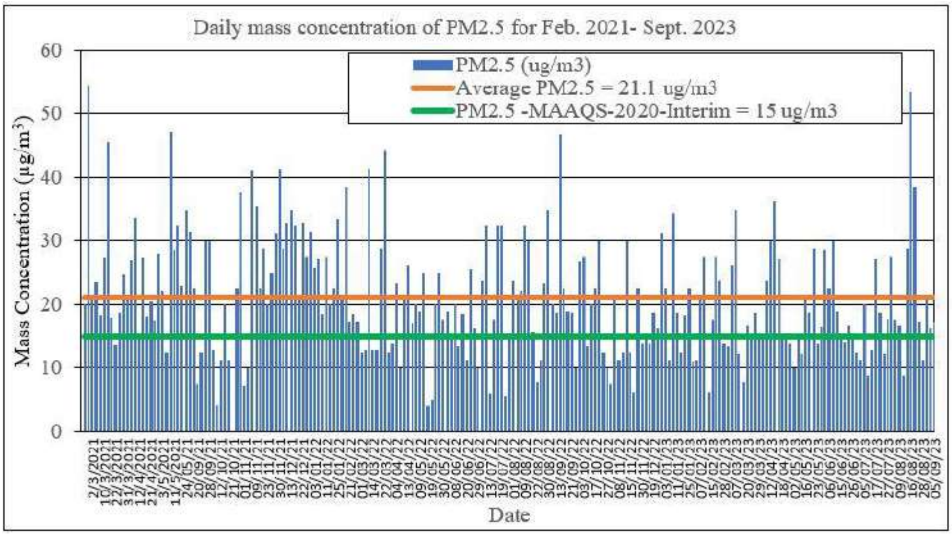

Figure 1: Analysis result of mass concentration of $PM_{2.5}$ in air filter

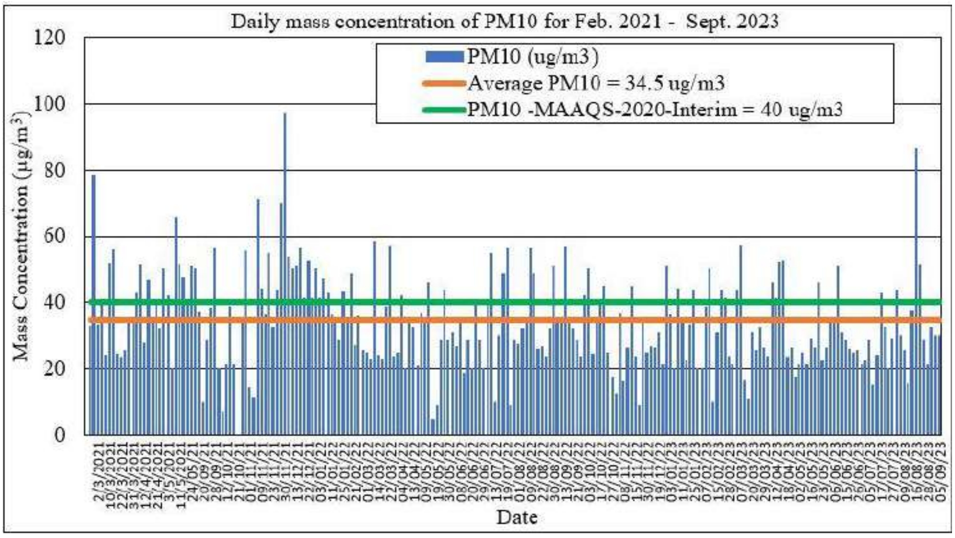

Figure 2: Analysis result of mass concentration of PM_{10} in air filterr

4 Conclusion

The average mass concentration of $PM_{2.5}$ for air quality in Kuala Lumpur, is higher than the Malaysian ambient air quality standard 2020 (MAAQS-2020), whilst the average mass concentration of PM_{10} is lower compared to MAAQS-2020.

References

S. Abdul Rahman, Mohd S. H., Abdul K.W., Md S. E., Nazaratul A. A. S., and Ezwiza S. 2011. Sources apportionment of fine and coarse aerosol in Klang Valley, Kuala Lumpur using positive matrix factorization. *Atmospheric Pollution Research*, 2:197 – 206.

Department of Environment Malaysia. 2020. Environmental Quality Report 2020. *Ministry of Environment and Water*, pages 36 – 105.

S. A. Rahman, M. S. Hamzah, M. S. Elias, N. A. A. Salim, A. Hashim, S. Shukor, W. B. Siong, and A. K. Wood. 2015. A long term study on characterization and source apportionment of particulate pollution in Klang Valley, Kuala Lumpur. *Aerosol and Air Quality Research 2009 (August 1991)*, pages 2291 – 2304.

Elemental Pollution in Soil Samples Collected From Klang Industrial Area

Md Suhaimi Elias
Waste Technology and Environmental Division
Malaysian Nuclear Agency
43000 Kajang, Selangor
mdsuhaimi@nm.gov.my

Abstract

Studies of elemental pollution in the soil were collected from the Klang industrial area to determine the concentration level in that area. The average concentration of heavy metals (As, Sb, Cr, Zn) in the soil of the Klang industrial area exceeded the average concentration in granitic igneous rocks. The geo-accumulation (Igeo) index was applied to identify the pollution status.

Keywords: geo-accumulation index, soil, Klang, neutron activation analysis.

1 Introduction

In Malaysia, rapid development and urbanisation have become issues related to the release of heavy metals into the environment. In general, sources of heavy metals pollution in soil mainly originate from two sources, namely anthropogenic activities and geogenic processes. The major activities that contribute to anthropogenic pollution are industrial waste, mining, logging, land clearing, road construction, processing and manufacturing, domestic waste, sewage, agriculture (crops, palm oil and rubber), fuel burning, livestock farming and shipping, activities (Ashraf et al., 2017; Elias et al., 2020). Meanwhile, the geogenic process occurs with weathering of soil and rocks, soil erosion, terrestrial runoff and atmosphere deposition (Elias et al., 2020). Studies of heavy metal contamination in the soil of Malaysia have been done by various agencies and locations. The objective of this study is to determine the concentration, distribution and pollution level of heavy metals in the soil sample of the Klang Industrial area. The study of heavy metals and pollution levels in the soils is vital due to their capability to be uptake by plants, vegetation and crops. Heavy metals can be transferred through the food chain and could have an adverse effect on human health at high concentrations.

2 Methods

2.1 Sampling and analysis of soil samples using Neutron Activation Analysis (NAA) technique

Fourteen locations in the Klang Industrial areas were selected for the sampling of soil samples. The soil samples were collected at 0 – 15 cm depth using an auger and dried at 60°C in an oven, followed by ground using agate mortar. Approximately 0.20 grams of soil samples were weighed and placed into polyethylene vials. The soil samples, standard reference materials (SRM) and blank were irradiated for six hours at the PUSPATI TRIGA Research Reactor facility of the Malaysian Nuclear Agency and allowed for a decay process of two to four days, followed by one hour of counting. The counting process of the irradiated soil samples, SRM, and blank was performed using a gamma spectrometer.

2.2 Contour Map

The contour maps of heavy metal concentrations were generated using Surfer software. Kriging interpolations were applied to illustrate the contour map of heavy metal concentrations in the Klang Industrial area.

3 Results and Discussion

3.1 Concentration of heavy metals in the soil of the Klang industrial area

The elemental concentrations of As, Cr, Zn and Sb were ranged from 3.8 – 428.7, 5.5 – 130.5, 25.7 – 866.6 and 0.5 – 18.5mg/kg, respectively. The average concentrations of heavy metals (As, Cr, Zn and Sb) were higher than the igneous granitic rock of the respective elements. This indicates the additional and accumulation of heavy metals in the soil of the Klang industrial area. The possible sources of heavy metal pollution likely originated from anthropogenic activities and natural land-based (landslides and terrestrial runoff).

3.2 Geo-accumulation index (I_{geo}) of heavy metals in the soil

I_{geo} values of As and Sb elements were ranged from 0.4 – 7.2 and 0.6 – 5.9, respectively (I_{geo} class = class 1 to class 6). This indicates that the elements of As and Sb in the soil sample of the Klang industrial area can be categorised as uncontaminated to moderately contaminated and as extremely contaminated. I_{geo} values of Cr ranged from – 2.6 to 2.5 (I_{geo} class = class 0 to class 3), indicating that the Cr in the soil sample can be categorised as uncontaminated and as moderately to strongly contaminated. Element of Zn can be classified as uncontaminated to strongly contaminated with I_{geo} values of – 2.7 to 3.3 (I_{geo} class = class 0 to class 4) as shown in Figure 1.

3.3 Contour map for distribution of heavy metals concentration in soil

The contour maps of the distribution of heavy metal concentrations in the soil of the Klang industrial area are depicted in

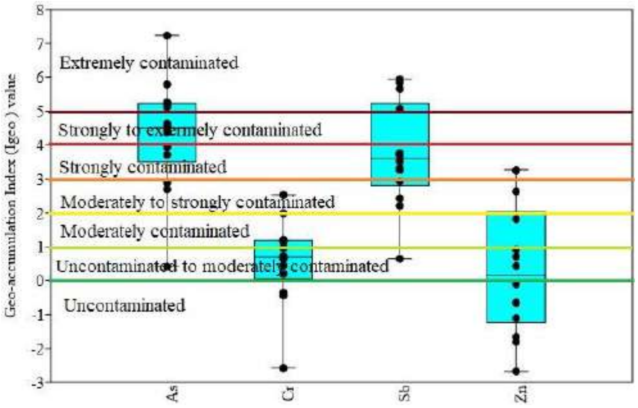

Figure 1: Geo-accumulation index (I_{geo}) status of heavy metals in the soil of the Klang industrial area.

Figure 2. The As element showed higher in SL11, which is located of shop lots, vehicle workshops and residential. The elements of Cr and Sb showed higher in SL14, where the Axis Industrial Park was located, which related to the activities of food and beverage manufacturers, rubber, recycling centres, paper, chemical, and plastic industries. Zn concentration showed slightly elevated in SL07 and SL08 locations.

4 Conclusion

The arsenic (As) showed a higher concentration in the SL11 location, which is located a residential, shop lots and vehicle workshops. Zn concentration showed more elevated in the SL07 and SL08 locations which, located workshop, concrete, manufacturing, plastic, motor and machine industries. The Cr and Sb showed higher concentrations in the SL14 location. The geo-accumulation (Igeo) index values of As and Sb can be categorised as uncontaminated to moderately contaminated and as extremely contaminated and the Igeo index of Cr and Zn can be categorised as uncontaminated to strongly contaminated.

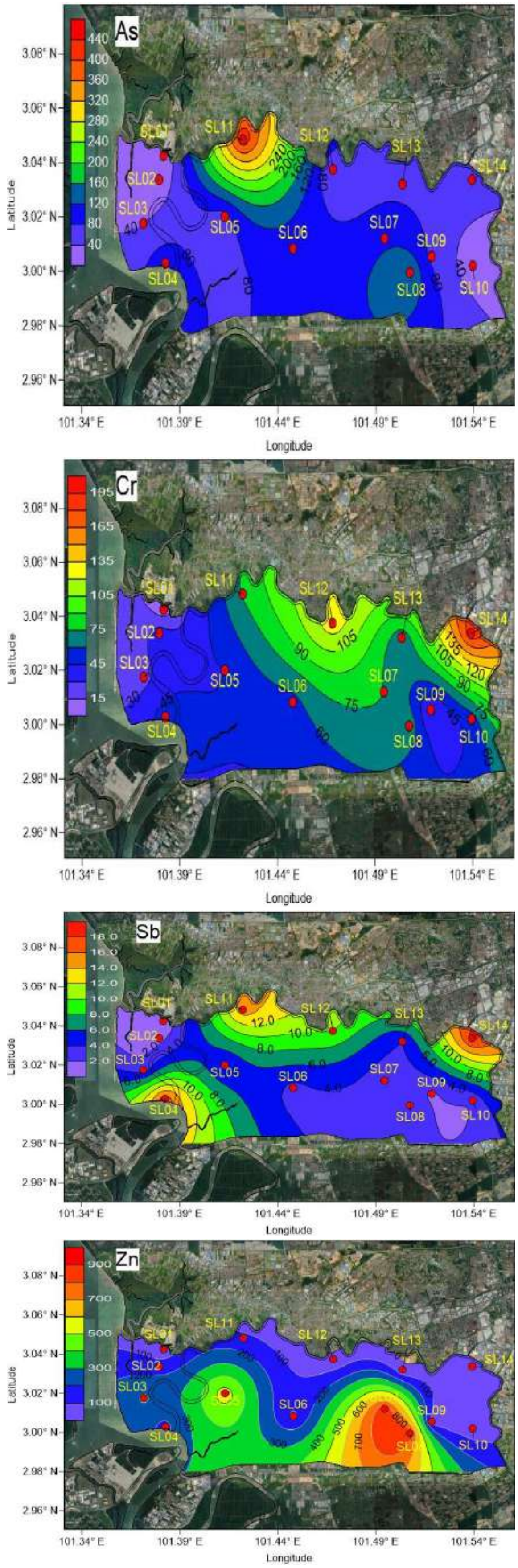

Figure 2: Distribution of heavy metals in soil (As element)

References

A. Ashraf, E. Saion, E. Gharibshahi, H. M. Kamari, C. K. Yap, M. S. Hamzah, and M. S. Elias. 2017. Distribution of trace elements in core marine sediments of Coastal East Malaysia by Instrumental Neutron Activation Analysis. *Applied Radiation and Isotopes*, 122:96 – 105.

M. S. Elias, S. Ibrahim, K. Samuding, J. A. D. Daung, N. Kantasamy, S. A. Rahman, and A. Hashim. 2020. Distribution, sources and modified degree of contamination of trace elements in Linggi estuary surface sediments, Malaysia. *Journal of Sustainability Science and Management*, 15(4):109 – 119.

Individual Research Contribution Review, 2023, 1(1): 105–106

Global Network of Isotopes in Precipitation (GNIP)

Mohamad Syahiran Bin Mustaffa
Waste Technology and Environmental Division
Malaysian Nuclear Agency
43000 Kajang, Selangor
syahiran@nm.gov.my

Abstract

The Global Network of Isotopes in Precipitation (GNIP) was initiated in 1958 by International Atomic Energy Agency (IAEA) and World Meteorological Organization (WMO), and became operational in 1961. The objective was a systematic collection of basic spatial data on the isotope content of precipitation across global scales to determine temporal and spatial variations of both environmental stable isotopes and tritium in precipitation. While the initial driver, was to monitor atmospheric thermonuclear test fallout through the determination of the radioactive hydrogen isotope (Tritium), however since the 1970s the focus changed to become observation network of stable hydrogen and oxygen isotope data for hydrological studies.

Keywords: Isotope, Precipitation, Tritium

1 Introduction

For over 50 years, GNIP has provided global isotope data for the use in hydrological studies such as water resources investigation, planning, conservation and development. Although these primary objectives remain as an important feature, over the past decade other scientific disciplines have increasing made use of this invaluable and unparalleled isotope database, including:

i. Verifying and improving atmospheric circulation models,

ii. Studying global, regional, spatial and temporal climate (climatology),

iii. Studying the interactions of water between atmosphere and biosphere, or as an input to hydrological studies (hydrology) and

iv. Providing baseline information for the authentication of commodities, ecology and for forensic purposes

The isotope data from by Malaysian Nuclear Agency, although patchy in some periods and areas, is compliant with GNIP in terms of the sampling strategy and methodology. Potential outliers in data quality have been highlighted in the attached spreadsheet; however, apart from the high d–excess and some of the tritium samples, this first evaluation did not reveal any systematic mistake or inconsistency that impeded entry into the GNIP database. Some additional meteorological data would be needed or useful to improve the record and its statistics.

1.1 Sample Measurement

Stable isotope compositions were determined for water samples and reported as δ values and denoted as ‰ or permil/per mill, which is relative to a standard of known composition (e.g., Vienna Standard Mean Ocean Water, VSMOW for δ^2H and δ^{18}O analyses). The δ values are calculated using the equation below, for example, in this case, ^{2}H:

$$\delta^2 H(‰) = \frac{R_{Sample} - R_{Standard}}{R_{Standard}} \times 1000$$

where R represents the ratio of heavy to light isotope (^{2}H/^{1}H), and R$_{Sample}$ and R$_{Standard}$ are the isotope ratios in the sample and the standard, respectively.The sample is described as depleted (more negative) if the δ values are lower, and enriched (more positive) if the δ values are higher with respect to a reference (IAEA, 1983; Clark and Fritz, 1997; Kendall and Caldwell, 1998).

2 Methods

Monthly composite precipitation samples were collected using a rain gauge, which was permanently installed by the Malaysian Nuclear Agency at all of the GNIP rainfall stations at the Malaysian Meteorological Department (Met Malaysia) state office compound together with their meteorological instruments. Stable isotopes (^{2}H and ^{18}O) and tritium (^{3}H) were measured in monthly rainwater samples collected at designated stations. The rain amount is estimated using the equation below:

$$\text{Rainfall amount}(mm) = \frac{10V}{\pi r^2}$$

where V = volume of rainwater collected (ml) and r = funnel radius (cm).

2.1 Sampling Location

As far as sampling in 2013 is concerned, initiatives taken by Malaysian Nuclear Agency constitute a laudable effort to improve GNIP coverage over Asia. The network is well designed, incorporating various climatic regimes and topographic features of peninsular Malaysia.

Currently, nine (9) active stations was installed in Peninsular Malaysia, Sabah and Sarawak for sample collection. These

Figure 1: Precipitation Totalizer (table tennis ball) Rain Gauge Collector (IAEA, 2014)

nine stations were chosen based on accessibility, the monsoon, altitude, and a crucial factor affecting the isotopic composition of precipitation, particularly in the tropics. In future there have six (6) potential stations must take to account as an additional stations for sampling.

Figure 2: Active and Additional (in future) GNIP Stations in Malaysia

3 Result and Discussion

Isotope ratios of deuterium or $^2H/^1H$ (δ^2H) and oxygen–18, $^{18}O/\ ^{16}O$ ($\delta^{18}O$) in precipitation are closely related, lying on a single line known as the Meteoric Water Line (MWL). Initially, the relationship between δ^2H and δ^{18}O in precipitation and non–marine surface waters, established from ~400 samples distributed from all over the world, is defined as:

$$\delta^2 H = 8\delta^{18}O + 10‰\text{SMOW} \qquad \text{((Craig, 1961))}$$

In Malaysia, isotope hydrology techniques were introduced in the early 1980s. The Malaysian Meteoric Water Line (MMWL) was established in 1981 with 3 rainfall stations covering only the northern part of Peninsular Malaysia. There were no stations in East Malaysia or Borneo Island. The study continued in the 1990s until mid–2000s, with irregular sampling intervals resulting in intermittent data. The number of rainfall stations also varied during the entire study period, with only 5 stations remained by the end of the study, mostly located on the upper half of Peninsular Malaysia. Overall, the Malaysian Meteoric Water Line was established as:

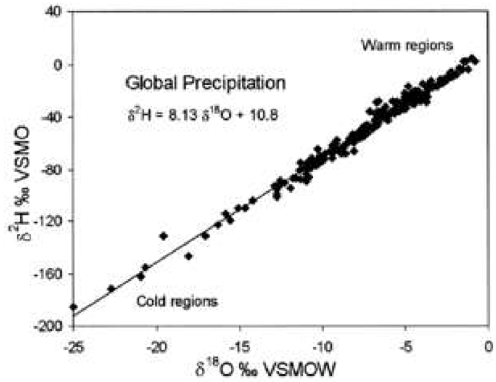

Figure 3: (Clark and Fritz, 1997) p. 37, as compiled in Rozanski et al. 1993, modified by permission of American Geophysical Union)

$$\delta^2 H = 8\delta^{18}O + 13.255 \qquad \text{((Ayub, 2006))}$$

A database containing the results from 2013 to 2021 has already been published to the IAEA Wiser GNIP. The isotopic composition of water, the deuterium excess, the sources and transport of precipitation, the characteristic of precipitation isotopes, seasonal and temporal variations, and their applications will all be discuss further in this research project.

4 Conclusion

The current demand to close the knowledge gaps in isotope hydrology research in Malaysia is fueled by the study's results, which were motivated by the need for a database of δ^2H, δ^{18}O of precipitation and local meteoric water lines. In addition to the database, this study effectively identified the meteorological and environmental components that influence local and regional climates.

References

M.S. Ayub. 2006. Malaysian meteoric water line. *MINT R&D Seminar. Bangi, Malaysia.*

I.D. Clark and P. Fritz. 1997. Environmental isotopes in hydrology. *Lewis Publishers, New York.*

H. Craig. 1961. Isotopic variations in meteoric waters. *Science*, 133:1702 – 1703. https://doi.org/10.1126/science.133.3465.17 02.

IAEA. 1983. Reference and intercomparison materials for stable isotopes and light elements. IAEA-TECDOC-825. https://www-pub.iaea.org/MTCD/Publications/PDF/te_825_prn.pdf.

IAEA. 2014. IAEA/GNIP precipitation sampling guide. IAEA, Vienna.

C. Kendall and E.A. Caldwell. 1998. Fundamentals of isotope geochemistry. pages In: Kendall C, McDonnell JJ (eds) Isotope Tracers in Catchment Hydrology. Elsevier, Amsterdam.

Individual Research Contribution Review, 2023, 1(1): 107–108

Determination of Natural Radionuclides (NORM) and Heavy Metal Elements Concentration with an Assessment of Absorbed Dose and Radiation Hazard Index from Soil Around Sembrong, Catchment Area, Johor

Mohd Izwan Bin Abdul Adziz
Waste Technology and Environmental Division,
Malaysian Nuclear Agency
43000 Kajang, Selangor
izwan@nm.gov.my

Abstract

Sources of natural radioactive material contribute to radiation exposure to humans and the environment. The increase in natural radioactive material, especially in the soil, needs to be given attention, as it is one of the routes of exposure to humans and communities. Continuous research and monitoring are done on the distribution and determination of these natural radionuclides activity as a guide and reference and are very useful, especially in an accidental exposure. Surface soil samples from several locations that have been identified around the Sembrong Dam water catchment area were taken for the study. Measurements of radioactive concentrations in soil samples were performed using a gamma spectrometer counting system equipped with a HPGe detector.

Keywords: Gamma Spectrometer, Soil, Natural Radioactive Material, HPGe detector, Catchment Area.

1 Introduction

This research project is one of the sub-projects aimed at supporting the implementation of the main project, namely the IAEA/RCA RAS/5/084 Project "Assessing and Improving Soil and Water Quality to Minimize Land Degradation and Enhance Crop Productivity Using Nuclear Techniques." The project was conducted from June 2019 to June 2022 (36 months). This study is an initiative by project members to develop a baseline data that can be used as a reference for determining the current conditions or status of the concentration of naturally occurring radioactive material (NORM) and heavy metal concentrations in the study area, specifically around the water catchment area in Sembrong, Johor Darul Takzim. Furthermore, the development of this database also includes data across various parameters for the determination of the Radiation Hazard Index in the study area. This research project builds upon the success of previous phases (phase 1) conducted in the Timah Tasoh reservoir area, Perlis, specifically funded under the RMK-10 special fund (PKA0514D003). The continuation is planned for phase 3 (Kuala Selangor Nature Park) and phase 4 (Kemaman, Terengganu) in the upcoming stages.

The objectives of this research project are:

i. To determine the concentration and distribution of naturally occurring radioactive materials (NORM) such as ^{238}U, ^{232}Th, ^{40}K, ^{226}Ra, and ^{228}Ra, as well as several trace metals in soil and sediment samples collected in the study area.

ii. To determine the radiation hazard index in the surrounding areas of the study.

iii. To generate maps depicting the concentration of NORM radioactive activity and exposure dose rates in the study area.

2 Methods

Sampling was carried out twice: once during the rainy season in December 2019 and again during the dry season in September 2020. This involved various areas surrounding the Sembrong water catchment. In total, 144 soil and sediment samples were collected from 12 sampling stations. The collected samples were transported to the laboratory, where they underwent processing and analyze using Gamma Spectrometry with a calibrated HPGe detector. For the determination of heavy metal concentrations, analysis was conducted using WD-XRF. The parameters of the Radiation Hazard Index were calculated using a recognized and established formula (Adziz and Khoo, 2018).

Figure 1: Study area map indicating the positions of 12 sampling stations

3 Results

The results obtained showed that the radioactivity concentration of ^{238}U ranged between 17.83 - 31.80 Bq/kg, ^{232}Th ranged between 23.18 - 40.64 Bq/kg, ^{226}Ra ranged between 20.09 -

32.80 Bq/kg, ^{228}Ra ranged between 21.20 - 38.88 Bq/kg and ^{40}K ranged between 9.11-51.39 Bq/kg with average values of 21.45 Bq/kg, 28.17 Bq/kg, 24.00 Bq/kg, 27.43 Bq/kg and 24.01 Bq/kg respectively. These obtained values are low compared to the world average values and the values of globally applied standards (UNSCEAR, 2000). It was found that the concentration of Manganese (Mn) was high compare to other trace elements for each sampling station with the highest value being at 430ppm at sampling station S12.

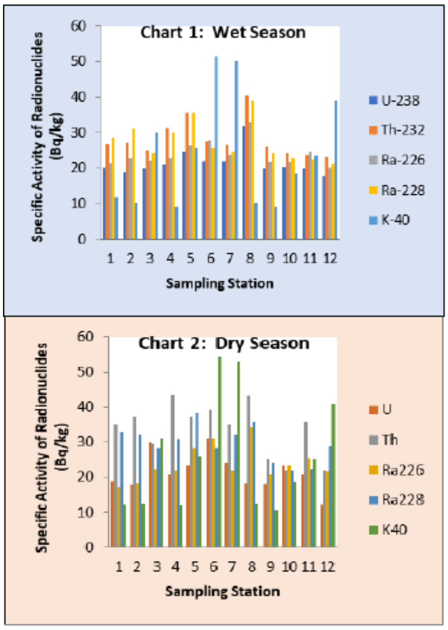

Figure 2: The concentration of specific radionuclide activity (Bq/kg) in soil samples for two seasons in the study area.

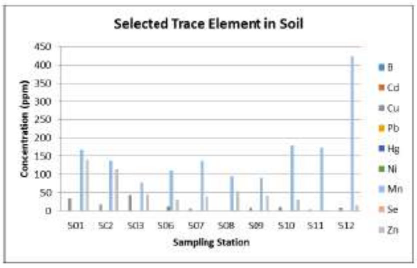

Figure 3: The concentration of several metals (trace elements) in soil samples in the study area.

The mean/mean values obtained for the four parameters of the Radiation Hazard Index, namely radium equivalent activity (Ra_{eq}), external dose rate (D), annual effective dose and external hazard index (H_{ex}) were 66.37 Bq/kg, 29.13 nGy/h, 20.16 10^{-6}Sv and 0.18 respectively.

4 Discussions/Conclusion

The study shows that the radioactivity in the area is low, similar to global averages and specific places in Malaysia. The radiation hazard index values are also low compared to global standards and some areas in Malaysia (Saffuwan et al.,

Samples	Specific activity of radionuclides (Bq/kg)				Reference
	^{238}U	^{226}Ra	^{232}Th	^{40}K	
Sembrong, Johor	**21 (17.83 – 31.80)**	**24 (20.09 – 32.80)**	**28 (23.18 – 40.64)**	**24 (9.11 – 51.39)**	*Present study*
Repository Facility, Bukit Kledang, Perak	-	21	33	21	Adziz, M. I. & Khoo, K. S 2017
Kinta District, Perak	12–426	-	246	-	Lee *et al.* 2007
Pulau Pinang	-	64 - 799	16 - 667	-	Almayahi *et al.*, 2012
Dengkil, Selangor	31.64 – 449.15	-	27 - 103	-	Yasir, S. M. *et al.*, 2007
Malaysia	66	67	82	310	UNSCEAR Report, 2000
Bangladesh	-	34	-	350	
Thailand	114	48	40	400	
Japan	29	33	28	310	
China	33	32	41	440	
India	29	29	64	400	
Egypt	37	17	18	320	
Iran (Islamic Rep. of)	-	28	22	640	
Belgium	-	26	27	380	
Denmark	-	17	19	460	
Switzerland	40	40	25	370	
Spain	-	32	33	470	
Argentina	-	-	-	650	
United States		40	35	370	
Worldwide mean	35	33	36	474	

Sampling Station	Radiation Hazard Index				References
	Radium Equivalent Activity (Bq/kg)	External Dose Rate (nGy/j)	Annual Effective Dose (10^{-6} Sv)	External Hazard Index	
Sembrong Catchment Area, Johor.	66.37 (56.23 – 91.70)	29.13 (24.46 – 40.13)	20.16 (17.15 – 28.53)	0.18 (0.15 – 0.25)	Present study
Repository Facility, Bukit Kledang, Perak.	68.74 (44.70 – 89.87)	30.03 (19.46 – 39.69)	36.91 (23.87 – 48.68)	0.18 (0.12 – 0.24)	Adziz, M. I. & Khoo, K. S. 2018.
LYNAS Rare-earth Procecing Plant, Gebeng, Pahang.	139.6 (19.00 – 335.9)	64.2 (8.6 – 157.1)	-	0.39 (0.05 – 0.94)	W.M. Zal U'Yun et al., 2017.
Worldwide, UNSCEAR	-	57.0 (18.00 – 93.00)	-	-	UNSCEAR Report, 2000 [13]
Worldwide, UNSCEAR	370	-	-	-	UNSCEAR Report, 1982 [12]
Worldwide	-	-	480	-	Saffuwan et al., 2015 [7]
Worldwide (Unity Value)	-	-	-	<1.0	Krieger, 1981 [17]

Figure 4: Comparison of the average specific radionuclide activity and radiation hazard index in the study area with other locations in Peninsular Malaysia and globally.

2015). It was discovered that the Mn concentration stood out among other trace elements at every sampling station, with the highest recorded value of 430ppm at station S12.

References

M. I. A. Adziz and K.S. Khoo. 2018. An assessment of absorbed dose and radiation hazard index from soil around repository facility at Bukit Kledang, Perak, Malaysia. *IOP Conf. Ser.: Mater. Sci. Eng.*, 298(012001).

M. J. Saffuwan, A. A. T. Saiful, and E. Zaidi. 2015. The gamma dose assessment and pH correlation for various soil types at Batu Pahat and Kluang districts, Johor. AIP Conference Proceedings (iNUSTEC 2015).

UNSCEAR. 2000. Radiation sources and effects of ionizing radiation. New York: United Nations Scientific Committee on the Effect of Atomic Radiation.

Individual Research Contribution Review, 2023, 1(1): 109–110

Using Stable and Radioactive Isotopes to Assess Hydrological Connectivity on Freshwater Wetland Lakes, River Systems and Shallow Groundwater Source

Mohd Muzamil Bin Mohd Hashim
Waste Technology and Environmental Division
Malaysian Nuclear Agency
43000 Kajang, Selangor
muzamil@nm.gov.my

Abstract

A study was carried out at the Paya Indah Wetland in Dengkil, Selangor, by using stable and radioactive isotopes. The primary goal of this study was to assess the wetland area's hydrological connectivity to water sources. Throughout the dry and wet seasons, a series of sampling activities were carried out to collect the surface water, groundwater, and precipitation. The stable isotope results indicate that the compositions of the surface and groundwater were close to the meteoric water line (LMWL). This implies that precipitation is the primary source of groundwater in the Paya Indah Wetlands.

Keywords: Isotope, Hydrology, Wetland

1 Introduction

The effects of climate damage can be found in all parts of the world and no country is immune from the impacts of climate change. The expected changes shall be reflected in higher temperatures, widespread changes in precipitation patterns, increased risk of drought, rising ocean levels, and increased frequency of bad weather. Water isotope data can be used for atmospheric circulation model development, calibration and validation (Stadnyk et al., 2013; Gibson et al., 2021). The analysis of water and environmental isotope variabilities offers fundamental information for hydrological and environmental investigations (Shamsuddin et al., 2018; Syakir et al., 2018). Commonly used stable isotopes (H-2, 0-18 and C-13) and radioactive isotopes (H-3 and C-14) in water have their own advantage for fingerprinting and trace water origin, age, flow, transport, and the complex hydrological mechanism involving water sustainability, quantity and quality.

2 Objectives

The objectives of this project are to map the spatio-temporal variability of water isotopes (stable and radioactive) composition and hydrochemical pattern in rivers, lakes, and shallow groundwater sources over multiple seasons and years and to formulate an improved conceptual understanding of the hydrological processes, sources, interaction and pathways in groundwater systems and linked wetlands based on the isotopic signatures.

3 Study Location

The project was conducted at the Paya Indah Wetlands. Paya Indah Wetland is his 450.76-hectare Wetland Reserve and Recreational Park in Dengkil District, Selangor, Malaysia. The Paya Indah Wetlands has 11 lakes and consists of tin mining degraded lakes, cleared peat swamp forests and large open lakes. The rest of the land is dominated by a variety of plant species, most of which are planted as part of wetlands reserve management and corporate social responsibility efforts to restore the wetlands. This wetland is managed by the Malaysian Wildlife and National Parks Authority.

Figure 1: The study area located at Paya Indah Wetlands, Dengkil, Selangor.

4 Methods

Integration of conventional hydrogeological techniques, stable isotopes (H-2, 0-18 and C-13) and radioactive isotopes (H-3 and C-14) will be applied in field and laboratory-based experiments. Paya Indah Wetland has been chosen as the pilot site for this research study. The field-based experiment will consist of geophysical application, GIS and on-site physical parameters to determine large scale information on the surface and subsurface materials. In the laboratory experiments, water samples will be collected and analysed on their isotope signature and chemical characteristics using IRMS, ICP-MS, liquid water isotope analyser (LWIA), tritium enrichment system, Direct CO_2 absorption method, LSC and WD-XRF. Sampling for surface water, groundwater and rainwater will be carried out during the dry and wet seasons. Lake or pond water samples will be collected at several depths below the surface using a water sampler, groundwater samples will be obtained at the identified tubewell in the wetland and vicinity area. Rainwater samples were collected every month using a rainwater collector which was installed permanently in the wetland area.

5 Result

Stable isotopes (^{18}O and ^{2}H) and physical characteristics of water samples were obtained from the analysis of stable isotopes in the laboratory and in-situ measurements at the sampling locations. Two sets of data (dry season and wet season) were used to identify the seasonal effects on the isotope ratio of water and the physical characteristics of the water in the wetland area.

A local meteoric water line (LMWL), which serves as a reference line, was generated from the local precipitation isotopic values. The nearest GNIP (Precipitation Global Network) Station is 20 km from Paya Indah Wetlands. The GNIP station is located at the Malaysian Nuclear Agency. LWML: δ^2H=7.66x + 8.91 is a least-squares method generated from annual precipitation isotope data in the GNIP database.

For the dry seasons, the δ^2H and δ^{18}O ratio in surface water ranged from –46.70 to –27.00‰ and from –6.31 to –3.67‰, respectively. The δ^2H and δ^{18}O in groundwater ranged from –48.3 to –35.3‰ and from –7.35 to –5.23‰ respectively. Surface water's δ^2H and δ^{18}O ratios during the wet season varied from 56.10 to -33.70‰ and 7.85 to -3.17‰, respectively. The ranges of δ^2H and δ^{18}O for the groundwater samples were, respectively, -58.5 to -35.0‰ and -8.39 to -4.86‰.

Physical parameter data show that groundwater and surface water temperatures for the dry and wet seasons, respectively, ranged from 26.24 to 31.13°C and 24.53 to 34.38°C. For the dry season and rainy season, respectively, the pH ranges of surface water and groundwater were 5.21 to 7.75°C and 4.75 to 7.62°C. For the dry season and the wet season, respectively, the conductivity values of surface water and groundwater ranged from 10 to 3681 μS/cm and 27 to 1287 μS/cm. A significant difference appears in the conductivity values. The dry season values for two groundwater samples (MW03 and BKLT10) are 3681 and 2311 μS/cm respectively. On the other hand, the wet season values for two groundwater samples (MW03 and BKLT10) are 1009 μS/cm and 1287 μS/cm, respectively.

6 Discussion

The isotopic data shows that the isotope ratio of δ^2H and δ^{18}O was more enriched in the dry season and more depleted in the wet season. The comparison of the compositions of δ^2H and δ^{18}O isotopes for the surface water and groundwater revealed that the δ^2H and δ^{18}O isotopes from the surface water and groundwater water had compositions that were close to the meteoric water lines (LMWL). This means that the source of the groundwater in the Paya Indah Wetlands is mainly from the rainwater.

7 Conclusions

The use of stable and radioactive isotopes in this project was successfully applied to identify hydrological connections between surface water and groundwater in the Paya Indah Wetlands area.

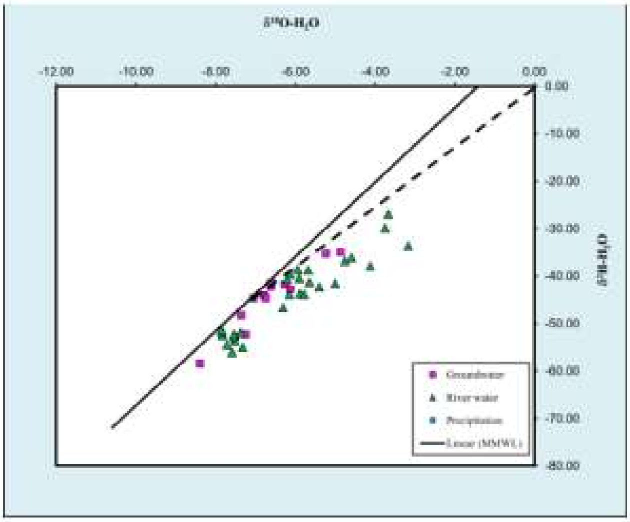

Figure 2: Stable isotope signatures of water samples taken during the wet season and the dry season.

References

J.J. Gibson, T. Holmes, T.A. Stadnyk, S.J. Birks, P. Eby, and A. Pietroniro. 2021. Isotopic constraints on water balance and evapotranspiration partitioning in gauged watersheds across Canada. *Journal of Hydrology*, Regional Studies(37):https://doi.org/10.1016/j.ejrh.2021.100878.

M.K.N. Shamsuddin, W.N.A. Sulaiman, M.F. Ramli, F.M. Kusin, and K. Samuding. 2018. Assessments of seasonal groundwater recharge and discharge using environmental stable isotopes at Lower Muda River Basin, Malaysia. *Applied Water Science*, 8:120. https://doi.org/10.l007/sl3201–018– 0767–x.

T.A. Stadnyk, C. Delavau, N. Kouwen, and T.W.D. Edwards. 2013. Towards hydrological model calibration and validation: Simulation of stable water isotopes using the isoWATFLOOD model. *Hydro!*, Processes(27):3791 – 3810.

M. I. Syakir, N. S. Jamian, M.H. Jaafar, and et al. 2018. A review of environmental isotopes: Its prospective applications in disaster-risk management of watershed. *J. Phys. Sci.*, 29(3):121 – 147. https://doi.org/10.213l5/jps2018.29.3.l0.

Individual Research Contribution Review, 2023, 1(1): 111–112

Global Radium-226 Management Initiative

Mohd Zaidi Ibrahim
Waste Technology and Environmental Division
Malaysian Nuclear Agency
43000 Kajang, Selangor
mohd_zaidi@nm.gov.my

Abstract

Malaysia joining Global Radium-226 Management Initiative as a provider country with the objective to send out legacy ^{226}Ra to recipient country for reprocessing with zero cost to Malaysia. Justification - not having Ra-226 or final disposal of Ra-226. This initiative gives opportunities to Malaysia to eliminates a waste liability at no cost and at the same time contributes to global healthcare. Implementation will be conducted through collaboration agreement between Malaysian Nuclear Agency (Nuklear Malaysia) and Canadian Nuclear Laboratories (CNL).

Keywords: Radium-226, global management

1 Introduction

Many countries have legacy stocks of ^{226}Ra, which may present a long-term management challenge for some of them. The IAEA understands this challenge presented by long-lived radionuclides and continues to seek suitable solutions for the stored legacy ^{226}Ra. Conversely, several countries may have a use for such legacy ^{226}Ra stocks, particularly, in the field of targeted alpha therapy in nuclear medicine. The treatment of cancer cells through the application of radiotracers with ^{225}Ac shows very promising results, and using ^{226}Ra as a feedstock material is an effective production route for the ^{225}Ac.

Considering the above, the IAEA coordinate an activity focusing on ^{226}Ra recycling referred as the "Global Radium-226 Management Initiative". In the frame of this initiative, a platform to facilitate information exchange between countries possessing legacy ^{226}Ra sources and countries with capabilities and suitable recycling facilities is being established. In this context, the IAEA ready to assist the safe and secure transport of ^{226}Ra sources from its holder to the recipient country.

2 Methods

This project or activities will be implemented in three (3) phases as follows:

2.1 Phase 1 - Contracting

a) Malaysia will dismantle and send CNL a list of dismantled Ra-226 sources in full details.

b) CNL will send draft template nondisclosure for review by Nuklear Malaysia.

c) Nuklear Malaysia will sign NDA for information sharing by CNL.

d) CNL will send draft template contract for review by Nuklear Malaysia and Ministry's Legal Advisor.

e) Declaration participation in Global Ra-226 Initiative as undertaking letter will be provided to regulatory body.

f) Contract will be sent to the Ministry or Cabinet Approval.

g) Contract signing between Nuklear Malaysia and CNL.

h) Finalized the list under the project after visit by CNL and communication with regulatory body.

2.2 Phase 2 - Preplanning

a) CNL will send procedures to Nuklear Malaysia.

b) CNL advance team site visit.

c) Updating the statement of ownership.

d) CNL apply for import permit.

e) Nuklear Malaysia apply for export permit.

2.3 Phase 3 – Execution

a) CNL deliver shipping containers to Nuklear Malaysia.

b) Local packaging operations by CNL.

c) Shipping the packages to CNL.

d) CNL and Nuklear Malaysia updating the statement of ownership.

3 Results

A few virtual meetings between Nuklear Malaysia and CNL have been conducted to carried out this project.

Malaysia was sent CNL a list of conditioned Ra-226 sources full details including the activities. CNL was sent draft template nondisclosure agreement (NDA) for review by Nuklear Malaysia, and the NDA was sign by the person in charge of this project from Nuklear Malaysia.

Currently, CNL was sent a draft template contract for review by Nuklear Malasyia. The contract was sent to Ministry's Legal Advisor for review and bring up to minister OR Cabinet for approval.

Nuklear Malaysia was sent an undertaking letter to the regulatory body as a declaration for Malaysia participation in

Global Ra-226 Initiative and as a letter of intent to send out ^{226}Ra from Malaysia to Canada.

The rest of activities will be carried out after agreement signed by Nuklear Malaysia and CNL. And currently both parties are waiting for approval from the Ministry of Cabinet.

4 Discussion/Conclusions

Global management Radium-226 initiative can consider as pilot project for send out DSRS to other country for reprocessing. Beside eliminating a waste liability and contributes to global healthcare, this project also will establish the procedure for export of DSRS to other country for reprocessing.

References

Richard Dufour and Peter D'Amico. 2023. Turning waste into medicine: International Radium 226 Turnkey Recovery Program. Canadian national Laboratories. *A presentation to Nuklear Malaysia*.

EVT2205305. 2023. Technical Meeting on the Global Radium-226 Management Initiative. IAEA's Headquarters, Vienna, Austria, from 5 to 9 June 2023.

Mohd Zaidi Ibrahim. Global Radium-226 management initiative. *A presentation to Nuklear Malaysia's Top Management*.

Individual Research Contribution Review, 2023, 1(1): 113–114

Implementation of Borehole Disposal of Disused Sealed Radioactive Sources System (BOSS) in Malaysia

Mohd Zaidi Ibrahim
Waste Technology and Environmental Division
Malaysian Nuclear Agency
43000 Kajang, Selangor
mohd_zaidi@nm.gov.my

Abstract

Implementation of BOSS has started on early Jan 2022 after Triparted Agreement between Malaysia Nuclear Agency, International Atomic Energy Agency (IAEA) and Groundwater Solutions Sdn. Bhd. enter into force on December 30, 2021. Implementation can be divided into dismantling of disused sealed radioactive sources (DSRS), waste package preparation (conditioning), sealing of 2 investigation boreholes, construction of disposal borehole, disposal of waste packages, borehole closure and licensing process. But this article only covers the scope from dismantling up to installation of disposal borehole casing (part of borehole construction process).

Keywords: Borehole, DSRS, Disposal

1 Introduction

The borehole disposal of disused sealed radioactive sources system (BOSS) is a detailed, engineering level system which allows the safe and permanent disposal of disused sealed radioactive sources (DSRSs) in specially created boreholes. BOSS has been developed as part of the IAEA/AFRA project and is intended for use in countries that own DSRSs, but do not have the necessary infrastructure to manage them.

The BOSS is a solution to the problem of DSRS that are too long lived for decay storage and yet cannot be returned to their manufacturer. Malaysia is the first country in the world to implement the BOSS for disposal DSRS categories 3 to 5.

2 Methods

The implementation of BOSS involves the activities of DSRS dismantling, preparation of waste packages (conditioning), construction of boreholes, disposal of waste packages, closure of boreholes and post-disposal monitoring. LEM/TEK/72, Guideline for Licence Application for Radioactive Waste Disposal Facilities (Borehole Disposal) is the main document that has been followed while carrying out these activities.

Dismantling of DSRS and waste package preparation was carried out in accordance with the procedures for the recovering, conditioning, containerization and disposal of low activity disused sealed radioactive sources in a borehole disposal facility using the Mobile Tool Kit Facility (IAEA, 2016).

Borehole construction was carried out in accordance with the Statement of Work - Construction of a Disposal Borehole for Disused Sealed Radioactive Sources in Malaysia (IAEA, 2018) and Method Statement - Construction of A Disposal Borehole for Disused Sealed Radioactive Sources in Malaysia (GWS, 2021). Borehole closure also will be carried out in accordance with the documents. Sealing of investigations and failed boreholes at the site were carried out in accordance with the guideline JMG.GP.27 from Mineral and Geoscience Department Malaysia (JMG, 2020).

Disposal of waste packages will be carried out accordance with disposal procedures that will be established by IAEA experts during disposal training for operators.

Post disposal monitoring program will be carried out in accordance with the Environmental Monitoring Plan for Borehole Disposal Facility (Malaysia, 2015).

3 Results

3.1 Dismantling of DSRS and waste package preparation

Figure 1: DSRS conditioning using MTKF.

As many as 12,894 units of DSRS with total activities 25.6 Ci have been dismantled and conditioned in 42 units of waste package. The activity for the waste packages ranged from 0.69 μCi to 7.79 Ci. The DSRSs have been conditioned in according to the type of radionuclides, but a few units of the waste packages containing mixtures of radionuclides (Figure 2).

The waste packages are temporarily store in storage facility until the borehole ready for disposal.

Figure 2: Waste packages for disposal in borehole.

3.2 Borehole construction

Two (2) unit of investigation borehole was successfully sealed before borehole drilling started. First two attempt to drill a borehole were failed and the boreholes ware sealed with compacted native soils. A borehole with 180 m depth successful drilled on the third attempt. HDPE casing was successfully installed until 176 m depth. The liner was grouted until 114 m depth. Several attempts to remove water inside the casing have failed due to deformation of the HDPE casing.

Figure 3: Borehole construction using Foremost Dual Rotary DR 24 mounted drilling rig truck.

4 Conclusion

4.1 Dismantling of DSRS and waste package preparation

Dismantling of DSRS category 3 to 5 can be conducted in existing conditioning room. While Mobile Tools Kit Facility (MTKF) provide tools, equipment, and safe space for the workers to conduct conditioning proses for DSRS with activity up to a few curries. The process was successfully conducted without any issue or accident involving physical injuries or overdose exposure to radiation.

4.2 Borehole construction

A borehole was successfully constructed until installation of HDPE casing stage, but the final stage could not be continued until now due to technical problem. Specification of this actual borehole is slightly different with the proposed design and its construction take much longer than planned timeline due to the technical problems during construction. These results suggest that the borehole design and the construction procedure need to be review again to overcome the issues during the construction. Lithology of the site, such as type of rock, availability of groundwater, etc., need to be consider during design of the borehole and development of drilling procedure. The siting process should also consider issues and limitations related to borehole construction as site selection criteria.

References

AELB. 2016. Guideline for licence application for radioactive waste disposal facilities (Borehole disposal). LEM/TEK/72.

GWS. 2021. Method statement - Construction of a disposal borehole for disused sealed radioactive sources in Malaysia. Groundwater Solution Sdn. Bhd.

IAEA. 2016. Procedures for the recovering, conditioning, containerization and disposal of low activity disused sealed radioactive sources in a borehole disposal facility using the Mobile Tool Kit Facility. Ver. 1, October 2016.

IAEA. 2018. Statement of work - Construction of a disposal borehole for disused sealed radioactive sources in Malaysia.

JMG. 2020. Garis panduan pembinaan telaga tiub untuk tujuan eksplorasi, pemantauan dan pengeluaran dalam penggunaan sumber air bawah tanah. *Jabatan Mineral dan Geosains Malaysia*, JMG.GP.27.

Nuklear Malaysia. 2015. Environmental monitoring plan for borehole disposal facility. *Malaysia Nuclear Agency, April 2015.*

LEXSYG SMART- Thermoluminescence Optically Stimulated Luminescence (TL OSL) Reader at Nuclear Dating Laboratory, Malaysia Nuclear Agency

Mohd Zuhair Mohd Sanusi
Waste Technology and Environmental Division
Malaysian Nuclear Agency
43000 Kajang, Selangor
zuhair@nm.gov.my

Abstract

LEXSYG SMART is an advance Thermoluminescence Optically Stimulated Luminescence (TL OSL) reader for dating in application of variety of fields. The main advantage of this reader is it can perform luminescence measurement up to 40 sample at once. In addition, this reader is equipped with an irradiation source, which has high activity. The Beta sources with an activity 1.85 GBq delivery dose rate range 120 mGy/s are placed on reader. For thermal luminescence stimulation (TL) a plated ceramic contact heater reaching up to 700°C is implement to this reader. Optical stimulation can be achieved by equipped laser diode/LED which has different wavelength such as infrared, violet and blue in range of 400-950 nm. Thus, LEXSYG SMART provide added value on the development of dating technique for crystal mineral sample based such as ceramic, rock and sediment.

Keywords: Thermoluminescence, Optical Stimulated Luminescence, LEXSYG SMART

1 Introduction

Nuclear Dating Laboratory located at Malaysian Nuclear Agency aims to conduct a study on dating mineral based material. This laboratory is located at Block 19 under the supervision of Radiochemistry and Environment Group (RAS), Waste Technology and Environmental Division (BAS).

This laboratory is established in 1983 via collaboration between Isotope Hydrology Unit with International Atomic Energy Agency (IAEA), Australian Atomic Energy Commission (AAEC) and Pusat Penyelidikan Atom Tun Ismail (PUSPATI). In 2003, BAS took over this laboratory after being advised by the management. Due to several critical problems regarding the equipment, the laboratory cannot fully function in order to provide archaeology dating service. Therefore, further initiative was taken to redevelop this laboratory under Malaysia Development Plan 11 (RMK-11) RP4 2020 (Abdullah et al., 2021). The budget allocation was used to purchase advance thermoluminescence (TL) Optically Stimulated Luminescence (OSL) reader from Freiburg, Germany and the reader was fully installed in November 2021. All basic training was successfully conducted in December 2021 to meet the scope of human capital development under this budget. This article aims to discuss the technical aspect related to LEXSYG SMART reader.

2 The Advance LEXSYG SMART

The advance LEXSYG SMART reader is the combination TL and OSL for luminescence measurement. This combination can provide advantages in the application of dating minerals. This reader system is very sensitive to changes, up to several millimetre scale through depthluminescence profile (Ageby et al., 2022). Thus, the reader can provide dating age from 100 years up to 200,000 years or even older with precision range 5-10% (Feathers, 2008). In addition, this reader only requires small aliquot sample in preservation of archaeology material (Brill and Tamura, 2020). Therefore, the advantages this reader can be fully utilise to perform luminescence measurement in the nuclear dating laboratory.

3 Component of LEXSYG SMART System

LEXSYG SMART is developed by Freiburg Instrument. It is used to determine luminescence profile efficiently for a large number of samples. The sample wheel in the reader can run the measurement up to 40 sample simultaneously. This factor considered as an advantage in terms of time saving and efficient.

3.1 Radiation Source

LEXSYG SMART reader is capable to execute variety protocol in luminescence measurement. Among the crucial procedure in SAR protocol is the irradiation of sample to ionizing radiation. Therefore, this reader is equipped with a beta radiation source for absorbed dose purposes. The beta source itself have been stored in radiation source module. It is fixed permanently and only movement of shutter for function of irradiation. The main objective of this concept is for accuracy of radiation dose applied to sample. The technical specification of the beta sources is shown in Table 1.

Table 1: Technical aspect on irradiation source.

Technical Aspect	Specification
Type of radiation	Beta
Radioisotope	Strontium-90 (Sr-90)
Activity	1.85 GBq
Form	Sealed (302 capsule)
Factory	Eckert & Ziegler Nuclide GmbH

3.2 Thermal stimulation

The reader is equipped with heating ceramic plat for thermal stimulation. The heating ceramic plate on the reader can reach a temperature operational up to 700°C. The advantage of this heating plate is to allow the sample to gain thermal stimulation homogenously, repeatably and definitively. A part of the main concern in stimulation is to ensure the heating from plat necessity to penetrate sample in disc approximately 0.5 mm thickness. However, disc sample is a heat conductor because it is made up of aluminium and stainless steel. Thus, it is allowed a stable heating to sample in order to assure the stimulation consistently.

3.3 Optical stimulation

LEXSYG SMART reader system is equipped with an OSL stimulation for optical stimulation. It is consisting of several unit of variance wavelength that acquire the usage up to three difference wavelengths as a choice either LED or laser diode. The optical stimulation unit incorporate of a total 15 LED/laser diode position that execution as optical source to implement a high unity of light excitation. All these optical stimulations are presented in Table 2.

Table 2: The optical stimulation including variance of wavelength and type.

Colour	**Wavelength (nm)**	Type
Blue	445/458	Laser diode/LED
Green	525	LED
Yellow	590	LED
Infrared	850	Laser diode/LED
Violet	405	Laser diode

4 Conclusion

The LEXSYG SMART reader system is an advance tool for luminescence measurement. This is due to numerous advantages in technical aspect. The major component has higher activity of radiation sources about 1.85 GBq. The equipped of heating plat is capable to generate an operational temperature up to 700°C and variance of wavelength of OSL stimulation ranging 400 to 950 nm in order to accomplish required thermal and optical stimulation. Thus, existence of this advance TL OSL reader is adequate to develop dating technique at Malaysia Nuclear Agency for sample such as ceramic, rock and sediments.

References

N. Abdullah, N.@Muhammad Mohamed, M.Z. Mohd Sanusi, Salahuddin Muhamad, M.N. Sawon, M.T. Ishak, and M.I.M. Ramli. 2021. Pembangunan aliran sintesis benzena di Makmal Tentu Umur Radiokarbon, Agensi Nuklear Malaysia. *Seminar NTC 2021, Bangi, Selangor, 26 – 28 Oktober 2021*.

L. Ageby, D. E. Angelucci, D. Brill, F. Carrer, H. Brückner, and N. Klasen. 2022. Dating drystone walls with rock surface luminescence: A case study from the Italian Alps. *Journal of Archaeological Science*, 144:105625.

D. Brill and T. Tamura. 2020. Chapter 32 - Optically stimulated luminescence dating of tsunami and storm deposits. In M. Engel, J. Pilarczyk, S. M. May, D. Brill, E. Garrett (Eds.),. *Geological Records of Tsunamis and Other Extreme Waves*, pages 705 – 727. Elsevier.

J. Feathers. 2008. LUMINESCENCE DATING. In D. M. Pearsall (Ed.),. *Encyclopedia of Archaeology*, pages 1590–1592. Academic Press.

Study on Heavy Metals and Trace Elements Distribution Around Heavy Industries in Klang Valley

Muhammad Azfar Azman
Waste Technology and Environmental Division,
Malaysian Nuclear Agency
43000 Kajang, Selangor
m_azfar@nm.gov.my

Abstract

Anthropogenic activities are one of the main contributing on environment and health issues in populated areas especially in or near heavy industries in Klang Valley. This study were focus on to determine actinides, heavy metals and rare earth elements distributed in the soils and crop samples using Neutron Activation Analysis technique.

Keywords: : Elemental Analysis, Heavy Metals, Neutron Activation Analysis, Environmental Analysis

1 Introduction

The Klang Valley, which is located in the state of Selangor and the Federal Territory of Kuala Lumpur in Malaysia, is one of the most densely populated regions in the country. The region is home to a range of anthropogenic activities, including urbanization, industrialization, and transportation, which have contributed to an increase in heavy metal and toxicity in the environment. In this study, the concentration of heavy and toxic elements is the main concern as it could impact on human health. Up to the total of 15 elements were analyzed in this study. The elements are consist of heavy metals and actinides (As, Cr, Sb, Th, U and Zn) and also rare earth elements (REEs) which focus on Ce, Dy, Eu, La, Lu, Nd, Sm, Tb and Yb.

2 Methods

Location for sampling were determined based on the criteria of industrial area as targeted area, near to industrial area and residential area as control area. Therefore, 34 locations have predetermined based on those criteria. Two matrices of samples were collected which is soil sample and crop sample to understand the possible intake of elements in daily life. This study used Neutron Activation Technique (NAA) technique and counted using Hyper-Pure Germanium Gamma Spectrometer. The obtained results were then calculated to get concentration of the elements.

2.1 Sample Collection

Soil samples were collected throughout multiple area in each 34 locations to get distribution of elements in the soil using an auger. Plant samples however were collected depends on the availability of the type of particular plant in the locations. In this study, the type of plants that included tapioca (pucuk ubi), lemongrass (serai) and pandan leaves.

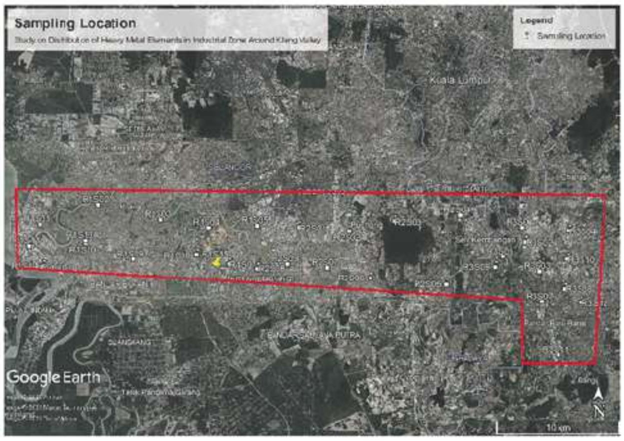

Figure 1: Sampling location throughout Klang Valley

2.2 Sample Preparation

The collected samples were cleaned and dried using an oven at 65°C until dried before ground into powder using a ball mill. Samples were then sieved using 0.2 mm sieve and were weighted approximately 0.10 g for a soil sample, while 0.50 g for flora samples. Each sample was prepared in duplicate to better analytical results. For each batch of irradiation, certified reference materials were co irradiated to get viable results.

2.3 Sample Irradiation

The samples were irradiated using the Pneumatic Transfer System of Triga Mark II Puspati Research Reactor operated at 750 kW with thermal neutron flux of about 2.0 x 10^{12} n.cm^{-2}.s^{-1}. Each polyethylene vial was inserted into each rabbit tube. The rabbit tube was then inserted into the PTS chamber before setting it off to the reactor. The travel time from the chamber to the PTS port in the reactor is 3 seconds. Each sample was irradiated for 30 seconds and was cooled down for 10 minutes behind lead brick inside the fume hood. To determine long lived radionuclide another batch of samples were irradiated for 5 hours through Rotary Rack (RR). After irradiation, samples were cooled down for 3-4 days in a lead storage container before counted

2.4 Sample Counting

For short lived radionuclides, the samples were then counted using the ORTEC HPGe detector of a high-resolution gamma spectrometry system for 5 minutes using GammaVision software. The detector has a relative efficiency of 20% with a resolution of 2.0 keV at 1332 keV. The ADC system connected to the PC analyzed the output signal from the detector. Samples were then counted the next day for 1 hour to get K, Mn and Na. For long lived radionuclide, after cooling of 3-4 days, the samples were counted using ORTEC HPGe detector for 1 hour. Samples will then later counted after 21 days since irradiation to determine long lived radionuclides.

2.5 Sample Analysis

Equation 1 shows the mathematical calculation of elemental concentrations in the sediment sample (Joel et al., 2018).

$$C_{sample} = \frac{A_{sample}}{A_{standard}} \times \frac{W_{sample}}{W_{standard}} \times C_{standrad} \quad (1)$$

where C_{sample} is the concentration of element in sample (mg/kg), A_{sample} is the net area count of an element in sediment sample, $A_{standard}$ is the net area count of an element in a standard, $W_{standard}$ is the standard weight, W_{sample} is the sediment sample weight and $C_{standard}$ is the concentration of an element in standard (mg/kg).

3 Results and Discussion

In the study, R1S02 have the highest arsenic content in soils at 417 ± 1 ppm and at the lowest in R1S12 at 3.81 ± 0.24 ppm. The reason why the As concentration is high on R1S02 is due to the villagers usage of pesticides to kill weeds on the empty field since the weeds are tall and unmanageable. R1S12 have lower concentration due to the untouched land besides the road. Cr is another main heavy and toxic elements that is the focus of this study. In soil sample, Cr at its highest in R1S05 at 196 ± 1 ppm while at its lowest in the same area at R1S12 with only 5.52 ± 0.62 ppm recorded. R1S05 are situated in Taman Sri Muda which is very near to heavy industrial zone of Hicom. Antimony (Sb) are both high in R3S08 and R3S12 which both area are near with each other where one in Sg Ramal and another one in Sg Chua around 1.2km. Sb can enter into the environment through several pathways and one of them due to smelting and combustion of coal to the air. Both area have steel industries and steel production is a highly energy-intensive process that involves the use of large amounts of coal and other fossil fuels, which can release antimony into the environment. R3S08 have high concentration of REEs in its soil which exempt the Neodymium which is lower than detection limit. Thorium are averagely less than 15 ppm which are relatively small amount in the environment but there is high concentration of Zn in R1S08 which is in AMJ Industrial Park. In that area, the sample were took at an empty field surrounded with small industries but the park are also near to heavy industries such as plastics, manufacturing, food, steel, motor and machine industries. The high concentration of Zn could be contributed from the industries. As differently as the soils sample, the concentration of the elements in the crops are drastically lower if compared to the soils. This is due to the intake of the crops are different and it only take some portion from the soils or its environments. For an instance, even though the As content in soils are high at R1S02, but the As content in Tapioca Leaves is 0.979 ± 0.036 ppm and Lemongrass is only at 0.248 ± 0.025 ppm. The highest As content in crop is in R1S10 which is pandan leaves at 2.046 ± 0.205 ppm. According to Akta Makanan 1983 (Pindaan 2010), the acceptable As content in vegetable is only at 1 ppm. This means that pandan leaves collected in R1S10 is higher than the permissible limit. Both R1S02 and R1S10 are situated at residential area which are 5 kilometers from Port Klang. It is also might be possible the usage of pesticides by the locals. Antimony (Sb) content in pandan leaves in R2S08 are also 4 times higher than the acceptable limit set by KKM which only 1 ppm. In crop samples, the highest recorded Cr level is lemongrass at R1S15 at 5.84 ± 0.02 ppm and the lowest at 0.09 ± 0.01 ppm. R1S15 situated in Taman Sepakat are near to Taman Perindustrian Bukit Kemuning. However it should be mention that there are no limitation sets for Cr in food by KKM, but European Food Safety Authority (EFSA) has established a tolerable daily intake (TDI) for chromium of 0.05 milligrams per kilogram of body weight per day (mg/kg bw/day).

4 Conclusions

As for conclusion from this study, it is known that several places have higher concentration of certain elements which could impose health risk to the human especially from food intake. From the outcome of this study, it is hopefully that this research could be a stepping stone for further research and focusing on more sampling point to generate proper mapping database for future use.

References

E. S. Joel, O. Maxwell, O. O. Adewoyin, C. O. Ehi-Eromosele, Z. Embong, and F. Oyawoye. 2018. Assessment of natural radioactivity in various commercial tiles used for building purposes in Nigeria. *MethodsX 5*, 8 – 19.https://doi.org/10.1016/J.MEX.2017.12.002.

Individual Research Contribution Review, 2023, 1(1): 119–120

Quality Control of Hardened Self-Compacting Concrete Using Non-Destructive Testing Method (NDT) for the Borehole Disposal Facility Concept in Malaysia

Muhammad Fathi Sujan
Waste Technology and Environmental Division
Malaysian Nuclear Agency
43000 Kajang, Selangor
fathi@nm.gov.my

Abstract

Borehole Disposal Concept (BDC) is a disposal facility that comprises of putting Disused Sealed Radioactive Sources (DSRS) into the waste package to more than 100m depth of borehole before covered it with a self-compacting concrete functioning as a chemical barrier and separator for the waste package. Nuclear Malaysia will do a quality control using NDT method to verify the test result based on already purchased materials, equipment, condition and disposal procedure developed with IAEA experts. Three tests were conducted to determine the compressive strength, ultrasonic pulse velocity and effect on additional water. The results indicated that concrete with 0.43 water to cement ratio has the best compressive strength. The findings also revealed that by adding additional water on the concrete mixture, it does affect the compressive strength of the concrete. It can be deduced that concrete mixture with 0.43 water to cement ratio can be used for this project and the amount of additional water in the borehole must be less than 3%.

1 Introduction

Disused Sealed Radioactive Sources are defined by International Atomic Energy Agency (IAEA) as source that are no longer used and there is no intention of using them again in the practices they were authorized for. In Malaysia, the policy for managing of DSRS only have two option which are need to be returned to the purchasing country or sent it to Nuclear Malaysia. Waste Technology Development Centre (WasTeC) is a responsible centre to manage and store radioactive waste in Malaysia and have done so since 1984. BDC have been initiated because the concern of safety and security with the increasing of DSRS volume in the Interim Storage.

Concrete is one of the important security functions for the BDC as a chemical barrier to slow down the development of corrosion to the waste package. Concrete also functioning as a separator between each waste package inside the BDC to minimize the chain reaction. Self-compacting concrete (SCC) chosen because the uniqueness of it, thanks to its excellent deformability, can be placed and compacted under its own weight without the need for any vibration effort. NDT used because it does not damage testing part or alter it in any way that would prevent it from being used again.

2 Methods

2.1 Research design

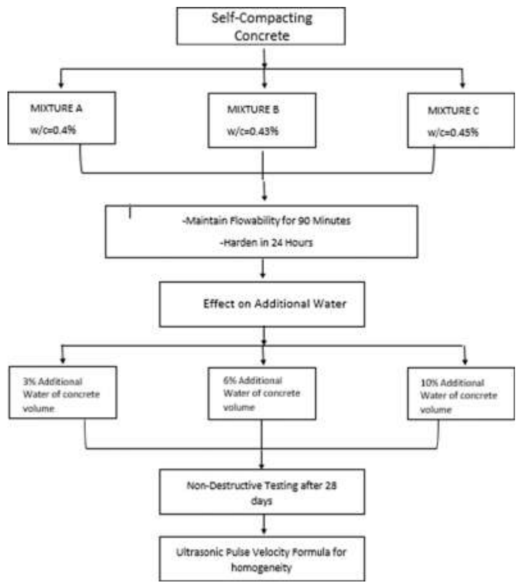

Figure 1: Overall research methodology.

2.2 Concrete Mix Design

- Stage 1: Determining the mixture for Self-Compacting Concrete.
- Stage 2: Determining the Water to Cement ratio.
- Stage 3: Determining the mixing procedure.

2.3 Composition of materials

Table 1: Weight of additional water.

Mixture	Weight of additional water (kg)
3%	0.159
6%	0.318
10%	0.530

Table 2: Composition of components used in the mixture.

Component	Content (kg/m^3)
Water	300.8
Sand	937.05
MasterGlenium629	3.008
Boric Acid	1.504
OPC	188
GGBS	564

2.4 Test Conducted

- Physical observation
- Conducting UPV Test
- Conducting compressive strength test

Figure 2: Pundit PL-200.

3 Data and Results

3.1 Concrete Production

Figure 3: All samples of concrete.

3.2 Direct Ultrasonic Pulse Velocity (UPV) Test

Refer Figure 4.

3.3 Compression Strength Test

Refer Figure 5.

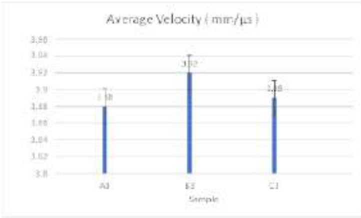

Figure 4: Comparison of the UPV measurements between concrete tested.

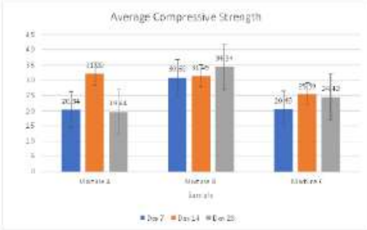

Figure 5: Average compressive strength.

4 Discussion and Conclusion

All objectives have managed to be achieved. The mixtures produced were all able to maintain flowability for 90 minutes and become completely hardened after 24 hours.

By using ultrasonic pulse velocity test, all mixtures were considered as good quality concrete. The findings presented indicate that all concrete samples are of excellent quality and are anticipated to possess high strength and durability. The UPV test outcome suggests that the samples are less prone to defects such as voids or cracks, which could affect their performance negatively over time.

Findings for compression test align with the trend observed in SCC, wherein a lower water to cement ratio generally results in a higher compressive strength due to the enhanced bonding between aggregate particles. Nonetheless, the compressive strength of SCC is not solely dependent on the water to cement ratio as other factors, including the specific workability required for the application, can also impact the concrete's strength.

In summary, the results presented in this study offer valuable insights into optimizing the mix design of SCC to achieve the desired strength and performance characteristics for various applications. Therefore, this formula could be recommended to Nuclear Malaysia to be used as backfill cement for the borehole disposal concept.

References

M. I. Ojovan. 2022. Approaches to disposal of nuclear waste. *Energies, no. Treatment of Radioactive Waste and Sustainability Energy*.

M. H. Z. and Y. F. Wong. 1996. Effect of couplant condition on ultrasonic pulse velocity measurements of concrete. *ACI Materials Journal*.

Individual Research Contribution Review, 2023, 1(1): 121–122

Drilling of Borehole Disposal for Disused Sealed Radioactive Sources

Nazran Harun
Waste Technology and Environmental Division
Malaysian Nuclear Agency
43000 Kajang, Selangor
nazranharun@nm.gov.my

Abstract

The borehole disposal facility is part of Nuklear Malaysia's effort to ensure that its disposal activity is conducted in a manner that will protect and maintain environmental quality. The construction phase is physically estimated to commence in a month from 30th May 2023. Updating activity records are necessary documents in compliance with requirements imposed by the Department of Atomic Energy Malaysia for Class G license. The update status is set out to record construction activities comprising drilling, constructing and sealing of a disposal borehole for disused sealed radioactive sources (DSRS) in Malaysia following the specific requirements outlined by the International Atomic Energy Agency (IAEA) and Department of Atomic Energy Malaysia, in the optimum time, in the most viable and safe manner to the satisfaction of all parties involved. After the construction phase is completed, the disposal phase will take place starting with provisional and cold testing IAEA expert mission before waste emplacement is conducted on the borehole disposal facility.

Keywords: borehole, disposal, DSRS, construction

1 Introduction

The primary objective of drilling Borehole Disposal for Disused Sealed Radioactive Sources (DSRS) is to drill a vertical and straight disposal borehole with 260mm diameter and a target depth of 175m below ground surface, so that disposal containers containing DSRS can be safely emplaced and sealed in the borehole. The borehole drilled with adequately straight and vertical less than 5° as stated in Statement of Works (SOW), and temporary mild steel and permanent HDPE casing were installed to ensure borehole stability and support waste emplacement operations. 2 soils investigations borehole nearby the area has been sealed before borehole disposal drilled. There are 2 attempts drilling the final borehole due to the technical events happened during the drilling worked for borehole 1 (BH 1) and borehole 2 (BH 2). The final drilled borehole (BH 3) as shown in Figure 1 has been successfully drilled and flushed up to 186m depth on 5 Aug 2023.

2 Methods

The borehole was drilled using Foremost DR-24, which utilizes a Dual Rotary Drilling method as shown in Figure 2.

Figure 1: Location of drilled boreholes

The primary distinguishing feature of a Dual Rotary drilling rig is its lower rotary drive that is used to advance steel casing through unconsolidated overburden. Rotational forces are transmitted to the casing via power-operated jaws. A carbide-studded shoe, welded to the end of the first piece of casing, enables the casing to cut its way through the overburden. Overburden is determined as formation above the hard rock. Overburden is typically made up of a variety of materials, including fine particles of silt and clay and larger particles of sand and gravel. A top drive rotary head simultaneously handles a drill string equipped with either a down-the-hole hammer, drag bit or rolling cone bit to drill the center.

2.1 Drilling

Mild steel casing was drilled and installed using dual rotary method (lower and top drive rotary insert simultaneously). First, primary surface casings with outer diameter 355.6mm (14 inch) were used to drill to a depth of 30m. Surface casings were installed to ease removal of temporary casing. Then, drill, temporary casings with outer diameter 304.8mm (12 inch) were installed up to stable formation of 120m (depends on hardness of lithology). Open hole drilling was continued using DTH Hammer bit with diameter of 260mm (10 inch) up to 176m depth.

Figure 2: Dual Rotary Drilling method

2.2 Testing

Verticality test has been done to asses borehole orientation at various depths. Data logging from inclinometer has been taken at depth of 50m only due to equipment cable limitation available in Malaysia. The verticality test then continued using Trushot tools up to 186m depth and data logged at interval of 10m. Post drilling completion measurements within the borehole was carried out to confirm that it has been drilled to the target depth 176m and diameter of 10”. The caliper survey has been done to ensure that the roughness of the Borehole walls will not limit emplacement of HDPE casing and to confirm a precise annular volume for grouting calculations.

2.3 Site Supervision

The progress while drilling and installing temporary mild steel casing as necessary in the Borehole has been monitor by minimum 2 Nuklear Malaysia Site Officers to record any activities and to ensure borehole stability and prevent collapse. There are 23 persons combination from Waste Technology Development Centre (WasTeC), Environmental Tracers Application Group (ETAG) and Engineering Division had been appointed working shiftly as site supervisor to monitor the physical working progress. Site Supervisor were responsible to deliver progress reports to Atomic Energy Department regularly.

2.4 Quality Assurance

Daily progress works were recorded and documented daily by site supervisor as part of quality assurance.

3 Discussion

The drilling works has been successfully done from 13th June 2023 till 7th July 2023 as shown in actual design in Figure 3. Due to collapsing of the wall at the depth of 120m to 130m. The flushing and related works has been carried out from 7 July 2023 till 2nd Aug 2023.

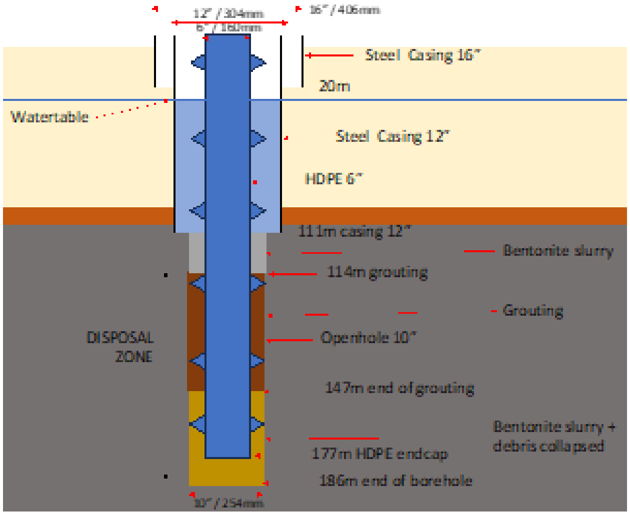

Figure 3: Actual design of borehole drilling

4 Conclusion

The complexity of drilling borehole disposal is depending on the lithology. The more simple and homogenous rock will make the drilling work more easy to be done.

References

Jabatan Tenaga Atom. 2016. LEM/TEK/72 Guideline for licence application for radioactive waste disposal facilities (Borehole disposal).

Groundwater Solutions Sdn Bhd. 2022. Construction of a disposal borehole for disused sealed radioactive sources in Malaysia.

IAEA. 2009. Borehole disposal facilities for radioactive waste. SSG-1.

IAEA. 2018. Statement of work construction of a disposal borehole for disused sealed radioactive sources in Malaysia.

Laws of Malaysia. 1984. Act 304 Atomic Energy Licensing.

Individual Research Contribution Review, 2023, 1(1): 123–124

Determination of Mercury in Water Sample in Accordance with American Public Health Association (APHA) 3125 Method: A comparative study between APHA 3030E (hot-block) and APHA 3030K (microwave) Digestion Method

Munirah Abdul Zali
Waste Technology and Environmental Division
Malaysian Nuclear Agency
43000 Kajang, Selangor
munirahzali@nm.gov.my

Abstract

Mercury contamination is among the key concern in aquatic environment. Within this requirement, analytical laboratories must be able to quantify this element in accurate and precise. In this study, the determination of mercury (Hg) in method performance and method detection level (MDL) samples was conducted using American Public Health Association (APHA) 3030E (hot-block digestion) and APHA 3030K (microwave digestion). The quantification of Hg was done using inductively coupled plasma- mass spectrometer (ICP-MS) (APHA 3125). Based on the result, the APHA 3030K method offer better method performance recovery than the APHA 3030E method. The MDL for Hg in water sample based on APHA 3030E method was unable to quantify due to poor recovery of method performance samples. The MDL for Hg in water sample based on APHA 3030K was at 20 μg L^{-1}. This study provides an insight for alternative digestion method for precise and accurate Hg quantification in water sample.

Keywords: water, mercury, digestion, ICP-MS

1 Introduction

Mercury (Hg) is recognized as a toxic and may cause severe health issues. Hg is also persistent element and high mobility due to its volatility in the environment (Gworek et al., 2020). The determination of Hg in water was crucial in order to fulfill environmental guidelines for nature conservation. To accomplish the environmental protection, suitable established method must be applied for the precise and accurate Hg quantification. Among the methods are, cold vapour atomic absorption spectrometry (CV-AAS) technique and inductively coupled plasma mass spectrometry (ICP-MS).

Based on American Public Health Association (APHA), the recommended method for Hg quantification was APHA 3112 by using CV-AAS. However, APHA also allows Hg quantification using APHA 3125 (ICP-MS) with implementation of strict quality assurance (QA) and quality control (QC) procedure. Principally in the APHA 3125 method, the water sample is introduced into an argon-based, high-temperature radio frequency plasma by using pneumatic nebulization. The energy from the plasma transfers to the water sample and causes desolvation, atomization, and ionization of elements. Ions generated by these energy-transfer processes are extracted from the plasma by the vacuum interface, separated based on mass-to-charge ratio by the mass spectrometer, counted and process by instrument software.

Among the method performance criteria recommended in the APHA method, every analysis requires the determination of method blank (MB), laboratory fortified blank (LFB), laboratory fortified matrix (LFM) and laboratory fortified matrix duplicate (LFMD) in every batch sample in order produce a reliable result ((APHA), 2022). Furthermore, QC APHA also requires the determination of method detection level (MDL) in every method to set acceptable level for reporting limit for Hg in water samples. This study aims to determine and compare the method performance and MDL for Hg in water samples using APHA 3030E and APHA 3030K techniques prior to ICP-MS quantification (APHA 3125). The findings of this study can be applied in the reporting of Hg in the water samples and can be used to implement further action in environmental protection improvement.

2 Methods

In this study, the 10 μg ml^{-1} Hg calibration standard was purchased from CPAChem. 10 μg ml^{-1} Hg for calibration verification standard and QC samples was purchased from Inorganic Ventures. Single standards of rhodium (Rh) was obtained from the Scharlau brand for internal standard purposes during analysis. Concentrated nitric acid with trace metal grade was purchased from Fisher Chemical. Deionized water (DIW) for washing, soaking and sample preparation was based on the high-quality reagent water specification based on the APHA 1080 method ((APHA), 2022).

2.1 Preparation of Quality Control Samples for APHA 3030E and APHA 3030K method

In this research, two metal digestion methods were used to compare the quality control (QC) samples consisting of method performance and MDL samples for Hg determination in water samples. The first method is the APHA 3030E method. For method performance, two blank, laboratory fortified blank (LFB) at 25 μgL^{-1} of Hg, unspike sample, laboratory fortified matrix (LFM) at 25 μgL^{-1} of Hg, and laboratory fortified matrix duplicate (LFMD) at 25 μgL^{-1} of Hg, samples were prepared for method performance samples of the APHA 3030E digestion technique. The seven portions of MDL samples for the APHA 3030E method were also prepared and analyzed together with method performance samples. Briefly, for the APHA 3030E method, 10 ml of quality QC samples were added to the 50 ml tube. The samples were added with 0.5 ml of concentrated nitric acid and placed in the block heater. The temperature of the block heater was adjusted to 105°C. The tube caps for all the samples were placed on top of the tube without screwing. The samples were digested for a minimum of 2 hours and more concentrated nitric acid was added until observation of clear solution. Upon complete digestion, the sample volume was adjusted and recorded for calculation.

The second digestion technique for QC samples consisted method performance and MDL determination is APHA 3030K. The concentration of blank, LFB, unspike sample, LFM and LFMD were prepared similar with APHA 3030E QC samples. Briefly 45 ml of quality control samples were added into microwave digester teflon vessels. Then the samples were added with 5 ml of concentrated nitric acid. The vessels were capped, tightened with vessel holders and placed in microwave digester turntable. The digestion procedure was programmed in the microwave digester system. The samples were heated to 160 ± 4 for 25 minutes for the first stage of digestion. For the second stage, the samples were digested with a slow rise to 170 ± 4 in 10 minutes. The vessels were allowed to cool and the solution was transferred into clean polypropylene tube.

2.2 Analysis of REE using Inductively Coupled Plasma-Mass Spectrometry (APHA 3125)

The determination of Hg in the QC samples for both digestion procedures was carried out using ICP-MS (APHA 3125). Two calibration points of calibration blank and 200 μg l^{-1} were established with correlation of coefficient more than 0.995. The calibration verification standard with concentration at 100 μg l^{-1} was analyzed for every ten samples and the values ranged between 90 and 110%. The recovery calculations for LFB, LFM, LFMD and MDL were explained in details in ((APHA), 2022).

3 Results and Discussion

Table 1 shows the method performance and MDL results for both digestion method. Based on APHA 3030E digestion method, the spike recovery for LFB and LFM were at 4.3% and 1.6% respectively. Both results were not within allowable range of APHA requirement. In contrast the LFB and LFM spike recovery for APHA 3030K method were 89.2% and 89.4% respectively. Therefore, APHA 3030K method was able to determine the Hg in water sample with good recovery and minimum loss during digestion compare to APHA 3030E method.

The poor recovery for hot block digestion technique (APHA 303E) compare to microwave digestion technique may due to the loss of Hg during semi-open heating of the hot block. Meanwhile, microwave digester is a closed system and able to prevent volatilization of Hg during digestion (Alsehli, 2021).

The MDL for APHA 3030E in water sample was unable to quantify due to the poor spike recovery for LFB and LFM. Meanwhile, the MDL for Hg in the water sample based on APHA 3030K was calculated at 20 μg L^{-1}. However, the MDL in this study was higher than the recommended Hg analytical method by using CV-AAS based on Environmental

Table 1: QC sample results for APHA 3030E and APHA 3030K methods

QC sample	APHA 3030E	APHA 3030K	Allowable range
LFB spike recovery (%)	4.3 ± 0.0001	89.2 ± 0.0005	85-1155
LFM spike recovery (%)	1.6 ± 0.0004	89.4 ± 0.0005	70-130
MDL Hg (μg L^{-1})	NA	20.0	

Protection Agency (EPA) Method 245.1 (EPA, 1994).

4 Conclusion

In this research, two digestion techniques (APHA 3030E and APHA 3030K) for Hg determination in water sample were conducted to determine method performance and MDL for each method. Based on method performance criteria, APHA 3030K method offers better LFB and LFM recovery compared to APHA 3030E method. The MDL of Hg in water sample was unable to quantify for APHA 3030E method due to poor recovery for LFB and LFM. The Hg determination in water sample can be digested using APHA 3030K and quantified using APHA 3125 with precise and accurate result.

References

B. R. M. Alsehli. 2021. Evaluation and comparison between a conventional acid digestion method and a microwave digestion system for heavy metals determination in mentha samples by ICP-MS. Egypt. *J. Chem.*, 64:869 – 881.

American Public Health Association (APHA). 2022. Quality control practices, in: Baxter, W.C.L.E.B.B.-H.T.E.(Ed.), Standard methods for the examination of water and wastewater. 190.

EPA. 1994. EPA 245.1, Revision 3: Determination of mercury in water by cold vapour atomic absorption spectrometry.

B. Gworek, W. H. Dmuchowski, and A. Baczewska-Dabrowska. 2020. Mercury in the terrestrial environment: A review. *Environ. Sci. Eur.*

Individual Research Contribution Review, 2023, 1(1): 125–126

Linking Rice to the Provenance Origin Through Multi-Element Relationship in Soil-Rice Matrix

Nazaratul Ashifa Abdullah Salim
Waste Technology and Environmental Division
Malaysian Nuclear Agency
43000 Kajang, Selangor
shifa@nm.gov.my

Abstract

Multi-element concentration in rice able to show relationship to their concentration in soil. An integrated analysis using chemometric approach visualized the linking between concentrations of multi-element in rice and soil. High correlation of between soil and rice enable validation of rice to the reproduction area. Hence, this approach may assist in the verification of rice geographical origin.

Keywords: multi-element, soil-rice, chemometric

1 Introduction

Proof of provenance has become an important topic in the context of food safety, quality, traceability and consumer protection. Proof of rice's geographical origin becomes important particularly for premium varieties that are frequently targets of fraud. The conventional documentation along the supply chain is susceptible to modification and misrepresentation. The packaging's authentic label might be forged to indicate a different rice quality or variety. Then, verification of rice variety by morphological inspection or genetic information has limitations and may not necessarily reflect the provenance of the rice.

Multi-element concentrations in rice provide a unique profile due to the environment of cultivation. Soil characteristics are one of the primary factors that influence rice growth. An assistance by chemometric analysis allows verifying the contribution of each variable (single-element) to the verification model, and its capacity to discriminate one category from another as well. Thus, this study aims (i) to quantify the multi-element in rice and soil and (ii) to assess the inter-relationship of the multi-element between rice and soil cultivated at different geographical origin.

2 Methods

Samplings of soil and rice were conducted on two phases by different locations; (i) Kedah, Selangor and Langkawi cultivated with variety MR220CL, (ii) Sawah Sempadan, Selangor and Kota Belud, Sabah with several rice varieties. Approximately, 1 kg of soil and rice were sampled in the same coordinate by a simple random sampling technique. Both samples were processed by cleaning, drying and grinding into powdered form.

2.1 Neutron Activation Analysis (NAA)

The multi-element concentration of the soil and rice was determined based on (A. et al., 2013). Briefly, approximately 100 mg of soil and rice were sealed in small polyethylene vials before undergoing irradiation and γ-ray counting procedures. The irradiations of all samples and reference materials were performed with the PUSPATI TRIGA Mark II. Then, an HPGe detector (E&G ORTEC, USA) with a resolution of 2.0 at 1332 keV (^{60}Co) and relative efficiency of 40% was used to count γ-ray activities of element Al, As, Br, Ca, Cl, Fe, K, Mg, Mn, Na, Rb and Zn.

2.2 Energy Dispersive X-ray Fluorescence (ED-XRF)

Element of Ca and Fe were quantified by ED-XRF (Thermo-Fisher, Quant X, USA) due to insensitive measurement by NAA technique in the rice matrix.

2.3 Data Analysis and Chemometric

Univariate analysis was performed using the freeware PAST3 (ver. 3.23, (Ø. et al., 2001)). Data were checked for normal distribution for each element. Non-parametric data were log-transformed. Then, analysis of variance by the Kruskal-Wallis and Dunn-Bonferroni post-hoc test was carried out to determine the differences in element concentration. Further evaluation of the relationship of variables between the soil and rice matrix was performed by chemometric generalized Procrustes analysis (GPA) and canonical correlation Analysis (CCA). This analysis was performed using InfoStat software (ver. 2014, National University of Cordoba, Argentina).

3 Results

Relationship of multi-element concentrations between soil and rice was assessed in accordance to the sampling regions.

3.1 Kedah, Selangor and Langkawi

Three regions cultivated with the same variety show the evaluation of the soil and rice matrix by GPA obtained 100% variability between sample (Figure 1). This result shows that the rice data has significance consensus (98%) with the elements in the soil, because both the data set projects the area in a similar way to the plane defined by its first two principal axes. CCA analysis showed a significant positive correlation (r^2=0.88; $p<0.001$) between soil and rice profiles that revealed the variability in elemental content in rice can be attributed to paddy soil (Figure 2). The detail on this project area was published in (Salim et al., 2023)

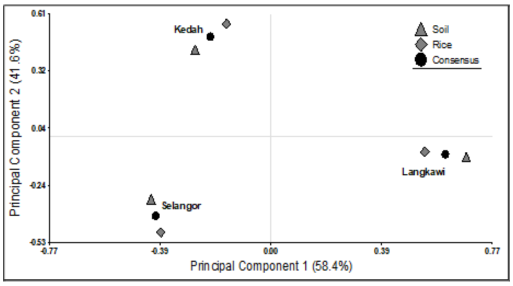

Figure 1: GPA discriminate the cultivation regions

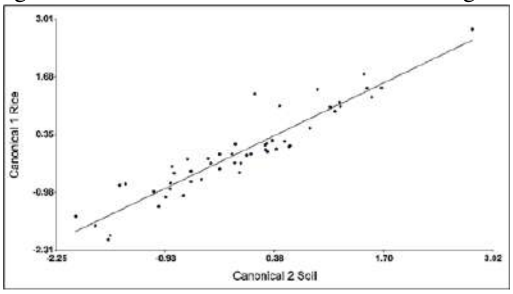

Figure 2: Correlation between soil-rice matrix by CCA

3.2 Selangor and Sabah

Different rice varieties cultivated in Selangor was distinguished from Kota Belud rice cultivated in low- and high-land fields. GPA verified the significant ($p<0.0001$) discrimination of rice and soil between regions with 93% consensus value (Figure 3). CCA showed highly positive correlation ($r^2=0.96$; $p<0.001$) between rice and soil profile (Figure 4).

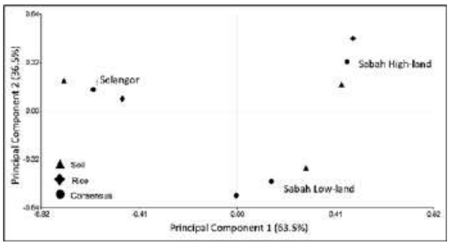

Figure 3: Discrimination of Selangor and Sabah cultivated regions

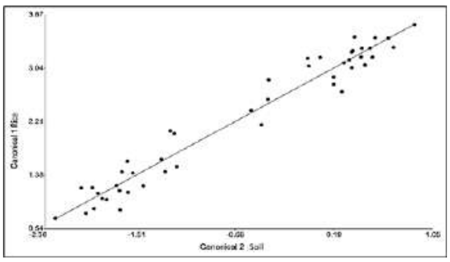

Figure 4: Correlation between soil-rice matrix by CCA

4 Discussion and Conclusion

The evaluation by the chemometrics approach of GPA and CCA provides reliable evidence that links the soil and rice to their provenance origin. Previously, the combination of multi-element analysis and chemometric was successfully assess the relationship between soil and agricultural products such as wine, honey and milk (Di Paola-Naranjo et al., 2011; Baroni et al., 2015; Griboff et al., 2019). Variability of the profile of elements with a substantial influence on the soil-grain interaction, such as rice and wheat, could reflect the effect of plant growing environment as well as species or variety differences.

This study may provide significant evidence to farmers or producers who seek Geographical Indication (GI) certification. The rice verification on the geographical origin can be useful for marketing strategy purposes and contribute to consumer confidence in the quality of rice products. The establishment of reference data on quality properties shall assist in preventing contamination or mixing with lower-grade products, guaranteeing product authenticity and assisting the national food surveillance program. Ultimately, the authentication aspect of agro-food is a prerequisite to ensure consumer health, successful global trade and sustain the development of agricultural resources, as addressed in National Food Safety Policy 2002 and National Agro-food Policy 2021.

References

Salim N. A. A., Hamzah M. S., Elias M. S., Siong W. B., Rahman S. A., Hashim A., and Shukor S. A. 2013. Instrumental neutron activation analysis of marine sediment in-house reference material. *Journal of Nuclear Science and Technology*, 10(1):1 – 7.

M. V. Baroni, N. S. Podio, R. G. Badini, M. Inga, H. A. Ostera, M. Cagnoni, E. A. Gautier, P. P. García, J. Hoogewerff, and D. A. Wunderlin. 2015. Linking soil, water, and honey composition to assess the geographical origin of Argentinean honey by multielemental and isotopic analyses. *Journal of Agricultural and Food Chemistry*, 63(18):4638 – 4645.

R. D. Di Paola-Naranjo, M. V. Baroni, N. S. Podio, H. R. Rubinstein, M. P. Fabani, R. G. Badini, M. Inga, H. A. Ostera, M. Cagnoni, E. Gallegos, E. Gautier, P. Peral-García, J. Hoogewerff, and D. A. Wunderlin. 2011. Fingerprints for main varieties of Argentinean wines: Terroir differentiation by inorganic, organic, and stable isotopic analyses coupled to chemometrics. *Journal of Agricultural and Food Chemistry*, 59(14):7854 – 7865.

J. Griboff, M. V. Baroni, M. Horacek, D. A. Wunderlin, and M. V. Monferran. 2019. Multielemental + isotopic fingerprint enables linking soil, water, forage and milk composition, assessing the geographical origin of Argentinean milk. *Food Chemistry*, 283:549 – 558.

N. A. A. Salim, N. M. Daud, J. Griboff, and A. R. Harun. 2023. Elemental assessments in paddy soil for geographical traceability of rice from Peninsular Malaysia. *Rice Science*, 30(5):486 – 498.

Hammer Ø., Harper D. A. T., and Ryan P. D. 2001. PAST: Paleontological statistics software package for education and data analysis. *Palaeontologia Electronica*, 4(1)(1):1 – 9.

Individual Research Contribution Review, 2023, 1(1): 127–128

Method Verification on Determination of Pb-210 in South China Sea Sediment Core

Nooradilah Abdullah
Waste Technology and Environmental Division
Malaysian Nuclear Agency
43000 Kajang, Selangor
nooradilah@nm.gov.my

Abstract

This project focuses on the method verification for the determination of Pb-210 in sediment cores from the South China Sea. The study will compare three distinct analytical methods: direct gamma counting, alpha counting *via* Po-210, and beta counting *via* Bi-210 to determine the radioactivity of Pb-210 in the samples. The accuracy and reliability of Pb-210 measurements is critical for understanding sedimentation rates and environmental processes. Results obtained indicate that the methods provide reliable measurements of Pb-210 radioactivity.

Keywords: Pb-210, sedimentation rate

1 Introduction

Radionuclides are very useful tools as tracers to study a large variety of processes in the oceans. Radioactive isotopes present in the environment, such as uranium-236 (U-236), lead-210 (Pb-210), caesium-137 (Cs-137) and carbon-14 (C-14), were used to study present-day sedimentation in seas and oceans (Periáñez et al., 2023; Ferreira et al., 2020). The study of sediments in coastal areas has great importance to understand the interaction between human activities and marine system. Apart from that, combining radionuclide dating methods with detailed sedimentological investigations allows sedimentary events to be correlated with well-documented earthquakes or volcanic eruptions (Arnaud et al., 2006).

Pb-210 is well-known as environmental radiotracer in various processes such as sediment resuspension (Baskaran et al., 2020), carbon and nitrogen cycle quantification (Yang et al., 2011) and particle cycling (Zhong et al., 2023). The half-life of Pb-210 is 22.3 years which can be used for dating on material from a year up to 150 years old. The origin of Pb-210 can be divided into two, unsupported Pb-210 which formed in the atmosphere due to the decay of Rn-222 and the other is supported Pb-210 which formed from the decay of Rn-222 arising from the natural Ra-226 contained in the sediments. Another source of Pb- 210 could be from anthropogenic sources such as from waste.

Several analytical techniques are available for the measurement of Pb-210 based on different chemical and physical principles, namely direct gamma counting, alpha counting *via* Po-210, and beta counting *via* Bi-210. They differ concerning the reachable detection limit, selectivity, analytical error reproducibility and stability against different chemical composition and levels of others natural radionuclides. In this study, Pb-210 in sediment core samples was designed to be determined by using these three methods. However, due to some technical limitation, gamma measurement results will not be discussed here.

2 Methods

2.1 Pre-treatment of sediment samples

All sediment samples were dried in an oven at 60°C until constant weight was achieved and re-weighed for calculation of porosity. Dried sediments then were grounded into fine particles until homogenous. Sediment sub-samples were retained for analyses of grain size and organic carbon content.

2.2 Laboratory methods

2.2.1 Alpha spectroscopy

Radiochemical separation of Po-210 was performed and polonium isotopes was spontaneously plated on silver disc before its activities was determined using alpha spectrometer. The activities of Pb-210 was determined by assuming that Po-210 and Pb-210 has reached secular equilibrium.

2.2.2 Gas proportional counter

The samples underwent sequential Po-210/Pb-210 radiochemical separation on Sr-resin column. After at least 14 days, the activity of Bi-210 beta emission was measured by using a low background gross alpha/gross beta counter. The activity of Po-210 was determined by using alpha spectrometer.

2.3 Sedimentation rate calculation

The sedimentation rate by using the three methods was determined using two different mathematical models, constant initial concentration (CIC) and constant rate of supply (CRS). The calculation is based on Turner and Delorme, 1996.

3 Results and Discussions

3.1 Verification of Pb-210 Determination using Beta Counter

Table 1 shows the activity concentration of Pb-210 and Po-210 in IAEA-385 determined by the sequential method. The radioactivity of Pb-210 was determined by measuring the beta emission of Bi-210, at least 14 days after the chemical separation to ensure secular equilibrium of Pb- 210 and Bi-210. The activity of Po-210 was measured by using alpha spectrometer.

Determination of Po-210 in IAEA-385 was also carried out without using Sr resin separation. The information values for activity concentrations of Pb-210 and Po-210 as reported in RS_IAEA- 385[Rev.04] / 2019-10-23 is (28.5 ± 1.9) Bq/kg and (29 ± 2) Bq/kg respectively.

Table 1: Activity Concentration of Pb-210 and Po-210 analysed in IAEA-385

Sample No.	Pb-210 (Bq/kg)	Po-210 (Bq/kg)	Po-210 (Bq/kg) (without resin)
1	33.32	30.32	28.00
2	31.69	25.14	28.81
3	30.86	33.05	30.10
4	31.99	27.39	30.80
5	33.35	26.44	29.30
6	32.36	30.55	28.30

The values obtained for Pb-210 lies on the upper range of the informational values with recovery more than 50%. On the other hand, the value obtained for Po-210 determined using sequential method tend to be distributed on both range of the informational value with recovery ranges from 25.1% to 77.8%. Determination of Po-210 without the use of Sr resin shows better recovery with a better precision. Losses of Po-209 tracer from the hot acid mixture before dissolution of Po-210 from the sediment is complete may lead to this lower recovery (Vrecek et al., 2003).

3.2 Determination of Pb-210 in Sediment Core

Determination of Pb-210 in the sediment core sample by using these methods show no significant difference in the radioactivity value. This shows that these two methods are reliable in determining the radioactivity of Pb-210. Determination of Pb-210 by using gamma spectrometer will be carried out in the future.

4 Conclusion

Results obtained indicate that these methods provide reliable measurements of Pb-210 radioactivity in sediment core sample. There are few factors that needs to be considered before a method is chosen, such as amount of sample, interest radionuclides and also chemical and instrument availability.

References

F. Arnaud, O. Magand, E. Chapron, S. Bertrand, X. Boës, F. Charlet, and M.A. Mélières. 2006. Radionuclide dating (210Pb, 137Cs, 241Am) of recent lake sediments in a highly active geodynamic setting (Lakes Puyehue and Icalma—Chilean Lake District). *Science of The Total Environment*, 366(2-3):837 – 850.

M. Baskaran, R. Mudbidr, and L. Schweitzer. 2020. Quantification of Po-210 and Pb-210 as tracer of sediment resuspension rate in a shallow riverine system: Case study from southeast Michigan, Usa. *Journal of Environmental Radioactivity*, 222(106339).

P.A.D.L. Ferreira, R.C.L. Figueira, S.C. Goya, and M.M.D. Mahiques. 2020. Insights on the marine sedimentation of the continental shelf and upper slope off SE Brazil during the 20th century with natural radionuclides. *Regional Studies in Marine Science*, 39(101466).

R. Periáñez, U. Abascal-Ruíz, J.M. López-Gutiérrez, and M. Villa-Alfageme. 2023. Sediments as sinks and sources of marine radionuclides: Implications for their use as ocean tracers. *Marine Pollution Bulletin*, 194(115316).

L.J. Turner and L.D. Delorme. 1996. Assessment of 210Pb data from Canadian lakes using the CIC and CRS models. *Environmental Geology*, 28(2):78 – 87.

P. Vrecek, L. Benedik, and B. Pihlar. 2003. Determination of 210Pb and 210Po in sediment and soil leachates and in biological materials using a Sr-resin column and evaluation of column reuse. *Applied Radiation and Isotopes*, 60:717 – 723.

W.F. Yang, Y.P. Huang, M. Chen, Y.S. Qiu, H.B. Li, and L. Zhang. 2011. Carbon and nitrogen cycling in the Zhubi coral reef lagoon of the South China Sea as revealed by 210Po and 210Pb. *Marine Pollution Bulletin*, 62(5):905 – 911.

Q. Zhong, W. Guo, H. Wang, J. Ji, J. Lin, J. Du, D. Huang, and T. Yu. 2023. 210Po and 210Pb as tracers for particle cycling in a shallow semienclosed bay of Taiwan Strait. *Deep Sea Research Part II: Topical Studies in Oceanography*, 207:105228.

Individual Research Contribution Review, 2023, 1(1): 129–130

Development of Marine Radioactivity Database in Peninsular Malaysia, Sabah, and Sarawak Seas

Noor Fadzilah Yusof
Waste Technology and Environmental Division
Malaysian Nuclear Agency
43000 Kajang, Selangor
fadzilah@nm.gov.my

Abstract

Radiochemistry & Environmental Laboratory (RAS) has undertaken numerous collaborative marine expeditions with local authorities and research universities aimed at establishing a comprehensive database on radioactivity levels in various components of the marine environment. The resulting dataset will play a crucial role in the development of simulation and prediction models. Presently, access to existing marine radioactivity data is restricted to internal personnel, limiting its availability for scientific research and investigation. Ongoing development including data clean up, compiling and verifying are expected to refine and expand the database's capabilities in ensuring its integrity of data for future research endeavors.

Keywords: Marine radioactivity, database, database design

1 Introduction

Radiochemistry & Environmental Laboratory (RAS) has actively collaborated with organizations such as local authorities and research universities to conduct multiple marine expeditions. The primary objective of these expeditions is to establish a comprehensive database on radioactivity levels in sediment, water, biota, and plankton within the marine environment (Jaffary et al., 2015). This data plays a crucial role in assessing environmental radionuclide levels in Malaysia's marine ecosystem, and serves as a basis for evaluating radiation exposure for local, regional, and global populations, as well as marine life. This comprehensive data will be instrumental in developing simulation and prediction models.

Despite Malaysia not currently operating a Nuclear Power Plant (NPP), it is crucial to monitor the presence and distribution of radioactive materials in the marine environment to assess potential radiological impacts on human life. This data will serve as a foundational reference for potential future nuclear endeavors in Malaysia or neighboring countries. Currently, the existing marine radioactivity data could only be assessed by internal personnel and not widely available for scientific research and investigation except for published data (Sulaiman et al., 2023). Due to this conditions, presentation and availability of the data can be argued by stakeholders. Therefore, development of marine radioactivity database system is proposed.

2 Methods

The initial phase of digitizing marine radioactivity database focused on data processing involving data cleaning, compiling, verifying and standardizing according to the database design. The standardizing and normalizing the data aimed to create a suitable data model for seamless conversion and transfer to a new shared database platform.

3 Results and Discussions

Based on the data clean up and verification, the marine radioactivity data for baseline dated in 2003 to 2004 have been compiled, cleaned up, verified and tabulated in Microsoft Excel for further action. The radioactivity data includes several coastal and deep sea with variation of radionuclides (Po-210, Pb-210, uranium and thorium isotopes, plutonium isotopes, Cs-137, Ra-226 and Ra-228) and sample types (seawater, sediment, biota and plankton) for East Coast and West Coast Peninsular Malaysia, Sabah and Sarawak.

Besides, on the database design (Figure 1), eight entities has been included in the marine database model including location, sample, sample-type, radioactivity, nuclide-type and three types of samples (Sulaiman et al., 2023).

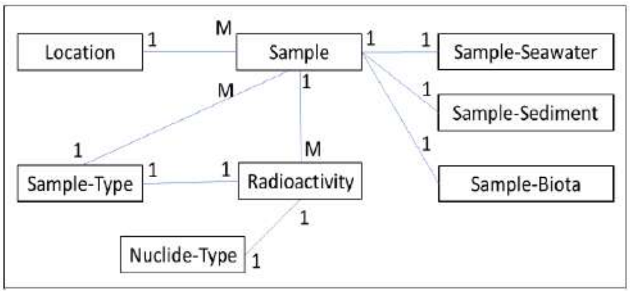

Figure 1: Normalized entity relationship model for marine database

4 Conclusion

Overall, with eight main entities identified, ongoing development activities will refine and expand its scope. Rigorous analysis and careful preparation are crucial for ensuring the integrity of the data. The widespread use of this database is anticipated to enhance social well-being through advancements in radiation protection, safety and security worldwide.

References

Nurrul Assyikeen Md. Jaffary, Yii Mei Wo, Abdul Kadir Ishak, Noor Fadzilah Yusof, Kamarozaman Ishak, Maziah Mahmud, Nor Aza Hassan, Khairul Nizam Razali, Nooruzainah Abu Hassan, Narizan Sanusi, Mohamad Fikri Mohamad Puad, Maimunah Hashim, Zulkifli Daud, and Noordin Mohd Noor. 2015. Monitoring of radionuclide contamination in food samples in Malaysia due to Daiichi Reactor accident in Fukushima, Japan. *Jurnal Sains Nuklear Malaysia*, 27(1):14–20 ISSN: 2232–0946.

M.S. Sulaiman, N. F. Yusof, S. N. Abd. Ghani, N. Hamdan, Yii Mei Wo, Jalaj Sharib@Sarip, and Norfaizal Mohamed@Muhammad. 2023. Digitalization of marine radioactivity data in Malaysia. *Konvensyen Inovasi dan Teknikal Nuklear Malaysia (NITC), Agensi Nuklear Malaysia*.

Individual Research Contribution Review, 2023, 1(1): 131–132

Estimating the Recurrence Periods of Earthquake Using the International Monitoring System (IMS) Data of the Comprehensive Nuclear-Test-Ban Treaty Organization (CTBTO)

Nor Dalila Desa
Waste Technology and Environmental Division
Malaysian Nuclear Agency
43000 Kajang, Selangor
nordalila@nm.gov.my

Abstract

Sabah represent the most seismically active state in Malaysia. It recorded more significant number of moderate seismological activities for the previous decades, as compared to other states in the country. The seismicity map of Sabah reveals the presence of two (2) zones of distinctive seismicity, which are Ranau in Kota Kinabalu and Lahad Datu in the south-east. The International Monitoring System (IMS) network setup by the Comprehensive Nuclear-Test-Ban Treaty Organization (CTBTO) has successfully detected seismic events occurred in Sabah for the previous decades. This study aims at quantifying the recurrence periods and probabilities of occurrence of an earthquake at any given magnitude in Sabah using seismic IMS data. This study utilized seismic data from the CTBTO International Data Centre and analysed it to identify the related seismicity parameters such as magnitude, depth, and intensity. The Extreme Value Distribution Type-I has been applied to evaluate the maximum magnitude data. The results of the analysis have enabled the quantification of recurrence periods and probabilities of occurrence of an earthquake at any given magnitude.

1 Introduction

Seismic technology is one of three waveform technologies which are part of the International Monitoring System (IMS) of the Comprehensive Nuclear Test Ban Treaty (CTBT). For this study, the data of earthquake events occurred around Sabah region (bounded by 3.95°N to 7.16°N latitude and 115.4°E to 119.3°E longitude) from January 2002 to June 2020 have been taken from the CTBT's Reviewed Event Bulletin (REB). In order to study the earthquake risk, probability of occurrence and return periods, the earthquake data distributed over 19 years periods has been divided into one year time interval such as at least one event in each year duration is observed. The region of Sabah has suffered several earthquakes of moderate magnitude, where of these events have caused structural damage to buildings and other infrastructures and injuries to humans. Based on the above facts, seismic hazard assessment (SHA) for Sabah is essential in order to mitigate the effects of potential large earthquake that may occur in the future.

2 Methods

The method of Extreme Value Distribution Type-I, which is also known as Gumbel's Type I, has certain clear and advantages If compared with other methods requiring the whole data set, and rarely completely reported. The Gumbel's need only part of the event data, such as, the largest earthquakes i.e. extremes. The CTBTO IMS data represent a continuous and complete set of annual maximum magnitude events, thus, it is very useful to apply such method for the calculation process of this study.

3 Result and Discussion

The annual maximum magnitudes of seismic events recorded in the considered region from the year 2002 to 2020 are shown in Table 1. Figure 1 shows the variation of maximum magnitude with years, which indicates that the maximum magnitude increases with time in the considered region.

Table 1: Calculations of Gumbel's Annual Maximum Distributions.

Extremes	Rank (j)	Plotting Position G(m)	Reduced Statistics In (-In(G(m)))
3.5	1	0.05000	1.09719
3.5	2	0.10000	0.83403
3.6	3	0.15000	0.64034
3.6	4	0.20000	0.47588
3.6	5	0.25000	0.32663
3.7	6	0.30000	0.18563
3.7	7	0.35000	0.04862
3.7	8	0.40000	-0.08742
3.8	9	0.45000	-0.22501
4	10	0.50000	-0.36651
4	11	0.55000	-0.51444
4	12	0.60000	-0.67173
4	13	0.65000	-0.84215
4.1	14	0.70000	-1.03093
4.1	15	0.75000	-1.24590
4.3	16	0.80000	-1.49994
4.4	17	0.85000	-1.81696
5.2	19	0.95000	-2.97020

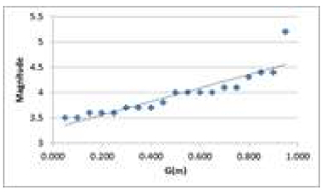

Figure 1: Variation of maximum magnitude with year

Figure 2 demonstrates the mean Line of Expected Extreme (LEE) to study the probability of largest extreme magnitude in

Table 2: Estimated Gumbel's Parameters α and β

Statistics	Value
Slope (-β)	-2.5039
β	2.504
Intercept(In(α))	9.3885
α	11950.16

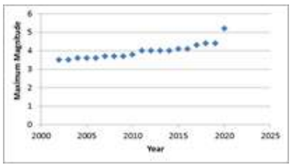

Figure 2: Variation of extreme magnitude with probability

Sabah. The values of estimated Gumbel's parameters α and β are then estimated from a least-square fit to the Reduced Linear Variation Equation, as described in Figure 3. These values of α and β are summarized in Table 2. The earthquake yearly numbers and their return period for different magnitude expected in Sabah region are calculated and summarized in Table 3. From the histories of maximum earthquake magnitude recorded, earthquake hazard probabilities for different magnitudes with time are calculated for 10, 20, 30, 50, 75 and 100 years periods. The results are summarized in Table 4. The relation between of these yearly numbers of earthquakes, their return periods and the calculated earthquake hazard is further illustrated in Figure 3 and Figure 4. The general interpretation of this curve reveals that the probability of an earthquake of magnitude 4.1 occurring in the considered region with 20-years period is estimated to be 0.999. From Table 3, the design earthquake recurrence period with 90% probability is calculated and the values are presented in Table 5. The 90% probability recurrence period could be understood that in Sabah region, there is 90% probability in 29 years period that at least one earthquake of magnitude 4.5 or greater will occur and conversely that 10% probability an earthquake of the same magnitude or more will not occur.

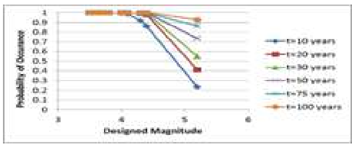

Figure 3: Variation of probability with year

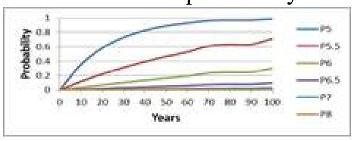

Figure 4: Earthquake hazard in Sabah region for different period

4 Conclusion

The results of analysis have enabled the quantification of recurrence periods and probabilities of occurrence of earthquake at any given magnitude in Sabah using seismic IMS data.

Table 3: Predicted yearly number of earthquakes and their return periods

Magnitude	N_m	T_m
3.5	1.867965642	0.535341752
3.5	1.867965642	0.535341752
3.6	1.454205854	0.687660552
3.6	1.454205854	0.687660552
3.6	1.454205854	0.687660552
3.7	1.132095054	0.883318054
3.7	1.132095054	0.883318054
3.7	1.132095054	0.883318054
3.8	0.881332728	1.134645257
4	0.53413853	1.872173497
4	0.53413853	1.872173497
4	0.53413853	1.872173497
4	0.53413853	1.872173497
4.1	0.415825302	2.404856065
4.1	0.415825302	2.404856065
4.3	0.252014147	3.968031205
4.4	0.196192285	5.097040379
4.4	0.196192285	5.097040379
5.2	0.026469026	37.78000723
3	6.532566815	0.153
3.5	1.867965642	0.535
4	0.53413853	1.872
4.5	0.152735127	6.547
5	0.043674099	22.897
5.5	0.012488463	80.074
6	0.003571034	280.031
6.5	0.001021125	979.312
7	0.000291987	3424.806
8	2.38745E-05	41885.712

Table 4: Most probable largest earthquake hazard Ht (m) for Different Magnitudes and Time Periods (t=10, 20, 30, 50, 75 and 100 years)

Magnitude	H_{10}(m)	H_{20}(m)	H_{30}(m)	H_{50}(m)	H_{75}(m)	H_{100}(m)
3.5	0.999999992	1	1	1	1	1
3.5	0.999999992	1	1	1	1	1
3.6	0.999999516	1	1	1	1	1
3.6	0.999999516	1	1	1	1	1
3.6	0.999999516	1	1	1	1	1
3.7	0.999987884	1	1	1	1	1
3.7	0.999987884	1	1	1	1	1
3.7	0.999987884	1	1	1	1	1
3.8	0.9999851262	0.999999978	1	1	1	1
4	0.995210768	0.999977063	1	1	1	1
4	0.995210768	0.999977063	1	1	1	1
4	0.995210768	0.999977063	1	1	1	1
4	0.995210768	0.999977063	1	1	1	1
4.1	0.984365152	0.999755552	0.999996	1	1	1
4.1	0.984365152	0.999755552	0.999996	1	1	1
4.3	0.919551775	0.993528083	0.999479	0.999997	1	1
4.4	0.859412169	0.980235062	0.997221	0.999945	1	1
4.4	0.859412169	0.980235062	0.997221	0.999945	1	1
5.2	0.23255638	0.41103029	0.547999	0.733785	0.862644	0.92913

Table 5: Design earthquake Recurrence Period with 90% probability

Magnitude (m)	Return Period (years)	Recurrence Period (years)
3	0.153	0.69
3.5	0.535	2.40
4	1.872	8.40
4.5	6.547	29.39
5	22.897	102.78
5.5	80.074	359.42
6	280.031	1256.96
6.5	979.312	4395
7	3424.806	15372.71
8	41885.712	188009.73

Generally, it can be summarized that the methodology of the Gumbel's Type I extreme distribution could provide future seismic and hazard status of the region, and the availability of CTBTO's IMS complete earthquake data sets leads to reliable results that the study aimed for.

References

https://access.ctbto.org/portal/index.html.

Enhancing Regional Capabilities for Marine Radioactivity Monitoring and Assessment of the Potential Impact of Radioactive Releases from Nuclear Facilities in Asia-Pacific Marine Ecosystems (RCA), RAS/7/028

Norfaizal bin Mohamed
Waste Technology and Environmental Division
Malaysian Nuclear Agency
43000 Kajang, Selangor
norfaizal@nm.gov.my

Abstract

RAS/7/028 project commenced in 2017 and was due to finish at the end of 2020. However, the impact of the pandemic in 2020 and 2021 has resulted in the postponement of project related activities and the finish date has been extended to the end of 2022. The main objective of this project is to improve the integrated regional quality-assured capabilities for marine radioactivity monitoring and for impact assessment of routine and accidental releases of radioactivity into the marine environment. Data obtained from this project was published in eight scientific papers and submitted to ASPAMARD and MARiS.

Keywords: RAS7028, radioactivity monitoring, marine environment

1 Introduction

The Asia-Pacific region includes a vast expanse of the marine coastline and its economies depend on ocean resources (seawater, sediments and marine biota) for livelihood and economic growth. This area is vulnerable to a range of issues including anthropogenic contaminant discharges, climate change, coastal erosion, population pressures and degradation of marine resources. In recent times, the 2011 accident at the Fukushima Daiichi Nuclear Power Plant, and recent plan for discharge of stored water, have emphasised the importance of monitoring radionuclides in the Asia-Pacific region's marine environment.

The plans for future expansion of nuclear power as the clean energy option further emphasise the importance of maintaining a sound capability to assess potential radiological impacts on the marine environment. According to these plans, more than 100 new nuclear power plants could be built in the Asia/Pacific region in the next few decades. For any future releases, atmospheric transport and regional ocean currents will disperse radionuclides throughout the region (transboundary contamination) which can have detrimental impacts on national economic zones, international waters and regional economies. Therefore, a continuing to build and maintain monitoring capabilities and coordinate in a harmonised regional approach is essential. The RAS/7/028 project has been implemented to improve the capabilities of regional countries and to optimise and coordinate the application of the skills and resources available in the region to generate monitoring data that is both reliable, directly comparable and exchangeable between the participating Government Parties (GPs).

2 Project Objectives

i. Enhanced regional skills in marine environmental sampling of seawater, sediments and biota.

ii. Advanced regional skills in marine radiochemistry/radiometry for reliable monitoring and evaluation of radioactive discharges from nuclear power plants and other nuclear facilities into the marine environment.

iii. Developed regional skills in radioecology and radiobiology studies of radionuclides in marine biota endemic to the Asia-Pacific region.

iv. Enhanced regional capabilities in dose assessment and risk analysis modelling.

3 Project Outcomes

i. A total of 7 training courses, 4 workshops and 2 expert mission were conducted under the project. Total of 147 persons were trained, which led to significantly enhancing the regional capacity in marine radioactivity monitoring.

ii. Six Proficiency Tests have been conducted from 2017-2022, and which helped the laboratories to monitor and enhance their analytical capability.

iii. Through the implementation of RAS/7/028, Quality Management System in all laboratories was maintained and improved significantly. The project supported the fulfilment of requirements for maintaining the accreditation of 8 laboratories in the region.

iv. A total of more than 76,680 samples of seawater, sediment and biota were collected by all the participating GPs and analysed for radionuclides like Cs-137, Sr-90, Po-210, Ra- 226 and H-3 etc. (this total includes 2017- 2022 post-Fukushima monitoring in Japan and other countries).

v. The detailed Guidelines for 'Sampling, Preparation and Radio-analysis of Marine Matrices' was developed in collaboration and made available for use by the GPs. The guidelines document enables conducting marine radioactivity monitoring in a harmonised manner and supports regional data comparability.

vi. A total of 3,923 data were submitted to the ASPAMARD database during the period of 2017-2022. The database provides the reference baseline radioactivity levels in the region.

vii. Marine radioactivity databases have been established or updated within each country.

viii. The capabilities for assessing radiological dose and risk to humans and the environment were improved via three training courses, and a collaborative workshop where the RAS/7/028 data were used to evaluate dose for the background baseline and a range of potential nuclear release scenarios.

ix. A total of 74 reports and scientific papers related to marine radioactivity were published during the course of the project.

x. The achievement of RAS 7028 has been appreciated and used by the National Authority in preparation of the policy for marine environment management.

4 Country Report (Malaysia)

Sampling activities were carried out at 40 sampling stations (2019 – 22 stations; 2020 – 15 stations; and 2022 – 3 stations) at selected coastal areas in the country to collect seawater, surface sediment and biota (pelagic and demersal). These sampling activities were carried out in collaboration with IAEA/CRP project entitled "Behaviour and Effects of Natural and Anthropogenic Radionuclides in the Marine Environment and their use as Tracers for Oceanography Studies (K41017)" and with Environmental Quality Monitoring Program (EQMP) under the Department of Environment. The samples collected were analysed to determine the concentration of both anthropogenic and natural radionuclides such as Cs-134, Cs-137, Sr-90, and K-40, Ra-226, Ra-228, K-40, Po-210 and H-3.

Malaysia had participated in all training courses held under this project (7 regional training courses and 4 regional workshops) and proficiency test exercises organised by IAEA-RML since 2018. A national database had been established but it is not running effectively due to some administrative problems and all analysed data until 2020 was submitted to ASPAMARD (2021) and MARIS (2020). Eight publications were published in various scientific journals and the data can also be shared with Malaysian authorities such as the Department of Atomic Energy, the Department of Environment and the Department of Fisheries.

5 Conclusion

Based on the country report, it was concluded that the project had successfully implemented and achieved the objectives set out. There has been demonstrated improvements in the capabilities of GPs in marine radiological monitoring. Numerous new data has been developed and shared. A new "best practice" guidelines document had been produced for use throughout the region and internationally, and numerous reports and scientific papers have been published. The project facilitated improved coordination, communication and collaboration among participating members.

Figure 1: Participants in IAEA/RCA TC Project RAS/7/028 Final Review Meeting, 7 to 11 November 2022, Singapore

References

W.M. Zal Uyun, M. Norfaizal, M.W. Yii, A. Nooradilah, A.T. Dainee Norfadzila, M. Salahudin, H. Maslan, I. Mohd Tarmizi, S. Mohamad Noh, and R. Muhammad Izzat Muammar. 2019a. Seawater, biota and sediment partitioning of ^{137}cs in the east coast of Peninsular Malaysia. *Journal of Radioanalytical and Nuclear Chemistry*, 322:2119 – 2128, https://doi.org/10.1007/s10967–019–06881–3.

W.M. Zal U'yun, A. Nooradilah, M. Norfaizal, I. Mohd Tarmizi, and R. Muhammad Izzat Muammar. 2019b. Distribution of po-210 in seawater, biota and sediment in the east coast of Peninsular Malaysia. *Jurnal Sains Nuklear Malaysia*, 31(2):59 – 68, ISSN: 2232–0946.

W.M. Zal U'yun, M.S. Mohd Zuhair, M.W. Yii, M. Norfaizal, A. Nooradilah, and S. Kamarudin. 2020a. Potential radiological significance of NORM in marine sediments from the East Coast of Peninsular Malaysia. *Global Scientific Journal (November 2020)*, 8(11):1429 – 1440, ISSN 2320–9186.

W.M. Zal U'yun, A. Nooradilah, Yii M. W., and M. Norfaizal. 2020b. Sediment distribution of Ra-226 and Ra-228 in the east coast of Peninsular Malaysia. *AIP Conference Proceedings 2295 (International Conference of Isotopes (ICI), Kuala Lumpur*, 020011:https://doi.org/10.1063/5.0031492.

W.M. Zal U'yun, Y. Rahman, M.W. Yii, M. Norfaizal, A. Nooradilah, A.T. Dainee Norfadzila, I. Mohd Tarmizi, S. Mohamad Noh, R. Muhammad Izzat Muammar, and M. Salahuddin. 2020c. Level, trends and effects of natural radionuclides in sediment from the east coast of Peninsular Malaysia. *Global Scientific Journal*, 8(3):1773 – 1791, ISSN 2320–9186.

Individual Research Contribution Review, 2023, 1(1): 135–136

Levels, Trends and Effects of Natural and Anthropogenic Radionuclides in the Malaysian Marine Environment

Norfaizal bin Mohamed
Waste Technology and Environmental Division
Malaysian Nuclear Agency
43000 Kajang, Selangor
norfaizal@nm.gov.my

Abstract

This research project is a project that was inspired at the national level as one of the sub-projects to support the implementation of the IAEA/CRP project "Behaviour and Effects of Natural and Anthropogenic Radionuclides in the Marine Environment and their use as Tracers for Oceanography Studies". It was implemented in 2017 to 2023. The overall objective of the project is to provide an overview of the distribution of natural and anthropogenic radionuclides in the marine environment. The data obtained is used for dose assessment to humans and biota, and also to provide a source of information in the investigation of ocean processes through the use of radionuclides.

Keywords: marine environment, dose assessment, ocean processes

1 Introduction

The marine environment is a major recipient of natural and anthropogenic radionuclides released by both atmospheric and aquatic pathways. Occurrence of natural specific radionuclides such as Naturally Occurring Radioactive Material (NORM) in marine environment normally from the weathering and mineral recycling of the terrestrial rocks and then supplied by river water. The distributions of natural radionuclides in marine environment particularly in sediment are mostly related to their physical, chemical and geochemical properties. While, sources for anthropogenic radionuclides in the marine environment are from nuclear weapon tests, radioactive releases from nuclear facilities, radioactive waste dumping, and nuclear accidents such as the Chernobyl and the Fukushima.

Determination of baseline levels of these radionuclides in the marine environment is very important and necessary before one attempt to study their behaviour, and to monitor and control their occurrences. Thus, it is important to determine the levels and trends of the radionuclides in different marine environmental compartments before any un-expected level is detected. Level of radionuclides also can be used as tracers to study oceanography processes such as sedimentation, water masses circulation in the open oceans, biological productivity and radioactive pollution indicator. Scientific and public interest in marine radioactivity and the mechanisms through which radionuclides are transported to large distances by ocean currents, diluted and taken up by marine organisms has increased in recent years, particularly after the Fukushima accident in 2011. Furthermore, recent developments in modelling of the dispersal of radionuclides through the marine environment, indicates the general need to substantially improve models. Model predictions are essential for reliable forecasting in accidental situations and assessment of doses through marine exposure pathways.

Malaysia in the past has routinely monitored the radioactivity in its coastal areas and within its territorial waters and has developed a database for future reference. However, the radionuclides studied and biota species selected were not consistent between each project which resulted in difficulties in the overall analysis to see the trends and to make comparison. Therefore, in this project, a more systematic approach with better data quality management is adopted. The new data set could be compared with available data from other studies carried out in the North Pacific Ocean. The data had been contributed to Asia-Pacific Marine Radioactivity Database (ASPAMARD) and IAEA's Marine Information System (MARiS) database.

2 Methods

2.1 Sampling

Sampling activities were carried out at 40 sampling stations from 2019 until 2022 at selected coastal areas in the country (Figure 1) to collect seawater, surface sediment and biota (pelagic and demersal). The biota samples were collected at some stations through manually fishing and most of them were purchased from local fishermen.

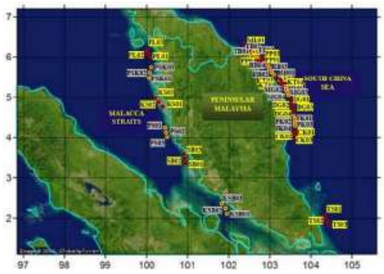

Figure 1: Map shows the sampling points

2.2 Laboratory Analysis

2.2.1 Cs-134, Cs-137

20 L water samples were taken using a Niskin sampler and preserved by adding nitric acid until pH 2. In laboratory, KNiFC-PAN resin was used to absorb radiocaesium from seawater.

After rinsing, KNiFC-PAN resin is transferred into counting container and counted using a high-purity germanium (HPGe) spectrometer. For marine sediment, it was dried in the oven, ground and transfer into 250 mL Marinelli counting container. Biota sample was subjected to the similar sample preparation and analysis procedures as the sediment sample.

2.2.2 U-238, Ra-226, Ra-228, K-40

Samples were transferred into 250 mL counting container, sealed and stored for a period in excess of 30 days to establish secular equilibrium between Ra-226 and Ra-228 and their respective radioactive progenies prior to gamma counting. All samples were counted using a HPGe spectrometer.

2.2.3 Po-210

Radiochemical separation of Po-210 was performed and polonium isotopes was spontaneously plated on silver disc before its activity was determined using alpha spectrometer.

2.2.4 H-3

100 mL of water samples were distilled with sodium hydroxide and potassium permanganate, then the distillate was transferred into a counting vial and mixed with liquid scintillator solution (Ultima Gold-LLT cocktail), and is counted in the liquid scintillation counting system.

3 Result and Discussion

Generally, the partitioning of Cs-137 in surface seawater, biota and surface sediments collected from the nearshore zone in the east coast of Peninsular Malaysia, reflecting variability in its concentration in all type of samples. Align with that, the activity concentration of Cs-137 in respectively were ranged from MDA to 2.70 ± 0.37 Bq m^{-3} (seawater), MDA to 0.34 ± 0.10 Bq kg^{-1} fw. (biota) and MDA to 1.61 ± 0.19 Bq kg^{-1} dw. (sediment). The partition coefficient (CF and K_d) of Cs-137 for biota and sediment were ranged of 0.59–2.95 ($\times 10^2$) L kg^{-1} and 4.44–18.51 ($\times 10^2$) L kg^{-1}, respectively. This condition may be associated with the variability in the characteristics of the seawater, biota and sediment. Additionally, this can be concluded that the levels of Cs-137 in seawater, biota and sediment remain in the background level and there is no new input of Cs-137 into this region (Zal Uyun et al., 2019a).

On the other hand, Po-210 activity concentration is found to be the highest at sampling point nearest to the coastal area that received more input of Po-210 source from the terrestrial. This result is also probably due to the sea condition during sampling which might changes in Po-210 activity concentration. Pelagic fishes have higher activity concentration of Po-210 compared to demersal fishes. These variations of Po-210 activity concentrations may be because of the different habitat and species, location and feeding behaviour of the fishes. The variation levels of Po-210 in sediment are probably affected by the change of redox condition of iron and manganese in the sediment. During the anoxic period, the level of Po-210 in sediment can be significantly increased. The results of the study indicated CF of Po-210 for pelagic fish was relatively high than demersal fish, probably depends on the factors of the physical and chemical properties of the ambient water, behaviour of fishes and related to their species; and geographical regions. Meanwhile, the variation of Kd values for Po-210 most probably due to the sediment particle size (Zal U'yun et al., 2019b).

The activity concentrations of Ra-226 and Ra-228 were comparable to previous studies and even lower than other regions. Thus, it can be confirmed that these radionuclides were mainly supplied and transported from terrestrial sources. Other factors that can be concluded to affect the variation of these radionuclide activity concentrations and their activity ratios were strictly related to their half-life, other potential input sources, geological formation of the study area, environment origin and behavior.

The radioactivity concentrations level of U-238, Th-232, Ra-226 and Po-210 in surface sediment collected in the east coast of Peninsular Malaysia were ranged of 3.81 ± 0.29 –32.58 ± 7.63 Bq/kg dw., 12.51 ± 1.65 – 63.29 ± 8.24 Bq/kg dw., 7.21 ± 0.59 – 64.93 ± 7.63 Bq/kg dw. and 22.28 ± 0.99 –69.14 ± 3.09 Bq/kg dw., respectively. Meanwhile, their radioactivity trends and distribution found to be higher toward the coastal area. This result due to terrestrial play an important role as a main source for supplying these radionuclides to studied area. The mean radium equivalent activity concentration index and other radiological hazard parameter were lower than their maximum permissible limits. Therefore, the sediments in the east coast of Peninsular Malaysia confirmed were not posed radiological risks to the surrounding people, fisherman, divers or who-else presence in this area owing to harmful effects of ionizing radiation from the natural radionuclides in sediment. Furthermore, these sediments are suitable and safe to use as road or building construction materials (Zal U'yun et al., 2020).

4 Conclusion

This project has been successfully carried out. The results obtained showed that the level of marine radioactivity in Malaysia does not pose radiological risks to human and the environment.

References

W.M. Zal Uyun, M. Norfaizal, M.W. Yii, A. Nooradilah, A.T. Dainee Norfadzila, M. Salahudin, H. Maslan, I. Mohd Tarmizi, S. Mohamad Noh, and R. Muhammad Izzat Muammar. 2019a. Seawater, biota and sediment partitioning of ^{137}cs in the east coast of Peninsular Malaysia. *Journal of Radioanalytical and Nuclear Chemistry*, 322:2119 – 2128, https://doi.org/10.1007/s10967–019–06881–3.

W.M. Zal U'yun, A. Nooradilah, M. Norfaizal, I. Mohd Tarmizi, and R. Muhammad Izzat Muammar. 2019b. Distribution of po-210 in seawater, biota and sediment in the east coast of Peninsular Malaysia. *Jurnal Sains Nuklear Malaysia*, 31(2):59 – 68, ISSN: 2232–0946.

W.M. Zal U'yun, Y. Rahman, M.W. Yii, M. Norfaizal, A. Nooradilah, A.T. Dainee Norfadzila, I. Mohd Tarmizi, S. Mohamad Noh, R. Muhammad Izzat Muammar, and M. Salahuddin. 2020. Level, trends and effects of natural radionuclides in sediment from the east coast of Peninsular Malaysia. *Global Scientific Journal*, 8(3):1773 – 1791, ISSN 2320–9186.

Individual Research Contribution Review, 2023, 1(1): 137–138

Determination of Polonium-210 in Various Environmental Samples Using Auto-deposition Technique and Measurement by Alpha Spectrometry

Nurrul Assyikeen Md. Jaffary
Waste Technology and Environmental Division
Malaysian Nuclear Agency
43000 Kajang, Selangor
assyikeen@nm.gov.my

Abstract

Research has carried out on the method validation and verification of ^{210}Po in Radiochemistry and Environmental Laboratory (RAS), Malaysian Nuclear Agency. An easy and accurate method for the determination of ^{210}Pb and ^{210}Po in various environmental samples such as soil, sediment, and biota using ^{210}Po spontaneous deposition onto a silver disk is proposed and assessed for its detection capabilities according to the ISO Guide for the expression of uncertainty in measurement (GUM) based on the alpha spectrometric measurement. Several studies conducted on ^{210}Po analysis in various sample types are highlighted.

Keywords: Polonium, radioactivity, radiochemistry, alpha spectrometry

1 Introduction

Polonium-210 (^{210}Po) is a naturally occurring alpha emitter and exists in the environment as a result of ^{210}Pb decay within the ^{238}U decay chain. Po-210 decays to its stable daughter isotope, ^{206}Pb. Being part of the ^{238}U decay series, ^{210}Po is ubiquitous in our environment. Its environmental distribution results from two main processes:

i. the release of ^{222}Rn from the earth's crust, and

ii. the dissolution of ^{226}Ra in seawater

which scatters radioisotopes through various environmental compartments (Matthews et al., 2007). Industrial activities such as oil-fired power plants (Vaasma et al., 2017), and phosphate industries (Bory lo et al., 2013).

Po-210 is one of the most toxic naturally occurring radionuclides and important environmental radionuclides due to its wide distribution and potential for human radiation exposure through ingestion and inhalation. The measurement of ^{210}Pb and ^{210}Po activities in environmental samples is important in the field of health physics, geochronology and environmental science. The main research areas were the prevalence of ^{210}Po in the atmosphere, marine, terrestrial, and food chains. This study aimed to validate the ^{210}Po test method and improve the method to be reliable to various sample types.

2 Methods

The radiochemical procedure of polonium determination includes the following stages: sample digestion, auto deposition on silver disc, and measurements using alpha spectrometry. Considering all stages, the developed method was assessed and its performance studied to determine its suitability for the analysis of ^{210}Po in environmental sample. Different certified reference materials with a wide range of compositions from the International Atomic Energy Agency (IAEA) were used for quality control measurement. Traceable radiotracer of ^{209}Po with available radioactivity value was used in this study for the recovery check. The quality assessment of the measuring method by evaluating the uncertainty according to the ISO Guide for the Expression of Uncertainty in Measurement (GUM) (1995) has been made.

3 Results and Discussion

The method validation of the ^{210}Po test method in soil and sediment was so convincing using the IAEA-384, IAEA-385 and IAEA-410, with the relative standard deviation, RSD value less than 10%. The average value obtained for the reference material is close to the certified value, with the Uscore value less than 1.5, showing no significant bias of this method. The method validation has also demonstrated that this measuring technique is robust in terms of physical and chemical aspects (Jaffary et al., 2023c).

The measurement's confidence level, an estimate of the measurement's uncertainty must be combined with its reporting value. The quantification of ^{210}Po uncertainty is extensively documented using the spreadsheet method (Kragten's method) (Jaffary et al., 2023d). The study found that the uncertainty variables for sample peak area, tracer peak area and tracer activity are the main contributors to the ^{210}Po radioactivity's uncertainty value. Uncertainty estimation of Uranium isotopes using alpha spectrometry has been reported for a better understanding of Kragten's approach (Jaffary et al., 2023b).

River sediment and soil along the Pekan, Kuala Sungai Baru, and Pulau Indah river estuary have been analysed for ^{210}Po (Jaffary et al., 2021a). Study has identified factors that influenced its distribution:

i) The distribution of ^{210}Po activity in river sediments at estuary areas is influenced by the salinity value, and correlated with the inclusion of the parent radionuclide ^{238}U.

ii) Po-210 activity in the western region of peninsular Malaysia is higher than the eastern region of peninsular Malaysia because the western area is closer to the volcanic range in Sumatra.

iii) The average reading of ^{210}Po activity in the river sediment sample (supported and unsupported ^{210}Po) is higher than the soil sample(unsupported ^{210}Po).

Po-210 is a radioactive compound present in nature, hence it can also be found in the human body. A study was conducted to assess any contaminants among radiochemistry laboratory radiation workers to better understand the baseline level. The urine excretion is used to estimate doses resulting from ^{210}Po or a combination of ^{238}U chain radionuclides that comprises ^{210}Po. The ^{210}Po of radiochemistry laboratory workers in this study were measured to be between 1.33 mBqL^{-1} and 49.84 mBqL^{-1} (Jaffary et al., 2021b).

Po-210 can accumulate in high concentrations in various marine species. Due to its radiotoxicity, determining ^{210}Po in seafood become very crucial. A study was conducted utilising certified reference material (CRM) IAEA-414 (Mixed Fish) to discuss the primary factors that influence the ^{210}Po determination in a biota sample. An improvement of the test method has been made and is to be used in analysing biota at the Radiochemistry and Environmental Group (RAS), Malaysian Nuclear Agency (Jaffary et al., 2023a).

4 Conclusions

Ongoing development activities on the determination of ^{210}Po in various environmental will be able to ensure reliable reporting data and expand the scope of analysis across multiple sample types. The continuous work on method development, validation, and verification will benefit the research world and the field of radiation protection. This study may fulfil demand by local authorities, industrial companies and research universities to ensure the reliability of the reported data requested.

References

A. Bory lo, G. Olszewski, and B. Skwarzec. 2013. A study on lead (210Pb) and polonium (210Po) contamination from phosphogypsum in the environment of Wiślinka (northern Poland). *Environmental Sciences: Processes and Impacts*, 15(8):1622–1628. Available at: https://doi.org/10.1039/c3em00118k.

N.A.M. Jaffary, N.Z. Azlan, J.S. Sarip, M.T. Ishak, N. Shaharudin, and et al. 2021a. Determination of the presence of Polonium- 210 in sediment and soil samples by auto deposition and alpha spectrometry analysis. *Konvensyen Teknikal Nuklear Malaysia (NTC 2021), 26 - 28 Oktober 2021.*

N.A.M. Jaffary, N.Z. Azlan, J.S. Sarip, M.T. Ishak, Z. Daud, and et al. 2021b. Po determination in urine samples among radiation workers by alpha spectrum analysis. *Malaysian Journal of Analytical Sciences*.

N.A.M. Jaffary, J.N.G. Li, and et al. 2023a. Improving measurement of Polonium-210 in biota samples at Radiochemistry and Environmental Group, Malaysian Nuclear Agency. *Konvensyen Inovasi dan Teknikal Nuklear Malaysia (NITC) 24-26 Oktober 2023*.

N.A.M. Jaffary, A. Chriscius, and et al. 2023b. Kragten's method approach to estimate the uncertainty of uranium isotopes radioactivity using alpha spectrometry. *Konvensyen Inovasi dan Teknikal Nuklear Malaysia (NITC) 24-26 Oktober 2023*.

N.A.M. Jaffary, M.H. Kamarozaman, and et al. 2023c. Robustness of Polonium-210 test method in terms of physical and chemical aspects. *e-Jurnal Sains Nuklear Malaysia*, 35(1):29 – 36.

N.A.M. Jaffary, Sarip J.S, and C. Anthonius. 2023d. Uncertainty measurement for radioactivity analysis of Polonium-210 environmental sample using alpha spectrometry system. *NUKLEARMALAYSIA/L/2023/75.*

K.M. Matthews, C. Kim, and P. Martin. 2007. Determination of Po in environmental materials : A review of analytical methodology. 65:267–279. Available at: https://doi.org/10.1016/j.apradiso.2006.09.00 5.

T. Vaasma, Jüri Loosaar, Francis Gyakwaa, Madis Kiisk, Banu Özden, and Alan H. Tkaczyk. 2017. Pb-210 and Po-210 atmospheric releases via fly ash from oil shalefired power plants. *Environmental Pollution*, 222:210–218. Available at: https://doi.org/10.1016/j.envpol.2016.12.054..

Individual Research Contribution Review, 2023, 1(1): 139–140

Assessing the Water Quality of Putrajaya Constructed Wetlands and Lakes

Nurul Fairuz Diyana
Waste Technology and Environmental Division
Malaysian Nuclear Agency
43000 Kajang, Selangor
nurulfairuz@nm.gov.my

Abstract

An assessment of water quality in Putrajaya Wetlands and Lakes was conducted to evaluate the water quality of Putrajaya Constructed Wetlands and Lakes against the established Malaysian Water Quality Index (WQI) standards. The results revealed that the parameters consistently met the stipulated standards of Class IIB water quality, as defined by the Department of Environment for primary body contact during water recreational activities. Stable isotope analysis suggested that rainwater was the primary source of water in this system, further confirming the uncontaminated nature of the water. The absence of any interaction with contaminated materials further supported the suitability of Putrajaya Wetlands and Lakes for water recreational activities.

Keywords: constructed wetlands, stable isotopes

1 Introduction

Constructed Wetland (CW) is recognized as an ecological technology for wastewater treatment, encompassing substrate, aquatic plants, animals, and microorganisms (Vymazal, 2010). This innovative approach has gained prominence globally over the last few decades, proving effective in purifying diverse sources of pollution such as domestic sewage, urban runoff, and industrial effluents (Vymazal, 2011). Notably, the Putrajaya Wetlands and Lakes (101.6883°E and 2.936361°N) exemplify the successful implementation of this technology. Established in 1997–1998, these 200 hectares constructed wetland system, featuring six arms with 24 cells, was designed to address surface runoff resulting from development and agricultural activities in an upstream catchment before it reaches the expansive Putrajaya Lake, spanning 400 hectares (Majizat et al., 2010). Assessing the water quality of Putrajaya Constructed Wetlands and Lakes is of paramount importance. Regular water quality assessments not only help identify any potential threats to the ecosystem but also inform necessary remedial actions. Furthermore, evaluating water quality provides a valuable assessment of the effectiveness of these CWs in removing pollutants and contributing to the overall health of the waterway. This study aims to comprehensively evaluate the water quality of Putrajaya Constructed Wetlands and Lakes in relation to the established Malaysian Water Quality Index (WQI) standards.

2 Methods

In situ measurements of dissolved oxygen (DO), pH, temperature, salinity and conductivity were carried out at Putrajaya Constructed Wetlands and Lakes as shown in Figure 1 using a YSI 6600 multi-parameter probe. Water samples were collected before being stored, preserved and transported to the laboratory for stable isotopes analysis.

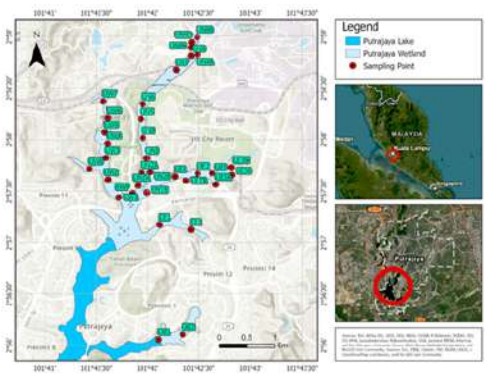

Figure 1: Distribution map of sampling points in Putrajaya Wetlands and Lakes.

3 Results and Discussion

An assessment of water quality in Putrajaya Wetlands and Lakes demonstrated that the parameters consistently meet the stipulated standards of Class IIB water quality, as defined by the Department of Environment for primary body contact during water recreational activities (Table 1).

Table 1: DOE Water Quality Classification for Class IIB (2012)

Parameter	Class IIB (DOE)
Temp (°)	28°C, Normal ±
pH	6 - 9
Conductivity (us/cm)	1000
Salinity (ppt)	1
Dissolved Oxygen (DO, mg/L)	5 - 7

Moreover, the range of water quality parameters presented in Table 2 indicates the overall stability and acceptability of water quality within the study area. This is important because it suggests that the water quality is not likely to fluctuate significantly over time, which would reduce the risk of adverse health effects for water users. Notably, the results of the analysis demonstrated the absence of any interactions with contaminated materials further reinforcing the suitability of Putrajaya Wetlands and Lakes for water recreational activities.

Table 2: Ranges of water quality data for Putrajaya Wetlands

Parameter	UN	UW	UE	LE	UB	CW
Temp (°)	29	29	29	29	29	29
pH	7-9	7.6	7.4-7.7	7.4-7.7	7	7.3
Conductivity (us/cm)	80	80	76-82	50-89	70-90	74
Salinity (ppt)	0.04	0.04	0.03-0.04	0.02-0.04	0.03-0.04	0.03
DO, mg/L	3	3	3	3	3-4	3

Figure 2 show the plot of δ^{18}O vs δ^{2}H for Putrajaya Lakes and Wetlands. The plot of δ^{18}O vs δ^{2}H exhibits a clear trend, indicating a mixing of different water sources.

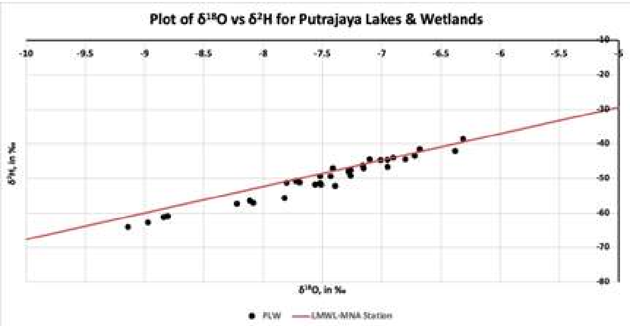

Figure 2: Plot of δ^{18}O vs δ^{2}H for Putrajaya Lakes and Wetlands.

This observation aligns with the fact that the water system draws from a combination of surface runoff, groundwater seepage, and treated wastewater. Consequently, the results demonstrate that isotope ^{18}O/^{16}O distribution can effectively unravel the interactions within water systems, providing a comprehensive understanding of ecological and hydrological dynamics. Stable isotope analysis indicates that rainwater is the primary source of water in this system. However, some points deviate from the LMWL line due to ongoing desilting activities. Desilting, a meticulously planned and impactful approach to river management, aims to enhance hydraulic performance and safeguard the natural balance of these critical water systems.

4 Conclusion

Constructed wetlands in Putrajaya effectively treat wastewater, meeting Class IIB water quality standards. This study supports the use of constructed wetlands as a sustainable wastewater treatment alternative. Additionally, continuous monitoring provides valuable data for assessing the long-term impact of the constructed wetlands on water quality and ecological conditions.

References

A. Majizat, R. Sahat, N. Noordin, N. A. Rahaman, and Y. Muhamad. 2010. Tasik Putrajaya and Wetlands, Putrajaya, Lake Brief. In: Managing lakes and their basins for sustainable use in Malaysia. *Lake briefs report series I, Akademi Sains Malaysia, Kuala Lumpur*, pages 139 – 169.

Department of Environment Malaysia (DOE). 2012. Malaysia Environmental Quality Report 2012.

J. Vymazal. 2010. Constructed wetlands for wastewater treatment: Five decades of experience. *C R C Crit Rev Environ Control*, 31:351 – 409.

J. Vymazal. 2011. Constructed wetlands for wastewater treatment: Five decades of experience. *Environ. Sci. Technol.*, 45:61 – 69.

Individual Research Contribution Review, 2023, 1(1): 141–142

Climate Influence on Pollutant Mobilization and Emerging Risks in Selangor River Basin

Nurul Syazwani Yahaya
Waste Technology and Environmental Division
Malaysian Nuclear Agency
43000 Kajang, Selangor
syazwani@nm.gov.my

Abstract

Climate change is expected to enhance the mobilization of pollutants in the surface as well as the subsurface environment(Miller and Hutchins, 2017; Jarsjö et al., 2020). More frequent floods will affect mobilization of contaminated floodplain sediments to other areas, turning floodplain from being the sink of pollutants to the source of pollutants (Ponting et al., 2021). In Selangor, the fast-blooming industrial activities, including in the upstream areas has brought forth increasing release of toxic waste materials into the environment (Najat et al., 2018). In recent years, river pollution incidences due to illegal dumping of industrial waste has often cause disruptions to water supplies in the Selangor and Kuala Lumpur area (Chowdhury et al., 2018).

1 Introduction

Over the last few decades, the Selangor River basin have been under rapid development, including expansion of industrial areas. Respectively, studies performed in the area showed a strong gradient of heavy metal concentrations moving from upstream to downstream (Daniel and Kawasaki, 2016). In the Rawang sub-basin, an upstream area where many heavy industries are located, river water samples were found to be more polluted than other parts of the river with average concentration of some heavy metals exceed the national standards (Faridah et al., 2018; Sakai et al., 2017; Daniel and Kawasaki, 2016). Persistent organic pollutants associated with plastic manufacturing industries are also quite prominent in the Selangor River (Santhi and Mustafa, 2013). Incidences involving industrial pollutants are commonly reported that often caused disruptions to water supplies in Selangor and Kuala Lumpur area. As flood events aggravated under the impact of climate change and the extent of flood prone area expanded, there may be an increasing risk of floods towards potential point sources of the pollutants, especially in areas that have never been flooded before or when flood level/magnitude is higher than the level that facilities were built to prepare for (Kumasaki and King, 2020). An assessment on projected 100-year flood for year 2030 and 2050 for Malaysia shows an increase of flood-prone areal extent by 38.3% and 39.6% respectively (NC3, 2018). Therefore, identifying the potential pollutants as well as the exposure of the potential point sources towards floods is a crucial first step towards a better understanding and management of the possible cascading risks on humans, resources and the environment. The study aims to identify potential pollutants, their sources and susceptibility of exposed elements in the Selangor River basin under the influence of climatic hazards.

2 Methods

The potential pollutants and their point sources within the Selangor River basin (SRB) were identified using content analysis of published government and local reports. The flood and coastal hazards susceptible areas are delineated from the local soil map using the GIS tool. Soil map is a classical but still relevant approach that is both fast and economic to estimate areas subject to flooding where there is no significant alteration to the stream regimen from man-made works (Cain and Beatty, 1968; Sangwan and Merwade, 2015). The distribution of the potential point sources was then identified from reports as well as from open sources, and were plotted to overlay with the flood and coastal hazards susceptible areas within the SRB. The exposure analysis to identify the potential point sources that are exposed to floods and coastal hazards were then performed based on the overlay.

3 Results

Based on the content analysis, heavy metals and inorganic pollutants were found to be the most prominent group of pollutants for the Selangor River. Other significant group of pollutants microbiological, physical, pesticides and organic. The potential point sources comprise industrial areas/factories, livestock farm, aquaculture, wet markets, and landfills. Based on the exposure analysis of the identified potential point sources, 66 manufacturing industry sites are exposed to floods, 38 are exposed to landslides and 6 are exposed to coastal hazards. Many communities and resources are found near industrial areas, where some of the areas are exposed to floods, landslides, and coastal hazards.

4 Discussion

The screening of the flood and coastal hazards-exposed potential point sources provides an initial step towards managing/controlling pollutants mobilization under the risk of the climatic hazards. To ensure higher efficacy in appraising future risks of pollutant mobilization, more inclusive monitoring of the sources of pollutants would be necessary (both from the point-sources and non-point sources). In addition to tackling immediate impacts of pollution (e.g. water supply disruptions), the longer-term impacts of pollution (e.g.

land degradation) on resources should also be appropriately addressed. Local-level actions proposed to ensure resilience to emerging climate include construction of retaining walls at exposed industrial sites, government's strategic policy and hazard warning systems, community awareness and actions, as well as risk communication by subject matter experts from academia and professional bodies.

References

J.M. Cain and M.T. Beatty. 1968. The use of soil maps in the delineation of flood plains. *Amerika Syarikat: Water Resources Research*, 4-1.

M. S. U. Chowdhury, F. Othman, W. Z. W. Jaafar, N. C. Mood, and M. I. Adham. 2018. Assessment of pollution and improvement measure of water quality parameters using scenarios modeling for Sungai Selangor Basin. *Bangi: Sains Malaysiana*, 47(3).

R. Daniel and N. Kawasaki. 2016. The distribution of heavy metals and nutrients along Selangor River and its adjacent mining ponds, Malaysia. *India: International Journal of Advances in Agricultural and Environmental Engineering*, 3(2).

Othman Faridah, M. S. U. Chowdhury, Wan Jaafar Wan Zurina, E. M. Mohammad Faresh, and S. M. Shirazi. 2018. Assessing risk and sources of heavy metals in a tropical river basin: A case study of the Selangor River, Malaysia. *Poland: Polish Journal of Environmental Studies*, 27(4).

J. Jarsjö, Y. Andersson-Sköld, M. Fröberg, J. Pietroń, R. Borgström, Å. Löv, and D. B. Kleja. 2020. Projecting impacts of climate change on metal mobilization at contaminated sites: Controls by the groundwater level. *Science of the Total Environment*, 712.

M. Kumasaki and M. King. 2020. Three cases in Japan occurred by natural hazards and lessons for Natech disaster management. *International Journal of Disaster Risk Reduction*, 51.

J. D. Miller and M. Hutchins. 2017. The impacts of urbanisation and climate change on urban flooding and urban water quality: A review of the evidence concerning the United Kingdom. *Journal of Hydrology: Regional Studies*, 12.

Masood Najat, N. Halimoon, A. Z. Aris, M. P. Zakaria, V. Vaezzadeh, S. M. Magam, S. Mustafa, M. M. Ali, M. Keshavarzifard, S. A. A. Alkhadher, C. W. Bong, and M. A. Alsalahi. 2018. Seasonal variability of anthropogenic indices of PAHs in sediment from the Kuala Selangor River, west coast Peninsular Malaysia. *Environmental Geochemistry and Health*, 40(6).

NC3. 2018. Malaysia: Third National Communication and Second Biennial Update Report to the UNFCCC. *Putrajaya: Ministry of Energy, Science, Technology, Environment and Climate Change.*

J. Ponting, T. J. Kelly, A. Verhoef, M. J. Watts, and Sizmur T. 2021. The impact of increased flooding occurrence on the mobility of potentially toxic elements in floodplain soil – A review. *Science of the Total Environment*, 754.

N. Sakai, Z. Alsaad, N. T. Thuong, K. Shiota, M. Yoneda, and M. Ali Mohd. 2017. Source profiling of arsenic and heavy metals in the Selangor River basin and their maternal and cord blood levels in Selangor State, Malaysia. *Chemosphere*, 184.

N. Sangwan and V. Merwade. 2015. A faster and economical approach to floodplain mapping using soil information. *Journal of the American Water Resources Association*, 51(5).

V. A. Santhi and A. M. Mustafa. 2013. Assessment of organochlorine pesticides and plasticisers in the Selangor River basin and possible pollution sources. *Environmental Monitoring and Assessment*, 185(2).

Coal Power Plant Fly Ash Characterization Assessment for Geopolymerization Process

Nurul Wahida Ahmad Khairuddin
Waste Technology and Environmental Division
Malaysian Nuclear Agency
43000 Kajang, Selangor
nwahida@nm.gov.my

Abstract

This paper presents the physical and chemical properties of fly ash obtained from two coal power plants; the Sultan Salahuddin Abdul Aziz Power Plant in Kapar, Selangor and Sultan Azlan Shah Power Plant in Manjung, Perak. The moisture content for Kapar and Manjung fly ash were at 0.41% and 0.11%, respectively. XRF result showed that Kapar fly ash sample is of class C due to the total percentage of SiO_2, Al_2O_3, and Fe_2O_3 being less than 70% while Manjung fly ash sample is of class F due to the total percentage of SiO_2, Al_2O_3, and Fe_2O_3 more than 70%. Gamma spectrometry analysis indicated presence of ^{226}Ra, ^{232}Th, and ^{40}K in the samples.

Keywords: fly ash, radionuclide, geopolymer

1 Introduction

This article is aimed to discuss the characterisation of fly ash for making a geopolymer for development of a conditioning method of radioactive waste at a laboratory scale. Geopolymers are made by adding aluminosilicates which can be sourced from fly ash to concentrate alkali solutions (Jaarsveld et al., 2000).

It uses polycondensation of silica and alumina precursors to achieve structural strength instead of calcium silicate hydrate (CSHs) like in Portland/pozzolanic cement (Jaarsveld et al., 2000). Cementitious materials such as Portland cement are hydraulic binders which are commonly used in the conditioning of radioactive waste.

It is expected that by reusing this by-product from electric power plants will have an overall positive impact on the total energy demand for producing concrete as well as the greenhouse gas emissions into the atmosphere (Harjito and Tsen, 2008). The rock-based geopolymer cement is ideal for environmental applications, such as the permanent encapsulation of radioactive wastes (Geopolymer Technology, 2009). Before geopolymerization takes place, the fly ash feed materials need to be characterized to determine factors contributing to its synthesis behavior and overall end product quality. Geopolymer binders have similar characteristics to Portland cement. It can set and solidify at room temperature and achieve reasonable strength in a short period of time.

2 Methods

Moisture content of fly ash was determined according to the BS EN 1097-5 (1999). Approximately 10g of fly ash were placed onto a weighing boat, weighed, and later dried in an oven at 105°C until a constant weight was achieved (in triplicate). The sample was weighed several times throughout the drying process until there was no more reduction in mass with further drying time to ensure dry mass was achieved. Moisture content was determined by the difference between the wet and the dry mass of the sample.

Particle size was measured using a PCScope PCS 81x digital microscope and Microtrac X-100 particle size analyzer. Morphology was checked using Zeiss GeminiSEM Field Emission Scanning Electron Microscopy (FESEM). Wavelength Dispersive X-Ray Fluorescence (WDXRF) was used to identify constituent elements of fly ash samples. Analysis of Radionuclide Content measured using Ortec hyper-pure germanium (HpGe) gamma spectrometer system with 30% relative efficiency and a resolution of 1.74 keV at 1.33 meV of ^{60}Co.

3 Results and Discussion

The moisture content of fly ash samples from Sultan Salahuddin Abdul Aziz Power Plant, Kapar Selangor, and Sultan Azlan Shah Power Plant, Manjung, Perak which were 0.48% and 0.11%, respectively. Smaller water content increases compressive strength and reduces of apparent porosity and pore size (Vitola et al., 2020). The Kapar fly ash has a particle size range between 1.06-209.3 μm and the median particle size of 20.64 μm. While Manjung fly ash has a particle size range of 0.75 – 104.70 μm and the median particle size of 11.37 μm. Particle size of fly ash needs to be 80-90% lower than 45 μm to obtain the optimum binding effect (Fernández-Jiménez and Palomo, 2003).

The XRF result, shows that Kapar fly ash is of class C fly ash due to the total percentage of SiO_2, Al_2O_3, and Fe_2O_3 of more than 50% and SO_3 percentage content of less than 5%; while Manjung fly ash is of class F fly ash due to the total percentage of SiO_2, Al_2O_3, and Fe_2O_3 of more than 70%. Ideal fly ash source material for geopolymerization should have low calcium content, Fe_2O_3 content of no more than 10% and 40-50% silica content (Fernández-Jiménez and Palomo, 2003). This fact establishes Kapar fly ash as being more superior than Manjung fly ash as source material.

Rietveld refinement of XRD pattern was performed on the profile fit to determine percentage of constituent phases. Results are as shown in Figure 1. Both samples contain almost similar percentage of quartz. Significant content of mullite which are 20.4% and 35.9% were found for Kapar and Manjung samples, respectively. The remaining phases were determined to be of either iron or aluminium. This result is in good agreement with results from XRD analysis whereby Manjung sample contains higher percentage of aluminosilicates than Kapar sample.

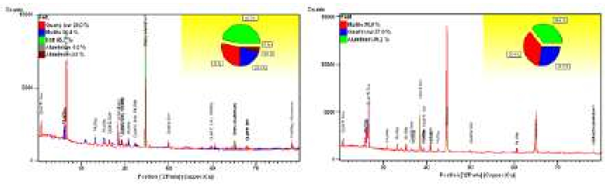

Figure 1: Phase identification of sample. Left: Kapar smple and right: Manjung sample.

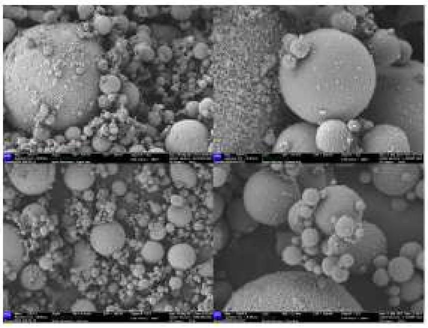

Figure 2: MIcrostructure of materials analyzed using field emission scanning electron microscopy (FESEM), Clockwise from top-left corner: Kapar sample at 1,500X magnification, Kapar sample at 7,000X magnification, Manjung sample at 1,500X magnification and Manjung sample at 7,000X magnification.

Field Emission Scanning Electron Microscope (FESEM) scanners were used to obtain the morphology of Kapar and Manjung fly ash. As shown in Figure 2, the particles of fly ash of Kapar and Manjung are spherically shaped. The diameter of Kapar fly ash ranges from 1μm to 50 μm; while for Manjung sample, the size ranges from 0.2 μmup to 13 μm in diameter with the average particle size of 9.8 μm. The microstructure of Kapar and Manjung fly ash is similar to that reported by Davidovits (Davidovits, 1994). According to (Pacheco-Taorgaln et al., 2008), spherical microstructure of fly ash will promote bonding within the matrix and will also reduce permeability. This theory is also supported by (Ammar et al., 2013) who stated that the spherical shape of the fly ash improves the workability of the concrete mix, while its small particle size acts as a space filler to produce a compact and durable concrete.

4 Conclusion

Kapar fly ash posesses superior characteristics in terms of composition, noting that Kapar fly ash is of class C fly ash while Manjung fly ash is of class F fly ash. Meanhile Manjung fly ash is superior in terms of physical characteristics such as particle size and moisture content. Study also showed presence of ^{226}Ra, ^{232}Th, and ^{40}K radioactivity in the fly ash which makes the feed materials slightly radioactive although still below the regulatory limit to be classified as such. This characterization of fly ash is important as a basis to develop fly ash-based geopolymer.

References

M. Ammar, S. Vineet, K. Ravishankar, N. Praveena, and D.B. Raijiwala. 2013. Alkali activated flyash based geopolymer concrete. *Intl. J. of Emerging Tech. and Adv. Eng.*, 3(1).

J. Davidovits. 1994. High-alkali cements for 21st century concretes, in: P.K Metha, Concrete Technology, Past, Present and Future American Concrete Institute, Farmington Hills, Michigan. *Key Engineering Materials*, 908 683:383–397.

A. Fernández-Jiménez and A. Palomo. 2003. Characterisation of fly ashes-potential reactivity as alkaline cements. *Fuel*, 82(18):2259–2265.

D. Harjito and M.Z. Tsen. 2008. Strength and thermal stability of fly ash-based geopolymer mortar. *The 3rd International Conference-ACF/VCA*, pages 144–150.

J.G.S. Van Jaarsveld, J.S.J. Van Deventer, and G.C. Lukey. 2000. The effect of composition and temperature on the properties of fly ash and kaolinite-based geopolymers. *The Chemical Engineering Journal*, 89(1-3):63 – 73.

F. Pacheco-Taorgaln, J. Castro-Gomes, and S. Jalali. 2008. Alkaliactivated binders: A review part I. Historical background, terminology, reaction mechanisms and hydration product. *J. Constr. Build Mater*, 22:1305–1314.

Geopolymer Technology. 2009. An opportunity to enhance the sustainability of the mining and construction industries. *Geopolymer Alliance*.

L. Vitola, I. Pundiene, J. Pranckeviciene, and D. Bajare. 2020. The impact of the amount of water used in activation solution and the initial temperature of paste on the rheological behaviour and structural evolution of metakaolin-based geopolymer pastes. *Sustainability*, 12.

Individual Research Contribution Review, 2023, 1(1): 145–146

Radioactive Waste Inventory for Borehole Disposal Facility in Malaysia

Nurul Wahida Ahmad Khairuddin
Waste Technology and Environmental Division
Malaysian Nuclear Agency
43000 Kajang, Selangor
nwahida@nm.gov.my

Abstract

This paper presents the conditioning of disused sealed radioactive source (DSRS) in Malaysia. In Malaysia, sealed radioactive sources (SRS) are widely used in Malaysia especially in industry, medicine and research. Once SRS are no longer in use, they are declared disused and managed as radioactive waste. In order to reduce the risk associated with disused sealed radioactive sources (DSRS), the first priority would be to bring them under appropriate controls. This paper describes the experience developed and activities performed by Nuclear Malaysia throughout the period in conditioning of DSRS as well as future programme to further enhancing the infrastructure. Currently, Malaysia has in possession about 16612 unit of DSRS categories 3-5 and 5 units of DSRS category 2 sources which being stored at the interim storage facility Nuclear Malaysia. A national activity was implemented for the on-the-job training of personnel tasked with the conditioning of DSRS, at the Waste Technology Development Centre (WasTeC) facilities. This is part of "cradle-to-grave" control of radioactive sources to protect the workers and public from the hazards of ionizing radiation.

Keywords: DSRS, inventory

1 Introduction

Disused Sealed Radioactive Sources (DSRS) has been stored at Nuclear Malaysia since 1985. This encompasses the whole range of activity, from micro curie to kilocurie level and from usage in small consumer products up to high activity teletherapy for medical application. There are more than 16000 units of DSRS in storage, with a whole spectrum of sources from category 1 to category 5. Currently, there are only 5 DSRS in Category 1 and Category 2 and the others are in Category 3-5. The current priority is to dispose the Category 3-5 DSRS under the borehole disposal concept. Management of DSRS with activities below 1 Ci (37 GBq) (based on maximum activity for Co-60) can be done in a lightly shielded facility using standard lead brick.

Currently, the inventory about all types of radioactive wastes including DSRS has been recorded and safely kept in the spread sheet form at Waste Technology Development Centre, Nuclear Malaysia. The spread sheets contained the most important information of DSRS including the type of radionuclides, activities with reference dates, the last user that transferred the DSRS to the WasTeC (as a Waste Management Centre of Nuclear Malaysia), manufacturer, type and model of the devices and serial number.

Radioactive waste characterization should be done if there are any waste records or inventory data which are not completely documented and verified. This kind of aspect is important because all the DSRS that has been planned to be put in the borehole must be identified and well documented by the waste operator and the regulatory body should verify the safety assessment aspects of the waste management strategies and plans which will be provided by the waste operator. Identifying and effort to complete all the related information such as DSRS source dimension will be the key parameter of the inventor which will enable the first screening to be done in the point of view for safety assessment aspect critically in the development of borehole disposal facility in Malaysia.

2 Inventory Requirement for the Borehole Disposal Facility

For Malaysia, the disposal of DSRS is only considered for DSRS in categories 3 to 5. Thus, DSRS in Category 1 and 2 will not be disposed of in the facility although the IAEA BDF concept does not restrict the disposal of DSRS in those categories in such facility. The typical dimension of sealed sources has been adopted and revised from the IAEA publication for the identification of radioactive sources and devices (IAEA, 2007). Other types of waste that will not be accepted for disposal in the planned borehole are as follows:

a. 5 unit Co-60 of Spent High Activity Radioactive Sources (SHARS) from Teletherapy Devices (Theratronic Model)

b. Unsealed sources in the form of powder (eg: CsCl) or gas (eg: Krypton)

c. Liquid waste either aqueous, chemicals, acid or alkali

d. All types of neutron sources such as Am-Be, Pu-Be or Ra-Be

e. Plutonium and its isotope

f. Uranium and thorium including depleted Uranium

g. Sources that for some reason, did not fit into the capsule.

h. 100 units consist of irretrievable Ra-226 (from needles that have already been conditioned)

i. 11 units of gas-filled Kr-85

All of them are also excluded from the screening process for the preliminary safety assessment calculation for a borehole disposal facility.

The amount of DSRS from our inventory records that have been considered to be disposed of in the borehole disposal facility is 13137 units of radioactive sources in total (as shown in Table 1). From this figure, 10980 units of Am-241 are smoke detectors that have been dismantled from their devices.

Table 1: Inventory of DSRS considered for Borehole Disposal Facility from 1984-2022

Radionuclide	Half-life (years)	DSRS (Units)	Current Activity (Ci) (2022)
Co-60	5.27	433	2.04E-01
Kr-85	10.7	47	1.20E+01
Sr-90	29.1	502	1.38E+00
Cs-137	30	164	8.90E+00
Am-241	432	11886	1.99E+00
Co-57	221.7 days	2	1.08E-20
Fe-55	2.7	17	1.03E+00
Cd-109	1.27	12	4.98E-04
Ni-63	96	8	1.14E-01
Se-75	120.4 days	4	4.90E-05
Pm-147	2.6	2	3.71E-05
Tl-204	3.78	20	1.12E-06
Po-210	0.379	1	4.43E-24
Na-22	2.6	22	2.10E-05
Bi-207	32.9	14	1.63E-05
Total Activity (Ci)	**2.56E+01**		
Total DSRS	**13137**		

3 Characterization, Dismantling and Conditioning of the DSRS

Characterization, dismantling and conditioning of DSRS in capsules and containers are part of the work done before disposal in a borehole facility. The DSRS inventory is a basis for characterizing and sorting the DSRS. Additional information extracted during these activities will complement and update the DSRS inventory.

The identification of the radionuclide which is presented in the sources and the activity has been considered the most important data for the characterization of disused sealed radioactive sources. The activity of the sources has been estimated by measuring the dose rate at a certain distance from the sources and 1 meter from the source. The type of source and possible application (for sources where this information was unknown), were approximately identified considering similar sources stored at the facility.

4 Conclusion

13137 units of DSRS consisting of 15 radionuclides are planned to be disposed into the borehole disposal facility. The radionuclides are Fe-55, Co-57, Cd-109, Ba-133, Pm-147, Tl-204, Po-210, Co-60, Ni-63, Kr-85, Sr-90, Cs-137, Pb-210, Ra-226 and Am-241. However, eight radionuclides will be further used in safety assessment calculation in the main screening calculation. The DSRS inventory shall be updated accordingly from the characterization, dismantling, and conditioning activities. This will complement the available information before these activities. Details of the sources can also be verified periodically which can be retained for future planning of the disposal facility in terms of traceability. They should also be managed properly according to the quality assurance (QA) so, that the information obtained will be more reliable and also can be used for safety assessment and safety case development of borehole disposal facility.

References

IAEA. 2007. Identification of radioactive sources and devices. IAEA Nuclear Security Series No. 5, IAEA, Vienna.

Individual Research Contribution Review, 2023, 1(1): 147–148

Repatriation of Disused Sealed Radioactive Sources (DSRS) of Radium-226 (Ra-226) under the Global Radium-226 Management Initiative

Nurul Wahida Ahmad Khairuddin
Waste Technology and Environmental Division
Malaysian Nuclear Agency
43000 Kajang, Selangor
nwahida@nm.gov.my

Abstract

The Global Radium-226 Management Initiative coordinated by the IAEA focuses on recycling radium-226 as an effort to wisely manage legacy radium sources such as radium needles used for targeted alpha therapy in nuclear medicine. The accumulation and storage of legacy radium sources without any further purpose may pose long-term management concerns if not managed safely and effectively. With a considerably huge number of legacy radium sources in its possession, Malaysia has decided to participate in this program to support the sustainable management of these radium sources. The Canadian National Laboratory (CNL) is interested in cooperating with Malaysia in recycling legacy radium sources. The legacy radium sources were mostly conditioned in stainless steel capsules and stored in the interim storage facility. 100 pieces of radium needles with a total activity of 157 mCi were conditioned in two cemented drums. This paper shares the working procedures for demolishing the cemented drums to retrieve the radium needles for transfer to CNL. Protection against occupational exposure is also described. This mission is a collaboration between the Waste Technology Development Centre (WasTeC) and the Health Physics Group (KFK).

Keywords: DSRS, inventory

1 Introduction

A radioactive source that is no longer in use, or not intended to be used, for the practice for which authorization has been granted, is deemed as disused. These DSRS of Ra-226 must be properly managed to ensure the whole life cycle is safe and secure, cost-effective, and the impact on the environment is minimized. The current interim policy related to radioactive waste management in Malaysia adopted by Jabatan Tenaga Atom (Atom Malaysia) in one of the following ways (Table 1).

As Malaysia has a legacy stock of Ra-226, which may present a long-term management challenge in the facility, repatriating to the recipient country seems like a good solution. This measure is not only able to reduce congestion in storage stores, but it can also support the Ra-226 recycling program under the Global Radium-226 Management Initiative coordinated by the International Atomic Energy Agency (IAEA).

Table 1: Radioactive Waste Management Policy in Malaysia

Waste generator	Types of waste	Policy	Licensing Requirement
Industry	Sealed sources	Return to the supplier	Undertaking letter from the supplier to accept back the waste
Hospital/ university/ research institute	Sealed sources	Return to the supplier	Undertaking letter from the supplier to accept back the waste
	Liquid waste	Sent to Malaysian Nuclear Agency	Undertaking letter from the supplier to accept back the waste
Activities related to TERNORM	Solid waste	Stored by user	Waste storing facility which must comply with AELB criteria
	Liquid waste	Stored by user	Waste storage tank

Paragraph 14 of the IAEA Code of Conduct on the Safety and Security of Radioactive Sources specifies that “every State should encourage the reuse or recycling of radioactive sources, when practicable and consistent with considerations of safety and security”. The IAEA understands this challenge presented by long-lived radionuclides and continues to seek suitable solutions for the stored legacy Ra-226. Conversely, the IAEA notes that several Member States may have a use for such legacy Ra-226 stocks, particularly, in the field of targeted alpha therapy in nuclear medicine. The treatment of cancer cells through the application of radiotracers with Actinium-225 shows very promising results and using Ra-226 as a feedstock material is an effective production route for the Actinium.

As a Member State of the IAEA, the Malaysian Nuclear Agency is committed to managing radioactive waste in a safe, secure, and sustainable manner by internationally recognized principles related to nuclear and radiation safety. The Waste Technology Development Centre (WasTeC) of Nuclear Malaysia is given the responsibility to collect all institutional waste within the country for processing, treatment, and storage.

In light of the above, the IAEA is coordinating an activity focusing on Ra-226 recycling referred to as the ”Global

Radium-226 Management Initiative". In the frame of this initiative, a platform to facilitate information exchange between Member States possessing legacy Ra-226 sources and Member States with capabilities and suitable recycling facilities has been established.

Canadian National Laboratory (CNL) is one leading laboratory in producing Actinium-225 for use in nuclear medicine and seeking the legacy Ra-226 from another country.

As Malaysia currently possesses a large number of Ra-226, CNL is interested in accepting our legacy of Ra-226 for recycling. In this particular task, the radiation safety and security aspect has to be in consideration. It will involve not only radiation workers and workplace monitoring, transportation, and packaging of DSRS but also an approval process from the regulatory authorities which is outlined in the radiation protection program. Therefore, this repatriation activity will be carried out together with the Health Physic Group, Radiation Health and Safety Division (BKS) throughout the whole repatriation process of the Ra-226 sources to the CNL.

2 Characterization, Dismantling, and Conditioning of Ra-226

Characterization, dismantling, and conditioning of Ra-226 in capsules and containers are part of the work done before repatriating Ra-226 to the recipient country. Detailed procedures for the recovery of DSRS from the devices are specific to the type and model of the device. These procedures are described in the Technical Manual on Dismantling Industrial Gauges, Recovering and Conditioning of Associated Radioactive Sources, IAEA. The dismantling of the smoke detector will be conducted by the work instruction for Dismantling of Smoke Detectors (WasTeC-W23). The identification of the radionuclide which is presented in the sources and the activity has been considered the most important data for the characterization of disused sealed radioactive. Figure 1 and 2 shows the dismantling and retrieval of Ra-226 for the repatriation program.

Figure 1: The dismantled Ra-226 from check sources and lightning arrester.

Figure 2: The retrieval of radium needles from 2 cemented drum.

3 Results and Discussion

The DSRS will be first characterized to get sufficient information for process control and to assure that the DSRS meets the acceptance criteria for conditioning, containerization, storage, and transport. The information will be recorded as appropriate to enable the DSRS to be identifiable, traceable, and safely handled. Individual records will include information, as appropriate, on the:

a) Location, both before and after disposal;
b) Radionuclide content;
c) Radioactivity on the manufacturing date;
d) Manufacturing date;
e) Serial number or unique identifier;
f) Source manufacturer;
g) Dose rate on a current date

The total number of Ra-226 which were characterized and dismantled is 1116 pieces with a total activity of 1.07e+3 mCi. Table 2 shows the total inventory of Ra-226 for repatriation to CNL.

Table 2: Inventory of Ra-226 considered for Repatriation

R/N	**QTY**	**Activity (mCi)**	**Remark**
Ra-226	182	1.20E+00	LIGHTNING ARRESTOR
	87	4.10E-01	CHECK SOURCE
	65	4.00E-02	CUP SOURCES
	225	1.05E+00	LIGHTNING ARRESTOR
	109	1.23E+02	LIGHTNING ARRESTOR + RADIUM NEEDLES + CHECK SOURCE
	77	3.85E-01	CHECK SOURCE
	100	1.57E+02	RADIUM NEEDLES
	78	1.87E-01	SMOKE DETECTOR, CHECK SOURCE
	19	4.97E+00	LIGHTNING ARRESTOR, CHECK SOURCE
	174	7.83E+02	RADIUM NEEDLES (CONDITIONED IN STAINLES STEEL CAPSULES)
	1116	**1.07E+03**	

4 Conclusion

1116 units of Ra-226 are planned to be repatriated to CNL under the Global Radium-226 Management Initiative coordinated by the IAEA. The Ra-226 mostly results from activities in nuclear medicine/hospitals (radium needles), industrial applications such as lightning arresters, smoke detectors, and education institutes (check source).

References

IAEA. 2004. Code of conduct on the safety and security of radioactive sources. IAEA/CODEOC/2004.

Individual Research Contribution Review, 2023, 1(1): 149–150

Potential Impact of Climate Change Including Extreme Events on Small Modular Reactor Site – A Review of Sabah, Malaysia

Rahman Yaccup
Waste Technology and Environmental Division
Malaysian Nuclear Agency
43000 Kajang, Selangor
rahman@nm.gov.my

Abstract

Climate change and increased urban population are two major concerns for society. Moving towards more sustainable energy solutions in the urban context by integrating renewable energy technologies supports decarbonizing the energy sector and climate change mitigation. This review provides an overview of and insight into the potential hazards that may occur due to climate change which is expected to bring new challenges to small modular reactor (SMR) sites. A case study in Sabah will be discussed in this paper as the potential site for SMR in Malaysia.

1 Introduction

Climatic hazards are expected to increase as a result of climate change due to extreme rainfall, strong winds, and storm surge as well as sea level rise (Stocker et al., 2013; Masson-Delmotte et al., 2018). Recently, the climatic impact on nuclear power plants has become an important issue in the planning and designing of new nuclear power plants or small modular reactors (SMR). SMR is part of a new generation of nuclear power plant designs being developed in several countries. In Malaysia, there are only a few potential sites for SMR. In this paper, the Sabah region will be deliberated more detail. Sabah is located in the north-eastern part of the island of Borneo and has an area of approximately 73,631 km^2. Sabah is mainly formed by sedimentary and igneous rocks, with a minor occurrence of metamorphic rocks. The rock units in Sabah have been divided into two groups: the Rijang Group and the Kinabatangan Group (Collenette, 1958). Granitic rock is dominant in the centre and southwest of Sabah, while sandstone covers more than 80% of Sabah's area. The alluvium is found along the shoreline (Figure 1). The granitic and schist rocks are highly preferred for the SMR siting because their physical properties are very hard and strong compared to other rocks. The purpose of this study is to describe the impact of future climatic hazards on SMR.

2 Potential Hazards

Several potential hazards were listed, including flooding, landslides and minor earthquakes in the study area. Malaysia has an equatorial climate with hot and humid weather all year round, followed by a rainfall distribution that is strongly influenced by topography and monsoon winds. The annual rainfall intensity in Sabah ranges from 2,000 mm to 4,000 mm (Figure

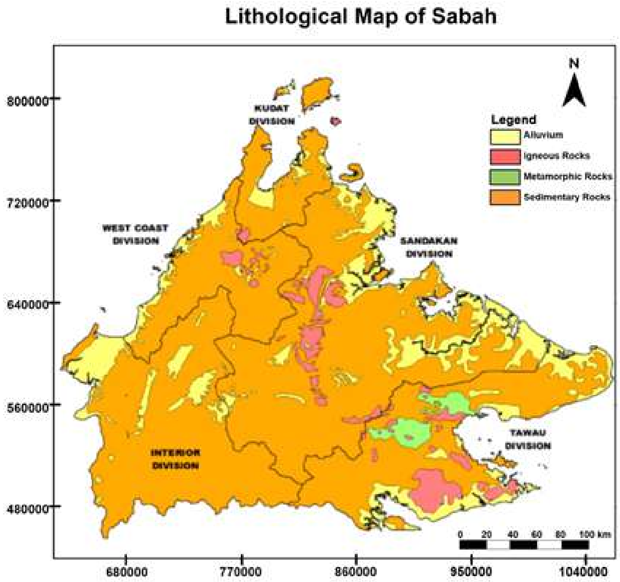

Figure 1: Lithological Map of Sabah

2. During the northeast monsoon, the northeast of Sabah can sometimes experience heavy rains that can last up to three days, sometimes resulting in severe flooding. In comparison, the southwest monsoon is drier. During the inter-monsoon seasons, heavy rains occur in the late afternoon and evening hours due to convective showers and thunderstorms. AELB reported that the best area for SMR should be located in a non-flooding area and have the best surface drainage features (AELB, 2011).

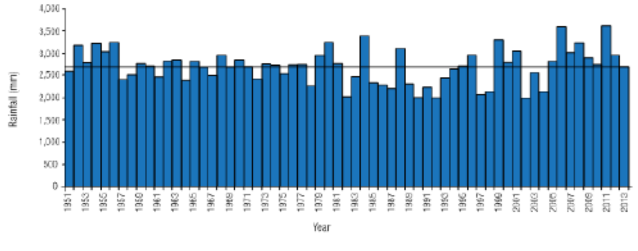

Figure 2: Annual Rainfall Trend for Sabah from 1951-2013 (Climate Risk Country Profile: Malaysia, 2021)

Figure 3 shows the map of flood risk in Sabah. Heavy rainfall in Sabah and steep slopes contribute to the widespread

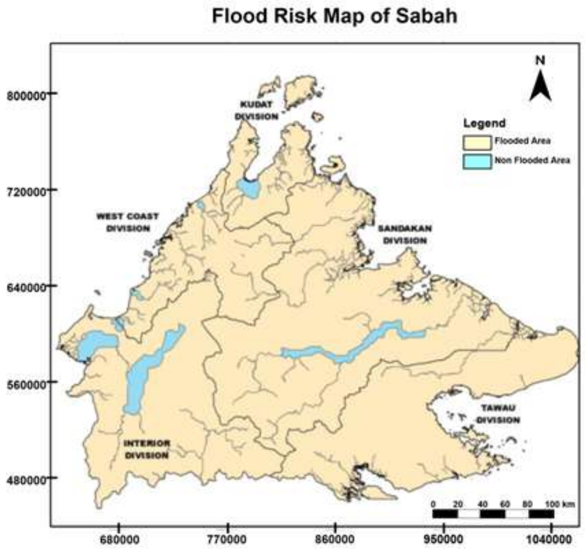

Figure 3: Flood Risk Map of Sabah

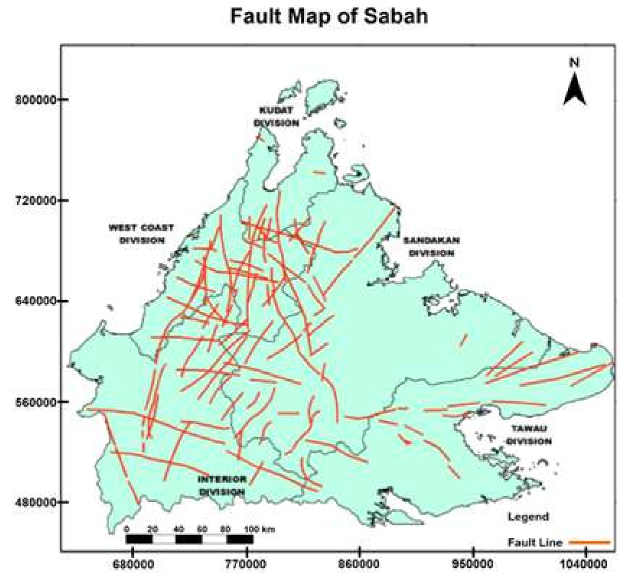

Figure 4: Fault Map of Sabah

occurrence of landslides. However, most of these landslides occur in remote areas away from larger settlements. The construction of highways through the mountainous region, cutting through steep slopes, has to some extent made landslides more frequent and visible. Tongkul & Rodeano (2009) reported that rapid development activities on hilly slopes in urban areas have also contributed to the frequent occurrence of landslides (Tongkul and Roslee, 2009). Three areas are prone to landslides: Kundasang, Kota Kinabalu and Sandakan. Lineament and other geological structures must be avoided as they can trigger landslides in the event of an earthquake. The higher the density of lineament, the greater the risk of landslides, especially during the monsoon season. Figure 4 shows the location of fault lines in the study area. Areas with fewer lineaments are preferable compared to the densest area. Christopher H. Scholz (2002) mentioned that a minimum buffer of 2.5 km around the fault line should be maintained when developing SMR for safety (Christopher, 2002). Besides, the other potential hazard will include the minor earthquake in Mt. Kinabalu with 6.0 *Mw* that occurred in 2015 (Wang et al., 2017).

3 Conclusion

There is much to be prepared to build the resilience of ecosystems, assets, and communities surrounding a SMR that could be impacted due to climate change.

References

Atomic Energy Licensing Board AELB. 2011. Guideline for site selection for Nuclear Power Plant. LEM/TEK/63.

H.S Christopher. 2002. The mechanics earthquakes and faulting. 2nd Edition:The University of Cambridge. United Kingdom. ISBN 0521652235.

P. Collenette. 1958. The geology and mineral resources of the Jesselton-Kinabalu area, North Borneo. *Br. Bomeo Geol. Surv*, Mem. 6.

Climate Risk Country Profile: Malaysia. 2021.

V Masson-Delmotte, P Zhai, H-O Pörtner, D Roberts, J Skea, PR Shukla, A Pirani, W Moufouma-Okia, C Péan, R Pidcock, S Connors, JBR Matthews, Y Chen, X Zhou, MI Gomis, E Lonnoy, T Maycock, M Tignor, and T Waterfield (eds.). 2018. An IPCC special report on the impacts of global warming of 1.5°c above pre-industrial levels and related global greenhouse gas emission pathways, in the context of strengthening the global response to the threat of climate change, sustainable development, and efforts to eradicate poverty. *IPCC.Summary for policymakers*, 24:World Meteorological Organization, Geneva, Switzerland.

T.F. Stocker, D. Qin, G.-K. Plattner, M. Tignor, S.K. Allen, J. Boschung, A. Nauels, Y. Xia, V. Bex, and P.M. Midgley (eds.). 2013. The Physical Science Basis. Contribution of Working Group I to the Fifth Assessment Report of the Intergovern-mental Panel on Climate Change. *IPCC. Climate Change 2013*, 1535:Cambridge University Press, Cambridge, United Kingdom and New York, NY, USA.

F. Tongkul and Rodeano Roslee. 2009. Landslide disasters in Sabah, Malaysia: Issues and challenges. Centre for Natural Disaster Studies, Universiti Malaysia Sabah.

Y. Wang, S. Wei, and X. et al Wang. 2017. The 2015 Mw 6.0 Mt. Kinabalu earthquake: An infrequent fault rupture within the Crocker fault system of East Malaysia. *Geosci. Lett.*, 4(6):https://doi.org/10.1186/s40562–017–0072–9.

Individual Research Contribution Review, 2023, 1(1): 151–152

Upgrading and Enhancement the Performance of the Thermal Plasma Pilot Plant in Malaysian Nuclear Agency

Rohyiza Baan
Waste Technology and Environmental Division
Malaysian Nuclear Agency
43000 Kajang, Selangor
rohyiza@nm.gov.my

Abstract

In this work, the thermal plasma pilot plant that was built and commissioned in 2014 was upgraded to improve the plant's processing performance to dispose low and intermediate level radioactive waste (LILW). Therefore, the provision of maintenance of the systems and equipment and spare parts can be provided to ensure the ability of plasma pilot plant and enables to function more effectively and ensures that it continues to perform in good condition.

Keywords: Thermal plasma pilot plant, plant's processing performance, low and intermediate level radioactive waste

1 Introduction

The plant consists of a non-transferred arc torch, plasma chamber reactor, plasma forming gas system, line system of Nobel gases, cooling system, air pollution control system, power supply, and instrumentation and control system. The plant upgrading system was covered related repair works, replacement, reconditioning, spare parts change, consumables, services, and maintenance of the whole existing system including hardware and software control unit system that were broken and malfunctioned.

2 Methods

The upgrading work were consisting of sub systems but not limited to the modification and upgrading of the Plasma Reactor Chamber, Additional Noble Gas Line (Nitrogen), Recondition and upgrading of Air-Cooling Line System, Recondition and upgrading of Air Treatment System and Upgrading of the Instrumentation and Control System Unit.

2.1 Modification and upgrading of the Plasma Reactor Chamber

The chamber was modified and designed for the maximum capacity and maximum possible dimension to suit the crucible size. The design was come with 60° degree mounting for the plasma torch, 60° degree waste feeder funnel, connection ducting to the air pollution control unit, and provision for cleaning and removing the vitrified material. The door chamber designed with window of suitable material for optical observation (suitable glass window 5"x 5") and camera compatibility to attached near chamber to view through the glass window.

2.2 Additional Noble Gas Line (Nitrogen)

2 units storage Nitrogen gas with capacity of $7m^3$ to $10m^3$ and operated at 0.2-0.5 g/s was installed at the plant. The gas line has been integrated with plasma torch and capable to separate the existing air line for pyrolysis treatment process. Both air and gas supply can be integrated with the monitoring and control system from control room.

2.3 Recondition and upgrading of Air-Cooling Line System

The upgrading air cooling system covers the observation, repair, service and re-install the air-cooling line to recondition the piping, the insulation, establish connection between pump, cooling tower, cooling fan and control system. The suitable size of new piping and the type of stainless steel (304 or 316) to meet the pressure and flow and corrosion resistant for the optimum of plasma torch to be operate or while operating. A recirculation system for the cooling water to promote water saving.

2.4 Recondition and upgrading of Air Treatment System

The upgrading air treatment system covers the observation, repair, service or re-install the air treatment line either to recondition the piping, the hose, the insulator, refurbish or replace new Heat Exchanger, Air pollution filter Trap, condenser, flow sensors, pressure sensors, temperature sensors and establishing connection between those equipment and tools to the control system.

2.5 Upgrading of the Instrumentation and Control System Unit

The upgrading of the instrumentation and control system unit covered observe, service or re-install the existing software and hardware control of the system and sub-system, so that the newly installed will be operable in an optimal condition. The control system OS (operating system) image or clone backup and easily deployed to the new computer.

3 Results

The reactor chamber was designed with adequate lining to reduce heat loss, permissible external body temperature and safe operation. Dimension inner chamber can be adjustable up and down platform.

The flue gas can be treated through a series of Air Pollution Control System before final emission in to the environment.

The newly installed system shall feature a liquid trap for sampling and overflow that can be operable via gravity.

The Vapor Air filter such as High Temperature Resistant HEPA Filter that meet the Environmental Requirement Procedure to be use in Air Filter Trap before releasing to environment.

3.1 Schematic Graphics of Process

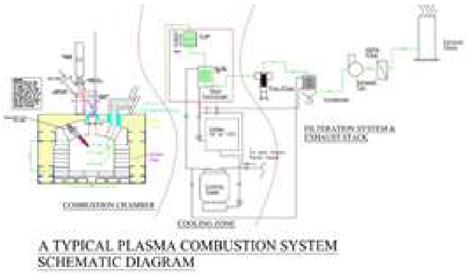

Figure 1: Schematic Diagram of Plasma Combustion System.

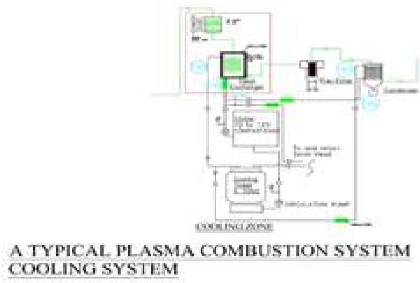

Figure 2: Cooling System Schematic Diagram.

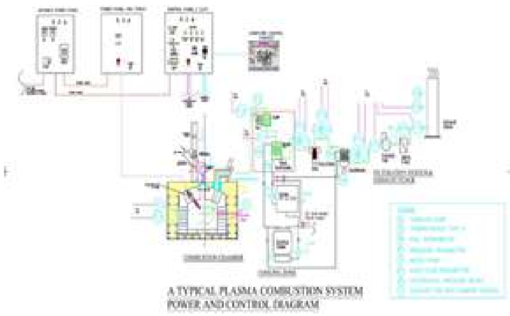

Figure 3: Combustion Process and Control Schematic Diagram.

3.2 Components of Plasma Torch

A supply system with sufficient capacity from the combustion chamber to the air monitoring system with a total voltage of 415V and a total of 250 A of electrical requirements (Figure 4).

4 Discussion/Conclusions

A plasma reactor chamber is designed based on the type of plasma application whether it is a melting, coating, waste destruction, vitrification, pyrolysis or other processes. A non-transferred plasma arc torch contains two electrodes, (front and rear). A direct current between these electrodes creates

Figure 4: 50kW Direct Current Power Supply.

an ionized-gas plasma stream which, is constrained to the end of the torch. The heat generated from this is more dispersed compared heat generated from a transferred arc plasma torch suiting the non-transferred design for a wide range of applications. Therefore, upgrading and enhancement of the plant's performance need to be ready to fulfill the objective of RMK budget.

References

I. G. Choi. 1992. Mathematical modeling of radioactive waste glass. *Westinghouse Savannah River Company, Savannah River Site, South Carolina.*

Li J., Liu K., Yan S., Li Y., and Han D. 2016. Application of thermal plasma technology for the treatment of solid wastes in China: An overview. *Waste Manag*, 58:260 – 269. doi: 10.1016/j.wasman.

Samal Sneha. 2017. Thermal plasma technology: The prospective future in material processing. *Journal of Cleaner Production.*

Zhang and Solonenko O.P. 2016. Thermal plasma torches and technology. *Plasma Torches: Basic Studies and Design Retrieved from books.google.com.*, 1.

Individual Research Contribution Review, 2023, 1(1): 153–154

Stable Isotope Characteristics of Precipitation in Malaysia: Establishment of Local Meteoric Water Line

Roslanzairi Mostapa
Waste Technology and Environmental Division
Malaysian Nuclear Agency
43000 Kajang, Selangor
roslanzairi@nm.gov.my

Abstract

This paper discussed the use of stable isotope compositions of precipitation (δ^2H and δ^{18}O) to understand its characteristics and the parameters controlling meteorological conditions in Malaysia. The meteoric water line for Malaysia, or MMWL established in this study are δ^2H= (7.43±0.05)δ^{18}O + (7.33±0.11) (n=595, r^2=0.97) for individual values, and δ^2H= (7.07±0.20)δ^{18}O + (4.90±0.75) (n=51, r^2=0.96) for annual precipitation weighted means.

Keywords: Stable isotope, precipitation, Malaysian meteoric water line

1 Introduction

The lack of localized detailed investigations related to the use of stable isotopes, i.e., deuterium (^{2}H) and oxygen–18 (^{18}O) in water resources study conducted previously in Malaysia are mainly due to insufficient knowledge in isotope technique, unavailability of Isotope Ratio Mass Spectrometer (IRMS), and the lack of a database of stable isotope compositions of precipitation to act as a reference point. In light of the abovementioned facts, this study aims to develop a δ^2H and δ^{18}O database of precipitation to elucidate various components of the water cycle and groundwater evolutions. Stable isotope tracers of water can be used for this purpose due to their unique 'fingerprint' of sources often preserved within the subsurface. The precipitation process has a geographically–specific isotopic fingerprint inherited by the local groundwater (Kortelainen, 2011). By collecting information, establishing a database on stable isotopes of hydrogen and oxygen of meteoric water, and analyzing the groundwater and surface water together with the hydrogeological information, an evaluation can be made to define the source and origin of groundwater, surface water, and groundwater interactions and groundwater dynamics. Recharge, sources of groundwater salinity, and the mass balance in the study area can also be determined (Yeh et al., 2009).

2 Methods

Rainwater samples were collected monthly for 6 years (January 2013 to December 2018) from nine IAEA GNIP rainfall stations located in Kuching, Senai, Malaysian Nuclear Agency, Kuantan, Cameron Highlands, Kuala Terengganu, Kota Kinabalu, Kota Bharu, and Alor Setar as illustrated in Figure 1.

Figure 1: GNIP rainfall sampling stations

2.1 Sample Measurement

Stable isotope compositions were determined for 595 samples and reported as δ values and denoted as ‰ or permil/per mill, which is relative to a standard of known composition (e.g., Vienna Standard Mean Ocean Water, VSMOW for δ^2H and δ^{18}O analyses). The δ values are calculated using the equation below, for example, in this case, ^{2}H:

$$\delta^2 H(‰) = \frac{R_{Sample} - R_{Standard}}{R_{Standard}} \times 1000$$

where R represents the ratio of heavy to light isotope (^{2}H/^{1}H), and R_{Sample} and $R_{Standard}$ are the isotope ratios in the sample and the standard, respectively.

2.2 Weighted Means

The weighted arithmetic mean is similar to an ordinary arithmetic mean, except that instead of each of the data points contributing equally to the final average, some data points contribute more than others, i.e., the isotope data are weighed in this study by the amount of precipitation. Weighted means of the isotope data are calculated by multiplying the isotope values by the amount of precipitation monthly or annually. The weighted mean values can be calculated using the equation below (IAEA, 1992):

$$\bar{\delta}_{Weighted} = \frac{\sum_{i=1}^{n} P_i \delta_i}{\sum_{i=1}^{n} P_i}$$

where P_i and δ_i represent the daily or monthly precipitation and its δ value, respectively.

3 Results

The annual weighted means and long–term annual weighted means of δ^{18}O, δ^{2}H and deuterium excess for the precipitation samples of the Malaysian GNIP stations are summarized in Tables 1 and 2, respectively. Most of the discussions of stable isotope characteristics in precipitation will be focused on δ^{18}O as δ^{2}H values will involve those with similar relationships and therefore will not be shown here.

Table 1: Annual precipitation weighted means of δ^{18}O, δ^{2}H, and deuterium excess (d).

	2013			2014			2015			2016			2017			2018		
	δ^{18}O (‰)	δ^{2}H (‰)	d (‰)	δ^{18}O (‰)	δ^{2}H (‰)	d (‰)	δ^{18}O (‰)	δ^{2}H (‰)	d (‰)	δ^{18}O (‰)	δ^{2}H (‰)	d (‰)	δ^{18}O (‰)	δ^{2}H (‰)	d (‰)	δ^{18}O (‰)	δ^{2}H (‰)	d (‰)
Alor Setar	−5.30	−36.30	6.1	−5.91	−34.34	13.0	−3.32	−18.41	8.2	−6.51	−42.37	9.7	−8.14	−53.33	11.8	−7.07	−44.02	12.5
MNA	−6.74	−44.64	9.3	−7.08	−44.39	12.3	−5.52	−32.27	11.9	−7.01	−44.95	11.1	−7.87	−50.98	12.0	−6.76	−42.95	11.1
Senai	−5.50	−37.07	6.9	−6.27	−40.45	9.7	−4.43	−25.54	9.9	−5.46	−34.36	9.3	−7.39	−49.47	9.6	−6.03	−36.28	11.9
C. Highlands	−3.32	−19.30	7.3	−7.28	−45.30	12.9	−7.34	−43.50	15.2	−8.27	−51.87	14.3	−9.88	−62.84	14.6	−7.93	−49.55	13.9
Kota Bharu	−3.57	−23.53	5.0	−4.90	−32.86	6.4	−5.60	−31.78	13.0	−5.88	−36.29	10.7	−6.34	−40.07	10.7	−5.54	−32.37	12.0
Kuala Terengganu	−4.90	−31.87	7.3	−6.13	−39.75	9.3	−4.63	−27.73	9.3	−5.75	−35.31	10.5	−6.86	−44.02	10.9	−5.38	−31.95	11.1
Kuantan	−5.74	−38.89	7.0	−6.13	−37.72	11.3	−5.10	−31.99	8.8	−6.03	−38.29	9.9	−7.37	−47.90	11.0	−6.31	−40.39	10.1
Kuching	−4.86	−31.83	7.1	−6.08	−38.41	10.3	−6.81	−44.35	10.1	−6.38	−39.28	11.7	−8.19	−55.18	10.4	−7.30	−47.34	11.1
Kota Kinabalu	−4.32	−24.72	9.8	−5.69	−34.20	11.3	−4.87	−26.74	10.6	−5.60	−31.27	13.6	−7.71	−50.28	11.4	−4.97	−28.58	11.2

Table 2: Summary of long–term annual precipitation weighted means of δ^{18}O, δ^{2}H, and deuterium excess.

	δ^{18}O (‰)					δ^{2}H (‰)					Deuterium excess, d(‰)				
	Min	Max	SD	Wt. mean	SD	Min	Max	SD	Wt. mean	SD	Min	Max	SD	Wt. mean	SD
Alor Setar	−11.34	0.01	2.28	−6.04	1.65	−78.1	5.5	16.7	−38.13	11.75	−0.3	15.0	3.6	10.2	2.7
MNA	−11.19	0.31	2.44	−6.83	0.76	−76.3	4.4	18.8	−43.36	6.11	2.0	15.0	2.4	11.3	1.1
Senai	−13.61	−1.43	2.14	−5.85	0.99	−95.2	−3.5	16.5	−37.19	7.82	−1.8	13.8	2.6	9.6	1.6
C. Highlands	−13.83	−1.24	2.25	−8.10	0.97	−96.4	4.2	18.4	−50.57	7.52	6.9	17.4	1.8	14.2	0.9
Kota Bharu	−10.28	−0.79	2.22	−5.65	0.52	−71.4	1.3	16.4	−34.67	3.49	−2.8	15.6	3.5	10.6	2.5
Kuala Terengganu	−8.96	1.92	2.27	−5.60	0.82	−61.8	14.2	16.7	−35.10	5.93	−1.2	15.3	2.6	9.7	1.4
Kuantan	−10.25	0.51	2.30	−6.11	0.75	−70.8	0.1	16.7	−39.20	5.14	−10.3	18.8	3.8	9.7	1.6
Kuching	−11.52	−1.68	2.41	−6.95	0.83	−83.2	−1.5	18.9	−44.91	6.81	2.3	15.8	2.7	10.7	0.7
Kota Kinabalu	−13.91	1.62	2.74	−5.49	1.21	−95.5	17.9	20.9	−32.62	9.26	3.8	16.9	3.1	11.3	1.2

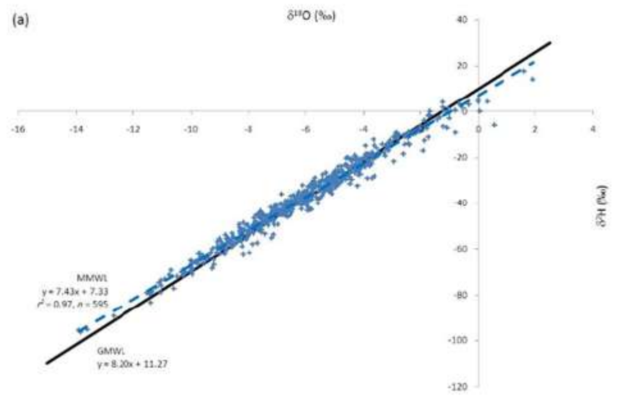

Figure 2: δ^{2}H–δ^{18}O linear relationship for precipitation derived from all the Malaysian IAEA GNIP network stations.

4 Discussion/Conclusions

4.1 The δ^{2}H–δ^{18}O linear relationship and Local Meteoric Water Line (LMWL)

Based on the 595 precipitation samples collected from nine stations of the International Atomic Energy Agency (IAEA) Global Network of Isotopes in Precipitation (GNIP), the Malaysian meteoric water line (MMWL) established in this study is δ^{2}H= (7.43±0.05)δ^{18}O + (7.33±0.11) (n=595, r^2=0.97) for individual values (Figure 2). A close relationship between δ^{2}H and δ^{18}O is evident, as most of the samples' plots are very close to the global meteoric water line, indicating that the precipitation condensed under saturated conditions from the ocean water–sourced vapor. Slightly lower slope values relative to GMWL imply small variations in precipitation temperature under the Rayleigh process at liquid–vapor equilibrium and some sub–cloud raindrops secondary evaporation (Dansgaard, 1964; Liu et al., 2014; Crawford et al., 2017). In contrast, the noticeable low intercept values indicate a significant evaporation process occurred at the water vapor source regions, i.e., South China Sea and Indian Ocean. During NEM, the continental dry cold air of the polar air mass originating from the north inducing the evaporation process above the South China Sea before progressive rainout over the east coast part of Peninsular Malaysia.

The need for a database of δ^{2}H, δ^{18}O of precipitation and local meteoric water lines led to this study, and the results garnered from this study contribute to the current demand in closing the knowledge gaps in isotope hydrology research in Malaysia. Besides the database, this study also successfully delineated the meteorological and environmental factors of the climatic conditions locally and regionally; for example, rainfall amount and temperature manifested poor correlation but considerable influence with the stable isotope signals in precipitation. Moisture sources between the two monsoons were also differentiated, where the NEM was slightly more negative than the SWM. Isotope values in precipitation were characterized by the water vapor transport trajectories, where longer pathways resulted in more depleted values, similar to the fractionation mechanism caused by the orographic effect. The seasonal behavior of the isotopes was quite clear with an insubstantial amount effect, in contrast with the temporal variations, which are indistinguishable. This study also captured the clear signals of El Niño and La Niña events indicated by heavier and lighter rainfall isotopes, respectively.

References

J. Crawford, S.E. Hollins, K.T. Meredith, and C.E. Hughes. 2017. Precipitation stable isotope variability and subcloud evaporation processes in a semi–arid region. *Hydrol Process*, 31:20 – 34.https://doi.org/10.1002/hyp.10885.

W. Dansgaard. 1964. Stable isotopes in precipitation. *Tellus*, 16:436 – 468. https://doi.org/10.3402/tellusa.v16i4.8993.

IAEA. 1992. Statistical treatment of data on environmental isotopes in precipitation. *Technical Reports*, Series No. 331:IAEA, Vienna.

N. Kortelainen. 2011. Isotope tracing in groundwater applications. *Geol S Finl*, 49:279 – 284.

J. Liu, X. Song, G. Yuan, X. Sun, and L. Yang. 2014. Stable isotopic compositions of precipitation in China. *Tellus B*, 66:22567:https://doi.org/10.3402/tellusb.v66.22567.

H. Yeh, C. Lee, K. Hsu, P. Chang, and C. Wang. 2009. Using stable isotopes for assessing the hydrologic characteristics and sources of groundwater recharge. *Environ Eng Manag J*, 19(4):185 – 191.

Individual Research Contribution Review, 2023, 1(1): 155–156

Landslide Susceptibility Map using Factor Analysis Model

Rozilawati Mohd Japar
Waste Technology and Environmental Division
Malaysian Nuclear Agency
43000 Kajang, Selangor
rozilawati@nm.gov.my

Abstract

The main objective of this study is to produce the latest geological map, to determine the factors that caused the landslides in the study area, to analyze and produce landslide susceptibility map using the Factor Analysis Model and also to recommend appropriate mitigation measures for hazardous slopes.

Keywords: Landslide, Susceptibility, Hazardous

1 Introduction

Landslides are geological events that encompass much of the movement of earth, such as rock falls, slope failures and debris flows. While gravity acting on steep slopes is the main cause of landslides, there are other factors such as erosion by rivers creating steep slopes of rock or weak soil due to heavy rainfall saturation, excessive weight from accumulated rain, piles of rocks or human-built structures that apply pressure to weak slopes leading to collapse and groundwater pressure that renders slopes unstable.The study area chosen for this study is Apas-Balung area located in Tawau, Sabah. The software used to produce the landslide susceptibility map is ArcGIS. The aim of this article is to show the potential for the occurrences of landslide from the susceptibility map of landslide produced.

2 Methods

2.1 Identification of Landslide Disasters (LHIP)

For laboratory analysis in LHIP, all soil and rock samples obtained from the field are analyzed and assessed to determine engineering properties in line with the standards proposed by ISRM (1979a; 1979b & 1985) and BS1377-1. After completing all the laboratory analysis, in combination with fieldwork including surveying parameters in FAM and observing information about landslide hazards, laboratory studies and GIS data extraction, 7 thematic maps have been generated: slope angle, lithology, rainfall, susceptibility, landuse, compressive strength values and soil types.

2.2 Assesment of Landslide Disasters (LHAP)

The calculation of LSL (Landslide Susceptibility Level) is done through a combination of parameterized map inputs with GIS operations using a grid database. The result of LSM (Landslide Susceptibility Model) was compared and validated with data from LDM (Landslide Data Model). The highest probability values for various scenarios are chosen for each pixel and the final LSM is constructed. After LSL in the final LSM has been turned into a singular value in each cell of the raster map, it facilitates the reclassification of values based on the standardization method by Voogd (1983) and Papathoma et. Al (2007).

(0.29*slope angle) + (0.17*lithology) + (0.14*soil type) + (0.12*rainfall) + (0.11*susceptibility) + (0.09*compressive strength) + (0.08*landuse).

Table 1: Stability levels according to the range of landslide susceptibility (LSL).

Level	Range of Landslide Susceptibility	Classification
I	<0.185	Very low
II	0.185-0.370	Low
III	0.370-0.555	Moderate
IV	0.555-0.740	High
V	0.740-0.930	Very High
VI	>0.930	Extremely High

3 Results

After generating 7 thematic maps for each parameter, a landslide susceptibility level map for the chosen study area was produced by combining all the analyzed maps with their respective weights. Figure 1 illustrates the results of the soil susceptibility assessment in the study area. The landslide susceptibility level has been categorized into 5 stages: low, moderate, high, very high and dangerous according to classification established by previous researchers (Roslee et al., 2012). Areas with the highest landslide susceptibility are those with steep slopes and elevated altitude. Almost the entire study area comprises a significant portion within the high and very high levels on the landslide susceptibility level map. These areas should be monitored as they are primarily used for oil palm agriculture and the occurrence of disasters would have more severe impacts.

4 Discussion and Conclusion

4.1 Discussion

Based on the analysis of landslide susceptibility conducted, the landslide vulnerability level indicates that 37.605% of the

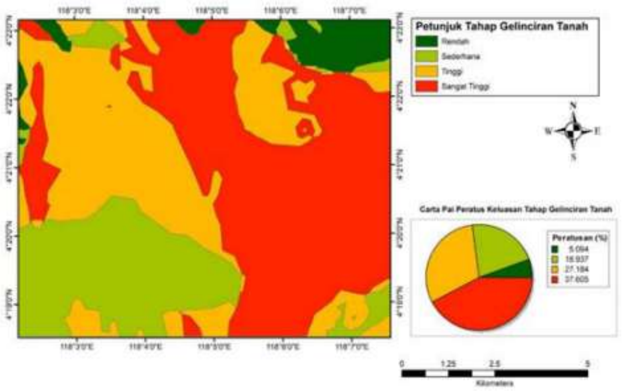

Figure 1: Map of Landslide Susceptibility Levels in the study area.

study area is categorized as having a very high level of landslide susceptibility, 27.184% as high susceptibility, 18.937% as moderate susceptibility and 5.094% as low susceptibility. Overall, the study area falls within the range of moderate to very high landslide susceptibility zones. The results from the generated landslide susceptibility map also show that areas in the low susceptibility zone are concentrated in the northeast part of the map, while areas highly prone to landslides are concentrated in the southeast region of the map.

4.2 Mitigation Recommendations

The mitigation steps that can be taken including Masonry structure, sheet piles, surface sealing, surface drainage systems and installing early warning systems in the study area. While non-structural approaches that should be considered include seeking advice from experienced and qualified engineering geologists or engineers to design developments based on existing risks from hazards and consequences, disaster preparedness, public awareness, physical non-structural adaptations, environmental control and behavioral adaptions, disaster preparedness and public awareness.

References

A. Carrara, M. Cardinali, F. Guzzetti, and P. Reichenbach. 1995. GIS technology in mapping landslide hazard. Geographical information systems in assessing natural hazards. *Kluwer Academic Publishers, Dordrecht, The Netherlands*, pages 135 – 175.

Rodeano Roslee, Tajul Anuar Jamaluddin, and Mustapa Abd. Talip. 2012. Landslide Susceptibility Mapping (LSM) at Kota Kinabalu, Sabah, Malaysia using Factor Analysis Model (FAM). *Journal of Advanced Science and Engineering Research*, 2:80 – 103.

Y. Thiery, J.P. Malet, S. Sterlacchini, A. Puissant, and O. Maquaire. 2007. Landslide susceptibility assessment by bivariate methods at large scales: Application to a complex mountainous environment. *Geomorphology*, 92(1):18.

Individual Research Contribution Review, 2023, 1(1): 157–158

Characterization and Radiometric Mapping of Langkawi Black Sand as Natural Tracer for Sediment Transport

Shakirah Abd Shukor
Waste Technology and Environmental Division
Malaysian Nuclear Agency
43000 Kajang, Selangor
shakirah@nm.gov.my

Abstract

Characterization and radiometric mapping of Langkawi black sand as a natural tracer for sediment transport was performed in this study. The Langkawi black sand was characterized in terms of its physical properties and leaching behaviour. A radiometric survey was also conducted to quantify and map the natural radioactivity levels within Langkawi black sand, focusing on the radionuclides Ra-226 and Ra-228. The activity concentrations of Ra-226 and Ra-228 in black sand from Pasir Hitam beach were 955 ± 115 Bq/kg and 530 ± 85 Bq/kg, respectively. The concentration of K-40 was 150 ± 41.5 Bq/kg. It was also reported that about 22 elements were detected in Langkawi black sand. The black sand consists of 4% ilmenite, 5.1% magnetite, 6.1% monazite, 14.1% albite, 41.4% anorthite, and 28.3% tourmaline.

Keywords: Langkawi black sand, natural tracer, radiometric mapping

1 Introduction

Climate change and rising ocean levels are unavoidable phenomena that pose a significant threat to coastal and riverine communities worldwide, increasing the risk of soil erosion, landslides, and floods. In Malaysia, these issues have raised concerns among government agencies, prompting the need for proactive measures beyond mere precautions. Prevention strategies, such as constructing stone or sand banks along coastlines and rivers, are crucial to mitigate these risks. However, the use of artificial radiotracers to track sediment movement has raised concerns about potential environmental radiological risks. In some countries, strict regulations govern the use of artificial radioactive tracers, and only a limited number of research reactors produce them. Tracers are tools employed to track mass soil movement using rare earth elements (REE) or radioactive elements. Black sand, commonly found in areas with volcanic activity, is a promising natural tracer material. While black sand is not abundant in Malaysia, which lies outside the Ring of Fire, Langkawi Island possesses a unique non-volcanic black sand beach. Notably, no studies have yet been conducted in Malaysia to assess the suitability of Malaysian black sand as a sediment transport tracer. Therefore, this study aims to comprehensively characterize Langkawi black sand and utilize radiometric mapping techniques to identify and evaluate its potential as a natural tracer for studying sediment transport dynamics.

2 Methods

2.1 Sample analysis

Black sand samples were collected along the shoreline of Black Sand Beach in Langkawi. The samples were collected from 32 locations along a straight line spanning 3 km along the beach. At each sampling point, approximately 3 kg of sand were collected from a depth of 5 cm below the surface. The samples were air-dried and subsequently analysed using Neutron Activation Analysis (NAA) for U/Th, gamma spectrometry for Ra-226, Ra-228, and K-40, X-ray diffraction (XRD) for mineral composition, and ICP-MS for leaching studies.

2.2 Radiometric mapping

The study employed a NaI detector for radiometric mapping. The detector was mounted on a custom-designed trolley to facilitate movement and positioning. Additionally, the detector could be carried by hand to traverse challenging terrains or navigate around boulders on the beach. At each location, three readings were taken for a duration of 60 seconds each. All readings were recorded and stored for subsequent mapping and distribution analysis.

3 Results and Discussion

Table 1 presents the results of radionuclide concentrations in Langkawi black sand. The activity concentrations of Ra-226, Ra-228, and K-40 were 955 ± 115 Bq/kg, 530 ± 85 Bq/kg, and 150 ± 41.5 Bq/kg, respectively. Compared to the activity concentration of Ra-226 in sand from Batu Ferringhi, which was 34 ± 2 Bq/kg (Shuaibu et al., 2017), the black sand in Langkawi exhibited significantly higher Ra-226 levels. This is attributed to its higher heavy mineral content (Khandaker et al., 2018).

Table 1: Radionuclides concentration in Langkawi Black Sand

Radionuclides	Activity Concentration (Bq/Kg)
Ra-226	955±115
Ra-228	530±84
K-40	150±41.5
U	896.71
Th	623.21

Table 2 presents the mineral contents of Langkawi black sand. The results indicate that the predominant mineral components in Langkawi black sand are anorthite (41.4%) and tourmaline (28.3%). This suggests that anorthite and tourmaline possess unique mineralogical compositions that can be readily distinguished from other minerals in the sediment. This characteristic facilitates their identification and tracking in sediment samples when employed as natural tracers. Furthermore, the feldspar minerals (albite and anorthite) and tourmaline are chemically stable and resistant to weathering and alteration. This means that they will remain intact and recognizable over long periods of time, making them reliable tracers for sediment transport studies.

Table 2: Mineral composition in Langkawi Black Sand

Mineral Composition	**Percentage (%)**
Quartz	1
ilmenite	4
Magnetite	5.1
Monazite	6.1
Albite	14.4
Anorthite	41.4
Tourmaline	28.3

Leaching analysis is conducted to investigate the recovery of elements in black sand for characterization. While previous studies have employed acid leaching with varying temperature and time parameters to specifically extract titanium (Ti) (Begum et al., 2012), this study utilizes deionized water leaching to extract a broader range of elements for comprehensive characterization. The results of the leaching analysis are presented in Figure 1. The results showed that sulfur (S) is the most leachable element in leaching studies of Langkawi black sand.

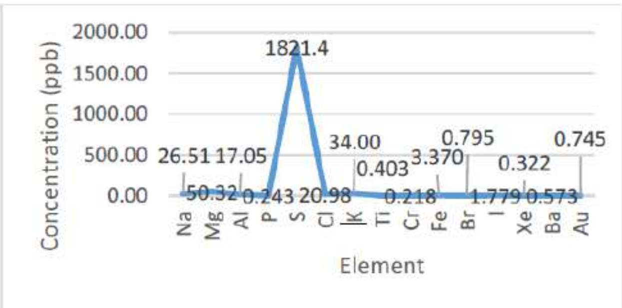

Figure 1: Elemental composition in Langkawi Black Sand leaching study using deionized water

Figure 2 presents a GIS map of Black Sand Beach in Langkawi. The distribution of black sand was determined using in-situ analysis with a NaI detector. The collected data was analyzed using GIS software and plotted in units of counts per second (CPS). The map shows several red spots, indicating high CPS values. These spots represent areas where black sand is abundantly distributed. Consequently, GIS maps provide a clear visual representation of black sand distribution patterns, allowing for easy identification of concentrated areas.

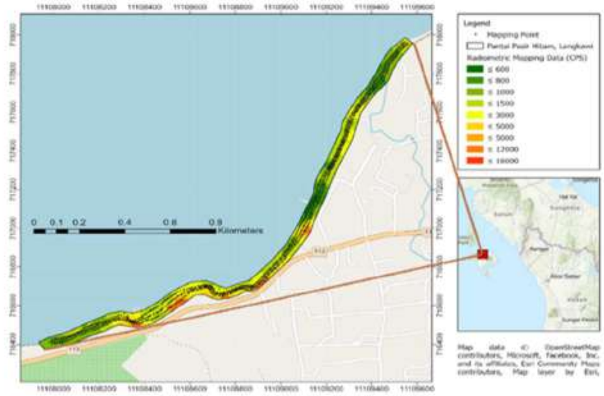

Figure 2: GIS mapping for Black sand Beach, Langkawi

4 Conclusion

In conclusion, this study provides a comprehensive assessment of Langkawi black sand as a natural tracer for sediment transport studies. The combination of mineralogical characterization, radiometric mapping, and leaching analysis highlights the potential of Langkawi black sand as a valuable tool for tracking sediment movement and understanding coastal processes.

References

Noorzahan Begum, Adilah Maisyarah, Fazlul Bari, Khairel Rafezi Ahmad, and Nur Hidayah. 2012. Leaching behaviour of Langkawi black sand for the recovery of titanium. *Procedia APCBEE*, 3:1 – 5. Elsevier.

Mayeen Uddin Khandaker, Khandoker Asaduzzaman, Abdullah Fadil Bin Sulaiman, D.A Bradley, and Matthew Omoniyi Isinkaye. 2018. Elevated concentration of naturally occurring radionuclides in heavy mineral-rich beach sand of Langkawi Island, Malaysia. *Marine Pollution Bulletin*, 127:654 – 663. Elsevier.

Hauwau Kulu Shuaibu, Mayen Uddin Khandaker, Tareq Alrefae, and D.A. Bradleyh. 2017. Assessment of natural radioactivity and gamma-ray dose in monazite rich black sand beach of Penang Island, Malaysia. *Marine Pollution Bulletin, Elsevier.*

Individual Research Contribution Review, 2023, 1(1): 159–160

Traceability and Authenticity of Kelulut Honey in Peninsular Malaysia through Elemental Profile using Neutron Activation Analysis (NAA) and Inductively Coupled Plasma Mass Spectrometry (ICPMS)

Siti Aminah Bt Omar
Waste Technology and Environmental Division
Malaysian Nuclear Agency
43000 Kajang, Selangor
sitiaminah@nm.gov.my

Abstract

This research focuses on developing database of elemental data of 50 kelulut honey collected from various location in Peninsular Malaysia. 32 multi-elements were successfully analyzed using NAA and ICP-MS. The database built were then subjected to chemometric analysis via PCA and OPLS-DA to form the geographical origin model of the kelulut honey based on its production location. From the chemometric analysis, the elements that were responsible for the separation between different production location of kelulut honey can be identified (fingerprinting elements).

Keywords: honey, multi-elements, NAA, ICPMS, traceability

1 Introduction

The concept of geographical origin in food products has expanded globally in recent years. Honey with a clear geographical origin not only provides recognition in terms of quality but also authenticity of the honey itself. Purity is one of the main issues in the honey market. This refers not only to counterfeit honey but also encompasses the mixing of low-quality honey with high-quality honey sold as premium honey, as well as honey sold with incorrect labels regarding the type of honey, geographical origin, and botanical origin.

The chemical composition of honey is closely related to its environmental factors such as soil, weather, climate, humidity, and types of flora. Different geographical areas will yield different chemical compositions of honey. Hence, the relationship between honey and its geographical production area can be verified. Honey with a clear geographical identity can add value to producers, allowing the marketed honey to be sold at higher prices. At the consumer level, honey marketed with the correct geographical origin label will increase consumer trust, thus leading to an even broader market.

Due to the importance of determining the geographical origin of honey for both consumers and honey producers, this research project to determine the geographical origin of kelulut honey was conducted with the aim of establishing a geographical model for kelulut honey in Peninsular Malaysia and obtaining its unique fingerprint profile.

2 Methods

Fifty samples of kelulut honey were collected from various states in Peninsular Malaysia. These samples were directly taken from the kelulut honey hives and stored in bottles. Subsequently, the kelulut honey samples were transported to the laboratory and stored in a refrigerator at a temperature of approximately 4°C until analysis was conducted. The samples underwent multi-element analysis using ICP-MS (inductively coupled plasma mass spectrometry) and NAA (neutron activation analysis). A comprehensive explanation of the methodology employed for both techniques is provided in SOP NUKLEARMALAYSIA/M/2022/16(S) and NUKLEARMALAYSIA/M/2022/17(S).

Following this, statistical analysis using PCA (principal component analysis) and OPLS-DA (orthogonal partial least squares discriminant analysis) were performed utilizing the soft independent modelling of class analogy (SIMCA-15; Umetrics, Umea, Sweden) software.

3 Data/Results

In this study, a total of 32 elements were analyzed. These elements include Al (aluminum), As (arsenic), Ba (Barium), Ca (calcium), Cd (cadmium), Ce (cerium), Co (cobalt), Cr (chromium), Cs (cesium), Cu (copper), Fe (iron), K (potassium), La (lanthanum), Li (lithium), Mg (magnesium), Mn (manganese), Mo (molybdenum), Na (sodium), Ni (nickel), Pb (lead), Rb (rubidium), Sb (antimony), Sc (scandium), Sm (samarium), Sr (strontium), Th (thorium), Ti (titanium), U (uranium), V (vanadium), Zn (zinc), Cl (chlorine), and Br (bromine).

The geographical model of kelulut honey based on its elemental profile is depicted in Figure 1, Figure 2 and Figure 3 below:

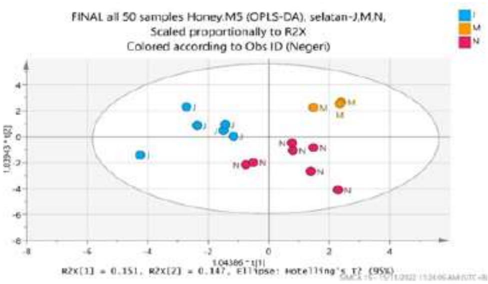

Figure 1: The OPLS-DA for Southern region (J = Johor, M = Melaka, N = Negeri Sembilan).

Elements that contributes to the classification of kelulut honey collected from the southern zone consist of Al, Ti, Ba, Mo, Cs, Mn, Th, V, Cd, Co, Br, La, and Pb.

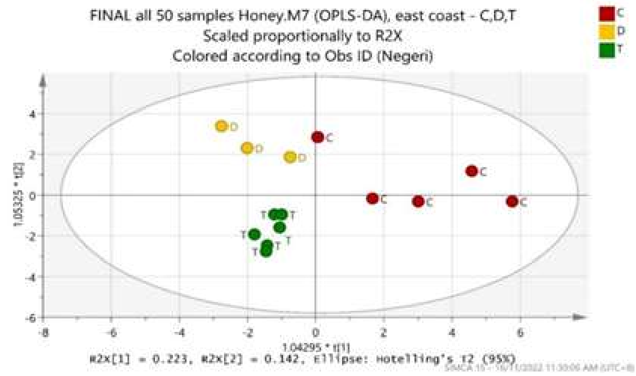

Figure 2: The OPLS-DA for East Coast region (C = Pahang, D = Kelantan, T = Terengganu))

Elements that contributes to the classification of kelulut honey collected from the east coast zone consist of Th, La, Ba, Al, Sr, Ni, Cd, Pb, Li, Cs and Ca.

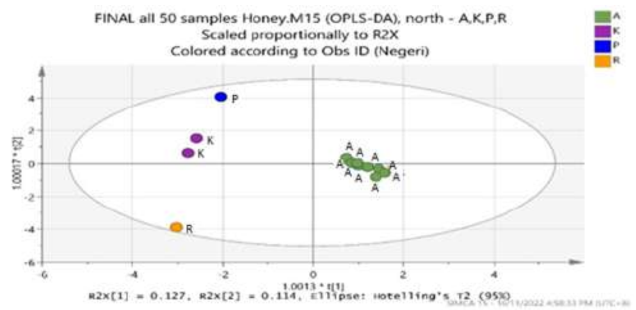

Figure 3: The OPLS-DA for Northern region (A = Perak, K = Kedah, P = Pulau Pinang, R = Perlis)

Elements that contributes to the classification of kelulut honey collected from the northern zone consist of Ba, Sb, La, Pb, Ni, Na, Cu, K, Sr, Zn, Mg and Mn.

4 Discussions/Conclusions

The database for 32 multi-elements from 50 kelulut honey samples collected from various locations in Peninsular Malaysia was successfully developed in this study. Overall, the geographical origin of the kelulut honey could be classified into 3 main zones: the southern zone, the east coast zone, and the northern zone. From the data collected, the main issue identified was that the model produced differentiation with a relatively low Q2 value. This indicates that the differentiation achieved was only at a moderate level. Therefore, the following suggestions are proposed to yield better results:

i. Use a larger number of samples for each state with an equal ratio. It is recommended to use around 10 to 20 samples for each state

ii. Conduct more sampling based on seasons to reduce sampling bias

iii. Utilize other parameters in addition to the analysis of elemental concentrations, such as stable isotope analysis and specific Sr and Pb isotope analyses.

These additional steps are aimed at enhancing the differentiation and accuracy in identifying the geographical origin of kelulut honey.

References

Kek S. P., Chin N. L., Tan S. W., Yusof Y. A., and Chua L. S. 2016. Classification of honey from its bee origin via chemical profiles and mineral content. *Food Analytical Methods*, 10(1):19 – 30.

Chua L. S., Abdul-Rahaman N. L., Sarmidi M. R., and Aziz R. 2012. Multi-elemental composition and physical properties of honey samples from Malaysia. *Food Chemistry*, 135:880 – 887.

Individual Research Contribution Review, 2023, 1(1): 161–162

Radioactivity Concentration, Effective Dose and Associated Cancer Risk Arising from the Consumption of Foods for Malaysian Adults

Yii Mei-Wo
Waste Technology and Environmental Division
Malaysian Nuclear Agency
43000 Kajang, Selangor
yii@nm.gov.my

Abstract

Consuming foods containing radionuclides may contribute to radiation dose and poses higher cancer risk to human. Study was conducted to determine the radionuclides concentration present in more than 400 commercial foods using Gamma Spectrometry technique. Based on the Malaysian adults' consumption rate, annual effective dose and the associated cancer risk were estimated. Activity concentrations of 40K were found to be one to three order of magnitudes higher than other radionuclides of ^{226}Ra, ^{228}Ra, ^{232}Th, ^{238}U, ^{134}Cs and ^{137}Cs. Calculated effective doses due to the intake of radionuclides was between 0.1 – 217 μSv/y, with potential of cancer risk incurrence up to 76 cases in every 100,000 people. Overall, dose received by population still below recommended limit of 1 mSv/y set by WHO and ICRP for radiological safety.

Keywords: Radionuclides, effective dose, cancer risk

1 Introduction

Assessing radionuclides contamination in diet is important to ensure food safety. Radionuclides can originate from either naturally occurring, such as primordial in mother nature, or through cosmogenic formation or by human activities, such as the release from nuclear weapons testing or accidents (UNSCEAR, 2000). These radionuclides enter human body via two main routes, i.e. inhalation of radon gas and ingestion of contaminated food (Jemii and Mazouz, 2020). Ingestion of foods containing natural (^{40}K, ^{226}Ra, ^{228}Ra, ^{232}Th, ^{238}U) and artificial (^{134}Cs and ^{137}Cs), radionuclides contribute large fraction of internal radiation exposure (UNSCEAR, 2008; Alamoudi, 2013; Godyn´ et al., 2014; Desideri et al., 2014; Uwatse et al., 2015; Sahar et al., 2016). Depending on radionuclide's chemical properties, they will behave differently inside the human body. For instance, radiums absorbed to the bone and teeth (VKM et al., 2017). Potassium-40 and caesiums assimilated into the tissues of all plants and animals and then distributed uniformly in the body (VKM et al., 2017). Typical annual effective dose ranges from the food ingestion are between 0.2 – 1 mSv (UNSCEAR, 2008). International Commission on Radiological Protection (ICRP) recommended 1 mSv as the annual effective dose for a member of public due to the operation of nuclear facilities and from the applications of radiation and radionuclides. Cancer and heritable effects are the most important health effects of ionising radiation at relatively low doses and dose rates. Depending on cancer types, latency period can range from 2 to 30 years (VKM et al., 2017). This study quantified several radionuclides concentration in commercial foods, estimate the annual effective dose and associated cancer risk in Malaysian adults (> 17 y).

2 Experimental

2.1 Activity concentration of radionuclides

Activity concentration of natural (^{40}K, ^{226}Ra, ^{228}Ra, ^{232}Th, ^{238}U) and artificial (^{134}Cs, ^{137}Cs) radionuclides in over 400 various food samples were measured with same unit of HPGe gamma spectrometry for 15 hours each. Sample was prepared in a 350 ml cylindrical container, sealed with PVC tape and stored for a month to achieve secular equilibrium. Sample preparation and minimum detectable activities (MDA) for this experiment was as reported earlier in (Yii et al., 2022). Equipment set-up and radionuclides identification also as reported earlier by (Yii, 2019).

2.2 Calculation of annual effective dose

The annual effective dose due to radionuclides intake was calculated using the formula (Alam et al., 1999):

$$A_D = A_C * C_F * A_I \quad (1)$$

where:
A_D is the annual effective dose (Sv/y) to an individual due to the ingestion of radionuclides,
A_C is the activity concentration of radionuclides in the ingested foods (Bq/kg),
C_F is the dose conversion factor for ingested radionuclides (Sv/Bq) (ICRP, 1995), and
A_I is the annual intake of foods (kg/y) for Malaysian (for Public Health, 2014).

2.3 Calculation of relative cancer risk

According to (Lin, 2010), one Sievert carries a 5% excess risk of death from cancer and this is extrapolated linearly for lower doses. Effective dose from consumption of each sample and the 5% chance of cancer risk was used for calculation of cumulative dose and risk up to the age of 70 years for the public. Calculation was performed using online calculation spreadsheet provided under Wise Uranium project.

3 Results and Discussion

3.1 Activity concentration of radionuclides

Generally, radionuclides concentrations were found in decreasing order of ^{40}K >> ^{238}U > ^{226}Ra > ^{228}Ra, ^{232}Th > ^{137}Cs, ^{134}Cs. K-40 was detected in all samples and was in one to three order of magnitudes higher when compared to other radionuclides. It varied between 2.9 – 1360 Bq/kg. Meanwhile, activity concentration for other natural radionuclides of ^{226}Ra , ^{228}Ra, ^{232}Th, ^{238}U, was ranged between 0.5 – 7.9 Bq/kg, 0.5 – 12 Bq/kg, 0.5 – 9.8 Bq/kg and 0.5 –21 Bq/kg, respectively. Most of these radioactivities values found were significantly lower than the mean levels reported by UNSCEAR (2000) in soil (33 and 45 Bq/kg, for ^{226}Ra and ^{232}Th, respectively). Meanwhile, artificial radionuclides ^{134}Cs was less than 1 Bq/kg while ^{137}Cs was between 1.0 – 6.3 Bq/kg. Radionuclides are believed to be transferred from the soil to the plants, then to the final products (UNSCEAR, 2008). For some radionuclides, their detection in some samples does not necessarily simply their absence in the others (below MDA). It is well understood that background levels and system MDA could conceal the minor photopeaks during counting (Knoll, 2000).

3.2 Annual effective dose

The total annual effective dose (sum of total radioactivities dose) for adults consumed the foods were performed with Eq. 1 above. The estimated annual effective dose ranged between 0.1 – 217 μSv/y. Only ten samples (2.5%) were found to have dose value more than 100 μSv/y which mostly were the fungus/herbal extracted pre-mix beverages. Generally, consumption of the commercial foods tested in this experiment would be considered giving insignificant health hazard to human. Overall, the estimated annual dose from the food's consumption was below the ICRP's recommended reference value of 1.0 mSv (ICRP, 1995).

3.3 Excess lifetime cancer risk

From the annual effective dose value, the cumulative lifetime cancer risk was calculated using the Wise program spreadsheet. The highest effective dose of 217 μSv/y arouse from consumption of a beverage that would have potential cancer risk occurrence of 76 cases in every 100,000 people. Radiation hazard associated with drinking this particular beverage may face greater health risk as compared to other foods. Most of the cancer risk probability found here were comparable or lower than those reported elsewhere (Moon et al., 2016; Priharti and Samat, 2016).

4 Conclusions

Based on Malaysian adults' foods consumption rate, annual cumulative internal dose due to the foods intake were calculated. Total annual effective dose in adult due to the ingestion of all radionuclides was estimated along with the excess lifetime cancer risk. The largest contributor to the dose received by people was due to the ingestion of fungus/herbal extracted pre-mix beverage with the highest effective dose of 217 μSv/y that gave potential risk of cancer occurrence at 76 cases in every 100,000 people. Drinking this particular beverage facing greater radiation health risk as compared to the other foods. Basically, when accumulated dose is higher, so do the cancer risk. Overall, potential doses received by the population are still below the 1 mSv/y radiological safety recommendation limit given by WHO and ICRP.

References

M.N. Alam, M.I. Chowdhury, M. Kamal, S. Ghose, M.N. Islam, and M. Anwaruddin. 1999. *Radiat. Prot. Dosimetry*, 82:207 – 214.

Z.M. Alamoudi. 2013. *J. Am. Sci.*, 9:267 – 273.

D. Desideri, M.A. Meli, C. Roselli, N. Forini, A. Rongoni, and L. Feduzi. 2014. *J. Radioanal. Nucl. Chem.*, 299:1461 – 1467.

Institute for Public Health. 2014. MOH/S/IKU/46.15(RR). *Ministry of Health Malaysia, Kuala Lumpur*, page 143pp.

P. Godyn´, A. Do lhan´czuk-S´ro´dka, Z. Ziembik, and E. Moliszewska. 2014. *J. Radioanal. Nucl. Chem.*, 299:1359 – 1364.

ICRP. 1995. ICRP Publication 72, Ann. ICRP. *Pergamon, Oxford*, 26(1).

E. Jemii and M. Mazouz. 2020. *J. Environ. Prot. Sci.*, 11:682 – 689.

G.F. Knoll. 2000. ISBN: 0-471-07338-5. *John Wiley Son Inc, New York.*, page 802pp.

E.C. Lin. 2010. *Mayo Clin. Proc.*, 85(12):1142 1146.

E.K. Moon, W.H. Ha, S.W. Seo, Y.W. Jin, K.H. Jeong, H.J. Yoon, H.S. Kim, M.S. Hwang, H. Choi, and W.J. Lee. 2016. *J. Korean Med. Sci.*, 31:9 – 12.

W. Priharti and S.B. Samat. 2016. *Malays. J. Anal. Sci.*, 20(6):1247 – 1253.

A.A. Sahar, M.S.M. Al-kafaje, and R.R. Al-Ani. 2016. *J. Nat. Sci. Res.*, 6:112 – 115.

UNSCEAR. 2000. pages United Nations, New York.

UNSCEAR. 2008. pages United Nations, New York.

O.B. Uwatse, M.A. Olatunji, M.U. Khandaker, Y.M. Amin, D.A. Bradley, M. Alkhorayef, and K. Alzimami. 2015. *Environ. Eng. Sci.*, 32:1 – 9.

VKM, J. Alexander, Brantsæter A.L., G. Brunborg, C.K. Fæste, A. Jaworska, M. Komperød, I.T.L. Lillegaard, C. Rosseland, L. Skuterud, L.F. Andersen, E.O. Elvevoll, B. Hjeltnes, M. Hofshagen, Å. Krogdahl, T. Källqvist, H.G. Opsahl-sorteberg, T. Rafoss, I. Skaar, J.U. Skåre, I-L. Steffensen, V. Vandvik, Y. Wasteson, and G-I. Hemre. 2017. VKM report 2017:25, ISBN: 978-82-8259-282-6. *VKM, Oslo,*, page 150pp.

M.W. Yii, D.N.F. Ahmad-Tugi, M. Mahmud, N.A. Hassan, and M.A. Ramli. 2022. *Seminar RD 2022, 4 – 6 Oktober 2022, Nuklear Malaysia, Bangi.*

M.W. Yii. 2019. *J. Radioanal. Nucl. Chem.*, 320(1):193 – 199.

Individual Research Contribution Review, 2023, 1(1): 163–164

Radiological Source Characterization for Nuclear Forensic Applications

Zalina Laili
Waste Technology and Environmental Division
Malaysian Nuclear Agency
43000 Kajang, Selangor
liena@nm.gov.my

Abstract

An examination was conducted on radiological sealed radioactive sources to assess their applicability for nuclear forensic purposes. Focus was placed on three specific types: ^{60}Co, ^{137}Cs, and ^{241}Am. The physical, macroscopic, and radiological properties of these sources were analyzed to determine their distinct signatures. The analysis revealed clear physical and radiological features that set these sources apart. This information has the potential to be valuable for the establishment of a National Nuclear Forensic Library (NNFL) in Malaysia, contributing to the enhancement of nuclear forensic investigations.

Keywords: nuclear forensics, radiological sealed radioactive sources, signatures

1 Introduction

Various methods can be used to study radiological sealed radioactive sources and understand their unique characteristics, whether related to their physical, chemical, or radiological properties. Notably, there have been no prior nuclear forensic studies in Malaysia. This current research focuses on characterizing sealed radioactive sources containing ^{60}Co, ^{137}Cs, and ^{241}Am, aiming to discover their distinct properties. These findings are valuable for nuclear forensic analysis in Malaysia, particularly in the context of creating a national nuclear forensic library (NNFL).

2 Methods

Four different types of radiological sealed radioactive sources were characterized in this study. The sources are two ^{60}Co sources (Source 1: rod shape and Source 2: cup style), one ^{137}Cs source (Source 3: cylindrical plastic disc), and one ^{241}Am source (Source 4: cup style). All the sources were characterized based on their physical and radiological characteristics (IAEA, 2015). For gamma spectrometric analysis, all the sources were measured high-resolution coaxial high-purity germanium (HPGe) detector, which has a relative efficiency of 25% with a resolution of 1.9 keV at 1332.5 keV of ^{60}Co. Radiographic studies were conducted on the sources using an X-ray machine, which featured a directional X-ray tube capable of generating up to 200 kV and operating at a constant current of 5 mA.

3 Results

Upon visual examination, notable differences were observed in the structure and design of each radioactive source. These variations included differences in the shielding materials used for the sources, with some sources being encased in sealed stainless-steel capsules, while others were composed of metal foils or discs (see Figure 1). The radiological source also exhibited embossing and engraving on its surface, providing information about the radionuclide and its initial activity. Green carbonate rust, a clear indicator of ongoing corrosion, occurred on one of the stainless steel-type sources.

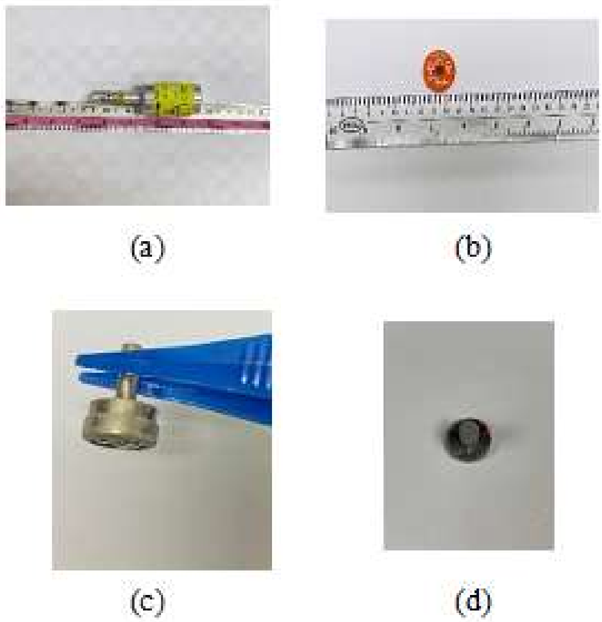

Figure 1: (a) A cylinder ^{60}Co source in the metal holder, (b) Plastic disc ^{137}Cs source with embossing and engraving on the source, (c) ^{60}Co source enclose in metal foil and has wire mesh and (d) corrosion occurred can on the stainless steel-type sources.

A scattering peak was notably detected in the cylindrical ^{60}Co source (Figure 2) and the ^{137}Cs disk source (Figure 3) within the energy range of 200-500 keV. However, it was not observed in the cup-style ^{241}Am source (Figure 4). The Compton edge was observed in both the ^{137}Cs plastic disc source at 1321.3 keV (Figure 3) and the ^{241}Am cup-style source at 125.3 keV (Figure 4). The gamma spectra obtained from the ^{60}Co, ^{137}Cs, and ^{241}Am sources exhibited extra peaks that cannot be attributed to these sources' emissions.

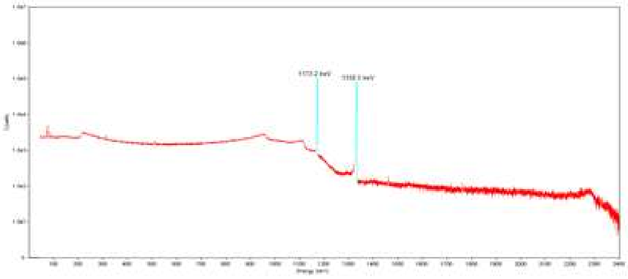

Figure 2: Gamma-ray spectrum of the ^{60}Co source (185 kBq)

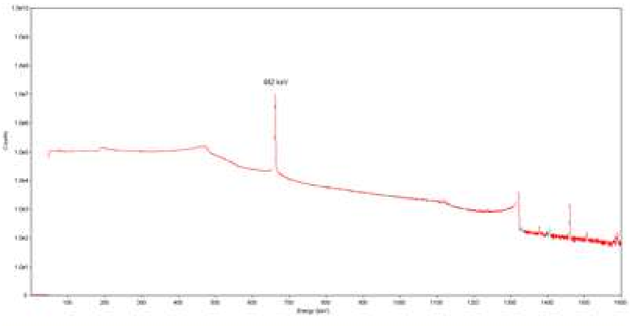

Figure 3: Gamma-ray spectrum of the ^{137}Cs source (185 kBq)

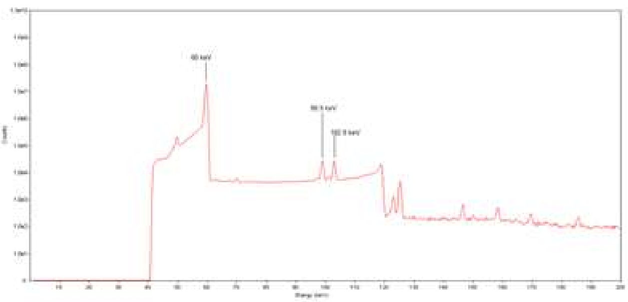

Figure 4: Gamma-ray spectrum of the ^{241}Am source (185kBq)

Figure 5 (a) offers valuable information about into the internal composition of the disc-shaped radioactive sources. The X-ray image precisely illustrates the positions and active regions of the ^{241}Am and ^{60}Co radioactive sources contained within the discs.

4 Discussions

Physical attributes serve as valuable markers for identification in nuclear forensic investigations. Variations in the construction and design of radioactive sources provide crucial information about their intended use and handling. Understanding the incident gamma ray energy is essential for source identification and comprehending its radiation characteristics.

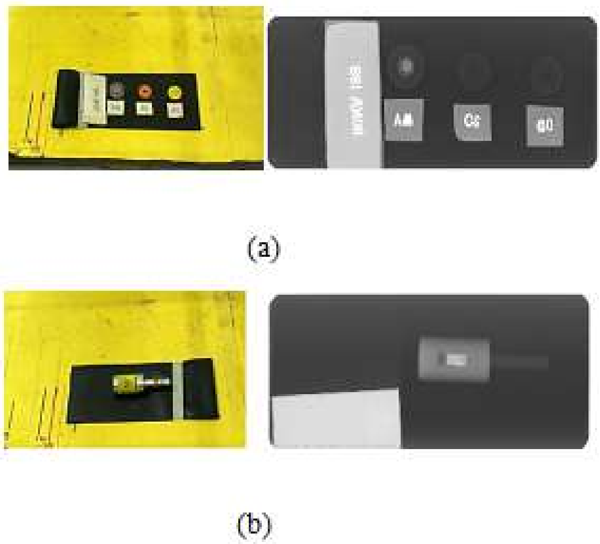

Figure 5: X-ray images of (a) ^{241}Am, ^{137}Cs plastic and ^{60}Co disk source and (b) the ^{60}Co cylindrical source contained within an aluminum shield

The presence of unexpected peaks in gamma spectra can be a significant indicator of impurities or the potential contamination of the radioactive sources. Additionally, X-ray imaging plays a pivotal role in verifying the authenticity of radioactive sources, evaluating their condition, and confirming their composition. Therefore, the precise portrayal of the location and active area within these source discs significantly enhances the effectiveness of nuclear forensic investigations.

5 Conclusion

In summary, the physical and radiological characteristics of sealed radioactive sources (^{60}Co, ^{137}Cs, and ^{241}Am) are essential for identification and analysis. This supports the development of a National Nuclear Forensic Library (NNFL) and enhances Malaysia's capabilities for radioactive source identification and analysis.

References

IAEA. 2015. Nuclear forensic in support investigation. *IAEA Nuclear Security Series*, No. 2-G (Rev. 1):Vienna. International Atomic Energy Agency.

Individual Research Contribution Review, 2023, 1(1): 165–166

Preliminary Trial Test of Trisodium Phosphate Produced from Malaysian Monazite Alkali Digestion

Abdul Rahman Norazumin
Industrial Technology Division, Malaysian Nuclear Agency
43000 Kajang, Selangor
abdrahman@nm.gov.my

Abstract

Monazite contains valuable substances which can be recovered by alkaline digestion. From literature review, there is a characterization of monazite by using Field Emission Scanning Electron Microscope Energy Dispersive X-ray (FESEM-EDX), X-ray Diffraction (XRD) and Particle Size Analyzer (PSA) to determine the mineral characterization. Using X-ray Diffraction (XRD), it was found that monazite is a type of Cerium Phosphate ($CEPO_4$). From experiment, it was found that the phosphorus content in monazite is 11.6% (FESEM-EDX) and the average size of monazite is 194.66mm (PSA). In addition, there is a white solution of trisodium phosphate produced after washing is carried out through alkaline digestion.

Keywords: Monazite, Alkali digestion, Trisodium Phosphate

1 Introduction

Monazite is a unique phosphate deposit with (Ce, La, Nd, Th) (PO_4, SiO_4) chemical properties. This commonly appears as small separated grains, throughout igneous and metamorphic rocks like granite, pegmatite, schist, and gneiss. All such grains also weather-resistant and become distributed from the host rock in downslope soils and sediments. There also exploited by the rare earth and thorium value.

The discovery of trisodium phosphate using alkaline digestion of monazite was pioneered by (Rohden et al., 1950), at the Battelle Memorial Institute. A total of one ton of monazite was used and one ton of sodium hydroxide was used in alkaline digestion. One ton of sodium hydroxide is prepared in a concentration of 65% and heated up to 140°C to 140°C for two to five hours. A total of one and a half tons of trisodium phosphate was produced through the crystallization of trisodium phosphate. Another researcher from the Battelle Memorial Institute, (Calkins and Bohlmann, 1957), performed alkaline digestion in open-air digestion by using stainless steel reaction vessel fitted with external heaters. A solution of sodium hydroxide with a concentration of 75% was prepared with the ratio of sodium hydroxide to monazite being 1.5. While the ratio of water to monazite was 1.7. The solution heated to 138°C for 3 hours. After the reaction took place, the slurry of sand and sodium hydroxide was dissolved in water with sodium hydroxide at a concentration of 20% and digested at 104°C for one hour before being filtered. The hydrous cake obtained contains 96.9% uranium, 100% thorium, 100% rare earth, and 0.3% phosphorus. The following is the equation of the chemical.

$$RePO_4 + 3NaOH = Re(OH)_3 + Na_3PO_4 \qquad (1)$$

$$Th_3(PO_4)_4 + 12NaOH = 3Th(OH)_4 + 4Na_3PO_4 \qquad (2)$$

2 Methods

Malaysian Monazite is collected from Universal Mineral Trading Sdn. Bhd., Chendriang, Perak. Samples were stored at room temperature before digestion work was carried out. Malaysian Monazite raw material will be characterized to identify the chemical composition before the experiments are conducted. Alkali digestion using sodium hydroxide purchased from LabChem Sdn. Bhd. Sodium hydroxide should be stored at room temperature and dried to avoid any reactions. Sodium hydroxide used flake type with 99% purity. Distilled water is used to dissolve the flake into a liquid.

The element content in monazite was determined using Carl Zeiss brand Field Emission Scanning Electron Microscope Energy Dispersive Energy X-ray (FESEM-EDX). Approximately 5mg of the sample was used in the analysis and placed in a sample tray after being crushed. After that, the sample tray will be placed inside the device and the experiment will be conducted for 5 minutes. X-ray diffractometer (XRD) is used to determine the presence of chemical composition in monazite samples. In this study, the X-ray spectrum used the PANalytical brand. Approximately 5 mg of sample was crushed when the test was performed. The sample will be placed on the sample tray and then an X-ray beam will be bombarded to the sample. The results of the spectrum will indicate the chemical composition of the monazite used. A particle size analyzer was used to identify the size distribution in monazite using Honeywell brand. Approximately 5mg of monazite sample was placed in the sample tray. The sample tray will be placed in the tool for 5 minutes. The granulometric graph will show the element distribution in the monazite sample.

The experiment was carried out by preparing a concentrated sodium hydroxide solution in a 3 L beaker. The weight of monazite added to the beaker was determined based on the weight ratio of monazite to sodium hydroxide 1: 1.5. The digestion time and temperature of the heated solution is 3 hours and 140°C. The solution will be heated on a hot plate and will be stirred with a magnetic stirrer bar throughout the experiment to ensure that the solution is well blended. Leaching will be carried out after the digestive reaction has been completed. The alkaline solution will be poured into a 3L beaker containing the weight of water based on the liquid to solution 3 ratio set. The monazite slurry will be stirred for 1 hour at 90°C and will be filtered using a Buchner funnel to separate the soluble trisodium phosphate and the insoluble hydroxide cake. The hydroxide cake will be washed with hot distilled water to remove aqueous sodium hydroxide. The washing process is carried out until the neutral value of pH is constant.

3 Results

Monazite was obtained from Universal Mineral Trading Sdn. Bhd., Chendriang, Perak used in the experiments were analyzed and characterized by several characterization methods. Energy Dispersive X-ray (EDX) was used to identify the types of elements contained in the monazite before the experiments were carried out. This is to ensure that the phosphorus element is contained in the monazite so that alkaline digestion does not waste time. From the result, there is a phosphorus element in this monazite with a content of 11.6%. Among the other elements in monazite are Cerium 23.5%, Lanthanum 10.1%, Neodymium 9.7%, Thorium 8.3%, and Oxygen 27.3%. The molecular composition in monazite can be determined by using X-ray Diffraction (XRD). It is found that the monazite content contained in this sample is cerium type monazite because shows a peak at 28.78°. In addition, there is a phosphate content in this sample that allows alkaline digestion to be carried out further. The result of the granulometric analysis using particle analyzer indicates that the concentration of 194.66 μm means diameter in the sample. So that grinding and sieving need to be done because use 100% passing 0.0045mm for digestion. Figure 1 shows a white trisodium phosphate solution after washing with hot distilled water on mixed hydroxide.

Figure 1: Preliminary trial-test –Trisodium Phosphate before crystallization

4 Discussion

Based on Energy Dispersive X-ray (EDX) and X-ray Diffraction (XRD) results showed monazite contains phosphorus and phosphate content. The reading value indicates that monazite contains 11.6% of the element phosphorus. This is important and needs to be studied first before trisodium phosphate can be produced from alkaline digestion. A white solution of trisodium phosphate was visible after washing was performed as shown in Figure 1.

References

G.D. Calkins and E.G. Bohlmann. 1957. Processing of monazite sand. *U.S. Patents*, US 2815264.

C.De Rohden, N. Seine, and M. Peltier. 1950. Treatment of monazite. *U.S. Patents*, US 2783125 A.

Individual Research Contribution Review, 2023, 1(1): 167–168

Study on Possibility of Using Aerogel as an Additive in Solvent-Based Paint as Alternative to Enhance Heat Resistance Characteristic

Ahmad Hambali Ismail
Industrial Technology Division, Malaysian Nuclear Agency
43000 Kajang, Selangor
hambali@nm.gov.my

Abstract

Plant Assessment Technology Group (PAT) specialize in application of sealed and unsealed radioactive sources and provide scanning services to the industry. However, common situation in industry is exposure to the high temperature surrounding that may cause some effect on the functionality of the detector and reduce shelf life. Thus, in this study, PAT group is studying the possibility to improve heat resistance characteristic by adding aerogel to the solvent-based paint. The study is conducted by adding variation percentage of aerogel (1%, 3%, 5%, 10% and 20%) and then coated on a steel plate to expose it to the variation of heat (25°C, 50°C, 100°C, 200°C and 400°C) for heat transfer performance evaluation. The coated samples also will be characterized using Thermogravimetric analysis and Fourier Transform Infra-Red.

Keywords: Aerogel, solvent-based paint

1 Introduction

PAT Group from Malaysian Nuclear Agency is one of the groups in Industrial Technology Division. PAT group is a group that leads in research and development and also application of sealed and unsealed radioactive sources. This nuclear technique application is also known as non-destructing testing (NDT) because it does not interfere with the ongoing and current process. PAT group is a service provider which specialize in detecting the abnormalities in the plant. The scanning services provided are distillation column scanning, pipe scanning, level scanning and application of radiotracer.

Whenever conducting NDT services in industries (petrochemical, fertilizer, chemical industry and many more), there is always a place which consist of high temperature such as a vessel consist of high temperature liquid, distillation column and high temperature multiphase flow in pipeline to deal with. The heat produced might have caused some effect on the detector which will reduce the functionality of the detector and this will probably reduce the shelf life. Therefore, one solution might be able to overcome it by applying thermal insulation coating. Thermal insulation coating is a layer or liquid that applied on the surface of material that can provide heat resistant. For this application, aerogel is identified as the material for this application.

Aerogel is gel that consist of a microporous solid that dispersed phase is a gas (McNaught and Wilkinson, 2007). Aerogel is proved to be the material that exist with low densities (0.003 – 0.15 kg/m3) with low density nano-porous solids with a fine, open pore structure, large porosity and large surface area (500 – 1000 m2/g) (Smirnova and Gurikov, 2018). It is also proved having low thermal conductivity and excellent transparency (Dorcheh and Abbasi, 2008). These characteristics provide wide range of aerogel usage in building application as thermal and acoustic applications and other sectors such as absorbents, shock absorber, nuclear waste storage, batteries and catalyst etc. (Baetens et al., 2011).

With the characteristics of high porosity and nanometer pores size, aerogel seems to be a material with very low thermal conductivity (Smirnova and Gurikov, 2017) and alternatively, it may be possible to be used as an additive in paint to produce thermal insulation paint. By referring to some study before, aerogel was introduced in water-based paint and the result shows that the thermal insulation performance was increased (Lu et al., 2022). Hence, in this study, PAT group had proposed with the initiative to use aerogel as an additive in solvent based paint to enhance the heat resistance characteristic to produce the thermal insulation paint. The variation of aerogel percentage will mix with the paint and the performance against heat will be evaluated.

2 Methods

In this study, the methods are divided into two parts which are experimental and characterization.

2.1 Formulation and performance evaluation

Variation of percentage of aerogel (1%, 3%, 5%, 10% and 20%) used to mix with solvent-based paint. The physical appearance of the solvent-based then observed including the viscosity changes. The viscosity is compared with the viscosity of the original formulation. The formulated solvent paint then coated on stainless steel plate and tested using variation of heat (25°C, 50°C, 100°C, 200°C and 400°C). The plates are exposing to the heat with the duration of 1 hour. The experiment is carried out in 3 replicates. The data are recorded using thermocouple.

2.2 Formulation and performance evaluation

2.2.1 Thermogravimetric Analysis (TGA)

The formulated solvent-based paint characterized using TGA to determine and observe the thermal stability of the samples.

2.2.2 Fourier Transform Infrared

The formulated solvent-based paint characterized using FTIR to observed the chemical bonding of the coated samples.

3 Data/ Results

The result on this study is to determine the effect of addition of variation percentage of aerogel to the solvent-based paint. We hypothesize that the viscosity of the solvent-based paint will shows an increasing trend as we increase the percentage of aerogel.

Second, this study is to determine the performance of new added formulation of aerogel-paint against the variation of heat. We hypothesize that decreasing trend or heat that can pass through for temperature 25°C, 50°C and 100°C. Then for 200°C and 400°C, we predict that there is no significant difference for the heat that pass through.

4 Discussion

If the result supported the hypothesis, it can be suggested that by adding the aerogel, it may show an increase in viscosity of the solvent-based paint. Other than that, the heat pass through also predicted to be reduced. These findings are aligned with the study that had been done before (Lu et al., 2022) that shows viscosity acceptance is within 20% of addition of aerogel and also decreasing of heat that pass through.

However, if the result is deviates from the hypothesis, potential reasons that contribute are include type of paint used, thickness of the coating and source of the aerogel. This study will show a contribution to knowledge on aerogel as heat barrier and thermal insulation coating. Other than that, it will show the opportunity to commercialize the aerogel as an additive in thermal insulation paint to the current market.

5 Conclusion and Attention

In conclusion, this study aims to evaluate the performance of aerogel in solvent-based paint in which it can enhance the heat resistant characteristic. Although the experimental and data collection process is not done yet, we believe that it can show positive outcome in enhance heat resistance characteristics. However, if the expectations are not as predicted, the findings will be used as reference data and future research can be propose to overcome the limitations.

References

R. Baetens, B.P. Jelle, and A. Gustavsen. 2011. Aerogel insulation for building applications: a state-of-the-art review. *Energy and Buildings*, 43(4):761–769.

A. Soleimani Dorcheh and M. H. Abbasi. 2008. Silica aerogel; synthesis, properties and characterization. *Journal of Materials Processing Technology*, 1199(1):10–26.

Yanru Lu, Zihe Liu, Xiaodong Li, Xi Jiang Yin, and Handojo Djati Utomo. 2022. Development of water-based thermal insulation paints using silica aerogel made from incineration bottom ash. *Energy Buildings*, 259:111866.

A. D. McNaught and A. Wilkinson. 2007. Compendium of chemical terminology, IUPAC goldbook, PAC. *Blackwell Science, Oxford, Cambridge, UK,*, 2nd edition.

I. Smirnova and P. Gurikov. 2017. Aerogels in chemical engineering: strategies toward tailormade aerogels annu. *Rev. Chem. Biomol.*, 8(4):307–334.

Irina Smirnova and Pavel Gurikov. 2018. Aerogel production: Current status, research directions, and future opportunities. *The Journal of Supercritical Fluids*, 134:228–233.

Individual Research Contribution Review, 2023, 1(1): 169–170

Asphalt Layer Determination using Ground Penetrating Radar

Amer Hazreq Bin Haron
Industrial Technology Division, Malaysian Nuclear Agency
43000 Kajang, Selangor
amer@nm.gov.my

Abstract

Ground Penetrating Radar (GPR) is a non-destructive method used to photograph and explore subsurface layers, such as asphalt layer thickness. The data revealed four layers in the asphalt profile which aligns with the Malaysian Public Works Department (JKR) standards, but variations can be attributed to meteorological factors such as temperature and recipitation. Further research and ongoing surveillance are recommended to evaluate weather conditions and asphalt layer integrity.

Keywords: GPR, Non-destructive, asphalt.

1 Introduction

GPR use radar technology, an acronym for ”Radio Detection and Ranging” to transmit high-frequency electromagnetic pulses into the subsurface, often within the microwave or radio wave spectrum. When these pulses encounter alterations in subsurface materials such as soil layers, rock formations, bodies of water, or concealed objects, a portion of the energy is reflected back to the surface. The evaluation of asphalt layer thickness using conventional techniques is frequently characterised by a significant investment of time and financial resources. The utilisation of GPR technology offers a non-intrusive means of photographing and exploring subsurface layers. By releasing electromagnetic waves into the ground and analyzing the resulting reflections or echoes from subsurface objects and structures, GPR technology can effectively boost the precision of determining asphalt layers. Through the examination of the temporal discrepancy between the transmitted signal and the received signal, GPR has the capability to generate a profile of the subsurface. The aforementioned technology exhibits versatile applications across multiple disciplines, encompassing civil engineering, archaeology, geology, environmental science, and forensics.

2 Methods

The GSSI 900 MHz Antenna was chosen for this project due to its extensive use in various industrial sectors. The antenna type and dimensions were customized to suit the specific purpose, with high frequency antennas having limitations in depth penetration. A GPR device was used to examine subsurface utility infrastructure, specifically for evaluating asphalt layer depth. The frequency range used is from 500 MHz to 2.6 GHz.

A control unit or computer equipped with GPR software was used to acquire and process data, while a cart with a GPS system was used for precise placement during the survey. The primary experiment location was at Evaluation and Verification Facility, Block 60, Malaysian Nuclear Agency where the thickness of the asphalt layer was constructed as the standard of Malaysian Public Works Department. The selection of the survey section was based on factors such as pavement condition, traffic volume, and evaluation objectives.

Chalk was used to demarcate precise testing points within designated locations, and the GPR scans were performed at regular intervals ranging from 1 to 5 feet (0.3 to 1.5 meters). The calibration of the GPR system was essential for providing accurate data, and calibration markers or established reference points of asphalt thickness were used.

The GPR antenna was affixed to the survey truck or cart at an optimal height and orientation, ensuring parallel alignment with the ground surface throughout the survey. Radar waves penetrated the asphalt layer and reflected when encountering interfaces between different materials, producing data profiles that provide information on layer thickness and anomalies.

Data was collected from the GSSI 900 MHz GPR antenna, which included comprehensive details about underlying strata and irregularities. This data was then analyzed and evaluated using Radan 7 software, which helped identify patterns and irregularities within the asphalt layer. The data was organized into a structured table, facilitating effective data cross-referencing and establishing connections between insights from GPR analysis and other sources of data.

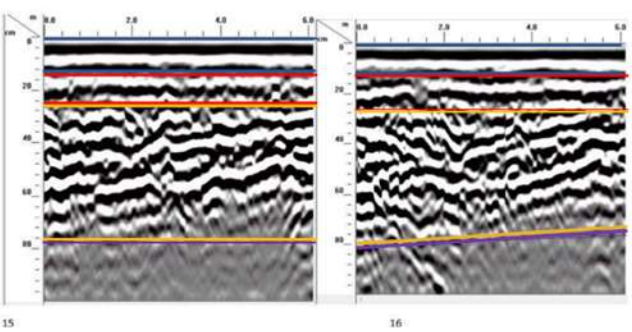

Figure 1: An example of GPR radargram profile after being processed and analysed using Radan 7 software by GSSI.

3 Results

Different layers in the asphalt profile were clearly distinguished in the GPR radargram. 4 layers were identified as Wearing Course (1^{st} layer, blue line), Binder Course (2^{nd} layer, red line), Crusher Run (3^{rd} layer, orange line) and Sand Bedding (4^{th} layer, purple).

The top and bottom depth of each interval were determined by analysing different pattern from the GPR response. Similar approach was done by Amran et al.in inspecting highway condition focusing on the structural integrity and pavement condition (Amran et al., 2021).

4 Discussion

After conducting a thorough examination of the data obtained from GPR scans and comparing it with the Malaysia Standard Specification outlined by the Malaysia Public Works Department (JKR), it is apparent that the thickness of the asphalt layer in our designated research location displays fluctuations that align with the prescribed standards. While a number of data points exhibit a strong correlation with the prescribed standards, as seen by their near measurements, there are also instances where the thicknesses depart from the set values. The observed variations can be ascribed to a multitude of causes, encompassing the influence of meteorological circumstances. It is imperative to recognise that meteorological variables, specifically fluctuations in temperature and precipitation, can exert a substantial impact on the thickness of the asphalt layer. The occurrence of extreme temperatures has the ability to induce thermal expansion and contraction, hence potentially influencing the reported thickness. The presence of water saturation resulting from inclement weather conditions may also have an impact on the attenuation of the GPR signal, hence influencing the gathering of GPR data.

5 Conclusion and attention

As a conclusion, the adherence of the asphalt layer to JKR requirements may vary as a consequence of various external circumstances. It is advisable to conduct additional inquiries and maintain ongoing surveillance in order to evaluate the enduring effects of weather conditions and the integrity of the asphalt layer. This will enable the implementation of proactive maintenance and repair procedures if deemed necessary.

References

T S T Amran, M S M Amin, M R Ahmad, N M Azreen, S Sani, M A K Adnan N A Razak, and S Sayuti. 2021. NDT methods in inspecting road and highway structures. *IOP Conference Series: Materials Science and Engineering*, 1106(012034).

Individual Research Contribution Review, 2023, 1(1): 171–172

Simulating Inspection of Flange Face Corrosion (FFC) using Phased Array Ultrasonic Testing

Amry Amin Abas
Industrial Technology Division, Malaysian Nuclear Agency
43000 Kajang, Selangor
amry@nm.gov.my

Abstract

Flanges are a component that joins two section of pipes together to achieve a contained flow of product through it. However flanges are susceptible to flange face corrosion due to various factors. One of the methods of Non-destructive testing that has potential to detect FFC is phased array ultrasonic testing (PAUT). In this article, the method of simulating PAUT inspection of flanges to detect FFC using CIVA software is discussed. The objective of this research is to optimize inspection parameters and Probability of Detection (POD) without compromising on practicality of inspection. From the initial simulation, it is found that a model has been successfully established that enables further optimisation work to be furthered.

Keywords: Flange Face Corrosion, Phased array ultrasonic testing, Non-destructive testing

1 Introduction

Flanges are components which joints two pipes together without the need to weld them together. The purpose is for easiness of fitting and ability to service sections of the pipeline. There are many types of flanges such as weld neck, slip on, threaded and etc with different flange face such as raised joint, flat face and ring type (Didik, 2017). Between the flanges, a layer of gasket is placed to ensure tightness and prevent loss of containment. However, due to the closed air environment, there is a high possibility of crevice corrosion occurring especially at the flange face in contact with the gasket surface. Material investigation showed that the chemical composition and mechanical properties of the flange were all in accordance with the corresponding parameter requirements, and the corrosion phenomenon was mainly attributed to CO_2 corrosion. High temperature and high medium flow rate also had a big influence on the acceleration of the corrosion process. Corrosion of the sealing groove end face was attributed to galvanic corrosion, the corrosion potential difference between the flange and gasket was the main reason for the galvanic corrosion (Nan et al., 2023).

Currently there are no methods of detecting FFC. It is only discovered during maintenance or when a loss of containment (LOCA) occurs. PAUT has been proposed as the technique to be able to detect FFC and could potentially reduce down time of production.

2 Methods

A model of a carbon steel flange was developed using a CAD software as dimensional accuracy is required to achieve reliable results. The model is then imported into the CIVA UT 2023 version in 3D format. The flange used in this simulation is made of carbon steel with weld neck and a raised face with 8 inches face diameter. This model is based on the readily available flange specimen which will be used to validate this simulation results. The inspection parameters are then selected based on the range that has been decided based on the relevant codes and standards such as ASME BPVC 2023. The probe selected is 5L16A10 with a SA10-0L wedge attached. Sectorial scanning is utilised to ensure sufficient coverage while the optimized resolution shall be determined from the simulation results in accordance to the interval range input. A side drilled hole reflector with diameter of 5 mm was placed at the raised face inner surface.

3 Results and Discussion

The model has been successfully developed in 3D format and with the inspection setup visualised as in Figure 1. The model also shows the beam profile and provides information on coverage of scan.

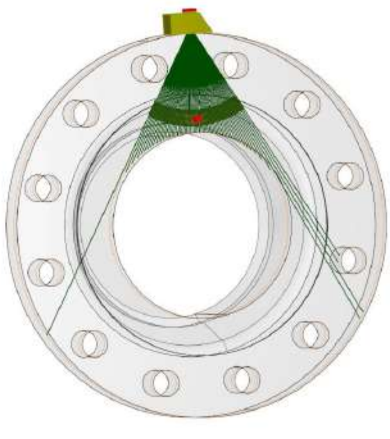

Figure 1: Model of flange inspection setup with a side drilled hole (red) and indication of beam coverage (green)

From the simulation, it is found that the inspection setup that has been developed has managed to provide sufficient detection of the side drilled hole as in Figure 2.

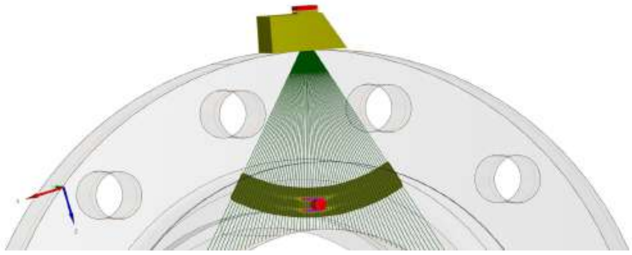

Figure 2: Indication from reflection of waves from the side drilled hole

Currently, this ongoing research only provides qualitative data and further study needs to be done focusing on certain parameters such as scanning sweep resolution and limits of beam angle. Further simulation should also be done on the multiple locations of reflectors and establishing the POD. Subsequently, the simulation shall have to be validated by applying the optimised parameters to inspect actual flange specimen.

4 Conclusion

Simulating inspection of flanges for detection of FFC using CIVA simulation software has been demonstrated to be useful in this research. Inspection parameters can be optimised while ensuring high POD.

References

F. A Didik. 2017. Phased array ultrasonic testing for internal corrosion detection on the flange joint. *Proceedings Indonesian Petroleum Association Forty First Annual Convention Exhibition*, IPA17-83-F.

J. Nan, L. Changliang, W. Peng, Z. Lijuan, and F. Chun. 2023. Corrosion cause analysis of a surface pipeline flange. *Journal of Physics: Conference Series*, 2468 012171.

Individual Research Contribution Review, 2023, 1(1): 173–174

Thermal Damage Evaluation on Hybrid Composite Via Advanced NDT Imaging: Formulation Kenaf/ Kevlar Composites

Asyraf Arif Bin Abu Bakar
Industrial Technology Division, Malaysian Nuclear Agency
43000 Kajang, Selangor
asyrafarif@nm.gov.my

Abstract

Composites now become vital components used in various industries such as automotive and aerospace. The integrity of components must be evaluated to ensure the components are saved. In this article, hybrid composites between Kenaf and Kevlar are fabricated and exposed to high temperatures to induce thermal damage. Later, the NDT method was used to evaluate the damage.

Keywords: Hybrid composites, Thermal damage, NDT

1 Introduction

Thermal or heat damage typically could occur to composites due to fire or during service operation, exposing them to hot gasses, lightning strikes, and others. These could lead to the degradation of the composites and affect their overall structural integrity (Shireesha et al., 2019). The challenge with thermally damaged composites lies in the physical nature of the damage itself, i.e. barely visible and can be undetected by visual inspection (Amir et al., 2019). Thus, it is pivotal to understand and characterize such damage using advanced NDT imaging modalities.

2 Methods

The method of this study involves experimental work consisting of sample preparation of Kenaf/ Kevlar hybrid composite, thermal damage, and advanced NDT imaging modalities. The hand lay-up method will be used to make the Kenaf/ Kevlar composite sample with dimensions 15cm x 10cm. Each ply of kenaf fibre will be stacked in layers between Kevlar to form the hybrid composite.

A heat gun or fire torch will be used as the heat source to introduce thermal damage to the fabricated hybrid composite samples. The samples will be heated between 200°C to 400°C, with a constant exposure time of 5 minutes. During the heating, the passive infrared thermography technique will be used to observe and evaluate the thermal damage in real time by mapping spatial and transient temperature changes in the area of interest. In the post-thermal damage stage, active thermography (vibrothermography) and digital radiography will be applied to the composite sample to detect and evaluate defects.

Figure 1: From left Kevlar, Kenaf

3 Formulation

The hand lay-up technique was chosen to fabricate Kenaf/ Kevlar composites. The mould for the fabrication of the samples is made of 450 cm x 20 cm mild steel plates. The fabrication of mould was done by Pusat Pembangunan Prototaip dan Loji, Agensi Nuklear Malaysia.

To ensure the ply of Kenaf and Kevlar are stacked in layers between them, an epoxy and hardener will be applied to the mould. Hence, there is a need for a formulation to fabricate the composites. Each ply of Kenaf and Kevlar is weighed using measure balance. The total weight of both fibre is equivalent to 25% of the total weight of the composite. The rest 75% is the ratio composition of epoxy and hardener which is 2:1 respectively. The formulation is given in Equation:

$$\text{(Kenaf ply + Kevlar ply) g} = 25\% \text{ total weight} \tag{1}$$

$$\frac{\text{(Epoxy + Hardener) g}}{75\%} = \frac{\text{(Kenaf + Kevlar) g}}{25\%} \tag{2}$$

The composite will undergo a curing process which will be left at room temperature, with pressure introduced on top of the composites for 24 hours.

4 Future Works

Different configurations of hybrid composites will be prepared using a combination of different numbers of plies (1,

Figure 2: Stainless steel mould

3 and 5) of the kenaf fibre with different grades of Kevlar. For each combination, six samples will be fabricated for the experiment. These samples will be heated to represent different damage phenomena and a few advanced NDT imaging modalities will be used for real time and post thermal damage assessment.

References

Siti Madiha Muhammad Amir, M.T.H. Sultan, Mohammad Jawaid, Ahmad Hamdan Ariffin, Shukri Mohd, Khairul Anuar Mohd Salleh, Mohamad Ridzwan Ishak, and Ain Umaira Md Shah. 2019. Nondestructive testing method for Kevlar and natural fiber and their hybrid composites. *Durability and Life Prediction in Biocomposites, Fibre-Reinforced Composites and Hybrid Composites*, 16.

Yegireddi Shireesha, Govind Nandipati, and KiranKumar Chandaka. 2019. Properties of hybrid composites and its applications: A brief review. *International Journal of Scientific Technology Research*, 8(08).

Individual Research Contribution Review, 2023, 1(1): 175–176

Characterization of Tropical Expansive Clays and Their Suitability as Natural Sealing Layer in Nuclear Waste Repository System: A Preliminary Study

Azlan Shah Nerwan Shah@Nintin
Industrial Technology Division, Malaysian Nuclear Agency
43000 Kajang, Selangor
azlanshah@nm.gov.my

Abstract

The establishment of a repository with minimum risk of hazards, specifically in regards to human well-being, environmental safety and cost implications is a significant concern associated with nuclear waste. Expansive clay has distinct characteristics that are readily available in the environment and can serve as a natural barrier (sealing system) against the migration of radioactive and chemical pollutants. This article focuses on the assessment of the physico-chemical properties, mineral composition, microstructure, and dispersion behavior of tropical expansive clays.

Keywords: dispersion, radioactive waste, tropical expams

1 Introduction

Generally, expansive clay soil is composed of relatively fine particles (<0.002 mm) that are susceptible to volumetric changes (swelling-shrinking) that are directly related to changes in water content, with an abundance of expanding clay minerals such as montmorillonite and vermiculite (Kumari and Mohan, 2021). This characteristic poses a significant risk to many civil engineering buildings, leading to damage. Nevertheless, these unique attributes possess the capacity to function as a natural barrier (sealing system) against the migration of radioactive and chemical pollutants, notably within a nuclear waste storage system. Hence, this study aims to investigate the physicochemical and microstructural features of clay minerals and the possibility of these clays as natural sealing in nuclear waste repository systems, particularly for future near-to-intermediate type repositories.

2 Methods

Two (2) samples of disturbed tropical clayey soil were collected for this study in Sabah, Malaysia. The physicochemical characteristics of the soils were assessed using the following tests according to the specific standards: soil specific gravity (SG), pH test, particle size distribution analysis (PSD), Atterberg limit/Consistency test (plastic limit (PL), liquid limit test (LL), and plasticity index (PI)), clay activity (A), linear shrinkage test (Ls), free swelling index (FSI), sodium adsorption ratio (SAR) and exchangeable sodium percentage (ESP). By analyzing the microstructure morphology of clay minerals using Field Emission Scanning Electron Microscopy (FESEM) analysis and X-Ray Diffraction Analysis (XRD) with the DIFFRAC.EVA software, the type of clay mineral composition is identified.

Based on the water flow rate (mL/s), effluent turbidity level, and diameter of the drilled specimen hole (mm), a pinhole dispersion analysis (a cylindrical shape with a diameter of 32 mm and a length of 38 mm) in accordance with ASTM D4647/4647M-13 can be used to assess the degree of dispersion of clayey soil according to the degree of dispersion, the analysis indicators range from dispersive (D1) (high erodibility) to non-dispersive (ND1) (resistance to erosion).

3 Results

Table 1 displays the index properties of samples of clayey soil. In comparison to montmorillonite, vermiculite clay soil has higher LL, PL, and PI values and demonstrates higher soil consistency (LL>50%; PI>30%). However, montmorillonite clay exhibits greater clay activity than vermiculite, as determined by the ratio of PI and clay fraction, revealing the soil's swelling potential when reacting with water; the higher the value of A (Clay Activity), the greater the swelling potential, which supported by the FSI value. Montmorillonite exhibit greater values of SAR > 13 and ESP > 20, compared to vermiculite (SAR<1; ESP<5).

Table 1: Index properties of tropical expansive clay soil.

Index Properties		Montmorillonite Soil	Vermiculite Soil
Gs		2.60	2.45
pH Value		8.50	7.20
PSD	Sand (%)	70	56.8
	Silt (%)	8	1.2
	Clay (%)	22	42
PL(%)		35.04	51.97
LL(%)		79.60	97.50
PI(%)		44.56	45.53
A		2.03, Active	1.08, Normal
FSI(%)		95	80
Ls(%)		26	30
SAR		18.1	0.5
ESP(%)		26.3	1.5
Soil Classification		Clayey Sand	Clay

Figure 1 depicts the results of XRD and FESEM analyses of soil. In accordance with the data, quartz (silica), montmorillonite, albite, and kaolinite predominate in montmorillonite clay soil. In contrast, vermiculite clay soil is dominated by vermiculite clay minerals and contains a negligible amount of quartz. At 30k magnification, FESEM analysis reveals that the microstructure of clay is predominantly composed of layered or stacked microaggregates formed by agglomeration of flaky morphology. Compared to montmorillonite, vermiculite clay has a notably flaky morphology and a porous structure.

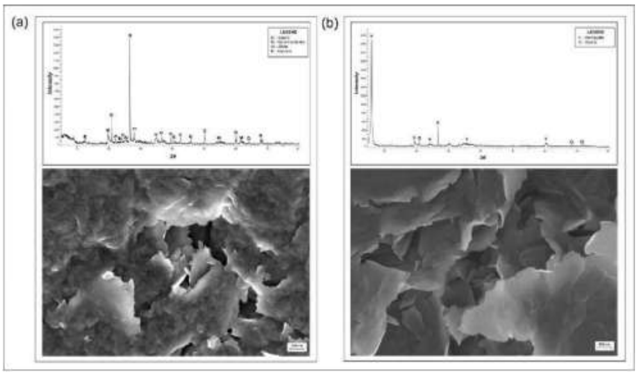

Figure 1: The figure illustrated XRD and FESEM analysis of soil samples: a) Montmorillonite soil sample; and b) Vermiculite soil sample

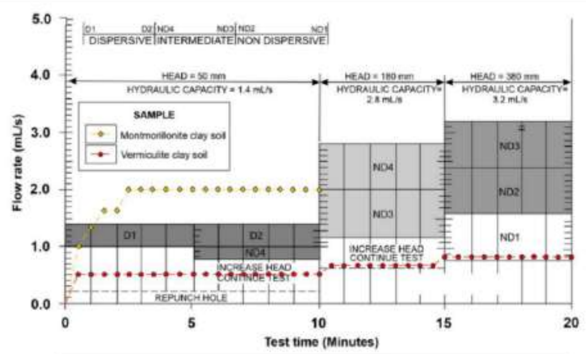

Pinhole dispersion analysis					
Soil sample	*Test duration (min)*	*Final hydraulic head (mm)*	*Effluent flow rate (mL/s)*	*Hole diameter (mm)*	*Soil dispersion level*
Montmorillonite	10	50	>2.00	>2	D1
Vermiculite	20	380	<0.80	<1.5	ND1

Figure 2: Pinhole dispersion analysis of soil samples.

Figure 2 represents the results of a pinhole dispersion test for analyzing soil dispersion. The size of the specimen hole is directly proportional to the effluent flow rate vs the duration of the test, with a greater erosion rate resulting from a higher effluent flow rate. The montmorillonite clay soil samples were classified as dispersive (high erodibility) (D1) with a final specimen hole size greater than 2 mm and a final effluent flow rate greater than 2.0 mL/s. Vermiculite clay soil is classified as non-dispersive (ND1) when the effluent flowing out of the specimen hole is completely clear and the change in diameter of the final specimen hole is 1.5 mm at a hydraulic height of 380 mm with a final effluent flow rate of 0.80 mL/s after 20 minutes.

4 Discussion

Theoretically, montmorillonite and vermiculite are classified as 2:1 crystalline structure, consisting two silica tetrahedral sheets and a central alumina octahedral layer. These characteristics, which include robust mechanical and chemical stability, high porosity, large surface area, high ion exchange capacity, high plasticity, and high porosity, can be considered when assessing the soil's, the suitability for natural sealing in nuclear waste repository systems. However, due to its ability to disperse when reacting with water via reaction with monovalent cations (Na+), a Montmorillonite clay soil sample exhibited more extreme erodibility properties compared to vermiculite. The presence of higher Na+ ions is likely due to the presence of albite mineral (Na-plagioclaserich mineral) (Shah et al., 2022). The erosive nature of dispersive soil makes it a significant role in increasing the instability of foundations or slopes. This erosion can occur either as internal erosion or pipe erosion, typically induced by soil cracking that occurred under hot climatic conditions.

5 Conclusion and Way Forward

In conclusion, expansive clay dominated by montmorillonite and vermiculite have the potential to be utilized as a natural sealing in repository system due to their unique properties. However, montmorillonite clay tends to disperse when it reacts with water, resulting in severe erosion (tunnel/internal erosion), as opposed to vermiculite clay soil, which is resistant to erosion. Further research on the chemical (radionuclide adsorption capacity), geo-mechanical (maximum swelling pressure), and laboratory (self-healing ability from surface cracking due to desiccation) factors, emphasizing soil adaptability to tropical climates that are wet and humid annually is suggested to obtain more comprehensive data on the soil's suitability for a future national radioactive waste repository in Malaysia. This research can be broadened to assess the dispersion phenomena in soil related to landslide mechanisms and the possibility of non-erosive soil to disperse as a result of continuous injection of salt reagents in rare earth elements (REEs) mining areas.

References

ASTM D4647/D4647M-13. 2020. Standard test methods for identification and classification of dispersive clay soils by the pinhole test. *West Conshohocken, PA: ASTM International*.

N. Kumari and C. Mohan. 2021. Basics of clay minerals and their characteristic properties. *Clay and Clay Minerals*, IntechOpen Book Chapter:1–29, https://doi.org/10.5772/intechopen.97672.

A.S.N. Shah, N.S.M. Nazer, and M.I. Harris. 2022. Morfologi hakisan dan sifat serakan lempung kaolinit dan montmorilonit di kawasan tropika. *Sains Malaysiana*, 51(12):3879–3896.

Individual Research Contribution Review, 2023, 1(1): 177–178

Electrocatalytic and Photocatalytic Assessment of Metal-Oxide Nanoparticles through Hydrogen Evolution Reaction Electrochemical Test

Choo Thye Foo
Industrial Technology Division, Malaysian Nuclear Agency
43000 Kajang, Selangor
ctfoo@nm.gov.my

Abstract

This study focuses on utilizing the hydrogen evolution reaction (HER) electrochemical test to assess the electrocatalytic and photocatalytic properties of metal-oxide nanoparticles, with a particular emphasis on elucidating their overpotential values within the context of HER. The objective of this study is to develop a straightforward and precise technique capable of concurrently evaluating both the electrocatalytic and photocatalytic characteristics of metal-oxide nanoparticles.

Keywords: Electrocatalytic, Photocatalytic, Assessment Nanoparticles.

1 Introduction

Assessing the catalytic capabilities of metal-oxide nanoparticles commonly involves evaluating their electrocatalytic and photocatalytic performance. This entails determining the catalytic characteristics of the nanoparticles both under light source irradiation and in the presence of an electrical potential. Degradation of organic dyes is a widely used method to evaluate the photocatalytic activity of metaloxide nanoparticles. In this approach, metal-oxide nanoparticles are introduced to a solution containing an organic dye, and their capacity to decompose the dye under UV or visible light exposure is tracked and quantified through spectrophotometric analysis. It's important to note, though, that this technique is specifically designed for assessing photocatalytic activity and is unable to evaluate the electrocatalytic performance of metal-oxide nanoparticles. Hence, a straightforward and precise technique capable of simultaneously evaluating both the electrocatalytic and photocatalytic characteristics of metal-oxide nanoparticles need to be developed.

2 Methods

ZnO nanoparticles prepared through different calcination temperatures of 500°C, 600°C, 700°C, and 800°C were employed in this investigation. To assess the electrocatalytic activity of these ZnO samples, linear sweep voltammetry (LSV) was conducted at the potential corresponding to the onset of the hydrogen evolution reaction (HER). The electrochemical analysis was carried out using a potentiostat (PCI4/300, Gamry Instruments) that was controlled by the Gamry Framework data acquisition software (version 6.33). The potentiostat was configured as a three-electrode system, with a rotating disk electrode as the working electrode, an Ag/AgCl reference electrode, and a platinum counter electrode. A N2-saturated 0.5 M Na_2SO_4 solution served as the electrolyte. These measurements were conducted at room temperature, and the LSV scan rate was set at 5 mV/s. The working electrode was prepared by blending 4 mg of ZnO powders with a solution comprising 225 μL of isopropyl alcohol, 225 μL of ultrapure water, and 50 μL of Nafion in a plastic vial. This solution was sonicated for 30 minutes, after which 3 μL of the mixture was evenly applied and dried onto a rotating disk electrode with a glassy carbon surface area of 0.1963 cm^2. Furthermore, to evaluate the photocatalytic activity of the synthesized ZnO, the difference in HER overpotentials of ZnO under standard room lighting conditions and with additional UV light irradiation was measured. A UV sterilizer lamp (5 W, UV-C) was used as the source of UV light. Commercial ZnO powder (Fluka) was also tested under the same conditions for comparison.

3 Results

In Figure 1, polarization curves obtained through linear sweep voltammetry (LSV) for both synthesized and commercial ZnO in a N_2-saturated 0.5 M Na_2SO_4 solution at 25°C are displayed. These curves reveal that ZnO synthesized at 500°C, 600°C, and 700°C exhibit lower overpotentials compared to ZnO synthesized at 800°C and the commercial ZnO. Specifically, ZnO synthesized at 500°C, 600°C, and 700°C achieved a current density of -10 mA/cm^2 at a potential of -1.18 V, while ZnO synthesized at 800°C and the commercial ZnO required higher overpotentials of -1.22 V and -1.21 V, respectively. A similar trend was observed at current density of -30 mA/cm^2. These results indicate that ZnO synthesized at temperatures of 500°C, 600°C, and 700°C exhibits superior electrocatalytic activity in the HER. Lower overpotentials signify lower energy requirements for initiating the HER and producing hydrogen gas. This enhanced electrocatalytic activity can be attributed to the small particle sizes of the synthesized ZnO. Smaller ZnO particles offer numerous advantages for electrocatalytic activity, including increased surface area, improved accessibility of active sites, and faster charge transfer kinetics, all contributing to improved catalytic performance.

The photocatalytic activities of both the synthesized and commercial ZnO samples were also assessed. The HER overpotentials were measured for the synthesized ZnO under normal room lighting conditions and with additional UV light irradiation. All the ZnO samples showed a decrease in

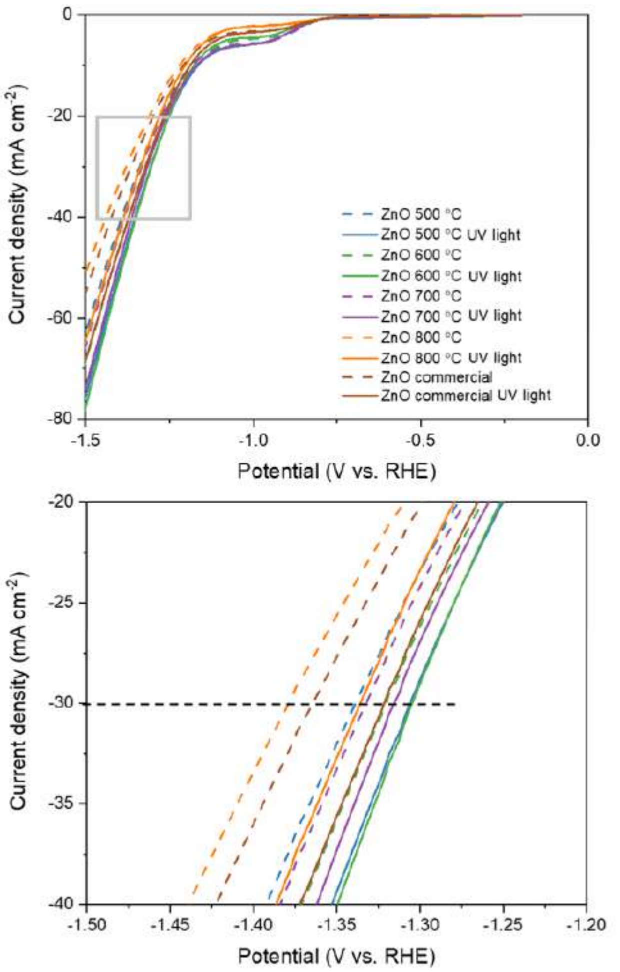

Figure 1: The upper figure displays a comparison of HER polarization curves between the synthesized ZnO and commercial ZnO in a 0.5 M Na_2SO_4 solution. In the lower figure, an enlarged view of the region highlighted by the gray square in the upper figure. Dotted lines correspond to LSV tests conducted under standard conditions, while solid lines represent LSV tests carried out under the influence of additional UV light irradiation.

HER overpotential under UV light irradiation. This reduction is attributed to the generation of photoexcited charge carriers (electrons and holes) when ZnO is exposed to UV light. These charge carriers actively participate in electrochemical reactions, leading to a decrease in the overpotential required for the HER. The differences in HER overpotentials under normal room lighting conditions and with additional UV light irradiation, highlighting variations in photocatalytic activity among different ZnO samples. Notably, at a current density of -10 mA/cm^2, the ZnO synthesized at 800°C and the commercial ZnO exhibit higher differences in HER overpotentials of 0.02 V and 0.04 V, respectively, compared to 0.01 V for ZnO synthesized at temperatures of 500°C, 600°C, and 700°C. At a higher current density of -30 mA/cm^2, the differences in HER overpotentials become more pronounced, with the ZnO synthesized at 800°C and the commercial ZnO displaying even greater variations, suggesting higher photocatalytic activity.

4 Discussion

The obtained results align with recent research. In a study by S.H. Ferreira (Ferreira, 2021b), different ZnO samples were calcined at various temperatures (300, 500, and 700°C). This research revealed that ZnO calcined at the highest temperature (700°C) exhibited the most significant photocatalytic activity when degrading rhodamine B under UV light irradiation. The authors attributed this enhanced photocatalytic activity to the material's high crystallinity and the resulting low concentration ratio of bulk to surface defects. Similarly, another investigation by N.S. Ferreira (Ferreira, 2021a) showcased superior photocatalytic performance in the degradation of methylene blue dye for samples calcined at a high temperature (700°C). Conversely, ZnO samples synthesized at temperatures of 500°C, 600°C, and 700°C demonstrated increased electrocatalytic activity in the hydrogen evolution reaction (HER). This was attributed to the presence of nanosized ZnO particles, which offer a substantial surface area, enhanced accessibility to active sites, and rapid charge transfer kinetics.

5 Conclusion

The hydrogen evolution reaction (HER) electrochemical technique proves to be a valuable approach for the simultaneous and precise assessment of both the electrocatalytic and photocatalytic properties of metal-oxide nanoparticles. It serves as a favorable alternative when compared to the organic dye degradation technique.

References

N.S Ferreira. 2021a. Visible-light-responsive photocatalytic activity significantly enhanced by active [VZn+VO$^+$] defects in self-assembled ZnO nanoparticles. *Inorganic Chemistry*, 60:4475–4496.

S.H Ferreira. 2021b. High UV and sunlight photocatalytic performance of porous ZnO nanostructures synthesized by a facile and fast microwave hydrothermal method. *Materials (Basel).*, 14:2385.

Individual Research Contribution Review, 2023, 1(1): 179–180

Elemental Characterization Analysis of Thorium Extracted from Local Monazite

Cik Rohaida Che Hak
Industrial Technology Division, Malaysian Nuclear Agency
43000 Kajang, Selangor
rohaida@nm.gov.my

Abstract

There is growing interest in REE and Th extraction from monazite minerals. Both materials are widely used in many industries such as automotive, electronics, energy, and other manufacturing industries. REE and Th extraction processes involved with complex processing routes and require variety of chemicals. One of the challenges in this R&D work is to determine the presence of Th, U and REE at each processing step due to its similarities of chemical composition and physical properties. The aim of this paper is to use several X-ray characterization techniques to identify elemental composition obtained at each processing route. Results show that the final product contains 85wt% of ThO_2 in thorianite phase and has nano rod morphology.

Keywords: Malaysia Monazite, Alkali Digestion, Characterization, X-ray Analysis

1 Introduction

In Malaysia, monazite mineral is obtained from tin mining byproducts called ‘amang’ that underwent various stages of mechanical and physical separation. In our previous study, Malaysian monazite mineral (obtained from Perak) was determined as (Ce, Nd, La, Gd)-PO_4 minerals contained about 28wt% Cerium (Ce), 14wt% phosphorus (P), 13.4wt% lanthanum (La), 8.2wt% neodymium (Nd), 3wt% of other REE such as gadolinium (Gd), samarium (Sm), praseydium (Pr) and dysprosium (Dy), 7 wt% Th, 0.2 wt% U and the rest are metal element at lower concentration (Hak et al., 2020). Th or REE can be extracted from monazite via 4 main steps: digestion, separation, extraction, and purification. In general, digestion can be done either through acid or alkaline route. Although acid leaching is proved to have high extraction efficiency of Th or REE, however the use of acids is well known to results in bad environmental effect and loss of phosphate as H_3PO_4, low solubility if the sulphates formed, high-cost maintenance and poor separation of Th and REEs (Kumari et al., 2015). In this work, we report the extraction of Th from Malaysian monazite using alkaline digestion technique with caustic soda. The objective of this paper is to characterize the Th extracted from Malaysian monazite (Hak et al., 2022).

2 Experimental Methods

In this study, monazite was first ground using industrial milling to reduce its particle size and was labelled as GM. The GM underwent digestion with sodium hydroxide (NaOH) at a defined temperature and time. The obtained slurry was then leached and filtered to separate the insoluble hydroxide cake (labeled as iHC1) with soluble phosphate. The iHC1 underwent hydrochloric acid (HCl) dissolution and filtration to separate the insoluble hydroxide cake 2 (labeled as iHC2) and soluble RECl solution. The iHC2 underwent HCl dissolution and filtration to separate the soluble thorium chloride solution (TCS) and insoluble waste. The TCS underwent several acid dissolutions for extraction of Th, followed by filtration process. This extraction process was repeated to purify the Th. Finally the Th solution was added with acid oxalic to precipitate it to thorium oxalate (labeled as ThOx). The ThOx was then calcined at temperature above 900 °C to form thorium oxide (ThO_2). To study the extraction of Th from monazite, the elemental analysis using WDXRF, XRD and EDX was done on GM, RECl, ThOx and ThO_2 samples.

3 Discussion and Conclusions

3.1 Th and REE extraction

Table 1 shows the elemental composition obtained from WDXRF analysis on the GM, RECl, ThOx and ThO_2 samples. There is a tremendous increase of Th content from 3.66wt% in GM up to 73.4wt% in the final product ThO_2. Meanwhile, the content of light REE (LREE) decreases from 64.82wt% in GM to 4 wt% for sample ThO_2. The major elements of LREE in GM and RECl are Ce, Nd, and La. These results show that alkaline digestion was successful to separate REE and Th from monazite. The acid dissolutions process show Th can be extracted out and purified. There is also a great decrease of P content from 23.14 wt% in GM to 0.17wt% in ThOX. This indicate that the P was completely solubilized after HCl dissolution.

Table 1: Element composition analysis of 4 samples using WDXRF.

Sample	Element composition(wt%)					
	Na	O	P	LREE	HREE	Th
GM	-	-	23.14	64.82	2.17	3.66
ReCl	-	22.6	5.63	53.02	4.79	7.26
ThOx	0.09	16.21	0.17	19	2.2	58.11
ThO_2	-	13.91	0.13	4.19	5.34	73.47

3.2 Determination of ThO_2

ThO_2 was formed after the ThOx underwent sintering at above 900°C. The formation of ThO_2 was investigated by using WDXRF, XRD and EDX. Graph in Figure 1(a) shows WDXRF data of ThO_2 amount increases tremendously from 6.65 wt% in GM to 66.12 wt% in ThOx and 85.53 wt% in ThO_2. This increment is accompanying with the significant decrease of all major RE oxides as compared to GM. Figure 1(b) shows the EDX spectrum indicating that Th is the major element with concentration of about 68.3 wt%, followed by heavy REE (HREE) such as yttrium, gadolinium and dysprosium, at concentration between from 1 to 5wt % and also P is detected at less than 1 wt%. This data corresponds to the one obtained from WDXRF analysis. Figure 1(c) shows the XRD spectrum of the ThO_2, with the energy peaks are detected at 27.86°, 31.99°, 57.29° and 76.56°, match with the thorianite phase (ICDD-98-006-3060). These results confirmed that the powder obtained after sintering of ThOx is thorium oxide (ThO_2).

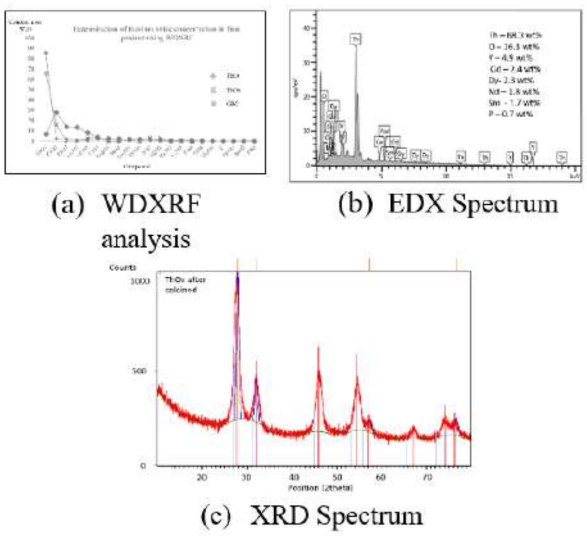

Figure 1: (a) Purity of ThO_2 in comparison with Th compound in GM, and ThOx; (b) EDX spectrum for ThO_2; (c) XRD spectrum of ThO_2

4 Conclusion

Four stages of chemical processing have been used to extract ThO_2 from monazite. The first and second stages are for removal of phosphorus and RECl that contained REE. Whereas third until fourth stages are for Th extraction. WDXRF, XRD and EDX analytical techniques confirmed the formation of ThO_2 after calcination of ThOx.

References

Cik Rohaida Che Hak, Sarimah Mahat, Ismail Mustapha, and M.S. Susan. 2020. Quantification of thorium and rare earth elements in Perak's ex-mining monazite. *Jurnal Sains Nuklear Malaysia*, 32(1):10–19.

Cik Rohaida Che Hak, Zakiuddin Januri, Ismail Mustapha, and Sarimah Mahat. 2022. Extraction of Thorium Oxide (ThO_2) from Malaysian Monazite through alkali digestion: Physical and chemical characterization using x-ray analysis. *Key Engineering Materials*, 908.

Archana Kumari, Rekha Panda, Manis Kumar Jha, J. Rajesh Kumar, and Jin Young Lee. 2015. Process development to recover rare earth metals from monazite mineral: a review. *Miner. Eng.*, 79:102 – 115.

Individual Research Contribution Review, 2023, 1(1): 181–182

Polymer Nanocomposites Functionalised with Nanocrystals of Zeolitic Imidazolate Frameworks as Ethylene Control Agents

E. M. Mahdi
Industrial Technology Division, Malaysian Nuclear Agency
43000 Kajang, Selangor
mahdiezwan@nm.gov.my

Abstract

This paper focuses on the potential applications of nanocomposites of metal-organic frameworks (ZIFs). ZIFs, characterized by their exceptional porosity and structural versatility, are posited as highly effective in gas separation processes, particularly in separating carbon dioxide (CO_2) and methane (CH_4) and ethylene (C_2H_4). However, its fragile nature necessitates the formation of MOF-composites to make it viable for more rigorous application. This paper discusses an innovative application of MOF-composites (ZIFs and Matrimid and Polyurethane) in the agricultural sector, specifically in enhancing the ripening and storage processes of fruits. This dual focus indicates the paper's exploration of both environmental and agricultural implications of ZIFs.

1 Introduction

The growing necessity for efficient gas separation methods is imperative in today's increasingly globalized supply chain. This need is underscored by the global challenges of environmental pollution and the search for sustainable energy solutions. The paper critiques the limitations of conventional gas separation materials, such as their lower efficiency and limited range of applications. MOFs are introduced as a groundbreaking alternative, with a focus on their unique structural properties, including high surface areas and customizable pore sizes. These characteristics are presented as the key to MOFs' potential in gas separation, offering a solution to the limitations of traditional materials. The introduction sets the stage for a detailed exploration of MOFs, positioning them as a significant advancement in material science with wide-ranging applications, while also highlighting that MOFs are not standalone components, and must be deployed in the form of composites in order to safeguard its structural fragility. ZIFs have proven themselves to be highly viable for separation of CO_2 and CH_4, while the composites formed using ZIFs and Matrimid and Polyurethane has been reported elsewhere, and thus utilized for this work.

2 Materials and Methods

The ZIFs and ZIF composites were prepared using methods discussed in a previous research. The samples were then characterized using thermo-mechanical methods, such as DMA, TGA, and DSC, and also mechanical characterization techniques such as stress-strain tests and nanoindentation. These samples were then used for the adsorption experiments using a specially prepared BET apparatus, modified to use CO_2, and CH_4, C_2H_4, and N_2 gases. The results of the characterization methods and also adsorption tests were collated and compared, and the correlation between thermo-mechanical properties and gas sorption properties were determined using the available data.

3 Results and Discussions

The results indicate that ZIFs and ZIF-composites exhibit superior performance in separating CO_2 and CH_2, surpassing traditional materials. The data suggest that this efficiency is due to the ZIFs' high porosity and the ability to tailor their pore structures for specific gases. The adsorption of C_2H_4 and its retention within the internal structure of the polyurethane and Matrimid based ZIF composites offer an interesting perspective, which render these composites suitable for passive controlled release of trapped gases.

The transport of fruits and other produce throughout the global supply chain relies on the use of ethylene (C_2H_4) for ripening in transit. This process relies on the active use of gases and gas canister, which is rather energy intensive. The ability of these ZIF-composites to retain and release trapped ethylene gases via subtle manipulation of pressure and temperature, per the data collected from the adsorption of gases of the modified BET apparatus, confirms a viable alternative to a passive and energy efficient approach towards produce ripening; via fluctuating pressure and temperature, controlled amounts of ethylene will be released and come into contact with the produce, thus instigating the ripening process. This approach eliminates the need for the gas canisters and an intricate gas system to deliver ethylene to the produce.

The discussion also addresses potential limitations and areas for future research. While ZIFs show great promise, there are challenges related to their stability and scalability that need addressing for widespread commercial adoption. The section concludes by reflecting on the broader implications of ZIFs in environmental and energy sectors, emphasizing their transformative potential.

4 Conclusion

This paper synthesizes its findings, reaffirming the significant potential of ZIFs in both gas separation and agricultural applications. The authors reiterate the advantages of ZIFs over traditional materials, particularly in terms of efficiency and the possibility of targeted customization. The conclusion also

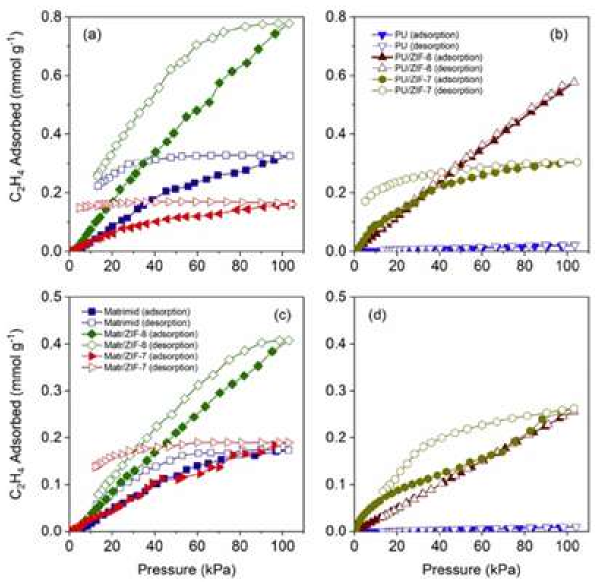

Figure 1: Adsorption plots of ZIF-composites

points to future research directions, emphasizing the need to enhance MOF stability for practical applications. It highlights the potential for MOFs to contribute significantly to environmental protection and sustainable energy solutions, aligning with global efforts to address climate change and energy efficiency.

The paper ends by considering the long-term implications of ZIFs in various industries, suggesting that their unique properties could lead to breakthroughs in material science and technology. The authors express optimism about ZIFs role in addressing critical global challenges, positioning them as a key material in the pursuit of sustainable and innovative solutions.

Overall, the paper presents a thorough and compelling examination of ZIFs, detailing their properties, applications, and potential for future development. It offers a comprehensive perspective on ZIFs, not just as a scientific curiosity but as a material with significant practical implications across various sectors. The paper contributes to the broader understanding of ZIFs, paving the way for further research and development in this exciting field.

References

E.M. Mahdi and J.C. Tan. 2016a. Dynamic molecular interactions between polyurethane and ZIF-8 in a polymer-MOF nanocomposite: microstructural, thermo- mechanical and viscoelastic effects. *Polymer*, (97):31–43.

E.M. Mahdi and J.C. Tan. 2016b. Mixed-matrix membranes of zeolitic imidazolate framework (ZIF-8)/Matrimid nanocomposite: thermo-mechanical stability and viscoelasticity underpinning membrane separation performance. *J. Membr. Sci.*, (498):276–290.

Individual Research Contribution Review, 2023, 1(1): 183–184

Structure-Property Relationship as Revealed by Small and Wide Angle X-ray Scattering Technique (SWAX)

Hafizal Yazid
Industrial Technology Division, Malaysian Nuclear Agency
43000 Kajang, Selangor
hafizal@nm.gov.my

Abstract

We have demonstrated the significant use of the Small and Wide Angle X-ray Scattering (SWAX) technique in elucidating the structure-property relationship of materials. Advantages of a direct technique in reciprocal space include average measurement, characterization in the native state of the sample, ease of sample preparation, and fast results. The end of 2016 marked the beginning of the operation of the instrument at the Malaysian Nuclear Agency. The instrument resolution is 0.035 nm^{-1}, known as q min. Biological and solid-state samples were illustrated as examples. The success of the technique was dictated by its capability to correlate the structure and the properties of the studied materials.

Keywords: SWAX, structure-property relationship, native state.

1 Introduction

Materials scientists employ analytical (as opposed to spectroscopic) methods called Small-Angle Xray Scattering (SAXS) and Wide-Angle X-ray Scattering (WAXS) to examine the structure of materials at the atomic and nanoscales, respectively. In both cases, a sample scatters X-rays, and the resulting scattering patterns reveal important details about the material's atom or molecular structure.

The primary use of SAXS is the investigation of nanoscale structures. Because of the material's density variations, X-rays interact with the sample and scatter at small angles (usually 0.1 to 10 degrees). The diffraction pattern formed by the dispersed X-rays provides details about the dimensions, composition, and arrangement of the sample's nanoscale structures. Numerous soft and hard materials, such as polymers, colloids, biological macromolecules, nanoparticles, and more, are studied extensively using SAXS. It aids in the understanding of a material's nanostructure by giving details on the distribution, size, and form of its particles. Specialised X-ray scattering equipment is used in SAXS experiments. The sample is usually in a solid, liquid, paste or powder state, and measurements are taken over a range of scattering angles to generate a scattering profile.

Unlike SAXS, WAXS is more concerned with larger scattering angles, usually greater than 10 degrees. The X-rays' interaction with the sample's crystal lattice produces diffraction patterns that provide details about the material's atomic structure. Studying crystalline materials, such as metals, ceramics, and some biological crystals, is where WAXS is especially helpful. It offers comprehensive details regarding the arrangement of atoms within the crystal lattice, crystal flaws, and crystal symmetry. X-ray scattering devices are also used in WAXS studies, frequently in tandem with SAXS. The crystallographic structure of the material can be ascertained by analysing the diffraction pattern produced by a crystalline sample of WAXS. In certain investigations, the same sample is subjected to both SAXS and WAXS in order to fully comprehend its structure. The combination gives scientists the ability to look at both atomic- and nanoscale aspects, giving them a more full understanding of the material's characteristics.

2 Methods

The samples were characterised using a point collimation SAXS instrument from Anton Paar. The X-ray source was Ni-filtered $CuK\alpha$ radiation with a wavelength of 0.154nm. The instrument was operated at 50 kV and 1 mA, coupled with an Eiger CMOS 2-D detector. The scattering vector q covered from 0.035 to 5nm^{-1}. All measurements were corrected for sample thickness, transmission, and background scattering.

Table 1: Samples

No.	**Sample**
1	Human hair (D1 & D curly)
2	Nanocomposite (B_4C in polymer blend)
3	Graphene powder

3 Results

Figure 1 shows the result of hair samples. Three peaks are observed for D1 & D curly, at q = 0.72, 0.96 and 1.36 nm^{-1}. In the case of hair sample, these three peaks might correspond to lattice parameter, axial stagger and lipid layer distance respectively (Yazid and Takirin, 2022).

For nanocomposite samples, B_4C fillers were found not to form agglomeration in the composite samples as indicated by the radius of the gyration result (Table 2)(Yazid et al., 2022).

Figure 2 shows the aluminium wire composite resistance. The values were highly correlated to graphene thickness (obtained by SAXS) (Yazid et al., 2023).

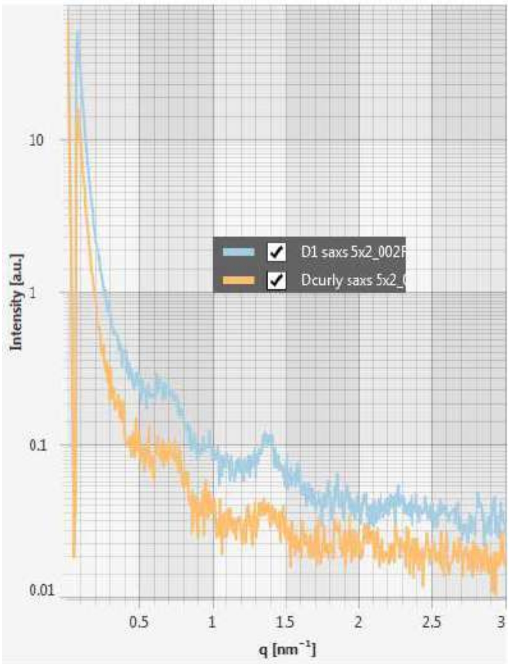

Figure 1: 1D scattering profile of D1 & D curly after normalization of beam intensity (SAXS).

Table 2: Radius of Gyration of Fillers

Samples	Radius of Gyration, R_t (nm)
Nanocomposite 2	4.7 ± 0.2
Nanocomposite 4	4.5 ± 0.2
Nanocomposite 6	4.8 ± 0.2
Nanocomposite 8	4.6 ± 0.2
Nanocomposite 10	4.9 ± 0.1

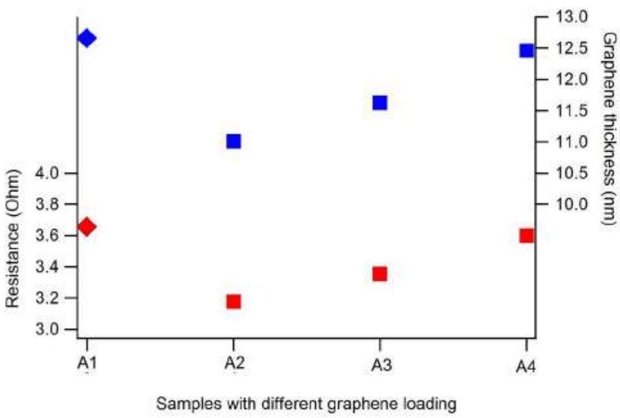

Figure 2: Resistance and graphene thickness relationship.

4 Conclusion

In conclusion, SAXS and WAXS are complimentary methods that are essential for characterising a variety of materials and providing information on their structural characteristics across a range of length scales.

References

Hafizal Yazid and Ummi Amimah Takirin. 2022. Small and wide angle x-ray scattering of hair samples. *NUKLEAR-MALAYSIA/L/2022/112(S)*.

Hafizal Yazid, Umar A. Anwar, A. Siti Zaubidah, M. Nurulizzati, Maria Sabtu, M. Julie Andrianny, M.Z. Nurazila, M. Rawi M. Zin, R.S. Chen, and Sahrim Ahmad. 2022. A combined method to probe the behaviour of the filler in polymer blend nanocomposites via x-ray diffraction and thermal measurement. *Nano-Structures Nano-Objects*, 32(100906).

Hafizal Yazid, Ummi Tamimah Takirin, and Azlan Shah Nerwah Shah. 2023. I-V measurement characteristic of graphene in aluminium tape. *NUKLEAR-MALAYSIA/L/2023/29(S)*.

Individual Research Contribution Review, 2023, 1(1): 185–186

Simulating Point-Source Detection through Varied Geometrical Arrangements for iSPECT System

Hanafi Ithnin
Industrial Technology Division, Malaysian Nuclear Agency
43000 Kajang, Selangor
hanafi_i@nm.gov.my

Abstract

Single Photon Emission Computed Tomography (SPECT) has demonstrated its reliability in imaging radiotracer distribution within opaque systems. Given the limited availability of detection tools, this study involves an assessment and comparison of different detection arrangements for the development of an industrial SPECT system (iSPECT) suitable for imaging in industrial conditions. Hexagonal, octagonal, and nonagonal iSPECT arrangements were modeled and simulated using the MCNPX code. The reconstructed images for a single point source are evaluated and compared across all three systems. The results indicate that, among the three iSPECT arrangements, the nonagonal system exhibits the best image resolution and the ability to detect the position of single-point sources within the region of interest.

Keywords: Industrial SPECT, Point-source Imaging, MCNPX Simulation

1 Introduction

Numerous studies have explored the potential application of SPECT systems in addressing industrial challenges. Legoupil et al. (Legoupil et al., 1997) conducted pioneering work in this area, developing an experimental SPECT system for dynamic fluid flow analysis. The results were promising, with successful construction of a 2D image depicting radiotracer distribution. Subsequent efforts encompassed the development of various industrial SPECT systems through a combination of experimental work and modeling simulations (Mesquita et al., 2020; Park et al., 2014a; Park et al., 2013). More recent contributions by Park et al. (Park et al., 2014b) involved the creation of an industrial SPECT system featuring a 12-gonal diverging collimator, which was compared to 24-gonal and hexagonal SPECT systems. The findings indicated that the 12-gonal system outperformed the others, offering a detection-efficiency map devoid of edge artifacts, superior image resolution, and accurately reconstructed images providing multi-source information. This underscores the need for tailoring the setup of industrial SPECT systems to the specific problems of interest, considering different numbers of detectors and arrangements of detector arrays.

The current study focuses on modeling and simulating three arrangements of an industrial SPECT system, iSPECT, namely hexagonal, octagonal, and nonagonal systems. The simulation aims to evaluate the accuracy of positional mapping for a single point source within a 20 cm region of interest. In this study, a Cesium-137 gamma-ray source with an energy of 622 keV is employed to simulate the point source.

2 Methods

This study employs the MCNPX code (Pelowitz et al., 2008) to model and simulate the iSPECT system. The code is specifically utilized here to model the iSPECT detectors and the gamma-ray detection. The number of detectors is capped at a maximum of 36 NaI scintillation detectors. The simulations for the iSPECT system involve three distinct arrangements: hexagonal (6x6) - featuring six arrays of six detectors, octagonal (8x4) - incorporating eight arrays of four detectors, and nonagonal (9x4) - comprising nine arrays of four detectors. Figure 1 illustrates the iSPECT model used for this study.

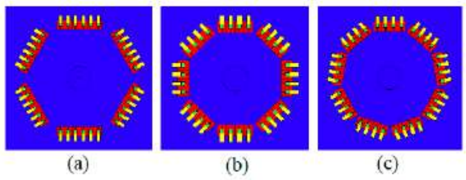

Figure 1: Three different model of iSPECT system used in this study; (a) hexagonal (6x6), (b) octagonal (8x4) and (c) nonagonal (9x4)

2.1 Image Reconstruction and Point-source Simulation

As the number of detectors is limited in each array, this study opts for the iterative reconstruction method to generate a high-resolution image. Specifically, the Maximum Likelihood – Expectation Maximization (ML-EM) method is employed in this study for the reconstruction of the iSPECT image.

For each of the three arrangements, the pixel interval is set as 0.5 cm for 20 cm diameter of a circular region of interest, ROI. Thus, a total of 1245 points source response needed to be calculated, as shown in Figure 2(a). This point-source response is the input for the system matrix, h, in the ML-EM algorithm used for calculating the reconstructed image of radiotracer distribution.

For each of the three iSPECT arrangements, the positional accuracy of a static Cesium Cs-137 point source is assessed by reconstructing images for the source positioned at the center of the Region of Interest (ROI), 5 cm along the radius, and at 10 cm, which is at the edge of the ROI (depicted by the

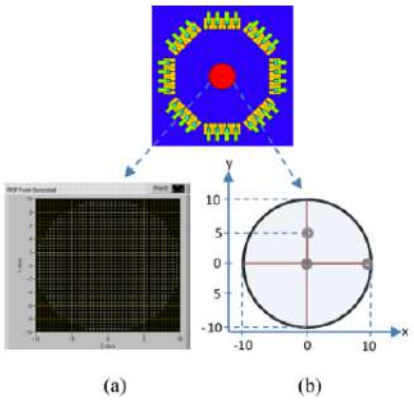

Figure 2: (a) 1245-point-source response generated inside ROI and (b) Different static point-source placement for positional accuracy detection.

grey circle in Figure 2b). All image reconstruction processes utilize ML-EM software developed in LabVIEW.

3 Results

3.1 Point-source Image

Figure 3 illustrates the outcomes of nine reconstructed images resulting from three distinct configurations of the iSPECT system and three different placements of a static point source. The three rows of horizontal images depict various arrangements of the iSPECT system, specifically showcasing (a) hexagonal, (b) octagonal, and (c) nonagonal structures. Simultaneously, the three vertical images correspond to different point source placements: (i) point source at the origin, (ii) point source positioned 5 cm from the origin, and finally, (iii) point source at 10 cm from the origin, signifying the source at the edge of the Region of Interest (ROI). The green circle serves as a reference for the ROI's circumference with a radius of 10 cm. Brighter pixels indicate a higher probability of locating the origin of gamma radiation or the source, while darker pixels signify the absence of gamma radiation.

The images presented in Figure 3 demonstrate that all three simulated systems can accurately detect a point source at the specified positions. The bright white pixels in the reconstructed images signify the successful detection of the point source position as simulated. The sharper the white pixel, the more precise the point source detection. Conversely, the darker or blue regions surrounding the point source represent noise in these reconstructed images, and fewer blue areas indicate higher-quality reconstructions.

4 Conclusion

Three different arrangements of the iSPECT system were modeled and simulated to assess their capability in mapping static single point-source images. The findings indicate that all three arrangements successfully detect the single point source at the coordinate (0,0), (5,10), and (0,10) inside the ROI. Among the three systems, the reconstructed images of the hexagonal arrangement exhibit less noise. Concurrently, despite the presence of noise, the nonagonal arrangement demonstrates superior overall image resolution compared to the other two systems. Based on these results, it can be concluded that the nonagonal arrangement of the iSPECT system is optimal for imaging a 20 cm ROI for point-source detection. Further studies will explore the detection process with different radiotracer sources and source shapes to enhance the applicability of the iSPECT system in industrial environments.

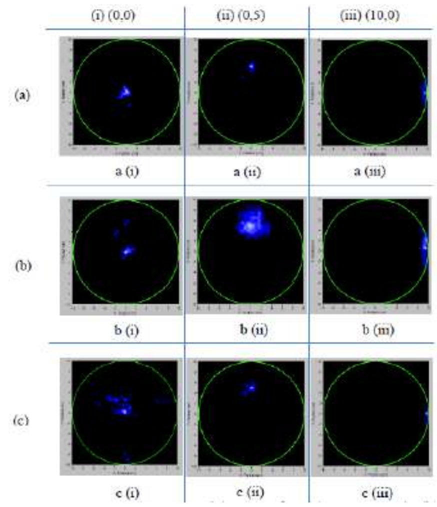

Figure 3: Reconstructed images for (a) Hexagonal, (b) Octagonal and (c) Nonagonal with (i) point-source at origin (0,0), (ii) point-source at 5 cm from origin (0,5) and (iii) point-source at 10 cm from origin (10,0).

References

S. Legoupil, G. Pascal, D. Chambellan, and D. Bloyet. 1997. An experimental single-photon emission computed tomograph method for dynamic 2d fluid flow analysis. *Appl. Radiat. Isot*, 48:1507–1514.

C.H. Mesquita, A.F. Velo, W.P. Calvo, D.V. Carvalho, and M.M. Hamada. 2020. Emission and transmission tomography system applied to analyze industrial process inside chemical reactors. *Nuclear Inst. And Methods in Physics Research*, 954(3):161847.

J.G. Park, C.H. Kim, M.C. Han, S.H. Jung, J.B. Kim, and J. Moon. 2013. Optimization of detection geometry for industrial spect by monte carlo simulations. *Journal of Instrumentation*, 8(4).

G. Park, S.H. Jung, J.B. Kim, J. Moon, Y.S. Yeom, and C.H. Kim. 2014a. Performance evaluation of advanced industrial spect system with diverging collimator. *Applied Radiation and Isotopes*, 94:125–130.

J.G. Park, S.H. Jung, J.B. Kim, J. Moon, M.C. Han, and C.H. Kim. 2014b. Development of advanced industrial spect system with 12-gonal diverging-collimator". *Applied Radiation and Isotopes*, 89:159–166.

D.B. Pelowitz, J.W. Durkee, J.S. Elson, M.L. Fensin, J.S. Hendricks, M.R. James, and R.C. Johns. 2008. Mcnpx user's manual 2.6 extensions. *No. LA-CP-07-1473. Los Alamos National Lab. (LANL), Los Alamos, NM (United States).*

Nuklear Malaysia as a Scientific Hub for Cultural Heritage Characterization and Preservation

Hishamuddin Husain
Industrial Technology Division, Malaysian Nuclear Agency
43000 Kajang, Selangor
hishamuddin@nm.gov.my

Abstract

Malaysian Nuclear Agency (Nuklear Malaysia) has carried out activities involving the study of cultural heritage since the beginning of year 2000. It involves collaboration with the department related to cultural heritage, namely the Department of Museums and Antiquities (JMA). Starting from that, cultural heritage research activities using nuclear science and technology continued to be developed. Several scientific tools were introduced, especially in material characterization. With various studies conducted together as well as knowledge gained through training at home and abroad, the researchers' experience continues to grow. In addition to the existing collaboration with the Department of Museums Malaysia, several other collaborations are also carried out, such as with the Department of National Heritage and Melaka Museums Corporation. This effort is also supported by the Ministry of Science, Technology and Innovation (MOSTI). With the experience, expertise and facilities available, Nuklear Malaysia can be a scientific hub for cultural heritage studies.

Keywords: Cultural heritage, characterization, disinfection and consolidation

1 Introduction

Cultural heritage is a legacy artifact from a community group that is inherited from previous generations, maintained and preserved for future generations. In addition, cultural heritage artifacts can contribute to boosting the country's source of income through the tourism sector.

The application of nuclear science and technology is the most popular method used in characterization and preservation of artifacts. Nuclear technology has great potential, is safe to use, non-destructive, and has proven to be accurate in the preservation and conservation of tangible cultural heritage artifacts. The potential applications of nuclear technology were proven in several major studies, such as authenticity verification, artifact origin investigation, dating, conservation, and restoration.

Therefore, Nuklear Malaysia as a leading agency in the research and development of nuclear technology should play a big role in promoting and advancing the scientific method in cultural heritage study.

2 Scientific Equipment and Facility

The application of scientific equipment can be divided into three major activities. Figure 1, 2 and 3 show the previous activities in collaboration with the Department of Museums Malaysia (JMM) related to the characterization and conservation of the artifacts. These include exploration and excavation, material characterization and conservation, and preservation. Table 1 shows some of the equipment and facilities in Nuklear Malaysia that are used in cultural heritage characterization and preservation.

Figure 1: Characterization and conservation of old cannon

Figure 2: Characterization and conservation of old boat

3 Strength and Advantages

Nuklear Malaysia has established strong links with institutions dealing with the country's cultural heritage. There are several joint projects that have been discussed and put into action. It is an opportunity to take advantage of those particular

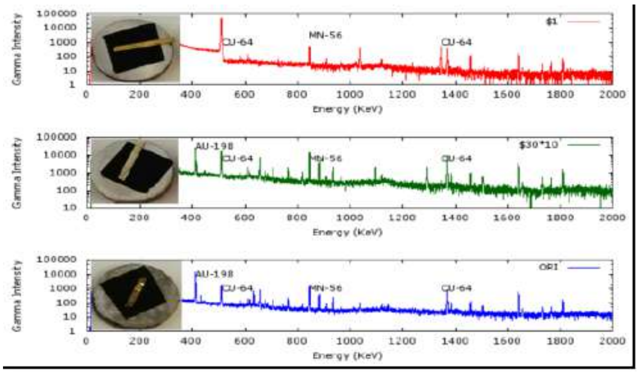

Figure 3: Elemental analysis of old textile using NAA technique

Table 1: Main activities and equipment commonly used in cultural heritage study

Activity	Equipment/Facility
Exploration and excavation	Ground Penetrating Radar (GPR), surveymeter, Gamma spectrometer
Materials characterization	Neutron, X-ray and Gamma Radiography, X-ray Florescence (EDXRF, WDXRF), Scanning Electron Microscope (SEM/EDAX), X-ray Diffraction (XRD), Neutron Activation Analysis (NAA / PGNAA) and other Non-Destructive Techniques (NDT) such as Eddy current and Ultrasonic testing
Dating	Radiocarbon and Thermoluminescence dating laboratory
Preservation	Gamma irradiation for disinfection and consolidation

links to propose and continue the use of nuclear techniques to good effect in the field of characterization that has already been developed. It is also a good approach to promoting nuclear technology to the public through joint outreach programs. Nuklear Malaysia has actively participated in several projects under the IAEA related to cultural heritage. Through the IAEA projects, researchers have the opportunity to acquire knowledge from other member countries, especially on new technology, as well as share our knowledge and technology. Besides having competent and trained researchers, Nuklear Malaysia has a variety of scientific equipment and irradiation facility which would contribute in characterization and preservation of the cultural heritage artifacts.

4 Future Challenges

Nuklear Malaysia as a premier nuclear research institution has a responsibility to expand the application of nuclear techniques in cultural heritage study. At the regional level, most of the neighbouring countries realise the importance of nuclear techniques in the characterization and preservation of artifacts, and some of the countries have started the preservation of artifact using gamma irradiation. Since there is an interest in using the disinfection and consolidation of the artifacts from the institutions dealing with cultural heritage in Malaysia, it is a great opportunity for us to expand our capacity in these areas. There are some countries that have the advanced facilities such as synchrotrons. Through our existing networking, we need to gain knowledge of advanced characterization and analysis to obtain valuable and more accurate data. Most of the available equipment used are getting older and need to be properly maintained or replaced existing old equipment to ensure that its service is not affected. Acquisition of new advanced equipment can enhance research capabilities. In conservation and preservation, there is a lot of room for improvement that needs to be considered. These areas include identification, maintenance, preservation, restoration, reconstruction, adaptation, and interpretation of artifacts. It involves researchers, historians, conservators and scientists.

5 Conclusion

Nuklear Malaysia has great potential to become a scientific hub in cultural heritage characterization and preservation. Besides having competent and trained researchers, Nuklear Malaysia has a variety of scientific equipment and irradiation facility. There are a few things that need to be considered to improve our capability. The available equipment needs to be properly maintained to ensure that the service of the equipment is not affected. The acquisition of equipment with advanced techniques can improve research capabilities. The development of gamma ray irradiation facilities for disinfection and consolidation needs to be developed in order to be a regional hub in cultural heritage preservation.

References

IAEA. 2011. Nuclear techniques for cultural heritage research. *IAEA Radiation Technology*, series no. 2.

Individual Research Contribution Review, 2023, 1(1): 189–190

Eddy Current Thermography for Quantitative Evaluation of Angular Defects

Ilham Mukriz Zainal Abidin
Industrial Technology Division, Malaysian Nuclear Agency
43000 Kajang, Selangor
mukriz@nm.gov.my

Abstract

Eddy current thermography employs a combination of eddy current and thermographic Non-Destructive Testing (NDT) techniques. This work considers the capabilities of eddy current thermography for obtaining quantitative information about cracks set at an angle to the surface. The investigation is implemented by simulating the transient thermal distribution for angular slots, via time-stepping 3D finite element analysis (FEA), with experimental work undertaken for verification. With the identification of the slot angle, quantification of the length/depth of the slot inside the sample can then be made through a maximum temperature amplitude feature. Experimental studies have been undertaken for evaluation of the numerical simulation and transient feature extraction methods.

Keywords: NDT, eddy current thermography, finite element

1 Introduction

Eddy current thermography combines eddy current and thermographic non-destructive testing (NDT) techniques to provide a fast and efficient method for defect detection and characterisation over a relatively wide area. The technique uses induced eddy currents to heat the material being tested (Riegert et al., 2004; Zenzinger et al., 2005; Netzelmann and Walle, 2008; Oswald-Tranta, 2007) and defect detection is based on the changes of the induced eddy current flows revealed by the thermal visualisation captured by an infrared (IR) camera.

In this work, features from the temperature distributions of eddy current thermography investigations were extracted to gain quantitative information about angular slots. FEA multiphysics simulations were carried out for eddy current thermography to provide initial results and analyses of the technique capabilities for 3D defect characterisation. A basic understanding and explanation of the heating mechanism surrounding an angular defect has been made through the multiphysics simulations which provides the platform for a complete defect assessment.

2 Details of the study

Numerical simulations for eddy current and temperature distribution were performed using COMSOL Multiphysics simulation software via the Electro-Thermal module which combines the application mode for induction currents and general heat transfer.

The governing equations introduced were solved numerically using a time-stepping method in finite element method (FEM) for an accurate description of the heating mechanism around a particular defect. This study also provides a base for the analysis of features for slot characterisation and thermographic discrimination of angular slots from the transient thermal responses. Experimental work was completed to verify the simulation results and analyses.

In the simulations, a numerical package was used to simulate the thermographic response to angular slots in an aluminium sample. The aluminium sample dimensions were 80 x 150 x 5mm. The angular slots had lengths of 1.5mm, 2.0mm, 2.5mm and 3.0mm and a constant width of 0.25mm with angles, of 0°, 22.5°, 45° and 67.5°. Figure 1 shows an illustration of an angular slot inside a sample with its length, and angle. The initial temperature was set at 19.85°C for every case of the simulation. The electrical and thermal parameters for aluminium used in the simulations are shown in Table 1.

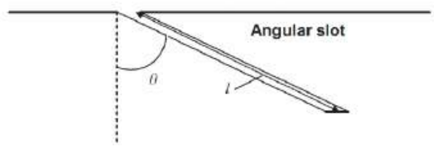

Figure 1: Illustration of an angular slot inside a sample

Table 1: Electrical and thermal parameters for Aluminum

Parameters	Aluminium
Conductivity δ (S/m)	3.7736E-07
Temperature coefficient (K^{-1})	2.31E-05
Density d (kg/m^3)	2700
Heat capacity C_p (J/kg K)	897
Thermal conductivity k (W/m K)	237
Thermal diffusivity $\propto$(=k/dC_p) (m^2/s)	9.7857E-05

3 Results

3.1 Simulation results

Figure 2 shows the resulting temperature distribution after 100 ms of heating for the cases in Figure 3. For 0° which is actually a straight slot, a build-up of heat can be observed at either side of the slot which shows a symmetrical distribution of heating pattern due to the presence of the slot. Slots with certain angles show heating distribution which is dominant in the slot direction inside the sample. The figures also show an increase in temperature contrast with increased angle. This can be explained by Figure 3 where it can be seen that with angular slots having a wider angle; more heat tends to accumulate at the slanted area, thus contributing to a higher temperature contrast at the surface of the sample.

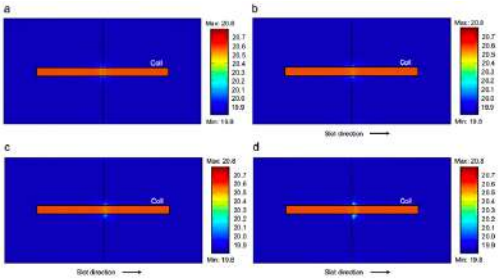

Figure 2: Simulated temperature distribution after 100ms of heating from top view

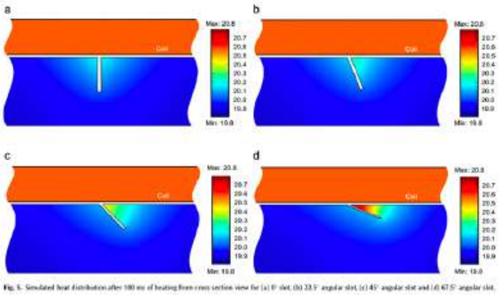

Figure 3: Simulated temperature distribution after 100ms of heating from cross section view

In order to investigate the temperature profiles of angular slots, temperature linescans at the sample surface taken directly beneath the induction coil were acquired for 22.5°, 45° and 67.5° angular slots after 100 ms of heating for different slot lengths of 1.5 mm, 2.0 mm, 2.5 mm and 3.0 mm (Figure 4). The aptitude of the features i.e. slope inclination and the maximum temperature amplitude feature, extracted from the temperature distribution for angular slot characterisation have shown the ability to provide geometrical information for a thorough and accurate assessment of a defect.

3.2 Experimental verification

Slope inclination and maximum temperature amplitude, were obtained from experimental investigations for each of the angular slots. Having determined the angle of a slot, the maximum temperature amplitude feature can then be used to quantify the length/depth by comparison of amplitudes between slots having the same angle. Figure 5 shows the comparison between the simulation and experimental results for the slope inclination and maximum temperature amplitude features based on the angular slots geometrical parameters investigated in the experiment.

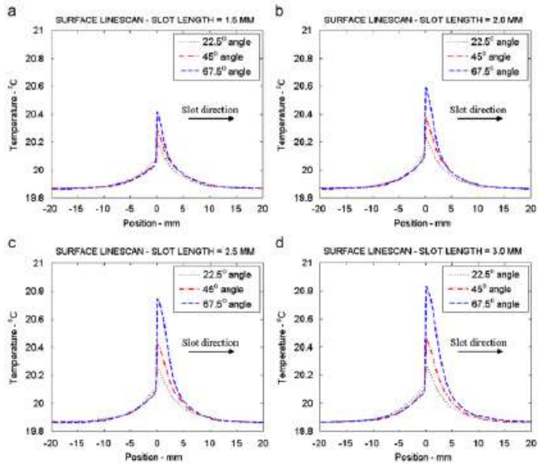

Figure 4: Temperature linescan for angular slots at different lengths

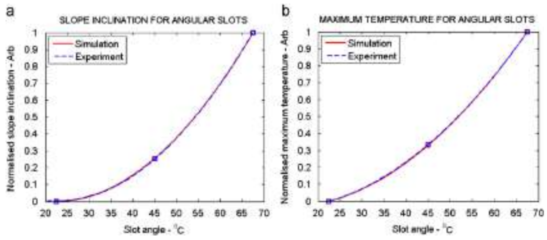

Figure 5: Comparison between simulation and experiment

4 Conclusions

An integrative NDT technique which combines the eddy current and thermography has been shown to be a useful for the characterisation and quantitative evaluation of angular defects. In these numerical studies, features of the eddy current thermography simulated temperature distribution have been analysed and extracted for the identification of a slot/defect angles and subsequently its lengths inside the investigated sample. Experimental measurements show a good agreement with the simulations. Quantitative information gathered by utilising the features identified by the simulations form the basis for the development of inverse model for defect quantification and 3D defect characterisation of an unknown slot or angled defect inside a sample or component under inspection.

References

U. Netzelmann and G. Walle. 2008. Induction thermography as a tool for reliable detection of surface defects. *17th World Conference on Nondestructive Testing, Shanghai China.*

B. Oswald-Tranta. 2007. Thermo-inductive crack detection'. *Nondestructive Testing and Evaluation*, 22(137- 153).

G. Riegert, Th. Zweschper, and G. Busse. 2004. Lock-in thermography with eddy-current excitation. *Quantitative Infra Red Thermography Journal*, 1(21-32).

G. Zenzinger, J. Bamberg, M. Dumm, and P. Nutz. 2005. Crack detection using eddytherm. *Review of Progress in QNDE*, 24(1646-1653).

Individual Research Contribution Review, 2023, 1(1): 191–192

Acoustic Emission-Based Classification of Ball Valve Leakage Levels: A Machine Learning Approach

Ismail Bin Mustapha
Industrial Technology Division, Malaysian Nuclear Agency
43000 Kajang, Selangor
ismail@nm.gov.my

Abstract

A non-destructive testing technique called acoustic emission (AE) in valve systems to detect level valve opening. This process requires the installation of AE sensors across the valve system to identify acoustic vibrations produced by fluid flow turbulence. In this article, valve opening detection based on the signal and then classification is done to categorize the signal and test the best classifier.

Keywords: Classification, Acoustic Emision, Valve

1 Introduction

Acoustic emission (AE) is a widely used non-destructive testing (NDT) technique for measuring valve leakage. It has high sensitivity and can detect weak signals without hindering operations. Researchers have studied the characteristics of AE signals in the process of valve leakage. Studies have shown that AE technology can qualitatively detect leakage in pipelines, indicating different characteristics of check valves, internal fluid leakage, and intelligent portable non-invasive instruments. These findings suggest that AE technology can be a valuable tool for detecting valve leakage without affecting operations (Zhao et al., 2020).

Internal leakages in valve pipeline systems are a common example of an acoustic emission phenomenon. The test evaluates acoustic signals produced by plastic deformation, crack propagation, leakage, burning, and fracture. The elastic wave frequency affects the signal's frequency. The AE technique analyses elastic waves from acoustic emission sources as electrical signals, converted by AE sensors, to determine the flow rate in pipeline systems. This process provides informative information and validates the existence of leakages in pipeline systems or valve failure. In this project, acoustic emission (AE) will be used to detect the flow rate of the pipeline system. Flow measurement using acoustic emission (AE) signal is a technique that relies on the generation and detection of acoustic waves to estimate fluid flow rates. Acoustic emission is the release of transient stress waves that occur when two a material undergoes deformation, such as crack propagation, fracture, or fluid flow turbulence. The principle behind using AE for flow measurement is based on the fact that fluid flow in pipelines or channels can generate acoustic emissions due to the turbulence and interactions between the fluid and the surrounding structure. By analysing the characteristics of these AE signals, it is possible to infer information about the flow rate.

2 Methods and Materials

Classification is a technique used to categorize the data obtained into several types of classes. The main purpose of classification is to identify some problems that occur during the classification. This is for the classification of data that will be categorized into several classes where the new data obtained is placed into which category. In this study, six types of classifiers were used, namely KNN, SVM, MLP, LR, RF and DNN classifiers.

In the field of machine learning and in particular statistical classification problems, the confusion matrix, also known as the error matrix is a special table layout that allows the visualization of the performance of an algorithm, usually supervised learning (in unsupervised learning it is usually called a matching matrix). Each row of the matrix represents an occurrence in the actual class while each column represents an occurrence in the predicted class, or vice versa.

Performance measurements TP, TN, FP, FN are parameters used in the evaluation of specificity, sensitivity and accuracy. TP or True Positive is the number of valve types and valve opening levels that are perfectly identified. The true negative or TN is the number of valve types and valve opening levels that are detected perfectly. False Positives or FPs are the number of valve types and valve opening levels falsely detected as positives that are not actually valve types and valve opening levels. False Negatives or FN are the number of valve types and valve opening levels detected incorrectly.

3 Result and Discussion

A study was conducted on the degree of valve opening for ball valves by comparing six types of classifiers. Evaluation is done by evaluating the performance of each type of classifier for ball valves as in Table 1. The SVM classifier showed high performance on all types of evaluations. It achieved high values for precision at 96.24%, recall at 95.73%, F1 score at 95.76%, MCC at 95.49% and precision at 95.92%. These results show that SVM performs well in identifying valve opening levels.

The KNN classifier also exhibits competitive performance on performance evaluation. It achieved relatively high values for precision (92.45%), recall (91.88%), F1 score (91.99%), MCC (91.33%) and precision (92.28%). KNN shows its effectiveness in correctly classifying valve opening levels and maintaining a high level of accuracy.

LR classifier shows lower performance compared to SVM and KNN where It has values for performance (40.84%), recall (45.86%), F1 score (42.34%), MCC (41.93%) and precision (44.53%). This result shows that LR cannot accurately predict the degree of valve opening and causes the accuracy results to be low.

The RF classifier consistently performed best on all types of evaluations. It achieved very high values for retention (99.06%), recall (99.00%), F1 score (99.02%), MCC (98.92%) and precision (98.98%). The RF classifier was also used by Shen & Cheng (2022) to assess pipe leakage and the results obtained were at 99.82% accuracy. The RF classifier also outperforms other models and shows its effectiveness in accurate classification and accurate prediction.

The MLP classifier outperforms the other classifiers in most evaluation performances. It has lower values for retention (23.65%), recall (36.36%), F1 score (26.19%), MCC (26.22%) and precision (37.29%). These results indicate that MLP cannot distinguish the degree of valve opening.

DNN classifiers show high performance on evaluation performance. It achieved relatively high values for precision (96.19%) and recall (92.72%), demonstrating its ability to identify valve opening levels. However, DNN has lower values for F1 score (91.79%), MCC (92.52%) and accuracy (92.94%) compared to RF classifier and SVM classifier.

From the overall results obtained, the RF classifier showed the best performance on all types of evaluations performed. SVM and DNN also show competitive performance.

Table 1: Performance of classifier.

Classifier/Performance	SVM	KNN	LR	RF	MLP	DNN
Precision	96.24	92.45	40.84	99.06	23.65	96.19
Recall	95.73	91.88	45.86	99	36.36	92.72
F1-score	95.76	91.99	42.34	99.02	26.19	91.79
MCC	95.49	91.33	41.93	98.92	26.22	92.52
Accuracy	95.92	92.28	44.53	98.98	37.29	92.94

From the performance analysis performed on the RF classifier, a comparison of the actual value and the predicted value is performed to identify errors in the predicted value. Figure 1 shows the error in the forecast value at openings of 1%, 6%, 7%, 9% and 10%. There is a predicted value of 1 at a 6% opening that is predicted to be at a 9% opening. This low error of the prediction value shows that the RF model is able to identify almost exactly the degree of valve opening.

4 Conclusion and Attention

Overall, the accuracy evaluations show that the RF classifier consistently performs the best of all the classifiers that were used. Furthermore, Support Vector Machines (SVM), Logistic Regression (LR), Multilayer Perceptron (MLP), and Deep Neural Networks (DNN) exhibit different degrees of accuracy, which are comparatively lower than those of other classification methods

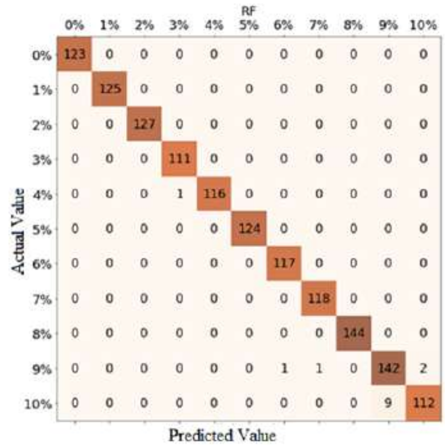

Figure 1: Confusion matrix for Random Forest (RF)

References

Hanxue Zhao, Zhenlin Li, Shenbin Zhu, and Ying Yu. 2020. Valve internal leakage rate quantification based on factor analysis and wavelet-bp neural network using acoustic emission. *Applied Sciences (Switzerland)*, 10(16).

Individual Research Contribution Review, 2023, 1(1): 193–194

Material Properties of Shipwreck Pottery for Cultural Heritage Studies

Izura Izzuddin
Industrial Technology Division
Malaysian Nuclear Agency, 43000 Kajang, Selangor
izura@nm.gov.my

Abstract

Pottery, categorized under traditional ceramics and frequently discovered in shipwrecks, serves as valuable artifact material. The analysis of material properties not only enhances our understanding of pottery but also contributes to authenticity, conservation, and preservation processes. This study aims to characterize the crystal structure, morphology, and microstructure of the pottery. In general, the x-ray diffractogram reveals that all samples closely resemble the crystal structure of kaolin clay. The morphological and microstructure images from FESEM characterization indicate that samples from England and the Netherlands are identical, while Ming Dynasty samples exhibit a greater number of pores.

Keywords: shipwreck, pottery, material properties, XRD, FESEM

1 Introduction

Shipwrecks and their contents represent invaluable national heritage treasures that warrant conservation and preservation efforts. The Straits of Melaka, renowned for numerous discovered shipwrecks because it became a vital maritime silk route during the 15th and 16th centuries. At once, Melaka also serving as a prominent trading center, attracted diverse traders from around the globe. Nowadays, continuous series of excavation activities have been undertaken to preserve this precious treasure. Items predominantly crafted from ceramics, such as pottery and tableware, are frequently uncovered during these excavations. An intriguing aspect of these ceramic materials lies in the shapes and motifs carved upon them. According to archaeologists or historians specializing in the study of such artifacts, these motifs typically serve as indicators of the origin and play a role in describing the trading activities in the Straits of Malacca centuries ago. By incorporating elements of science and technology into these artifacts, more information can be extracted from them. This information is valuable for establishing a fingerprint, contributes to the authentication process as well as conservation and preservation of the artifacts. A possible approach to enhancing this endeavor involves studying the material properties of these ceramics. Beyond imparting better intrinsic value, these findings could assist in comprehending the ceramics manufacturing processes during that era. This study will provide information on the crystal structure and morphological properties of the discovered ceramic materials.

2 Experimental Methods

Potteries fragments were taken from the excavation site of shipwreck. The end of each fragment was tapped using a hammer. Only the inner part of the pottery was selected and ground into a powder form using a mortar and pestle. The samples were then characterized using XRD and FESEM instruments.

3 Results and Discussions

Figure 1 displays the photographic image of the pottery's fragments collected from the excavation site of shipwreck. Referring to the motif, it is possible to assume that the pottery originated from: (a) the England, (b) the Netherlands, and (c) the Ming Dynasty. The similarity that can be observed among the potteries is that they all feature a white base color. This suggests that they were likely produced using kaolin clay.

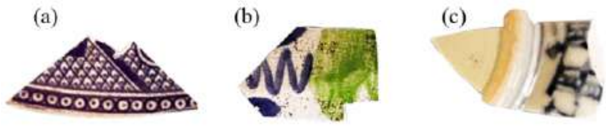

Figure 1: Photographic image of the pottery's fragments

Potteries are a form of traditional ceramics. Therefore, X-ray Diffraction (XRD) characterization was carried out to identify their crystal structure. In general, all samples exhibit a similar XRD spectrums, but with varying intensity levels as depicted in Figure 2. The diffractograms indicated that all samples exhibit a nearly identical spectrum of kaolin clay (Macaria et al., 2021). Meanwhile, the difference in intensity generally reflects difference degree of crystallinity in each sample.

To gather further information about the potteries, their microstructure and morphology were examined using Field Emission Scanning Electron Microscopy (FESEM). At a 500x magnification, both sample (a) and (b) displayed similar morphological properties ((a) & (b)), while sample (c) exhibits a higher number of pores (Figure 3).

The variation in microstructure observed may be attributed to differences in the production process, possibly stemming

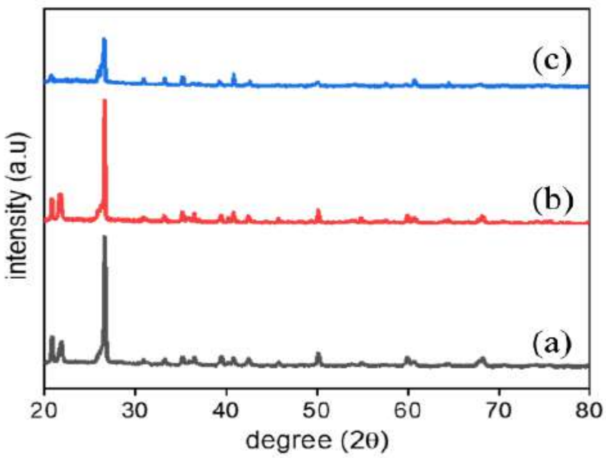

Figure 2: Diffractogram of pottery's fragments

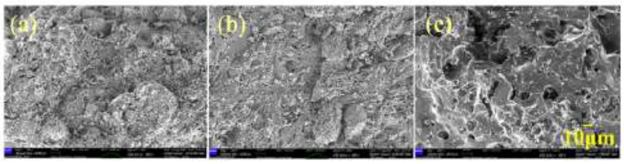

Figure 3: Microstructure and morphology image of pottery's fragments

from varying heating times and temperatures during pottery manufacturing. It is conceivable that these divergences in production processes are influenced by the specific regions where the pottery is created. Considering the preliminary findings, with the assumption that pottery (a) and (b) originated from the western region and pottery (c) from the eastern region (Asia), it suggests the potential for distinct ceramic production methods between the West and the East (Asia).

4 Conclusion

The results obtained were significant in providing information about the pottery, simultaneously adding higher value to this historical material. It can serve not only as a fingerprint but also contributes to the authenticity process of the artifacts. Additionally, a better understanding of the nature of this pottery aids in conservation and preservation purposes. However, a more detailed analysis and additional characterizations will be conducted to attain a more precise information of the potteries.

References

H.C. Macaria, Marissa V. R., Ana M. H. G., Jesús G. S, Alejandro C. R., José A. R. S., and Ricardo G. S. A. 2021. Thermodynamic analysis of the influence of potassium on the thermal behavior of kaolin raw material. *Physicochem. Probl. Miner. Process.*, 57(1):39–52.

Individual Research Contribution Review, 2023, 1(1): 195–196

Separation of Cerium from Rare Earth Hydroxide Concentrate using Oxidation Method

Jacqueline Kones
Industrial Technology Division, Malaysian Nuclear Agency
43000 Kajang, Selangor
jacqueline@nm.gov.my

Abstract

Cerium can be found along with other rare earth elements such as neodymium and lanthanum. Separation of cerium is important to enhance the extraction of other rare earth elements since its presence can affect the process. Oxidation is one of the methods that can be used to separate cerium from other elements.

Keywords: Cerium, rare earth elements

1 Introduction

Malaysian monazite contains light rare earth elements, namely cerium, lanthanum, neodymium and praseodymium. These elements can be used in a wide variety of applications such as for hard drives, speakers, electric motors, and power generators. The demand for rare earth element has also been increasing each year since these elements can enhance the properties of the equipment. For example, neodymium magnet is stronger than conventional permanent magnet and it is more resistance to demagnetization.

Separating and extracting rare earth elements from its ore is one of the important stages before the final device can be produced. Processing monazite started from beneficiation process of the tin tailing or amang followed by a series of steps to separate any potential by-products before rare earth elements obtained in the desired purity or concentration. One of the methods to process monazite is through alkali digestion process. The process started by treating the monazite in caustic soda reaction to remove phosphate followed by leaching the rare earth elements into acidic media before the radioactive and the rare earth elements can be done.

Rare earth concentrate obtained can be extracted to produce high purity of the required elements. Cerium, however need to be separated from the other elements because its presence can affect the extraction process. Unlike other rare earth elements that only can form +3 oxidation state, cerium has the ability to form +4 oxidation state. Therefore, through oxidation of Ce (III), cerium can be separated from others.

Oxidation of Ce (III) has been demonstrated by few studies (Formiga and Morais, 2016; Sauber, 2018; Purwani and Trinopiawan, 2019) but, there is a need to investigate on how to do it properly. This study aims to study the suitable pH range for the oxidation to occur.

2 Experimental Methods

Rare earth concentrate used in this study was obtained from Malaysian monazite. Alkali digestion process was used to remove the phosphate followed by acid leaching using hydrochloric acid. The pregnant leached solution then treated with ammonia solution at selected pH level to separate thorium from the rare earth elements. The rare earth concentrate was obtained as hydroxide contains cerium, lanthanum and neodymium.

Cerium separation started by dissolving the rare earth concentrate in acidic media. Hydrochloric acid or nitric acid can be used. pH of the pregnant leach solution was adjusted by adding sodium carbonate solution until pH 3. Potassium permanganate was added to start the oxidation of Ce (III) to Ce (IV) while adding sodium carbonate for pH adjustment. The pH for this reaction was maintained at around 3-4 by adding more sodium carbonate if the pH drops after potassium permanganate added. Ce (IV) concentrate filtered and the remaining rare earth elements were retrieved by adding ammonia solution until no precipitation formed.

Elemental analysis of the products obtained were analysed using energy dispersive X-ray fluorescence spectrometer.

3 Data/Results

Results obtained as shown in Table 1.

Table 1: Comparisons of element obtained

Elements	Ce concentrate	Other REE concentrate
Ce	71.2 %	n.d.
Nd	15. 2 %	37.6 %
Mn	7.7 2%	n.d.%
La	n.d.	31.1 %
Pr	n.d.	12.6 %
Cl	4.2 %	11.6 %
Other REEs	0.8 %	6.8 %
Other elements	0.7 %	0.3 %

4 Discussion and Conclusions

Oxidation of cerium

Potassium permanganate is more stable at pH more than 2.5. However, the more Potassium permanganate added, the pH of the solution will be reduced and eventually will affect the oxidation process. This could be explained by the formation of

H+ ions as described in Equation 1. Therefore, to maintain the pH, Na_2CO_3 need to be added. The oxidation process of Ce (III) with $KMnO_4$ was described in Equation 2 – 4. It showed that apart from forming Ce (IV) as Ce $(OH)_4$, manganese (IV) oxide will be produced as impurity, hence affecting the purity of cerium. Fortunately, MnO_2 can be removed by dissolving it in dilute HCl.

$$3Ce^{3+} + MnO^{4-} + 10H_2O \leftrightarrow 3Ce(OH)_4(\text{s}) + MnO_2(\text{s}) + 8H^+(\text{aq}) \quad (1)$$

$$3Ce(NO_3)_3 + KMnO_4 + 2H_2O \leftrightarrow 2Ce(NO_3)_4 + Ce(OH)_4 + KNO_3 + MnO_2 \quad (2)$$

$$Ce(NO)_3 + 4H_2O \leftrightarrow Ce(OH)_4 + 4HNO_3 \quad (3)$$

$$HNO_3 + Na_2CO_3 \leftrightarrow NaNO_3 + H_2O + CO_2 \quad (4)$$

$$2MnO^{4-} + 8H^+ + 6Cl^- \leftrightarrow 2MnO_2 + 3Cl_2 + 4H_2O \quad (5)$$

From this study, it was found that no cerium was detected in the remaining REE concentrate suggesting oxidation of Ce (III) to Ce (IV) was successful. Therefore, this study had explained what the other researchers have done on how to do the oxidation of cerium for separation from other REEs. Also, it is recommended to conduct elemental analysis using inductive coupled plasma (ICP) spectroscopy to determine concentration of the remaining cerium if any. The other rare earth concentrate can therefore be processed further without any of cerium present.

References

T. Formiga and C.A. Morais. 2016. Cerium separation from light rare earth concentrate by liquid-liquid extraction. *World Journal of Engineering and Technology*, (4):129–137.

M.V. Purwani and K. Trinopiawan. 2019. Separation of Ce, La, and Nd in Rare Earth Hydroxide (REOH) by Oxidation with Potassium Permanganate and precipitation. *J. Pys.: Conf. Ser.*, (1198 032003).

M. E. Sauber. 2018. Oxidative removal of Cerium from rare earth elements mixed chloride solution. *Extraction 2018, The Minerals, Metals Materials Series*.

Individual Research Contribution Review, 2023, 1(1): 197–198

Synthesis and Characterization of Carbon Aerogel (CA) for Hydrogen Storage Applications

Julie Andrianny Murshidi
Industrial Technology Division, Malaysian Nuclear Agency
43000 Kajang, Selangor
julie@nm.gov.my

Abstract

The carbon aerogel (CA) has been synthesized by the sol-gel method using resorcinol (R) and formaldehyde (F). RF wet gel has been dried using ambient pressure drying. To avoid shrinkage during this mode of drying, organic catalyst triethylamine (C) has been used. In order to find out the effect of using gamma irradiation on structural and microstructural of the synthesized CA, X-Ray Diffraction (XRD), Field Emission Scanning Electron Microscopy (FESEM) and Small Angle X-ray Scattering (SAXS) analysis have been studied.

Keywords: Carbon Aerogel, Structural, Microstructural

1 Introduction

The increase in global energy consumption has led to an increase in greenhouse gaseous emissions and climate change. To rectify this, research is being undertaken to evaluate and refine alternative energy carriers that are green, environmental friendly with zero CO_2 emission. Among these, significant interest has been associated with hydrogen. Materials based hydrogen storage has demonstrated the ability to increase the density of hydrogen by a factor of more than twice that of liquid hydrogen, resulting in hydrogen densities of up to 21.1 MJ/L hydrogen (McWhorter et al., 2011). Of the wide variety of materials based hydrogen storage, Carbon Aerogels (CAs) were chosen as the primary focus of this project. More recently, the excess wt% of H_2 in CA was reported to have reached 5.3 wt% (Kabbour et al., 2006). The reported value is close to the 2010 US Department of Energy (DOE) gravimetric hydrogen storage density target of 6 wt% H_2. This project is focused on optimum preparations conditions, microstructure and hydrogen sorption capacity of CA as a hydrogen storage medium.

2 Methods

The starting reagents were Resorcinol (Thermo Scientific, 98%), formaldehyde (R&M, 36–41%) and triethylamine (R&M, 99%). All solutions were prepared from water which had been deionized. A typical gel formulation contained 0.29 M resorcinol, 0.57 M formaldehyde and 0.00029 M triethylamine. The molar ratio of formaldehyde:resorcinol was held at a constant value of 2. Table 1 displays the formulation examined in this study. The precursor ingredients were mixed using magnetic stirring for 2 h and then gamma irradiated at 20 kGy.

Table 1: RF gel samples formulation.

Formulation	Concentration of molar		
	R	F	C
(R:F = 1:2 ; R/C = 1000)	0.29	0.58	0.00029

The acetone was replaced with fresh acetone every 24 h. The carbonization was done in the Argon atmosphere (Ar flow rate of 10 ml/min) by following a specific heating program. Thus heating from ambient temperature to 350°C at a heating rate of 2°C/min and then up to 900°C/min heating rate 5°C/min were deployed. The sample was kept at 900°C for 2 h. It was then cooled to room temperature through ambient cooling. The as-prepared CA was powdered in an agate mortar and KOH powder was mixed in 3(KOH):1(CA) molar ratio. This mixture was heated under Ar flow (10 ml/min). The heating was done at the rate of 5°C/min up to 350°C and then 3°C/min up to 900°C. The temperature of 900°C was maintained for 3 h under Ar flow. Afterward, the temperature was lowered to room temperature under Ar atmosphere.

2.1 Characterization

PANalytical X'Pert PRO MPD PW 3040/60 diffractometer was used for phase identification of crystalline RF gel samples. Cu Kα1 radiation source (λ = 1.54060Å) with a 2θ range of 20° to 80° with a step size of 0.0334° under a voltage of 40 kV and a current of 30 mA were applied. Microstructural observations were conducted on a Carl Zeiss Gemini SEM 500 FESEM using a secondary electron detector whilst operating at 15 kV. The microscope was coupled with an Oxford energy dispersive X-Ray spectrometer (EDS) for elemental analysis. Samples were not coated prior to imaging in the FESEM. SAXS experiments were performed using Anton Paar Saxpoint instrument, operated at 50kV and 1mA with the point collimation geometry. The radiation used was a Ni filtered CuKα radiation of wavelength 0.154 nm. The intensity profiles are recorded using a CMOS 2-D detector (Eiger) and the scattering vector q, covers from 0.035 to 5 nm^{-1}. Sample to detector distance is 575.5 / 271 mm and sample exposure to the source is 600 seconds. All experiments are carried out at room temperature, 20°C.

3 Data/Results

3.1 XRD

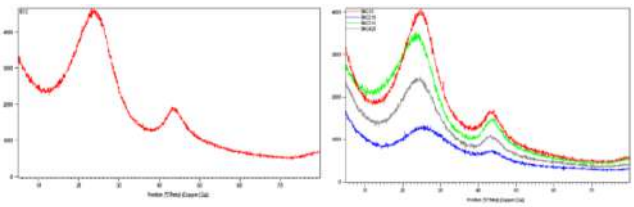

Figure 1: XRD pattern of non-irradiated (left) and gamma-irradiated (right) CA samples.

3.2 FESEM

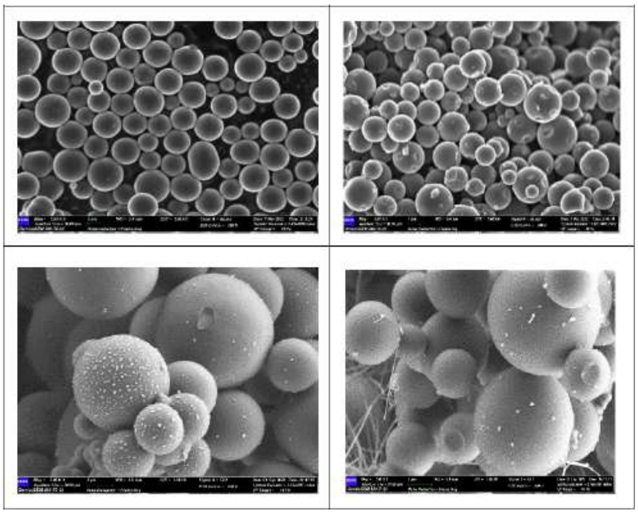

Figure 2: FESEM images of non-irradiated (above) and gamma-irradiated (below) CA samples.

3.3 SAXS

Table 2: SAXS analysis in Porod region of non-irradiated and gamma irradiated CA samples.

Sample	**Specific surface (m^2/g)**
Non-irradiated	426.54
Gamma-irradiated	724.43

4 Discussion/Conclusions

Figure 1 shows XRD pattern of non-irradiated and gamma-irradiated CA samples. The XRD peak between 2θ = 24° to 25° corresponds to (002) planes of graphite-like carbons. XRD peaks are broad, bringing out the disordered nature of the arrangement of carbon atoms for CAs. The next XRD peak located between 44.0° and 44.5° represents (101) planes of graphite carbon. It may be pointed out that because of the disorder the exact position of the Bragg angle for (002) and (101) have been determined within the range of ±1°. The 2θ range is in consistence with the graphitic carbon structure.

FESEM images in Figure 2 show the CA morphology is dominated by pearl-like particles. The microstructures reveal the configuration of particles and the intervening pore structure. As can be seen, the particles have nearly spherical geometry. All the particles of CAs are under the category of the large particles (>1 mm). Interparticle spaces forming pores correspond to macropores.

The total surface area for non-irradiated CA samples as determined by the SAXS porod region (Table 2) have been found to be 426.54 m^2/g. For gamma-irradiated CA samples the above parameters have been found to be 724.43 m^2/g.

References

M. Aegerter, N. Leventis, and M. Koebel. 2011. Aerogels handbook (advances in sol-gel derived materials and technologies).

H. Kabbour, T.F. Baumann, J.H.Jr. Satcher, A. Saulnier, and C.C. Ahn. 2006. *Chem. Mater*, 18.

J.H. Lee and S.J. Park. 2020. Recent advances in preparations and applications of carbon aerogels: A review. *Carbon N Y*, 163:1–18.

S. McWhorter, C. Read, G. Ordaz, and N. Stetson. 2011. Current opinion in solid state and materials science. 15.

A. P. Pandey, A. Bhatnagar, V. Shukla, P. K. Soni, S. Singh, S. K. Verma, M. Shaneeth, V. Sekkar, and O.N. Srivastava. 2020. Hydrogen storage properties of carbon aerogel synthesized by ambient pressure drying using new catalyst trimethylamine.

S. Singh, A. Bhatnagar, V. Dixit, V. Shukla, M.A. Shaz, and A.S.K. Sinha et al. 2016. Synthesis, characterization and hydrogen storage characteristics of ambient pressure dried carbon aerogel. *Int J Hydrogen Energy*, 41:3561–3570.

H.Y. Tian, C.E. Buckley, S. Mul'e, M. Paskevicius, and B.B. Dhal. 2008. Preparation, microstructure and hydrogen sorption properties of nanoporous carbon aerogels under ambient drying. *Nanotechnology*, 19.

H.Y. Tian, C.E. Buckley, S.B. Wang, and M.F. Zhou. 2009. Enhanced hydrogen storage capacity in carbon aerogels treated with KOH. *Carbon N Y*, 47:2128–2130.

H.Y. Tian, C.E. Buckley, D.A. Sheppard, M. Paskevicius, and N. Hanna. 2010. A synthesis method for cobalt doped carbon aerogels with high surface area and their hydrogen storage properties. *Int J Hydrogen Energy*, 35:13242–13246.

H.Y. Tian, C.E. Buckley, M. Paskevicius, and D.A. Sheppard. 2011. Acetic acid catalysed carbon xerogels derived from resorcinol furfural for hydrogen storage. *Int J Hydrogen Energy*, 36:671–679.

Individual Research Contribution Review, 2023, 1(1): 199–200

Digital Laminography for Evaluating Weld Discontinuities

Khairul Anuar Mohd Salleh
Industrial Technology Division, Malaysian Nuclear Agency
43000 Kajang, Selangor
khairul_anuar@nm.gov.my

Abstract

Decades of research have unveiled the potential of 3D radiographic imaging, with Computed Tomography (CT) finding applications in Non-Destructive Testing (NDT) across industries. However, CT's need for unrestricted access poses challenges when inspecting large, flat objects. This study explores Coplanar Translational Laminography (CTL) as an alternative technique for characterizing welding imperfections on welded carbon steel plates. Comparisons with Phased Array Ultrasonic Testing (PAUT) highlight CTL's advantages for clustered porosities. Assessment of a test phantom and carbon steel plate, along with image quality evaluations, demonstrates CTL's reliability. It proves to be a valuable 3D measurement technique with the potential to overcome CT's limitations in NDT applications.

Keywords: Non-Destructive Testing (NDT), Computed Tomography (CT), Coplanar Translational Laminography (CTL)

1 Introduction

Over the past three decades, extensive research has provided valuable insights into using three-dimensional (3D) radiographic imaging for depth information. Initially applied in healthcare, Computed Tomography (CT) has extended to assess internal 3D structures in Non-Destructive Testing (NDT) areas like composite materials and structures, manufacturing, aerospace, and weld inspection. However, CT demands unrestricted object access, complicating the inspection of large, flat items (Liu et al., 2015; Boateng et al., 2016). Laminography excels in such cases, examining objects with varying dimensions (Bullinger et al., 2016; Ewert et al., 2017). A laminography technique has been developed to address this. This paper assesses Coplanar Translational Laminography (CTL) in characterizing welding imperfections on flat-welded carbon steel plates and compares CTL with Phased Array Ultrasonic Testing (PAUT).

2 Methods

The CTL (Ewert et al., 2015; Ahmad Hamidi et al., 2021) was applied to an in-house fabricated 50 mm x 15 mm x 9.5 mm test phantom and a known 300 mm x 250 mm welded carbon steel plate with a base metal thickness of 8.0 mm containing artificial discontinuities such as clustered porosity, lack of fusion (LOF), and slag inclusions. These imperfections underwent Ultrasonic Testing (UT), complemented by visual inspection to confirm the absence of surface defects. The welded plate and test phantom, equipped with seven small-diameter (1 mm) carbon steel wires spanning from 1.0 mm to 7.0 mm, were subjected to X-ray exposure. A 2D digital radiograph acquisition utilized a calibrated Digital Detector Array (DDA) with a 100μm pixel size and 16-bit analog-to-digital converter (ADC).

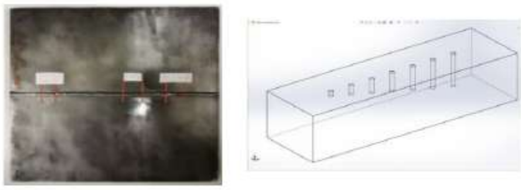

(a) (b)

Figure 1: Specimens and CLT assessment tool used (a) Welded plate (b) schematic of test phantom.

Before 3D volume reconstruction, contrast, sensitivity, and basic spatial resolution (SR_b) were assessed based on ISO 17636-2. The 3D volume of the sample was reconstructed using a fast shift-average algorithm, with parameters conforming to a 0.1 mm x 0.1 mm x 0.1 mm scaling in alignment with the DDA pixel size. The 3D volume of the sample was reconstructed using a fast shift-average algorithm, with parameters conforming to a 0.1mm x 0.1mm x 0.1mm scaling in alignment with the DDA pixel size. The CTL manipulator (Figure 2) was designed and documented elsewhere (Ahmad Hamidi et al., 2021). Each projection represented the 3D object volume from a distinct angle, with comprehensive details on system development available elsewhere (Ewert et al., 2015; Ahmad Hamidi et al., 2021).

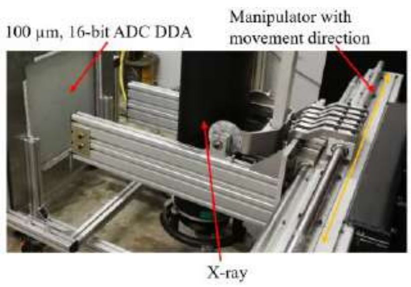

Figure 2: Exposure setup for the Coplanar Translational Tomography (CTL) showing the manipulator movement direction

Exposure parameters are tabulated in Table 1 and Table 2, respectively.

Table 1: Exposure Parameters for the welded plate.

Technique	X-ray voltage peak (kVp)	X-ray current (mA)	Exposure/ Frame time (sec)	SDD (mm)	ODD (mm)	No. of frames	No. of projection	Scan angle
RT-D with DDA	160 kV	5.0	2.0	650.0	10.5	1	-	0°
CTL	160 kV	5.0	2.0	650.0	10.5	1	750	30°

Table 2: Parameters for RT-D for test phantom.

Technique	X-ray voltage peak (kVp)	X-ray current (mA)	Exposure/ Frame time (sec)	SDD (mm)	ODD (mm)	No. of frames	No. of projection
RT-D with DDA	120 kV	2.5	10.0	1000.0	7.5	10	-
CTL	90 kV	2.0	2.0	650.0	5.0	1	700

3 Results and Discussion

The acquired 2D image, shown in Figure 3, is high-pass filtered to improve the visibility and interpretation of discontinuities. The image shows and confirms all three artificial discontinuities mentioned previously.

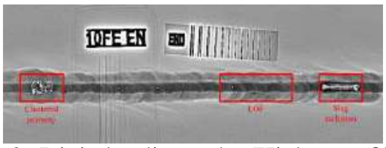

Figure 3: Digital radiographs (High-pass filtered)

Table 3 tabulates the image quality assessment on the original image of Figure 3 to assess the contrast, sensitivity, and image sharpness using single and duplex IQI wires, respectively. The result demonstrated that the image quality of 2D images is well above the minimum requirement of ISO 17636-2 (testing Class A).

Table 3: Comparison of image quality parameters

	Single wire	Duplex wire	SR_b^{image} mm	SNR_N at weld centre
ISO 17636-2 (Class A)	W12	D8	0.16	>70
RT-D with DDA (raw image)	W15	D10	0.10	143

Figure 4 illustrates the reconstructed image of the steel wires in the XY plane, and Table 4 suggests no significant difference in the wire length with CTL. The maximum percentage difference is up to 9.0%, which is acceptable for industrial practices.

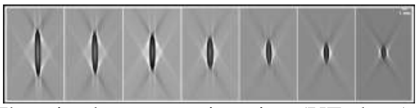

Figure 4: The wires' cross-section view (YZ plane) at different lengths (a – g).)

The CTL and PAUT measurements in Table 5 show a significant difference (about 40%) in the depth and height of the lack of fusion and the height of slag inclusion. These differences could be due to the exposure condition, detector properties, geometrical, and the measurement of CTL at one location only.

4 Conclusion

The analysis involved a carbon steel plate with artificial welding flaws and a test phantom, utilizing RT-D with DDA and CTL. The 2D image of the welded plate met standard requirements, detecting artificial discontinuities with high contrast sensitivity and image quality. However, RT-D's quantitative measurements lacked depth information. While CT was impractical for such structures due to scanning limitations, CTL proved to be the best 3D measurement technique. It demonstrated good agreement with PAUT for clustered porosity but showed differences in characterizing other artificial discontinuities like lack of fusion and slag inclusion. Measurement uncertainties influenced the physical appearance of imperfections for both techniques.

Table 4: Comparison depth of steel wire of test phantom

No.	Depth (mm)		
	RT-D with DDA	CTL	Error (%)
Wire 1	7.12	7.10	0.3
Wire 2	6.10	6.16	1.0
Wire 3	4.70	4.87	3.6
Wire 4	4.06	4.10	1.0
Wire 5	3.11	3.00	3.5
Wire 6	2.10	2.09	0.5
Wire 7	1.00	1.09	9.0

Table 5: Comparison of results

Type	PAUT				
	Position (S)	Length (L)	Depth^a(D)	Height (H)	(D)+(H)
Clustered Porosity	48.0	13.0	3.4	3.3	6.7
Lack of Fusion	163.0	33.0	4.0	5.2	9.2
Slag Inclusion	230.0	26.0	4.1	2.6	6.7

Type	RT-D with DDA & CTL				
	Position (S)	Length (L)	Depth^a(D)	Height (H)	(D)+(H)
Clustered Porosity	47.0	14.0	2.5	3.6	6.1
Lack of Fusion	167.0	29.7	2.8	1.7	4.5
Slag Inclusion	223.0	22.9	4.4	4.8	9.2

References

S. Ahmad Hamidi, A. Muad, K. Mohd Salleh, and M. Wahab. 2021. Development of a manipulator system for x-ray imaging laminography. *Elektrika*, 20(2-3):117–120.

F. Boateng, U. Ewert, T. Kannengiesser, U. Zscherpel, A. Griesche, A. Kromm, S. Hohendorf, and B Redner. 2016. Real-time radiography for observation of crack growth during GTA welding. *Welding in the World*, 60:931–937.

O. Bullinger, U. Schnars, D. Schulting, B. Redmer, M. Tschaikner, and U. Ewert. 2016. Laminographic inspection of large carbon fibre composite aircraft- structures at airbus. *19th World Conference on Non- Destructive Testing*.

U. Ewert, K.-U. Thiessenhusen, A. Deresch, C. Bellon, S. Hohendorf, S. Kolkoori, and B. Redmer. 2015. Reconstruction methods for coplanar translational laminography applications. *Digital Industrial Radiology and Computed Tomography (DIR 2015)*.

U. Ewert, M. Tschaikner, B. Redmer, A. Deresch, F. Hille, S. Hohendorf, and O. Paetsch. 2017. Digital x-ray cross laminography for evaluation of crack fields in large concrete blocks after impact. *General Assembly of Academia NDT International*.

B. Liu, Z. Wei, C. Wei, Y. Wang, L. Yuan, Y. Shu, and L. Wei. 2015. An industrial computed laminography imaging system. *Digital Industrial Radiology and Computed Tomography (DIR 2015)*.

Individual Research Contribution Review, 2023, 1(1): 201–202

Characterisation of Multiphase Hold-Up of Packed Bed Reactor Using Gamma Densitometry: Preliminary Study

Lahasen@Normanshah Dahing
Industrial Technology Division, Malaysian Nuclear Agency
43000 Kajang, Selangor
shah@nm.gov.my

Abstract

Multiphase flow is commonly encountered in chemical reactors and quantifying the hold-up of each phase is important for reactor design and performance evaluation. Packed bed reactors, filled with catalyst particles, are widely used in the chemical and petrochemical industries. Knowing the behaviour and characterizations of the process inside the column is very important to indicate the performance of plant. This study focuses on using gamma densitometry to determine the density profile of gas, liquid, and solid phases for preliminary study in a Plexiglas packed bed column with a 2m tall and 5cm inner diameter. Gamma densitometry utilizes the different gamma ray attenuation characteristics of each phase to quantify hold-up. A packed bed column was constructed with a gamma ray source and detector installed at two axial locations. The effects of gas and liquid flow rates on hold-up were investigated. The preliminary results demonstrate that gamma densitometry can be used (successfully) determine multiphase hold-up in packed beds. Further work is suggested to explore effects of particle shape, size distribution and packing geometry on hold-up using gamma densitometry.

Keywords: Gamma Densitometry, Hold-up, Packed Bed

1 Introduction

Packed bed reactors are widely used in chemical, petrochemical and nuclear industries for gas-liquid-solid reactions. Understanding the hydrodynamics of multiphase flows in packed beds is critical for reactor design and performance evaluation. A key hydrodynamic parameter is the hold-up, defined as the fraction of reactor volume occupied by each phase. Accurately quantifying hold-up remains a challenge due to the opaque nature of packed beds. Numerous techniques have been explored for hold-up measurement. Pressure drop methods can determine overall hold-up but cannot distinguish between phases. Invasive sampling and tracer techniques provide phase-wise data but disturb the flow. Recent advances have made non-invasive gamma densitometry a promising technique for multiphase hold-up characterization in packed beds.

Gamma densitometry utilizes the different gamma ray attenuation properties of each phase to quantify hold-up. Early studies by Kumar et al. (Kumar et al., 1995) demonstrated the applicability of gamma densitometry for hold-up measurement in bubble columns. Van Baten and Krishna (Van Baten and Krishna, 2001) later extended the technique to trickle bed reactors by installing a gamma source and scintillation detector at two axial locations. They reported good agreement between the hold-up values from gamma densitometry and invasive sample collection.

Recent work has focused on using dual-energy gamma densitometry for simultaneous estimation of gas and liquid hold-up in packed beds. Kantzas et al. (Kantzas et al., 1988) first proposed using dual-energy gamma rays to discriminate between phases. This was successfully implemented by Islam (Islam, 2008) for trickle beds by combining a 241Am source with a 137Cs source. The effects of flow rates, packing properties and column inclination angle on hold-up were characterized.

While past literature has established gamma densitometry for trickle beds, relatively few studies have applied it to highly gas-liquid-solid three-phase flows in packed bed reactors. Therefore, the present work aims to demonstrate the use of single energy gamma densitometry for measuring density profile in a packed bed reactor under varied flow conditions. The results will provide insights into packed bed hydrodynamics and aid in reactor design.

2 Methods

The plexiglas packed bed column consisted of a 2 m tall with a 5 cm inner diameter. The column was packed with carbonate of 5 mm diameter up to a height of 1.5m. A 10 mCi 137Cs gamma ray source and a NaI scintillation detector were installed at two axial locations along the column to measure the gamma ray attenuation.

The gas and liquid flow rates into the column were controlled using rotameters. Air was used as the gas phase and water as the liquid phase. Experiments were performed over a range of superficial gas velocities from 0.05 to 0.5 m/s and liquid velocities from 0.02 to 0.1 m/s.

The output signals from the detector were acquired using a data acquisition system and logged continuously on a computer. Pulse height analysis was used to generate the gamma ray attenuation spectrum. For each flow condition, the measurements were made after steady state was attained.

3 Results and Discussion

The effects of gas and liquid flow rates on the density profiles were analyzed. Figure 3 shows the density profiles of the

Figure 1: Gamma densitometry system with Plexiglas packed bed column

Figure 2: The gamma ray source and detector are mounted in two axial locations with motorized parallel movement.

empty column, column with water, and column with catalyst. The graph shows density profiles where not symmetry because of catalyst were not fully packed and observe of air between the catalyst.

Figure 4 shows similar results of density profiles of various condition of the flow rates of gas and liquid. Unsymmetrical density profiles also observed. This is indicating liquid and gas channelling occur due to the catalyst was not properly packed in the column. Further experiment will be conducted to examine and fixed the catalyst packed in the column.

4 Conclusion

In summary, this preliminary study demonstrates that gamma densitometry can be an effective technique for non-invasively determining the density profile in packed bed reactors. The key advantages of gamma densitometry are its non-invasive nature, ability to distinguish between phases, and applicability to opaque multiphase reactor systems. Further work should explore the effects of factors like particle properties, packing

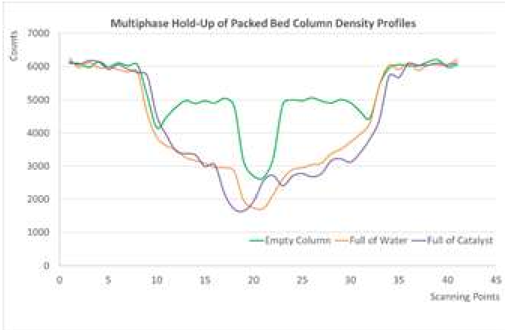

Figure 3: Area on the step wedge used for contrast sensitivity calculation

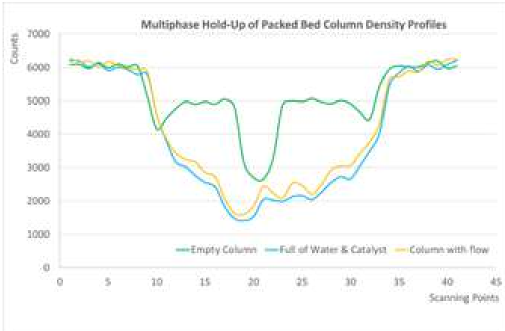

Figure 4: Area on the step wedge used for contrast sensitivity calculation

geometry and column inclination on the hold-up. Overall, this study demonstrates gamma densitometry to be a promising technique for packed bed characterization and performance improvement.

References

C. Boyer, A. Koudil, P. Chen, and M.P Dudukovic. 1990. Study of liquid spreading from a point source in a trickle bed via gamma-ray tomography. *Industrial Engineering Chemistry Research*, 29(7):1288–1295.

M.A. Islam. 2008. Unified measurement technique for the hydrodynamic parameters in trickle-bed reactors using gamma-ray densitometry. *Chemical Engineering Science*, 63(7):1889–1902.

A. Kantzas, B.B. Halvorsen, and J.R. Grace. 1988. Multiphase flow measurement techniques. *The Canadian Journal of Chemical Engineering*, 66(4):529–541.

S.B. Kumar and M.P Dudukovic. 1997. Computer assisted gamma and x-ray tomography: Applications to multiphase flow systems. *Noninvasive Instrumentation and Measurement in Medical Diagnosis*, pages 28–84.

S.B. Kumar, M.P. Dudukovic, and B.A. Toseland. 1995. Measurement techniques for local and global fluid dynamic quantities in two and three phase systems. *Non-Invasive Monitoring of Multiphase Flows*, pages 1–78.

J.M. Van Baten and R. Krishna. 2001. CFD simulations of mass transfer from taylor bubbles rising in circular capillaries. *Chemical Engineering Science*, 56(4):1117–1126.

Individual Research Contribution Review, 2023, 1(1): 203–204

Electron Beam Irradiated TiO_2 Nanorod Thin Films for Photoelectrochemical Water Splitting (Hydrogen Generation)

Masliana Muslimin
Industrial Technology Division, Malaysian Nuclear Agency
43000 Kajang, Selangor
masliana@nm.gov.my

Abstract

Photoelectrochemical (PEC) water splitting holds great promise for harvesting solar energy. We found that the high energy electron beam (EB) irradiation has a strong influence on the photoelectrochemical water splitting performance of TiO_2 nanorods thin films (TiNRTF) under UV light illumination. TiO_2 nanorods thin films were grown by using facile hydrothermal route on FTO substrate and subjected to electron beam irradiation (3 MeV) afterwards. The influences of the EB on the photocurrent density of the TiNRTF were investigated. TiNRTF irradiated with 1300 kGy have a higher photocurrent density than TiNRTF irradiated with 1000 and 1100 kGy as well as unirradiated TiO_2. This work proposes that the EB irradiation technology can effectively alter the photocatalysts to significantly improve the water splitting activity.

Keywords: TiO_2 nanorods, e-beam, PEC water splitting

1 Introduction

Hydrogen fuel can be produced from clean and renewable energy sources and, thus, its life cycle is clean and renewable. Solar is one of the major sources of renewable energy and they are also the promising sources for renewable hydrogen production. However, presently, renewable energy contributes only about 5% of the commercial hydrogen production primarily via water electrolysis, while other 95% hydrogen is mainly derived from fossil fuels. Renewable hydrogen production is not popular yet because the cost is still high. Alternatively, photocatalytic water-splitting using TiO_2 for hydrogen production offers a promising way for clean, low-cost and environmentally friendly production of hydrogen by solar energy.

Nanostructured titanium dioxide (TiO_2) attracts considerable current interest because of its modified electronic and optical properties which have numerous applications that include photovoltaic cells, photocatalytic processes and gas sensors (Rajamanickam and Ramachandran, 2020; Wang et al., 2020; Maziarz, 2019). Surface nano-structuring of a TiO_2 thin film is of great importance as the morphology of the film, to a great extent, determines many of its properties. Nowadays, electron beam (EB) irradiation is known as a valuable and innovative tool for the engineering and modification of materials at the nano/atomic scales. A highly energetic EB irradiation offers unique capabilities for structuring materials and for tailoring functional properties. When high energy EB irradiation is applied to oxide samples under high-vacuum conditions, defect sites, such as oxygen vacancies, tend to form in the surface structure, modifying the electronic structure of the oxides (Chung et al., 1977). In this study, we demonstrated that post-treatment with high energy EB irradiation for TiO_2 nanorods is an effective photoelectrode approach for efficient PEC water splitting devices.

2 Experimental Methods

On FTO substrate, TiO_2 nanorods were grown via the facile hydrothermal route and they were then post treated with EB irradiation (3 MeV). 10 ml of concentrated hydrochloric acid, HCl were dissolved in 10 ml of deionized (DI) water, to make growth solution for TiO_2 nanorods. Then, 0.7 ml of titanium butoxide was added using micropipette and vigorously stirred for 15 minutes. The hydrothermal process was then started by pouring the solution into the autoclave with a Teflon-made liner. The hydrothermal reaction occurs at 170°C and last for 30 minutes. The autoclave was then removed from the oven and allowed to cool to room temperature. The sample was subsequently rinsed with DI water and heated on a hotplate for 5 minutes at 100°C.

The prepared samples were subjected to 3 different doses of electron bombardment (1000 kGy, 1100 kGy and 1300 kGy). PEC measurements were carried out in a conventional three-electrode configuration, with a saturated calomel reference electrode, platinum plate counter electrode, and the TiO_2 films as the working electrode, in a quartz-windowed cell. We used 0.5 M Na_2SO_4 as the electrolyte. An electrochemical workstation (CHI660D) and a 5 W UVC lamp were used for photocurrent density e-potential measurements. Linear sweep voltammetry of OER were obtained for the samples before and after irradiation to determine the photocurrent density for the reactions. All electrochemical characterizations were carried out using 020018-2 Autolab PGSTAT128N at scan rate of 10 mVs^{-1}. All potentials vs Ag/AgCl were converted to reversible hydrogen electrode (RHE) using the formula below:

$$V(RHE) = V(Ag/AgCl) + 0.6106V \tag{1}$$

3 Results

Figure 1 shows the linear sweep voltammetry (LSV) curves, represent the PEC performances of the unirradiated and irradiated TiO_2 nanorods electrode, respectively. When illuminated by the UVC lamp, irradiated TiNRTF photoanode shows a remarkable enhancement in photoresponse. It is observed that the unirradiated TiO_2 electrode displays a relatively low photo-response over the whole potential window with a photocurrent density of 0.4 mA/cm^{-2}. While the irradiated TiO_2 electrode exhibits a remarkably increase in photocurrent density (0.7, 0.6 and 1.1 mA/cm^{-2}) for 1000 kGy, 1100 kGy and 1300 kGy accordingly. As the highest doses give the highest value of photocurrent. In addition, irradiated TiNRTF (1300 kGy) photoelectrode exhibited a cathodic shift of the onset potential of 1.23 V. This negative shift of potential increases the overpotential for charge transfer, suggesting the less hole transfer barrier at the irradiated TiO_2/electrolyte interface (Bian et al., 2015). In terms of photocatalytic activity, all the samples show oxygen evolution reaction (OER) improvement under the UV light irradiation, attributed to the generation of photoexcited charge carriers. This result demonstrates that the introduction of EB irradiation onto TiO_2 can significantly improve the PEC efficiency.

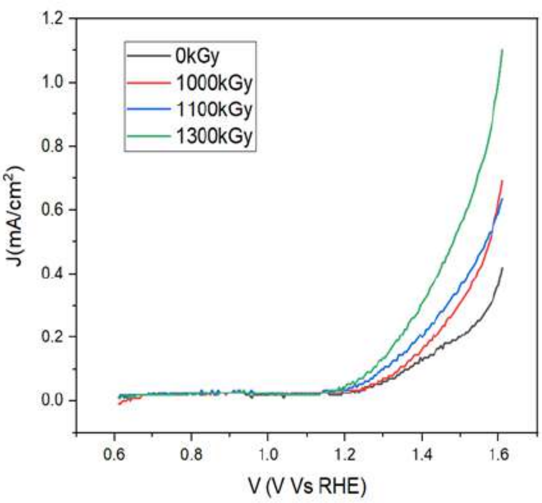

Figure 1: LSV curves of unirradiated and irradiated TiO_2 nanorods

4 Conclusion

In summary, hydrothermal synthesized TiNRTF have been irradiated by EB and used as working electrodes in PEC studies for hydrogen generation from water splitting. Irradiated TiNRTF (1300 kGy) has a higher photocurrent density than unirradiated TiO_2 or other irradiated TiO_2. In the future, studies will be conducted to quantitatively compare the PEC performance of TiNRTF produced by EB irradiation post-treatment with different strategies including doping and sensitization.

References

J. Bian, Q. Li, C. Huang, J. Li, Y. Guo, M. Zaw, and R.Q. Zhang. 2015. Thermal vapor condensation of uniform graphitic carbon nitride films with remarkable photocurrent density for photoelectrochemical applications. *Nano Energy*, 15:353–361.

Y. W. Chung, W. J. Lo, and G. A. Somorjai. 1977. Low energy electron diffraction and electron spectroscopy studies of the clean (110) and (100) titanium dioxide (rutile) crystal surfaces. *Surface Science*, 64(2):588–602.

W. Maziarz. 2019. Tio_2/sno_2 and tio_2/cuo thin film nano-heterostructures as gas sensors. *Applied Surface Science.*, 480:361–370.

N. Rajamanickam and K. Ramachandran. 2020. Improved photovoltaic performance in nano Tio2 based dye sensitized solar cells: Effect of TiCl4 treatment and Sr doping. *J. of Colloid and Interface Science.*, 580:407–418.

S. Wang, Z. Ding, X. Chang, J. Xu, and D.-H. Wang. 2020. Modified nano-tio_2 based composites for environmental photocatalytic applications. *Catalysts*, 10(7):759.

Individual Research Contribution Review, 2023, 1(1): 205–206

A Study on The Appropriate Elevation from The Ground Using the Neutron Backscatter Technique before In-Situ Measurement Performed

Md Fakarudin Ab Rahman
Industrial Technology Division, Malaysian Nuclear Agency
43000 Kajang, Selangor
fakarudin@nm.gov.my

Abstract

This paper provides the appropriate distance measurement using neutron backscattered technique during measurement of the sample from the surface before the measurement can be performed. It is a very important measurement to avoid incorrect decision from the measurement taken during in-situ measurement. Americum 241/Berylium (Am-Be 241) fast neutron source with 50mCi in activity has been chosen.

Keywords: Neutron Backscattered, fast neutrons

1 Introduction

Three sources can produce neutrons: isotope sources, nuclear reactors, and neutron generators. Consequently, in the absence of any interaction with the electric fields of electrons or nuclei, neutrons can penetrate matter relatively deeply. Fast neutron will be thermalized when collide directly with an atom of a light element, like a hydrogen nucleus. This is due to very light neutrons preferentially exchange momentum and energy with similar sized particles. Rapid neutrons with energies between 0.5 and 11 MeV have the potential to "thermalize," or slow down, and lose energy to become thermal neutrons, which have energies of 0.25 eV.

The thermal neutron that was created during the thermalization process had a brief travel path but was dispersed in all directions. The detector counts the neutrons that are scattered back towards the scanning head from among these thermal neutrons. Higher concentrations of hydrogen will reflect more neutrons back to the detector. Any hydrogenous substance, such as water, hydrocarbons and concrete can be determined.

Several industrial processes like petroleum, chemical and power generation industries require continuous measurement of interface level to operate efficiency and guarantee uniform product quality. Determination of moisture exists in certain location of the wall in process vessel or storage tank is also considered as extremely important for the assessment and improvement of the plant performance. The technology used in measurement of interface level is known as the 'neutron backscattered' technique which is based on measuring the hydrogen concentration of material. This technique is a non-destructive method where a slow-level radioactive source is used to generate the high-energy neutrons, collide with hydrogen atom, slowed down, and the backscattered neutron (part of thermal neutron) bounced back toward the source and measured by a thermal neutron detector. The detector response is recorded as count rate on the portable electronics gauging system.

2 Methods

The Am-Be 241, 50mCi fast neutron produced during the thermalization process had a short travel path but was scattered in all directions. Among these thermal neutrons, the detector counts the neutrons that are scattered back towards the scanning head. The scattering process is responsible for energy loss and slowing down of neutrons. If neutron energy before collision is denoted by E_1, neutron energy after collision is denoted by E_2, and A is the mass number of nucleus, it is possible to show that the energy transferred to the nucleus in a head-on collision is (Md Fakarudin Ab Rahman, 2012):

$$\frac{E_2}{E_1} = (\frac{A-1}{A+1})^2 \tag{1}$$

From Equation (1), it can be seen that it is possible for a nucleus to lose all its kinetic energy in head-on collision with hydrogen nucleus. It is clear that the hydrogen is the major factor in the slowing down of fast neutrons (Md Fakarudin Ab Rahman, 2012). When in use, the measuring probe (comprising fast neutrons) positioned adjacent to slow neutron detector is suspended at the material. The detector will count the resulting flux. The detector count rate displayed on the electronic unit depends directly on hydrogen concentration of the surrounding medium. The equipment used for NBT is portable Hydrotector which uses Americium- 241/Beryllium (Am/Be) as the neutron source.

2.1 Device

Portable electronics gauging system has been used for this experimental including:
i) Detector: CPN MCM2- DETECTOR
ii) Radioactive source: Americium-241: Beryllium
iii) Type of radiation: neutron
iv) Survey meter calibration
v) Height marking tools
vi) Measuring tape

2.2 Procedures

1. The portable electronics gauging system is set up as follows:

(i) The readout display unit is connected to the pole assembly by plugging the cable into the readout display unit.
(ii) STD is pressed then STEP then ENTER. STEP is pressed again to view CHI ratio. This is statistical measurement which should fall between 1.25 and 0.75 for a properly working unit.
(iii) To start a new check count, STEP is pressed again. The screen will display NEW CHK. To START the test, ENTER is pressed.
(iv) The detector assembly is pushed against the ground.

2. Measuring tape is used to mark the height starting from the 0 from the ground and elevate with the range 5 cm each at height marking tools for slow neutron count/8sec.

3. The portable head is then placed closed to the bottom ground. The count is taken 3 times and the average is calculated.

4. The portable is elevated 5cm and the count is taken.

5. Step 5 is repeated until the highest position from the surface.

6. The recorded counts are plotted into graph and are analyze.

3 Data/Results

The standards an air counts refer to slow neutron counts/8sec have been taken as references measurement.

3.1 Standard and air counts

Table 1: Standard Count

No. of measurement	Slow neutron counts/8sec
s1	26602
s2	26502
s3	24495
s4	25327
Average	**25736**

Table 2: Air Count

No. of measurement	Slow neutron counts/8sec
1	495
2	390
3	375
Average	**420**

3.2 Neutron counts/8se for every height

The table of neutron counts for every 2cm have been recorded in table 3 below.

Table 3: Elevation Counts

Height (cm)	Neutron Counts/ 8sec			
	1	2	3	average
5	2955	3053	3368	3125
10	1898	2018	2155	2023
15	1470	1208	1528	1402
20	938	1155	1170	1087
25	923	1065	990	992
30	690	945	803	812
35	893	743	653	763
40	638	705	585	642
45	615	635	593	614
50	593	630	465	562
55	443	638	683	588
60	615	495	518	542
65	518	503	495	505
70	368	585	530	494
75	420	488	473	460
80	360	525	690	525

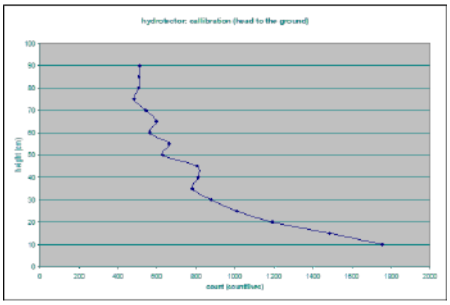

Figure 1: Graph elevation vs neutron count/8sec

4 Discussion/Conclusions

4.1 Discussion

A study has been established on the proper appropriate elevation from the ground using the neutron backscatter technique before in-situ measurement performed. We can understand from the measurement graph that as the slow neutron counts decreased after portable electronics gauging system elevated. The results revealed that ground measurement has been affected by hydrogen concentration presence. The slow neutrons decreased as it elevated and almost to the air counts.

4.2 Conclusion

As concluded, the appropriate height or elevation of the portable gauging system of neutron backscattered technique during in-situ measurement is not less than 30cm from the ground.

References

D. J. Abdullah. 2005a. Gamma scanning can aid in troubleshooting and optimisation of distillation columns. *Malaysian Institute for Nuclear Technology Research*, pages 1–4.

D. J. Abdullah. 2005b. Poliscanner, neutron backscatter technique. *Malaysian Institute for Nuclear Technology Research*, pages 1–4.

I. M. Md Fakarudin Ab Rahman. 2012. Detection of pipeline by neutron device. *Jurnal Sains Nuklear Malaysia*, pages 35–42.

P. Priyada, M. Margret, R. Ramar, and Shivaramu. 2012. Intercomparison of gamma ray scattering and transmission techniques for fluid-fluid and fluid-air interface levels detection and density measurements. 70(3):462–469.

Individual Research Contribution Review, 2023, 1(1): 207–208

Application of Silicon Photomultiplier (SiPM) in Scintillator Based Gamma Detector

Megat Harun Al Rashid Megat Ahmad
Industrial Technology Division, Malaysian Nuclear Agency
43000 Kajang, Selangor
megatharun@nm.gov.my

Abstract

A silicon photomultiplier (SiPM) operating at 30V was evaluated as a replacement for photomultiplier tube (PMT) in a scintillator based gamma detector. A Bismuth Germanate (BGO) single crystal was used as the scintillator and placed on top of SiPM in a photon tight small container with simple electronics for data collection. Pulse signal of the SiPM was monitored on an oscilloscope when this system was exposed to gamma sources. Initial findings show the SiPM exhibits superlative performance allowing the possibility of building small low voltage small compact size gamma spectrometer.

Keywords: SiPM, scintillator, ionizing radiation, sensor

1 Introduction

Radiation spectrometry based on scintillation traditionally used photomultiplier tube (PMT) that utilizes series of dynodes to multiply the small amount of photons produced by the scintillator million of times. This type of PMT usually requires hundreds of volts in operating voltage that may not be suitable to be used in industrial premise because of safety precaution. The current alternative to this classical PMT is Silicon Photomultipliers (SiPM) that can be operated in tens of volts only. The SiPM is an already established photodetector having used in many fields of basic scientific research (F and S., 2019). The SiPM is a solid state semiconductor photodetector made of an array of hundreds or thousands of single-photon avalanche diodes (SPADs) or Geiger-mode avalanche photodiodes (Gm-APD). All these SPAD are independent and connected to a common readout. A SPAD can generates a large electric output signal even when exposed to a single photon due to internal avalanche multiplication.. Herewith, we evaluate an SiPM as a replacement for PMT in a simple radiation detection setup using a single crystal Bismuth Germanate (BGO) scintillator. Detection pulses characteristics from the SiPM were then analyzed.

2 Methods and Materials

The SiPM (SensL MICROFC-SMTPA-30035-GEVB) was placed on a breadboard inside an in-house designed photon tight container. The teflon covered BGO was placed on top of the SiPM array cell. A generic bias filter was used to stabilize the input voltage from a 9V battery (Energizer Max) that amplified to 29.5V breakdown overvoltage using a DC to DC converter (XL6009E1). Direct measurement were carried out using an oscilloscope (Tektronix TDS 2004B). Small gamma radiation sources (^{60}Co and ^{137}Cs) were then used to observe pulses from the oscilloscope by placing them right on top of the BGO scintillator.

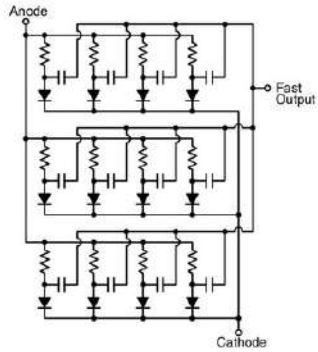

Figure 1: An SiPM consists an array of SPADs with sum outputs (ONSEMI publication AND9970/D).

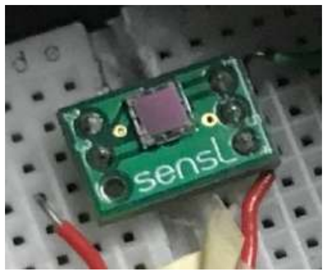

Figure 2: The SiPM board used on a breadboard.

Table 1: Specifications of SiPM used.

Specifications	Values
Area Size (mm^2)	9
Cell size (μm^2)	35
Breakdown voltage (V)	24.2 – 24.7
Spectral range (nm)	300 - 950
Peak Wavelength (nm)	420

Table 2: BGO scintillator properties.

Properties	Values
Size (w x h x l, mm)	5 x 25 x 10
Max emission (nm)	480
Cutoff (nm)	320
Primary decay time (ns)	300
Light yield (photons/keV)	8 - 10

3 Discussion and Conclusion

Pulses obtained show a variation in height. ^{60}Co pulses are mostly higher compare to ^{137}Cs pulses indicating the energy discriminating capability of SiPM. Some of the lower height pulses resulted from scintillation caused by photons from Compton inelastic scattering and photoelectric effect as well as pair production in the case of ^{60}Co source. All pulses have a decay time of about 2μs.

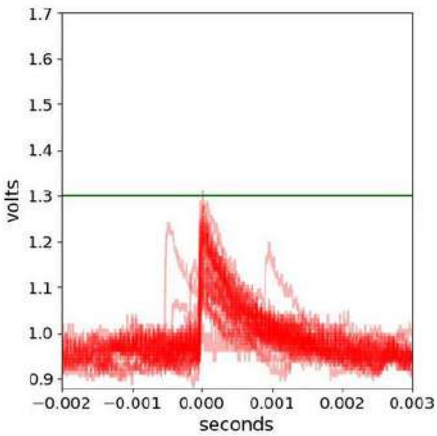

Figure 3: Pulses of ^{137}Cs

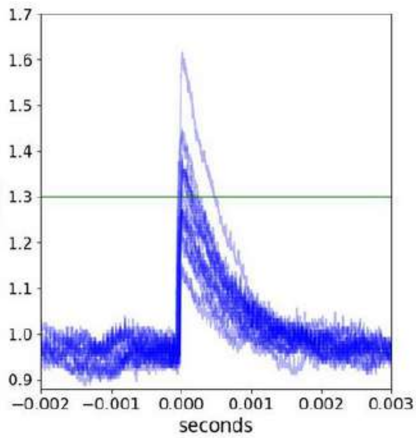

Figure 4: Pulses of ^{60}Co

Some data contained more than one pulse per measurement. This event as well as the shape and height of the pulses allows us to properly design the signal processing electronics later on. This initial work also provides further insight on development of other scintillator based particle detectors in particular for neutron scattering and muon tomography as well as using SiPM in photonic based analogue computation.

References

Acerbi F and Gundacker S. 2019. Understanding and simulating SiPMs. *Nuclear Instruments and Methods in Physics Research Section A*, 926:16–35.

Individual Research Contribution Review, 2023, 1(1): 209–210

Ionizing Radiation Detection Algorithm for CMOS Sensor from Consumer Camera Device

Megat Harun Al Rashid Megat Ahmad
Industrial Technology Division, Malaysian Nuclear Agency
43000 Kajang, Selangor
megatharun@nm.gov.my

Abstract

Laplacian of Gaussian (LoG) algorithm was applied as counting algorithm to quantify ionizing gamma events on CMOS sensor in a webcam. The webcam camera was fully covered allowing only gamma radiation to reach the CMOS sensor and none of the visible lights. The CMOS was operated to record movie of ionizing events by exposing the webcam to a 241 Am gamma source. Scikit image software library was used to perform the LoG algorithm on the frame by frame movie data collected to identify cluster of bright pixel values that correspond to charge collection for individual ionizing event. The very thin thickness of CMOS nevertheless hindered the building of gamma spectrum based on these charge collection values alone.

Keywords: Laplacian of Gaussian, CMOS, ionizing radiation, sensor

Figure 1: The webcam used for capturing ionizing events in a movie frame.

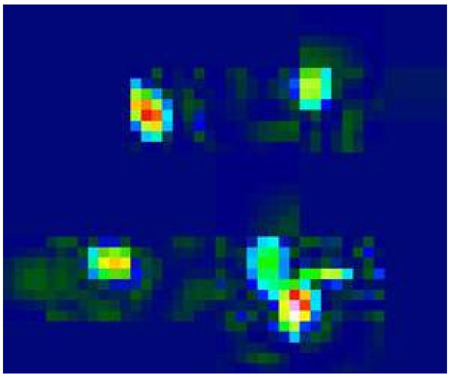

Figure 2: Cluster of bright pixels captured on a movie frame (enlarged area).

1 Introduction

Inexpensive and readily available consumer camera device with CMOS sensor has been shown able to detect ionizing radiation (Ahmad et al., 2021). An ionizing event on this detector can be observed as clustering of bright pixels on the detector image frame which are quite similar in appearance to bright celestial objects in astronomical image observation. Similar method for detecting these astronomical objects therefore can be applied to detect ionizing events on CMOS image frame. The Laplacian of Gaussian (LoG) algorithm is one of the technique quite commonly used for astronomical objects identification by edge detection. Herewith, we applied the LoG to identify the central pixel position for each ionizing events on the CMOS image frame allowing us to quantify and give a reference area coordinate for further data computation of charge collection values that can be used to discriminate energy spectrum.

2 Methods and Materials

The description of CMOS sensor used and experimental procedure were the same in previous report (Ahmad et al., 2021) with modifications i.e. the CMOS sensor instead functioned as a camera in which a movie of ionizing events was first taken for each radiation exposure before data processing and this resulted in more data frame per exposure time. The movie recording cycle was about 3.3 seconds (total of 99 frames or 30 frames/second). Three measurements were carried out for each source to detector distance of 0 to 5 cm. Noise removal from all image data frames were done by subtracting each pixel values with the frame median value. The source of radiation used was ^{241}Am (100μCi). The movie was later processed frame by frame using the LoG function in scikit-image python library. The software tool for experimental control and details of data processing can be found in Ref (https://doi.github.com/puspati2Ion/cmos-radiation detector,).

Table 1: Common photon (gamma and *X-rays) energies.

Source (Nuclide)	Energies, keV (photons/100 disintegration)
^{241}Am	59.54 (35.92), 26.34 (2.31), 33.20 (0.12), *11.89-22.2 (37.66)

3 Discussion and Conclusion

The thin layer of the CMOS indicates that the probability of any ionizing event is very low. The ^{241}Am source used with its relatively low energy gamma photons allowed higher ionizing event to be captured for better statistics.

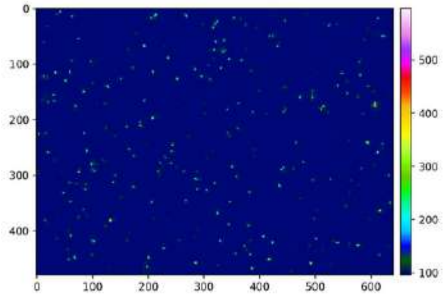

Figure 3: Summation of all ionizing events of all frames for a measurement at 5 cm source to detector distance.

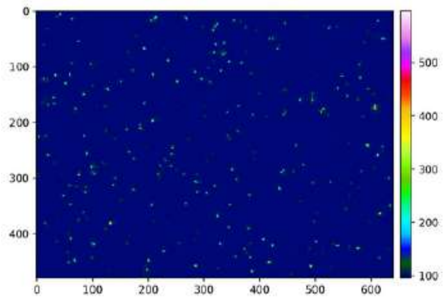

Figure 4: LoG identification of these ionizing events coordinates (shown as enlarge rings).

The output of LoG algorithm in scikit-image python library provides a list of image coordinates (center of rings as shown in Figure 4). Charge collection value was then calculated by summing all pixel intensities in the pixel area of 441 (21 x 21). Summation value for all the bright pixels inside the cluster area were then discriminated into channels to obtain a ^{241}Am spectrum for evaluation.

Two visible peaks can be discerned in Figure 5 spectra for 0 and 1 cm source to detector distances. These peaks are at around 700 and 1300 of charge collection values. At much larger source to detector distances, no discernible peaks can be seen because of insufficient ionization events and thus poor statistics. These two peaks perhaps represent gamma energy at 59.5 and 11-22 keV.

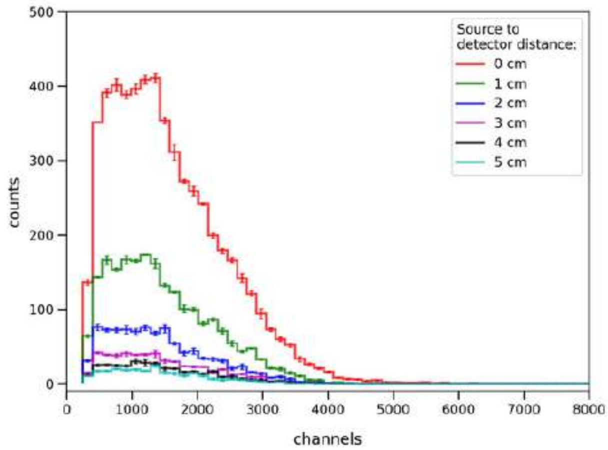

Figure 5: Spectra of ^{241}Am

References

Megat Harun Al Rashid Megat Ahmad, Glam Hadzir Patai Mohamad, Ishak Mansor, Abul Adli Anuar, Norizam Saad, Noryana Abdul Razak, Abdul Bakhri Muhamad, Shaharuddin Sayuti, and Shukri Mohd. 2021. Detection of ionizing radiations using cmos sensor from consumer camera device. *TechRxiv*, page https://dpi.org/10.36227/techrxiv.13705414.v1.

https://doi.github.com/puspati2Ion/cmos-radiation detector.

Individual Research Contribution Review, 2023, 1(1): 211–212

Research Acoustic Emission Testing on Selected Marine Valves

Mohamad Ridzuan Ahmad
Industrial Technology Division, Malaysian Nuclear Agency
43000 Kajang, Selangor
ridzuan_a@nm.gov.my

Abstract

The AET was conducted from 30th Nov to 1st Dec 2018 on Main IG 4C Valve, IG Purge 4C Valve, and IG Purge 5S of FPSO Bertam as in Figure 2. Minimum of eight AE sensors are used for the inspections where four sensors are placed on the body of the valves with two sensors have been attached on each of upstream and downstream of the valves. Two days are needed to complete the AET on all three valves, due to inspection window availability afforded by Offshore Marine Department (Operation). The opportunity to perform AET on these Marine Valves is due to the delayed COT4C tank entry for the supposed inspection of COT4C frames structure.

Keywords: Classification, Acoustic Emision, Valve

1 Introduction

Acoustic Acoustic Emission testing (AET) is a non-destructive testing method that has been applied in the petrochemical industry since the early 1980s with several well-proven codes and standards. In shipping and marine industry, the method has been applied in oil tankers and containerships. The Acoustic Emission process begins when forces acting on a body that result in changes in the stress field and localized deformation at defect sites. These localized deformations produce Acoustic Emissions, elastic waves that travel outward from the source, echoing through the body until they arrive at a remote sensor. The elastic waves manifest themselves as in-plane and out-of-plane displacements that cause the sensor to produce an electrical signal, which is passed to electronic equipment for further processing.

2 Methods

The acoustic emission system has Vallen AE-Suite Software which is made up of individual modules. A module can contain a standalone application, e.g. VisualAE, VisualTR, VisualClass, etc or enhancements to existing software (e.g. location-and data processor modules). If a module consists of a number of applications – which is usually the case – it is also referred to as a software package. A module of package provides certain functionality, such as data acquisition, hardware management, data analysis, system verification, etc.

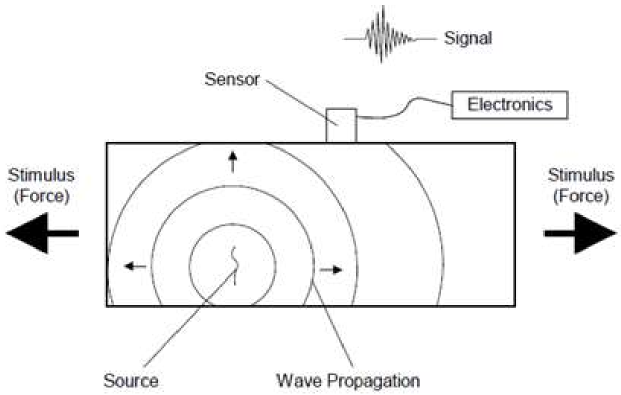

Figure 1: Schematic Diagram of Acoustic Emission Technique.

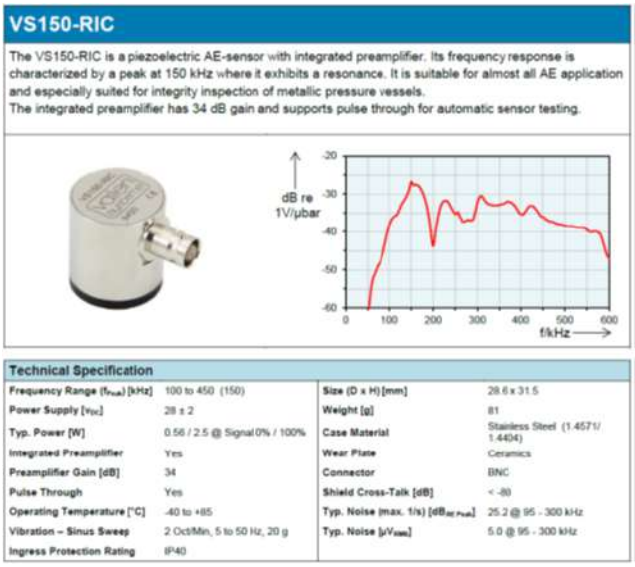
VS150-RIC

The VS150-RIC is a piezoelectric AE-sensor with integrated preamplifier. Its frequency response is characterized by a peak at 150 kHz where it exhibits a resonance. It is suitable for almost all AE application and especially suited for integrity inspection of metallic pressure vessels.
The integrated preamplifier has 34 dB gain and supports pulse through for automatic sensor testing.

Technical Specification

Frequency Range (f_{Peak}) [kHz]	100 to 450 (150)	Size (D x H) [mm]	28.6 x 31.5
Power Supply [V_{DC}]	28 ± 2	Weight [g]	81
Typ. Power [W]	0.56 / 2.5 @ Signal 0% / 100%	Case Material	Stainless Steel (1.4571/ 1.4404)
Integrated Preamplifier	Yes	Wear Plate	Ceramics
Preamplifier Gain [dB]	34	Connector	BNC
Pulse Through	Yes	Shield Cross-Talk [dB]	< -80
Operating Temperature [°C]	-40 to +85	Typ. Noise (max. 1/s) [$dB_{AE\ Peak}$]	25.2 @ 95 - 300 kHz
Vibration – Sinus Sweep	2 Oct/Min, 5 to 50 Hz, 20 g	Typ. Noise [μV_{RMS}]	5.0 @ 95 - 300 kHz
Ingress Protection Rating	IP40		

3 Result and Discussion

The pressure noise from body of the valve indicated higher AE noise compared to the background from the upstream and downstream of the valve. The high pressure noise shows that the valve is passing and form the turbulence flow. 20dB difference from the valve body with respect to upstream and downstream indicates medium passing occurrence.

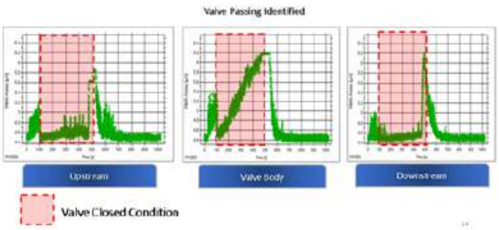

Figure 12: RMS Signal at Main IG 4C

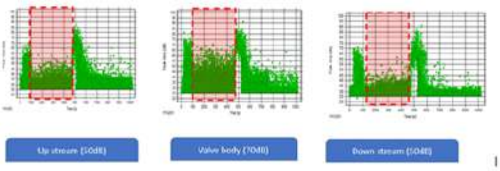

Figure 13: Hit Signal at Main IG 4C

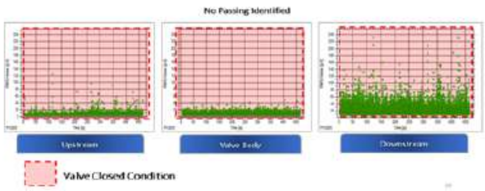

Figure 14: RMS Signal at IG Purge 4C

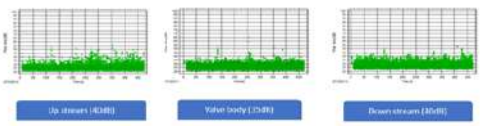

Figure 15: Hit Signal at IG Purge 4C

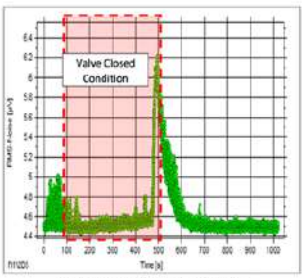

Annex 3: Downstream Background Noise of Main IG 4C

The measured pressure noise at body of the valve recorded lower RMS signal compared to the background noise at the downstream of the valve. Hit signal at body is lower compared to hit signal to upstream and downstream indicating there are no turbulence flow occurred, the valve in good condition.

4 Conclusion and Attention

AE sensors are used to determine valve passing from the measured pressure noise and background noise of the inspected valves. Three valves consist of Main IG 4C, IG Purge 4C, and IG Purge 5S have been inspected for the valve passing test.

RMS level for the measured noise in body of the valve is used to determine the event of valve passing. As the result, valve passing has been identified at the Main IG 4C while no passing was identified from the rest two valves.

References

Hanxue Zhao, Zhenlin Li, Shenbin Zhu, and Ying Yu. 2020. Valve internal leakage rate quantification based on factor analysis and wavelet-bp neural network using acoustic emission. *Applied Sciences (Switzerland)*, 10(16).

Individual Research Contribution Review, 2023, 1(1): 213–214

Development of International Standard (ISO) on Measurement of Fluid Flow Rate in Closed Conduits – Radioactive Tracer Methods

Mohd Amirul Syafiq Mohd Yunos
Industrial Technology Division, Malaysian Nuclear Agency
43000 Kajang, Selangor
syafiq@nm.gov.my

Abstract

International Standards mean that users can have confidence that their products and services are safe, reliable and of good business quality in troubleshooting processing plant problems and anomalies especially involving the flow measurement that measure the unpredictable differences in flow rate of liquid and gas flowing through the pipelines. This international standard development defines the use of radioactive tracer methods in the measurement of homogeneously single-phase fluid (gas or liquid) flows in closed conduits. This method of measurement is applicable only to single-phase homogeneous fluid mixtures in order to measure the fluid flow rate accurately. This International Standard Organization (ISO) standard is developed to fill the need for a generalized reference based on fundamental principles to measure fluid flow using radioactive tracer methods. It defines the terms and principles needed for intelligent consideration of radioactive tracer methods for any single-phase fluid flow flowing in closed circuits.

Keywords: Fluid flow rate, Radioactive tracer, Pipelines, Single phase, Standards

1 Introduction

The performance of industrial process systems can be examined and diagnosed with great benefit from the application of industrial radiotracer technology. When it comes to industry applications, radiotracer technology is an effective method because of its ability to offer real-time measurement.

Radioactive tracer methods are very competitive and sometimes unique for online measurement of flow rate in single phase flows flowing inside closed conduits. Radioactive tracer methods are already well accepted from industrial end users and established in routine service worldwide. Maintaining fluid flow quality performance in the systems depends on the flow rate or fluid velocity measurement.

ISO standards are basic elements of quality control and accreditation for recognition and cooperation in national and international market. There have been proposed several ISO standards dealing with radioactive tracer methods for measurement of water and gas flows in closed conduits during last five decades:

(i) ISO2975/VII Measurement of water flow in closed conduits – Tracer methods: Transit time method using radioactive tracers.

(ii) ISO4053 Measurement of gas flow in conduits – Tracer methods.

The ISO standards ISO2975 and ISO4053 issued in 1975-1977 addressed radioactive tracer methods respectively for water and gas flows. The ISO2975 is limited to water phase only, while ISO4053 dealt with gas phase, was withdrawn in 2001 leaving a void on this subject. The new development of ISO standard will replace both of them and focus on single-phase fluid.

2 Methods

Three methods for flow rate measurement are described in this ISO standard development which is pulse velocity or transit time method, constant rate injection method, and pulse injection integration method.

2.1 Transit Time Method

The transit time method, determines the flow rate by measuring the time it takes the radioactive tracer to travel between two detector locations or between the injection point and a detector location along the conduit. The method involves instantaneous injection of a gamma-emitting radiotracer into the pipeline at a selected location and monitoring its passage at two or more than two downstream locations using externally mounted radiation detectors as shown below.

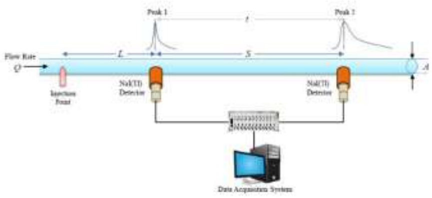

Figure 1: Illustration of flow rate measurement using transit time or peak to peak method

The first detector is mounted at sufficiently downstream location from the injection point at which complete lateral mixing of the radiotracer is achieved. The first moment of the radiotracer concentration curve is determined using the equation.

The geometric volume (V) between the two monitoring locations is determined from the distance (L) and the cross-sectional area (A) of the pipeline. Knowing the geometric volume V, and mean transit time $\bar{t}$, the volumetric flow rate (Q) is calculated from the following simple relation:

$$Q = \frac{L.A}{\bar{t}} = \frac{V}{\bar{t_2} - \bar{t_1}} \quad (1)$$

Where $\bar{t_1}$ and $\bar{t_2}$ are first moments of tracer concentration curves recorded at two monitoring locations.

2.2 Constant Rate Injection Method

The constant rate injection method, applies a well-known constant rate injection of a radioactive tracer, and measuring the concentration of diluted radioactive tracer in the downstream conduit. In dilution technique, a tracer solution of known concentration (C_1) is injected into the flow stream at a constant rate (Q_1) for a particular duration of time. Samples are collected from a sufficiently downstream location, where the tracer is completely mixed within the flow. The tracer concentration (C_2) in the collected samples is measured. The discharge rate (Q_2) of the flow stream is calculated by following tracer balance equation:

$$Q_2 = Q_1 \frac{C_1}{C_2} \quad (2)$$

2.3 Pulse Injection Integration Method

The integration method, determines the flow rate by total counting of pulses of the radioactive tracer response crossing the radiation detector located downstream the conduit. This method known as total count method where the radiotracer is injected instantaneously and its concentration is recorded at a downstream sampling point during the entire passage of the tracer. The sampling point is selected in such a way that the radiotracer is completely mixed within the entire cross-section of the system. If A is the amount of injected radiotracer, then the tracer balance equation is calculated as below:

$$A = Q \int_0^\infty C(t)dt \quad (3)$$

The mixing criterion in this case is similar to that in the transit time method, that $\int_0^\infty C(t)dt$ is constant at any point in the flow cross-section at the sampling or measuring station. The total counts recorded during the passage of the tracer pulse are determined either in situ or by sampling method, although sampling yields better accuracies.

3 Analysis & Discussions

As with any measurement of a physical quantity, the determination of a flow rate in a conduit by tracer methods is subject to uncertainties related either to systematic errors due to errors in the measuring apparatus or in the measuring process used, or to a random error obtained by random variations in the flow system, or in the measuring equipment.

Uncertainty of a flow rate measurement using radiotracers and transient time method is composed by two components: the first one is characterized by the variance evaluated from residence time distribution (RTD) curves and the other is calculated from the statistical distribution of the results of series of measurements (injection) and can be characterized by statistical standard deviations.

3.1 Systematic Error

Although these cannot be estimated precisely, careful injection, collecting, counting analysis, and dilutions, as well as correction formulae for electrical frequency variations, dilution and counting systematic errors, or water density variation with temperature, practically guarantee that the systematic error of the result is very small, for example, less than 0.2%. It should be highlighted that by calibration and the application of correction factors, the components of error related to the utilized equipment or to verifiable procedures such the dilution of injected solution samples can be reduced to the minimum amount necessary. However, the conduit's dilution process can create faults that are more challenging to verify.

3.2 Random Error

The reliability and accuracy of the methods in this standard have to achieve statistical estimation of the tolerance (for 95% confidence limits), under general conditions of use. Thus, this standard development procedure includes the formulation development, testing, and verification. For gaseous fluids, the repeatability of flow must be examined, and in particular, the intervals of fluctuation of flow parameters must be determined beforehand in order for the aforementioned statistical laws to be applicable. The goal of uncertainty analysis is to quantify the variability of the output caused by the variability of the input such as error in mean count rate of collected samples, dilution ratio, uncertainty in half-life and error in infection rate includes the limit error of pump discharge rate, frequency, and density measurement.

4 Conclusion

In general, a higher total number of counts is required to obtain a statistical uncertainty of 1% at 95% confidence. Additionally, the calibration factor and the injected activity are also measured with an uncertainty of ±1%. Thus, a combined uncertainty of ±(1-2)% can be successfully achieved when measuring the flow rate. By achieving better accuracy in flow rate measurement, this ISO document has been accepted and published on 20 September 2023 titled as ISO24460:2023 – Measurement of fluid flow rate in closed conduits–Radioactive tracer methods. This document defines the measurement of single-phase fluid flow rate in closed conduits using radioactive tracer methods

References

ISO 2975-7. 1977. Measurement of water flow in closed conduits-tracer methods. Part 7: Transit time method using radioactive tracers.

Chmielewski A. et al. 2019. Radiotracers and nucleonic control systems applied in industry—polish case. *World Journal of Nuclear Science and Technology*, 9:27–66.

ASME MFC-13M. 2006. Measurement of fluid flow in closed conduits: Tracer methods. *The American Society of Mechanical Engineers*, New York, NY 10016.

H.J Pant, A. Kundu, and K.D.P Nigam. 2001. Radiotracer applications in chemical process industry. *Rev. Chem. Eng.*, 17:165–252.

Acoustic Emission Conditioning Monitoring of an above Ground Storage Tank Floor

Mohd Fajri Bin Osman
Industrial Technology Division, Malaysian Nuclear Agency
43000 Kajang, Selangor
fajri@nm.gov.my

Abstract

Acoustic emission (AE) is a non-destructive method used to measure tank and vessel condition. It detects acoustic vibrations from fluid flow turbulence. AE sensors detect defects using signal-based methods, and signal classification helps determine the most effective classifier. This technology reduces the need for inspection of tank floors due to the non-intrusive nature of AE.

Keywords: Tank, Vessel, Acoustic Emision

1 Introduction

Acoustic emission (AE) refers to the spontaneous generation of transitory elastic waves caused by sudden localised changes in stress or strain within a body. The stress changes that occur during crack propagation or plastic deformation can generate elastic waves. These waves can occasionally have a significant amplitude, making them detectable by transducers that are mounted to the surface of the body. This technology offers a non-invasive approach to ascertain the current state of corrosion on tank floors, eliminating the requirement to open, clean, and inspect them.

2 Methods

After isolating the tank, sensors are affixed to the tank's perimeter using magnetic holders. The sensitivity of the sensors was then tested on-site, ensuring a minimum sensitivity level of +/- 2db on average for all sensors. The tank was observed for a minimum test time of twelve hours, in accordance with the established Tank Floor testing technique for Acoustic Emission testing of Above Ground Storage Tank Floors. After the gathering of data, various sorts of analysis can be conducted for each tank. Standard or routine analyses include location analysis and cluster analysis.

i. The tank's activity is monitored and saved. It is then evaluated and categorised as A, B/C or D based on established criteria. This evaluation takes into account factors such as the tank's type, size, test threshold, and the type of product being stored. Before the evaluation, any irrelevant data is removed from the recorded information.

ii. The activities observed on the bottom of the tank, such as corrosion, leakage, and over-stress, can be identified by analysing the tank plots in the "All Data" report and conducting routine Cluster and Location Analysis.

iii. The data analysis reveals that severe corrosion and potential leak sources are more prevalent in the "Potential Leak" tank plots.

iv. Additional assessment of any sources with significant activity may be necessary in order to enhance the precision of the location. Tests a are conducted according to the company's existing test method, and the first test data is retained as a record for quality control purposes. The statistics, tank, and test data portions of this report provide comprehensive information and results regarding the storage tank.

This method is fundamentally routine and relies on expertise. It has the ability to accurately determine the general condition of the floor, particularly in terms of its activity. The tank assessment can result in three possible evaluations:

i. Good - A Grade : no additional measures needed;

ii. Intermediate - B and C Grades : indicating either overall activity or potential leak sources; or

iii. Poor - D Grade : necessitating interior inspection and repair.

This method aids in assessing the need for additional (internal) examination and repairs, making it an exceptionally efficient tool for maintenance planning. This tool is not primarily designed for leak detection or location purposes. Several sources of acoustic emission have been identified, although caution should be exercised when utilising this knowledge. The provided information does not include details on the remaining thickness of the floor plate. However, it is capable of distinguishing between tank floors that are severely corroded and those that are not corroded.

Insignificant leaks can be identified and do not have a substantial impact on the assessment or recommendation of the test. If the floor is actively corroding, even little leaks may be concealed. Although it is possible to identify significant leaks, they are likely to obscure other activities occurring on the floor.

3 Result and Discussion

The assessment encompasses all floor activities, such as corrosion noise and any other identifiable source on the tank

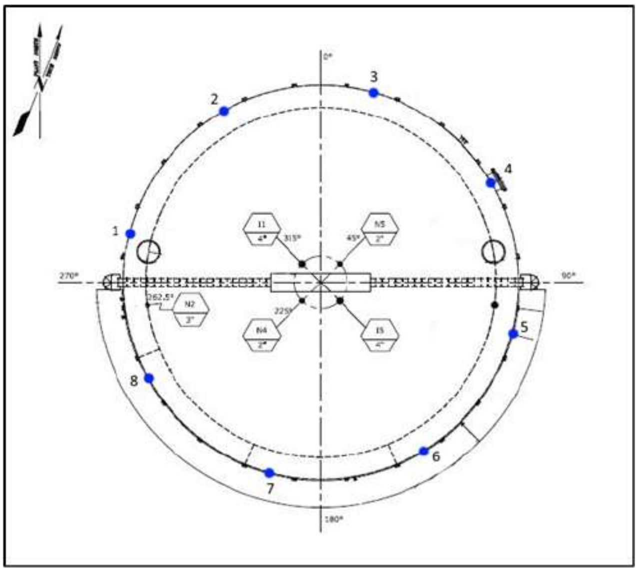

Figure 1: Acoustic Emission sensors arrangement setup

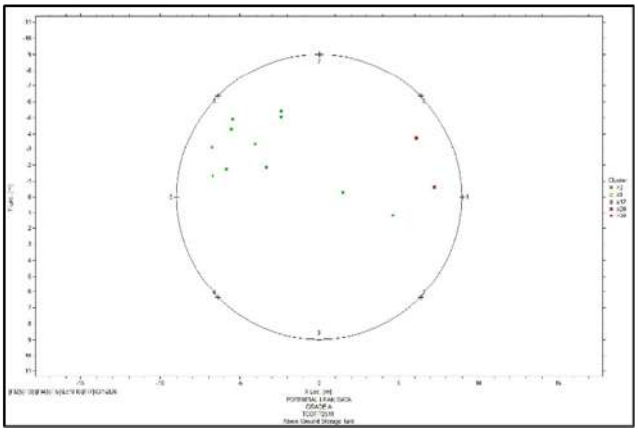

Figure 2: Potential Leak Data

floor, while ensuring that any irrelevant noise is eliminated if detected.

The manifestation of a possible leak is characterised by distinct features, typically displaying significant levels of energy or amplitude. Additionally, it may present as deep pitting or corrosion, along with locations that could potentially serve as sources of the leak.

4 Conclusion and Attention

During the experiment, it was found that the state of the stabilisation product did not match the required standards. Errors in the location were estimated to have happened, and it is recommended to repeat the process in order to achieve the best possible outcome. There is rusting or corrosion present surrounding the annular ring. The recommended re-test interval for maintenance planning purposes, using the Acoustic emission test, is normally 5 years, providing the tank is not opened

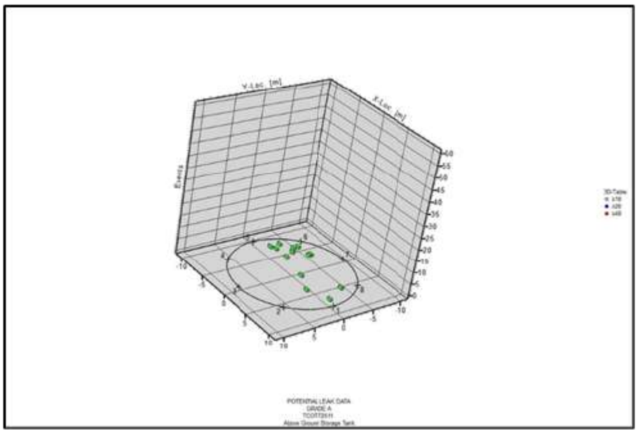

Figure 3: Potential leak data in 3D View

for inspection. Currently, there is no recommended course of action for Plant Maintenance/Inspection to undertake in terms of opening the tank and examining the floor.

References

Hanxue Zhao, Zhenlin Li, Shenbin Zhu, and Ying Yu. 2020. Valve internal leakage rate quantification based on factor analysis and wavelet-bp neural network using acoustic emission. *Applied Sciences (Switzerland)*, 10(16).

Conversion of Fortran Code for Process Tomography Image Reconstruction to Python

Mohd Fitri Abdul Rahman
Industrial Technology Division, Malaysian Nuclear Agency
43000 Kajang, Selangor
fitri@nm.gov.my

Abstract

Process tomography is an imaging technique used in industrial applications to visualize the internal characteristics of an object. Image reconstruction algorithms play a vital role in generating accurate tomographic representations. Traditionally, Fortran programming language has been used to implement such algorithms due to its computational efficiencies. However, Fortran lacks modern software capabilities and integration tools compared to advanced languages like Python. This work presents the conversion of Fortran code for an expectation-maximization (EM) based tomography image reconstruction technique to Python. The reconstructed images obtained from the Python implementation matched those from the original Fortran code. Python provided faster image processing and better visualization abilities. Additional techniques like gamma scanning experiments were also implemented in Python. The conversion enabled leveraging Python's vast libraries and tools for tomography image analysis. The work demonstrates Python's suitability for scientific computing and merits in reconstructing process tomography images.

Keywords: Fortran, Pyhton, Image Reconstruction

1 Introduction

Process tomography is an imaging technique used to visualize the internal characteristics of an object under observation. It involves capturing projections from multiple angles and using computational algorithms to reconstruct cross-sectional images representing the interior. Tomography finds extensive use in industrial applications like visualizing multi-phase flows in packed bed reactors, determining liquid distribution in trickle bed columns, and inspecting pipelines in oil and gas infrastructure (Kuzeljevic and Dudukovic, 2012; Roy et al., 2005).

Image reconstruction is a critical step in deriving high-fidelity tomographic representations from the captured projection data. Different analytical and iterative algorithms like filtered back-projection, algebraic reconstruction, and expectation-maximization (EM) have been developed for this purpose (Toze et al., 2020). Traditionally, the Fortran programming language has been utilized to implement such image reconstruction algorithms given its computational speed and ability to handle large matrices (Toye et al., 1997). However, Fortran lacks object-oriented capabilities, easy integration with external libraries, and advanced data visualization tools offered by more modern languages like Python.

This work focuses on converting existing Fortran code for an EM-based image reconstruction technique to Python. The key objectives are to leverage Python's vast ecosystem of tools and libraries for scientific computing, achieve modular and readable code, enable better data analysis and visualization, and lay the foundation for future extension and improvement of the reconstruction algorithms. The paper discusses the methodology for translating the core EM algorithm and the results obtained from the Python implementation. Additional techniques like column scanning simulations and gamma scanning experiments relevant to process tomography applications are also implemented. The work demonstrates the benefits and suitability of using Python for tomographic image reconstruction in an industrial setting.

2 Methods

The original image reconstruction code was implemented in Fortran based on the expectation-maximization (EM) algorithm for computed tomography (Shepp and Vardi, 1982). The key steps involved in the algorithm are:

i. Transmission ratio calculation: The ratio of radiation counts obtained by scanning the object versus counts for air is computed. This generates the projection data.

ii. Geometry matrix creation: The scan area is discretized into pixels and corresponding geometry coefficients are calculated.

iii. Initial guess: Start with an initial guess for the attenuation coefficient of each pixel.

iv. Image reconstruction: Implement the iterative EM update equations to estimate pixel attenuation coefficients.

v. Post-processing: Obtain phase fraction images and average azimuthally.

The core EM algorithm was translated from Fortran to Python while retaining the overall workflow. The NumPy library was leveraged to port the matrix and vector operations. Matplotlib was used for image visualization and analysis. The I/O handling was modified to use Python's built-in file operations.

Figure 1: Example coding for Averaging Process

To validate the Python code, test cases were generated using simulated projection data in text files. The images reconstructed from the Python code were compared to the original Fortran output for the same inputs. Additional techniques relevant to process tomography such as column scanning simulation and gamma scanning experiments were implemented in Python. This demonstrated integration with data acquisition and experimental validation aspects.

The Python implementation aimed to achieve modular functions, better readability via coding best practices, simplified data passing between steps, and efficient processing by utilizing NumPy vector operations. The goal was to reproduce the original Fortran output while enhancing maintainability, extensibility and leveraging the Python ecosystem.

3 Results and Discussion

The Python implementation of the expectation-maximization algorithm was validated using simulated test cases for process tomography analysis. The reconstructed images obtained from the Python code showed excellent agreement with the original Fortran output, thus verifying the accuracy of the translation. Figure 1 illustrates instances of Phyton programs that have undergone translation.

The modular structure and readability of the Python code allows for easier understanding, debugging and extension of the implementation. The ablation study conducted by removing certain sections of the code demonstrated the self-contained functionality enabled by the modular approach.

The performance of the Python implementation was comparable to the original Fortran code. While the compilation process in Fortran results in faster execution, the vectorized operations in NumPy combined with just-in-time compilation in Python reduced this gap significantly. The total execution time for a sample case was 1.2X faster for Fortran, indicating Python's suitability for scientific computing applications.

Python provided greater flexibility in analyzing the reconstructed images and intermediate outputs. Integration of matplotlib for plotting the EM iteration convergence helped visualize the trends. The scikit-image library enabled filtering, segmentation and quantitative characterization of the reconstruction output. Python's versatility in data analysis is a key advantage over Fortran. The work also demonstrated leveraging Python's numerics stack to implement related techniques like the column scanning simulation model and analysis of gamma scanning experiments relevant to process tomography. This showcases Python's ability to unify different aspects of the imaging pipeline under a common programming environment.

Certain memory-intensive operations were observed to be faster in Fortran, highlighting an area for further optimization using packages like Cython. Overall, the results indicate Python's viability as an alternative to replace aging Fortran code for image reconstruction while gaining modern software engineering advantages.

4 Conclusion

This work demonstrated the conversion of legacy Fortran code for process tomography image reconstruction to Python. The implementation in Python matched the output of the original Fortran code while providing better readability, modularity and integration with modern analysis libraries.

The results verified Python's capability to deliver the computational performance needed in reconstruction algorithms, making it a viable alternative to replace Fortran for such scientific computing tasks. Python's extensive tools and community support will enable easier extension of this work to incorporate newer reconstruction techniques and handle emerging data modalities.

By transitioning the tomography reconstruction codebase to Python, this project paved the path for enhanced visualization, quantitative characterization, experiment integration and overall improved maintainability. The work highlights the maturity of Python as a platform for not just prototyping but also production-grade scientific computing and industrial imaging applications.

Future efforts will focus on optimizing the performance gaps compared to Fortran as well as leveraging GPU computing to accelerate the reconstruction. Integrating deep learning models for image analysis and quality enhancement is another promising direction. The converted Python code established a modular and extensible foundation to support research and translation of process tomography techniques.

References

Z. V. Kuzeljevic and M. P. Dudukovic. 2012. Computational modeling of trickle bed reactors. *Industrial Engineering Chemistry Research*, 51(4):1663–1671.

S. Roy, A. Kemoun, M. H. Al-Dahhan, M. P. Dudukovic, T. B. Skourlis, and F. M. Dautzenberg. 2005. Countercurrent flow distribution in structured packing via computed tomography. *Chemical Engineering and Processing*, 44(1):59–69.

L. A. Shepp and Y. Vardi. 1982. Maximum likelihood reconstruction for emission tomography. *IEEE Transactions on Medical Imaging*, 1:113–122.

D. Toye, P. Marchot, M. Crine, and G. L'Homme. 1997. Computer-assisted tomography for liquid imaging in trickle flow columns. *In Computer Tomography for Industrial Applications*, pages 105–139.

M. Toze, N. Barradas, and A. Senos. 2020. Industrial process gamma tomography: A review of image reconstruction techniques. *Measurement*, 152:107263.

Individual Research Contribution Review, 2023, 1(1): 219–220

The Application of Ultrasonic Reflected Energy Technique for Concrete Structures Inspection

Mohd Noorul Ikhsan bin Mohamed@Ahmad
Industrial Technology Division, Malaysian Nuclear Agency
43000 Kajang, Selangor
ikhsan@nm.gov.my

Abstract

Low frequency piezocomposite transducers have been used in combination with pulse compression methods to penetrate 35 cm into concrete-type materials. A chirp signal with a frequency range 100 – 200 kHz and of 10 ms duration was used to excite a pair of 54 mm diameter piezocomposite transducers in patch-catch mode. The centre frequency of the transducers was 170 kHz. Using this arrangement, good signals could be obtained, but there was a problem with variability due to the high degree of scattering – even small changes in transducer location changed the measurement. Thus, an additional signal processing technique called reflected energy was introduced, whereby the total energy reaching the receiver was calculated as a function of time from the cross-correlation outputs.

Keywords: Pulse compression, cross correlation, piezocomposite, bandwidth, concrete inspection

1 Introduction

It is very difficult to inspect thick sections of concrete and related material using ultrasound (Philippidis and Aggelis, 2005). The problem is mainly scattering from aggregate and other types of inclusions. This often limits the depth of penetration, but also causes a poor signal to noise ratio (SNR) to be present in a single-sided inspection (Gaydecki et al., 1992; Venkatraman and Rao, 1996). The objective was to develop a system at low frequencies (100-400 kHz), which had good penetration, but which also had a reasonable bandwidth and SNR. This required the correct combination of transducer, excitation waveform and an additional signal processing method, so that the resolution of the method in terms of defect location could be optimised.

2 Methods

As will be shown below, it was sometime difficult to use pulse compression alone to determine sample thickness, due to excessive back-scatter. It was thus decided to define statistical quantities which could highlight the location of a major reflection site, such as a back wall or a major fracture in concrete. The idea was to analyze the spatial and temporal distribution of the reflected energy in order to understand if there are noticeable variations when performing measurement on concrete samples of different length. When used with piezocomposite transducers and long-duration coded waveforms, it gives an advantage especially on materials such as thick and concrete sample with uneven surfaces within which backscatter and attenuation levels are high.

In this method, the total integrated energy is obtained by summing the contributions scattered back to the top surface from each incremental depth into the material. A plot is produced as the value of this total reflected/back-scattered energy increases with time (and hence distance into the sample). Eventually this reaches a maximum saturation level. A threshold level for the cumulative amount of the reflected energy is then chosen – in this case at 70% of the maximum level. The depth within the sample at which this energy is reached is then obtained from each individual measurement. This is then repeated by moving the transducer pair to different positions on the top surface, so that ten different values of the threshold distance are recorded. The data is then plotted as a histogram of the number of measurements that reached this 70% level at a particular depth into the sample. In this way, it is hoped statistically to determine the location of the main reflection of energy back to the surface or the back wall of the sample. This was done for Samples 1 and 2, where the depth of the concrete was to be estimated. For sample 3, it could be used to determine possible location of the v-notch at the bottom surface.

3 Results

Figure 1 shows a histogram result from the data analysis technique that utilized reflected energy. The data has been plotted into a histogram from ten repetitive measurements of the same sample. The histogram is of the number of measurements that reached this 70% level at a particular depth into the sample. This result shows that the analysis is capable of determining the thickness of a concrete material even at significant depths. From the two samples of concrete with thickness of 15 cm each, the resultant values obtained were 17 cm and 13 cm from samples 1 and 2 respectively.

4 Conclusion

Tests have shown that the developed pulse compression system at low frequencies is capable of testing difficult materials such as thick concrete. Pulse compression techniques without further processing could be used to give a fairly consistent estimate of sample thickness at depths of up to 15 cm. This is an achievement because it could in future be applied to detect

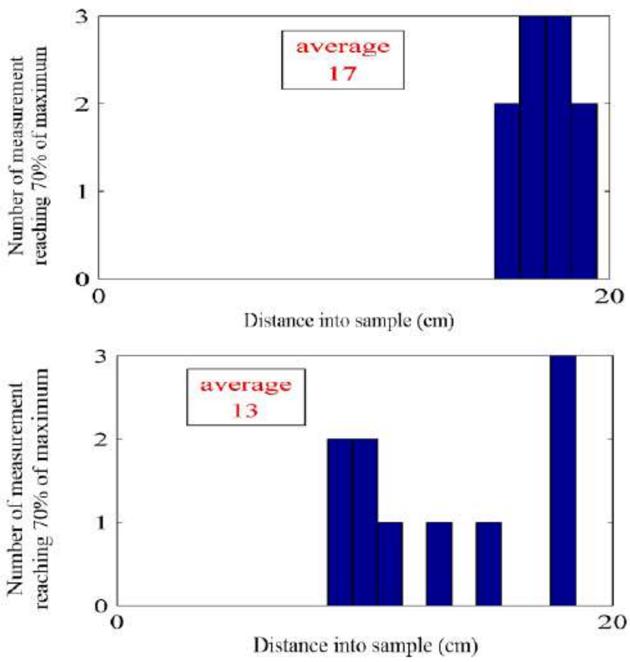

Figure 1: The results of reflected energy technique; 150 mm (15 cm)

the presence of reinforcement bars and crack-like defects in concrete materials. The new reflected energy technique seems to give a good indication of the likely position within a sample of a major change, such as a change in thickness or a major through-thickness fracture.

References

P.A Gaydecki, F.M Burdekin, W. Damaj, and D.G John. 1992. The propagation and attenuation of medium-frequency ultrasonic waves in concrete : A signal analytical approach. *Meas. Sci. Technol.*, 3:126–134.

T.P. Philippidis and D.G. Aggelis. 2005. Experimental study of wave dispersion and attenuation in concrete. *Ultrasonics*, 43:584–595.

S. Venkatraman and N.A.K.H Rao. 1996. Combining pulse compression and adaptive drive signal design to inverse filter the transducer system response and improve resolution in medical ultrasound. *Med. Bio. Eng Comp*, 34:318–32.

Individual Research Contribution Review, 2023, 1(1): 221–222

Fabrication of Composite Nanofibers of Carboxymethyl Starch/Poly(l-Lactide) Acid/β-Tricalcium Phosphate for Biomedical Applications

Mohd Reusmaazran Yusof
Industrial Technology Division, Malaysian Nuclear Agency
43000 Kajang, Selangor
reusmaazran@nm.gov.my

Abstract

A natural polymer of carboxymethyl starch (CMS) was used in combination with the inorganic mineral of Tricalcium Phosphate (β-TCP) and Poly l-lactide (PLLA) to prepare composite nanofibers with the potential to be used as a biomedical membrane. β- TCP contents varied in the range of 0.25% to 1% in the composition of PLLA and CMS. A mixed composition of these organic and inorganic materials was electro-spuned to produce composite nanofibers.

Keywords: poly l-lactide (PLLA); carboxymethyl starch (CMS); β-tricalcium phosphate (β-TCP); electrospinning; nanofibers

1 Introductions

In biomedical engineering areas, nanofibers prepared via electrospinning provide valuable properties since the nanofibers mimic the extracellular matrix (ECM) which is important as a cell platform. Electrospinning involves three major components a high voltage, a collector, and a syringe pump (Yalcinkaya et al., 2016). Presently, numerous types of composite nanofibers have been developed, such as synthetic–synthetic polymers, natural–synthetic polymers and natural–synthetic–particulate nanofibers. Natural polymers have become a great interest of many researchers due to a number of advantages such environmental friendliness, low costs, and easy extraction from a natural resources that are available in many countries. In industrial applications, a natural polymer of carboxycellulose nanofibers derived from jute has exhibited a very high mechanical strength compared to the raw jute fibers in nanopaper applications.

2 Methods

The composite PLLA/CMS/β-TCP polymer solution was placed into a 1 mL syringe with a 0.6 mm diameter of a blunt needle tip. Distance between the needle and collector was set to 12 cm and connected to a high voltage source. Voltage was set to 10 kV, and the syringe pump was placed vertically. The flow rate of the polymer jet was set to 0.006 mL/min, and the nanofiber mat was collected on an aluminum foil. The surface of fibers was characterized by using a scanning electron microscope. The images were collected with magnification at 10 kV. The chemical interaction analysis was performed by using Fourier transform infrared (FTIR) spectroscopy. The FTIR spectrum was measured in the spectral range of 400 to 4000 cm^{-1}, which was performed at 16 scans per sample.

3 Result and Discussions

Figure 1 demonstrates the micrographs of the composite PLLA/CMS/β-TCP with different concentrations of the β-TCP particles in the nanofibers. A low content of β-TCP (0.25% to 1 wt %) was added to avoid possible fiber breaking during the electrospinning. It can be observed that smooth, beadless, homogenous, continuous, and randomly oriented nanofibers were obtained. A highly porous and interconnected pore structure were also obtained via this method. A cluster was observed in the nanofibers with the presence of β-TCP particles indicating that a combination interaction had occurred between the particles. As a comparison in morphology observations, the addition of 6 wt % of β-TCP was found to deface the nanofibers structure due to the higher content of the particles in the polymer structure. The presence of a higher content of the particles led to the agglomeration in the nanofibers. This agglomeration defaces the formation of nanofibers due to the stretching of the jet polymer during the electrospinning process and results in the discontinuation and breakage of nanofibers. Agglomeration also hinders the movement of jet polymers and the formation of the Taylor cone at the nozzle which leads to non-uniform nanofibers.

The agglomeration that formed clusters in nanofibers has been found at a content as low as 0.75 wt % of β-TCP. The distribution of nanofiber diameter generally changed in the range of 20 to 400 nm for PLLA/CMS with the content of 0.25 to 0.75 wt % of β-TCP. The diameter distribution was increased to approximately 500 nm when the concentration was raised to 1 wt %. The distribution was shifted to the right, as shown, indicating that the diameter of nanofibers was increased with the increase in the composition of β-TCP particles.

Chemical interactions between the matrix and other component of the composite nanofibers were analyzed by FTIR, as indicated in Figure 2. β-TCP can be characterized by the absorption bands of 946 and 1023 cm^{-1} that rises from the stretching of symmetry and anti-symmetry of P–O bonding, respectively. The O–P–O bond was indicated at 601 and 547 cm^{-1} of the absorption band. The low intensity peak of 1085 cm^{-1} was rising from the portion of crystal structure in the amorphous region. The absorption band of the CMS hydroxyl group appeared at 3200–3400 and 1550–1660 cm^{-1}, and was attributed to the $COO^{-}Na^{+}$; whereas the absorption peaks of

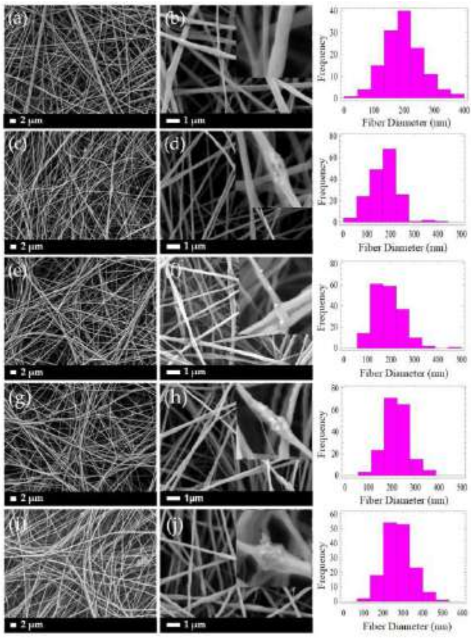

Figure 1: Morphology of the PLLA/CMS/β-TCP composite nanofibers with different compositions of β-TCP at different magnifications of 2000x and 10,000x (**a,b**) PLLA/CMS (**c,d**) 0.25% β-TCP, (**e,f**) 0.5% β-TCP, (**g,h**) 0.75% β-TCP and (**i,j**) 1% β-TCP in PLLA/CMS.

2995 and to 2945 cm^{-1} corresponded to C–H in PLLA. Peaks at 1767, 1453, and 1383 attributed to C=O presence in PLLA. The peak of 1023 cm^{-1} was observed to budge at 1036 cm^{-1} after the addition of β-TCP into PLLA/CMS.

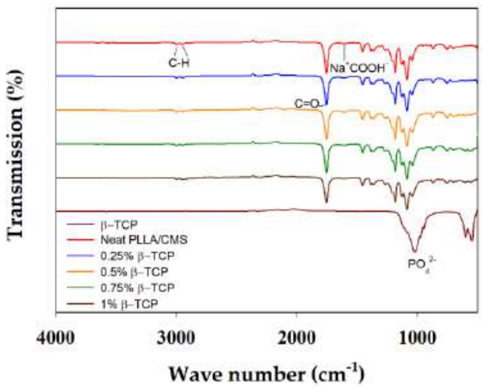

Figure 2: IR Spectrum of composite nanofibers with the different concentrations of β-TCP.

A similar reaction was observed by Chen et al (Chen et al., 2006), a formation of complex bonds on the surface by the cation transfer between OH groups in CMS and O group in alumina. This condition has resulted in the budging and widening of the FTIR spectroscopy absorption band. The peaks of 839 and 702 cm^{-1} corresponding to CMS structure were found to vanish, which is attributed to the changes in C–C bond in the polymer network of CMS.

4 Conclusion

In this study, we prepared and optimized a composite of synthetic–natural–inorganic mineral nanofibers with the potential to be applied as biomedical membranes, such as guided bone regeneration (GBR) membranes. The composite nanofiber mat was successfully electrospun to uniform non-woven nanofibers. The combination of natural polymers and β-TCP mineral improved the hydrophilic behavior of the PLLA but a higher concentration of the β-TCP led to decreases in mechanical strength and an increment in fiber size. Agglomeration may restrain the performance of the uniform and smooth nanofibers. Overall, the engineered electrospun nanofibers prepared in this works are promising candidates for bone tissue engineering applications such as the GBR membrane.

References

Y. Chen, S. Liu, and G. Wang. 2006. Kinetics and adsorption behavior of carboxymethyl starch on α-alumina in aqueous medium. *J. Colloid Interface Sci.*, 303:380–387.

F. Yalcinkaya, M. Komarek, D. Lubasova, F. Sanetrnik, and J. Maryska. 2016. Preparation of antibacterial nanofibre/nanoparticle covered composite yarns. *J. Nanomater.*, page 1–7.

Individual Research Contribution Review, 2023, 1(1): 223–224

Optical Phase Measurement for Laser Interferometry Phase Stepping Technique

Mohd Yusnisyam Bin Yusof
Industrial Technology Division, Malaysian Nuclear Agency
43000 Kajang, Selangor
yusnisyam@nm.gov.my

Abstract

This paper discusses the optical phase measurement of interference pattern from coherent light Nd:YAG 532nm laser source for phase stepping technique in laser interferometry. The accuracy of optical phase measurement of three-phase stepping and four-phase stepping are discussed.

Keywords: Phase, Fringe Pattern, Phase Shift

1 Introduction

In this paper, the Phase shift interferometry (PSI) techniques is used for the phase measurement instruments. The basic idea of the PSI technique is that, if the phase difference between two beams is made to vary in some known manner, the initial phase can be derived from three or more intensity measurements. The most common way to vary the phase difference between two beams is to apply a voltage to a piezoelectric transducer (PZT) on which the reference mirror is mounted. The voltage applied is a step voltage with equal period and equal increment or a ramp voltage. In this case, the PZT is used to achieve the required phase shift of the fringe pattern. The different voltages are applied to a PZT for measurement of three-phase stepping and four-phase stepping procedures.

2 Methods

The schematic optical arrangement of the Twyman-Green Interferometer for phase stepping calibration is shown in Figure 1.

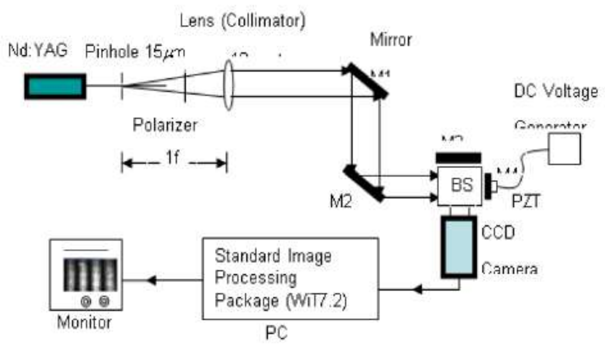

Figure 1: Phase shifting interferometry system.

The fringe density and fringe orientation as depicted on monitor screen is controlled by the rotation of M3. In this experiment the number of fringe density is chosen for approximately 4.5-fringe order number or about 9π phase change. The orientation of fringe is set to be in vertical position. The phase stepping mechanism is employed by PZT that generated by DC voltage.

In phase-shifted interferometry technique, three and four phase shifted sinusoidal fringe patterns are shifted onto an object surface with phase shifted by $2\pi/3$ and $\pi/2$ respectively. The following algorithms are used to represent successive intensity distributions with phase shift between each frame.

3 Phase Step Image Frame Intensity

$$I_1(x,y) = a(x,y) + b(x,y) + cos\varphi(x,y)$$
$$I_2(x,y) = a(x,y) + b(x,y) + cos[\varphi(x,y) + \frac{2\pi}{3}]$$
$$I_3(x,y) = a(x,y) + b(x,y) + cos[\varphi(x,y) + \frac{4\pi}{3}] \quad (1)$$

4 Phase Step Image Frame Intensity

$$I_1(x,y) = a(x,y) + b(x,y) + cos\varphi(x,y)$$
$$I_2(x,y) = a(x,y) + b(x,y) + cos[\varphi(x,y) + \frac{\pi}{2}]$$
$$I_3(x,y) = a(x,y) + b(x,y) + cos[\varphi(x,y) + \pi] \quad (2)$$
$$I_4(x,y) = a(x,y) + b(x,y) + cos[\varphi(x,y) + \frac{3\pi}{2}]$$

Where a(x,y) is the average intensity, b(x,y) is the intensity modulation, and φ(x,y) is the optical phase. By solving Equation 1 and Equation 2 simultaneously, the phase φ(x,y) at point (x,y) in the image can be obtained as given by the following equations:

3 Phase Step Image Frame Technique

$$\varphi(x,y) = \arctan\sqrt{3}\frac{I_1(x,y) - I_3(x,y)}{2I_1(x,y) - I_2(x,y) - I_3(x,y)}$$

4 Phase Step Image Frame Technique

$$\varphi(x,y) = \arctan\frac{I_4(x,y) - I_2(x,y)}{I_1(x,y) - I_3(x,y)} \quad (3)$$

The phase φ(x,y) results in a principal value of 2π phase shifted regardless of the actual value of the phase.

3 Data and Results

Figure 2 shows the wrapped experimental phase maps of images data with 3-frame intensity phase stepping and followed by 4-frame intensity phase stepping in one run while Figure 3 shows the wrapped phase of 4 frames followed by 3 frames intensity phase stepping.

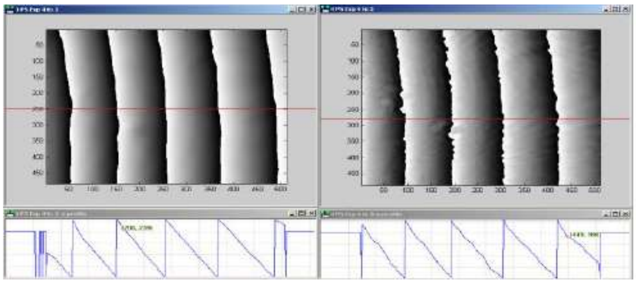

Figure 2: Experimental image data of wrapped phase maps 3-intensity phase step followed by 4-intensity phase step

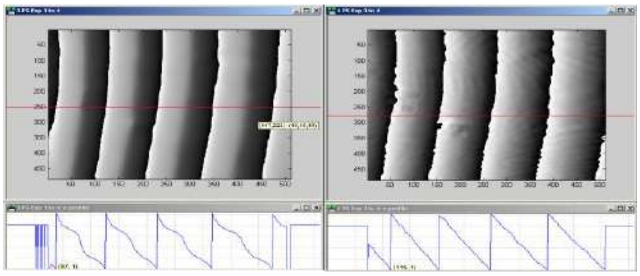

Figure 3: Experimental image data of wrapped phase maps 4-intensity phase step followed by 3-intensity phase step

Four sets of phase step procedures were experimentally performed using the calibrated voltage of phase stepping interferometry (PSI) method. The fringe order number measured is tabulated in Table 1.

Table 1: Measurement of Fringe Order Number Using 3-Frame Intensity Phase Step and 4-Frame Intensity Frame Phase Step

Experiment	**No.1**		**No.2**		**No.3**		**No.4**	
	3-PS followed by 4-PS		4-PS followed by 3-PS		3-PS followed by 4-PS		4-PS followed by 3-PS	
Phase Step Procedure	3	4	3	4	3	4	3	4
No. of Fringe	4.62	4.73	4.93	5.08	4.86	5.10	4.74	4.90
Different (%) 3- to 4-frame procedure	2.4		2.9		4.9		3.3	

Experimental result indicates that the number of fringe order number using 4-intensity phase stepping procedure is about 2.4% to 4.9% higher than the fringe order number using 3-intensity phase stepping procedure. This trend is in an agreement to theoretical phase calculation analysis hence error in phase measurement could be minimized with the number of frame used. The error value in theoretical calculation is slightly higher than the minimum deviation of experimental phase analysis. This figure is due to the theoretical error that refers to actual input of the fringe number while the experimental analysis is the relative value refers to phase data of 4-frame intensity phase step. The similar trend of phase deviation with the number of intensity frame number is reported elsewhere with error or nonlinearity in the phase shifter will decrease as the number measurement increase. The high deviation values in the experimental data are due to the system error in the measurement such as miscalibration of the phase shifter, nonlinearities of the detector, quantization of the detector signal, the reference surface, air turbulence, and vibrations. Air turbulence and vibrations are dynamics variables that contribute to both the system measurement precision and the accuracy.

4 Discussion and Conclusion

The phase calibration procedures of PZT (Piezosystem jena 72507) using Twyman-Green interferometer is established and the voltage required to complete one fringe shifted is measured as 8.8 Volts. It had been shown experimentally that the 4 frames intensity phase stepping technique contributes less error in comparison with 3 phase stepping technique. The experimental result is theoretically validated. The experiment also concludes that the 4-frame phase shifting procedure provides better accuracy in the quantitative phase analysis for use in shearography and other interferometric measurements.

References

Yeou-Yen Cheng and James C. Wyant. 1985. Phase shifter calibration in phase-shifting interferometry. *Applied Optic.*, 24(18).

K. Creath. 1988. Phase measurement interferometry techniques. *Progress in optics XXVI*, pages 349–393.

Yongjian Zhu, Liren Liu, Zhu Luan, and Jianfeng Sun. 2007. Discussions about fft-based two- step phase-shifting algorithm. *Opt. Int. J. Light Electron. Opt.*

Detection of Passive Buried Defects in Carbon/ Carbon Sample using Magnetostrictive Transducer-based Vibrothermography

Mohd Zaki Umar
Industrial Technology Division, Malaysian Nuclear Agency
43000 Kajang, Selangor
zaki@nm.gov.my

Abstract

This study presents the use of magnetostrictive transducer-based Vibrothermography to detect six passive buried defects in a carbon/carbon (C/C) plate. The rise in surface temperature caused by heat emitted at the defect zone during ultrasonic stimulation was monitored and quantified using an infrared camera. It's worth mentioning that all six passive buried defects are detectable. The results show that the approach method can successfully reveal passive buried defects in C/C composites.

Keywords: Passive buried defects, Carbon/Carbon, magnetostrictive, Vibrothermography

1 Introduction

Carbon/carbon (C/C) composites have been widely used in aircraft, aerospace, and automotive structures. The use of C/C composite is driven by the need for strong and lightweight materials. However, besides their low oxidation resistance, another major concern to widespread the use of C/C composite is they are susceptible to impact damage. Despite several efforts to automate inspection, existing NDT techniques utilised for impact damage detection are still time-consuming and expensive. These drawbacks can be mitigated by employing Vibrothermography. This paper presents the attractiveness of the magnetostrictive-based VT system to detect low energy impact damages that act as passive buried defects including kissing bond which present a difficult problem for many other NDT methods (1−3).

2 Method

Experiments were carried out on a 440 x 350 x 7 mm−dimension bi−directional C/C plate containing 6 areas of impact damage of varying energy 5, 10, 15, 20, 25, and 30 J act as buried defects (shown in Figure 1). The test plate was ultrasonically stimulated for 10 s using a magnetostrictive−based VT system which is developed by Tomsk Polytechnic University, Russia. The system is based on using a magnetostrictive device with a ball−like indenter (frequency 22 kHz with a deviation of ±100 Hz, tuneable power up to 2.5 kW, vibration amplitude ±7 m, and pulse duration from 0.1 to 20 s). The maximal electrical energy applied by the ultrasonic generator to the transducer was 2 kW. Test results were recorded on the front surface as a sequence of thermograms by using an NEC TH 9100 IR camera (long wave IR cam with temperature resolution 0.06°C) for 15 s. These thermograms were then analyzed with ThermoFit Pro program to obtain the absolute differential temperature, $\Delta T(\tau)$. Figure 2 presents the described setup.

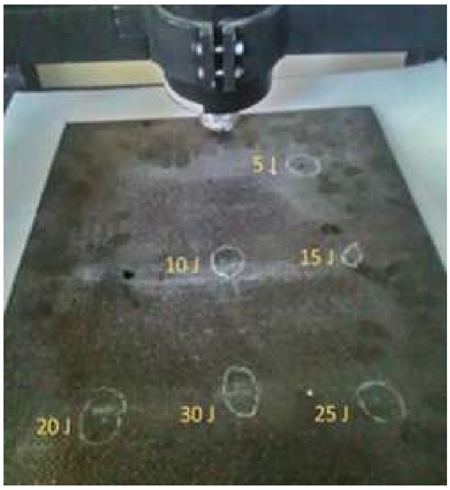

Figure 1: A 440 x 350 x 7 mm bi−directional C/C test plate with 6 locations of simulated impact damage defects.

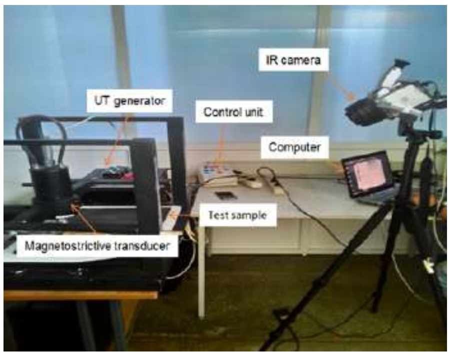

Figure 2: Photo of the experimental setup.

3 Results and Discussion

Figure 3 demonstrated that all six buried defects produced observable temperature readings. Figure 4 depicts the progression of $\Delta T(\tau)$ for each fault, and Table 1 displays the corresponding value. The findings clearly demonstrated that flaws caused by higher energy impacts are characterized by higher intensity thermal emission due to more effective conversion of acoustic energy into thermal radiation. It is worth mentioning that thinner and, in particular, kissing bond−like defects (two surfaces in intimate contact but not bound together) generate more heat energy due to internal friction when subjected to ultrasonic stimulation. This phenomenon may be responsible for higher temperature signals produced by smaller defects and, hence, larger defect indications even in the case of lower impact energy. To illustrate, the 25 J impact zone showed larger indication (lateral size is approx. 80 mm) as compared to the 30 J impact (lateral size is approx. 74.3 mm), as shown in Figure 5.

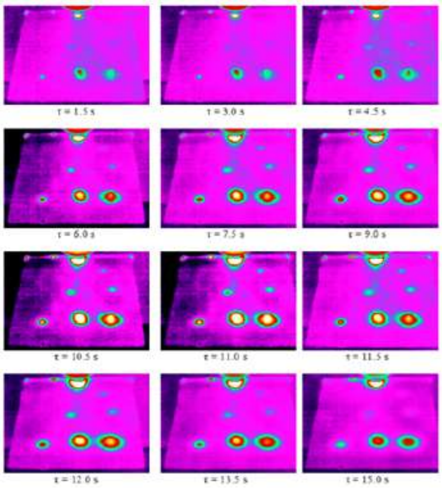

Figure 3: IR thermogram sequences of temperature evolution (only to show 12 out of 450 images).

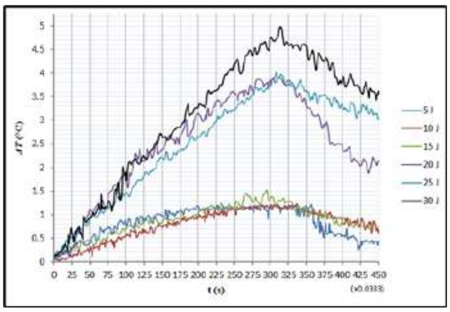

Figure 4: Evolution of $\Delta T(\tau)$ for each defect.

4 Conclusion

The usefulness of magnetostrictive transducer−based VT for detecting low energy impact damages that behave as passive buried defects in composite was demonstrated in this work. This advanced thermal NDT approach should be viewed as a quick and dependable inspection technique for assessing the technical state of various types of composite constructions. However, the physics driving the heat generation process in the defective zone is still poorly understood. More research is needed to help explain the heating mechanisms and their relationship with the structure's resonance pattern, especially when complex geometries are considered, such as stimulation power, ultrasonic frequency, and so on.

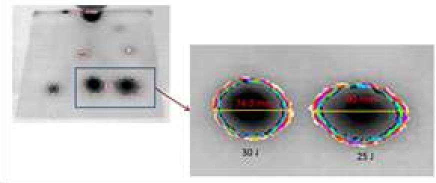

Figure 5: Enlarged image of impact zone for 25 J and 30 J (with the maximum SNR value).

Table 1: The values of $\Delta T(\tau)$ maximum

Impact Energy (J)	$\mathbf{\Delta T}(\tau)_{max}$
5	1.219°C
10	1.229°C
15	1.525°C
20	3.915°C
25	4.016°C
30	4.983°C

References

Andrzej K. and Micha l Z. 2006. Influence of the impactor geometry on the damage character in composite structures. *Composite Structures*, 49:33–39.

Umar MZ., Vavilov VP., H. Abdullah, and Ariffin AK. 2019. Quantitative study of local heat sources by ultrasonic infrared thermography: An approach for estimating total energy released by low energy impact damage in C/C composite. *Composites Part B: Engineering*, 165:167–173.

Guo X. and Vavilov V. 2013. Crack detection in aluminium parts by using ultrasound-excited infrared thermography. *Infrared Physics and Technology*, 61(5):149–156.

Individual Research Contribution Review, 2023, 1(1): 227–228

Simulation Study to Identify Muons from Heavy Flavor Mesons in Proton-Proton and Lead-Lead Collisions at LHC ALICE Run 3

Muhamad Noor Izwan Bin Ishak
Industrial Technology Division, Malaysian Nuclear Agency
43000 Kajang, Selangor
noorizwan@nm.gov.my

Abstract

The Quark Gluon Plasma (QGP), a unique state of matter believed to have existed shortly after the Big Bang, is the central focus of this study. Specifically, the paper explores the production of heavy flavor B and D mesons in both pp and Pb-Pb collisions. The integration of the Muon Forward Tracker (MFT) into the ALICE (A Large Ion Collider Experiment) detector at LHC energies enhances precision in measuring the kinematic properties of muons. The simulation results concentrate on particles in the forward rapidity region (-3.6<η< -2.5) with momentum exceeding 4 GeV/c, with a particular emphasis on evaluating the parameters of distance of closest approach (DCA) and transverse momentum (p_T).

Keywords: Quark Gluon Plasma, Muon Forward Tracker, ALICE, distance of closest approach, transverse momentum

1 Introduction

This research aims to uncover the characteristics of the Quark Gluon Plasma (QGP) phase formed in heavy ion collisions - a state akin to conditions shortly after the Big Bang. The QGP study provides crucial insights into the core properties of matter and the universe's evolution. The focus is on investigating the traits of individual heavy flavor B and D meson particles in relativistic heavy ion collisions, with a specific emphasis on their decay. Originating from hard-scattering processes in early heavy-ion collisions, these heavy quarks decay into muons and electrons, contributing vital information about the QGP phase. For more in-depth QGP studies, it's essential to separate the contributions of beauty (from B mesons) and charm (from D mesons) to muon yield. Analyzing charm and beauty elliptic flow aids in comprehending in-medium parton energy loss and thermalization.

The substantial production yield of heavy quarks at the LHC sparks significant interest in studying heavy flavor production in heavy-ion collisions. Measuring both charm and beauty hadrons in comparable kinematic ranges allows for a direct "double" nuclear modification factors comparison. Assessing the total production cross section of heavy quarks in heavy ion collisions becomes a crucial benchmark for investigating modifications in quarkonia (charmonia and bottomonia) production yield, intricately linked to the corresponding heavy quark production cross section.

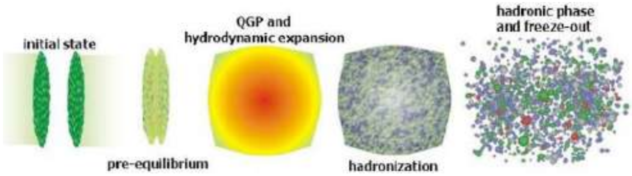

Figure 1: QGP production in Pb-Pb collision and hadronization process

2 Methods

In the context of LHC Run 3, the spotlight is on the O2 (Online-Offline) framework, taking a central role in simulations and analysis. Specifically, attention is directed towards studying the decay of heavy flavor hadrons such as B and D mesons into muons ($B,D \rightarrow \mu X$). MFT can be used in c/b muon separation by detecting the passage of charged particles and providing information on the distance of closest approach of the muon track from the primary vertex (The ALICE Collaboration,2013).

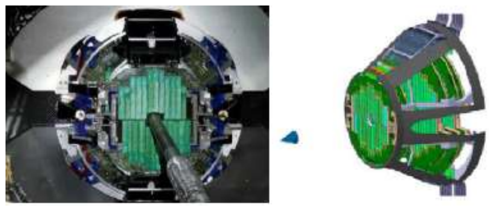

Figure 2: MFT half-disks (left) and MFT geometry (right)

Performance evaluations hinge on HIJING for simulating background events, predominantly consisting of pions and kaons, complemented by signals from a PYTHIA 8 parametrization embedded within HIJING events (The Alice Collaboration,2015). Ensuring an accurate representation of the experimental setup, the GEANT 4 detector simulation software is utilized to simulate the interaction between generated particles and the ALICE detector. These tools play pivotal roles in advancing our comprehension of heavy flavor decays and other phenomena in heavy-ion collisions within the ALICE experiment.

When it comes to determining the transverse momentum of B mesons and D mesons, various techniques are employed, contingent on the experimental setup. One prevalent approach involves measuring the curvature of the particle trajectory within a magnetic field. The relationship between transverse

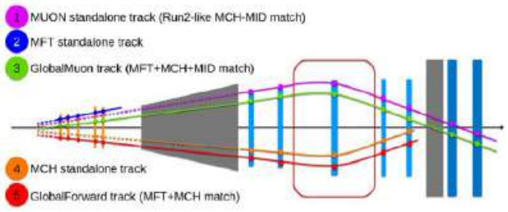

Figure 3: Track reconstruction in the Muon spectrometer and MFT

momentum (p_T) and curvature is expressed by the equation $p_T = qB\rho$, where p_T signifies transverse momentum, q is the particle's charge, B denotes the magnetic field strength, and ρ represents the radius of curvature. Alternatively, another method involves assessing the distribution of decay products in the laboratory frame and extracting transverse momentum from the momentum conservation equation.

Examining muon tracks with minimal DCA_T values suggests close proximity to the primary vertex and a heightened likelihood of originating from a B or D meson decay. By gauging the displacement between the primary vertex and the track's point of closest approach, the decay length can be estimated. In this study, we analyze the DCA_T distribution of specific particles, determining optimal ranges for maximizing muon signal extraction while effectively excluding background muons from other sources.

3 Data/Results

Proper DCA_T results were obtained from a simulated kinematic MC (Monte Carlo) file, proving its reliability compared to MFT and GM (Global Muon Track) files for DCA_T calculations. The MC track simulation has shown better DCA_T distribution results for B and D mesons compared to GM track simulation, suggesting the influence of multiple scattering in ALICE detector components affecting accuracy of the track matching. At $DCA_T > 0.1$ cm, muons from pion and kaon decays dominate the DCA_T distribution with mostly wider distribution, while at $p_T > 1$ GeV/c, muons from charm-hadron and beauty-hadrons decays dominate for small DCA_T values ($DCA_T < 0.1$ cm).

Cutoff optimization with p_T and DCA_T information were conducted, and signal yield and background calculations are obtained (Figure 4 and 5). The analysis has shown a high statistical significance of signal muons compared to background muons near $DCA_T < 0.03$ cm so we have decided that would be a good separation point. To separate muons from pions and kaons below $DCA_T < 0.03$ cm and maximize signals (from B and D mesons) while filtering background (from other muons), rejection techniques are implemented. Also, MC track shows that prompt muons from light mesons (ρ, ϕ, η, and ω mesons) are concentrated at $DCA_T = 0$ cm.

4 Discussion/Conclusions

Based on the results, it can be concluded that muons from the decay of B mesons and D mesons have been effectively distinguished from pions and kaons in the low transverse momentum region ($p_T \leq 4$ GeV/c). However, certain challenges need to be addressed. The low count of B mesons poses an obstacle for meaningful analysis, while the high count of charm mesons necessitates the rejection of minimum bias from charmonium to enhance accuracy. Additionally, the calculation of true matching is crucial to assess how false matching tracks can influence the overall measurement efficiency.

In the actual experiment, MFT plays a crucial role in the study of charm and beauty mesons' decay muons by providing vertexing capabilities at forward rapidity. It effectively separates muons from charm-hadron and beauty-hadron decays from the light-flavor background, with respective p_T cutoffs of about 0.5 GeV/c and 2 GeV/c. Notably, the longer lifetime of beauty hadrons results in muons from beauty-hadron decays having a larger average separation from the primary vertex compared to those from charmed hadrons.

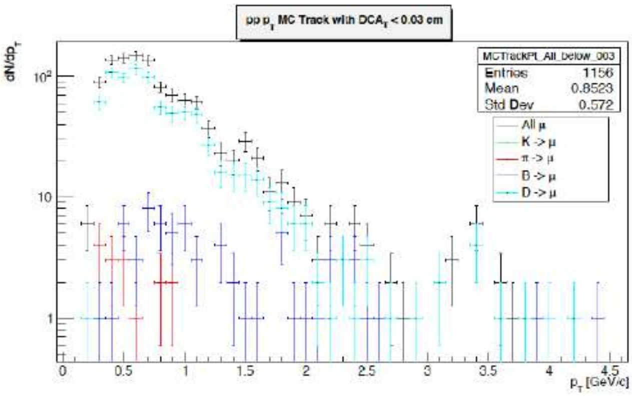

Figure 4: p_T distributions for all muons for MC track of pp after cut-off optimization ($DCA_T < 0.03$ cm)

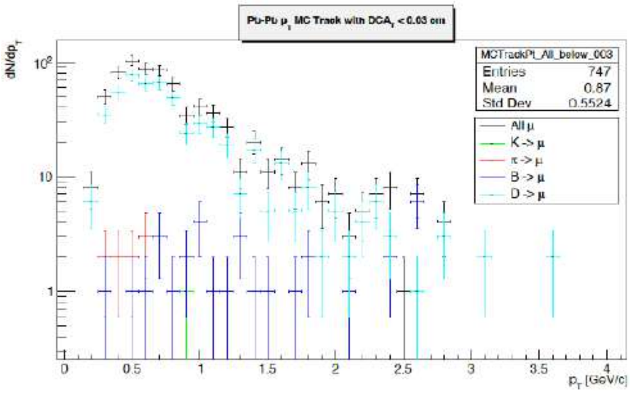

Figure 5: p_T distributions for all muons for MC track of Pb-Pb after cut-off optimization ($DCA_T < 0.03$ cm).

References

The ALICE Collaboration. 2013. Upgrade of the alice experiment: Addendum to the letter of intent. CERN.

The ALICE Collaboration. 2015. Technical design report for the upgrade of the online–offline computing system. ALICE-TDR-19(CERN-LHCC-2015-006).

Individual Research Contribution Review, 2023, 1(1): 229–230

Cellulose Fibers Integrity and Color Changing Effect due to Gamma Irradiation at Higher than Recommended Disinfection Dose

Nadira Binti Kamarudin
Industrial Technology Division, Malaysian Nuclear Agency
43000 Kajang, Selangor
nadira@nm.gov.my

Abstract

Most crucial preservation challenges of rare books and manuscripts is biodeterioration. Microorganisms and insects that consume cellulose, pose a significant threat to materials and the health of conservators. The current method of chemical fumigation using ethylene oxide and methyl bromide has limited effectiveness due to only surface disinfection and poses safety and environmental concerns. The potential of gamma radiation as an alternative to disinfect has raised some controversy. The fear of irradiation damage towards cellulose based artifacts is the main reason that this technique is not so popular among archivers and curators. The research aims to demonstrate that the irradiation damage only occurs when higher that recommended dose of gamma irradiation is applied.

Keywords: Cellulose, Radiation Damage, Gamma Irradiation.

1 Introduction

Biodeterioration is the most common source of degradation of files and books in tropical and subtropical countries (Area and Ceradame, 2011). The common method used to handle this is fumigation which involves handling of a dangerous gas that poses hazard towards health and the artifact itself. Ethylene oxide used in fumigation makes paper much more super sensitive to mold (Valentin, 1986). The effectiveness of fumigation is only on the surface of the artifact is not suitable for borrowing insects (silverfish) infested rare books.

Gamma radiation proved could eliminates insects, microbes and fungi in the paper and cellulose based artifact. Gamma radiation involves no residual toxicity or pollution in addition of large volumes of material can be handled in short time (IAEA, 2017). Experiments have been conducted to find the lowest gamma radiation dose needed to inactivate fungi (Dasilva et al., 2006) and basic dose to in activate microbes, insects and fungi already establish and reported (IAEA, 2017).

Degradation of the cellulose macromolecules can be brought about with various kinds of energy input, such as chemical, thermal, mechanical, or radiation energy. Recent experiments have been focused on the study the effects of radiation on paper properties, especially those related to strength and appearance of paper (Moise et al., 2017; Bicchieri et al., 2016; Jiménez-Reyes et al., 2018; Moise et al., 2019).

2 Method

The materials that use in this study are commercial 80grm paper. The samples are irradiated in Co-60 research loop irradiation facility in Sinagama, Malaysian Nuclear Agency. Selected dose from 10 kGy which is the maximum dose recommended for disinfecting microbes, fungi and insects for cultural heritage artifacts up to 120 kGy was applied to each sample. Sufficient sample is prepared and packed in polyethylene envelopes before irradiation. Field emission scanning electron microscopy (FESEM) is used to detect changes in fiber structure. Color changes of the irradiated paper are analyzed using spectrophotometer.

3 Results

The micrograph of samples with doses applied to commercial 80 grm paper is shown in Figure 1. The control sample was not irradiated and shows that naturally the fibers and additives in the paper intact well. Irradiation at 10 kGy show that the additive on the paper is dryer than control sample. At 120 kGy, radiation damage shown as micro tears of fibers and dryness of additives. This will increase the surface roughness and induce brittleness.

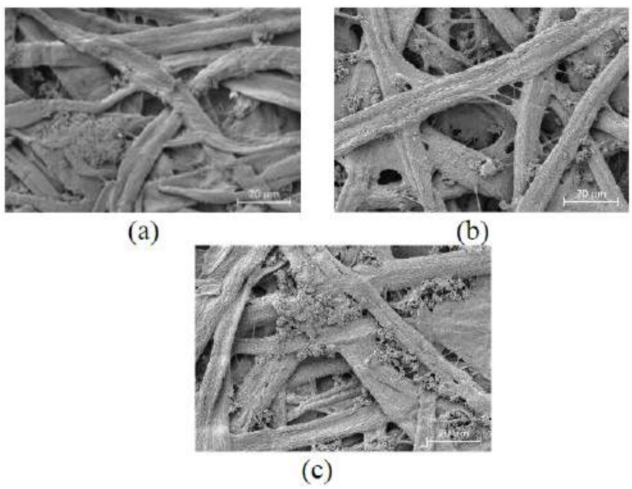

Figure 1: Micrographs of commercial 80 grm paper applied different doses (a) Control (not irradiated), (b) 10 kGy and (c) 120 kGy.

Results of spectrophotometer analysis is shown in Figure 2.

The graph shows that the brightness of the sample decreases with the increasing if applied dose. While the yellowness of the sample increases with the increasing of applied dose.

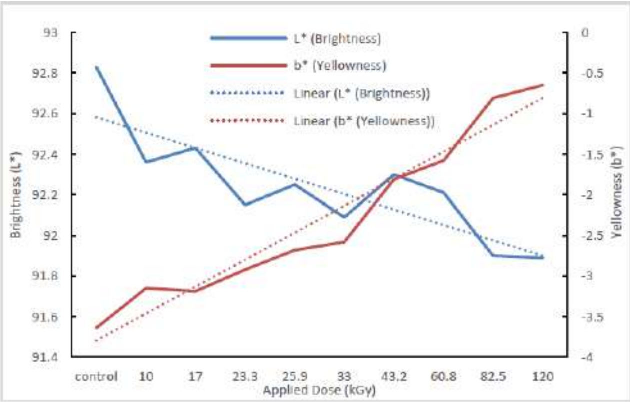

Figure 2: Brightness and yellowness of sample exposed at high dose.

4 Discussion

Radiation can have various effects on cellulose materials depending on the dose applied. Ionizing radiation can break chemical bonds and ionize atoms within the cellulose structure. This can lead to structural changes, degradation, and even complete breakdown of the material over time. Exposure to high levels of ionizing radiation to cellulose-based materials like paper, can result in yellowing, embrittlement, and a reduction in mechanical strength. The extent of damage also depends on factors such as the radiation dose, duration of exposure, and the specific type of cellulose material.

5 Conclusion

The use of gamma radiation for disinfection of cellulose materials involves a trade-off between microbial inactivation and potential damage to the material itself. Doses up to 10 kGy is sufficient to disinfect cellulose based cultural heritage artifacts and does not pose any harm towards cellulose base material. Careful consideration of radiation dosage and duration is essential to strike a balance between achieving disinfection goals and preserving the structural integrity of the cellulose.

References

M. C. Area and H. Ceradame. 2011. Paper aging and degradation: recent findings and research methods. *BioResources*, 6:5307–5337.

M. Bicchieri, M. Monti, G. Piantanida, and A. Sodo. 2016. Effects of gamma irradiation on deteriorated paper. *Radiation Physics and Chemistry*, 125:21–26.

M. Dasilva, A. Moraes, M. Nishikawa, M. Gatti, M. Vallimdealencar, L. Brandao, and A. Nobrega. 2006. Inactivation of fungi from deteriorated paper materials byradiation. *International Biodeterioration Biodegradation*, 57(3):163–167.

M. Jiménez-Reyes, D. Tenorio, M. Rojas-Robles, and G. García-Rosales. 2018. Physicochemical behavior of several kinds of paper under gamma irradiation. *Radiation Physics and Chemistry*, 148:13–18.

I. V. Moise, M. Ene, C. D. Negut, M. Cutrubinis, and M. M. Manea. 2017. Radiation processing for cultural heritage preservation: Romanian experience. *Nukleonika*, 62.

I. V. Moise, M. M. Manea, S. Vasilca, C. Pintilie, M. Virgolici, M. Cutrubinis, I.R. Stanculescu, and V. Meltzer. 2019. The crosslinking behaviour of cellulose in gamma irradiated paper. *Polymer Degradation and Stability*, 160:53–59.

N. Valentin. 1986. Biodeterioration of library materials. Disinfection methods and new alternatives. *The Paper Conservator*, 10:40–45.

Individual Research Contribution Review, 2023, 1(1): 231–232

Advancements in First-Generation Gamma-Ray Tomography: Development to Improved Imaging

Nazrul Hizam Yusoff
Industrial Technology Division, Malaysian Nuclear Agency
43000 Kajang, Selangor
nazrul_yusoff@nm.gov.my

Abstract

Gamma-ray tomography, as a non-invasive imaging technique, has witnessed significant progress since its inception as a first-generation technology. This extended abstract provides an overview of the development of first-generation gamma-ray tomography and highlights key advancements that can contributed to its continuous improvement. Results on two layers scanning system also presented as one of the ongoing advancements for the first-generation gamma-ray CT system.

Keywords: Computed Tomography, Gamma-ray CT, Image Reconstruction

1 Introduction

First-generation gamma-ray tomography emerged in the mid-20th century, pioneering the application of gamma rays for non-destructive imaging. Early implementations primarily focused on industrial applications, particularly for monitoring processes involving pipelines and chemical reactors. The foundational principles of using gamma-ray sources and detectors to capture attenuation data formed the basis for subsequent developments.

The initial systems utilized basic gamma-ray sources, often isotopes like Cobalt-60, Cesium-137 or Barium-133, coupled with simple detector configurations. These early implementations faced challenges related to resolution, data acquisition speed, and computational limitations (Abdullah et al., 2003; Denison et al., 1997; Jansen et al., 2001; Rossi et al., 2000; Abdullah et al., 2013). Despite these challenges, first-generation gamma-ray tomography provided valuable insights into the internal structures of objects and processes.

The early systems faced limitations in terms of spatial resolution and the ability to discriminate between materials with a slight difference in densities.

Time taken for each tomographic scanning also a challenge in developing parallel gamma-ray tomography system (Abdullah et al., 2015). Additionally, safety concerns associated with the use of radioactive isotopes prompted a search for alternative sources and methods to enhance both safety and imaging capabilities.

2 Methods

The development and improvement of first-generation gamma-ray tomography involved a series of methodological advancements in radiation source design, detector technology, and computational algorithms.

2.1 Advancements in Source and Detector Technology

Advancements in radiation source technology have led to the development of more sophisticated gamma-ray emitters with improved stability and safety profiles. Likewise, detector technologies have evolved, incorporating higher sensitivity and efficiency. These enhancements have contributed to better data quality and more accurate imaging.

2.2 Computational Improvements

The computational aspects of gamma-ray tomography have undergone substantial improvements. Advanced algorithms for image reconstruction, inspired by developments in medical imaging, have significantly enhanced the accuracy and speed of three-dimensional image generation. These algorithms address challenges such as data noise, limited-angle measurements, and incomplete data sets.

2.3 Simultaneous Scanning Method

An initial lab work had been done by measuring the effect of radiation counts on the different angle and distance from the gamma-ray source. With simultaneous counts from a single source is expected from the proposed two-layers CT system, this initial experiment will give an initial picture on how well the second layer measurement to be measured. The experiment also intended to measure the extend of the range for a reliable distance and angular spread for the second layer detector placement. Figure 1 illustrates the experimental setup for measuring the gamma-ray counts from the sealed source. In this experiment, Ba-133 source and 1-inch NaI detector were used. Both source and detector were collimated using Lead collimator with 0.5 cm circular aperture.

3 Results

Results presented here is one of the ongoing improvements done for the first-generation gamma-ray CT system. Figure 2 shows the results from this experiment plotted on two sides A and B. The results show there are differences on both side measurements. This indicates that there is angular effect from the source emission at different angle. Further experiments are in progress to investigate and explained this phenomenon. This is important so that the reading of the second layers in relation to the first is constant.

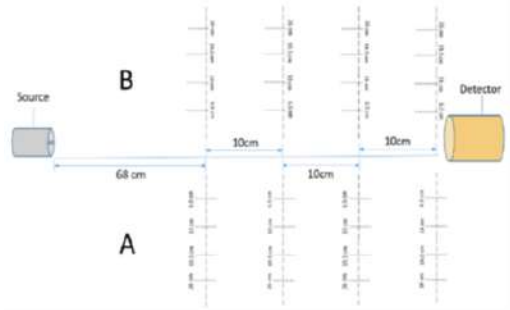

Figure 1: Gamma-ray measurement at different distance and right-angle position from the sealed source

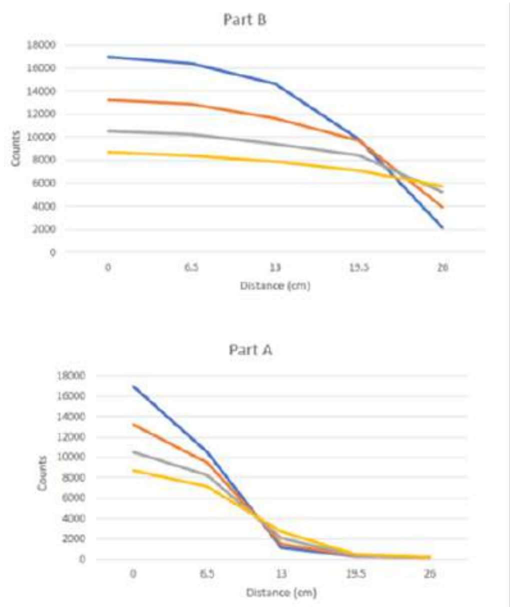

Figure 2: Different angular and distance counts from Ba-133 sealed source.

3.1 Reconstructed Images

The second layer collimator and detector holder had been successfully installed on the GammaSpider system as shown in Figure 3. Currently, the lab work on scanning and testing the ability of the second layer detection is in progress. The preliminary image from the scanning for first and second layer presented in Figure 4. Although from the reconstructed images suggest there are not much difference in the reconstructed image, the maximum and minimum count for each scanning and the relation to the pixel value still need to be investigate. Thus, detailed analysis is ongoing with more data and image need to be gathered before accurate analysis can be presented.

4 Conclusion

First-generation gamma-ray tomography laid the foundation for a powerful imaging technique that has evolved and improved over the decades. Advancements in radiation sources, detectors, and computational methods have addressed initial limitations, broadening the scope and enhancing the applica-

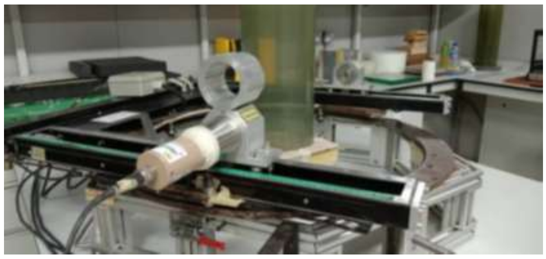

Figure 3: Two layers NaI detector holder for 1st Gen gamma-ray CT system

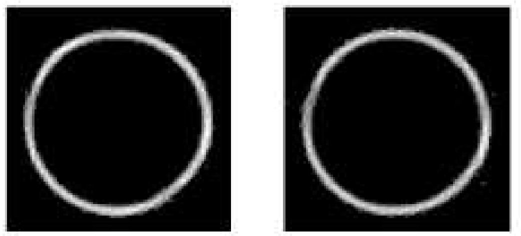

Figure 4: Reconstructed image of top (left) and bottom (right).

bility of gamma-ray tomography. One of the improvements presented here is by simultaneously scanning two-layers of tomographic image. promising This result demonstrate the ability for the 1st gen gamma-ray CT system to be advanced. The journey from its early industrial roots is ongoing commitment to innovation in non-destructive imaging technologies.

References

J. Abdullah, G. H. P. Mohamad, M. A. Hamzah, M. S. M.Yusof, M. F. A. Rahman, F. Ismail, and R. M. Zain. 2003. Development of a portable computed tomographic scanner for on-line imaging of industrial piping system. *Proceedings of the 5th National Seminar on NonDestructive Testing*.

J. Abdullah, Hearie Hassan amd Mohamad Rabaie Shari, Salzali Mohd, Mahadi Mustapha, Airwan Affendi Mahmood, Shahrizan Jamaludin, Mohd Rosdi Ngah, and Noor Hisham Hamid. 2013. GammaScorpion: Mobile gammaray tomography system for early detection of basal stem rot in oil palm plantations. *Opt. Eng.*, 52(3):036502.

J. Abdullah, H. Hassan, M.R Shari, M.M Ibrahim, N. Yussup, H. Ithnin, and A.A Mahmood. 2015. Development and implementation of a portable nucleonic computed tomography system with clamp-on-features for engineering inspection. *Jurnal Teknologi*, 77(17).

C. Denison, W. D. Carlson, and R.A. Ketcham. 1997. Three dimensional quantitative textural analysis of metamorphic rocks using high-resolution computed Xray tomography: Part i. methods and techniques. *Journal of Metamorphic Geology*, 15(3):29–44.

R.J. Jansen, H.F.W. Koens, C.W. Neeft, and J. Stoker. 2001. CT in the archaeologic study of ancient greek ceramics. *Radiographics*, 21:315–321.

M. Rossi, F. Casali, and D. Romani. 2000. Investigation of small egyptian mummies by 3D computed tomography. *Proceedings of the 15th World Conference on NonDestructive Testing*.

Individual Research Contribution Review, 2023, 1(1): 233–234

Ultrahigh Performance Concrete as Radiation Shielding with Mixture of High Density Mineral

N.M. Azreen
Industrial Technology Division, Malaysian Nuclear Agency
43000 Kajang, Selangor
noorazreen@nm.gov.my

Abstract

Radiation shielding linear attenuation coefficients μ (cm^{-1}) is highly depends on the density of the material used. Previous studies have shown the mineral known as barite can be effectively used to increase the specific density of concrete structures. Barite in Malaysia is limited; therefore, a locally available alternative source must be identified to meet the requirements of high−density concrete for radiation shielding. With the aim to explore the possibilities, to be further developed for the application in the hot cell, radiation generating equipment and storing radioactive waste. This study selected steel fiber−reinforced ultra−high-performance concrete (UHPC) samples with different inert materials, namely, silica sand (2700kg/m^3), amang (4000kg/m^3), hematite (2967kg/m^3), barite (4400kg/m^3) and lead glass (3038kg/m^3), as the study object and tested them experimentally for their mechanical properties and radiation absorption capabilities. The UHPC samples showed compressive strength values exceeding 155 MPa at 28 days. Meanwhile, UHPC with lead glass underwent decreased of compression strength in a long period, and UHPC with amang caused an issue related to radiological safety despite that it was effective as a γ−ray shield, UHPC with hematite and barite is very good in radiation absorption but cause an issue of practicality and country reserve. Thus, the use of UHPC with silica sand is practical for constructing nuclear facilities because of the abundance and cost-effectiveness of the involved materials.

Keywords: Ultrahigh Performance Concrete (UHPC), high density mineral, gamma radiation shielding.

1 Introduction

Concrete has proven to be an excellent and versatile material as radiation shielding. However, with unpredictable climate, heavy monsoon rain leads to heavy flood where the most devastating disaster in Malaysia (D/iya, Barzani Gasim, Ekhwan Toriman, & Abdullahi, 2014). Therefore, it is importance to carry on research to give better solution on the public safety to avoid leaching and migration of the radionuclides to surroundings.

The most advanced concrete technology nowadays is the invention of Ultrahigh Performance Concrete (UHPC) where this cementitious composite can achieve compressive strengths and flexural strength beyond 100 MPa respectively (Richard & Cheyrezy 1995) ductility comparable to steel (Kusumawardaningsih et al. 2015). Conventional reinforced concrete material normally has a specific density range between 2300 kg/m^3 to 2400 kg/m^3, which might be an issue on safety, toughness and durability if being used in severe environment. The previous research only uses concrete containing high density coarse aggregates (Akkurt et al. 2006) for radiation shielding. However, there have yet to find any research on UHPC. Therefore, in this research the usage of high density minerals have been selected as a replacement to sand in the mixture with UHPC.

Other than that, this research also focus on the maintenance program of UHPC due to lack of quality control methods (Shi et al. 2015) using non-destructive test mainly using ultrasonic pulse velocity (UPV). The results obtain will give bigger picture of UHPC quality and uniformity compared to steel and normal concrete. Previous research only focus on Ultrasonic Pulse Velocity value on concrete containing course aggregates. However, there have yet to find any research on UPV value on UHPC. The information gathered in this study gives input on the baseline data which useful for future research.

2 Methods

Five different types of fine aggregates were prepared for each UHPC mix based on reference of research done by R. Yu (2014) named as code B−UHPC for barite mix, H−UHPC for hematite mix, A−UHPC for Amang mix, LG−UHPC for lead glass mix and SS−UHPC for silica sand mix. The ideal proportion for each blend is based on UHPC done by Shi (2015) using only silica sand. Each UHPC mix were represented by twelve 100 mm cubes, three 75 mm ∅ × 150 mm long cylinders, seven 100 mm × 100 mm × 500 mm prisms and six 30 mm × 100 mm × 500 mm prisms. Based on the total sample, total volume is calculated and used in designing the UHPC mix proportion. Volume for each UHPC mix used in this research is 0.0667 m^3 after adding 10% of total volume to make sure that the mix design is enough to fill all the moulds. 28 specimens for each UHPC mix were prepared for this research and sum up to 140 specimens as total.

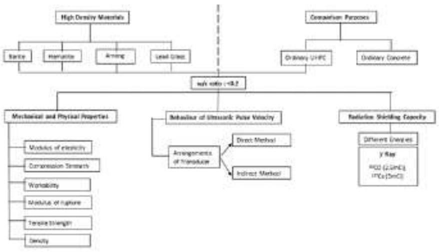

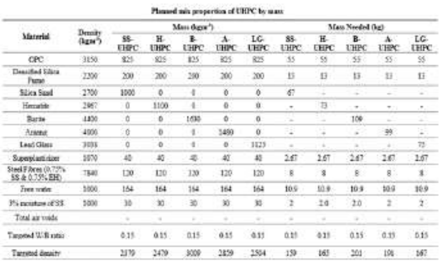
Planned mix proportion of UHPC by mass

Material	Density (kgm^{-3})	Mass (kgm^{-3})					Mass Needed (kg)				
		SS-UHPC	H-UHPC	B-UHPC	A-UHPC	LG-UHPC	SS-UHPC	H-UHPC	B-UHPC	A-UHPC	LG-UHPC
OPC	3150	825	825	825	825	825	55	55	55	55	55
Densified Silica Fume	2200	200	200	200	200	200	13	13	13	13	13
Silica Sand	2700	1000	0	0	0	0	67	-	-	-	-
Hematite	2967	0	1100	0	0	0	-	73	-	-	-
Barite	4400	0	0	1690	0	0	-	-	109	-	-
Aramid	4000	0	0	0	1480	0	-	-	-	99	-
Lead Glass	3038	0	0	0	0	1123	-	-	-	-	75
Superplasticizer	1070	40	40	40	40	40	2.67	2.67	2.67	2.67	2.67
Steel Fibres (0.75% SS & 0.75% EH)	7840	120	120	120	120	120	8	8	8	8	8
Free water	1000	164	164	164	164	164	10.9	10.9	10.9	10.9	10.9
3% moisture of SS	1000	30	30	30	30	30	2	2.0	2.0	2	2
Total air voids		-	-	-	-	-	-	-	-	-	-
Targeted W/B ratio		0.15	0.15	0.15	0.15	0.15	0.15	0.15	0.15	0.15	0.15
Targeted density		2379	2479	3009	2859	2504	159	165	201	191	167

3 Result and Discussion

The workability, W/B ratio and density of all UHPC samples are presented in Table 1. Measurements for the studied mixtures were compared with those for a UHPC mix with only silica sand.

Table 1: W/B ratio, workability, density and average pore size of UHPC mixtures.

UHPC Mix	W/B ratio	Workability (mm)	Density (kg/m^3)	Average pore ∅(nm)
SS−UHPC	0.15	210	2401	83.96
A−UHPC	0.16	190	3036	11.72
LG−UHPC	0.16	250	2479	98.9
H−UHPC	0.18	160	2602	7.82
B−UHPC	0.15	210	3112	148.8

Significantly, H−UHPC shows the lowest workability which is 160 mm even though it has the highest W/B ratio. According to a laboratory study done using Brunauer–Emmett–Teller theory, which aims to determine the average pore ø of materials, the decrease in workability of UHPC mixes was considerably attributed to a reduced pore ∅. Pores with small ∅ produce large surface areas, thereby causing additional water to be absorbed and consequently reducing workability (Vaitkevičius et al. 2014).

The average curing of 1, 7, 28 and 56 days to determine compressive strength for each UHPC mixes are presented in Figure 1. The test was carried out using 2500 kN compression testing machine at a loading rate of 80 MPa/min.

In such an environment, glass powder will encounter alkali silica reaction (ASR). This shows that at the condition whereby the compression strength of LG−UHPC significantly dropped by 6% on day−56 compared to day−28. B. Topçu & Canbaz (2004) claimed that waste glass contains high NA2O and shows signs of amorphousness (reactive non-crystalline), which causes ASR eventually. This reaction will cause the expansion in the altered aggregates through the swelling gel of the C−S−H formed. This gel when mixed with water will increase in volume and exerts expansion in pressure inside the material, which will cause spalling and weaken the concrete.

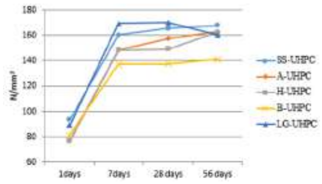

Figure 1: Compressive strength for each UHPC mixes

The mass attenuation coefficient has an unit of cm^2/g and it can be written as $\mu m = \mu/\rho$, where μ is the linear attenuation coefficient come with an unit of cm^{-1} and ρ is the density with an unit of g/cm^3. The μm value is an important parameter to assess the radiation absorption ability of a material. The higher the μm value the better its absorption to radiation. Figure 2 below shows mass attenuation coefficient of all UHPC samples with different γ−ray energy.

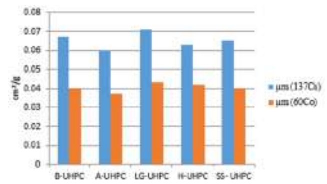

Figure 2: Mass attenuation coefficient of all UHPC samples with different γ−ray energy

4 Conclusion

Compression strength of LG−UHPC dropped by 6% on day−56 and continuous dropped to 21% at day 610 compared to day−28 is not due to ASR but caused by non−homogenous portlandite, elongated and flattened nature of LG particles. It is found that UPV value for UHPC only applicable for classification of concrete quality and control deterioration. All the UPV value of all UHPC mixes achieved 4000 m/s which concludes high quality and uniformity. UPV data on 7 days, 14 days, 28 days and 56 days shows varying of velocity in range 4000 – 5000 m/s. Due to its practicality and cost efficiency, it is found that SS−UHPC is the better choice to be used as a shielding material in nuclear facilities as compared to the other UHPC. Besides the overall radiation shielding ability of SS−UHPC is only slightly lower than B−UHPC, H−UHPC, A−UHPC and LG−UHPC. In term of abundance and economy, SS−UHPC has a larger availability than the other four material.

References

Refer to Construction, Building Materials 172 (2018) 370−377, Construction, Building Materials 263 (2020) 120161, Construction, and Building Materials 262 (2020) 120567.

Individual Research Contribution Review, 2023, 1(1): 235–236

Application of Computed Radiography (CR) Tangential Technique for Wall Thickness Measurement

Noorhazleena Azaman
Industrial Technology Division, Malaysian Nuclear Agency
43000 Kajang, Selangor
hazleena@nm.gov.my

Abstract

Wall thickness assessment, with Radiography Testing (RT) is normally used to inspect such discontinuities and can be performed with two approaches; (a) center line beam technique (b) tangential technique. The latter is a method of choice for this work.

Keywords: Nondestructive Testing (NDT), radiography testing (RT), computed radiography (CR), tangential radiography technique

1 Introduction

The introduction of powerful computers and reliable imaging technologies has significant impact on the currently used NDT methods. New radiologic imaging technique in Digital Radiography; Computed Radiography (CR) with phosphor imaging plates have increased the capacity and accuracy for visualization and measurement of defects.

A typical application for Computed Radiography (CR) is the quantification of corrosion effects in pipe walls (shadow technique or projection radiography). The inspection for corrosion in pipes is one of the most important NDT precautions measures in the chemical industry.

2 Methods

Two techniques recommended for making tangential radiograph. There are radiation source located on the pipe centre line as Figure 1 and radiation source located offset from the pipe centre line as Figure 2. The suitable technique used in this validation, application and inspection is the technique TA where there are intended for tangential radiography of generalized wall loss and the radiation source is located offset from the pipe centre line.

For tangential radiography, the choice of radiation source should be determined by the maximum penetrated thickness of the pipe, W_{max} which occurs for the path forming a tangent to the pipe inner diameter, as shown in Figure 3.

3 Results

Image from the Figure 4 below shows the result from the simulation. At the area where the 45% groove is created, the thickness calculated is 4.95mm. It is mean the value for measured and calculated is equal. Here, the simulation of Computed Radiography (CR) tangential technique for wall thickness measurement of 10 inch carbon steel pipe was identified and determined.

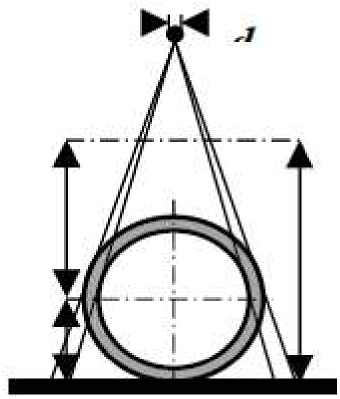

Figure 1: Test arrangement and distances for tangential radiography with the source located on the pipe centre line

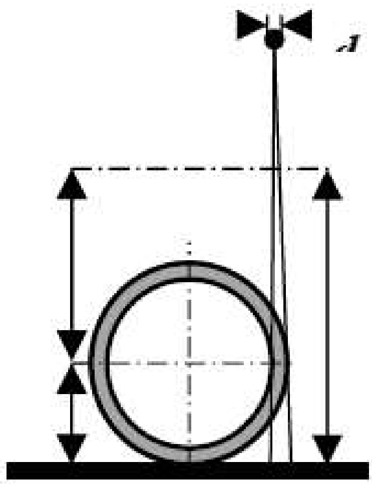

Figure 2: Test arrangement and distance for tangential radiography with the source offset from the pipe centre line

4 Discussion

From the results, it gives the reliable data for the wall thickness measurement of 10 inch carbon steel pipe.

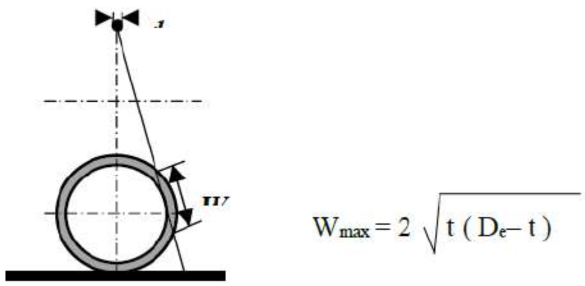

Figure 3: Maximum penetrated thickness, W$_{max}$, for the tangential radiography technique

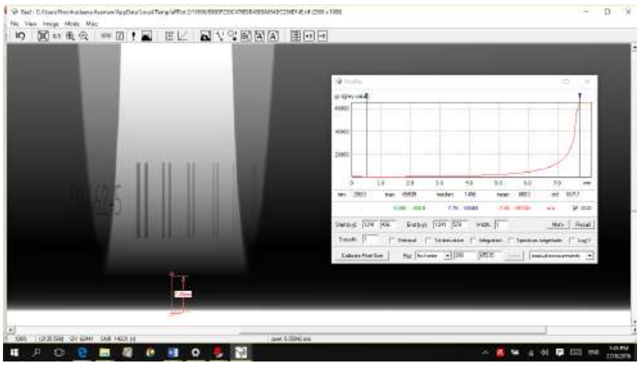

Figure 4: Result radiography image from simulation

5 Conclusion

The image of radiography for simulation and real exposure (experiment) were analysed. The result image from simulation shows that the calculated and measured pipe with groove 4.95mm thickness results are equal. The result calculated is according to the standard of ISO 20769-1 for tangential radiography.

References

ISO 20769-1. 2018. Non-destructive testing - radiographic inspection of corrosion and deposits in pipes by X- and gamma rays - Part 1: Tangential radiographic inspection.

Individual Research Contribution Review, 2023, 1(1): 237–238

Development of Smart RT-NEMO Capsule for Leak Detection in Underground Pipeline Application

Noraishah Othman
Industrial Technology Division, Malaysian Nuclear Agency
43000 Kajang, Selangor
noraishah@nm.gov.my

Abstract

The detection of leakage in underground pipeline is significant challenge to many industries, in particular oil and gas industry. Therefore, Radiotracer Technology (RT) is adopted to solve the issue.

Keywords: Radiotracer Technology, Leakage, Underground pipeline

1 Introduction

RT is the introduction of radioactive material inside the domain and the tracing of gamma radiation emitted by this material is conducted externally using scintillation detector. Any drop of velocity along the pipeline is susceptible to potential leak area. RT is very sensitive, effective and competitive for on-line leak detection and widely used for on-line leak detection. However, the conventional RT is very expensive, requires a lot of manpower, cumbersome and very time consuming.

Thus, SMART RT-NEMO is introduced to overcome the aforementioned problems as well as to localize and verify the leakage of industrial underground pipeline. This state-of-art system utilizes a silicon photomultiplier (SiPM), a semiconductor photo-detector coupled with NaI scintillator detector to act as gamma detector. SiPM is used as an alternative to PMT for scintillator readout and has a higher photon detection efficiency which creates larger signals.

2 Methods

In SMART RT-NEMO has 2 modules which are radioactive tracer Module (M1) and Positioning Module (M2) respectively.

2.1 Radiotracer Module (M1)

M1 comprises of SiPM coupled with NaI scintillator detector as the sensor and data logger to acquire and save the radiation signals. Data logger is made up of Raspberry Pie 3B+ to acquire the radioactive signals and also to save the data in the system, Real Time Counter (RTC) is embedded in order to ensure the time polling from SiPM to data logger is synched. M1 will be powered up by Lithium battery.

2.2 Positioning Module (M2)

Module 2 consists of three odometer attached to the wall of the system to localize the position travelled by the system and also integration board (IB) which acts as the common platform to integrate data from data logger and odometers. The integration board is powered up by the 12V DC lithium battery. The integrated data will be extracted using work station using wireless or cable. All the components are encapsulated using stainless steel material and compressible polyurethane (PU) rubber cup to seal the pipeline. Figure 1 shows the general architecture of the SMART RT-NEMO.

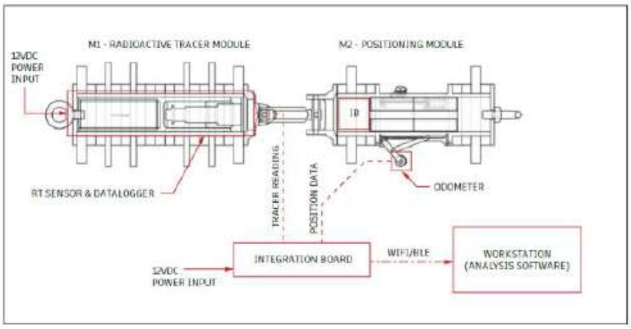

Figure 1: General Schematic Architecture

2.3 Development of experimental rig

Experimental rig is developed to execute RT-NEMO testing. The rig consists of two skids which are the 2 10” x 4.5m length of carbon steel pipe and 2 x 1m pipe attached to S-bend pipe as shown in Figure 2.

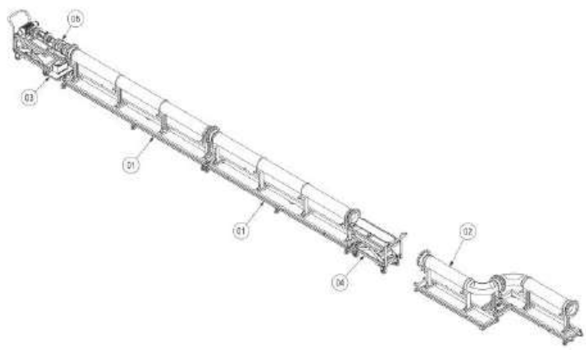

Figure 2: Experimental Rig

3 Data/Results

SMART RT-NEMO will be launched at the upstream of the 10 inch underground or buried pipeline and retrieved at the other end of the pipeline.

3.1 Application

The system will be mobilized using winch at designated speed. Moreover, the system can be used not only in the straight pipe but also at bend radius 1.5D for 10” pipe size as shown in Figure 3.

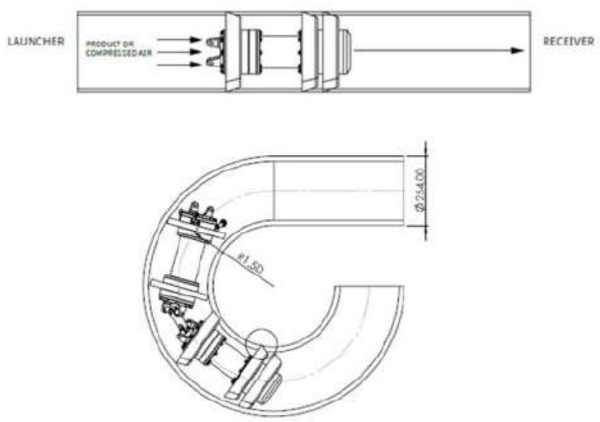

Figure 3: Movement of RT-NEMO inside the pipe

4 Discussion/Conclusions

The analysis from the experimental result is the main objective of the development of SMART RT-NEMO. The results should show the ability and capacity of SMART-RT-NEMO in order to acquire and store radioactive signals as well as to track the distance travel by RT-NEMO at designated speed. The speed of RT-NEMO will be controlled by winch. The radioactive source Cs-137 with various activities will be used as mimic of the leak occurrence since the work only involves dry experiment and align with TRL 3-4 which does not involve actual industrial environment.

4.1 Graphical User Interface (GUI)

The results of operating parameters can be observed from the GUI developed by team and can be completed at the end of the project.

References

Hills AE. 2001. Practical guidebook for radioisotopes-based technology in industry. 2nd edition. *IAEA/RCA RAS/8/078*.

IAEA. 2001. Radiotracer technology as applied to industry. *IAEA-TECDOC1262*.

IAEA. 2004. Radiotracer applications in industry: A guidebook. *IAEA Technical Reports Series No. 423*.

IAEA. 2008. Radiotracer residence time distribution method for industrial and environmental applications. *IAEA TECDOC Series No.31*.

IAEA. 2009. Leak detection in heat exchangers and underground pipelines using radiotracers. *IAEA-TCS-38*.

Individual Research Contribution Review, 2023, 1(1): 239–240

Effect of Low Doses Gamma Irradiation on XRD Crystallization of Commercial Silicate Glasses Containing High Lead

Nor Hayati Alias
Industrial Technology Division, Malaysian Nuclear Agency
43000 Kajang, Selangor
norhayati@nm.gov.my

Abstract

Irradiation has a significant impact on the structures and properties of glasses, potentially altering their chemical, physical, and mechanical characteristics, as well as their crystallization behaviors. This study focuses on investigating the effects of low-dose gamma irradiation on the XRD (X-Ray Diffraction) crystallization properties of shielding glasses, using commercial lead silicate glasses as a typical example. Irradiation strongly influences the structural connectivity of the glasses, leading to a decrease in the crystallinity index in irradiated glasses. Predominantly, lower crystalline phases are formed in glasses subjected to higher low doses. The results presented here illustrate how even lower doses of irradiation can contribute to changes in the crystallization of silicate glasses containing a high concentration of lead.

Keywords: Irradiation, silicate and crystallization

1 Introduction

The study focuses on the structural alterations in glass resulting from irradiation, even at lower dose concentrations. Most of these changes remain inconspicuous to the naked eye under normal conditions. In contrast, the investigation of transparent materials as radiation shielding has elevated the demand for glasses in this domain compared to concrete. The preference for glasses is attributed to numerous advantages, as highlighted by Mahmoud et al. (Mahmoud et al., 2023) and Sayyed et al. (Sayyed et al., 2020), encompassing ease of processing, competitive pricing, optical clarity in the visible spectrum, and a diverse range of composites suitable for intended applications.

In this study, XRD spectroscopy is employed to observe changes in crystallization behavior in commercial glasses at doses of 0, 0.007Sv, 0.035Sv, 0.07Sv, 0.105Sv, and 0.14Sv. The samples are denoted as C0, C1, C2, C3, C4, and C5, respectively. The observed changes are recorded using the XRD Crystallinity Index (CI), where a higher CI indicates stronger structural bonding in the glass.

2 Methods

Origin software was utilized to integrate the crystallinity region within the amorphous peak of glass. The Crystallinity Index (CI) for both unirradiated and irradiated samples was determined using Origin software. The crystallinity index is calculated by determining the ratio of the integrated area of crystalline peaks to the total integrated area under the XRD peak (Schroeder et al., 1986).

$$CI\% = \frac{\text{area of all crytalline peaks}}{\text{total area of all crystalline and amorphous peaks}} \times 100\%$$

Figure 1 display the observed spectral characteristics in commercial glasses before and after irradiation. The results of the crystallinity index, expressed as percentage values, are shown in Figure 2.

3 Results

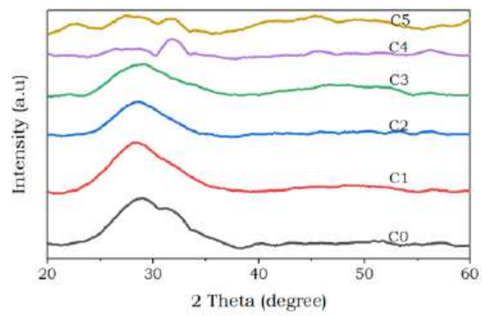

Figure 1: XRD of sample before and after irradiation

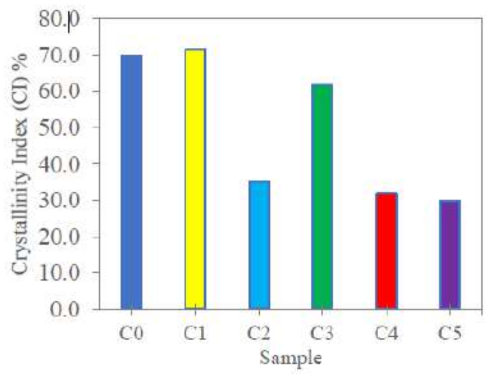

Figure 2: Plot of Crystallinity Index (CI) versus sample

4 Discussion

The glass displays an amorphous nature, characterized by the absence of long-range order and the presence of dual humps (Marzuki et al., 2023) for samples C0 to C3. Amorphous regions lack a well-defined crystal lattice, and the structural arrangement is more random. A further reduction in the crystallinity index after irradiation implies a higher proportion of amorphous or disordered regions in the glass material. This indicates an increase in short-range order in glass amorphous bonding, particularly at 0.105 Sv and 0.14 Sv. The disappearance of the broader hump peak near 25 to 30 degrees is observed at these irradiation doses, resulting in a smaller single hump. Samples of irradiated glass with a crystallinity index below approximately 30% exhibit a higher likelihood of forming smaller humps, as indicated in conditions C4 and C5 at 0.105 Sv and 0.14 Sv, respectively.

5 Conclusion and Attention

When dealing with glass, X-ray diffraction (XRD) may not be the most suitable technique for determining crystallinity due to its amorphous nature. Nevertheless, for glass, a low crystallinity index is expected because of its amorphous nature, reflecting the absence of a well-defined crystalline structure and the unique disordered arrangement of atoms or molecules in glass. A decrease in the crystallinity index (CI) from approximately 70% to lower than 30% in glass after irradiation suggests a significant change in the material's structure. The irradiation may have caused structural disruptions in the glass, leading to a reduction in the ordered arrangement of atoms. This could involve further breaking of bonds or the creation of defects, introducing more disorder into the material and thus lowering the crystallinity index of irradiated glass, resulting in the formation of much smaller humps. Samples C4 and C5 are indicative of these structural changes caused by enhance low doses irradiation.

References

K. Mahmoud, M. Sayyed, D. Aloraini, A. Almuqrin, A. Abouhaswa, and C. Chantler. 2023. Impacts of praseodymium (iii, iv) oxide on physical, optical, and gamma-ray shielding properties of boro-silicate glasses. *Radiation Physics and Chemistry*, 207:110836.

A. Marzuki, T. Sasmi, D. E. Fausta, H. Harjana, V. Suryanti, and I. Kabalci. 2023. Radiation physics and chemistry. 205(December 2022):110722.

M.I. Sayyed, M.H.M. Zaid, N. Effendy, K.A. Matori, H.A.A. Sidek, E. Lacomme, K.A. Mahmoud, and M.M. AlShammari. 2020. The influence of PbO and Bi_2O_3 on the radiation shielding and elastic features for different glasses. *J. Mater. Res. Technol.*, 9:8429–8438.

L. R. Schroeder, V. M. Gentile, and R. H. Atalla. 1986. Nondegradative preparation of amorphous cellulose. *Journal of Wood Chemistry and Technology*, 6(1):1–14.

Individual Research Contribution Review, 2023, 1(1): 241–242

Energy Dispersive X-Ray Fluorescence (ED-XRF) Analysis on Acids and Deionized Water Used for Impurities Removal from Rare Earth-Loaded Organic

Norhazirah Azhar
Industrial Technology Division, Malaysian Nuclear Agency
43000 Kajang, Selangor
norhazirah@nm.gov.my

Abstract

Removing impurities after solvent extraction during the rare earth purification process is crucial to avoid any interference in the stripping process afterwards. The acids used to remove impurities via liquid-liquid extraction are HNO_3 and HCl at low concentrations. While deionized water is used to remove of impurities at different temperatures. This paper will discuss on results of impurities removed from the rare earth-loaded organic via Energy Dispersive X-ray Fluorescence (ED-XRF).

Keywords: ED-XRF, liquid-liquid extraction, scrubbing, rare earth, tributyl phosphate

1 Introduction

Rare earth element (REE) consists of fifteen elements in the lanthanide group including yttrium (Y) and scandium (Sc). REEs become a vital component in various products due to their unique physicochemical properties (Devi and Sukla, 2019) and applied in various fields whilst presently having no substitution which makes them more essential (Goodenough et al., 2018).

Monazite, bastnaesite and xenotime are some examples of minerals that contains REE and they are also known as rare earth minerals. In this paper, the focus is made on Malaysian xenotime mineral that was obtained from local by-products of tin mining. REE was recovered from xenotime via the recovery process that starts with cracking, leaching until selective precipitation. The precipitated rare earth product in oxalate form was then purified further in the purification process.

During purification, solvent extraction was done to extract elements of interest from the oxalate in acidic media. The extractant used is tributyl phosphate (TBP) mixed with kerosene as diluents. After the extraction process, this REE-loaded TBP/Kerosene (RE-loaded organic) will undergo scrubbing process.

Scrubbing is a process of which unwanted elements (impurities) such as calcium, sulphur, potassium, sodium, chlorine, iron etc. will be removed from the solution of interest. Scrubbing is done to improve the efficiency of the upcoming process (stripping of desired element) by removing elements that may cause interference during stripping process.

Various acids were studies to remove these impurities from organic solvents such as using HCl (Zhou et al., 2021), HNO_3 (Bae et al., 2020) and also via deionized water (Jorjani and Shahbazi, 2016).

In this study, scrubbing of unwanted elements was done via HCl and HNO_3 and via deionize water. Efficiency of scrubbing process will be measure via Energy Dispersive X-ray Fluorescence (ED-XRF).

2 Methods

2.1 Scrubbing via HNO_3 and HCl of different concentrations

Scrubbing media was prepared using HNO_3 and HCl at concentrations of 0.01, 0.1, 0.3, 0.5 and 0.7M. Rare earth-loaded organic (Tributyl Phosphate/ Kerosene) was retrieved from previous extraction process. Scrubbing process was done by mixing scrubbing acid with RE-loaded organic of ratio 1:1 in a beaker and stirred for 15 minutes. The mixtures were transferred into a separatory funnel and allowed for separation into two distinct layers. Both solutions transferred back into each sample bottles.

2.2 Scrubbing via deionized water at different temperatures

Scrubbing media was prepared using deionized water. Rare earth-loaded organic (Tributyl Phosphate/ Kerosene) was retrieved from previous extraction process. Scrubbing process was done by mixing scrubbing acid with RE-loaded organic of ratio 1:1 in a beaker and stirred for 15 minutes with presence of temperature at room temperature, 40, 50, 60, 70 & 80°C. The mixtures were transferred into a separatory funnel and allowed for separation into two distinct layers. Both solutions transferred back into each sample bottles.

2.3 ED-XRF Analysis

All samples were analyzed via Energy Dispersive X-ray Fluorescence (ED-XRF) before and after scrubbing process and recorded as the initial and final reading respectively.

3 Data/Results

3.1 Scrubbing via HNO_3

Figure 1 shows that at 0.7M HNO_3, about 50% of Cl was successfully removed from the RE-loaded organic despite becoming the least favorable concentration for S scrubbing. Lowest concentration of HNO_3 (0.01M) resulting in optimum Ca scrubbing. When the concentration increases, the percentage of Ca removed decreases. Conversely, S is only selective

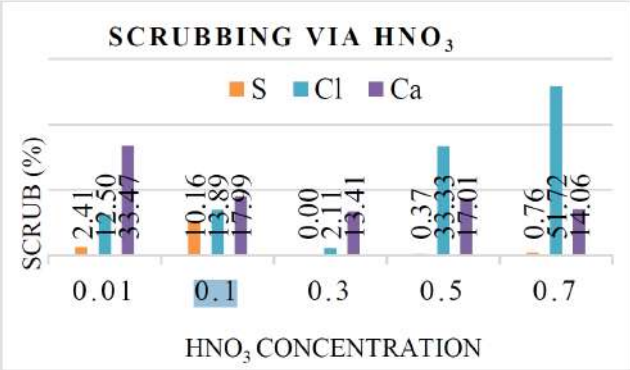

Figure 1: Scrubbing Efficiency at different HNO_3 concentrations

when HNO_3 is lower than 1.0M, with a 10.16% scrubbing. Sulphur appears very little or almost absent from the acid concentration higher than 0.3M.

3.2 Scrubbing via HCl

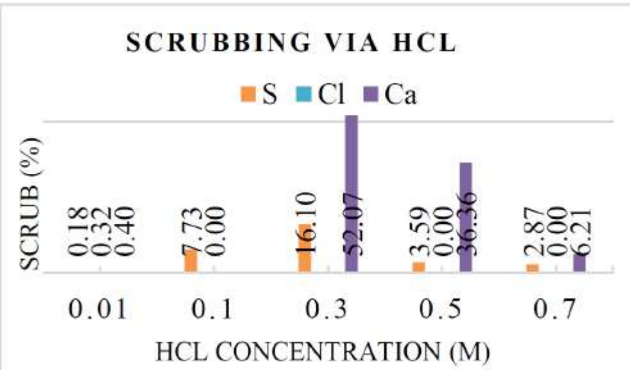

Figure 2: Scrubbing Efficiency at different HCl concentrations

Figure 2 shows that HCl unable to remove Cl from RE-loaded organic at every concentration except at 0.01M with percent scrubbing of 0.32%. Removal of S shows increasing trend from 0.01M to 0.3M and decrease afterwards. The scrubbing of C only achieves at concentration of 0.3M and reduces as the concentration increases. To conclude, optimum concentration for removal of Ca and S is at 0.3M HCl. However, HCl appears unsuitable for removal of Cl from TBP/Kerosene system.

3.3 Scrubbing via deionized water at different temperatures

The process of impurities removal via deionized water (Figure 3) shows that only potassium (K) can be removed successfully in general, with percent scrubbing between 78 – 97%. The optimum condition is at 60°C, where 97% of K is removed from the RE-loaded organic.

4 Discussion/Conclusion

The optimum concentration of HNO_3 for scrubbing of S at 0.1M, for Cl at 0.7M and Ca at 0.01M. On the other hand, the

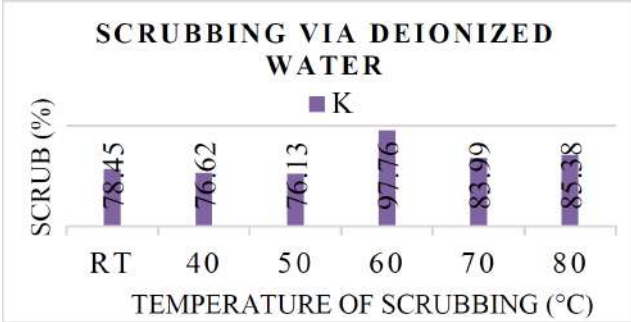

Figure 3: Scrubbing Efficiency via deionized water at different temperatures.

optimum HCl concentration for removing impurities, especially Ca and S, from the REE-loaded TBP/Kerosene system is at 0.3M HCl. The optimum condition for deionized water as scrubbing media is at 60°C.

References

M. Bae, J. chun Lee, H. Lee, and S. Kim. 2020. Recovery of nitric acid and gold from gold-bearing aqua regia by tributyl-phosphate. *Separation and Purification Technology*, 235, https://doi.org/10.1016/j.seppur.2019.116154.

N. Devi and L. B. Sukla. 2019. Studies on liquid-liquid extraction of yttrium and separation from other rare earth elements using bifunctional ionic liquids. *Mineral Processing and Extractive Metallurgy Review*, 40(1):46–55, https://doi.org/10.1080/08827508.2018.1481058.

K. M. Goodenough, F. Wall, and D. Merriman. 2018. The rare earth elements: Demand, global resources, and challenges for resourcing future generations. *Natural Resources Research*, 27(2):201–216, https://doi.org/10.1007/s11053–017–9336–5.

E. Jorjani and M. Shahbazi. 2016. The production of rare earth elements group via tributyl phosphate extraction and precipitation stripping using oxalic acid. *Arabian Journal of Chemistry*, 9:S1532–S1539, https://doi.org/10.1016/j.arabjc.2012.04.002.

X. Zhou, Y. Shen, J. Peng, and Q. Liu. 2021. Separation of Fe(iii) and Al via tributyl phosphate and 2-octanol in the comprehensive recovery process of metals from hydrochloric acid leaching solution of fly ash. 28(1).

Individual Research Contribution Review, 2023, 1(1): 243–244

The Pilot Mineral Processing Plant: Installation and Operation

Nor Pa'iza bin Mohamad Hasan
Industrial Technology Division, Malaysian Nuclear Agency
43000 Kajang, Selangor
norpaiza@nm.gov.my

Abstract

The alkaline cracking method involves digesting monazite in caustic soda to convert phosphorus into water-soluble tri-sodium phosphate (WSTSP), leaving the rare earth and thorium as insoluble hydroxides. WSTPS is removed and crystallized as a profitable byproduct. The insoluble hydroxide is treated with hydrochloric acid to separate the rare earth from salable rare earth chlorides. The remaining hydroxide dissolves as thorium chloride, leaving the insoluble silica as a solid residue. Then, this Thorium chloride precipitation is subjected to a solvent extraction system, followed by precipitation in oxalic acid, and finally calcined to produce high purity thorium oxide. The Malaysian Nuclear Agency (Nuklear Malaysia) is considering processing local monazite using alkaline methods to produce high-value rare earth products.

Keywords: Thorium, monazite, extraction

1 Introduction

Nuklear Malaysia has developed a pilot mineral processing plant based on the extraction of elements using an alkaline method developed in-house. This method extracts thorium from local monazite raw materials through five production lines. The pilot plant can handle up to 100 kg of monazite raw material with an expected yield of 6 kg of thorium oxide at the end of the process.

2 Methods and Operations

The overall Thorium extraction process from raw Monazite minerals follows the Alkali Cracking Method. It can be divided into five stages: trisodium phosphorus (TSP) production, rare earth (RE) carbonate production, sodium diuranate production, thorium oxide production, and finally, purification of thorium oxide production. Figure 1 shows the flow process to produce thorium oxide.

2.1 Trisodium Phosphate (TSP) Production Line

This process can be divided into seven sub-units: monazite grinding, monazite digestion, leaching, filtration of leachate solution, evaporation of TSP solution and crystallization in a centrifuge which will be operated sequentially unit by unit.

First, raw monazite is crushed and reduced to particles up to 300# mesh size (>95%). Monazite is pre-treated with caustic

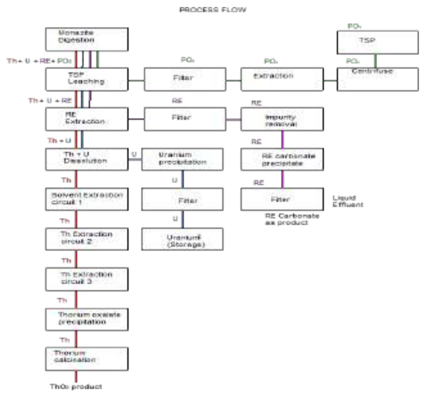

Figure 1: Process flow for thorium extraction and purification

soda and digested in a jacketed reactor at 140-1600°C. The literature has reported that monazite particles smaller than 300# mesh show satisfactory digestion efficiency.

2.2 Rare Earth (RE) Carbonate Production Line

This line consists of two processes: RE dissolution & filtration and RE Carbonate deactivation, precipitation and crystallization steps. The feed to the RE Carbonate production line is a mixed hydroxide cake obtained from the TSP Production line.

In this process, the mixed hydroxide solid mass is collected in a simple filtration system. Measured quantities of mixed hydroxide slurry and hydrochloric acid are treated in an extractor to extract rare earth metals. The pH of rare earth extraction was controlled in the range of 2.9–3.1 to obtain >99% extraction efficiency. The extraction temperature was controlled below 70°C to avoid the generation of aggregated compounds. Then, the rare earth chloride solution is treated with high molecular poly electrolytes and animal glue to remove suspended solids. Thorium Hydroxide is filtered and the weak rare earth chlorides are recycled. Radium, lead, iron, and barium sulfate are removed during settling. After settling, a deactivated rare earth chloride solution is removed. The precipitated solid lead-barium-radium sulfate slurry is filtered and the weak rare earth chloride solution is recycled.

2.3 Sodium Diuranate (SDU) Production Line

In this line, thorium and uranium hydroxide cakes received from the previous section are processed by dissolving in 1.5M hydrochloric acid. This section is intended to selectively dissolve thorium and uranium while leaving other impurities in solid form. Both thorium and uranium chloride solutions are then subjected to liquid-liquid extraction, where uranium is separated by extraction using tri-isobutyl amine (TOA) solvent. The extracted uranium is then stripped with water before being precipitated with sodium hydroxide into salable sodium diuranate (SDU).

In this section, the mixed solid of thorium+uranium hydroxide is subjected to the dissolution of hydrochloric acid into a solution of thorium and uranium chloride. The dissolution process is controlled at a pH below 1 and the temperature is maintained at <70°C, preferably at around 65°C. The resulting clear thorium chloride solution is pumped to a storage tank and the remaining insoluble solids are removed by filtration. Solid waste is packed in HDPE containers for disposal.

2.4 Thorium Oxalate Production Line

The thorium chloride solution produced from the previous process was treated in a counter current acid-proof FRP mixer settler using diethyl-hexyl phosphonic acid. The thorium chloride solution is extracted and stripped with sulfuric acid in a mixer settler. This operation aims to recover thorium as oxalate. After that, the thorium oxalate is treated and prepared for purification in the downstream operation.

At this line, thorium chloride solution with 40-60g/L thorium oxide is subjected to conversion to crude thorium oxalate. Thorium firstly extracted with a diethyl-hexyl phosphonic acid at an organic to aqueous ratio of 2:1. Then followed by a stripping process with weak sulfuric acid as a stripping agent. This solvent extraction system removes thorium as crude thorium sulfate and leaves other impurities as rare earth raffinates. Then, the thorium sulfate solution is further treated with oxalic acid. From there on, thorium is converted to oxalate, producing spent sulfuric acid. The spent sulfuric acid separated from this process is recycled in the extraction system. Thorium slurry is about 70-100 L with 5-15% solids.

2.5 Thorium Nitrate Purification and Thorium Oxide Production Line

Thorium nitrate solution is extracted using tributyl phosphate (TBP) and refined as pure thorium nitrate during solvent extraction system. The thorium nitrate is again refined with a final solvent extraction system consisting of extraction, scrubbing and stripping stages. The purified thorium nitrate solution is then precipitated into thorium oxalate before being calcined to produce thorium oxide (ThO_2) as the final product.

The stripped thorium stream is then evaporated and concentrated before being crystallized in a stainless steel batch operated centrifuge with a capacity of 30 kg per batch to separate thorium nitrate crystals. The mother liquor is sent to an acidic effluent tank. The above thorium nitrate crystals are dissolved in nitric acid with a concentration adjusted to 150-250 g/L and 1.5-2 N nitric acid equivalent to a 6% HNO_3 solution. This thorium nitrate solution is treated with analytical grade barium nitrate and magnesium nitrate to remove sulfate impurities.

3 Results

The results obtained from the operation line are started upon completion of the reaction, the reacting mass is transferred into a leaching reactor where soluble trisodium phosphate is separated from the mixed hydroxide solids using single or multi-stage leaching methods. This is followed by filtration of the trisodium phosphate solution to separate the TSP solution from the mixed hydroxide. The clear trisodium phosphate filtrate is stored in a clear TSP solution tank. At the Rare Earth (RE) Carbonate Production Line, Deactivated rare earth chloride solutions are precipitated and produced as rare earth carbonates which are salable byproducts of thorium extraction from the monazite mineral process.

In the Sodium Diuranate (SDU) Production Line,Thorium chloride solution containing thorium and uranium is subjected to a solvent extraction system. The solvent extraction system separates the uranium and then dilutes it with water. This thorium chloride solution typically contains about 2-3gpl heavy metals, 10-30gpl rare earths and 50-80gpl ThO_2.

In the thorium Oxalate Production Line, Crude thorium oxalate is finally prepared for purification by treatment in sodium hydroxide into thorium hydroxide before dissolution in nitric acid into thorium nitrate solution. Dissolution occurs by maintaining 1.5-2M nitric acid equivalent to 6% HNO_3.

In the thorium Nitrate Purification and Thorium Oxide Production Line, sulfate-free thorium nitrate is processed. Finally, pure thorium oxalate is calcined as thorium oxalate (ThO_2) and packaged in 20 liter polyethylene-lined metal containers.

4 Conclusion and Attention

Most of the equipment in the pilot mineral processing plant is static equipment, such as tanks, mixer settlers, and filters, except for the stirrer, agitator, and motors. The moving parts, such as the agitator and pump, are not operating simultaneously. These operations will be carried out on a cycle basis. The plant can be operated with the complete installation. This plant can operate up to 100 kg of raw material from monazite, and the estimated end of the process will achieve 6 kg of thorium oxide.

References

M. Eskandari Nasab, A. Sam, and S.A. Milani. 2011. Determination of optimum process conditions for the separation of thorium and rare earth elements by solvent extraction. *Hydrometallurgy*, 106:141–147.

Hafni Lissa Nuri, Abdul Jami Prayitno, and M. Pancoko. 2014. Preliminary design needs for a pilot plant of Monazite processing into thorium oxide (Tho2). *Eksplorium*, 35(2):131–141.

Farzaneh Sadri, Fereshteh Rashchi, and Ahmad Amini. 2017. Hydrometallurgical digestion and leaching of Iranian monazite concentrate containing rare earth elements Th, Ce, la and Nd. *Int. Journal of Mineral Processing*, 159:7–15.

S. Sethi, P. Anupama, L. M. Gantayet, and M. P. Bellary. 2002. Pilot plant experience of recovery of rare, natural protactinium from the insoluble muck: Installation and operation. *BARC Newsletter, Founder's Day Special Issue*.

Individual Research Contribution Review, 2023, 1(1): 245–246

Synthesis and Characterization of Nickel Oxide Nanoparticles

Nurazila Mat Zali
Industrial Technology Division, Malaysian Nuclear Agency
43000 Kajang, Selangor
nurazila@nm.gov.my

1 Introduction

Nickel oxide (NiO) has attracted great interest in many research areas due to its unique electrical, optical, magnetic and catalytic properties (Wei et al., 2009). NiO has been widely used in various applications including catalysis, gas sensors, fuel cell electrodes, magnetic materials, photovoltaic devices and electrochemical capacitors (Gomaa et al., 2021; Li et al., 2002; Garcia-Miquel et al., 2003; Manthiram et al., 2017; Ghosh et al., 2006; Borgstrom et al., 2005). Most of these applications require particles with a small size and a narrow size distribution. A reduction in particle size to nanometer scale results in various interesting properties compared to their bulk-sized particles.

So far, many methods have been attempted to synthesize nanosized NiO such as hydrothermal synthesis, ultrasonic radiation, microwave plasma, sol-gel method and electrodeposition (Du et al., 2012; Torkzadeh-Mahani et al., 2019; Awais et al., 2011). However, most of the reported techniques for the synthesis of NiO require a high- temperature process to obtain the desired products. The most important disadvantages of the high-temperature process are that the products obtained generally possess inhomogeneity, low surface area and agglomerated particles (Liu et al., 2015). Hence, it is important to develop a way to produce high-quality nanoparticles with a low-temperature process.

In this work, we report the use of freeze-dried precursor to produce NiO nanoparticles at low temperatures. The thermal decomposition process of freeze-dried $Ni(OH)_2$ to form NiO nanoparticles was evaluated. The results of the morphological and structural analysis of the products were also discussed.

2 Methods

$Ni(OH)_2$ precursors were first synthesized using the precipitation method. In this method, 1M nickel (II) chloride hexahydrate ($NiCl_2.6H_2O$) solution was added dropwise into 2M sodium hydroxide, NaOH in a sonicator. The greenish hydroxide precipitate obtained was repeatedly washed and rinsed with deionized water using a centrifuge. The precipitate was then freeze-dried at a pressure of 28 mTorr and temperature of -100°C in a benchtop Pro Freeze Dryer (SP VirTis). Then it was calcined at 200°C and 350°C for 2 hours to form nickel oxide nanoparticles.

To investigate the thermal evolution of the precursors, thermogravimetric analysis (TGA) was performed in N_2 between room temperature and 850°C at a heating rate 10°C min^{-1} using NETZSCH-TG 209 F3 Tarsus. X-ray diffraction (XRD) patterns of the samples were recorded by using PANalytical X'Pert PRO with monochromated CuKα radiation (λ= 1.54184Å) to study the structure and phase present in the samples. The morphology of the samples was observed using GeminiSEM 500 FESEM and the size of the particles was measured using Image J software. Elemental composition was determined via energy dispersive X-ray spectroscopy (EDX) using an X-Max 80 EDS detector.

3 Results

The thermal decomposition of the samples was analyzed using TGA and the variation in weight loss was recorded. Figure 1 shows the TGA and DTG curves graph of the sample after freeze-dried. Two weight loss regions can be observed. The first region is below 170°C where the loss of any interfacial-adsorbed water molecules. The second region is between 170°C to 320°C corresponding to the decomposition of nickel hydroxide into nickel oxide. The weight loss of the two regions is about 4% and 16%, respectively.

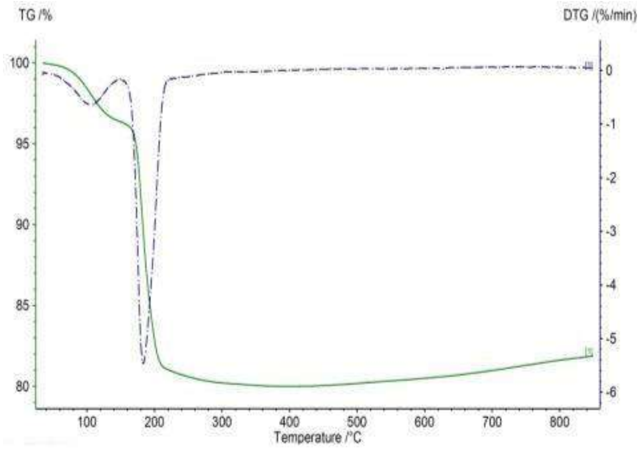

Figure 1: TGA-DTG graph of the precursor

The XRD patterns of the precursor and the calcined samples are shown in Figure 2. After calcination at 200°C and 350°C, diffraction peaks appear at 2θ=37.2, 43.2, 62.8,75.3 and 79.3 which indexed to (111), (200), (220), (311) and (222) respectively, corresponding to the cubic crystal system of NiO (PDF# 00-047-1049). These results show that the $Ni(OH)_2$ has already decomposed into crystalline NiO at 200°C.

Figure 3(a) and 4(a) displays the morphology of NiO nanoparticles from FESEM micrographs at 50000x magni-

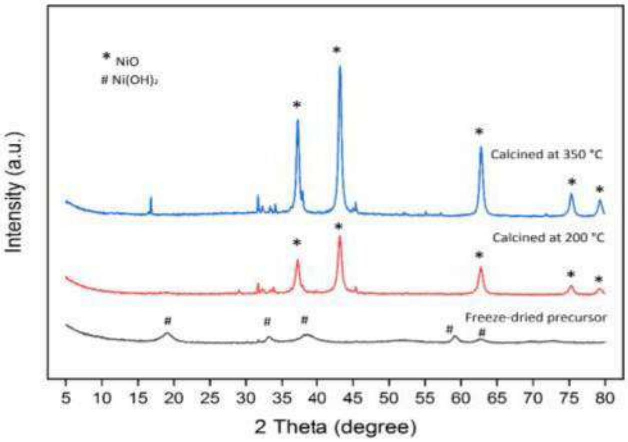

Figure 2: XRD patterns of the precursor and calcined samples

fication while Figure 3(b) and 4(b) shows the EDX spectrum and the elemental composition in the samples. FESEM micrographs revealed uniform spherical NiO nanoparticles with average particle size in the range of 17 to 19 nm. The EDX analysis confirmed the presence of Ni and O elements. Sample calcined at 200°C shows the atomic percent of Ni is 53.2 at% and O is 46.8 at% while for the sample at 350°C calcination temperature shows 49.4 at% Ni and 50.6 at% O.

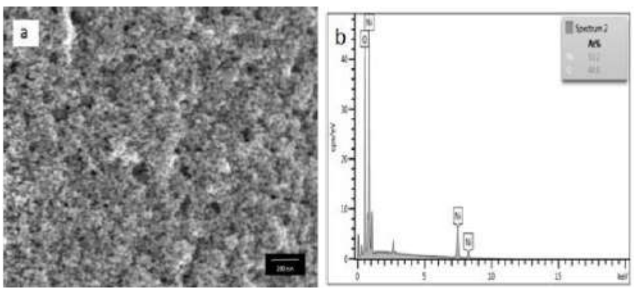

Figure 3: (a) FESEM micrographs and (b) EDX spectrum of the sample calcined at 200 °C

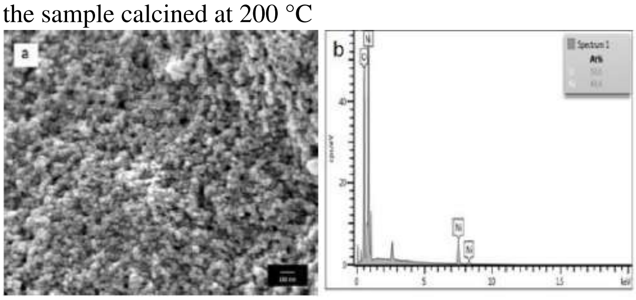

Figure 4: (a) FESEM micrographs and (b) EDX spectrum of the sample calcined at 350°C

4 Conclusion

Nanostructured nickel oxide was successfully produced via thermal decomposition of the freeze-dried precursor at low temperatures. The prepared NiO nanoparticles were characterized by TGA, XRD and FESEM-EDX. TGA results showed the decomposition region of the $Ni(OH)_2$ to form NiO is between 170°C to 320°C with 16% weight loss. The XRD results revealed the crystalline phase of NiO starting at calcination temperature of 200°C. The uniform spherical NiO nanoparticles have an average particle size in the range of 17 to 19nm.

References

M. Awais, M. Rahman, J. M. Don MacElroy, D. Dini, J. G. Vos, and D. P. Dowling. 2011. *Surface Coatings Technology*, 205:S245–S249.

M. Borgstrom, E. Blart, G. Boschloo, E. Mukhtar, A. Hagfeldt, and L. Hammarstrom. 2005. *J. Phys. Chem. B*, 109(22928).

Y. Du, W. Wang, X. Li, J. Zhao, J. Ma, Y. Liu, and G. Lu. 2012. *Mater. Lett.*, 68.

J. L. Garcia-Miquel, Q. Zhang, S. J. Allen, A. Rougier, A. Blyr, and H. O. Davies. 2003. *Thin Solid Films*, 424:165–170.

M. Ghosh, K. Biswas, A. Sundaresan, and C. N. R. Rao. 2006. *J. Mater. Chem.*, 16(106).

M. M. Gomaa, M. H. Sayed, V. L. Patil, M. Boshta, and P. S. Patil. 2021. *Journal of Alloys and Compounds*, 885(160908).

F. Li, H.Y. Chen, C. M. Wang, and K. S. Hu. 2002. *J. Electroanal. Chem.*, 531(53).

Y. Liu, R. Wang, and X. Yan. 2015. *Sci Rep 5*, 11095.

A. Manthiram, B. Song, and W. Li. 2017. *Energy Storage Materials*, 6:125–139.

R. Torkzadeh-Mahani, M. Mehdi Foroughi, S. Jahani, M. Kazemipour, and H. Hassani Nadiki. 2019. *Ultrasonics Sonochemistry*, pages 183– 192.

W. Wei, X. Jiang, L. Lu, X. Yang, X. Wang, and J. Hazard. 2009. *Mater.*, 168(838).

Individual Research Contribution Review, 2023, 1(1): 247–248

Synergistic Solvent Extraction of Cerium from Monazite Mineral

Nurliana Roslan
Industrial Technology Division, Malaysian Nuclear Agency
43000 Kajang, Selangor
nurliana_r@nm.gov.my

Abstract

Synergistic extraction with the mixed extractants has been developed as the promising method, which could improve the extraction capability and durability as well as to produce high selectivity of REEs. The effectiveness of extraction and separation process of monazite was affected by the size of the particle. The objective of this study is to determine the performance of synergist extractants on the extraction of Cerium (Ce). The experiments were carried out under aqueous phase of acidic solution and organic phase of extractants at organic-to-aqueous (O/A) phase ratio of 1. It was found that the synergist extractant of Cyphos IL 104 and D2EHPA (SE01) have better extraction efficiency compared to synergist extractant of TBP and D2EHPA (SE02).

Keywords: Synergistic, Extraction, Monazite

1 Introduction

Monazite mineral is one of the major sources for REEs including thorium and uranium. In particular, monazite contains a high amount of REEs which contribute about 54–60%, 3.1–11.34% of thorium and a small amount of uranium (0.2–0.4%) (Mohd Salehuddin et al., 2019). Solvent extraction is a conventional technique that applies various types of organic extractants which expected to produce high purity single REEs solutions or compounds. However, these extractants offer several drawbacks such as the tendency of extractant loss into the aqueous phase due to the acts of multiple contacts and the formation of emulsion due to a high viscosity of extractant that declines the extraction efficiency (Hidayah and Zainal Abidin, 2019; Gupta and Krishnamurthy, 2005). Therefore, synergistic extraction with the mixed extractants has been developed as the promising method, which could improve the extraction capability and durability as well as to produce high selectivity of REEs.

2 Methods

2.1 Sampling

Monazite mineral used in this study were originally obtained from 'amang', a by product from tin mining at processing factory in Ipoh, Perak. Monazite was undergo milling and sieving process as the pre-treatment methods for the particle size refinement. Monazite leach solution were further prepared by digesting monazite in NaOH solution.

2.2 Synergistic Extraction

Solvent extraction experiments were carried out at room temperature (298 K) by contacting equal volumes (10 ml) of organic-to-aqueous phases (O/A=1) in a covered Erlenmeyer flask. The content was shook vigorously using a mechanical shaker with the help of magnetic stirrer to mix the two-phase mixture for a period of 15 minutes to reach equilibrium. After equilibration, the contents were allowed to stand for at least 10 minutes for separation of phases. Synergistic extraction between different extractant including Trihexyl(tetradecyl) phosphonium bis(2,4,4trimethylpentyl) phosphinate (Cyphos IL 104), Di-(2-ethyl hexyl) phosphoric acid (D2EHPA) and Tributyl phosphate (TBP) was prepared with ratio 1:1 as shown in Table 1.

Table 1: Synergist extractant between Cyphos IL 104, D2EHPA and TBP

Sample ID	Ratio	Extractant 1	Extractant 2
SE01	1:1	Cyphos IL 104 (ionic liquid)	D2EHPA (acidic organophosphorus)
SE02	1:1	TBP neutral	D2EHPA (acidic organophosphorus)

The concentrations of Ce(IV) in the aqueous phase before and after extraction were obtained by analysis with XRF. The extraction efficiency, E of synergist extractant was determined using Equation 1.

$$E = \frac{C_{\text{before}} - C_{\text{after}}}{C_{\text{before}}} \tag{1}$$

where C_{before} is the initial concentration of Ce in aqueous phase and C_{after} is the final concentration of Ce in aqueous phase.

3 Results

The physical observation of monazite samples for before milling and after milling and sieving is presented in Figure 1.

It can be seen that the colour of RM looks like yellowish brown to reddish brown and exhibited a coarse-grained surface texture. After milling and sieving (MM-Lab), the colour of monazite looks like slightly greyish- yellow and the texture become smoother and looks like fine powder particles.

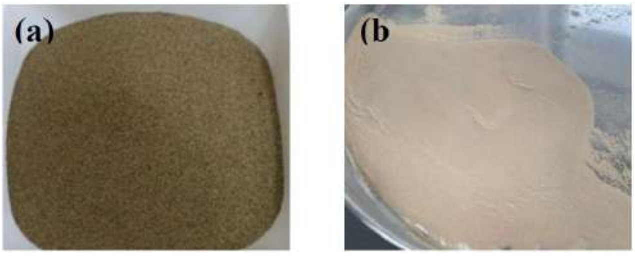

Figure 1: Monazite samples (a) before milling (RM) (b) after milling and sieving (MM-Lab)

Table 2 shows that, in general, the chemical composition of synergist extractant analysed by XRF. It is obviously seen that the chemical composition of REEs was increased after the synergistic extraction compared to single extraction.

Table 2: Chemical composition of synergist extractant by XRF

Sample/Element	Single Cyphos IL 104	D2EHPA	TBP	SE01	SE02
		Wt%			
P	0.044	0.751	0.206	0.78	0.32
Nd	0.024	0.173	0.003	0.197	0.025
Ce	0.019	0.155	0.006	0.197	0.019
Th	0.041	0.081	-	0.084	0.045
La	0.008	0.057	0.002	0.069	0.002
Y	0.009	0.028	0.020	0.034	0.016
Pr	0.005	0.026	-	0.030	-
Ca	0.008	0.023	0.008	0.025	0.010
Cu	0.006	0.005	0.003	0.005	0.003
Se	0.003	0.002	-	0.003	0.001
Fe	0.023	0.039	0.006	-	0.008
K	-	0.751	-	-	0.001
Zn	0.003	-	-	-	-

4 Discussion

Organic phase which plays significant role in REE extractant contains the main extractant and diluents. In this research, organic phase used is a synergist between D2EHPA with Cyphos IL 104 and TBP extractants. Kerosene is acting as diluents for this extraction. The chemical composition data of synergist extractant including Cyphos IL 104, D2EHPA and TBP are tabulated in Table 2. From the result, it was found that the extraction of Ce from the aqueous phase using synergist extractants is slightly higher compare to a single extractant. The performance of SE01 was compared with SE02 and the results shows that the higher efficiency at Ce extraction was achieved using SE01 compared to SE02. It can be seen that there is a significant of Ce extraction between SE01 and SE02.

5 Conclusion and attention

The pre-treatment method for the REEs recovery of the monazite samples was successfully optimized by milling and sieving process. Particle size analysis was carried out as a preliminary characterization to study the size distribution present in the monazite samples. The effect of particle size distribution of monazite on the physicochemical properties was studied using WD-XRF, XRD and FESEM-EDX analysis. In this study, pretreatment of monazite was chosen as an ideal sample for further digestion and extraction process because resulted in a smaller particles size and gave highest REEs composition. The extraction of Ce using three kind of synergist extractants of Cyphos IL 104, D2EHPA and TBP at 1:1 ratio finalised with SE01 to be better synergist extractant compare to SE02.

References

C.K. Gupta and N. Krishnamurthy. 2005. Chapter 3: Resource processing. *Extractive Metallurgy of Rare Earths, CRC Press*, pages 172–174.

N.N. Hidayah and S. Zainal Abidin. 2019. Extraction of light, medium and heavy rare- earth elements using synergist extractants developed from ionic liquid and conventional extractants. *Comptes Rendus Chimie*, 22(11-12):728–744.

AH.J. Mohd Salehuddin, A. Fazli Ismail, C.N.A. Che Zainul Bahri, and E.S. Aziman. 2019. Economic analysis of thorium extraction from monazite. *Nuclear Engineering and Technology*, 51:631–640.

Individual Research Contribution Review, 2023, 1(1): 249–250

A Finite Element Method Simulation of Pulsed Eddy Current Technique for Defect Evaluation in Non Ferromagnetic Material

Nurul A'in Binti Ahmad Latif
Industrial Technology Division, Malaysian Nuclear Agency
43000 Kajang, Selangor
nurul_ain@nm.gov.my

Abstract

Pulsed eddy current (PEC) is an advanced Non-Destructive Testing (NDT) technique that uses transient waveform for their coil excitation. It has the advantage of gathering different depth information in a single excitation process, thus provide the solution towards the drawbacks by both single and multi- frequency eddy current testing. In this work, simulation investigations on PEC were conducted to establish the correlation between PEC signals and different defect i.e. crack, depths. Initial FEM simulation work has provided understanding of the underlying phenomena of the PEC results through the visualisation of the induced eddy current and defect interaction in the SS 304 sample. Features from the differential magnetic field transient profiles have provided information of the crack in terms of its depth and location.

1 Introduction

The wideband pulse in PEC excitation consists of a series of frequency components leading to richness of information gathered about the defect (Angani et al., 2016; Johnston et al., 2018; Tian and Sophian, 2005). The technique has the advantage that it is equivalent to a multitude of single frequency with simultaneous injection of sinusoidal inputs (Sophian et al., 2017; Zhang et al., 2018). In PEC, the signals are represented in the time domain, rather than the more familiar impedance plane diagram, as is the case for conventional eddy current testing. In order to get better understanding of the PEC results especially for the quantitative evaluation of defects, simulation and experimental works are conducted to establish the correlation between PEC signals and different defect i.e. crack, depths. Such investigations would be very helpful in understanding and interpreting the PEC responses though the transient profiles of the magnetic flux density from the eddy current and crack interaction in the sample. This will facilitates not only forward problem but also inverse solution (Latif et al., 2023) for 3D reconstruction (Sha et al., 2021) and pattern recognition of defects through the establishment of linkages between experiment and simulation (Chandran et al., 2019).

2 Methodology

A series of finite element method (FEM) numerical modelling simulations are conducted to build the relationship between the acquired magnetic field transient profiles and the induced eddy currents with different crack geometrical characteristic i.e. depth. Through the simulation, the underlying phenomena of PEC can be understood and the acquired results can be explained through the visualization of the induced eddy currents inside the tested sample. To implement this study, a current driven with a rectangular waveform of 1A amplitude to generate a varying magnetic field. A 20 mm thick stainless steel sample with different crack depths of 2 mm, 4 mm, 6 mm, 8 mm and 10 mm were introduced in the study. The time step of the pulse waveform is 10 ms with 5 ms excitation pulse width and pulse repetition frequency is 100 Hz. All simulations were performed using COMSOL.

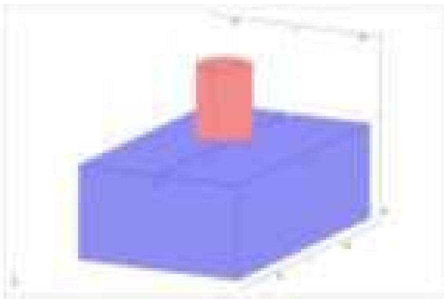

Figure 1: 3D model of the PEC coil and stainless steel with a defect

For a cylindrical PEC coil located over a conductive sample, the magnetic field, within the vicinity of the sample is given by Equation 1.

$$B_x = B_z^e - \triangle B_z \tag{1}$$

where B_x denotes the magnetic field at x-component, B_z^e is the field produced by the coil and $\triangle B_z$ is the field change caused by the sample.

3 Results and Discussion

Figure 2 shows the acquired transient profiles for different crack depths. These are the resultant net magnetic field from the interaction between the primary magnetic field coming from the coil and the secondary magnetic field produced by the induced eddy current inside the stainless steel sample. Crack with 10 mm depth exhibits the highest followed by the 8 mm, 6 mm, 4 mm and 2 mm, in the respective order.

The results show that as the depth of the crack increases, the amplitude of the respective profiles increases.

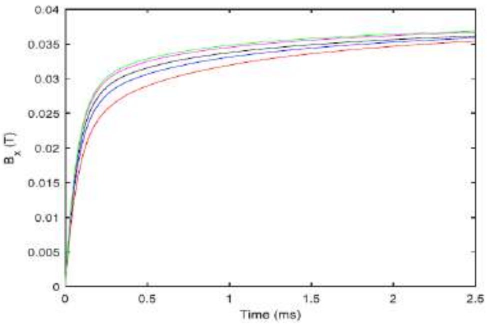

Figure 2: Net magnetic field, B_x acquired at different crack depths

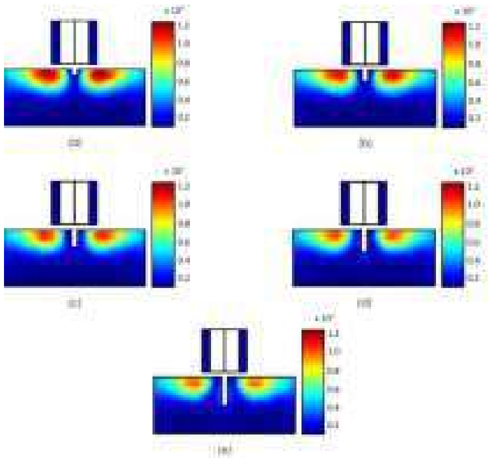

Figure 3: Simulated visualisation of eddy current density at different crack depth of a) 2 mm, b) 4 mm, c) 6 mm, d) 8 mm and e) 10 mm

The cross section view of the stainless steel sample for every crack depth are presented in Figure 3. This signals were acquired at steady state of transient signal at 2.5 ms. From the visualization provided by the simulation, it can be observed that the eddy current density is changing with different crack depths. The presence of a crack inside the stainless steel sample will perturb the flow of the induced eddy currents and changes its overall density at that particular area. With the increase of crack depths, the flow of the eddy currents will increasingly be perturbed thus results in reduced in eddy current density as shown in Figure 3a to Figure 3e. This in turn increase the net B_x acquired from the sample by the PEC coil with increase crack depth, as presented in Figure 2.

4 Conclusion

This paper has presented the work on PEC technique and the correlation between acquired PEC signals with cracks having different depths in a stainless steel plate sample. Through the FEM simulation, the underlying phenomena of the PEC responses and the relationship between the acquired magnetic field transient profiles with the induced eddy currents have been explained.

References

C. S. Angani, H. G. Ramos, A. L. Ribeiro, and T. J. Rocha. 2016. Evaluation of transient eddy current oscillations response for thickness measurement of stainless steel plate. *Measurement: Journal of the International Measurement Confederation*.

P. Chandran, M. Rantatalo, J. Odelius, H. Lind, and S. M. Famurewa. 2019. Train-based differential eddy current sensor system for rail fastener detection. *Measurement Science and Technology*, 30(12):125105.

D. P. Johnston, J. A. Buck, P. R. Underhill, J. Morelli, and T. W. Krause. 2018. Pulsed eddy current detection of loose parts in steam generators. *IEEE Sensors Journal*, 18(6):2506–2512.

N. A. A. Latif, I. M. Z. Abidin, N. Zaki, and N. Jamaludin. 2023. Experimental investigation and finite element method simulation of time domain pulsed eddy current technique on non- ferromagnetic conductivity plates. *Defence S and T Technical Bulletin*, 16(1):37–45.

J. Sha, M. Fan, B. Cao, and B. Liu. 2021. Noncontact and nondestructive evaluation of heat-treated bearing rings using pulsed eddy current testing. *Journal of Magnetism and Magnetic Materials*, 521(P2):167516.

A. Sophian, G. Tian, and M. Fan. 2017. Pulsed eddy current nondestructive testing and evaluation: A review. *Chinese Journal of Mechanical Engineering (English Edition)*, 30(3):500–514.

G. Y. Tian and A. Sophian. 2005. Defect classification using a new feature for pulsed eddy current sensors. *NDT and E International*, 38(1):77–82.

K. Zhang, Y. He, and Z. Dong. 2018. Pulsed eddy current nondestructive testing for defect evaluation and imaging of automotive lightweight alloy materials. *Journal of Sensors*.

Individual Research Contribution Review, 2023, 1(1): 251–252

Recovery of Rare Earth Elements (REE) and Valuable Elements from Local Resources via Alkaline Fusion and Related Techniques

Roshasnorlyza Hazan
Industrial Technology Division, Malaysian Nuclear Agency
43000 Kajang, Selangor
roshasnorlyza@nm.gov.my

Abstract

Malaysia has been blessed with its local resources such as Xenotime and Ilmenite mineral. These minerals are rich with precious rare earth elements (REE) and other valuable elements. This REEs and valuable elements are commercially need in this industrial revolution (IR) 4.0 era to be used in many high technology instruments such as microwave filters for radar, white LED lights, superconductors, fuel cells and radioactive isotope to cure cancer. Thus, effort needs to eliminate impurities that may affects the materials characteristic and product efficiency. Therefore, mineral processing in mid-stream sector is crucial and has been adapted in my research work. The work starts with alkaline fusion, leaching, selective precipitation, separation and solvent extraction at the end in order to obtain enriched interested element.

Keywords: Alkaline fusion, Ilmenite, Iron, Rare earth elements (REE), TiO_2, Xenotime and Yttrium

1 Introduction

Tin mining business in Malaysia produce many types of by product such as xenotime, monazite, zircon and ilmenite. Ilmenite is one of the crucial materials that helps the growth of economy in Malaysia (Chen and Tu, 2012). The recovery of REE and valuable elements from unconventional sources have potential to be sustainable source for nano-materials and renewable energy applications.

As considering Malaysia to be one of REE supplier in the future, xenotime mineral seems to be as promising mineral to be explore. Xenotime is one of a rare earth phosphate mineral which have 40-50% yttrium content together with others REEs (Prameswara et al., 2020). Abundant of xenotime can be easily retrieved from abandoned tin mine in Kinta Valley, Perak (Meor Sulaiman, 2010). In addition, there are several REEs contained in xenotime, such as Dysprosium (Dy), Erbium (Er), Terbium (Tb), Ytterbium (Yb), Thorium (Th), and Uranium (U) (Prameswara et al., 2020). As there are radioactive elements, Th and U, hence xenotime is categorized as radioactive mineral. Whereas Ilmenite composition can provide titanium dioxide (TiO_2) which can be used in many industries such as painting and iron oxide (Fe_2O_3 or Fe_3O_4) for catalytic and magnetic industries (Mendili et al., 2016). Therefore in this study, extractive metallurgy method was used in order to enhanced REE and valuable elements purity.

2 Methods

Mineral cracking was done by mixed mineral with NaOH beads and fused in furnace at elevated temperature (250–550°C) for 3 hours. After washing and filtration process, the solid sample undergo selective acid leaching process. The leaching was done in air atmosphere at 70-80°C for 6 hours. Different acid type (HCl, HNO_3 and H_2SO_4) and molarity (0.2–14M) was introduced in this step and the solution was quickly separated by vacuum filtration. Then, the filtrate was separated by selective precipitation and solvent extraction. Different precipitation agents and organic solvents were use in this stage.

The samples either solid or liquid obtained after leaching step and co-precipitation were characterized using Energy Dispersive X-Ray Fluorescence (EDXRF). Selected samples also tested with X-ray Diffraction (XRD) for phase identification, Raman spectrometer for chemical bonding identification, simultaneous thermal analysis (STA), particle size analysis and FESEM for morphological study. However, just few results were selected and reported in this extended abstract.

3 Results and Discussion

3.1 Xenotime mineral

Xenotime react with NaOH in alkaline fusion process. Table 1 shows elemental analysis of samples when through mineral processing steps. Both XRF and EDAX analysis gave mostly similar heavy REE (HREE) content.

Figure 1 shows selected FESEM micrographs in which it was observed that the HREE particles were found to consist flake-like crystals upon precipitation with oxalic acid and calcined at 550°C for 3 hours. The size of the particles was typically in 10μm in both length and width.

3.2 Ilmenite mineral

Elemental analyses of ilmenite raw material, products after acid leaching and selective precipitation are presented in Table 2. High purity of titanium (94.32%) could be possessed after acid leaching step. In the other hand, high purity of iron (93.30%) could be obtain after selective precipitation.

Table 1: Major element analysis by XRF and EDAX after mineral processing of Xenotime mineral (Hazan, 2023)

Elements	Weight%	
	XRF analysis	EDAX analysis
Yttrium (Y)	**75.23**	**77.99**
Dysprosium (Dy)	**12.49**	**9.68**
Erbium (Er)	**ND**	**8.21**
Holmium (Ho)	**3.26**	**3.08**
Thulium (Tm)	**1.28**	ND
Ytterbium (Yb)	**0.89**	ND
Gadolinium (Gd)	**0.69**	ND
Cobalt (Co)	3.79	ND
Nickle (Ni)	1.11	ND
Silicon (Si)	ND	0.45
Chlorine (Cl)	0.64	0.31
Calcium (Ca)	0.26	ND
Potassium (K)	0.21	0.16
Copper (Cu)	ND	0.12
Sulphur (S)	0.16	ND
Total HREE	**93.84**	**98.96**

**ND = not detected*

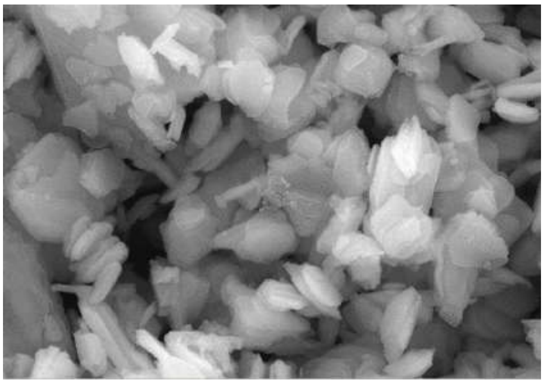

Figure 1: Microstructure image of HREE particle after calcination process (Hazan, 2023)

Table 2: Major element analysis after mineral processing of Ilmenite mineral (Hazan et al., 2020; Hazan et al., 2023)

Elements	Weight%		
	Raw ilmenite	After acid leaching	After selective precipitation
Titanium (Ti)	52.48	**94.32**	1.02
Iron (Fe)	30.35	1.85	**93.30**
Chlorine (Cl)	ND	ND	0.31
Manganese (Mn)	2.48	0.01	2.73
Silicon (Si)	5.28	0.25	ND
Aluminium (Al)	2.00	ND	ND

4 Future Direction

There is a greater need to intensify our research for REE cracking and extraction. Based on recent research, it is believed that separation of REE and valuable elements into single element could be enhanced with some adaptation on advanced separation technologies through ionic liquid separation and electrodeposition in the future. Also, these elements need to undergo proof of concept study in down-stream sector, such as nanotechnology application, batteries, permanent magnet, renewable energy which can be employed.

5 Conclusions

A technological mineral processing of REE and valuable elements recovery from Malaysian Xenotime and Ilmenite has been formulated. The results of this study provided knowhow evidence to recover precious elements which could be useful in interest element recovery for various applications. Due to the unique magnetic, luminescent, chemical and physical properties of these elements, are essential ingredients for many high-technology applications, and there still will be demand for them in the mere future. Especially since their significant use is related to the production of clean energy, which nowadays is a very important issue.

References

Y. H Chen and K. J. Tu. 2012. Thickness dependent on photocatalytic activity of hematite thin films. *International Journal of Photoenergy*, 80595, doi:10.1155/2012/980595.

R. Hazan, M. A. Muhamad Yusop, W. Paulus, and K. Mohamed Takip. 2020. Obtaining tio2 and fe2o3 from ilmenite via alkaline fusion method. *Materials Science Forum*, 1010:385–390.

R. Hazan, A. A. S. Shahul Hameed, N. H. H. Jaidi, W. A. H. Wan Ahmad Khalid, N. A. Sapiee, W. Paulus, M. A. Md Harashid, S. Ahmad, R. S. Chen, A. F. Ismail, and M. Z. Ahmad. 2023. Reducing impurities in fe compound via selective precipitation and heat treatment. *International Conference on X-ray Application in Research and Industry (ICXRI 2023), Selangor, Malaysia.*

R. Hazan. 2023. Study on valuable element recovery from local mineral via alkaline fusion. *Kolokium Unit Mineral dan Nadir Bumi, MTEG, BTI, Agensi Nuklear Malaysia, Selangor, Malaysia.*

Y. Mendili, J. F. Bardeau, N. Randrianantoandro, J. M. Greneche, and F. Grasset. 2016. Structural behavior of laser-irradiated -fe2o3 nanocrystals dispersed in porous silica matrix: fe2o3 to -fe2o3 phase transition and formation of -fe2o3. *Science and Technology of Advanced Materials*, 17(1):597–609.

M. Y. Meor Sulaiman. 2010. Recovery of uranium from malaysian non-conventional sources. *Journal of Nuclear and Related Technologies*, 7:55–65.

G. Prameswara, I. Trisnawati, H. Poernomo, P. Mulyono, A. Prasetya, and H. T. B. M. Petrus. 2020. Kinetics of yttrium dissolution from alkaline fusion on zircon tailings. *Mining, Metallurgy Exploration*, 37:1297–1305.

Individual Research Contribution Review, 2023, 1(1): 253–254

Image Optimization Using Predetermined Voltage and Filter on the 1172 Micro Computed Tomography (MicroCT) System

Roslan Yahya
Industrial Technology Division, Malaysian Nuclear Agency
43000 Kajang, Selangor
roslan_yahya@nm.gov.my

Abstract

In MicroCT systems, choosing the correct voltage and filter settings for scanning different samples is crucial for achieving the best image quality and contrast. While past studies are typically consulted for guidance, variations in MicroCT systems can make these references less accurate. This discrepancy often leads to a time-consuming trial-and-error process. To address this, systematic studies are necessary to find the optimal combination of settings for specific samples and imaging goals. By methodically adjusting parameters and evaluating resulting images, researchers can minimize the trial-and-error approach, streamline the scanning process, and enhance the efficiency of MicroCT imaging research.

Keywords: Micro Computed Tomography (MicroCT)

1 Introduction

Micro computed tomography (MicroCT) is a non-destructive imaging technique that allows detailed exploration of the internal structures of small objects in three dimensions, based on the principles of conventional computed tomography (CT) but with higher resolution. The 1172 MicroCT, manufactured by SKYSCAN (now owned by Bruker), is a prominent MicroCT model widely used in scientific research and industrial applications for analyzing various materials. In the MicroCT process, multiple x-ray transmission images of a sample are captured from different angles. Placed between an x-ray source and a detector, the sample influences the attenuation or absorption of x-rays based on its density and composition, resulting in a series of recorded shadow images. Computer algorithms then reconstruct cross-sectional slices from these images, revealing the internal structure at different depths. By assembling these slices, a 3D representation or volume rendering is created, enabling a detailed examination of the intricate internal features of the sample.

2 Methods

In order to enhance the optimization of MicroCT imaging, the first objective involves the development of a comprehensive database that encompasses a range of voltage settings from 20kV to 100kV, paired with corresponding filter usage information. This database is intended to serve as a valuable resource for researchers and operators aiming to achieve the best possible image quality and contrast for specific samples. Once established, the second objective focuses on the practical utilization of this database for image optimization. By referencing the database, researchers and operators can efficiently select the most appropriate voltage and filter settings tailored to the characteristics of their samples, minimizing the need for a time-consuming trial-and-error process. This streamlined approach ensures that MicroCT imaging procedures are conducted with precision and effectiveness, ultimately contributing to improved efficiency and accuracy in research or analysis.

The project at hand involves the creation of a phantom, a material designed for the calibration and quality assurance of diverse imaging systems, particularly in the context of microCT. This phantom is composed of a specific material with varying densities, ranging from 0.46g/ml to 2.70g/ml (Table 1), each likely representing different compositions or variations found in microCT samples.

Table 1: Phantom number with specific density

Serial no.	Phantom no.	Density ρ (g/cm^3)
QSA-926.1	1	0.46 ± 0.02
QSA-926.2	2	1.08 ± 0.02
QSA-926.3	3	1.47 ± 0.02
QSA-926.4	4	1.88 ± 0.02
QSA-926.5	5	2.70 ± 0.02

Beyond density variations, the phantom also possesses distinct dimensions, measuring 33mm in length. Notably, the diameter of the phantom exhibits a staggered pattern, starting wider at one end (20mm) and gradually tapering down to a narrower end (2mm). This design enables the phantom to mimic the diverse geometric characteristics encountered in actual microCT samples. Overall, the development of such a phantom serves as a crucial tool for ensuring accurate calibration and quality control in microCT imaging systems, contributing to the reliability and precision of the obtained results.

3 Results

Considering that the custom phantom just been received at the end of September 2023, only preliminary findings have been obtained so far. These results are obtained for Phantom 1, Phantom 3, and Phantom 5, with the goal of determining the percentage of x-ray radiation that passes through at specific phantom sizes. The tests were conducted at voltages of

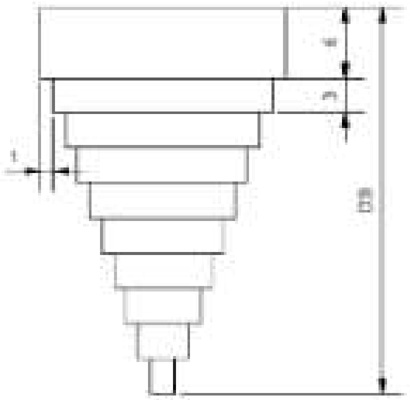

Figure 1: Phantom dimension in millimeter (mm)

40kV, 60kV, and 80kV for each filter configuration. The setup involves conditions without a filter, with a 0.5mm aluminum filter, and a combination of a 0.5mm aluminum filter and a 0.5mm copper filter. All results are recorded and are representing in Figure 2, Figure 3 and Figure 4 respectively for Phantom 1, Phantom 3, and Phantom 5.

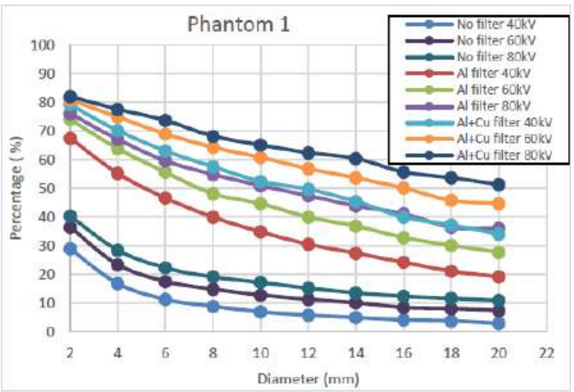

Figure 2: Percentage of x-ray passing through Phantom 1

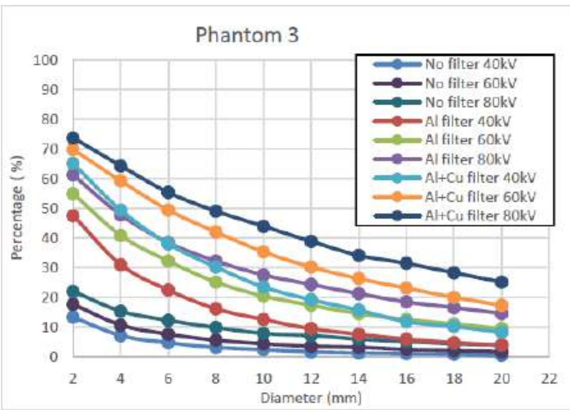

Figure 3: Percentage of x-ray passing through Phantom 3

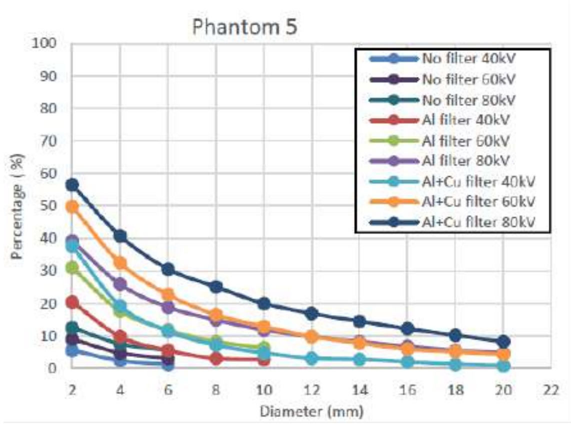

Figure 4: Percentage of x-ray passing through Phantom 5

4 Discussion

The findings indicate that, for each phantom, the introduction of a filter increases the percentage of x-rays passing through a specific diameter, while, for a given filter, x-ray attenuation decreases with higher voltage (kV). When comparing the phantoms, Phantom 5 demonstrates higher attenuation than Phantom 3, which, in sequence, has higher attenuation than Phantom 1, aligning with their decreasing density order (5>3>1). In summary, the data highlights essential connections between x-ray beam attenuation, the addition of filters, phantom density, and voltage. Denser phantoms and lower energy x-rays experience more noticeable attenuation. The anticipation is that more comprehensive results will emerge after successfully gathering data from all five phantoms.

References

Bruker MicroCT method note. Flat-field corrections (MCT-129).

Bruker MicroCT method note. SkyScan 1172 microCT scanner operation (MCT-029).

Individual Research Contribution Review, 2023, 1(1): 255–256

Characterization and Evaluation of Flat Panel Detector for Industrial Application

Sapizah Rahim
Industrial Technology Division, Malaysian Nuclear Agency
43000 Kajang, Selangor
sapizah@nm.gov.my

Abstract

Special test phantoms can be used to quantitatively measure the performance of flat panel detectors for radiographic imaging. Several parameters have been measured, including basic spatial resolution (SR_b), contrast sensitivity (CS), efficiency, specific material thickness range (SMTR), and image lag. These tests are very important for tracking longterm stability and lifetimes of industrial digital detector systems.

Keywords: Flat panel detector, parameter, phantom

1 Introduction

A flat panel is a digital detector array (DDA) system that converts ionizing radiation into an electrical signal to form a digital image. It is widely used in the oil and gas industries, especially for weld and casting inspection, as well as corrosion and erosion control in pipelines. The electronic response plays an important role in determining the limitations and characteristics of the flat panel system. Long-term stability tracking and lifetime are also determined to ensure the accuracy and reliability of digital images during inspection. The essential parameters in digital images that should be considered are shown in Equation 1 below:

$$\frac{CNR_N}{\nabla w} = \frac{\mu_{\text{eff}}.SNR_{I_{\text{total}}}}{SR_b} \tag{1}$$

where CNR is for contrast-noise ratio, ∇w is visibility of small flaws, μ_{eff} is effective attenuation coefficient, SNR is signal-noise ratio and SR_b is effective pixel size in the image. Thus, a flat panel system can be characterized and evaluated using these parameters.

2 Methods

Each measurement has used a specific phantom according to ASTM E2597. However, the choice of phantom depends on our equipment limitations, such as the maximum energy of the X-ray machine and the environmental conditions. The parameters that will be measured include interpolated basic spatial resolution (iSR_b, the smallest geometric details that can be resolved), efficiency (DDA responds toward radiation energy), achievable contrast sensitivity, Specific Material Thickness Range, and image lag. In this report, the Durr flat panel system with the ISOVOLT Titan E X-ray machine have been evaluated. For example, contrast sensitivity was measured using a step wedge with a center groove in each step and was placed at 600 mm from the detector (Figure 1). The energy was set to 160 kV, and the images were acquired by averaging frames to obtain effective exposure times of 1s, 4s, 16s, and 64s.

Figure 1: Experimental setup for contrast sensitivity measurement

3 Results

The different mean signal levels between two image areas and the standard deviation of the signal levels of step wedge (Figure 2) was used to determine contrast sensitivity as shown in Equation 2.

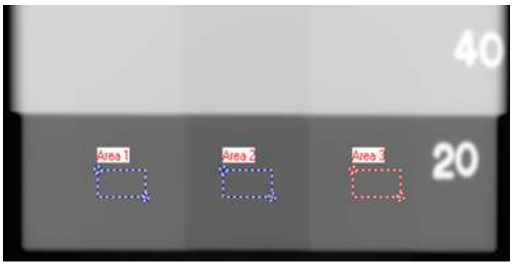

Figure 2: Area on the step wedge used for contrast sensitivity calculation

$$\text{CNR} = \frac{0.5 \times (\text{signal (area 1)} + \text{signal (area 3)}) - \text{signal (area 2)}}{0.5 \times (\text{noise (area 1)} + \text{noise (area 3)})} \tag{2}$$

In this work, the contrast sensitivity measured can determine the limit of visibilities for materials such as aluminum. The flat panel enables distinguishing wall thickness changes of up to 1/1000 of the penetrated material thickness 1. However, complete flat panel system characterization can be presented as quality numbers according to Table 2 in ASTM E2597

(Figure 3). Therefore, each parameter can be summarized as a spider web chart to identify potential application and limitation for the flat panel system (Figure 4).

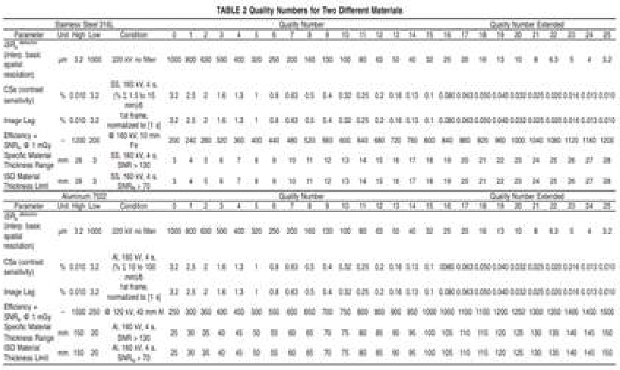

TABLE 2 Quality Numbers for Two Different Materials

Stainless Steel 316L					Quality Number																	Quality Number Extended									
Parameter	Unit	High	Low	Condition	0	1	2	3	4	5	6	7	8	9	10	11	12	13	14	15	16	17	18	19	20	21	22	23	24	25
iSR_b (Interp. basic spatial resolution)	µm	3.2	1000	220 kV no filter	1000	800	630	500	400	320	250	200	160	130	100	80	63	50	40	32	25	20	16	13	10	8	6.3	5	4	3.2
CSa (contrast sensitivity)	%	0.010	3.2	SS, 160 kV, 4 s, (% ≥ 1.5 to 15 mm)/8	3.2	2.5	2	1.6	1.3	1	0.8	0.63	0.5	0.4	0.32	0.25	0.2	0.16	0.13	0.1	0.080	0.063	0.050	0.040	0.032	0.025	0.020	0.016	0.013	0.010
Image Lag	%	0.010	3.2	1st frame, normalized to [1 s]	3.2	2.5	2	1.6	1.3	1	0.8	0.63	0.5	0.4	0.32	0.25	0.2	0.16	0.13	0.1	0.080	0.063	0.050	0.040	0.032	0.025	0.020	0.016	0.013	0.010
Efficiency = $dSNR_n$ @ 1 mGy	–	1200	200	@ 160 kV, 10 mm Fe	200	240	280	320	360	400	440	480	520	560	600	640	680	720	760	800	840	880	920	960	1000	1040	1080	1120	1140	1200
Specific Material Thickness Range	mm	28	3	SS, 160 kV, 4 s, SNR > 130	3	4	5	6	7	8	9	10	11	12	13	14	15	16	17	18	19	20	21	22	23	24	25	26	27	28
ISO Material Thickness Limit	mm	28	3	SS, 160 kV, 4 s, SNR_n > 70	3	4	5	6	7	8	9	10	11	12	13	14	15	16	17	18	19	20	21	22	23	24	25	26	27	28
Aluminum 7022					Quality Number																	Quality Number Extended									
Parameter	Unit	High	Low	Condition	0	1	2	3	4	5	6	7	8	9	10	11	12	13	14	15	16	17	18	19	20	21	22	23	24	25
iSR_b (Interp. basic spatial resolution)	µm	3.2	1000	220 kV no filter	1000	800	630	500	400	320	250	200	160	130	100	80	63	50	40	32	25	20	16	13	10	8	6.3	5	4	3.2
CSa (contrast sensitivity)	%	0.010	3.2	Al, 160 kV, 4 s, (% ≥ 10 to 100 mm)/8	3.2	2.5	2	1.6	1.3	1	0.8	0.63	0.5	0.4	0.32	0.25	0.2	0.16	0.13	0.1	0080	0.063	0.050	0.040	0.032	0.025	0.020	0.016	0.013	0.010
Image Lag	%	0.010	3.2	1st frame, normalized to [1 s]	3.2	2.5	2	1.6	1.3	1	0.8	0.63	0.5	0.4	0.32	0.25	0.2	0.16	0.13	0.1	0.080	0.063	0.050	0.040	0.032	0.025	0.020	0.016	0.013	0.010
Efficiency = SNR_n @ 1 mGy	–	1500	250	@ 120 kV, 40 mm Al	250	300	350	400	450	500	550	600	650	700	750	800	850	900	950	1000	1050	1100	1150	1200	1250	1300	1350	1400	1450	1500
Specific Material Thickness Range	mm	150	20	Al, 160 kV, 4 s, SNR > 130	25	30	35	40	45	50	55	60	65	70	75	80	85	90	95	100	105	110	115	120	125	130	135	140	145	150
ISO Material Thickness Limit	mm	150	20	Al, 160 kV, 4 s, SNR_n > 70	25	30	35	40	45	50	55	60	65	70	75	80	85	90	95	100	105	110	115	120	125	130	135	140	145	150

Figure 3: Quality Number for different material

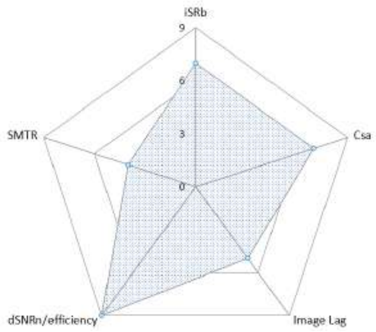

Figure 4: Summary plot for Duur DDA system

4 Discussion

The measurement of this parameter enables a flat panel system to be evaluated and interpreted to determine its limitations and whether it is suitable for use in welding inspection, profiling, or casting specimens. The acquired web spider provides guidance to the user to select and differentiate the characteristics of a flat panel/DDA in terms of its quantitative capabilities while conducting the examination.

5 Conclusion and attention

All types of flat panel or DDA systems, whether direct or indirect, can be evaluated using the parameters discussed. However, the measurements are limited by the energy of the X-ray and the limitations of the X-ray machine itself.

References

ASTM E2597:14. Standard practice for manufacturing characterization of digital detector arrays.

ASTM E2597:22. Standard practice for manufacturing characterization of digital detector arrays.

Sapizah Rahim, Khairul Anuar Mohd Salleh, and Norhazleena Azaman. 2020. Quantitative evaluation and characterization of digital detector array system. *Proceeding in R&D Seminar 2020*.

Individual Research Contribution Review, 2023, 1(1): 257–258

Failure Investigation on Natural Fiber Hybrid Composites due to Low Velocity Impact

Siti Madiha Muhammad Amir
Industrial Technology Division, Malaysian Nuclear Agency
43000 Kajang, Selangor
madiha_amir@nm.gov.my

Abstract

Hybrid composites of synthetic fibers has shifted to natural fiber hybrid composites. This is due to its environmental friendly solution without compromising its stringent engineering requirements. Like any other materials natural fiber hybrid composites also experiencing damage due to low velocity impact. This paper provides failure investigation of natural fiber hybrid composites using Infrared Thermography Non Destructive Testing Methods. From the investigation, the surface crack from the samples could be detected. However, there exist limitations in detecting the surface crack using the Infrared Thermography method especially for impacted energy less than 3J.

Keywords: Natural Fiber Hybrid Composites, Low Velocity Impact, Infrared Thermography

1 Introduction

In the current scenarios, hybrid composites are mainly made up of synthetic hybrid composites; such as from glass fiber, carbon fiber and Kevlar. However, trends show that natural fibers are replacing the commercial hybrid composites. This is due to growing global demand for new and overcoming eco-friendly solutions for future sustainability without compromising its unique characteristics; lightweight and low-density nature, high strength to weight ratio, good molding flexibility, and cost-effectiveness (Najeeb et al., 2023). However, exposure to damage have been reported. Common damage in composite materials is low velocity impact damage.

Non Destructive Testing (NDT) is a vital tools to use for assessing damage for the low velocity impact event, eg. Ultrasonic testing, Eddy current testing, magnetic particle testing among others. Choosing the appropriate NDT methods is crucial to prevent any misleading or misinterpretation of defects especially from low velocity impact damage. In this paper, infrared thermography NDT method is executed to investigate the defect failure on natural fiber due to low velocity impact event.

2 Methods

In this work, the hybrid composites of kenaf/glass fibers were used. The hybrid composites were fabricated using hand lay up method with weight to weight ratio of kenaf/glass hybridization at 30:70. This fibre loading condition exhibited a balanced mechanical properties between kenaf and glass fibers (Sharba et al., 2016). The low velocity impact test were performed using an Instron CEAST 9340 drop weight impact testing machine with different impact energy. The impacted hybrid composites were provided by the Aerospace Engineering Faculty, UPM, Malaysia.

In investigating the damage, infrared thermography method was conducted (Boccardia et al., 2017). The experimental setup is shown in Figure 1.

Figure 1: Experimental setup for reflection infrared thermography method.

Halogen lamp was used as a heat source to the samples. The samples were heated for 60 seconds. Images were taken during the cooling down of the samples after the halogen lamp were switched off. Optrix software were used to capture the images.

3 Discussion/Conclusions

3.1 Results and Discussions

Figure 2, 3, 4, 5, 6 and 7 show the results of the images captured using the infrared thermography camera for sampleswith various impacted energy.

In impact damage, the main three (3) types failures that occur are namely matrix cracking that appear at the surface of the samples, delamination and internal fiber cracks. However, the types of damages occur very much depending on the impact energy and the process of the fabrication.

From the observation, the samples with impacted energy higher that 4J experienced severe matrix crack as shown in Figure 2, 3, 4 and 5. Impact energy of 3J and below experienced less severe matrix crack as shown in Figure 6 and 7. From the investigation, the matrix cracking that appear at the surface of the samples could be detected using the reflection

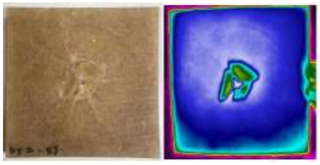

Figure 2: Physical sample and the thermogram at impact energy 8J.

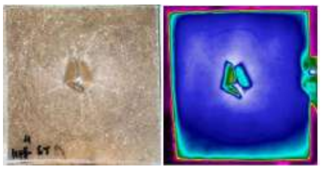

Figure 3: Physical sample and the thermogram at impact energy 6J.

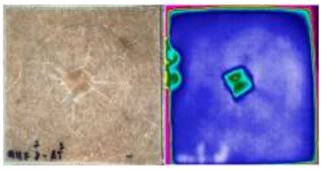

Figure 4: Physical sample and the thermogram at impact energy 5J.

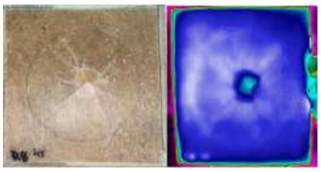

Figure 5: Physical sample and the thermogram at impact energy 4J.

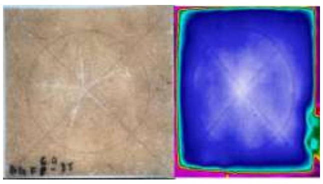

Figure 6: Physical sample and the thermogram at impact energy 3J.

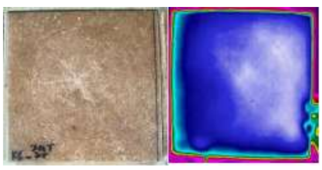

Figure 7: Physical sample and the thermogram at impact energy 2.4J.

infrared thermography method. Delamination and internal damage such as internal fiber crack were not detected. The surface crack that could be observed were samples with impact energy higher than 3J as shown in Figure 2, 3, 4 and 5. However, at impact energy 3J and below, the surface crack were not detected by the infrared camera as shown in Figure 6 and 7. This may due to low energy impacts do not significantly alter the surface temperature, thus the low temperature changes do not cause noticeable thermal difference from the surrounding materials.

From the investigation, it is concluded that infrared thermography has the ability to detect the failure due to low velocity impact with some limitations. Since detection of defect at lower energy is important, hence further investigation need to be conducted. The applications on other NDT methods or hybrid NDT approach (Chaki et al., 2016) could be other alternative to detect failure at lower than 3J energy impact.

References

Simone Boccardia, Natalino D. Boffaa, Giovanni M. Carlomagnoa, Carosena Meola* a, Fabrizio Riccia, Pietro Russob, and Giorgio Simeolid. 2017. Infrared thermography to impact damaging of composite materials. *Health Monitoring of Structural and Biological Systems*, 10170.

Salim Chaki, Walid Harizi, Patricia Krawczak, Gérard Bourse, and Mohamed Ourak. 2016. Structural health of polymer composites: Non-destructive diagnosis using a hybrid ndt approach. *JEC Composites Magazine*, 107(53):62–65.

Muhammad Imran Najeeb, Agusril Syamsira, Siti Madiha Muhammad Amir, Tabrej Khand, and Tamer A. Sebaeyd. 2023. Failure analysis of plant fibre-reinforced composite in civil building materials using non-destructive testing methods: Current and future trend. *Journal Of Natural Fibers*, 20(2):1:16.

Mohaiman J. Sharba, Zulkiflle Leman, Mohamed T. H. Sultan, Mohamad R. Ishak, and Mohammad A. Azmah Hanim. 2016. Partial replacement of glass fiber by woven kenaf in hybrid composites and its effect on monotonic and fatigue properties. *BioResources*, 11(1):2665–2683.

Individual Research Contribution Review, 2023, 1(1): 259–260

Commercialisation Progress of NuRust in 2023

Siti Radiah Mohd Kamarudin
Industrial Technology Division, Malaysian Nuclear Agency
43000 Kajang, Selangor
Radiah@nm.gov.my

Abstract

The commercialisation of the corrosion-protection R&D product, NuRust has been carried out with the collaboration with Venerable Precision Sdn. Bhd. in January 2023. Since then, commercialisation activities such as promotional work, facilities set up, material and equipment procuring, NuRust testing and market study have been carried out actively by the company as well as Nuclear Malaysia. In this article, all the achievements as well as progress in this work are presented.

Keywords: Commercialisation, NuRust, progress

1 Introduction

NuRust is a water-based compound that coats over rusty ferrous-based metals. It chemically converts rust into a more stable protective layer that seals out moisture and protects against future corrosion. The research and development of NuRust started in 2006 and a final product with good properties and quality was achieved in 2016. In the year 2019, 600 litres of NuRust were produced. In January 2023, Venerable Precision Sdn. Bhd. has agreed to buy all the 600-litre NuRust that has been produced and signed the agreement for the commercialisation of NuRust. This article aims to report the achievement and progress of the commercialisation of NuRust in 2023.

2 Methods

The facility for the production of Nurust is set up at No. 52-1, Jalan BM 2/1, Bandar Bukit Mahkota, 43000 Kajang, Selangor. The renting of the shop lot starts in March 2023, with the renovation and installation of equipment at the facility finished in June 2023. The promotional work of NuRust started in March with a technical presentation given to Enquest Petroleum Production Malaysia Ltd on the 15th of March 2023. Following this, Venerable Precision was given an order of 3000 litres of NuRust from Enquest Petroleum. Participation at the Oil & Gas Asia exhibition (13th - 15th September 2023) was also an effort to promote NuRust to the global market. NuRust has been tested on the oil rig platform of Enquest Petroleum since March 2023 and other field tests were also carried out at Shell Sarawak and Petronas MLNG. To ensure a smooth production, a trial run which consisted of 6 mixing of NuRust with the new raw materials was carried out by the Nuclear Agency. Apart from the promotional and production work, activities to improve the product readiness level, such as the completion of the material safety data sheet (MSDS), and testing from the international certification body SGS (the world's leading, testing and certification company) were also carried out. Numerous characterisation techniques were also carried out at Nuclear Malaysia; corrosion properties measurements (linear polarisation resistance (LPR), Tafel polarisation, electrochemical impedance spectroscopy (EIS), corrosion potential (Ecorr), thermogravimetric analysis (TGA) as well as MEK rub test (ASTM D4752, 2003). The influence of temperature on NuRust performance and storage condition was studied as well. Non-destructive testing (NDT) techniques, radiography and phased array ultrasonic (PAUT) (ASME BPVC) were also carried out to evaluate the effect of the NuRust layer on the structure surface. For morphological studies, scanning electron microscopy (SEM) and an optical microscope were used. Analysis of the sample surface compound was also carried out using Raman spectroscopy. All the samples tested were pre-corroded mild steel.

3 Results

From the activities of commercialisation of NuRust in 2023, the achievement and progress can be categorised in terms of; production facility, production of NuRust, promotional work as well as testing and field tests. In July 2023 (11th – 17th July 2023), the production of 1000 litres of NuRust was carried out at the company's production facility at Bukit Mahkota. Before that, 200 litres of co-NuRust was prepared for the production of 3000 litres of NuRust at Nuclear Malaysia. The production of the remaining 2000 litres will be completed later this year. Results from the field tests have shown very promising feedback; Petronas MLNG said NuRust is the best product and only needs to solve the precipitation problem at the bottom of the bottle, whereas, Shell Sarawak said that it was easy to apply as well as an environmentally friendly. Some of the results from this work are shown in Figure 1, 2 and 3. Raman spectroscopy in Figure 1 shows peaks for the uncoated (highlighted in orange) and NuRust-coated (highlighted in dark blue) samples. The Raman database revealed that the uncoated spectrum matched with iron oxide. Figure 2 shows the corrosion potential of the NuRust-coated samples at room temperature, 50°C, 75°C, and 100°C as well as commercial product (KURUST) and bare metal.

Corrosion potentials of approximately –0.37 V to -0.27 V were recorded for NuRust coated samples, whereas, com-

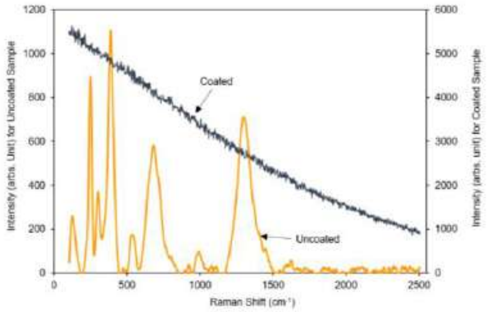

Figure 1: Raman spectrums of the coated and NuRust-coated samples

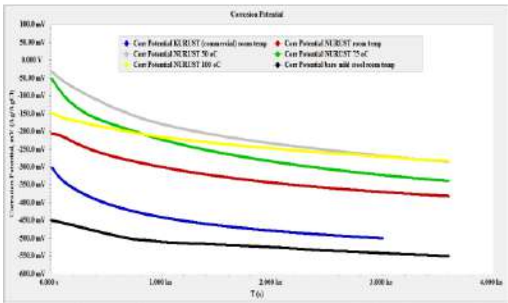

Figure 2: Potential of NuRust-coated, commercial and bare metal samples at room temperature, and NuRust-coated samples at 50°C, 75°C, and 100°C

mercial product and bare metal exhibited corrosion potential values of approximately -0.55 V and –0.50 V respectively.

Figure 3 of the PAUT inspection analysis shows the uncoated (Figure 3a) and NuRust-coated (Figure 3b) samples. The results displayed that both samples have similar signal patterns. Results from the other characterisation techniques also revealed promising findings of the NuRust performance.

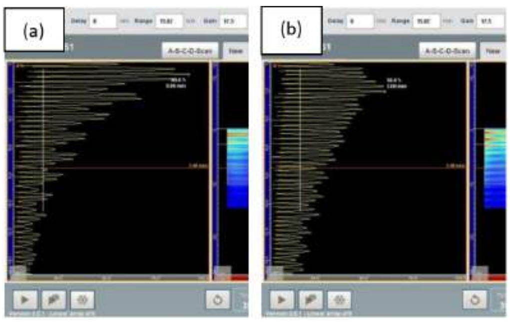

Figure 3: PAUT analysis of the (a) uncoated , and (b) NuRust-coated sample

Radiography image revealed no significant difference between the coated and uncoated area, which is in agreement with the PAUT analysis, while SEM and optical surface morphological studies displayed the formation of a polymeric-like layer on the NuRust-coated surface. The hightemperature effect on NuRust has shown that even after a week of storage at 50°C, NuRust still has its original form and colour. Results from the EIS test have clearly shown that the impedance value (Z) of the NuRust-coated sample is higher than bare metal, indicating better corrosion resistance. In addition, TGA analysis of the hardened NuRust layers treated at 50°C, 75°C, and 100°C revealed that all samples exhibited thermal stability up to approximately 180°C before they rapidly decomposed when heated up to 800°C.

4 Discussion

The disappearance of the iron oxide spectrum from Raman spectroscopy results indicates the effectiveness of NuRust in converting the iron oxide compound to a passive layer on the sample surface. Observation at higher temperatures (50°C, 75°C, and 100°C) found that corrosion potential increased as the temperature increased. Even at room temperature, the NuRust-coated sample exhibited higher corrosion potential compared to the commercial product (KURUST) and bare metal, indicating a better corrosion protection of NuRust-coated samples, which is in agreement with electrochemical behaviour results that show a higher impedance value (Z) for the NuRust-coated sample compared to bare metal. Additionally, TGA results showed that NuRust-coated surfaces can withstand operating temperatures up to 180°C. From the observation of the PAUT inspection, the results suggest that NuRust does not interfere with the sound wave during the inspection, while, the NuRust-coated layer is not highly resistant to the MEK chemical. However, results from the MEK rub test showed that the NuRust-coated surfaces were able to pass 50 double rubs without exposing the bare metal surface.

5 Conclusion and Attention

Based on the results and findings, NuRust is a promising corrosion protection product that can be used in many industries and applications. It works by converting the rust to a passive surface layer that protects the metal surface against future corrosion attacks. All the data/results presented in this article are particularly useful in determining the performance of NuRust.

References

ASTM D4752. 2003. Standard test method for measuring MEK resistance of ethyl silicate zinc-rich primers by solvent rub. 2003.

ASME BPVC Sec. V Art. 4 & 5.

Individual Research Contribution Review, 2023, 1(1): 261–262

Fabrication and Characterization of Nickel Oxide Nanofibers by Electrospinning Technique

Siti Salwa Zainal Abidin
Industrial Technology Division, Malaysian Nuclear Agency
43000 Kajang, Selangor
sitisalwa_za@nm.gov.my

1 Introduction

One-dimensional metal oxides nanostructures such as nanofibers, nanowires, nanotubes, nanorods, have a great potential application in various functional devices (Iqbal et al., 2018). Among various metal oxides, p-type semiconducting material such as nickel oxide, NiO with a band gap (3.7-4.0) is widely use in the several applications. The nickel oxide nanofibers are one of the promising candidates for many applications due to high surface area, psuedo-one dimensional structure and semiconducting characteristics (Khalil et al., 2016).

A variety of methods have been used to synthesize Ni nanofibers. In comparison to the various physico-chemical synthesis pathways mentioned above, this process has several advantages: efficiency, reproducibility, high yield, simplicity, low cost, and high adaptability. Additionally, the preparation of electrospun materials can be easily scaled up due to the availability of setups with multiple needles or needle-less electrospinning (Ercolano et al., 2016). Electrospinning technique is considered the simple, efficient and easy ways among others. It is the technique to produce fibers with diameters down to tens of nanometers from various materials such as polymers, metal oxides and composites (Fridrikh et al., 2003; Khalil and Hashaikeh, 2014; Park et al., 2018).

There are three basic components to be used in an electrospinner a high voltage supply, a needle of small diameter with syringe that is connected to a syringe pump and a collector (Ercolano et al., 2016; Fridrikh et al., 2003; Khalil and Hashaikeh, 2014; Park et al., 2018). It has been shown that electrospinning can be synthesis pure NiO nanofibers using suitable polymer such as PVP and PVA. In a typical electrospinning process, a polymer solution or melt is injected from a small nozzle under the influence of an electric field as strong as several kV/cm. (Iqbal et al., 2018; Khalil et al., 2016; Ercolano et al., 2016; Fridrikh et al., 2003; Khalil and Hashaikeh, 2014; Park et al., 2018). In the electrospinning, the viscosity of solution is the important factor to make the uniform nanofibers without beads. In this work, the formation of NiO nanofibers prepared by electrospinning technique were studied.

2 Experimental

The materials used in this experimental was nitrate acetate dihydrate Ni $(CH_3COO)_3 \cdot 2H_2O$ mix with polyvinylpyrrolidone, PVP (Mw = 1300000) in ethanol with volume ratio of 1:1. All chemicals are used as received without any further purification.

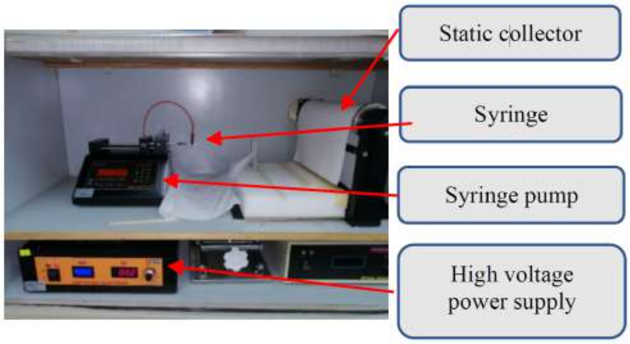

Figure 1: The equipment set up for electrospinning process.

The samples were characterized using field emission scanning electron microscope [FESEM] (Carls Zeiss Gemini SEM 500) and X-ray diffraction (XRD) using PANAlytical Xpert Pro MPD with Cu Kα irradiation (λ=1.5418$\mathring{A}$). The set up of equipment are shown in Figure 1.

3 Results and Discussion

The NiAc/PVP NFs were appear in light green colour due to the present of Nickel ions, Ni^{2+} that were prepared by electrospinning process. Then after the calcination process white colour of nanofibers obtained. The NiAc/PVP NFs were investigated with by two different techniques such FESEM and XRD.

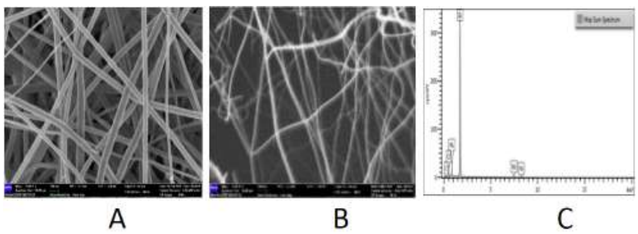

Figure 2: (A)The morphology of the NiAc/PVP nanofibers and (B) the images of NiO nanofibers after calcination with magnification 25kX. Also (C) The EDS analysis of NiO nanofibers.

Figure 2 shows the FESEM images and EDS spectrum NiAc/PVP NFs obtained by electrospinning. The nanofibers were in uniform and with smooth surface without any beads

(NiAc/PVP) Figure 2(A). While Figure 2(B) show the calcined NiO nanofibers. After calcined at 500°C, the nanofibers remained continuous but the diameter becomes thinner, due to the decomposition of polymer. The EDS analysis shown in Figure 2(C) proved that the presence of Ni was composed with Oxygen element and the highest peak presence of Silicon which was used as a substrate for collecting the nanofibers.

Figure 3 shows the XRD spectrum of NiAc/PVP NFs before and after calcined. It is found that NiAc/PVP NFs shows no apparent diffraction peak and exhibited a similar XRD pattern with the ITO substrate, suggesting that the nanofibers were still in amorphous phase. This indicate that there are no metal oxides formation occurs prior to heat treatment process. However, the peaks for NiO are present in the XRD spectra after the calcination process. NiAc/PVP NFs shows two sharp peaks at 37.32° and 43.32° which corresponding to (003) and (012) for NiO (ICSD code: 98-005-9081). This was expected that the calcination of NiAc/PVP NFs will eliminate the polymer and decompose to form the oxide material. This had further strengthened the existence of metal oxide in the nanofibers formed as supported by the FESEM and EDS results mention before. Also, ITO glass peaks, $In_4O_{12}Sn_3$ (ICSD code: 98-003-9963) is observed after the heat treatment process at 30.56°, 35.34°, 50.64° and 60.49° which correspond to (211), (322), (214) and (143) respectively.

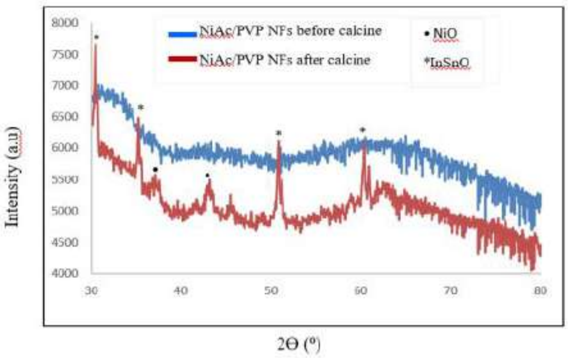

Figure 3: The XRD spectra of obtained NiO nanofibers

4 Conclusion

The characterization results show that the metal oxides (NiO) nanofibers can be easily prepared via versatile and cost-effective electrospinning. The nickel oxide nanofibers were fabricated by electrospinning of NiAc/PVP NFs followed with calcination process. Further investigation on the electronspun NiO nanofibers is compulsory to get the optimum parameters. The study parameters of the solution such as concentration, mixing ratio, molecular weight, viscosity and voltage parameter are important to fabricate this nanofiber. The electrospinning technique to fabrication of NiO nanofibers is useful for application such as renewable energy, water treatment and sensor.

References

G. Ercolano, F. Farina, S. Cavaliere, D. J. Jones, and Rozière. 2016. *J. Nanomaterials*, 6(12):1–12.

S.V. Fridrikh, J.H. Yu, M.P. Brenner, and G.C. Rudledge. 2003. *Phys. Rev. Lett.*, 90:1–4.

M. J. Iqbal, S. Khan, K. Hayat, Y. Iqbal, and S. Ali. 2018. *Mater. Res. Express.*

A. Khalil and R. Hashaikeh. 2014. *R. Materials Charac.*, 95:65–71.

A. Khalil, J. J. Kim, H. L.Tuller, G. C. Rutledg, and R. Hashaikeh. 2016. 227:54–64.

J. Park, Y-C. Kang, S. W. Koh, and J. Chosun. 2018. *Nat. Sci.*, 11(1):14–18.

Individual Research Contribution Review, 2023, 1(1): 263–264

Density Assessment of Materials Using Gamma Transmission Technique

Soleha Mohamat Yusuff
Industrial Technology Division, Malaysian Nuclear Agency
43000 Kajang, Selangor
soleha@nm.gov.my

Abstract

In this work, the transmission rates of various materials were observed via gamma-ray transmission technique using Ba-133, Cs-137, and Co-60 as gamma radioisotope sources. Results found increasing thickness and density of materials reduced the transmission rates for all materials using different gamma sources. This finding shows that the gamma-ray transmission technique was compatible with predicting the density of various materials.

Keywords: Transmission, Density, Gamma

1 Introduction

Density is a vital characteristic of materials (Carvalho et al., 2023) in identifying the purity, modification, or any material changes. Conventionally, density is determined by dividing the mass of an object by its volume (Nor et al., 2019). However, under various circumstances, the researcher found nuclear techniques application such as gamma-ray transmission technique for density measurement offers many advantages (reducing labor-intensive, time-consuming, and material preparation without material destruction) (El-Mesery et al., 2019). This study aims to measure the transmission rate of various samples with different thicknesses and densities using the gamma-transmission technique and low-activity gamma sources.

2 Methods

2.1 Materials and equipment

The instruments required for intensity measurements are a detector (Thallium doped Sodium Iodide, NaI(TI) scintillation crystal optically coupled to a 38 mm diameter photomultiplier tube (PMT)), collimator for a detector, collimator for a gamma source, 5 m long wire cable, ratemeter (LUDLUM 2200 scaler), low activity (<1 mCi) of gamma sources (Ba-133, Co-60, and Cs-137), blocks of lead, USB 2.0 to RS232 serial DB9 9 pin adapter cable, laptop, and G-frame. G-frame ensures correct geometry for gamma measurement. A ratemeter took readings every 6 seconds by setting up the threshold dials at 1, a multiplier at x.1, and a numerical value at 1. Figure 1 shows the experimental setup for the stability test and transmission rate study.

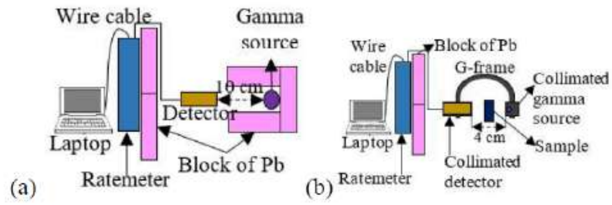

Figure 1: Experimental setup for stability test (a) and transmission rate study (b).

2.2 Stability test study

The stability test was conducted by measure the intensity without and with gamma source by placing each gamma source in distance of 10 cm opposite to gamma detector.

Intensity count was recorded as high voltage (HV) dial setting increased by 0.01 starting from 0 until the intensity count reached the plateau result. The optimum HV dial setting for each gamma source were determined from intensity against HV dial setting graph using Equation 1.

$$\text{optimum } HV = \frac{2}{3}(V_f - V_i) + V_i \tag{1}$$

where V_i and V_f are first and last HV found from the plateau line, respectively. Then, the chi-squared test was conducted by performing twenty replications of intensity measurements using optimum HV dial setting. The chi-squared value is determined using the formula in Equation 2.

$$x^2 = \sum (C_I - C_E)^2 / C_E \tag{2}$$

where x^2 is chi-squared value, C_I is observed intensity count value, and C_E is expected or average intensity count value.

2.3 Transmission rate study

The transmission rate study was performed by using optimum HV dial setting and acceptable chi-squared value. The experimental setup for transmission rate study were followed Figure 1(b). Thickness of stainless-steel plates, aluminium plates, polyethylene (PE) plates, acrylic plates, plywood plates, meranti block, kempas block, and keranji block were measured using veneer clipper. All intensity measurements were conducted three times for accuracy at three different points.

3 Results

The stability test is necessary to obtain accurate radiation measurements using a detector and scaler ratemeter at a proper high voltage while indicating measurement validity and the proper operation of the counting system when applying random pulses from a radioactive source (Susiapan et al., 2015). From the stability test study, the optimum HV dial setting for Co-60, Ba-133, and Cs-137 were 2.8 (700V), while the chi-squared value for Cs-137 (14.38) and Ba-133 (14.35) lies in the acceptable chi-squared range of 3.33 and 16.92. The chisquared value for Co-60 (18.41) is larger than 16.92 and may result from spurious pulses from random electrical noise, unstable power supply, temperature changes, or electronic faults, thus indicating faulty performance (IAEA,1988). The stability study results demonstrate that the 2.8 HV dial setting (700V) using the Na(I) detector was appropriate for achieving stable, dependable, and valid measurements for Ba-133 and Cs-137 (661.6 keV) gamma sources. Figure 2 illustrates the transmission rate (I/Io) of PE, acrylic, aluminum, and steel using Co-60, Ba-133, and Cs- 137 at different thicknesses. The transmission rate reduces as the sample thickness increases for all samples.

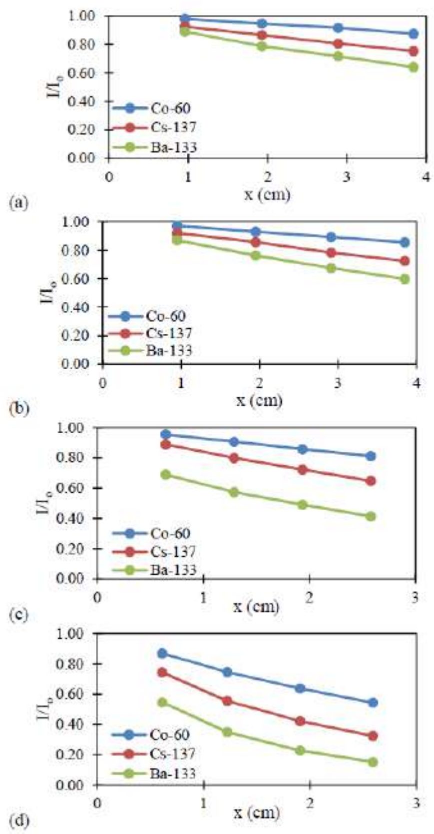

Figure 2: Transmission rates against PE (a), acrylic (b), aluminium (c), and steel (d) thickness using gamma sources.

The PE with lower density gave a higher transmission rate followed by acrylic, aluminum, and steel. Table 1 also shows the order of the wood blocks according to their decrease in transmission rates over the density material, Meranti>Kempas>Keranji.

Table 1: Transmission rates of materials with previous density.

Sample	x (cm)	ρ (g/cm^3)	I/I_o		
			Co-60	Cs-137	Ba-133
PE	3.84	0.950	0.88	0.75	0.64
Acrylic	3.85	1.180	0.86	0.73	0.60
Aluminium	2.58	2.710	0.81	0.65	0.42
Steel	2.59	7.750	0.54	0.32	0.15
Keranji	4.10	1.180	0.85	0.71	0.59
Kempas	4.20	0.815	0.88	0.76	0.65
Meranti	3.60	0.418	0.92	0.84	0.75

4 Discussion

The photon energy of gamma sources decreases when gamma-ray interacts with material regarding the absorbance effect of the materials (Turgay, 2021). The absorbing effect or attenuation of photons is different for each material due to the density and elemental composition of the material. Thus, increasing the thickness and density of materials reduces the transmission rates obtained.

5 Conclusions

The gamma transmission technique was capable of assessing the density of materials based on transmission rate results. Future research work will explore the attenuation coefficient parameter and density for Malaysian timber products using low activity of gamma sources to support radiation gauging applications in forestry management, timber quality control, and radiology.

References

INTERNATIONAL ATOMIC ENERGY AGENCY. 1988. Quality control of nuclear medicine instruments. *IAEA-TECDOC-602*.

Ellen C.D. Carvalho, Bruno C. Souza, Marília S. Silva, Bruno S. Menezes, Fernando R. Martins, Francisca S. Araújo, and Arlete A. Soares. 2023. Xylem anatomical traits determine the variation in wood density and water storage of plants in tropical semiarid climate. *Flora*, 298(1):152185.

Hany S. El-Mesery, Hanping Mao, and Abd E.F. Abomohra. 2019. Applications of non-destructive technologies for agricultural and food products quality inspection. *Sensors*, 19(4):846.

Fazrul M. Nor, Abd R. Tamuri, and Abd K. Ismail. 2019. Fake gold: Gold purity measurement using non destructive method. *International Journal of Engineering Technology)*, 8(1.1):65–172.

Yvette Susiapan, Ruzairi A. Rahim, Rasif M. Zain, Ahmad R. Wahab, Herman Wahid, Mohd H.I. Ishak, Salinda Bunyamin, Yusri Yunus, and Leow P. Ling. 2015. Stability test for NaI(TI) scintillation detector. *Jurnal Teknologi (Sciences Engineering)*, 77(17):27–30.

Muttalip E. Turgay. 2021. Comparison of gamma sources (Cobalt and Cesium) for density measurement of metals and alloys via using transmission technique. *Journal of Engineering Technology and Applied Sciences*, 6(1):37–43.

Individual Research Contribution Review, 2023, 1(1): 265–266

Synthesis and Characterization of Metal Decorated Graphene

Suhaila Hani Ilias
Industrial Technology Division, Malaysian Nuclear Agency
43000 Kajang, Selangor
suhaila_hani@gov.my

Abstract

Hydrogen is a good candidate that fulfills this requirement but a major challenge to its usage is its storage. In the safest mode, hydrogen can be stored as solid state by combining with materials through physisorption or chemisorption mechanism (Nagar et al., 2017). In this research, we focus on metal decorated graphene materials that involves studying for the right formulation for hydrogen storage as well as to optimize their properties and evaluate their performance with the appropriate analytical tools.

Keywords: Graphene, metal nanoparticles, gamma irradiation

1 Introduction

Graphene and metal hydride through physical and chemical treatments can be optimized for higher hydrogen storage capacities. Metal like Palladium (Pd) nanoparticles can take up large volumetric amounts of hydrogen at normal room temperature and atmospheric pressure. Pd nanoparticles were synthesized using precipitate method and then functionalized with exfoliated graphene using gamma radiation.

In this work, gamma (γ) radiation is used to reduce metal ions to metal particles. Compared to other reduction methods, γ-radiation reduction method has several advantages such as no toxic chemical reducing agent or undesired oxidation products are involved. The reaction induced by radiation is well defined and thus the particle size and shape can be controlled. It is also a simple and clean technique that provides metal particles in fully reduced, high purity and stable state with no disturbing impurities produced, thus making the γ-irradiation a harmless and environmentally friendly technique to be used (Liu et al., 2019).

2 Experimental Methods

Electrochemical exfoliation is a promising process for synthesizing graphene from graphite. It is cheaper, greener and potentially capable of mass production with few layers of graphene. In this process, an applied voltage drives ionic species to intercalate into graphite lattices where they form gaseous species that expand and exfoliate into individual graphene sheets.

The quality and quantity of the synthesized graphene (graphene layer numbers, O contents, lateral size, edge or sheet defects) can be obtained by controlling the process parameters (applied electrical potential, current, processing time, composition of electrolytes) (Murshidi et al., 2020).

Graphene decorated with palladium nanoparticles have been synthesized based on a chemical approach using ascorbic acid as an eco-friendly reducing agent. PVA plays a significant role as a capping agent to control the nanoparticle size. Raman spectroscopy analysis can determine the quality and quantity of graphene and determine the peak of metal. The spectra of graphene and metal samples has been characterized by 532 nm laser wavelength. The integral intensities and full width half maximum (FWHM) of the bands assigned to the vibrations of graphitic band (G band) and defect band (D) used to calculate the layers and its quality.

3 Results

The mechanisms behind electrochemical exfoliation depend principally on the type of potential applied: anodic or cathodic. Anodic exfoliation involves the intercalation of anions as well as other co-intercalating species involved in the reaction mixture into the graphite lattices.

For anodic potential, a positive bias withdraws electrons from the graphite (anode), creating a positive charge. On the other hand, a negative bias allows electrons to the Pt (cathode), creating a negative charge. This negative charge drives the reduction of water molecules at the cathode, producing hydroxyl ions (OH^{-1}). OH^{-} can attack graphite (anode) at the edges and grain boundaries (Murshidi et al., 2020)]. This oxidation at anode leads to the expansion of graphite layers at the edges, opening up the lattices for intercalation by sulfate ions (${SO_4}^{2-}$) and also possibly more water molecules. After the electrochemical intercalation and expansion of graphite, the gaseous species (e.g. SO_2 and O_2) produced (e.g. from oxidation of water molecules and from reduction of ${SO_4}^{2-}$ anions) will then exfoliate and separate the graphite lattices into graphene.

Figure 1 shows the Raman spectrum for synthesis palladium metal decorated graphene exfoliated using gamma radiation. From the spectra, D peak for palladium is located at 700 cm^{-1}. From the graft, only Pd with PVA and exfoliated graphene have the G and 2D peak. G peak is located at 900 cm^{-1} and 2D peak is located at 1900 cm^{-1}. The intensity of the D peak depends on the disorder of the graphene. The G peak represents the E_{2g} phonons vibrations mode in the center of the Brillouin Zone and is a characteristic peak of carbon material (S.H.Ilias et al., 2020). The ID/IG ratio, which gives information about

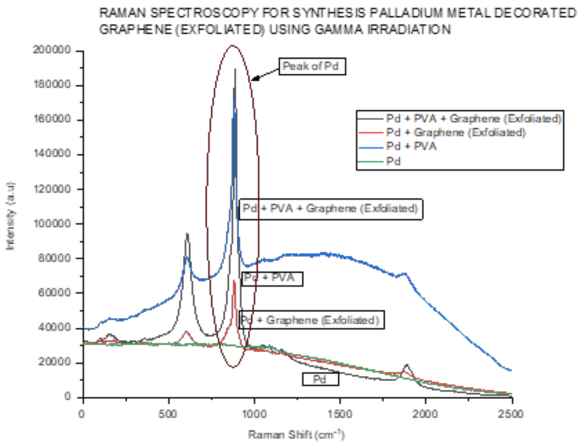

Figure 1: Raman spectrum for synthesis palladium metal decorated graphene exfoliated using gamma radiation.

the amounts of defects in graphene, was found to be 0.47. This ratio allows to distinguish graphene from multi layered graphite. The intensity I2D/IG ratio, which represents the number of graphene layers, for exfoliated graphene was 0.22 respectively.

4 Discussions

Polyvinyl alcohol (PVA) is a water soluble and was used as a binder of the sample. It is one of the promising representatives of polymer materials that have high clarity, lack of charge density proper and excellent durability. The hydroxyl groups attached to the polymer backbone exert a significant effect on the solubility (S.H.Ilias, 2011). It contains a carbon chain backbone with hydroxyl groups attached to metal nanoparticles and graphene using a precipitation method. These OH groups can be a source of hydrogen bonding hence the assistance in the formation of blend.

In this work, gamma (γ) radiation is used to reduce metal ions to metal particles. The major advantages of radiation processing are neither oxidizing agent is used to polymerize PVA nor surfactant agent is needed to functionalize graphene with Palladium (Pd). In the synthesis process, the reduction of graphene and the formation of nanoparticles are accomplished simultaneously such that the metal nanoparticles are uniformly anchored on the surfaces of individual graphene to prevent the restacking of graphene, resulting in good dispersibility in solvents. The interactions of Palladium metal nanoparticles with graphene have been examined using Raman spectroscopy. In fact, there is a notable shift of the G and D bonding configurations, in addition to the variation in the relative intensities of those characteristic peaks when the metal was deposited on graphene. The spectral shifts in G and D bands show meaningful trends with ionization energies of the metals as well as charge transfer energies between metal particles and graphene.

5 Conclusion

In conclusion, the successful synthesis of graphene was achieved through the electrochemical exfoliation of a graphite rod, utilizing a higher concentration of electrolyte (H_2SO_4:KOH volume ratio of 90:10). This optimized approach resulted in a superior yield, lower oxygen content, and minimized defects. Subsequently, the synthesized graphene was decorated with palladium using gamma radiation. Selection of a suitable electrolytes is thus important to tune the quantity and quality of the graphene. The present study provides a proficient approach to synthesize cost effective and environment friendly of metal palladium decorated graphene.

References

Fei Liu, Chaojun Wang, Xiai Sui, Muhammad Adil Riza, Meiying Xu, Li Wei, and Yuan Chen. 2019. Synthesis of graphene materials by electrochemical exfoliation: Recent progress and future potential. DOI: 10.1002/cey2.14.

J.A. Murshidi, K.K.Ying, S.H.Ilias, and U.T.Tukirin. 2020. Synthesis of graphene materials by electrochemical exfoliation of graphite. *NUKLEARMALAYSIA/L/2020/126*.

Rupali Nagar, Bhaghavathi P. Vinayan, Sai Smruti Samantaray, and Sundara Ramaprabhu. 2017. Recent advances in hydrogen storage using catalytically and chemically modified graphene nanocomposites. *Royal Society of Chemistry*, pages 22897–22912.

S.H.Ilias, J.A. Murshidi, K.K.Ying, and U.T.Tukirin. 2020. Synthesis of graphene materials by effect of electrolyte concentration on the synthesis of graphene by electrochemical exfoliation process. DOI: 10.1088/1757-899X/1106/1/012013.

S.H.Ilias. 2011. Gamma radiation induced synthesis and optical characterization of cobalt and nickel nanoparticles stabilized in polymer.

Individual Research Contribution Review, 2023, 1(1): 267–268

Characterization of Ultrasonic Signals from Welding Defects

Suhairy Bin Sani
Industrial Technology Division, Malaysian Nuclear Agency
43000 Kajang, Selangor
suhairy@nm.gov.my

Abstract

Inspecting weld structures is crucial to determine the quality of welds to prevent failure in daily operations. Ultrasonic testing (UT) is an effective and non-destructive test that has become one of the most suitable methods for detecting defects in welded structures. This work presents a method to determine the most suitable feature extraction using full-wave pulse echo (FWPE) to distinguish the various types of weld defects in single V−joint plates. The outcomes revealed that characteristic extraction for the time domain, maximum amplitude, depth, number of peaks and skew can be used to determine the type of defect on the welded specimens tested. Scanning both sides of the weld provides additional information that helps distinguish the type of defect in terms of orientation and position.

Keywords: Ultrasonic testing (UT), full-wave pulse echo (FWPE), weld defects, signal features extraction.

1 Introduction

Structural weld inspection is a crucial method for determining whether the quality of welds meets the quality standards for operation. Defects in welds can affect their condition. This depends on three factors, which are the type, size and location of the defect. One of the most widely used non−destructive evaluation (NDE) methods of weld defects is ultrasonic testing (UT). The UT method, consisting of pulse−echo, is the most reported method applied to characterize A−scan weld defects. The UT pulse−echo method utilizes high frequency sound wave pulses that can be transmitted into a weld. Any weld defects will cause echoes in pulses. The signal patterns are then processed to obtain information on the size, shape and orientation of the defects. The two types of A−scan signal patterns used to characterize weld defects are unrectified and full rectification signals. They are commonly known as RF−wave pulse−echo (RFPE) and full−wave pulse−echo (FWPE) respectively. However, the FWPE method for the characterization of welding defects is always used as a standard procedure in the practical training of ultrasonic inspection. In this study, UT is obtained by inspecting V−welded steel plates through manual transverse probe movement. The aim of this study is to determine the most valuable extraction features for comparing different types of weld defects; i.e.,

i. center crack (CCr);
ii. slag inclusion (SI);
iii. lack of fusion (LOF);
iv. cluster porosity (Po);
v. lack of penetration (LOP); and
vi. root crack.

Feature data for normal conditions (N−no defects) is also used as the baseline reference.

2 Methods

This study utilised specimens of six different weld defects in single V−butt weld plates (Sonaspection International Ltd.). Figure 2 presents the specimens that only contain a specific type of defect in each plate. These specimens are composed of carbon steel with a thickness of 10 mm. The defects are about 25 mm in length. Ultrasonic measurements of these defects were conducted using a 60° angle beam ultrasonic probe (GB Inspection Systems Ltd.) and a portable USBUT−350 ultrasonic pulser / receiver with an analogue to digital converter. The frequency employed for all the experiments is 4 MHz. An in−house device control and data acquisition system was developed in C# programming language for data acquisition. The system was applied to obtain the pulse−echo signals used to generate the B−scan results at a sampling rate of 50 MHz and scanning sensitivity of 43 dB. Calibration of the sensor sensitivity was conducted using a V2 block prior to the scanning process. The processed signal underwent two types of filters before characterisation was performed. The first filter is the low−pass filter (LPF), which can be appropriately selected from the data acquisition card. The second filter is the moving average filter (MAF), symmetrically used to further smoothen the signal until a single peak appears. Scanning was accomplished from half skip distance (HSD) to full skip distance (FSD) as well as half of the weld cap on both sides (Figure 1).

The FWPE data measurement was processed in Python programming language to extract the features of signals and display the results in the form of data images (B−scans) as shown in Figure 2. The feature extraction in the developed software was obtained using the maximum peak in the signal processing. Data was extracted from FWPE, equal or above 10% of the full screen height (FSH). The extracted data is represented by the blue line in the Figure 3.

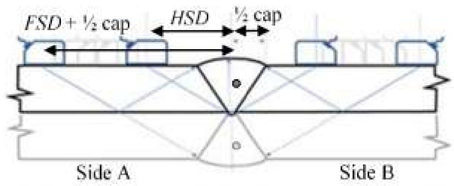

Figure 1: Diagram of the weld specimen

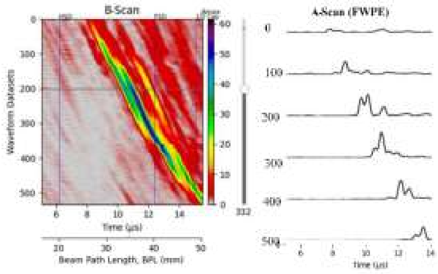

Figure 2: B-scan data waveform and A-Scan envelops.

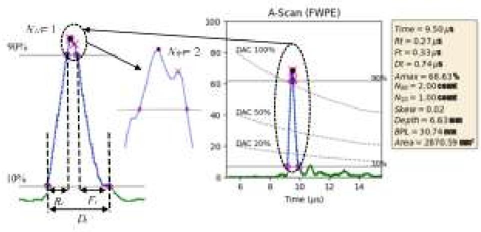

Figure 3: Features extraction from FWPE.

Note: Rise time (*Rt*), Fall time (*Ft*), Duration time (*Dt*), Maximum amplitude (*Amax*), FWPE ≥ than 10% of the FSH (N_{10}), FWPE ≥ than 90% of the FSH (N_{90}).

3 Results and Discussion

Principal component analysis (PCA) was performed to determine the correlation between feature extraction parameters and weld defect types, as shown in Figure 4. Both axes describe a cumulative variance of 80.39% and the symbols represent the types of defects on both sides of the weld. All defects and N are in almost identical clusters, except LOF and RCr, which are isolated between the two sides. The first component describes 59.34% of variation and separates the extraction of the highest value traits for CCr and Po from the other defects, while N is at the lowest position for all the defects as the reference data. Po shows the extraction of the highest N_{10}, N_{90}, *Rt, Ft, Dt* values and skew, followed by CCr and N. The second component describes the 12.17% variance and separates the extraction of the highest value features for LOF−A, CCr and LOP from the other defects. The *Amax* extraction exhibited the highest values for LOF−A (on side A). RCr−B (on side B) is with the LOP cluster, indicating that the relationship has similar characteristics, where the signal obtained is almost the same due to the position of the defect orientation.

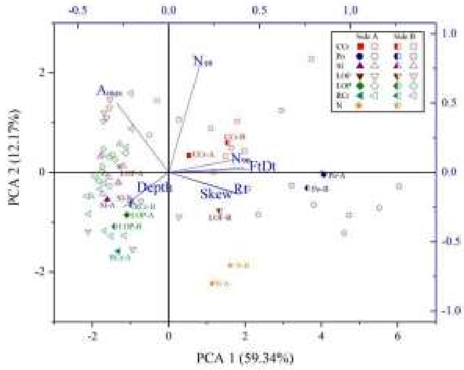

Figure 4: PCA for all tested weld specimens.

4 Conclusion and Attention

The results of the investigation revealed that the characteristic extraction parameters were influenced by the presence of defects. The findings from these experiments proved the capability of the UT method using the transverse scan technique to detect the presence of different defects in V−butt welded specimens with the following conclusions:

a) UT offers the potential to detect and identify different weld defects and evaluates the entire welded structure on both sides A and B.

b) From the extraction of features tested in this study, the time-domain (*Rt, Ft* and *Dt*), number of peaks (N_{10} and N_{90}), depth, skew and Amax were found to be the main parameters in detecting the presence of weld defects.

c) Analyzing the number of peaks was found to be a good detection indicator for detecting Po and CCr defects. Depth characterization can further distinguish LOP and RCr from other defects.

d) Scanning on both sides (A and B) of the weld as a recommended standard is essential to distinguish the types of LOF and RCr defects since they are influenced by defect orientation.

e) Although the SI defect is quite difficult to identify, its symmetric pattern shows low skew values. The comparison of mean values for N_{10}, N_{90} and *Amax* revealed identical distribution values on both sides A and B.

References

Suhairy Sani, Mohamad Hanif Md Saad, Nordin Jamaludin, Norsalim Muhammad, Siti Fatahiyah Mohamad, and Megat Harun Al Rashid Megat Ahmadi. 2022. Evaluation of weld defects signal features using ultrasonic full wave pulse echo methods. *Defence S and T Technical Bulletin*, 15:110–123.

Individual Research Contribution Review, 2023, 1(1): 269–270

Gamma Ray Imaging of Concrete Material

Susan Maria Sipaun
Industrial Technology Division, Malaysian Nuclear Agency
43000 Kajang, Selangor
susan@nm.gov.my

Abstract

A first generation translate-rotate gamma ray computed tomography system was designed and built in Malaysian Nuclear Agency. This CT system is movable; it is used at a fixed station in the laboratory or on-site locations. Several industrial applications of this CT scanner have been carried out to study materials and object defects. In this work, CT images were obtained from gamma ray CT scans of 7cm and 14.5cm diameter concrete cylinders, 10cm^2 and 15cm^2 concrete blocks with embedded metal rebar.

Keywords: Gamma ray, Tomography, Concrete, Rebar

1 Introduction

Gamma ray computed tomography (CT) system produces cross sectional images of objects, which enables users to analyse and observe the objects' internals. Typical radioisotopes used in gamma CT are Am-241 (59.54keV), Ba-133 (356keV), and Cs-137 (662keV) with activities ranging from several MBq to a few GBq. Gamma ray CT has been used to investigate gas-liquid distribution at varying gas volume fractions in a centrifugal pump. It is able to reconstruct gas holdup distribution images inside the rotating impeller wheel, hence giving information on its operational behaviour. This system utilised 320 scintillator detectors and a fan beam gamma ray from 180GBq Cs-137 source (Schafer et al., 2015). A high speed gamma CT system studied the implementation of imaging rapid changes in multiphase hydrocarbon flow regimes (Maad et al., 2010). It is designed to capture images of gas bubbles that are 10% smaller than the pipe diameter. This system has five units of 500mCi Am-241 source and five detector modules, each consisting of 17 CdZnTe detectors. These CT systems utilised multiple detectors to capture dynamic and moving body, and used algebraic reconstruction technique (ART) (Schafer et al., 2015) and iterative least squares technique (ILST) algorithm (Maad et al., 2010). A movable gamma CT system was designed at Agensi Nuklear Malaysia for the purpose of on-site inspection of objects up to 100cm large. This CT system utilised single source-single detector in a translate-rotate configuration. It was used to detect basal stem rot due to Ganoderma disease in oil palm plantation using 50mCi Cs-137 (Abdullah et al., 2013). A smaller movable CT system was used to inspection pipe and concrete. It was used to detect material deposition, corrosion in pipes as well as concrete objects. The radioisotope 10mCi and 15mCi Ba-133 were used in the inspections. The filtered back projection algorithm was use to reconstruct the cross-sectional images (Abdullah et al., 2015; Sipaun et al., 2022; Sipaun et al., 2020). This paper discusses the CT imaging on cylindrical and cubic concrete blocks using the gamma CT system at Agensi Nuklear Malaysia. This work was done in preparation for the application of gamma ray tomography examination of materials in concrete structures especially building pillars.

2 Methods

Attenuation data is collected at each translate and rotate movement location, (translate position, rotation angle). For a 15cm sample size, we select the field of view (FOV) to be 20cm. There is a 5cm gap for air count measurements, whereby if the 'Set Linear Motion' is 0.5cm, there shall be at least two (2) air count data collected within a single line scan. The set linear motion is the translation interval in data collection, for example 0.5cm means attenuation data is collected at every 0.5cm. If the FOV is 20cm, the total number of translation data per degree is (20cm/0.5cm)+1 = 41. The 'Set Rotation Motion' correspond to rotation interval, for example for 5° the data is collected every 5° beginning at 0° and ends at 180°, total rotation data is (180°/5°) +1 = 37. The +1 is added so that there is always a centre data. The total number of data for a 20cm FOV is 41 x 37 = 1517. CT images are reconstructed using data from multiple projections. The filtered back projection algorithm has been discussed elsewhere and is not repeated here (Abdullah et al., 2013; IAEA, 2008). Concrete samples were cylindrical cement with aggregates (7cm diameter) and homogenous cement (14.5cm diameter), and cubic cement (10cm^2) with four embedded rebar (21, 17, 15 and 13 mm) and cubic cement (15cm^2) embedded with two same-size metal rebar (8mm). These samples were chosen as to obtain operational scan parameters in preparation for on-site inspection on building pillars (cylindrical and rectangular).

3 Results

CT images reveal the constituent materials within the concrete. The cross-sectional images allow us to distinguish metal rebar, air/void, aggregate and concrete and its structural form. The square and circular shapes are clearly seen. The dark shades represent air, the white shade represent the denser materials, i.e. metal rebar and aggregates, and the grey shade is the concrete mix. It is suggested that for small sizes of concrete, Ba-133 is sufficient, however, for larger structures higher energy radioisotope such as Cs-137 and Co-60 is more suitable.

3.1 Cylindrical concrete

Results from the CT scan of cylindrical cement samples are shown in Figure 1. It is found that both images show good fidelity to objects whereby the shapes and material constituents can be distinguished. Some artifacts are seen for the larger sample due to the difference in density between concrete and air (Figure 1-left.

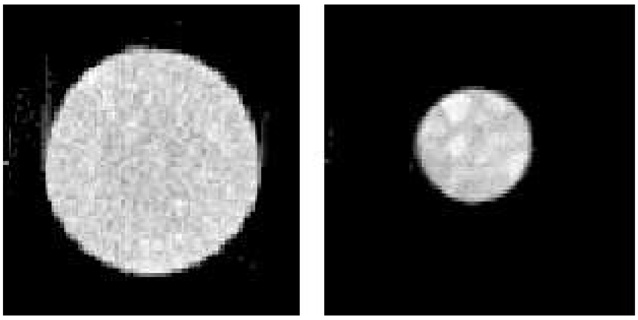

Figure 1: Cross sectional image of the 14.5cm cylindrical homogenous cement sample (left). Image of the 7cm cylindrical cement with aggregates (right)

3.2 Cubic concrete

In Figure 2, the left image shows a homogenous cement and the two rebars of the same size. We used a standard concrete mix in this sample and embedded two 8mm metal rebars. The right image shows the cross section of each rebar of sizes 21, 17, 15 and 13mm. This concrete mix is a fibre-reinforced ultra-high-performance concrete (UHPC) designed for radiation shielding.

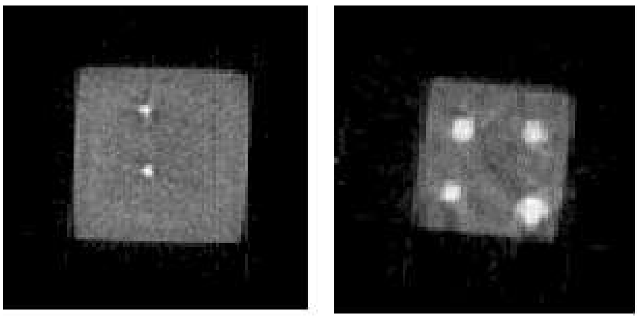

Figure 2: Cross sectional image of the cubic cement (15cm^2) embedded with two same-size metal rebar (8mm) (left) and cubic cement (10cm^2) with four embedded rebar (21, 17, 15 and 13 mm) (right).

4 Conclusion

Tomographic imaging allows non-invasive examination of material distribution, internal shapes and object structure. This gamma CT system provided images of concrete and metal rebar at reasonable resolution and contrast. It can produce realistic image fidelity to object. This CT system is suitable for determining rebar sizes above 8mm, and can be used to estimate the rebar sizes for concrete structures between 7cm and 15cm.

References

J. Abdullah, H. Hassan, and R.Shari Mohamad. 2013. Gamma scorpion: mobile gamma-ray tomography system for early detection of basal stem rot in oil palm plantations. *Optical Engineering*, 52(3).

Jaafar Abdullah, Hearie Hassan, Mohamad Rabaie Shari, Maslina Mohd Ibrahim, Nolida Yussup, Hanafi Ithnin, and Airwan Affandi Mahmood. 2015. Development and implementation of a portable nucleonic computed tomography system with clamp-on-features for engineering inspection. *Jurnal Teknologi*, 77(17):121–127.

IAEA. 2008. Industrial process tomography. *IAEA TECDOC 1589*.

Maslina Ibrahim, Jaafar Abdullah, Nolida Yussup, Nur Aira Abdul Rahman, M. Mokhtar, Hanafi Ithnin, and Hearie Hassan. Development of software for automation and data acquisition system for Gamma Spider and SPECT.

G.A. Johansen. 2015. "Gamma Tomography" in industrial tomography systems and applications. *Woodhead Publishing Series in Electronic and Optical Materials*, pages 197–222.

M. Khorsandi and S.A.H. Feghhi. 2016. Gamma-ray CT as a complimentary technique for structural inspection of tray-type distillation columns. *Measurement*, 78:1–8.

R. Maad, B.J. Hjertaker, G.A. Johansen, and Ø. Olsen. 2010. Dynamic characterization of a high speed gamma-ray tomograph. *Flow Measurement and Instrumentation*, 21(4):538–545.

Thomas Schafer, Andre Bieberle, Martin Neumann, and Uwe Hampel. 2015. Application of gamma-ray computed tomography for the analysis of gas holdup distributions in centrifugal pumps. *Flow Measurement and Instrumentation*, 46(B):262–267.

Susan Sipaun, Md Fakarudin Ab Rahman, Nor Azreen Masenwat, and Hearie Hassan. 2020. Examination of corrosion under insulation using gamma ray computed tomography. *IOP Conf. Ser.: Mater. Sci. Eng.*, 785:785 012039.

Susan Sipaun, Hearie Hassan, Mohamad Rabaie Shari, Airwan Affandy Mahmood, and Nurliyana Abdullah. 2022. A technical comparison between gamma ray and x-ray CT for industrial materials examination. *Jurnal Fizik Malaysia*, 43(1):10009–10017.

Underground Utility Inspection using Ground Penetrating Radar

Tengku Sarah Tengku Amran
Industrial Technology Division, Malaysian Nuclear Agency
43000 Kajang, Selangor
sarah@nm.gov.my

Abstract

Subsurface utility inspection is crucial for urban planning, building, and public safety, as it helps in accident prevention, minimizes construction delays, and reduces service disruptions. It reduces the likelihood of accidents, injuries, and deaths by identifying potential risks such as gas leaks, live electrical wires, and unstable ground conditions. Ground penetrating radar (GPR) is a technique used to accurately locate and map pre-existing underground infrastructure, such as water pipelines, gas conduits, sewage networks, and communication cables, before construction or excavation activities. This helps prevent unplanned damage to these vital components, which can be costly to repair and disrupt essential services. GPR uses electromagnetic fields to investigate lossy dielectric materials and detect changes in material characteristics. The transmitter antenna emits a subterranean electromagnetic pulse, while the receiver detects backscatter and reflected waves.

Keywords: GPR, Non-destructive, subsurface utility

1 Introduction

Subsurface utility inspection is crucial for urban planning, building, and public safety, as it helps prevent accidents, minimize construction delays, and reduce service disruptions. It helps identify potential dangers like gas leaks, live electrical wires, and unstable ground conditions. Ground penetrating radar (GPR) is a technique used to accurately pinpoint the location of pre-existing underground utilities, such as water pipelines, gas conduits, sewage networks, and communication cables, before construction or excavation activities. This prevents unplanned harm to these vital infrastructure components, which can be costly to repair and disrupt essential services. GPR uses electromagnetic fields to investigate lossy dielectric materials and detect changes in material characteristics. The transmitter antenna emits a subterranean electromagnetic pulse, while the receiver detects backscatter and reflected waves. The residual electromagnetic waves persist and penetrate subterranean layers, making it suitable for detecting artefacts in the subsurface.

2 Methods

This experiment was held at the evaluation verification facility (EVF) in Malaysia Nuclear Agency. The scanning area was divided into two parts which consisted of 1^{st} phase and 2^{nd} phase. The dimensions of the scanning area was 13m × 6m with 22 line profile for vertical scan and 9 line profile for horizontal scan for the 1^{st} phase scanning area. For the 2^{nd} phase scanning area was 5.9m × 14m with 9 profiles for the vertical scan and 18 profiles for the horizontal scan. The GPR used was a GSSI 400MHz shielded antenna. Data was collected using SIR 4000 and then processed using RADAN 7 software. For comparison, the contractor's as-built drawing has been used for validation purposes. The depth of mild steel pipe has been used as a reference depth (1.15m).

Figure 1: (a) Evaluation Verification Facility (EVF) (b) 1^{st} phase scanning area (c) 2^{nd} phase scanning area

The experiment was divided into two parts, named Experiment 1 and Experiment 2, where the difference is the scanning area. Experiment 1 was to capture radargram for the 1^{st} phase while experiment 2 was to capture radargram for the 2^{nd} phase. After a complete scan for each phase. The collected data has been transferred into the PC then it will be assembled as a 3D file for each phase.

3 Results

The data was obtained from radargram by using SIR4000 and then was processed by Radan 7 software. 31 radargram was obtained for experiment 1 and 27 radargram was obtained for experiment 2. From the radargram, the average depth was obtained for mild steel pipe. The average depth from the radargram is 1.075m with a tolerance of ±0.095m. Compared with the reference depth of 1.15m, we get the accuracy using GPR is 1.075/1.15 x 100% = 93.48%. For comparison, the 3D file from Radan 7 software shows the pattern of mild steel pipe below the ground.

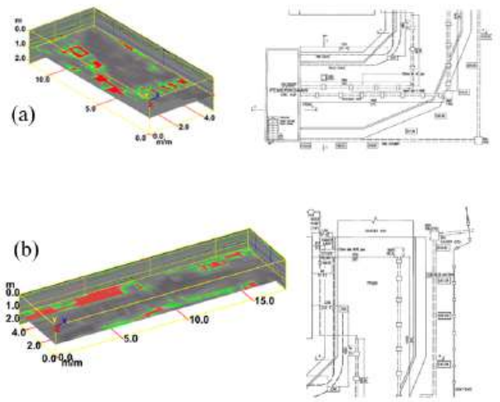

Figure 2: (a) The 3D view for 1^{st} and 2^{nd} phase scanning area (b) Contractor's as-built drawing for reference 1^{st} and 2^{nd} phase

These 3D files were obtained from the combination of radargrams in X and Y direction. Every radargram has the detail of the image below the surface. From that, using radargram can observe the potential area that has the underground utility that has been desired for inspection. Below are several examples of the radargram:

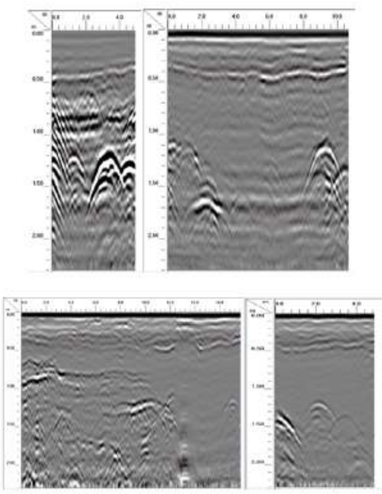

Figure 3: Radargram for X direction 1^{st} & 2^{nd} phase and Radargram for Y direction 1^{st} & 2^{nd} phase

4 Discussion

Based on the radargram, the images captured beneath the ground can be obtained directly using ground penetrating radar. This radargram shows a depth of approximately 2 meters. It also shows the distance of the data taking makes the user easier to identify the targeted area for marking and point reference. Therefore, based on data processing, it can be concluded that the application of GPR is a non-destructive, fast, and economical method for evaluating road structures (Zainal et al., 2023). Through different data acquisition and processing techniques, results show that there is great success when using GPR for collecting information for verifying the state and condition of the materials (Spears et al., 2023). It breaks through the limitation of the insufficient number of cavity samples for 3D radar detection on the intelligent learning model training, reduces algorithm training costs, and improves identification accuracy (Li et al., 2023).

5 Conclusion and attention

The study used ground penetrating radar to assess the subsurface utility of mild steel pipe. The data was extracted into RADAN 7 software for 3D view, allowing layer-by-layer detection and identifying underground areas. The radar's link with radio frequency locator provides accurate information for mapping subterranean utilities. The study found that ground penetrating radar is effective for obtaining comprehensive photographs of subsurface structures, providing precise measurements of depth and coordinates.

References

D. L. Moffatt andR. J. Puskar. 1976. A subsurface electromagnetic pulse radar. *Geophysics*, 41(3):506–518.

A. P. Annan. 2002. Subsurface sensing technologies and applications. 3(4):253–270.

Chlaib Hussein, Abdulnaby Wathiq, and Abd Najah. 2014. Application of the ground penetrating radar to detect weapons caches and unexploded ordnance: laboratory experiments. *IOSR Journal of Applied Geology and Geophysics*, 2:41–50.

Siow Wei Jaw and Mazlan Hashim. 2013. Locational accuracy of underground utility mapping using ground penetrating radar. *Tunnelling and Underground Space Technology*, 35:20–29.

F. Li, F. Yang, X. Qiao, W. Xing, C. Zhou, and H. Xing. 2023. 3d ground penetrating radar cavity identification algorithm for urban roads using transfer learning. *Measurement Science and Technology*, 34.

J. Pande, A. Singh, A. Gupta, K. Singh, and A. Sharma. 2022. Miniaturised ultra-wideband rectangular shaped slot antenna for ground penetrating radar applications. *Frequenz*, 77:107–114.

M. Spears, S. Hedjazi, and H. Taheri. 2023. Ground penetrating radar applications and implementations in civil construction. *Journal of Structural Integrity and Maintenance*, 8:36–49.

M. Zainal, R. Raihan, M. Yanis, and M. Umar. 2023. The mapping of road pavement structure around the seismically active regions by using ground penetrating radar. *Key Engineering Materials*, 940:145–152.

Individual Research Contribution Review, 2023, 1(1): 273–274

Phenotypic Analysis of Drought Resistance Trait in Rice Mutant Lines NMR151 AND NMR152

Affrida Abu Hassan
Agrotechnology and Biosciences Division, Malaysian Nuclear Agency
43000 Kajang, Selangor
affrida@nm.gov.my

Abstract

Drought is the most major problem facing by rice farmers in Malaysia. Development of new variety that tolerant towards this abiotic stress is crucial in rice production. Two potential drought resistance rice mutant lines namely NMR151 and NMR152 have been developed through induced mutation using gamma irradiation. The phenotypic analysis of these mutants has been carried out to elucidate the drought resistance trait. Both mutant varieties NMR151 and NMR152 showed good agro-morphophysiological and yield contribution traits under drought stress and non-stress during reproductive stages.

Keywords: Rice, drought resistance, phenotyping

1 Introduction

Drought is the most major problem in Malaysia resulting in a reduction of rice yields. For many decades, Malaysia's climate has been predictable. However, due to the effect of climate change, the El-Nino phenomenon is becoming common causing widespread drought in rice cultivating areas. Rice and other agricultural crop yields are declining due to climate change (Vaghefi et al., 2016). One of the alternative solutions to improve rice production during El-Nino is the introduction of drought tolerant rice variety. Mutation induction by gamma rays has contributed for improving of crops (Mustikarini et al., 2016). This technique has proven to be effective and used widely by the plant breeder for developing a new plant variety with desirable traits in a short time compared to conventional method. Two potential drought resistance rice mutant lines namely NMR151 and NMR152 have been developed through induced mutation using gamma irradiation. Thus, the characterization of drought resistance traits in these mutant lines is essential in understanding the mechanism of drought tolerance. Phenotypic analysis was carried out to elucidate the drought resistance trait in these advanced rice mutant lines.

2 Methods

2.1 Plant Material

Seeds of the advanced mutant lines NMR151 and NMR152 and its parent MR219 were obtained from Nuclear Malaysia seed collection.

2.2 Phenotyping

Phenotyping experiment were conducted at the glasshouse in Malaysian Nuclear Agency and rice field in Sekinchan, Selangor as follows:

- **Glasshouse Evaluation**

The pre-germinated seeds were sown in trays containing wet soil. Seedlings were transplanted into pots 24 days after germination with 3 replications. For drought stress treatment, water was drained at 60 days after transplanting (DAT) and was re-irrigated periodically when soil water tension fell below -50kPa. As for the control (non-stress) (NS), seedlings were continued to grow with standing water until maturity.

- **Field Evaluation**

The experiment was conducted for two planting seasons and a protocol by Site et al. (Site et al., 2012) was adapted. Alpha Lattice Experimental Design (Patterson and Williams, 1976) was applied with two replications. The control (NS) trial was managed like an irrigated lowland condition where no water stress was applied. Whilst, for the drought-stress trial, an artificial drought stress was imposed during the reproductive stage. Standard agronomic practices were employed for plant maintenance. Observations was recorded at different stages of crop growth until maturity from both the control (non-stress) and drought stress treatment.

2.3 Data collection

Phenotypic data were recorded at reproduction stage. Data includes days to 50% flowering (DTF), plant height (PH), spikelet fertility (SF), grain yield (GY), number of tillers, flag leaf area, panicle length and days to maturity. Visual score of leaf rolling (LR) and leaf drying (LD) were recorded according to IRRI's Standard Evaluation System for rice (IRRI, 1996).

3 Results and Discussions

The effect of drought was observed in drought stress plants in the glasshouse (Figure 1). Leaf rolling is one of drought avoidance mechanism to divert the effect of water deficit during drought in rice, the result marked a point for NMR152 as a drought tolerant variety. NMR152 has low score for both LR and LD (Table 1). Both of LR and LD are closely related to plant water status (RWC).

Additionally, both drought resistant mutant lines, NMR151 and NMR152 showed good yield contribution traits under

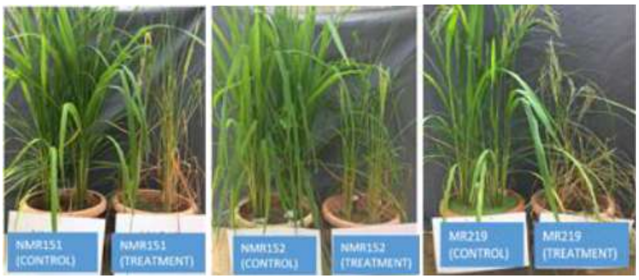

Figure 1: The effect of drought stress on NMR151, NMR152 and MR219.

Table 1: The score for leaf rolling (LR) and leaf drying (LD) of NMR151, NMR152 and MR219

Variety	LR Score	LD Score
NMR151	5	1
NMR152	3	1
MR219	7	7

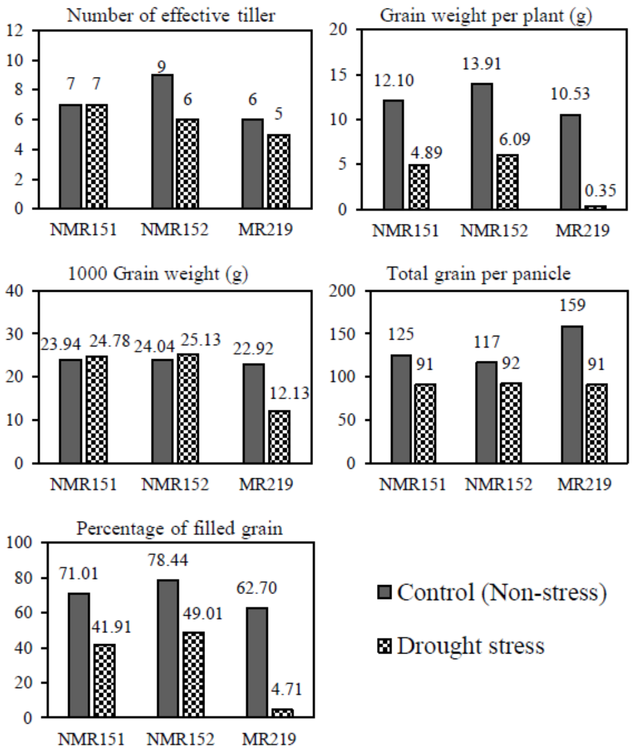

Figure 2: Yield contribution traits for NMR152, NMR151 and MR219 under control (non-stress) and drought stress.

drought condition compare to its parent (MR219). The result for yield contribution traits is shown in Figure 2.

Field planting of NMR151 and NMR152, with its parent were done entirely for two seasons (February-June 2021 and September-December 2021). From the result, both mutant lines, NMR151 and NMR152 showed good agro-morphophysiological traits under drought stress and non-stress (NS) during reproductive stages (Figure 3).

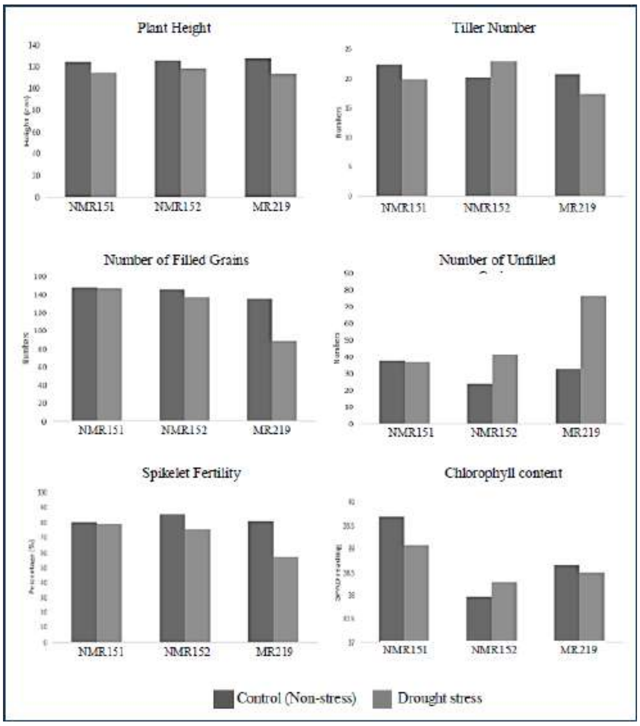

Figure 3: Yield contribution traits for NMR152, NMR151 and MR219 under control (non-stress) and drought stress.

4 Conclusion

Mutant varieties NMR151 and NMR152 showed good agro-morphophysiological and yield contribution traits under drought stress (RS) and non-stress (NS) during reproductive stages.

References

IRRI. 1996. IRRI's standard evaluation system for rice.

Eries D. Mustikarini, Noer Rahmi Ardiarini, Nur Basuki, and Kuswanto Kuswanto. 2016. The improvement of early maturity red rice mutant trait for drought tolerance. *Int J Plant Biol*, (7):6345–6345.

H. D. Patterson and E. R. Williams. 1976. A new class of resolvable incomplete block designs. *Biometrika*, 63(83-90).

A.R. Site, T.H. Borromeo, N.C. Altoveros, and A. Kumar. 2012. Growth performance of selected malaysian rice germplasm under drought stress environment. *J. Trop. Agric. And Fd. Sc.*, 40(2):169–179.

Negin Vaghefi, Mad Nasir Shamsudin, Alias Radam, and Khalid Abdul Rahim. 2016. Impact of climate change on food security in malaysia: economic and policy adjustments for rice industry. *J. Integr. Environ. Sci.*, 13(1):19–35.

Individual Research Contribution Review, 2023, 1(1): 275–276

Greenhouse Gases Emission and Mitigation Under Climate Smart Agricultural Practices in Rice Ecosystem Using Direct Analytical and Stable Isotope Techniques

Ahmad Nazrul Abd Wahid
Agrotechnology and Biosciences Division, Malaysian Nuclear Agency
43000 Kajang, Selangor
a_nazrul@nm.gov.my

Abstract

This project was initiated in 2023 with the aim to evaluate greenhouse gas (GHGs) emissions and finding mitigation measures for GHGs emission reduction through the climate-smart agricultural practices in rice crop ecosystem. In this project, several climate-smart agricultural practices will be implemented such as alternate wetting and drying irrigation (AWD), biochar application and optimal nitrogen fertilizer application will be evaluated as an effort to reduce the emission of methane (CH_4), carbon dioxide (CO_2) and nitrous oxide (N_2O). This project also aims to produce several related SOPs and produce for a new and efficient method for GHGs sampling and measuring in the field by using direct analytical technique.

Keywords: Greenhouse Gases, Alternate Wetting and Drying, Biochar, Nitrogen Optimization

1 Introduction

In the agricultural sector, rice covers 11% of the world's arable land and is responsible for 10.1% of total agricultural emissions and approximately 1.3%–1.8% of global anthropogenic GHG emissions (Meijide et al., 2017). Rice cultivation has contributed to global climate change through the release of CO_2, CH_4 and N_2O gases into the atmosphere. Rice fields act as a source of CH_4 and N_2O emissions depending on soil organic matter status, land management and cropping intensity, irrigation and drainage water, fertilizer management, soil microbial population and activity and soil properties (Wang et al., 2017). In Malaysia, GHGs emission has been increasing year by year for the over past 10 years. this may occur due to excessive use of fertilizers, less efficient water and soil management.

Malaysia aims to reduce the intensity of greenhouse gas (GHG) emissions across the economy by 40% based on Gross Domestic Product (GDP) in 2030. The former Prime Minister, Dato' Seri Ismail Sabri Yaakob said that the reduction in intensity was made unconditionally and was 10% higher than the previous target. The current Prime Minister, Dato' Seri Anwar Ibrahim also stated that Malaysia needs to reduce CH_4 production by 40% by 2023. Climate change has had a bad impact on the country as well as affecting the national economy varieties which can perform well in local condition especially in terms of biomass yield are highly needed.

As the research agency, Nuclear Malaysia will take the initiative in the implementation of the National Climate Change, National Agrofood 2021-2030 (NAP 2.0) and Sustainable Development Goals (SDG) policy that have been formed by the Government of Malaysia. A study related to climate smart agricultural practices in the scope of soil, water and nutrition management in the rice plant ecosystem will be conducted. The measurement of greenhouse gases in the rice plant ecosystem will be made through a more recent and sophisticated method, different from the manual method that has been carried out as before. The use of direct measurement equipment, "Laser Spectrometer" and "LSE N2O-4405 Analyzer" will be used. The role of nuclear technology is to use stable isotopes technique at enriched and natural abundance levels precisely quantifies fertilizer use efficiency, biological nitrogen fixation, and identifies the sources of greenhouse gases (GHGs) to exert more control on their mitigation.

2 Methods

2.1 Field preparation

The locations for study will be conducted in Nuclear Malaysia Rice Research and Breeding Site. This site was built in 2021 in Malaysian Nuclear Agency with the purpose of breeder seed and rice research.

2.2 Greenhouse Gas Sampling and Measurement

Stainless steel closed chamber will use to trap GHGs in rice field. The chamber septum will connect directly via 3-way stopcock to the Laser Spectrometer and LSE Analyzer using teflon tube. Laser Spectrometer and LSE N2O-4405 Analyzer will setup in site provided for direct measurement from the chamber directly to the instrument. A distributer system consisting of a sampling control panel and a teflon tube will be built to facilitate the simultaneous reading of CO_2, CH_4 and N_2O on the instruments.

2.3 Climate Smart Agricultural Practices

- **Alternate Wetting and Drying (AWD)**

A water tube/pipe made of PVC is usually used to monitor the water depth. After the irrigation in the crop field, the water depth gradually decreases because of evapotranspiration, seepage, and percolation. When the water level drops 15 cm below the soil surface, irrigation should be applied in the field to re-flood to a depth of 5 cm. During the flowering stage of the rice, the field should be kept flooded. After flowering, during the mid-season and late season (grain filling and ripening stages), the water level is allowed to drop below the soil surface to 15 cm before re-irrigation.

- **Biochar Application**

The crushed charcoal wood will use as a soil amendment in this study. Biochar will apply with top dressing method onto soil in rice plot 1 week before watering and planting.

- **Optimum N-fertilizer Application**

The optimum nitrogen fertilizer application will be obtained through the use of isotope tracer techniques. Urea 5% atom access will be used to evaluate the efficiency of N use by rice plants in the study area. Use of microplots to differentiate normal urea and urea isotope fertilization areas. The NUE data will be entered into Mitscherlic crop response model to obtain the most optimal N fertilizer application.

3 Results and Discussions

The experimental results for effect of CF and AWD irrigation on CH_4 and CO_2 emission are summarized in Figure 1 and 2.

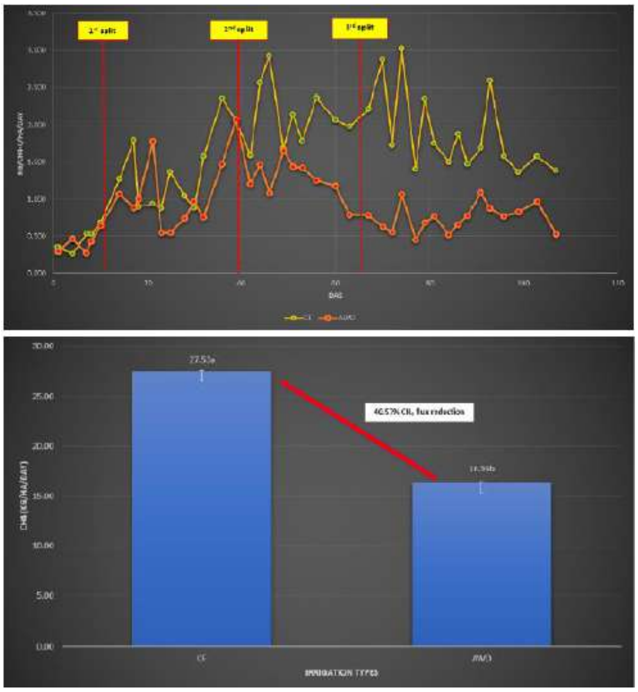

Figure 1: Effect of CF and AWD Irrigation Methods on CH_4 Emission and Cumulative in Planting Season

CH_4 and CO_2 fluxes from all treatments were observed in 2 days after transplanting (DAT). Early observation shown CH_4 and CO_2 fluxes on the 2 – 10 DAT at CF and AWD were almost similar. After fertilizer application, both CH_4 and CO_2 fluxes was increased. The figure also shown, AWD treatment has caused CH_4 emissions was reduced until the end of the season. But for CO_2 emission shown, no significant fluctuation rate has occurred to both treatments. This can be explained further through the cumulative data of CH_4 and

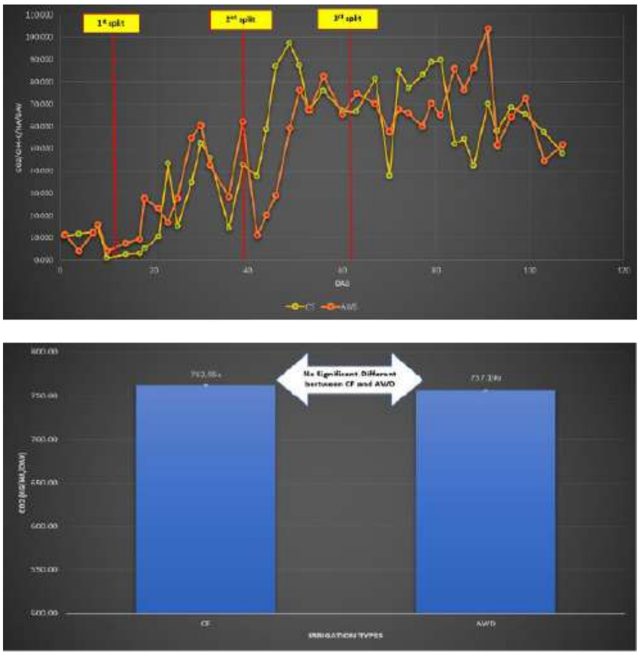

Figure 2: Effect of CF and AWD Irrigation Methods on CO_2 Emission and Cumulative in Planting Season

$CO_2$where the application of AWD irrigation on rice plants has reduced by 45.7% of the CH_4 emission but the opposite happened to the CO_2 emission where, the cumulative CO_2 for both treatments has shown no significant difference.

References

A. Meijide, C. Gruening, I. Goded, G. Seufert, and A. Cescatti. 2017. Water management reduces greenhouse gas emissions in a Mediterranean rice paddy field. *Agriculture, Ecosystems Environment*, 238:168–178.

Chun Wang, Derrick Y. F. Lai, Jordi Sardans, Weiqi Wang, Congsheng Zeng, and Josep Peñuelas. 2017. Factors related with CH_4 and N_2o emissions from a paddy field: Clues for management implications.

Individual Research Contribution Review, 2023, 1(1): 277–278

Antimicrobial activity of γ-Synthesised Silver Nanoparticles Against *Dickeya zeae*, the Causal Pathogen of Bacterial Heart Rot in Pineapple

Anis Nadia Mohd Faisol Mahadeven
Agrotechnology and Biosciences Division, Malaysian Nuclear Agency
43000 Kajang, Selangor
anisnadia@nm.gov.my

Abstract

Pineapple is regarded as one of the premium crops in Malaysia. However, pineapples are susceptible to plant diseases such as *Dickeya zeae* that causes bacterial heart rot resulting in reduced agricultural productivity and economic losses. The employment of nanoparticles in agriculture field with some beneficial effects to the crops will be promising step toward nano-revolution in agriculture field. This study aims to explore the potential use of silver nanoparticles against *D. zeae*. Bacterial pathogen *D. zeae* is subjected to silver nanoparticles to assess the susceptibility of *D. zeae* against silver nanoparticles using agar diffusion method – well variant. Different concentrations of silver nanoparticles are compared to Gentamicin disk as control.

Keywords: Bacterial heart rot, pineapple, *Dickeya zeae*

1 Introduction

In pineapple, including the MD2 varieties, one of the common diseases is the bacterial heart rot caused by the bacteria *Dickeya zeae*. This disease was first reported in Malaysia and has since been described in Costa Rica, Brazil, and the Philippines (Kaneshiro et al., 2008). The pathogen into the fruits is via the open flowers and that the main source of inoculum is from freshly collapsed fruits and heart rot tissues ((Sahilah et al., 2008). Once a pineapple plant is infected with this pathogen, they are infected for life. One of the control measures are through chemical ways using pesticides and fungicides. However, excessive use of pesticides and fungicides also pose threat to the environment thus there is a need to find an alternative measures to minimize the plant diseases (Krishnakumar and Bai, 2015).

Although the amount of antibiotics used against plant pathogens is little, antibiotic resistant plant pathogens have still emerged which makes it more difficult to manage. Therefore in contrast to conventional antibiotics, application of nanoparticles is most important strategy to manage plant diseases (Abbas et al., 2015). Silver nanoparticles have a high surface area and fraction of surface atoms; as a result have high antimicrobial effect as compared to the bulk silver. It can be synthesized from physical, chemical and biological methods therefore; there is a growing interest to utilize antimicrobial property of silver nanoparticles for plant disease management (Duhan et al., 2017). Silver nanoparticles also exhibit multiple mode of action against plant pathogens; therefore they can be used for controlling various plant diseases in relatively safe way than the synthetic chemicals.

2 Methods

2.1 Synthesis of silver nanoparticles

For the synthesis of Ag/Kln NPs, six different doses of irradiation is used. The $AgNO_3$ solution was prepared at five concentrations (10, 20, 30, 40 and 50 ppm) the samples are irradiated at 5, 10, 20, 30, 40 and 50 kGy. The suspensions were centrifuged, filtered and washed twice using distilled water to remove the silver ion residue, and dried in an oven. All the experiments were conducted at ambient temperature similar to the above. Gamma irradiations were carried out in Co-60 gamma chamber having a radiation dose rate of 4 kGy hr-1 determined using Fricke dosimetry (Moosa et al., 2018).

2.2 Preparation of microbial suspension

Prepare 5 ml overnight culture of *D. zeae* in nutrient broth medium from nutrient agar plate using aseptic technique and incubate at 28°C for 24 hours. After incubation for 24 hours, prepare 1 ml of 1:50 dilution of the culture using nutrient broth and determine the cell number spectrophotometrically at OD_{600} using sterile broth as blank. A serial dilution up to 10^{-7} is performed and plated on nutrient agar plates. The agar plates are incubated at 28°C for 24 hours.

After 24 hours, the number of colonies are counted and the concentration (cfu/ml) of *D. zeae* is determined. A correlation between OD_{600} readings and the cfu/ml are determined and is used throughout the experiment. Suspension is diluted accordingly to prepare an inoculum containing 25 ml of $1x10^6$ cells.

2.3 Antimicrobial susceptibility testing

Nutrient agar plates are dried and labelled accordingly. Holes are punched on the agar with a 6-mm cork borer using aseptic technique then remove agar plugs using a scalpel to make wells. Next 100 μl of *D. zeae* inoculum is pipetted onto the agar and spread using an L-shape cell spreader aseptically. Sample solutions are mixed thoroughly then 50 μl of Ag-NP solutions of different concentrations and irradiation doses are dropped into respective wells with Gentamicin 10 μg and solution containing 10 ppm Ag-NP with Kaolin (Kln) used as control. The testing is done in triplicates. Solutions in each well is left to dry before incubating the plates at 28°C for 24 hours. After overnight incubation, the diameter of the inhibition zone in measured and the data is recorded.

3 Results and Discussions

The susceptibility of microorganisms to silver nanoparticles was evaluated by measuring the zone of inhibition and the results are as shown in Table 1.

Table 1: Diameter of inhibition zone of *D. zeae* with different concentration of Ag-NP and different irradiation doses.

Concentration (ppm)	**Irradiation Dose (kGy)**					
	5	10	20	30	40	50
10	-	-	-	-	-	-
20	-	-	-	-	-	-
30	-	-	-	-	-	-
40	-	-	-	-	-	-
50	-	8.2	8.8	8	7.8	7.3
Control (Gm, 10 μg)	9.7					

The diameter of the inhibition zone is proportional to the antimicrobial activity. Based on the results no inhibition was observed for all concentrations at 5 kGy irradiation dose, while the other irradiation doses showed antimicrobial activity at 50 ppm. The highest inhibition was observed at 20 kGy.

There are four established antimicrobial mechanism of Ag-NPs namely through (1) adhesion of Ag-NPs onto the surface of cell wall and membrane, (2) penetration of Ag-NPs inside the cell subsequently damaging the intracellular structures and biomolecules (3) generation of reactive oxygen species (ROS) and free radicals which induces cellular toxicity and oxidative stress, and (4) modulation of signal transduction pathways. Ag-NPs also orchestrate inflammatory response, which further aid in inhibition of microorganisms (Dakal et al., 2016). The bacterium used in this study, *D. zeae* is a Gram-negative bacterium, hence making it more susceptible to the antibacterial action of Ag-NPs due to its thin cell wall (Linlin et al., 2017). Singh and Mijakovic (Singh and Mijakovic, 2022) found that positively charged Ag-NPs adheres to the negatively charged surface of the cell wall and membrane leading to the shrinkage of the cytoplasm and membrane detachment. This will then lead to rupture of the cell wall. They have also reported that the porins on Gram-negative bacteria are responsible for Ag-NPs uptake. After penetration, Ag-NPs may interact with cellular components such as proteins, lipids, and DNA, further confirming the damaging effects.

4 Conclusion

Further studies to determine the antimicrobial activity in vivo, mechanism of action is, dose optimization and toxicity study are needed explore the application and use of these nanoparticles to formulate novel antimicrobial materials in combating plant diseases.

References

A. Abbas, S. S. Naz, and S. Alam. 2015. Antimicrobial activity of silver nanoparticles (agnps) against erwinia carotovora pv. carotovora and alternaria solani. *International Journal of Biosciences (IJB)*, 6(10):9–14, https://doi.org/10.12692/ijb/6.10.9–14.

T.C. Dakal, Kumar A., Majumdar R.S., and Yadav V. 2016. Mechanistic basis of antimicrobial actions of silver nanoparticles. *Front. Microbiol.*, 7:1831, doi: 10.3389/fmicb.2016.01831.

J. S. Duhan, R. Kumar, N. Kumar, P. Kaur, K. Nehra, and S. Duhan. 2017. Nanotechnology: The new perspective in precision agriculture. *Biotechnology Reports, 15(December 2016)*, pages 11–23, https://doi.org/10.1016/j.btre.2017.03.002.

W. S. Kaneshiro, M. Burger, B. G. Vine, A. S. De Silva, and A. M. Alvarez. 2008. Characterization of erwinia chrysanthemi from a bacterial heart rot of pineapple outbreak in hawaii. *Plant Disease*, 92(10):1444–1450, https://doi.org/10.1094/PDIS–92–10–1444.

S. Krishnakumar and V. D. M. Bai. 2015. Extracellular biosynthesis of silver nanoparticles using terrestrial streptomyces sp-sbu3 and its antimicrobial efficiency against plant pathogens. *International Journal of TechnoChem Research*, 01(02):112–118.

W. Linlin, H. Chen, and S. Longquan. 2017. The antimicrobial activity of nanoparticles: present situation and prospects for the future. *International Journal of Nanomedicine*, 12:1227–1249, https://doi.org/10.2147/IJN.S121956.

S. Moosa, A. N. Mohd Faisol Mahadeven, and K. Shameli. 2018. A comparative study of chemical and gamma-ray irradiation method for synthesis of silver nanoparticles in kaolinite.

A. M. Sahilah, L. Rozeita, U. Kalsum, and R. Son. 2008. Typing of erwinia chrysanthemi isolated from josapine pineapple in malaysia using antimicrobial susceptibility, plasmid profiles, eric-pcr and rflp analysis. *International Food Research Journal*, 15.

P Singh and I Mijakovic. 2022. Strong antimicrobial activity of silver nanoparticles obtained by the green synthesis in viridibacillus sp. extracts. *Front. Microbiol.*, 13(820048. doi: 10.3389/fmicb.2022.82004).

Individual Research Contribution Review, 2023, 1(1): 279–280

Evaluation of Microbial Diversity and Stable Isotope Content in Nuklear Malaysia Mutant Paddy NMR152 Cultivation Soil Applied with Biofertilizer M99

Asma Aris
Agrotechnology and Biosciences Division, Malaysian Nuclear Agency
43000 Kajang, Selangor
asmaaris@nm.gov.my

Abstract

Rice (*Oryzae sativa* L.) is one of the most staple food in the world that feed nearly half the world population. However, Malaysia paddy cultivation has been suffering from various challenges which include poor soil fertility as well as nutrient management, poor soil heterogeneity and increase soil degradation. Soil is a very dynamic area which regulated by complex of interactions between plants and microorganisms. Microbe functionally acts as stores and sources of active soil nutrients owing to their wide biochemical activities. In this study, Biofertilizer M99 was applied into mutant Nuklear Malaysia Rice (NMR152) cultivation soil to see the interactions of complex biological processes in the rhizosphere. Microbial diversity evaluated by using 16S rRNA amplicon sequencing demonstrated potential plant growth promoting rhizobacteria (PGPR) responsible for the plant growth. Quantifying stable isotopes content by using Isotope Ratio Mass Spectrometry (IRMS) in the cultivated soil portrays its essential nutrient consumption. Rhizobia activity in the soil depends on it adaptation to nutrient available in order to enhance plant growth.

Keywords: rice, biofertilizer, NMR152, PGPR

1 Introduction

Paddy cultivation begins in the early 60s with smallscale farming. Increase in world population triggers the rice global demand. Since then, Malaysia rice production unable to provide adequate supply to the consumers. Moreover, the pandemic Covid-19 strikes up the insufficiency of global food supply. This phenomenon leads a concern to escalate our rice production. Incessant progress of the paddy cultivation has led to various alternatives as a way to increase crop yield. This activity opens up a way to an intensive use of chemical feretilizer. The use of chemical fertilizers above threshold level pollutes the water bodies, reduce soil fertility and increase soil degradation. These accelerates the acidification of soil and reduces the composition of soil microorganisms which act as key indicator of soil bioactivity. The microorganism plays complex biological processes and the rhizosphere is where it inhabited and benefited the host plant particularly in terms of nutrient availability, encountering stress resistance, and defense against soil-borne pathogens (Bai et al., 2015). Microbe communities play a crucial role in most biogeochemical processes in terrestrial ecosystems, including, organic matter decomposition, nitrogen fixation and mineralization, and plant productivity (Zhang et al., 2022). Rice mutant cultivar NMR152 is a product of mutation breeding by Nuklear Malaysia through gamma radiation at 30 Gy has a high yield potential. Application of Biofertilizer M99 act as growth enhancer to fit the low input cultivation mission. Hence, in this study we evaluate the potential microbes and essential nutrients inhabitant in the rhizosphere for a better rice production system in the future.

2 Material and Methods

Pseudomonas putida used as test strain in the biofertilizer was provided by EGI Agrotek Sdn Bhd. The experiment was carried out using randomized complete block design and protective lines. The experiment started on Jun 2023 in Kg. Sanglang, Kodiang, Kedah. Two treatments, control and biofertilizer application trials on two varieties; NMR152 and NMR191. The control group treated with farmer's practice fertilizer without biofertilizer and the other group treated with 25% of farmer's practice fertilizer with biofertilizer. The area of cultivation plot is 100 m^2 (length x width: 10 m x 10 m). Seeds sown for 20 days, prior to transplanting into cultivation plot. Three seedlings per hill were transplanted into soil with distance between hills of (length x width) 25 cm x 25 cm. 8 x 8 (rows x columns) of hill were arranged in a plot. Three replicates performed and labelled as R1, R2, R3 for each treatment. Experiment was conducted in two seasons; humid or main season (August until February) and dry or off-season (March-July). Soil samples randomly obtained from 0 – 2 cm depth. Total DNA was extracted from 500 mg soil sample. Targeted DNA were amplified and the sequence analysis involved OTU classification using UCLUST (V5.1.221) and principal component analysis (PCA) bu R software (V3.2.0). Prior to stable isotopes analysis, soil samples were ball mill grinded and weighted into tin capsule before introduce into the IRMS analyzer.

3 Results and Discussions

Agronomics data which includes yield (kg/ha), culm height (cm), number of panicle/plants, panicle length (cm), leaf area (cm^2), chlorophyll content and total tiller have been recorded and analyzed showing NMR152 and NMR191 significantly higher compared to controls (Figure 1 and Figure 2). By using a 97% sequence similarity cutoff, total operational taxonomic unit (OTUs) of controls expected to show lower counts than the treated soils. Comparison of the community composition at the species level showing relative abundance is expected to be significant.

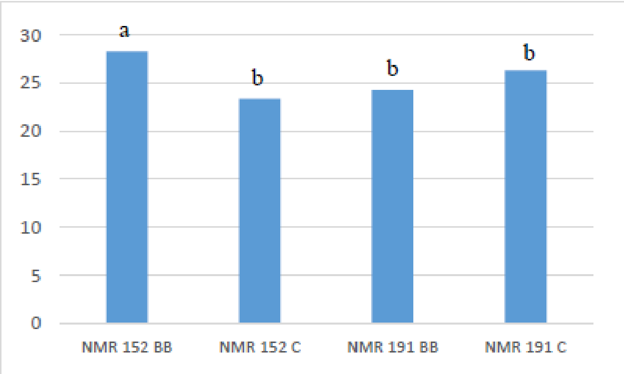

Figure 1: Weight of 1000 grains

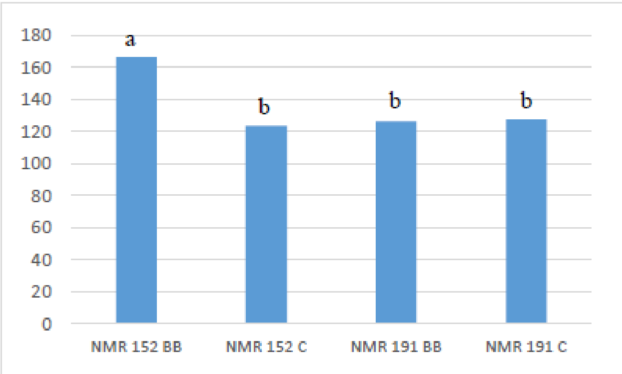

Figure 2: Filled grains

4 Conclusion

The application of Biofertilizer M99 increased mutant varieties NMR152 and NMR191 agronomic yields. The yield should hypothetically increase with microbial diversity in the soil. Soil microbial and nutrient heterogeneity significantly enhance plant growth compared to homogenous soil.

References

Y. Bai, D.B. Muller, G. Srivinas, R. Garrido-Oter, E. Potthoff, M. Rott, P.C. Dombrowski, N.and Munch, S. Spaepen, M. Remus-Emsermann, B. Huttel, A.C. McHArdy, J.A. Vorholt, and P. Schulze-Lefert. 2015. Funtional overlap of the Arabidopsis leaf and root microbiota. *Nature*, 528:364–369.

J. Wang, L. Liu, X. Gao, J. Hao, and M. Wang. 2021. Elucidating the effect of biofertilizers on bacterial diversity in maize rhizosphere soil. *Plos One*, 16(4: e0249834).

R. Zhang, Li, L. Yulin, X. Zhao, Degen A.A., X. Lian, J. nd Liu, Y. Li, and L. Duan. 2022. Fertilizers have a greater impact on the soil bacterial community than on the fungal community in a sandy farmland ecosystem. *Inner Mongolia. Ecology Indicators*, 140:108972.

Individual Research Contribution Review, 2023, 1(1): 281–282

Development of Smart Mushroom House (SMH)

Azhar Mohamad
Agrotechnology and Biosciences Division, Malaysian Nuclear Agency
43000 Kajang, Selangor
azhar_m@nm.gov.my

Abstract

Mushrooms becoming a valuable commodity in Malaysia. Malaysian Nuclear Agency has developed a smart mushroom house (SMH) in 2022. The purpose of this SMH is to become a model facility towards commercialization of fresh fruiting body mushroom. The use of sensors and programmed systems control temperature, humidity, and ventilation through application system in managing the SMH. The system was tested on Pleurotus pulmonarius. Humidity required for mycelium development and fruiting is 70% and 80% respectively. Whereas, the temperature should be controlled bellow 30°C. At both stages, good aeration is important in balancing between O_2 and CO_2 to enable vigorously production of fruiting bodies and mycelium. This, this study allows the development of smart mushroom house towards commercial production.

Keywords: Edible mushroom, sensors, humidity, temperature, IOT

1 Introduction

Mushroom is a significant superfood in Malaysia as it has been classified as one of the high-value commodities due to the increasing demands and benefits. However, global warming with unstable weather such as very hot temperature and uncertain wet season had become a threat to the cultivation of mushrooms in Malaysia. The unpredictable weather would directly affect the mushrooms quality and quantity, besides of affecting the mushrooms byproducts (Muhammad and Aizan, 2022). Thus, it is crucial to provide optimum environment to enhance the mushroom production. Cultivation methods began to undergo a transformation process towards the use of controlled cultivation systems.

The development of SMH is the best solution to overcome these problems. In the system, sensors are used to control humidity, temperature and ventilation system. SMH is a structured mushroom house that was equipped with appropriate parameters to promote the best and/or optimum condition for high yield fruiting body (controlled environment) in mushroom production. All undesired environmental factors can be eliminated in SMH. Thus, the SMH is important and ways to get consistency production of mushroom fruiting body in sustaining commercial demand for mushroom industry.

Figure 1: Local edible mushroom in Malaysia

2 Material and Methods

Development of high technology equipment such as IoT (Internet of Things) is important to improve management, production and operational of many plants' cultivation. Thus, the application of this system was implemented for mushroom cultivation. The development process involved:

i. Facility Design
ii. IOT System Design
iii. System Controlled Environment Optimization
iv. Mushroom Cultivation Optimization

The SMH was designed for three mushroom species known as *Pleurotus florida*, *Plourotus pulmonarius* and *Volvarela volvacea*. These species have certain specificities for temperature and humidity for their growth.

Figure 2: Smart Mushroom House (SMH)

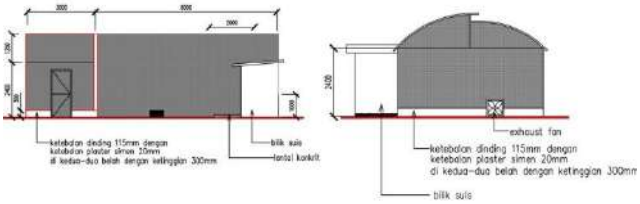

Figure 3: Design for SMH with good ventilation system and misting system supported by sensors and IOT applications.

(A) (B)

Figure 4: Mushroom blocks (A) in SMH during optimization mapping controlled by IOT system (B). At one time, 8000 blocks can be allocated in the SMH

3 Results and Discussions

It was found that optimum growth and development of mycelium by *In vivo* growth required temperatures between 25-30°C for *Pleurotus* sp.

(A) (B)

Figure 5: Fresh (A) and Dried (B) fruiting body due to low humidity, and high temperature in the SMH.

In Figure 5, the difference of mushroom fruiting body can be immediately observed after 3 days pinning. It was revealed that integration of ventilation and water misting were important in controlling environment of SMH accordingly. The process was detected by sensors followed by the IOT system activation to trigger the fan and misting accordingly (Ten et al., 2021; Mohamad Suhaimi et al., 2023)

According to Islam et al. (Islam et al., 2017), even under controlled humidity, contaminations can occur up to 30%. In controlling the problem, good ventilation at certain air flow is significant to balance the moisture in the SMH.

Data collection can be easily obtained by datalogger connected to IOT. Moreover, it is also convenient as less workers are needed to operate the mushroom smart house. Therefore, the construction of mushroom smart house is the best idea

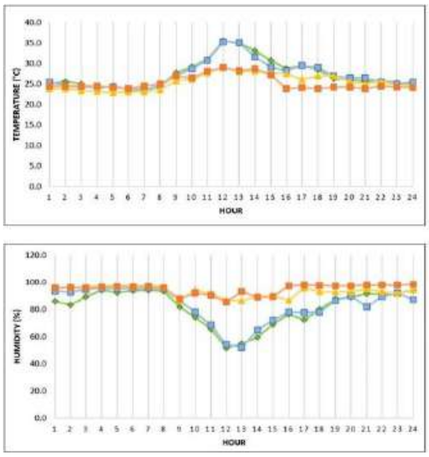

(A)

(B)

Figure 6: The graph shows on how temperature (A) and humidity (B) were controlled in SMH by the IOT sytem. The red and yellow lines showed the condusive environment during system activation.

to provide an optimum environment in producing high yield mushroom fruiting body.

4 Conclusion

The IoT system was successfully installed, commissioning and managed to control environment in SMH accordingly. Further study is still required to improve yield and increase harvesting cycles for high yielding mushroom. High technology applications in the agricultural sector would help to improve the food production (quantity) and quality. The development of high technology equipment such as IoT (Internet of Things) would greatly improves the management and operation of the mushroom cultivation.

References

M. T. Islam, Z. Zakaria, Mohd Ishak M. A. Hamidin, N., and Fern C. S. 2017. The management of humidifying treatment for low contamination risks during indoor cultivation of grey oyster mushroom (Pleurotus pulmonarius). *MATEC Web of Conferences*, 97:01080.

Y. Mohamad Suhaimi, M. Azhar, S. Mohamad Safuan, A.A. Mohd Dzul, S. Nordin, A.M. Mohamad Fazreen, A. N. Mohd Hafiz, Y. Juhari, M. Sa, and P.S. Tan. 2023. Designing and instalation of IOT system form smart mushroom house. *NITC Proceeding. Nuclear Malaysia.*

H. M. H. Muhammad and U. Aizan. 2022. Mushroom house monitoring system using internet of things (IoT). *Evolution in Electrical and Electronic Engineering*, 3(1):545–553.

S. T. Ten, K. Ganisan, A. K. Khairul, M.T. Muhd Akhtar, H. Mohamad Hafiz, and K. Syaliyana. 2021. Automated controlled environment mushroom house. *Adv Agri Food Res J*, 2(2):a0000230, https://doi.org/ 10.36877/ aafrj.a0000230.

Mutation Breeding for Local Edible Mushroom

Azhar Mohamad
Agrotechnology and Biosciences Division, Malaysian Nuclear Agency
43000 Kajang, Selangor
azhar_m@nm.gov.my

Abstract

Mutation breeding in edible mushroom is an alternative way in generating new mushroom strains with desirable traits. Both monokaryon and dikaryon mycelium were exposed to selected dose of acute gamma radiation revealed high growth performance rate in the edible mushroom strains. Mycelium tolerance to gamma rays depends on mushroom species, mycelium types and subculture stages. Samples for mutation induction were varied from spores, mycelium, grain seedling and/or substrate seedling. LD_{50} was used as referral dose in acute gamma radiation to find effective doses of the mutation induction technique.

Keywords: Edible mushroom, gamma radiation, mutation breeding

1 Introduction

Fungi are eukaryotes with complex cellular organization. Cells contain a membrane-bound nucleus where DNA is wrapped around histone proteins. Mushroom is a fungi group which bear fruiting body. There are various techniques in producing new mushroom strains such as conventional mating between monokaryon hyphal, protoplast fusion and transformation. However, the biggest challenge in these processes is related to compatibilities type amongst the cells.

Mutation breeding is an alternative way in generating new strains of mushroom. Gamma rays is the most common process in mutation breeding that can make alterations at mushroom genome. The fact is conventional mushroom cultivation and propagation is difficult in sustaining superior traits for selection and collections of the mushroom strains. Induced mutations by ionizing radiations such as gamma rays resulted a wide spectrum of alterations, metabolite changes and is becoming important tool in creating genetic variants and diversity amongst species. (Jan et al., 2012; Tayebeh et al., 2021).

2 Material and Methods

Spores were isolated and exposed to specific acute gamma rays from selected matured mushroom fruiting body. The spores were diluted in sterile distilled water in selecting vigorous, clean, and healthy single spore prior to irradiation.

The spores were geminated on freshly prepared potato dextrose agar (PDA) media, prepared according to manufacturing manual. Dose respond for both monokaryon and dikaryon were found significantly different in responding to different dose strength. Based on LD_{50}, specific doses were selected for the mutation induction. Selection and screening were made based on the mycelium growth performance.

Figure 1: Local edible mushroom in Malaysia

Mutated mushroom strains were detected by using molecular Inter single sequence repeat (ISSR) primer marker technique.

Figure 2: Type of sample appropriate for mutation induction technique

3 Results and Discussions

Mutant lines of dikaryon mycelium (MLDM) produced high compatible mating for the edible mushroom. High clamps formation was found after exposed to acute gamma radiation at certain dose.

LD_{50} is an important referral in finding an effective dose for any type of samples for acute gamma radiation. Higher doses

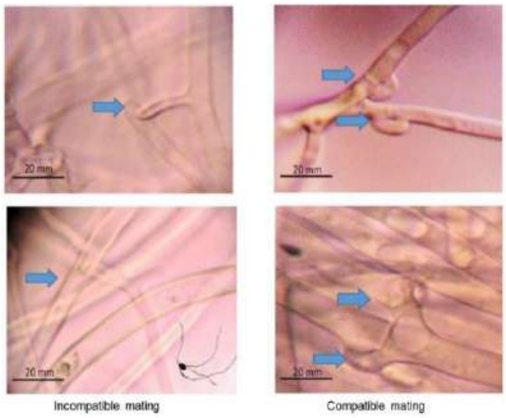

Figure 3: High clamps formation discovered for compatible mating of irradiated (Clamps refer to blue arrows) under 40x magnification

Table 1: Dose response for mushroom species are significantly different. LD_{50} can be used as referal in mushroom mutation induction. (Azhar et al., 2018; Ibrahim et al., 2017)

Species	Local name	LD_{50}(Gy)
Pleurotus sp.	Grey Oyster	1050
Volvariella sp.	Jerami Padi	1860
Auricularia sp.	Black Jelly	1530
Lentinular sp.	Shiitake	1360

can change phenotypic characters but also altering genetic background of the strains and will affecting genotypic characters. Radiation enghances the production of clamps which lead to high growth performance and activation of multicellular cells. The irradiation process involves two stages, laboratory stage and the farm stage. At the laboratory stage, identification of strains from superior species, irradiation, screening, and selection were done intensively by *in vitro* propagation. While *in vivo* cultivation was done in multiple locations at mushroom farm.

In vitro propagation was important in propagating the mycelium towards doubling quantity of required materials and seedling preparation proposes. However, continuously subculture can damage the viability and vigorously of the mycelium. This behaviour was varied amongst mushroom species. Commonly, after 7^{th} subculture, the symptom can be observed significantly. Radiation treatment was carried out at 3^{rd} subculture as at this stage the mycelium found stable, healthy and active.

Overall process of *in vitro* mushroom propagation phases can be interpreted into subculture analogy:

Persistent: Phase after initiation where small portion of mycelium was isolated from fruiting body. Cells are slow growth as intact mycelium tissue is adjusting to new media

Adaptation: Improvise growth as mycelium is adapting to new media. Mycelium was formed from the initial tissue

Stability: Mycelium is growing vigorously and consistent in growth as mycelium is comfortable to grow onto new media. This stage differed among species.

Survival: Inconsistent growth is the stage whereby the mycelium is trying to keep the cells survive under continuously grown on the same media formulation. At this stage the growth performance of the mycelium is not consistent.

Radiation shock is important for mycelium improvement and selection of variants. More variants can be observed with small changes at genetic levels but yet stable to inherit the traits. The mushroom is unique, besides radiation environment stress might also affects the growth performance and changes from vegetative to reproductive stage. However, the characteristics of the mushroom fruiting body that was altered after the radiation process remains.

4 Conclusion

The induction of mutations in mushrooms by acute gamma radiation occurs randomly which can make changes at the genotypic level but remains the phenotypic characterization at the fruiting body stage. These changes inherit and continuously stable for next generation. The process supports breeders, growers, scientists, and people interested in the mushroom industry as more sources of quality with desirable traits from new breed mushroom strains become available.

References

M. Azhar, D. J. Prisca, P. Puvan, W. M. N. Maizatul, and F. N. Nurul. 2018. Improvement of Volvariella strains through low dose acute gamma irradiation. *Nuclear Malaysia RD Seminar 2018*.

M. Ibrahim, M. Azhar, D. Fauzi, A.K. Zaiton, J. N. Hing, H. H. Hisham, W. A.R. Wan Safina, O.B. Airianah, and F. Shazrul. 2017. Variants production of Lentinula edodes spores monokaryon mycelium and dikaryon mycilium by gamma radiation. *Malays. Appl. Biol.*, 46(1):77–82.

S. Jan, T. Parween, and T.O. Siddiqi. 2012. Effect of gamma radiation on morphological, biochemical, and physiological aspects of plants and plant products. *Environmental Reviews*, 20(1):17–39.

H. Tayebeh, A. Motallebi-Azar, F. Rasouli, and F. Zaare-Nahandi. 2021. Induced mutation in Agaricus bisporus by gamma ray to improve genetic variability, degradation enzyme activity, and yield. *Int. J. of Radiation Biology*, 97(7):1020–1031, DOI: 10.1080/09553002.2021.1913528.

Individual Research Contribution Review, 2023, 1(1): 285–286

Determining Greenhouse Gas Emission from Agricultural Activity (Paddy Field)

Azilah Abdul Malek
Agrotechnology and Biosciences Division, Malaysian Nuclear Agency
43000 Kajang, Selangor
azilah@nm.gov.my

Abstract

Agricultural activities often contribute to the rising of greenhouse gas such as the nitrous oxide, methane, and carbon dioxide. In this study, the nitrogen transformation in paddy plot (fertilizer residue) was evaluated by determining the nitrate concentration using Kjedahl method. From the result, nitrate yielded low concentration with 6 mg/L using nitrate probe. This indicates that the fertilizer residual on the paddy field did not contribute much to the nitrous oxide emission into the atmosphere.

Keywords: Ammonium; Nitrate; Greenhouse gas; Nitrogen

1 Introduction

Nitrogen (N_2) is a very important element to help plant growth and development. This is because nitrogen is involved in the formation of proteins (amino acids), DNA (nucleic acids), and plant chlorophyll in addition to promoting the absorption of other important fertilizers such as phosphorus and potassium. However, excessive nitrogen fertilizers can be toxic to plants, animals and the environment. Nitrogen will go through transformation processes such as nitrification, denitrification, immobilization, mineralization, etc. in the soil and produce nitrate, nitrite, nitric oxide and indirectly produce greenhouse gases such as nitrous oxide (N_2O) into the air (Grzyb et al., 2021). N_2O gas has a heating power 300 times higher than carbon dioxide (CO_2) (Stanford News,2020). It has no color and is able to stay in the environment for 114 years where it responsible for the thinning of the stratospheric ozone layer further exposing the earth to higher radiation and damaging plants and human health.

As much as 60% of N_2O gas emissions occur naturally, while the rest is caused by human activities from agricultural land management, wastewater treatment, transportation, stationary combustion, and industry (Environmental and Energy Study Institute, 2022). In order to control the emission of N_2O gas, the use of nitrogen must be monitored. This is because the nitrogen cycle in the soil is very complex and makes it difficult to control the emission of this greenhouse gas. Nitrogen in urea fertilizer will undergo a fixation process and produce ammonium (NH^{4+}) or through a nitrification process to produce nitrite (NO^{2-}) and nitrate (NO^{3-}). Next, this transformation process will continue until it produces N_2O gas and threatens the earth.

2 Methods

2.1 Land Preparation

Labeled urea was prepared in a solution and evenly spread on the microplot using 21G syringe. Then, the soil was squeezed using to ensure even distribution. The soil was left for 4 hours. Auger was used for soil sample collection and transferred to the laboratory for the next step. Soil temperature and moisture was recorded.

2.2 Ammonium Concentration

Ammonium concentration was determined using Kjedahl method. 125ml of potassium chloride was added to a 50g of soil mixture and incubated for 2 h. Later, the soil was filtered. 0.7g of magnesium oxide was added to the soil filtrate and the tube was fitted into the Kjedal distillation system. 20ml of boric acid indicator was filled in the conical flask in the Kjedahl distillation system. At the end of the distillation process, the boric acid indicator was titrated using 0.01N sulphuric acid indicating the ammonium formation.

2.3 Nitrate Concentration

0.4g Devarda alloy powder dan 0.25 magnesium oxide was added to the ammonium solution in the distillation tube earlier and the tube was fitted into the Kjedal distillation system. 20ml of boric acid indicator was filled in the conical flask in the Kjedahl distillation system. At the end of the distillation process, the boric acid indicator was titrated using 0.01N sulphuric acid indicating the nitrate formation. Nitrate concentration was determined using a nitrate probe.

3 Results and Discussions

3.1 Nitrate Concentration

The results showed low amount of nitrate concentration in the unused paddy plot. This indicated that the fertilizer residual in the paddy plot degraded over time and does not significantly contribute to the emission of greenhouse gas.

4 Conclusion

Nitrate probe is not sufficient in determining the nitrate concentration in soil. Advance device such as IRMS should be applied to and carried out in this project to obtain accurate result.

References

Environmental and EESI Energy Study Institute. 2022. Laughing gas is no joke: The forgotten greenhouse gas. *Retrieved from https://www.eesi.org/articles/view/laughing-gas-is-no-joke-the-forgotten-greenhouse-gas*.

A. Grzyb, A. Wolna-Maruwka, and A. Niewiadomska. 2021. The significance of microbial transformation of nitrogen compounds in the light of integrated crop management. *Agronomy*, 11(7):1415.

Individual Research Contribution Review, 2023, 1(1): 287–288

Microbe Beads – A New and Eco-friendly Biofertilizer Using Plant Growth-Promoting Rhizobacteria

Chong Saw Peng
Agrotechnology and Biosciences Division, Malaysian Nuclear Agency
43000 Kajang, Selangor
sawpeng@nm.gov.my

Abstract

Chemical fertilizers have negative impacts on soil health and the environment, including soil erosion, water pollution, and greenhouse gas emissions. Therefore, PGPR-based biofertilizer is a promising biofertilizer due to its ability to enhance soil health, promote plant growth, and reduce the environmental impacts of agriculture.

Keywords: Microbe beads, plant growth-promoting rhizobacteria, biofertilizer

1 Introduction

Biofertilizers are defined as microorganisms that enhance plant growth and nutrient uptake by improving soil fertility. Bacteria-based biofertilizers are one type of biofertilizer that utilizes bacteria to improve soil quality and promote plant growth (Daniel et al., 2022). These bacteria are responsible for nitrogen fixation, phosphorus and potassium solubilization, and the production of plant growth-promoting substances (PGPS), which are essential for plant growth and development (Saeed et al., 2021). This group of beneficial bacteria also known as Plant Growth-Promoting Rhizobacteria (PGPR) colonize the rhizosphere, the soil region around the roots of plants, and promote plant growth. PGPR have gained attention as a potential biofertilizer because of their ability to enhance plant growth and yield, improve nutrient uptake, and suppress plant pathogens (Vacheron et al., 2013).

2 Methods

The rhizobacteria strain was isolated from chili plants in a shade house from the Malaysian Nuclear Agency, Bangi, Selangor, Malaysia, and was cultured on a nutrient agar (NA) plate for further research use and storage purposes. A single colony of pure biofertilizer bacteria was selected from the NA agar plate and cultured with 100 mL of nutrient broth (NB). Bacteria culture grew in NB at 28±2°C in an orbital shaker at 120 rpm for 16-20 hours. The bacteria culture reached a concentration $\geq 1 \times 10^{10}$ cfu/ml and was ready to be used. Shelf-life test was carried out on the microbe beads at different storage temperatures including 4°C and ambient temperature. The cfu/ml of one microbe bead from each storage temperature was carried out using the total plate count method with 5 replicates per test.

The performance of microbe beads was measured through the seed's germination rate and plant height. The seed used for the test was the tomato seed. The soil used for the planting was sterilized by autoclaving at 121°C for 20 minutes. The sterile soil was divided into two with 10 kg each. The 10 kg of sterile soil was mixed with a volume of 200 mL microbe beads and treated for 14 days before planting. Another 10 kg of sterile soil was mixed with 200 mL of sterile water and left it for 14 days to use as a control. Approximately 30 tomato seeds were sowed in the treated soil. The seed's germination rate and plant height were measured to determine the performance of microbe beads.

3 Results and Discussions

Figure 1: Microbe beads shelf-life test at different storage temperatures, 4°C, and ambient temperature (25°C).

Shelf-life test was carried out on the microbe beads at different storage temperatures including 4°C and ambient temperature (25°C). The result showed that at the beginning 6 months of storage, microbe beads stored at ambient temperature gave higher bacteria in cfu/ml than those stored at 4°C with $>1 \times 10^6$ cfu/ml. However, their cfu dropped faster than those stored at 4°C from 7 to 12 months with roughly 1×10^3 cfu/ml after 12 months of storage compared to 4°C storage of about 1×10^4 cfu/ml (Figure 1). Based on the result, the most suitable storage temperature for microbe beads is at ambient temperature after including the consideration of the storage cost.

The performance of microbe beads was measured through the seed's germination rate and plant height. The results showed that 100% of the tomato seeds germinated after 21 days after sowing (DAS) for both soils with and without microbe beads (Figure 2). Although there was a slight delay

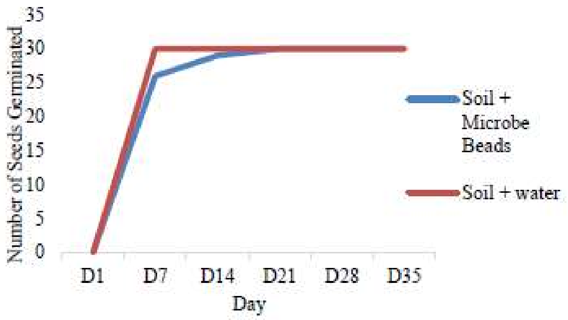

Figure 2: Microbe beads performance on tomato seeds germination.

in the seed's germination in soil with microbe beads due to the adaptation of seeds to the presence of microbes, the final germination rate reached 100%.

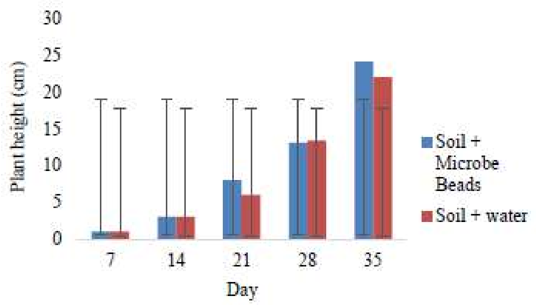

Figure 3: Microbe beads performance on tomato plant growth. The data were analyzed using One-Way ANOVA online software (Social Science Statistics) with a total standard deviation of 8.5031. The p-value is 0.90522. The result is not significant at $p < 0.05$.

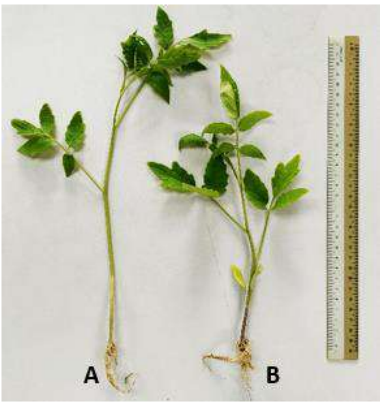

Figure 4: The tomato plant grew after 35 DAS, (A) was planted in soil without microbe beads (control) and (B) was planted in soil with microbe beads. The differential was shown in the plant stem, the control had a thin green stem and the fertilized plant had a red, thick, and sturdy stem.

The performance of microbe beads in the plant height as shown in Figure 3, both with or without microbe beads treatment showed a significant increase in plant height after 35 DAS. However, the plants applied with microbe beads showed a stronger stem compared to the control. They had a red, thick, and sturdy stem compared to the control plant which had a thin green stem (Figure 4). This proved that the biofertilizer bacteria used in this study were able to fix and solubilize the nitrogen and potassium that help to stimulate plant growth.

4 Conclusion

PGPR-based biofertilizers are an effective and environmentally friendly way to improve soil fertility. Their ability to promote plant growth, improve nutrient uptake, and suppress plant pathogens can lead to higher crop productivity and reduce the environmental impact of agriculture. By using PGPR-based biofertilizers, farmers can improve plant growth and yield while reducing their dependence on synthetic fertilizers and pesticides, making them an essential tool in sustainable agriculture.

References

A.I. Daniel, A.O. Fadaka, A. Gokul, O.O. Bakare, O. Aina, S. Fisher, A.F. Burt, V. Mavumengwana, M. Keyster, and A. Klein. 2022. Biofertilizer: The future of food security and food safety. *Microorganisms*, 10(6):1220, doi: 10.3390/microorganisms10061220.

Q. Saeed, W. Xiukang, F.U. Haider, J. Kučerik, M.Z. Mumtaz, J. Holatko, M. Naseem, A. Kintl, M. Ejaz, M. Naveed, M. Brtnicky, and A. Mustafa. 2021. Rhizosphere bacteria in plant growth promotion, biocontrol, and bioremediation of contaminated sites: A comprehensive review of effects and mechanisms. *Int J Mol Sci.*, 22(19):10529, doi: 10.3390/ijms221910529.

J. Vacheron, G. Desbrosses, M.L. Bouffaud, B. Touraine, Y. Moënne-Loccoz, D. Muller, L. Legendre, F. Wisniewski-Dyé, and C. Prigent-Combaret. 2013. Plant growth-promoting rhizobacteria and root system functioning. *Front. Plant Sci.*, 4:356, doi: 10.3389/fpls.2013.00356.

Individual Research Contribution Review, 2023, 1(1): 289–290

Development of Early Maturing and Submergence-Tolerance Rice Through the Crossing between NMR152 and MR220CL2

Faiz Ahmad
Agrotechnology and Biosciences Division, Malaysian Nuclear Agency
43000 Kajang, Selangor
faiz@nm.gov.my

Abstract

Development of early-maturing rice varieties could be the most sustainable approach to reduce the impacts of abiotic and biotic stress. Furthermore, submergence tolerance rice genotypes were also desired to withstand under submergence which has increasing in the frequencies due to global climate change. Therefore, a study was conducted to develop early maturing submergence tolerant rice for Malaysia by crossing a newly released submergence-tolerant mutant rice, NMR152 with an early maturing mega-variety, MR220CL2. The purity of F_1 population were confirmed using polymorphic SSR markers. The selection of early-maturing and submergence-tolerant individuals were performed in F_2 and F_3 generations through screenings them under vegetative stage submergence stress (VSS). For VSS, 18 days-old seedlings were completely submerged in a water tank for 14 days. The survival rate (SR in percentage) were recorded 10 days after de-submerged. Survived individuals were transplanted into the individual pot and morpho-agronomical traits were recorded. About 75% of putative F_1 individuals were confirmed hybrid and were selfed to generate F_2 population. Through VSS screening, 488 from 2000 F_2 individuals (24.4%) were identified as submergence tolerance. 72 of them were also flowered early such as their MR220CL2 parent. In F_3 generation, only 70 from 544 F_3 lines (12.87%) showed more than 75% SR under VSS. 53 lines were further selected and transferred into the field to obtain their morpho-agronomical data. The result shows that 54.72% of the selected lines had maturity period similar to MR220CL2 parent. These early-maturing and submergence-tolerant F_3 lines will be further screened for several generations until the uniform and fix promising lines are obtained.

Keywords: Oryza sativa, Mutant rice, Submergence tolerance, Early maturity rice

1 Introduction

Climate change affects direct and indirectly rice yield production worldwide. In Malaysia, submergence is the examples of the abiotic stress limiting rice production. Additionally, about RM 2 million total loss facing rice farmers in Rompin, Pahang, due to flooding at the end of 2019. Low yield production causes the 2019 self-sufficiency level (SSL) for rice in Malaysia to be around 63%, respectively. Thus, developing a new rice variety adaptable to submergence stress is highly needed to overcome the problem, especially in the problematic area.

Nuclear Malaysia has released and commercialized one mutant rice variety, namely NMR152, which can adapt to submergence conditions and is high yielding. Unfortunately, these mutant varieties are considered an intermediate in terms of days of maturity, which is about 108 days. Thus, improving these high-yielding rice mutant varieties by crossing with short maturity, MR220CL2 is highly recommended. The objectives of this study is to develop early-maturing and submergence tolerant rice for Malaysia by crossing a newly released submergence-tolerant mutant rice, NMR152 with an early maturing mega-variety, MR220CL2.

2 Methods

2.1 Plant Materials

Mutant rice cultivar NMR 152 (Submergence tolerant) and early maturity rice cultivar (MR220CL2) were used in this study.

2.2 Hybridisation of parental lines and confirmation of F_1 plants

The crossing procedures were conducted at the glasshouse of Nuclear Malaysia using the hybridization techniques by Jenning Coffman and Kauffman (Jennings et al., 1979). Mutant cultivar NMR152 was used as recipient parent, while MR220CL2 was used as donor parent. After 30 days, the naked putative F_1 seeds were harvested and were kept at 4°C chiller to maintain their viability. The confirmation of F_1 plants were confirmed using polymorphic SSR Markers.

2.3 Screening of submergence tolerant in F_2 and F_3 populations

Submergence were imposed at early vegetative stage. 14 days old seedlings will be submerged and de-submerged after a majority of susceptible checks plants died (14-21 days of complete submergence). Agronomical data are 1000 grain weight (GW), grain length (GL), biomass (BIO) and grain yield (GY) while morphological traits that will be recorded are days to flowering (DTF), number of panicle (NP), plant height (PH).

2.4 Selection of early maturity and promising lines

The promising rice lines that showed improvement of desirable traits such as days to maturity, and submergence tolerant will be selected for further screening.

3 Results and Discussion

3.1 Confirmation of F_1 plants

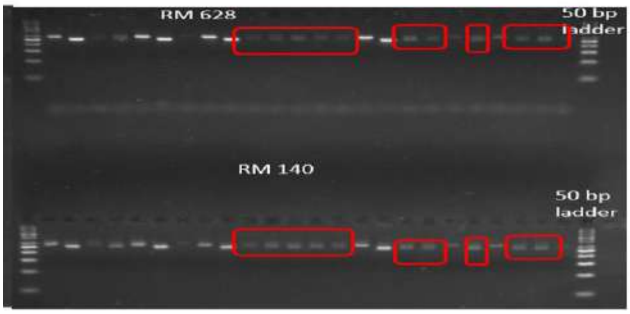

Figure 1: F_1 hybrids confirmation using SSR markers, RM628 and RM140

About 75% of F_1 plants have been identified as F_1 hybrids using SSR markers, RM 628 and RM 140.

3.2 Screening of submergence tolerant in F_2 and F_3 populations

Table 1: Survival rate under submergence stress in F_2 populations

Population F_2	Survival rate under submergence stress		
	Resistant (R)	Susceptible (S)	Total
	484	1516	2000

About 484 or 24.2% of total 2000 F_2 individual showed tolerance to submergence stress. Meanwhile, about 75.8% or about 1516 F_2 individuals showed susceptible to submergence stress.

Table 2: Survival rate under submergence stress in F_3 populations

Survival percentage under submergence stress	Total lines
All died (0%)	132 (24.26%)
1-49%	212 (38.80%)
50-74%	130 (23.90%)
More than 75%	70 (12.87%)

3.3 Selection of promising lines in F_3 populations

About 29 potential lines which showed early maturity and submergence tolerant will be used further evaluated for yield and good agro-morphological traits.

4 Conclusion

- Early-maturing and submergence tolerant lines have been identified from F_3 populations. About 29 lines showed both early maturing and submergence tolerant.
- These early-maturing and submergence-tolerant F_3 lines will be further screened for several generations until the uniform and fix promising lines are obtained.

References

P.R Jennings, Coffman W.R, and Kauffman H.E. 1979. Rice improvement. *Manila: International Rice Research Institute*.

Individual Research Contribution Review, 2023, 1(1): 291–292

Procedure for Isolation of Nitrate-Reducing Bacteria from Palm Oil Mill Effluent

Jong Bor Chyan
Agrotechnology and Biosciences Division, Malaysian Nuclear Agency
43000 Kajang, Selangor
jongbc@nm.gov.my

Abstract

Palm oil mill effluent (POME) is rich in organic matter and has been found to have high levels of nitrate. Thus, POME is a potential source of water pollution as nitrate is an excellent nutrient source for bacterial and algae growth in water. Nitrate-reducing bacteria have the ability to reduce nitrate into nitrite or/and other nitrogenous compounds. The objective of this study was to determine a procedure to isolate bacteria from POME, after which the nitrate reducing ability and the concentration of nitrite were determined. Samples were collected directly from a palm oil mill in Dengkil, Selangor. Bacterial isolates were cultured on nitrate broth and nitrate reduction tests were conducted. The red colour formed was measured with a spectrophotometer to determine absorbance at 540 nm. From the standard nitrite curve, the concentration of nitrite was obtained. A total of 60 isolates were obtained from the POME sample and 55% were identified to be nitrate-reducing bacteria. Among the isolates, AEP H24, POM H7, POM H11 and POM H14 produced the highest amount of nitrite (>32 mg/L). These isolates will be studied in strain improvement experiments using radiation mutagenesis.

Keywords: Palm oil mill effluent, nitrate reduction, nitrite

1 Introduction

Malaysia is the second major producer of oil palm in the world and produced 23% of total global palm oil in 2019 (Food and Agricultural Organization of the United Nations 2020). Palm oil is an important commodity in the country; the industry contributed about 37% of Malaysia's agricultural sector GDP (Department of Statistics Malaysia,2021). A persisting environmental issue in the palm oil industry is to ensure effective treatment of Palm Oil Mill Effluent (POME) to avoid polluting water sources after discharge. For every tonne of crude palm oil produced, around 2.5 - 3.5 tonne of POME will be generated. POME consist of about 0.6 - 2% oil, 2 – 5% suspended solids and 94 - 96 % water. The high organic content is due to residue plant materials from palm oil processing. Raw POME are commonly detected to have high levels in parameters such as biochemical oxygen demand (BOD), chemical oxygen demand (COD), colour intensity, residual oil content, nitrogen and phosphorus content. Concentrations of total nitrogen and ammoniacal nitrogen in raw POME were 750 mg/L and 35 mg/L, respectively.

Nitrate pollution cause negative effects to human health and the environment. High levels of nitrate in drinking water will result in a condition named methaemoglobinaemia which mainly affects infants due to conversion of nitrate to nitrite in the body. People affected by methaemoglobinaemia or also known as the blue baby syndrome will experience a lack of oxygen in the body. Methaemoglobinaemia occurs when the ferrous irons are converted to the ferric state and thus haemoglobin changed to methaemoglobin. Other effects to human health including respiratory problems, birth defects, tumours growth, higher risk of cancer and abortions. Excess nitrate in water will accelerate the growth of bacteria, algal and other aquatic plants causing eutrophication. As the plants used up much of the oxygen in the water, the fishes and coral reefs will begin to die.

Nitrate-reducing bacteria or denitrifying bacteria play a major role in the biological treatment of nitrate in POME. Nitrate-reducing bacteria reduce nitrate to nitrite and further to nitric oxide, nitrous oxide or nitrogen gas. The Griess test or nitrate reduction test is performed to detect nitrate-reducing bacteria. The combination of sulfanilic acid and alpha-napthylamine reagents in nitrite solution produces a red azo dye (Buxton, 2011).

2 Methods

Bacteria were isolated from Palm Oil Mill Effluent (POME) and Aerobic Pond (AEP) collected from a Palm Oil Mill in Dengkil, Selangor. Isolates were grown on nitrate agar [composition (g/L): bacteriological peptone 5, 'Lab-Lemco' powder 3, potassium nitrate 1, agar bacteriological 12, distilled water 1 L, pH 7.0 ± 0.2] and incubated at 30°C. After 24 hours, plates were observed and the bacterial morphologies recorded. Nitrate broth [composition (g/L): bacteriological peptone 5, 'Lab-Lemco' powder 3, potassium nitrate 1, distilled water 1 L, pH 7.0 ± 0.2] were prepared and 10 mL broth were poured into 25 mL-Universal bottles with a Durham tube inverted. Each isolate from POME or AEP was transferred to 3 universal bottles and incubated at 30°C for 24 hours. The Durham tubes were observed for bubbles (gas production).

From the uiversal bottles, 1 mL of culture was transferred to 1.5 mL centrifuge tubes. The nitrate reduction was detected by pipetting 50 μL of each Nitrate Reagent A (1-Naphthylamine Solution) (Sigma-Aldrich, St. Louis, MO, USA) and Nitrate Reagent B (Sulfanilic acid Solution) (Sigma-Aldrich) into the sample and left for 3 minutes. The sample was observed for colour changes to red (positive). A tiny amount of zinc powder was added to samples with no colour change. After addition of zinc, colour changes to red will indicate a negative result. The optical density of samples with positive results will be measured with a spectrophotometer at 540 nm. The concentrations of nitrite in samples were determined from the standard nitrite curve.

3 Results

A high number of bacteria isolated from POM and AEP have nitrate-reducing ability. Nitrate reduction test conducted on samples from POME and AEP revealed 56% and 58% of the isolates were able to reduce nitrate (Figure 1).

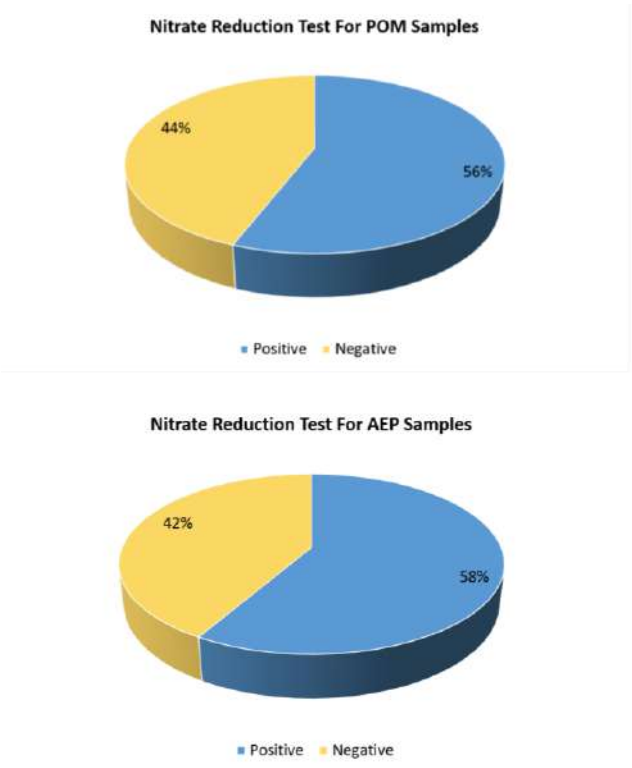

Figure 1: Percentage of POM (Total isolates = 34) and AEP (Total isolates = 24) isolates with positive and negative results for nitrate reduction.

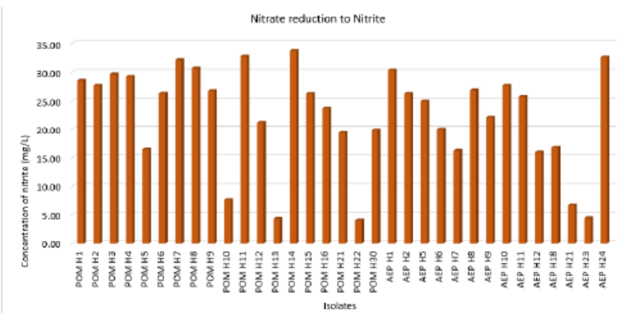

Figure 2: Nitrite produced from reduction of nitrate

4 Discussion/Conclusions

Isolates AEP H24, POM H7, POM H11 and POM H14 (Figure 2) were determined to have high nitrate reducing to nitrite efficiency compared to other isolates. These isolates will be further characterised and improved in radiation mutagenesis experiments.

References

R. Buxton. 2011. Nitrate and nitrite reduction test protocols. *American Society for Microbiology*, pages 1–20.

Department of Statistics Malaysia DOSM. 2021. Press release selected agricultural indicators. page https://www.dosm.gov.my.

Individual Research Contribution Review, 2023, 1(1): 293–294

Aerial Multispectral Imaging: NDT Technique for Precision Agriculture

Mohamad Syafiq bin Mohd Amin
Agrotechnology and Biosciences Division, Malaysian Nuclear Agency
43000 Kajang, Selangor
syafiqamin@nm.gov.my

Abstract

The purposes of this extended abstract in to present the current progress of the work associated with aerial multispectral imaging technique for various agriculture study. Remote Sensing Lab in Agrotechnology and Bioscience Division currently carries out research using Unmanned Aerial Vehicle (UAV) with multispectral sensor to evaluate plant health of Harumanis Mango in Perlis. In this study, aerial multispectral images that have been acquired once every month for the last 13 months from altitude of 30 meter is presented. All the data presented have been computed by subscribed software and corelated with actual field data.

1 Introduction

Traditionally, manual plant health monitor is a very time consuming task that will make early disease detection impossible. Non destructive testing, NDT via remote sensing data permits measurement of biophysical and biochemical parameters of plants for nondestructive monitoring of plant growth and health (Lu et al., 2015; Sankaran et al., 2010; Sankaran et al., 2012).

Precision agriculture (PA) then continue this process by collecting and evaluating field and real-time environmental data in order to develop a predictive management. (Lum et al., 2016)

Combining Unmanned Aerial Vehicle (UAV) and remote sensing data like multispectral imaging is becoming one of the technique that enable fast and accurate plant health monitoring for large scale agriculture farm.

The primary goal of this study is to develop a database of indices map that can be use for plant health monitoring, phenological stages study, development yield model, and others.

2 Aerial Multispectral UAV

In this study, we employ an DJI Phantom 4 Multispectral UAV (Figure 1) that carry a multispectral sensor which include 6 spectrum such as Blue (B): 450 nm ± 16 nm; Green (G): 560 nm ± 16 nm; Red (R): 650 nm ± 16 nm; Red edge (RE): 730 nm ± 16 nm; Near-infrared (NIR): 840 nm ± 26 nm and visible light spectrum.

Figure 1: DJI Phantom 4 Multispectral UAV.

3 Results and Discussions

The study was carried out at Malaysian Department of Agriculture facility in Bukit Temiang, Perlis.

Aerial Multispectral Mapping at Bukit Temiang Harumanis Plot covered 4 research plot sizing 5.99 hectare or 59,891 m^2 (Figure 2).

Figure 2: Orthomosaic Map of Harumanis Research Plot

For every fly mission, 6 indices maps (one for each spectrum) was created using photogrammetry software and the been analyze into required index map such as Normalize Differential Vegetative Index (NDVI), Landsat Enhanced Vegetation Index (EVI), Normalized Difference Red Edge Index (NDRE) using geographic information system,GIS application (Figure 3).

All index map will then be crop using each plant/area boundary which will produce specific index value for each plant or area (Figure 4).

The index value of each plant/area then will be collected

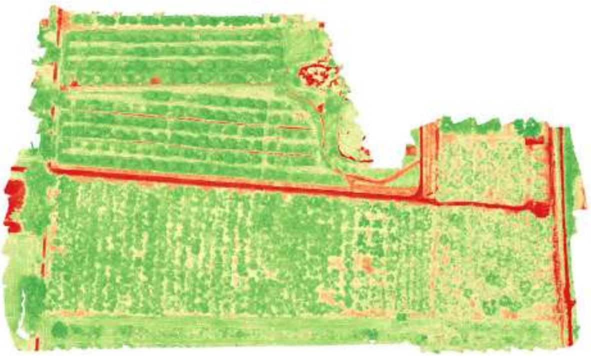

Figure 3: NDVI Map

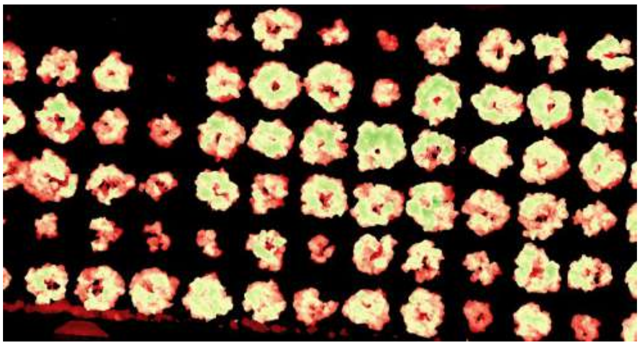

Figure 4: NDVI Map after soil removal and plant isolation process

and compile into database system which can be use to various study. Figure 5 show individual value of NDVI for selected Harumanis plant.

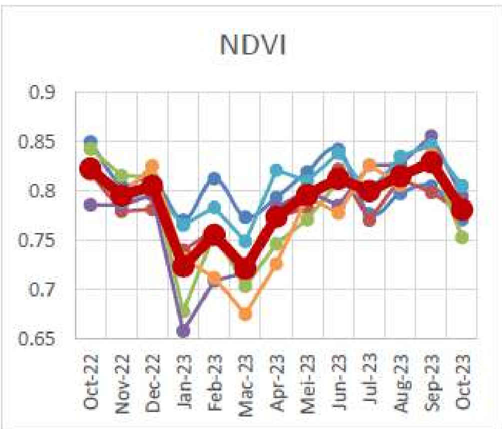

Figure 5: Individual plant NDVI value

This individual plant multispectral index data will then be correlated with manual measurement data that provided by Malaysian Department of Agriculture personnel.

Based on our current finding, although there is a pattern regarding the correlation of NDVI value with actual yield data and NDVI value with plant growth, we still need to collect more data to further proof our correlation in order to develop any prediction or estimation model (Figure 6).

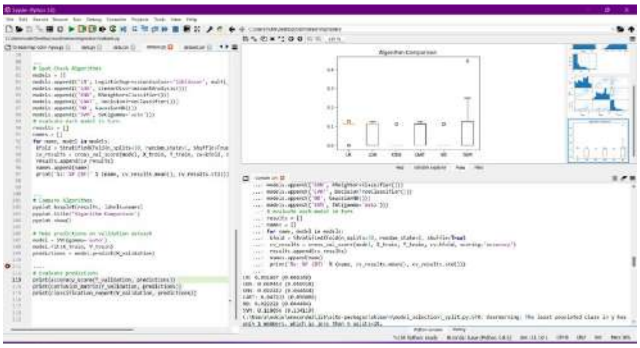

Figure 6: Correlation between multispectral data and manual data using Phyton programming.

4 Conclusion

As a conclusion, the results presented in this extended abstract have shown the capability of aerial multispectral imaging to monitor plant health, predict yield and assist on phenological stages study in the long run.

References

S. Lu, X. Lu, W. Zhao, Y. Liu, Z. Wang, and K. Omasa. 2015. Comparing vegetation indices for remote chlorophyll measurement of white poplar and Chinese elm leaves with different adaxial and abaxial surfaces. *Journal of Experimental Botany*, 66(18).

Christopher Lum, Madison Mackenzie, Charlie Shaw-Feather, Elaiza Luker, and Matthew Dunbabin. 2016. Multispectral imaging and elevation mapping from an unmanned aerial system for precision agriculture applications.

S. Sankaran, A. Mishra, R. Ehsani, and C. Davis. 2010. A review of advanced techniques for detecting plant diseases. *Computers and Electronics in Agriculture*, 72(1).

S. Sankaran, R. Ehsani, S.A. Inch, and R.C. Ploetz. 2012. Evaluation of visible-near infrared reflectance spectra of avocado leaves as a non-destructive sensing tool for detection of laurel wilt. *Plant Disease*, 96(11).

Discovery of MicroRNA-Target Gene Pairs Related to Mahsuri Mutant Rice Resistance to *Magnaporthe oryzae*

Mohammad Malek Faizal Azizi
Agrotechnology and Biosciences Division, Malaysian Nuclear Agency
43000 Kajang, Selangor
malek@nm.gov.my

Abstract

The lack of resistant rice cultivars to blast disease is a contributing factor to the increase of outbreaks in major rice granary areas in Malaysia. One solution to understand the genetic basis and genes that contribute to rice plant resistance against *Magnaporthe oryzae* is to study rice germplasms that are resistant to blast. In 1979, Malaysia initiated a significant project to release the Mahsuri mutant through gamma irradiation. A mutant line in Malaysia has gained recognition for its high resistance to blast disease and its favorable rice quality. This variety is not released or planted by farmers due to its late maturity and tall plant height. Mutant lines exhibit strong resistance to blast pathogen. The systemic information regarding miRNAs during the interaction between Mahsuri mutant-*M. oryzae* is currently unknown. Small RNAs (sRNA) play a vital role in regulating plant immunity against various diseases. The study used sRNA sequencing analysis to identify miRNAs involved in the interaction between Mahsuri rice mutant and *M. oryzae*. Identifying miRNA that contributes to durable blast resistance in rice genotypes is a promising approach for studying broad-spectrum mechanisms against blast disease.

Keywords: Mahsuri mutant, miRNA, blast disease, *Magnaporthe oryzae*

1 Introduction

M. oryzae is a pathogen known for causing rice blast, a major disease in Asian rice. In Malaysia, several rice varieties that are resistant to major rice diseases like blast and blight have been released. This is part of the ongoing efforts to develop improved rice varieties that can withstand both biotic and abiotic stresses. The Mahsuri mutant is considered the most important mutant line out of all the mutants created through induced mutations. The aim of the research was to assess the effectiveness of mutation techniques in rice breeding. The Mahsuri mutant was developed through gamma irradiation. A mutant line in Malaysia has been recognized as the most significant due to its enhanced blast resistance and high eating quality. There is currently no available information on the systemic immunity of Mahsuri mutants against *M. oryzae* and their interaction. MicroRNA (miRNA) is a type of small RNA molecule that is naturally produced by genes in plants. They play a role in regulating various biological processes in plants (Zhang et al., 2018). miRNA is important for regulating plant growth, development, and their ability to resist environmental stress and diseases caused by bacteria, fungi, and other microorganisms. The study by Campo at al. (Campo et al., 2021) found that editing miR812w using CRISPR/Cas9 improves disease susceptibility in rice, while overexpressing Osa-miR812w enhances resistance to *M. oryzae*. The findings suggest that miRNAs play a crucial role in regulating important plant defense genes. The study's important finding will aid in the advancement of miRNA-based breeding strategies in the future.

2 Materials and Methods

Seeds of the Mahsuri Mutant genotype will be supplied by the Malaysian Nuclear Agency. Mahsuri Mutant rice variety plants are cultivated under natural conditions in the greenhouse. The leaves of plants with a growth period of about 14 days are used for *M. oryzae* inoculation and miRNA expression assays. *M. oryzae* isolates are cultured and propagated at 18–20 °C in petri dishes containing potato dextrose agar medium. Plates containing *M. oryzae* isolates mycelium (grown for approximately seven days) are filled with ddH_2O and scraped to collect sporangia. The sporangia are filtered through a nylon mesh of 300 mesh, the spores are collected through a nylon mesh 1200 mesh, and the spore concentration is adjusted to $1x10^5$ mL^{-1} under a microscope for rice leaf inoculation. For the preparation of Mahsuri Mutant, rice leaves sRNA-seq samples, a spore suspension is equitably sprayed on the back of the leaves, and samples are collected at 8, 24, 48, 72, and 96 hours. Three biological samples containing ten leaves are prepared for each time point. The samples are quickly flash-frozen in liquid nitrogen and will be stored at 80 °C for future use. Leaves of un-inoculated Mahsuri mutant plants will be used as control samples.

The Mahsuri Mutant rice leaf samples are sent to Apical Scientific Sdn. Bhd. for various processes including RNA isolation, small RNA library construction, and next-generation sequencing. The procedure described below outlines the analysis of raw data from sRNA sequences. Blastn is a tool that is used to remove short sequences of various types of RNA, including tRNA, rRNA, snoRNA, and snRNA. RNA sequences were aligned to the Mahsuri rice genome sequencing and the *M. oryzae* reference genome using bowtie. The script psrobot_tar is used to predict the target genes of miRNAs using the reference genome sequences of rice and *M. oryzae*.

The miRNA sequence was aligned with the target transcript sequence, and the binding site was determined based on the complementary base sequence.

The total leaves RNA is extracted with a TransZol kit (Trans, Beijing, China), and the cDNA is synthesised with a miRNA 1st Strand cDNA Synthesis Kit by stem-loop (Vazyme Biotech Co., Ltd., Nanjing, China). The miRNA Universal SYBR qPCR Master Mix (Vazyme Biotechnology Co., Ltd., Nanjing, China) is utilised for quantitative real-time PCR (qPCR). The reference control gene for the miRNA qRT-PCR analysis is U6 snRNA. At each *M. oryzae* inoculation time point, nine rice leaves of each variety are sampled, and three leaves are combined into one biological replicate, resulting in three biological replicates. The levels of gene expression are analyzed using the $2^{-\triangle CT}$ method with U6 as the reference gene.

The samples will be analyzed at different time points following inoculation. The data will be sent to the NCBI database. DESeq was used to identify differentially expressed genes based on certain criteria, including an adjusted FDR of 0.01 and a minimum fold-change of 1 in log2FPKM. The transcriptome will be used to screen for miRNA target genes. The software Toolbox for Biologists uses a color scale to show variations in the expression of candidate genes. The user plans to use qRT-PCR analysis to confirm the expression of candidate genes in Mahsuri mutant rice leaves that have been infected with *M. oryzae*. The user plans to design qRT-PCR primers for the target gene using Beacon Designer 7.0. The U6 will be utilized as an internal control to standardize the outcomes. Each biological replicate was performed with three technical replicates.

All data and statistical analysis are performed using one-way ANOVA and pairwise or multiple comparisons with the Statistical software suite (SAS). All presented values and error bars are means SD or SEM of at least three experimental replicates.

3 Results and Discussions

miRNA-mediated gene silencing is a powerful regulatory mechanism that plays a key role in plant responses to pathogen infection. It acts as a master modulator of gene expression. During the interaction between rice and the pathogen *M. oryzae*, both compatible and incompatible infections lead to distinct changes in gene expression of endogenous small RNAs (sRNAs). These changes are caused either by the infection of the pathogen or by the natural defense mechanisms of the host. Therefore, the regulation of gene expression by these small RNAs may either promote the development of diseases or enhance resistance to diseases. Hence, it is imperative to identify the small non-coding RNAs (sRNAs) that play a role in the interaction between *M. oryzae* and Mahsuri mutant rice. Additionally, studying the roles of the target genes is essential in uncovering key immune components in rice that can combat the blast disease. Prior research has demonstrated that miR160a and miR398b play a role in the natural defense mechanisms of rice against blast disease. When these genes are overexpressed, it leads to a notable increase in disease resistance (Li et al., 2014).

4 Conclusion

The progress in the cross-kingdom transfer of miRNAs holds significant promise for manipulating a plant's disease response. The information on miRNAs offers novel perspectives on the cross-kingdom immune regulation in the interaction between Mahsuri mutant rice and *M. oryzae*. This knowledge will aid in the development of a new strategy to combat blast disease. These findings indicate that the MicroRNAs of the Mahsuri mutant and its target genes are ideal target for breeding crops with both disease resistance and high yield.

References

S. Campo, F. Sánchez-Sanuy, R. Camargo-Ramírez, J. Gómez-Ariza, P. Baldrich, L. Campos-Soriano, and B. San Segundo. 2021. A novel transposable element-derived microRNA participates in plant immunity to rice blast disease. *Plant biotechnology journal*, 19:1798–1811.

Y. Li, Y. G. Lu, Y. Shi, L. Wu, Y. J. Xu, F. Huang, and W. M. Wang. 2014. Multiple rice microRNAs are involved in immunity against the blast fungus magnaporthe oryzae. *Plant physiology*, 164:1077–1092.

X. Zhang, Y. Bao, D. Shan, Z. Wang, X. Song, Z. Wang, J. Wang, L. He, L. Wu, Z. Zhang, D. Niu, H. Jin, and H. Zhao. 2018. Magnaporthe oryzae induces the expression of a microRNA to suppress the immune response in rice. *Plant Physiology*, 177:352–368.

Individual Research Contribution Review, 2023, 1(1): 297–298

Stable Isotope Analysis of The Major Bioelements for Authentication of Malaysian Kelulut Honey for *Trigona itama*

Mohd Noor Hidayat Adenan
Agrotechnology and Biosciences Division, Malaysian Nuclear Agency
43000 Kajang, Selangor
hidayat@nm.gov.my

Abstract

Over 50% of legitimate honey traders' income is affected by fake Kelulut honey in the local market. The stable isotope is a promising nuclear method for combating fraud and determining the origin of Kelulut honey. Honey isotopic fingerprints of carbon, oxygen, nitrogen, and hydrogen can verify labelling claims and product authenticity within regulations such as non-permitted use of exogenous sugar syrups.

1 Introduction

Kelulut honey or Malaysian stingless bee honey is a valuable superfood which contributed RM66 million to the agriculture industry annually. The issue of adulterated or fake honey is a global concern and has been reported in various countries, including Malaysia. Adulteration can involve adding syrups or other substances to honey to increase volume and decrease production costs. Stable isotopes profiles serve as reference databases, aiding in the verification of Kelulut honey authenticity and origin. Any deviation from the expected isotopic signatures may indicate potential adulteration or misrepresentation.

Fractionation, caused by isotopes' slightly varied physical properties, is the cause of nature's isotope ratio fluctuation. By combining source material with climatic circumstances and other isotope ratio-affecting elements (water, soil, plant type, etc.), such methods can precisely determine its origin and type. This provides sample-specific fingerprints that may be "read" to determine the authenticity and sample history of Kelulut honey.

2 Methods

The project involves sampling of authentic Kelulut honey samples (*Trigona itama*), analysis, and compilation of chemical properties of samples. Multivariate statistical tool (SIMCA) will be used to analyze and interpret the data.

2.1 Sampling of Malaysian Kelulut honey (*Trigona itama*)

A total of 50 samples of SBH (*Trigona itama* species) have been collected from multiple locations in Peninsular Malaysia. There were 11 states, namely Perak, Selangor, Pahang, Kelantan, Johor, Malacca, Negeri Sembilan, Terengganu, Perlis, Kedah, and Penang, involved in the sampling activities during the study.

2.2 Protein Extraction

Sodium tungstate and sulphuric acid are the important chemicals for protein extraction in the study. The carbon isotope ratio values of raw honey (without extraction) were compared with the carbon-13 values of extracted protein for authenticity evaluation purposes.

2.3 Elemental Analyzer Isotope Ratio Mass Spectrometer (EA-IRMS) Analysis

Carbon, nitrogen, oxygen, and hydrogen stable isotopes were analyzed using Elemental Analyzer Isotope Ratio Mass Spectrometer. USGS 40 and 41a were used as certified reference materials for carbon-13 and nitrogen-15 analysis. Analysis of oxygen-18 and hydrogen-2 were performed using EMA P1 and EMA P2 certified reference materials. The isotope ratios were expressed in δ‰ against international standards (Vienna Peedee Belemnite= ^{13}C, Nitrogen Air= ^{15}N, Vienna Standard Mean Ocean Water= ^{18}O and ^{2}H and Vienna-Canyon Diablo Troilite= ^{34}S) according to the following equation:

$$\delta^{13}C(‰) = \frac{R_{sample}}{R_{standard} - 1} x1000 \tag{1}$$

R = ratio of ^{13}C/^{12}C

2.4 Identification of Authentic SBH

The apparent %C4 sugar addition is calculated by:

$$\text{Adulteration}(\%) = \frac{100[\delta^{13}C(\text{protein}) - \delta^{13}C(\text{wholehoney})]}{[\delta^{13}C(\text{protein}) - (-9.7)]} \tag{2}$$

2.5 Multivariate Statistical Analysis

The stable isotopes data were analyzed using Soft Independent Modelling Class Analogy (SIMCA) software. This software consists of principle component analysis (PCA) for pattern distribution of variables and identification of outliers. The data was further analyzed using orthogonal partial least square discriminant analysis (OPLS-DA) model in SIMCA to distinguish the samples according to the set class or group in the study (states or zone).

3 Data/Results

3.1 Authenticity Analysis of Kelulut Honey

All the 50 samples were categorized as authentic Kelulut honey since the carbon-13 calculation values for extracted proteins and raw honey are below 7%.

3.2 Traceability Model Development

The SIMCA software was used first to develop Malaysian Kelulut honey model as described in Figure 1. The model shows that all of the samples were correctly class as Malaysian Kelulut honey.

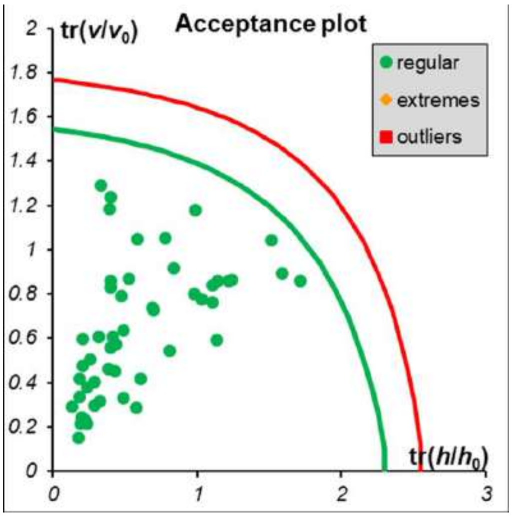

Figure 1: Malaysian Kelulut honey model by SIMCA

Figure 2 shows discrimination of two regions by SIMCA. Region 1 are Perak, Selangor and Pahang while Region 2 are Kelantan, Johor, Malacca, Negeri Sembilan, Terengganu and Northen states (Kedah, Perlis and Pulau Pinang). Two markers differentiated these two regions using this model are carbon-13 and nitrogen-15.

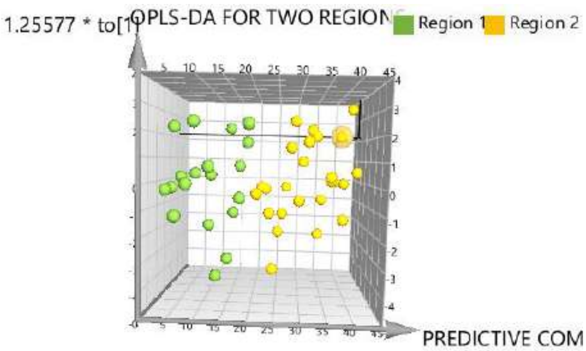

Figure 2: OPLS-DA model of two regions by SIMCA

4 Discussion/Conclusions

All the samples are proven to be authentic Kelulut honey in the study. Apparently, based on the results, carbon-13 and nitrogen-15 are the main isotopes to discriminate the samples into unique classes. Carbon-13 usually relates with soil characteristics in a location while nitrogen-15 represents the farmers practices such as fertilization and the use of chemical pesticides for plantation in an area. (Philip, 2016)

References

Philip. 2016. From production to consumption: tracing C, N, and S dynamics in Brazilian agroecosystems using stable isotopes. *Pesq. agropec. bras., Brasília*, 51(9):1039–1050.

Individual Research Contribution Review, 2023, 1(1): 299–300

IRCR

Optimization of Multiple Shoot Induction Media of Grain Corn

Muniroh Md Saad
Agrotechnology and Biosciences Division, Malaysian Nuclear Agency
43000 Kajang, Selangor
muniroh@nm.gov.my

1 Introduction

Malaysia imports almost 100% of its grain corn requirement every year to meet the local demand of around 3.7 million MT per year as our yearly production is only 80,000 metric tons. Over the past decades, grain corn supply for the local animal feed industries has been entirely dependent on importation, mainly from Argentina and Brazil (Yazid et al., 2021; Zahari and Wong, 2009). To reduce dependency on imports, Malaysia has taken the initiative to locally mass-cultivate grain corn. To further strengthen this effort, grain corn has also been recently gazetted by the Malaysian Ministry of Agriculture and Food Industries as one of the five new wealth-generating crop commodities as announced in the Malaysian 2018 budget (Bank Negara Malaysia, 2018). This research supports the National Agrofood Policy (NAP) 2.0. The NAP 2.0 under the third focus was aimed to increase the production of grain corn with a 30% increment by 2032 to reduce the dependency on the importation. This goal is in line with the principle of the Sustainable Development Goals (SDG) 2030 under zero hunger goals and National Nuclear Technology Policy (DTNN) 2030.

The reason why grain corn farming has not taken off in Malaysia is no available high-yielding variety suitable for Malaysian climates. Therefore, it is important to develop a new variety that can adapt to Malaysia's climate. Screening the grain corn in the field is tedious because it is an openly pollinated crop. Each plant has to be individually bagged during the pollination period. To overcome this issue, the tissue culture technique is used in the early screening of mutant plants. Therefore, this current study was conducted to evaluate the potential effects of 6-Benzylaminopurine (BAP) (cytokinin) with 1-Naphthaleneacetic acid (NAA) (auxins) combinations at different concentrations for in vitro multiple shoot induction of grain corn plantlets.

2 Methodology

2.1 Plant Material and Seed Sterilization

Healthy and mature viable seeds (Zea mays L.) GWG 888 was collected from Green World Genetics Sdn. Bhd. (GWG). Surface sterilization of seeds was carried out according to the method described by Pathi et al. (Pathi et al., 2013) with little modifications.

2.2 Seed Germination and Collection of Split Node Explants

For seed germination, surface-sterilized seeds were cultured on Murashige and Skoog medium supplemented with 3% sucrose, lacking plant growth regulators, and incubated in the light at 25±2°C. The nodal region of 7-day-old seedlings, approximately 0.5 cm above and below the node, was excised and split longitudinally into two halves. These split pieces were placed on a regeneration medium containing different concentrations of Naphthaleneacetic acid (NAA) and 6-Benzylaminopurine (BAP), and incubated under 16 hours of light at 25±2°C.

2.3 Multiple Shoot Induction from Split Node Explants

The split node explants were transferred onto a regeneration medium containing 30 g/l sucrose and 2.6 g/l agar augmented with various concentrations of NAA and BAP (Table 1). The pH of the medium was adjusted to 5.8 before autoclaving. The cultures were maintained at 25±2°C under a 16-hour photoperiod.

Table 1: Treatment combinations of NAA and BAP for multiple shoot induction medium.

Treatment	NAA(mg/L)	BAP(mg/L)	Treatment	NAA(mg/L)	BAP(mg/L)
T1 (control)	0	0	**T9**	0.5	0
T2	0	0.5	**T10**	0.5	0.5
T3	0	1.0	**T11**	0.5	1.0
T4	0	2.0	**T12**	0.5	2.0
T5	0.2	0	**T13**	1.0	0
T6	0.2	0.5	**T14**	1.0	0.5
T7	0.2	1.0	**T15**	1.0	1.0
T8	0.2	2.0	**T16**	1.0	2.0

2.4 Statistical Analysis

Data of shoot regeneration percentage, the number of shoots per culture, and mean shoot length were recorded after 4 weeks. The data were statistically analyzed using Duncan's multiple range test (DMRT) with SAS Software.

3 Results and Discussion

The study described here examined the tissue culture response of split-node explants of maize for direct organogenesis, to establish an efficient and reproducible regeneration protocol for further in vitro mutagenesis studies. Freshly harvested nodal explants collected from 7-day-old seedlings were found to be suitable sources of explants for culture establishment.

When split nodal explants were incubated on MS media with 1.0 mg/l BAP and 0.2 mg/l NAA (T7) or 1.0 mg/l BAP and 0.5 mg/l NAA (Treatment 11), 100% of the explants responded after around 14 days of culture. When split node explants were placed on a medium with different concentrations of only BAP (0.5, 1.0, and 2.0 mg/l), the response of regeneration was very low, but the shoots were regenerated, and the mean number of shoots was lower (0.4–0.7).

Recent reports have described the regeneration of maize plants from embryogenic and organogenic calli derived from split node explants of maize (Pathi et al., 2013). As per our knowledge, no such reports have been discussed regarding the efficient regeneration of hybrid maize (GWG 888) via direct regeneration from mature seeds. Here, the direct regeneration of shoots from split node explants without an intervening callus phase was reported. For direct shoot regeneration from split node explants, different concentrations of NAA and BAP were tested. Cytokinin and auxin treatments showed the ability to induce shoot regeneration and recorded the highest response (up to 100% of responsive explants). Of all the treatments, the addition of 1.0 mg/L BAP and 0.2 mg/L NAA (T7) promoted the highest number of shoot multiplications (3.20±0.41) (Figure 1a). The inclusion of 0.5 mg/L BAP (T2) into MS30 triggered the longest shoots (6.37±1.63 cm), but the mean number of induced shoots was lower in this treatment (Figure 1b). The efficiency of direct shoot regeneration varied with the PGR concentrations used in the study. Shoot initials developed from the cut ends of split node explants and further developed into shoots. This was a common morphogenic response witnessed in all regenerating cultures.

Figure 1: Plant regeneration from split node explants of maize **(a)** direct regeneration of multiple shoots from split node explants on MS medium containing 1.0 mg/L BAP and 0.2 mg/L NAA (T7) **(b)** direct regeneration of multiple shoots from split node explants on MS medium containing 0.5 mg/L BAP (T2)

4 Conclusion

In this study, mature seeds were used as a novel explant, and regeneration was achieved through direct organogenesis. To the best of our knowledge, no reports have discussed the efficient regeneration of hybrid maize (GWG 888) via direct organogenesis from mature seeds. This investigation employed split node explants derived from 7-day-old seedlings to achieve reliable and efficient direct regeneration without the intervening callus phase. The inclusion of 1.0 mg/L BAP and 0.2 mg/L NAA (T7) into MS30 supplemented medium triggered a high frequency of regeneration response (100%) from split node explants with a maximum number of shoots (3.20 ± 0.41) obtained directly within 4 weeks of culture. Thus, the present study suggests that among all treatments, MS30 medium supplemented with 1.0 mg/L BAP and 0.2 mg/L NAA (T7) could be the best option for multiple shoot induction of grain corn. Direct shoot organogenesis achieved from split node explants could be valuable for establishing, rapidly propagating, and conducting in vitro mutagenesis studies of maize plants. However, for the next study, we need to optimize other parameters such as rooting media and acclimatization process for in vitro grain corn plantlets. All the optimized protocol will be used for in vitro mutagenesis of grain corn.

References

BNM Bank Negara Malaysia. 2018. The 2018 budget speech. available online: https://www.mof.gov.my/portal/arkib/budget/2018/bs18.pdf. (accessed on 31 january 2023).

Krishna Mohan Pathi, Suresh Tula, Kazi Md. Kamrul Huda, Vineet Kumar Srivastava, and Narendra Tuteja. 2013. An efficient and rapid regeneration via multiple shoot induction from mature seed derived embryogenic and organogenic callus of Indian maize (Zea mays l.). *Plant signaling behavior*, 8(10).

Siti Nur Ezzati Yazid, Wan Jing Ng, Jinap Selamat, Siti Izera Ismail, and Nik Iskandar Putra Samsudin. 2021. Diversity and toxigenicity of mycobiota in grain corn: A case study at pioneer grain corn plantations in Terengganu, Malaysia. *Agriculture*, 11(3):237.

Zahari and Wong. 2009. Research and development on animal feed in malaysia. *WARTAZOA. Indonesian Bulletin of Animal and Veterinary Sciences*, 19(4):172–179.

Individual Research Contribution Review, 2023, 1(1): 301–302

Development of New Grain Corn Variety by Gamma Irradiation

Mustapha Akil
Agrotechnology and Biosciences Division, Malaysian Nuclear Agency
43000 Kajang, Selangor
mustapha@nm.gov.my

Abstract

Grain corn is typically utilized as a key ingredient in animal feed destined for ruminants, poultry and swine. In Malaysia, grain corn supply for the local animal feed industries has entirely depended on importation. The huge increase in the grain corn import of 3.7 million tons in 2020-2021 has substantially contributed to the country's economic burden. Since the 1980s, grain corn has been cultivated in Malaysia, but there is no available variety suitable for Malaysian climates thus causing the yield obtained to be unsatisfactory. Mutation breeding has played an important role in the development of new crop varieties. Gamma Cell Biobeam GM8000 facility is available at Nuclear Malaysia Agency and was used to irradiate the corn's seeds for radio-sensitivity test and mutation induction. The newly developed variety through mutation breeding was expected to have a high yield, good seed quality, disease-tolerance characteristics, and be adaptable to climate change. Thus, procedure on grain corn mutation breeding is important to help breeders in developing new varieties according to the desired characteristics.

Keywords: Grain corn, Mutation breeding, Gamma radiation, radio-sensitivity.

1 Introduction

Grain corn is an important commodity for the livestock industry in Malaysia as it is the main ingredient for animal feeds. Corn provides between 40% and 60% of energy sources for animals (Nazmi et al., 2021). More than 85% of feed ingredients are imported, while another 15% are produced locally, such as rice bran, palm oil, and palm kernel cake. At the same time, Malaysia produces more than six million tons of animal feed valued at more than RM9 billion every year. However, the local feed industry is heavily dependent on imported feed ingredients and feed supplements. Currently, the farmers in Malaysia does not have many options for domesticated grain corn varieties that can fully adapted to the country's climate. Therefore, it is a suitable time to start for development of a new variety of grain corn with good characteristics such as high yield, good seed quality, adaptability to climate change, and disease tolerance. Mutation breeding is a very well-known option to develop new plant variety. This technique can improve crop development by generating and utilizing genetic variability through the application of mutagenic agents (Oladosu et al., 2016). In addition, gamma ray application is simple, with great reproducibility and high mutation occurrence. It also has less disposal problem (Chahal and Gosal, 2002). Thus, this paper will discuss the procedure for mutation breeding of grain corn.

2 Materials and Methods

2.1 Seed Germination Test

The seed germination test needs to be conducted to ensure the seeds are viable and suitable to be used for mutation breeding. The percentage of germination rate must be above 90% to guarantee the grain corn seeds are good for further use. The germination rate was calculated using the formula below:

$$\%\text{Germination rate} = \frac{\text{Germinated seed}}{\text{Total number of seeds}} \times 100 \tag{1}$$

2.2 Radio-sensitivity Test

Grain corn seeds were irradiated using BioBeam GM8000 facilities at the Malaysian Nuclear Agency with Ceasium-137 as the radioactive source. Different doses were used to irradiate the seeds i.e. 0, 50, 100, 150, 200, 300, 400, 500, 600, 700, 800, 900, 1000 and 1200 Gy . Each dose consists of 3 biological replicates with 15 technical replicates.

Following irradiation, the seeds were planted in troughs filled with mixed soil for 16 days and watered twice daily. Data on survival rate, plant height, and number of leaves were recorded in the glasshouse while data of root length, leaves area, leaves length, average leaves width, and maximum leaves width were recorded in the laboratory using Leaf Area Meter. Analysis of variance (ANOVA) was performed using Statistical Analysis System (SAS) version 9.2.

2.3 Mutation Induction and Development of M5 Mutant Lines Population

The seeds (M0) (approximately 2000 seeds) will be irradiated to induce mutations at the optimal dose before being planted and self-pollinated to create M1 seeds. The M1 seeds will then be sown and self-pollinated to produce M2 seeds. In the M2 generation, mutants will be screened and selected depending on desirable traits. To investigate the genetic stability of the desired features, the selected mutants will be planted in M3 to M5 generations (self-pollination). M5 mutant lines with target traits will be selected and propagated. Cultivation of each line will be conducted at different times to avoid cross-pollination between lines. Subsequently, solid mutant plants will be identified and screened for nutritive quality and disease tolerance.

3 Results and Discussions

LD (Lethal Dose) is the primary metrics used to determine the optimal dose to be used for irradiation by performing radio-sensitivity test. It is a measurement that determines the percentage of the population that will die due to effect of irradiation. LD_{50} means 50% of the irradiated samples die because of irradiation (Albokari et al., 2012) and at the same time, the other 50% is survived. LD_{50} normally creates high frequency of mutation while some scholars used LD_{25} (Ghasemi-Soloklui et al., 2023; Muhammad et al., 2021) that can be considered as well for mutation induction. High doses are generally reported to affect the entire genome which can lead to cell death, normally cause abnormalities and disadvantageous changes, whilst low doses produce the least effect on the plant genome which also could result in morphological variations (Álvarez Holguín et al., 2019). Therefore, based on the LD_{50} value obtained, the determined doses of irradiation are used to induce diversity in plants and obtain the desired characteristics (Hanafiah D.S. and Putri, 2017). From the results obtained as illustrated in Figure 1 and Figure 2, the same trend was seen for both of survival rate and the plant height formed which is found inversely proportional against irradiation doses. It was found that doses above 700Gy have caused the population died entirely. From statistical analysis, it was shown that doses below 400Gy did not show significant changes in comparison with control plant whilst doses above 500 Gy showed significant differences compared to control plant. The higher the dose given, the more the plant population died and reduction of other parameters such as plant height due to cell damage caused by the effects of irradiation.

4 Conclusion

In summary from the experimental results, gamma ray at different doses has adverse effect to significantly alter the morpho-physiological characteristic of grain corn. From the early observation, LD_{50} is calculated approximately 527Gy for grain corn and can be used in the next subsequent mutation induction. The development of a new variety of grain corn using mutation breeding is essential to reduce the country's dependency on grain corn importation and strengthen our national food security.

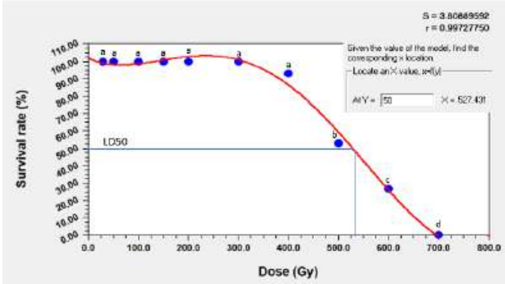

Figure 1: Survival rate (%) of irradiated and non-irradiated grain corn seedlings at 16 days after planting and LD50 determination based on the Curve Expert 1.3

Figure 2: Comparison of non-irradiated (control) and irradiated grain corn at 16 days after planting

References

M.M.A Albokari, S.M. Alzahrani, and A.S. Alsalman. 2012. Radiosensitivity of some local cultivars of wheat (Triticum aestivum l.) to Gamma irradiation. *Bangladesh J. Bot.*, 41(1):1–5.

G.S Chahal and SS Gosal. 2002. Principles and procedures of plant breeding. *Alpha Science International Ltd.*, pages 399–412.

A.A Ghasemi-Soloklui, M. Kordrostami, and R. Karimi. 2023. Determination of optimum dose based of biological responses of lethal dose (LD25, 50, 75) and growth reduction (GR25, 50, 75) in 'Yaghouti' grape due to gamma radiation. *Sci Rep 13*, page 2713.

Luhtfi Azis Mahmud Siregar Hanafiah D.S. and Mutia Dinulia Putri. 2017. Effect of Gamma rays irradiation on M1 generation of Roselle (Hibiscus sabdariffa L.). *Int. J. of Agricultural*, Res 12:28–35.

Ismaila Muhammad, Mohd Y. Rafii, Muhamad Hazim Nazli, Shairul Izan Ramlee, Abdul Rahim Harun, and Yusuff Oladosu. 2021. Determination of lethal (LD) and growth reduction (GR)doses on acute and chronic gamma- irradiated Bambara groundnut (Vigna subterranea (L.) Verdc.) varieties. *Journal of Radiation Research and Applied Sciences.*, 14(1).

M.S. Nazmi, R. Abu Dardak, R. Abdul Rani, and M.R. Rabu. 2021. Benchmarking Indonesia for the development of the grain corn industry in Malaysia. *FFTC Agricultural Policy Platform (FFTC-AP).*

Y. Oladosu, M.Y. Rafii, N. Abdullah, G. Hussin, A. Ramli, H.A. Rahim, G. Miah, and M. Usman. 2016. Principle and application of plant mutagenesis in crop improvement: a review. *Biotechnology and Biotechnological Equipment.*, 30(1):1–16.

A. Álvarez Holguín, C. R. Morales-Nieto, C. H. Avendaño-Arrazate, R. Corrales-Lerma, F. VillarrealGuerrero, E. Santellano-Estrada, and Y. Gómez-Simuta. 2019. Mean lethal dose (LD 50) and growth reduction (GR 50) due to gamma radiation in Wilman lovegrass (Eragrostis superba). *Revista Mexicana De Ciencias Pecuarias*, 10(1):227–238.

Individual Research Contribution Review, 2023, 1(1): 303–304

In Vitro Mutagenesis through Acute and Chronic Gamma Irradiation for Improvement of Local Cassava Variety

Norazlina Noordin
Agrotechnology and Biosciences Division, Malaysian Nuclear Agency
43000 Kajang, Selangor
azlina@nm.gov.my

Abstract

Cassava (Manihot esculenta) belongs to the family Euphorbiaceae. Cassava which also known as Tapioca and called *Ubi Kayu* locally, is a tropical root or tuber crop suitably grown on mineral or peat soil for fresh consumption or processed food. Cassava varieties have either sterile genotypes or produce orthodox sexual seeds which are highly heterozygous with poor flowering, hence genetic improvement through crossbreeding or open pollination is difficult. Micropropagation of cassava varieties in Malaysia is also relatively new with very few studies have been reported. To meet the rising demands of cassava for food consumption and security in agro-based products, it is vital to develop a new variety through efficient protocols of mutation induction and associated biotechnologies such as tissue culture and genomic tools for ensuring a sustainable cassava industry. In this study, micropropagation process of Ubi Putih was established and the aseptic explants were used for the *in vitro* mutagenesis with acute and chronic gamma irradiation.

Keywords: Cassava, Ubi Putih, micropropagation, acute gamma, chronic gamma, mutagenesis

1 Introduction

In Malaysia, cassava is considered as one of the most important root crops, it covers an area of 3,053 hectare. In 2019, Malaysian Department of Agriculture and FAO recorded about 2,450 ha of tapioca grown in Malaysia, producing about 42,267 metric tonnes valued at RM40 (FAO, 2000). Currently, the cassava industry for production of starch, chip and snack production has been increasing in demand and becoming a source of income generation for the small-scale farmers. Domestic demand and local consumption for cassava -based products are very high and profitable according to the Department of Agriculture (DOA) Sarawak (2015). The important problems for cassava industry in Malaysia are poor flowering, limited germplasm, low multiplication rate and low storage ability of the cuttings. Therefore, to meet the rising demands of cassava for food consumption and security in agro-based products, it is vital to develop a new variety with attractive agronomic traits.

At present, there is no report on the use of radiation to induce mutation for the improvement of agronomic traits such as yield, root size, early harvesting of local cassava varieties in Malaysia. Micropropagation of cassava varieties is also relatively new in our country with very few studies have been reported. To meet the rising demands of cassava, it is vital to develop new varieties through mutation induction and associated biotechnologies such as tissue culture and genomic tools for ensuring a sustainable cassava industry. In this project, tissue culture propagation technique and mutagenesis were carried out using acute and chronic gamma irradiation to further improve local cassava varieties. Genetic variation amongst potential mutants of cassava var. Ubi Putih obtained will be evaluated by using Whole Genome Sequencing (WGS).

2 Method

2.1 Micropropagation of cassava var. Ubi Putih

Young and healthy stems from Ubi Putih plants were harvested and surface sterilized by immersing in 70% ethanol followed in commercial bleach solution (active ingredients: 5.25% Sodium Hypochlorite). The sterile stem cuttings were aseptically excised into 1.0-1.5 cm inter-nodes. These internodes were used as the starting materials and cultured in MS (Murashige and Skoog, 1962) media supplemented with Benzylaminopurine (BAP) and 1-Naphthaleneacetic acid (NAA) for shoot bud initiation.

2.2 *In vitro* mutagenesis using acute and chronic gamma irradiation

A radiosensitivity test was conducted using acute gamma irradiation (Bio Beam) and chronic gamma irradiation (Gamma Greenhouse) to study radiation sensitivity of cassava var. Ubi Putih. *In vitro* shoot tips and nodal cuttings of Ubi Putih were used as explants. These explants were irradiated at different acute and chronic gamma ray doses of 0,10, 20, 30, 40, 50, 60, 70, 80, 90, 100 Gy. Survival and shoot regeneration rate were recorded accordingly. Data for radiosensitivity test, LD_{50} and effective/optimal doses for mutagenesis were determined

3 Results and Discussions

3.1 Micropropagation of cassava var. Ubi Putih

Initial shoot buds formed for shoot multiplication. Subculturing of shoot tips and inter-nodes were carried out routinely. The in vitro shoot tip and nodal cuttings of Ubi Putih were used as explants for mutation induction using acute and chronic gamma irradiation

3.2 *In vitro* mutagenesis using acute and chronic gamma irradiation

It was observed that as the dose increases, the survival rate declined. Lethal Dose 50 (LD_{50}) was determined based on the survival rate using CurveExpert 1.4 Software which was at the range of 13- 20 Gy for acute and 30- 45 Gy for chronic. Thus, the suggested optimal doses of gamma irradiation for mutagenesis of cassava are in the range of 10 to 50 Gy. Determination on LD_{50} and optimal doses from this study is vital for future mutagenesis and improvement of local cassava varieties.

Survived *in vitro* shoot tips and nodal cuttings from the selected optimal doses were sub-cultured and used for the *in vitro* mutagenesis of cassava var. Ubi Putih. Subsequently, each growing shoot were separately cultured until M1V4 and then allowed to root (3 to 4 weeks). Irradiated population of rooted plantlets (>M1V5 population) were advanced to acclimatization phase and used for screening in the field.

4 Conclusion

A Protocol on in vitro propagation of cassava var. Ubi Putih has been developed. Database on radiosensitivity, LD_{50} and optimal doses of acute and chronic gamma irradiation for mutation breeding of cassava have been determined. Irradiation population is currently being developed for planting, evaluation and screening in the field.

References

FAO. 2000. *Cassava*, Retrieved 22nd October 2015, from:http://www.fao.org/ag/agp/agpc/gcds/.

T. Murashige and F. Skoog. 1962. A revised medium for rapid growth and bioassay with tobacco tissue culture. *Physiol. Plant.*, 15:473–497.

Department of Agriculture (DOA) Sarawak. 2015. Pakej teknologi penanaman ubi kayu. Sarawak: Malaysia: Jabatan Pertanian Sarawak:1–24.

Individual Research Contribution Review, 2023, 1(1): 305–306

Isolation and Characterization of Cadmium-Tolerant Bacterial as Potential Microorganism for Bioremediation of Heavy Metal in Contaminated Agricultural Soil

Nur Humaira' Lau Abdullah
Agrotechnology and Biosciences Division, Malaysian Nuclear Agency
43000 Kajang, Selangor
humaira@nm.gov.my

Abstract

Heavy metal contamination in agricultural soils has become a global concern. Cadmium is one of the most toxic and mobile heavy metal. Accumulation of cadmium in agricultural products will enter the human body through food chain and cause health risk. Bioremediation of heavy metal contaminated soil is relatively economical compared to physical and chemical techniques. This study aimed to isolate and characterize cadmium-tolerant bacteria from open farming agricultural soil as potential bacteria for bioremediation of cadmium contaminated soil. Cadmium-tolerant bacteria were isolated using spread plate method. The isolated bacteria were characterized based on colony morphology, Gram-staining and cadmium tolerant ability. Eight potential cadmium-tolerant bacteria were isolated and all of them were Gram-negative. The bacterial isolates showed tolerance to cadmium with IC_{50} ranging from 6.637 x 10^{-6} to 348.2 mg/L. Isolate KF4 has the potential for further evaluation in bioremediation of cadmium due to its high tolerance to cadmium.

Keywords: Cadmium, Tolerant, Bacteria, Bioremediation

1 Introduction

Heavy metal contamination has become a global concern (Prosad et al., 2019). Cadmium is one of the most toxic and mobile heavy metal in the environment (Kubier et al., 2019). Cadmium has been reported being accumulated in edible part of different vegetables such as cauliflower, spinach, radish and lettuce (Gupta et al., 2019). The accumulation of cadmium in agricultural products will enter the human body through food chain and cause health risk. Remediating metal-contaminated soils is important to ensure food safety. Bioremediation is relatively economical compared to physical and chemical remediation techniques (Khalid et al., 2017). In this study, potential bacteria for bioremediation of cadmium were isolated and characterized based on their tolerance to cadmium.

2 Methods

2.1 Sampling of soil samples

Two soil samples of approximately 1 kg each were collected randomly from two open farming agricultural land at Cameron Highlands in January 2022. The soil samples were stored at room temperature upon arrival at the laboratory.

2.2 Isolation and characterization of cadmium-tolerant bacteria

Soil sample (10 g) was weighed and transferred aseptically into Schott bottle (250 mL) containing sterilized RO water (90 mL). The bottle was agitated at 150 rpm and 28°C for 2 hours (Muzammil et al., 2021). After mixing, a loopful of the soil solution was taken and streaked onto NA containing cadmium chloride (60 mg/L) (Burke et al., 1991). The plates were incubated at 28°C. The growth of microorganisms was observed daily. The phenotypically distinct single colony grown on the plate was purified to obtain pure culture. The colony morphology of the bacterial isolates grown on NA was characterized by observing the colony size, shape, edge and opacity. Gram-staining was carried out using fresh culture of the isolates.

2.3 Cadmium toxicity test

The metal tolerant ability of the bacterial isolates was determined in the metal-containing liquid media using 96 well microplate. The filter-sterilized cadmium chloride stock solution was added into the wells to give concentration ranging 50-700 mg/L. The fresh culture of the isolates was added into the well as 5% (v/v) inoculum. The mixture was incubated at ambient temperature and the growth was monitored daily for a week by measuring optical density at 600 nm using a microplate reader (EnSpire® Multimode Plate Reader, PerkinElmer).

3 Results

3.1 Isolation and characterization

Isolation of cadmium-tolerant microorganisms had been carried out from the open-farming agricultural soil samples. Eight potential cadmium-tolerant bacteria were isolated and purified. Table 1 shows the bacterial isolates obtained and their characteristics. Two of the bacterial isolates were Gram-negative rods and the remaining were Gram-negative cocci. All the bacterial isolates were translucent except one which appeared opaque. Additionally, isolate KF3 appeared as slimy colony while isolate KF4 produced diffusible pigment (pigment secreted into the agar environment) (Figure 1).

3.2 Cadmium toxicity test

Toxicity test of cadmium was performed for all the bacterial isolates. Table 2 shows the 7-day half inhibitory concentration

Table 1: Characteristics of bacterial isolates purified from open-farming agricultural soil.

Bacterial isolates	Morphology of colony			Gram	Shape of cell
	Margin	Size (mm)	Opacity		
B2	Smooth	4	Translucent	Negative	Cocci
B3	Smooth	1	Translucent	Negative	Rod
B4	Smooth	1	Translucent	Negative	Cocci
KF1	Smooth	2	Translucent	Negative	Cocci
KF2	Smooth	1	Translucent	Negative	Cocci
KF3	Smooth	Pinpoint	Opaque	Negative	Cocci
KF4	Smooth	3	Translucent	Negative	Rod
KF6	Smooth	2	Translucent	Negative	Cocci

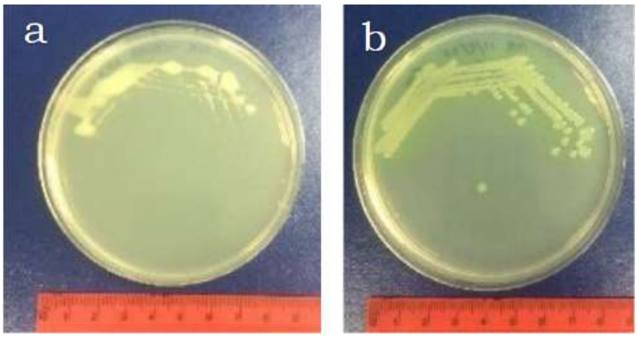

Figure 1: The colony of the pure culture of a) slimy isolate KF3 and b) isolate KF4 with diffusible pigment.

(IC_{50}) value of cadmium for tested isolates in NB. The growth responses of the bacterial isolates in the presence of cadmium in NB were different from each isolates. Isolate B2 was the least tolerant bacterium as it had the lowest IC_{50} values for cadmium i.e. 6.637 x 10^{-6} mg/L. On the other hand, the most tolerant bacterium to cadmium in this study was isolate KF4 with its IC_{50} values was 348.2 mg/L.

Table 2: 7-day IC_{50} values of cadmium for the bacterial isolates.

Bacterial isolate	**IC_{50} of cadmium (mg/L)**
B2	6.637 x 10^{-6}
B3	176.8
B4	164.4
KF1	248.2
KF2	269.9
KF3	183.0
KF4	348.2
KF6	321.5

4 Discussion

In this study, eight cadmium tolerant bacteria were isolated using NA supplemented with 60 mg/L of cadmium as cadmium chloride. All the Gram-negative soil bacterial isolates showed tolerance to cadmium with IC_{50} ranging from 6.637 x 10^{-6} to 348.2 mg/L. Gram-negative bacteria are known to have two layers of cell membrane. This help them to tolerate and grow at higher metal concentration (Stachurska et al., 2020). A 15-min IC_{50} of 0.537 mg/L cadmium for P. phosphoreum T3S, a Gram-negative was reported by Zeb et al.(Zeb et al., 2017). The tolerance of soil bacteria to cadmium enable them to survive in contaminated environment and make them potential candidate for cadmium bioremediation.

This current study demonstrated that the tolerance to cadmium varied among bacteria even though they were isolated from the same soil. Isolate KF4 has the potential for further evaluation in bioremediation of cadmium due to its high tolerance to cadmium.

References

B. E. Burke, K. W. Tsang, and R. M. Pfister. 1991. Cadmium sorption by bacteria and freshwater sediment. *Journal of Industrial Microbiology.*, 8:201–208.

N. Gupta, K.K. Yadav, V. Kumar, S. Kumar, R. P. Chadd, and A. Kumar. 2019. Trace elements in soil-vegetables interface: Translocation, bioaccumulation, toxicity and amelioration- a review. *Science of the Total Environment.*, 651:2927–2942.

S. Khalid, M. Shahid, N. K. Niazi, B. Murtaza, I. Bibi, and C. Dumat. 2017. A comparison of technologies for remediation of heavy metal contaminated soils. *Journal of Geochemical Exploration.*, 182:247–268.

A. Kubier, R.T. Wilkin, and T. Pichler. 2019. Cadmium in soils and groundwater: A review. appl. *Geochem.*, 108:1–16.

S. Muzammil, M. H. Siddique, F. Mureed, R. Andleeb, F. Jabeen, M. Waseem, S. Zafar, H.F. Rehman, T. Ali, and A. Ashraf. 2021. Assessment of cadmium tolerance and biosorptive potential of bacillus cereus gcfsd01 isolated from cadmium contaminated soil. *Braz. J. Biol.*, 81(2):398–405.

R. Prosad, M. S. Islam, T. Kormoker, M.S. Bhuyan, M.A. Hanif, N. Hossain, R. Roy, and A.C. Sharma. 2019. Contamination of heavy metals in agricultural soils: Ecological and health risk assessment. *SF J Nanochem Nanotechnol.*, 2(1):1012.

X. Stachurska, B. Sroda, K. Dubrowska, J. Jablonska, M. Roszak, and J. Karakulska. 2020. Tolerance of environmental bacteria to heavy metals. *Acta Sci. Pol. Zootechnica.*, 9(2):63–74.

B. Zeb, C. Ping, Q. Mahmood, Q. Kin, A. Pervez, M. Irshad, M. Bilal, Z. A. Bhatti, and S. Shaheen. 2017. Assessment of combined toxicity of heavy metals from industrial wastewaters on photobacterium phosphreum t3s. *Appl Water Sci.*, 7:2043–2050.

Individual Research Contribution Review, 2023, 1(1): 307–308

Developing Laboratory Scale Rearing of Oriental Fruit Fly *Bactrocera dorsalis* (Diptera: Tephritidae)

Nur Siti Aisyah Zarimin
Agrotechnology and Biosciences Division, Malaysian Nuclear Agency
43000 Kajang, Selangor
nursiti@nm.gov.my

Abstract

Oriental fruit fly, *Bactrocera dorsalis* (Hendel), is an invasive insect that infest varied range of fruits and vegetables. Sterile insect technique (SIT) have been introduced to reduce fruit fly's population without harming the environment. One of the components in SIT is mass rearing that aimed for increasing fruit fly population before irradiation. Therefore, rearing fruit fly in laboratory-scale has been conducted for the development of SIT. The objectives are to optimize the fruit fly feeding regimen, determine the rearing duration of each stage in fruit fly's life cycle, and examine the morphology of the fruit flies. This study was carried out under laboratory condition at room temperature and were provided with artificial diets and 10% sugar solution. Its morphology was observed using digital microscope. As a result, the artificial diet was changed twice a week while the 10% sugar solution was changed once a month. The duration of each phase of the fruit fly's life cycle was determined: 10 to 12 days from egg to third instar larvae, 5 to 14 days from third instar larvae to pupa formation, and 7 to 10 days from pupa to adult fruit fly. The complete life cycle took about 22 to 36 days. In conclusion, this fruit fly rearing procedure can help maintain the *B. dorsalis* population in the laboratory prior the development of SIT.

Keywords: *Bactrocera dorsalis*, laboratory rearing, artificial diet, SIT

1 Introduction

B. dorsalis has become a threat to agricultural sector in Malaysia. The fruit production has declined about 4% since 2013 due to fruit fly infestations and decrease in the export of fruits due to high levels of insecticide residues. In Malaysia, there have been reports of severe attacks by *B. dorsalis* on various economically valuable crops such as papaya, mango, guava, and star fruit (Mohamed et al., 2020). Controlling the fruit fly population during the larval stages is challenging because they actively bore into and consume the flesh inside the fruits. The fruit itself acts as a safe environment for them from any control methods. Sterile Insect Techniques (SIT) are environmentally friendly and species-specific approaches utilized in the management of pests (Zhao et al., 2022). SIT has shown promising potential as a strategy for the biological control of *B. dorsalis* (Zhao et al., 2013).

2 Methods

2.1 Collection of Parental Stock of *Bactrocera dorsalis*

The parental stock of *B. dorsalis* used in this study originated from infested guava fruits collected from a guava orchard in Selangor, Malaysia. The infested guava was chosen and plucked out by hand after being observed for signs of infestation on its fruit surface. The number of parental larvae was not recorded as the larvae were already inside the fruit.

2.2 The Insectary

The experiment was conducted in the insectary of the Entomology Laboratory at the Malaysia Nuclear Agency from March to July 2023. The rearing conditions were maintained at temperatures of 31 ± 3 °C and 71 ± 7% humidity, with a natural light phase of 14 hours of light and 10 hours of dark condition in a cycle.

2.3 Supplements

Semi-solid artificial diet in Petri dish was placed inside the rearing cage as food supplement. The composition for semi-solid artificial diet were referred from Kaur et al. (Kaur et al., 2021). A 10% sugar solution was also provided in the rearing cage.

2.4 Oviposition Device

An oviposition device is a tool designed to facilitate the process of egg-laying by female insects. In this experiment, an orange was used as an oviposition device. The females that had already mated were attracted to the citrus scent of the oranges. They immediately landed on the fruit surface and prepared to lay eggs.

2.5 Insect Rearing

The oviposition device was left for 12 days inside the rearing cage. Eggs usually took half a day to hatch and enter the larval stage. Usually day 12, the third instar larvae exited the oranges and began searching for a suitable spot to pupate. To prevent the third instar larvae from pupating within the rearing cage, the egg-laying device was removed after being left in the cage for 12 days and was ready to be cut open for extracting the third instar larvae. Third instar larvae were carefully extracted using a scalpel and each larva was transferred into a paper container and supplied with semi-solid artificial food.

3rd instar larvae progressed into the pupal stage. Each individual pupa was carefully collected from the paper container using forceps and then placed inside a glass vial. The glass vials were sealed with Parafilm, and pointed forceps were used to puncture the Parafilm, providing air circulation. These procedures facilitated sex separation and the emergence of virgin females and males.

The pupae inside the glass vials then emerged into adults and introduced into the rearing cage. Before being released, their sexes were identified and recorded. Following a span of 10 days post-pupal emergence, the adults became ready for mating.

3 Results and Discussions

The pre-oviposition stage represents the period before fruit flies lay their first eggs. The complete life cycle took about 22 to 36 days. It took 10 days after the adults emerged to reach sexual maturity, mate, and start laying eggs, which was consistent with previous reports by Ni et al. (Ni et al., 2020). After 10 days, when the adults emerged, the oranges were placed inside the rearing cage for egg laying. *B. dorsalis* goes through three larval stages or instars, but in this experiment, only 3rd instar larvae were observed due to a limited initial parental stock. The duration from the 3rd instar larvae stage to pupation ranged from 5 to 14 days, while the duration from pupation to the emergence of adults varied from 7 to 10 days. These findings were in line with the report by Steiner (Steiner, 1957), who noted that adults typically emerged in about 10 days. Figure 1 showed observation on life cycle of fruit fly from egg to adult and Figure 2 showed the emergence of individual virgin male and female adults.

Figure 1: Complete life cycle of fruit fly from rearing in laboratory scale.

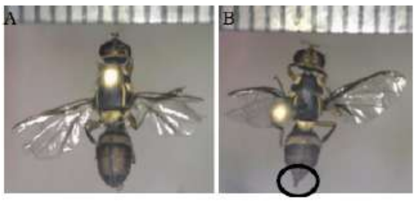

Figure 2: Successfully emerges adult of *Bactrocera dorsalis*. (A) Male adult. (B) Female adult with ovipositor at the end of the abdomen.

The effectiveness of the semi-solid artificial diet was observed from Day 1 to Day 12. The results indicated that from Day 1 to Day 4, the texture and color remained consistent, displaying a light brownish hue with a gel-like texture. Adult fruit flies were observed consuming the artificial diet, as evidenced by the presence of bubbling saliva stains on the cage cloths. However, starting from Day 5, the color began to intensify, progressively darkening as the days passed (Figure 3).

Figure 3: Observation of semi-solid artificial diet from Day 1 to Day 12 in room temperature.

Over the course of one month, the volume of the sugar solution decreased from 50 mL to 10 mL. Nevertheless, if any mold growth was detected on the cotton wool, the sugar solution and conical flask would be replaced with new ones.

4 Conclusion

In conclusion, the primary objective of the experiment was to establish a laboratory-scale rearing method for *B. dorsalis*, resulting in the successful progression of three consecutive generations through this procedure. Although this study was conducted on a small scale in the laboratory, all the collected data will serve as reference information for the potential large-scale rearing of *B. dorsalis* in SIT-based methods. Further investigation, such as studying eggs, 1st instar larvae, and 2nd instar larvae, will be necessary to strengthen the laboratory rearing procedure.

References

S. Kaur, S. Singh, P. Mohanpuria, and Z. Li. 2021. Successful rearing of bactrocera dorsalis on a semi-solid artificial diet. *Indian Journal of Agricultural Sciences*, 91(9).

S.N. Mohamed, Y. NurulFatihahM., M. Hilmi, and N. Norhayati. 2020. Growth and development of oriental fruit fly, Bactrocera dorsalis Hendel (Diptera: Tephritidae) reared on sweet potatoes (Ipomoea batatas l.) based artificial diet. *Serangga*, 25(2):96–107.

M. Ni, K. Gu, D.and Zheng Y.and Qi Y. Hassan, B.and Ning, and Y. Xu. 2020. Effect of oviposition by bactrocera dorsalis on the antioxidant activity of orange juice. *Brazilian journal of biology = Revista brasleira de biologia.*

L. F. Steiner. 1957. Field evaluation of oriental fruit fly insecticides in Hawaii. *J. Econ. Ent.*, 50:16–24.

J. Zhao, S. Chen, Y. Deng, H. Rirong, J. Ma, F. Liang, and M.Y. Hu. 2013. Sperm precedence pattern and the effect of irradiation on male mating competition in the oriental fruit fly, Bactrocera dorsalis. *Cell Bio.*, 1:1–5.

J. Zhao, S. Li, X. Li, C. Liu, Q. Li, Y. Dewer, and K. Wu. 2022. Effects of x-ray irradiation on biological parameters and induced sterility of Ephestia elutella: Establishing the optimum irradiation dose and stage. *Frontiers in Physiology*, 13.

Individual Research Contribution Review, 2023, 1(1): 309–310

Traceability of Malaysian Cocoa Beans using Stable Isotope and Related Techniques

Nurul Elma binti Sabri
Agrotechnology and Biosciences Division, Malaysian Nuclear Agency
43000 Kajang, Selangor
nurulelma@nm.gov.my

Abstract

Theobroma cacao L., or well-known as cocoa beans, are the key raw material for chocolate production. The geographic origin is one of the major sources of the sensory, flavours and the quality of the chocolate. The isotopic profile for $\delta^{13}C$, $\delta^{18}O$, $\delta^{2}H$ and $\delta^{15}N$ was used to define the origin of cocoa beans where the climate and altitude are the factors that influencing the isotopic composition of $\delta^{13}C$ and water precipitation for $\delta^{18}O$ and $\delta^{2}H$, whereas $\delta^{15}N$ usually affected by farmer's practices.

Keywords: Cocoa Beans, Stable Isotope, Origin Traceability

1 Introduction

The consumption of chocolate by Malaysians is approximately 0.5 kg/year/person according to Malaysian Cocoa Board and it is expected that this demand will continue to increase over time as Malaysian nowadays aware of the benefits of cocoa and chocolate. Quality standard for cocoa beans and products in Malaysian Cocoa Industry are based on Standards and Industrial Research Institute of Malaysia (SIRIM). The criterias such as contaminants, fat content, physical test, moisture content and beans count were carried out by other project members from Malaysian Cocoa Board. For geographical traceability of Malaysian cocoa beans, we are using a nuclear technique such as Isotope Ratio Mass Spectrometry (IRMS). According to Park et al (Park et al., 2019), previous studies stated that stable isotope ratio analysis has been employed in geographical origin authentication of food, especially honey and cereal grains. Adulteration of commercial honey was identified by elemental analyzer and liquid chromatography coupled to isotope ratio mass spectroscopy (Dong et al., 2016). Stable isotope data combined with elemental composition and a multi-elemental approach provide better discrimination for geographical origin (Park et al., 2019). There were some studies on the origin of cocoa beans using stable isotope ratio analysis performed by Bindereif et al., Perini et al., Diomande et al. and Bertoldi et al. (Bindereif et al., 2019; Perini et al., 2016; Diomande et al., 2015; Bertoldi et al., 2016) found it possible to discriminate the samples by five subcontinental origins by investigating the geographical traceability of cocoa beans using a multi-elemental fingerprinting approach. There is no study on traceability and authenticity of the origin of Malaysian cocoa beans until now, as stated by Malaysian Cocoa Board. Thus, this study will help to establish an appropriate database of the geographical origin of Malaysian cocoa beans where the main objective of this study is to identify the geographical origin of Malaysian cocoa beans grown in different regions in Malaysia based on the different contents of different elements such as C, N, O and H.

2 Methods

Eleven (11) fermented and dried cocoa beans samples listed in the Premium Cocoa Beans Validation Program were provided by Malaysian Cocoa Board on 22nd Mac 2023. The 11 cocoa samples comprise of 5 samples from Sabah, 3 from Sarawak, 3 from Peninsular areas and one sample is labelled as organic reference. The dried cocoa beans were pulverised using a mortar and pestle and subsequently processed in a blender to achieve a finely powdered texture. The fine powder samples were sieved two times with a mesh width of 125μm in 5 minutes with 80 amplitudes using a Retsch Test Sieve (Retsch, German) to get homogeneous cocoa powder. The fine and homogeneous cocoa powder was stored in a desiccator prior to analysis.

3 Data/Results

A 2.0 mg of homogenous cocoa powder were weighed into tin capsule and analysed using Elemental Analyzer – Isotope Ratio Mass Spectrometry (EA-IRMS) in CNS mode to analyze isotopic values of $\delta^{13}C$ and $\delta^{15}N$. $\delta^{15}N$ and $\delta^{13}C$ values for all samples are tabulated in Table 1.

The values were expressed according to the IUPAC protocol which follows the formula δ = (Rsample – Rstandard)/Rstandard, where R is the ratio between the heavier isotope and the lighter one, against international standards Vienna-Pee Dee Belemnite (VPDB) for $\delta^{13}C$ and Air for $\delta^{15}N$. For $\delta^{15}N$ and $\delta^{13}C$, the isotopic values were calculated and calibrated against international reference materials; L-glutamic acid USGS 40 and USGS 41a for $^{13}C/^{12}C$ and $^{15}N/^{14}N$.

4 Discussion/ Conclusions

4.1 Isotopic values of $\delta^{13}C$ and $\delta^{15}N$

For 11 Malaysian cocoa beans, $\delta^{15}N$ ranged from 3.29‰ to 7.78‰. The results were in accordance with Perini et al. (Perini et al., 2016) who reported the $\delta^{15}N$ values in their study were 2.6‰ to 7.2‰. Variation in $\delta^{15}N$ found between cocoa-producing areas are likely the result of different agricultural

Table 1: $\delta^{15}N$ and $\delta^{13}C$ values for 11 Malaysian Cocoa Beans

FARMER	LABEL	STATE	$\Delta^{15}N$ (AIR)	$\Delta^{13}C$ (VPDB)
SIK KIM SOON	SKS	Kelantan	7.78	-30.48
			7.74	-30.52
			7.75	-30.57
KG GOSHEN	KGS	Sabah	5.61	-30.89
			5.7	-30.92
			5.61	-30.87
QC TAWAU	QCT	Sabah	5.94	-30.15
			6.03	-30.16
			5.92	-30.13
CYRIL ANAK LANGIN	CAL	Sarawak	4.38	-30.24
			4.36	-30.28
			4.47	-30.27
LKM MADAI	LKM	Sabah	5.58	-30.98
			5.4	-31.05
AHMAD ABDUL AZIZ	AAA	Johor	4.96	-30.1
			4.81	-30.15
			5.45	-30.1
NASARUDDIN NGU ABDULLAH	NNA	Sarawak	3.73	-31
			3.85	-31.02
			3.68	-31
MISPARI RAMLI	MR	Selangor	6.14	-30.9
			6.15	-30.85
			6.14	-30.86
ESON LUPAN	EL	Sabah	4.67	-30.47
			4.88	-30.44
			4.81	-30.45
JANDA AK JELIAN	JAJ	Sarawak	3.46	-30.85
			3.31	-30.87
			3.29	-30.87
GOFRI LIANG	GL	Sabah	7.22	-29.63
			7.17	-29.67
			7.07	-29.61

practices (Bindereif et al., 2019). The isotopic values of ^{13}C isotope are between -31.05‰ to -29.61‰ for the cocoa bean samples. The results are comparable with Acierno et al (Acierno et al., 2020) which found the isotopic values of $\delta^{13}C$ for their samples were -32.2‰ to -27.7‰.

As illustrated in Figure 1, all samples could be clustered into six different groups based on the C and N isotopic values. Groups labelled I, II, and III belong to Gofri Liang, Sik Kim Soon, and QC Tawau, respectively. Ahmad Abdul Aziz, Cyril Anak Langin, and Eson Lupan were grouped together and labelled as IV, whereas Mispari Ramli, KG Goshen, and LKM Madai were grouped together and labelled as group V. Meanwhile, the last group VI consists of Nasaruddin Ngu Abdullah and Janda Ak Jelian.

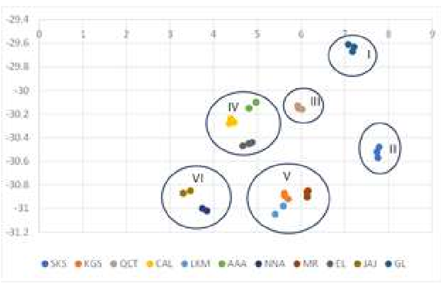

Figure 1: Data distribution of $\delta^{15}N$ and $\delta^{13}C$ values for 11 Malaysian cocoa beans from different geographical origins

QC Tawau is recognized as a certified agricultural establishment that cultivates organic cocoa beans by Malaysian Cocoa Board. This certification indicates that the farmer uses organic fertilizers in their cultivation practices. Based on Figure 1, QC Tawau is near the point x=6. As stated above, variation in N isotopic values might be the result of different agricultural practices. Thus, the nearest to the point x=6 is Mispari Ramli, which we could say that this farmer's agricultural practice is almost like the QC Tawau.

5 Summary

Currently, we only gather the information of C and N isotopic values for eleven Malaysian cocoa beans. To develop a good model, bigger sample size (at least 150 samples) is necessary for database of Malaysian cocoa beans. To identify the geographical origin, soil and water samples of the same origin of cocoa beans are compulsory. Soil and water samples are required to establish the origin which is the main objective for this project.

References

V. Acierno, L. D. Jonge, and S. V. Ruth. 2020. Sniffing out cocoa bean traits that persist in chocolates by ptr-ms, icp-ms and ir-ms. *Food Research International*, 133(109212).

D. Bertoldi, A. Barbero, F. Camin, A. Caligiani, and R. Larcher. 2016. Multielemental fingerprinting and geographic traceability of theobroma cacao beans and cocoa products. *Food Control*, 65:46–53.

S. G. Bindereif, F. Brauer, J. M. Schubert, S. Schwarzinger, and G. Gebauer. 2019. *Food Chemistry*, 299(125105).

D. Diomande, I. Antheaume, M. Leroux, J. Lalande, S. Balayssac, G. S. Remaud, and I. Tea. 2015. Multi-element, multi-compound isotope profiling as a means to distinguish the geographical and varietal origin of fermented cocoa (theobroma cacao l.) beans. *Food Chemistry*, 188:576–582.

H. Dong, D. Luo, Y. Xian, H. Luo, X. Guo, C. Li, and M. Zhao. 2016. Adulteration identification of commercial honey with the c-4 sugar content of negative values by an elemental analyzer and liquid chromatography coupled to isotope ratio mass spectroscopy. *Journal of Agricultural and Food Chemistry*, 64(16):3258–3265.

J. H. Park, S. H. Choi, and Y. S. Bong. 2019. Geographical origin authentication of onions using stable isotope ratio and compositions of c, h, o, n, and s. *Food Control*, 101:121–125.

M. Perini, L. Bontempo, L. Ziller, A. Barbero, A. Caligiani, and F. Camin. 2016. Stable isotope composition of cocoa beans of different geographical origin. *Journal of Mass Spectrometry*, 51(9):684–9.

Individual Research Contribution Review, 2023, 1(1): 311–312

Developing Standard Guidelines for Gram Positive and Negative Bacteria Mutagenesis by Using the Gamma Irradiation Technique

Phua Choo Kwai Hoe
Agrotechnology and Biosciences Division, Malaysian Nuclear Agency
43000 Kajang, Selangor
phua@nm.gov.my

Abstract

Gamma irradiation by gamma cell is a powerful tool for mutagenesis to improve the functionalities of microbes. However, microbe mutagenesis is complex and is affected by various factors. Effects of gamma irradiation on Gram positive and negative bacteria are different. There is no standard and information in this study. It is important to have a standard optimum dose and LD_{50} data as guidelines for gamma cell mutagenesis.

Keywords: Mutagenesis, Gamma irradiation, Biofertilizer

1 Introduction

Mutagenesis of microorganisms is used to improve microbial activities to meet market needs (Satoh and Oono, 2019). The advantage of mutagenesis is it does not require genetic knowledge to determine the desired features before starting. It is a process of mutation induced by a mutagenic agent. The two types of mutagens used for microorganism mutagenesis are chemical mutagen and physical mutagen (Ram et al., 2019). Microorganism mutagenesis is mostly applied in fermentation and cellulose enzyme industries. In agriculture, microorganism mutagenesis is mainly applied for biological control. Trichoderma sp., Fusarium sp., and Bacillus sp. are widely used in mutagenesis through gamma irradiation (Haggag, 2002; Haggag and Mohamed, 2002; Baharvand et al., 2014; Naseripour et al., 2014).

The effects of irradiation can be measured via two means, namely, decimal reduction dose (D_{10} value) and lethal dose (LD_{50}). D_{10} value is the radiation dose (kGy) required to reduce the number of microorganisms by 10-fold (one log cycle) or the radiation dose required to kill 90% of the total number of microorganisms (Atique et al., 2013; Satoh and Oono, 2019). Studies on mutagenesis applied the lethal dose (LD_{50}), where 50% of irradiated cells died. Both values can be obtained by plotting the survival curve.

Gamma irradiation by gamma cell is a powerful tool for mutagenesis to improve the functionalities of microbes. However, microbe mutagenesis is complex and is affected by various factors. Effects of gamma irradiation on Gram positive and negative bacteria are different. There is no standard and information in this study. It is important to have a standard optimum dose and LD_{50} data as guidelines for gamma cell mutagenesis.

2 Methods

2.1 Culture collections

Gram negative bacteria were collected from Nuclear Malaysia and Gram positive bacteria were collected from Universiti Putra Malaysia.

The bacterial strains were identified by using the 16S rRNA method. Stock bacteria were cultured in Merk, United Stated nutrient agar (NA). Gram staining were done by using Gram staining kits. Plant growth activities screen by using selective media. All culture collection kept in -20 °C stock.

2.2 Gamma irradiation experiment and determination of LD_{50}

Mutagenesis experiment was done by using gamma cell (Gamma Cell Biobeam GM8000, Germany) in Nuclear Malaysia. The mutagenesis experiment utilised gamma rays (50–400 Gy) from the gamma cell in accordance with a modified version of the method used by Rugthaworn et al.(Rugthaworn et al., 2007). The bacterial strains were cultured on NA in 50 mm diameter Petri dishes. There were four replications for each radiation treatment and the experiment was repeated twice. The plates were incubated at 28 ± 2 °C for 24 h. Culture plates were wrapped with aluminum foil and irradiated in the gamma cell. Non-irradiated plates were used as controls. Dose mapping of gamma cell were done before gamma irradiation was carried out. Fricke dosimetry was used. Afterward, the plates were incubated at 28 ± 2 °C for 24 h. The bacterial cultures were suspended in sterile distilled water and adjusted to the same concentration at OD_{620nm} = 0.2 (Gram negative bacteria) and OD_{620nm}= 1.5 (gram positive bacteria) with a spectrophotometer (Shimadzu UV mini-1240, Japan). Serial dilution and plate count methods were used to determine the lethal dosage (LD_{50}) and plot the survival curve (Liner regression) by using Statistical Package for the Social Sciences (SPSS) software version 22.

3 Data/Results

Eight Gram negative bacteria and two Gram positive bacteria with various plant growth activities such as nitrogen fixation, phosphate solubilization, potassium solubilization etc. were isiolated (Table 1). LD_{50} were determine. LD_{50} for Gram negative bacteria in range 400 to 500 Gy and Gram positive in range 800 to 1100 Gy (Table 2).

Table 1: Bacterial designation, organism identification, gram stain and plant growth promoting activities

Isolates designation	Organism identification	Gram Stain	Plant growth promoting activities
M100	*Acinetobacter calcoaceticus*	Negative	• N_2 fixation • Phosphate solubilisation • Potassium solubilisation
AP1	*Acinetobacter beumannii*	Negative	• N_2 fixation • Phosphate solubilisation • Potassium solubilisation
AP2	*Klebsiella pneumoniae*	Negative	• N_2 fixation • Phosphate solubilisation • Potassium solubilisation • IAA production
AP3	*Enterobacteriaceae* bacterium	Negative	• N_2 fixation • Phosphate solubilisation • Potassium solubilisation
C2	*Pseudomonas putida*	Negative	• Phosphate solubilisation • Potassium solubilisation
V3	*Pantoea stewartii*	Negative	• Phosphate solubilisation • Potassium solubilisation
V15	*Pseudomonas putida*	Negative	• Phosphate solubilisation • Potassium solubilisation
M99	*Pseudomonas putida*	Negative	• N_2 fixation • Phosphate solubilisation • Potassium solubilisation
UPM10	*Bacillus sp.*	Positive	• Produce IAA (phytohormone) • Fix atmospheric nitrogen (BNF) • Solubilise phosphate (PSB) • Solubilise potassium (KSB) • Produce siderophore • Produce hydrolyzing enzymes (celluase and pectinase)
UPM06	*Bacillus proteolyticus*	Positive	• Produce IAA (phytohormone) • Fix atmospheric nitrogen (BNF) • Solubilise phosphate (PSB) • Solubilise potassium (KSB) • Produce siderophore • Produce hydrolyzing enzymes (celluase and pectinase) • Produce exopolysaccharide (EPS) • Flocculation yield • Produce biofilm • Uptake sodium • Able to promote growth and yield on rice under saline and non-saline conditions

4 Discussion/Conclusions

The effects of irradiation can be measured via LD_{50}. Studies on mutagenesis applied the LD_{50}, where 50% of irradiated cells died. Effects of gamma irradiation on Gram-positive and Gram-negative bacteria are different. A study on the survival of bacterial isolates under radiation doses of 1 kGy to 10 kGy was conducted. Streptococcus sp. continued to grow even up to 9 kGy, but all the isolates died at 10 kGy. Thus, Gram-positive bacteria can tolerate high doses of radiation. By contrast, all Gram-negative isolates, such as Pseudomonas sp., died after exposure to 5 kGy (Atique et al., 2013). An investigation on the effect of acute gamma irradiation of Gram-positive bacteria (Bacillus sp.) and Gram-negative bacteria (Escherichia coli) were conducted. The LD_{50} for Bacillus megaterium NMBCC50018, Bacillus subtilis NMBCC50025 and E. coli were 1.2 kGy, 0.2 kGy and 0.03 kGy, respectively. Gram-positive bacteria were more resistant to gamma irradiation in comparison to Gram-negative bacteria (Hing et al., 2022). In view of these results, LD_{50} from this study for Gram negative bacteria in range 400 to 500 Gy and Gram positive in range 800 to 1100 Gy show Gram positive bacteria more resistant to gamma irradiation. These results are use to develop a guidelines for mutagenesis of microorganisms involving gamma irradiation.

Table 2: LD_{50} values of gamma irradiated biofertilizer microorganisms

Isolates	Organism identification	LD_{50} value (Gy)
M100	*Acinetobacter calcoaceticus*	448.5
AP1	*Acinetobacter baumannii*	483.5
AP2	*Klebsiella pneumoniae*	506.5
AP3	*Enterobacteriaceae* bacterium	417.5
C2	*Pseudomonas putida*	381.5
V3	*Pantoea stewartii*	406.5
V15	*Pseudomonas putida*	404.0
M99	*Pseudomonas putida*	445.5
UPM10	*Bacillus sp.*	815.0
UPM06	*Bacillus proteolyticus*	1154.0

References

F. B. Atique, K. T. Ahmed, S. M. Asaduzzaman, and K. N. Hasan. 2013. Effects of gamma irradiation on bacterial microflora associated with human amniotic membrane. *BioMedResearch International*, page 1–6.

A. Baharvand, S. Shahbazi, H. Afsharmanesh, M. A. Ebrahimi, and H. Askari. 2014. Investigation of gamma irradiation on morphological characteristic and antagonist potential of Trichoderma viride against M. phaseolina. *International Journal of Farming and Allied Sciences*, 3(11):1157–1164.

W. M. Haggag and H. A. A. Mohamed. 2002. Enhancement of antifungal metabolites production from gamma-ray induced mutants of some Trichoderma species for control onion white rot disease. *Plant Pathology*, 11:45–56.

W. M. Haggag. 2002. Induction of hyperproducing chitinase Trichoderma mutants for efficient biocontrol of botrytis cinerea on tomato and cucumber plants growing in plastic houses. *Arab Journal of Biotechnology*, 5(2-July):151–164.

J.N. Hing, B. C. Jong, P.W.Y. Liew, E.E. Rashid, and S. Shamsudin. 2022. Gamma radiation dose-response of Gram-positive and Gram-negative bacteria. *Malaysian Applied Biology*, 51(5):107–112.

T. Naseripour, S. Shahbazi, and H. Askari. 2014. The impact of γ-radiation on morphological characteristics and antagonist potential of Trichoderma harzianum against Rhizoctonia solani. *International Journal of Agriculture and Crop Sciences*, 7(8):454–461.

H. Ram, P. Soni, P. Salvi, N. Gandass, A. Sharma, A. Kaur, and T. R. Sharma. 2019. Insertional mutagenesis approaches and their use in rice for functional genomics. *Plants*, 8(310):1–14.

P. Rugthaworn, U. Dilokkunanant, S. Sangchote, N. Piadang, and V. Kitpreechavanich. 2007. A search and improvement of actinomycete strains for biological control of plant pathogens. *Kasetsart Journal (Natural Science)*, 41:248–254.

K. Satoh and Y. Oono. 2019. Studies on application of ion bean breeding to industrial microorganisms at TIARA. *Quantum Beam Science*, 3(11):1–16.

Detection of Selected Irradiated Dried Food using Photostimulated Luminescence (PSL) technique

Ros Anita Ahmad Ramli
Agrotechnology and Biosciences Division, Malaysian Nuclear Agency
43000 Kajang, Selangor
anita@nm.gov.my

Abstract

This research was conducted to find the ability of photostimulated luminescence (PSL) to detect selected irradiated dried food such as dried mushroom, dried shrimp, dried Indian Threadfin and dried dates fruit. All the samples were irradiated at 0 (control), 1 kGy, 3 kGy and 5 kGy. The PCs of irradiated samples showed a general trend of increase with increasing doses. However, the signal intensity response to irradiation dose varied with samples and this is possibly attributed to the varying quantity and quality of silicate minerals present in each sample. The results of this study provide a useful database on the applicability of PSL technique for the detection of Malaysian irradiated dried food.

Keywords: Food irradiation, detection, photostimulated luminescence, dried food

1 Introduction

To date, health and safety authorities in over 60 countries worldwide have approved the irradiation of over 60 kinds of foodstuffs. Global production of irradiated foods, while still small in volume, has increased steadily in recent years, from 300,000 tonnes in 2000 reaching to 405,000 tonnes in 2005 (Kume et al., 2009). In 2013, Malaysia has developed detection of irradiated food using PSL technique to support Food Irradiation Regulations 2011 which require labeling of irradiation food on sale. A major constraint for the acceptability of irradiated food in the international market is the conformance of the applied regulations requiring effective and reliable detection methods. The development of analytical methods for correct identification of irradiated samples from non-irradiated samples has thus become important for upholding regulatory controls, checking compliance against labeling requirements, facilitating international trade, and reinforcing consumer confidence.

Since 1980, extensive research was undertaken in development of a range of test methods determining the irradiation status of a wide variety of foods (Delincée., 2002). Currently, there are 10 different standardized methods endorsed by the Codex Alimentarius. The methods are classified as screening and confirmatory techniques depending on their specificity, reliability, reprehensibility, and ease of use (Chauhan et al., 2009). Unfortunately, there is no single method with the potential to be applied to all kinds of foods. Hence, the use of different techniques is usually suggested in available resources.

Photo-stimulated luminescence (PSL) is one of the promising physical methods for detecting irradiated food. PSL measurement is based on emission of light or luminescence properties of contaminating minerals present on the food. When food is irradiated, the radiation energy absorbed is stored in charge carriers at structural, interstitial or impurity sites which, upon stimulated by light, produces a measurable luminescence signals recorded by PSL detector (Chauhan et al., 2009).

Thus, the objective of this study was to further investigate the applicability of this physical detection methods PSL on irradiated selected dried food (mushroom, thread fin, shrimps and dates fruit) samples. These investigations will help to improve the testing of selected irradiated dried food on the market in Malaysia as required by food irradiation regulations 2011. However, the international legislation requires labeling of irradiated food to facilitate international trade and to meet consumer's rights of choice. Therefore, development of potential detection methods to classify marketed foods as irradiated or nonirradiated is of paramount interest (Arvanitoyannis, 2010).

2 Materials and Methods

Three types of dried food, mushroom, shrimps, Indian threadfin and dates fruit (Figure 1) were purchased from local supermarket near Bandar Baru Bangi. The samples were exposed to γ-radiation at doses ranging 1, 3 and 5 kGy using a cobalt-60 gamma source. The doses were selected in the range used for dried food, including a very low value (1 kGy) to check the detection limit of the method. Before measurement, all samples (non-irradiated and irradiated) were stored inside their packaging under dark conditions.

Figure 1: Samples analysis - dried food (shrimps, mushroom, Indian threadfin and dates fruit)

The PSL of the control and irradiated samples were measured using a PSL Irradiated Food Screening System at Malaysian Nuclear Agency. The PSL measurements were performed according to EN 13751 (2009). Sample was placed in

50 mm diameter disposable petri dish (Figure 2). The PSL signals (photon counts, PCs) of the samples were recorded in the measuring mode at the rate of counts/60s and were presented at PCs/ 60s. All measurements were done in duplicates.

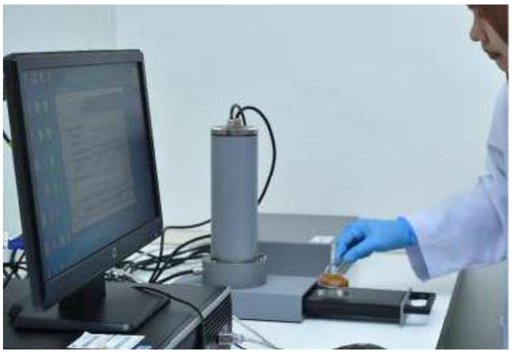

Figure 2: Analysis on detection of irradiated dried food using photostimulated luminescence

Table 1, samples producing signals below the lower threshold value of 700 counts/60s (T_1) are categorized as non-irradiated (negative) while above the upper threshold of 5000 counts/60 s (T_2) suggests irradiated samples (positive). Samples with signal levels between the two thresholds (700-5000 counts/60s) were classified as intermediate (M).

Table 1: Decision-making scheme for the classification of the sample with the EN 13751 method

Total Count	Response	Classification
total counts < T_1	negative	not irradiated
T_1 < total counts < T_2	intermediate	intermediate
total counts > T_2	positive	probably irradiated

3 Results and Discussions

The effect of radiation dose on signal intensity shows a general trend of increasing PCs with increasing dose up to 5 kGy. The PSL photon counts (PCs) for all samples, measured as a function of irradiation dose, are presented in Figure 3. The PCs of the 1-5 kGy irradiated dried food such as mushroom, shrimps, Indian threadfin and dates fruit measured were higher than the upper threshold value (T_2 = 5000 counts/60s) indicating irradiation treatment, making it possible to discriminate them from non-irradiated ones. The result also showed a trend of increasing PCs with increasing dose in all the dried foods. The result of this study agrees with the finding for 19 different herbs reported by Sukdeb et al. (Sukdeb et al., 2010). This clearly shows that PSL methodology, although simple to perform, is suitable only to some types of food products, for example, such as dried food. Through PSL technique, all the samples were correctly distinguished between non-irradiated and irradiated based on photon count (PC) values (Ramli et al., 2016).

The other hand, the PCs of foods at dose 1 kGy and 5 kGy, were increase 278202 to 637054 PCs (mushroom), 62715 to 272929 (shrimp), 9578431 to 19211423 (Indian threadfin) and 26902 to 119016 (dates fruit). Respectively, which were upper threshold values 5000 counts/60s indicated the samples irradiated (EN 13751: 2009).

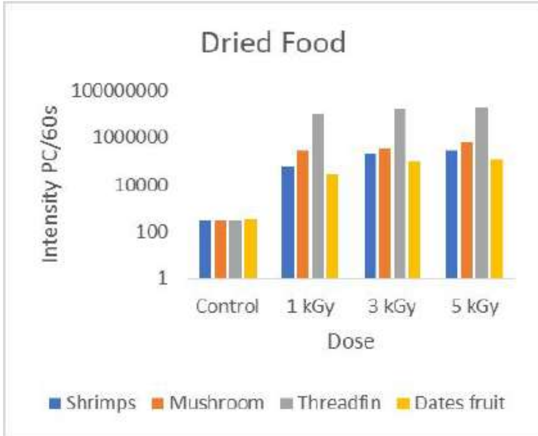

Figure 3: The signal intensity of non-irradiated and irradiated dried food (Shrimps, mushrooms, Indian threadfin and dates fruit)

4 Conclusion

Using screening PSL, all the samples were correctly distinguished between non- irradiated and irradiated samples at doses (1, 3 and 5 kGy) based on photon count values. The PCs of irradiated samples showed a general trend of increase with increasing doses.

References

I.S. Arvanitoyannis. 2010. Irradiation of food commodities: Techniques, applications, detection legislation, safety and consumer opinion. *Academic Press, Cambridge, MA*, 763.

H. Delincée. 2002. Analytical methods to identify irradiated food - a review. *Radiat. Phys. Chem.*, (63):455–458.

European Committee for Standardization. 2009. Foodstuffs – detection of irradiated food using photostimulated luminescence. *Brussels: European Committee for Standardization*, (EN 13751:2009).

Grzegorz Piotr Guzik and Jacek Michalik. 2021. European inter-comparison studies as a tool for perfecting irradiated food detection methods. *NUKLEONIKA 2021*, 66(3):91–97, doi: 10.2478/nuka–2021–0013.

T. Kume, M. Furuta, Uenoyama S., M. Kikuchi N., and Y. Kobayashi. 2009. Status of food irradiation in the world. *Radiat. Phys. Chem*, pages 222–226.

Ros Anita Ahmad Ramli, Muhamad Samudi Yasir, Zainon Othman, Wan Saffiey Wan Abdullah, Foziah Ali, and Zainab Harun. 2016. Detection of irradiated tubers (ginger and potato) using photostimulated luminescence (psl) technique. *Nuclear Malaysia RD Conference*.

P. B. Sukdeb, K. Kim, W.Y. Kim, M.J. Kim, H.A. Ki, W.S. Kang, Kang I. H., S. J. Kang, and J. M. Song. 2010. Pulsed photostimulate and thermo-luminescence investigations of -ray irradiated herbs. *Food chemistry 122*, pages 1290–1297.

Individual Research Contribution Review, 2023, 1(1): 315–316

Authentication of Malaysian Honey Using Stable Isotope Techniques

Salmah Moosa
Agrotechnology and Biosciences Division, Malaysian Nuclear Agency
43000 Kajang, Selangor
salmahmoosa@nm.gov.my

Abstract

The Official method of honey analysis (AOAC, 1999) is based on the stable-isotope ratio mass spectrometry analysis to detect the addition of C4 plant derived sugars, such as cane sugar. This method is used as the primary C4 sugar adulteration test around the world. We are now developing our own Malaysian honey standards through collaboration with Ministry of Health Malaysia, From the database collected, a predictive model in authentication and discriminate Malaysian honey by applying multivariate statistical analysis was developed. The model developed according to the AOAC test will reduce false identification of C4 sugars and can be used as a traceability tool to support surveillance control of honey and an effective tool to detect adulteration of honey products on Malaysian market shelves by Ministry of Health Malaysia.

Keywords: Honey authenticity; stable isotope ratio; C4 sugar; adulteration; authentication

1 Introduction

Honey is nature's most gratifying hand-out which comes power packed with health benefits, and it is one of the top ten most falsified food products in Europe (García., 2018). In Malaysia, about 80% of the honey in Malaysian market is direct adulteration with sugar which can be harmful to the health of consumers especially diabetics (Elflein and Raezke, 2008). While indirect adulteration occurs when the honeybees are fed with sucrose or other sugars by irresponsible beekeepers due to the demand of a competitive market. The most widely used method for honey analysis is undoubtedly chromatographic technique using LCMS and GCMS, but they are generally time-consuming, expensive, and unable to distinguish honey from bees fed with sugar.

IRMS is quite a well-established technique in the field of food authenticity because not only it can detect added sugar, but it can also determine the origin of the honey product (Pita-Calvo et al., 2017). The purpose of this method is to detect sugars from C4 plants (sugar cane) in honey. According to this procedure, honey is adulterated, if the C4 sugar percentage is ≥ 7%. honey involving the addition of sugar. The aim of the present study is to determine the C4 sugars in multifloral honey samples from Malaysia and to find a possible correlation between these two parameters.

2 Methods

2.1 Sampling of Honey

Sampling of honey were completed and the location of all the 52 samples in peninsular Malaysia are shown in Figure 1.

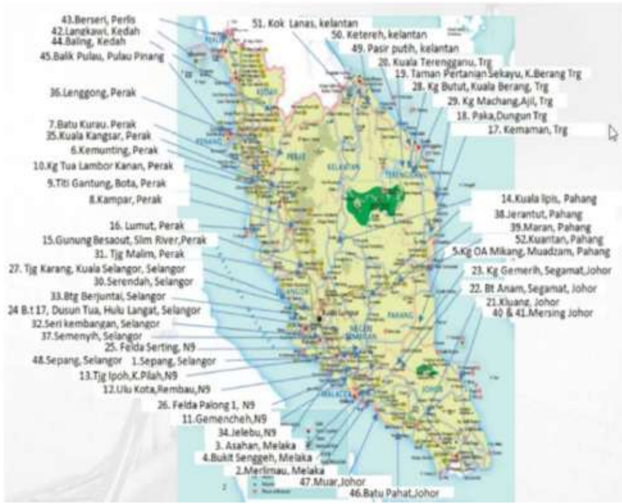

Figure 1: Location of the sampling of honey for 52 locations in Peninsular Malaysia

2.2 Sample Preparation for the analysis of stable ssotope carbon (δ13C) and nitrogen (δ15N) using IRMS

Extraction of honey is required to isolate the protein from sugar contents. 2 mL of 10% sodium tungstate and 2 mL of 0.33 M sulphuric acid were added to into 10-14 mL of honey in 50 mL tube. The tubes were then placed in water bath until visible floc forms with clear supernatant. The samples were washed several times steps by centrifugation. The final products, sugar and protein of the honey will be dried in an oven at 70°C and analyzed for 13C stable isotope delta value. Honey samples will be weighed (1.1–1.2 mg) into a tin capsule (5 x 9 mm), folded and compressed to contain the sample and minimize any air present before analysis by IRMS to determine C, N, O, and H contents and isotope ratios. Data will be recorded in the delta notation relative to an established standard.

For the EA-IRMS (determination of 13C values of honey and protein) analysis, the following procedures were applied: (a) For honey samples, 1 g honey sample were weighted and dissolved with 1 ml ultrapure water in a centrifuged tube and centrifuged for 5 min at 3500 rpm to remove insoluble impurities, then 3 μL of original honey sample was pipetted into a tin capsule. (b) For honey protein samples, 30–35 g of honey sample was mixed well with 20 mL of water in a 50 mL centrifuge tube. Then 3 mL of 100 g/L sodium tungstate solution and 3 mL of 0.335 mol/L sulfuric acid solution were added and mixed well. The centrifuge tube was subsequently placed in an 80°C water bath for at least 30 min until a visible protein floc had formed, with the tube being swirled for 20 s at 5–10 min intervals during the heating process. Then the tube was centrifuged for 5 min at 3500 rpm and the supernatant were decanted. This procedure was repeated three times to get the precipitated protein. 100–200 μg of each protein were weighed in small tin capsules using an MX-5 ultra-microbalance from Mettler-Toledo, Giessen, Germany. (AOAC Official Method 998.12, 1999).

3 Results and Discussions

3.1 Determination of Stable Isotope carbon (13C), nitrogen (15N) delta value (δ) in honey using IRMS.

The results indicated δ13C stable isotope analysis of raw stingless bee honey met the detection criteria as C3 plant source and as pure honey. All the samples are correctly verified as Kelulut honey from the Peninsular of Malaysia. The database was analyzed using Principal Component Analysis then, Orthogonal Partial Least Squares Discriminant Analysis (OPLS-DA) were used to classify samples into group as well as to build the authenticity model. To verify the authentication model developed for honey, market samples were obtained and analysed for authentic evaluation. Results of the analysis are shown in Figure 2.

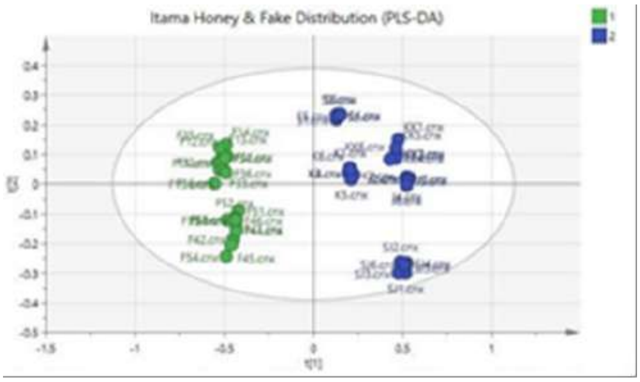

Figure 2: Distribution of the selected honey products from market compared to authentic and synthetic control with white sugar

There was a clear difference between raw stingless bee honey and synthetic honey.

4 Conclusion

IRMS is more efficient in detecting indirect adulteration from sugar fed honey compared to the other methods. In the current context of honey adulteration, IRMS is a more advanced techniques that must be further developed and harnessed at every stage of the supply chain, to combat honey adulteration.

References

AOAC. 1999. C-4 plant sugars in honey, internal standard stable carbon isotope ratio method. *AOAC official methods of analysis, 44.4.18A, Method 998.12 (1999, rev. 2013).*

E. Aries, J. Burton, L. Carrasco, O. De Rudder, and A. Maquet. 2016. Scientific support to the implementation of a coordinated control plan with a view to establishing the prevalence.

L Elflein and K. P. Raezke. 2008. Improved detection of honey adulteration by measuring differences between 13C/12C stable carbon isotope ratios of protein and sugar compounds with a combination of elemental analyzer-isotope ratio mass spectrometry and liquid chromatography-isotope ratio mass spectrometry 13C/12C-EA/LC–IRMS). *Apidologie*, 39(5):574–587.

Norberto L. García. 2018. The current situation on the international honey market. *Bee World*, 95(3):89–94.

Walter Lachenmeier. 2018. Application of nmr for authentication of honey, beer and spices. *Current Opinion in Food Science*, 19:pp. 57–6, ISSN 2214–7993.

Pita-Calvo, Consuelo, María Esther Guerra-Rodriguez, and Manuel Vazquez. 2017. Analytical methods used in the quality control of honey. *Journal of agricultural and food chemistry*, 65.4:690–703.

Application of Nuclear Technology in Extending Storage Time of Dried Mushrooms

Seri Chempaka Bt. Mohd. Yusof
Agrotechnology and Biosciences Division, Malaysian Nuclear Agency
43000 Kajang, Selangor
seri@nm.gov.my

Abstract

Gamma irradiation has the ability for decontamination of powdered dried mushrooms (*Pleurotus pulmonarius* and *Volvariella volvacea*) and reliable process for edible mushrooms storage in commercial industries. The mushrooms were dried at temperature of 45-55ºC, powdered and given gamma irradiation at 0 (control), 2, 5 and 10 kGy. At 2 kGy the ability to reduce the microbial loads (bacterial and fungal colonies) in powdered dried mushrooms and there was no presence of microbes after irradiated at 5 and 10kGy. Irradiation at dose 5 and 10kGy are suitable in maintaining the quality of the powdered dried samples and also extended the storage period.

Keywords: Gamma, Irradiation, Mushroom, Microbial, Storage

1 Introduction

Mushrooms have been consumed for century as food or food supplement due its delicate taste, flavour and therapeutic effects (Chockchaisawasdee et al., 2010). Literally, there are less than 25 species of edible mushroom out of more than 2000 species that exists. Oyster mushrooms (Pleurotus species) are commercially produced mushroom in the world and are cherished due to their culinary, nutritional, as well as medicinal properties (Singh et al., 2012; Deepalakshmi and Mirunalini, 2014).

Mushrooms are soft textured, highly perishable and prone to deterioration shortly after harvest if not stored properly. In view of their short shelf life under normal ambient conditions of temperature and humidity, it is imperative to preserve it by processing to extend shelf life for off season use. Drying is one of the common methods used for mushrooms for preservation owing to its easiness and economical nature (Kumar et al., 2013). According to Labuza and Altunakar (Labuza and Altunakar, 2007), the principle behind drying is primarily reduction of moisture to levels low enough to inhibit microbial growth and also slow down enzymatic and other biological reactions that may contribute to food spoilage. A common problem in the mushroom industries is related to storage period after drying procedures. Gradually in time dried mushrooms will be degraded by microbes after certain time in storage containment.

Food irradiation is the intentional exposure of food to ionizing radiation (such as gamma and electron beam) in order to enhance its shelf life without any detrimental effect on food quality as well as the safety of food. After decades of research, development, public debate and consumer acceptance trials in many countries, irradiation has emerged as a safe and viable technology for ensuring the safety and quality of food and for combating food-borne diseases. According to IAEA (IAEA, 2009) it is currently the best available technology according to as suitable for treating raw and partially raw food products and those countries which adopt it will benefit greatly in both domestic and international markets.

2 Methods

Powdered dried *Pleurotus pulmonarius* and *Volvariella volvacea* mushrooms were packed each 10gm in plastic packages, sealed, packed in boxes and sent for irradiation with doses 2 kGy, 5 kGy and 10 kGy. The control samples (0 kGy) and all irradiated samples were stored at room temperature for 0, 3, 6 and 9 months.

Samples (2g) in duplicates from the irradiated and their corresponding non-irradiated control batches were aseptically homogenized for 1 min with 225 ml sterile saline in a Stomacher (Seward Medical, UK). Appropriate serial dilutions of the homogenate were carried out. Total plate count by spread plate method, was determined using Plate Count Agar incubated at 30°C for 48 hours and Potato Dextrose Agar for molds (incubated at 30°C for 5 days). The results were expressed as colony forming units per gram (cfu/g).

Proximate composition analysis of the samples were carried out to determine the content (gram) of moisture, ash, protein, fat and carbohydrate using standard procedures according to the Association of Official Analytical Chemists (AOAC, 2002). Colour changes of the products were recorded using Colorimeter (Minolta) with L, a, b values i.e. Lightness (L), redness (a) and yellowness (b).

3 Results and Discussions

Irradiation at 2 kGy reduced the microbial and fungal loads in both powdered dried Pleurotus pulmonarius and Volvariella volvacea samples and there was no presence of microbes and fungi in samples irradiated at 5 and 10 kGy (Table 1 and 2). After storage at 3, 6 and 9 months, the fungal loads increased in the control samples but maintained low in samples irradiated at 2, 5 and 10 kGy. Although there were some changes observed for proximate compositions due to the gamma irradiation, the results obtained were no significant differences ($P<0.05$) and showed that the integrity of these compositions in the mushrooms were minimally affected as no adverse effects were observed.

Table 1: The number of fungal colonies in powdered dried *Pleurotus pulmonarius* samples after irradiation with different doses and storage time.

Doses(kGy)	Number Of Fungal Colony (CFU/g) - *Pleurotus pulmonarius*			
	Months Of Storage			
	0	3	6	9
0	$3.33x10^3$	$5.8x10^3$	$6.4x10^3$	$11.3x10^3$
2	$2.4x10^2$	$3.2x10^2$	$4.3x10^2$	$5.2x10^2$
5	0	$1.7x10^2$	$1.7x10^2$	$1.8x10^2$
10	0	$5.0x10^1$	$3.0x10^1$	$4.0x10^1$

Table 2: The number of fungal colonies in powdered dried *Volvariella volvacea* samples after irradiation with different doses and storage time.

Doses(kGy)	Number Of Fungal Colony (CFU/g) - *Volvariella volvacea*			
	Months Of Storage			
	0	3	6	9
0	$6.87x10^3$	$4.1x10^3$	$5.8x10^3$	$9.2x10^3$
2	$3.1x10^2$	$3.9x10^2$	$5.0x10^2$	$6.4x10^2$
5	0	$1.5x10^2$	$4.0x10^2$	$1.5x10^1$
10	0	$5.0x10^1$	$3.0x10^1$	$5.0x10^1$

There was significant reduction of lightness and increment of redness of both powdered dried mushroom samples after irradiation. However, there was no significant changes ($P<0.05$) in lightness and redness of all samples during storage. There was no significant increment of yellowness of both powdered dried mushroom samples after irradiation. There were also no significant changes ($P<0.05$) in yellowness of all samples during storage. Irradiation dose of 5kGy and 10kGy completely decontaminate the dried mushroom samples, but high doses are not recommended for food products as it would affect the taste and coloration. Irradiating with more than 7kGy negatively affect organoleptic features and meat quality including colour, flavour & oxidation rate (Rahimi et al., 2013). Irradiation with low doses (<5kGy) is suggested for reducing microbial load of food product.

The highly penetrative ionising energy has the ability to inactivate spoilage and disease-causing microorganisms without causing harmful changes to the products. The ionising energy passes completely through the products and their packaging. Thus, the products can be irradiated in their final packaging ready for the end-user. This process is a cold treatment and suitable to retain the acceptability of the products. Other food preservation methods such as chemical and heat treatment can kill microorganisms including pathogens. However, chemical leaves residues and heating treatment can change the texture, colour and flavour of the products .

Kortei et. al. (Kortei et al., 2017) stated that current research demonstrates the ability of gamma irradiation to be used in the preservation of nutritional qualities of foods as changes that occurred due to gamma irradiation were minimal irrespective of the packaging material used. Non-irradiated dried mushroom last not more than 6 months because of insect and pests damage. Additionally, gamma irradiation eliminated all these insects and pests to prolong its shelf life to 12 months. Gamma irradiation with its enormous attributes could be employed in food manufacturing industries to enhance product quality and shelf life.

4 Conclusion

Irradiation in conjunction with drying process inhibits fungal and microbial growth in powdered dried mushrooms and prolonged their shelf life. The ability of gamma irradiation to decontamination of dried powdered mushrooms (*Pleuratus pulmonarius* and *Volvariella volvacea*) is effective and reliable process for edible mushrooms storage in sustaining commercial industries sources.

References

AOAC. 2002. Official Method of Analysis. *16th Edition, Association of Official Analytical, Washington DC.*

S. Chockchaisawasdee, S. Namjaidee, S. Pochana, and C.E. Stathopoulos. 2010. Development of fermented oyster-mushroom sausage. *Asian Journal of Food and Agro-Industry*, 3:35–43.

K. Deepalakshmi and S. Mirunalini. 2014. Pleurotus ostreatus: an oyster mushroom with nutritional and medicinal properties. *J Biochem Tech.*, 5(2):718–726, ISSN: 0974–2328.

IAEA. 2009. Irradiation to ensure the safety and quality of prepared meals. *Vienna, Austria*, page 375.

N. K. Kortei, G. T. Odamtten, M. Obodai, and M. Wiafe-Kwagyan. 2017. Nutritional qualities and shelf-life extension of gamma irradiated dried Pleurotus ostreatus (Jacq. Ex. Fr.) Kummer preserved in two different storage packs. *Food Science and Technology*, 5(1):9–16.

A. Kumar, M. Singh, and D. Singh. 2013. Effect of different pretreatments on the quality of during solar. *J. Food Sci. Tech.*, 50(1):165–170.

T.P. Labuza and B. Altunakar. 2007. Diffusion and sorption kinetics of water in foods. In G. V. Barbosa-Canovas, A. J. Fontana, S .J. Schmidt T.P. Labuza, (Eds), Water activity in foods, fundamental applications. *Blackwell Publishing Ltd, Oxford*, pages 215–238.

MINTec-SINAGAMA. Food irradiation - A technology to preserve and improve food safety (pamphlet).

E. Rahimi, R Faghihi, M. Baradaran-Ghahfarokhi, A. Alavaian-Ghavanini, H. R. Baradaran-Ghahfarokhi, Z. Siavashpour, A. Farshadi, and F. Rafie. 2013. Effects of gamma irradiation on microbial load and quality characteristics of veal. *Adv Biomed Res.*, 2(11).

V. K. Singh, Y. Patel, and R. Naraian. 2012. Medicinal properties of Pleurotus species (oyster mushrooms). *World Journal of Fungal and Plant Biology*, 3(1):1–12.

Individual Research Contribution Review, 2023, 1(1): 319–320

Application of Nuclear Technology in Extending Storage Time of Selected Shelf Stable Fermented products

Seri Chempaka Bt. Mohd. Yusof
Agrotechnology and Biosciences Division, Malaysian Nuclear Agency
43000 Kajang, Selangor
seri@nm.gov.my

Abstract

Fresh packed fermented products were obtained from local producers and irradiated at doses of 2.0 kGy, 5.0 kGy and 10 kGy, using 60Co gamma irradiation source at MINTec-Sinagama. The irradiated and non-irradiated samples were displayed at room temperature storage periods for 2 weeks, 1 month, 3 months and 6 months. Microbiological analysis was carried out to determine status of bacteria and fungi counts. Colour changes were recorded and acceptability of the irradiated fermented products were determined through sensory evaluation by using 30 members (male and female) of untrained panellists. The fungal and microbial counts in both samples irradiated at 5 and 10 kGy were more lowered than samples irradiated at 2 kGy and increased after 3 months storage but maintained low in both irradiated samples. Both irradiated samples at 2 kGy and 5 kGy were more accepted in sensory evaluation especially the texture and taste and no significant changes ($P<0.05$) in lightness, redness, and yellowness of fermented cabbage samples during 3 months storage. Irradiation reduced the bloatness in the packaged fermented cabbages by reducing the count of bacteria in the products. These results showed the ability gamma irradiation for decontamination of selected fermented food and reliable process for food storage in commercial industries.

Keywords: Gamma, Irradiation, Mushroom, Microbial, Storage

1 Introduction

Irradiation offers a potential effort to enhance microbiological safety and quality of food through shelf-life extension. Fermented products are highly popular in Asian and African countries as the basic ingredients of the daily diet and lactic fermentation is a simple and often the only method for preservation of fruits and vegetables (Tamang, 2012). Fermented vegetable such as cabbage has an important role in the diet and nutrition and has become popular throughout the world. However, it has a very short shelf life because its microbiological and enzymatic activity which result in a quality deterioration due to a sour and bitter taste, off-order and softening. Mushrooms are appreciated for their organoleptic qualities as well as the presence of many different bioactive substances exhibiting healing and health-promoting properties(Jab lońska-Ryś et al., 2019). Edible mushrooms have a short shelf life due to rapid post-harvest changes. Therefore, lactic acid fermentation of wild and cultivated mushrooms is a cheap and efficient method of preservation. Generally, local fermented mushrooms (Pekasam cendawan) can be kept in room temperature and under chilled condition only for one and three days respectively. Local fermented cabbages require chilled condition for storage to avoid the packages bloated with CO_2 gas generated upon displayed and storage. Therefore, an inactivation of fermentative microorganisms is essential for the preparation of shelf stable foods. Studies were carried out to overcome arisen problems and to evaluate the suitability of irradiation in preserving local fermented mushrooms and cabbages.

2 Methods

Fresh packed fermented products were obtained from local producers and irradiated at irradiation doses of 2 kGy, 5 kGy and 10 kGy, using ^{60}Co gamma irradiation at MINTec-Sinagama. Until irradiation was over, non-irradiated samples (control) were kept in refrigerator. The irradiated and non-irradiated samples were displayed at room temperature storage period of 3 months. Samples (25g) in duplicates from the irradiated and their corresponding non-irradiated control batches were aseptically homogenized for 1 min with 225 ml sterile saline in a Stomacher (Seward Medical, UK). Appropriate serial dilutions of the homogenate were carried out. Total plate count by pour plate method, was determined using Plate Count Agar incubated at 30°C for 48 hours and Potato Dextrose Agar for molds (incubated at 30°C for 5 days). The results were expressed as colony forming units per gram (cfu/g).

Colour changes of the products were recorded using Colorimeter (Minolta) with L, a, b values i.e. Lightness (L), redness (a) and yellowness (b). Acceptability of the irradiated fermented products were determined through sensory evaluation using 30 members (male and female) of untrained panellists. A 5-point hedonic rating scale was used with 5 points as the most acceptable and 1 point as the most unacceptable. The attributes evaluated were colour, aroma, shape, texture, taste, chewiness, juiciness and overall acceptance. Statistical analysis using ANOVA test and comparisons were made by Duncan's multiple range tests.

3 Results and Discussions

Irradiation at 2 kGy reduced the fungal (Table 1) and microbial loads in irradiated local fermented cabbages (local kimchi) and samples irradiated at 5 and 10 kGy were more lowered and maintained low after storage at 3 months. Samples irradiated at 2 and 5 kGy were more accepted in sensory evaluation especially the texture and taste.

Table 1: The number of fungal colonies in fermented cabbages irradiated with different doses and storage time.

Doses(kGy)	Fungal count (cfu/g) 0 month	Fungal count (cfu/g) 3 months
0 (control)	2.4 x 10^3	3.6 x10^3
2	5.4 x10^2	7.4 x10^2
5	3.2 x10^2	4.6 x10^2
10	6.4 x10^1	8.1 x10^1

Samples irradiated at 10 kGy were totally changed in the texture and taste acceptance. However, there were no significant changes (P<0.05) in lightness, redness and redness of all samples after 3 months storage. The control samples generate gases during display and storage and the packaging became bloated. This is because the growth of lactic acid bacteria in the fermented products keep increasing and emit gases (Hong-sun et al., 2003). In this studies irradiation at 2, 5 and 10 kGy prevented the bloat in the packaging of fermented cabbages by reducing the count of bacteria in the products.

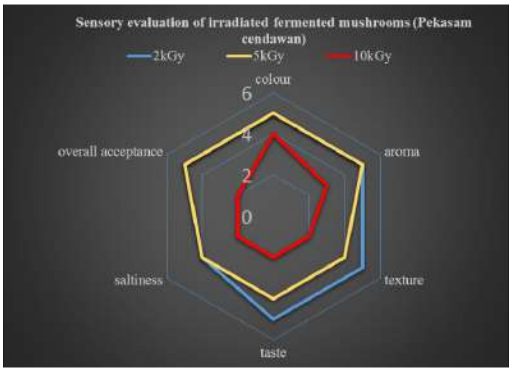

Figure 1: Sensory evaluation of irradiated fermented mushrooms (Pekasam cendawan) samples after 3 months storage.

Irradiation at 5 kGy reduced the fungal and microbial loads in irradiated local fermented mushrooms (Pekasam cendawan) samples compared to the control samples and maintained low after 3 months storage. The control samples were spoiled after being displayed one day in room temperature and the fungal and microbial loads increased and spoiled after being kept in chilled temperature for 3 months. Samples irradiated at 2 and 5 kGy were more accepted in sensory evaluation especially the texture and taste. However, samples irradiated at 10 kGy were not acceptable due to changes in texture (soften) and taste (Figure 1). Samples irradiated at 5 and 10 kGy become darker after 3 months storage. Earlier studies have been carried out to control the fermentation process using various treatments such as high pressure treatment, heat treatment, antimicrobial agents, chemical additives and microbial additives (Jang et al., 2015). Although they could retard the fermentation slightly, it is difficult to control the microbial and enzymatic activities during storage, distribution and to keep the product intact (Jeong et al., 2020). Ionizing irradiation is one of the food preservation techniques with minimum interruption to the functional, nutritional, and sensory properties of food products at lower doses. However, high dose irradiation, especially higher than 10 kGy, can lead to physicochemical changes and significantly deteriorate sensory properties of foods (Kim et al., 2006). It is considered a more effective and appropriate method to enhance food stability and safety, when compared to other processing methods like heat and chemical methods (Arapchesk et al., 2020).

4 Conclusion

Irradiation at dose 2 and 5 kGy was suitable in preserving local fermented mushrooms (Pekasam Cendawan) and local fermented cabbages as shelf stable products and accepted in morphology and sensory evaluation. These products can be displayed or kept at room temperature for 1 to 3 months (maximum). These results showed the ability of gamma irradiation for decontamination of selected fermented food and reliable process for food storage in commercial industries.

References

M. Arapchesk, H. Spasevska, and M. Ginovska. 2020. Effect of irradiation on food safety and quality. *Current Trends in Natural Sciences*, 9(18):100–106, DOI:10.47068/ctns.2020.v9i18.014.

Y. Hong-sun, K. Dong-Ho, S. Hyun-Pa, L. Hyun-Ja, and B. Myung-Woo. 2003. Effect of gamma irradiation on the fermentative microorganisms and lactate dehydrogenase activity in kimchi at different fermentation stages. *J. Food Sci Nutr.*, 8:265–269.

E. Jab lońska-Ryś, K. Skrzypczak, A. S lawińska, W. Radzki, and W. Gustaw. 2019. Lactic acid fermentation of edible mushrooms: tradition, technology, current state of research: a review. *Journal of Comprehensive Reviews in Food Science and Food Safety*, 18(3):655–669.

J. Y. Jang, M. E. Lee, H. W. Lee, J. H. Lee, H. W. Park, H. J. Choi, Y. R. Pyun, and Kim. T. W. 2015. Extending the shelf life of Kimchi with Lactococcus lactis strain as a starter culture. *Food Sci. Biotechnol.*, 24(3):1049–1053, DOI 10.1007/s10068–015–0134–8.

S.G. Jeong, J. E. Yang, J. H. Park, S.H. Ko, I. S. Choi, Ho Myeong Kim M., H. H. Chun, M. J. Kwon, and H. W. Park. 2020. Gamma irradiation improves the microbiological safety and shelf-life of kimchi seasoning mixture. *LWT- Food Science and Technology.*, 134(110144, https://doi.org/10.1016/j.lwt.2020.110144).

J. G.and Kim J. H.and Park J. N.and Lee H. J. Kim, M. J.and Park, W. G. Kim, J. W. Lee, and M. W. Byun. 2006. Combined effect of heat treatment and gamma irradiation on the shelf- stability and quality of packaged Kimchi during accelerated storage condition. *Korean Journal of Food Preservation*, 13:531–537.

J. P. Tamang. 2012. Plant-based fermented foods and beverages of Asia. In Y.H. Hui (Ed.). *Handbook of plant-based fermented food and beverage technology*, pages pp. 49–90, Boca Raton, FL: CRC Press.

Individual Research Contribution Review, 2023, 1(1): 321–322

Mutation Breeding of Napier Grass (*Pennisetum purpureum*) using Acute Gamma and Chronic Irradiation for High Quality Animal Feed

Shakinah Salleh
Agrotechnology and Biosciences Division, Malaysian Nuclear Agency
43000 Kajang, Selangor
shakinah@nm.gov.my

Abstract

Napier is among the most important feed resources for livestock. Even though it was introduced into Malaysia almost a century ago, very little research on breeding for improvement of this species has been reported in this country. A mutation breeding programed for Napier grass using acute and chronic gamma irradiation was carried out to generate new improved varieties with good biomass yield and nutritive quality for livestock. Two varieties which are cultivar Dwarf and Taiwan were irradiated using acute gamma ray at doses 0 (non-irradiated control), 10, 20, 30, 40, 60, 80 and 100 Gy; and chronic gamma (Gamma Greenhouse) with the total of accumulated doses ranging from 0 (control) to 1089.86 Gy. Survived cuttings after irradiation treatments were propagated and frequently screened for potential mutant lines which are high in biomass yield, vigorous growth, good nutritional contents and resistance to pest and diseases.

Keywords: Napier, *Pennisetum purpureum*, mutation breeding

1 Introduction

Napier grass was first introduced to Malaysia in the 1920's. Napier grass is one of most popular fodder grass in dairy and feedlot production systems. Some popular cultivars are Taiwan Napier, Dwarf Napier, King Grass and Red Napier. According to Halim et al (2013), there are morphological differences between the varieties and clearly divided into two distinct group based on the plant height which are greater than 139 cm (taller varietis) or less than 95 cm (Dwarf varieties). Some of the taller varieties are King Grass, Common Napier and Taiwan Napier; and Dwarf varieties are Dwarf Napier, Dwarf 'Mott' and Australian Dwarf. The Dwarf varieties were leafier and also had higher nutritive quality than the taller varieties.

Very little research on breeding program for improvement of Napier grass has been reported in Malaysia. Therefore, there is a high need to initiate a mutation breeding programmed for Napier grass using acute and chronic gamma irradiations in order to improve its yield and nutritive values for livestock. Gamma radiation is a promising method to induce genetic variation in variable crops (van Harten, 1998) including vegetative propagated crop. The ultimate aim of this study is to improve Napier grass through mutation breeding with targeted breeding traits such as high biomass and high protein content for ruminant consumption. These are among the important traits needed to produce high quality animal feed.

The mutation breeding work was carried at Malaysian Nuclear Agency using two facilities for mutation induction in plants for both acute (high dose) and chronic (low dose) irradiation. Both irradiators use consist of Caesium-137 as the radioactive source. Biobeam GM8000 gamma cell is the acute gamma irradiation facility that produces high dose radiation whilst Gamma Greenhouse (GGH) is a chronic gamma irradiation facility that provides low dose radiation. Chronic gamma irradiation produces a wider mutation spectrum and useful for minimizing radiation damages towards obtaining new improved traits for research and commercial values.

2 Methods

2.1 Plant Material

Two varieties of Napier grass used in this study (cv. Dwarf and cv. Taiwan) were obtained from Malaysian Agricultural Research and Development Institute (MARDI) collection. The healthy and uniform size stems for each variety were cut into approximately 25 cm segments that contain 2 to 3 nodes. The cuttings were cleaned and sent for irradiation at Malaysian Nuclear Agency.

2.2 Gamma Irradiation

- **Acute Irradiation**

Acute irradiation was carried out using Gamma Cell (Biobeam GM8000, Germany). The cuttings were packed and loaded into BB13-5 container of 29.2 cm height and 10 cm diameter. A total of eight dose treatments were used in this study which were 0 (non-irradiated control), 10, 20, 30, 40, 60, 80, 100 Gy at the dose rate of 15.7 Gy/min. Each treatment was consisted of 25 cuttings. Irradiated cuttings were then planted into polybag for germination and subsequently cut for multiplication for several generations in the glasshouse.

- **Chronic irradiation**

The cuttings were exposed to chronic radiation at Gamma Greenhouse (GGH). GGH is a circular greenhouse of 15-meter radius consisting of 15 isodose rings in which every ring has different dose rate per hour. For this study, ten treatments which were 0 (non-irradiated control), ring 2 (0.66 Gy/h), 3

(0.33 Gy/h), 4 (0.17 Gy/h), 5 (0.11 Gy/h), 6 (0.07 Gy/h), 7 (0.05 Gy/h), 8 (0.04 Gy/h), 9 (0.03 Gy/h), 11 (0.02 Gy/h) and 12 (0.02 Gy/h) were involved. A total of 12 cuttings were planted in containers in each ring. The accumulated dose for each ring was calculated based on dose rate and time of exposure. Due to the low dose rate nature of chronic gamma irradiation, the cuttings were exposed for three consecutive months in GGH before being transferred to a regular glasshouse for germination and multiplication for mutant selection.

2.3 Morphological and physiological evaluation of potential mutant plants

At M1V4 generation, a total of 129 variant lines were selected based on morphological variation and vigorousness among the irradiated population. These selected variant lines were further planted at M1V5 generation for evaluation of their major morphological and physiological characteristics in the glasshouse. At M1V5 generation, mutant lines are considered phenotypically stable. Measurement on main morphological and physiological traits of the potential mutant lines were focused on the number of leaves, plant height, stem diameter, inter-node length, leaf area, leaf length, average leaf width, maximum leaf width and chlorophyll content. All studied characters of the potentials mutants were analyzed and compared with the control.

3 Results and Discussions

From this study, a total of 29 potential mutant lines which produced higher biomass than the control were selected as below.

No	Mutant lines	Type of Radiation	Dose (Gy)	Traits
	cv. Dwarf			
1.	DA20A	Acute	20	Higher biomass
2.	DA20B	Acute	20	Higher biomass
3.	DA20C	Acute	20	Higher biomass
4.	DA30.5	Acute	30	Higher biomass
5.	DA40A	Acute	40	Higher biomass
6.	DA40B	Acute	40	Higher biomass
7.	DA40C	Acute	40	Higher biomass
8.	DA40D	Acute	40	Higher biomass
9.	DA40E	Acute	40	Higher biomass
10.	DA40.4	Acute	40	Higher biomass
11.	DA60A	Acute	60	Higher biomass
12.	DA80A	Acute	80	Higher biomass
13.	DA80B	Acute	80	Higher biomass
14.	DA80C	Acute	80	Higher biomass
15.	DA100A	Acute	100	Higher biomass
16.	DA100.2	Acute	100	Higher biomass
17.	DA100.5	Acute	100	Higher biomass
18.	DA140A	Acute	140	Higher biomass
19.	DA180A	Acute	180	Higher biomass
20.	DA180B	Acute	180	Higher biomass
21.	DC80.2	Chronic	80	Higher biomass
22.	DC95.3	Chronic	95	Higher biomass
23.	DC150.5	Chronice	150	Higher biomass
24.	DC409.5	Chronic	409	Higher biomass
	cv. Taiwan			
25.	TC65.1	Chronic	65	Higher biomass
26.	TC178.3	Chronic	178	Higher biomass
27.	TC178.4	Chronice	178	Higher biomass
28.	TA20.5	Acute	20	Higher biomass
22.	TA30.3	Acute	30	Higher biomass

All these potential mutants will be further planted in the field to obtain the DUS (Distinctiveness, Uniformity and Stability) data. The DUS data is important for filing and registration of New Plant Variety with the Malaysian Department of Agriculture before the mutant can be used for further commercialization.

Figure 1: Greenhouse screening of potential Napier mutants.

References

Halim R.A., Shampazurini S., and Idris A.B. 2013. Yield and nutritive quality of nine napier grass varieties in malaysia. *Malaysian Journal of Animal Science*, 16(2):37–44.

A. M. van Harten. 1998. Mutation breeding: Theory and practical applications. *Cambridge, UK: Cambridge University Press.*

Individual Research Contribution Review, 2023, 1(1): 323–324

Study on the Effectiveness of AWD Water Management Method in Rice Cultivation

Shyful Azizi bin Abdul Rahman
Agrotechnology and Biosciences Division, Malaysian Nuclear Agency
43000 Kajang, Selangor
shyful@nm.gov.my

Abstract

A study was conducted in rice observation plots at the Rice Seed Production Center, Sungai Burong, Selangor, covering an area of 2.57 acres (1.04 hectares) for three seasons. The aim was to compare the crop yields between conventional continuous flooding (CF) and Alternate Wetting and Drying (AWD) practices. Results showed that, there was no significant difference (P>0.05) in yields between T0 (CF) and T1 (AWD). However, there was a notable difference in the total amount of water input and water use efficiency between the two practices. Despite achieving similar yields, fertilizer uptake, w.r.t nitrogen, was lower in AWD compared to CF.

Keywords: AWD, CF, rice

1 Introduction

The Alternate Wetting and Drying (AWD) method is an irrigation approach used in rice cultivation, allowing the initial standing water level to recede for several days until it dries (water level below the soil surface) before rewatering to the original level. The number of non-submerged days varies from 1 to 5 days, depending on the soil type. This method can significantly reduce water usage compared to conventional practices involving continuous flooding throughout the growing season. The technology has proven effective in decreasing methane emissions which generated in anaerobic condition by methanogenic bacteria in soil. However, further studies are needed to assess the suitability of this method in terms of yields, as well as water and nutrient efficiency.

2 Methodology

Land preparation and experimental design for the study:

2.1 Plot Design

Refer Figure 1.

2.2 AWD Tube Design

Refer Figure 2.

2.3 15N Experimental Design

Refer Figure 3.

3 Data/Result

The data obtained throughout the study:

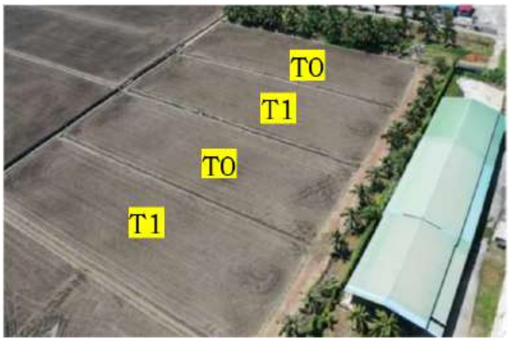

Figure 1: Design and plot arrangement

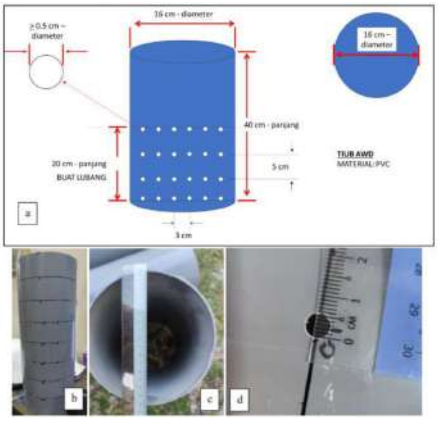

Figure 2: The design of the Alternate Wetting and Drying water level monitoring tube (AWD Tube) using PVC pipes.

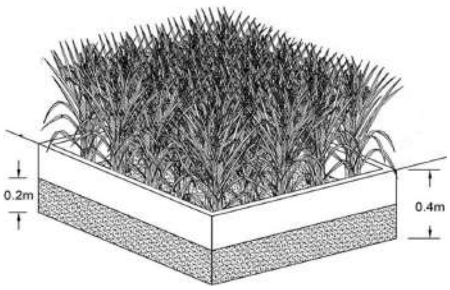

Figure 3: Perspex material Microplot (1m x 1m) for nitrogen uptake study using 15N labelled urea fertilizer.

3.1 Water level monitoring

Refer Figure 4.

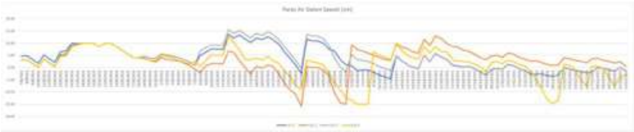

Figure 4: Example of water level data (Season 1/2022). There were 2 periods where the water was below the soil surface in the AWD treatment plot (T1).

3.2 Water usage

Refer Table 1.

Table 1: Water usage per kg of grain yield

Treatment	Season 1/2021: Total water use per kg of grain yield	Season 2/2021: Total water use per kg of grain yield	Season 1/2022: Total water use per kg of grain yield
CF (T0)	6891.19	9265.50	8205.11
AWD (T1)	5898.71	4990.10	5235.19

3.3 Yield components

Refer Figure 5.

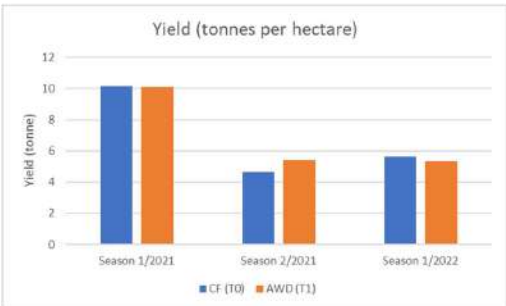

Figure 5: Yield in 3 seasons for CF (T0) and AWD (T1)

3.4 15N analysis

Refer Figure 6.

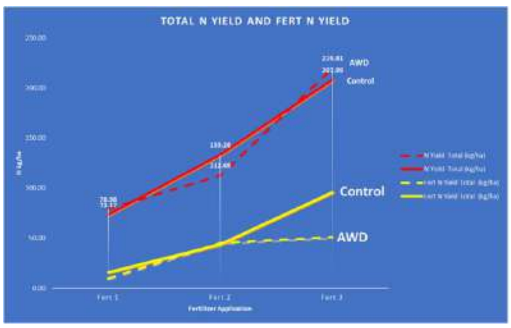

Figure 6: Nitrogen uptake derive from fertilizer and total nitrogen uptake.

4 Discussion/ Conclusion

4.1 Water use efficiency

The water usage for the AWD method across all three seasons is significantly lower compared to the conventional method, with a reduction ranging from 20 to 40 percent. The AWD method is highly suitable for reducing water consumption, especially in limited water supply areas.

4.2 Yield comparison

The results revealed no significant difference in yields between the AWD and CF methods across all three seasons. The decrease in yields during the second and third seasons was attributed to pest infestation. This suggests that the AWD method can be employed without negatively impacting crop yields.

4.3 Nitrogen use efficiency

The AWD method results in reduced nitrogen uptake. Nevertheless, the total nitrogen uptake by plants remains consistent for both treatments. This suggests that under certain period of aerobic conditions (AWD method), nitrogen based organic compounds decompose and become available to plants. Additional research is advisable to explore the potential reduction in nitrogen fertilizer input for the AWD method.

References

International Atomic Energy Agency. 2001. Use of isotope and radiation methods in soil and water management and crop nutrition. *Training Course Series No. 14. Vienna, Austria*.

B.A.M Bouman, R.M. Lampayan, and T.P. Tuong. 2007. Water management in irrigated rice: Coping with water scarcity. *International Rice Research Institute. Los Baños, Philippines.*

Siopongco JDLC, Wassmann R, and Sander BO. 2013. Alternate wetting and drying in philippine rice production: feasibility study for a clean development mechanism. *IRRI Technical Bullettin, Los Banos, Philippines: International Rice Research Institute (IRRI)*, 17.

Richards M. and Sander B. O. 2014. Alternate wetting and drying in irrigated rice: Implementation guidance for policymakers and investors. *Climate Change, Agriculture, and Food Security Info Note. International Rice Research Institute. Los Baños, Philippines.*

Individual Research Contribution Review, 2023, 1(1): 325–326

Production of Polysaccharide (*Pleurotus* sp. and *Auricularia* sp.) in Submerged Culture Fermentation Using UVC for Applications in Biotechnology Industries

Shaiful Azuar Mohamad
Agrotechnology and Biosciences Division, Malaysian Nuclear Agency
43000 Kajang, Selangor
azuar@nm.gov.my

Abstract

The submerged culture fermentation (SCF) has been proven to be a viable option to produce products to be used in various applications. Various benefits also have been reported regarding the applications of *Auricularia* sp. and *Pleurotu*s sp, hence its production is being explored using SCF. *Auricularia* sp. and *Pleurotus* sp. mycelium were cultured in the petri dish from the stock culture. Ultraviolet C (UVC) irradiation was then applied to the petri dish and then the mycelium was transferred to the shake flask. The shake flasks were then harvested for its biomass. The irradiated biomass of *Auricularia* sp. increased by approximately 26-30% compared to the control. However the biomass of *Pleurotus* sp. was not affected by the UVC. Thus, UVC irradiation was able to increase its biomass of *Auricularia* sp., hence polysaccharide. The β-glucan content of the *Auricularia* sp. showed at 8.66 mg/100mg, whilst the *Pleurotus* sp showed at 7.70 mg/100mg samples.

Keywords: submerged culture fermentation, ultraviolet C irradiation, Auricularia sp, Pleurotus sp., biomass

1 Introduction

Various benefits also have been reported regarding the applications of *Auricularia* sp. and *Pleurotus* sp. such as anti-tumor, antioxidant, anti-coagulant and immunomodulating effects on human. Other properties such as antimicrobial, antibacterial, antitumor activities as well as anti-hypercholesteremic were reported by Bandara et al. (Bandara et al., 2019) and Miao et al. (Miao et al., 2020) whilst Sun et al. (Sun et al., 2016) reported the production of melanin from *Auricularia auricula*. These properties indicated that *Auricularia* sp. contained beneficial sources for pharmaceutical products. Various reports also explained in detail about *Pleurotus* sp, applications (Kozarksi et al., 2014).

The submerged culture fermentation (SCF) has been proven to be a viable option to produce polysaccharides to be used in various applications. Mohamad et al. (Mohamad et al., 2015) has reported the production of *Pleurotus flabellatus* successfully using bioreactor to be used in the industry.

Ultraviolet irradiation has been reported to be able to enhance the production of mushroom biomass in SCF through elicitation process. Past research had showed that the use of UVC irradiation on mycelia can produce high biomass as well as antimicrobial activities (El-Fallal et al., 2013; Tetiana et al., 2018).

2 Methods

Auricularia sp. and *Pleurotus* sp. mycelium was cultured in the petri dish from the stock culture. UVC dose mapping was done to determine the dose at mapped locations in a biosafety cabinet. Then UVC irradiation was applied to the petri dish at calculated doses between 0-2.28 J/cm^2 when the petri dish was half full. After irradiation the mycelium was allowed to grow in the petri dish. After allowing to settle 3 more days in the petri dish, the mycelium was then transferred to the shake flask (250ml working volume) and then harvested for its biomass after 14 days. The biomass was dried in a drying oven before its dry weight measured. The dried biomass was then extracted using hot water extraction and its β-glucan (1,3:1,6) content was determined using assay kit by Megazyme (Mohamad et al., 2015).

3 Data/Results

Table 1 showed the the dry weight of Auricularia sp. obtained from the shake flask.

Table 1: Biomass harvested at different UVC doses

Doses (J/cm^2)	Biomass in Flask (g)					Sum (g)	Mean (g)	Increase (%)
	1	2	3	4	5			
Control	1.46	2.36	2.56	2.04	2.39	10.81	2.162	NA
0.57	1.70	2.74	2.51	3.80	3.85	14.60	2.920	25.96
1.14	3.13	2.74	2.84	2.83	3.96	15.50	3.100	30.26
2.28	2.93	2.65	3.75	2.76	2.52	14.61	2.922	26.01

The irradiated biomass increased by approximately 26-30% compared to the control. Thus, UVC irradiation is able to increase its biomass, hence polysaccharide.

The biomass of *Pleurotus* sp. however was not affected by the UVC.

Table 2 showed the β-glucan content of the *Auricularia* sp. endopolysaccharides obtained after hot water extraction of the biomass.

From the assay-kit, the total glucan of the endopolysaccharides was determined to be 14.97g/100g sample whilst the α-glucan was determined to be 6.31g/100g. Thus the β-glucan was determined to be 8.66g/100g.

Table 3 showed the β-glucan content of the *Pleurotus* sp. endopolysaccharides obtained after hot water extraction of the biomass.

Table 2: β-glucan content of the *Auricularia* sp. endopolysaccharides

Sample	Total glucan (g/100g)	α-glucan (g/100g)	β-glucan (g/100g)
Control	50.33	0.312	52.02 (Std 49%)
EndoP	14.97	6.31	8.66

Table 3: β-glucan content of the *Pleurotus* sp. endopolysaccharides

Sample	Total glucan (g/100g)	α-glucan (g/100g)	β-glucan (g/100g)
Control	63.98	2.38	61.61 (Std 58.5%)
EndoP	17.54	9.84	7.70

From the assay-kit, the total glucan of the *Pleurotus* sp. endopolysaccharides was determined to be 17.54g/100g sample whilst the α-glucan was determined to be 9.84g/100g. Thus the β-glucan was determined to be 7.70g/100g.

4 Discussion/ Conclusions

In the case of the control experiment both controls showed very close value to the standard supplied from the kit. which showed that the test was done according to the established method provided with the assay-kit.

The biomass can be produced consistently in bioreactor and early indication showed that UVC can be utilized to increase the biomass production of *Auricularia* sp. but not *Pleurotus* sp. Both polysaccharide contained β-glucan which indicated that the research should be continued further for its efficacy.

References

A. R. Bandara, S. Rapior, P. E. Mortimer, P. Kakumyan, K. D. Hyde, and J. Xu. 2019. A review of the polysaccharide, protein and selected nutrient content of Auricularia, and their potential pharmacological value. *Mycosphere*, 10(1):579– 607, https://doi.org/10.5943/mycosphere/10/1/10.

A.A. El-Fallal, A.K.A. El-Sayed, and H.M. El-Gharabawy. 2013. Improving yield and productivity of oyster mushroom (Pleurotus columbinus) using ultra violet mutation. *Journal of Environmental Sciences*, 42(2):241–253.

M. S. Kozarksi, A. S. Klaus, M. P. Niksic, L. J. L. D. Van Griensven, M. M. Vrvic, and D. M. Jakovljevic. 2014. Polysaccharides of higher fungi: biological role, structure and antioxidative activity. *Hemijska Industrija*, 3:305–320.

J. Miao, J. M. Regenstein, J. Qiu, J. Zhang, X. Zhang, H. Li, H. Zhang, and Z. Wang. 2020. Isolation, structural characterization and bioactivities of polysaccharides and its derivatives from Auricularia-A review. *International Journal of Biological Macromolecules*, 150:102–113, https://doi.org/10.1016/j.ijbiomac.2020.02.054.

S.A. Mohamad, M.R. Awang, R. Ibrahim, C.Y. Keong, M.Y. Hamzah, R. Abdul Rashid, S. Hussein, K. Abdul Rahim, F. Daud, A. Abdul Hamid, and W.M. Wan Yusof. 2015. Production of Endopolysaccharides from Malaysia's local mushrooms in air-lift bioreactor. *Advances in Bioscience and Biotechnology*, 6:456–462.

S. Sun, X. Zhang, S. Sun, L. Zhang, S. Shan, and H. Zhu. 2016. Production of natural melanin by Auricularia auricula and study on its molecular structure. *Food Chemistry*, 190:801–807.

K. Tetiana, B. Victor, K. Tetiana, K. Hanna, A. Hanna, and T. Olena. 2018. Effect of ultraviolet c irradiation on growth and antibacterial activity of Fomitopsis betulina (Bull.) b.k. cui, m.l. han and y.c. dai. *GSC Biological and Pharmaceutical Sciences*, 04(03):001–006.

Individual Research Contribution Review, 2023, 1(1): 327–328

Development and Commercialization of Climate-Resilient Rice Varieties to Increase National Yield Production

Sobri Hussein
Agrotechnology and Biosciences Division, Malaysian Nuclear Agency
43000 Kajang, Selangor
sobri@nm.gov.my

Abstract

Malaysia's National Agrofood Policy (NAP 2.0) was formulated with a special focus on improving the food production sector including rice, and strengthening country food supply and food security. Even though Malaysia is still depending on imported rice to fulfil consumer's demand, rice industry has always been a national priority based on its strategic importance as a staple food commodity. Nevertheless, the rice industry in Malaysia is hampered by several challenges such as global climate change, flash flooding, rising prices of pesticides, unauthorized seeds, rapid development in rural area, lacking new variety, insufficient certified and high-quality seeds, emerging of major diseases such as Bacterial Panicle Blight (BPB), Leaf Blast, drought season, decreasing of planting area, lost interest of the farmers due to high cost of rice production and many others. Apart from that, according to the local newspapers, currently, farmers are facing huge problem with the flash flood and plant disease caused by brown planthopper. To increase the country's rice self-sufficiency ratio (SSR), Malaysia needs to increase the current average rice yield (3.64 tonnes per hectare) in order to reduce dependence on rice imports. Besides the increase in population, climate change and global geopolitical conflicts have also affected the cost of agricultural production and the sustainability of the food supply.The development of new high-yielding rice cultivars resistant to abiotic and biotic stresses can provide a more sustainable long-term solution and increase the income of farmers in Malaysia, the majority of whom belong to low-income groups. This study aims to find solutions through the development and commercialization of new high-yielding, early-maturing rice cultivars that are resistant to global climate change using mutation breeding and molecular assisted breeding (MAB).

Keywords: Gamma Irradiation, Ion Beam, Mutation Breeding, MINT, NMR152, NMR151 & Rice.

1 Introduction

In Malaysia, rice industry has always been a priority based on strategic importance of rice as a staple food commodity. Although the production of rice is increasing towards population increase, Malaysia still depends on imported rice to meet the consumer's demand. Malaysia managed to achieve 72% self-sufficiency level in rice with the current average rice yield of 3.7t/ha/season. In this situation, about 28% of the local demand will have to depend on imported rice. In Peninsula Malaysia, rice production depends largely on the irrigated lowland production system. Currently, there are 241,741ha of irrigated rice in Peninsula Malaysia, which contributes more than 85% of the national rice production. Induced mutation is an important supplementary approach to plant breeding, particularly when it is desired to improve one or two easily identifiable traits in an otherwise good lines or varieties. The successful use of plant breeding for improving crops requires the existence of genetic variation of useful traits. Unfortunately, the desired variation is often lacking. However, radiation can be used to induce mutations and thereby generate genetic variation from which desired mutants may be selected. Mutation induction has become a proven way of creating variation within a crop variety.

2 Materials and Methods

Evaluation of mutant lines derived from gamma irradiation

The seeds of popular local variety, MR219 were irradiated with 300Gy of gamma radiation from the Cobalt-60 (^{60}Co source) at Malaysian Nuclear Agency. Irradiated seeds were sown at Mardi Research Station in Tanjung Karang, Selangor. The M1 seedlings were transplanted into the field with 25cm x 25cm planting distance. A total of 10,000 M1 seedlings were planted to produce M2 seeds and a total of 5,250 plants were selected from which 2 panicles per hill were randomly harvested from each hill. After M6 generation, the best selected mutant line were further evaluated for MLT (Multi Location Trial), LVT (Local Verification Trial), disease screening, morphology and agronomy characteristics. The best selected line were planted for 4 seasons and the data on culm height, panicle length, number of panicle per plant, flowering time, day of maturity, weight for 1000 grain seed, seed length, width length and yield in t/ha were collected. This study was conducted in collaboration with MARDI (Malaysian Agriculture Research and Development Institute), MADA (Muda Agricultural Development Authority), KADA (Kemubu Agricultural Development Authority), IADA (Integrated Agricultural Development Area), Department of Agriculture Malaysia (DOA), HMN (M) Sdn Bhd), BAYER Co (M) Sdn. Bhd. and farmers. The locations for field trial were inclusive of Northern part until Southern part of Peninsular Malaysia with the planting area of approximately one hectare per variety.

3 Results and Discussions

Evaluation of mutant lines derived from gamma irradiation

Malaysian Nuclear Agency has moved one step forward in the area of mutation breeding by signing the Memorandum of Understanding (MoU) with Certified Seed Company HMN (M) Sdn. Bhd and Bayer Co. (MALAYSIA) Sdn. Bhd. on 29 April 2019. With this agreement, HMN (M) Sdn. Bhd. will collaborate with Malaysia Nuclear Agency to produce certified seeds, multiply and commercialize the rice mutants. Meanwhile, Bayer Co. (MALAYSIA) Sdn. Bhd. will be responsible in coating the mutant seeds with plant growth promoters. This collaboration will add value to NMR 151 and NMR 152 mutant seeds and result in more competitive seeds as compared to other varieties in the market. In addition, from 2016 until 2020, several local verification trails (LVT) and multi-location trial (MLT) were also conducted from the Northern part until the Southern part of Peninsular Malaysia (Table 1). The data obtained from the field trial at Sekinchan, Selangor revealed that NMR 152 consistently produced between 9-10 t/ha in granary area as compared to 6 t/ha produced by other varieties within the same planting areas. Field trials also showed that the production cost was reduced by 10%, mainly due to the reduction in fertilizer and pesticide usage. At the same time, the yield could be increased between 40 - 60%, depending on the planting areas (Table 1). Table 2 shows the yield of NMR 152 using different evaluation methods in the farmers' field. The data revealed that Wheel method that introduced by the Agriculture Department is the most accurate methods in estimating the yield of mutant rice in an open field.

Table 1: Yield increment in different state of Malaysia as compared with data from MOA

Location (State)	**Average Yield From MOA (Agro-food Statistics 2018)**	**Average Yield NMR152 (PBR 0156)**	**Yield Increment (t/ha)/(%)**
Perlis	5 t/ha	7 t/ha	2 (40%)
Kedah	5 t/ha	8 t/ha	3 (60%)
Penang	5 t/ha	7 t/ha	3 (60%)
Perak	3 t/ha	5 t/ha	2 (67%)
Pahang	2 t/ha	6 t/ha	4 (67%)
Selangor	6 t/ha	10 t/ha	4 (67%)
Johor	3 t/ha	5 t/ha	2 (67%)

(Note: PBR = Certificate of registration of new plant variety and grant of breeder's right, MOA = Ministry of Agriculture and Food Industries, Malaysia)

4 Conclusion

In summary, the data obtained from the farmers revealed that NMR 152 had consistently produced between 9-10 t/ha in granary area as compared to 6 t/ha produced by other varieties within the same planting areas. Field trials also showed that the production cost was reduced by 10%, mainly due to the reduction in fertilizer and pesticide usage. At the same time, the yield could be increased between 40 - 60%, depending on the planting areas. Ion beam irradiation at 60 Gy significantly induced the genetic variability in physicochemical characteristics and nutritional compositions. The estimation of glycemic index revealed that two mutant lines could be consumed by diabetic patients. The two mutant lines (ML3 and ML30) were recorded to have normal glucose reading which was identified to have a moderate GI of 65 and 66, respectively. As low and moderate GI foods are recommended for diabetic patients, these two mutants (ML3 and ML30) have a high potential for their consumption. The findings also raise the value of knowing the GI in our food for awareness. Further study should be carried out on ML3 and ML30 by testing these mutant lines on diabetic patients. As for mutation induction from variety Pongsu Seribu2 using ion beam, data from the M6 generation showed that the highest yield was significantly observed in MINT 4 (10.04 ± 3.38 t/ha) and followed by MINT 3 (9.52 ± 2.80 t/ha), MINT 10 (9.42 ± 3.24 t/ha), MINT 5 (8.68 ± 2.99), MINT 9 (8.46 ± 0.43). In conclusion, mutation breeding is still one of the promising techniques for the development of new and novel varieties in combination with advanced molecular genetics that can bring plant mutation breeding into new era. The mutant and organic input will help in mitigating production issues (low yield, less water resources, soil fertility) in rice cultivation affected by environment impact as a result of climate change.

References

I.K. Asma, M.Y. Rafii, H. Sobri, L.P.K. Anna, A.H. Rahim, T.M.M. Mahmud, Z.S. Siti, R. Asfaliza, and Y. Oladosu. 2019. Physicochemical characteristics and nutritional composition of MR219 mutant rice and their effects on glycaemic responses in BALB/c mice. *International Food Research Journal*, 26(5):1477–1484.

Y. Hase, Tanaka., T. Baba, and H. Watanabe. 2000. FRL1 is required for petal and sepal development in Arabidopsis. *Plant Journal*, 24:21–32.

J. Hidema, M. Yamamoto, T. Kumagai, Hase, A. Sakamoto, and A. Tanaka. 2003. Biological effects of carbon ion on rice (Oryza sativa l.). *JAERI-review*, pages 85–87.

H. Sobri, H. Abdul Rahim, M Azhar, S. Shakinah, A. Zaiton, A Sakinah, A. Faiz, L.A Nur Humaira, A. R. Shyful, Azizi, A.W Ahmad Nazrul, Latiffah N., T. Atsushi, L. P. K. Anna, Y. Mohd Rafii, and R. Kogeethavani. 2018. Mutation breeding in Malaysia. *3rd World Biotechnology Congress 2018, São Paulo, Brazil.*

Individual Research Contribution Review, 2023, 1(1): 329–330

Transcriptome Sequencing Method for The Discovery of Submergence Tolerance Genes in Mutant Rice Cultivar NMR152

Wan Dalila Wan Chik
Agrotechnology and Biosciences Division, Malaysian Nuclear Agency
43000 Kajang, Selangor
wandalila@nm.gov.my

Abstract

Rice (Oryza sativa L.), as the most important food crop for human consumption, provides a stable food supply for more than half of the world's population. In Malaysia, climate change posing a threat to the production levels of rice and this is expected to have an adverse impact on the nation's rice security. The effects of climate change are being felt increasingly in recent years as the higher risk of occurrence of natural disasters such as floods and prolonged dry spells have influenced water availability. To meet increasing of the food demand, breeders and scientists aim to improve the yield and quality of major food crops. Malaysian Nuclear Agency has developed many advanced rice mutant lines through gamma radiation mutagenesis such as NMR152 variety. These rice mutant lines have been identified with traits such as high-yielding and adaptable to abiotic stress conditions such as drought and submergence. These mutant lines will be used in this study and are also believed associated to other stress conditions such as submergence in water for few weeks. To date, no gene that regulates the adaptable to submergence stress and drought condition has been identified in rice. An advanced mutant rice genotypes, NMR152, subjected to the submergence condition was analysed in order to understand the molecular regulation and the associated genes. Transcriptome profiling by RNA-Seq was used to compare the advance mutants with the local rice variety, MR219. The results provided valuable information for candidate genes identification and help to build a foundation for stress tolerance determination in rice. The information also important in supporting rice mutation breeding program.

Keywords: rice, transcriptome, NMR152

1 Introduction

In 2023, it was estimated that Malaysia would consume approximately 2.91 million metric tons of rice in total, a slight increase in the annual consumption from the previous year (Saali, 2023 August 1). However, Malaysia is currently facing challenges in achieving adequate rice production. Several factors contribute to this circumstance, including the delayed production of new paddy varieties and the exacerbation of climate change that lead to occurrences of drought and flooding. Farmers in Malaysia currently cultivate high-yielding rice cultivars that exhibit the susceptibility to both drought and submergence. Submergence tolerance was defined as the capability of a plant to survive a period of complete submergence lasting between 10 and 14 days. The growth process continues even after the flood recedes in minimal damage to plant morphology (Singh et al., 2017). Malaysian Nuclear Agency had successfully developed one drought and submergence tolerant mutant cultivar, NMR152 through a series of stringent phenotypic and genotypic selections based on its parental line MR219 using gamma irradiation at 300 Gy. To date, no information of NMR152 transcriptomic sequences has presented a significant challenge to the advancement of research on mutant rice varieties. To address these issues, we have assembled a high-quality transcriptomic sequence of NMR152 using RNA-Seq method. The resulted sequences were compared to local variety, MR219. The identified genes and their sequence information will also assist in the development of suitable markers to be used in marker assisted breeding (MAB) and genetic engineering program towards generating new rice varieties.

2 Materials and Methods

Two rice genotypes comprising one mutant rice cultivar (NMR 152) and its parent (MR219, negative check), were used in this experiment. The mutant line is derived from breeding improvement program of Malaysia popular Mega variety MR219. The program aimed to develop a new variety that resilient to climate change. The seed is supplied by Malaysian Nuclear Agency (MNA) and Malaysian Agricultural Research and Development Institute (MARDI). Later, all genotypes were screened under vegetative stage submergence stress (SS) and non-stress (NS) conditions. Plants are grown under direct seeded condition. Generally, 14-18 days old seedlings are completely submerged under 70-80 cm of water. The lines to submergence, generally, show less elongation and remain inside the water and survive the stress. Finally, number of survivors is counted after 10 days of de-submergence. About 2 mg of leaves was collected from each NMR152 and MR219 duringvegetative states prior RNA extraction process. The extraction was performed in three replicates. Total RNA was extracted using a Trizol reagent according to the manufacturer's protocol (Takara Bio Inc., Otsu, Japan). The integrity and purity of the RNA was determined by using the Agilent 2100 RNA 6000 Kit and electrophoresis on 1% agarose gel. RNA sequencing was performed using Illumina HiSeq

4000 according to the manufacturer's instructions (Illumina, San Diego, CA, USA). The methods of mapping of RNA-Seq reads, transcriptome assembly and sequence clustering, unigene function annotation and gene expression profiling screening were described in detail in a previous study (Sun et al., 2020). The results were used to determine the differentially expressed genes (DEGs), gene ontology (GO) and Kyoto Encyclopedia of Genes and Genomes (KEGG) pathway. The details workflow is shown in Figure 1.

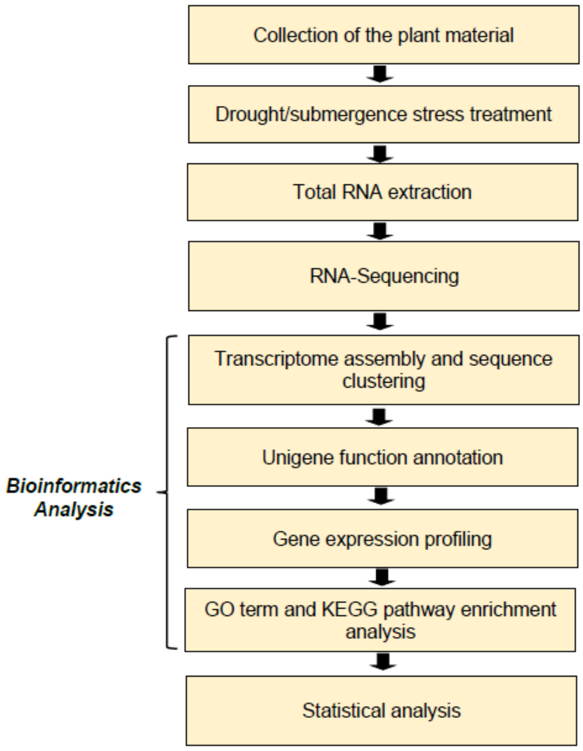

Figure 1: Transcriptomic sequencing analysis workflow

3 Results and Discussions

In this study, we have used submergence tolerant mutant cultivar, NMR152 developed by Malaysian Nuclear Agency and its parental line MR219. Transcriptomics analysis is employed to measure the relative activity of identified target genes. The data analysis was presented by the coexpression Venn diagram showing the number of genes that are uniquely expressed within each sample. After the gene expression was quantified, statistical analysis of the expression data was performed to identify the most targeted genes. We have identified five highly expressed genes in NMR152 during the submergence treatment. The targeted genes were associated with the chloroplast organelle that is responsible for photosynthesis, intracellular signalling, and the production of various compounds (Leister et al., 2017). Chloroplasts are plant organelles that are responsible for the process of photosynthesis, producing various metabolites, and sensing changes in the external environment. In the GO enrichment analysis results, the most significant 30 Terms were selected. The results showed the significance level of GO Term enrichment where higher values correspond to higher significance. The different colors represent the three GO subclasses of biological processes (BP), cellular components (CC) and, molecular function (MF). Cellular components such as chloroplast thylakoid and photosynthesis membrane were the most significant terms effected during the submergence stress condition of NMR152.

4 Conclusion

The application of transcriptome sequencing contributed to the identification of submergence tolerance genes in the NMR152 rice cultivar. During the submergence stress condition, it was observed that the expression levels of five genes associated with chloroplast and photosynthesis membranes were highly expressed. This study provides an in-depth understanding of the transcriptomic responses to submergence stress in NMR152 rice cultivar.

References

D. Leister, L. Wang, and T. Kleine. 2017. Organellar gene expression and acclimation of plants to environmental stress. *Frontiers in Plant Science*, 8(387).

M. S. B. Saali. 2023, August 1. NST leader: Five-season padi. *NST Online*.

L. Sun, D.-W. Di, G. Li, Y. Li, H. J. Kronzucker, and W. Shi. 2020. Transcriptome analysis of rice (Oryza sativa L.) in response to ammonium resupply reveals the involvement of phytohormone signaling and the transcription factor OsJAZ9 in reprogramming of nitrogen uptake and etabolism. *Journal of Plant Physiology*, 153137:246–247.

Individual Research Contribution Review, 2023, 1(1): 331–332

Field Evaluation Trials for Assessing Distinctiveness, Uniformity and StabilitY (DUS) on Morphological and Agronomic Characteristic of Kenaf Mutant Lines Generated through Mutation Breeding

Zaiton Ahmad
Agrotechnology and Biosciences Division, Malaysian Nuclear Agency
43000 Kajang, Selangor
zaitonahmad@nm.gov.my

Abstract

A project to develop new varieties of kenaf (*Hibiscus cannabinus* L.) with good agronomic traits using mutation breeding technology was started in December 2015 with a collaboration with LKTN. In this project, 30 potential mutant lines with promising agronomic traits (high fiber and seed yield) were selected from M5 population at LKTN field plot, Perlis. Subsequent activities were carried out in collaboration with UPM to generate F1 hybrids between 2019 and 2021. In October 2022, a new project was formulated with LKTN to evaluate 13 potential mutant lines and 2 mutant hybrids for assessing distinctiveness, uniformity and stability (DUS) of their agronomic traits for 4 seasons in the field.

Keywords: Kenaf, *Hibiscus cannabinus* L., mutation breeding

1 Introduction

Kenaf (*Hibiscus cannabinus* L.,) is a high value fiber plant commonly used as a raw material for various industries such as pulp, paper, furniture, construction and automotive. Kenaf was first introduced into Malaysia in the early 2000, as part of the government effort to replace tobacco plants in Kelantan and Terengganu areas. Depending on soil and weather conditions, kenaf fiber yield in Malaysia can reach up to 20 tons per hectare in experimental plots, (Lembaga Kenaf and Tembakau Negara, 2013) but generally, the yield in plantation areas is still low which is around 5 to 10 tons per hectare. The highest yield achieved in plantation areas was about 9.8 tons per hectare from V36 (Basri et al., 2014).

A number of research on kenaf has been carried out in Malaysia, mainly in the aspects of screening of suitable varieties adaptable to local weather, development of good agronomic practices, mechanization of planting and harvesting processes. One of the problems faced by kenaf industry in Malaysia is the lack of kenaf varieties that are suitable to Malaysian climate. Most areas are still planted with the same variety which is V36. Therefore, new varieties which can perform well in local condition especially in terms of biomass yield are highly needed.

Approximately 30 potential mutant lines from M5 population were selected in 2018 at LKTN Plot in Beseri, based on with high fiber and seed yield traits (Zaiton et al., 2018). Further field evaluation trials were carried out and mutant hybrids were developed under a collaboration with UPM (Al-Mamun et al., 2022). In this project, 13 potential mutant lines and 2 mutant hybrids are being evaluated in the field to assess the distinctiveness, uniformity and stability of the mutated traits. At the end of the project, the mutant lines that show uniform and consistent traits especially in fiber and seed yield will selected for establishment of new varieties and eligible for filing for Plant New Variety Protection.

2 Methods

2.1 Field preparation

The locations for field trials were Beseri and Chuping, Perlis and the plots were prepared according to the standard practice by LKTN.

2.2 Field planting for seed production

The first season of planting will be focused on seed production only. The main objective is to obtain enough seeds for subsequent DUS evaluation. Seeds obtained from season 1 was used for DUS evaluation in Season 2 and 3.

2.3 Field planting for DUS evaluation (2 seasons)

Each mutant line will be evaluated separately in a Randomized Complete Block Design (RCBD) with 3 replications in two (2) locations, in the second and third seasons. Morphological and agronomic characters for each mutant lines will be recorded. Seeds from this planting season will be kept for subsequent planting. The evaluation will be done for two (2) planting seasons.

2.4 Identification of stable mutants

Morphological and agronomic data from both planting seasons will be analysed to identify and select stable mutant varieties with good morphological and agronomic traits.

- **Morphology:** leaf shape, leaf size, leaf colour, stem size, stem colour, seed pod shape etc
- **Agronomy:** fiber yield, flower/fruit maturity, seed yield

2.5 Seed production for selected stable mutant varieties

Field planting of selected stable mutant varieties will be carried out to mass produce their seeds for future use (filing for Plant Variety Protection, pre-commercialization trial etc)

2.6 Filing for Plant New Variety Protection

Once stable mutants are identified, application will be made for Filing of Plant New Variety Protection and granting of Breeder's Right with Department of Agriculture Malaysia. Target: 5 new varieties.

3 Results and Discussions

For this study, a total of 13 mutant lines, 2 hybrids (F2) and 1 control variety (V36) were used. The details of the seeds used are as follows;

No	Mutant	Dose (Gy)	Traits
1	ML5	300	High fiber, palmate leaves
2	ML9	300	High fiber
3	ML10	300	High fiber
4	36-3	300	High fiber
5	36-8	300	High fiber
6	36-11	300	High fiber
7	36-20	300	High fiber
8	36-10	300	High fiber
9	36-21	800	High fiber, seed and palmate leaves
10	36-24	1300	High fiber
11	36-25	1300	High fiber
12	36-27	1300	High fiber
13	ML Ring 4	230	High fiber
14	ML36-25 x LR4P2	-	Hybrid, tall plant
15	ML36-24 x BJR1	-	Hybrid, tall plant, palmate leaves
16	V36	0	Check variety

Seed germination was done on 3 Feb 2023. The plants were allowed to grow on the nursery trays for about 10 days before being transferred to the plot. Land preparation and pre-germination treatment were done on 13 Feb 2023 and transplanting of seedlings was completed on 15 Feb 2023. The second planting was completed on June 2023 (Chuping) and November 2023 (Beseri). Maintenance of the plants follows the standard practice by LKTN.

In the first season, the mutants maintained leaf and flower morphological traits. All mutants have ovate leaves except ML5, 36-21 and ML36-24 x BJR1 (hybrid) that have palmate leaves. For flowers, all mutants have flowers with purple throat, except ML5 which has yellow throat (Figure 1). Data collection on agronomic traits (fiber and seed yields) is still ongoing.

Figure 1: Example of leaf and morphological traits of mutants, Mutant 36-11 (left) and ML5 (right)

References

Md Al-Mamun, Mohd Y. Rafii, Yusuff Oladosu, Azizah Binti Misran, Zulkarami Berahim, Zaiton Ahmad, Md Mahmudul Hasan Khan, and Fatai Arolu. 2022. Genotypic variability, correlation and path analysis among yield components in kenaf mutants under tropical conditions. *Journal of Natural Fibers, DOI: 10.1080/15440478.2022.2073499*.

M.H.A. Basri, A. Abdu, N. Junejo, H.A. Hamid, and K. Ahmed. 2014. Journey of kenaf in Malaysia: A review. *Scientific Research and Essays*, 9(11):458–470.

Lembaga Kenaf dan Tembakau Negara. 2013. Manual penanaman, pemprosesan dan pengendalian hasil kenaf (edisi kedua).

Ahmad Zaiton, Ahmad Faiz, Akil Mustapha, Sani Zulmadi, Abu Hassan Affrida, and Romli Mohammad Nazri. 2018. Agronomic performance of ten selected potential kenaf mutant lines at Beseri, Perlis. *Transaction of Persatuan Genetik Malaysia*, 10:1–6, ISBN 978–967–16583–2–1; eISBN 978–967–16583–3–8.

Individual Research Contribution Review, 2023, 1(1): 333–334

Ion Production Diagnostics in a 2.3kJ Malaysian Nuclear Agency-Plasma Focus (MNA-PF)

Abd Halim bin Baijan
Technical Support Division, Malaysian Nuclear Agency
43000 Kajang, Selangor
ahalim@nm.gov.my

Abstract

This work is an introduction of ion beam diagnostics suitable for Malaysian Nuclear Agency- Plasma Focus (MNA-PF) device. Currently, there are two diagnostics that will be tested to the plasma focus (MNA-PF) device. The diagnostics are biased ion collector and Faraday cup.

Keywords: Plasma Focus, Ion collector

1 Introduction

Malaysian Nuclear Agency-Plasma Focus (MNA-PF) configuration has enable the generation of hot and dense plasma through the pinch effect. This event will also produce radiation such as neutron, X-rays and ion beam. In order to verify the quality of the ion beam a diagnostic tool is needed. At this moment two basic method for the measurement of ion beam will be implemented. They are faraday cup and biased ion collector methods.

1.1 Faraday Cup

Faraday cup is a metal cup (conductive) designed to collect charged particles in vacuum. It was named after Michael Faraday who founded ions around 1830s. The ion hitting the metal in the cup will generate current and then it will be measured to determine the number of ions it received.

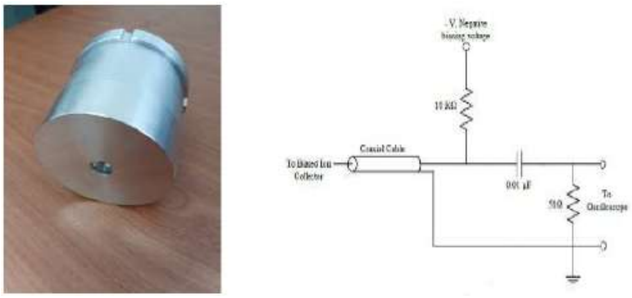

Figure 1: Faraday Cup with negative biased circuit

1.2 Biased Ion Collector

Biased ion collector basically is made from a piece of copper plate as the charge collector and negatively biased to certain potential as shown in Figure 2, (Kuan, 2017). The device works when the ion hitting the copper plate, spike of voltage will be observed at the oscilloscope. From the signal, the numbers of charges being carried in the ion beam can be determined upon analysis.

Figure 2: Ion Collector with biased circuitry

2 Methodology

The arrangement of the diagnostics and the plasma focus is shown in Figure 3. The collectors will be placed on top of the MNA-PF vacuum chamber flange. The orientation is arranged in such a way as the plasma focus electrodes is pointed to the top of the vacuum chamber flange. Theoretically the plasma pinch occurs slightly at the end of the electrodes. When the pinch occur ion beam will be emitted spontaneously. The ion than will be travel and hit the collector and gives a signal to the oscilloscope.

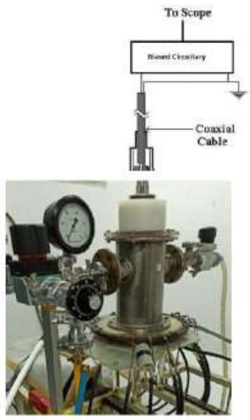

Figure 3: The ion collectors will be placed on top of the flange

3 Result and Discussions

There are three diagnostics signals shown in the graph above, each one represents current diagnostic, voltage diagnostic and ion diagnostic. The graph shows the signal for each diagnostics the occurring of plasma pinch at 10.0 kV with am Argon gas pressure at 1.5 mbar.

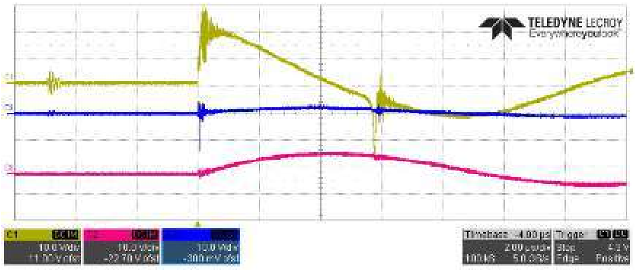

Figure 4: A) current from Rogowski coil, (B) Signal from biased ion collector, and (C) voltage signal from voltage probe

References

L.L. Kuan. 2017. Low pressure plasma for deuteron beam generation. *Faculty of Science, University Malaya, Kuala Lumpur. PhD Theses*.

Individual Research Contribution Review, 2023, 1(1): 335–336

N-FIT for assisting RTP Fuel Cladding Visual Inspection

Ahmad Nabil Bin Ab Rahim
Technical Support Division, Malaysian Nuclear Agency
43000 Kajang, Selangor
ahmadnabil@nm.gov.my

Abstract

N-FIT is a new structure designed and fabricated for improving the visual inspection activity conducted in Reactor TRIGA PUSPATI in a more efficient manner and with safety factors consideration during design stage and application in the RTP tank.

Keywords: SS304 Cladding, Image processing, RTP

1 Introduction

In general, RTP fuel inspection has been conducted using fuel inspection tool to assess the failure criteria of elongation limit and visual inspection using underwater camera to assess the physical condition without detail assessment.

Due to aging degradation mechanism, the physical condition of the RTP Fuel cladding surface should be monitored closely. The conventional image record did not have details on the physically changed appearance dimension such as length and color tone. Development of this image processing system will enable us to characterize cladding degradation phase of the fuel element and thus monitor pattern of the effected zone at the fuel cladding surface.

N-FIT is a very important structure in assisting the task for improvement of fuel visual inspection in RTP.

2 Methods

The main project of fuel cladding assessment will involve two components. The first one is on the development of mechanical structure to support fuel element, the image recorder and lightings inside the reactor tank. This will involve with many design consideration limitations in the working environment. Selection of material is also an important consideration due to the radiation environment.

Another component of the project is on the image processing capability development using image processing. This will involve with image preprocessing, development of segmentation model, classification model and characterization of cladding condition. The figure below is the main concept toward achieving the project goal.

This paper will focus only the first part of successful development of the Cladding Imaging Rig (N-FIT). The stages involve during the design were:

1. Recognizing the needs to perform visual inspection using underwater camera. The images recorded then would enable the analyst to identify and describe any visual finding in accurate manner.

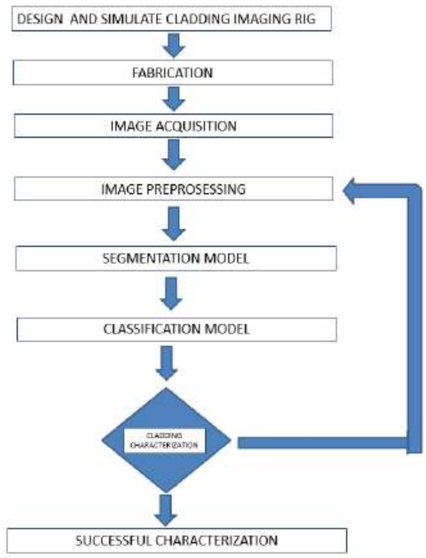

Figure 1: RTP Fuel Cladding Assessment

2. Problem or challenges are fuel is material that has radiation and dangerous to human and potential hazard to sensitive electrical equipment, challenge of maneuvering under water with the depth about 6 meters and we have to minimize the risk of any object falling into the reactor core.

3. Design requirement must be established base on the following constraints:
   (a) installed underwater
   (b) allow the fuel to be inserted and removed
   (c) must be able to hold irradiated fuel
   (d) able to viewed without any obstruction
   (e) considerable safety margin

4. Design Considerations also included such as:
   (a) Location Selection
   (b) Depth Justification
   (c) Fuel Rest Design
   (d) Assembly rest
   (e) Lighting Condition
   (f) Additional (Strength, Reliability, Cost, Ergonomics, Manufacturability, Safety, Weight, Shape, Size, Flexibility, and Surface Finish

The main concern should be the strength of the main body structure and joint part assembly structures. Design with similarity to FIT considered as the main concept since the structure has been used since 1982 that has shown safe performance throughout its lifetime.

3 Results

Figure 2 is displaying the main structure of N-Fit component.

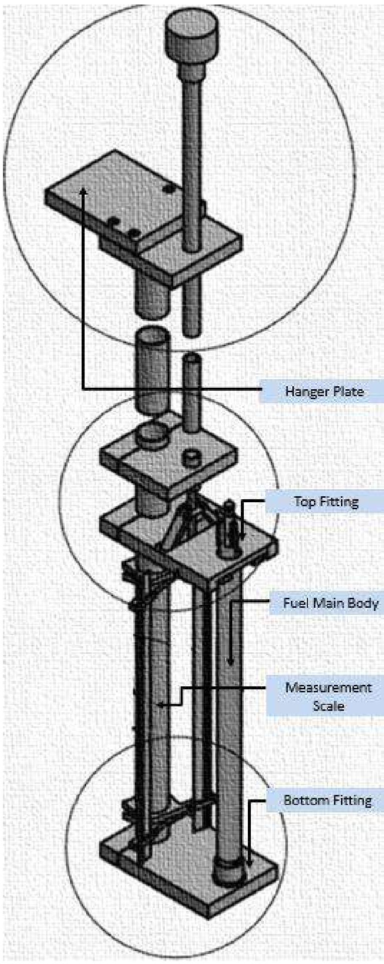

Figure 2: N-FIT main component

Figure 3 is showing the N-FIT is being installed safely inside RTP tank with lighting arm manipulator to assist fuel inspection in the future.

4 Discussion/ Conclusion

N-FIT has successfully designed and fabricated for RTP Fuel Inspection to provide additional assessment on fuel element positioning and provided with lighting capability. N-FIT has successfully demonstrated and tested for fuel inspection during RTP annual maintenance. RTP fuel integrity inspection can be further enhanced with the application of N-FIT in the future.

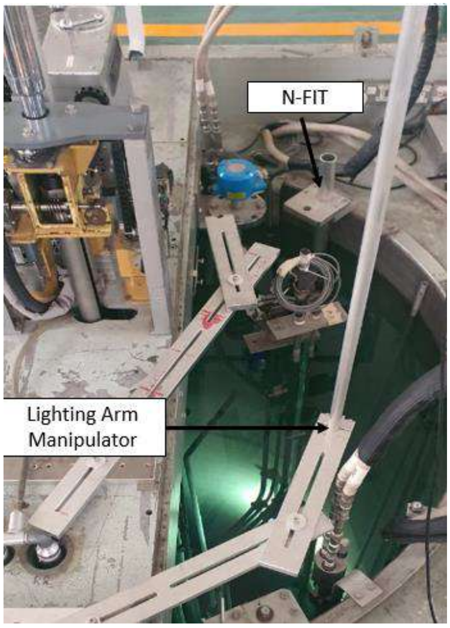

Figure 3: N-FIT inside RTP tank

References

A.N. Ab Rahim, M.K Arif, N.S. Hamzah, A.S. Ligam, N. Ramli, M.F. Zakaria, and M.F. Abdul Farid. 2017. Selected puspati triga reactor fuel cladding displacement trending behavior. *Nuclear Technical Convention 2017, Nuklear Malaysia*.

A.N. Ab Rahim, M.S. Minhat, M.H. Hussin, Y. Ismail, A.S. Ligam, N.A. Joha, T. Lanyau, and R. Abdul Mutalib. 2020. Rtp fuel cladding surface integrity visual inspection test rig design concept. *Seminar RD 2020, Agensi Nuklear Malaysia*.

Individual Research Contribution Review, 2023, 1(1): 337–338

Conceptualization of Nuklear Malaysia Business Continuity Resilience using Predictive Analytic Tools

Amy Hamijah binti Ab. Hamid
Technical Support Division, Malaysian Nuclear Agency
43000 Kajang, Selangor
amyhamijah@nm.gov.my

Abstract

We are proud to declare that the Malaysian Nuclear Agency (Nuklear Malaysia) is a solely national government research agency certified in ISO 22301:2012 Standard in the competence of Business Continuity Good Practice Guidelines implementations. Nuklear Malaysia is obliged to be operated that refers to Act 304, Directive 20, International Atomic Energy Agency (IAEA) guidelines and so forth. This paper discussed the Business Continuity (BC) management effectiveness in accordance with predictive radiological and operational management of dedicated facilities in Nuklear Malaysia as a comparative case study. This discussion prior to the business impact analysis consequences of the dedicated facilities' organizational resilience using predictive analytic in suppressing any challenging disruptive events such as electrical outage. From the conceptualized Business Impact Analysis (BIA) strategy chart can be transformed into feasible actual real-time and digitized simulation modelling tool. This research identified from the real-time exercised simulation drill outcome of the dedicated Facility A resilience utilization results between the estimated BIA strategy chart and the ARENA© digitized results are quite similar with the difference of 11% which are 80% and 91% accordingly. This paper concluded that BIA strategy chart most likely accommodated digitized BCMS simulator development as the follow through in preparation for future predicaments mitigation and recovery.

Keywords: safety, security, resilience, business continuity, and disruptive events.

1 Introduction

Nuklear Malaysia is among the pioneering public agencies to be certified in Business Continuity Management System (BCMS) according to ISO 22301:2012 for the provision of services related to critical service centers such as SINAGAMA, RAYMINTEX, Radiation Metrology Group (KMS), Waste Technology Development Centre (WasTeC) and Radioactivity Measurement - Radiochemistry and Environment Laboratory (RAS) in 7 January 2019 (Hamid, 2018; International Organization for Standardization, 2019).

The Nuklear Malaysia's BCMS effectiveness focusing on how-to achieve organizational resilience in our Business Continuity Strategy Program and Plan (BCSP). Our BCSP is incorporated to identify our strength and effectiveness of the following capabilities as (1) the capability to prevent an accident from occurring; (2) the capability to prevent that an occurred accident spreads its impacts; and (3) the capability to recover to the normal state, after an occurred accident (Giacchero et al., 2013).

2 Methods

Main principles to achieve a resilience Business Continuity Management (BCM) Strategic Plan is to understand exactly the main critically acclaimed business requirements in order to survive an unexpected event. Second, we should know how to plan suppressing challenges that could appear at any time. Nuklear Malaysia has adopted the conceptualization of the BIA strategic chart into a digitized Business Continuity Recovery Response Simulator (BCRRS©) by using Radiation and Nuclear Emergency Planning Framework (RANEPF©) (A.H.A., 2018; Hamid et al., 2018b; Hamid et al., 2018a; Zalil, 2019). The simulator was developed using ARENA© as an application for building simulation model accordingly.

3 Results and Discussions

Nuklear Malaysia implemented several simulation drills manually and digitally in 2018 and 2019 in order to achieve at least 60% of the recovery objectives using the Business Impact Analysis for two service centers at least once a year. The BIA strategy chart was mathematically formulated using MS Excel© according to tailored Nuklear Malaysia BCMS critically acclaimed requirements and business processes through mutual understanding and approval by consulted subject matter expert, certified auditors and stakeholders. The outcome of the conceptualized BIA strategy chart is transformed into BCRRS© (Zalil, 2019).

Figure 1 depicted the BIA strategy chart estimating 80% utilization of the Facility A resilience compared to 91% utilization rate using BCCRS© in Table 1. The difference is only 11% between them accordingly (Zalil, 2019).

4 Conclusions

As a conclusion, this research had successfully identified and analyzed the key requirements and success factors of Nuklear Malaysia BCMS are critically acclaimed and feasibly incorporated with our capacities and capabilities in order to achieve organizational and radiological operational resilience by using appropriate framework and development tools.

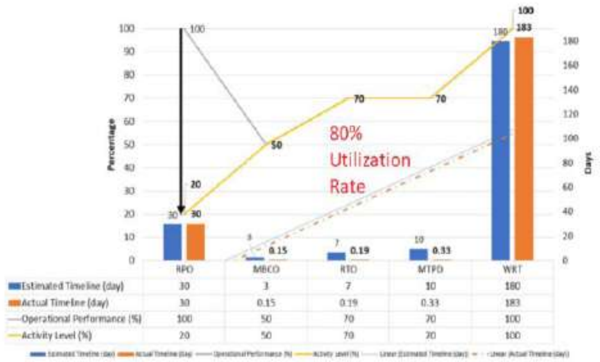

Figure 1: Business Continuity Simulation Drill Results using BIA Strategy Chart

Table 1: Digitized Business Continuity Drill Results using ARENA© Simulation Development Software

Facility A

Entity/Process	Number In/Out	Average VA Time (minutes)	Average Total Time of Completion (minutes)	Work in Process (%)	Utilization (100%)
Lorry/Send Lorry	1	1.795	21.795	20	2
Sample/Send Sample	1	101.13	111.13	100	91
Report/Send Report	1	5.242	19.242	17	5

References

Hamid A.H.A. 2018. Limitations and challenges towards an effective business continuity management in Nuklear Malaysia. *IOP Conference Series: Materials Science and Engineering*, 298(012050):11.

A Giacchero, F Giordano, and M Schiraldi. 2013. From business continuity to design of critical infrastructures: ensuring the proper resilience level to datacentres. *Int. J. of Eng. and Tech. (IJET)*, 5(4):3544–3553.

Amy Hamijah Ab. Hamid, Mohd Zaidi Abd Rozan, Roliana Ibrahim, Safaai Deris, Ali Selamat, and Norita Md. Norwawi. 2018a. Reflective multi-agency user acceptance analysis: Contextualize evaluation of the Malaysian radiological incidents response simulation system. *4th Visual Informatics International Seminar 2018 (VIIS '18), Universiti Kebangsaan Malaysia*.

Amy Hamijah Ab. Hamid, Mohd Zaidi Abd Rozan, Roliana Ibrahim, Safaai Deris, Ali Selamat, and Muhd. Noor Muhd. Yunus. 2018b. Requirements engineering of Malaysian radiological medical emergency response simulator. *Journal of Information and Telecommunication (JIT)*, 2(3):305–321.

Nurain Fitri Zalil. 2019. Predictive analytics: Analyzing effectiveness of the business continuity recovery response simulation system (BCRRSS) in Nuklear Malaysia [practicum report]. Universiti Utara Malaysia.

Does Recovery Team Matters in Safeguarding Information Technology Incident Management in Nuklear Malaysia?

Amy Hamijah binti Ab. Hamid
Technical Support Division, Malaysian Nuclear Agency
43000 Kajang, Selangor
amyhamijah@nm.gov.my

Abstract

This paper discussed some key issues and success factors in validating disaster recovery teams scope, roles and responsibilities prior to the Nuklear Malaysia's certified Business Continuity Management System (ISO 22301:2012) and Information Technology Management System (ISO/IEC 27001:2013) accordingly known as BCMS and ISMS. This paper discussed on the Business Continuity Plan (BCP) and Disaster Recovery Plan (DRP) implementation issues from the scope of Job Hazard Analysis. As a concluding remark, it is at best that Nuklear Malaysia highlighted the integral capacities and capabilities of the Information Technology (IT) Recovery Team within these safety and security standards to prevent any misleading and misunderstanding in managing any future information technology incident management.

Keywords: safety, security, business continuity, information security

1 Introduction

Nuklear Malaysia is among the pioneering public agencies to be certified in BCMS according to ISO 22301:2012 for the provision of services related to critical service centers such as SINAGAMA, RAYMINTEX, Radiation Metrology Group (KMS), Waste Technology Development Centre (WasTeC) and Radioactivity Measurement - Radiochemistry and Environment Laboratory (RAS) in 7 January 2019 (Hamid, 2018; International Organization for Standardization, 2019). These prioritized facilities shall be aided by other supporting divisions such as technology commercialization, engineering, instrumentation and automation services and information technology support. In addition, the initially certified BCMS is also in competence of the Business Continuity Good Practice Guidelines implementations.

Meanwhile, Nuklear Malaysia's Information Technology Management System (ISO/IEC 27001:2013) is initially certified since 2014, focusing on e-SSDL System credentials located at our data center for the provision of data management, web application services, and also, in managing e-SSDL server and network management (Agensi Nuklear Malaysia, 2023; International Organization for Standardization, 2013).

The exclusion differences between BCMS and ISMS implementations, whereby, BCMS did not included any product development and verification, and also, critical and not urgent activities and processes. As for ISMS implementation does not related to e-SSDL customers and business partner.

The Nuklear Malaysia's BCMS effectiveness validation focusing on how-to achieve organizational resilience in our Business Continuity Strategy Program and Plan (BCSP). Our BCSP is incorporated to identify our strength and effectiveness of the following capabilities as (1) the capability to prevent an accident from occurring; (2) the capability to prevent that an occurred accident spreads its impacts; and (3) the capability to recover to the normal state, after an occurred accident (Giacchero et al., 2013). This validation based on the Business Impact Analysis (BIA) strategy charts for the critically acclaimed processes and activities of the dedicated facilities mentioned above (Zalil, 2019).

Meanwhile, the Nuklear Malaysia's ISMS effectiveness validation based on DRP according to the act of maintaining and minimizing system downtime during any disaster and crises that must be restored within 24 hour Recovery Time Objective (RTO) for applications (i.e. e-Client and e-SSDL) and 14 days restoration for network and storage credentials.

2 Methods

This paper will discussed the recovery team issues regarding to BCMS and ISMS implementation from the Job Hazard Analysis perspectives according to BCP and DRP execution (Hamid et al., 2014; Hamid, 2018).

3 Results and Discussions

Disaster Recovery is the subset of the Business Continuity which addressing the e-SSDL and other IT technical components recovery such as IT infrastructure core systems, data and communication technologies and business support. Meanwhile, Business Continuity is the recovery planning of the dedicated facilities processes and activities that might causing significant organizational and functional interruption which includes emergency response, business continuity, disaster recovery and also, managing crises. Business continuity involved a bigger picture of handling recovery planning for Nuklear Malaysia rather than information technology disaster recovery. If any disaster disrupted our business continuity competencies, we might tarnished our image, loss of profit, stakeholders, customers, business partners and also, depleting our research and industrial commercialization gain.

Figure 1 depicted proposed Business Continuity Management Team (BCMT) organizational chart, whereby, IT recovery team should be assisted by another teams which are the

Business Recovery Team (BRT) and System/Application Recovery Team (SRT) (Hamid, 2018). During any unexpected disruption, any decision making process and suggestion will be given by the top management officers with the guidance of the Crises Command Team (CCT) such as Unit Keselamatan Fizikal (UKF), Bahagian Keselamatan dan Kesihatan Sinaran (BKS) and Jawatankuasa SHE. BRT is among the dedicated facilities' members (SINAGAMA, RAYMINTEX, BKS-KMS, WasTeC and RAS) responsible to operate the recovery processes and activities. Meanwhile, SRT such as Bahagian Kejuruteraan (BKJ) is responsible to support core infrastructure and utility services. Besides that, Administrative Support Team (AST) such as Bahagian Khidmat Pengurusan (BKP) is essential in sustaining and providing logistic and managerial support for recovery processes and activities of Nuklear Malaysia's core business related to the dedicated facilities. Most likely, Bahagian Pengkomersilan Teknologi (BKT) is the main role-player organizing, integrating the Business Continuity Program, and also, reporting the whole recovery processes and activities known as the Coordinator Team (CT).

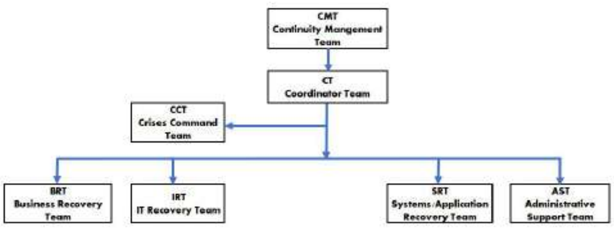

Figure 1: Proposed Business Continuity Management Team (BCMT)

The proposed BCMT in Figure 1 was initiated during the previous BCMS implementation in 2018 and 2019. In order to fulfil the effectiveness validation of both BCP and DRP, we have applied a walk through procedural and digitized simulation drill using ARENA© (Hamid, 2018; Ab.Hamid et al., 2018b; International Organization for Standardization, 2019; Zalil, 2019). The validation is significant to confirm conditions or elements, such as location, time, temperature, and culture in which the recovery process and activities operates or needed for the business processes to be normalized in those facilities.

4 Conclusions

As a conclusion, this research identified and analyzed key requirements and success factors of Nuklear Malaysia BCMS and ISMS implementations can be do-able and achievable organizational and operational resilience by using appropriate framework and digitized development tools.

References

Amy Hamijah binti Ab. Hamid, Mohd Zaidi Abd Rozan, Roliana Ibrahim, Safaai Deris, Ali Selamat, and Norita Md. Norwawi. 2018. Reflective multi-agency user acceptance analysis: Contextualize evaluation of the Malaysian radiological incidents response simulation system. *4th Visual Informatics International Seminar 2018 (VIIS '18), Universiti Kebangsaan Malaysia*.

International Organization for Standardization. Information technology - security techniques - information security management systems - requirements ISO/IEC 27001. Second Edition 2013-10-01.

International Organization for Standardization. Security and resilience - business continuity management systems - requirements ISO 22301. Second Edition 2019 -10.

A Giacchero, F Giordano, and M Schiraldi. 2013. From business continuity to design of critical infrastructures: ensuring the proper resilience level to datacentres. *Int. J. of Eng. and Tech. (IJET)*, 5(4):3544–3553.

AHA Hamid, MZA Rozan, R Ibrahim, S Deris, and MN Muhd Yunus. 2014. Framing a nuclear emergency plan using qualitative regression analysis. *Journal of Nuclear and Related Technologies (JNRT)*, 11(1):27–45.

Amy Hamijah Ab. Hamid, Mohd Zaidi Abd Rozan, Roliana Ibrahim, Safaai Deris, Ali Selamat, and Muhd. Noor Muhd. Yunus. 2018. Requirements engineering of Malaysian radiological medical emergency response simulator. *Journal of Information and Telecommunication (JIT)*, 2(3):305–321.

A.H.A. Hamid. 2018. Limitations and challenges towards an effective business continuity management in Nuklear Malaysia. *IOP Conference Series: Materials Science and Engineering*, 298(012050):11.

Agensi Nuklear Malaysia. 2023. Dokumen ISMS. https://spkms. nuclearmalaysia.gov.my/teknikal/bst/itc/isms/sitepages/dokumenisms.aspx.

Nurain Fitri Binti Zalil. 2019. Predictive analytics: Analyzing effectiveness of the business continuity recovery response simulation system (BCRRSS) in Nuklear Malaysia [practicum report]. Universiti Utara Malaysia.

Individual Research Contribution Review, 2023, 1(1): 341–342

Nuklear Malaysia Business Continuity Predictive Analytics using ARENA

Amy Hamijah binti Ab. Hamid
Technical Support Division, Malaysian Nuclear Agency
43000 Kajang, Selangor
amyhamijah@nm.gov.my

Abstract

We are proud to declare that the Malaysian Nuclear Agency (Nuklear Malaysia) is a solely national government research agency certified in ISO 22301:2012 Standard in the competence of Business Continuity Good Practice Guidelines implementations. Nuklear Malaysia is obliged to be operated that refers to Act 304, Directive 20, International Atomic Energy Agency (IAEA) guidelines and so forth. This paper discussed the Business Continuity (BC) management effectiveness in accordance with predictive radiological and operational management of dedicated facilities in Nuklear Malaysia as a comparative case study. This discussion prior to the identified 7% business process utilization differences between facility A (98% utilization) and facility B (91% utilization). This paper concluded that dedicated business process key requirements according to Nuklear Malaysia capacities and capabilities can be facilitated for further enhancement using digitized simulation modelling following through future challenges afterwards.

Keywords: safety, security, resilience, business continuity, disruptive events

1 Introduction

Nuklear Malaysia is amongst the pioneering public agencies to be certified in Business Continuity Management System (BCMS) according to ISO 22301:2012 for the provision of services related to critical service centres such as SINAGAMA, RAYMINTEX, Radiation Metrology Group (KMS), Waste Technology Development Centre (WasTeC) and Radioactivity Measurement - Radiochemistry and Environment Laboratory (RAS) in 7 January 2019 (Hamid, 2018; International Organization for Standardization, 2019).

The Nuklear Malaysia's BCMS effectiveness focusing on how-to achieve organizational resilience in our Business Continuity Strategy Program and Plan (BCSP). Our BCSP is incorporated to identify our strength and effectiveness of the following capabilities as (1) the capability to prevent an accident from occurring; (2) the capability to prevent that an occurred accident spreads its impacts; and (3) the capability to recover to the normal state, after an occurred accident (Giacchero et al., 2013).

2 Methods

Main principles to achieve a resilience Business Continuity Management (BCM) Strategic Plan is to understand exactly the main critically acclaimed business requirements in order to survive an unexpected event. Second, we should know how to plan suppressing challenges that could appear at any time. Most likely, whenever we ensure principle awareness in achieving resilience BCM Program on disaster recovering by mitigating on how to monitor the indicated performance, therefore, we are also, being prepared on what to expect of the anticipated future threats. The business continuity resilience framework is referring to Radiation and Nuclear Emergency Planning Framework (RANEPF©) (Hamid et al., 2018b; Hamid et al., 2018a).

3 Results

Nuklear Malaysia have conducted manually and digitally simulated disruptive events drills within our vicinity in 2018 and 2019 specified to our BCMS scope and conduct as follows: (1) To achieve at least 60% of the recovery objectives using the Business Impact Analysis for two service centers at least once a year and, (2) To achieve at least 70% attendance during the Awareness Program. This paper will highlighted on the first objective. The outcome of the digitized BCM drill simulation highlighted was produced by ARENA© as an application for building simulation model which is integrated with RANEPF© framework known as Business Continuity Recovery Response Simulator (BCRRS©)(Hamid, 2018; Hamid et al., 2018b; Hamid et al., 2018a; Zalil, 2019).

Table 1 depicted the sample irradiation service in Facility A had achieved 98% utilization. Meanwhile, the sample counting service in Facility B had achieved 91% utilization (Zalil, 2019).

Table 1: Simulation Results

Facility A

Entity/Process	Number In/Out	Average VA Time (minutes)	Average Total Time of Completion (minutes)	Work in Process (%)	Utilization (100%)
Lorry/Send Lorry	4	0.0598	1.206	46	2
Sample/Send Sample	1	10.341	10.508	100	98
Report/Send Report	2	0.0716	0.245	5	1

Facility B

Entity/Process	Number In/Out	Average VA Time (minutes)	Average Total Time of Completion (minutes)	Work in Process (%)	Utilization (100%)
Lorry/Send Lorry	1	1.795	21.795	20	2
Sample/Send Sample	1	101.13	111.13	100	91
Report/Send Report	1	5.242	19.242	17	5

4 Discussion and Concluding Remarks

Main research recommendations for both facilities starts with Facility A, whereby, this facility need to improve their process throughput to average number of flow units processed over time to be operated 100 time units equivalent to 400 items per unit, or (100x4) (Zalil, 2019).

The following Facility B is suggested to be operated for 100 time units should be 100 items per unit time, or (100x1). Secondly, the average VA Time (value added time) for each process in Facility A to achieve 100% performance is 4 minutes per process. Meanwhile in Facility B, it is suggested 51 minutes per process (Zalil, 2019).

This research concluded that it has successfully identified and analyzed Nuklear Malaysia BCMS are critically acclaimed and feasibly incorporated with our capacities and capabilities in order to achieve organizational and functional radiological operational resilience.

References

International Organization for Standardization. Security and resilience - business continuity management systems - requirements ISO 22301. Second Edition 2019 -10.

A Giacchero, F Giordano, and M Schiraldi. 2013. From business continuity to design of critical infrastructures: ensuring the proper resilience level to datacentres. *Int. J. of Eng. and Tech. (IJET)*, 5(4):3544–3553.

Amy Hamijah Ab. Hamid, Mohd Zaidi Abd Rozan, Roliana Ibrahim, Safaai Deris, Ali Selamat, and Norita Md. Norwawi. 2018a. Reflective multi-agency user acceptance analysis: Contextualize evaluation of the Malaysian radiological incidents response simulation system. *4th Visual Informatics International Seminar 2018 (VIIS '18), Universiti Kebangsaan Malaysia*.

Amy Hamijah Ab. Hamid, Mohd Zaidi Abd Rozan, Roliana Ibrahim, Safaai Deris, Ali Selamat, and Muhd. Noor Muhd. Yunus. 2018b. Requirements engineering of Malaysian radiological medical emergency response simulator. *Journal of Information and Telecommunication (JIT)*, 2(3):305–321.

A.H.A. Hamid. 2018. Limitations and challenges towards an effective business continuity management in Nuklear Malaysia. *IOP Conference Series: Materials Science and Engineering*, 298(012050):11.

Nurain Fitri Binti Zalil. 2019. Predictive analytics: Analyzing effectiveness of the business continuity recovery response simulation system (BCRRSS) in Nuklear Malaysia [practicum report]. Universiti Utara Malaysia.

Individual Research Contribution Review, 2023, 1(1): 343–344

Mobile Hot Cell for Handling Category 1 and 2 Sealed Sources

Anwar A Rahman
Technical Support Division, Malaysian Nuclear Agency
43000 Kajang, Selangor
anwar@nm.gov.my

Abstract

Mobile Hot Cell is a shielded enclosure facility with remote handling equipment in which the high activity Disused Radioactive Sources (DSRS) can be safely examined and conditioned. The term mobile for Mobile Hot Cell is referring to capability of the facility to be transported, assembled and dismantled at anywhere in the world and this facility is independent on its own. There are only 3 units available in the world, which are in South Africa, China and Malaysia. The Mobile Hot Cell project is a collaboration project between Malaysia Government and International Atomic Energy Agency (IAEA). The project was funded under the $10^{th}/11^{th}$ Malaysia Plan, and the training and expertise for 14 Malaysian Nuclear Agency operators was provided by IAEA. In 2023, the facility was granted for operational license approval by Atomic Energy Licensing Board (AELB) after a successful second International Peer Review in 2018. Then, the new journey of the MHC will begin to provide services for Malaysia and regional country with Research and Development.

Keywords: MHC, Hot Cell, DSRS, Category 1, Category 2, Spent Source

1 Introduction

Mobile Hot cell (MHC) is the facility used for conditioning of Spent High Activity Radioactive Sources (SHARS) in Category 1 and 2. The high activity sources is referring to sealed source that are used in medical and industry either for diagnostic, treatment, irradiation or research. There are many of the sources is no longer used in the world and requires safe management in handling and storage. Some of the sources has been returned back to the original country but the government has to spent high cost on the returned shipment. The issues of abandoned or orphan sources need to handle by the local experts and specialties in securing the sources. Mobile Hot Cell is one of the solution proposed by IAEA to handle SHARS and currently three countries owned the MHC namely South Africa, China and Malaysia.

In Malaysia, the project was started in 2015 with the assistance of IAEA and used 10th Malaysia Planning programme for the budget. The facility capable to handle up to equivalent 2000 Curie Cobalt 60 sources. For more than 2000 Curie, Cobalt 60 the special arrangement for the operation will be discussed with the local authority before proceed to the actual operation.

Since MHC is the mobile facility, the facility can be transported, assembled, operated and dismantled at any site. This independent facility can fit into two 40 foot container and capable to be transported by sea, land and air. The facility developed in Malaysia will be used in the Asia region (if requested) to cater the issue of SHARS in their country. Long Term Storage Shield (LTSS) has been introduced to store the SHARS until further process (reuse or disposal). LTSS capable to store up to equivalent 10,000 Curie Co-60 into the 4 drawers. The introduction of LTSS into this programme can reduce the space required to store the radioactive sources and it can be retrieved back anytime using the MHC.

2 Equipment

Mobile Hot cell (MHC) main component is consist of shielding, handling equipment, supporting system, detection system and in cell equipment.

Shielding is consist of 3 main component namely the shielding wall, roof and window. MHC shielding wall were constructed from the sand with metal plate in between to contain the sand and maintain the thickness of the shielding wall. The sand act as shielding material to reduce the high radiation during operation. The sand density is 1.5 g/cm^3 (minimum) and the wall thickness is 1.5 meter. For the roof, 5 set of the concrete roof are aligned at the top of MHC with the specific thickness of the concrete. The concrete roof act as a shielding on the top and also will reduce the sky shine effect.

Window is the main viewing component for the hot cell. The operator used the window to view the operation inside the hot area. For the MHC, Zinc Bromide is used to fill the window enclosure. The Zinc Bromide ($ZnBr_2$) liquid is transferable from the drum to the enclosure vice versa with the assistance of the pump.

There are 3 main handling equipment for MHC. Master Slave Manipulator (MSM) is the main handling equipment for the operation of the Mobile Hot Cell. The MSM for the MHC capable to handle up to 12kg for vertical lifting and 7kg of weight in any direction. The slave side can cover almost all the side of the operation area. The MHC MSM was manufactured by Automotor, Chengdu China. The operator was trained by the manufacturer to safely operate the equipment.

For the weight more than 12kg, one jib crane was installed inside the operation area to assist heavy handling. The jib crane capable to handle up to 300kg of weight and its supported by the steel channel fixed at MHC structure. The coverage of jib crane covers most of the area of operational area.

The A Frame Crane is handling equipment installed at the outside area of MHC containment. The 3000kg hoist is used to handle heavy equipment such as teletherapy head and irradiator. The light weight A Frame made by aluminium is easy to assemble and dismantle by the operator. The A frame travels along the guide rail placed at the front and back of the MHC.

The supporting system is the system that support the MHC operation. One of the main equipment is the nuclear ventilation system. The purpose of the nuclear ventilation system for MHC is to ensure the containment is under slightly negative pressure. This is mandatory requirement so that the personnel and environment are kept safe from any contamination if exist.

The CCTV system plays important role in supporting the operation to ensure the clear view inside the MHC by operator. Lighting system is important to visualize the operation inside MHC because, there is almost zero visibility inside the hot cell when the MHC closed by the roof.

Long term storage shield or LTSS provide long term non-permanent storage for the source. The design of LTSS was based on MDS Nordion F147 transport container. The lead shielding can hold up equivalent to 10000 Ci of Co-60 sources. There are 4 (four) capsules inside rotatable drawer with double door system and it will allow variety of source size to be stored inside the drawer. The LTSS shall be aligned properly with LTSS chute to ensure smooth transfer between LTSS and MHC containment. The LTSS was equipped with locking screw to prevent unauthorised access to the source drawer.

The radiation detector is the monitoring equipment not only for detection but it's also for the measurement of source activity. There are two fixed detector for the MHC. The outside detector used to monitor the dose rate at the operator area (window) and the inside detector is used to measure the dose rate and then, it will convert to current activity of the sources for record purpose.

The in cell equipment is the equipment or tools that requires for operational and conditioning of sources inside the MHC. Welding machine and leak test equipment together with special modified engineering tools (plier, screwdriver hammer, cir clip etc.) are the equipment for the assisting the retrieval and conditioning process. The equipment is specially design to suit with the MHC operation. Some of the in cell equipment was developed onsite based on the case by case basis.

3 Mobile Hot Cell Operation

There are 5 main procedures for the operation of Mobile Hot Cell namely preparation, assembly, facility commissioning, operation and dismantling. There are two team involved in MHC operation which consist of 14 personnel. The responsibility of the personnel was based on the specialties stated in the Quality Management System.

4 Current Status

There are two successful operations of MHC has been done in Nuclear Malaysia during two peer review mission. The purpose of operation on 2017 and 2018 is to review the MHC readiness, the team preparation and the documentation. The peer review was done by IAEA and experts from various countries. The peer review on 2017 was not successful. The issues of documentation was highlighted by the panels and need to be solved.

In 2018, the team member with the assistance from IAEA developed the Quality Assurance Programme. This programme and document successfully completed on October 2018 and pass the Peer Review on the same year.

The document has been submitted to AELB (local authority) for operational licensing and MHC was granted the full operation in 2023. Nuclear Malaysia looking to provide assistance for regional operation in 2024 after all the requirement by IAEA for the regional mission has been fulfilled.

5 Research Planning

The facility will provide the wide area of research for PDC in the project related to the sealed source. Some of the project in planning are:

a. Reuse and Recycle of Spent Source

b. Development of equipment for handling the spent sources

c. Irradiation equipment

d. Assistance in forensic research

e. Source storage

The research and development above was covered in National Nuclear Technology Policy (DTNN) and Nuclear Malaysia Vision 2030 (WNM 2030).

6 Conclusion

The mobile hot cell facility will provide the research and development opportunity for PDC in the area of sealed source. This opportunity will benefit of Malaysia in order to support the industry especially in waste management, tool and equipment, source handling and others.

References

Anwar A Rahman et al. 2018. Mobile hot cell for conditioning of category 1 and 2 sources. *Proceeding Radiation Protection Conference Workshop, 28th November 2018, Langkawi.*

Anwar A Rahman et al. 2019. Mobile hot cell in handling category 1 spent high activity sources. *Proceeding Nuclear Technical Covention, 22nd October, 2019, Malaysia.*

Design and Fabrication of Nuclear Malaysia Survey Meter for Education

Azraf Azman
Technical Support Division, Malaysian Nuclear Agency
43000 Kajang, Selangor
azraf@nm.gov.my

Abstract

The main purpose of this article is to shed some information during the design and fabrication of a casing for a survey meter. The perspective of a design standpoint is to generate appropriate designs and, from the machining standpoint is the requirement to achieve the required quality of the machine part.

Keywords: Design, Fabrication, CAD,CAM

1 Introduction

Design and fabrication is a common process to translate an idea to produce physical forms or patterns. It involved several tools such as Computed Aided Design (CAD), Computed Aided Manufacturing (CAM), and machines whether through conventional or modern machining methods. The objectives of this article are to show the design and fabrication flow for educational survey meter casing.

2 Methods

The process flow chart for casing design and fabrication is described in Figure 1. To design a survey meter casing, a detailed study of the components, the geometry of the circuit board, and the placement of the components. This will determine the size of the casing for the device. Inventor from Autodesk is a Computed Aided Design software used in this design stage. Whereas Edgecam is a Computed Aided Manufacturing software that was used to simulate the machining process. The simulation code then is uploaded to a Computed Numerical Control (CNC) milling machine. The CNC milling will physically do the machining according to the shape required. Installation, assemblies, and retrofit of the casing are required to ensure the electronic board and components fit within the casing. The assembled components will undergo a series of tests to ensure the functionality of the device according to the required specifications.

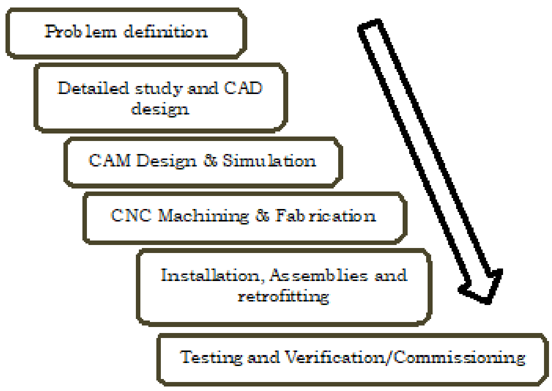

Figure 1: Process flow chart for design and fabrication of casing

3 Results

The survey meter casing was produced based on the flow process for design and fabrication. The casing material is made of acrylic also known as Plexiglass, the top casing dimensions were 160 mm (length) x 110 mm (width) x 18 mm (depth) as shown in Figure 2, and for the bottom casing was 160 mm (length) x 110 mm (width) x 24 mm (depth). The casing was machine using a CNC Milling machine and also test fit using an electronic circuit board. The machining and fitting process took about two weeks to complete for 20 units of casing. Whereas, it took a week to complete a unit of the casing by using a conventional milling machine.

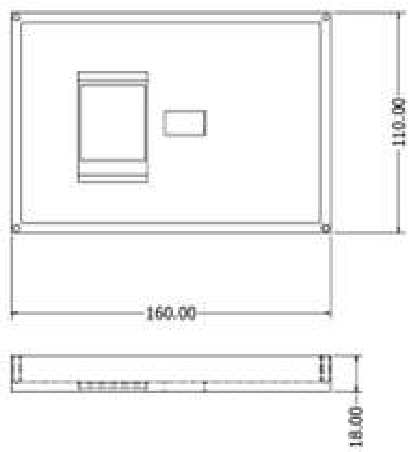

Figure 2: CAD drawing for top casing

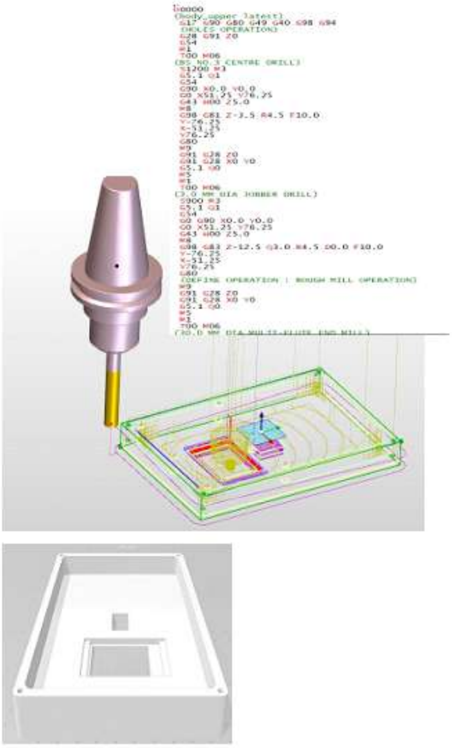

Figure 3: Edge cam codes and simulation

Figure 4: Product of the survey meter casingn

4 Conclusion

The design and fabrication of the survey meter casing was able to be manufactured and delivered according to the required specification. Modern tools (CAD, CAM, and CNC) introduced in the design and fabrication process accelerate manufacturing and improve the accuracy and precision of products.

References

Ehmann K. F., Kapoor S.G., DeVor R. E., and Lazoglu I. 1997. Machining process modeling: A review. *ASME. J. Manuf. Sci. Eng. November 1997*, 119(4B):655–663. https://doi.org/10.1115/1.2836805.

Individual Research Contribution Review, 2023, 1(1): 347–348

Ultraviolet Irradiator for Latex Vulcanization

Chai Chee Keong
Technical Support Division, Malaysian Nuclear Agency
43000 Kajang, Selangor
chai@nm.gov.my

Abstract

Latex vulcanization via ultraviolet irradiation was proven scientifically viable. Numerous studies have shown the methods and ultraviolet radiation devices for latex vulcanization. Some of these findings were internationally patented. Malaysian Nuclear Agency has attempted to innovate latex formulation for vulcanization by ultraviolet radiation and gained positive results. Hence, it is crucial to demonstrate the feasibility and viability of the findings for industrial benefits. This article discusses the design of an ultraviolet irradiator prototype for latex vulcanization.

Keywords: Ultraviolet irradiator, Latex vulcanization, Prototype

1 Introduction

Scientific studies have shown the capability of ultraviolet radiation in vulcanizing latex (Lazim et al., 2021; Hansupalak et al., 2016). Methods and ultraviolet radiation devices for latex vulcanization have been internationally patented (Schaller et al., 2006). There are also publications about the use of thin layer photoreactor and falling film photoreactor for latex vulcanization using ultraviolet radiation (Schlogl et al., 2010). The patented and published designs for UV irradiation apparatus are shown in Figure 1(a). Realizing the potential of ultraviolet radiation technology in latex vulcanization and its potential impact to the latex production and latex dipped product manufacturing industries in Malaysia, the Malaysian Nuclear Agency has endeavored to conduct research and development for a novel ultraviolet radiation technology, related expertise and devices. Laboratory studies have shown positive results in latex vulcanization using innovative latex formulation that is based on hybrid ultraviolet radiation – peroxide vulcanization (Ibrahim et al., 2023).

In order to benefit the related industries, it is crucial to upscale the laboratory formulation and setup to demonstrate the feasibility and viability of these research findings beyond laboratory scale through a well-designed prototype. However, it is also important to ensure the novelty of the prototype to avoid patent infringement issues. This paper discusses the design of a pilot-scale ultraviolet irradiator prototype for latex vulcanization, which will be used to test the feasibility of the laboratory findings and obtain preliminary data for industrial-scale prototype in the future.

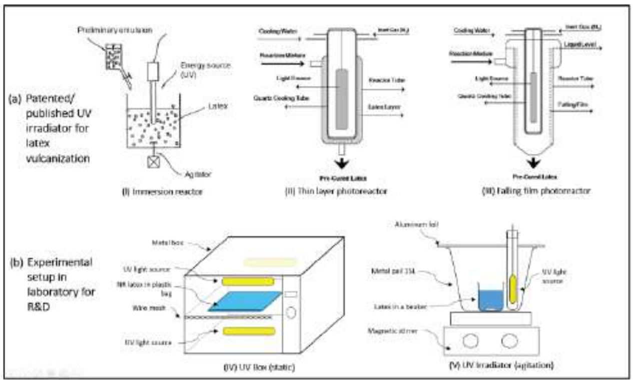

Figure 1: (a) Patented/ published UV irradiator for latex vulcanization and (b) experimental setups in laboratory for R&D.

2 Methods

The ultraviolet irradiator setup used for previous laboratory studies is shown in Figure 1(b). There were two experimental setups involved that simulate or mimic the situations of UV irradiation on still latex and agitated latex. The former was performed in a metal box where the formulated latex sample was sealed in a plastic bag and placed on a wire mesh in between two UV light sources. While the latter was done in a metal bucket attached with UV light source inside and placed on a magnetic stirrer, and the formulated latex was stirred with a magnetic bar place at the bottom of the bucket. These setups were used for studies to determine the formulation and parameter for UV vulcanization of latex. The design of the UV irradiator prototype was based on the experimental outcome obtained from these two experiment setups.

3 Results and Discussion

The whole idea of an ultraviolet irradiator for latex vulcanization is to exposure the latex to a sufficient amount of ultraviolet radiation in an effective manner. One of the main limitations of ultraviolet radiation is depth penetration that caused a big challenge to irradiate the latex in bulk. Hence, the design of a UV irradiator prototype for latex vulcanization in pilot scale must take into consideration of this limitation. The proposed UV irradiator prototype shown in Figure 2 is an attempt to vulcanize formulated latex in bulk. It combines the ideal of both UV irradiation on thin static latex layer and latex in beaker while stirring. According to the design, formulated latex will be channeled to a UV irradiation chamber which is a narrow cavity made of glass and sandwiched by an array of UV lamps. While passing through the cavity, the formulated latex will be exposed to a predetermined amount of UV radiation and vulcanized. The irradiated latex can be re-channeled to the UV irradiation chamber if needed for prolong exposure to UV. The latex is transported through the UV irradiation chamber from the bottom. The reason for this bottom-up route of latex transport is to ensure novelty of this design.

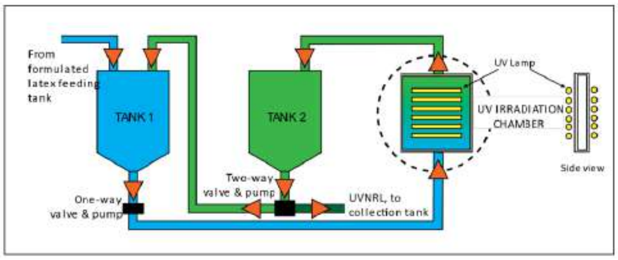

Figure 2: Design of UV irradiator prototype for latex vulcanization

4 Conclusion

An UV irradiator for latex vulcanization at pilot scale was carefully designed based on the experimental outcome of UV irradiation on latex in static and agitated mode. The UV irradiator prototype combined the idea and novelty of exposing thin layer of formulate latex bulk while flowing from bottom up through a cavity.

References

N. Hansupalak, S. Srisuk, P. Wiroonpochit, and Y. Chisti. 2016. Sulfur-free prevulcanization of natural rubber latex by ultraviolet irradiation. *Industrial & Engineering Chemistry Research*, 55(14):3974–3981.

S. Ibrahim, C.K. Chai, M.H. Bahrin, H. Sham, M.N.M. Lazim, A.A. Rahman, A.B.A. Kadir, N.M.R. Brahin, K.H.M. Yusop, H. Maseri, S.H. Said, W.I.W. Yusof, M.N. Atan, and N.H.M. Ali. 2023. Effect of ultraviolet irradiation dose on mechanical properties of hybrid ultraviolet-peroxide prevulcanized natural rubber latex. *Nuclear Technical Convensyen 2023*.

M.N.M Lazim, A.F. Mohd, C.K. Chai, and N. Ibrahim. 2021. The effects of HDDA and n-BA & TMPTMA on physical, and thermal properties of UV irradiation vulcanization natural rubber latex. *International Transaction Journal of Engineering, Management, & Applied Sciences Technologies*, 12(9)(12A9F):1–11.

R. Schaller, A. Holzner, R. Ehrenfeldner, M. Hochtl, W. Kern, F. Stelzer, and A. Temel. 2006. Method for producing a crosslinked elastomers. EP1762586A2, European Patent Office.

S. Schlogl, A. Temel, R. Schaller, A. Holzner, and W. Kern. 2010. Prevulcanization of natural rubber latex by UV techniques: a process towards reducing Type IV chemical sensitivity of latex articles. *Rubber Chemistry and Technology*, 32(2):133–148.

Assessment of Structural Integrity of Biological Shielding Structure at RTP

Hasniyati Bt Md Razi
Technical Support Division, Malaysian Nuclear Agency
43000 Kajang, Selangor
hasniyati@nm.gov.my

Abstract

The TRIGA PUSPATI Reactor (RTP), a crucial research facility for nuclear science and technology, relies on a robust biological shielding structure to contain radiation and ensure the safety of personnel and the environment. Over time, factors such as aging, radiation exposure, and environmental conditions can degrade the structural integrity of this vital shielding. The aim of this project is to evaluate and assess the condition of the biological shielding structure at the RTP. The overall average value of the rebound number across the walls of the RTP (excluding the results from the rebound test on the thermal column) amounts to 39.2. This finding indicates that, on average, the concrete quality of the RTP wall aligns with the characteristics of a highly durable and resilient hard layer, signifying its quality as being very good. These findings are in line with theoretical expectations and provide valuable insights into the structural integrity of the TRIGA PUSPATI Reactor.

Keywords: Structural integrity, Safety assessment

1 Introduction

The reactor core structure of the RTP is equipped with several barriers as defense-in-depth measures to protect humans and the environment against radiological hazards. The first layer was held by its fuel matrix, subsequently, the fuel cladding, reactor core tank and coolant, were surrounded by a thick layer of high-density concrete as its biological shielding. The fission process released neutrons and other ionizing radiation which interact directly with the reactor core structure and materials. Consequently, the activated materials were builtup and accumulated over the time span.

The greatest concern most likely comes from the release of hazardous fission products if the fuel cladding loses its function to contain and confine the radioactive materials. The ageing process can potentially result in the deterioration of structural integrity, raising the likelihood of failures in the barriers. If biological shielding, particularly in concrete, by long-term exposure to radiation, its ability to contain and to prevent the release of radioactive materials may be compromised.

Assessing and evaluating the condition of the biological structure can provide valuable insights into its quality and its ability to fulfil its intended function. One of the probable assessment methods is by surface inspection to the biological shielding. The purpose of the surface inspection is to verify the near-surface flaws while the volumetric inspection is to indicate the depth or size of cracking that involves radiographic, ultrasonic or eddy current techniques. The high-density concrete can be affected by radiation interactions with material and heating the concrete by the absorption of the radiation energy. Severe damage from radiation is not expected for nuclear research reactor operations conditions. However, it is very important and significantly needs to be investigated to understand the physical condition of the systems.

2 Methods

2.1 Location Mapping

The RTP biological shielding concrete structure is 6.6-meter in diameter and 6.5-meter height. For this assessment, 14 different locations have been identified where 7 locations were located at both bottom at top segment of the RTP concrete structure. Only two segments of the RTP were not able to be accessed because of some limitations. The location mapped was distributed into two segments as described in Figure 1.

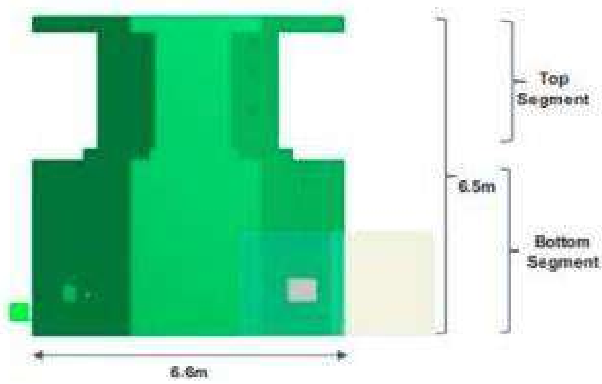

Figure 1: Segments of RTP

2.2 Rebound Hammer Test

Rebound Hammer measured the surface hardness of concrete and provides an estimation of surface compressive strength, uniformity, and quality of concrete. The calibration report of rebound hammer meets the requirement of ISO/DIS 8045, EN 12504-2 and BS 1881 Part 202. The rebound distance is typically measured as the distance the hammer's plunger moves back after impact, expressed as a percentage of the initial impact distance as in Figure 2.

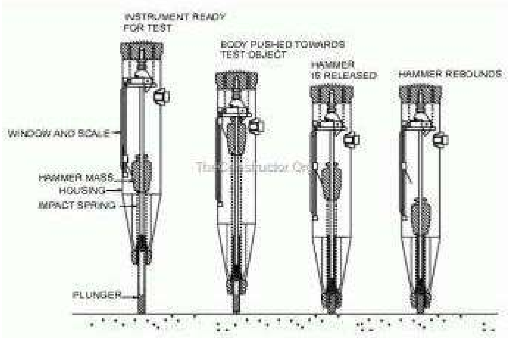

Figure 2: Rebound Hammer Testing

3 Results

3.1 Rebound Hammer Test

A comprehensive assessment of the RTP wall's structural integrity involved conducting the rebound hammer test, and this assessment extended across a substantial area. Specifically, this examination covered the entire surface of the RTP wall, excluding the TC wall, BP2. In total, an impressive 344 individual test points were meticulously examined and subjected to the rebound hammer test.

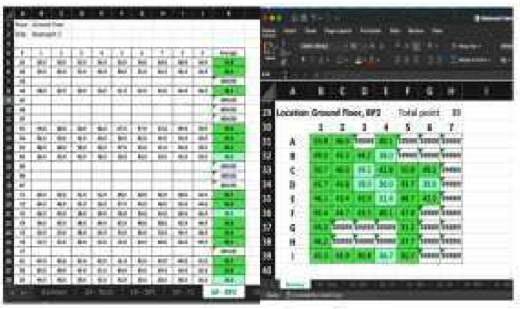

Figure 3: Rebound Hammer Test data

Table 1 shows the rebound values obtained from rebound hammer tests at various locations in the reactor control structure.

4 Discussion

The overall average value of the rebound number across the walls of the TRIGA PUSPATI Reactor amounts to 39.2. This finding indicates that, on average, the concrete quality of the RTP wall aligns with the characteristics of a highly durable and resilient hard layer, signifying its quality as being very good. Furthermore, it is essential to mention that the estimated comprehensive strength value for the average rebound number at RTP (39.2) approximately translates to 39.5 N/mm2. In the upper segment, these readings fall below the overall average value, signifying a very good hard layer. Conversely, the average rebound numbers for each part of the wall in the lower segment surpass the overall average value, indicating a good layer.

Table 1: Rebound values

Test Location	Average Rebound Number	Quality of Concrete
Bottom Segment		
Radial Neutron Flow (BP1) / Small Angle Neutron Scattering (SANS)	43.6	1
Thermal Column (TC)	NA	NA
Tangential Neutron Flow (BP2)	44.2	1
Sample Storage	42.0	1
Radial Neutron Flow (BP3) / Neutron Radiography (NuR)	42.9	1
Between BP3 dan BP4 (BP3-4)	43.2	1
Piercing Neutron Flow (BP4)	42.2	1
Top Segment		
Radial Neutron Flow (BP1) / Small Angle Neutron Scattering (SANS)	37.8	2
Thermal Column (TC)	33.0	2
Tangential Neutron Flow (BP2)	32.7	2
Sample Storage	33.0	2
Radial Neutron Flow (BP3) / Neutron Radiography (NuR)	34.3	2
Between BP3 dan BP4 (BP3-4)	33.9	2
Piercing Neutron Flow (BP4)	34.1	2

Theoretically, objects in closer proximity to the reactor core should experience higher radiation dose exposures. Surprisingly, the total number of reflections in the lower segment exceeds that in the upper segment. This phenomenon can be attributed to the greater thickness of the concrete wall in the lower level compared to the upper level. Consequently, despite the lower reflection readings, the concrete quality in the upper segment aligns with the characteristics of a good coating.

5 Conclusion

In summary, the RTP wall, emphasizing its overall robustness and durability (solely based on the result of rebound hammer test). Despite minor instances of damage and variations in rebound numbers, the concrete quality meets or exceeds the required standards for its role as a protective biological shield within the reactor environment. These findings are in line with theoretical expectations and provide valuable insights into the structural integrity of RTP.

Individual Research Contribution Review, 2023, 1(1): 351–352

Neutron Flux Profiling at the End-Of- Cycle (EOC) RTP Core Configuration

Hasniyati Bt Md Razi
Technical Support Division, Malaysian Nuclear Agency
43000 Kajang, Selangor
hasniyati@nm.gov.my

Abstract

The neutron flux profiling is important for determine thermal, epithermal, and fast neutron flux distribution in a reactor as Reactor TRIGA PUSPATI, Malaysia is at the end of cycle (EOC) of 15th core configuration. The thermal, epithermal, and fast neutron fluxes were determined by the foil activation method. The experimental samples with and without a cadmium cover were irradiated at in-core irradiation facility in RTP reactor core. The induced activities in the samples were measured by gamma ray spectrometry with a high purity germanium detector. Thermal flux, epithermal and fast flux profile peaked at the center of the aluminum rod which represent the middle of fuel rod in reactor core as expected and gradually decreased towards the end of the fuel. The effect of graphite rods on the core flux shape are also noticeable where the thermal, epithermal, and fast flux give a lower value at this position.

Keywords: Neutron Flux, Core Configuration

1 Introduction

Neutron flux parameter is crucial for the analysis of nuclear reactors because it affects the reaction rate and fuel burnup. Generally, neutron activation analysis (NAA) method is widely used to measure neutron flux at various research reactor irradiation facilities around the world. Aurum wire (gold) and Cadmium tube are among the activation neutron detectors used for a qualitative and quantitative measurement. The Aurum (Au) wire has only one stable isotope that can absorb a wide energy range of neutrons while Cadmium tube is used to separate thermal dan epithermal neutrons. To analyze the reaction rates of neutrons with Au wire or Cd tube samples, a special device such as high-pure germanium (HPGe) detector was used. The Malaysian 1MW Reactor TRIGA PUSPATI (RTP) was designed to effectively implement the various fields of basic nuclear research and education. It incorporates facilities for advanced neutron and gamma radiation studies as well as for isotope production, sample activation and student training. RTP reached its criticality on 28 Jun 1982 with excess reactivity of \$0.15. The neutron flux at RTP's irradiation facilities was initially measured after the commissioning of the reactor in 1980's and re-measured when nuclear fuels inside the reactor core undergo reconfiguration or reshuffling process. At present, the reactor core has changed 15th times, consisting of 111 Uranium Zirconium Hydrate (UZrH1.6) nuclear fuels, 10 dummy elements, 4 control rods and 5 in-core irradiation facilities.

2 Methods

A set of 10 activation samples were prepared in the form of Aurum-Bare (Au-Bare) and Aurum covered with Cadmium tube (Au-Cd). Au wire was cut approximately into a size of 1 mm length while Cd tube was cut slightly longer, about 3 mm each. All samples were then inserted into aluminum rod as in Figure 1 and were irradiated inside in-core irradiation facilities as shown in Figure 1. Aluminum rod A was placed at hole between fuel C9-C10-B5-B6 while aluminum rod B at hole between fuel B3-B4-A1-B2. All the samples were irradiated at a power level of 750 kW for 20 minutes based on suitability of irradiation time and samples handling process.

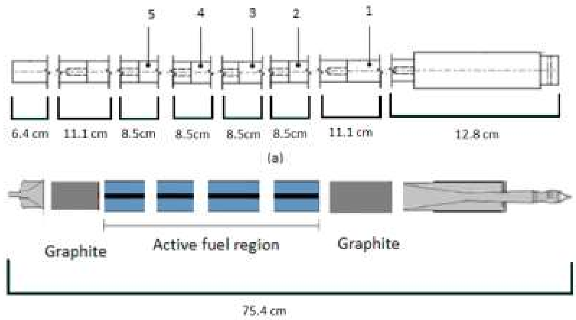

Figure 1: (a) Aluminum rod (b) RTP fuel dimension

The activity of samples for irradiation process can be determined by using following equation:

$$Au_b, Au_{b+Cd} = \frac{\frac{\text{(net peak area)}}{\text{mass}} \times \lambda}{\epsilon\gamma(\exp^{-\lambda t_{\text{decay}}})(1 - \exp^{-\lambda t_{\text{meas}}})} \quad (1)$$

where λ is the decay constant of the nuclide, ϵ is the efficiency of the detector γ is the intensity of Au t_{decay} is the time decay during cooling t_{measure} is the time decay during irradiation.

To obtain accurate results, it is essential to determine the efficiency of the detector prior to the analysis of the samples. The efficiency of detector was determined at geometry 20 cm by using Americium-241 (Am-241), Barium-133 (Ba- 133), Caesium-137 (Cs-137) and Europium-152 (Eu-152).The counting time was set at 1 hour to obtain minimum photo-peak fitting errors. Once the detector efficiency is determined, Au-bare and Au-Cd samples were fixed horizontally facing the center of the detector. The counting process was conducted for 10 minutes while the detector dead time was kept below 20%.

3 Results

3.1 Detector Efficiency

The efficiency of the detector was determined by using Americium-241 (Am-241), Barium-133 (Ba-133), Caesium-137 (Cs-137) and Europium-152 (Eu-152) where Am-241 emit gamma at energy 59.67 keV, Ba-133 emit gamma ray at energy 81.02 keV, 303.19 keV and 356.36 keV, Cs-137 emit gamma ray at energy 661.66 keV and Eu152 emit gamma at energy 121.84 keV, 344.62 keV, 411.49 keV, 779.48 keV and 964.6 keV at 20 cm distance from detector. The detector efficiency was calculated using equation below:

$$\text{Efficiency}, \epsilon = \frac{\text{Net Area}}{(\text{Live Time})(\text{Activity})(\text{Yield})} \tag{2}$$

The efficiency calibration curve was plotted as in Figure 2.

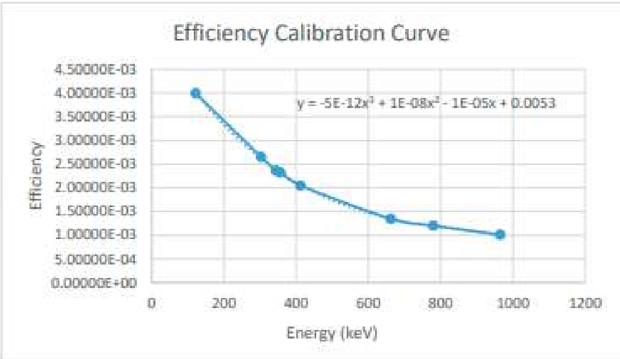

Figure 2: Efficiency Calibration Curve

Using the equation obtained by the graph, for Aurum-198 with gamma energy 412 keV, the efficiency of detector, ϵ is 0.002528.

3.2 Neutron Flux Distribution

The thermal, epithermal, and fast fluxes at in-core irradiation facility are calculated using below:

$$\phi_{\text{th}} = \frac{A_{\text{th}}}{N\sigma(1 - e^{-\lambda t_{\text{irr}}})}$$

$$\phi_{\text{epi}} = \frac{A_{\text{cd}}}{N\sigma(1 - e^{-\lambda t_{\text{irr}}})}$$

$$\phi_{\text{total}} = \frac{A_{\text{bare}}}{N\sigma(1 - e^{-\lambda t_{\text{irr}}})}$$

where A_{th} is specific activity of Au-bare minus specific activity of Au-Cd, A_{cd} is specific activity of Cd, A_{bare} is specific activity of Au-bare, N is Avogadro's number, λ is decay constant, σ is the cross section of Au-197 and t_{irr} is irradiation time in second. The summary of neutron flux distribution for these three irradiation facilities at power level 750kW are shown in Table 1.

Table 1: Summary of neutron flux distribution

Position at Reactor Core	Thermal Flux Ø0 x 1012 (n/cm2.s)	Epithermal Flux Ø0 x 1012 (n/cm2.s)	Fast Flux Ø0 x 1012 (n/cm2.s)
A1	0.70±0.007	0.01±0.009	0.86±0.003
A2	9.89±0.001	0.18±0.0001	1.41±0.007
A3	11.29±0.009	0.22±0.008	13.40±0.004
A4	6.93±0.005	0.08±0.006	6.67±0.004
A5	5.27±0.008	0.06±0.009	0.94±0.007
B1	0.69±0.001	0.02±0.002	0.09±0.007
B2	6.67±0.005	0.10±0.01	2.14±0.005
B3	11.40±0.001	0.15±0.008	5.03±0.009
B4	4.36±0.003	0.08±0.0001	1.27±0.001
B5	1.12±0.001	0.01±0.001	0.27±0.001

4 Discussion

Based on Table 1, the thermal flux, epithermal and fast flux profile peaked at the center of the aluminum rod (A3 and B3) which represent the middle of fuel rod in reactor core as expected and gradually decreased towards the end of the al rod. The significant peak at the core center is also because it has larger water volume compared to other location of measurements. Hence, more moderation process occur which increased thermal neutron flux at the core center. The effect of graphite rods on the core flux shape are also noticeable where the thermal, epithermal, and fast flux give a lower value at this position.

5 Conclusion

By using Aurum-Bare and Aurum-Cadmium samples, thermal, epithermal, and fast neutron fluxes of RTP was successfully obtained. The detector efficiency was determined prior to the neutron flux measurement using Americium-241 (Am-241), Barium-133 (Ba-133), Caesium- 137 (Cs-137) and Europium-152 (Eu-152) at geometry 20 cm. The detector efficiency was found to be 0.002528. The thermal flux, epithermal and fast flux profile peaked at the center of the aluminum rod (A3 and B3) which represent the middle of fuel rod in reactor core as expected and gradually decreased towards the end of the fuel. The effect of graphite rods on the core flux shape are also noticeable where the thermal, epithermal, and fast flux give a lower value at this position.

Neutron Image Deblurring Using Blind Deconvolution

Khairiah Yazid
Technical Support Division, Malaysian Nuclear Agency
43000 Kajang, Selangor
khairiah@nm.gov.my

Abstract

This project deals with the deblurring of neutron radiography images. The neutron radiography images produced from small research reactor like TRIGA MARK II PUSPATI research reactor (RTP) are inherently blurred due to certain physical limitations at the reactor as low beam collimation and blurring from the imaging detector. This study proposes a new approach in a blind deconvolution framework specifically for neutron image deblurring.

Implementation: A coarse-to-fine multi-layer iterative blind deconvolution approach is implemented within the MAP estimation blind deconvolution framework.

Results: The proposed method demonstrates a fast and accurate PSF estimation using only one blurred neutron image, without the need for any edge phantoms or edge selection procedures. Visual inspection shows significant improvement in restoration quality and robustness compared to conventional methods.

Keywords: PSF Estimation; blind deconvolution; neutron images and image restoration

1 Introduction

Neutron radiography, a non-destructive imaging technique that utilizes neutron radiation to probe the internal structure of objects, similar to X-ray radiography. This imaging technique excels in materials characterization, defect detection, and analysis of various opaque objects particularly useful for imaging materials that are difficult to penetrate with X-rays, such as metals or materials with high atomic numbers. Neutrons have high penetration capabilities into all types of materials, including heavy metals, and sensitive to many light elements, especially hydrogen.

Blurring associated with a lack of collimation in the beam gives rise to blurring in neutron images. A collimator in neutron radiography plays a crucial role in controlling, shaping, and focusing the neutron beam to achieve highquality images. The beam collimation *L/D* ratio in neutron radiography facility is illustrated in Figure 1. The *L/D* ratio is where the *L* is the length between the smallest diameter of the collimator and the sample, and D is smallest diameter of the collimator. This *L/D* ratio defines the geometrical blurring of the neutron imaging facility. In general, the *L/D* ratio of state-of -arts neutron radiography facilities generally lie in the range of 100 to 500.

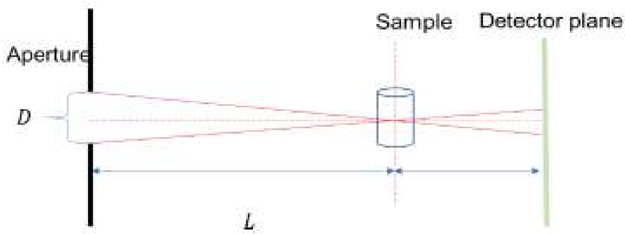

Figure 1: The beam collimation, (***L/D***) ratio in neutron radiography facility.

In contrast to the X-ray imaging system, the source of neutron radiography is not a point source but an extended aperture. This to the finite size *D* of aperture is the main reason for geometrical blurring. The main reason for using this extended aperture at low- power reactor is to guarantee that enough flux reaches the sample position. Increasing the *L/D* ratio in most facilities is not a viable option due to the necessity for facility reconstruction.

However, the *L/D* ratio is the main but not the only challenge connected with blurring in neutron radiography. The scintillator- based digital detectors used in neutron radiography also have limitations in terms of spatial resolution and sensitivity. This can result in blurry images and difficulties in distinguishing fine details or small defects. Hence, the imaging detector and large aperture neutron source are the main contributors to the blurring of the neutron images.

1.1 Neutron Radiography Facility at RTP

All neutron images presented in this work are acquired at Malaysia Nuclear Agency which houses the Research TRIGA PUSPATI (RTP) reactor. The neutron radiography facility at the RTP was constructed at the one of the radial beam-port. Since the neutron entrance aperture diameter is 3 cm and the distance between the inlet aperture to the image plane is 312 cm, this gives the *L/D* ratio of approximately is 104. This low *L/D* ratio is the main reason for the degradation of neutron images as previously explained.

The imaging detector is CCD/scintillator type, using 16-bit cooled CCD camera. The neutron beam strikes a 0.1 mm thick green scintillation screen. The lights produced by the scintillation screen were recorded on the CCD comprising of

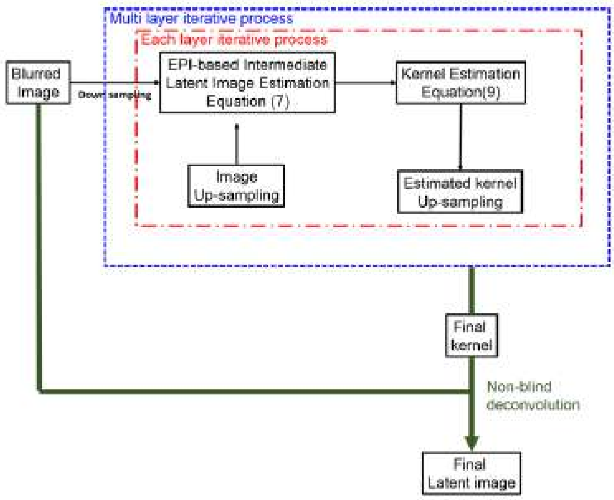

Figure 2: Overall flowchart multi-level scheme of proposed method

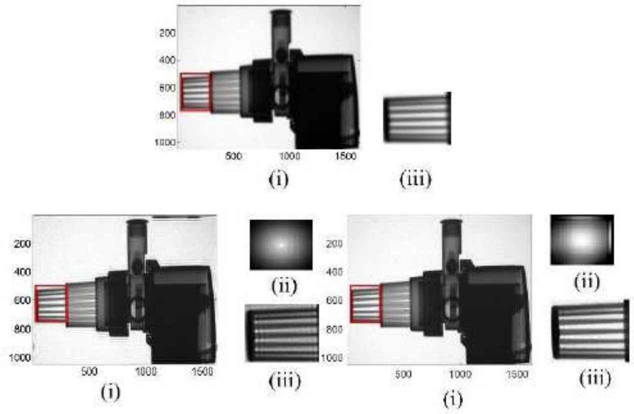

Figure 3: Iterative image deblurring comparing conventional and proposed methods. (i) neutron image, (ii) the estimated PSF and (iii) selected regions are zoomed-in to highlight small and fine details in red box, (a) blurred image, (b) and (c) are restored image by the conventional and proposed methods respectively.

2200x2750 active pixels. A double surface coated was used to keep the camera away from the direct neutron beam. Additional shielding was used to protect the electronic parts from the direct neutron beam. There are limitations in the imaging system. This type of standard detector suffers blurring from the lens system due to the large distance between the scintillator and the lens system.

All acquired neutron images were processed using open source ImageJ software to remove the significant noise mainly added during acquisition. Then the low dynamic range image contrast is adjusted to widen the dynamic range. Because of neutron image was too big in size and causing the algorithm to run very slow therefore the original image is cropped for selected area. Then, the denoised blurred image is normalized between 1 and 0 from the original 16-bits digital values.

2 Results and Discussion

In the following, we present some experiment deblurring results using the proposed method and compared with the conventional edge-based neutron image deblurring method. As discussed above, ESF-based method for PSF estimation and iterative RL deconvolution for final restoration in common practice within the neutron community. In both methods, the estimated PSF is then input into a non-blind deconvolution method. In this study, 15 iterations were used for final deblurring.

3 Conclusions

This paper describes a robust method for deblurring from a single blurred neutron image. A coarse-to-fine multi-layer iterative blind deconvolution approach is implemented within the MAP estimation deblurring framework. Compare to conventional method, the new approach in this study demonstrated fast and accurate PSF estimation method using one single blurry neutron image without any edge phantom or edge selection method. Visual inspection of produced images illustrate that the proposed scheme improves the restoration quality efficiently and possesses a robust performance.

Individual Research Contribution Review, 2023, 1(1): 355–356

Towards Advanced Neutron Imaging: A Planned Upgrade for Neutron Radiography and Computed Tomography (NuRCT)

Khairiah Yazid
Technical Support Division, Malaysian Nuclear Agency
43000 Kajang, Selangor
khairiah@nm.gov.my

Abstract

The article describes about the upgraded neutron imaging facility at 1 MW PUSPATI TRIGA Research Reactor in Malaysian Nuclear Agency, Malaysia. The imaging facility at the radial beam port has undergone upgrades, resulting in a maximum L/D ratio of 110 and thermal neutron flux of approximately 10^5 ncm^{-2}s^{-1} at sample position. The significant enhancement in this upgraded facility is the incorporation of an affordable CCD-based detector for standard neutron radiography and tomography. This article outlines various activities conducted at the RTP, focusing on the qualitative and quantitative results achieved, as well as the advancements made in developing a neutron tomography system.

1 Introduction

Neutron radiography, a non-destructive imaging technique that utilizes neutron radiation to probe the internal structure of objects, similar to X-ray radiography. This imaging technique excels in materials characterization, defect detection, and analysis of various opaque objects particularly useful for imaging materials that are difficult to penetrate with X-rays, such as metals or materials with high atomic numbers. Neutrons have high penetration capabilities into all types of materials, including heavy metals, and sensitive to many light elements, especially hydrogen.

1.1 Neutron Radiography Facility at RTP

The imaging detector is CCD/scintillator type, using 16- bit cooled CCD camera. The neutron beam strikes a 0.1 mm thick green scintillation screen. The lights produced by the scintillation screen were recorded on the CCD comprising of 2200x2750 active pixels. A double surface coated was used to keep the camera away from the direct neutron beam. Additional shielding was used to protect the electronic parts from the direct neutron beam. There are limitations in the imaging system.

2 Results and Discussion

2.1 Neutron Computed Tomography

The NuRCT system integration at the RTP was successfully completed in early October 2023. The camera box and sample manipulator systems are controlled through a combination of C++ and Python software.

Figure 1: Layout neutron radiography components at RTP

Table 1: Main parameters of the neutron facility at RTP

Parameters	
Beam line	Radial
Neutron spectrum	Thermal
Flux at sample position	10^4ns^{-1}cm^{-2}
Length collimator [cm]	232
Distance outer collimator to sample [cm]	80
L/D	104

Figure 2: The biological shielding of NuRCT

3 Conclusions

A tomography system, NuRCT is being developed at RTP. This system would be capable to perform nondestructive assays after 2D images acquired on a real or quasi real time basis as well as 3D tomographic images reconstructed from the

(i)

(ii)

Figure 3: NuRCT system (i) control system and (ii) sample manipulator

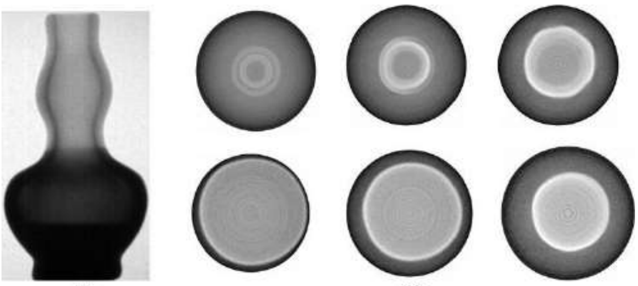

(i) (ii)

Figure 4: (i) neutron projection (ii) The reconstructed neutron CT slices

two-dimensional ones.

The operation time for RTP in steady state is limited at three hours. Consuming time for a projection was over one minute (exposure, change of position for object, manual control of every action, image save etc.). These constraints limited the number of projections for an investigation.

Individual Research Contribution Review, 2023, 1(1): 357–358

Overview of Reactor TRIGA PUSPATI (RTP) Seismic Monitoring System

Khairul Anwar Bapujee
Technical Support Division, Malaysian Nuclear Agency
43000 Kajang, Selangor
k_anwar@nm.gov.my

Abstract

The Reactor Digital Instrumentation and Control System (ReDICS) plays a crucial role in monitoring and controlling Reactor TRIGA PUSPATI (RTP). It encompasses a seismic monitoring system that captures seismic information, including time history data and peak ground acceleration levels at the reactor building basement. This system features selfdiagnostic, testing capabilities and alerts plant operators following an event to assure continuous system and simplicity of operation and maintenance for Reactor TRIGA PUSPATI (RTP). The seismic monitoring system is capable of detecting and recording spike readings that exceed predetermined threshold levels and are saved as event data. In this study, the analysis of recorded event data used R Programming open source and it entails data preprocessing and event frequency. This study aims to assess and discuss the current performance of the seismic monitoring system employed in Reactor TRIGA PUSPATI (RTP).

1 Introduction

In recent years, Malaysia has experienced a variety of seismic events of varying magnitude and frequency, reflecting the region's dynamic geological landscape. While the details of recent seismic events may vary, their significance highlights the critical importance of robust monitoring systems. Inside the TRIGA PUSPATI (RTP) reactor, the seismic monitoring system ensures the safety and stability of critical infrastructure during these geological activities. The seismic monitoring system is to obtain seismic information such as time history data, and peak ground acceleration level at the reactor building floor. It is not related to the reactor operation but is available to display the information of the earthquake event. This system not only records earthquake information such as time history data underground of the reactor building and peak values of ground acceleration but also has self-diagnosis and inspection functions. Its central role is to immediately alert the plant operator after an event, ensuring continuous system reliability, ease of operation, and ease of maintenance of the Reactor TRIGA PUSPATI. A key aspect of this monitoring system is the ability to identify and record peak values that exceed a predetermined threshold and save them as important event data. Through a careful review and insightful analysis, this study identifies the system strengths, potential improvements, and systems for the safety and reliability of TRIGA PUSPATI (RTP) reactors in the face of seismic events.

2 Methods

In this study, the seismic monitoring system involves data acquisition and data analysis. The seismic monitoring system collects data from seismic sensors (X, Y, Z) and will show in digital seismometers such as history data, peak ground acceleration level, and alarm indicator. This system also possible to send data to other external systems. The characteristics and technical specifications of this seismic monitoring system also be identified and verified. This project utilizes an event frequency analysis approach to assess the performance of the seismic monitoring system at Reactor TRIGA PUSPATI (RTP) in detecting earthquakes. Data collected from the AK-2000-12 seismic monitoring system at RTP, including event frequency and peak-toground acceleration data were used to be processed using R-programming and the data obtained was tabulated in the graph.

3 Results and Discussion

The seismic monitoring system consists of a seismic acceleration sensor and a seismometer. A seismic acceleration sensor is a portable seismometer that requires no power supply. Its battery-free sensor is an over-damped acceleration sensor and is housed in a drip-proof case. This is the best seismometer for earthquake observation in places where only a limited power supply can be obtained or for temporary permanent earthquake observation in places where no power supply is available.

Figure 1: RTP Seismic Monitoring System

This system requires no power and is housed in a drip-proof case. It can be used in the various severe environments in which earthquake observation is often involved. The earthquake motions monitored will be output as an acceleration waveform with three components (two horizontal and one vertical). The sensor used is compact, lightweight, easy to install, and suitable for temporary or other earthquake observation in which it is necessary to move sequentially to another observation point. The combined use of this sensor and a data logger will allow the establishment of a seismic wave observation system. This includes a built-in amplifier type, which is best suited for accurate detection of minor earthquake motions.

Table 1: Technical Specification of Digital Seismometer and Seismic Sensor

Digital Seismometer	
Content	Specification
Model	AK-2000, Korea
Converter Precision	24bit 129dB
Channel number	3 channel - 12 channel (1 sensor – 6 sensor)
Alarm output	±10V, 4-20mA Relay control signal
Data acquisition & transmission	TCP/IP, Data recording & real time transaction
Temperature & humidity condition	-10 ~+70ºC
Sampling	100Hz, 20Hz
Memory capacity	280 GB
Correction function	Sensor signal error detect(A/D Convert correction function)
Data recording time	• Based on trigger point (30 second ago) work storage up to 60 sec • 60 day continuous recording
Installation Method	- Monitor: MCR of the DESK - Sensor: Reactor Hall Ground Floor

Seismic Sensor	
Content	Specification
Model	JEP-6A3
Type	Overdamped type accelerator
Direction of earthquake detection	X, Y, Z (Three orthogonal components)
Sensitivity	1.1 V/9.8m/s^2 ±10%
Frequency characteristics	0.07 to 100 Hz
Maximum displacement in movable section	2mm p-p
Natural frequency	3±0.5Hz
Linearity	0.1%
Operating temperature	-20 to 50ºC
Water resistance	Drip – proof construction
Mass	Approx. 2kg

The time frame of data collected is from 28th August 2013 until 13th July 2023, in which large sets of data span over 10 years. Most data detected below 50 gal due to low seismic noise caused by the noise of the RTP working environment and vehicles outside of the facility. The high density of detection happening during working hours (8 am-6 pm) proves man-made noise created during that period had been detected by seismic sensors. There was also a gap in the data due to two separate events of power supply for the seismic monitoring system loss. The seismic monitoring system works as usual when new power supply units are connected to the system.

The sensitivity of the monitoring system needs to be properly set to its baseline. This is crucial because the sensor outputs the strengths of the earthquake as an electronic signal. A slight deviation in system sensitivity will give incorrect readings. Proper calibration and maintenance action also need to be performed over a specific time to ensure the reliability and performance of the RTP seismic monitoring system.

4 Conclusions

For data analysis utilize R programming for statistical analysis of RTP's data. Methods include descriptive statistics, hypothesis testiig, and visual comparisons to assess the accuracy of RTP's seismic monitoring system in detecting earthquakes. The seismic monitoring system at RTP demonstrated high accuracy in detecting earthquakes within the research region. The high accuracy of RTP's system in earthquake detection is a promising finding,

In conclusion, the RTP Seismic monitoring system has demonstrated the capability to detect seismic motion; however, it primarily registers a low number of seismic events. This may be attributed to the system's sensitivity in detecting low seismic noise, including man-made induced events. Several improvements needed to be performed to achieve a more robust and reliable seismic monitoring system at RTP. This will enable RTP can further strengthen its capabilities and contribute to enhanced earthquake preparedness and safety in the region.

References

P.R Johnson and M.L Garcia. 2019. Performance evaluation of seismic sensors in a nuclear facility. *Seismological Research Letters*, 90(2):214–228.

Chen Q. and Wang H. 2021. Assessment of seismic monitoring systems in nuclear facilities: A case study of reactor TRIGA PUSPATI. *Proceedings of the International Conference on Seismology (ICOS 2021)*, pages 143–156.

Individual Research Contribution Review, 2023, 1(1): 359–360

Accelerator: Technologies and Applications

Leo Kwee Wah
Technical Support Division, Malaysian Nuclear Agency
43000 Kajang, Selangor
leo77@nm.gov.my

Abstract

This paper provides the development and basic information of the accelerator technologies and its application.

Keywords: Accelerator, Technologies, Applications

1 Introduction

Particle accelerator is a scientific instrument consists of various advanced technologies such as source technology, acceleration technology, vacuum technology etc and science principle that boosts up the kinetic energy of the charged particles (beam) by an electric field and the applications of accelerator are very broad (Leo and Hashim, 2019). Typically, in Malaysian Nuclear Agency, several electrostatic electron accelerators such as EPS-3000, ELV-4, Curetron and localized Low Energy Electron Accelerator (LEEA) (Leo et al., 2021b) were established and operating to serve for various applications. The next section will introduce the various technologies or systems of accelerator based on the LEEA development.

2 Methods

A local made low energy electron accelerator was initiated in 2006 so-called as Baby-Electron Beam Machine (EBM), with the initial energy of 140. This project was started by coupling an accelerator tube obtained from the BINP and high voltage power supply (HVPS) of an unused Philips x-ray machine of model MG-160. The application of the 140 keV machine is limited. Therefore, for application enhancement, the energy of this machine has been upgraded from 140 keV to 200- 250 keV with a localized made low energy electron accelerator (LEEA) as shown in Figure 1.

Figure 1: 200 keV Low Energy Electron Accelerator

The accelerator is comprised of many technologies, it must be developed individually and integrated to form a complete set of accelerator. The technologies/elements of accelerator are elaborated based on the LEEA development as below:

(i) Source: Electron gun of LaB_6 material to produce the electron beam when heating up by a powers supply.

(ii) Accelerating elements:
- High voltage power supply (HVPS): To provide the kinetic energy to the electron beam. This component is a heart of the accelerator. (Leo et al., 2019)
- Accelerating tube: Accelerating element composed of the number of electrodes and potential divider components. (Leo et al., 2020)

(iii) Vacuum system: To provide the vacuum environment inside the accelerating tube. This system consists a rotary pump, turbo molecular pump and vacuum gauge.

(iv) Scanning system:
- Scanning horn: to provide an irradiation space and sustain the vacuum environment. This is a crucial part which must hold a micron meter thickness titanium foil in 10^{-6}–10^{-7} mbar pressure over the atmosphere pressure. (Leo et al., 2021b)
- Scanning power supply: To avoid the heat at the titanium window and dose uniformity. This unit is required to supply the desired excitation currents and frequencies to exciting the magnetitic coils horizontally and vertically. (Leo et al., 2020)

(v) Window cooling system: To provide the cooling along the window and avoid break down of the window. (Leo et al., 2018)

With the integration of those individual systems, the energetic beam will be passing through the window and hit the target or irradiation sample. (Leo et al., 2021a)

3 Applications

Basically, the type of ion species and beam energy is determined by the type of accelerators as shown in Figure 2. Whereby the user could identify the type of accelerator based on their application. Therefore, as a user this is essential to understanding the basic mechanism and principle of the accelerators. Although the machine itself is very costly and complicated but accelerator is indeed is very useful and could support various kind of mankind activities from health, environmental, security, high technology research and etc as elaborated in following section.

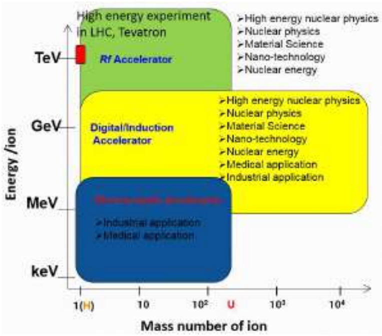

Figure 2: Energy Region explored by type of Accelerators

3.1 Promising Technology: Medical Applications

- Medical Radio-isotope Production

  Typically, medical radio-isotope production widely produced by using cyclotron. For example, when the energetic beam bombarded with the specific target, the nuclear reaction will produce the required radio-isotope by using the accelerator technology.

- Cancer Therapy

  Cancer therapy by X-ray is to use the high energy X-ray (photon) which is created by an electron accelerator with tens of MeV and collides with the metallic target and used for cancer treatment. Whereby the cancer therapy by using heavy ion is to use the heavy charge particles such as proton and carbon in few hundred MeV to deliver to the cancer cell and kill it.

3.2 Promising Technology: Agriculture Applications

- Mutation Breeding

  Mutation breeding is a process of new mutant's generation with desirable traits to bed into other cultivars by using the chemical or radiation techniques. Mutation breeding facility or Radioactive Isotope Beam Facility (RIBF) has been developed by the accelerator community to increase the quantity of plantation and to create the notable species of plantation with high quality, substantiality yield production.

3.3 Promising Technology: Industry Applications

- Scission, Cross-Linking and Grafting

  Particles beam is capable to induce the reaction inside the polymers by scission, cross-linking and grafting. Which are mainly dependent on the type of polymers and the energy deposition

- Surface Curing and Coating

  Besides of the 3 MeV electron accelerator, 200 keV electron accelerator so-called curetron is utilized to improve the damage resistance and hardness of the material surface.

3.4 Promising Technology: Nuclear Applications

- Accelerator Driver System (ADS)

  ADS promotes the subcritical reactor concept based on the accelerator technology. A driven proton beam with typically energy of ~1GeV will hit the spallation target and the neutron will be generated. The neutron will be reacted with the surrounding reactor core and the nuclear reaction will be occurred. In such concept, the safety of this kind of subcritical reactor is reserved by the driven proton beam. Whereby, the neutron production is terminated with the cut off of the proton beam.

- Neutron generator

  Recently, neutron generator based on the accelerator technology is developed by many companies rapidly. By using the neutron source-based accelerator technology, the safety feature is much promising than the nuclear reactor.

4 Discussion/Conclusions

Particles accelerator is a very costly but it is an advanced technology with the capability to overcome the environment pollution, climate change, energy and security issues. As a developed country, Malaysia should pursuit a national accelerator center (Leo and Takayama, 2020) to support the technology and science development and the economic growth of the nation.

References

K. W. Leo and S. A Hashim. 2019. Applications of accelerator. *Jurnal Sains Nuklear Malaysia*, 31(1):48 – 66.

K. W. Leo and K. Takayama. 2020. Proposed malaysian national accelerator facility: Multipurpose cyclotron. *AIP Conference Proceedings*, 2295(020005).

K.W. Leo, R.M. Chulan, S.A. Hashim, M. Azhar, Y. Dalim, M. Mokhtar, A. H. Baijan, R. M. Sabri, M. Faiz, A. Azaman, and R.C. Rosli. 2018. Study on the window cooling system of the 300 keV electron accelerator. *IOP Conf. Series: Materials Science and Engineering*, 298(012045, doi:10.1088/1757-899X/298/1/012045).

K.W. Leo, M. Azhar, R.M. Chulan, S.A. Hashim, M. Mokhtar, Khaidawaton, A. H. Baijan, and R. M. Sabri. 2019. Study on the filament power supply of the 300 keV electron accelerator. *IOP Conf. Series: Materials Science and Engineering*, 555 012022.

K.W. Leo, M. Azhar, R.M. Chulan, S.A. Hashim, M. Mokhtar, Khaidawaton, A. H. Baijan, and R. M. Sabri. 2020. Study on the scanning power supply of the 300 keV electron accelerator. *IOP Conf. Series: Materials Science and Engineering 785*, 012037.

K.W. Leo, M. Azhar, R.M. Chulan, S.A. Hashim, M. Mokhtar, Khaidawaton, A. H. Baijan, and R. M. Sabri. 2021a. Study the dose profile of low electron accelerator. *IOP Conf. Series: Materials Science and Engineering*, 1106(012023).

K.W. Leo, S.A. Hashim, R.M. Chulan, M. Mokhtar, M. Azhar, A. H. Baijan, R. M. Sabri, and M. Faiz. 2021b. Succeed story of low energy electron accelerator. *5th Annual Conference of Women in Nuclear (WiN)*.

Individual Research Contribution Review, 2023, 1(1): 361–362

IRCR

Assorted Electronics for Nuclear Instrumentation

Lojius bin Lombigit
Technical Support Division, Malaysian Nuclear Agency
43000 Kajang, Selangor
lojius@nm.gov.my

Abstract

A low-cost and a high-end version of survey meters were produced. Both suffer from post-development technical issues. A new breed of room-temperature semiconductor detectors became available and requires a bespoke front-end amplifier for readout. This article describes the post-developmental fixes of radiation survey meters and the proposal for assorted electronics for future handheld nuclear instrumentation. The technical issues were addressed by identifying the root cause via on-board measurement, and the proposed electronics were designed and simulated. Results are presented and discussed.

Keywords: radiation survey meter, high voltage circuit, front-end amplifier

1 Introduction

Two variants of radiation survey meters based on a Geiger-Muller detector were produced. The low-cost survey meter (LCSM) used a low-cost GM tube with minimal electronic sub-system and was intended as an educational tool for Malaysian secondary schools. The high-end version, dubbed the *G2 Tag Radig meter* (G2Tag), follows the international standard for handheld radiation survey meters and is equipped with a GPS locator. Both prototypes suffer from inconsistent readings, high voltage (HV) problems, and linearity issues in the high-dose region. Issues were addressed by examining the circuit design, physical examination of the electronic components, and performing onboard signal measurement. The problems were properly identified, the fix was implemented, and the post-remedial result was verified.

A new design for a low-power consumption HV circuit for future battery-operated nuclear instrumentation was proposed. It was based on the micro-power DC-DC boost regulator, commonly used in battery-operated instruments. A new breed of radiation detectors based on room-temperature compound semiconductors, such as 4H-SiC and CdTe/CZT become available. An electronics scheme was proposed as a potential front-end amplifier for these detectors.

2 Methods

2.1 LCMS & G2Tag issues

For both cases, the circuit and PCB diagrams were examined to find the possible cause of the problem. On-board measurements of the component values, wiring/interconnections, and low-level/HV sections were measured with a multimeter. Output signals at various points in the board were checked with an oscilloscope. The survey meters were also tested with a calibration source at the NM SSDL to verify the accuracy of the reading.

2.2 High voltage and front-end analogue circuits

Both circuits were designed using parameters defined by circuit requirements. The HV circuit shall deliver an adjustable low-ripple DC voltage between 450V to 600V from 3V to 5V input. This HV value is typical for GM tubes for industrial applications.

The CdTe and 4H-SiC semiconductor detectors require $\approx$ 4.4 eV and 7.8 eV to generate electron-hole pairs (Owens and Peacock, 2004). A charge amplifier comprised of pre-amp and quasi-gaussian shaper was proposed. The amplifier's dynamic range was designed to accommodate the energy deposition of γ-rays with energy below 100 keV. This range would be a realistic energy range that this detector could detect.

Small-footprint SMD components were used in both circuits to minimise noise and PCB layout. The circuit simulation was performed using the LTSpice[1] circuit simulator.

3 Data/Results

3.1 LCMS & G2Tag remedial

The LCMS suffers from poor PCB layout design, with no separation between the high-frequency HV and the digital sections (see Figure 1(a)). This leads to excessive noise, causing erratic readings in the LCMS. The GM's output pulse width is too large due to a mismatch in the capacitive coupling, causing high dead time (Figure 1(b)). An improved PCB layout and fixing the capacitive mismatch solve the technical issues in the LCMS.

Only one out of six tested G2Tag survey meters produced acceptable calibration results. Others show inconsistent results with early saturation (see Figure 2). Found that the maximum HV in failed units was under 500 V, the recommended HV for the LND 7121[2] GM tube. The problem was due to the mismatch of components in the HV circuit. Moreover, the GM output pulse width is large, causing early saturation. Solutions will be implemented in the next version of the G2Tag.

[1]https://www.analog.com/en/design-center/design-tools-andcalculators/ltspice-simulator.html
[2]https://www.lndinc.com/products/geiger-mueller-tubes/712-2/

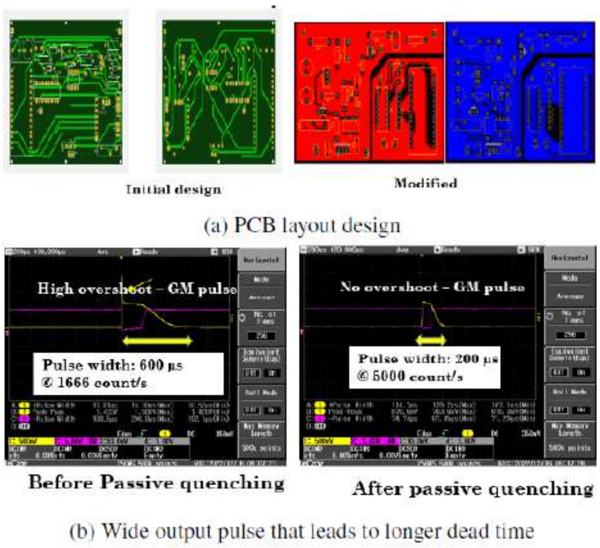

(a) PCB layout design

(b) Wide output pulse that leads to longer dead time

Figure 1: Technical issues and remedial in the LCMS design.

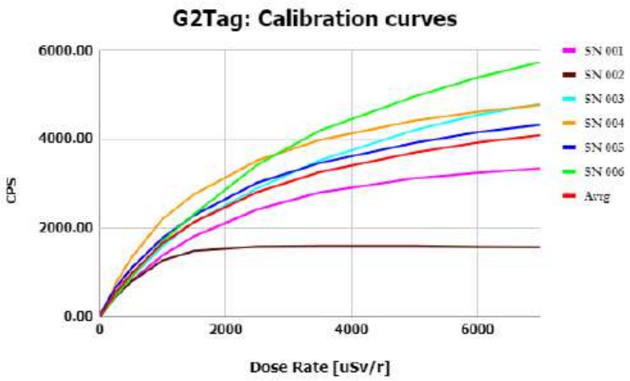

Figure 2: Inconsistent calibration curves in the tested G2Tag survey meters.

3.2 HV and front-end amplifier simulation

The HV circuit (see Figure 3(a)) is based on LT1615 (Technology,), a micro-power step-up Dc-DC converter from Analog Devices/Linear Technology[3]. An LPR6235-253L step-up transformer from Coilcraft[4] ramp up the voltage up to 280VAC and converted to 550VDC via voltage doubler.

The front-end amplifier (see Figure 3(b)) is a charge-sensitive pre-amp followed by a quasi-Gaussian shaper based on the circuit in (Lombigit et al., 2012). The feedback capacitor is set at 0.1 pF, which deliver $\approx$ 27mV for a 60 keV γ-rays.The quasi-gaussian shaper produced a Gaussian pulse with a width of $\approx$ 25 μs. A gain amplifier and buffer at the final stage amplify the signal up to 3 V.

4 Discussion/Conclusions

Technical issues hindering the LCMS and G2Tag survey meters have been identified. Afix in the LCMSwas implemented in the new design. The solution will be implemented in the next iteration of the G2Tag survey meter. An improved HV circuit and front-end amplifier were proposed for nuclear instrumentation in the future.

[3]https://www.analog.com/en/index.html
[4]https://www.coilcraft.com/

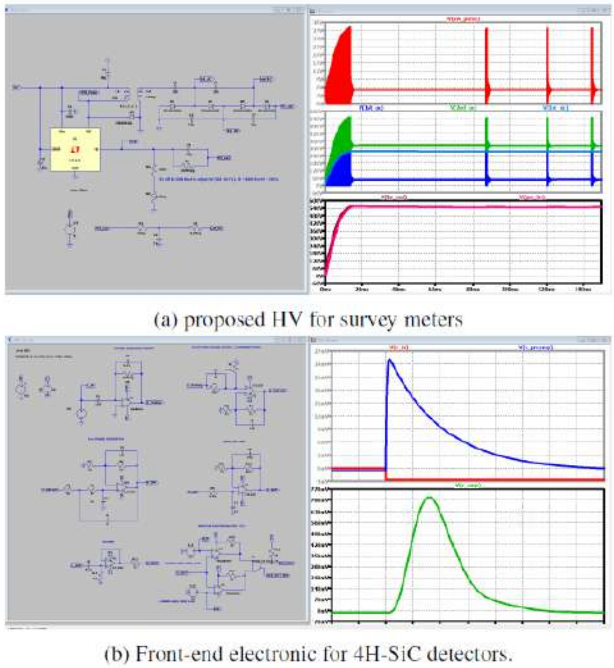

(a) proposed HV for survey meters

(b) Front-end electronic for 4H-SiC detectors.

Figure 3: Electronics for future nuclear instrumentation.

References

Lojius Lombigit, Mohd Nizar Bin Hamidon, Mohd. Ashhar Khalid, and Nasri Bin Sulaiman. 2012. Low cost front-end readout electronic for instrumentation used in neutron experiments. *International Journal of Physical Sciences*, 7:2812–2817.

Alan Owens and A. Peacock. 2004. Compound semiconductor radiation detectors. *NIM A*, 531.

Linear Technology. Lt1615/lt1615-1:micropower step-up dc/dc converters in thinsot. *https://www.analog.com/media/en/technical-documentation/ data-sheets/16151fas.pdf.*

Individual Research Contribution Review, 2023, 1(1): 363–364

Hybrid Pixel Detectors with Exotic Sensors

Lojius bin Lombigit
Technical Support Division, Malaysian Nuclear Agency
43000 Kajang, Selangor
lojius@nm.gov.my

Abstract

A hybrid pixel detector is highly desirable for future particle physics experiments because the sensor and readout electronics can be optimised separately. This article described the characterisation and application of a hybrid pixel detector based on a Timepix3 readout ASIC coupled to exotic pixelated sensors. Three exotic sensors were used in this work: **L**ow **G**ain **A**valanche **D**etector (LGAD), inverse LGAD (iLGAD), and CdTe. The (i)LGAD sensors were envisaged as future detectors for particle physics experiments and were investigated for electrical properties and radiation response. The potential application was explored by demonstrating a single-layer Compton camera (SLCC) with a 1mm thick CdTe bonded to Timepix3 readout ASIC. Key findings were presented and discussed.

Keywords: pixel detectors, LGAD, Compton camera

1 Introduction

A pixel detector consists of individual microscopic sensors, each with readout electronics and arranged in 2D grid pattern called a pixel (Campbell, 2001). In a hybrid pixel detector, the sensor element and readout electronic are separate components that are bonded together. Three hybrid pixel detectors were explored, each with an exotic sensor bonded to a Timepix3 readout ASIC (Poikela et al., 2014). A novel silicon sensor with a small intrinsic gain called the LGAD (Pellegrini et al., 2014) has been identified as one of the technologies for the ATLAS[1] phase-II upgrade (Casado., 2022) and LHCb[2] VELO upgrade II (Rodr´ıguez, 2023). Two prototypes were realised: the 50 μm thick LGAD and 250 μm thick inverse LGAD. Each prototype was fabricated as multiple sizes pad detectors and pixelated versions with 55, 110, and 220 μm-pixel pitches. The pad detectors were used as test devices for measuring the electrical properties and signal gain. The pixelated version was bonded to Timepix3 readout ASIC and characterised with a micro-focused synchrotron beam.

A prototype hybrid pixel detector with a high-Z semiconductor detector was also produced. The single-layer Compton camera (SLCC) (Turecek et al., 2020), a novel gamma camera that relies on the Compton scattering kinematic.

[1]A Toroidal Large Hadron Collider Apparatus
[2]Large Hadron Collider Beauty

2 Characterisation techniques

2.1 Electrical characterisation and gain measurement

The iLGAD pad detectors shown in Figure 1(a), fabricated in various sizes and gain. Electrical properties via current-voltage (I-V) and capacitance voltage (C-V) were measured.

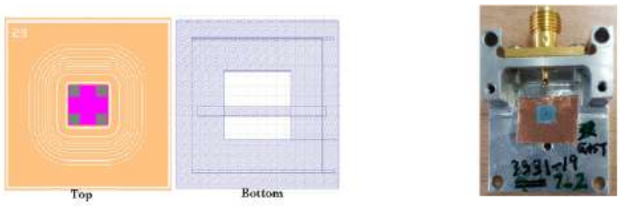

(a) (b)

Figure 1: (a) A sample of a mask of an LGAD pad detector and (b) device-under-test (DUT) assembly: the pad detector was glued onto an A1 mounting and wire-bond for the TCT measurement

The Transient Current Technique (TCT) (Kramberger, 2001) was used to investigate the detector's signal gain at various temperatures.

2.2 Characterisation with synchrotron beam

The iLGADs with 55, 110 and 220 μm-pixel pitches were bonded to Timepix3 Readout ASIC and characterised with a synchrotron beam at Beamline B16, Diamond Light Source facility. The test beam investigates inter-pixel charge sharing, homogeneity response, and pixel signal gain. A monochromatic beam with energy of 15 keV and with beam focus of $\approx$ 2 μm (FWHM) was used.

2.3 Single-Layer Compton camera

The hybrid pixel detector used in this example is a 1mm thick, 256 × 256 pixels with 55 μm-pixel pitch CdTe bonded to Timepix3 readout ASIC. A 122 keV γ-rays from ^{57}Co was used, placed $\approx$ 64mm above and $\approx$ 50mm (in x- and y-axes) outside the detector field of view. The aim was to demonstrate the image shift in the reconstructed images.

3 Results

3.1 Electrical properties and signal gain

Table 1 shows the summary of electrical properties of the 50 μm thick LGAD pad detectors. Depending on the doping concentration, the measured breakdown voltages were between 150V to 280 V, which were 5 to 9 times higher than the full depletion voltages. This implies a higher voltage can be used to obtain higher signal gain. Also, it requires a slightly higher voltage (29V to 30 V) to deplete the highly doped detector.

Table 1: Electrical characteristics and signal gain of the LGAD pad detectors.

Doping	Breakdown Voltage (V)	Full depletion voltage (V)	Signal gain @-20°C
High	≈ 200	29 - 30	≈ 12
Medium	150 - 200	26 - 27	-
Low	≈ 280	26 - 28	-

Figure 2 shows a strong influence of temperature and pixel size on the signal gain in LGAD detectors. A higher gain was due to the impact ionisation rate is greater at lower temperatures. The pixel size affects signal gain in LGAD with junction termination extension (JTE) structure due to the small pixel effect as explained in (Moffat and Bates, 2021).

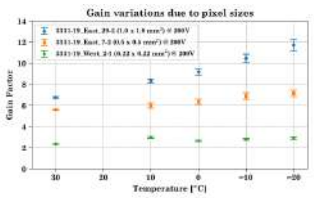

Figure 2: The influence of temperature and pixel sizes on the signal gain in the 50 μm thick LGAD pad detectors.

3.2 Synchrotron beam test

Figure 3 shows pixel responses across 3 PoIs of LGAD and iLGAD sensors. A signal gain was observed in the 110 μm-pitch LGADs, but only occurred in the central area of the pixel (see Figure 3(a)). This is due to the JTE structure reduced the fill factor in LGAD devices. The iLGAD used different structural configurations and was devised as a technological solution to overcome the fill factor limitation of an LGAD detector. Figure 3(b) shows a signal gain with a significantly large fill factor in the 55 μm iLGAD detector.

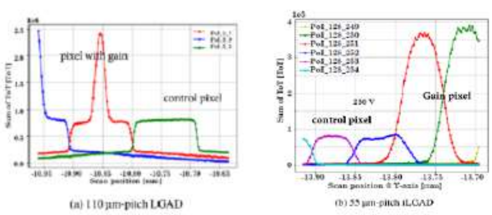

Figure 3: Pixel response of the hybrid pixel detectors with (a) LGAD and (b) iLGAD sensors

3.3 Single-layer Compton camera

The demonstration of SLCC is shown in Figure 4, where the origin of the photon source was properly indicated in

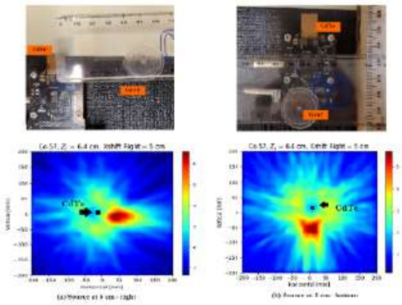

Figure 4: The reconstructed Compton camera images from the two experiments.

both projected images. Images lacked sharpness due to the limited number of valid Compton events available for image reconstruction, primarily because of the thin nature of the CdTe used. Moreover, images were projected without any image enhancement processing algorithm, commonly used in the conventional gamma camera system.

4 Discussion/Conclusions

The (i)LGADs were proven as viable detectors for future particle physics experiments. Signal gains were demonstrated in both detectors, and the iLGAD was proven to be a viable technological solution to overcome the fill factor limitation of an LGAD detector. The hybrid pixel detector with a high-Z sensor was demonstrated as a feasible detector for a single-layer Compton camera in the future.

References

M Campbell. 2001. Electronics for Pixel Detectors. *CERN-2001-005*, 11.

M. P. Casado. 2022. A high-granularity timing detector for the atlas phase-II upgrade. *NIM A*, 1032(166628)).

Gregor Kramberger. 2001. Signal development in irradiated silicon detectors. Ph.D. thesis, University of Ljubljana.

Niel Moffat and Richard Bates. 2021. Simulation of the small pixel effect contributing to a low fill factor for pixellated low gain avalanche detectors LGAD. *NIM A*, 1018(165746)).

G. Pellegrini, P. Fernández-Martínez, M. Baselga, and C. Fleta et al. 2014. Technology development and first measurement of low gain avalanche detector (LGAD) for high energy physics applications. *NIM A*, 765:12 – 16.

T. Poikela, J. Posila, T. Westerlund, and M. Campbell et al. 2014. Timepix3: A 65k channel hybrid pixel readout chip with simultaneous toa/tot and sparse readout. *JINST*, 9(C05013).

Efrén Rodríguez Rodríguez. 2023. Silicon vertex detector with timing for the upgrade II of LHCb. *NIM A*, 1048(167965).

D. Turecek, J. Jakubek, E. Trojanova, and L. Serfc. 2020. Single layer compton camera based on timepix3 technology. *JINST*, 15(C01014).

Individual Research Contribution Review, 2023, 1(1): 365–366

I2NS: A Framework on Applying Big Data Analytics for Nuclear Security

Maizura Ibrahim
Technical Support Division, Malaysian Nuclear Agency
43000 Kajang, Selangor
maizura@nm.gov.my

Abstract

The problem with the nuclear security systems in most nuclear facilities in the world today is that un-integrated data management is causing sub-optimal efficiency in the detection of malicious acts involving nuclear/radioactive materials. Therefore, in this paper, we present a conceptual framework of big data analytics for nuclear security to integrate all the data from the nuclear security systems at the facilities level and national level so that the data can be analyzed to get insights to increase the accuracy of decision-making, enhance situational awareness, hence increase the efficiency of detection, prevention and response process related to nuclear/radioactive malicious event.

Keywords: Nuclear Security, Big Data Analytics, Security System, situational awareness

1 Introduction

Development in IT contributes to the improvement of the quality of security systems, speeding up getting data for security monitoring purposes, effective security management, emerging novel forms of security systems, improving communication and interaction between security personnel, and providing access to a wide range of information for further security improvement. A concept to combine nuclear security strategy with big data analytics technology could be formulated to provide solutions for the problems faced by most of the nuclear facilities in the world, i.e. a 'silo' data management practice for a nuclear security system that is causing a sub-optimal nuclear security system (WINS, 2015b; WINS, 2015a).

2 Methods

In the context of a data management point of view, the conceptual framework is formulated based on a holistic methodology to integrate all data of the nuclear security systems at the facilities level and national level so that the data can be easily analyzed to derive insights, appropriate patterns, increasing the accuracy of decision-making, hence increase the efficiency of prevention, detection, and response to the malicious nuclear security event. The elements in the framework are designed based on the nuclear security elements stated in the International Legal Nuclear Security framework (IAEA, 2013b; IAEA, 2013a; IAEA, 2015; IAEA, 2008; IAEA, 2020) and the need to perform autonomous analysis of the data for the enhancement of the nuclear security system's situational awareness.

3 Result - The conceptual framework

This framework is called the integrated and intelligent nuclear security, I2NS framework. It is developed on two levels shown in Figures 1 and 2, each for the implementation at the nuclear facilities and state level by the related state regulators. In Figure 1, data visualization is adapted into the framework from the big data analytics concept. However, at this stage, the focus of this framework is only limited to physical security (IAEA, 2013b; IAEA, 2013a), personnel security (IAEA, 2015; IAEA, 2008), and nuclear/radioactive materials accounting and control systems (IAEA, 2020) which are critically important for digitalization. All components are integrated to facilitate an online alert system so that a trigger can be initiated whenever an abnormality is detected.

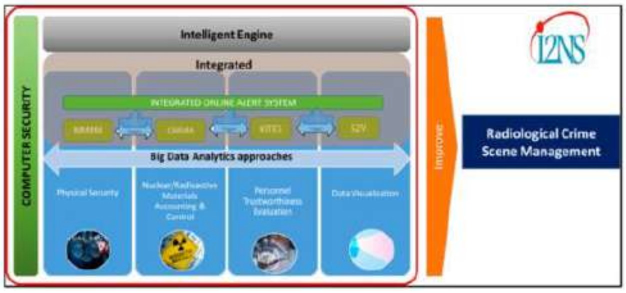

Figure 1: Facilities Level

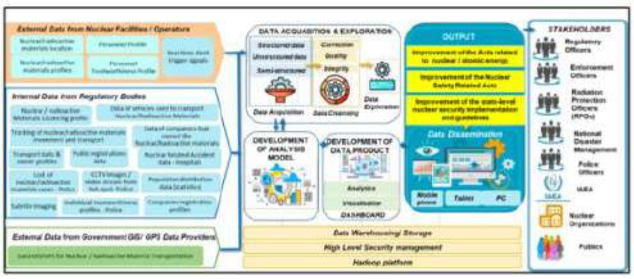

Figure 2: State-level

Figure 2 shows the state level of the I2NS framework that was developed based on a literature review and research by (Ibrahim et al., 2017; Ibrahim et al., 2018; Ibrahim et al., 2020a; Ibrahim et al., 2020b). The framework depicts the flow of data acquisition needed from different parties to be integrated and explored to derive new insights that could benefit different nuclear security stakeholders.

4 Discussion

This framework is tailored to the statement that security must be viewed and operated as an enterprise-wide activity and be fully integrated into other business processes and objectives (WINS, 2015b; WINS, 2015a). For each of the components, the related back-end databases must be integrated to form the data pond/lake, depending on the needed data storage capacity for the respective facility/operator, but for our work, we utilized an open-source Hadoop platform (https://hadoop.apache.org, November 13 2020).

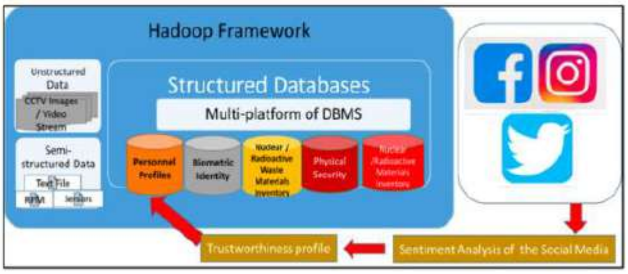

Figure 3: Integrated back-end databases

Figure 3 shows three types of data that must be dealt with at the facilities/operators' level, which are, structured data, semi-structured data, and unstructured data.

5 Conclusion and Future Work

In this paper, we proposed a conceptual big data analytics framework for nuclear security. The framework is developed in the context of a data management point of view. This framework has yet to be implemented as a pilot case study, especially at the facilities level. Therefore, our future work is to develop a facility-level pilot system for the proof-of-concept.

References

https://hadoop.apache.org. November 13, 2020.

International Atomic Energy Agency IAEA. 2008. Implementing guide: Preventive and protective measures against insider threats. *IAEA Nuclear Security Series 8 (Vienna, Austria).*

International Atomic Energy Agency IAEA. 2013a. Implementing guide: Nuclear security systems and measures for the detection of nuclear and other radioactive material out of regulatory control. *IAEA Nuclear Security Series 21 (Vienna, Austria).*

International Atomic Energy Agency IAEA. 2013b. Nuclear security fundamentals: Objective and essential elements of a state's nuclear security regime. *IAEA Nuclear Security Series 20 (Vienna, Austria).*

International Atomic Energy Agency IAEA. 2015. Implementing guide: Risk-informed approach for nuclear security measures for nuclear and other radioactive material out of regulatory control. *IAEA Nuclear Security Series.24-G (Vienna, Austria).*

International Atomic Energy Agency IAEA. 2020. Implementing guide: Preventive and protective measures against insider threats. *IAEA Nuclear Security Series (Rev. 1) 8-G (Vienna, Austria).*

M Ibrahim, Ismail S, Haris M F, Hamdan S N, Sulaiman M S, Hamid A H A, Aris S N M, Aslan M D A, Ghani N F A, and Hassan H. 2017. A proposal on adaptation of big data analytics framework in nuclear security toward development of integrated, real-time, and intelligent nuclear security system. *Nuclear RD Seminar 2017.*

Ibrahim, Ismail, Haris M F, Hamdan S N, Sulaiman M S, Hamid A H A, Aris S N M, Aslan M D A, Ghani N F A, and Hassan H. 2018. The integrated intelligent nuclear security (i2ns) system: A progress report for 2018. *Technical Report No.Nuklearmalaysia/L/2018/173.*

M Ibrahim, Ismail S, Haris M F, Hamdan S N, Sulaiman M S, Hamid A H A, Aris S N M, Aslan M D A, Ghani N F A, , and Hassan H. 2020a. Malaysian nuclear agency integrated and intelligent nuclear security (i2ns) system: A progress report 2019. *Technical Report No.Nuklearmalaysia/L/2020/10.*

M Ibrahim, Ismail S, Haris M F, Hamdan S N, Sulaiman M S, Hamid A H A, Aris S N M, Aslan M D A, Ghani N F A, and Hassan H. 2020b. Big data analytics for nuclear security: a literature review. *Nuclear R D Seminar 2020, 16 -19 Nov. 2020.*

World Institute of Nuclear Security WINS. 2015a. Big data in motion, how real-time integrated data management could support nuclear security. *WINS Special Report Series Vienna, Austria.*

World Institute of Nuclear Security WINS. 2015b. Data analytics for nuclear security, how real-time integrated data management could support nuclear security. *WINS Special Report Series, Vienna, Austria.*

Individual Research Contribution Review, 2023, 1(1): 367–368

I2NS: Design and Development of the Ontologies to Model the Existing Personnel Trustworthiness Evaluation Process

Maizura Ibrahim
Technical Support Division, Malaysian Nuclear Agency
43000 Kajang, Selangor
maizura@nm.gov.my

Abstract

Most organizations implemented a background checking process for personnel trustworthiness evaluation. The process is done manually, by screening a personnel's background data, by a security personnel in the Security Department. The process raised issues because there is human intervention in the process. The screening result could be biased based on the human perception or the relationship of the evaluator to the personnel that is being evaluated. Therefore, an artificial intelligence (AI) system could be used to overcome the problem by autonomously evaluating the personnel's trustworthiness, thus eliminating human bias. Therefore, this paper presents an ontology, namely, the Personnel Trustworthiness Evaluation Ontology (PTEO) to model the existing personnel trustworthiness evaluation process.

Keywords: Insider threats, Artificial Intelligence, Knowledge-based System, Ontology, Personnel Trustworthiness.

1 Introduction

In Artificial intelligence, the term ontology means one of two related things. Ontologies are content theories about the sorts of objects, properties of objects, and relations between objects that are possible in a specified domain of knowledge. They provide potential terms for describing knowledge about the domain. In other words, ontology is defined as a shared understanding of some domain of interest, which is often realized as a set of classes (concepts), relations, functions, axioms, and instances. Based on the I2NS framework (Ibrahim et al., 2021), apart from the CARMA System, another base system component that is critical to be digitalized is the Personnel Security Screening process because Personnel trustworthiness is an important task to mitigate insider threats in the nuclear security regime (Ibrahim et al., 2022; IAEA, 2020). The rest of this paper presents and discusses the PTEO.

2 Methods

A method proposed by Noy et al. (Noy and McGuinness, 2001) is followed in the design and development of the PTEO because it adopted a simple knowledge-engineering methodology. Figure 1 illustrates the steps that are used in the PTEO design and development.

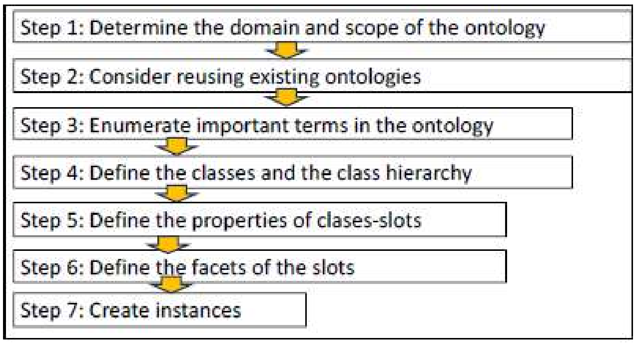

Figure 1: Steps used in PTEO Design and Development

Apart from that, the core domain set of classes (concepts), relations, functions, axioms, and instances are designed and developed based on the international best practices published by IAEA (IAEA, 2020) and Landers (Landers, 2022). Protégé version 5.5.0 (Musen, 2015) is used as an ontologydeveloping environment for PTEO.

3 Result - Personnel Trustworthiness Evaluation Ontologies (PTEO)

The insiders can be identified based on three attributes namely, access, authority, and knowledge (IAEA, 2020). Figure 2 shows the upper-level taxonomy of PTEO that modeled those three attributes.

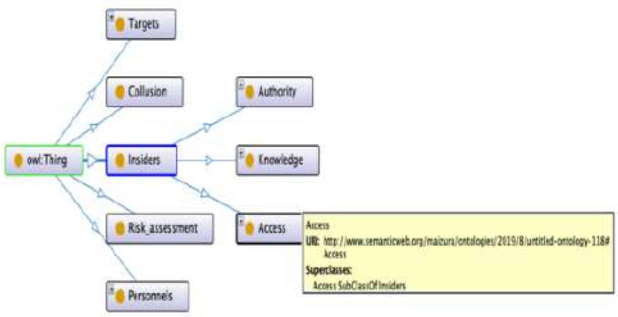

Figure 2: An Upper-Level Taxonomy of PTEO

Figure 3 depicts ten indicators that are modeled by the PTEO in assessing personnel trustworthiness over time. The workplaces, organizational, boundary, trustworthiness metrics, psychology, life, cognitive/physical, life, divided loyalty, and IT/Technical indicators are adopted from the trustworthiness & reliability indicators checklist published (Landers, 2022). The full taxonomy of PTEO is shown in Figure 4. The radial diagram shows how the relationship between entities is crafted into a knowledge-based or graph-based database that can potentially be used for insider threat mitigation intelligent systems.

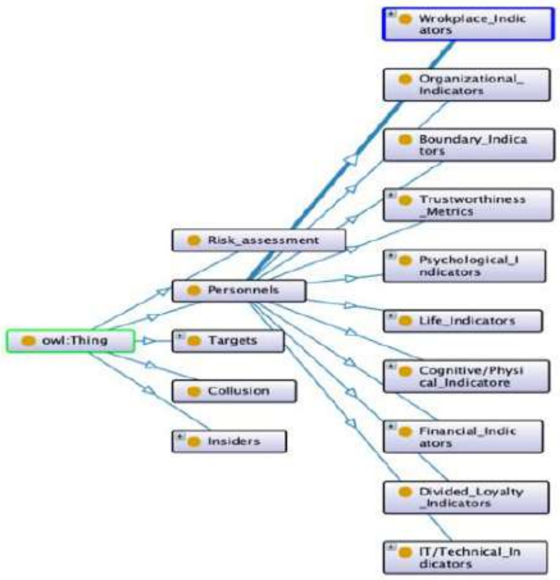

Figure 3: The Second-level Hierarchy of PTEO

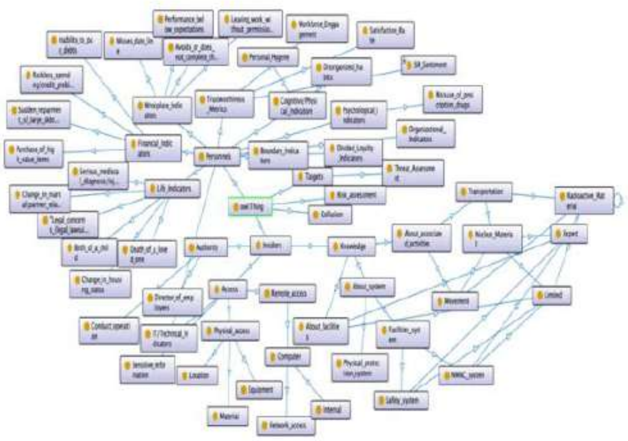

Figure 4: PTEO Taxonomy in Radial Diagram

4 Conclusion and Future Work

In this paper, we have presented an ontology to model the process of evaluating personnel trustworthiness and identify potential insiders based on existing international best practices. The ontology is named based on the function it serves, which is the Personnel Trustworthiness Evaluation Ontology (PTEO) version 1.1. We also presented a methodology used during the ontology development and gave justification for why the method was adopted. The potential application of the PTEO is that it can be used in AI systems to autonomously assess the personnel's trustworthiness periodically and create situational awareness so that early steps can be taken to mitigate the risk or insider threat to protect the nuclear/radioactive material, associated facilities, and associated activities.

References

International Atomic Energy Agency IAEA. 2020. Implementing guide: Preventive and protective measures against insider threats. *IAEA Nuclear Security Series No.8-G (Rev.1), Vienna, Austria.*

Maizura Ibrahim, Siti Nurbahyah Hamdan, Saa'idi Ismail, Mohd Fauzi Haris, Mohamad Safuan Sulaiman, Sufian Norazam Mohamed Aris, Mohd Hasnor Bin Hasan, MohdDzul Aiman Aslan, Nur Fatini Abdul Ghani, and Amy Hamijah Ab Hamid. 2021. Big data analytics nuclear security framework. *Journal IOP Conf. Series: Materials Science and Engineering*, 1106:012026.

Maizura Ibrahim, Nur Fatini Abdul Ghani, and Mohd Safuan Sulaiman. 2022. A knowledge-based model for personnel trustworthiness evaluation. *Research and Development Seminar 2022, Bangi (Malaysia).*

J.E Landers. 2022. Trustworthiness & reliability indicator checklist. *Office of International Nuclear Security (INS), National Nuclear Security Administration Learning Sciences, Nuclear Nonproliferation Division, National Security Sciences Directorate, Oak Ridge National Laboratory, USA.*

M.A. Musen. 2015. The protégé project: A look back and a look forward. *AI Matters. Association of Computing Machinery Specific Interest Group in Artificial Intelligence*, 1(4, DOI: 10.1145/2557001.25757003).

N.F. Noy and D.L McGuinness. 2001. Ontology development 101: A guide to creating your first ontology. *Stanford Knowledge Systems Laboratory Technical Report KSL-01-05 and Stanford Medical Informatics Technical Report SMI-2001-0880.*

Individual Research Contribution Review, 2023, 1(1): 369–370

I2NS: Designing A Base System for the Digitalization of Nuclear/Radioactive Material Accounting and Control Process

Maizura Ibrahim
Technical Support Division, Malaysian Nuclear Agency
43000 Kajang, Selangor
maizura@nm.gov.my

Abstract

Based on the I2NS framework, one of the base system components that critically needed to be digitalized is the Nuclear/Radioactive Material Accounting and Control process (NRMAC). A web-based application system namely the Computerized Automation of the Nuclear/Radioactive Materials Accounting (CARMA) is designed to digitalize and automate the process of record keeping and inventory of nuclear/radioactive materials, hence fulfilling the scope of improving security measures by controlling and monitoring the balance sheet of nuclear/radioactive materials. This paper exposed an initial stage of CARMA System design based on KRISA.

Keywords: Nuclear Security, Big Data Analytics, situational awareness, NRMAC, KRISA.

1 Introduction

Many security systems, either manual security systems or computer-based security systems are established in Nuklear Malaysia to protect nuclear/radioactive materials, associated facilities, and associated activities. A manual security system is defined as a human-managed nuclear security system without any automated computer-aided system such as the existing inventory of radioactive materials recorded in the inventory log book, utilizing the Microsoft Excel application, or Inventory Cards to record, perform, and monitor the Nuclear/Radioactive Material Accounting (NRMAC) related activities. A manual system needs human intervention in every step of the procedure, such as updating the inventory card and log book, hence performing the calculation of the inventory to produce the balance sheet of the NRMAC. This kind of system is highly exposed to error-prone made by careless and neglecting behavior. Apart from that, it lacks benefits in terms of aiding situational awareness of nuclear/radioactive materials security because no automated alert could be generated if an imbalance in inventory happens.

Based on the I2NS framework (Ibrahim et al., 2021), one of the base system components that critically needed to be digitalized is the Nuclear/Radioactive Material Accounting and Control process (NRMAC). The rest of this paper presented a design of the CARMA System.

2 Methods

The CARMA design is accomplished following the Public Sector Application System Engineering Guide Book (Buku Panduan Kejuruteraan Sistem Aplikasi Sektor Awam, KRISA) published by MAMPU in 2019 (MAMPU, 2019). Figure 1 shows the stages of the development. The design process covers stages 1 to 3 is adopted.

Figure 1: The Development Stages based on KRISA

3 Result - The CARMA System Design and Discussion

Figure 2 shows the context diagram that illustrates the CARMA system interactions with eight external entities namely the Stakeholders, System Administrator Team Members, Internal Auditors, External Auditors, licenses, other I2NS sub-systems, and Input/Output Devices. Each of these external entities must be detailed to achieve the clarity of the system modules.

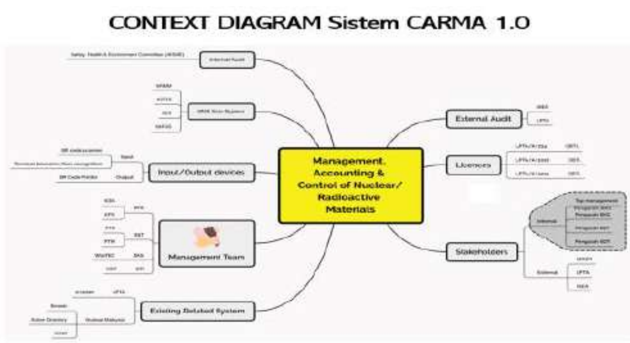

Figure 2: The CARMA Context Diagram

Table 1 lists the stakeholders and the related description to clarify the degree of involvement that is used as the basis for designing the role-based access control (RBAC) module for the CARMA system.

Table 1: CARMA Stakeholders and Descriptions

Stakeholders	Descriptions
Top Management of MOSTI	The Top Management of Ministry of Science Technology & Innovation (MOSTI) are the officers responsible for monitoring the Key Performance Indicators of services related to nuclear safety and security.
Radiation Safety Division	Process owner to the business domain in the system to be developed.
Top Management of Nuklear Malaysia	The Top Management of ANM are Director General (DG) and two Deputy DGs the who are responsible for ensuring direction and monitoring activities related to the management of nuclear and radioactive materials.
Internal Research Officers	Research officers of the Malaysian Nuclear Agency who make applications for the procurement of radioactive materials and nuclear materials, responsible for updating the ownership status and location of materials periodically, and ensuring that the safety level of the materials owned is guaranteed.
External agencies that will interact with the system: Auditor: i) LPTA ii) IAEA	An external agency that performs audits on material safety. They are responsible for: 1. Conduct an audit 2. Inform the Malaysian Nuclear Agency as soon as possible (in writing) if there is any matter or event that may affect the safety of the material; 3. Comply with all instructions from time to time given by the Malaysian Nuclear Agency in relation to the implementation of the audit; 4. Provide recommendations for equipment and modules required for material safety 5. Provide any information to the Malaysian Nuclear Agency related to the safety of nuclear/radioactive materials from time to time when required by the Malaysian Nuclear Agency

Apart from that, the list of users must also identified and used as the basis for the RBAC module. Furthermore, the business environment model, functional business model, and process flow diagram (PFD) must be developed and verified to facilitate the mutual understanding achievement between the developer team and system owner. Figure 3 depicts one of the PFDs for the Radioactive Materials Registration Module.

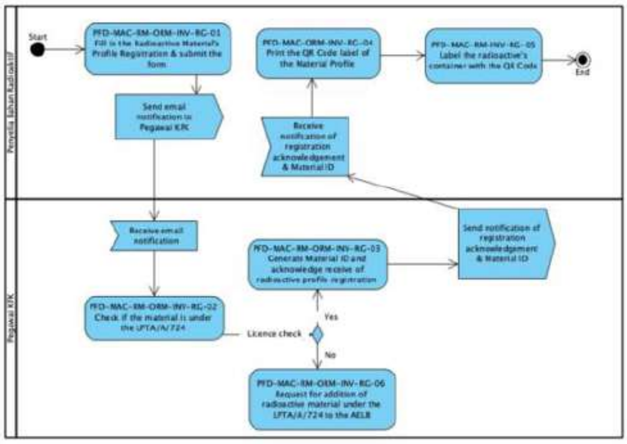

Figure 3: PFD for Radioactive Material Registration Module

4 Conclusion and Future Work

In this paper, we present the initial stage design of the CARMA System based on the KRISA approach. Currently, the design stage is almost completed but has yet to be verified by the system owner. Therefore, our future work is to conduct verification sessions with the system owner and then develop a database and programming code for the CARMA System version 1.0.

References

Maizura Ibrahim, Siti Nurbahyah Hamdan, Saa'idi Ismail, Mohd Fauzi Haris, Mohamad Safuan Sulaiman, Sufian Norazam Mohamed Aris, Mohd Hasnor Bin Hasan, Mohd Dzul Aiman Aslan, Nur Fatini Abdul Ghani, and Amy Hamijah Ab Hamid. 2021. Big data analytics nuclear security framework. *Journal IOP Conf. Series: Materials Science and Engineering*, 1106:012026.

Jabatan Perdana Menteri Malaysia MAMPU. 2019. Buku panduan kejuruteraan sistem aplikasi sektor awam (KRISA).

Revamp, Refactor and Refine (3R) Reactor TRIGA PUSPATI Operating Hour (OptOur) System

Mazleha Maskin
Technical Support Division, Malaysian Nuclear Agency
43000 Kajang, Selangor
mazleha@nm.gov.my

Abstract

Since RTP reach criticality, the operational data for RTP has been diligently recorded manually into RTP operational logbook. To report and summarized on what had been logged into the logbook, an operating hour (OptOur) system was used. However, since OptOur's deployment in 2010, the accuracy and the integrity of the data has never been examined from the point view of the system developer. This paper describes the activities involved in revamping, refactoring, and refining the OptOur system. The goal is to improve and enhance OptOur with the aim of ensuring data integrity, which data integrity is mainly, the accuracy, completeness, and quality of data as it's maintained over time and across formats. The System Development Life Cycle (SDLC) methodology has been chosen as a guide to modify OptOur system.

Keywords: IMS, online, TRIGA PUSPATI, ShareFolder, SharePoint

1 Introduction

Since reaktor TRIGA PUSPATI (RTP) reach criticality in 1982, operational data for RTP has been diligently recorded. Initially, all data was manually logged into RTP operational logbook. Among the parameters involved are operational hours, released energy, number of samples, and reactivity changes.

In 2008, the Pusat Teknologi Reaktor (PTR) research team develop a revised edition of ANADATA, namely OptOur using Microsoft Access. which was subsequently fully deployed in 2010. OptOur boasts several benefits, including a user-friendly interface, comprehensive data recording, and the ability to generate instant reports as needed.

Microsoft Access (Access) is a relational database management system (RDBMS), which are collections of related data organized in a structured format. One of the key features is its ability to create relational databases, where data in different tables can be linked together based on common fields. Figure 1 portrays OptOur relationship between Tables.

2 Problem Statements

OptOur interrelated objects consists of 15 Tables, 21 Queries, 27 Forms, 13 active Reports (out of 22) and 5 Macros. Since OptOur's deployment in 2010, the accuracy and the integrity of the data has never been examined from the point view of the system developer.

In first diagnosed, two tables (01 OPTHR and 01 OPTHR Trainee as in Figure 2) are referring to name of operators with their position whether as Licensed Operator or Trainee. This existing two tables is a mistake and resulting in errors to queries calculation and reporting. To solve this, the two tables need to be merged into one with several fields need to be added, deleted, and merge.

In Figure 2, the absence of name selection options (selecting from List box) in two columns: RO (OPTHR: Rx Operator) and Trainee (OPTHR: Trainee) causes operators to input names as they please. These resulted in non-unique names appeared in reports and lead to error in calculating numbers of both operations and reactivities.

The lack of mandatory data, such as the sequence number of the reactor auto-scram (Figure 3), and the significant human errors in data entry (Figure 4(a) and (b)), need to be addressed as top priority in need to review and amend.

Therefore, the process of revamping, refactoring and refining OptOur is essential, as the reports generated by OptOur, which need to indicate data preciseness, are utilized in the following contexts:

1. Inspection by the Jabatan Tenaga Atom (JTA) and IAEA.
2. Fuel burnup calculation input.
3. Yearly report to JTA:

a) Operational Report.
b) Safety Performance Indicators Report.
c) Annual Maintenance Report.
d) Semi-Annual Maintenance Report.

4. Stack monitoring input.

3 Methods

Since the scope of this project is small, the System Development Life Cycle (SDLC) method has been chosen as a guide to modify OptOur system. There are five important phases or stages in this methodology that need to be followed and these phases are illustrated in Figure 4 below.

1. First Phase

The first phase is planning objectives and identifying problems. This aims to avoid unexpected problems arising during or after the construction of this system. In this project, all planning, objectives, and problems have been identified in advance. This is done by differentiating the existing manual system with the online system that will be built.

2. Second Phase

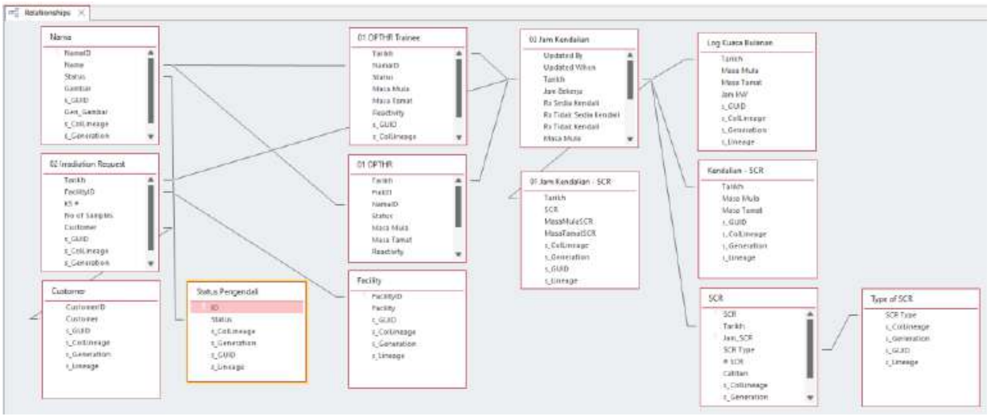

Figure 1: OptOur relationship

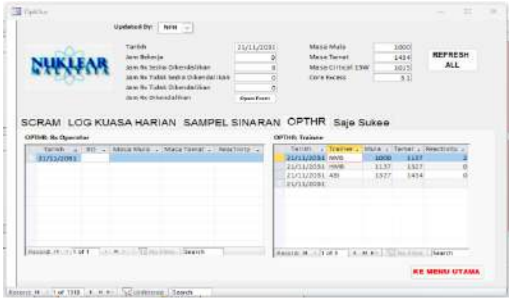

Figure 2: OptOur primary data interface

Figure 3: Absence of important data: #SCR

(a) value at ❶ and ❷ should be the same

(b) upcoming date

Figure 4: Human error in data entry

The second phase is to analyze the system requirements. In this phase, the analysis of the system needs to be done in detail so that the process of revamping OptOur can run smoothly without facing any problems. Among the analyzes carried out are the hardware requirements and the software that is suitable to be used.

3. Third Phase

The third phase is re-designing and re-modifying the system relationship. Every angle needs to be examined, to meet the more user-friendly as well as the objective requirements.

4. Fourth Phase

The fourth phase is to implement the system. In this phase, implementation and testing of the completed system will be done. This is very important so that the resulting system can run perfectly without problems. It is also the last phase to go back to the previous phase if problems arise.

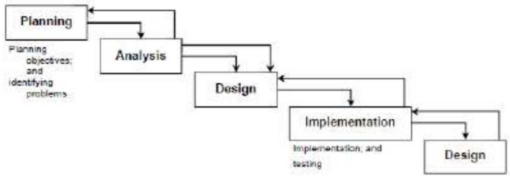

Figure 5: System Development Life Cycle (SDLC) method

5. Fifth Phase

The fifth and final phase is the fully function OptOur system. In this phase, the system is completely completed, and this is the point of no return to the previous phase.

4 Conclusions

In general, the goal of this project is to improve and enhance OptOur with the aim of ensuring data integrity, which mainly is, the accuracy, completeness, and quality of data as it's maintained over time and across formats.

References

K. Beyls and E.H D'Hollander. 2009. Refactoring for data locality. *Computer*, 42(2):62–71, https://doi.org/10.1109/MC.2009.57.

B. Shah (Ed.). 1988. Revamping the examination system. *Northern Book Centre*.

P. Gardiner and C. Morgan. 1991. Data refinement of predicate transformers. *Theoretical Computer Science*, 87(1):143–162, https://doi.org/10.1016/0304–3975(91)90029–2.

G.O Ogundajo, Odunayo J., Osunsusi A. K., Desi A., and Oyedokun G. E. 2023. Digitalized accounting system: Revamping small and medium enterprises financial reporting system. *The American Journal of Humanities and Social Sciences Research (THE AJHSSR)*, 6(3):99–113, https://doi.org/10.56805/ajhssr.

L. Sawyer. 2001. Revamping a teacher evaluation system. *Educational Leadership*, 58(5):44–47.

Individual Research Contribution Review, 2023, 1(1): 373–374

The RTP-MS Evolution from ShareFolder to Online-Based Management: An Alternative Document Accessibility

Mazleha Maskin
Technical Support Division, Malaysian Nuclear Agency
43000 Kajang, Selangor
mazleha@nm.gov.my

Abstract

This paper describes the structure of document management, specifically the evolution of Reactor TRIGA PUSPATI Management System (RTP-MS) from ShareFolder to online-based management using SharePoint. Employing the Integrated Management System (IMS) approach, which characterizes documents based on a hierarchy of importance, the development and utilization of Nuclear Malaysia's long-standing SharePoint website has served as a pivotal shift for officials at the Reactor Technology Center (PTR) in the quest for enhanced document accessibility and updates. The migration initiative commenced in 2020, coinciding with the onset of the COVID-19 pandemic, and it remains an ongoing process. The objective of this paper is to share how PTR utilizes SharePoint as an alternative digital document management system, with the scope of this study focuses on the existing Nuclear Malaysia SharePoint and the local reactor ShareFolder under NAS3. PTR officers have enthusiastically adopted the SharePoint platform, especially during audit sessions with regulatory agencies and for document sharing. This preference is due to SharePoint's utilization of a graphical user interface that acts as a navigation panel, in contrast to ShareFolder's method of displaying a document list.

Keywords: IMS, online, TRIGA PUSPATI, ShareFolder, SharePoint

1 Introduction

The increasing intricacy of the TRIGA PUSPATI reactor (RTP) documentation, which consists of procedures, work instructions, technical instructions, forms, and reports, coupled with stringent standards, poses a considerable challenge to the Reactor Technology Center's (PTR) management. Retrieving and updating documents becomes particularly challenging, especially during the COVID-19 pandemic era, due to the use of shared folders on the local network that cannot be accessed via the internet at all. Hence, working from home seems not to be working for PTR personnel where accessibility of documents is the mainstay especially for auditing purposes.

Storing documents in an individual workstation ends up with multiple different versions for each officer (Bergman et al., 2014; Whittaker, 2011), which later increase confusion on which version of the file is the most up-to-date. Once updated and all the comments have been incorporated, there may emerge multiple document versions, each containing slight differences and several repetitive elements resulting from the feedback. However, manually juxtaposing the documents is not an efficient method for identifying discrepancies (Accusoft, 2021). In an effort to maintain only one document for all PTR staff to work on, Google Drive was used and links were shared using email addresses in an effort to control documents only to be shared among involved staffs, as well as upholding safety culture (T. Erickson, 2006). Unfortunately, despite the humongous benefits, Google Drive does have some disadvantages in terms of security, as listed by Campaigns of The World (of The World, 2023) on their website. Thus, instead of selecting Google Drive as a substitute for ShareFolder, the PTR management opted for SharePoint. However, Google Sheets and Google Forms are extensively utilized for data collection and streamlining the process of summarizing data.

The aim of this document is to elucidate how PTR leverages SharePoint as an alternative system for managing digital documents. This paper specifically delves into the management of operational and maintenance documents within RTP, encompassing the utilization of the existing Nuclear Malaysia SharePoint platform and the local reactor ShareFolder located under NAS3.

2 Methods

In order to ensure the comprehensive inclusion of vital documents in the entire RTP management system, the approach employed in this study aligns with the guidelines set forth by Smallwood (Smallwood, 2013) as detailed below:

1. Assessment and Planning: (a) Inventory: Identify all existing documents and data stored in ShareFolder; and (b) Categorization: Documents are grouped based on the RTP-MS hierarchy of priority.
2. Configuration and Setup: Configure the SharePoint environment, including document libraries, sites, subsites, and user access.
3. Migration: (a) Data Transfer: Manually transfer selected documents and data from ShareFolder to SharePoint; and (b) Permissions: Ensure that access permissions are correctly configured in SharePoint, which are currently managed by the Information Technology Center (ITC).
4. Training and User Briefing: Provide training and briefings to users on how to navigate and effectively utilize SharePoint for accessing documents.

5. Optimization: Continuously assess and optimize the SharePoint environment based on user feedback and evolving document management needs.

3 Results and Discussion

This segment illustrates the portion of RTP-MS SharePoint content that can be contrasted with the traditional RTP-IMS ShareFolder as shown in Figure 1.

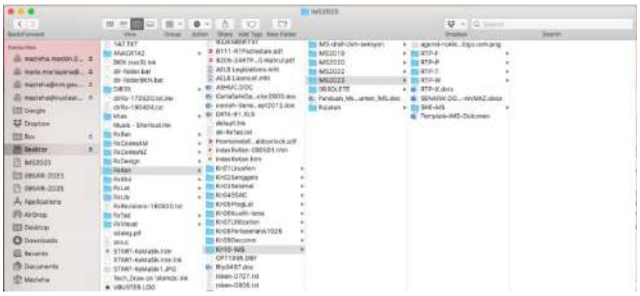

Figure 1: Reactor ShareFolder in NAS3

3.1 RTP-MS Content Management

The key functionalities and features framework of RTP-MS SharePoint has been organized to mirror the RTP-MS hierarchy. It starts with an introduction to PTR and IMS, followed by information on referenced regulatory and safety documents. Additionally, links to Act 304, BSRP and SHEMS local website are also provided.

3.2 Knowledge Management Sharing

In addition to the RTP-MS documentation framework, RTP-MS SharePoint also encompasses an effective knowledgesharing interface. Among the readily accessible information are RTP publications, RTP commemoration events, IAEA missions, and student supervision.

3.3 Impact to Audit Activities

RTP-MS SharePoint offers a more user-friendly method for accessing documents in contrast to ShareFolder due to its graphical user interface functioning as a navigation tool instead of simply presenting a document list. This valuable feature is particularly beneficial when dealing with auditors in high-pressure situations, making it easier to locate specific documents.

Another noteworthy effect of the RTP-MS SharePoint is on the results of audits conducted by Atom Malaysia. Figure 2 illustrates the audit outcomes by Atom Malaysia between 2017 and 2023. The utilization of RTP-MS SharePoint for audits commenced in 2021, and during this period, a noticeable decrease in the instances of corrective actions and opportunities for improvement has been observed.

4 Conclusions

In general, RTP-MS in SharePoint has had a positive impact on PTR personnel, primarily by improving the efficiency of document retrieval and enhancing document management in terms of accessibility. Another notable criterion of RTP-MS

Figure 2: Audit result by Atom Malaysia from 2017 to 2023

SharePoint is its graphical user interface, which functions as a navigation tool instead of merely presenting a document list (ShareFolder). In the near future, a brief survey among PTR personnel will be conducted to gather authentic feedback and evaluate the effectiveness of RTP-MS SharePoint in supporting daily tasks, reporting, competency, as well as identifying areas for further improvement. Finally, PTR management would like to recommend that ITC can assist the person in charge of SharePoint with training to enhance website development management and workflow.

References

Accusoft. 2021. What is document comparison? https://www.accusoft.com/resources/blog/what-isdocument- comparison/.

O. Bergman, Whittaker S., and Falk N. 2014. Shared files: The retrieval perspective. *Journal of the Association for Information Science and Technology*, 10(65):1949–1963, https://doi.org/10.1002/asi.23147.

M.L Johnson, Bellovin S. M., Reeder R. W., and Schechter S.E. 2009. Laissez-faire file sharing: Access control designed for individuals at the endpoints. *Proceedings of the 2009 Workshop on New Security Paradigms Workshop (NSPW '09)*, page 1–10.

S. Khumalo and M. Mearns. 2019. Sharepoint as enabler for collaboration and efficient project knowledge sharing. *South African Journal of Information Management*, 21(1):1–9, https://doi.org/10.4102/sajim.v21i1.1044.

Campaigns of The World. 2023. The dark side of Google: A closer look at privacy concerns and user data collection. https://campaignsoftheworld.com/news/the-dark-side-ofgoogle/.

R.F Smallwood. 2013. Managing electronic records: Methods, best practices, and technologies. *John Wiley Sons, Inc.*

T T. Erickson. 2006. From PIM to GIM: Personal information management in group contexts. *Communications of the ACM*, 49(1):74–75, https://doi.org/10.1145/1107458.1107495.

S. Whittaker. 2011. Personal information management: From information consumption to curation. *Annual Review of Information Science and Technology*, 45(1):3–62.

Individual Research Contribution Review, 2023, 1(1): 375–376

Data Collection and Analyse for Establishing Initial Noise Levels Database in RTP Plant Room and Basement

Mohamad Amirudin Mohamad Rosli
Technical Support Division, Malaysian Nuclear Agency
43000 Kajang, Selangor
amirudin@nm.gov.my

Abstract

The primary focus of this study is to collect data on noise levels in the RTP plant room and basement, which is essential for the establishment of a comprehensive noise database. Excessive noise in a machine or piece of equipment can result in malfunctioning and damaged equipment, causing risks to personnel safety, equipment functionality and overall operating effectiveness. Accurate and thorough noise level measurement in these areas is critical for ensuring the longevity of the euipments. The data is being collected using noise detection equipment and will be compared to other device to get precise reading. The aims of this research is to provide insights into the analysis techniques required to establish a robust initial noise database.

1 Introduction

The maintenance and condition monitoring of machine are very important factors in saving cost and energy conservation in industries (Supachai et al., 2017). By monitoring the machine or equipment, preventive measure can be taken earlier thus save cost, manpower and prolong the life or machine and equipment. The machine will eventually fail to do its functionality for several reasons beyond one's control, such as mechanical wear and tear issues, including but not limited to bearing failure, metal fatigue, and corrosion (Rashad et al., 2023). There is no noise database exist at Reaktor TRIGA Puspati (RTP) to do comparison with surrent data collected. This data collection is for establishing initial database for future reference and comparison. One of method can be used for collecting data of noise level is by recording of sound (dBA) of machine or equipment. Obeserving the noise level by plotting the graph can predict and study the trend of every machine and equipment.

2 Methods

Preparing for this experiment is simple. The surrounding environment must be kept in low noise as possible. Turn off any machine or equipment that running to achieved ambient surrounding as the foreign noise must not be captured during the recording of data. When the surrounding ambient have been setup, place the recording device UNI-T (UT 353 BT) near the motor or pump that need to be tested. Recorded the noise from the motor or pump for two (2) minutes. Recording should be done with 3 phase initial condition, operating condition (peak load) and shutting off condition. If the recording data captured foreign noise the experiment need to be restart until only the noise from motor or pump recorded.

Figure 1: Flow chart noise collection database

The recording device has a function that can be connected using Bluetooth with smartphone. The recording data will be recorded and save into the smartphone storage. After the experiment is done, the saved data then will be extracted to excel using computer. Using the saved data, graph of noise level (dBA) against time (sec) will be plotted. The trend of plotted graph will be analyzed and the result will be stored to be able to compare to future data.

3 Results and Discussion

Figure 2 shows the plotted graph for emergency motor #1 and #2 which located at plant room of RTP. Noise trend at RTP plant room for emergency pump #1 and #2 measure at 3 phase initial condition, operating condition (peak load) and shutting off condition. Similar noise level trend during start-up was recorded which was 63-65 dBA. Upon reaching operating condition (peak load), motor #1 and #2 show different reading. Amplitude difference may due to piping design causing more

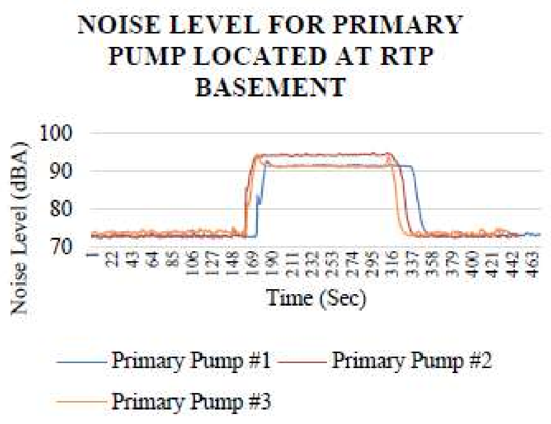

Figure 2: Noise level for primary pump

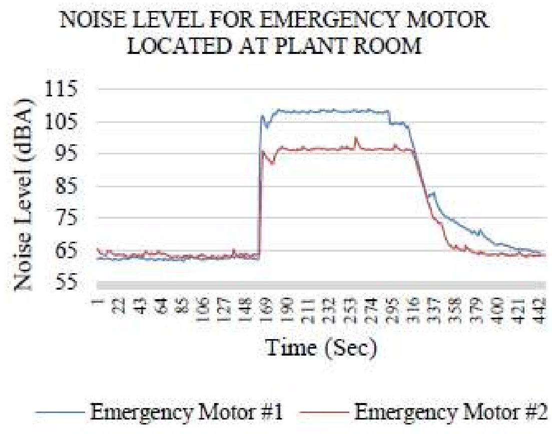

Figure 3: Noise level for emergency motor

air resistance. During shutting down, noise level for both motor show similar trend.

Figure 3 shows that, during peak load, primary pump #1 graph trend is normal, while primary pump #2 and #3 show slight difference in graph trend. Initially, all three pumps recorded 73 – 75 dBA of noise level. The trend shows it different at operating condition (peak load). Every motor or pump should have in-rush current supply during starting of the equipment. In-rush current is the high amount of electrical current that flows into an electric motor when it is first turned on or starts operating. This surge of current occurs during the initial moments when the motor is accelerating from a standstill to its normal operating speed. primary pump #2 peak load recorded noise level average at 94 dBA and show no in-rush current involve. Primary pump #3 show normal graph trend until at the end of peak load. Before primary pump #3 shutting off the recorded noise level spike a little and continued to reduce until shutdown.

4 Conclusions

From data collected the slight difference of the noise level in the emergency motor #1 and #2 is due to the piping structure causing air resistance. Primary pump #2 and #3 need further analysis with more data collection because difference in amplitude of graph. Data recorded will be use as a guide of a future trend noise level of the measured equipment. More data need to be measured to compare the noise trend and the noise level consistencies throughout their lifetime.

References

R.S Rashad, S.A Ahmad, and M.K Ismail. 2023. Fault detection in rotating machinery based on sound signal using edge machine learning. *IEEE Access*, 11:6665–6672.

P. Supachai, W. Santi, and T. Satean. 2017. Detection mechanical fault of induction motor using harmonic current and sound acoustic. *International Electrical Engineering Congress (iEECON)*, pages 1–4.

Individual Research Contribution Review, 2023, 1(1): 377–378

A Micro-sized High-temperature Thorium Reactor with Duplex TRISO Fuel with Enhanced Thorium Utilization Compared to the SBU Configuration

Mohamad Hairie Rabir
Technical Support Division, Malaysian Nuclear Agency
43000 Kajang, Selangor
m_hairie@nm.gov.my

Abstract

This study compares two cores - one duplex fueled and the other Seed-and-Blanket-Unit (SBU)-fueled - in a micro- modular high temperature reactor (MMR-HTR) using the MCNPX 2.7 code. Both cores had the same Th:U ratio and initial fissile mass but differed in thorium and uranium distribution. The duplex core showcased superior neutron performance with a higher core conversion ratio, enhanced long-term ^{233}U production, more negative fuel temperature coefficient (FTC) value, and lower rod peaking factors. These results highlight the significance of optimizing the distribution of fertile and fissile materials for advanced thorium reactor designs.

Keywords: HTR; Micro Modular Reactor; Thorium Reactor; TRISO-Duplex

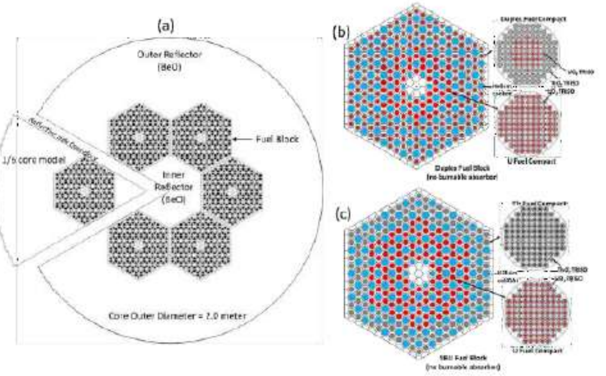

Figure 1: Illustration of the core (and 1/6 core model for burnup calculation) (a), the Duplex '30-L5' (b) and SBU (c) fuel block configurations

1 Introduction

This paper evaluates the TRistructural ISOtropic (TRISO) duplex fuel concept for enhancing thorium consumption in the MMR-HTR. It conducts a comprehensive neutronics analysis of the Duplex TRISO fuel at the core level within the framework of a 10 MWth U-Battery micro reactor using a 6*4 core configuration. The study compares cores utilizing duplex fuel versus SBU fuel, aiming to select the optimal duplex core based on power level and outer reflector thickness. All simulations were conducted using MCNPX 2.7 with the ENDF/B-VII Release 0 cross-section data library.

2 Methods

The comparative analysis of core neutronics relies on identical initial thorium mass ratios (Th:U, 50:50) in both the duplex-fuelled and SBU-fuelled cores. A simplified SBU-fuelled core, analogous to the duplex-fuelled core, could be constructed by populating only the first three layers of the fuel block with thorium rods. Figure 1 illustrates the core (a), the duplex fuel block (b), and the SBU fuel block (c). Maintaining consistent initial masses of ^{232}Th, ^{238}U, and ^{235}U in these core models emphasizes the distinctions between these configurations within an MMR-HTR context.

3 Results

Results are presented in Figure 2. Figure 2 (a) shows k_{eff} trend comparisons in which the duplex and SBU core are nearly identical. The rapid decrease in k_{eff} value during the early stages of the core cycle is caused by the accumulation of xenon poison. The k_{eff} trend difference appears between 2 and 5 EFPY for duplex-fuelled and SBU-fuelled cores. Both have the same burnup trend and almost identical heavy metal mass changes, as shown in Figures 2 (b) and (c). Both have a lower accumulation of plutonium compared to ^{233}U. The duplex-fuelled core has a slightly higher ^{233}U buildup trend after 2 EFPY, which is likely why it has a slightly higher k_{eff} trend during this time period. Although this is an advantage over the SBU-fuelled core, both cores have become subcritical during this time period. Therefore, prolonging the cycle length or maintaining longer criticality would aid in obtaining the benefits of thorium fuel for thorium reactors generally as well as for the duplex-fuelled core. Since both cores contain the same amount of ^{232}Th and uranium, the difference is due to the different effects of uranium and thorium spatial distribution.

The power distribution (Figure 3 (a)) in the duplex core is concentrated in the UO2 rods group in the centre of the fuel block, with a peak power of 1.5. With a value of 0.8, the maximum duplex rod power peaking was at the periphery (inner reflector side). The distribution of power at BOC and EOC is not significantly distinct. The power distribution in the SBU-fuelled core is concentrated in the UO_2 rods area, with a maximum rod power peaking at 1.8 at BOC. At EOC, the distribution of SBU core power changed, with maximum power peaking at 1.6 and ThO_2 rod power peaking is 0.0 at

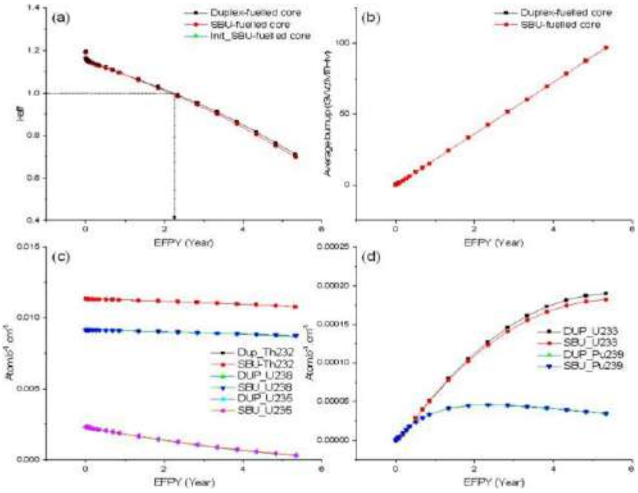

Figure 2: Comparison of the Duplex and SBU fueled core's cycle length, burnup, and selected actinides

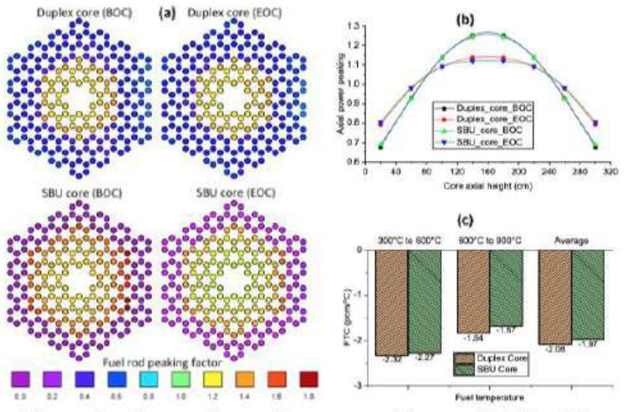

Figure 3: Comparison of power peaking and FTC of the Duplex and SBU cores

BOC and 0.2 at EOC. Since the difference and heterogeneity of the two reactor cores are only radially distinct, but axially identical, the axial power peaking is also identical. Figure 3 (b) illustrates the axial power at BOC and EOC for duplex-fuelled and SBU-fuelled cores. Higher burnup at the middle plan of the reactor's height decreases the axial peaking power from 1.26 at BOC to 1.15 at EOC.

Figure 3 (c) depicts the FTC differences for the duplex and SBU cores for 300 - 600 °C, 600 - 900 °C, and averaged. In comparison to the SBU-fuelled core, the duplex-fuelled core exhibits slightly stronger negative FTC. In a thermal spectrum reactor, when the fuel temperature rises, the Doppler effect causes the resonance region to broaden and more neutrons to be absorbed before reaching thermal energy, causing reactivity to drop. The effect occurs in ^{238}U and is significantly stronger in ^{240}Pu, which is produced via neutron absorptions in ^{238}U and ^{239}Pu. As is well known, the resonance energy range of the ^{238}U is greater than that of the ^{232}Th. Consequently, the likelihood of resonance capture increases as the ^{233}U mass is distributed more evenly, such as in a duplex core. This explains why duplex-fuelled cores have a lower FTC than SBU-fuelled cores.

4 Conclusions

In conclusion, the study on the use of conceptual design, duplex TRISO fuel in micro-sized HTRs based on the 6*4 U-Battery configuration was conducted successfully. The MCNPX 2.7 Monte Carlo code was used to model and determine the optimal fuel block pattern and neutronic characteristics of the micro-sized HTR core that uses duplex TRISO fuel. The results obtained and discussed above indicate that not only is duplex TRISO fuel feasible, but it also offers neutronic advantages over a core based on the seed and blanket configuration or SBU where both have the same Th:U ratio and initial fissile mass. Evenly distributed thorium and uranium mass via the use of Duplex TRISO fuel has been shown to benefit in terms of safety and neutronics. In comparison to the SBU core, this configuration allows for more balanced power per fuel rod distribution and a better FTC value. It increases the epithermal region of the neutron spectrum, allowing for more resonance captures, particularly during the early cycle length period.

References

Mohamad Hairie Rabir, Aznan Fazli Ismail, and Mohd Syukri Yahya. 2023. A micro-sized high- temperature thorium reactor with duplex TRISO fuel with enhanced thorium utilization compared to the SBU configuration. *Fuel*, 354:129316.

Individual Research Contribution Review, 2023, 1(1): 379–380

Neutron Characteristics Profiling at the RTP In-core and Beamport Irradiation Facilities

Mohamad Hairie Rabir
Technical Support Division, Malaysian Nuclear Agency
43000 Kajang, Selangor
m_hairie@nm.gov.my

Abstract

Neutron flux at the in-core PUSPATI TRIGA reactor (RTP) has been measured through experiments. The neutron activation technique was used to measure neutron flux by irradiating gold wire samples. These measurements were then compared to the neutron fluxes calculated using the developed MCNPX reactor model, and the results were found to be in good agreement. The neutron flux in its beam ports and thermal column facility will be measured and simulated as well.

Keywords: RTP; Neutron Flux; Neutron Spectrum; MCNPX

1 Introduction

Research conducted at the PUSPATI TRIGA Research Reactor (RTP) in Malaysia may vary over time, and it typically covers a broad range of scientific disciplines related to nuclear science and technology. Some common areas of research and applications at research reactors like RTP include; neutron radiography, neutron activation analysis, and the production of radioisotopes for medical, industrial, and research purposes. Determining neutron flux in a research reactor is crucial because neutrons play a fundamental role in various experimental and practical applications within the realm of nuclear science and technology. Neutron flux refers to the density or rate of neutron flow in a specific area, and it is measured in neutrons per unit area per unit time.

2 Methods

The neutron activation technique for flux estimation entails irradiating some samples with a known amount of nuclei and then measuring the activation rate. Radioisotopes are mostly produced by neutron capture during neutron activation and usually decay with simultaneous emission of gamma-rays. The activation rate is then assessed using gamma-ray spectroscopy with High Purity Germanium (HPGe) detectors by measuring the -rays emitted by the isotopes. The following equation describes the relation between the neutron flux, φ and the activation rate:

$$R = N \int \varphi(E)\sigma(E)dE \quad (1)$$

Where N represents the number of precursor isotopes in the irradiated sample and σ is the activation cross section. In this study, gold wire samples are irradiated in various positions among the fuel elements, the Rotary Rack, and the Central Thimble.

The RTP core detail geometry was created in a three dimensional Cartesian coordinate system. Detailed engineering drawings of the reactor were used to build an MCNPX input deck. Individual cells were explicitly defined for each reactor component. All simulations were conducted using MCNPX 2.7 with the ENDF/B-VII Release 0 cross- section data library. All simulations generate statistical errors, which can be reduced by changing the number of neutron histories. Flux is calculated using the cell volume tally and the meshtally.

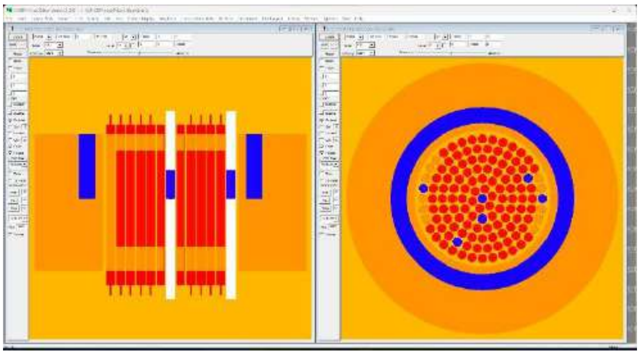

Figure 1: Illustration of the RTP core model

3 Results

The comparative findings are illustrated in Figure 2 and Figure 3, wherein neutron flux measurements were conducted at a core power level of 500 kW. Figures 4 and 5 depict the estimated neutron spectrum and spatial thermal neutron flux distribution within the RTP core. It is noteworthy that, in the MCNPX simulation, all data have been normalized based on a core power level of 500 kW. It should be noted that the thermal energy group in this work is defined as neutrons less than 0.025 eV and epithermal neutrons between 0.025 eV and 0.4 eV.

As evident from the contrast between measurement outcomes and simulation results, the observed discrepancies may arise from the simplification of temperature distribution, cross- sectional data, and cell tally methodology in the MCNPX model. However, a substantial disparity in the epithermal outcomes could stem from inaccuracies in the burnup and radionuclide inventory listing within the MCNPX model.

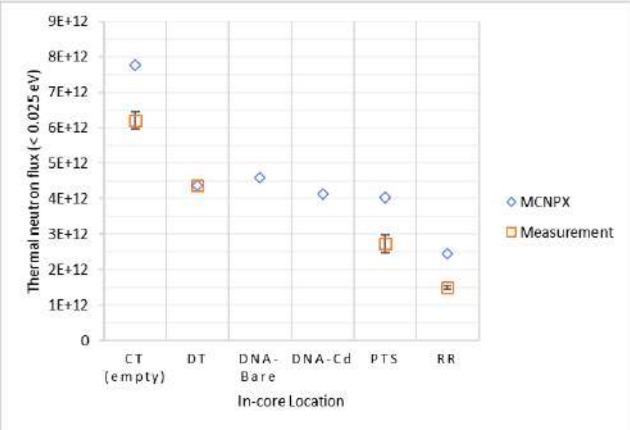

Figure 2: Thermal neutron flux comparison

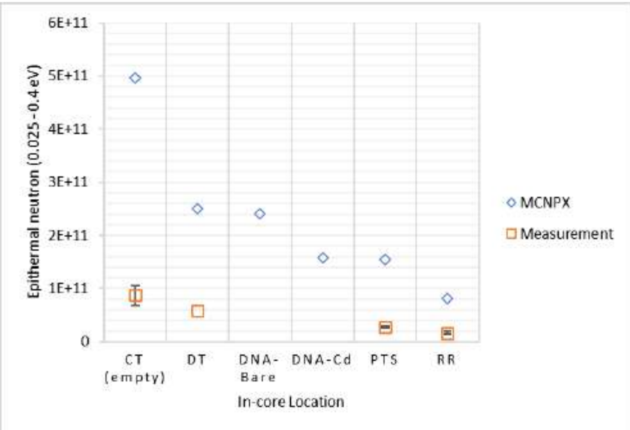

Figure 3: Epithermal neutron flux comparison

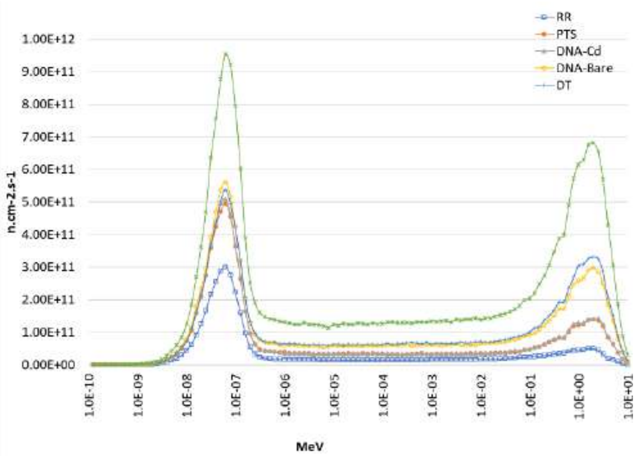

Figure 4: In-core facility neutron spectrum simulation

4 Conclusions

The determination of in-core flux in RTP has been undertaken through both measurement employing the activation method and simulation utilizing the MCNPX code. The simulated and measured thermal neutron flux exhibits a relatively satisfactory concordance; however, notable discrepancies are observed in the epithermal results. Further scrutiny of this divergence will be conducted. Additionally, future iterations of this study will encompass the inclusion of the out-core facility.

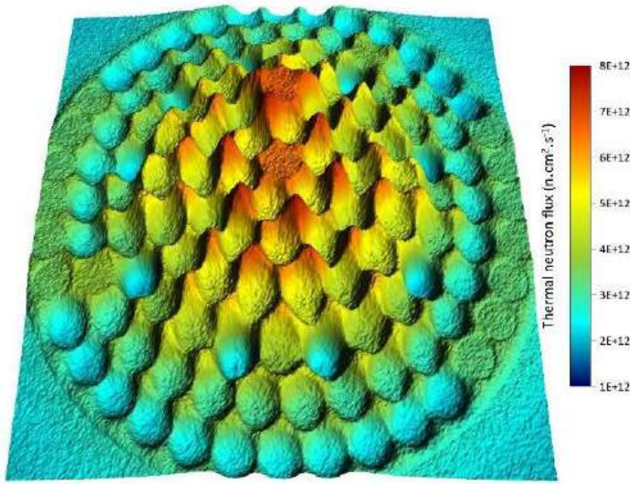

Figure 5: In-core neutron distribution simulation

References

Davide Chiesa, Massimiliano Nastasi, Carlo Cazzaniga, Marica Rebai, Laura Arcidiacono, Ezio Previtali, Giuseppe Gorini, and Christopher D. Frost. 2018. Measurement of the neutron flux at spallation sources using multi-foil activation. *Nuclear Instruments and Methods in Physics Research Section A: Accelerators, Spectrometers, Detectors and Associated Equipment*, 902:14–24.

Individual Research Contribution Review, 2023, 1(1): 381–382

Neutron Flux and Activation Determination Inside the PUSPATI TRIGA Reactor Biological Shielding to Support Future Decommissioning Plan

Mohamad Hairie Rabir
Technical Support Division, Malaysian Nuclear Agency
43000 Kajang, Selangor
m_hairie@nm.gov.my

Abstract

The activation of the biological shield holds significance in the context of waste management for nuclear facilities. The determination of the final activity involves estimation through modeling, specifically utilizing the neutron flux density via the MCNPX code. In a series of MCNPX simulations conducted at the PUSPATI TRIGA reactor (RTP), it is observed that the flux density on the inner surface of the biological shield ranges around 109 n.cm^{-2}.s^{-1} at maximum power. However, it is noteworthy that this value is markedly influenced by the configuration of reactor installations. The derived data enable the assessment and estimation of the final waste categorization of the concrete in accordance with safety legislation.

Keywords: RTP; Neutron Flux; Neutron Spectrum; MCNPX

1 Introduction

RTP stands as the sole operational nuclear research reactor in Malaysia, achieving its first criticality in 1982. Since then, it has maintained an average annual utilization of 20 MWdays. RTP serves as a host for various research endeavors associated with reactor physics, radiochemistry, neutron physics, and education. The reactor, characterized by a height of 6.55 m and a width of approximately 7 m, is predominantly constructed using heavy concrete. During standard operations, the reactor operates within the range of 500 - 750 kWth, corresponding to a maximum neutron flux density of 1013 n.cm^{-2}.s^{-1} in the central irradiation tube. In the context of decommissioning, it becomes imperative to ascertain the activity of the biological shield to adhere to regulatory stipulations for radioactive waste. This undertaking involves an analysis of the neutron flux, which will be utilized to predict the activation of the biological shield.

2 Methods

The RTP core and biological concrete shielding detail geometry was created in a three-dimensional Cartesian coordinate system, as illustrated in Figure 1. Detailed engineering drawings of the reactor were used to build an MCNPX input deck. Individual cells were explicitly defined for each reactor component. All simulations were conducted using MCNPX 2.7 with the ENDF/B-VII Release 0 cross- section data library. All simulations generate statistical errors, which can be reduced by changing the number of neutron histories. Flux is calculated using the meshtally. Owing to challenges in obtaining an adequate number of neutrons that penetrate deeply into the RTP concrete shield, the entire model underwent modification, adopting a layered approach wherein volumes were delineated with increasing neutron importance from the central to the outer regions of the shielding, as illustrated in Figure 2.

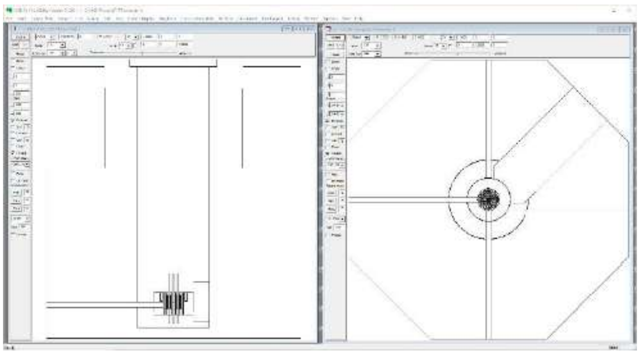

Figure 1: Illustration of the RTP core and biological concrete shielding model

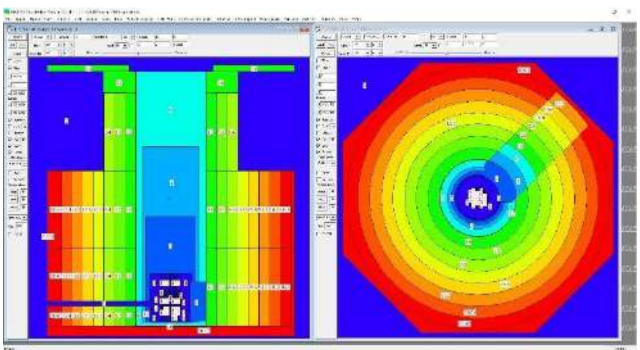

Figure 2: Illustration of increasing neutron importance with colour changes from blue to red

3 Results

The total neutron flux calculation results are illustrated in Figure 3 and Figure 4, wherein all data have been normalized based on a core power level of 750 kW.

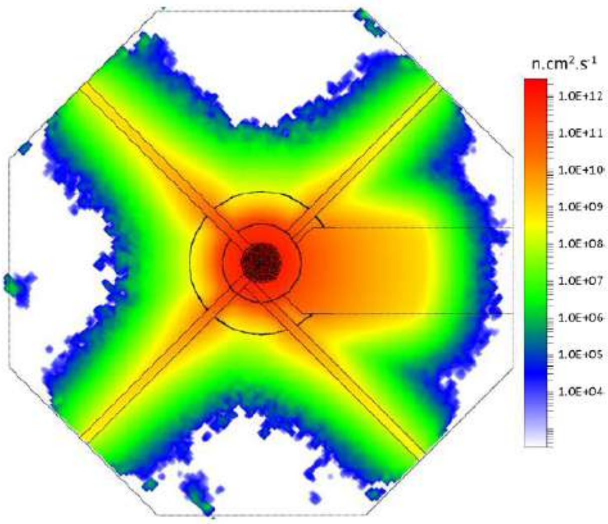

Figure 3: Top view neutron flux map

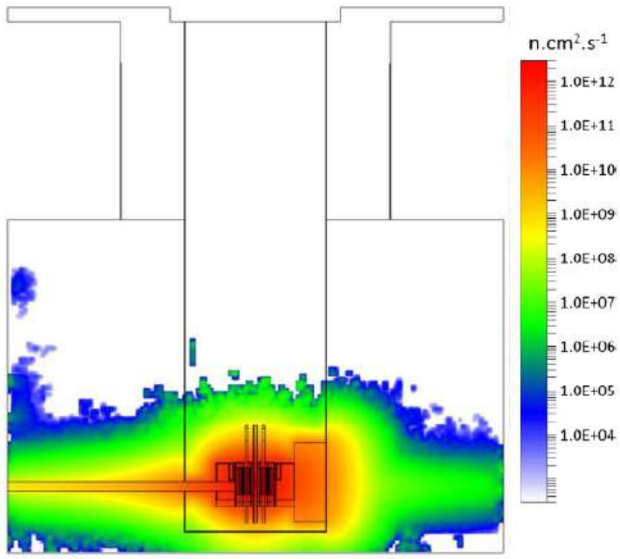

Figure 4: Side view neutron flux map

4 Conclusions

The assessment of the overall neutron flux within the biological shielding of RTP was conducted through simulation, employing the MCNPX code. Despite representing approximately 30% of the overall progress in evaluating the shielding structure's activation, the data presented offered crucial insights into the affected concrete volume. Subsequently, the next phase involved incorporating all structures, encompassing the specific configuration of each beamport facility, including its collimator, shielding structure, and components external to the biological shielding. The subsequent step entails utilizing Origen for the determination of radionuclide inventories.

References

Stefan Merz, Mile Djuricic, Mario Villa, Helmuth Böck, and Georg Steinhauser. 2011. Neutron flux measurements at the TRIGA reactor in Vienna for the prediction of the activation of the biological shield. *Applied Radiation and Isotopes*, 69(11):1621–1624.

Individual Research Contribution Review, 2023, 1(1): 383–384

Neutronics Characterization of the RTP Core-16

Mohamad Hairie Rabir
Technical Support Division, Malaysian Nuclear Agency
43000 Kajang, Selangor
m_hairie@nm.gov.my

Abstract

The Reaktor TRIGA PUSPATI (RTP), a Malaysian research reactor, underwent core reshuffling to boost core excess reactivity. Accurate neutronics data for the RTP core is vital for safety, operation, and future reshuffling planning. Using MCNPX 2.7, a computational model of the new 16th core configuration was created to estimate key neutronics parameters and validate against operational data for core excess.

Keywords: Neutronics, TRIGA reactor, MCNPX, PUSPATI

1 Introduction

The RTP has been reshuffled 15 times since 1982. For ongoing study and irradiation, new core was proposed to increase excess reactivity and improve neutronics parameters. The new Core-16 configuration requires fuel position changes. The optimal configuration was determined based on the core's excess reactivity and peak power (Rabir et al., 2022). This paper provides a summary of the key findings from neutronic investigations conducted on the new RTP core configuration at 500 kW. In section 2, the computational tools used for analysis are described. In section 3, the key neutronic parameters, whereas in section 4, the principal conclusions of the presented work are drawn. This paper can be especially helpful for future research and development (R&D) studies linked to neutronics and safety analysis of the PUSPATI TRIGA Reactor because it describes the current status of the neutronic studies for the RTP Core- 16.

2 Methods

Analyses of the neutronics of the RTP core have been conducted using deterministic and Monte Carlo code. TRIGLAV is a deterministic code based on the diffusion approximation of the transport equation that employs the WIMSD program to calculate an averaged unit cell cross section. Core and individual fuel element (FE) burnup will be determined using the TRIGAV code. FE will have a distinct burnup value due to its initial composition, loading history, and location within the core. Then, the MCNPX code will be utilized to generate the nuclide inventory of each FE based on the burnup calculation from the TRIGLAV code. In the end, MCNPX fuel and core model of RTP Core-16 is developed using the nuclide inventories obtained previously (Rabir et al., 2017). Figure 1 depicts the MCNPX simulation's layout of the RTP core and surrounding water.

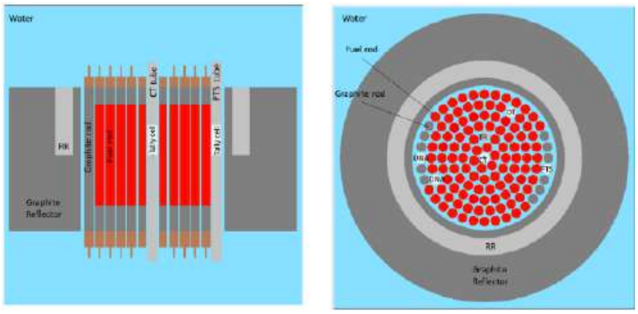

Figure 1: MCNPX simulation model

3 Results

Results are presented in Figure 2. Thermal neutrons reach their maximum concentration in water, exhibit a more uniform distribution in empty volumes and graphite, and experience a significant reduction within fuel rods. Fast neutron flux achieves its peak within the central fuel rods, with lower intensities in water and graphite. The highest kW/FE output is generated by the 12 wt. % fuel element in the C-ring and the 20 wt. % fuel element in the E-ring. The predominant neutron flux is thermal in all simulated facilities, with the ratio of thermal-to-fast neutrons increasing as the distance from the core increases. The neutron spectrum analysis showed that the thermal neutron flux had its highest point at an energy of 0.0631 eV in the RTP core, while the fast neutron flux peaked at 2 MeV, suggesting a hardening spectrum.

4 Conclusions

In this study, Monte Carlo N-Particle eXtended version 2.7 (MCNPX 2.7) was employed to construct a computational model of the new 16th core configuration at 500 kW, facilitating the determination and estimation of key neutronics parameters. The developed core physics model strived for the practical level of accuracy, encompassing fuel and core dimensions, fuel burnup and nuclide inventory, as well as core structure material composition. It is recommended that these results be compared to the measurement results, as well as a comparison of the effect with and without axial burnup.

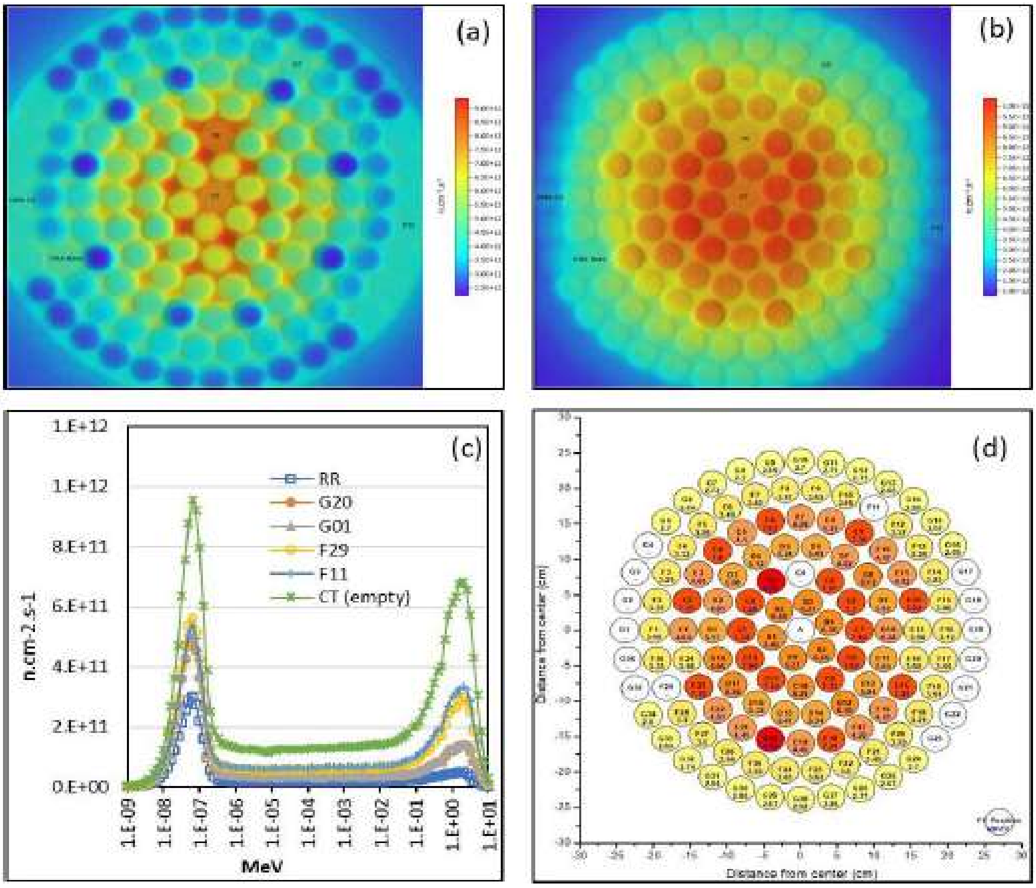

Figure 2: MCNPX simulation results; (a) thermal and (b) fast neutron flux distribution, (c) neutron spectrum in main irradiation facility and (d) total energy produced per FE

References

M.H. Rabir, Mohamed Zin M.R., Abdul Karim J., Jalal Bayar A.M, Usang M.D., Mustafa M.K.A., Hamzah N.S., Mohd Said N., and Jalil M.H. 2017. Neutronics calculation of RTP core. *AIP Conference Proceedings*, page 020009.

M.H. Rabir, Muttaqin A. Bayar J., and Karim J.A. 2022. In-core RTP fuel relocation and criticality behaviour using MCNP5 / XCODE. *J. Nucl. Relat. Technol.*, 19:8–18.

Individual Research Contribution Review, 2023, 1(1): 385–386

IRCR

Radiation Dose Map Simulation in Teletherapy Room with a 2000 Curie Co-60 Source using the MCNPX Code

Mohamad Hairie Rabir
Technical Support Division, Malaysian Nuclear Agency
43000 Kajang, Selangor
m_hairie@nm.gov.my

Abstract

Any preliminary evaluation of a radiation shielding assessment requires the simulation data. In this case, the dose distribution was simulated in a teletherapy room with a 2000 Curie Co-60 source using MCNPX code. This study highlights important results and a proposal for a shielding structure as an overview of early data that will be used in the future.

Keywords: Dose map, Shielding, Teletherapy, Simulation, MCNPX

1 Introduction

A teletherapy room at Nuklear Malaysia consists of a 2k Ci Co-60 source encapsulated in a shield structure (source head). The source is primarily used for radiation detector calibration, and the room is currently being refurbished for optimal use. One critical aspect of the project is obtaining detailed data on radiation dose distribution. Although a measurement method could be used, a detailed map of gamma dose from the source could allow for better planning. As a result, the MCNPX code was used to simulate the data and obtain early recommendations on optimal shielding design inside the room.

2 Methods

Analyses start with detail model development of the room and the source head geometry and materials. MCNPX simulation was performed with SDEF source cards and mesh tally. All statistical error were kept below 1% by controlling the number of gamma history. Illustration of the models shown in Figure 1 and Figure 2. The teletherapy room wall is 50 cm thick high density concrete, while the roof is the same material but 30 cm thick. The proposed shielding structure included a sourcehead collimator and a stopper made of lead.

3 Results

The results are shown in Figures 3, 4, and 5. Aside from direct beam dose, it can be seen that scattered gamma contributes significantly to dose distribution, particularly at the back and top of the sourcehead.

4 Conclusions

According to the MCNPX simulation, the upper floor's maximum surface dose can reach 80–100 uSv/h. Radiation scattering plays a major role, particularly above and behind the sourcehead. Although the suggested collimator and stopper design is merely conceptual and needs more research, it could help reduce scatter gamma.

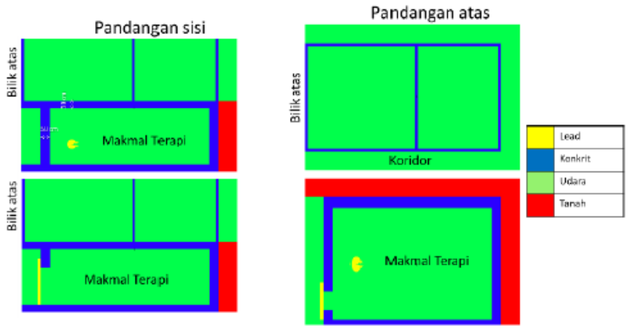

Figure 1: 2D top and side view of simulated room

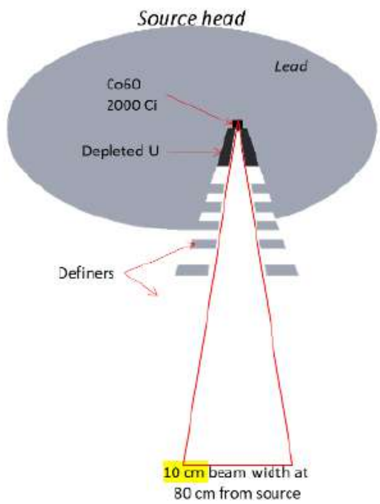

Figure 2: Source head model

References

M.H. Rabir. 2023. Simulasi kasar taburan dos di Makmal Terapi blok 32 menggunakan kod MCNPX. *Laporan Teknikal: NUKLEARMALAYSIA/L/2023/183*.

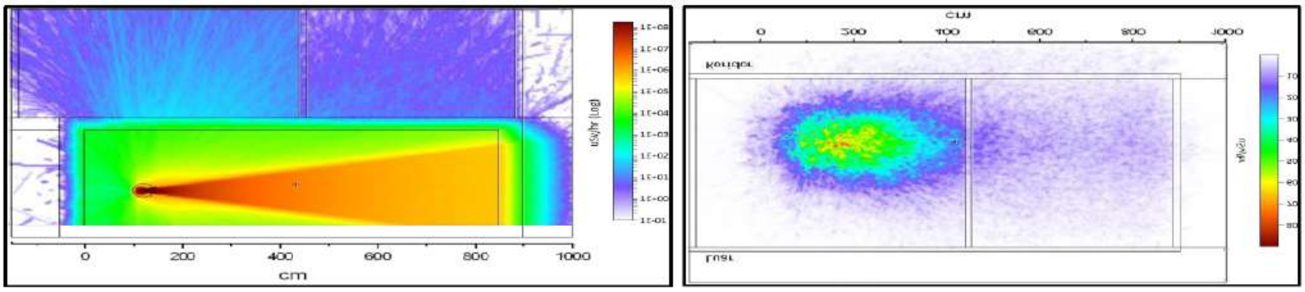

Figure 3: MCNPX 2d side and top (upper floor surface dose) view simulation map

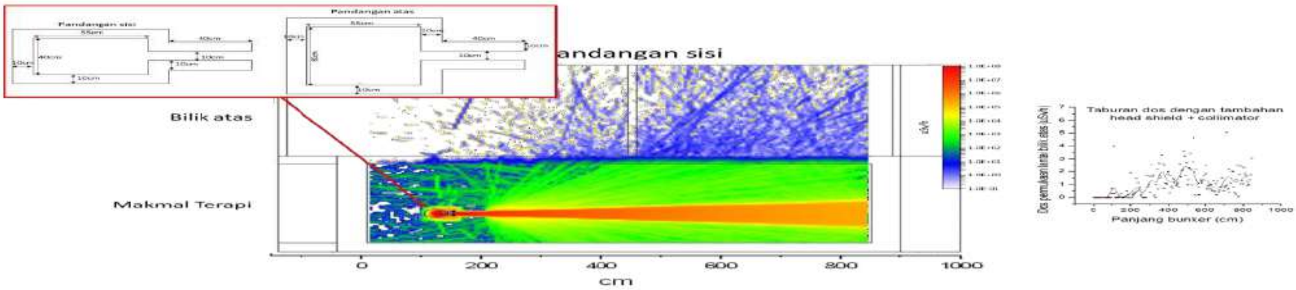

Figure 4: Dose map with sourcehead collimator

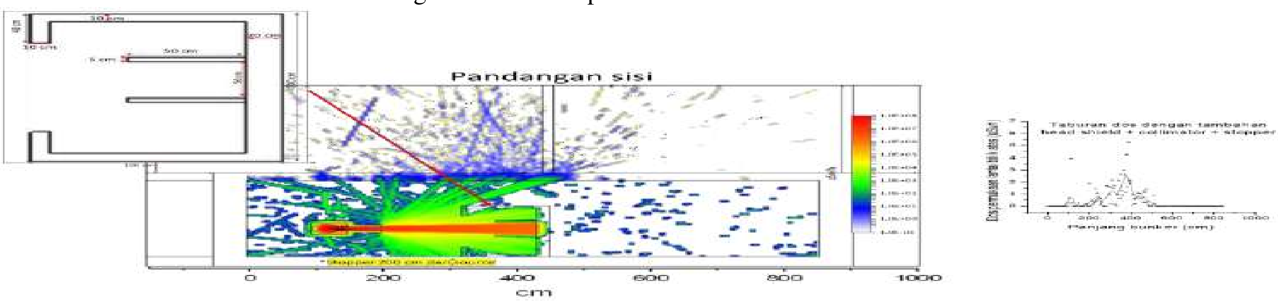

Figure 5: Dose map with sourcehead collimator and stopper

Individual Research Contribution Review, 2023, 1(1): 387–388

Development of Database Architecture for Microbiology Laboratory Test Management System (MBioTest)

Mohamad Safuan Sulaiman
Technical Support Division, Malaysian Nuclear Agency
43000 Kajang, Selangor
safuan@nm.gov.my

Abstract

Through a project called MBioTest, a structured database architecture has been developed to support the MBioTest system. Previously, data used for Microbiology Laboratory test were in the text-based files and unstructured. The unstructured data leads to unproductive data usage and retrieval. This paper presents the development of database architecture used in the Microbiology Laboratory test information system (MBioTest). The database architecture is design based on two type of microbiological test procedures, namely Sterility and Bacterial Endotoxin Test. Those tests were conducted to ensure the safety of radiopharmaceutical product used in cancer screening. The emphasize is on the generalization of the database architecture design which is able to be replicated to some other application of similar type of laboratory information management.

Keywords: MBioTest, Database Architecture, Microbiology Laboratory, Laboratory Information System

1 Introduction

This project is an R&D join venture project between IT Center (Tech. Support Division) and Medical Technology Division of Nuklear Malaysia. Microbiology Quality Control Laboratory is one of the Nuclear Malaysia's service centers which offers microbiology test includes Sterility test, Bioburden test (bacteria or fungus), Bacteria Endotoxin test using gel clot technique and Environmental Monitoring Test to internal and nationwide customers. A system called VBMikrotestV01 has been used to manage the tests' information. As time goes by the system hardware is ageing and similarly the software comes to the end of support. Besides, data in previous system were not well structured, stored in text files that has limited and unmanaged control and less efficient of data design and relational that affect some module malfunction in the system.

Due to this conditions, this paper studies the existing data system and proposed new database architecture as the preparation to develop a new system called MBioTest to improve the legacy of VBMikrotestV01.

2 Method

Development of MBioTest is using Agile System Development Life Cycle (ASDLC). The general understanding of the method as in Figure 1.

Figure 1: Agile SDLC Methodology (Johnivan, 2022; Tyagi, 2020)

At planning and Design stage, detail user and system design requirements are acquired as much as possible before a complete database design architecture could be proposed. In addtition, forms used in the process of the microbiology test have also been studied to get appropriate understanding of the data model.

3 Data/Results

As a result, the proposed database architecture for MBioTest system as in Figure 2.

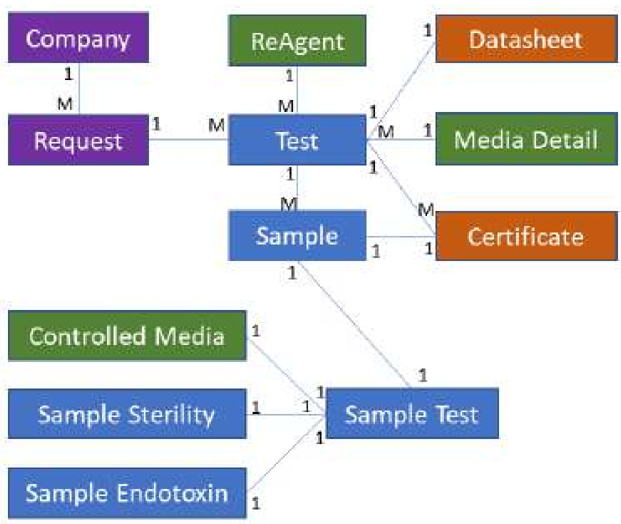

Figure 2: E-R Diagram or Proposed Database Architecture for MBioTest

4 Discussion/Conclusions

From Figure 2, twelve (12) entities have been identified for MBiotest database. Data of Company, Request, Test, Reagent, Sample, Datasheet, Media Detail, Certificate, Sample Test, Controlled Media, Sample Sterility and Sample Endotoxin should be kept in database to ensure the system could fulfill the new user requirement. Instead, the relationship of each entity should be appropriately designed so that data could be easily and accurately retrieved once detail statistical analysis is needed, during the process of generating dashboard report and result of sample certificate.

As conclusion, 12 entities have been proposed for the MBioTest database architecture based on information acquired from user and system design requirements. The proposed structured database architecture is designed in such a way to improve data usage and retrieval and to ease the process of generation of reports and certificates. In the next study, the design could be applied to similar type of laboratory work system and tested for future expension in terms of replication of the usage.

References

J.R. Johnivan. 2022. Agile software development methodology & principles - https://project-management.com/10-key-principles-of-agile-software-development/ - accessed on 7 Dec 2023.

Neelam Tyagi. 2020. Types of agile methodologies - https://www.analyticssteps.com/blogs/7-types-agile-methodologies - accessed on 7 Dec 2023.

Individual Research Contribution Review, 2023, 1(1): 389–390

Digitalization of Marine Radioactivity Data in Malaysia

Mohamad Safuan Sulaiman
Technical Support Division, Malaysian Nuclear Agency
43000 Kajang, Selangor
safuan@nm.gov.my

Abstract

Marine radioactivity data in Malaysia were acquired many years ago. It began with manual recording process using paper, pen, and pencil. From 2003 onwards it has been consistently recorded and stored in MS Excel sheet. Due to limited access to the document, less structured, scattered and conducted with less systematic way, presentation and validation of the data could be argued and may not comply with the requirement of radiological assessment standard of practice. Therefore, this paper presents the idea of digitalization through development of an appropriate database system as a solution.

Keywords: Marine Radioactivity, Digitalization, Database System.

1 Introduction

In Malaysia, marine radioactivity data were acquired many years ago. It began with manual recording process using paper, pen, and pencil. Since year 2003, it has been consistently recorded and stored in MS Excel sheet. As time went by, the marine radioactivity data need to be accessible online and widely used for regional and international collaborations. For example, the data is shared at the international level such as the Global Marine Radioactivity Database (GLOMARD) (IAEA, 2000) organized by the IAEA Marine Environment Laboratory (MEL). The sharing of the data (Pavel et al., 2004) is important because it has been used as a basis for radiation dose assessment, provision of temporal trends and levels as well as finding the information gap at national, regional, and international levels. In Malaysia perspective, data in MS Excel sheet could only be accessed by Radiochemistry and Environmental Laboratory (RAS) (RAS, 2023) personnel, and not widely available for scientific research and investigation (except the published data). It is also less structured, scattered and conducted with less systematic way.

Due to those conditions, presentation and validation of the data could be argued and may not comply with the requirement of radiological assessment standard of practice. Therefore, development of an appropriate radioactivity database system that considering data from various matrices such as sediment, water, biota and plankton in sea and freshwater environment is proposed.

2 Method

This study is at the preliminary stage of the digitalization process which focuses on the marine radioactivity database development. The database development involves data standardization and normalization to produce appropriate data model that can facilitate data conversion and transfer to a new shared database platform. The database development uses relational database (Storey, 1991) technique to produce the data model. This technique is chosen because it could improve the data integrity and accuracy through appropriate data structure and relationship as the important aim of this study.

3 Data/Results

Through the relational database technique, the first result of the marine database model and relationship as in Figure 1. After detail analysis of the normalization the model and relationship has been improved as in Figure 2.

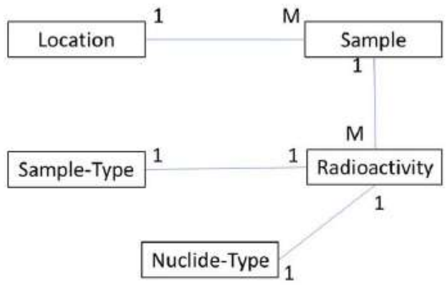

Figure 1: First Entity Relationship (E-R) Model For Marine Database

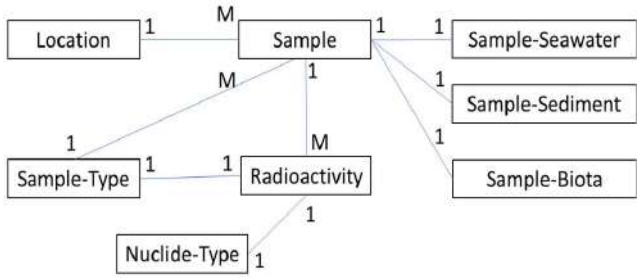

Figure 2: Normalized E-R Model For Marine Database

From ER Diagram as in Figure 1, only five (5) entities have been identified which includes 1. Location, 2. Sample, 3. Sample-Type, 4. Radioactivity and 5. Nuclide-Type.

While relationship between those entities are mostly one-to-one relationship except one-to-many for Location-Sample relationship. Detail description of each main entity as Table 1.

Table 1: Description of Entities in Marine Database

No.	Entity	Description
1	**Location**	Location is where the marin sample is collacted. Location data contains infomation of geographical location such as longitude and latitude.
2	**Sample**	Sample is the information of the sample collected such as time and date collected and distance from the shore
3	**Sample-Type**	Sample type contains information of sample type such as sediment, seawater or biota. This entity is created to standardized the sample type data used in the database, while detail data for each type of sample is contained in each entity of the sample namely **Sample-Seawater**, **Sample-Sediment** and **Sample-Biota**.
4	**Radioactivity**	Radioactivity contains information of the radioactivity from the sample collected. It records data such as weather, radioactivity and uncertainty
5	**Nuclide-Type**	Nuclide Type contains information of the nuclide found from the sample. This is entity is created to standardized the type of nuclide used in the database and has strong data relationship with Radioactivity

As the study going deeper, it is needed to add three more entities called 1. Sample-Seawater, 2. Sample-Sediment and 3. Sample-Biota.

The additional three sample entities are needed because, the main sample entity could not hold data from different variation of data. In this case sample data for seawater, sediment and biota have their own unique attributes. The difference of the attributes in each sample entity can be seen in Figure 3.

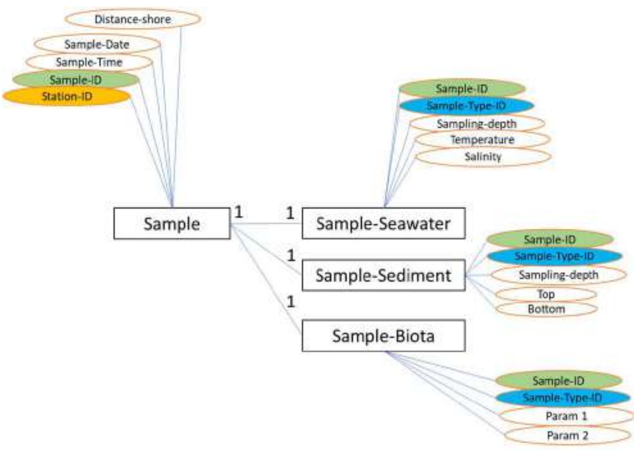

Figure 3: Attributes in each Sample Entity Relationship

In Figure 3, Sample-Seawater contains Sampling-depth, Temperature and Salinity. While, Sample-Sediment contains Sampling-depth, Top and Bottom; Finally, Sample-Biota contains Param1 and Param2.

4 Discussion/Conclusions

This preliminary study is at the very beginning stage of digitalization process and further development activities need to be worked out. Currently, eight (8) main entities were found to be included in the marine database. As the analysis progressing, tables and records are created and data in excel documents are further transferred into the database. Appropriate preparation of the marine database through rigor analysis is important to achieve higher integrity of data, at the same time facilitates the marine radioactivity data sharing and research collaboration at various levels. The outcome of the database usage is perceived to benefit the social wellbeing for global radiation protection, safety and security.

References

International Atomic Energy Agency IAEA. 2000. Global marine radioactivity database (GLOMARD). *IAEA TECDOC 1146, Vienna*.

P.P. Pavel, Katsumi H., Teruyuki H., Toshimichi I., E. Marian S., and Orihiko T. 2004. Spatial distribution of ^{3}H, ^{90}Sr, ^{137}Cs and ^{239,240}Pu in surface waters of the Pacific and Indian Oceans—GLOMARD database. *Journal of Environmental Radioactivity*, (76):113–137.

Nuklear Malaysia RAS. 2023. Introduction of radiochemistry and environment, https://www.nuclearmalaysia.gov.my/pagedesc.php?idmodul=4idpage=181.

Veda C. Storey. 1991. Relational database design based on the entity-relationship model. *Data Knowledge Engineering*, 7(1):47–83, ISSN 0169–023X,https://doi.org/10.1016/0169– 023X(91)90033–T. (https://www.sciencedirect.com/science/article/pii/0169023X9190033T).

Individual Research Contribution Review, 2023, 1(1): 391–392

Conceptual Design of 13 MeV Cyclotron Magnet

Mohd Azhar Ahmad
Technical Support Division, Malaysian Nuclear Agency
43000 Kajang, Selangor
mohdazhar@nm.gov.my

Abstract

This paper describes the conceptual design of 13MeV cyclotron magnet. The design process started with determining the initial design parameter which determining the magnet rigidity coefficient and pole radius considered with the RF cavity angle based on the harmonic number. Next, the geometry of the CAD magnet design is created based on the initial parameter condition and the design need going for shimming process using OPERA-3D Modeler to suit the isochronous magnetic curve. Modelling methods, mechanical design and some results are also presented. Finally, the Conceptual of 13MeV Cyclotron Magnet is suit the isochronous magnetic curve with the centre pole for ion source installation with a 35 mm radius.

Keywords: AVF Cyclotron, Magnet design, isochronous magnetic

1 Introduction

A cyclotron is a device that accelerates charged particles with the spiral orbit, and has been continuously developed since it was invented by Ernest O. Lawrence in 1931 (Lawrence and Edlefsen, 1931). The cyclotron accelerates protons or heavy ions, and the acceleration energy of particles ranges from few MeV to a few GeV. Various types of cyclotrons have been studied according to the acceleration energy, beam current, and particle species.

The classical type cyclotron defines as a fixed field magnetic field. Meanwhile, the azimuthal varying field (AVF) cyclotron has a sector focus on the magnetic field. The AVF magnetic field varies by radius depending on the energy of the particle motion. The geometry of the AVF magnet pole consists of wide and narrow gaps characterized as hill and valley, respectively. The basic principle of the cyclotron is the isochronous condition, which is that the centripetal and Lorentz forces should be the same in the cyclotron radius (Taufik et al., 2014).

In this study, the magnet design is based on three-dimensional magnetic field calculation. The purpose of this research is to obtain a design of the cyclotron magnet until the magnetic pole approached the isochronous curve which can be used as a basis for the construction of the 13 MeV proton cyclotron magnet.

2 Methods

This study was conducted initially by studying important parameters in mathematical formula which used to determine the design requirements of the cyclotron magnet. The next step is to create geometry computer-aided design (CAD) based on the initial parameter by using CATIA 3D software. The simulation started by importing the magnet CAD drawing into OPERA-3D Modeler followed by magnetic field calculations by Tosca module in the Opera 3D software. Simulation results were analyzed with the Python Programing to determine whether the parameters of the cyclotron magnet have met design requirements. Next is the magnetic pole shimming process (the CAD remodification process) performed to make the magnet design suit and approached the isochronous magnetic curve.

3 Results and Discussions

3.1 The Magnetic Design Calculation

From the calculation (can be referred to this full paper), it found that the rest energy of the proton E_0 is 939.375 MeV and magnetic rigidity is $0.5227Tm$. The magnet design is symmetrically four sectors and uses 4 as the harmonic number (h=4) with the RF oscillation of 80Mhz. The relativistic factor γ, the magnetic field at the centre pole B_0 and extraction magnetic field B_{ext} which found from the calculation is 1.0138, $1.311615T$ and $1.3297T$, respectively. So, the magnet pole radius was determined as 0.393 meters, but due to beam energy loss, the pole magnetic edge effect and ion source position in the centre pole was extended from 0.393 to 0.50 meters. Figure 1 represents the illustration of the isochronous magnetic field that has been calculated theoretically.

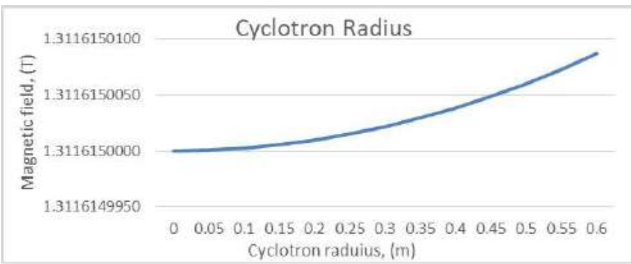

Figure 1: The isochronous magnetic field throughout the magnetic pole radius

3.2 CAD Design and OPERA-3D Simulation

The preliminary sector-focused CAD design has been created with a 50° hill and valley angle using CAD software. Initially, the radius of the magnet is ~ 0.4m. After considering the centre pole design and edge effect, the total radius becomes 0.5m. The hill gap was designed as 30mm. The initial mechanical model was analyzed using OPERA- 3D software.

3.3 The Magnetic Shim Process

For the first time running the simulation software, there is a substantial difference between the average magnet with the isochronous magnetic field. The edge of the hill pole was shimmed and the updated average magnetic field was replotted and compared to the isochronous graph. The initial and final of shimming process graph is shown in Figure 2.

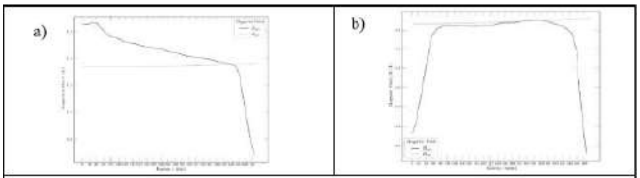

Figure 2: a) Initial b) Final: comparison of the isochronous field and average magnetic field.

3.4 The Final Design of Magnet

The final design of the 13 MeV cyclotron is shown in Figure 3. The centre pole was designed for ion source installation with a 35 mm radius. The initial hill design was at angle 50° and after the final shimming process the angle goes to 55°.

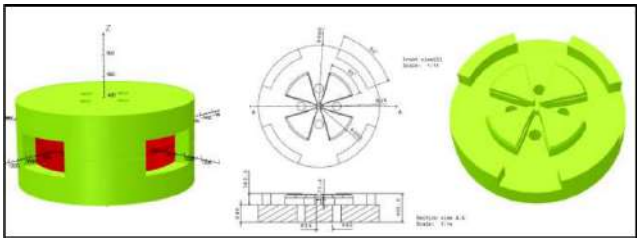

Figure 3: The 13 MeV AVF cyclotron dimension

4 Conclusions

This study, a four-fold symmetry 13 MeV isochronous cyclotron magnet was designed to suit and approached the isochronous magnetic curve. However, this magnet design needs to be further analyzed to cover beam dynamic design using CYCLONE equilibrium orbit code which used to analyse the beam stability and the equilibrium orbit tracking across all regions in a cyclotron.

References

E. O. Lawrence and N. E. Edlefsen. 1931. On the production of high-speed protons. *Science*, 72:376–7.

T. Taufik, A. Hermanto, P. Anggraita, and S. Santosa. 2014. Determination of magnet specification of 13 MeV proton cyclotron based on Opera 3D. *Atom Indonesia*, (2):69–75, doi: 10.17146/aij.2014.275.

Individual Research Contribution Review, 2023, 1(1): 393–394

Design and Construction of a Faraday Cup for Malaysian Nuclear Agency Plasma Focus Device (MNA-PF)

Mohd Azhar Ahmad
Technical Support Division, Malaysian Nuclear Agency
43000 Kajang, Selangor
mohdazhar@nm.gov.my

Abstract

A Faraday cup has been developed for measuring pulsed ion beam of a low energy plasma focus device. The faraday cup operating in biased ion collector mode have nanosecond response and these have been used to determine the energy spectrum and flux of ion beam emerging out of the pinched plasma column. Faraday cup consists of a conductive material with a shape like a cup to 'capture' ion particles in vacuum. The hitting of ion to the metal cup would generate a current, which can be used to determine the number of ions. Therefore, this paper describes specifically design, fabrication process, our findings and all related works for faraday cup based on our Malaysian Nuclear Agency Plasma Focus Device (MNA-PF).

Keywords: Faraday cup, ion collector, plasma focus device

1 Introduction

Faraday cup consists of a conductive material with a shape like a cup to 'capture' ion particles in vacuum. The hitting of ion to the metal cup would generate a current, which can be used to determine the number of ions.

Our group, ADC are developing Faraday Cup device to measure ion beam for our plasma focus device. Ion beam is an important source produced by this device. The ion beam is produced according to the type of gas filled inside the device chamber. The present diagnostics for the MNA-PF is still lacking in term of plasma diagnostics such as ion beam diagnostic. To measure the ion beam, Faraday cup is a good choice for this specific purpose.

2 Project Objectives

1. To develop an apparatus in order to investigate the ion emission from MNA-PF
2. To study the design and fabrication process of the Faraday cup suitable for MNA-PF
3. To determine the suitable materials for our FC by performing simulation study on its ion beam emission from MNA-PF

3 Simulation process

For plasma focus device, we have used SRIM in order to simulate the trajectory of ions inside the material for Faraday cup. According to the simulation, in general, copper is suitable as the penetration of the ion is very much lower than the thickness of the material (around 1 mm to 2 cm). Even in high ion energy (10 MeV ion), the penetration of copper only reached at below than 10 μm.

Comparison with other materials using SRIM and TRIM:

201 keV Argon Ion		
Metal	**Melting Temperature (°C)**	**Projected Range of ion inside the material (μm)**
Copper	1085	0.0862
Aluminium	660	0.176
Graphite	3527	0.167
304 Stainless Steel	1400-1450	0.088

In comparison with other material, copper can be considered as suitable for the material of Faraday cup in term of its ion penetration and melting temperature. The ion trajectories for this simulation as shown in Figure 1.

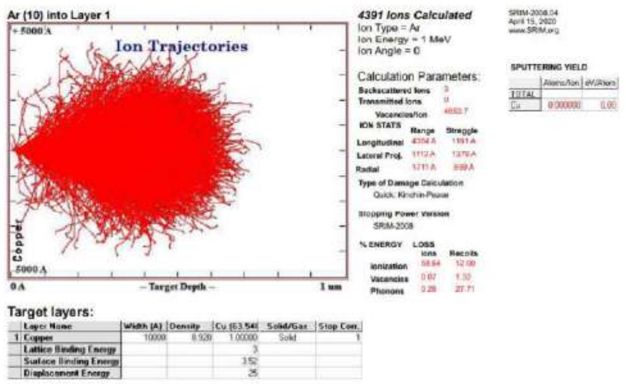

Figure 1: Ion trajectories in simulation process

4 Design of faraday cup

The faraday cup is designed by using 3D CAD software. The 3D CAD can ensure that all the dimensions will coincide with the desired measurement especially during fabrication process. The overview drawing and fabrication process of this faraday cup are shown in Figure 2 to Figure 6.

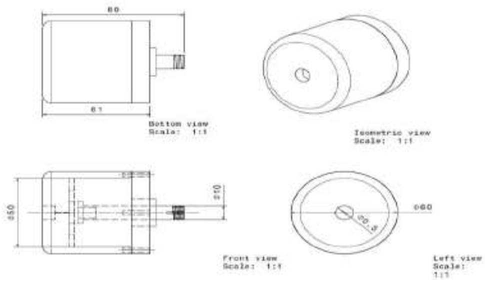

Figure 2: Dimension of 3D drawing faraday cup

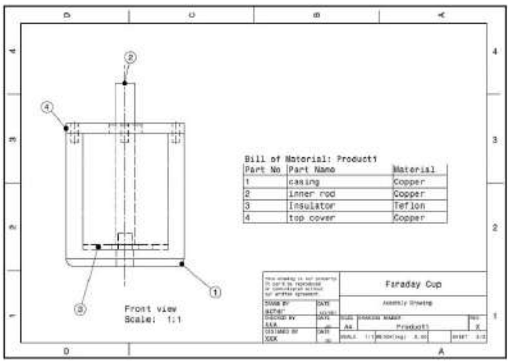

Figure 3: Material and part number

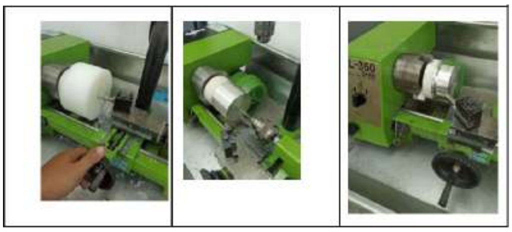

Figure 4: Machining process using lathe machine

Figure 5: Die, tap and flange fabrication process

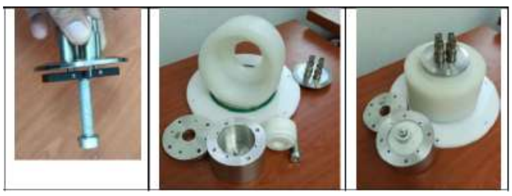

Figure 6: Completed fabrication process

5 Result

The design and fabrication process as shown in Figure 7 has been successfully carried out including the design of the electronic circuit for 100-250V bias negative voltage supply. As a result, testing the amount of ions produced by MNA-PF can be studied and carried out in next research.

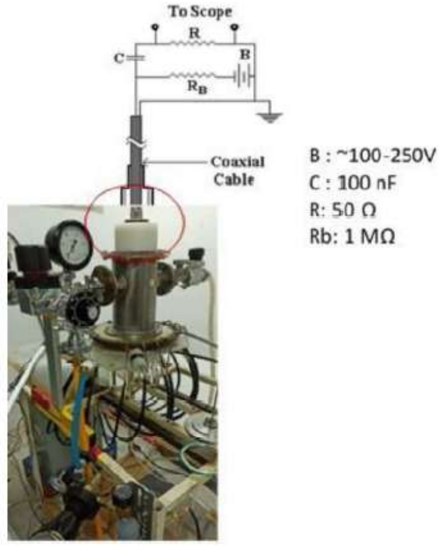

Figure 7: Installation of Faraday Cup on Plasma Focus Device (MNA-PF)

References

V. Damideh, J. Ali, S. H. Saw, R. S. Rawat, P. Lee, K. T. Chaudhary, and L. Sing. 2017. Fast faraday cup for fast ion beam tof measurements in deuterium filled plasma focus device and correlation with lee model. *Physics of Plasmas*, 24(6).

S. R. Mohanty, H. Bhuyan, N. K. Neog, R. K. Rout, and E. Hotta. 2005. Development of multi faraday cup assembly for ion beam measurements from a low energy plasma focus device. *Japanese journal of applied physics*, 44(7R):5199.

J. Moreno, D. Morales, G. Avaria, O. Cuadrado, and L. Soto. 2015, March. Ion emission study using visible spectroscopy and tof method in a plasma focus device of two kilojoules. *In Journal of Physics: Conference Series, IOP Publishing*, 591(1):012023.

Individual Research Contribution Review, 2023, 1(1): 395–396

Development of Nuklear Malaysia Source Code Repository System for Security Review and Backup

Mohd Dzul Aiman Bin Aslan
Technical Support Division, Malaysian Nuclear Agency
43000 Kajang, Selangor
dzulaiman@nm.gov.my

Abstract

In the contemporary era, the development of systems is now open to any company, organization, or individual. These developed systems serve to streamline the daily tasks of organizations. For organizations like Nuklear Malaysia, the emphasis on system development is currently not only centered around system effectiveness but also includes a keen focus on issues related to security and source code integrity. Within Nuklear Malaysia, there are more than 30 systems that have been developed in-house as well as using external resources. This paper presents the development of the Nuklear Malaysia Source Code Repository System (NMSRS) utilizing GitLab as a platform to enhance the security aspects of system development. NMSRS aims to provide a robust and trusted solution for reviewing and securely storing Nuklear Malaysia's source code, safeguarding intellectual property and sensitive information. Additionally, this paper elaborates on the design and implementation aspects of NMSRS, including key features such as code versioning, access control, issue tracking, and continuous integration/continuous deployment (CI/CD) capabilities, alongside code reviews for security concerns.

Keywords: Source Code, Security, Cybersecurity, Application Development

1 Introduction

Application system in Nuklear Malaysia has risen nowadays as a need for embracing technology. Nuklear Malaysia currently operates a substantial infrastructure comprising over 40 servers and 30 applications. These applications encompass a diverse spectrum, with 62% being internally developed, 28% outsourced, and the remaining 10% attributed to other functions or scripts. Preserving the integrity of these applications is essential, as they serve as invaluable assets for Nuklear Malaysia, playing a pivotal role in facilitating essential organizational processes on a daily basis. Notable systems in this portfolio include Localweb, eSSDL, eClient, eTAS, ePunhcard, JSNM, Nuklear Malaysia Portal, and various others.

2 Problem Statement

The decentralization of development application code is a prominent issue, with a majority of it residing on individual

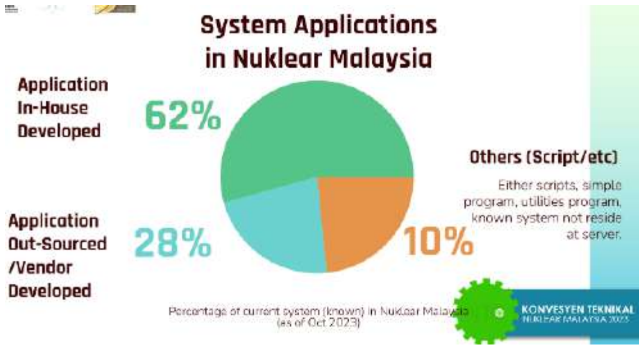

Figure 1: Application developed percentage over the type of development

and developer laptops or servers. This decentralized setup poses significant challenges for maintenance and security, relying heavily on external entities for code safeguarding. The absence of a dedicated review process for the source code exacerbates the situation, leaving standards unchecked and potential vulnerabilities undetected until much later, primarily known only to the original developer. Additionally, the critical absence of a backup process for the source code amplifies concerns, particularly in the face of unforeseen server incidents.

3 Method

This paper emphasis on development of source code repository system to ensure centralized, security and backup of the code can be done effectively. Four system will be tested that is Bioweb, Localweb, ePCv2 and python_infoGrabber will be the test case. The method has been divided into four phases that is:

(i) Identifying the best platform

(ii) Develop and configure Git

(iii) Implement to four system that consist of internal, external and script

(iv) Code Maintaining

During the phase 1, we have identified the system that can fulfil our requirement as of now that is Bit Bucket, GitHub and GitLab. The criteria we look into are whether it has open source version, the number of repositories it can hold,

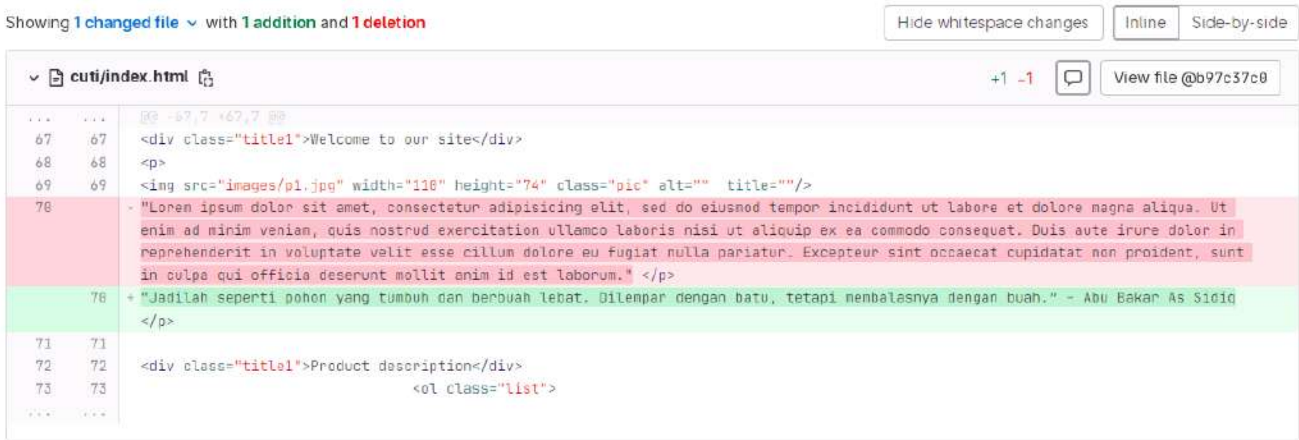

Figure 2: Changes to the code has been coloured. Red for removal, green for new added.

the number of contributors it allows, whether it can perform continuous integration and continuous delivery, and whether it meet industry standard. Among those, GitLab fulfil the criteria rather than those two.

Next on phase 2, we acquire open-source community edition GitLab (GitLab CE) and manage to get a dedicated virtual server for the system. We have carefully configured the following to the GitLab:

(i) Fully Qualified Domain Name (FQDN) : git.nuclearmalaysia.gov.my

(ii) Firewall and DNS to allow the system

(iii) Apache Webserver that serve the application via web

(iv) Ruby on Rails that run the application

(v) Corporate SSL/TLS Certificate that is DigiCert Wildcard Certificate Authority

(vi) Troubleshooting for misconfiguration and reconfiguration

The system can be access via: https://git.nuclearmalaysia.gov.my

On phase 3, we have implemented the code backup to four system that are is Bioweb, Localweb, ePCv2 and python_infoGrabber. All source code has been successfully uploaded to the system and initialized for future amendment. Phase 4 is when we invite several contributor or programmer to review any code and make amendments. The amendments were recorded into the system.

4 Results and Discussion

All of the source code for the tested system has successfully reviewed and backed up for security flaw and incident each for the current time.

With this implementation of source code repository system in Nuklear Malaysa, source code for the system is centralized, resulting in better view. Security of the source code is also improved as code checking can be done manually or automatically. As the system support collaboration, multiple collaborator from internal developer can contribute enhancing or reviewing the codes. Furthermore, there will be backed up of source code if the is any incident happen to the production server of the system itself. (Figure 2)

References

J.C. Cortés Ríos et al. 2019. A methodology for using GitLab for software engineering learning analytics. *IEEE/ACM 12th International Workshop on Cooperative and Human Aspects of Software Engineering (CHASE)*, pages 3–6, doi: 10.1109/CHASE.2019.00009.

Choudhury P., Crowston K., and Dahlander L. et al. 2020. GitLab: work where you want, when you want. *J Org Design* 9, 23.

M. Politze, U. Christoph, B. Decker, P. Hristov, I. Lang, M. Nellesen, and M. A. Yazdi. 2023. Supporting software development processes for academia with GitLab. *Proceedings of European University*, 95:229–238.

C. Vassallo, S. Proksch, A. Jancso, H. C. Gall, and M. Di Penta. 2020. Configuration smells in continuous delivery pipelines: a linter and a six-month study on GitLab. *In Proceedings of the 28th ACM Joint Meeting on European Software Engineering Conference and Symposium on the Foundations of Software Engineering*, pages 327–337.

In-Situ Fuel Burnup Determination of Reaktor TRIGA PUSPATI Core

Mohd. Fairus Abdul Farid
Technical Support Division, Malaysian Nuclear Agency
43000 Kajang, Selangor
m_fairus@nm.gov.my

Abstract

Reaktor TRIGA PUSPATI (RTP) has been operated for nearly forty years and the configuration of core has changed more than a dozen times due to the irradiation requirement. The percentage of uranium-235 (U-235) content in the nuclear fuel will experience burnup process every time the reactor operated. In this situation, considering the reactor has been operated many hours since 1982, the evolution of core configurations as well as the different in the U-235 composition, it is crucial to determine the burnup of each type of fuel element instead of taking the average core burnup. The burnup indicates the useful lifetime of the fuel in the reactor core. Fuel burnup also plays important role for reactor operation because of its capability to determine how long RTP can be operated each day at desired power and for how many hours of operation. Currently, determination of RTP core burnup has been based on simulation only using ORIGEN, TRIGLAV and MCNP computer codes. However, determination of burnup by experiment is rarely conducted and it is much more complex when the percentage of U-235 composition varies between fuel elements and also if core configuration always changed. In this case, measurement of fuel burnup for each fuel element is necessary not only due to safety reason such as fuel integrity but also the information obtained from the measurement are crucial for future planning of the reactor itself especially for the continuity of sufficient irradiation requirement. As a part of that, the study also will contribute to obtain information of fission products in the fuel as well as its properties.

Keywords: RTP, fuel burnup, fission products, experiment, simulation

1 Introduction

Malaysian Nuclear Agency (Nuklear Malaysia) is the only national research center having a nuclear reactor for research of non-power and peaceful applications; it is known as Reactor TRIGA PUSPATI (RTP). This reactor has reached its first criticality on June 28, 1982 and since then utilized mainly in neutron activation analysis, isotope production, in- core and out-core experiment as well as training. The reactor was designed to produce thermal power up to 1 megawatt, RTP has been safely operated where the reactor core consists of TRIGA fuel element with 19.99% enrichment. Using treated light water as moderator and coolant, this pool type reactor can easily operate and maintained. Vertical cross- section view of RTP is given in Figure 1.

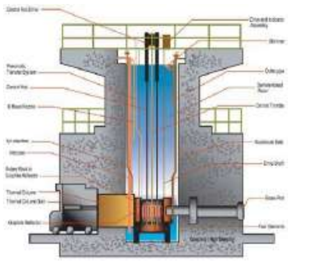

Figure 1: Cross-section of RTP

Figure 2: TRIGA fuel element

RTP has been operated for nearly forty years and the configuration of core has changed more than a dozen times due to the irradiation requirement. The percentage of uranium-235 (U-235) content in the nuclear fuel will experiencing burnup process every time the reactor operated. Furthermore, RTP core consists of three different types of fuel elements (moderating properties for thermal neutrons) with 8 wt%, 12.5 wt% and 20 wt% of U-235 compositions. Figure 2 shows the photo of fuel element using in RTP, namely TRIGA fuel element. TRIGA fuel is made from a unique blend of uranium mixed with zirconium hydride as well as a burnable poison, the resulting configuration created a fuel element whereby the primary basis for safety originates in the fuel itself (Reese, 2021).

In this situation, considering the reactor has been operated many hours since 1982, the evolution of core configurations as well as the different in the U-235 composition, it is crucial to determine the burnup of each type of fuel element instead of taking the average core burnup. The burnup indicates the useful lifetime of the fuel in the reactor core (R.Khan et al., 2010). Fuel burnup also plays important role for reactor operation because of its capability to determine how long RTP can be operate at desired power and for how many hours of operation. Currently, determination of RTP core simulation has been based on simulation (Rabir et al., 2017) only using ORIGEN, TRIGLAV and MCNP computer codes. From the literature review, it was found that there is no study had been carried out to determine burnup of TRIGA fuel by experimental method. Table 1 below shows a few related research papers to this proposal.

Table 1: Related research papers

Previous researches	Main highlights
M.Q. Huda, S.I. Bhuiyan, T. Obara (2008)	Fuel reshuffling at 20,000 MWh to provide highest core lifetime of the reactor
Anze Pungercic, Dusan Galic, Luka Snoj (2020)	TRIGLAV code is viable for TRIGA fuel management and burnup analysis
B.El Bakkari, T.El Bardouni, B.Nacir, et. al. (2013)	Fuel burnup analysis using in-house computer code. BUCAL1
T.makmal, O.Aviv, E.Gilad (2016)	Out-pool gamma spectrometry for MTRtype HEU burnup evaluation

2 Objective of Study / Problem Statement

The objectives of this study are:

1) To design and develop experimental tools and methodologies for the determination using gamma energy spectrum of radionuclide for each fuel elements inside the reactor pool.

2) To utilize the analysis method of gamma energy characterization for each radionuclide inside fuel element.

3) To determine the burnup of TRIGA fuels by using experimental approach

4) To compare and analyze the result obtained by simulation using a computer code such as ORIGEN, TRIGLAV etc.

Figure 3 shows the illustration of experimental setup at RTP and Figure 4 shows the compact gamma spectrometry system as a main tool.

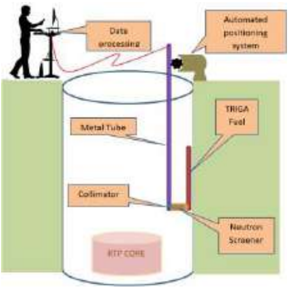

Figure 3: Experiment setup

Figure 4: Gamma Spectrometry System

Determination of TRIGA fuel burnup in RTP mostly done by computer codes and it is practiced worldwide among nuclear reactor community when the configuration of core is usually remained unchanged and the composition of U-235 is same. However, determination of burnup by experiment is rarely conducted and it is much more complex when the percentage of U-235 composition varies between fuel elements and also if configuration always changed. In this case, measurement of fuel burnup for each fuel element is necessary not only due to safety reason such as fuel integrity but also the information obtained from the measurement are crucial for future planning of the reactor itself especially for the continuity of sufficient irradiation requirement. As a part of that, the study also will contribute to obtain information of fission products in the fuel as well as its properties.

3 Scope of Study/ Theoretical Framework

The scope of study;

1) Designing and developing an experimental method at the reactor pool tank for the measurement of gamma energy spectrum of fission products from TRIGA fuel.

2) Measurement of in-situ gamma energy spectrum inside reactor pool without fuel element (background) and measurement of gamma energy spectrum for fuel elements (background and fission product inside fuel element).

3) Analysis method will be developed in determination of fission product radionuclide contributed to the burnup calculation and identification of radioisotope generated from fuel meat.

4) Analysis method will be developed in characterizing of each gamma energy spectrum for each fuel element for calculation of radionuclide concentration in determination of fuel burnup.

5) The measurement of gamma energy spectrum, analysis of spectrum will be conducted for at least 9 fuel elements for different U-235 composition of 8 wt12.5 wt% and 20%wt.

6) Data from experiment will be compared with the simulation using computer code ORIGEN, TRIGLAV or MCNP etc.

4 Impact and Contribution of Proposed Research

This study will contribute to new knowledge in the in-situ nuclear burnup measurement and calculation using nondestructive method approach. The value of fuel elements burnup is important input for decision making about the safety of the reactor and also decommissioning factor of reactor. The data of fuel burnup for each fuel is useful parameter for prediction of future nuclear waste generated from the RTP core fuel element. It can also be further used for next core configuration as well as future decommissioning plan for TRIGA reactor. In addition, this proposed research will also contribute towards human capital development in term of expertise and high skilled worker based on Malaysian Science, Technology, Innovation and Economy (MySTIE 2050) framework.

References

Mohamad Hairie B. Rabir, Muhammad Rawi B. Mohamed Zin, Julia Bt. Abdul Karim, and Bayar et al. 2017. Neutronics calculation of RTP core. *AIP Conference Proceedings*, 1799.

Steve Reese. 2021. TRIGA® reactors: A unique approach in research reactor fuel and design. *Encyclopedia of Nuclear Energy*, pages 182–190.

R.Khan, S.Karimzadeh, and H.Bock. 2010. TRIGA fuel burnup calculations and its confirmation. *Nuclear Engineering and Design*, 240:1043–1049.

Individual Research Contribution Review, 2023, 1(1): 399–400

Simulation of Fusion Neutron Emission for D_2-Ar Gas Mixtures in the MNA Plasma Focus

Mohd Faiz bin Mohd Zin
Technical Support Division, Malaysian Nuclear Agency
43000 Kajang, Selangor
faizzin@nm.gov.my

Abstract

This study focuses on the enhancement of fusion neutron production in MNA-PF by introducing argon into deuterium gas, a technique previously shown to increase neutron yield in plasma focus devices. To validate the potential benefits of deuterium-argon gas mixtures, the Lee Model Code was employed for simulation. While the Lee Model Code only support a single gas system, an enhanced version of the Lee Model Code, capable of handling double gas mixtures, was acquired. The simulation involved extensive fitting procedures and the manual adjustment of current traces to align them with measured data. The results demonstrate that mixing argon with deuterium gas significantly enhances neutron production, particularly at lower gas pressures. An 80% argon and 20% deuterium mixture at 1 mbar exhibited a remarkable 58-fold increase in neutron yield compared to pure deuterium at the same pressure. This study highlights the potential of gas mixing, particularly D_2-Ar mixtures, for improving fusion neutron generation in the MNA Plasma Focus device and suggests future research directions for optimizing gas ratios and pressures.

Keywords: plasma focus, fusion neutron, lee model, computational plasma

1 Introduction

The Malaysian Nuclear Agency Plasma Focus device (MNAPF) is a 3.3 kJ UNU-ICTP Mather-type device, emitting various radiation types like x-rays, electron beams, ion beams, and neutrons based on the gas used. This adaptability is valuable for various material exposure applications. Plasma focus devices like MNA-PF are advantageous for neutron production due to their ease of use, low charging voltage, safety features, and absence of radioactive source (IAEA, 2013). For neutron-based research, MNA-PF is capable to produce 10^3 neutrons in previous experiments (Zin et al., 2017). This value is considered relatively low compared to other similar type of UNU-ICTP devices. On the other hand, studies have shown that adding noble gases like argon to deuterium gas can substantially enhance neutron yield, mainly due to induced radiative collapse and improved plasma compression (Marciniak et al., 2022; Yap et al., 2005). To improve fusion neutron emission in MNA-PF, the Lee Model Code was employed for simulation, aiming to validate the potential benefits of deuterium-argon gas mixtures (Lee, 2014).

2 Methods

The Lee Model Code was employed for the analysis of pure D_2 discharges using total discharge current fitting techniques. In this technique, the current derivative was initially measured using two diagnostic systems, namely the Rogowski coil and the magnetic probe. Subsequently, the necessary fitting parameters were derived from the Lee Code through extensive fitting procedures. However, when working with D_2-Ar gas mixtures, gas mixture configurations were not inherently supported by the MNA-PF setup. Therefore, in this paper, the primary focus was placed on theoretical computations of D_2-Ar discharge scenarios. To simulate gas mixture in plasma focus device, an enhanced version of the Lee Model Code was obtained directly from its developer, Professor Lee Sing. This specialized code has the capability to handle double gas mixtures, a feature not publicly available. To facilitate data acquisition and analysis, the original Visual Basic for Excel (VBA) program was rewritten into Fortran code. This step allowed for code customization and provided a deeper understanding of the simulation process, particularly in relation to fusion neutron production. The output of this simulation shows various plasma parameters and neutron emission characterizations.

3 Results and Discussions

Figure 1 shows the computed fusion neutron emission for D_2-Ar mixture at different gas pressures. For mixture at total pressure below 2 mbar, there was an increase in total neutron emission when the argon fraction is raised relative to deuterium. On the other hand, for total pressure above 2 mbar, there were decreases in the total neutron emission with an increase in the fraction or pressure of noble gases within the mixture. From 6 mbar and above, the effect from argon fraction to the increase of neutron emission gradually reduced. At 13 mbar, the fraction of noble gas does not influence the total of neutron emission relative to the pure D_2.

Figure 2 shows the comparison of neutron emission between pure deuterium and D_2-Ar mixture across the total filling gas pressure with varying argon fraction percentage. The green dashed line indicates a neutron emission increment 50 times higher than that of pure deuterium, while the blue dashed line indicates the point of maximum emission for pure D_2 at 9 mbar. Generally, up to 9 mbar filling gas pressure,

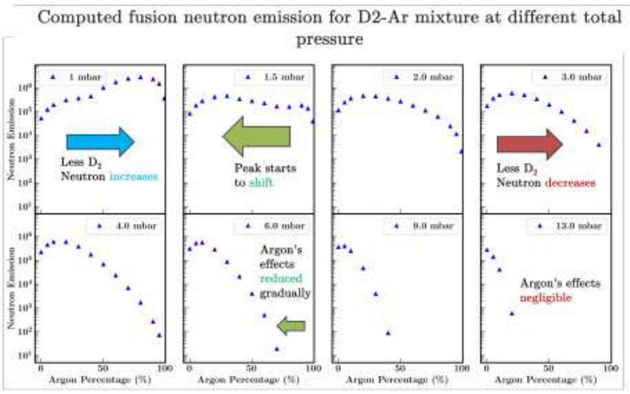

Figure 1: Computed fusion neutron emission for D_2-Ar mixture at varying argon (Ar) fraction across different total pressures.

D_2-Ar mixture exhibit significantly higher neutron emission compared to pure D_2. Furthermore, the maximum emission for pure D_2 occurs at 9 mbar. The most substantial increase in neutron emission due to argon doping is observed at 1 mbar, where an 80% argon and 20% deuterium mixture achieves about 58 times higher neutron emission than pure deuterium at 1 mbar. Interestingly, the highest neutron emission occurs when the deuterium fraction is at its lowest across the entire gas pressure range.

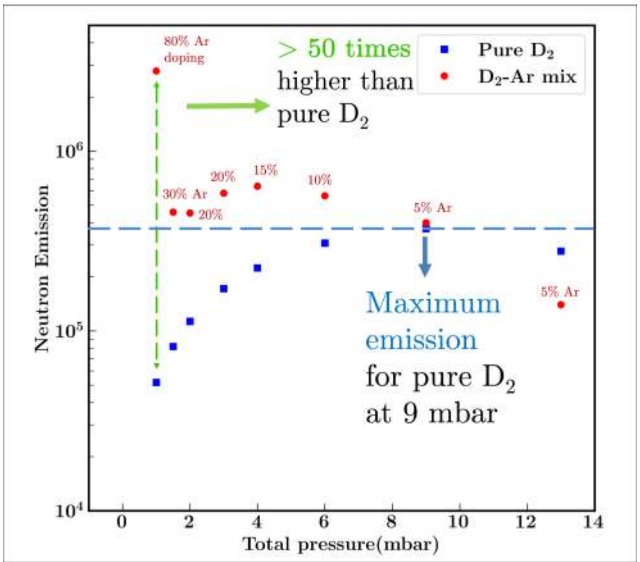

Figure 2: Neutron emission comparison between pure D_2 and D_2-Ar mixture across the total filling gas pressure.

In Table 1, an estimation of neutron emission per shot for MNA-PF is presented. According to the simulation and considering the previous measurement using pure D_2, it is estimated that MNA-PF can achieve 10^5 neutrons per shot for a mixture at 1 mbar with an 80% Ar fraction. This indicates that the mixing gas can increase by two orders of magnitude, from 10^3 to 10^5.

Table 1: Fusion neutron emission per shot for MNA-PF between previous measurement and estimated mixture measurement

Measurement for pure deuterium at 13 mbar	**Estimation for D_2-Ar at 1 mbar**
7.5×10^3 neutron	4.5×10^5 neutron

4 Conclusions

Simulation shows that mixing argon with deuterium gas in the MNA-PF device significantly increases neutron production, especially at lower total gas pressures. This gas mixing approach offers a cost-effective means to enhance fusion neutron emission. An 80% argon and 2% deuterium mixture at 1 mbar resulted in a remarkable 58-fold increase in neutron yield compared to pure deuterium at the same pressure. This method could enable the MNA-PF to produce approximately 4.5×10^5 neutrons per shot at 1 mbar. In summary, gas mixing, specifically D_2-Ar mixtures, holds great potential for improving fusion neutron generation in the MNA-PF device. Future research should focus on optimizing gas ratios and pressures for even better results.

References

IAEA. 2013. Integrated approach to dense magnetized plasmas applications in nuclear fusion technology. No. 1708 in TECDOC Series. INTERNATIONAL ATOMIC ENERGY AGENCY, Vienna.

Sing Lee. 2014. Plasma focus radiative model: Review of the Lee model code. *Journal of Fusion Energy*, 33(08).

L. Marciniak, M. Akel, A. Kuli´nska, S. Lee, M. Scholz, and S.H. Saw. 2022. Results of plasma radiative compression investigation in the PF-24 device operated with D2, Ar and (100%-x)D2+x%Ar mixtures obtained using the 5-phase Lee model code. *Applied Radiation and Isotopes*, 182(110118).

S. L. Yap, C. S.Wong, P. Choi, C. Dumitrescu, and S. P. Moo. 2005. Observation of two phases of neutron emission in a low energy plasma focus. *Japanese Journal of Applied Physics*, 44(11R:8125).

M. F. M. Zin, A. H. Baijan, V. Damideh, S. A. Hashim, and R. M. Sabri. 2017. Preliminary results of malaysian nuclear agency plasma focus (MNA-PF) as a slow focus mode device for argon and deuterium filling gas in correlation with Lee model code. *AIP Conference Proceedings*, 1824(1):020005,03.

Individual Research Contribution Review, 2023, 1(1): 401–402

Improving Research Reactor Interlocks and Trip Control System

Mohd Khairulezwan Abdul Manan
Technical Support Division, Malaysian Nuclear Agency
43000 Kajang, Selangor
khairule@nm.gov.my

Abstract

In Malaysia, Reactor TRIGA PUSPATI (RTP) is a nuclear research reactor that has been operating since 1982 with the thermal energy of 1MWth as a multi-purpose research reactor especially in neutron applications research. Since then, the RTP control system has had to undergo several parts replacement and upgrades to meet the requirements of the Regulatory Board known as Department of Atomic Energy (JTA) as the state regulator on safety operation of the nuclear reactor. Interlocks and trips control hardwarebased (analogue components) are common to the nuclear reactor instrumentation system and it is part of the safety-related component. Due to the ageing and shortage of hardware and spare parts availability in the market made all TRIGA reactor type users need to find the solution and that it with new design of interlocks and trips control system based on software control in order for the reactor can still be operated. First, the interlock and trip controls need to be identified from the existing system and then grouped into its functionality as the end of its operation all the control rods drop back into the reactor core. Second, developing trip and interlock logic using Laboratory Virtual Instrument Engineering Workbench (LabVIEW), a programming environment that can create programs using a graphical notation. Finally, all the interlock and trip function been tested by simulation in LabVIEW simulation software.

1 Introduction

The RTP reactor at Agensi Nuklear Malaysia is a research reactor has been used over 35 years. The reactor was made by General Atomic in the 1950s. General Atomic has stopped its nuclear reactor involvement as a vendor of their TRIGA reactor. However, there are a few countries still operates TRIGA reactors and that includes Malaysia. The RTP reactor cylindrical core uses less than 20% enriched uranium embedded in stainless steel cladding and surrounded by demineralized water as coolant and moderator. This enriched uranium collides with the thermal neutron and then causes a chain reaction. This chain reaction will increase the neutron population in the core and to control that is by using the control rods. The four control rods contain neutron absorption materials to control neutron populations during fission. The control rod moves vertically up and down from its core using a stepper motor connected to the driveshaft and connected to the interlock and trip system in the control console located in the control room. The interlocks function is to prohibit two or more control rods to withdraw at the same time as well as to prevent control rod withdrawal during square-wave mode operation. While trips function is to secure four control rod back into the core when abnormality happened and also when it is automatically or manually shutdown the operation.

2 Trip and Interlock Design

2.1 Trip Circuit Design

There are two channel of trip control system and each trip channel has four circuits. That four circuits are bistable circuit, coincidence circuit, initiation circuit and actuation circuit as shown in Figure 1.

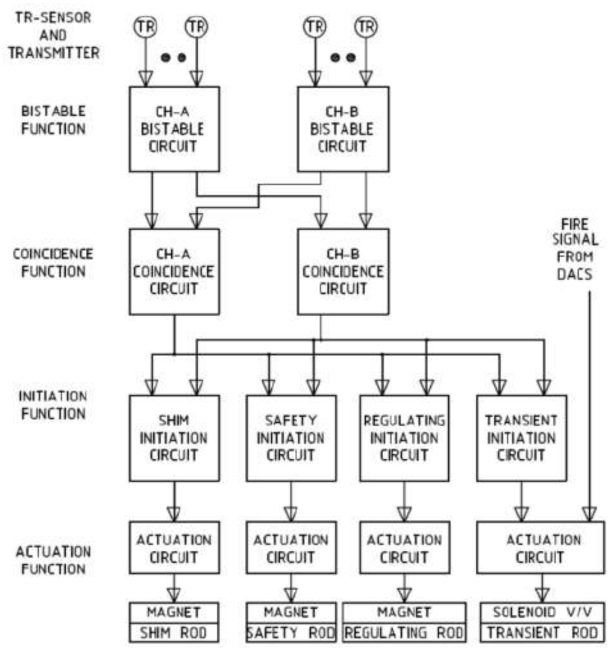

Figure 1: Trip block diagram

The bistable circuit generates bistable signals for the reactor trip. It based on the measurement channel value exceeding a setpoint. The bistable circuit provides bistable trip signals to coincidence circuit located in each channel to de-energize its associated coincidence trip relays when any trip parameter reaches its setpoint that can be set according to the safety operating conditions as stated in the Safety Analysis Report (SAR).

The coincidence circuit is redundant circuits and each component is installed in each channel for complying with single failure criterion. Each coincidence circuit evaluates the 1-out-of-2 logic based on the state of two bistable trip signals. The coincidence signals are used in the generation of the initiation signals for trip.

The initiation circuit is designed independently for each actuation circuit for complying with the single failure criterion. Each initiation circuit is a combination of relays to perform latch, trip reset, and manual individual rod trip functions. This circuit controls power interruption to the actuation relays.

The actuation circuit for the reactor trip is installed inside of the power path of rod dropping mechanism. The actuation relays disconnect their associated power source for dropping rods into the reactor when each initiation circuit sends initiation signal to related actuation circuit.

2.2 Interlock Design

The interlock circuit is designed to interrupt the power being applied to the rod drive magnets should any of the safety interlock criteria not be met. In this interlock design there is three events that will initiate this interlock function; Prevents control rod withdrawal at less than 2 counts per second (cps) which refer to neutron population to low, prevents TRANSIENT rod fire above 1 kWth (rod that operated by pneumatic system) and prevents simultaneous withdrawal of two rods. The interlocks circuit get the input signal from the instrument called Wide Range Neutron Measurement System (WRNMS) that connected to the detectors and sensors in the reactor core.

3 Results and Discussion

3.1 LabVIEW Simulation

The system is then designed using software that can be interfaced with hardware such as sensors. But in this study, it was only simulated for the purpose of the initial study before it can be validated with connection to the hardware. In this simulation, there are two graphical panels: front panel and block diagram panel as shown in Figure 2 and Figure 3.

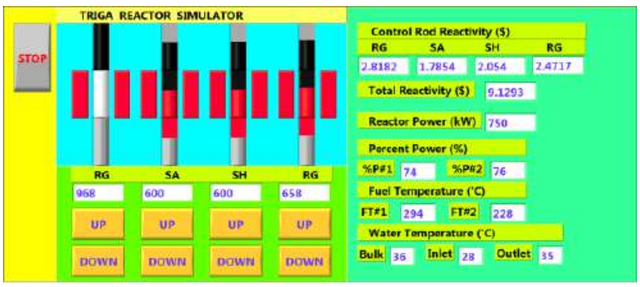

Figure 2: Front panel

From this simulation, it is functioning as expected (eg. one of the trip safety parameters in Figure 4 where trip occurred when fuel temperature exceeded 600°C). In this simulation only simplified dynamic reactor model is considered. This is because the actual operation is more complex due to the non-linear dynamic reactor behaviour depending on the neutronic and thermal-hydraulic models.

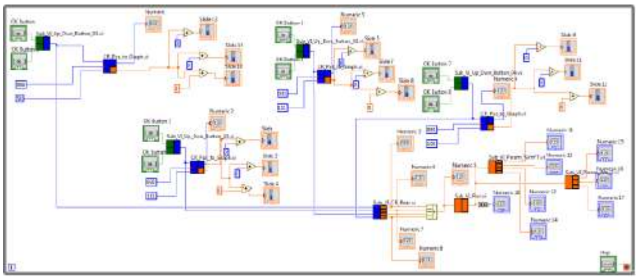

Figure 3: Block diagram panel

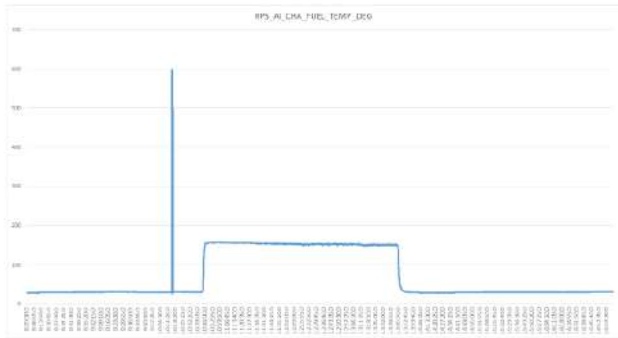

Figure 4: Fuel temperature trip at 600°C

4 Conclusion and Future Work

This study has concluded that the use of interlocks and trips system previously hardware-based can be upgraded using LabVIEW software-based control with the same functionality. The current interlocks and trips system are separately designed. In the future, the new architecture will be integrated design based on a combination of interlocks and trips system.

References

Mallicoat A. and Pope C. L. 2020. Design improvements to the ISU AGN-201 reactor SCRAM, interlock, and magnet circuits. *Annals of Nuclear Energy*, 136.

J. G. Choi and D. Y. Lee. 2012. Development of RPS trip logic based on PLD technology. *Nuclear Engineering and Technology*, 44(6):697–708.

M. Cocchiara, V. Bartolozzi, A. Picciotto, and M. Galluzzo. 2001. Integration of interlock system analysis with automated HAZOP analysis. *Reliability Engineering and System Safety*, 74(1):99–105.

Agensi Nuklear Malaysia. 2017. *Safety Analysis Report, Agensi Nuklear Malaysia*.

Individual Research Contribution Review, 2023, 1(1): 403–404

The Effect of Polyethyelene Glycol Diacrylate on Physical Properties of UV Irradiation Vulcanization NR Latex

Mohd Noorwadi Mat Lazim
Technical Support Division, Malaysian Nuclear Agency
43000 Kajang, Selangor
noorwadi@nm.gov.my

Abstract

The natural rubber (NR) latex was vulcanized by exposing it to ultra-violet irradiation for 1.5 hours with the presence of acrylate monomers 1, 6 hexanediol diacrylate (HDDA), low molecule weight oligomer Polyethylene Glycol Diacrylate (PEGDA) and 2–hydroxy-2-methyl-1-phenylpropanoid (Duracure 1173) was used as a photoinitiator. The effect of PEGDA at 0, 3, 5 and 8 phr on tensile properties of ultraviolet irradiation vulcanization natural rubber latex (UVNRL) was investigated. The tensile strength, modulus (M500% & M700%) and crosslink density were determined to study the physical properties while the Fourier transform infrared (FTIR) spectroscopy was used to determine the chemical interaction between PEGDA and NR. It was found that NR latex formulated with 8 phr had the highest tensile properties.

Keywords: UVNRL, PEGDA, HDDA, NR latex

1 Introduction

Natural rubber (NR) latex derived from the Hevea brasiliensis tree is a widely used natural polymer with applications in various industries. However, un-vulcanized NR exhibits low strength, poor elasticity, and limited resistance to chemicals. To enhance its properties, a vulcanization process is employed, creating vulcanized NR latex with improved tensile strength, elasticity, and chemical resistance. Three main vulcanization methods—sulfur, peroxide, and radiation are utilized, while sulfur vulcanization remains the most commonly favored method, concerns about carcinogenic by-products have led to the exploration of alternative technique. Latex allergy can be categorized into type I and type IV, poses additional challenges, encouraging researcher in the development of sulfur-free vulcanization processes like peroxide and radiation vulcanization.

The focus on sulfur-free methods aims to address toxicity concerns, environmental impact, and safety issues. However, these alternatives often come with drawbacks, such as poor aging stability, long vulcanization time, and higher production costs. A promising advancement is the introduction of ultraviolet irradiation vulcanization of NR latex (UVNRL). This technique eliminates the need for sulfur-based chemicals, offering good biocompatibility, operational safety, and lower energy consumption. The UVNRL process involves the initiation of a photo-initiator by UV light, leading to thiol-ene addition reactions and crosslinking in NR latex.

Factors influencing efficient UV irradiation include the type of UV lamp, photo-initiator, monomer type, and irradiation duration. Studies have explored different combinations, revealing optimal tensile properties and crosslink density. In this study, acrylate monomers, namely HDDA, and PEGDA along with a Duracure 1173 photo-initiator, were employed in UVNRL formulation using a medium pressure mercury UV lamp. The effects of this mixture at various phr of PEGDA on the tensile properties of UVNRL were analyzed.

2 Methods

A latex compounding formulation for UVNRL preparation using acrylate monomer; HDDA, n-BA and TMPTMA is shown in Table 1. The acrylate monomer, photo-initiator, potassium laurate and water were homogenized using an emulsifier machine before adding into the NR latex with gentle stirring.

Table 1: NR latex Formulation at different phr of PEGDA

Material	PHR
NR latex	100
HDDA	3
Photo-initiator (Duracure 1173)	2
PEGDA	0, 3, 5 , 8
KOH	0.25
Water	Reduce tsc 55%

Once the addition of emulsified chemicals was completed, the KOH solution was added into the latex mixture to stabilize the pH of the mixture in the range of 9 to 11. The latex mixture was kept stirred for 1 hour. It was then transferred into the reaction flask with an immersion well and exposed to UV irradiation for 1.5 hours. Each latex mixture was irradiated with UV light at 250-350 nm wavelength sourced from a medium pressure mercury lamp 3040 models with current supply 400W as shown in Figure 1. The latex mixture was kept stirred and cold water was continuously circulated in an immersion well at a set temperature of 20°C to reduce evaporation during UV irradiation. After UV irradiation was completed, the NR latex compound was known as UVNRL. The experiment was repeated for compounding formulation with the other acrylate monomer. The control sample was prepared by diluting NR latex with distilled water to reduce TSC from 60% to 45% and not exposed to UV irradiation.

The latex formulated without and with HDDA, n-BA and TMPTMA were labellled as NR, NR/HDDA, NR/n-BA and NR/TMPTMA respectively.

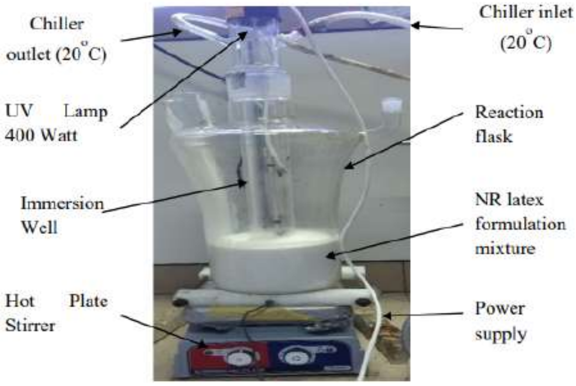

Figure 1: Lab scale set-up of UV irradiation vulcanization NR latex (UVNRL) using reaction flask with immersion well and UV lamp.

3 Result

Based on Table 2, the tensile strength of all samples formulated with PEGDA progressively increased as the amount of PEGDA increased. The NR (8phr of PEGDA) sample was the highest tensile strength followed by NR (5phr PEGDA) and NR (3phr PEGDA) with the lowest tensile properties. This indicated that UV irradiation to NR latex induced chemical reaction with the presence of PEGDA. The tensile strength value indicated that there was chain entanglement in NR which may be due to physical crosslink and chemical crosslink of HDDA and PEGDA. Both of these crosslinks contributed to better tensile properties. For NR, without the presence of HDDA and UV irradiation, the tensile strength clearly show there is no chemical crosslink occur and the value of tensile due to physical entanglements of polyisoprene chain in NR. For NR formulated with HDDA and PEGDA, the increases of tensile strength were contributed from chemical and physical crosslink. The chemical crosslink formed from grapfting of monomer at NR, HDDA and PEGDA chain, chain combination from free radical and direct crosslink during the termination stage. The physical crosslink occurred due to chain entanglement between NR and homopolymerization of HDDA and PEGDA in NR latex medium.

Table 2: The tensile strength of samples at different phr of PEGDA

Sample	PEGDA	Tensile Strength (MPa)
NR (unvulcanized)	0	4.95
NR	0	11.44
NR	3	13.79
NR	5	14.76
NR	8	15.63

4 Conclusions

NR latex can be effectively vulcanized by using the UV irradiation method as demonstrated in this work. The highest tensile strength can be achieved by NR latex formulated with 3 phr of HDDA, 2 phr of 2–ydroxy-2-methyl-1-phenylpropanone photo-initiator and 8 phr of polyethylene glycol diacrylate at 15.63 MPa. However, this is not the optimum strength and further extension on the amount of PEGDA should be carried out to find out the optimum tensile strength. It can be concluded that the enhancement of tensile strength is contributed by chemical and physical crosslinks. The strength of UVNRL may be due to homopolymerization of HDDA, grafted HDDA and PEGDA polymer to NR chain.

References

Ogl C. H. L. Prevulcanization of natural rubber latex by UV techniques: A process towards reducing type IV chemical. pages 133–148.

Hansupalak N., Srisuk S., Wiroonpochit P., and Chisti Y. 2016. Sulfur-free prevulcanization of natural rubber latex by ultraviolet irradiation. *Ind. Eng. Chem. Res.*, 55(14):3974–3981, https://doi.org/10.1021/acs.iecr.6b00076.

Wiroonpochit P., Uttra K., Jantawatchai K., and Hansupalak N. 2017. Sulfur-free prevulcanization of natural rubber latex by ultraviolet irradiation in the presence of diacrylates. https://doi.org/10.1021/acs.iecr.7b01133.

Schlögl S., Trutschel M. L., Chassé W., Letofsky-Papst I., Schaller R., Holzner A., Riess G., Kern W., and Saalwächter K. 2014. Photo-vulcanization using thiol-ene chemistry: Film formation, morphology and network characteristics of uv crosslinked rubber latices. *Polymer (Guildf)*, 55(22):5584–5595, https://doi.org/10.1016/j.polymer.2014.06.007.

Sandra Schlogl, Armin Temel, Raimund Schaller, and Armin Holzner W. K. 2012. Characteris of the photochemical prevulcanization in a faliing film photoreactor. *J. Appl. Polym. Sci.*, 124:3478–3486, https://doi.org/10.1002/app.

Multipurpose High Density Cell

Mohd Rizal Mamat @ Ibrahim
Technical Support Division, Malaysian Nuclear Agency
43000 Kajang, Selangor
m_rizal@nm.gov.my

Abstract

Prototype and Plant Development Center (PDC), Malaysian Nuclear Agency has developed a hot cell facility which is meant for research activities such as spent fuel inspection, fuel fabrication and post irradiation material examination/inspection. The hot cell is of alpha-gamma shielding hot cell type. The size of the hot cell is 4.4 x 3.9 x 3.825 meter. The 1-meter thickness hot cell wall consists of 89 pieces of interlocking curve design concrete blocks. The 1-meter hot cell roof consists of 41 pieces of square shape concrete blocks. The density of all concrete blocks is 2350kg/m^3. The hot cell is designed to handle up to 227.5 Ci ^{60}Co activity. The design of the shielding wall of the hot cell is briefly described.

Keywords: hot cell, spent fuel inspection, fuel fabrication, post irradiation material examination

1 Introduction

The semi-permanent concept is selected due to the ease/ possibility of assembling and dismantling work within the Nuclear Malaysia site. The basic design used is the Chevron brick-built wall and curved brick-built wall, the typical interlocking system in designing a semi-permanent hot cell.

The main original purpose for developing the hot cell is to provide the fuel fabrication preparation especially for thorium fuel research. In addition, the hot cell can also be used for spent fuel inspection (from TRIGA RTP) and post irradiation material examination/inspection.

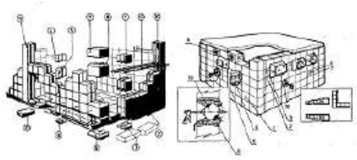

Figure 1: Chevron brick-built wall (left) and Curved brick-built wall construction concept.

2 Design Considerations

2.1 Radioactive Handling Capacity

The value of activity of 300 R/hr (equivalent to 227.5 Ci of Cobalt-60 (^{60}Co) and fission products of 50% burnup RTP 20wt% fuel type have been selected as the hot cell shielding design criteria based on relevant literature and studies of TRIGA RTP spent fuel.

2.2 Hot Cell Design Specifications

The design of a hot cell depends on the type of hot cell, the types of radioactive material to be handled, the expected level of activity to be handled, types of operations to be performed, the viewing system, shielding material selection, size of hot cell and etc.

Table 1: Multipurpose High Density Cell Design Specifications

Specification	Details
Type of Hot cell	Alpha-gamma shielding hot cell type (semi-permanent)
Overall size	4.4 meter x 3.9 meter x 3.825 meter (height)
Containment size	2.4 meter x 1.9 meter x 2.825 meter (height)
Shielding material	Wall: Concrete with density: 2.35g/cm^3 (Cement Grade 40) Door: Lead+Boronated HDPE (Lead density: 11.35g/cm^3, boronated HDPE: 1.08g/cm^3) Window: Zinc Bromide, $ZnBr_2$ 77% w/w Nuclear Optical Grade (density 2.55 g/ml @ 20^{o}C)
Shielding thickness	Wall and roof: 1 meter concrete - Wall: 89 pieces of interlocking curve design concrete - Roof: 41 pieces of square shape concrete Door: 200mm lead, 50mm boronated HDPE Window: 1 meter ($ZnBr_2$ Clear colourless solution, and 25mm polycarbonate plate each side)
Maximum weight one-piece concrete	1.25 tonne
Lead Door weight	3.186 tonne
Window	- Zinc Bromide, $ZnBr_2$ 77% w/w Nuclear Optical Grade - Density 2.55 g/ml @ 20^{o}C) - Clear colourless solution - Volume: 320Liter
Manipulator model	Walischmiller HWM model A201(2 units)
Radioactive handling capacity	227.5 Ci activity (Cobalt 60 equivalent), refer report MCNP
Research activity	- Spent fuel inspection - Fuel fabrication - Post irradiation material examination/inspection.
Target operating hour	2000 hour per year (Not higher than dose limit 20mSv/year for operator).

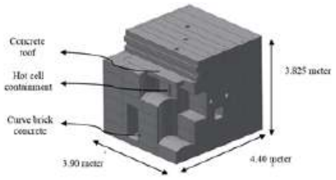

Figure 2: The conceptual hot cell design with interlocking concrete wall.

3 Monte Carlo N-Particle Transport Code (MCNP) Simulation

Monte Carlo radiation shielding simulations using MCNPX 2.7.0 Monte Carlo code with two different source terms (227.5 Ci Co-60 and 50% burnup RTP 20wt% spent fuel) have been conducted to assess the shielding characteristics of the designed hot cell.

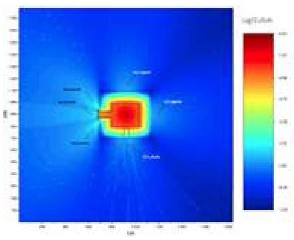

Figure 3: XY axis view, dose-rate map results for 227.5Ci ^{60}Co gamma sourcel.

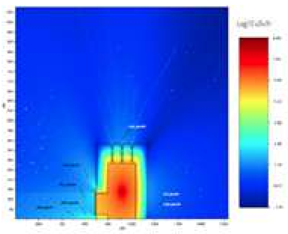

Figure 4: XZ axis view, dose-rate map results for 227.5Ci ^{60}Co gamma sourcel.

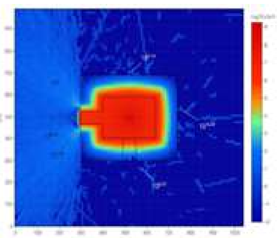

Figure 5: XY axis view, dose-rate map results for fission product's gamma used as source-term from RTP fuel.

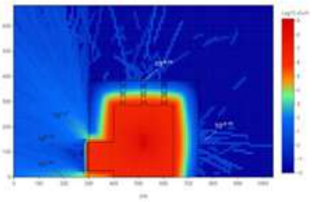

Figure 6: XZ axis view, dose-rate map results for fission product's gamma used as source-term from RTP fuel.

The results of the radiation simulations are shown in Figure 3 to Figure 6. The 1-meter concrete shield shows that it is capable of reducing the dose-rate from the inside the wall to the outside surface. The dose-rate at the outer surface of the concrete wall is reduced approximately more than 10 million times when compared to the inner wall surface, the reduced values are 12.1μSv/hr for gamma source and 0.65μSv/hr for RTP fuel fission product source.

Similar reduction of dose rate is observed at the $ZnBr_2$ windows, both for gamma and RTP fuel fission products. The highest dose rate value in front of $ZnBr_2$ window for gamma and RTP fuel fission product are 10.1μSv/hr and 2.04μSv/hr, respectively. However, the result shows that a relatively high radiation leaked through the door. The highest dose rate, located at lead door are 1570μSv/hr and 489μSv/hr for 227.5 Ci ^{60}Co source and RTP fuel fission product, respectively.

Scattered radiation are observed at the left and right side and also at the upper and bottom side of the door. The low energy gamma, dominant from fission products seems to be stopped by the door. However, the scattered gammas, even the low energy gammas could also escape through the left, right, top or bottom side. Therefore, additional shielding or modification is needed in the future especially at the gap between interlock concrete and the lead door in order to further reduce the dose rate.

4 Conclusion

Through the evaluation, the design of interlocking concrete wall with 1-meter thickness are able to act as a shielding for 227.5Ci ^{60}Co and fission products of 50% burnup RTP 20wt% fuel. However, a set of measurement data is still needed to verify the percentage of discrepancy for the simulation in future. This study proves that the hot cell with interlocking alpha-gamma shielding design, installed in controlled area or RTP Hall is fit to handle research activities.

References

IAEA. 1981 Edition. Book: Manual on safety aspects of the design and equipment of hot laboratories. *Procedures and Data, Safety Series No.30*, International Atomic Energy Agency (IAEA).

Sipaun Susan. 2017. Thorium fueled reactor. *AIP Conference Proceedings 1799*, 050012. https://doi.org/10.1063/1.4972946.

Individual Research Contribution Review, 2023, 1(1): 407–408

Radiation Measurement Instrument for Educational Tools

Mohd Shafiq Bin Sazali
Technical Support Division, Malaysian Nuclear Agency
43000 Kajang, Selangor
mohdshafiq@nm.gov.my

Abstract

This work was aimed to develop a device which is affordable and functional according to Malaysian secondary school syllabus. The Malaysian Ministry of Education (MOE) requires radiation measuring tools to assist school teachers. Thus, this article describes the design, fabrication, and testing of the radiation survey meter which is based on a Geiger-Muller (GM) detector.

Keywords: Radiation survey Meter, Geiger-Muller detectors

1 Introduction

The incident at Chernobyl in 1986 and Fukushima in 2011, it has brought an awareness to society that nuclear radiation protection is one of the important aspects especially to countries which have nuclear power plants (Yamaguchi, 2023). When referring to radiation, we knowthat alpha, beta and gamma are three most common types (Harvard., 2012). To detect these radiations, there are several radiation detectors used, but one of the most common detectors are called survey meter.

In order to design a budget-friendly or can be called as low-cost survey meter for educational purpose, the Information Management Division (BPM) has approached the Instrumentation and Automation Centre (PIA) to design a survey meter specifically for learning and teaching in schools. The survey meter specifications need to follow all the education and teaching standards and most important aspects is the price needs to be budget friendly.

Thus, the Instrumentation and Automation Centre (PIA), took the initiative to produce a radiation survey meter at a reasonable cost. Therefore, in this project, 20 survey meters with GM tubes will be develop which will involve on designing and fabricating the survey meters specifically on the printed circuit board (PCB), circuit testing and display development.

2 Methods

There are few aspects that need to be taken to design a low-cost survey meter. One of the important components that determine the general purpose of a survey meter is the Geiger-Muller (GM) detector. GM detectors are the most common and widely used due to its simplicity and reliability in detecting wide range radiation (Singseeta and Pencharee, 2017). Thus, to choose an affordable and effective detector, RD003 (SBM-20) model GM tubes are chosen.

The detector was developed by Vinca Institute of Nuclear Sciences (VINS) mainly to detect beta and gamma radiation. The tube window has a wall type with area density: mg/cm^2, effective length: 96 ± 2 mm, effective diameter: 10 mm, high voltage (HV): 360V. Also, the survey meter is powered with 6 x AA batteries.

3 Results and Discussion

The Malaysian Nuclear Agency has a Secondary Standards Dosimetry Laboratory (SSDL), which is a national facility assigned to calibrate radiation measurement devices like dosimeters that are used in radiotherapy centers and for radiation protection. All measurements and calibrations are referenced back to primary standard laboratories and other international standards.

Furthermore, SSDL plays a crucial role as an Individual Dose Monitoring center for radiation workers in Malaysia. This involves providing and analyzing OSL Badges, TLD Badges, and TLD rings. Additionally, SSDL supplies high dose dosimeters like Ceric Cerrous and Fricke for use in the radiation processing industry in Malaysia.

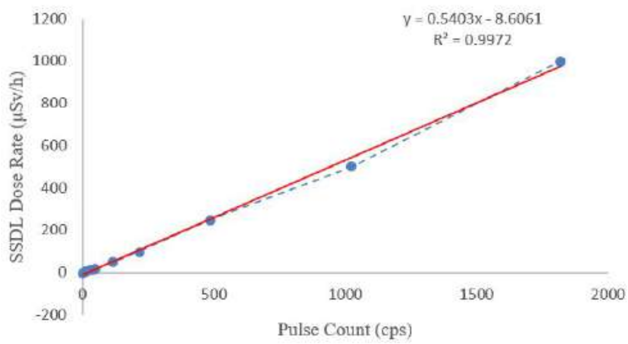

Figure 1: Conversion Factor on 1000 Sv/h.

In order to test the radiation response and identify the performance of LCSM, the calibration will be tested with 662KeV gamma-ray radiation using certified procedures at the SSDL until the performance meets the standards given along with LCSM improvements. Testing can be divided into 2 which are the conversion pulse count to Sv/hr and verification (Rajan and J.Izewska, 2019).

In order to convert the dosage rate in microsievert per hour (Sv/hr) from pulse count value, we need to identify the conversion factor (CF). The pulse count per one second (1s) for each activity is recorded for ten readings and averaged. Finally, the CF for each activity is calculated and based on the calculation, the result of CF value is 0.54 as shown on Figure 1.

Next, the accuracy of the survey meter is observed by performing measurement at few activity levels. Accuracy or acceptable values are defined by ratio values within the zero-error percentage and ± 20% tolerance. Thus, based on Figure 2, it is shown that the ratio value varies from 0.896 to 1.431; which are within the acceptable range.

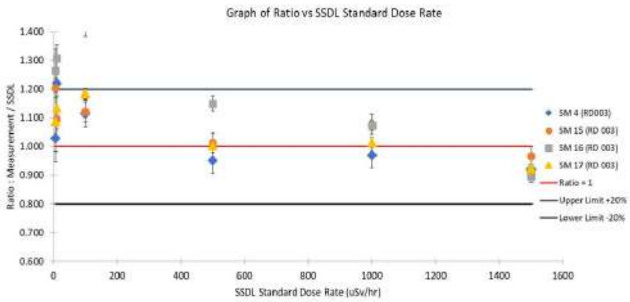

Figure 2: Ratio vs SSDL Standard Dose Rate.

4 Conclusions

The invention of the low-cost survey meter provides good tools to be used by teachers for school education and learning. Even though the survey meter is budget-friendly, the main purpose of it shall not be neglected. The survey meter is designed to be a battery-operated and portable device that has a detector to measure radiation in microsieverts per hour (Sv/hr) (Harvard., 2012) . By testing the survey meter on radiation response and verification, it can be concluded that the survey meter is able to work efficiently and provide accurate radiation measurement even with a low-cost price design.

References

Harvard. 2012. Radiation survey meter – how it works. *Harvard Campus Services, Environmental Health Safety*.

G Rajan and J.Izewska. 2019. Radiation monitoring instruments. *International Atomic Energy Agency*, 4.

Decho Thong-Aram Warut Singseeta and Somkid Pencharee. 2017. Design and construction of portable survey meter. *Department of Physics, Faculty of Science*.

Mari Yamaguchi. 2023. Events at fukushima daiichi nuclear plant since the 2011 earthquake, tsunami and nuclear disaster. *AP News*.

Individual Research Contribution Review, 2023, 1(1): 409–410

The Development of the Gamma Irradiator Control System

Mohd Zaid Hassan @Abd Rahman
Technical Support Division, Malaysian Nuclear Agency
43000 Kajang, Selangor
mohdzaid@nm.gov.my

Abstract

This study discusses the preliminary software development for the Gamma irradiator control system utilising supervisory control and data acquisition (SCADA) software. The radiation dose analysis studies the relationship between the initial loading source activity (Curie) and concurrent activity to perform the irradiation process. The current source activity calculation model is presented. The human-machine interface (HMI) was used to solve the mathematical calculation, task, and process overview.

Keywords: SCADA, Irradiator, Gamma, ALARA

1 Introduction

This paper demonstrates the reliability of a computer-based, real-time processing control system with an improved security structure and multiuser database. Recently, some irradiator operations have become significant. The proposed control system has been designed and is ready to integrate with the PDC Gamma Irradiator, which is still under development. The system controls the entire irradiation process, from the loading of products to the production of post-treatment reports. In addition to wholly automated control, remote monitoring of the facility operation, including radioactive area monitoring, is provided via the secure local LAN network.

2 Gamma Irradiator Facility

Gamma radiators were divided into two types: self-contained and panoramic irradiators. Self-contained irradiators are specially designed for research and applications requiring small doses and relatively small throughputs. Most of these are dry-storage irradiators, and the source activity is limited. For full commercial-scale irradiations, panoramic irradiators are used.

Refer to Figure 1 and Figure 2, the irradiator facility design has four sets of irradiation chambers that operate individually. The systems consist of one Programmable logic controller (PLC) with an Ethernet connection to an industrial panel personal computer (IPPC) and radiation area monitoring system (RARM).

3 Radiation Source Activity

The following formula was used to calculate the activity of a radioactive material at any point in time.

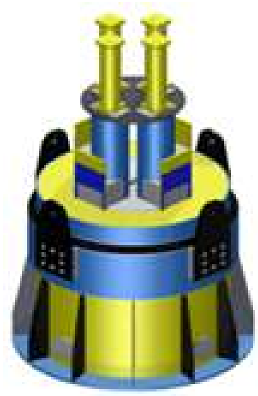

Figure 1: The PDC gamma irradiator facility design

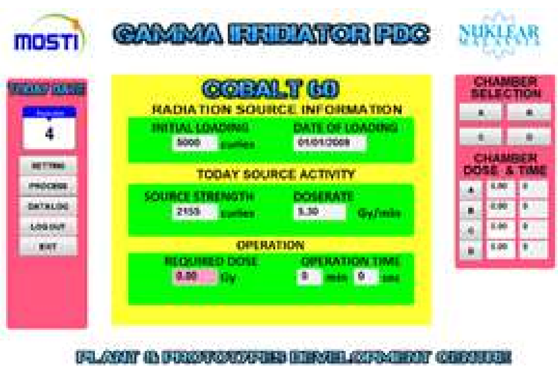

Figure 2: A Gamma Irradiator main menu and user login page

$$A = Aoe^{-\lambda t}$$

A = Activity remaining in the radioactive material over time (t) from when the initial activity was measured (at the time of purchase)
Ao= Initial Activity of the radioactive material (time of purchase)
e = Base of the natural logarithm
λ= Decay constant (ln2/$T^{1/2}$)
t = time (in days) since the initial activity was measured

4 Control System Features

The human-machine interface (HMI) has been developed and has excellent features. This GUI has security features; system status comprises overall system health and readiness.

Several techniques and methods deployed in the PDC gamma Irradiator protection systems regarding database management and safety interlocking systems are highlighted.

Several data can be calculated, such as preset exposure time, elapsed exposure time, and real-time clock time. This data plays an essential role in determining the success of an irradiation operation, as shown in Figure 3 and Figure 4.

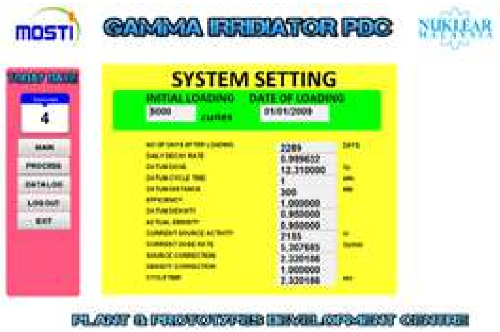

Figure 3: A Gamma irradiator system status

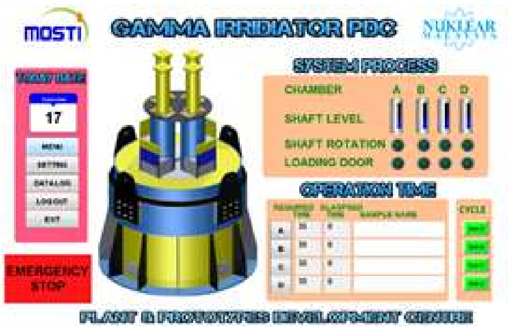

Figure 4: A Gamma irradiator operation time and process

5 Conclusion

In this paper, a GUI was developed to solve the security, safety, radiation dose calculation, irradiation task and process overview. Still, some efforts must be made to improve and maintain it with great care as it is vital in any aspect: security, safety, supervision, testing, and management.

References

Stuart A. Boyer. 2009. Scada: Supervisory control and data acquisition. *4th International Society of Automation, USA ©2009*, ISBN:1936007096 9781936007097.

Alejandro Castaneda. 2008. The use of software in safety-critical interlock systems of the lhc. *06 Instrumentation, Controls, Feedback Operational Aspects Proceedings of EPAC08, Genoa, Italy*.

PENG Dao-gang. 2008. Design and realization of modbus protocol based on embedded linux system. *The 2008 International Conference on Embedded Software and Systems Symposia (ICESS2008)*, 978-0-7695-3288-2/08.

Vujo DRN DARE VIC. 2008. Control of gamma irradiation facility with improved safety system. *Journal of NUCLEAR SCIENCE and TECHNOLOGY*, 45(4):361–367.

International Atomic Energy Agency (IAEA). 1996. Manual on panoramic gamma irradiators (categories II and IV). *IAEAPRSM-8, Vienna*.

American National Standards Institute. 2001. Safe design and use of panoramic, wet source storage irradiators (category IV). *ANSI-N43.10-1984, New York*.

Otani T. 1995. A SCADA system using mobile agents for a next-generation distribution system. *PowerTech, 2009 IEEE Bucharest*, 978-1-4244-2234-0.

Individual Research Contribution Review, 2023, 1(1): 411–412

Reusable Irradiation Capsule

Muhammad Hannan Bahrin
Technical Support Division, Malaysian Nuclear Agency
43000 Kajang, Selangor
hannan@nm.gov.my

Abstract

This paper discussed the preliminary proposal on aluminium capsule design for sample irradiation in the Reaktor TRIGA PUSPATI (RTP). The current irradiation capsule used by Bahagian Teknologi Perubatan (BTP) is a single-use type. There is also a limited number of usable capsules for the reactor group. Therefore, this aluminium capsule is designed to be reusable. In this study, several design proposals are produced, fabricated and tested with TRIGA central thimble (CT) condition. Tighten the capsule using the thread method is selected as the best design. An aluminium washer is used as a tightness medium between the capsule cap and capsule body. The best tightness setting is 25Nm torque with no leaking found at 5.5 water depth and 70°C heat condition.

Keywords: Design, Irradiation, watertight

1 Introduction

Radioisotopes are produced by exposing suitable target materials to the neutron flux in a nuclear reactor for an appropriate time. In Agensi Nuklear Malaysia, the Medical Technology Division (BTP) are producing long irradiation isotope such as Samarium 153 ($^{153}Sm_{62}$), Technetium-99m (^{99m}Tc), etc through the TRIGA PUSPATI reactor.

Target materials to be irradiated are sealed in primary capsules, loaded in specially designed irradiation capsules and then lowered to predetermined locations in the core for irradiation. However, the current existing irradiation capsule is not reusable and limited. If reused again, there is the possibility of leakage. Irradiation capsule leakage should be avoided because it can cause contamination to or from the irradiation sample. In addition, the current irradiation capsule is expensive and if it is used for a single use, it will increase the waste volume.

In this research study, the irradiation capsule is designed and fabricated to be reusable. Then, the irradiation capsule will be tested for water-tight and pressure tests to simulate real conditions inside the reactor pool.

The majority of the target is encapsulated in an aluminium capsule because the absorption cross-section is low (aluminium is considered nearly transparent to neutrons), radioisotopes produced in the aluminium capsule material are very short-lived hence post-irradiation handling and disposal are easy, good thermal conductivity hence heat produced in the target is easily transferred to the coolant and It is possible to make air/water tight container by cold welding a lid to the container with the target material inside. This has the advantage of not subjecting the targets to high temperature thus avoiding oxidation or decomposition of the target.

Several aspects need to be considered in the design of a watertight irradiation capsule such as the selection of material and the dimension of the capsule. In terms of material, Aluminium 6061 was selected for this study because it is available in-house. In terms dimensions of the capsule, all aspects will affect each other such as the thickness of the capsule, size and length of the capsule, the weight of the capsule and buoyancy effect, and the position of the capsule inside the reactor pool. The depth or water pressure toward the capsule depends on the position of the capsule during irradiation. The depth between the top of the pool to the central thimble (CT) in TRIGA PUSPATI is 5.5 meters will be used as a reference value for the water pressure experiment.

2 Methods

The proposed watertight capsule design is by tightening the capsule cap with the capsule body using the thread method. Concept 1 is that the capsule cap is tightened with the capsule body with a special thread. The tread for the capsule cap is on the outer surface, meanwhile, the thread for the capsule body is on the inner surface. To make sure these two pieces are tightened, both touching surface has tapered shape. This tapered shape will force both surfaces to become very close to each other once it is tight enough. Meanwhile, in concept 2, the aluminium washer is placed in between the capsule cap and capsule body. The aluminium washer will play the role of tightening the surface between the capsule cap and capsule body. Concept 2 is inspired by the car oil drain plug. Figure 1 shows the design between concept 1 and concept 2.

Figure 1: Concept 1 and Concept 2

A torque wrench will be used to measure the tightness between the capsule cap and the capsule body. The maximum torque allowed for aluminium materials is 44Nm (PUSPATI TRIGA Reactor User Guide book). Aluminium is a soft material, if the torque applied is more than 44Nm, the tread will become a permanent damage.

The sample size and position of the irradiation capsule inside the TRIGA reactor are the factors that will influence the design dimension of the irradiation capsule. Usually, the interest sample is placed and sealed inside 2ml ampoules.

Meanwhile, the possible position of the irradiation capsule inside the TRIGA reactor is in the Central thimble and Rotary Rack. Central thimble has a diameter of 33.8mm with a height of 704.86mm (fuel height). The Rotary Rack diameter is 31.7mm with a height of 274mm. To get higher flux from the reactor fuel, the irradiation capsule will be placed at the central thimble. The outer diameter of the irradiation capsule should be less than 31.7mm to fit on a central thimble or rotary rack. The internal diameter is more than 11mm to fit a 2ml ampoule size. The thicker irradiation capsule thickness is preferable as reduces the flux shielding. The height of the capsule is not more than 150mm.

To replicate the actual pressure condition of the irradiation capsule inside the TRIGA reactor, the irradiation capsule is submerged in 5.5meter height of water for 24 hours. The irradiation capsule is tightened using a torque wrench at 15Nm, 20Nm, 25Nm, 30Nm, 35Nm and 40Nm.

(a) Tightened the capsule (b) Take in and out the capsule (c) 5.5-meter depth of the pipe (d) Open the capsule

Figure 2: The experiment setup for the pressure test to the irradiation capsule

Figure 3: Concept 1 failed at the tapered surface

According to J. Abdul Karim et al, the TRIGA PUSPATI water temperature is in the range of 32°C to 67°C Therefore, to replicate the actual temperature condition of the irradiation capsule inside the TRIGA reactor, the irradiation capsule is submerged for 24 hours in water (70°C water temperature) inside a conical flask.

3 Result and discussion

At the pressure test, with a depth of 5.5 meters of water, the capsule is drowned at the bottom of the pipe. By calculation, the irradiation capsule is exposed to 1.55 bar pressure. The condition of concept 1 and concept 2 irradiation capsules during the pressure test experiment is shown in Table 1. Both design is drowned into the bottom of the pipe, with no issue of weight or buoyancy. Concept 1 is leaking at all tightness levels of the capsule cap, meanwhile, no leaking was found for Concept 2 after 25Nm tightness was applied. Concept 1 failed because of the uneven surface at the taper (maybe due to torque tightness, causing damage at the taper surface).

Table 1: Condition of the capsule during the pressure test

Torque	Concept 1	Concept 2
15Nm	10ml	1ml
20Nm	14ml	Just wet
25Nm	13ml	No leaking
30Nm	12ml	No leaking
35Nm	8ml	No leaking
40Nm	3ml	No leaking

Thus, at the heat test, concept 1 is no longer being tested due to failure and permanent deformation. The concept 2 design shows no leaking found at every tightness level. Therefore, concept 2 is a suitable design for reusable capsule design. The tightness setting is 25Nm torque which is good enough with no leaking found at the basis condition, pressure condition and heat condition.

4 Conclusions

In conclusion, the best design for reusable capsules is design concept 2. The aluminium washer is used as a tightness medium between the capsule cap and capsule body. Design concept 2 can be watertight at pressure conditions of 5.5 meters water depth and 70°C heat. No permanent deformation is observed for the design concept 2 irradiation capsule. The best tightness setting is 25Nm torque. However, in a real condition inside the TRIGA reactor, it is not advised to reuse the aluminium washer as the performance of the washer will drop and may cause leakage. There is no issue of buoyancy as the design with a weight of 135g can submerge into 5.5 meters of water depth. However, there is a requirement for the concept 2 irradiation capsule design to be tested in real conditions inside the TRIGA reactor.

References

Pro bolt Aluminium Information. https://www.pro-bolt.com/torque-information/.

Matteo F. 2019. Experimental study of consistency degradation of different greases in mixed neutron and gamma radiation. *Heliyon*.

Book: Manual for reactor produced radioisotopes. 2003. IAEA-TECDOC-1340, International Atomic Energy Agency (IAEA).

Book: PUSPATI TRIGA reactor user guide book. https://urtp.nuclearmalaysia.gov.my/files/TOC_PIC.pdf.

Osvaldo L. 2015. Study and evaluation of aluminium capsules to irradiation of gaseous samples in nuclear reactor. *Journal of Physical Science and Application*.

Individual Research Contribution Review, 2023, 1(1): 413–414

Reuse and Recycle of Radioactive Sources from Sinagama

Muhammad Hannan Bahrin
Technical Support Division, Malaysian Nuclear Agency
43000 Kajang, Selangor
hannan@nm.gov.my

Abstract

Sinagama irradiation plants have 362 Cobalt-60 (Co-60) pencil sources aged over 20 years. Currently, the Radioactive Waste Management Centre (WasTeC) is unable to manage and store Sinagama's Co-60 pencil sources. Based on the market survey, the cost to return the source to the original country is expensive. Meanwhile, the Raymintex irradiation plant requires additional Co-60 sources as the current activity is low. Therefore, this research paper will discuss the feasibility study on reusing and recycling Co-60 sources from Sinagama to Raymintex. Factors such as the activity of the Co-60 sources, source dimension, the transfer method, and the estimated cost of this project are discussed.

Keywords: Reuse and recycle, radioactive source

1 Introduction

Sinagama irradiation plants have 362 Cobalt-60 (Co-60) pencil sources aged over 20 years. The current activities for each source are between 10Ci to 900Ci, with an estimated activity of 76,745Ci (April 2023). In Radioactive Waste Management Centre (WasTeC), Malaysian Nuclear Agency, a dedicated plant to store the pencil source from Sinagama is not available. Meanwhile, sending the pencil source back to the original country will cost millions of Ringgit. The Raymintex irradiation plant requires additional Cobalt-60 sources as the current activity is only 13,000Ci (low). The best minimum activity for the Raymintex irradiation plant to operate is 70,000 Curie. Therefore, there is a potential to reuse and recycle the Cobalt-60 sources from Sinagama to Raymintex.

The International Atomic Energy Agency (IAEA) are encouraging member state to consider on reuse and recycling of disused sealed radioactive sources (DSRS).

The objective of this study is to collect information about the source activity, dimension, and possible method to transfer, transfer cask design/transport package and local technology available to support the project.

2 Methods

Sinagama plant are using Nordion C-188 Co-60 sealed sources. It was designed primarily for use in wet source storage at pool-type irradiator. The capsule is made from stainless steel or zircaloy. According to the C-188 Co-60 sealed sources safety evaluation document, this source can be used in dry source storage irradiators with less harsh environmental conditions. The dimension of the C-188 sealed source is 452mm in length with 11.2mm in diameter. Meanwhile, the Co-60 in Raymintex is in R1800 capsule or DIP rod. This capsule is suitable for wet or dry storage irradiation plants. The capsule is made from stainless steel type AISI 316L. Inside the DIP rod, there are 24 clusters of sources. The arrangement of sources inside the DIP rod is unknown. The dimension of a single Co-60 is 152mm in length with 6.35mm in diameter. The DIP rod dimension is 658mm internal length, 703mm overall length with 41.25mm diameter.

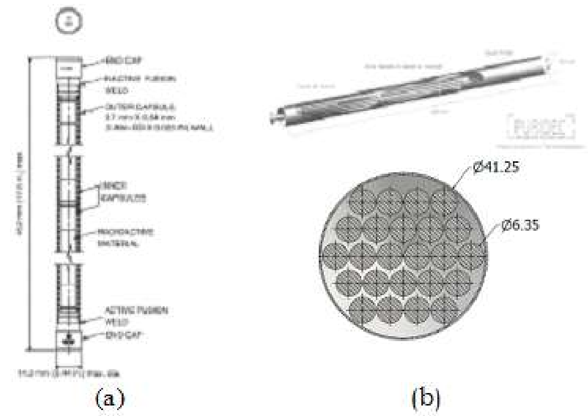

Figure 1: (a) C-188 Co-60 sealed sources at Sinagama, (b) R1800 capsule with Co-60 arrangement inside capsule

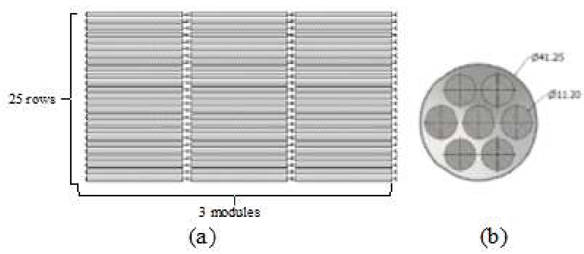

Figure 2: (a) Raymintex source rack arrangement, (b) 1 DIP rod can fit a maximum of 7 pieces of C-188 Co-60

Based on the source dimension, there is a possibility to arrange the C-188 Co-60 sealed source from Sinagama into the DIP rod of Raymintex as shown in Figure 2(b). Raymintex has 3 modules with 25 rows of racks. Overall, there are spaces for 75 DIP rods however, one DIP rod needs to be empty. In addition, 8 DIP rods are already filled with Co-60. Therefore, the available empty rack in Raymintex is 66 DIP rods. All the 362 C-188 sealed sources from Sinagama can be arranged in 52 DIP rods. In April 2023, the current activity of Co-60 in the Raymintex plant was 13,345 Curie, meanwhile, the spent Co-60 fuel in the Sinagama plant is 76,747 Curie. If all the spent Co-60 from the Sinagama plant is transferred to the Raymintex plant, the estimated Raymintex plant Co-60 activity would be increased to 90,093 Curie. However, this activity will decrease over time due to the half-life of Co-60.

Here are the general step-by-step operations for the reuse and recycling of Sinagama Co-60. First, unloading the C-188 Co-60 sealed source from the Sinagama pool by using the Sinagama transport cask. Then, the transport cask is placed into a Mobile Hot Cell (MHC) for source visual inspection, source integrity, serial number etc. After that, insert the C-188 Co-60 sealed source into the fabricated DIP rod and weld the DIP rod. Finally, transfer the DIP rod into the Raymintex transfer cask and align the transfer cask with the Raymintex plant loading port for source transfer.

Table 1: The operational activities and cost involved in transferring Co-60 from the Sinagama to the Raymintex

Unloading source from Sinagama Transfer Sinagama source into rental transfer cask (Option 1 and 2) / Fabricated transfer cask (Option 3)
MHC Operation - Transfer MHC to Dengkil and back to PDC - Assemble of MHC (1 week) - Modification of MHC to suit this activity - Site Preparation
Rental of Crane and transportation loader.
Fabrication: - DIP rod (52 units) - QC for DIP Rod and license - Welding set - Leak test machine
Transfer source from MHC into Raymintex loading (GB/3231A/B(U) Transport Cask) Option 1 Fabricated Transfer Cask (Option 2 and 3)
Other cost: - Manipulator spare part - Storage for rejected source / contaminated source - Consumable items and maintenance of MHC - HEPA filter

There are three options to transfer the Sinagama source to Raymintex. The first option is to rent two transport packages: transport cask Sinagama (Eg: Model F-168: CDN/2081/B(U)-96) and transport cask Raymintex (Eg: GB/3231A/B(U)). The second option is to rent a Sinagama transport cask and fabricate a new transport cask to align with the Raymintex plant. The third option is to fabricate a transfer cask that can be used for both activities in the Sinagama pool and Raymintex plant.

3 Result and discussion

The C-188 Co-60 sealed source from the Sinagama plant can be reused and recycled by arranging it into a DIP rod capsule of Raymintex. According to regulations SSR-6 (Rev-1, 2018), this new DIP rod capsule is considered a special form capsule and required to pass several tests such as impact test, percussion test, heat test, bending test and leaching test.

It is not compulsory to have a transport package type B(U) for the operation of unloading the Co-60 source from Sinagama to Raymintex because both of the plant is located at the same premises. However, currently, Agensi Nuklear Malaysia does not possess any transfer cask for loading and unloading activity for the Sinamaga and Raymintex plants. Thus, renting and fabricating own transfer cask is considered to be the only option.

Based on the list of operational activities of loading and unloading Co-60 from the Sinagama plant to the Raymintex plant, the estimated duration is 2 months. The estimated total costs are RM5,541,568, RM5,298,384 and RM5,468,000 for option 1, option 2 and option 3 respectively. Although all the estimated costs are almost the same, options 2 and 3 will benefit more to the agency as the transfer cask can be reused again in the future. The rental transport container will cost a lot and have no time flexibility during handling the operation of unloading and loading of the radioactive source.

4 Conclusion

There are a lot of challenges that have been identified such as approval from Jabatan Tenaga Atom, handling issues, manpower/expertise, time constrain (rental issues) etc. However, this project will be a starting point to increase Nuklear Malaysia's capability in handling radioactive transportation, transfer cask design, reuse and recycling of radioactive sources and much more. In addition, this project will open opportunities for Nuklear Malaysia to provide services to other Gamma processing facilities in Malaysia on the management of disuse radioactive sources. The spent Co-60 source can be reused and recycled again for other purposes and applications rather than sent back to the original country for long-term storage or disposal.

References

Regulations for the safe transport of radioactive material, SSR-6 (Rev.1), International Atomic Energy Agency (IAEA) 2018.

REVISS Services' product code: RSL1800, product information.

Book: Management of Disused Sealed Radioactive Sources. 2014. Technical Report, IAEA Nuclear Energy Series No.NW-T-1.3.

Individual Research Contribution Review, 2023, 1(1): 415–416

Maintenance and Repair Proposals Including Upgrading the Existing Probe System of the IV Tester

Muhammad Haziq bin Sayuti
Technical Support Division, Malaysian Nuclear Agency
43000 Kajang, Selangor
m_haziq@nm.gov.my

Abstract

Electrical characterization is one of the important testing in the fabrication process. There are two techniques commonly used for IV characterization; two probes and four probes method. Probe station used in Block 75; Nuclear Malaysia was using the two-probe method since 2018. This paper studied the possibility of this IV tester to be upgraded, using the four probes method by discovering the differences between these two methods. The double two probes method has also been suggested in the methodology part to reduce the cost for having the four probes method.

Keywords: : Electrical characterization, Two probes, Four probes

1 Introduction

Electrical characterization is one of the process consists in semiconductor fabrication device. There are two purpose of this process; to get the device perspective and also materials perspective to make sure the product that have been fabricated achieve the specification required. There is no issue to do an electrical measurement on a discrete component but there is a little challenge when it comes to have an electrical measurement on a wafer. Hence, there is a special station called "Probe Station" to do an electrical characterization on each of die. This Probe station usually consists of Source Measurement Unit (SMU), Micro positioners, solid plate or base, vacuum chuck, microscope, magnetic manipulators and the important one is probe tips. Figure 1 shows the complete setup for the probe station which located in Semiconductor Nuclear Detector Fabrication Laboratory, Block 75.

Figure 1: Full setup of probe station.

2 Basic Concept

There are two common techniques for the electrical characterization of semiconductor which are two probe method and four probe method. The most frequently is two probes because it is simple and inexpensive compared to the four-probe method (Caballo and A.Acebron, 2009). Figure 2 shows the general connection for the two-probe method whereas a pair of probes with conductive wires is attached to a specimen. These two probes are used for electrical current input, as well as for the voltage measure. While the resistance of the segment between the voltage contacts can be calculated through the Ohm's law:

$$R = \frac{V}{I}$$

Where, V and I are the voltage and current from the voltage and current contact respectively. For the four-probe method as depicted in Figure 3, the electrical current is passed through the outer probes and induces voltage in the inner probes. Based on the measured voltage and current, the resistance between the voltage contact is then calculated.

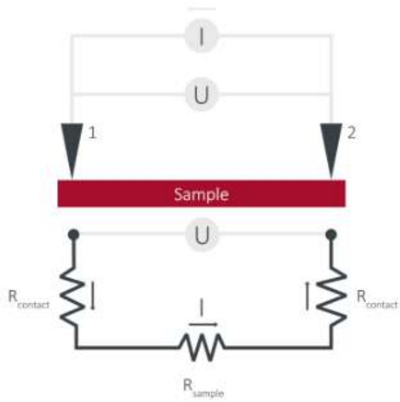

Figure 2: Two probe connection.

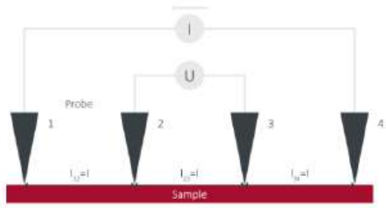

Figure 3: Four probe connection.

3 Literature Review

Probe station (brand Signatone) which owned by Nuclear Emerging Technology Centre (NET) was among of two-point probe type. Based on (SURAGUS, 2023) explanation, the contact and propagation are very high when using two probes which give an advantage to the four-point method. Four point has high accuracy measurements because the contact and propagation resistances of the voltage probes are very low. Furthermore, they said a two-point probe measures the combined resistivity of the sample, the contact resistance and the probe resistance whereas a four-point probe only measures the sample resistivity. It can only be achieved when two wires are used separately which is one for induced the current while the other to measure the drop in voltage.

(Singh, 2013) also discussed the electrical resistivity measurements regarding the differences of probes used in electrical characterization. He suggested to take advantage on the differences on both two probes and four probes measurements. For instance, he mentioned that two probes is the simplest method that can be used to measure resistivity. In addition, this method is really suit for a sample that has large resistance. On behalf four probes, it is applicable for resistivity measurements on the low resistive samples. In a summary, he recommends to choose an appropriate method which suit the nature of the material studied.

(Betty, 2023) published an article discovered the four-probe testing for the electrical characterization. He was agreed with (SURAGUS, 2023) on the four-probe technique can eliminate the effects of contact resistance which can cause errors in the measurement. Besides, he mentioned also that this technique can be used to measure electrical properties of biological tissues and cells such as conductivity of the skin. In addition, the electrical behavior of cells in response to different stimuli can be studied specifically using this four-probes technique.

Based on their studies, there will be more benefit on having both of the measurement methods whereas upgrading the two probes to four probes could be a solution for IV tester located at Block 75.

4 Methodology

There are two main concerns on upgrading this two probes method to four probes method for the Signatone IV Tester.

4.1 Addition number of Probes

The current IV tester is using the two probes method is suggested to be upgraded onto four probes method instead of buying a new item separately. In other word, it can be said that the electrical characterization will be done using double two probes method. Hence there will be another four probes desired (two for induce or measure while two for common) to be added to fulfill the general connection of the four probes method.

4.2 Need of an extra Source meter

Source Measuring Unit is the main item in order to simplify the measurement. This device is capable of sourcing, measuring and displaying resistance or resistivity in addition to measure voltage and current. However, SMU Model 2612B only can be used limited up to two probes method. Thus, when there is an addition of the probe numbers, there will be a connection required for the additional probe then it can be used to supply or measure either current or voltage. Thus, this item also needs to be added to proceed with this method upgrade.

4.3 Preventative Maintenance

Preventative maintenance (PM) should be done after some changes and modification has been done to an equipment. This is important to prevent an unexpected failure occurs in the future. Repairing or restoring the damaged item are also involved in PM activity. This Signatone 1160 Series Probe Station has two major problems which have been reported to the person in charge for the restoration. These two issues are; faulty Uninterruptible Power Supply (UPS) and malfunction of 12V adapter for the High Definition (HD) Display. Despite, these are the problems only noticed by the user. There must be other accessories that must be replaced or upgraded as all components has its own lifespan. Thus, PM will really be helped identifying those problems.

5 Conclusions

In this study, development of the IV tester have been studied as this equipment plays vital role on understanding the performance of a sample especially semiconductor components in micro sized. Improving machine and scientific equipment really important in order to increase the accuracy, consistency and performance.

References

Wang. Betty. 2023. Four-probe testing demystified: An introduction to the basics and beyond. Available at: https://www.linkedin.com/pulse/four-probe-testingdemystified- introduction-basics-beyond-betty-wang/.

Aldrich T. Caballo and Loremay A.Acebron. 2009. Implementation of the two probe method : A technique in measuring electrical properties. 14(3).

Y. Singh. 2013. Electrical resistivity measurements: A review. *International Journal of Modern Physics: Conference Series*, (22):745 – 756, doi:10.1142/s2010194513010970.

SURAGUS. 2023. Four point probe measurement method (2023) SURAGUS sensor & Instrumentation. Available at: https://www.suragus.com/en/technology/four-point-probe/.

Individual Research Contribution Review, 2023, 1(1): 417–418

Preventative Maintenance and Repair for the Computerized Numerical Control (CNC) Dicing Machine

Muhammad Haziq bin Sayuti
Technical Support Division, Malaysian Nuclear Agency
43000 Kajang, Selangor
m_haziq@nm.gov.my

Abstract

Wafer Dicing is the process by which die are separated from a wafer of semiconductor following the processing of the wafer. The dicing machine owned by Malaysian Nuclear Agency was equipped with software that allow users to choose suitable cutting parameters according to their needs. This machined was bought on 2014, at the same time there is no major maintenance been done for this machine. Thus, this study is mainly about the preventative maintenance (PM) which has been done to maintain the performance of the machine itself. Furthermore, there are also some enhancements have been done to increase the experimental efficiency while using this dicing machine. Nevertheless, this preventative maintenance will be continued with the calibration maintenance to make sure the accuracy of the controller part.

Keywords: : Preventative maintenance, Dicing machine

1 Introduction

Wafer Dicing is the process by which die are separated from a wafer of semiconductor following the processing of the wafer. The dicing machine owned by Malaysian Nuclear Agency was equipped with software that allow users to choose suitable cutting parameters according to their needs. SYJ-800 as depicted in Figure 1 is one of the CNC machines (Computerized Numerical Control) [1]. CNC machine means the machine tools or other device are operating automatically by the computer instead of a manually by an operator (Yasar and Essex, 2023). However, there are some parameters need to be set manually for enabling the user to choose their desired values by following the range provided. This machine needs to undergo the preventative maintenance mainly because there is a vibration issue with the spindle rotor speed when entering turn knob of 8.

2 Methodology

There preventative maintenance has been classified into two categories; service and restoration and also enhancement on the machine efficiency. The cleaning services and restoration works are:

a. Tube, fitting and hoses replacement for water and vacuum supply.

b. Ball bearing replacement for the rotor spindle speed (suspected this issue cause the vibration during spindle speed turn 8).

c. Water pump cleaning.

While the enhancement on the machine efficiency such as:

a. Modify the old knob for controlling the spindle rotor speed with the knob which has an indicator.

b. To install an internal cap inner rubber cover for the Oiless Vacuum Pump.

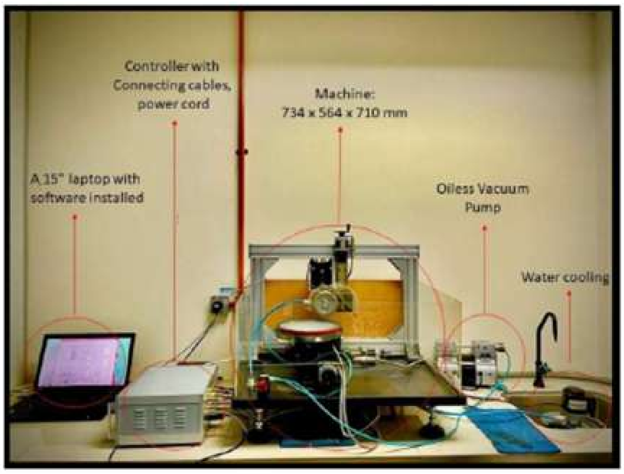

Figure 1: Full setup of the wafer dicing machine (SYJ-800).

3 Results

As per Table 1.

4 Conclusions

In a conclusion this preventative maintenance not only covered the repairing and restoration, but including also the enhancement on the machine performance. Despite having some changes and new spare-part, the performance of this machine still needs to be monitor time to time. Thus, this machine is

[1] Heavy Duty Coolant circulating tank with pump, 4 L for MTI cutting saw - eq-eco-430 (no date) MTI Corp - Leading provider of lab equipments and advanced crystal substrates. Available at: https://www.mtixtl.com/heavydutycoolantcirculati ngtankwith-pump6lformticuttingsaw.aspx (Accessed: 08 December 2023)

Table 1: Condition comparison for the SYJ-800 machine before and after preventative maintenance been done.

Before	After
	
Old tubes used for water and vacuum supply.	Replaced tubes for water and vacuum supply
	
Old fitting and hoses or connector between tube and piping.	New fitting and hoses.
	
Contaminated water pump.	Condition of the water pump after cleaning service.
	
Old control knob without indicator	New knob with indicator for controlling the spindle speed.
	
Oiless vacuum pump without an internal cap, which caused the pump vibrated and moved	Oiless vacuum pump with an internal cap (inner rubber cover)
	
Loosed ball bearing which caused vibration during high-speed	New ball bearing, made in Japan.

advised to undergo the calibration maintenance to make sure the speed of the spindle for example met the specification of the machine accurately to make sure the results produced with zero-error on behalf the technicality of the machine [2].

References

K. Yasar and D. Essex. 2023. What is computer numerical control (CNC)? – TechTarget definition, ERP. Accessed: 08 December 2023:Available at: https://www.techtarget.com/searcherp/definition/computer–numerical–controlCNC: :text=Computer

[2] Calibration and preventative maintenance procedures, Inst Tools. Available at:https://instrumentationtools.com/calibration-preventative-maintenance/ (Accessed: 08 December 2023)

Individual Research Contribution Review, 2023, 1(1): 419–420

Proof of Concept (POC) for Semiconductor Radiation Detector using Schottky Diode 4H-SiC

Muhammad Haziq bin Sayuti
Technical Support Division, Malaysian Nuclear Agency
43000 Kajang, Selangor
m_haziq@nm.gov.my

Abstract

4-Hexagon Silicon Carbide semiconductor has been used to fabricate a Schottky diode to be used in radiation detection. The optimization of its fabrication process is still undergoing however the role of this Schottky diode as a radiation detector must be prove. In this study, the concept is proven by using the theoretical analysis, software simulation and the experimental setup. There is a limitation when it comes onto the circuit prototype especially on the component selection. Hence, this study needs to be continued with the amplifier setup to complete the circuit designation using the printed circuit board (PCB) instead of using the breadboard or donut board.

Keywords: : preamplifier, Schottky diode, 4H-SiC

1 Introduction

Fabrication and characterization of the Silicon Carbide Schottky Diode for a radiation detector in Nuclear Malaysia have been developed in 2014. Silicon carbide was chosen because of its characteristic such as wide bandgap, high thermal conductivity, high breakdown field, high saturation electron velocity and high displacement threshold energy which lead to the radiation hardness to act as radiation detector (Mansor, 2013). The fabrication process of this Schottky diode has been done in laboratory of Newcastle University and have been tested with ultraviolet, alpha and gamma ray. This diode was succeeded to detect the UV but having problem on detecting the alpha and gamma ray due to the designation of the preamplifier itself. Radiation interaction usually been read by a preamplifier followed by pulse shaping amplifier which is the main amplifier. Thus, the objective of this study is to develop a suitable preamplifier with low noise as the first stage of the electronic readout. In order to meet this aim, the following circuit design requirements and testing methodologies must be satisfied:

i. To calculate the amount of charge produced with the expected output voltage of the preamplifier.

ii. To design and develop a Charge Sensitive Preamplifier (CSP) circuit design using the LT-Spice.

iii. To compare the calculation with the simulation result in term of the output voltage produced by the preamplifier.

iv. To develop a prototype circuit board to test directly with the radioactive material.

2 Background Theory

There are three (3) important elements in charge-sensetive preamplifier introduced by (Nakhostin, 2018). Those elements are simplified in Figure 1. In general, charge sensitive preamplifier consists of an operational amplifier, a feedback capacitor, Cf and also a reset circuit.

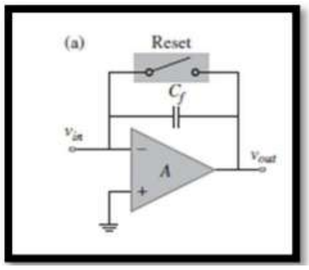

Figure 1: Basic elements of a charge-sensetive preamplifier.

3 Methodology

3.1 Theoretical Analysis

In the selection of a charge-sensetive preamplifier for a specific detector, output voltage is calculated using the formula derived using the relation between input and output of the operational amplifier. In CSP, operational amplifier used is in form of negative feedback. Based on sic characteristics studied by (Nava et al., 2008) they found that the pair creation energy for the sic is 7.8 eV. Now the voltage output of the preamplifier is fully dependent on the feedback capacitor. As mentioned by (Rogalski and Bielecki, 2006), charge sensitive preamplifier integrates the charge on the feedback capacitor. Its gain is not sensitive to a change in detector capacitance.

For example, calculation below shows the amount of charge produce, Q_o in a SiC detector when 60keV Υ-rays (241Am) are deposited. With Wi = 7.8 eV, the

$$Q_o = \frac{E_e}{W_t}, e = 1.602 \times 10^{-19} C$$

Amount of charge produce, Q_o

$$= \frac{(60 \times 10^3)(1.602 \times 10^{-19})}{7.8} = 1.23 fC$$

While the calculation of the charge sensitive preamplifier output produced is,

$$V_o max = -\frac{Q_i}{C_f}$$

In this part, the output voltage of the charge sensitive preamplifier is now depending only on the feedback capacitor. Thus, below are the comparison of the calculation for the output voltage with feedback capacitance = 1pF and 0.1pF.

if C_f *= 1pF,*

$$V_o max = -\frac{1.23fc}{1pF}$$

$$V_o max = 1.23mV$$

if C_f *= 0.1pF,*

$$V_o max = -\frac{1.23fc}{0.1pF}$$

$$V_o max = 12.3mV$$

3.2 Simulation Methodology Using LT-Spice

After that, the charge sensitive preamplifier is then simulated using the open source software (LT-Spice). Figure 2 shows the charge sensitive preamplifier developed completely with all the basic element of the charge sensitive preamplifier; 100 Mohm feedback resistor, 0.1pF feedback capacitor and operational amplifier specifically using the LT6268-10. Based on the CSP output calculation above, the value of the 0.1pF was selected to have maximum voltage of 12.3mV. Selection of this value also considering the availability of a component in the market. 100M ohm resistor was chosen as to enable the time constant to be 10μ seconds. In this study, pulse voltage (initially zero) is used to generated -1.23mV which is represent as the amount of charge produced after the radiation interaction. Then, two probes were inserted each for input and output of the charge sensitive preamplifier to compare their reading.

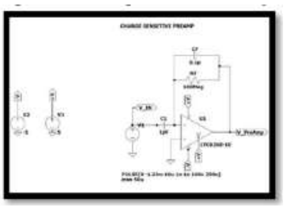

Figure 2: Developed Charge Sensetive Preamplifier using LT-Spice.

Figure 3 and Figure 4 show the simulation result based on circuit developed in Figure 2. Figure 3 depicted the voltage output produced (green colour) when 0.1pF of the reference capacitor is applied. The reading of the peak shown is 12.30mV exactly same as in the theoretical analysis part. Same goes to the feedback capacitor with 1.0pf, the reading in Figure 4 is 1.232mV as calculated in the previous calculation.

3.3 Experimental Setup

This study was continued with the experimental setup by using the breadboard and some components such as capacitor, resistor, operational amplifier and jumper. Nevertheless, those components with values needed cannot be fulfil due to challenges below:

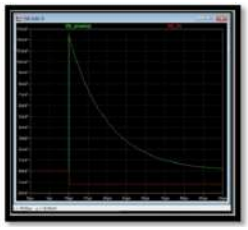

Figure 3: Result simulation of the charge sensetive preamplifier with Cf = 0.1pF

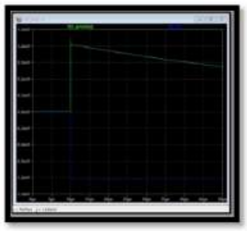

Figure 4: Result simulation of the charge sensetive preamplifier with cf = 1.0 pF

i. The feedback capacitor (Cf) and feedback resistance (Rf) both desired values are not available in the through hole component application. Thus, need to use surface mount device (SMD) component which require the designation of the charge circuit preamplifier on the printed circuit board (PCB)

ii. Ordering the PCB for this POC project consuming very high cost, thus this circuit designation was advice to be done until the signal amplifier (pulse shaping amplifier) which is the main amplifier.

4 Conclusions

In this study, the preamplifier of the radiation detector has been calculated and simulated but was stuck on the experimental part. A pulse shaping amplifier will be studied to be included in the printed circuit board to reduce the development cost of this detector. Thus, the design of this test circuit can be used in the future with other detector which require the application of the charge sensitive preamplifier.

References

Ishak Mansor. 2013. Fabrikasi dan pencirian diod schottky 4H-SiC [Preprint]. Unpublished doctoral thesis (Limited Thesis).

Mohammad Nakhostin. 2018. Signal processing for radiation detectors. pages 1st edn. Hoboken, USA: John Wiley amp; Sons.

F. Nava, Giuseppe Bertuccio, A Cavallini, and Ettore Vittone. 2008. Silicon carbide and its use as a radiation detector material. *Measurement Science and Technology*, 19(10):p. 102001. doi:10.1088/0957–0233/19/10/102001.

Antoni Rogalski and Zbigniew Bielecki. 2006. Detection of optical radiation.

Individual Research Contribution Review, 2023, 1(1): 421–422

Wafer Singulation by CNC Dicing Machine for Wafer Cutting Application in Nuclear Malaysia

Muhammad Haziq bin Sayuti
Technical Support Division, Malaysian Nuclear Agency
43000 Kajang, Selangor
m_haziq@nm.gov.my

Abstract

The miniaturization of devices has brought onto the fabrication of smaller and lighter chips. Thus, the singulation of a wafer into die plays a vital role in producing many and mini chips. Wafer Dicing is the process by which die are separated from a wafer of semiconductor following the processing of the wafer. The dicing machine owned by Malaysian Nuclear Agency was equipped with software that allow users to choose suitable cutting parameters according to their needs. In this study, a wafer of 100mm diameter, 2mm thickness was been cut using the 4 inches of the diamond blade. The result of cutting then was analyzed using the Axio-Scope A1 in term of the consistency of the kerf width and the formation of chipping width. These kerf and chipping width can be observed and measured directly with the I-Solution software. Based on the result produced, future study of the optimal parameter can be constructed in order to get the best cutting quality (with minimum chipping width) to be used for various types of semiconductor fabrication purpose especially for radiation detector application.

Keywords: : Wafer Dicing, Schottky Diode, Semiconductor Wafer, Fabrication, Kerf Width, Chipping

1 Introduction

Fabrication of electronic components in micro and nanoscale nowadays are due to the miniaturization of the electronic devices. Thus, wafer singulation plays an early and vital role in the quality of the final product. In order to have bulkier quantity and great quality of chips the precision in wafer cutting is the main focus. Moreover, todays silicon wafers are getting more thinner; very fragile, can caused crack and larger size of chipping during the cutting process. This study was aimed to give an overview on the complete process of wafer singulation which is a part of process in developing the radiation semiconductor detector.

2 Methods

Characteristics of the silicon wafer used for this study are N-type dopant with diameter of 100mm/4inch. Its thickness is 2000μm or 2mm. It was cut using the 4-inch sintered diamond blade. There are three parameters which affected the chipping size most; Spindle speed, Cutting speed and Cutting depth (Shi et al., 2022). In this study, the cutting speed used are for X, Y and Z axis are maximum value which X & Y axis;50 mm/min while Z axis;20mm/min, cut depth is 1mm (to observe the dicing street) and the spindle speed is 3333.0 rpm (turn 5). The spindle speed was half of the maximum speed. Most of researchers used 30000 to 60000 rpm however this machine has limitation as it only can exceed 6000 rpm.

3 Result

There are five different locations captured for the cutting analysis. Each picture is labelled with measurement of the kerf width and the largest chipping width produced during the cutting process. The data captured by the software were then classified into Table 1 and extracted into a graph as depicted in Figure 1. Based on this multiple Y graph in figure 1, kerf width generated by the diamond blade wereremain uniformly with value of 350.537 μm. While the chipping width were dramatically decreased along the cutting street. In the transient stage, the wafer is being cut with impact force and abrasion force from the diamond grits of the blade while only abrasion force during the steady stage; final part of cutting street which resulting to the minimal chipping (Lin and Cheng, 2014). There must be an optimal parameter to reduce the impact force so that the uniform cutting can be produced on both stages of the cutting street (Shen et al., 2019). Nevertheless, parameters setup are still depending on the wafer type of materials, thickness and also its diameter.

Table 1: Classification of Kerf width and chipping width according to the cutting distances.

Cutting distance (mm)	Kerf Width (μm)	Chipping width (μm)
0-15	350.537	84.946
15-30	350.537	68.817
30-45	350.537	61.215
45-60	350.537	52.688
60-75	350.537	43.387

4 Conclusions

The optimal parameter for a wafer dicing needs to be study time to time as the evolving of the wafer specification itself. Also, to study how to decrease the dicing street so that many

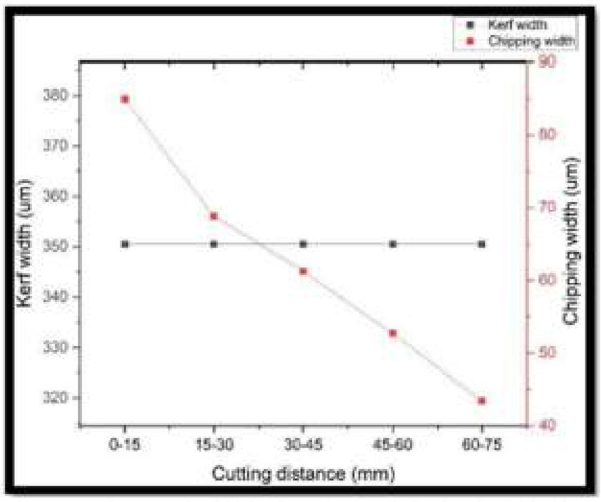

Figure 1: The trend of chipping size and the kerf width along the cutting distance.

components can be installed in a wafer to have larger production of semiconductor fabrication purposes including also the Schottky Diode (radiation detector).

References

J. W. Lin and M. H Cheng. 2014. Investigation of chipping and wear of silicon wafer dicing. *Journal of Manufacturing Processes*, 16(3):373–378, https://doi.org/10.1016/j.jmapro.2014.04.002.

J. Shen, X. Zhu, J. Chen, P. Tao, and X. Wu. 2019. Investigation on the edge chipping in ultrasonic assisted sawing of monocrystalline silicon. *Micromachines*, 10(9):https://doi.org/10.3390/mi10090616.

J. Shi, W. Liu, Z. Chen, W. Cao, and L. Zhou. 2022. Optimization method of cutting parameters of wafer dicing saw based on orthogonal regression design. *SN Applied Sciences*, 4(10):https://doi.org/10.1007/s42452– 022–05146–1.

Individual Research Contribution Review, 2023, 1(1): 423–424

Preliminary Results from the Field Trial of an Autonomous Robot for Radiation Mapping

Muhammad Izzuan Mohd Ghazali
Technical Support Division, Malaysian Nuclear Agency
43000 Kajang, Selangor
izzuan@nm.gov.my

Abstract

Utilising mobile robotics for radiation mapping can effectively reduce the potential for operator radiation exposure, while simultaneously generating comprehensive radiation maps of specific areas. Although this technology has potential benefits, its utilisation is now restricted and necessitates additional research. A earlier investigation involved the creation and development of an independent robot capable of mapping radiation. This paper describes the preliminary results of a field test on autonomous radiation mapping, which specifically examines the operational processes and problems encountered during the deployment of the robot. The text also covers the discussion of temporary measures implemented to address the difficulties. The findings will offer valuable insights for future researchers and operators involved in the development of mobile robotic technology for radiation mapping.

Keywords: Mobile Robot, Field Test, Radiation Mapping

1 Introduction

Radiation mapping is a technique that graphically illustrates the spatial distribution of radiation levels within a given region. The measurement of radiation levels is conducted using devices such as Geiger-Muller counters, scintillation detectors, and sophisticated monitoring tools. Subsequently, the gathered data is scrutinised in order to generate a map employing diverse hues or contour lines. Robotic radiation mapping employs specialised robots equipped with detection sensors to generate maps of radiation levels in perilous regions. This technology provides enhanced safety, efficiency, and precision when compared to manual techniques (Ravishankar et al., 2013). It enables the assessment of radiation hazards, detection of sources of contamination, surveillance of radiation levels, and implementation of appropriate measures to mitigate risks and safeguard the health of the public and the environment. The AMoRA project employs the Turtlebot2 as its designated mobile robot platform (Rahman et al., 2023).

2 Methods

2.1 Robot Description

The project, AMoRA, is an autonomous mobile robot for accurate radiation detection and mapping, using the Turtlebot2 platform and Kobuki for low-cost education and research purposes. The robot has a range of 1.2 meters to 3.5 meters and uses various navigation sensors. The system is paired with the Robot Operating System (ROS) for real-time data visualization. The radiation detection system uses the Geiger Muller (GM) detector LND7121, with an electronics module developed for it. The module connects to the AMoRA host computer via USB and uses the ROS package rosserial arduino for communication.

2.2 Radiation Mapping Procedures

The initial phase of automated radiation mapping involves a site survey to select suitable sites for the robot. This phase is crucial due to the AMoRA's dual wheels and the need for a smooth, indoor surface. Obstacles must be carefully assessed to maintain the accuracy of the final manually generated map. Asymmetrical site structure can lead to data overlap, requiring multiple attempts and editing.

After site selection, 2D mapping or manual mapping can be initiated, which involves connecting the robot and host computer, using input devices, and executing command prompts. Data clarity can be enhanced by rotating the robot at multiple locations. Data preservation is also essential. Autonomous radiation mapping is initiated by connecting devices, using manual maps, grid visualization, partition verification, and activating the GM detector. Parameters are configured, and the robot follows predetermined paths through the grid to measure radiation levels (Zakaria et al., 2017).

Upon completion of the autonomous process, a radiation map is generated based on visited grid locations. Comprehensive reports are generated, providing clear explanations and insights for future mapping needs or emergency responses. The manual and radiation map data collected are instrumental for present and future requirements, ensuring readiness for any future contingencies or needs.

The process of 2D mapping involves connecting the robot to a host computer and using input devices for long-distance control. Command prompts are used to establish connectivity and activate the Simultaneous Localization and Mapping (SLAM) algorithm. Data clarity is optimized by rotating the robot at multiple locations. Data preservation is done for easy retrieval. Autonomous radiation mapping is initiated by connecting devices and using a manual map. The robot follows predetermined paths through the grid to measure radiation levels. A radiation map is generated based on visited grid locations, with distinct color contours representing radiation intensity. Comprehensive reports are generated to enrich the data bank and facilitate future mapping needs or emergency responses. The manual and radiation map data collected are instrumental for present and future requirements.

3 Data/Results

Radiation mapping is an essential technique used to detect and quantify radiation sources at specific locations on a grid. Nevertheless, the sensor's limited capability to identify objects and obstacles that are less than 20 cm away is a noteworthy obstacle that necessitates the implementation of programming strategies to overcome. In order to achieve more precise statistics, it is recommended to carry out the 2D mapping technique manually in this study.

The AMoRA robot's mobility is restricted by its small wheels, which are specifically built for flat surfaces. As a result, it may not be able to navigate through rugged or uneven terrain or go over holes. To temporarily even out the surface, thin wooden or metal sheets were employed. The dimensions and stature of the AMoRA device surpass the half-meter threshold, so constraining its ability to reach confined regions and impeding its capability to measure grids situated in narrow places.

Figure 1: Challengers and Temporary Solution Implemented.

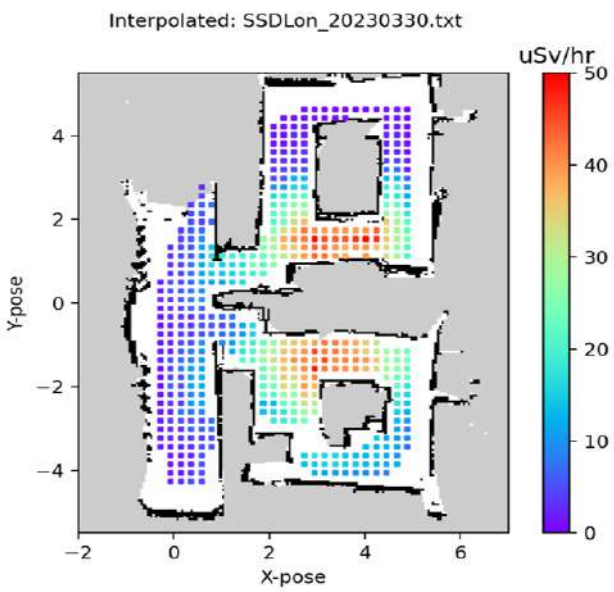

Figure 2: One Of the Final Result of the Attempts.

The limited battery life of both the robot and the host computer is a challenge for sustained operation, particularly for bigger locations that require extended periods of activity. Occasionally, the sensor may overlap data, leading to mistakes. Moreover, if automated mapping is not performed promptly after manual mapping and there are alterations in the object's configuration, the previously collected data may become unsuitable for the automated procedure due to environmental modifications.

To address the majority of issues and challenges faced in this study, it is advisable to utilise an upgraded iteration of the robot that possesses augmented capabilities and functionality, such as a robot operating on a robotic platform. The current AMoRA robot has proven its suitability throughout the experimental evaluation phase, and the existing version can be remedied either temporarily or permanently by employing an improved iteration of the robot with enhanced capabilities and accessibility.

4 Discussion/Conclusions

This study reported preliminary results from a field trial of the AMoRA autonomous radiation mapping robot. The experiment showcased the advantages of employing autonomous robots for radiation mapping, such as enhanced safety and increased precision of data. The process encompassed doing site surveys, performing manual two-dimensional mapping, and executing autonomous radiation mapping. Issues such as the limitations of item detection and constraints posed by the landscape were identified, and interim remedies were put in place. The results demonstrated the efficacy of autonomous radiation mapping, however enhancements are required. This research makes a valuable contribution to the area and lays the foundation for future progress in the mapping of radiation using robots.

References

Nur Aira Abd Rahman, Khairul Salleh Mohamed Sahari, and Mohd Zafri Baharuddin. 2023. The coverage and detection limit of a sampling point for robotics radiation mapping. *Applied Radiation and Isotopes*, 200:110968.

R. Ravishankar, T.K. Bhaumik, T. Bandyopadhyay, M. Purkait, S.C. Jena, S.K. Mishra, S. Sharma, V. Agashe, K. Datta, B. Sarkar, C. Datta, D. Sarkar, and P.K. Pal. 2013. Radiation mapping inside the bunkers of medium energy accelerators using a robotic carrier. *Applied Radiation and Isotopes*, 80:103–108.

Abd. Hafiz Zakaria, Yasir M. Mustafah, Jaafar Abdullah, Nahrul Khair, and Taufiq Abdullah. 2017. Development of autonomous radiation mapping robot. *Procedia Computer Science*, 105:81–86. 2016 IEEE International Symposium on Robotics and Intelligent Sensors, IRIS 2016, 17–20 December 2016, Tokyo, Japan.

Individual Research Contribution Review, 2023, 1(1): 425–426

IRCR

Spent Fuel Disposal Scenarios Option for Reactor TRIGA PUSPATI (RTP)

Muhammad Khairul Ariff bin Mustafa
Technical Support Division, Malaysian Nuclear Agency
43000 Kajang, Selangor
mkariff@nm.gov.my

Abstract

RTP has been in safe operation since 1982. For over 40 years, various experiments and utilizations has been conducted in RTP. RTP used standard TRIGA fuel element (FE). The fuels have been remained in the reactor core since it first criticality. When reactor need to be decommissioned, all the FE will be removed from the reactor and will be managed as the spent fuel also categorized as high-level waste (HLW). As Malaysian did not participate in Foreign Research Reactor Spent Nuclear Fuel Acceptance Program (FRR-SNF-AP), Nuklear Malaysia has responsibility to manage all the spent fuel in facility. A few scenarios have been considered to find the best solution for RTP spent fuel disposal. These scenarios have been modelled in BRIDE Tool introduced to Malaysia by IAEA in 2022 as a pilot project. BRIDE tool is a decision-making tool and the output may help the government to select the best option for the nuclear spent fuel disposal in the country. This paper will discuss about spent fuel disposal scenarios option for RTP that can be modelled in BRIDE tool.

Keywords: RTP, Spent fuel, disposal, BRIDE tool

1 Introduction

RTP has been in safe operation since 1982. For over 40 years, various experiments and utilizations has been conducted in RTP. RTP used standard TRIGA fuel element (FE). The fuels have been remained in the reactor core since it first criticality. When reactor need to be decommissioned, all the FE will be removed from the reactor and will be managed as the spent fuel also categorized as high-level waste (HLW). As Malaysian did not participate in Foreign Research Reactor Spent Nuclear Fuel Acceptance Program (FRR-SNF-AP), Nuklear Malaysia has responsibility to manage all the spent fuel in facility. These scenarios have been modelled in BRIDE Tool (Back end Research reactor Integrated Decision-making Evaluation) introduced to Malaysia by IAEA in 2022 as a pilot project. BRIDE tool is a decision-making tool and the output may help the government to select the best option for the nuclear spent fuel disposal in the country.

2 Methods

BRIDE, a multi-attribute utility methodology, serves as a tool for comparing options related to the disposition of research reactor (RR) spent nuclear fuel (RRSNF). It integrates non-economic factors with cost estimates to identify the optimum option. The process involves screening an initial scenario set to eliminate non-viable options. The remaining scenarios are then evaluated, considering both cost and various non-economic factors, leading to the selection of a preferred scenario as shown in Figure 1. BRIDE's structure ensures that the evaluation not only identifies the strengths and weaknesses of each scenario but also proposes measures to address any identified weaknesses.

To finalize the BRIDE process, the identification of scenarios for spent fuel management in Malaysia is crucial, as depicted in Figure 1 within the red box square. This identification is grounded in an assessment of technology and facility readiness both within Malaysia and globally.

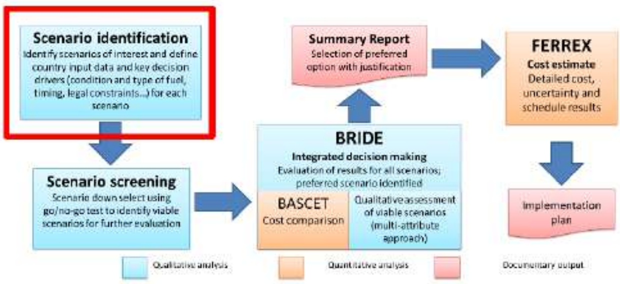

Figure 1: BRIDE flow chart

3 Result

Below are the spent fuel management scenarios has been developed as a part of BRIDE tool.

- **Scenario 1** - Direct Disposal in Borehole/ Geologic Repository. After the reactor stops operating and a cooling period of 5 years at the reactor site, SNF is transported to its immediate disposal of SNF in a Deep Borehole facility.

- **Scenario 2** - Interim Storage, Borehole/ Geologic Repository. After a cooling period of 5 years at the reactor spent fuel, the SNF is placed in a dry storage for 10 years, followed by transportation to disposal in a Deep Borehole facility.

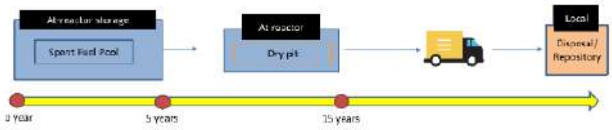

- **Scenario 3** - Conditioning and Borehole. During dry storage, a conditioning facility is built to bring the SNF into a simplified form. Efforts would be made so that the conditioned form meets the acceptance criteria of a conventional Borehole.

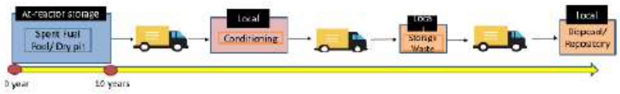

- **Scenario 4** - Reprocess and receive ILW. Engage the commercial reprocessing services of a third party who would return the equivalent intermediate level waste in a conditioned form.

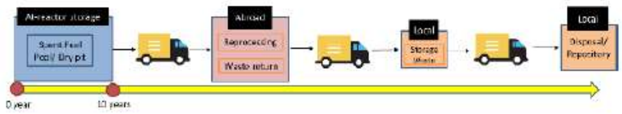

- **Scenario 5** - Transfer of waste. Engage the commercial reprocessing services of a third party to take full possession of the SNF, without waste return.

Different methods and facilities will be necessary for each scenario. International involvement is required for scenarios 4 and 5, adding complexity to the process due to the need for international legislation. The BRIDE tool will be utilized to calculate associated costs for each scenario, aiding the government in determining the most suitable option for spent fuel management in Malaysia based on scenarios and costs.

4 Conclusion

RTP has been operational for over four decades, with Nuklear Malaysia overseeing the management of all spent fuel. The BRIDE Tool will assist the government in selecting the optimal option, considering costs associated with spent fuel management.

References

Research reactor spent fuel management: Options and support to decision making. *IAEA Nuclear Energy Series No. NF-T-3.9*.

Individual Research Contribution Review, 2023, 1(1): 427–428

Centralized Interface System for Low Energy Electron Accelerator (LEEA)

Mukhlis B. Mokhtar
Technical Support Division, Malaysian Nuclear Agency
43000 Kajang, Selangor
mukhlis@nm.gov.my

1 Introduction

In Nuclear Malaysia, a localized own developed accelerator has started with Baby- EBM project in year 2002 with the initial energy of 140 keV (Ghazali et al., 2005) and then upgrade to Low Energy Electron Accelerator (LEEA) with initial energy of 250 keV. In the present status, this accelerator is under-commissioning status for upgrading the energy from 140 keV to 250 keV with the replacement of the high voltage power supply and development of the individual supporting systems such as scanning system, gas insulating system, window cooling system and etc. This replacement and upgrading subsystems need to be synchronize under one control system for an optimum energy output.

2 Methods

As illustrated in Figure 1, LEEA systems can be divided into independent subsystems, such as high voltage, vacuum system, electron gun, scanning system, and others. Scanner, high voltage, and vacuum subsystems all have their own microcontrollers that can be connected to the main program through serial communication. Once communication has been established, the main software can be used to retrieve all indication status and set operating parameters. A commercially available data acquisition boards (DAQs) is used for a subsystem that doesn't has microcontroller such as electron gun and interlock system.

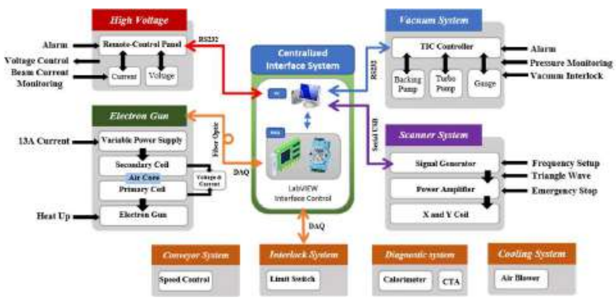

Figure 1: Block diagram of centralized interface system

3 Result and Discussions

Computer control software based on LabVIEW programming has been used to create a graphical user interface (GUI) and to control system hardware. LabVIEW is a data flow visual programming language that combines graphical development with the advantages of a programming language. It offers an intuitive environment, tightly integrated with data acquisition hardware, for user-friendly engineering solutions. Through various communication protocols, every component is connected to this software and functions as one system as a whole.

To operate all subsystems via various communication protocols, one customized LabVIEW software has been created (Figure 2). The sample irradiation process is controlled by this program, which is utilized to manage all operational parameters. This software makes it simple for the user to synchronize the subsystem.

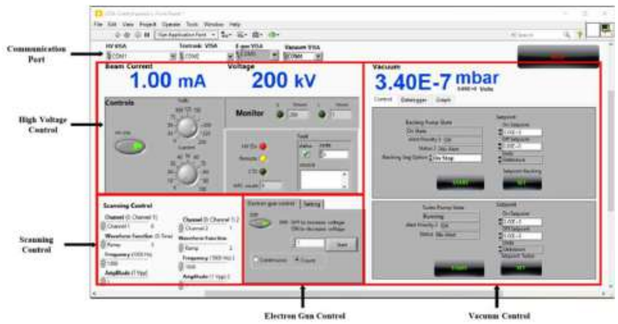

Figure 2: Front panel of centralized interface system / LEEA Control System

The software that runs an irradiation process goes through three steps. By selecting a comm port, the user first created a link between the PC and the subsystems. Once all interlock logic has been established, the next step in the procedure is to increase high voltage and electron gun current. Beam current is a function of the electron gun's heating process; as more electrons are emitted, the beam current will rise.Running a conveyor system is the third and last phase. By controlling the conveyor speed and timing, user may acquire the dose they want for their sample. As an additional safety measure, an emergency shut-off mechanism has been added in case the scanner system stops working or any interlock systems become inoperable (Ghazali, 2009).

For future works, artificial intelligence (AI) can be integrated into this control systems to enhance functionality, efficiency, and adaptability. AIpowered control systems leverage machine learning, data analysis, and decision-making algorithms to make autonomous and data-driven decisions.

4 Conclusions

By using centralized interface system, user can precisely control critical operation parameters of LEEA such as high voltage, electron gun, beam scanner and vacuum pressure. The system has incorporated user safety through an interlock system. The visual adaptability, user-friendly interfaces, dependability, and applicability to communicate with all subsystems via various communication protocols are the most crucial aspects of this centralized interface system.The centralized system has successfully irradiate lab scale sample from 10 to 100 kGy by synchronize beam energy and irradiation time.

References

A Bakar Ghazali, Razali H., S. Aiasah H, Rosli D., W Leo K, M. Rizal, Vadim V. P., M. Rizal C., M. Zahidee T., Lee C. H., and Ayub M. 2005. Some results on the development of electron beam machine. *International Meeting of Frontiers of Physics*.

Abu Bakar Ghazali. 2009. Intelligent fail safe design for failure operation of electron beam machine (EBM). *Technical Report for Nuclear Malaysia*.

Individual Research Contribution Review, 2023, 1(1): 429–430

Refurbishment and Calibration of the Conveyor for Low Energy Electron Accelerator (LEEA)

Mukhlis B. Mokhtar
Technical Support Division, Malaysian Nuclear Agency
43000 Kajang, Selangor
mukhlis@nm.gov.my

Abstract

A low-energy electron accelerator (LEEA) with energy of 200 keV and beam current of 10 mA has developed by Accelerator Development Center (ADC). At current status, LEEA has been served as an irradiation facility to support the research activities internally. For such irradiation services, a delivery system is required to ensure the absorbed dose of the sample can be determined. Therefore, a disposal conveyor system has been refurbished and calibrated. In this paper, the refurbishment and calibration process of conveyor with calibration result will be discussed.

1 Introduction

In Nuclear Malaysia, a localized own developed accelerator technology has started with Baby-EBM project in year 2002 with the initial energy of 140 keV (Figure 1a) and then upgrade to Low Energy Electron Accelerator (LEEA) with initial energy of 200 keV (Figure 1b). Since 2021, the activity to increase the energy from 140 keV to 250 keV has been initiated. With it, the high voltage power supply was replaced and individual supporting systems such as filament power supply, scanning system, gas insulating system and window cooling system were designed and developed. With the current capability of 200 keV and 10 mA, the potential applications of LEEA such as food irradiation, surface curing and coating have been identified. Such applications are required precise validated absorbed dose, therefore a delivery or conveyor system is required. Which the process of conveyor system development and calibration is discussed in next section.

1a 1b

Figure 1: **(a)** Baby-EBM Project, ~120keV, ~few μA. **(b)** Upgrading from Baby-EBM project, known as Low Energy Electron Accelerator (LEEA) 250 keV, maximum current 30mA

2 Hardware Configuration

Overall conveyor system (Figure 2) are divided to two subsystem, control subsystem (Figure 3a) and delivery system (Figure 3b) . All of the component are refurbish and redesign from existing conveyor. Control subsystem consist Hitachi L200 variable frequency drives. This is a compact motor drives and has a build in PID control function for adjusts motor speed automatically to maintain a process variable value.

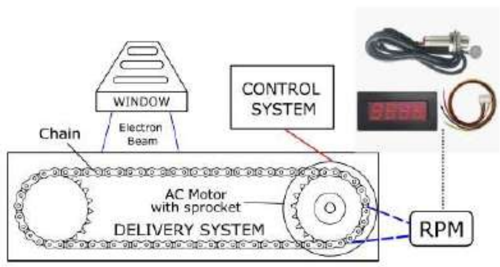

Figure 2: Conveyor system block diagram

3a 3b

Figure 3: **(a)** Control subsystem, **(b)** Delivery system

The L200 can connect to an external digital operator via the front panel (Figure 4) serial port connector. The separate keypad can be used to control conveyor. For this project, a switch and knob is connect direct to control logic terminal. Operator can control motor speed using a voltage knob (0V to 10V) and motor direction switch (forward/reverse). This control unit directly connect to a single phase motor. For future development,this L200 motor driver can be control by software via built-in RS-485 MODBUS RTU communication protocol (Hitachi Industrial Equipment Systems Co., 2004) .

For delivery system, the single phase motor is attached to metal sprocket and chain. Because of the limited space in radiation Front Panel bunker, maximum conveyor length is 2m. Later this conveyor can be upgrade to Lshape design.

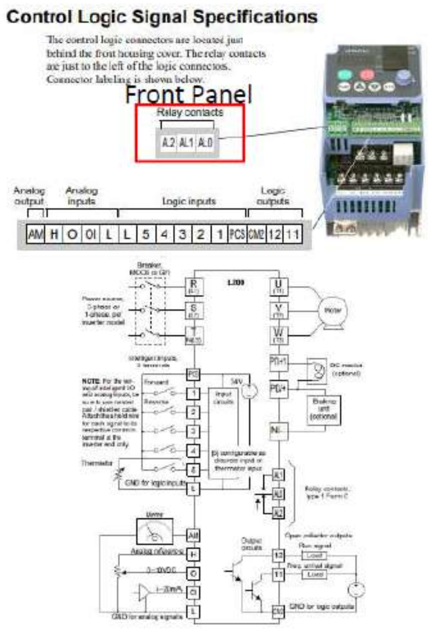

Figure 4: The control logic connectors Hitachi L200

Conveyor chain subsystem to deliver sample under electron beam window.

3 Experimental setup

One tachometer transducer was installed beside metal sprocket (Figure 2). This transducer display a revolutions per minute (RPM) on digital display. Reading from RPM are converted to speed by following formula;

$$\text{Chain speed} = \frac{T \times R.P.M}{K(\text{Ft. Per Min.})} \tag{1}$$

Where T = number of sprocket teeth,
Constant K (Pitches of Chain Per Foot)

PITCH	3/8”	1/2”	5/8”	3/4”	1”	1¼”	1½”	1¾”	2”	2½”	3”
K	32	24	19.2	16	12	9.6	8	6.85	6	4.8	4

4 Result and Discussions

Table 1 shown result conversion from RPM to speed [ms^{-1}]. This result is calculated using Equation 1 formula. Constant for T (number of sprocket) is 14 and constant K (Pitches of Chain Per Foot) is 19.2 (pitch 5/8”). Speed for foot per minutes was convert to speed per minute [$mmin^{-1}$] by divide the speed value by 3.281.

Operating voltage using Hitachi L200 inverter is from 0V to 10V, but initial voltage 3.021V is need to start AC motor. Maximum operating voltage is 10V, but starting from 8.010V, conveyor speed reach a maximum speed. Figure 5 shown a relationship between voltage and speed. From 3.021 V to 8.010V, increasing in voltage is linear with speed. This linearity can be describe as equation wheres y=0.041 x - 0.0036.

Table 1: Result conversion from RPM to speed [ms^{-1}]

Voltage	RPM	ft per min	S ($mmin^{-1}$)	S (ms^{-1})
3.021	31	22.604	6.889	0.115
3.562	37	26.979	8.223	0.137
4.000	42	30.625	9.334	0.156
4.510	48	35.000	10.667	0.178
5.006	53	38.646	11.779	0.196
5.503	58	42.292	12.890	0.215
6.011	64	46.667	14.223	0.237
6.510	69	50.313	15.335	0.256
7.010	74	53.958	16.446	0.274
7.500	79	57.604	17.557	0.293
8.010	85	61.979	18.890	0.315
8.520	85	61.979	18.890	0.315
9.000	85	61.979	18.890	0.315
9.530	85	61.979	18.890	0.315
10.060	85	61.979	18.890	0.315

Constant
T =14
K =19.2
Pitch= 5/8”

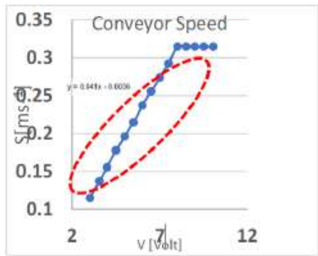

Figure 5: Speed (ms^{-1}) conversion from RPM transducer versus voltage control

5 Conclusion

Conveyor speed limited with current control. It can reach maximum speed 0.315 ms^{-1} with 8V control voltage. It is a short delivery system, wheres sample can deliver from start to the end of conveyor within 6 second (maximum speed). For targeted dose, it was accumulated during repetitive conveyor turn.

At a present setup, there is a scattering photon with conveyor metal supporting frame because of the limited space between conveyor and electron beam windows. This situation will be improved by time to time. For further work, this conveyor speed result will be use for dose mapping and PHITS (Particle and Heavy Ion Transport code System) simulation.

References

Sprocket engineering data design. *TAYLOR Material Handling and Conveyor*, page 13.

Individual Research Contribution Review, 2023, 1(1): 431–432

Autonomous Radiation Mapping: Unveiling Radiation Intensity with AMoRA

Nabilah Binti Ramli
Technical Support Division, Malaysian Nuclear Agency
43000 Kajang, Selangor
nabilah@nm.gov.my

Abstract

Autonomous radiation mapping involves employing autonomous robots to conduct radiation measurements and analysis within a specified area. Its main goal is to assess radiation intensity levels, unveil the distribution of radiation doses across the area and pinpoint potential hotspots. The experiments were conducted with a radiation mapping robot namely Autonomous Mobile Robot for Accurate Radiation Detection and Mapping (AMoRA).

1 Introduction

Radiation in work environments originates from diverse origins and if not appropriately handled, it can present health hazards to employees. Common sources include nuclear reactor and research facilities, radioactive materials, X-ray machines, and radiation therapy equipment. On top of that, there is a regulation that specifies that each licensee and employer engaged in activities associated with regular or potential occupational exposure is required to ensure the safety of their workers from occupational hazards (AELB, 2010).

In order to protect the workers from the harmful effects of radiation, it is imperative to implement safety measures and practices. These measures and practices encompass conducting risk assessments, monitoring radiation levels in the workplace and regularly inspecting and maintaining radiation-emitting equipment to ensure safety.

The primary goal of this study is to assess radiation distribution, enabling the identification of areas with higher radiation levels to be avoided during work at these facilities. This approach ensures that work activities in the selected areas can be more efficiently coordinated in accordance with the ALARA (As Low As Reasonably Achievable) principle.

2 Autonomous Radiation Mapping

AMoRA consists of a Turtlebot2 as a mobile robot platform together with a Geiger Mulller (GM) detector LND7121 as the radiation detector (Abd Rahman et al., 2020). The GM electronic module is connected to the Turtlebot2 host computer via USB connection as shown in Figure 1.

A 2D map of each selected site was created with Simultaneous Localisation and Mapping (SLAM) by running the Robot Operating System (ROS) *gmapping* package. The procedure was manually operated by personnel and created a 2D map.

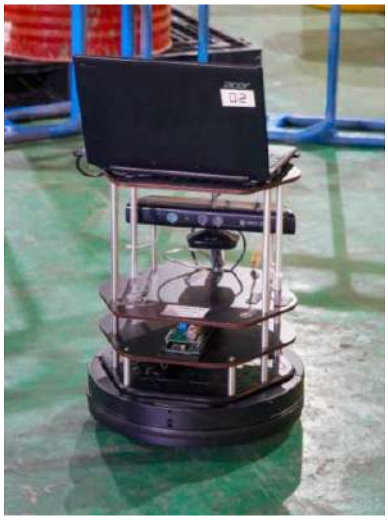

Figure 1: Complete set of AMoRA used in this study.

AMoRA is deployed to perform autonomous radiation mapping by executing the ROS *rad_mapper* package developed in the previous work (Abd Rahman et al., 2020). The *rad_mapper* divides the 2D map into a grid and generates sampling points at the centroid of each unoccupied grid cell. The counting time for data collection can be configured manually. Finally, the radiation map was generated and a corresponding report was produced.

3 Results and Discussion

The experiment was carried out at the facilities of the Malaysian Nuclear Agency under the guidance of professional supervision.

The radiation mapping at BTP Development Laboratory was executed twice. Initially during the rest state, where the radioactive material source remained in the generator with proper shielding. The result shown in Figure 2 demonstrate only background reading was detected at rest state.

After that, AMoRA was deployed again during the workload state. The workload state is the process where the radioactive source (Ga-68/Tc-99m) which is eluted from the generator and transferred into a shielded fume hood for research work. During the ongoing work, there is a concern from the employer regarding the effectiveness of the shielding in preventing radiation exposure to personnel. The results obtained clearly demonstrate the presence of radiation distri-

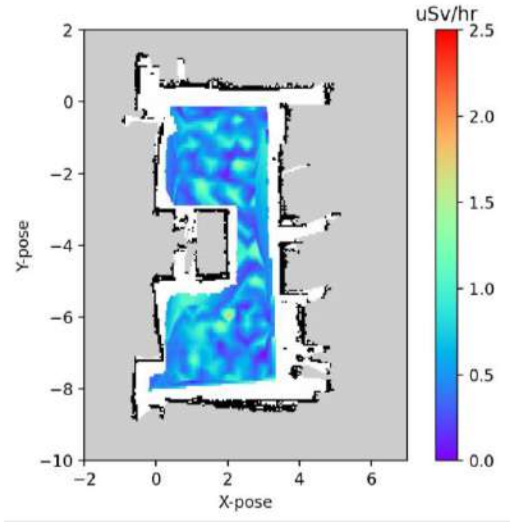

Figure 2: At rest state

bution during the work as shown in Figure 3. It proves that the radiation around the working area is slightly elevated.

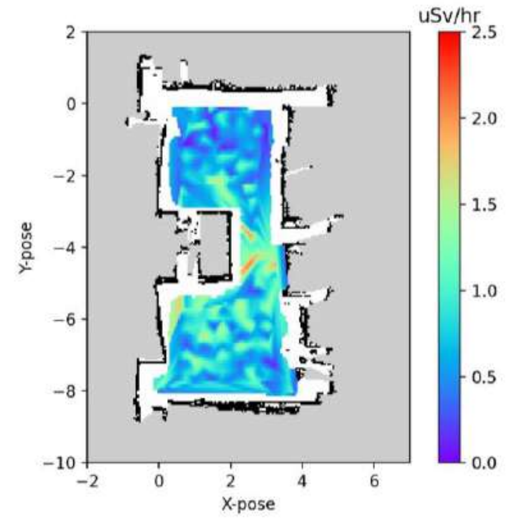

Figure 3: At workload state

Finding of this is useful for facility personnel to evaluate and coordinate the activities to ensure that the radiation exposure is within permissible limits. Based on the findings provided, employer can strategize to enhance shielding measures and restructure their work procedures to minimise radiation exposure.

4 Conclusion

As a conclusion, the results presented in this paper have demonstrated AMoRA capabilities to produce comprehensive radiation maps of the target areas. These radiation maps can be referred to effectively manage and minimise radiation exposure in the workplace, to ensure the safety compliance with local regulations and standards.

References

N. A. Abd Rahman, Sahari K. S. M., Jalal M. F. A., Rahman A. A., Abd Adziz M. I., and M. Z. Hassan. 2020. Mobile robot for radiation mapping in indoor environment. *In IOP Conference Series: Materials Science and Engineering*, 785(1):012021. IOP Publishing.

N. A. Abd Rahman, Sahari K. S. M., Hamid N. A., and Y. C. Hou. 2022. A coverage path planning approach for autonomous radiation mapping with a mobile robot. *International Journal of Advanced Robotic Systems*, 19(4):17298806221116483.

AELB. 2010. Atomic Energy Licensing (Basic Safety Radiation Protection) Regulations.

Individual Research Contribution Review, 2023, 1(1): 433–434

Radioisotope Identification System Performance Testing and Assessment at Reaktor TRIGA PUSPATI

Na'im Syauqi Hamzah
Technical Support Division, Malaysian Nuclear Agency
43000 Kajang, Selangor
naimsyauqi@nm.gov.my

Abstract

The performance of two-unit radioisotope identification systems at Reaktor TRIGA PUSPATI (RTP) were assessed using single radionuclide sealed sources, mixes sealed sources and standard fresh fuel element. The detection abilities were also test under high background level, different geometry set-up and presence of shielding materials.

Keywords: Radioisotope Identification System, Reaktor TRIGA PUSPATI, Radionuclide, Nuclear Material

1 Introduction

The detection and identification of radiological and nuclear threats is essential to support national nuclear defense and security programme. The radioisotope identification system must be able to reliably identify a wide range of radionuclides, including of natural occurring radioactive material (NORM), industrial and medical radioactive material, and special nuclear material (SNM). The growing sophistication, availability and adaptability of radioisotope identification systems that use algorithm embedded in the detector has been very useful to detector users. For instance, automatic background suppression and rejection function is able to discriminate surrounding background radiation data. The other way around, without clear understanding on the strength and limitation of how the decisions are made by the algorithm, this might lead to introduction of unintended effect of ignoring indication of possible threat and false identification of radionuclides.

2 Methods

The performance of radioisotope identification systems at Reaktor TRIGA PUSPATI were assessed using various disc shape radionuclide sealed sources and Standard TRIGA nuclear fuel element. The ^{235}U enrichment of SNM is about 19.9%. Among the radionuclide seal sources used are ^{60}Co, ^{137}Cs, ^{133}Ba, ^{152}Eu, and ^{241}Am. The proficiency of radioisotope identification systems was determined through numerous testing condition. This includes of testing the identification capability of single-nuclide sealed sources, multi-nuclide sealed sources and nuclear material. An additional testing was also performed to observe the detection capability under various geometry set-up (different distance of radionuclide to the detector), high radiation background condition and application of shielding materials.

3 Results and Discussion

Initially, the detection performance of identification system at RTP were determine using single and mixes sealed sources. As shown in Table 1 and Table 2, ORTEC and FLIR detectors were successfully identify all single radionuclides. Though, it was found that ORTEC detector measured higher count rate (cps) values compared to FLIR detector (approx. 2 to 4 times larger). For the following test, ORTEC detector was able to detect all five radionuclides in mix sealed source samples, whereas FLIR detector can only detect dominant / high radioactivity radionuclides (Cs-137 and Eu-152). At certain distant, FLIR detector identify Ba-133 radionuclide as a combination of Ba-133 and I-131 due its poor energy resolution characteristic. Another significant finding, ORTEC detector was able to identify radionuclides immediately whereas FLIR detector need longer period of time (<60 seconds).

Table 1: Detection capability of single and mix sealed sources for ORTEC detector

Distance	RADIONUCLIDES IDENTIFICATION STATUS					
	Am-241	Eu-152	Ba-133	Cs-137	Co-60	MIX
0 cm	✓	✓	✓	✓	✓	✓
5 cm	✓	✓	✓	✓	✓	✓
10 cm	✓	✓	✓	✓	✓	✓
15 cm	✓	✓	✓	✓	✓	✓
20 cm	✓	✓	✓	✓	✓	✓
25 cm	✓	✓	✓	✓	✓	✓
30 cm	✓	✓	✓	✓	✓	✓

Table 2: Detection capability of single and mix sealed sources for FLIR detector

Distance	RADIONUCLIDES IDENTIFICATION STATUS					
	Am-241	Eu-152	Ba-133	Cs-137	Co-60	MIX
0 cm	✓	✓	✓	✓	✓	✗
5 cm	✓	✓	✓	✓	✓	✗
10 cm	✓	✓	✓	✓	✓	✗
15 cm	✓	✓	✓	✓	✓	✗
20 cm	✓	✓	✓	✓	✓	✗
25 cm	✓	✓	✓	✓	✓	✗
30 cm	✓	✓	✗	✓	✓	✗

The detectors were then tested with SNM sources. Based on the result shown in Table 3 and Table 4, it was found that

ORTEC and FLIR detectors might reporting false results if the count rates are too low. FLIR detector start giving an unstable result at measurement above 100cm and completely unable to identify SNM from TRIGA fresh fuel at distance above 200cm.

Table 3: Detection capability of special nuclear material of standard TRIGA fuel

SOURCE	DISTANCE	FLIR	ORTEC
STANDARD TRIGA FUEL	10 cm	Uranium	U-235, U-238
	50 cm	Uranium	U-235, U-238
	100 cm	Uranium	U-235, U-238
	150 cm	Uranium, Ir-192,Eu-152, Na-22, Th-232/U-232	U-235, HEU, Co-60
	200 cm	Annh., Ir-292, K-40	U-235
	245 cm	unknown	U-235

Table 4: Detection capability of standard TRIGA fuel and Cs-137 radioactive source

SOURCE	DISTANCE	FLIR	ORTEC
STANDARD TRIGA FUEL & Cs-137	10 cm	Cs-137, Uranium	U-235, Cs-137
	50 cm	Cs-137, Uranium	U-235, Cs-137
	100 cm	Cs-137, Uranium, K-40	U-235, Cs-137
	150 cm	-	U-235, Cs-137, Co-60

From the result shown in Table 5 and Table 6, it can be concluded that the detection capability of radionuclides in shielding environment depends on several factors including of shielding thickness, types of shielding materials and gamma energy. As discussed previously, FLIR detector shown similar limitation on 'resolution' aspect and fail to identify Eu-152 and Ba-133 in certain experiment set-up. In the final test, as shown in Table 7, ORTEC detector was found to be able to identify low radioactivity radionuclides in high radiation background environment despite recording high 'dead time' values. Even so, repetition of similar measurement can potentially reduce the efficiency and life time of the detector.

Table 5: Detection capability in shielding environment for ORTEC detector

Plate Material	RADIONUCLIDES IDENTIFICATION STATUS				
	Am-241	Eu-152	Ba-133	Cs-137	Co-60
1pcs Pb	✗	☑	☑	☑	☑
1pcs Al	☑	☑	☑	☑	☑
1pcs Cu	☑	☑	☑	☑	☑
2pcs Cu	✗	☑	☑	☑	☑
5pcs Cu	✗	☑	☑	☑	☑
10pcs Al	☑	☑	☑	☑	☑

Table 6: Detection capability in shielding environment for FLIR detector

Plate Material	RADIONUCLIDES IDENTIFICATION STATUS				
	Am-241	Eu-152	Ba-133	Cs-137	Co-60
1pcs Pb	✗	☑	✗	☑	☑
1pcs Al	☑	☑	☑	☑	☑
1pcs Cu	☑	☑	☑	☑	☑
2pcs Cu	✗	✗	☑	☑	☑
5pcs Cu	✗	☑	☑	☑	☑
10pcs Al	✗	☑	☑	☑	☑

Table 7: Detection capability in high background environment

HIGH BACKGROUND SOURCE	SOURCE AND DISTANCE	FLIR	ORTEC
High radioactivity Cs-137 sealed source located at detector surface	Co-60 (0cm)	✗	☑
	Co-60 (15cm)	✗	☑
	Co-60 (30cm)	✗	☑
	Eu-152 (0cm)	☑	☑
	Eu-152 (5cm)	✗	☑
	Eu-152 (15cm)	✗	☑
	Eu-152(30cm)	✗	☑

4 Conclusion and Future Work

The radioisotope identification systems at Reaktor TRIGA PUSPATI are able to identify various radioactive and special nuclear material which subject to certain limitation of the detector proficiencies. In general, ORTEC detector was observed to have higher detection capability whereas FLIR detector was significantly lighter, mobile and able to work with high activity radionuclides (due to low dead time values). Both detectors were proficient to be used in routine safeguard inspection activities, but careful consideration must be taken in more complex emergency situations.

References

FLIR. 2015. Identifinder R400 user manual.

ORTEC. 2014. Portable neutron and gamma nuclide identifinder user manual.

Individual Research Contribution Review, 2023, 1(1): 435–436

Arduino Temperature Monitoring: Programming and System Implementation

Noor Farhana Husna Binti A Aziz
Technical Support Division, Malaysian Nuclear Agency
43000 Kajang, Selangor
farhanahusna@nm.gov.my

Abstract

The temperature monitoring system is designed to gather temperature-related data in a specific situation or environment. This study concentrates on implementing a temperature monitoring system tailored for observing temperature variations in High Purity Germanium (HPGe) semiconductor detectors during maintenance procedures. The project aims to streamline the data recording tasks for personnel, allowing them to monitor temperatures with minimal disruption to their workflow. This paper will explore the programming elements of the temperature monitoring system.

Keywords: Arduino UNO, Temperature, Monitoring

1 Introduction

Arduino, is an open-source microcontroller known for its ease of programming, erasing, and reprogramming. It was created to provide an affordable and straight forward solution for students and professionals to build devices that interact with the environment using sensors and actuators.

Arduino IDE can program Arduino microcontroller. Arduino IDE is a tool to write a program for Arduino boards. Arduino IDE is open-source software that can be downloaded and installed on the computer is free.

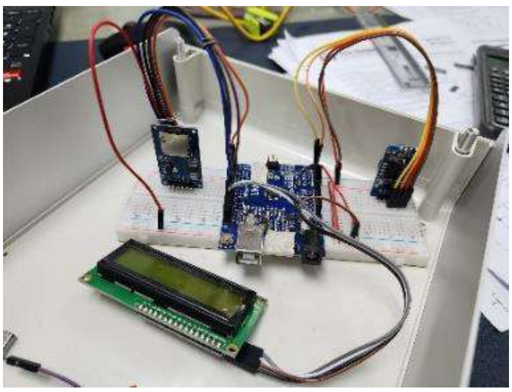

Figure 1: Completed installation module of temperature monitoring system.

Arduino IDE provides many ready-to-use libraries. Using these libraries Arduino developers will save a lot of time. In this project, we used Arduino UNO. The function of Arduino UNO is as the central hub for processing input signals. Figure 1 depicts the interconnection of an Arduino UNO with additional modules, forming a temperature monitoring system.

2 Methods

The main idea of this system is to display and save the resistance and temperature readings automatically and show the readings on the LCD including the current time. The project methodology is divided into two segments: hardware implementation and code description.

2.1 Hardware Implementation

The hardware configuration comprises a circuit connecting the Arduino UNO, a 1602A LCD Module, an RTC Module, and a Micro SD Card Module as shown in Figure 2. Information is acquired through the field effect transistor (FET) component of the HPGe, wherein resistance measurements are subsequently transformed into current temperature readings utilizing a predetermined equation.

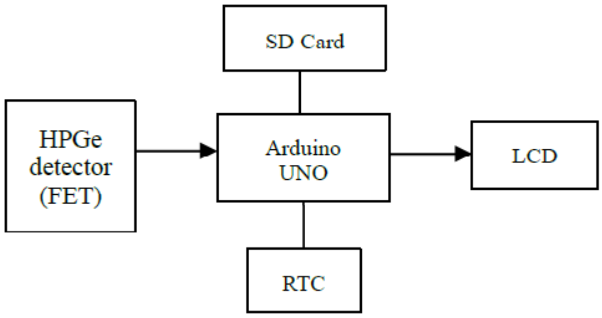

Figure 2: Block Diagram of Temperature Monitoring System.

Arduino UNO board is a microcontroller board based on the ATmega328. RTC is the system clock, that is necessary to make the device performs real time monitoring. The LCD serves as the unit for displaying system output, enabling users to view real-time measurements. The SD module is used as data logger.

2.2 Code Description

The program code written for Arduino is known as a sketch. The first process for code description is to determine the required libraries, relevant definitions and constant variables declaration as shown in Figure 3. In this system, we used four libraries and declare the variables integers (int) and floating-point numbers (float).

```
#include <LiquidCrystal_I2C.h>
#include <SPI.h>
#include <SD.h>
#include <RTClib.h>
```

```
int Vin = 5;
float Vout = 0;
float R1 = 360;
float Rfet = 0;
int a2d_data = 0;
float buffer = 0;
int i = 20;
```

Figure 3: Includes, Defines, Constant and variables declaration

There are two main functions in every sketch. The first function is, **void setup()**. The first function to be executed, mainly takes care of the pin mode configurations and displays as shown in Figure 4. It also contains the initialization of the serial monitor, display and SD card. A serial monitor is used to know the data that are being sent serially to any peripheral device.

```
void setup() {
  rtc.begin();
  lcd.init();
  lcd.backlight();
  lcd.createChar(0, omega);
  Serial.begin(9600);
  pinMode(A1, INPUT);
```

```
Serial.print("SD Card init...");
if (!SD.begin(4)) {
  Serial.println("init failed..")
  while (1);
}
Serial.println("init ok");
```

Figure 4: Code description in void setup()

The second function is **void loop()** This function is set to run repeatedly on the Arduino, commencing immediately after the completion of setup() and its associated subfunctions, and persisting until the program is stopped or reset. Consequently, any functions will be called from void loop() or its subfunctions will likewise be executed continuously.

This feature enables the mathematical calculations within this function. In this project, we used the interpolation formula from DME data to get the temperature reading, given in Equation:

Temperature = 0.506 (Resistance) - 256.19

```
void loop() {
  a2d_data = analogRead(A1);
  if (a2d_data) {
    buffer = a2d_data * Vin;
    Vout = buffer / (1023.0);
    buffer = Vout / (Vin - Vout);
    Rfet = R1 * buffer;
    float T = (0.506 * Rfet) - 256.1
  data.print(" Rfet: ");
  data.print(Rfet);
  data.print(" Ω ");
  data.print("      ");
  data.print("T: ");
  data.print(T);
  data.println(" C ");
```

```
if (i == 200) {
  SD.end(); // close SD card
  delay(10000); // wait 10 seconds
  SD.begin(4); // reinitialize SD card
  data = SD.open("data.txt", FILE_WRITI
  if (data) {
    DateTime now = rtc.now();
  lcd.print(T);
  lcd.setCursor(13, 1);
  lcd.print((char)223);
  lcd.print("C");
  delay(3000);
  lcd.clear();
```

Figure 5: Code description in void loop()

The void loop() function have been ordered in accordance to their order in the flow of execution of the program as shown in Figure 5. In this section as well, include "data.print" and "lcd.print" to store and display data on the LCD respectively. The program code for saving data every 10 minutes and displaying data every 3 seconds are also incorporated in this section.

3 Results and Discussion

The testing of the Arduino program code was carried out successfully. Each module has been thoroughly tested and has proven to function successfully. The resistance and temperature with time readings were effectively shown on the LCD display and data was stored in SD card as shown in Figure 6(a) and 6(b) respectively.

(a)

23/8/2023 12:34:42	Rfet: 336.18 Ω	T: -86.08 C
23/8/2023 12:53:42	Rfet: 318.23 Ω	T: -95.16 C
23/8/2023 13:4:6	Rfet: 318.23 Ω	T: -95.16 C
23/8/2023 13:14:31	Rfet: 295.38 Ω	T: -106.77 C
23/8/2023 13:24:56	Rfet: 281.60 Ω	T: -113.78 C
23/8/2023 13:35:22	Rfet: 264.28 Ω	T: -122.58 C
23/8/2023 13:45:47	Rfet: 257.92 Ω	T: -125.68 C
23/8/2023 13:56:12	Rfet: 247.72 Ω	T: -130.84 C
23/8/2023 14:6:37	Rfet: 238.83 Ω	T: -135.34 C
23/8/2023 14:17:2	Rfet: 232.09 Ω	T: -138.75 C
23/8/2023 14:27:27	Rfet: 223.65 Ω	T: -143.03 C
23/8/2023 14:37:52	Rfet: 215.44 Ω	T: -147.18 C
23/8/2023 14:48:18	Rfet: 193.80 Ω	T: -158.12 C
23/8/2023 14:58:43	Rfet: 190.49 Ω	T: -159.80 C
23/8/2023 15:9:8	Rfet: 189.67 Ω	T: -160.22 C

(b)

Figure 6: (a) Data display on the LCD (b) Data saved in SD Card

This Arduino programme code also successfully demonstrated the ability to display data every 3 seconds on LCD and store data every 10 minutes with time stamp.

4 Conclusion

The Arduino programme code was successfully programmed for temperature monitoring system. The system can monitor resistance and temperature in real time, record and save the data in an SD card for every 10 minutes while displaying the current reading for every 3 seconds on the LCD screen.

References

Alisher Shakirovich Ismailov and Zafar Botirovich Jo'rayev. 2022. Study of Arduino microcontroller board. *Science and Education Scientific Journal*, 3(3):172 – 179.

Kyi Kyi Khaing, K. Srujan Raju, G. R. Sinha, and Wit Yee Swe. 2020. Automatic temperature control system using Arduino. *Advances in Intelligent Systems and Computing*, 1090(1):219 – 226.

Leo Louis. 2016. Working principle of arduino and using it as a tool for study and research. *International Journal of Control, Automation, Communication and Systems.*, 1(2):21 – 29.

Individual Research Contribution Review, 2023, 1(1): 437–438

Proof of Concept for High Voltage Circuits for Radiation Detection Device

Nor Arymaswati Abdullah
Technical Support Division, Malaysian Nuclear Agency
43000 Kajang, Selangor
arymas@nm.gov.my

Abstract

Various detectors, such as ionizing chambers, proportional counters, Geiger Mueller (GM) counters, and luminescence detectors, are employed for ionizing radiation detection. The activation of ionizing radiation detectors involves applying high voltage. Each detector requires a specific high voltage during operation. Hence, the aim of this project is to proof a versatile high voltage module inhouse that capable of supporting detectors like HPGE or ion chambers, as well as smaller ones like the GM tube. The outcomes indicate that the module can generate high voltages up to 2,000V.

1 Introduction

Many ionizing radiation detectors rely on the application of high voltage to initiate their operational state. There are different types of detectors used in ionizing radiation detection such as ionizing chambers, proportional counters, Geiger Mueller (GM) counters, and luminescence detectors. Each of these detectors requires a different high voltage value when operating. Therefore, this project is to develop in-house of wide range high voltage (HV) modules. Not only to support for small detector such as GM tube but these modules will be able to support detectors such as HPGE or ion chamber as well. Hence, the objective of this project is to develop internally a versatile range of HV modules. These modules will not only cater to small detectors like GM tubes but also provide support for larger detectors such as HPGE or ion chambers. This initiative aims to not only save costs but also facilitate HV applications in other projects and foster in-house skill development.

2 Methodology

The circuits design for this study were based on (Abdullah et al., 2021) with higher voltage output. Next, is the selection of the components. This stage is crucial because in order to determine the PCB layout, performance, electronics design, etc. Numerous problems will occur due to poor component selection. Before fabricating the Printed Circuit Board (PCB) for the dedicated circuit, the components were assembled on the breadboard to test the circuits. This experimenting process can give the preliminary expected voltage output. Figure 1 shows the flow of the high voltage circuit process development.

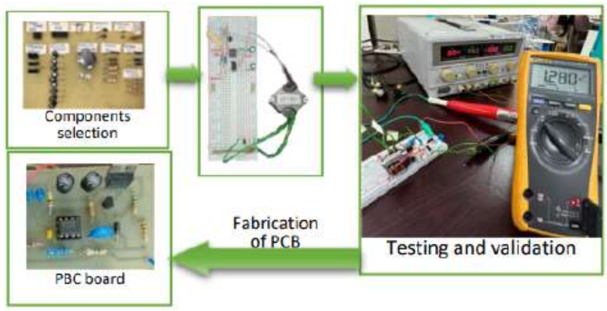

Figure 1: Flow of High Voltage Process Development

3 Results and Discussion

This paper shares two types of circuits. One circuit that uses a transformer integrated with a multiplier to increase the voltage up to 3000V and the other one is a circuit assembled with inductors to generate 450V and 500V. All of these voltages are identified based on GM tube specifications and the expected output based on HV in the detector used in Nuclear Malaysia (NM).

Nevertheless, due to limited access and availability of electronics components in the lab, the design process did not result in the expected output aligned with the objective. Therefore, these circuits require more exploration due their unstable output and relatively high power consumption, including noise that interferes with signal flow. Table 1 demonstrates the results for various transformer configuration and inductor in HV circuit.

4 Conclusion

As of now, the applications for 500V had been implemented in the Low Cost Survey Meter for Educational project. Due to optimum voltage of the new GM tube, the HV was modified into 450V from 500V. This circuit uses an inductor as a storage electric energy that supplied by the voltage source. On the other hand, the circuit utilizing the transformer step up the voltage at second winding of the transformer. This HV circuit have been prove that the circuit be able to produce up to 2911V. Figure 2 presents the application of the HV that were developed and utilized in NM products i.e. survey meters.

Table 1: Results for various transformer configuration and inductor in HV circuit

Transformer turn	Resistance (Ohm)	HV value (V)
15:3100	1.7:128k	1531
25:3100	1.2:285	2911
20:2600	2.0:243	2130
50:3100	4.2:280	1220
30:1000	2.2:112.9	1119
25:1500	2.3:112.9	1870
50:1500	3.3:121.3	1280
150:1700	9.4:138.3	234

Transformer turn	Resistance (Ohm)	HV value (V)
NIL (replaced with inductor)	19.95k	241
	17.66k	255
	11.04k	305
	6.29k	355
	2.77k	405
	3.8	455

Figure 2: The applications of HV in Nuclear Malaysia products

References

Nor Arymaswati Abdullah, Glam Hadzir Patai Mohamad, Nolida Yussup, Noor Farhana Husna, Nur Aira Abd Rahman, Khairul Salleh Mohamed Sahari, and Muhammad Fairuz Abdul Jalal. 2021. Power consumption comparison in three experimental circuits for radiation detection. *IOP Conf. Series: Materials Science and Engineering*, 1106:1 – 7.

Bob Dobkin and Jim Williams. 2011. Analog circuit design: A tutorial guide to applications and solutions. *Linear Technology and Newnes*.

Doug Sinclair and Jonathan Dyer. 2013. Radiantion effects and COTS parts in smallsats. *27th Annual AIAA/USU Conference on Small Satellites*, pages 1 – 12.

Individual Research Contribution Review, 2023, 1(1): 439–440

Boron Neutron Capture Therapy Implementation at Reaktor TRIGA PUSPATI

Norfarizan Mohd Said
Technical Support Division, Malaysian Nuclear Agency
43000 Kajang, Selangor
norfarizan@nm.gov.my

Abstract

Boron Neutron Capture Therapy (BNCT) is a promising cancer treatment modality that utilizes thermal neutrons to induce tumor cell death in less toxic environment. Research reactor is one of the reliable neutron sources for BNCT implementation. The use of research reactors has allowed researchers to optimize treatment parameters and develop more effective neutron capture agents. The study aims to propose Reaktor TRIGA PUSPATI (RTP) as a neutron source for BNCT procedure.

Keywords: Boron Neutron Capture, research reactor, cancer treatment

1 Introduction

RTP has been safely operated for more than 40 years and utilized for various R&D activities, irradiation services, and training programs. However, RTP has one available beam port and a thermal column being unutilized and ready for new applications. The motivation to conduct this study is to increase the utilization factor of the TRIGA MARK II reactor by housing a Boron Neutron Capture Therapy (BNCT) facility in Malaysia.

BNCT is a targeted radiation approach that enables the selective killing of malignant cells by sparring surrounding healthy cells. The technic is suitable for highly invasive tumors that difficult to treat and have particularly poor prognosis recurrence after radiotherapy. Reactor-based BNCT showed relatively good local control, tumor shrinkage, and favorable survival along with acceptable safety for recurrent and refractory high-grade tumor or cancer patients in poor condition. In order to give light on the viability of using RTP as the neutron source for BNCT, this study considers both the physical and biological aspects of the endeavor to establish the facility in Malaysia.

2 Methods

The study involved three phases as shown in Figure 1. The first phase is knowledge acquisition especially in terms of important physical and biological aspects of reactor-based BNCT, beam design and dose estimation and quantification of boron compound concentration and delivery agent for BNCT application.

The second phase is the model development and simulations which include RTP model with related specification of the thermal column and beam ports, verification using experimental results and from citation, and optimization of the beam design and dose estimation. Simultaneously, quantification of boron compound concentration and delivery agent will be performed using imaging technique and experiments. The final phase is the discussions of the results and analysis.

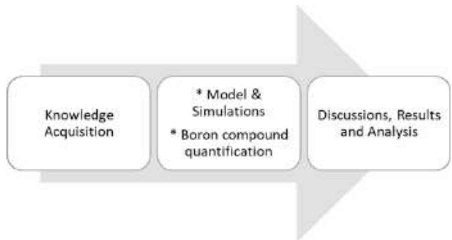

Figure 1: Flowchart showing the work phases

3 Results

A literature review has been conducted by looking into the physical and biological aspects of the reactor-based BNCT. The important physical factors determined are the neutron source, neutron beam and facility design. Meanwhile, boron compound, neutron beam optimization and characterization, and the biological effects are important factors need to be considered in biological aspects. The review paper has been presented in Norfarizan et al. (2023).

More details review on different design and characterization of BNCT facility available in other countries were reported in Norfarizan and Siti (2018). Neutron beam optic model and simulation for BNCT facility at RTP has been developed using McSTAS software and presented in Norfarizan et al. (2021). A research proposal were submitted for application of Fundamental Research Grant Scheme (FRGS) in the year 2020 were rejected at the final level of the Ministry of Higher Education (KPT) evaluation (Norfarizan et al., 2020).

Furthermore, several experiments utilizing human cell cultured were conducted to explore the impact of the neutron radiation exposure to the cells. The cultured cells used were MCF-7 and MDA-MB breast cancer cells, and glioblastoma brain cancer cells. Typical cell culture workflow is shown in Figure 2.

4 Conclusions

An efficient cell culture workflow involves checking the cell confluence, which is a routine measurement used to track

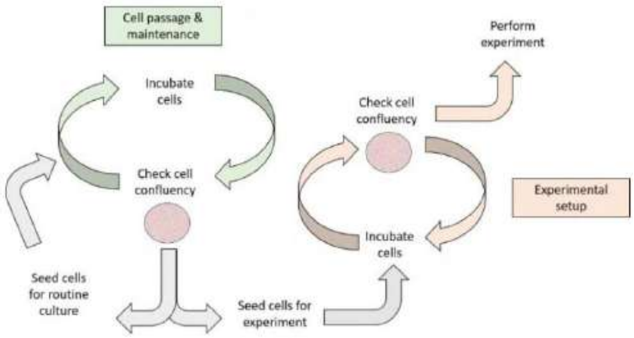

Figure 2: Typical cell culture workflow. (Image source: https://bitesizebio.com/63887/cell-confluency)

cell proliferation during cell culture before experimental use. Figure 3 shows the cell's figure in confluence condition under the microscope.

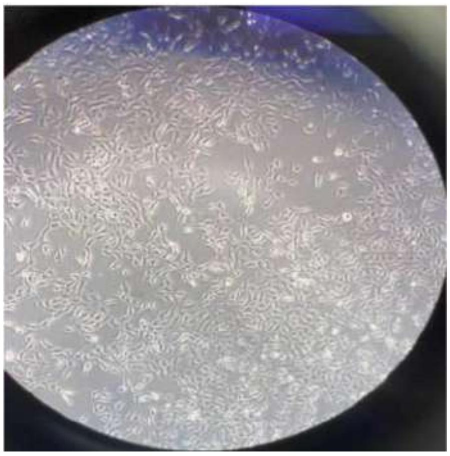

Figure 3: Cells in confluence condition

Clonogenic study was performed to observe the growth of the cells after the neutron irradiations. The result for MCF- 7 and MDA-MB cells were shown in Figure 4.

The investigation found that the growth of the irradiated cells had clearly declined especially for MCF-7 cells. However, this experiments are a preliminary approach to grasp the essence of the research.

The experiments were carried out under a project entitled "The impact of neutron radiation using RTP on the viability of tumor" which involved three industrial training students from University of Putra Malaysia (UPM) and International Islamic University Malaysia (IIUM). Two research officers from Agrotechnology and Biosciences Division (BAB) and Medical Technology Division (BTP), respectively, were also participated in the project.

5 Conclusions and Future Work

The feasibility study on BNCT implementation at RTP enquire thorough investigation on the physical and biological aspects. Some issues encountered during the experiments conduct brought to light a few crucial areas that needed to be

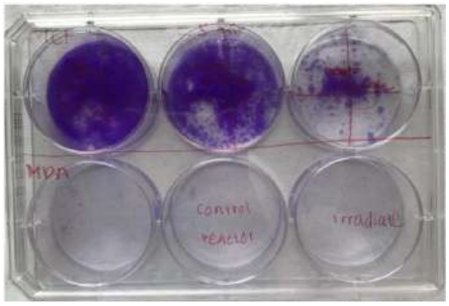

Figure 4: Clonogenic Study for MCF and MDA-MB breast cancer cells after five minutes irradiation

improved in order to carry out the study in the future. The study will enter the second phase in which more model development and simulations will be perform to investigate the physical aspects of the reactorbased BNCT implementation. Boron compound quantification and more experiments will also be conducted for the future work.

References

M.S. Norfarizan and F.M. Siti. 2018. Review on neutron beam instrumentation at research reactor: Boron neutron capture therapy. *NUKLEARMALAYSIA/L/2018/178*.

M.S. Norfarizan, A. Norma, M.I. Faridah, and S.Y. Siti. 2020. Invasion model of brain tumor cell and its response to boron neutron capture therapy using reaction-diffusion equation (Application ID: 355608).

M.S. Norfarizan, S.H. Naim, R. Nurhayati, M.I Faridah, and A.K. Julia. 2021. Neutron optic simulation for boron neutron capture therapy facility of TRIGA PUSPATI reactor using McSTAS. *[Online Paper presentation]. International Nuclear Science, Technology and Engineering Conference (iNuSTEC2023).*

M.S. Norfarizan, M.I Faridah, and A.K. Julia. 2023. Boron neutron capture therapy implementation at research reactor: Physical and biological aspects. *[Paper presentation]. International Nuclear Science, Technology and Engineering Conference (iNuSTEC2023).*

S.S. Nur. 2022. Student weekly log sheet, Biomedical practicum at Agensi Nuklear Malaysia.

A. Nurfarhanah. 2022. Engineering industrial training at Agensi Nuklear Malaysia report.

N.J. Nurin. 2022. Student weekly log sheet, Biomedical practicum at Agensi Nuklear Malaysia.

Individual Research Contribution Review, 2023, 1(1): 441–442

Digital Repository System of Reactor Experience, Expertise and Explicit Knowledge (DiR3X)

Norfarizan Mohd Said
Technical Support Division, Malaysian Nuclear Agency
43000 Kajang, Selangor
norfarizan@nm.gov.my

Abstract

Reaktor TRIGA PUSPATI (RTP) has been safely operated for more than 40 years. Throughout the years, the experience, expertise and explicit knowledge related to RTP have been shared and collected via several platforms such as seminar, symposium, physical documentations, databases, share folders and share point. However, the shared knowledge and collected information is not organized and controlled systematically. As a result, the location of the information is uncertain and difficult to find. Furthermore, same information in several different files is resulting in a loss of storage capacity. Therefore, we propose new digital repository system of reactor experience, expertise and explicit knowledge known as DiR3X.

Keywords: Knowledge management, digital repository system

1 Introduction

Digital repository is a significant instrument for knowledge management in modern technologically advanced world. It is a digital collection where content is added either by the owner, the author, or a third party, and the repository architecture handles both content and metadata. The digital items in the repository, which are the electronic equivalent of library stacks, require special storage and management to be properly preserved and to maintain their integrity over time.

DiR3X is developed to help in identifying, collecting, managing, disseminating, archiving and preserving the knowledge and information related to RTP in more systematic approach. It is created using the Python programming language as it offers flexibility and versatility, particularly in terms of interface design, architecture, display, and control settings. Prior to the code development, all available knowledge and information with its designated locations, are identified and categorized accordance with the predetermined modules. To ensure thorough, accurate and pertinent mapping and design of the repository, due diligence is performed.

2 Methods

The key feature of effective digital repositories is centralization. DiR3X offers a wide range of digital courseware that has been carefully selected from several sources and is held in a central location where it can be labelled and shared by users using a single, standardized interface.

This enables users to find the knowledge they require while also allowing repository administrators, the Reactor Technology Centre Knowledge Management Team (KMPTR), to maintain intellectual control. Thus, the repository is sustainable and trusted, well-supported and well-managed. The flowchart of the process is presented in Figure 1.

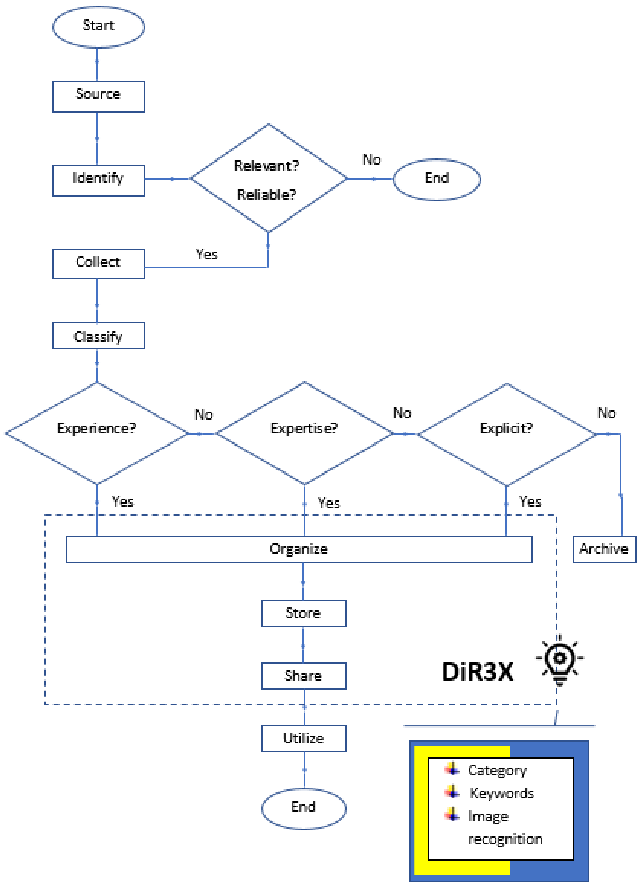

Figure 1: Flowchart of DiR3X process

3 Results

The project is conducted in phases. The early phase of the study is aim to determine the source of knowledge and information available in PTR and where it stored. It is figured out that some documents containing valuable information were stored only in physical folders. This condition increase the risk of losing them. Therefore, we decided to start digitalizing the information in order to preserve them. It also improves productivity by leveraging technology, processes, and organizational culture to better share, apply, create, capture and store knowledge. KMPTR is committed on deployment of transition from physical to virtual (Norfarizan and Nurhayati, 2021).

Some documents are available in share folders and share points. However, the storage capacity became an issue. We take the initiative to identify and make the sorting based on the relevancy and reliability of the documents. The documents and folders that fail to meet the specified criteria were removed. Meanwhile, the documents that meet the criteria are categorized according to the DiR3X system classification. External hard disk and server are also utilized to ensure smoother process. Currently, DiR3X were located in the reactor share folder as shown in Figure 2.

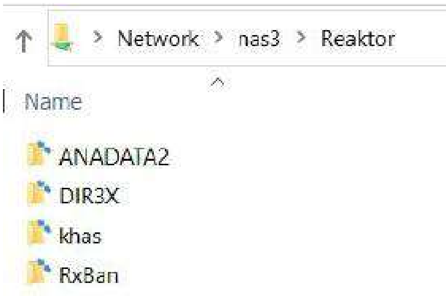

Figure 2: Location of DiR3X

One of the challenging part is dealing with the photos and images. The main reason for this is due to no standard ways were set to name the files. Therefore an exploration study are conducted on image classification technique which involve big data management and machine learning. The preliminary work are presented in Norfarizan et al. (2022).

4 Conclusions and Future Work

In conclusion, organized information, subject classification and indexing, quick and flexible discovery, information sharing discipline, and preservation of explicit knowledge are major characteristics of DiR3X and its significance to RTP's knowledge management system. Next phase of the project would be focused on the development of the graphic user interface (GUI) of the system and image classification tools.

References

M.S. Norfarizan and R. Nurhayati. 2021. Pusat Teknologi Reaktor (PTR) physical to virtual knowledge management. *Pertandingan Poster Hari Pengurusan Pengetahuan (KM).*

M.S. Norfarizan, Nurhayati R., Khairulezwan A.M., Muhammad Khairul Ariff Mustafa, Tonny Anak Lanyau, Na'im S.H., Mohd H.H., and Shahril M.S. 2022. Digital repository system of reactor experience, expertise and explicit knowledge (DiR3X). *Pertandingan Kreativiti Perkhidmatan, Hari Inovasi dan Kreativiti (HIKNM2022).*

Individual Research Contribution Review, 2023, 1(1): 443–444

Optimization of Si Back-to-Back Schottky Junction Diode Photolithography Process

Norizam Saad
Technical Support Division, Malaysian Nuclear Agency
43000 Kajang, Selangor
norizam@nm.gov.my

Abstract

In this paper, we discussed the photolithography process optimization of silicon (Si) back-to-back schottky diode (BBSD) using the photolithography system available at Semiconductor Nuclear Detector Fabrication Laboratory in Malaysian Nuclear Agency. The parameters affecting BBSD pattern developed on Si sample or substrate from identical to the BBSD pattern on the photomask are thoroughly analyzed and an economic approach improving the photolithography process is presented.

Keywords: Photolithography process, mask aligner, transfer pattern

1 Introduction

Photolithography or optical lithography is a process of creating patterns with photoresists that may achieve high product resolution (Ismail et al., 2023). It's often applied to semiconductor manufacturing of microchips and commonly used for fabricating micro-electro-mechanical-systems (MEMS) devices. A typical photolithography process contains several steps to fabricate device from layer grown on substrate or wafer that will discussed in the next topic.

Optimization is an act, process or methodology of making something such as a design, system, or decision as fully perfect, functional or effective as possible. In term of optimization process, it is adjusting a process to optimize that make the best or most effective use of some specified set of parameters without violating some constraints. The most common goals are minimizing cost and maximizing throughput and/ or efficiency. When optimizing a process, the goal is to maximize one or more of the specifications process, while keeping all others within their constraints (Wikipedia, 2023). Adapting to photolithography process; it is an act to adjusting the spin coating process in terms of spinning speed, time and temperature during soft baking, UV light exposure time, finally pattern development in terms of time and technique.

The objective of this study was aimed to obtain the best setting for photolithography system and technique to achieve BBSD pattern on Si sample that is identical to BBSD pattern on the photomask.

2 Methods

The 6” N-doped Si (n-Si) wafer having <111> orientation was procured from Siltronic AG Pte. Ltd (Singapore). The thickness of the wafer was 650 ± 25 μm and its resistivity was in the range of 1000 – 10000 Ω cm. The wafer was diced into square pieces of dimension ~2.0 x 2.0 cm and cleaned using 4 types organic cleaning method as described in photolithography process flowchart in Figure 1.

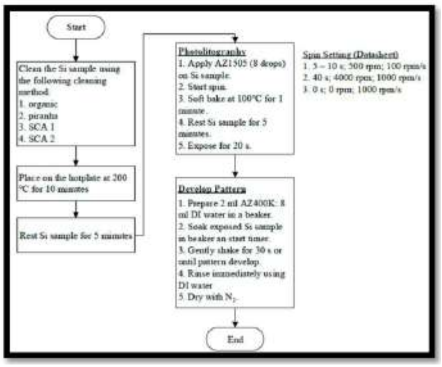

Figure 1: Photolithography process of Si BBSD.

Photomask is basically made from Soda Lime (SL), Quartz, and polyester film. Soda Lime and quartz are the most common substrates for photolithography masks, and typical glass mask sizes can range from 3 square inches to 7 square inches. Film photolithography masks have less constraints on size and can be made on sheets from 25 cm x 30 cm (10” x 12”) up to a huge 3 m long x 1 m wide (120” x 40”). The polyester base on the film is 0.18 mm thick (Elveflow, 2023). The photomask design is based on Si BBSD structure in Figure 2 and photoresist type.

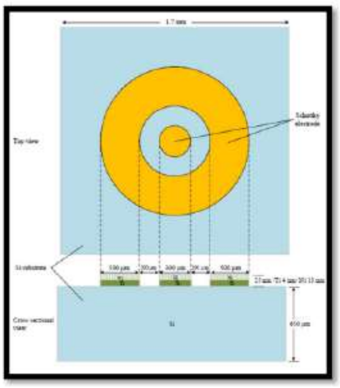

Figure 2: Si BBSD structure.

3 Results and Discussion

The developed Si sample that is ready for metal deposition process is shown in Figure 3.

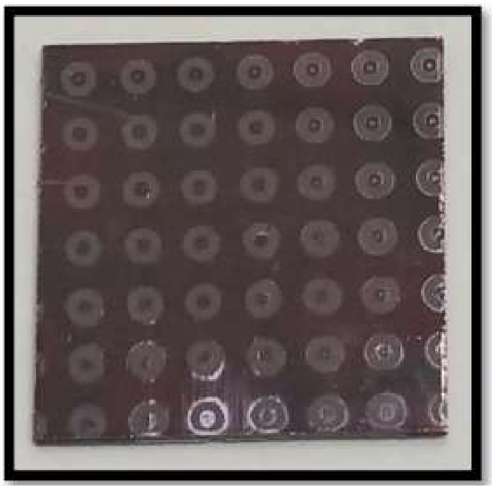

Figure 3: The developed Si sample.

The inspected BBSD pattern on Si sample compared to the BBSD photomask is shown in Table 1.

Table 1: Quality of the developed pattern on Si sample compared to the BBSD photomask.

Photomask	Developed Si sample
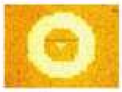 Bottom left	
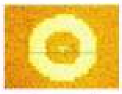 Bottom right	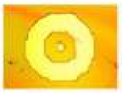
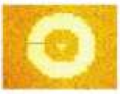 Center	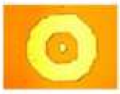
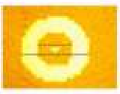 Top left	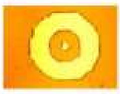
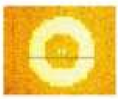 Top right	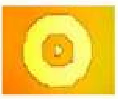

BBSD pattern on Si sample, which are bottom left, bottom right, center, top left and top right. were selected and inspected using metallurgical microscope then compared to the BBSD photomask. Referred to the images in Table 1, the pattern developed identical to the pattern in the photomask. Therefore, the developed Si sample can proceed to the metal deposition process.

There are three common problems existed during photolithography process that namely were inhomogeneous photoresist coating, double pattern and middle pattern was not perfectly round. he inhomogeneous photoresist coating of Si sample was solved by thoroughly cleaned the Si sample and bake at 200°C for 10 minutes to provide a hydrophobic surface as the photo resist will not have a good adhesion to a hydrophilic surface. Vibration of the photomask during UV light exposure that lead to double pattern developed was solved by contact printing method. Middle pattern not perfectly round was depending on the resolution of the printer used to print BBSD pattern on polyester film.

4 Conclusion

A photolithography process basically requires three basic materials, which light source, photomask, and photoresist. It's a very detail process that requires cleanliness, discipline and consistency to obtain an identical pattern to the photomask. Different types of sample or substrate, photoresist, developer and UV light source require different setting of the equipment and techniques. Therefore, it is a great importance to refer to a datasheet and specification of each materials and equipment before any photolithography process.

References

Elveflow. 2023. Introduction to photomasks in microfluidics. Source from "Microfluidic reviews" website https://www.elveflow.com/microfluidic-reviews/softlithography-microfabrication/introduction aboutphotomask-in-microfluidic/Accessed on 11 September 2023.

M. M. Ismail, B. R. Babu, M. Arivanandhan, and R. Jayavel. 2023. Rapidly emerging aspects & future R&D directions for supercapacitor. *in Hussain, C. M. and Ahamed, M. B. (eds.) Smar supercapacitors. United Kingdom: Elsevier*, pages 137 – 158.

Wikipedia. 2023. Process optimization (2023). Source from "Wikipedia" website. https://en.wikipedia.org/wiki/Process_optimization, Accessed on 21 September 2023.

Individual Research Contribution Review, 2023, 1(1): 445–446

Feasibility Study on Mobile Robot Deployment for Autonomous Radiation Mapping in Malaysian Nuclear Agency

Nur Aira Binti Abd Rahman
Technical Support Division, Malaysian Nuclear Agency
43000 Kajang, Selangor
nur_aira@nm.gov.my

Abstract

A feasibility study was conducted by the Malaysian Nuclear Agency, with a focus on exploring the use of mobile robots for autonomous radiation mapping in occupational safety inspections. A key benefit of this technology is its capacity to provide a detailed radiation map, which serves to validate work-area classifications and offers crucial support for planning work activities in alignment with permissible dose limits. An in-house developed mobile robot known as AMoRA (Autonomous Mobile Robot for Accurate Radiation Detection and Mapping) was employed. Presently, AMoRA has been deployed to six selected radiation facilities. Simultaneously, the limitations, challenges, and essential operational and technical requirements were identified. Finally, the findings will be analysed to devise the next action plan in this area of research.

Keywords: autonomous radiation mapping, mobile robot

1 Introduction

Radiation mapping is a critical process that involves comprehensive assessment of radiation levels across the target area, resulting in the creation of a radiation map. Conventionally, this task is carried out by radiation workers who manually collect data using survey instruments at predetermined sampling points. This process is relevant for a wide range of applications, including emergency response and mitigation activities, environmental monitoring, source search missions, and occupational safety inspections.

Previously, a research project was conducted under the MOHE grant (FRGS), entitled 'Path Planning Algorithm for Mobile Robot Autonomous Radiation Mapping in Cluttered Environment Using Radiation Detector and Navigation Sensors Data Fusion (FRGS/1/2019/TK04/UNITEN/01/2)'. In this research, an algorithm was developed to enable mobile robot to perform detailed measurements throughout the target area and produce the radiation map. The research was centralized on the computations of sampling points, path-planning for autonomous navigation, radiation parameters estimation, and hotspots localization. Subsequently, AMoRA (Autonomous Mobile Robot for Accurate Radiation Detection and Mapping) was constructed by integrating a small commercial mobile robot (Turtlebot2) with a GM detector module. The algorithm was implemented as the AMoRA brain. The performance and accuracy of the algorithm were evaluated and validated by simulation and real-world experiments in a known and controlled environment.

However, in order to deploy the robot in real-world applications, there are a few gaps and challenge that need to be considered and addressed. Among the issues are the mobile robot capability to navigate in unstructured and complex environment, control and autonomy, requirements of safety regulations and algorithm readiness for deployment. This project is the continuation of the FRGS project to evaluate the feasibility of mobile robot deployment for occupational safety application. For workplace safety assessment, the radiation map produced by the robot can be referred to assess the radiation dose distribution throughout the region of interest and to define boundaries between different class areas.

Therefore, the objective of this study is to perform experimental evaluation at selected radiation facilities in Nuclear Malaysia where AMoRA was deployed to perform radiation mapping and construct a detail radiation map of the target areas. Simultaneously, the limitations, challenges, and essential operational and technical requirements were identified. Finally, the findings will be analysed to strategize the next action plan in this topic of research.

2 Methods

Methodology of the experimental evaluation is presented in Figure 1. Initially, a list of potential sites was identified by the team members from the Health Physics Group based on the current work areas classifications as delineated in the 'Work Area Classification Guide According to the Atomic Energy Licensing (Basic Safety Radiation Protection) Regulations 2010 P.U (A) 46' document. Next, a site survey will. be conducted to obtain information of the location and to ascertain its suitability for the deployment of AMoRA. Presently, the selection of locations is restricted to indoor settings with smooth surfaces or flooring due to the limitations posed by AMoRA/Turtlebot2. In cases where deployment at a particular site is unfeasible, detailed reasons will be documented in the report for future analysis and potential enhancements of the deployment strategy.

Given that the site was deemed suitable for AMoRA deployment, a 2D mapping operation will be performed to generate the 2D occupancy map of the location. Next, AMoRA will be deployed to run the autonomous radiation mapping and construct the radiation map of the site. Finally a radiation mapping report will be generated. This report will detailed

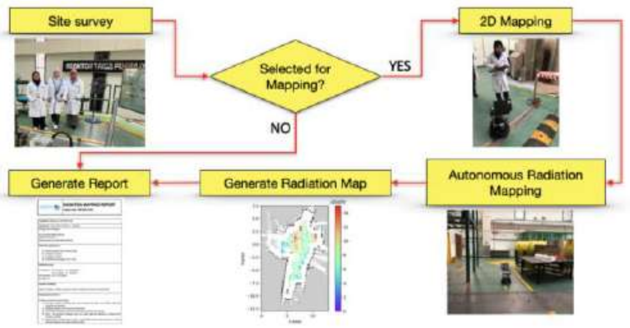

Figure 1: Methodology of the experimental evaluation

out the operation specifications, observations and limitations, as well as the overall mapping results and analysis.

2.1 Results and Discussion

In summary, a total of 15 sites have been visited and surveyed and 12 sites were identified suitable for AMoRA deployments for radiation mapping. Currently, AMoRA have been successfully deployed at 6 sites; including the Reactor Hall, Wastec Interim Storage, LENDT facility and SSDL facility. Radiation map has been constructed for each deployed site. The overall status is listed in Table 1.

Table 1: Overall site survey and AMoRA deployment status

No	Locations	Site Surveyed	AMoRA Compatible	AMoRA Deployed
1	PIA - Lab 005, 006, Americium	√	√	√
2	Reactor Hall	√	√	√
3	Reactor Control Room	√	√	X
4	SSDL Lab/Room	√	√	√
5	BTP R&D Lab	√	√	√
6	Wastec Interim Storage	√	√	√
7	BLENDT Facilities	√	√	√
8	Sinagama Bunker	√	X	X
9	Sinagama Research Loop	√	√	X
10	Gamma Green Housep	√	X	X
11	BTP Clean Room	√	√	X
12	BTP Hotcell	√	√	X
13	Wastec Sorting Room	√	√	X
14	Wastec Conditioning and Compacting Room	√	√	X
15	Wastec LLETP	√	X	X

The typical challenges recorded from the site visits and deployment includes small, tight and cluttered spaces, as well as uneven terrain (stairs, drains, bumps, and holes on the floor). AMoRA also faced difficulties to perform mapping on outdoor spaces where the movement and data measument were controlled manually. The robot specifications as well as control autonomy need to be revised to overcome this challenges.

Additionally, based on the observation, the original algorithm has been fine-tuned in terms of the partitioning algorithm and the partition sequence (with DBSCAN clustering and Nearest Neighbour). This has improved the sequence of autonomous radiation mapping and avoid the robot from skipping certain areas.

3 Conclusion and Recommendations

In conclusion, the field experiments conducted at the Malaysian Nuclear Agency demonstrate the feasibility and effectiveness of using a mobile robot for autonomous radiation mapping. Challenges and limitations identified highlight the need for further refinement and optimization. The current robot platform is limited to operating on smooth surfaces and indoor locations, prompting the need for the development of ruggedized versions to expand its applicability. Expertise is required in robotics design and technology, focusing on hardware and mechanical design, to optimize the robot's performance and reliability. Proficiency in radiation map interpolation techniques and validation methods is essential to guarantee the precision and dependability of the acquired data.

References

N.A. Abd Rahman, K.S. Mohamed Sahari, N. A. Hamid, and Y.C. Hou. 2022. A coverage path planning approach for autonomous radiation mapping with a mobile robot. *Int. J. Adv. Robot. Syst.*, pages 1 – 17.

Individual Research Contribution Review, 2023, 1(1): 447–448

Data Profiling of Safety-Related Parameters during 1MW RTP Operation with Associated Alarm Response

Nurfarhana Ayuni Joha
Technical Support Division, Malaysian Nuclear Agency
43000 Kajang, Selangor
nurfarhana@nm.gov.my

Abstract

Reactor TRIGA PUSPATI (RTP) has been in operation for more than four decades since 1982 without any accidents. Various strategies are taken to enhance safety of RTP which in line with international standards and practices in ensuring that this safe operation remains and continues for the future. RTP is equipped with digital instrumentation and control (I&C) system which is known as Reactor Digital Instrumentation and Control System (ReDICS). All ReDICS components are connected to the alarm log and displayed at the RTP control console. These alarm logs are very essential to reactor operators so that they alert to any early warnings related to abnormal reactor data, processes or systems. Any safety parameter that approaches or surpasses their prescribed operating limit triggers the trip system on ReDICS and shuts down RTP operation automatically. On the other hand, this study focuses on the reactor safety-related parameters that are not connected to the RTP trip system for instance reactor pool water temperature and reactor pool top radiation as well as alarm response that triggered during normal and abnormal operations. This study is very important to support the ability of reactor operators in determining the reactor behaviours and understanding the alarm system based on the messages in RTP alarm logs. Thus, RTP will always operate in a safe condition and in turn ensures the safety of RTP operating personnel and environment.

Keywords: RTP, reactor operation, safety-related parameters, alarm system.

1 Introduction

RTP operation is supported by several systems such as instrumentation and control (I&C) system, cooling system, water purification system, area radiation monitoring systems and so on. The I&C system is one of the crucial systems for RTP operation.

The digital alarm system at the RTP serves to provide an early warning to the reactor operator when parameters reach operational limits. Based on RTP operation records, the highest frequency of alarms is from the area radiation monitoring system at reactor pool top with readings exceed setpoint which is 10000 μSv/hour. Besides pool top radiation, heat removal from reactor also need to be monitored according to design basis for I&C system.

RTP control system is equipped with digital alarms that are vital to reactor operators so that they are aware of any early warning related to unusual system, process or reactor operating data. In-depth knowledge of the reactor alarm system is very important while operating a nuclear reactor to prevent any incident or accident and to ensure the sustainability of the reactor operation. Comprehensive knowledge on reactor operating parameters and alarm system displayed at the RTP control console are essential in ensuring the safety of radiation workers and their environments including preserving the lifespan of RTP components.

The objective of this study is to investigate reactor behavior by analyzing selected safety-related parameters which are reactor pool water temperature and pool top radiation during 1MW operation in normal and abnormal conditions.

The results of this study increase the extensive knowledge of the alarm system at RTP and at the same time ensure the safety of the reactor by protecting the equipment and components at RTP from any damage. This is one of the most cost- effective ways to solve problems or maintenance that may involve a large amount of budgeting.

2 Methods

RTP operating conditions for this study are as in Table 1. The power level of the reactor is at full power which is 1MW thermal. This study involves two types of operation, namely normal operation and abnormal operation.

For normal operation, the valves and pumps on the RTP primary cooling system are open and working normally. As for the abnormal operation, the valves and pumps on the RTP primary cooling system are closed. Data for both types of operation are analyzed to study trends and changes in reactor operating parameters.

Table 1: RTP operating condition

Item	**Normal operation**	**Abnormal operation**
Reactor power	1MW	1MW
Primary cooling system	Pump ON	Pump OFF (LOF)
Samples irradiated	NONE	NONE
Core configuration	Core-15	Core-15

Reactor operational data with activated alarms are obtained from the Data Acquisition and Control System (DACS) in the RTP control room using the RTP InTouch software. RTP safety-related parameters consist of reactor pool water temperature, radiation readings at the reactor pool top, negative pressure in the reactor hall, readings from the stack monitoring system, particularly readings of noble gases and particulates, seismic monitoring systems, radiation readings at the beamports and water conductivity. Data profiling in this study focuses on reactor pool water temperature, radiation readings at the reactor pool top and relates these two RTP safety related parameters to reactor power.

3 Results and Discussion

Figure 1 shows the reactor power level during operation including SCRAM test for over power.

Figure 1: Reactor power level during operation

Figure 2 shows that pool water temperature and pool top radiation is inversely proportional correlated. Considering the expected temperature rise of the water passing through the core, an immediate release of about 30% of the argon- 41 made could be expected during passage. It was found that the highest radiation reading was 13800 μSv/hour. At that point, the alarm will be activated because the reading exceeds the setpoint value of 10000 μSv/hour.

Pool top radiation may take lesser time to spike and immediately drop compared to pool water temperature that needs longer time to increase and decrease as shown in Figure 3. The reactor pool water temperature alarm system is activated indicating that the reactor pool water temperature has reached 45°C.

4 Conclusions

In conclusion, loss of flow due to failure in reactor cooling system may increase coolant temperature and activate the audible alarm at 45°C. Radiation reading at reactor pool top exceeds alarm setpoint which is 10000 μSv/hr during both normal and abnormal operation. Comprehensive knowledge of the reactor alarm system is very important when operating a nuclear reactor to prevent any incidents or accidents that may lead to damage of SSC.

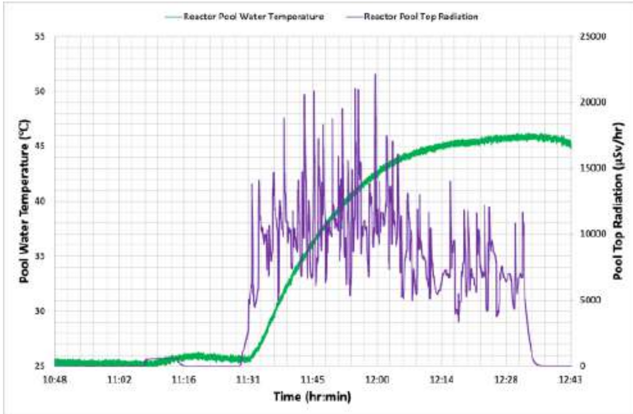

Figure 2: Comparison of reactor pool water temperature and reactor pool top radiation during normal operation

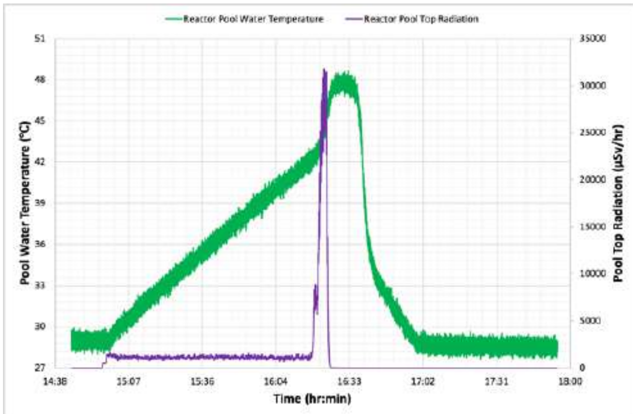

Figure 3: Comparison of reactor pool water temperature and reactor pool top radiation during abnormal operation

References

IAEA. International Atomic Energy Agency. 2016. History, development and future of TRIGA research reactors. Technical Reports Series No. 482.

Agensi Nuklear Malaysia. 2020. Safety analysis report for Reaktor TRIGA PUSPATI.

Individual Research Contribution Review, 2023, 1(1): 449–450

Development of ECPunch - Educational Course Puchcard System

Nur Fatini Binti Abdul Ghani
Technical Support Division, Malaysian Nuclear Agency
43000 Kajang, Selangor
fatini@nm.gov.my

Abstract

The implementation of ECPunch, an Educational Course Punchcard System, revolutionizes attendance tracking for PGEC students at Unit Khidmat Latihan (UKL). This system allows students to easily punch-in and punch-out via desktop or mobile, providing flexibility for attendance amendments. The personalized automated tracking system offers real-time reporting and a dashboard for Course Coordinators to monitor attendance efficiently. Employing the Software Development Life Cycle (SDLC), the system is cost-effective, adaptable, and integrates responsive web design, ensuring accessibility across devices. ECPunch replaces manual attendance methods, enhancing productivity, accuracy, and reinforcing attendance policies. The system's advantages include increased efficiency, ease of use, and insightful dashboard reporting, making it a reliable and superior alternative to traditional attendance tracking methods.

1 Introduction

Unit Khidmat Latihan or UKL has implemented a conventional method in order to take the attendance of their PGEC students. This inefficient method is very time consuming and need much effort to analyze the track record of their student attendance. By using ECPunch, PGEC student's may punch-in and/or punch-out their attendance by using their desktop or even a mobile. Students also are allowed to amend previous days' attendance details in case of late, absence or leave subject to authorization by their Course coordinator. Dashboard reporting allows viewing of who is currently punched in and out, and can see past attendance details. Course coordinator may check the student's attendance by generating the report automatically, and also verify every late attendance. It's simple, effective, and a time card solution that just makes sense.

2 Methodology

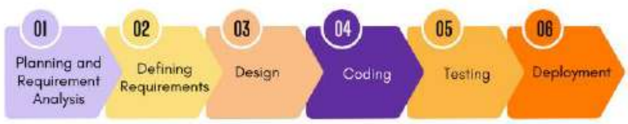

PTM follows the standard of Software Development Life Cycle (SDLC) (Pressman, 2020) to develop ECPunch. This structured process includes planning and requirement analysis involving both IT and UKL, defining detailed requirements through collaborative meetings, designing the system's architecture and functionality, coding by IT developers, and rigorous testing to ensure meeting specified requirements. Upon successful testing, ECPunch is deployed for recording PGEC student attendance.

3 Finding

Key Features of ECPunch:

(a) Personalized Automated Attendance Tracking and Reporting

ECPunch presents a revolutionary approach to attendance tracking and reporting, offering a personalized and automated system that allows for unparalleled flexibility in generating attendance summaries. UKL can effortlessly customize reports based on specific days or months, tailoring the system to their unique needs.

(b) Attendance Dashboard

Designed with simplicity and interactivity in mind, it allows users to apply filters for custom date ranges, ensuring a seamless and intuitive experience when accessing attendance data on a daily, weekly, or monthly basis.

(c) Current software development practices

ECPunch adopts an open-source framework incorporating MySQL database, PHP development tools, CSS, HTML, Apache Web server, and the Linux operating system. This approach not only ensures cost-effectiveness compared to proprietary software but also offers unparalleled flexibility for code modifications and the seamless integration of new features. ECPunch stands out as an adaptable solution, making the addition or modification of features significantly easier and more reliable.

(d) Responsive Web Design and Mobile-Friendly version

ECPunch is built on a foundation of responsive web design, ensuring a mobile-friendly version that caters to users across various devices (Almeida and Monteiro, 2017). Leveraging the Bootstrap framework, HTML5, CSS3, and jQuery plugins, it delivers a modern and responsive dashboard complete with interactive charts. Its adaptability to any viewport, including iPhones, iPads, Android phones, and tablets, underscores its commitment to providing a versatile (Almeida and Monteiro,

2017) and accessible attendance management solution. Picture below show the interface of ECPunch that employ responsive web design.

4 Conclusion

ECPunch provides significant benefit to UKL and the students such as:

(a) Increased Productivity & Efficiency

ECPunch demonstrates increased productivity and efficiency by minimizing the amount of work required for administrative tasks. While manual attendance proves time-consuming, error-prone, and prone to inconsistency, ECPunchstreamlines workforce utilization, reinforces attendance policies, and enables easy tracking of time violations and repeat absenteeism. Moreover, it offers flexibility and seamless integration with other in-house systems.

(b) Cost-effective

Manual Attendance necessitates more effort and physical space to manage attendance documents, whereas ECPunch presents itself as a cost-effective alternative to traditional paper timesheets.

(c) Ease-of-use

Manual Attendance relies on traditional paper timesheets, while ECPunch excels by being web browser and mobile phone-friendly, ensuring accessibility and convenience to UKL and students.

(d) Reliablity and Accuracy

ECPunch shine through when compared to Manual Attendance, which poses a high risk of human error and inaccurate reporting. ECPunch ensures greater precision, eliminating errors and providing insightful dashboard reporting for enhanced data accuracy.

In conclusion, the development of ECPunch as an Educational Course Punchcard System represents a significant leap forward for Unit Khidmat Latihan (UKL) in streamlining attendance management for PGEC students. The system's implementation aligns with modern software development practices, emphasizing cost-effectiveness, flexibility, and responsiveness. The novel features, such as personalized automated attendance tracking, an attendance dashboard, and mobile-friendly capabilities, provide clear advantages over manual attendance processes, enhancing productivity, accuracy, and ease-of-use. Looking ahead, potential future works could focus on refining and expanding features, ensuring continuous adaptation to evolving technological trends, and maximizing the system's potential for supporting educational institutions. The ECPunch system stands as an innovative solution, showcasing a dedication to efficiency, reliability, and user-centric design especially for program PGEC.

References

Fernando Almeida and J Monteiro. 2017. The role of responsive design in web development. *Webology*, 14:48–65.

Pressman. 2020. Software engineering: A practitioner's approach.

Individual Research Contribution Review, 2023, 1(1): 451–452

Implementation on New Features in BIOWEB and The Added Value

Nur Fatini Binti Abdul Ghani
Technical Support Division, Malaysian Nuclear Agency
43000 Kajang, Selangor
fatini@nm.gov.my

Abstract

Nuclear Malaysia's staff information system, now known as BIOWEB (Sistem Biodata Kakitangan berasaskan Web) has been in operation for many years under different names. This system plays an important role in managing staff profile information in which the business process is determined by the Management Services Division (BKP) as the owner of the system. In recent years, Bioweb has undergone continuous improvement and changes driven by novel technologies and also with a growing demand in its function. This paper will introduce the new features that has been implemented and improved in Bioweb and also where and how the new features generate 'added value' to the information.

1 Introduction of Bioweb

1.1 Background

Bioweb, initially designed for HR (Human Resource) management at Bahagian Khidmat Pengurusan (BKP), has transformed into a centralized employee database with enhanced user-friendly features. It efficiently handles staff information, including job details, salary, work history, education, and skills.Several trends have caused Bioweb to evolve to become more user-intensive. The new focused on Bioweb have focused on mechanism and strategies for Bioweb improvement which can generate added value not only to the system owner but also to entire organization. Some of the improvements in the Bioweb are due to following reasons:

- breaking down information siloed
- multiple, disparate Information Sources and Repositories
- inflexible report generation
- preserving the information confidentiality and integrity

2 Development Methodology

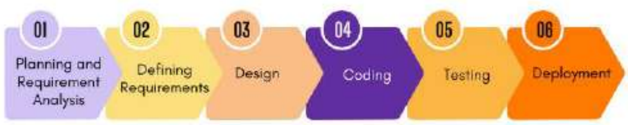

The development methodology involves standard system development methodology (Pressman, 2020) by PTM which involved planning, defining requirements from stakeholder such as BKP, UKF and BSM, design and coding by PTM, thorough testing, and ends with the deployment of the finalized system.

3 Result

The results demonstrate the incorporation of new features into bioweb, including: facilitating inter-departmental collaboration, serving as the single source of truth, embracing new system and information access control, implementing single sign-on with active directory credentials, introducing separation of duties,enhancing flexible report generation, and implementing audit trails.

(a) Facilitating Inter-Department Unit Collaboration

Below picture show other business unit that has access to Bioweb and what is their input that contributes to Bioweb information.

(b) Serving as Single Source Of Truth (SSOT)

Below picture shows a few systems with serving different functional areas that are currently integrated with Bioweb. Bioweb act as SSOT as a central and authoritative data source that is considered the reference for staff information within agency to ensures data consistency and integrity.

(c) Embracing New System and Information Access Control

Bioweb has enhanced its security access controls to prevent unauthorized access and protect sensitive information. The access controls in Bioweb prioritize the confidentiality and integrity of data through effective identification, authentication, and authorization mechanisms.

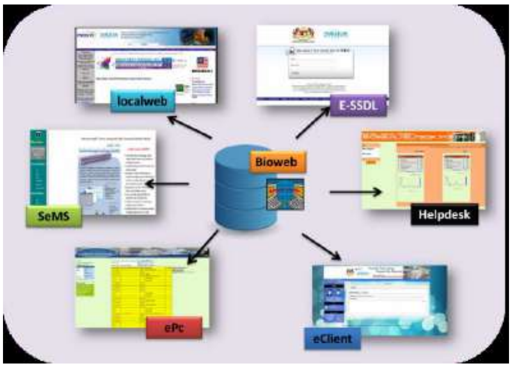

(d) Implementation on Single Sign-On with Active Directory Credentials

Enabling Single Sign-On with active directory credentials streamlines user authentication, allowing access to multiple systems with just one login. This enhances productivity and security, as users only need to log in once to navigate authorized applications seamlessly within Nuclear Malaysia.

(e) Introducing Separation of Duties

Upon user authentication, Bioweb ensures user receives appropriate access like Read, Write, or Full Control. This feature, such as only granting Unit Perkhidmatan the ability to update staff information, enhances security and controls user responsibilities.

(f) Enhancing Flexible Report Generation

Bioweb's enhanced flexible report generation module signifies a significant improvement in its capabilities. This upgraded feature allows for more dynamic and adaptable report creation, enabling users to generate customized reports efficiently.

(g) Implementation Audit Trails

Bioweb's audit trails feature records vital details, including date, timestamp, web address, and event status. This enhances system security, ensures accountability, and facilitates thorough monitoring of user interactions for analysis and compliance.

4 Conclusions and Further Work Recommendations

The new features in Bioweb provide significant added value and benefits.

(a) Capability of further processing staff information

Inter-department collaboration in Bioweb facilitates comprehensive reporting by consolidating staff information from various sources, unlocking insights, and promoting valuable insights for the organization. The flexibility and customization features ensure reports address specific business areas, preventing unnecessary information from being overlooked.

(b) Management of Information

Organizing information resources in Bioweb minimizes the risk of retrieving outdated data, enhancing overall organizational efficiency (Queiroz et al., 2024). The possibility of information integration ensures a comprehensive view of staff details, overcoming inefficiencies caused by scattered information. Bioweb's single source of truth consolidates data across systems, providing integrated and relevant user views, accessible to other systems, promoting organizational coherence.

(c) Capabilty Of Correction / Modifications / Evaluation Of Information

Bioweb's data processing advantage lies in its ability to modify, correct, and evaluate staff data elements across all records stored in the database. For instance, BSM can easily update staff academic details initially created by BKP, saving considerable time and effort. Consistent data entry enhances accuracy and ensures up-to-date staff information.

In conclusion, Bioweb emerges as a crucial asset for enhancing our organization's knowledge management. Its value grows with increased usage, aligning with the rising strategic importance of information over time. To stay relevant, Bioweb should adapt to the digital revolution and evolving user needs, seeking innovative solutions to enhance usability and extract valuable information for users.

References

Pressman. 2020. Software engineering: A practitioner's approach.

Magno Queiroz, Paul Tallon, and Tim. Coltman. 2024. Data value and the search for a single source of truth: What is it and why does it matter?

Individual Research Contribution Review, 2023, 1(1): 453–454

Key Elements of the Ageing Management for PUSPATI TRIGA Reactor

Phongsakorn Park Tom
Technical Support Division, Malaysian Nuclear Agency
43000 Kajang, Selangor
phongsakorn@nm.gov.my

Abstract

PUSPATI TRIGA Reactor (RTP) operated for 41 years and have intention to keep the reactor in operation as long as technically feasible. The preconditions of the long-term operation are the safety and reactor in good condition. In the paper, the review of ageing management covers the structures, systems and components (SSCs). Key elements of ageing management are identified and described. Proper level of understanding of the ageing phenomena is reached and adequate ageing management program. The practice and solution of identified ageing management issues will ensure the safety of long-term operation of RTP.

Keywords: Ageing Management, PUSPATI TRIGA Reactor, Long-term operation

1 Introduction

This Aging Management is part of the integrated management system as applied to ensure that the facility meets the requirements for safety as derived from the requirements of the regulatory body, design requirements and assumptions, the safety analysis report and operational limits and conditions. After several years of successful operation, some deterioration in components and associated systems of the reactor have been observed primarily due to ageing. Also, for some of the components, obsolescence is a major problem since spares for these old designs are no longer available in the market. Since then, several refurbishments work and upgrading activities have been carried out in order to extend the useful life and reliability of the systems for the safe operation of RTP.

Ageing is defined as a general process in which the characteristics of SSCs gradually change with time or use. Research reactors experience two kinds of time dependent changes: (1) Degradation of SSCs (physical ageing), i.e. gradual deterioration in their physical characteristics; (2) Obsolescence of SSCs (non-physical ageing), i.e. their becoming out of date in comparison with current knowledge, standards and technology.

In practice, the ageing management program (AMP) at a research reactor is accomplished by coordinating existing program, including maintenance, periodic testing and inspection programmers, as well as applying good operational practices, research and development (of material behavior, radiation effects, chemistry, etc.), and incorporating lessons learned from operating experience.

2 Tasks for Ensuring of Safe Long-Term Operation

The generic goal of the AMP is to ensure the cost effective and competitive production under stringent condition of safety. Generally, AMP covers all SSCs of the plant, also the infrastructure necessary for the functioning of the operating organization. Within the scope of the AMP program, ensuring the intended function of the safety classified SSC has the most important role. Independent form the regulatory framework related to the long-term operation (LTO), the required technical condition of the safety classified items and their intended function has to be ensured by proper ageing management, maintenance practice and reconstructions. For the acceptance of LTO it has to be demonstrated that the effects of aging will be adequately managed so that the intended safety functions will be maintained consistent with the current licensing basis for the period of extended operation.

3 Ageing Management Program Development Planning

Planning an orderly and planned development is crucial for the success of AMP. Figure 1 below shows the key elements for the success of the Plan Do Check Action (PDCA) cycle of AMP is systematic in RTP.

4 Coordination, Monitoring and Evaluation

Coordination, Monitoring and Evaluation is a fundamental part of the AMP where it will explain in detail the condition of SSCs in the reactor whether it can operate within it deems appropriate or safe. The following is an analysis - an analysis that must be met or implemented: 1. Objective Analysis,

2. System Analysis & components,
3. Analysis of staff training,
4. Analysis of In-Service Inspection,
5. Testing & Monitoring Program,
6. Spare part program,
7. Quality Plan,
8. Analysis of staff time,
9. Document time, after the above performed satisfactorily, it led to the suggestion that the approach can be used to move the SSCs and corrective measures of aging.

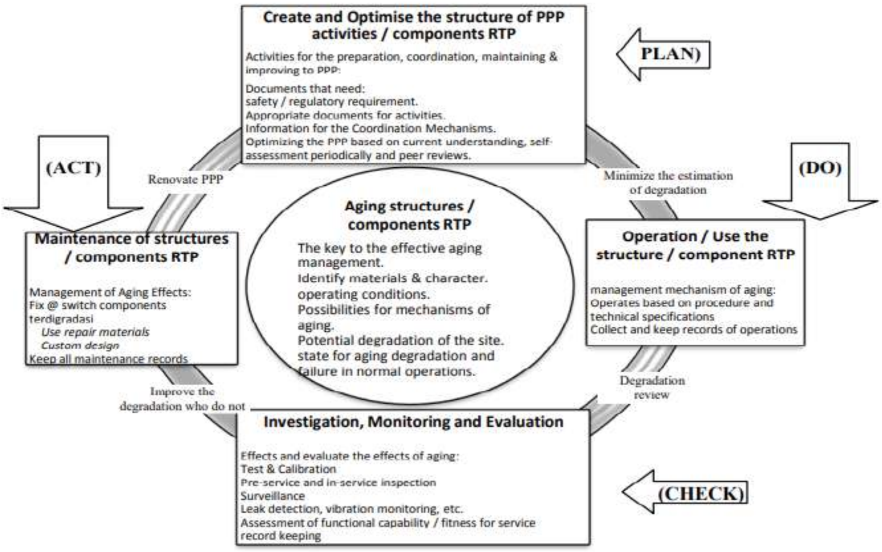

Figure 1: The elements of the PDCA cycle in order to achieve a systematic Aging Management Program in RTP

4.1 Aging Modification

Coordination is important for the effects of aging research reactor facility to enhance the integrity and safety of a reactor facility. To carry out the aging management program (AMP), several framework activities must be considered such as obtaining information from the design, maintenance and periodic testing SSCs of the reactor. The data should be recorded and kept for inspection and analysis. The program also needs to cover in your choice of equipment, details of the categories, surveillance and testing program, for data collection and management for further evaluation of the effects of aging. In addition, all major components of the system and the research reactor to be considered. In addition, analysis of the data collection mechanisms of aging is based on aging. Other factors should also be considered as failure to obtain the original information, inspection data is not updated, misinterpretation of aging and others that could shake the aging program.

4.2 Monitoring

Aging surveillance program is essentially a long-term program. This program should be implemented as early as possible and must be used during reactor operation. Monitoring programs in design, manufacturer specifications, operation and maintenance experience should be implemented together with the selection of equipment, the categorization process and qualification of equipment. This monitoring must be conducted regularly, two times a year.

4.3 Evaluation

Value in terms of inspection, monitoring and tests should be conducted in accordance with the propriety of a situation and must be controlled. The report should be standardized aging program and collected for analysis to identify the problems of aging reactor. This report must be in the form of technical reports, and it must include records of daily, monthly or yearly. It must refer to the components and parts that are involved in aging programs to ensure the safety of components and parts are in that situation is safe to operate. The report also must include records, such as renovation, maintenance and so on. This report must also indicate the methods for identifying problems, analysis and solutions.

5 Conclusion

The aging management program is focused on identifying the aging occurs, identify the parties involved in the program and further notes the problems of aging that can affect the safety of the reactor RTP. Significant for safe long-term operation structures, systems and components of RTP are identified. Proper level of understanding of the ageing phenomena is reached and adequate AMP were developed for ensuring the required status and intended function for long-term.

References

T.J. Katona et al. 2005. Key elements of the ageing management of the Wwer-440/213 type nuclear power plants. *18th International Conference on Structural Mechanics in Reactor Technology (SMiRT 18) Beijing, China*.

2020. Reactor TRIGA PUSPATI safety analysis report, Malaysian Nuclear Agency.

IAEA Specific Safety Guide No. SSG-10. 2010. Ageing management for research reactors, Vienna.

Individual Research Contribution Review, 2023, 1(1): 455–456

Study of Neutron Field Around Malaysian Nuclear Agency- Plasma Focus (MNA-PF) Using PHITS

Puteri Nuraliah Husna Mohd Tajuddin
Technical Support Division, Malaysian Nuclear Agency
43000 Kajang, Selangor
puteri@nm.gov.my

Abstract

Plasma Focus is a device that can produce neutron, x-ray, electron, and ion. The Malaysian Nuclear Agency employs a plasma focus device based on the UNU/ICTP PFF design of the Mather type. In this study, the Particle and Heavy Ion Transport Code System (PHITS) was used to model the neutron field in the plasma focus and simulate the neutron field in the chamber. As a result of employing the PHITS code, the effective dose rate will be compared with the result from the experiment that has been done to study the neutron field around the plasma focus device. The neutron flux and dose mapping also has been obtained from the PHITS code.

Keywords: Plasma focus, PHITS, effective dose rate

1 Introduction

In Malaysia, MNA-PF consists of a capacitor that is capable of storing energy up to 30μF with rated voltage of 15kV (Zin et al., 2017). Plasma focus devices can be used in many applications, so it is better to understand the fundamental process of the plasma. The neutron field has been simulated for a neutron with energy of 2.45 MeV and 14.1 MeV using PHITS code (Rahmani, 2016). The energies were obtained due to the reaction of Deuterium-Deuterium (D-D) and Deuterium-Tritium (D-T) reaction (Lang et al., 2018). Besides that, electrode geometry plays a big role in determining the neutron production (Akel et al., 2021). Due to this reason, the effective dose rate from this simulation has been compared to the experiment that has been done before in the Preliminary results of Malaysian Nuclear Agency Plasma Focus (MNA-PF) as a slow focus mode device for deuterium filling gas in correlation with Lee model code (Zin et al., 2017).

2 Methods

This work required the Particle and Heavy Ion Transport code System (PHITS) to run the simulation that has been used in many studies that includes the study of radiation. PHITS can be used to simulate the transport of all particles that include the neutron field in the plasma focus (Sato et al., 2018). The first step in starting using the PHITS is to define the geometry and the source used in the Plasma Focus Device. Next step is to determine the source in the MNA-PF. Plasma focus device is a device that does not require any radioactive source. But in this work, it was assumed that the neutron is produced due to the D-D reaction inside the chamber. D-D reaction is the collision of plasma with the deuterium gas. The neutron has 7500 neutrons/shot in the Source section. Lastly is determine the parameter used to run the code which is T-Track. The T-Track was used in the PHITS to obtain the neutron flux and effective dose rate in the plasma focus device.

3 Data/Results

The effective dose rate that has been obtained from the T-Track tally is 4.326 μSv/hr. This result, when compared to the result in the previous study which is 4.78 μSv/hr is almost the same. This proves that the calculation and experimental data from previous study can be used. Thus, the neutron yield that has been obtain from previous study which is 7.5E+03 can be used in the further study. Figure 1 shows that the effective dose rate is highest when the energy reaches 2.45 MeV and 14.1 MeV.

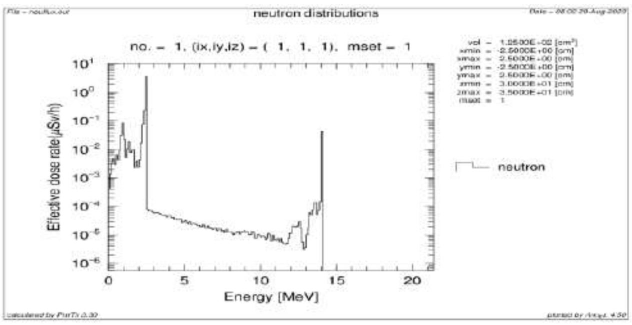

Figure 1: Effective dose rate VS energy for MNA-PF

Figure 2 also shows that the fluxes are highest when energies are 2.45 MeV and 14.1 MeV. These are the energies of neutrons that have been used in the code. When the energy reaches 2.45 MeV, the effective dose is 3.7033 μSv/hr and the flux is 2.3515E+02/cm^2/source. While, when energy reaches 14.1 MeV, the effective dose rate is 4.3569E-02 μSv/hr and the flux is 2.4103E+00/cm^2/source. These results show that energy of 2.45 MeV affected most of the total effective dose rate and flux of neutrons. From PHITS, the average relative error is 4%. Thus, these results can be accepted.

4 Conclusions

The effective dose rate, dose mapping, and neutron flux for MNA-PF have been obtained by using PHITS code. The

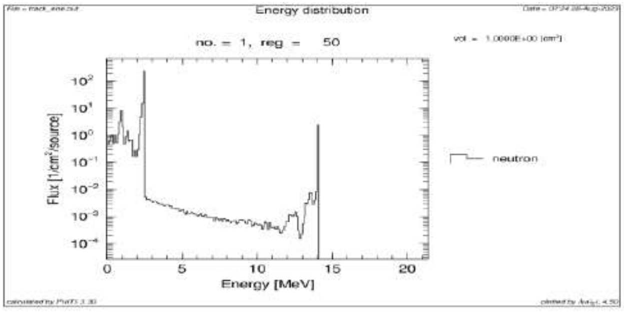

Figure 2: Flux VS energy for MNA-PF

result for effective dose rate has been compared with the result that has been published in Preliminary results of Malaysian Nuclear Agency Plasma Focus (MNA-PF) as a slow focus mode device for deuterium filling gas in correlation with Lee model code. The previous work has been done via experiment and calculation. From the result in the PHITS code, the effective dose rate obtained was almost the same as the result that has been done through experiment which is 4 μSv/hr. The average relative error from PHITS is 4%, which is lower than 5%. This error can be reduced more by increasing the number of batches and number of histories per batch. Therefore, it can be confirmed that the measurement neutron dose that emitted from MNA-PF is around 4 μSv/hr when the neutron yield from previous calculation and experiment has been used in the PHITS code.

References

M. Akel, P. Kubes, M. Paduch, and S. Lee. 2021. Comparison of measured and computed neutron yield from PF1000 plasma focus device operated with deuterium gas. *Radiation Physics and Chemistry*, 188(109633, https://doi.org/10.1016/j.radphyschem.2021.109633).

R. F. Lang, J. Pienaar, E. Hogenbirk, D. Masson, R. Nolte, A. Zimbal, S. Röttger, M. L. Benabderrahmane, and G. Bruno. 2018. Characterization of a deuterium–deuterium plasma fusion neutron generator. *Nuclear Instruments and Methods in Physics Research Section A: Accelerators, Spectrometers, Detectors and Associated Equipment*, 879:31–38, https://doi.org/10.1016/j.nima.2017.10.001.

F. Rahmani. 2016. Dose calculation for radiation safety assessment of plasma focus 2.5 kJ. *Journal of Fusion Energy*, 35(2):378–384, https://doi.org/10.1007/s10894–015–0043–0.

T. Sato, Y. Iwamoto, S. Hashimoto, T. Ogawa, T. Furuta, S. Abe, T. Kai, P.-E. Tsai, N. Matsuda, H. Iwase, N. Shigyo, L. Sihver, and K. Niita. 2018. Features of particle and heavy ion transport code system (PHITS) version 3.02. *Journal of Nuclear Science and Technology*, 55(6):684–690, https://doi.org/10.1080/00223131.2017.1419890.

M. F. M. Zin, A. H. Baijan, V. Damideh, S. A. Hashim, and R. M. Sabri. 2017. Preliminary results of malaysian nuclear agency plasma focus (MNA-PF) as a slow focus mode device for argon and deuterium filling gas in correlation with Lee model code. (020005, https://doi.org/10.1063/1.4978818).

Individual Research Contribution Review, 2023, 1(1): 457–458

Refurbishment of Automation System for Instrumented Delayed Neutron Activation Analysis (IDNAA)

Ridzuan Abdul Mutalib
Technical Support Division, Malaysian Nuclear Agency
43000 Kajang, Selangor
ridzuan@nm.gov.my

Abstract

Reconstruction of the IDNAA technique using PAUS equipment consists of three main parts; (1) sample activation control using a computer-based control module and sample detection card (2) electronic neutron counting equipment using a Canberra counter and a neutron detector filled with helium gas (3) automation system interface control program, data acquisition and storage using LabVIEW software.

Keywords: neutron activation analysis, computer-based control, automation system

1 Introduction

Instrumental Delayed Neutron Activation Analysis (IDNAA), is a special technique in NAA. This IDNAA technique is capable of quantitatively analyzing 2 elements that have a large atomic weight in the order of the periodic table which have fissionable properties, namely Uranium- 235 and Thorium-232 using neutron particles in a nuclear reactor. Uranium-235 (235U) is an isotope of uranium that makes up about 0.72% of natural uranium. Unlike the dominant uranium-238 isotope, 235U is fissionable by irradiation into neutron particles, i.e. can sustain fission chain reactions. It is the only fissionable isotope that is a primordial nucleus or found in large quantities in nature. Almost all thorium found in nature is the thorium-232 isotope (several other isotopes exist in trace amounts or can be produced synthetically). This radioactive material is relatively stable but cannot be fissile on its own, unless it can only be done in a nuclear reactor where the fission of uranium-233 (U233) and neutrons are formed which allow the fission chain process to continue.

2 Methods

Human Machine Interface (HMI) automation control program development using LabVIEW software signal flow graphics. Actuator control and monitoring is done using a PC through a virtual control panel consisting of main control panel as an interface with the user (HMI). Process control operations are generally performed sequentially to complete a necessary process, background, calibration or analysis and will repeat (loop) according to the number of samples as shown in Figure 1. Actuator sequence operation control requires an input signal from a timer on the PC and a digital input signal through the module (IO) that gets included from an interface card based on an Infrared photo detector, and a pressure switch control panel.

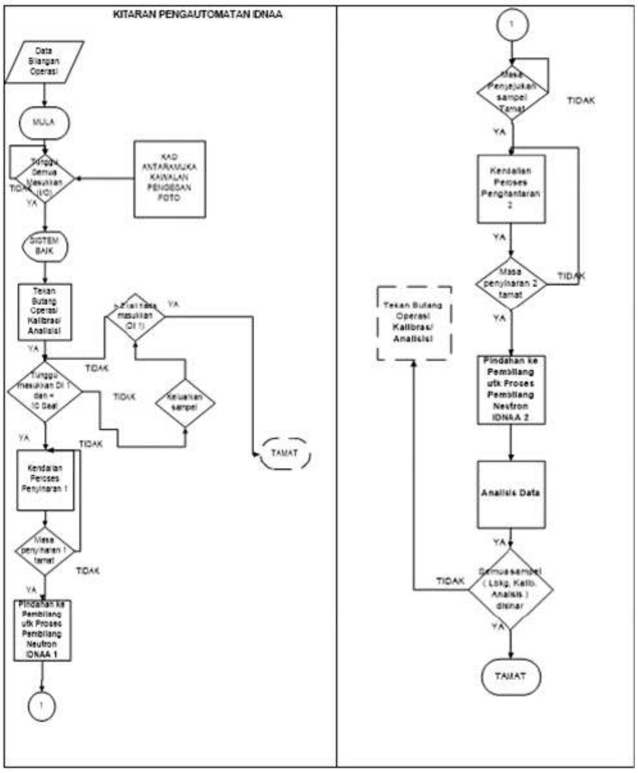

Figure 1: Flow chart of IDNAA automation

2.1 Main Control Panel

The main control panel has several sub-panels displaying PAUS system automation operation activities. The main display panel displays 2 fixed and variable displays where the process control button is permanently displayed on the left side and a simulation sub-panel or a start/stop operation indicator display (On/OFF) of the actuator, a delayed neutron data record display, a rabbit transmission time data record ' and a simple flow chart of the automation process is seen on the right as Figure 2 and Figure 3.

2.2 Problems

This initial development found several issues that have been observed, namely the automatic analysis operation has not been fully carried out, especially the process of analyzing

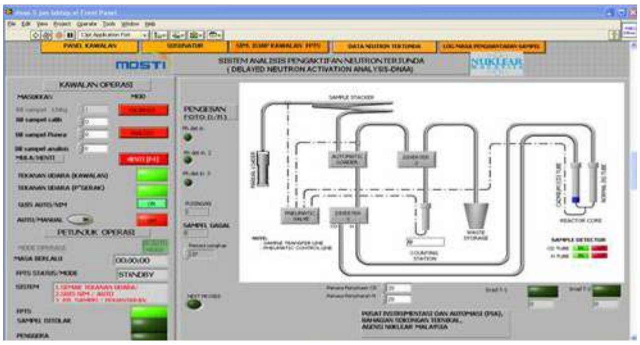

Figure 2: Virtual control and monitoring panel for PAUS

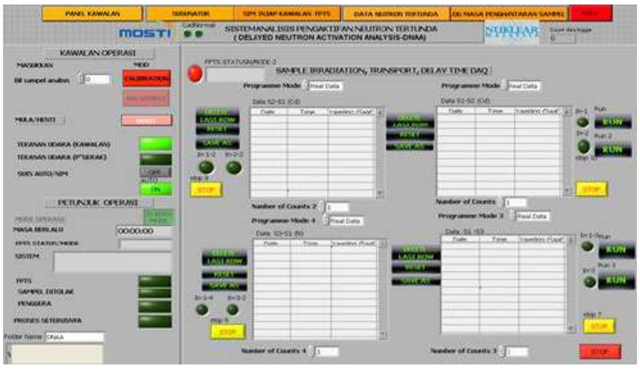

Figure 3: Sub-panel data acquisition of pneumatic effect on sample delivery time

the content of both radionuclides after the irradiation process, making the analysis results time-consuming to issue. The analysis is done manually using microsoft excell software. The development of phase one (1) recorded the automation of PAUS sample transfer parameter transmission found that from the inserter to the reactor core was 3251 ± 210 ms and from the reactor core to the counting chamber was 3264 ± 407 ms. While the results of the analysis using PAUS that was developed using the IAEA S14 standard material found an average of 235U, which is 18.28 ppm (parts per million) and 232Th, which is 439.55 ppm. This gives a relative error of analysis of 5.3 percent for 235U and 5.8 percent for 232Th.

2.3 Improvement Works

The automation control circuit of the PAUS system has been improved where the following works are carried out:

1. Replacement of 'PE tube-5mm' pneumatic system in the control panel and PE Tube-29mm diameter for sample storage and sample disposal and modify the existing 'fitting/bracket'.

2. Rewiring all control modules and components, panel grounding, power supply control switch (24V DC). Replacement Solenoid Air Control Valve, 2 units', Auto/manual selector switch 240V, 6A, On-off-On toggle switch (Miniature Toggle Switch PC Terminal 6A 25V-DC) and LED Indicator Lights and components related to manual control.

3. Provides a data processing system with Intel Core i5 32bit Processing specifications and a printer.

The software still uses the signal flow graphics of LabVIEW software. The operational procedures of the analysis did not change but the program code was reworked considering the weaknesses of the existing program structure which was found to have several weaknesses including the lack of sub vi where this 'sub vi' has many advantages.

3 Results

The functional test of the nuclear counter system was carried out at the PAT laboratory. 29 and found that the rough number of neutrons for 40 seconds resulting from the Am- Be 28 mCurie radioactive source is 500 including the background in the laboratory. The definition of 'Single- Channel Analyser'-SCA, the lowest detection limit of the Voltage or LLV signal is at 1.37 Volts and above and the operating voltage of the detector is 1100V. We encourage the selective use of tables and/or figures as appropriate.

The new software code will be designed by identifying sub-program modules (sub vi) based on functions such as pneumatic valve control, sample transfer data acquisition, sample neutron count data acquisition and analysis calculations and analysis report generation. This modulebased or sub-vi program allows the process of identifying problems (troubleshooting) and making upgrades or improvements easier in the future.

4 Conclusions

In general, phase 1 of the IDNAA system redevelopment is the first step in establishing a better IDNAA analysis facility. With the management's belief in supporting the wider use of reactor technology, the continuation of the ongoing second phase development when completed will and can be used by researchers in NM in particular and will be commercialized even more widely with the development of nuclear reactor applications.

References

Smit M. C. B. 1976. The determination of uranium in geological material by delayed neutron counting. *Report No. PEL–248. Atomic Energy Board, Republic of South Africa*.

Binney S. E. and Scherpelz R. I. 1978. A review of the delayed fission neutron technique. *Nuclear Instruments and Methods*, 154(3):413–431.

Abdul Ghaffar Ramli, Hasni Mohamad, and Meor Yusoff Sulaiman. 1987. Analisis uranium dan thorium melalui teknik analisis neutron tertunda. *Journal Sains Nuklear Malaysia*, 5(1):15–28.

Echo M. W. and Turk E. H. 1957. Quantitative determination of u-235 by delayed neutron counting. *Report PTR-143. The United States Atomic Energy Commission (AEC)*.

Individual Research Contribution Review, 2023, 1(1): 459–460

Correlation of MNA-PF Properties with The Anode Voltage

Rokiah Mohd Sabri
Technical Support Division, Malaysian Nuclear Agency
43000 Kajang, Selangor
rokiah@nm.gov.my

Abstract

The anode voltage has been used as basis for good focusing of the plasma. It has been observed that as the peak anode voltage increases, the current dip and the intensities of the charged particles also increase. The anode voltage signal has been recorded and compared simultaneously. The model and operational parameters of the MNA-PF encoded onto the Lee Model code excel file for simulation and computation. Correlations of intensities of the peak anode voltage have been found and observed. The data obtained are useful for enhancement and optimization of emission of charged particles.

Keywords: Plasma focus, Voltage signal, Current signal

1 Introduction

The Malaysian Nuclear Agency Plasma Focus (MNA-PF) is a compact version of a Mather-type machine MNA-PF device operated by a single 12.5 kV, 30 μF aimed to have a small cost-effective facility for the study of neutron production, x-ray production and understanding of the basic physics of the device. The design of MNA-PF device is based on UNU/ICTP PFF (The United Nation University/International Center For Theoretical Physics Plasma Focus Facility) in Asian– African Association for Plasma Training Network (AAAPT) program (S.Lee, 2014) and originated from University Malaya. The MNA-PF system is sufficiently simple in design and reliable in operation and production of ion beam, x-ray and neutron source.

The Lee Model code provides a beneficial tool to execute initial studies for a given plasma focus machine. It couples the electrical circuit with plasma focus dynamics, thermodynamics and radiation. The basic model (2-phase) with axial phase and radial phase was described in 1984. The model was written as a non-radiative model (3-phase) for an experimental program in 1991. The radiation part was included in a 5-phase code in 2000. The radiative (slow compression) phase will be added and a reflected shock phase is introduced to give a more reasonable start of the quasi equilibrium. The 5-phase code is not suitable for high static inductance (L0>100 nH) plasma focus devices because the computed current waveform in these devices has an extended dip beyond the regular dip so that the simulated current dip appeared less than the measured one. This problem was solved in extended 6-phase code by including the effects of the unusual resistances in a post-pinch phase.

2 Methods

The Lee model code simulates the total current, utilizing four model parameters: mass swept-up factor (f_m) and plasma current factor (f_c) for the axial phase, as well as mass swept-up factor (f_{mr}) and plasma current factor (f_{cr}) for the radial phases. These parameters are used to account for the experimentally observed mass loss and current loss in the axial and radial phases of discharge, respectively (percentages of total mass and current flowing between electrodes in axial and radial phases) (Lee and Saw, 2013). After each run, the user changes one of the model parameters to improve the fitting of the computed to the measured current trace for the next run. This fitting procedure is done sequentially, starting with f_m and f_c while inspecting the fit of the current trace in the axial phase before the current dip, and then proceeds to f_{mr} and f_{cr} while inspecting the fit of the current dip. Additionally, static inductance, L_0 and stray resistance, r_0 parameters may be fine-tuned from run to run during the fitting procedure of current traces. The plasma focus's current signal serves as a primary performance indicator. The Lee model provides insights into axial and radial phase dynamics, radiation yields, and outputs data on phase dynamics, pinch geometry, temperatures, densities, line radiation, and neutron yields. All experimental discharges are individually fitted with simulated ones using the four model parameters, as well as L_0 and r_0 parameters.

This paper reports the measurement of current output of Argon operating gas pressure, 1.5 mbar on plasma pinch properties in Malaysian Nuclear Agency Plasma Focus (MNA-PF), Mather type. The Lee Model code was used to carry out the numerical simulation on MNA-PF to compute current output at optimum voltage supply and filling gas pressure. All experimental discharges (experimental current traces) were fitted individually with simulated discharges (simulated current traces) using four model parameters.

2.1 Lee Model code

The numerical experiment is used to conclude some features of the pinch dynamics and plasma pinch as a function of operating gas pressure. To start with the numerical simulation, a discharge current signal of MNA-PF was selected and obtained by numerical integrating the output of dI/dt calibrated Rogowski coil. The 6-phase Lee Model code was used. To start fitting, the following parameters are used. Lee Model code configured to run the discharge short-circuited to generate a current trace for fitting to measured current waveform. The fitting process of the computed and measured current waveform shown in Figure 1.

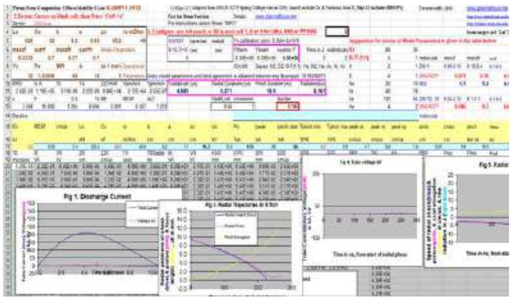

Figure 1: Lee Model code parameters to compute current trace

3 Results and Discussions

The measurements of the current and voltage waveforms on MNA-PF were investigated with Argon gas, Ar, at an optimum pressure of around 1.5 mbarr with high voltage applied 11.0 kV and 12.5 kV. In this work, the measured current traces were used to compute the plasma focus parameters, and ion and electron beam properties emitted from MNA-PF operated with Argon gas, Ar, using the Lee model code. The fitting procedures using the Lee model were investigated for each measured current step by step.

The experimental parameters of MNA-PF which have been set on the simulation of the Lee model code are static inductance, L_0 = 1430 nH, storage capacitance, C_0 = 25 μF, r_0 = 50 mΩ, cathode radius, b = 3.2 cm, anode radius, a = 0.95 cm, anode length, z_0 = 16 cm with operating voltage, V0 = 11.0 and 12.5 kV and initial pressure, p0 = 1.5mbarr for Argon gas. In the same manner, applying the adapted version of the Lee model code on the plasma focus device and considering the fitting procedures, the pinch plasma parameters and the properties of the electron and ion beams were determined for each shot.

Figure 2 and Figure 3 shown simulation results of 11.0 kV and 12.5 kV using Lee Model Code. Table 1 shows the data obtained through the parameters available from the simulation using Lee Model code. From the results, it is found that the increase in voltage supplied to the system affects the good concentration. The higher voltage is given, the better the concentration will be. However, it is well known that high voltage supplied at plasma focus device can play a dominant role in determining current distribution in plasma focus and will affect the focus mechanism.

4 Conclusions

Measurements of the ion beam flux, ion beam fluence and ion beam energy are calculated on the low energy MNA-PF device with Argon gas around the operational pressure 1.5 mbar during the experiment. The Lee model is adapted to the version of 6-phase code for studying the formed plasma, as well as the produced ion beams. The fitting procedures between the measured and computed current waveforms are applied for each shot. Then, numerical experiments are carried out using the Lee Model code.

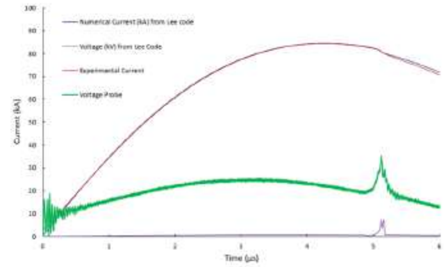

Figure 2: Simulation Lee Model Code result for 11.0 kV high voltage power supply

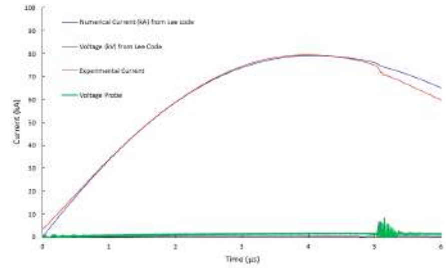

Figure 3: Simulation Lee Model Code result for 12.5 kV high voltage power supply.

Table 1: Data obtained through the parameters available from the simulation using Lee Model code

Voltage	11.0kV	12.5kV
Speed Factor	78.5	83.7
U (keV)	20.6	22.3
U*Zeff (keV)	170.0	201.0
Ion Flux ($m^{-2}s^{-1}$)	6.3x10^{26}	1.8x10^{27}
Ion Fluence (m^{-2})	1.1x10^{19}	3.4x10^{19}
Damage Factore ($Wm^{-2}s^{0.5}$)	2.2x10^{9}	7.9x10^{9}
FPS Energy %E0	2.7	2.6
FPS Speed (cm/us)	9.8	16.0
Number of Ions	6.8x10^{13}	9.1x10^{13}
Current Density (A/m^2)	8.3x10^{8}	2.6x10^{8}
Ion Speed 1 Charge (cm/us)	31.3	32.6
Ion Speed Zeff (cm/us)	90.1	98.0
Ion Current (kA)	5.2	7.0
ni pinch ($10^{23}/m^3$)	14.1	8.2
Pinch Duration (ns)	17.1	19.0
Ions/s	3.9x10^{21}	4.8x10^{21}
T Pinch ($\times 10^6$ K)	0.6	0.9
Beam Energy(J)	1.8	2.9

References

S. Lee and S.H. Saw. 2013. Plasma focus ion beam fluence and flux—for various gases. *Physics of Plasmas*, 20(6):062702.

S.Lee. 2014. Plasma focus radiative model: Review of the Lee model code. *Journal of Fusion Energy*, 33(4):319–335.

Individual Research Contribution Review, 2023, 1(1): 461–462

Measurement of Ion Beam in Malaysian Nuclear Agency Plasma Focus

Rokiah Mohd Sabri
Technical Support Division, Malaysian Nuclear Agency
43000 Kajang, Selangor
rokiah@nm.gov.my

Abstract

This study presents the computed ion beam properties (flux, fluence, and energy) of Argon gas with pressure variation in the Malaysian Nuclear Agency Plasma Focus device, MNA-PF. Numerical experiments are performed using the Lee code with the Argon gas in the pressure range of 1.5 mbar. The computed results of Argon gas show that the ion beam properties measured and calculated.

Keywords: Plasma focus, Ion beam

1 Introduction

The Malaysian Nuclear Agency Plasma Focus (MNA-PF) is a compact version of a Mather-type machine MNA-PF device operated by a single 12.5 kV, 30 μF aimed to have a small cost-effective facility for the study of neutron production, x-ray production and understanding of the basic physics of the device. The design of MNA-PF device is based on UNU/ICTP PFF (The United Nation University/International Center For Theoretical Physics Plasma Focus Facility) in Asian– African Association for Plasma Training Network (AAAPT) program (S.Lee, 2014) and originated from University Malaya. The MNA-PF system is sufficiently simple in design and reliable in operation and production of ion beam, x-ray and neutron source.

The application of a dense plasma focus device for various material processing utilizes high energy ions. The characterization of these ions beam is very important, not only for understanding the mechanism of the production of high-energy ions, but also for their applications in different fields, including plasma processing (ion implantation, surface modification, thermal surface treatment, ion assisted coating, device fabrication and thin film deposition).

2 Methods

2.1 Lee Model code

The discharge current waveform getting from MNA-PF operation can be considered a significant indicator of realistic simulation and analyze all the gross properties of a plasma focus. Using the Lee Model code, the important information (axial and radial phase dynamics and radiations) of a device can be traced quickly from the current flow through the plasma sheath. However, when the computed discharge current waveform is fitted with the measured one, the computed outputs of the code provide the following realistic data: the dynamics and energy in each phase, the geometry of pinch column, densities and temperatures, radiations, neutron yields, and ion beam. Therefore, to simulate a specific DPF device by this code, the measured discharge current waveform of the device is to be picked out from current discharged from a laboratory experiment. So, the extended 6-phase Lee Model code was used to study the ion beam generated in the MNA-PF device using the fitting procedures mentioned above for 12.5 kV voltage supply.

2.2 Ion Beam Flux Equation

To study the properties of the emitted ion beam from the pinch plasma in a DPF, the ion beam flux equation has been derived and inserted into the Lee code. At the time of simulation, the flux of the ion beam is estimated in the code with the following equation:

$$\text{Flux (ions } m^{-2}s^{-1}) = 2.75\times 10^{15}\left(\frac{f_e}{\sqrt{MZ_{\text{eff}}}}\right)\left(\frac{ln[b/r_p]}{{r_p}^2}\right)\left(\frac{I^2_{\text{pinch}}}{\sqrt{U}}\right) \tag{1}$$

2.3 The Ion Fluence Equation

The ion fluence is defined as the number of ions per unit cross-section of the pinch column. Since the beam emits from the focus pinch with slight divergence, fluence is the best way to characterize the ion beam. It is calculated as the flux multiplied by the pulse duration of the ion beam.

$$\text{Fluence (ions } m^{-2}) = 2.75\times 10^{9}\left(\frac{f_e}{\sqrt{MZ_{\text{eff}}}}\right)\left(\frac{ln[b/r_p]}{{r_p}^2}\right) \tag{2}$$

2.4 The Ion Beam Energy Equation

Ion beam energy (E) is estimated by using the following equation:

$$E(J) = Z_{\text{eff}}U \times \text{Number of ion in beam} \tag{3}$$

The Lee Model code computes the values of Z_{eff}, r_p, pinch duration, I_{pinch}, and U along with the ion beam flux followed by ion beam fluence and energy.

This paper reports the measurement of ion beam produced by Argon gas with operating gas pressure, 1.5 mbar in Malaysian Nuclear Agency Plasma Focus (MNA-PF). The Lee Model code was used to carry out the numerical simulation on MNA-PF to compute current output at 12.5 kV voltage supply to measure the ion beam production from MNA-PF device.

The experiment was performed at 12.5 kV with 1.5 mbar Argon gas using MNA-PF. To start with the numerical simulation, discharge current signal of MNA-PF was selected to find the output of dI/dt. The Lee Model code simulate and fitting the computed current trace.

3 Results and Discussions

The operating pressure of Argon gas and the corresponding flux, fluence, and energy of outgoing ion beam from pinch plasma in terms of I_{peak}, I_{pinch}, Z_{eff}, r_p, and U are obtained using the Equation (1), (2), and (3) through the Lee Model code. Table 1 shown the ion beam characteristics in MNA-PF. From the computed results, ion beam flux= 1.8 x 10^{27} $m^{-2}s^{-1}$, ion beam fluence= 3.4 x 109 m^{-2} and ion beam energy= 2.9 J.

Table 1: Ion beam properties with pressure Argon gas, 12.5 kV voltage supply in MNA-PF.

Voltage	**12.5kV**
Speed Factor	83.7
U (keV)	22.3
U*Z_{eff} (keV)	201.0
Ion Flux ($m^{-2}s^{-1}$)	$1.8x10^{27}$
Ion Fluence (m^{-2})	$3.4x10^{19}$
Damage Factore ($Wm^{-2}s^{0.5}$)	$7.9x10^{9}$
FPS Energy %E0	2.6
FPS Speed (cm/us)	16.0
Number of Ions	$9.1x10^{13}$
Current Density (A/m^2)	$2.6x10^{8}$
Ion Speed 1 Charge (cm/us)	32.6
Ion Speed Z_{eff} (cm/us)	98.0
Ion Current (kA)	7.0
ni pinch ($10^{23}/m^3$)	8.2
Pinch Duration (ns)	19.0
Ions/s	$4.8x10^{21}$
T Pinch ($\times 10^6$ K)	0.9
Ion Beam Energy, E (J)	2.9

4 Conclusions

Measurements of the ion beam flux, ion beam fluence and ion beam energy are calculated on the low energy MNA-PF device with Argon gas around the operational pressure 1.5 mbar during the experiment. The Lee model is adapted to the version of 6-phase code for studying the formed plasma, as well as the produced ion beams. The fitting procedures between the measured and computed current waveforms are applied for each shot. Then, numerical experiments are carried out using the Lee Model code.

References

M. Akel, S.A. Salo, S.H. Saw, and S. Lee. 2014a. Ion beam features produced by two plasma focus machines operated with different gases. *IEEE Transactions on Plasma Science*, 42(9):2202–2206.

M. Akel, S.A. Salo, S.H. Saw, and S. Lee. 2014b. Properties of ion beams generated by nitrogen plasma focus. *Journal of Fusion Energy*, 33(2):189–197.

S. Lee and S.H. Saw. 2013. Plasma focus ion beam fluence and flux—for various gases. *Physics of Plasmas*, 20(6):062702.

R.M.Sabri, A.H.Baijan, S.A.Hashim, M.R.M.Chulan, L.K.Wah, M.Mokhtar, A.Ahmad, and R.C.Ros. 2016. Plasma focus device as a x ray source for radiography applications in Nuclear Malaysia. *Jurnal Sains Nuklear Malaysia*, 28(1):30–33.

S.Lee and S.H Saw. 2012. Plasma focus ion beam fluence and flux—scaling with stored energy. *Physics of Plasmas*, 19(11):112703.

S.Lee. 2014. Plasma focus radiative model: Review of the Lee model code. *Journal of Fusion Energy*, 33(4):319–335.

Individual Research Contribution Review, 2023, 1(1): 463–464

Migration of Email from Zimbra to MyGovUC 2.0 - Towards Stable Email Communication and Information Security

Saaidi Bin Ismail
Technical Support Division, Malaysian Nuclear Agency
43000 Kajang, Selangor
saaidi@nm.gov.my

Abstract

The MyGovUC 2.0 platform (MyGovUC) is introduced as an integrated communication solution to enhance government service delivery methods and achieve comprehensive cost savings. It is also aimed at improving the security of information exchange and minimizing communication disruptions. There are 13 core services offered by MyGovUC, but this study specifically focuses on email communication. The Malaysian Nuclear Agency took 8 months (December 2022 to August 2023) to prepare for the implementation of technical, administrative, and change management transformations, as well as risk analysis.

Keywords: government service delivery methods, information exchange security, communication disruption.

1 Introduction

Malaysian Nuclear Agency (Nuklear Malaysia) has been using email as one of its communication methods since 1992. There have been six instances of changing email service providers to ensure that the delivery methods achieve their objectives. All previous platform changes were carried out internally by officers in Information Technology Center (ITC). However, for the transition to MyGovUC, external involvement (MAMPU) was introduced, requiring several changes, including unforeseen ones, while maintaining email communication. This transformation involves shifting from a communication approach focused solely on email to an email platform that includes additional delivery methods and information sharing through chat, video conferencing, collaborative storage, restricted document sharing, and the utilization of cloud storage technology.

2 Method

The initial technical discussion with MAMPU to assess readiness was conducted on February 9, 2023. The implementation was divided into three main activities, namely user information collection, technical preparation, and implementation activities.

The user information collection activity involved 896 individuals and took 3 days to complete. The data was extracted from the Infomint Biodata System, and additional information such as phone numbers and alternative email addresses took three months to compile. The technical preparation activity, including configuration and server changes, took 2 months as it involved approval and verification from relevant parties, scripting automation, and data sanitation.

The implementation activity took 3 months and included installation, changes in route configuration, dissemination of notifications regarding usernames and passwords, and verification of Two Factor Authentication (2FA). The longest process was the activation of 2FA, which was fully completed on August 7, 2023. Details of these activities can be seen in Figure 1 below.

Bil	Aktiviti	1st 2mth	2nd 2mth	3rd 2 mth	4th 2mth	Nota
1	Mesy Libaturus	4/11/22				
2	Perbincangan Teknikal	9/2/23		3/5/23		
3	Verifikasi langganan/ Pemohonan	10/2/23				
	XTVT 1					
4	Pengumpulan Maklumat Pengguna	20/1/23	12/4/23			4 kali warning
5	Serahan maklumat		17/4/23			
6	Backup data/archiving		17/4/23	18/5/23		
	XTVT 2					
7	Pewujudan akaun		18/4/23	10/5/23		
8	DNS Swing, Config CutOver,			18/5/23		tukar email
9	Ujian penerimaan			19/5/23	2/6/23	
	XTVT 3					
10	Hebahan username passwd,			14/5/23		
11	Taklimat pengguna			19/5/23	11/7/23	
12	2FA, konfig user, activate			19/5/23	7/8/23	sepanjang

Figure 1: Migration Activity

3 Result

Daily transactions on the Zimbra email platform for addresses with user@nuclearmalaysia.gov.my reached tens of thousands per day, including spam. However, with the transition to the MyGovUC platform using the address user@nm.gov.my, a significant and drastic decrease in email transactions was observed, totaling only in the thousands. This can be seen in Figure 2.

Figure 2 shows a decline in Zimbra email transactions starting from May 18, 2023, but an increase is detected on May 19, 2023, due to user email migration. It steadily decreases afterward, reaching an average estimated transaction range from tens of thousands per day to only thousands per day (27,000-91,000 per day to 3,000-6,000 per day).

However, the Zimbra platform is still utilized for internal system notifications such as autoreply, error notifications, server monitoring, and individual journal subscriptions. New subscriptions in 2024 are required to use the MyGovUC email. Examining the email issue statistics, it is reported as illustrated in Figure 3.

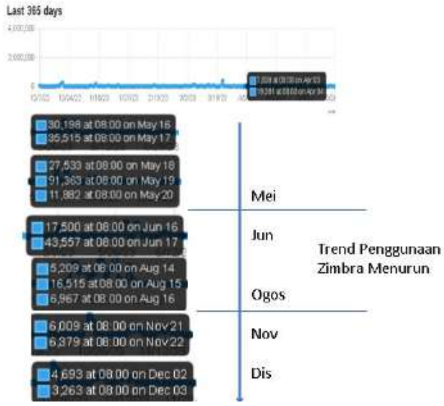

Figure 2: Zimbra transaction trend

Figure 3: Report on email issues based on Localweb HelpDesk.

4 Discussion/Conclusion

Based on the low number of email issue reports in Figure 3, considering the figures from June to December 2023, the transformation from Zimbra to MyGovUC can be considered successful, and issues such as spam have been effectively reduced. With the reduced incidence of spam, users will feel more secure, and the risk of clicking links in such spam is successfully mitigated earlier.

The usage of MyGovUC-Google Workspace for the address @nm.gov.my during the same period also increased, with a daily average of around 4,000-8,000 *GWS Report by PERNEC MAMPU.

References

https://localweb.nuclearmalaysia.gov.my. Dec 8, 2023. Server statistic: Localweb techdesk. *https://localweb.nuclearmalaysia.gov.my/helpdesk/v1/.*

https://mail.nuclearmalaysia.gov.my. December 7, 2023. Server statistik: Zimbra version 9. *https://mail.nuclearmalaysia.gov.my:7071/zimbraAdmin/.*

Individual Research Contribution Review, 2023, 1(1): 465–466

Speed Verification of Conveyors for Validation of an Irradiation Process at an Electron Beam Facility

Shalina Sheik Muhamad
Technical Support Division, Malaysian Nuclear Agency
43000 Kajang, Selangor
shalina@nm.gov.my

Abstract

Operational Qualification (OQ) is essential for the success of the application of radiation processing. Conscientious attention is given to demonstrate that the irradiator, as installed, is capable of operating and delivering appropriate doses within defined acceptance criteria. The Operational Qualification must be considered a critical activity for creating baseline data used for a full understanding of the process and relevant parameters, to compare after repairs/maintenance and after facility component replacement. The speed of conveyors used in radiation processing systems is one of the factors influencing absorbed dose and dose distribution to the flat surfaced product such as silicon wafer, facial mask, waste water and food. This work presents an operational qualification for monitoring and validation of the conveyor speed in an irradiation facility. The deviation values obtained help provide the quality control team with the periodic verification activity as consistency is important for OQ. It also helps the maintenance team to better plan for corrective actions such as disassembly and lubrication of the conveyor system.

Keywords: Operational Qualification, electron beam, irradiation facility, radiation process control, consistency

1 Introduction

Radiation processing is based on the concept of the dose deposited in a product. Measurement of the absorbed dose, in addition to the irradiation parameter controls, provides proof that the radiation processing has been carried out according to the required specifications. When using irradiation to disinfect, decontaminate or extend food shelf life, the main technical challenge is to achieve a uniform dose distribution throughout the product. Over-dosage is costly, while under-dosage can have massive safety implications (Ferreira et al., 2018). The uniformity of the applied energy of an accelerator beam (exposure time) to a product will define the dose received. In electron beam applications, factors that influence absorbed dose and dose distribution are electron beam current (and energy), conveyor speed, scan width/length and uniformity, number of passes, product geometry/density/orientation and process interruption (Kuntz, 2023). Thus, the conveyor speed under the output window of the electron beam, defines the effectiveness of the dose applied to the product. Bulk products can be distributed uniformly on a belt conveyor, and packaged products can be placed directly on a belt conveyor or in totes on a roller conveyor. The beams then scan across the products in the horizontal direction, as schematically shown in Figure 1.

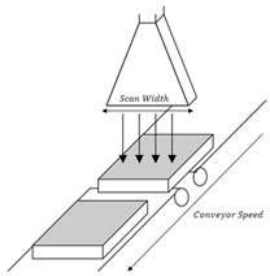

Figure 1: Typical schematic representation of the electron beam scanning configuration (Miller, 2005)

2 Methods

The objective was to evaluate both the speed and the percentage of variations in the speed of a conveyor over a range of required speeds. To measure the performance of the conveyor at various speed set points, an experimental device of a known length and time was set up. Since the length of the travel and the length of time it takes to pass a specific point were known, it was possible to calculate the average speed of the conveyor. The simplest method was to mount a pen and ruler in the defined location of the conveyor. The stopwatch and video recording started the timing function when the pen first passed and stopped when the pen had fully passed (Figure 2). This timing procedure must be repeated for each test speed (0.4 and 0.89 m/min).

3 Data/Result

Table 1 presents the travel time and average speed from the experiments. Table 2 represents the difference between the measured and target speeds in percentage. The acceptable value of the error is a criterion of the facility that owns the equipment.

4 Discussion/Conclusions

From Table 2, it can be seen that the actual speeds were significantly lower than the target speeds. The differences were

Figure 2: Pen and ruler positioned in the two conveyors.

Table 1: Travel time and average speed of the conveyor *Empty Tray

Target speed (m/min)	Distance (m)	Stop with Stop-watch (min)	Time with Video (min)	Calculated actual average speed (m/min)
0.20	0.3	NA	1.88	0.16
0.40	1.0	2.70	2.65	0.38
0.89	1.0	1.17	1.25	0.80

up to 25% lower for 0.2 m/min, 5% and 6.7% for 0.4 and 0.89 m/min respectively. By analysing the video and snapped pictures, the distance travelled by the tray according to elapsed time were plotted. Figure 3 shows the linear plot for the target speed of 0.4 m/min. From the linear plot of Figure 3, the *instant* speed at several locations was calculated as shown in Figure 4. From Figure 4, it could be seen that the instant speed varied significantly over the course of the conveying distance. At this speed setting (0.4 m/min) the average calculated speed was 0.38 m/min with a standard deviation of 0.03. The significant variations observed could impact the dose uniformity in conveying travel distance. Therefore, it is recommended to improve the consistency and stability of the conveyor.

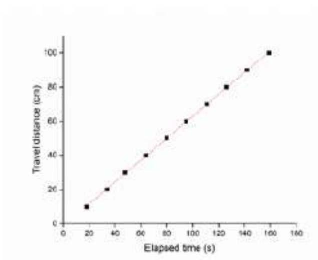

Figure 3: Travel distance and elapsed time for target speed of 0.4 m/min

The testing of conveyor system's speed is an essential process since allowable speed variations are a major factor in the management of quality and maintenance teams. This technical article has presented a procedure for speed verification

Table 2: The difference between measured and target speeds

Target speed (m/min)	Average measured speed (m/min)	Difference between measured and target (%)
0.20	0.16	25.0
0.40	0.38	5.0
0.89	0.83	6.7

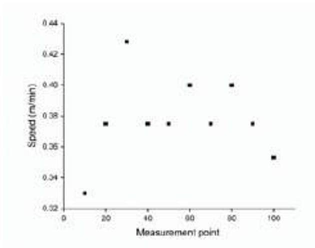

Figure 4: Instant speed of 0.4 m/min

of a conveyor system. By using a few basic pieces of equipment (pen, ruler, stopwatch and video recording) is possible to complete an effective proof of the process. It is proposed to run a periodic of speeds tests that allow the calculation of the average error of the system. It also can allow the maintenance team to adjust the motor's controller's software or predictive maintenance such as disassembly for lubrication. This method is valid and effective that works in a process with electron beam accelerators used for sterilization and polymerization. This article aimed at presenting the engineering teams with a simple procedure with an easy application that can be used for other processes and services.

The work presented reflects the qualification tests performed in EPS 3000 electron beam accelerator at ALURTRON, Nuclear Malaysia during IAEA expert mission with the aim of validation and verification of dosimetry system for sanitary and phytosanitary purposes. Based on the study, it shows that significant variations of conveyor speeds could impact the dose uniformity in conveying travel distance. Therefore, it is suggested to improve the consistency and stability of the conveyor.

References

Isabel C. F. R. Ferreira, A. L. A., and S. C. V. 2018. Food Irradiation Technologies Concepts, Applications and Outcomes. CPI Group (UK) Ltd.

F. Kuntz. 2023. Installation and Operational Qualification-IAEA RCA/RAS5087. Issue 01.

R. B. Miller. 2005. ELECTRONIC IRRADIATION OF FOODS An introduction to the technology. *Springer Science Business Media, Inc.*

Development of the Malaysian Nuclear Agency Radiation Worker Record Management System (SPPS)

Siti Nurbahyah Bt. Hamdan
Technical Support Division, Malaysian Nuclear Agency
43000 Kajang, Selangor
nurbahyah@nm.gov.my

Abstract

Under the Atomic Energy Licensing Act 1984 (Act 304), all licensees are required to be responsible for ensuring the safety and protection of radiation workers from ionizing radiation. Following that, each radiation worker has a radiation exposure record book that contains annual radiation exposure reading information by month. In addition, the Radiation Protection Officer (RPO) is responsible for monitoring health examination records and radiation safety-related training records for each radiation worker, which is once every 3 years.

This information needs to be updated and notified to the Atomic Energy Licensing Board (LPTA) periodically to fulfill part of the license compliance requirements. From the analysis of user needs, until January 2019, the Malaysian Nuclear Agency has a total of 395 radiation workers for both agency licenses. The Radiation Safety Division (BKS) manages the radiation worker exposure record book manually and relies on the MS Excel application to update information on health screening and radiation worker training.

Therefore, a radiation worker record system has been developed by integrating the eSSDL system and the existing Bioweb System to facilitate the management and monitoring of radiation exposure information of radiation workers. Through this system, the BKS can also monitor health check-up records and training records attended by radiation workers according to the set period.

1 Introduction

Every radiation worker needs to attend regular training and medical examination, which is once every three (3) years. While the exposure dose of radiation workers needs to be monitored every month. These things need to be recorded for LPTA audit purposes in meeting the requirements of the act. For now, occupational exposure doses for 395 radiation workers are recorded in the LPTA/BM/5 Medical Record Book (Section B) every month manually.

2 Method

The Linear Sequence methodology (Waterfall Methodology) has been used to develop the SPPS system. The system development approach using this predictive model requires a comprehensive study of user needs according to a series of structured phases before the system is designed and developed. Business process reengineering (BPR) has been implemented to set the functionality of the system to meet the needs of various levels of users from different business units. The relationship diagram between entities is illustrated as Figure 1 below.

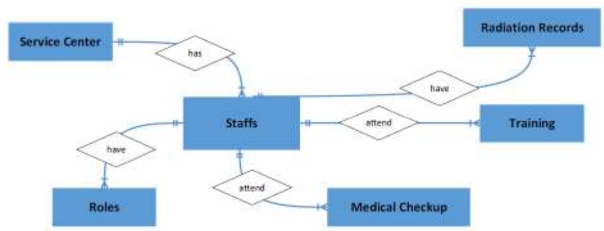

Figure 1: Entities Relationships Diagram

3 Result and Discussion

In order to ensure that the functionality of the SPPS system meets the needs of users and agencies, the integration process has been carried out between the SPPS and the Bioweb System and the eSSDL System.

Figure 3 shows the design of the SPPS physical architecture and its relationship with other systems. The information design of the SPPS system consists of 3 main components, namely users, business processes and information groups as illustrated in Figure 4. Four directly identified user groups for each process are:

(a) Radiation Workers,

(b) KFK Staff,

(c) Radiation Protection Officer
(based on three license categories), and

(d) System Administrator

Business process that has been identified for the automation of the radiation exposure record management process is as shown in the Figure 2 below.

Based on information requirements, the SPPS System is integrated with several other systems such as email, Active

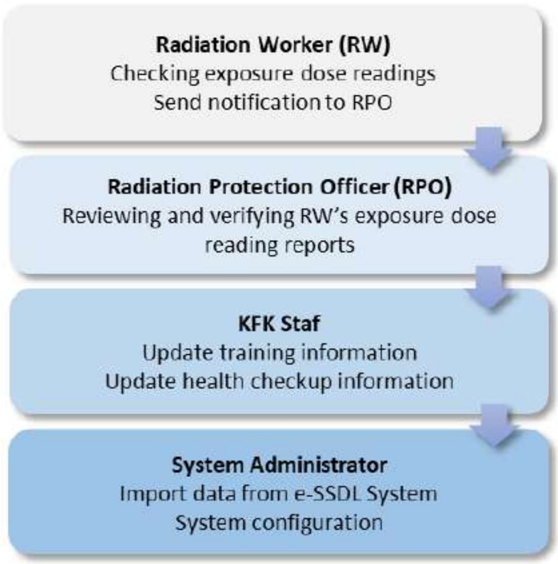

Figure 2: Business Process Components

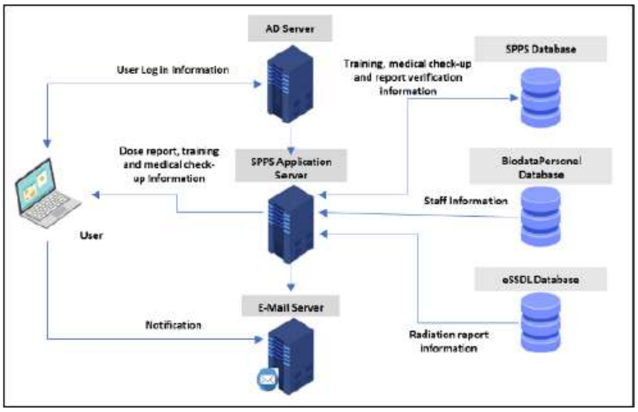

Figure 3: SPPS Physical Architecture Design

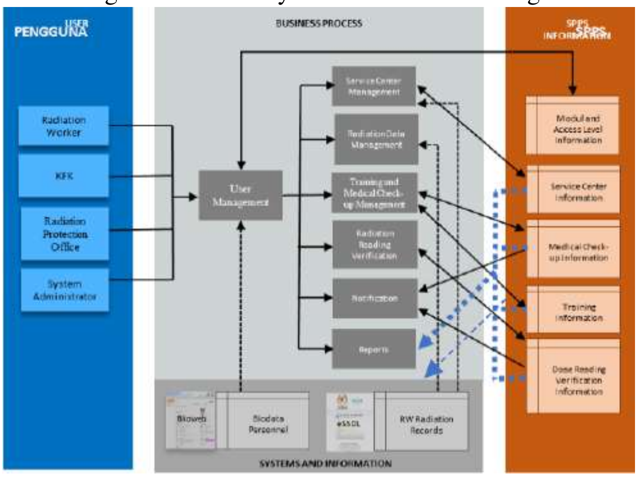

Figure 4: SPPS Information Design

Directory (AD), personnel Information database and e-SSDL System database.

SPPS System has been developed in the Internet Information Services (IIS) web server environment but has used the PHP programming language. The database software used is MSSQL. In addition, the Bootstrap CSS Framework has also been used to create a more responsive website that supports the mobile environment. Next, the system was tested and errors identified during testing phase were fixed. Proper training sessions have been given to users to ensure smooth use of the system.This system is maintained by the IT Center to ensure its running smoothly, efficiently and safely.

4 Conclusion

There are several issues that have been identified. Among them are issues related to data from the e-SSDL System. The user profile in the e-SSDL System is not synchronized with the BiodataPersonel user profile. Therefore, any change in user information in eSSDL will cause the user display in SPPS to be less accurate. System administrators should check this periodically. In addition, there are also restrictions on the exposure reading report that is displayed. This happened because of the system developer's difficulty in querying the data in the eSSDL database due to the data structure in the eSSDL system not meeting the SPPS exposure dose reading display requirements based on the LPTA radiation exposure record book. Exposure dose readings can be displayed according to the radiation license category available in Nuklear Malaysia. However for the license category under NDT, there is a slight difference in requirements in the training module. Developers need to review user specifications and modifications are underway.

References

Buku kejuruteraan sistem aplikasi sektor awam (KRISA). *https://sqa.mampu.gov.my/index.php/ms/garis-panduan/garis-panduan-pembangunan-aplikasi-krisa*.

Program perlindungan sinaran Agensi Nuklear Malaysia, lesen LPTA/A/724.

1984. Undang – undang Malaysia, Akta 304, Akta Perlesenan Tenaga Atom 1984.

2010. Peraturan-peraturan Pelesenan Tenaga Atom (Perlindungan Sinaran Keselamatan Asas) 2010.

Mark McMurtrey. 2013. A case study of the application of the systems development life cycle (SDLC) in 21st century health care: Something old, something new? 1(1, DOI: http://dx.doi.org/10.3998/jsais.11880084.0001.103).

Individual Research Contribution Review, 2023, 1(1): 469–470

The Importance of the Information System Maintenance Phase in the System Development Life Cycle (SDLC) and the Service Continuity Plan (PKP)

Siti Nurbahyah Bt. Hamdan
Technical Support Division, Malaysian Nuclear Agency
43000 Kajang, Selangor
nurbahyah@nm.gov.my

1 Introduction

The Malaysian Nuclear Agency (Nuklear Malaysia) is the main leader in research and development (R&D) of nuclear science and technology in Malaysia. Among the country's industry, Nuclear Malaysia is not left behind in playing a role by providing services and producing products based on radiation technology that have an impact on the country's economy and development. Therefore, Nuclear Malaysia needs an effective, reliable and safe delivery system landscape as the backbone of the agency to support R&D activities, operations, business transactions, decision-making processes and information and communication delivery channels to interact with stakeholders.

Nuklear Malaysia's information system is developed using the System Development Life Cycle (SDLC) methodology. SDLC provides a structured framework for managing operational automation processes and business processes within an agency. One of the most important and final phases in the SDLC is the maintenance phase. This phase is used to monitor the system that has been developed to function according to the requirements that have been set. In the maintenance phase as well, the system development group will fix any errors, provide technical support and identify the need for improvements to the system that need to be done for the benefit of users.

At the same time, Nuclear Malaysia is also implementing a public sector service continuity plan (Pelan Kesinambungan Perkhidmatan - PKP). PKP is implemented to ensure that agencies can maintain essential functions by minimizing the impacts of disruption that may affect agency's main activities. This extended abstract explores the important role of system maintenance in the SDLC and its relationship to the effectiveness of the implementation of the PKP strategy.

2 Method

The discussion in this paper uses a literature review approach and case study methodology. A number of existing literatures were reviewed, including scholarly articles, industry reports and case studies at the agency itself; to identify the relationship between system maintenance, SDLC and PKP. The analysis also considers technological, process and human factors that influence this relationship.

3 Result and Discussion

From the analysis conducted, several things have been found as follows:

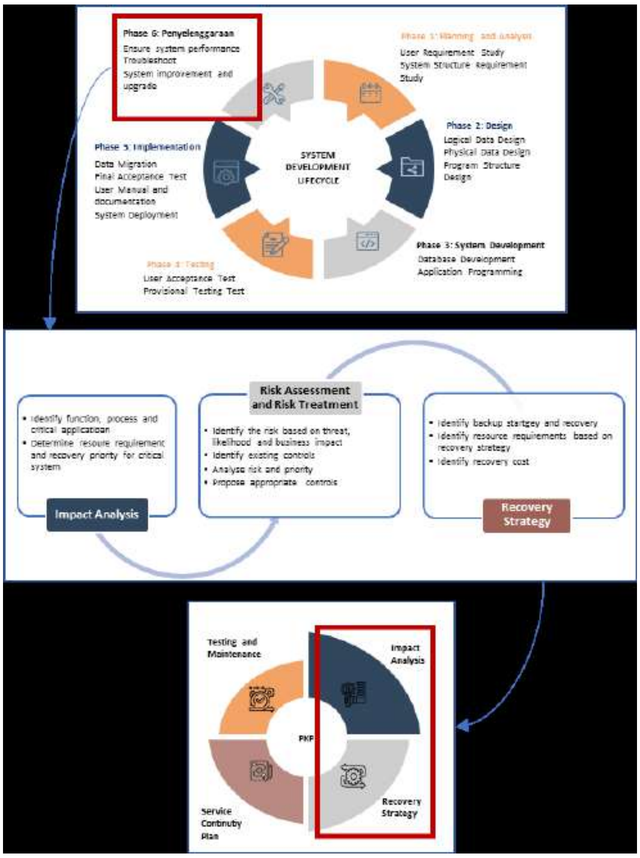

Figure 1: Maintenance activities provide input to the implementation of PKP

(i) Maintenance Strategy:

Agencies that practice proactive maintenance during the SDLC experience fewer disruptions to their business operations. An important component in proactive maintenance is updating the information system and system environment including hardware and software, updating patches, monitoring system security consistently. This contributes to the stability of the system, reduces risks related to data security and protects the system from cyber threats.

(ii) PKP Implementation:

Integrating maintenance practices into the PKP plan is important to minimize downtime during a disaster or crisis. This includes identifying system threats and vulnerabilities, identifying critical system components, establishing backup systems, and establishing efficient, effective, and secure recovery mechanisms.

(iii) Human Factor:

Awareness training programs for employees play an important role in ensuring that both system maintenance and PKP activities can run hand in hand. Trained employees are more likely to identify potential issues and risks earlier and respond effectively during system failures.

(iv) Use of latest technology:

Using modern technology such as predictive maintenance tools and automation can streamline the maintenance process, making it more efficient and cost-effective. These advances contribute to better system resilience. In addition, system backup technology and the availability of a disaster recovery site (disaster recovery site) can contribute to a faster, efficient and effective recovery process.

(v) Organizational Culture:

Organizations that foster a culture of continuous improvement and resilience tend to perform better in both maintenance and PKP. A culture that embraces adaptability and learning from failure (lessons learned) can lead to more robust system performance.

4 Conclusion

The integration of system maintenance in the SDLC and its alignment with the PKP is essential to ensure service continuity in Malaysia's complex and interconnected Nuclear environment. This extended abstract outlines the symbiotic relationship between system maintenance, SDLC and PKP. It emphasizes that system maintenance should not be seen as a routine operation but as one of the proactive strategies to reduce risk, increase overall system reliability and system strengthening.

References

Nurul Aisyah Sim Abdullah, Nor Laila Md Noor, and Emma Nuraihan Mior Ibrahim. 2015. Contributing factor to business continuity management (BCM) failure – A case of Malaysia public sector. *Proceedings of the 5th International Conference on Computing and Informatics, ICOCI.*

Asra Masrat, Mohammed Ammar Makki, and Hardika Gawde. April 24, 2021. Software maintenance models and processes: An overview.

Mark McMurtrey. 2013. A case study of the application of the systems development life cycle (SDLC) in 21st century health care: Something old, something new? 1(1, DOI: http://dx.doi.org/10.3998/jsais.11880084.0001.103).

Tamara Radjenovic and Snezana Zivkovic. 2022. *The Effectiveness of Business Continuity Management System in Enterprises.*

Monika Sethi and Anju. Sharma. 2013. Information system and system development life cycle. pages 118–127, 10.4018/978–1–4666–3679–8.ch007.

Howard Slomer and Alan Christie. 1992. Analysis of a software maintenance system: A CASE study. (CMU/SEI-92-TR-031). *Carnegie Mellon University, Software Engineering Institute's Digital Library, Software Engineering Institute.*

C. J. Stefanou. 2003. System development life cycle. *Encyclopedia of Information Systems*, pages 329–344, doi:10.1016/b0–12–227240–4/00176–3.

Individual Research Contribution Review, 2023, 1(1): 471–472

Effect of Ultraviolet Irradiation Dose on Mechanical Properties of Hybrid Ultraviolet-Peroxide Prevulcanized Natural Rubber Latex

Sofian Ibrahim
Technical Support Division, Malaysian Nuclear Agency
43000 Kajang, Selangor
sofian_ibrahim@nm.gov.my

Abstract

At present, there are three main vulcanization procedures being used in rubber latex industries; which is sulphur, radiation and peroxide vulcanization. However, another vulcanization technique that began to receive serious attention from researchers is UV vulcanization. This paper will discuss the effect of UV irradiation time and dose on the mechanical properties of hybrid UV and peroxidation vulcanizations.

Keywords: vulcanization, UV radiation, latex

1 Introduction

Over the past decade, researchers have begun to gain interest in ultraviolet (UV) vulcanization. According to the findings and report by Schlögl (2010), vulcanization of natural rubber latex through UV irradiation can be done by adding a photoinitiator into the latex formulation; this photoinitiator will form free radicals via the thiol-ene addition reaction when exposed to UV radiation.

The present work attempts to combine UV and peroxide vulcanizations with the presence of an acrylate coagent. Effects of the following factors on the mechanical properties (tensile strength) of the resulting prevulcanized natural rubber latex were assessed in order to determine the optimal UV dose for prevulcanization. This research output may trigger the diversification and encourage the use of sulphur-free prevulcanized natural rubber latex in local latex product industries and abroad.

2 Methods

2.1 Preparation of RVNRL compounding formulations

A 2.5 kg latex formulation was prepared by weighing NRL into a beaker. Then the beaker was covered using aluminum foil before slowly adding stabilizer, peroxide, activator, acrylate, photoinitiator and water (with gentle stirring) at room temperature in the dark as shown in Table 1 (Sofian et al., 2018; Wiroonpochit et al., 2017) Once the addition of the materials was completed, the latex mixture was left stirring for one hour. Then 500 g from the prepared latex formulation transferred into a 250 x 350 mm polyethylene bag and then sealed; a total of 5 samples. Each latex sample was then exposed to UVC light for 0, 15, 30, 45 and 60 minutes respectively. After exposure, the latex was made into a film by the coagulant dipping method and mechanical properties tests were performed.

Table 1: : Compounding formulation of Hybrid UVperoxide prevulcanized natural rubber latex

Materials	Part perhundred (Pphr)
NR Latex (62%*TSC)	100.0
Stabilizer	0.1
HDDA	2.0
t-BHPO	0.5
Irgacure 1173	2.0
HAC	0.5
Water	Add to 52% TSC

2.2 UV irradiation

Four commercial UVC lamps (Philips TUV PL-L 55W/4P HF 1CT) were used to irradiate the latex formulations, as illustrated in Figure 1. The intensity of the incident radiation at the surface of the plastic bag was 3707.9 μW/cm^2. The experiments were carried out in a dark room at a distance of 100mm between lamps and the latex sample surface.

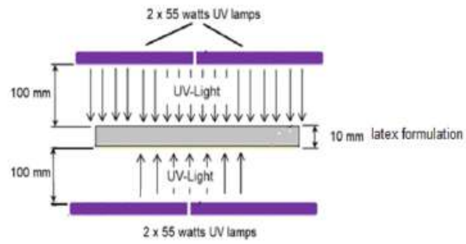

Figure 1: Experimental setup; The prepared latex contained in a plastic bag was irradiated using UV lamps from top (2 lamps) and below (2 lamps).

3 Results and Discussion

3.1 Effect of UV irradiation doses on mechanical properties of hybrid UV-peroxide prevulcanized natural rubber latex

In the process, a photoinitiator added to the latex will absorb UV light and create free radicals. Cross-links in polyisoprene will then be formed thanks to these free radicals. The UV dose that was provided to produce free radicals was calculated as Equation below:

UV dose = UV light intensity (μWsec/cm^2) x time (s)

Table 2: Mechanical properties of hybrid UVNRL-peroxide (median value from the tensile test)

Sample	**Exposure time (min)**	**Average sample's temperature (°C)**	**UV dose (mJ/cm^2)**	**Mod@500% (mPa)**	**Mod@700% (mPa)**	**Tensile strength (mPa)**
Hybrid UVNRL-peroxide (Control)	0	28	0.00	0.5	2.3	5.6
Hybrid UVNRL-peroxide	15	45	3337.11	2.1	5.5	24.1
Hybrid UVNRL-peroxide	30	59	6674.22	2.3	8.0	25.1
Hybrid UVNRL-peroxide	45	65	10011.33	2.5	8.1	23.5
Hybrid UVNRL-peroxide	60	73	13348.44	2.7	6.3	22.4

In addition, UV vulcanization also generated heat from the UV lamps. The intensity of the UVlamp and the duration of the exposure will contribute to the increment of the sample's temperature. Since peroxide is used as a co-sensitizer in the hybrid UVperoxide vulcanization process, the heat generated by the UV lamps will be manipulated to decompose the peroxide compounds' breakdown into radicals, which will help improve the hybrid UV-peroxide prevulcanized natural rubber latex's mechanical properties and cross-link density.

Table 2 showed the mechanical properties of control and hybrid UVNRL-peroxide samples that have been prepared at various time duration and tested as required by ASTM D412 standard. It was observed that rubber film obtained from irradiation at 30 minutes (6674.22 mJ/cm^2) had tensile strength, mod @ 500% and mod @ 700% of 25.1, 2.3 and 8.0 mPa respectively, which is more than 400% increment compared to control. It is suggested that increasing of UV irradiation dose and monogeneity reaction from the hybrid UV radiation and peroxide vulcanizations has enhanced the intraparticle crosslink density (chemical crosslinking). However, the mechanical properties of the hybrid UVNRL-peroxide start to decline with increasing of irradiation doses; 10011.33 mJ/cm^2 and above. We believed this happened when interparticle entanglement (physical crosslinking) decreased with the increasing dose. Makuuci (2003) suggested that interparticle entanglements depend on the free rubber chain ends at the surface of each latex particle. These chains interpenetrate during film formation and contribute to the strength of the film by means of entanglements. The length of the free rubber chain ends decreases with the increase of irradiation dose because it is equivalent to molecular weight between crosslinks. Thus, the tensile strength, mod @ 500% and mod @ 700% of the hybrid UVNRL-peroxide latex film increase up to a certain maximum level and then start to decrease with the increasing dose.

4 Conclusions

Hybrid UV-peroxide prevulcanized natural rubber latex with good tensile strength can be prepared by hybrid UV radiation and peroxidation vulcanizations. Irradiation of latex formulations based on 2.0 parts per hundred rubber (phr) of 2–hydroxyl-2-methyl-1-phenylpropanone (Irgacure 1173) as the photoinitiator, 0.5 phr of tert-butyl hydroperoxide (tBHPO) as the sensitizer, 2.0 parts per hundred rubber (phr) of hexanediol diacrylate (HDDA) as the co-sensitizer and 0.5 phr of hydroxyacetone (Hac) as the activator at UV irradiation dose of 6674.22 mJ/cm^2 (30 minutes) can produced rubber film with tensile strength of 25 mPa.

References

Siri Upathum C. and Sonsuk M. 1996. Development of an efficient process for radiation vulcanization of natural rubber latex using hydroperoxide with sensitizer. *Proceedings of the Second International Symposium On RVNRL, Kuala Lumpur, Malaysia*.

ASTM D412. 2016. Standard test methods for vulcanized rubber and thermoplastic elastomers—tension. *ASTM International, West Conshohocken, PA*.

Pairu I., Rusli D., and Wan Manshol W. Z. 2016. Radiation effects and defects in solidsn. 171:1006–1015.

Pairu I., Wan Manshol W. Z., Chai C. K., Sofian I., Mohd Noorwadi M. L., and Saadiah S. 2017. *Jurnal Sains Nuklear Malaysia*, 29(1):28–36.

Makuuci K. 2003. An introduction to radiation vulcanization of natural rubber latex. *T.R.I. Global Co. Ltd., Bangkok*.

Schlögl S., Temel A., and Schaller R. 2010. Rubber chemistry and technology. 83(2):133–148.

I. Sofian, Khairiah B., Chantara T. R., and Noor Hasni M. A. 2018. Radiation effects and defects in solids. 173:427–434.

P. Wiroonpochit, Uttra K., Jantawatchai K., Hansupalak N., and Chisti Y. 2017. Sulfur-free prevulcanization of natural rubber latex by ultraviolet irradiation in the presence of diacrylates. *Industrial Engineering Chemistry Research*, 56(25):7217–7223.

Individual Research Contribution Review, 2023, 1(1): 473–474

Effect of Low Voltage for Voltage Output of HV Circuit for Nuclear Detector in Radiation Survey Meter: A Review

Syirrazie Shaari
Technical Support Division, Malaysian Nuclear Agency
43000 Kajang, Selangor
syirrazie@nm.gov.my

Abstract

This study purposely to review characteristic of battery discharge and HV plateau. These characteristics are obtain from previous related studies. Both them are adapted each other to identify effect of low voltage for high voltage output of HV circuit in a radiation survey meter. Results shows that HV output signal is proportional with LV from DC battery.

1 Introduction

Implementing the right High Voltage (HV) operating range for a particular nuclear detector to ensure reliability of radiation detection and measurement. For radiation survey meter, the typical input DC voltage of a battery is up to low voltage of 9V. This battery could reliably to source up nuclear detector for a period of time subject to its capacity in mAh. Higher mAh, the longer period the battery could source up nuclear detector sufficiently. Thus, lower mAh, the shorter period the battery could source up nuclear detector. Sourcing up a nuclear detector with HV output from battery is processed using HV circuit.

2 Methodology

In order to source up nuclear detector sufficiently, a circuit of High Voltage is needed to step up low voltage from battery, 9V to be high voltage, maximum up to 650V for Geiger Muller (GM) detector that commonly used in radiation survey meter (Almutairi et al., 2021). This process is presenting as shown in Figure 1.

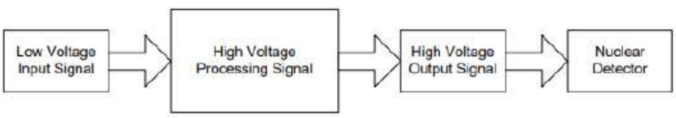

Figure 1: Producing Process of HV Output.

Then, effect of low voltage of battery in producing HV output is through reviewing battery discharging period and HV operating range of a nuclear detector (Root et al., 2017).

3 Results and Discussion

This study found that a battery voltage is significantly drop after 80,000 second as shown in Figure 2 subject to a particular battery capacity (Casanova et al., 2009). This dropped voltage shows that HV output for a nuclear detector also could decrease as decreasing battery voltage when applying for HV circuit.

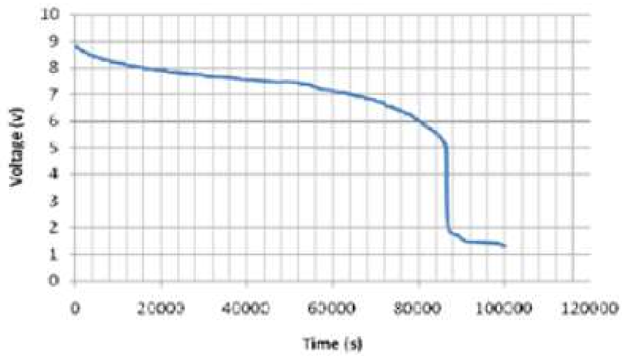

Figure 2: Battery Discharging.

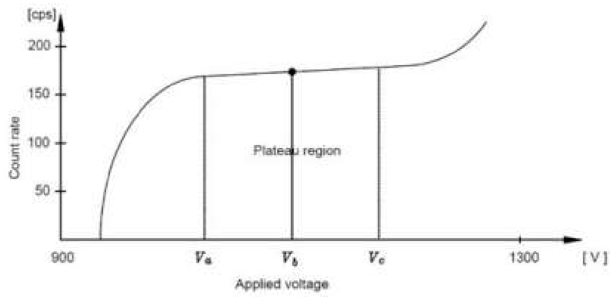

Figure 3: HV Plateau of Nuclear Detector.

If decreasing of HV output is remain within HV plateau region as shown in Figure 3, the detector still working effectively. Else, the detector could not working properly.

4 Conclusion

Higher battery capacity lead longer discharging process. Thus, applying this battery on a HV circuit could guarantee HV operating maintain in longer period as well. This is important to identify mAh of a battery to use for nuclear detector of a radiation survey meter subject to an essential period.

References

B. Almutairi, S. Alam, C. S. Goodwin, S. Usman, and T. Akyurek. 2021. Simultaneous experimental evaluation of pulse shape and deadtime phenomenon of GM detector. *Sci. Rep.*, 11(1):doi: 10.1038/s41598–021–81571–3.

A. M. Casanova, A. S. Bray, T. A. Powers, A. J. Nimunkar, and J. G. Webster. 2009. Battery power comparison to charge medical devices in developing countries. *Proceedings of the 31st Annual International Conference of the IEEE Engineering in Medicine and Biology Society: Engineering the Future of Biomedicine, EMBC 2009*, pages 931 – 934, doi: 10.1109/IEMBS.2009.5333717.

M. A. Root, H. O. Menlove, R. C. Lanza, C. D. Rael, K. A. Miller, and J. B. Marlow. 2017. Technical basis for the use of a correlated neutron source in the Uranium Neutron Coincidence Collar. *Nucl. Technol.*, 197(2):180 – 190, doi: 10.13182/NT16–50.

Individual Research Contribution Review, 2023, 1(1): 475–476

Design of Multi-Purpose Experimental Test Facility (M-PETF) for Reactor TRIGA PUSPATI

Tonny Lanyau
Technical Support Division, Malaysian Nuclear Agency
43000 Kajang, Selangor
tonny@nm.gov.my

Abstract

The Multi-purpose Experimental Testing Facility (M-PETF) was designed to demonstrate and find solutions to the ageing effects in the RTP structures, systems and components (SSCs). It might be cumbersome if not detected early, leading to severe problems if not verified. The M-PETF is a scaled-down facility that best reflects the RTP and can probe the SSCs' issues. The technical drawing was built using CAD software to visualize the engineering concept of the M-PETF. The difficulty level of the technical drawing was moderate because all sizes needed to be reduced using the available layout to correspond to the space provided. The actual development of M-PETF is expected based on the technical drawings that have been built and verified. This paper highlights the engineering aspects of the M-PETF.

Keywords: design, test, facility, structures, systems and components (SSCs), RTP

1 Introduction

After four decades of operation since first criticality in 1982, outstanding services of RTP is the pride of the country. The RTP is continuing its prime functions for training and education (E&T), research and development (R&D) in nuclear technology as well as radioisotopes producer for industry and medical applications. The needs and demands for RTP irradiation services are increasing since past few decades. For that reason, a lot of effort have been taken to ensure the RTP able to continuously provide its services. Amongst the focused effort are being carried out is ageing management activities.

Even though RTP has very comprehensive maintenance programme, sometimes the extension of shutdown period has to be adopted especially when the SSCs need for further actions including analysis and testing. The constraint arises when these activities cannot be done during the operation.

Therefore, the idea on establishing of the testing facility was proposed. A Multipurpose Experimental Testing Facility (M-PETF) has been designed to demonstrate and find solutions to the ageing effects in the RTP structures, systems and components (SSCs). The M-PETF is a scaled-down facility that best reflects the RTP and can probe the SSCs' issues.

The objectives of this paper are to design a scaled-down test facility for RTP's cooling system and to produce a blue print of multipurpose testing facility.

2 Methods

The design of the M-PETF is inspired from the RTP itself. The rough concept of it is to represent the vital systems of the RTP. The design methodology has been adopted in order to produce the best conceptual design of the facility. The flow of the design process is simplified in the Figure 1.

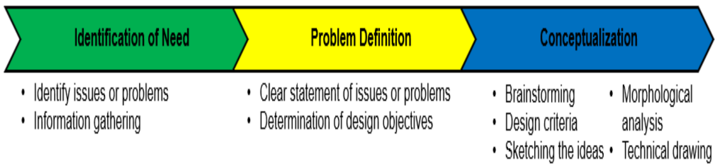

Figure 1: Design process of M-PETF

3 Result

The development of the M-PETF is needed to demonstrate and find solution for the ageing effects in the RTP. There are three design objectives have been identified. Firstly, to design the scaled-down testing facility that best reflects to the RTP. Secondly, to design the facility capable to perform verification and validation through experiment and testing. Thirdly, to design facility that able to accommodate education and training for operation and maintenance personnel, researchers and students.

The concept criteria for the design are size of the facility must be realistic for construction corresponding to the available space, equipment installed are like the RCS, coolant water flow circulation is like both primary and secondary loop. The design objectives and criteria of the M-PETF are shown in the Figure 2 and Figure 3 accordingly.

The size of the MPETF is limited by the available space of 3m (wide) x 4m (long) to accommodate the primary and secondary loop. Both loops have their own water tank, pump, pipes, valve and interconnected by heat exchanger. The design of MPETF does not include the water purification system for primary loop and cooling tower for secondary loop as in the real plant of RTP. These system and equipment were abolished based on consideration of the graded approach. In the primary loop, water tank is scaled to about quarter size of the RTP pool tank. Three electric water heaters were used as heat generator. These heaters are representing the nuclear fuel elements in the RTP.

Figure 2: Design objective of M-PETF

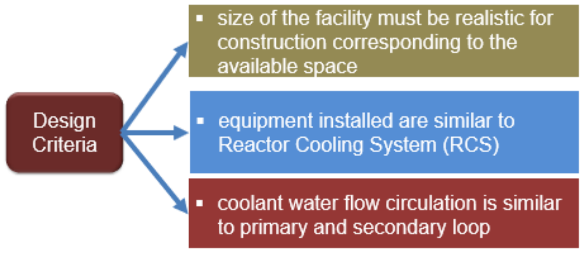

Figure 3: Design criteria of M-PETF

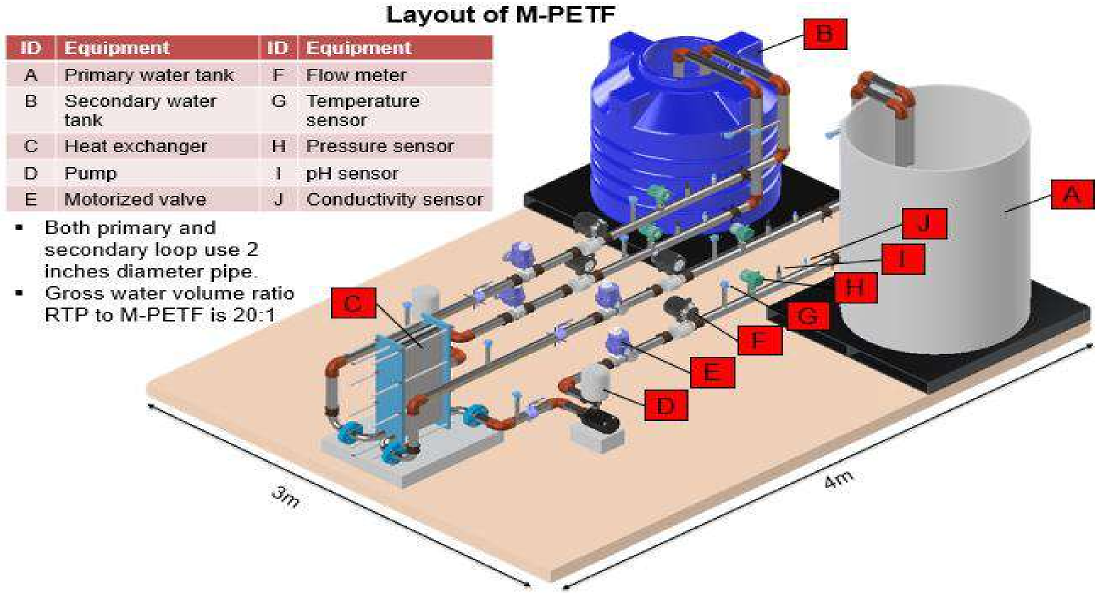

Figure 4: Layout of M-PETF

The heat generated by these heaters are deposited to the coolant water inside the primary water tank and circulated through the loop by water pump. The heat is then transfer to the secondary loop by the heat exchanger. The secondary water tank acts as cool water reservoir. The temperature of cool water is depending on the ambient temperature. The overall layout of the design as illustrated in the Figure 4.

4 Conclusion

The M-PETF design was inspired by the RTP cooling system. The scaled-down approach is based on water volume inside the reactor pool to M-PETF primary water tank.

References

IAEA. 2005. TRIGA reactor main systems. *Education and Training – Nuclear Safety and Training*.

Nuclear Malaysia. 2020. Reactor TRIGA PUSPATI safety analysis report.

Budynas R. and Nisbett K. 2020. Shigley's mechanical engineering design. *11th Ed. McGraw-Hill, ISBN: 0390764876*.

Individual Research Contribution Review, 2023, 1(1): 477–478

Cleaning and Dicing Silicon Wafer (Industrial Report)

Umi Zulaikha binti Mohd Azmi
Technical Support Division, Malaysian Nuclear Agency
43000 Kajang, Selangor
umizulaikha@nm.gov.my

Abstract

Industrial training is compulsory to students in certain programmes at all levels of higher education at the Institute of Higher Learning (IPT). This document provides information on activities, procedures, results and discussion that have been done by the student, Nur Wardina Syahirah Mohamad Fadil. The activities are cleaning silicon wafer using solvent clean, RCA-1, and HF dip, and dicing the wafer.

Keywords: Industrial training, cleaning wafer, wafer dicing

1 Introduction

The industrial training is compulsory for undergraduate students at the Faculty of Science, Universiti Teknologi Malaysia (UTM) in order to fulfil the requirements of the degree programme. The primary purpose of the industrial training is to introduce students to the industrial working environment. As a result, students will be able to comprehend the theories learned with more extensive and hands-on practise in a real-world employment environment. The industrial training programme provides students with learning opportunities in the industry where they may get practical experience and expand their knowledge that will be beneficial after graduation.

During the internship, the student was performed two main activities such as cleaning wafer and dicing the wafer. Apart from that, the student also required to perform a particle monitoring every week in order to monitor the cleanliness of the cleanroom. The cleaning wafer was carried out using two different methods and compare both methods. Two different methods are (i) piranha solution and (ii) solvent clean, RCA-1, HF dip. Effective method to clean the wafer is important as semiconductor devices are very sensitive due to the nanometer sizes. Finally, the student was asked to cut the wafer into certain size using a machine. There are several techniques to cut the wafer, but in this task, dicing machine was used to cut the wafer.

2 Materials and Methods

i. **Particle monitoring**
The particle counter, GT-321 was turned on and removed the rubber cap from inlet nozzle. Next, the 'Select' button was pressed and chose 0.3μ for particle size. Placed the particle counter at appropriate place with the inlet nozzle pointing upward. Then, the 'Start' button was pressed to start the measurement. The reading was recorded and repeated the measurement for another 4 times.

ii. **Cleaning silicon wafer (piranha)**
The silicon was cleaned using piranha solution. This step was explained in detail in another technical report entitled "Cleaning wafer using piranha solution".

iii. **Cleaning silicon wafer (solvent clean, RCA-1, HF dip)**
The silicon was cleaned using solvent clean, RCA1, HF dip. This step was explained in detail in another technical report entitled "Cleaning wafer using solvent clean, RCA-1, HF dip".

iv. **Wafer analysis**
After being cleaned, the wafer's surface was observed under microscope, MX-6R (China) to observe the cleanliness of the wafer.

v. **Dicing silicon wafer**
The SYJ-800 represents a precision CNC (Computerized Numerical Control) dicing/cutting saw specifically designed for research and development laboratories in the materials and microelectronics research sectors. It has parameters such as spindle rotor speed (0-6038.2 rpm/min), cutting speed (0-25mm/min), cut depth (mm depending on the blade's diameter), and moving speed (0-25mm/min). These parameters help maintain wafer cutting quality by choosing the optimum value for various wafer types, sizes, and thicknesses. The SYJ-800 is a machine with various features including a Z-axis stepper motor, water splash guard, sample holder stage, X-axis stepper motor, cutting blade, spindle motor, power on/off function, vacuum chuck valve, and 3-axis motion driver controller. It requires a stable worktable and correct water and vacuum supply connections. Operating involves configuring initial home points, setting cutting speed, blade assembly, spindle rotation speed, mounting the sample, and programming the machine using a computer interface. This knob has ten turns with an ultimate speed of 6000 rpm.

vi. **Observation of cutting quality**
The cutting quality is tested in this experiment using the Zeiss Axio Scope Al microscope. It was aided by the I-Solution programme, which was designed to provide accuracy measurements on a very tiny scale. The objective lens was set to 5x/0.16. The uniformity of the

kerf width and the creation of chipping width are the two primary items to be examined.

Chipping width and kerf width are terms used in the dicing industry to describe the width of a cut made by a dicing blade. Chipping width refers to the material removed from the workpiece during the dicing process, while kerf width refers to the cut made by the blade itself. Factors such as feed rate, blade speed, and blade stiffness can affect chipping width, while blade stiffness and maximum undeformed chip thickness can affect kerf width.

3 Result and Discussions

Wafer analysis after cleaning

After cleaned the wafers using both methods, the quality surface and cleanliness of the wafer was examined under microscope. From the observation, cleaning using solvent clean, RCA-1, and HF dip provides better surface cleanliness compared to piranha. This technique not only removes a potential source of contamination, but it also passivates the silicon surface.

Apart from that, the combination of these two methods to clean the wafer also was carried out. From the observation, the wafer shown significantly cleaner, and it shows that this combination method is an effective strategy in achieving a cleaner wafer surface.

Wafer dicing analysis

Figure 1 depicts the cutting outcome after approximately 1 hour of cutting time. The wafer was cut into six slices by dividing its diameter of 100mm by 15mm, and then rotated perpendicular to the previous cutting. The wafer was then split into six segments to make 15mm dies. The cutting process was monitored to assure constant water cooling, which was then employed to spray water over the moving blade.

Figure 1: Outcome after dicing.

Analysis of the kerf width and chipping width were studied using the software that mention in Materials and Methods section. From the study, it shows that the kerf width increases as the spindle speed increases whereas the chipping width produced decreases substantially along the cutting path. This conclusion is consistent with the findings of Zhou et al. (Zhou et al., 2012), who attempted to determine the effect of blade speed on chipping width and kerf width.

Another study is the relationship of kerf width and spindle speed. The kerf width shows a consistent result for each spindle speed. This consistency suggests the kerf width is virtually uniform throughout the cutting operation. When the kerf width remains constant, the cutting tool maintains a constant depth and width as it goes over the silicon wafer. This level of constancy is essential in industries requiring exact dimensions, such as semiconductor production.

4 Conclusion

In conclusion, cleaning silicon wafer using combination method piranha and solvent clean, RCA-1, HF dip provides a significantly cleaner surface compared to separate the methods. After cleaning, dicing the wafer into 1.5 cm x 1.5 cm size using mechanical sawing with variation of spindle rotor speed. The effect of spindle rotor speed (rpm) on chipping width and kerf width was studied using microscope. According to the results, a spindle speed of 3333 rpm generated the smallest chipping width for a 4 inches silicon wafer with a thickness of 2 mm. To summarise, minimising chipping width while cutting silicon wafers is crucial for ensuring semiconductor manufacturing operations' reliability, performance, and cost-effectiveness. It contributes to the quality of wafers and electrical devices made from them, eventually benefiting both producers and end users.

References

H. Zhou, S. Qiu, Y. Huo, and N. Zhang. 2012. High-speed dicing of silicon wafers conducted using ultrathin blades. *The International Journal of 58 Advanced Manufacturing Technology*, 66(5-8):947 – 953.

Individual Research Contribution Review, 2023, 1(1): 479–480

Cleaning Wafer Using Piranha Solution (Technical Report)

Umi Zulaikha binti Mohd Azmi
Technical Support Division, Malaysian Nuclear Agency
43000 Kajang, Selangor
umizulaikha@nm.gov.my

Abstract

Wafer needs to be cleaned from particle and chemical contaminants without damaging the surface of the substrate. that was formed on the surface. Piranha solution is a mixture of hydrogen peroxide and sulphuric acid, is used to remove organic and inorganic contaminants that presence on the substrate. However, piranha solution is dangerous and should be handling with care. Therefore, this document provides the procedure to clean a wafer using a piranha solution and necessary information to handle the solution safely.

Keywords: Cleaning wafer, piranha solution, semiconductor

1 Introduction

Silicon wafers play an important role in semiconductor devices, electronics, and even in several types of machinery and technologies. In semiconductor manufacturing, there are several processes need to go through, including wafer cleaning. Surface contamination is one of the biggest challenges in semiconductor industry. Therefore, cleaning silicon wafer before thermal oxidation, after patterning by etching, after ion implantation, and before and after film deposition are important due to the sensitivity of the semiconductor surface and nanometer sizes of the device features. In this document, the procedure of cleaning silicon wafer using piranha solution and the safety that need to be considered were provided (Kern, 2018).

2 Safety Consideration

Handling the chemical substances with care is important in order to prevent any accident. Therefore, prior to cleaning wafers, hazards of each chemical substance especially when mixing with different chemicals need to be familiarized.

Hazard overview

Piranha solution, also known as piranha etch, is a mixture of sulfuric acid (H_2SO_4) and hydrogen peroxide (H_2O_2) used to clean organic residues off substrates. The mixture is a strong oxidizing agent that removes most organic matter, and it will also hydroxylate most surfaces (add -OH groups), rendering them highly hydrophilic (water compatible). Acid piranha is a 3:1 mixture of concentrated H_2SO_4 with 30% H_2O_2. It is dangerous when hot.

The Piranha solution is very energetic, exothermic and potentially explosive. It is very likely to become hot, more than 100°C. Handle with care! When preparing the Piranha solution, always add the peroxide to the acid. Piranha solution reacts violently with any organic materials. Avoid mixing with incompatible materials such as acids, bases, organic solvents (acetone, isopropyl alcohol) or nylon. Always ensure that all substrates are rinsed and dried before placing them in a Piranha solution. Only use clean glass or Pyrex containers; Piranha solution is not compatible with plastic.

Piranha solution is a corrosive liquid and strong oxidizer. Piranhas burn (oxidize) organic compounds. If you provide sufficient fuel for them (i.e. photoresist, IPA), they will generate enormous quantities of heat and gas. Both liquid and vapor forms are extremely corrosive to skin and respiratory tract. Direct contact will create skin burns and will be extremely destructive to mucous membranes, upper respiratory tract and eyes.

3 Procedure

Here, the cleaning of silicon wafer was done by immersing in piranha solution. Firstly, piranha solution was prepared by mixing the concentrated of hydrogen peroxide (H_2O_2) and sulphuric acid (H_2SO_4) with ratio 1:3. Make sure that peroxide added into acid. Then, dipped the wafer in the piranha solution for 1 min in order to remove any contaminants on the wafer surface. After 1 min, the wafer was taken out using tweezer and rinsed in deionized water (DI) for 5 mins. Rinsed the wafer in DI again for another 2 times using different beaker, 5 mins. The wafer was dried using nitrogen gas and placed in desiccator if not in use.

4 Flow Chart

Refer Figure 1 on the process of cleaning wafer using piranha solution.

5 Conclusion

As a conclusion, cleaning wafer is an important step to ensure that the silicon wafer is free from any contamination. This technical report will give a benefit to laboratory staff.

References

W. Kern. 2018. Overview and evolution of silicon wafer cleaning technology. *In Handbook of Silicon Wafer Cleaning Technology*, pages 3–85, Elsevier Inc.

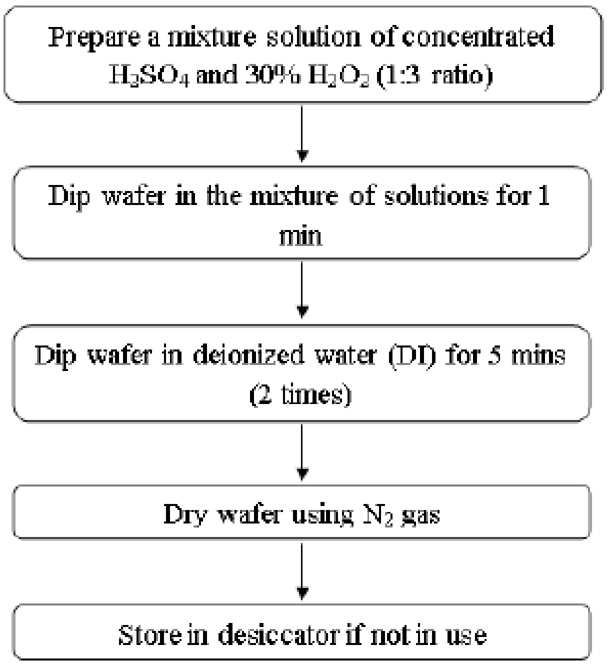

Figure 1: Flow chart for cleaning wafer using piranha solution.

Individual Research Contribution Review, 2023, 1(1): 481–482

Cleaning Wafer Using Solvent Clean + RCA-1 + HF Dip (Technical Report)

Umi Zulaikha binti Mohd Azmi
Technical Support Division, Malaysian Nuclear Agency
43000 Kajang, Selangor
umizulaikha@nm.gov.my

Abstract

Cleaning a silicon wafer is an important process in fabrication of semiconductor microelectronic devices. The aim of this process is to remove particle and chemical contaminants without altering or damaging the wafer surface or substrate. The surface of the wafer must be maintained not affected so that roughness, corrosion or pitting negates the results of the wafer cleaning process. Here, the procedure of cleaning silicon wafer by using solvent clean + RCA-1 + HF dip is implemented and documented. Besides that, necessary information also provided in order to help the staff to handle the chemicals safely.

Keywords: Cleaning wafer, solvent clean, RCA-1, HF dip

1 Introduction

Since the emergence of solid-state device technology in the 1950s, the significance of ensuring pristine substrate surfaces in manufacturing semiconductor microelectronic devices has been acknowledged. It is widely understood today that the performance, reliability, and yield of silicon circuits are profoundly impacted by the existence of chemical contaminants and particulate impurities on the wafer or device surface. Silicon native oxide also needs to be removed (Kern, 2018). Therefore, the cleaning silicon wafers by using solvent clean + RCA-1 + HF dip was implemented. Solvent clean can remove oils and organic residues while RCA-1 can remove organic residues. Besides that, the RCA-1 clean can oxidizes the silicon and provides a thin protective layer of oxide to the surface of the wafer. Finally, HF dip was implemented because it can remove native oxide and silicon wafer become pure silicon.

In this document, the procedure of cleaning silicon wafer using solvent clean + RCA-1 + HF dip was provided. Apart from that, the information on safely handling the chemicals also included.

2 Safety Consideration

Handling the chemical substances with care is important in order to prevent any accident. Therefore, prior to cleaning wafers, hazards of each chemical substance especially when mixing with different chemicals need to be familiarized.

Hazard overview

The cleaning process involves three main steps: solvent clean, RCA-1 clean, and HF dip. The solvent clean step uses acetone and methanol to remove oils and organic residues from the wafer, followed by an RCA-1 clean to remove any remaining organic residues and leave a thin oxide layer on the surface. Finally, the HF dip step removes the native silicon dioxide from the wafer. The cleaning process is conducted in INRF cleanroom facilities, adhering to the organization's safety and procedural regulations.

Acetone and methanol are flammable liquids, so handle them cautiously, avoid letting the solvent exceed 55°C, and avoid storing them near heat sources. Never leave the RCA process unattended. Hydrofluoric acid (HF) is an extremely toxic and dangerous acid.

3 Procedure

Here, the cleaning of silicon wafer was divided into three parts: parts: (i) solvent clean, (ii) RCA-1, and (iii) HF dip.

i. *Solvent clean*
Firstly, acetone and methanol were prepared in a separate beaker. Then, immersed the silicon wafer in a warm acetone (do not warm the acetone exceed than 55°C) for 10 mins. The wafer was removed and placed in methanol solution for 2-5 mins. Removed the wafer and rinsed in DI water. The wafer was dried using nitrogen gas.

ii. *RCA-1*
The RCA-1 solution was prepared by mixing 5 parts of DI, 1 part of 27% ammonium hydroxide (NH_4OH) and 1 part of 30% hydrogen peroxide (H_2O_2). Briefly, 40 mL of DI was mixed with 8 mL of NH_4OH, and heated it to 70°C. Then, put aside the beaker and added 8 mL of H_2O_2. The solution was bubbled vigorously after 1-2 mins, indicated that the solution is ready for use. Then, soaked the wafer in RCA-1 solution for 15 mins. Removed the wafer from solution and rinsed with DI water. Dried the wafer using nitrogen gas.

iii. *HF dip*
The 2% of HF solution was prepared by diluting the 49% HF in DI water. Briefly, 38.37 mL of DI was added into a propylene beaker. Then, added 1.63 mL of 49% HF into the DI water. Soaked the wafer in the solution for 2 mins. Finally, removed the wafer and rinsed in running DI water.

Hydrophobicity test

After dip the wafer in HF solution, the wafer should become hydrophobic, indicating the wafer is free from native oxide. Therefore, to confirm the hydrophobicity of the wafer, a little of DI water was poured on the wafer surface. If the water beads up and rolls off, the surface is hydrophobic, and water will not wet the wafer. After this test was done, dried the wafer using nitrogen gas and stored in a desiccator.

4 Result

Hydrophobicity test

Hydrophobicity test was done in order to confirm that the native oxide on silicon wafer was removed and became pure silicon. As shown in Figure 1, the water beading is not flat suggested that the surface of wafer is hydrophobic due to the HF dip process.

Figure 1: Water on silicon wafer surface.

5 Flow Chart

Figure 2, 3 and 4 show the flow charts of solvent clean, RCA-1 clean and HF dip.

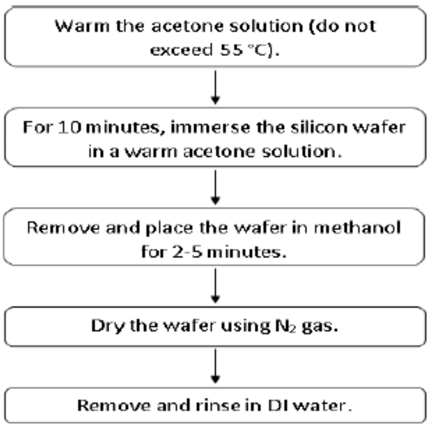

Figure 2: Flow chart of solvent clean

6 Conclusion

As a conclusion, cleaning wafer is an important step to ensure that the silicon wafer is free from any contamination and native oxide. This technical report also will give a benefit to laboratory staff to conduct a cleaning process for silicon wafer.

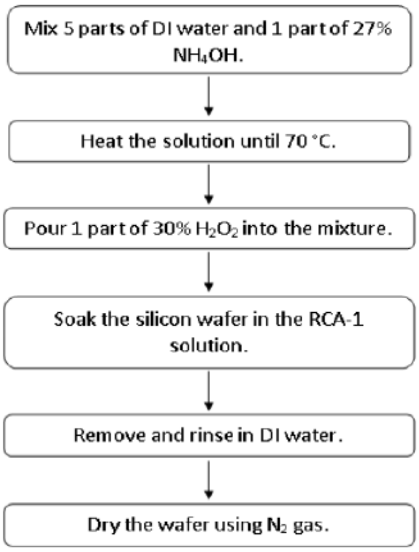

Figure 3: Flow chart of RCA-1 clean

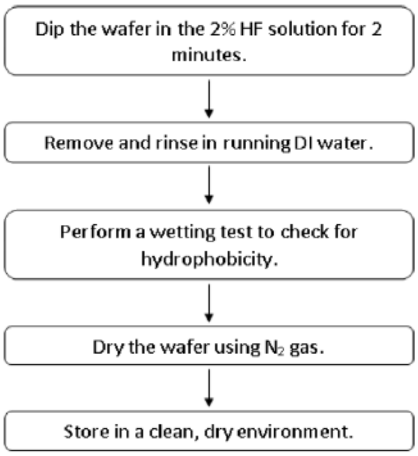

Figure 4: Flow chart of HF dip.

References

W. Kern. 2018. Overview and evolution of silicon wafer cleaning technology. *In Handbook of Silicon Wafer Cleaning Technology*, pages 3–85, Elsevier Inc.

Individual Research Contribution Review, 2023, 1(1): 483–484

Equipment Module Development for Semiconductor Nuclear Detector Fabrication Laboratory

Umi Zulaikha binti Mohd Azmi
Technical Support Division, Malaysian Nuclear Agency
43000 Kajang, Selangor
umizulaikha@nm.gov.my

Abstract

The Semiconductor Nuclear Detector Fabrication Laboratory is situated at the Malaysian Nuclear Agency Complex in Dengkil. It features two class of clean rooms—Class 100 and 1000, along with a Cleaning Room, Clean Enough Room, Changing Room, and Laboratory Preparation Room. This laboratory is also equipped with high-tech equipment for the purpose of fabricating nuclear detection devices such as Dicing Machines, High Temperature Furnaces, Photolithography Facilities, I-V Measurement System Tools (I-V Measurement Probe), Plasma Enhanced Chemical Vapor Deposition System (PECVD), Reactive Ion Etching Polymide System, Rapid Thermal Annealing (RTA), Integrated Coating System, Backside IR Mask Aligner and Sputtering System. This paper describes the functionality, specifications and current status of each piece of equipment in the Semiconductor Nuclear Detector Fabrication Laboratory, aiming to provide comprehensive understanding and knowledge. The goal is to open opportunities for research and development activities to all.

Keywords: Nuclear Detector Device

1 Introduction

The Nuclear Emerging Technology Center (NET) is a new unit under the Technical Support Division (BST), established on 24 January 2022. The Semiconductor Nuclear Detector Fabrication Laboratory is a research facility located in the Maintenance Technology and Research Operations Section (ROM) of NET. In addition to ROM, NET also has two other sections, namely the Semiconductor Nuclear Detector Technology Section (SND) and the Sensing and Emerging Technology Section (STE). The establishment of NET is a continuation of the research and development of Nuclear Detectors based on semiconductor technology. The main objective of the establishment of NET (Mohamed et al., 2022) is to conduct enhanced research and development activities in current science and technology development, adapted to new market strategies to improve capabilities, optimize initial production costs, and maximize product output. In line with the rapid development of manufacturing technology and opportunities to explore new markets and regional economic growth, especially in the field of semiconductors, NET aims for quality certification and the establishment of a National One-Stop Center Service, including the development of a Semiconductor Nuclear Detector Fabrication Laboratory at the national level.

2 Research Methodology

The research and development work process involving the fabrication of semiconductor nuclear detectors involves several phases as shown in Table 1 (Mansor, 2013).

Table 1: Nuclear Detector Fabrication Work Process Semiconductor

Phase 1: Determination of Material Properties and Preparation Process	Material Research activities: • Defect Mapping Process • Material Charactetization Process • Cleaning Process • Oxidation Process
Phase 2: Material Inspection • Measure the thickness • Study the structure • Surface inspection • Identification of defects and material character	Material Research Activities: • Mask aligner • Coating the substrate layer (Photoresist) • Doping Process • Metal Deposition
Phase 3: Formation of 4H-SiC Single Layer	Material Research Activities: Annealing Process and Surface Protection Process
Phase 4: Diode Design and Simulation of Mask Design	Material Research Activities: Electrical Characterization
Phase 5: Electronic Design: The Formation of preamplifiers and amplifiers	Material Research Activities: Material and Device Damage Analysis

3 Equipments

The following is a list of scientific equipment or machine facilities and the main functions of the equipment in general.

i. Digital Particle Counter (digital particle counter)
The Digital Particle Counter, GT-321 is used to measure particulate pollution in particles per cubic foot. This tool aims to monitor the number of particles in a clean room in a laboratory.

ii. Ultrasonic Tab Cleaner
The Ultrasonic Tub Cleaner is used to get a better cleaning and purification effect by converting the ultra-audio-frequency electrical signal produced by the ultrasonic generator into mechanical vibration with the frequency the same through the inverse change effect of the piezoelectric transducer.

iii. Wafer Dicing Machine
Wafer Cutting Machines are used to cut semiconductor chip wafers individually by using cutting blade points at high speed to produce chips according to a certain size for industrial use.

iv. Metallurgical Microscope
Metallurgical microscopes are mainly used in metallography, forensics, plastic processing, metal inspection, semiconductor materials, laser systems, solar cells using both thin film and wafer technology and many other areas of materials science.

v. De-Ionized Water System
The De-Ionized Water System is a ”crystal” water purification system to produce pure and ultrapure water that each complies with the ISO 3696 water requirements standard Grade II and Grade I.

vi. Photoresist Single Layer Coating Device
Spin coating is intended to form a thin coating of photoresist evenly across the entire wafer. This is done by using a spinner at high speed which allows a small amount of photoresist material in liquid form to spread evenly across the thickness of the wafer.

vii. Hot Plate Magnetic Stirrer
After the coating process, the resist layer has a residual solvent concentration of typically 10 - 35%, depending on the thickness of the layer and the solvent used. The purpose of softbake is to reduce the concentration of residual solvents.

viii. Mask Aligner
A mask aligner is a high precision machine tool used in the semiconductor manufacturing process to transfer patterns to wafers or substrates at the micro and nano scale.

ix. Tube furnace Controlled Atmosphere
To produce an oxide layer on the surface of the material.

x. I-V Measurement System Tool (I-V Measurement probe)
The IV measurement system is the equipment used for the IV characterization of electronic devices. It is a basic electrical measurement and is a way to understand the characteristics of the device under test (DUT).

xi. Plasma Enhanced Chemical Vapor Deposition System (PECVD)
This equipment is used for the process of depositing a dielectric thin film on a material or substrate. This process is crucial for the semiconductor industry and is widely used in microelectronics applications

xii. Reactive Ion Etching Polymide System
Reactive Ion Etching (RIE) is a dry etching technique widely used in semiconductor manufacturing, MEMS fabrication, microfabrication and nanotechnology to create patterns on the surface of various materials with high resolution and anisotropy.

xiii. Rapid Thermal Annealing
Rapid thermal anneals (RTA) is a process used in the fabrication of semiconductor devices to heat a single wafer in a short time which will affect the electrical properties of the material.

xiv. Integrated Coating System (ICS)
ICS is used to improve the appearance structure of new materials or restore damaged components. This is to increase protection and improve the appearance of parts and components.

xv. Backside IR Mask Aligner
Mask Aligner is an instrument that allows the photolithography process to occur, which is a microfabrication process to selectively remove portions of a thin film to create a specific pattern or design on a substrate.

xvi. Sputtering System
Sputtering is a process in which microscopic particles of a target material are removed from its surface using gaseous energetic ions or gas plasma.

4 Conclusion

These equipments are ready to be used by Malaysian Nuclear Agency staff for related R&D activities. The establishment of class 100 and class 1000 clean rooms as well as other related facilities at the Semiconductor Nuclear Detector Fabrication Laboratory is a privilege in conducting R&D activities, especially in the field of semiconductors where Malaysia is the main supplier of semiconductor devices in the world after China and Japan in 2022.

References

Workman D. 2022. Electronic circuit component exports by country. *World's Top Exports*.

Mohamed. K. et al. 2022. Nuclear emerging technology center (pusat teknologi emerging nuklear (net). *No Rujukan : BST/NET/2022/01,*.

Ishak Mansor. 2013. Fabrication and characterization of 4h-sic schottky diode. *Universiti Kebangsaan Malaysia: PhD Thesis*.

Individual Research Contribution Review, 2023, 1(1): 485–486

Maintenance Proposal and Restoration Works of Sputtering System Equipment (Technical Report)

Umi Zulaikha binti Mohd Azmi
Technical Support Division, Malaysian Nuclear Agency
43000 Kajang, Selangor
umizulaikha@nm.gov.my

Abstract

This technical report provides an overview of maintenance proposal and restoration work of Sputtering System equipment in Block 75, Agensi Nuklear Malaysia Branch Dengkil. This equipment was initially used by the TM Research & Development (R&D) and currently belongs to the Semiconductor Nuclear Detector Fabrication Lab.

Keywords: Sputtering System, Nuclear Detector Fabrication

1 Introduction

Sputtering System is a plasma-based deposition process in which energetic ions are accelerated towards a target. The ions strike the target and atoms are ejected (or sputtered) from the surface. These atoms travel towards the substrate and incorporate into the growing film.

2 Findings

2.1 Initial Observation

The inspection of the unit was conducted. The exterior of the Magnetron sputtering system was found to be in generally good condition, no corrosion in areas where the finish coat had been removed or damaged. Casing feet, bearing housing arms, flanges and casing mating half surfaces seem to be in very good condition. The TM pump and RVP pump interior was again found to be in good condition with only surface rust and the occasional flaked area without major corroded areas. The critical area around water system piping and gas piping requires total change to avoid any leakage.

Overall system looks quite outstanding but we could not be able to check a complete line by line the electrical connection system because we believe the inspection need to be very detail and deliberate, focusing on each line of attachment function for specific system control. This inspection will take most of our time, focus, detail & expertise and very time consuming because one operating control failure will affect overall system functioning.

As per the sputtering machine, almost all component are electrically control and very ahead of its time in 2005. Based on our initial inspection, unfortunately, the PLC or program to run the instrument are corrupted or lost (due to battery running out power) and need to be rebuild from professional and local manufacturer/coding programming like us that understand how the sputtering coating system and process works.

All the electronics are completely controlled by the HMI and PLC making this job is quite challenging but very doable.

2.2 Suggestions for Implementation

After all the component is sorted out, our next hurdle will be on the coating procedure and process for the sample running. We need to produce the plasma which is not a simple task as clicking some button. We will teach your researchers on how to fine tune and making the plasma and coating the best possible way plus your propose receipt development requirement.

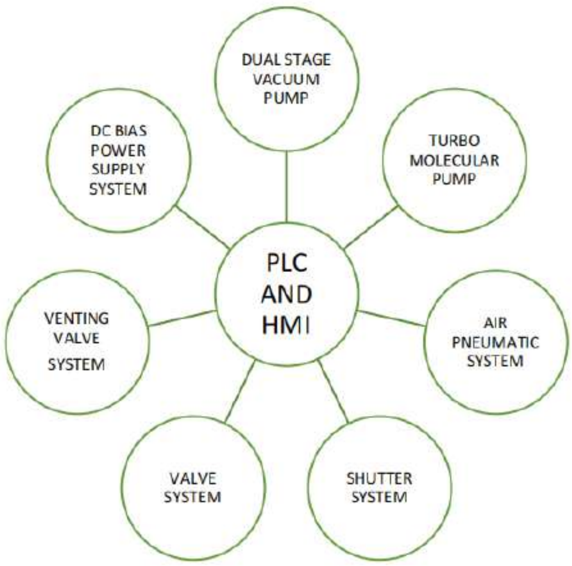

Figure 1: PLC connection.

3 List of Parts/Component

Refer Figure 2, 3 and 4.

4 Conclusion

As a conclusion, the Sputtering System is currently in dire need of maintenance and restoration works to fulfil its designated function. This manual will help to prioritize and determine the further plan for the research and development works in detector fabrication processes.

No.	NAME	QTY	PROPOSE PRICE	OPTIONAL PRICE
1	DC MAGNETRON POWER SUPPLY SYSTEM	1 set	3,000.00	27,000.00
2	HMI DISPLAY SYSTEM	1 set	7,000.00	0.00
3	PLC SYSTEM	1 set	35,000.00	0.00
4	CHAMBER	1 set	5,000.00	0.00
5	MASS FLOW CONTROLLER SYSTEM	2 unit with Controller	29,000.00	0.00
6	LOW VACUUM GAUGE PIRANI SYSTEM	2 set with Controller	15,000.00	0.00
7	BARATRON CAPACITANCE MANOMETER SYSTEM	1 set	29,500.00	0.00
8	HIGH VACUUM GAUGE (PENNING GAUGE)	1 set	4,000.00	0.00
9	ROTARY VACUUM PUMP	1 set	9,980.00	15,000.00
10	TURBOMOLECULAR PUMP	1 set	15,800.00	32,000.00
11	AIR PNEUMATIC SYSTEM	1 set	4,000.00	0.00
12	WATER COOLING SYSTEM	1 set	4,000.00	0.00
13	ROTARY STAGE	1 set	5,700.00	0.00
14	STAGE HEATER	1 set	7,600.00	0.00
15	ELECTRICAL SYSTEM	1 set	21,500.00	0.00
16	SPUTTER GUN SYSTEM	3 set	12,000.00	0.00
17	SHUTTER SYSTEM	1 set	4,000.00	0.00
18	VACUUM AND GAS ACCESSORIES	1 set	20,000.00	0.00
		TOTAL	232,080.00	74,000.00

Figure 2: List of parts/components with price.

DC MAGNETRON POWER SUPPLY SYSTEM

Power supply for sputtering gun to create Plasma

Unknown/Not tested

- Required Further Testing with Sputter Gun
- Will check & test the system with Sputter Gun & Test for several hours to ensure the component working & maintaining the power for at least 2 to 3 hours.
- Servicing and troubleshoot cost RM 3,000.00

If needed to change or MALFUNCTION for new equipment, costing approx, RM 27,000 (300W DC Magnetron Power Supply System with 3 sputter gun switching system).

Figure 3: DC Magnetron Power Supply System.

HMI DISPLAY

TO PROVIDE AN SYSTEM INDICATION & INTERFACE BETWEEN THE MACHINE AND ALL ELECTRICALLY COMPONENT

Need to Change for Different Brand

- The PLC hardware of the system partially power by battery during non-operation will have a battery power loss, thus all the downloaded software will be missing or deleted in the hardware. Battery power are warranted for 5 years and the system already more than 10 years.

- Need to replace HMI controller.
- The cost will be RM 7,000.

Figure 4: HMI Display.

References

Workman D. 2022. Electronic circuit component exports by country. *World's Top Exports*.

Mohamed. K. et al. 2022. Nuclear emerging technology center (pusat teknologi emerging nuklear (net). *No Rujukan : BST/NET/2022/01,*.

Mohamed. K. et al. 2023. Manual alat. *Nuclear Emerging Technology Center (NET)*.

Ishak Mansor. 2013. Fabrication and characterization of 4h-sic schottky diode. *Universiti Kebangsaan Malaysia: PhD Thesis*.

Individual Research Contribution Review, 2023, 1(1): 487–488

Maintenance The Air Quality to Standard Class 100 and 1000 (Technical Report)

Umi Zulaikha binti Mohd Azmi
Technical Support Division, Malaysian Nuclear Agency
43000 Kajang, Selangor
umizulaikha@nm.gov.my

Abstract

This technical report is a working instruction on maintenance the air quality to standard class 100 and 1000. Prior to maintenance, the measurement and monitoring air quality or cleanliness for cleanroom with standard Class 100 and 1000 is important. If abnormal condition occurs, then, maintenance is necessary to make the cleanroom clean as it is. Here, a laser diode-based particle counter was used to measure the particulate contamination in particles per cubic foot at designated sampling locations. From this measurement and monitoring, the contamination of air and, if appropriate, surfaces, can be controlled, which can be beneficial to contamination-sensitive activities.

Keywords: Particle monitoring, Cleanroom, Standard Class 100 and 1000

1 Introduction

A cleanroom is an enclosed area in which airborne particles (contamination) are restricted, monitored or eliminated. It is designed to minimize the introduction, generation, and retention of particles inside the area and where other relevant parameters, such as temperature, humidity, and pressure, are controlled as needed. Semiconductor fabrications require cleanrooms because small particles can affect the production and quality of a components or devices.

Semiconductors are found in practically every electronic device such as smartphone, vehicles, defence equipment, and spacecraft. This is because semiconductor wafers are particularly sensitive to environmental contamination. There are two classification that involve in this cleanroom which are standard class 100 and class 1000. The cleanrooms are required to meet ISO 14644-1, which mandates a maximum of 100 and 1000 particles for class 100 and class 1000 respectively at 0.3 μm or smaller per cubic meter of air (International Organization for Standardization, 2015). Therefore, they must implement air quality control to and maintain level of cleanliness based on the classification criteria.

This document provides a working instruction on monitoring air quality by measuring the number of particles in a cleanroom.

2 Measurement Equipments

A handheld particle counter, GT-321 is used to measure the particulate contamination in particles per cubic foot. It has 5 selectable size ranges of 0.3, 0.5, 1, 2 and 5 μm. This particle counter contains a laser diode-based sensor, NiCd battery pack, vacuum pump, microprocessor electronics, LCD display and user input keys all in one small package. The accuracy is certified according to ASTM and JIS standards and comparable to larger more expensive bench top particle counters. The fast 6-second response makes it especially useful for troubleshooting contamination problems and tracing contamination leaks to the source.

3 Sampling Location

The measurement shall be taken from three (3) sampling locations as listed below:

i. Cleaning room (Class 1000)

ii. Furnace and Sputter Coater area (Class 1000)

iii. Photolitography room (Class 100)

4 Sampling Frequency And Condition

The frequency of sampling is once per week, 2 times in 1 day (morning and evening). Additional counting shall be performed if needed.

5 Procedure

The main procedure in this document is particle monitoring because form this monitoring, we can know the status of cleanroom. If abnormal reading was recorded, actions will be taken. Here, there are three parts of sampling:(i) pre-sampling, (ii) during sampling, and (iii) post-sampling work.

i. **Pre-sampling**
The air ventilation was turned on for at least 15 mins prior to sampling. The battery of the particle counter (GT-321) should be checked prior to use. When the battery is low enough, a “Battery Low” message is displayed on the display and the pump will not turn on when the ‘Start’ key is pushed. This particle counter is rechargeable. The cleanroom should be ensured are well-function before sampling.

ii. **During sampling**
The rubber cap from particle counter inlet nozzle was

removed. Turned on particle counter and press 'Select' key. Select 0.3μ particle size. Then, place the particle counter at the appropriate place and press 'Start' key to start sampling. The reading was recorded. Measurement was performed for five times.

iii. **Post-sampling**
After done sampling, place a rubber cap back at inlet nozzle. Place GT-321 inside the provided box.

6 Flow Chart

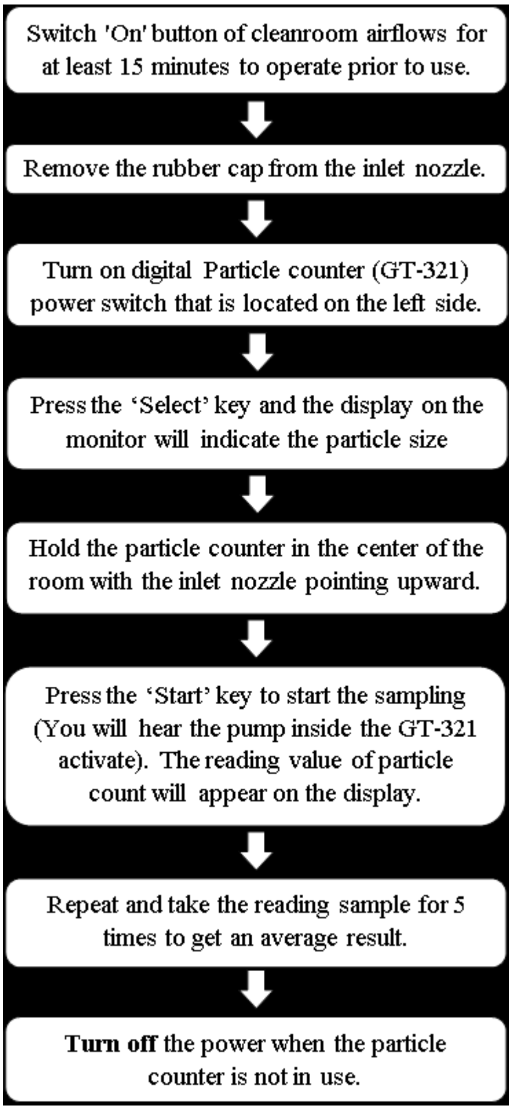

Figure 1: Flow chart of particle monitoring.

7 Conclusion

As a conclusion, thermal oxidation is necessary in fabrication of semiconductor in order to form a thin oxide layer on a substrate. This manual will help other researchers or officers to conduct a process using split tube furnace.

References

International Organization for Standardization (ISO). 2015. Cleanrooms and associated controlled environments — Part 1: Classification of air cleanliness by particle concentration. No. 14644-1.

Individual Research Contribution Review, 2023, 1(1): 489–490

Specification and Potential Applications of Split Tube Furnace

Umi Zulaikha binti Mohd Azmi
Technical Support Division, Malaysian Nuclear Agency
43000 Kajang, Selangor
umizulaikha@nm.gov.my

Abstract

Split tube furnace is a tube furnace that can be opened to allow for the easy installation and removal of work tubes and reaction vessels. Located in the cleanroom laboratory at Block 75, Dengkil Complex, it has the maximum temperature of 1200°C and maximum operating temperature of 1100°C. However, for the maximum continuous temperature is set at 1150°C. The main component in a tube furnace is heating chamber comprises of a circular furnace wall made of high-temperature ceramic. Kanthal Coil element are embedded into the ceramic by surround a central chamber for uniformly distributed heaters. This tube furnace has one (1) unit FUJI programmable temperature control with 64 ramps/soaks that fitted with type K thermocouple. This architecture guarantees the highest possible thermal uniformity for processing both inorganic and organic compounds. The tube furnace also provides the gas inlet/outlet in order to perform a reaction under a controlled atmosphere. In this study, the split tube furnace had been used to grow oxide layer on silicon wafer (SiO_2/Si) through dry oxidation method. From the study, the thickness and surface roughness of wafer were investigated.

Keywords: Split tube furnace; Horizontal furnace; Thermal oxidation

1 Introduction

Furnace is a container or enclosed space in which a very hot fire is made. It can be used for a broad range of thermal processes (Massoud et al., 1985; Jenkins and Mullinger, 2023). Split tube furnace is a type of furnace that can be opened to allow for the easy installation and removal of work tubes and reaction vessels. Located in the cleanroom laboratory at Block 75, Dengkil Complex, a model of VT Tube Furnace, STF-1200- 450-100 with maximum temperature of 1200°C and maximum operating temperature of 1100°C is ready to be used. Meanwhile, the maximum continuous temperature is set at 1150°C. This tube furnace is a single zone furnace, meaning that it has only one set of heating elements and controller. Kanthal Coil elements are embedded into the ceramic by surrounding a central chamber for uniformly distributed heaters. It has one (1) unit FUJI programmable temperature control with 64 ramps/soaks that are fitted with type K thermocouple. In this study, the split tube furnace has been used to grow the oxide layer on silicon (Si) wafer to form silicon dioxide (SiO_2) layer by using dry oxidation method. The thickness and surface roughness of wafers after different oxidation time have been studied.

2 Methods

2.1 Cleaning of Si wafer

Prior to oxidation, Si wafer was cleaned in order to eliminate any inorganic or organic contaminants on the surface (Dalila et al., 2020). Briefly, 5 mL of 30% H_2O_2 was mixed with 15 mL of concentrated H_2SO_4 (1:3) and immerse the wafer into the solution. Then, the wafer was rinsed using deionized water (DI) thoroughly. Finally, the wafer was dried using nitrogen gas because it is a preferred technique with less for particle recontamination (Kern, 2018). The wafer was immediately used for the oxidation process or else, placed it in a desiccator for further used.

2.2 Oxidation Experiments

Dry thermal oxidation process was carried out in a split tube furnace as shown in Figure 1(a). Firstly, heat up the furnace until 800°C. Then, put in the wafer inside the wafer boat and use a quartz push rod to push the boat inside the furnace until it reaches the centre of the tube as displayed in Figure 1(b). Next, flow the nitrogen gas until it reaches at certain 1000°C. After reaches at required temperature, stop flow the nitrogen and start flow the oxygen gas for certain time (30, 60, and 90 mins), or called oxidation time. After that oxidation time ended, stop flow the oxygen gas and cooling down the furnace. Then, put the oxidized wafer in a desiccator for further analysis.

a)
b)


Figure 1: (a) Image of split tube furnace located at Blok 75 which installed with opening valve and gas inlet/outlet, and (b) location of sample.

2.3 Analysis on surface of SiO_2

After being oxidized, the wafer's surface has been placed under microscope, MX-6R (China) to observe the colour changes and estimate the thickness using colour chart for SiO_2. Atomic force microscopy (AFM) also been used to investigate the surface roughness of SiO_2. This was done using Park System (South Korea) in a non-contact mode in order to prevent from surface damage.

3 Results and Discussion

In this experiment, thermal oxidation was conducted to grow oxide layer on Si wafer. Oxidation is one of the most important thermal processes in fabrication of semiconductor. It is a method in which oxygen is growth on a Si wafer to generate SiO_2 on the wafer surface. When Si reacts with oxygen, it undergoes an oxidation process. The reaction happens fast at first, but as the oxide layer on the surface grows, the oxygen must diffuse through the oxide before reaching the silicon and reacting.

Prior to thermal oxidation, the silicon wafer needs to be cleaned in order to minimize the chemical contaminants and particles on wafer surface. This is due to the extreme sensitivity of the semiconductor surface and the small sizes of the device features, which lead to the key technologies in the fabrication of ultra-large-scale integration (ULSI) Si circuits (Kern, 2018). After cleaning using piranha method, the Si wafer was observed under microscope and it shows less particles contamination compared to before cleaning. This may be due to several factors such as transient effects during rinsing and drying residues (Bearda et al., 2018).

3.1 Analysis on surface of SiO_2

The wafers were examined under a microscope after it undergoes the oxidation process to observe the colour changes. Then, the thickness of SiO_2 was estimated based on the observed colour using a colour chart for SiO_2. From the observations, the wafer that undergoes oxidation time for 30 mins shows the colour of royal blue which we assume that the thickness is around 125 nm. Meanwhile, 60 mins of oxidation show the colour of light blue which is around 150 nm and for 90 mins show a quite similar colour with 60 min oxidation time. Hence, the longer the wafers are exposed to the oxygen source, the thicker the oxide layer, coincides with the theory (Massoud et al., 1985). However, at 90 mins, the thickness started to be stagnant as 60 mins. Therefore, other parameters need to be done such as oxidation temperature, pressure of the O_2 gas and location of the wafer (near the gas inlet, in the middle or far from gas inlet).

The surface roughness of Si wafer before and after oxidation were also studied by using AFM. From the study, the surface roughness of Si wafer before oxidation was higher compared to after oxidation. The root-mean-square roughness (Rq) value before oxidation, 30 mins, 60 mins, and 90 mins oxidation were 0.0845 nm, 0.068 nm, 0.057 nm, and 0.047 nm, respectively.

4 Conclusion

As a conclusion, the split tube furnace successfully grows the oxide layer on silicon wafer by using thermal oxidation method. It was performed at various oxidation time with constant temperature which affecting surface of wafer in terms of thickness and roughness. From the study, the thickness of SiO_2 were increased as oxidation time increased. However, at 90 mins, the thickness of SiO_2 seems similar to 60 min which does not follow the theory. Therefore, several parameters need to be considered for future study. Meanwhile, the surface roughness of wafer was reduced as the oxidation time increased, which is good for fabrication of semiconductor.

References

T. Bearda, P. W. Mertens, and S. P. Beaudoin. 2018. Overview of wafer contamination and defectivity. *In Handbook of Silicon Wafer Cleaning Technology*, pages 87 – 149, Elsevier Inc. https://doi.org/10.1016/B978–0– 323–51084–4.00002–2.

N. R. Dalila, M. K. M. Arshad, S. C. B. Gopinath, M. N. M. Nuzaihan, and M. F. M. Fathil. 2020. Molybdenum disulfide—gold nanoparticle nanocomposite in field-effect transistor back-gate for enhanced C-reactive protein detection. Microchimica Acta, 187, 588. https://doi.org/10.1007/s00604-020- 04562-7.

J. Henrie, S. Kellis, S.M. Schultz, and A. Hawkins. 2004. Electronic color charts for dielectric films on silicon. *Optics Express*, 12(7):1 – 6.

B. Jenkins and P. Mullinger. 2023. Introduction in industrial and process furnaces. Elsevier. https://doi.org/10.1016/b978-0-323-91629-5.00005-7.

W. Kern. 2018. Overview and evolution of silicon wafer cleaning technology. *In Handbook of Silicon Wafer Cleaning Technology*, pages 3 – 85, Elsevier Inc. https://doi.org/10.1016/B978–0–323–51084–4.00001–0.

H. Z. Massoud, J. D. Plummer, and Irene E. A. 1985. Thermal oxidation of silicon in dry oxygen growth rate enhancement in the thin regime: 1. Experimental results. *Journal of The Electrochemical Society*, 132:2685.

Individual Research Contribution Review, 2023, 1(1): 491–492

Thermal Oxidation of Silicon (Industrial Report)

Umi Zulaikha binti Mohd Azmi
Technical Support Division, Malaysian Nuclear Agency
43000 Kajang, Selangor
umizulaikha@nm.gov.my

Abstract

Industrial training is compulsory to students in certain programmes at all levels of higher education at the Institute of Higher Learning (IPT). This document provides information on activities, procedures, results and discussion that have been done by the student, Nur Faatihah Ahmad Redzuan. The activities are particle monitoring in cleanroom and thermal oxidation of silicon wafer.

Keywords: Industrial training, particle monitoring, thermal oxidation

1 Introduction

The industrial training is a required course for all students pursuing a Bachelor of Science in Chemistry with Management at University Technology Mara (UiTM). This course is required for students to finish their bachelor's degree and graduate from UiTM. The primary purpose of industrial training is to introduce students to the industrial working environment. As a result, students will be able to comprehend the theories learned with more extensive and hands-on practise in a real-world employment environment. The industrial training programme provides students with learning opportunities in the industry where they may get practical experience and expand their knowledge that will be beneficial after graduation.

The activities that have been done by the student were particle monitoring in cleanroom and thermal oxidation of silicon wafer. Particle monitoring was performed in cleanroom standard class 100 and 1000 in order to maintain the level of cleanliness based on the requirement in ISO 14644-1. The requirements are 100 particles and 1000 particles for class 100 and 1000, respectively at 0.3μm or smaller per cubic meter of air. Another activity was thermal oxidation of silicon wafer. Thermal oxidation is one of the process to fabricate semiconductor. This process was used to grow oxide layer on the wafer surface which serves as a passivation and masking layer for silicon devices. Here, the student was conducted a dry oxidation method, whereby the pure oxygen was utilized as the oxidizing atmosphere. The silicon interacts with the surrounding oxygen during the dry oxidation process, resulting in the formation of silicon dioxide on the surface (Shi et al., 2011).

2 Materials and Methods

Particle monitoring
The particle counter, GT-321 (Figure 1) was turned on and removed the rubber cap from inlet nozzle. Next, the 'Select' button was pressed and chose 0.3μ for particle size. Placed the particle counter at appropriate place with the inlet nozzle pointing upward. Then, the 'Start' button was pressed to start the measurement. The reading was recorded and repeated the measurement for another 4 times.

Figure 1: Particle counter, GT-321.

Thermal oxidation of silicon wafer
Prior to oxidation, the silicon was cleaned using piranha solution. This step was explained in detail in another technical report entitled "Cleaning wafer using piranha solution".

After cleaning, dry oxidation method was carried out to grow oxide layer on the wafer. Firstly, the furnace needs to be heated up until 800°C. Then, put in the wafer inside the quartz boat and use a quartz push rod to push the boat inside the furnace. Next, flowed the nitrogen gas (20 psi) until it reached at 1000°C. After reached at 1000°C, stop the nitrogen and flowed the oxygen gas for certain time (30, 60, and 90 mins). After that time, stop the oxygen gas and cooling down the furnace. Then, put the oxidized wafer in a desiccator.

Surface analysis
After being oxidized, the wafer's surface was observed under microscope, MX-6R (China) to observe the colour and estimate the thickness using colour chart for SiO_2. Other than that, Fourier transform infrared (FTIR) spectrometer (Agilent/Cary 630) was used from the range 500-4000 cm^{-1} to

identify the chemical bonding that occurred on the substrate.

3 Result and Discussions

In this experiment, thermal oxidation was conducted to grow oxide layer on Si wafer. Oxidation is one of the most important thermal processes in fabrication of semiconductor. It is a method in which oxygen is growth on a Si wafer to generate SiO_2 on the wafer surface. When Si reacts with oxygen, it undergoes an oxidation process. The reaction happens fast at first, but as the oxide layer on the surface grows, the oxygen must diffuse through the oxide before reaching the silicon and reacting.

Prior to thermal oxidation, the silicon wafer needs to be cleaned in order to minimize the chemical contaminants and particles on wafer surface. This is due to the extreme sensitivity of the semiconductor surface and the small sizes of the device features, which lead to the key technologies in the fabrication of ultra-large-scale integration (ULSI) Si circuits (Kern, 2018). After cleaning using piranha method, the Si wafer was observed under microscope and it shows less particles contamination compared to before cleaning. This may be due to several factors such as transient effects during rinsing and drying residues (Bearda et al., 2018).

Analysis on surface of SiO_2

The wafers were examined under a microscope after it undergoes the oxidation process to observe the colour changes. Then, the thickness of SiO_2 was estimated based on the observed colour using a colour chart for SiO_2. From the observations, the wafer that undergoes oxidation time for 30 mins shows the colour of royal blue which we assume that the thickness is around 125 nm. Meanwhile, 60 mins of oxidation show the colour of light blue which is around 150 nm and for 90 mins show a quite similar colour with 60 min oxidation time. Hence, the longer the wafers are exposed to the oxygen source, the thicker the oxide layer, coincides with the theory (Massoud et al., 1985). However, at 90 mins, the thickness started to be stagnant as 60 mins. Therefore, other parameters need to be done such as oxidation temperature, pressure of the O_2 gas and location of the wafer (near the gas inlet, in the middle or far from gas inlet).

The chemical bonding that occurred on the surface of substrates were also studied. The results of four samples before oxidisation, after oxidisation for 30, 60, and 90 mins showed the absorption peaks around 790cm^{-1} which correspond to rocking mode and 1040cm^{-1} correspond to stretching mode. These two peaks are attributed to Si-O bonds in silicon oxide. Furthermore, the peak at 1040cm^{-1} which assigned to high-quality oxide and reveals the high quality of the film that was produced. Moreover, the peak appears around 1190cm^{-1} corresponds to Si-O-Si is cause by the splitting of longitudinal and transverse optical stretching motions (Kayed, 2022). Therefore, the appearance of the Si-O bond peak in silicon indicates that the sample has successfully undergone the oxidation process compared to before oxidizing.

4 Conclusion

As a conclusion, the split tube furnace successfully grows the oxide layer on silicon wafer by using thermal oxidation method. It was performed at various oxidation time with constant temperature which affecting surface of wafer in terms of thickness and chemical bonding. From the study, the thickness of SiO_2 were increased as oxidation time increased. However, at 90 mins, the thickness of SiO_2 seems similar to 60 min which does not follow the theory. Therefore, several parameters need to be considered for future study. Meanwhile, the FTIR spectrum showed that the surface of substrates have the chemical bonding of Si-O and Si-O-Si, which indicates the wafer has successfully undergone oxidation process.

References

T. Bearda, Mertens P. W., and Beaudoin S. P. 2018. Overview of wafer contamination and defectivity. *In Handbook of Silicon Wafer Cleaning Technology*, pages 87 – 149. Elsevier Inc.

K. Kayed. 2022. The effect of annealing temperature on the structural and optical properties of Si/SiO_2 composites synthesized by thermal oxidation of silicon wafers. *Silicon*, 14:5157 – 5163.

W. Kern. 2018. Overview and evolution of silicon wafer cleaning technology. *In Handbook of Silicon Wafer Cleaning Technology*, pages 3–85, Elsevier Inc.

H. Z. Massoud, Plummer J. D., and Irene E. A. 1985. Thermal oxidation of silicon in dry oxygen growth rate enhancement in the thin regime: 1. Experimental results. *Journal of The Electrochemical Society*, 132:2685.

Z. Shi, Shao S., and Wang Y. 2011. Improved the surface roughness of silicon nanophotonic devices by thermal oxidation method. *Journal of Physics: Conference Series*, 276:1.

Individual Research Contribution Review, 2023, 1(1): 493–494

Thermal Oxidation of Silicon Wafer (Technical Report)

Umi Zulaikha binti Mohd Azmi
Technical Support Division, Malaysian Nuclear Agency
43000 Kajang, Selangor
umizulaikha@nm.gov.my

Abstract

This technical report is a manual on how to conduct a process of thermal oxidation on silicon wafer by using split tube furnace. Thermal oxidation is a method to grow the oxide layer on silicon wafer surface to form silicon dioxide (SiO_2). Meanwhile, split tube furnace is a tube furnace that can be opened to allow for the easy installation and removal of work tubes and reaction vessels. The furnace was installed with two opening chamber and gas inlet/outlet which suitable for this process. This process including cleaning wafer and followed by thermal oxidation procedure.

Keywords: Thermal oxidation, Silicon wafer, Split tube furnace

1 Introduction

Thermal oxidation is a method to grow oxide layer on silicon substrate and become SiO_2 film. This thin film has become increasingly important recent years due to the continuing down-scaling of ultra-largescale integration (ULSI) metal oxide silicon fieldeffect transistors (MOSFETs). Besides that, these thin films also important for organic transistors where back-gating is needed (Kayed, 2022).

A split tube furnace which is located in the cleanroom laboratory at Block 75, Dengkil Complex has a horizontal oriented chamber with a furnace body that splits into two halves. A sample can be slowly moved during the experiment by opening the ends of the furnace tube. Besides that, gas inlet/outlet also provided in order to perform a reaction under controlled environment (pure oxygen or nitrogen). Gas will flow in one end of the tube and the gas (or any evolved gases) exits through the other site.

Here, a model of VT Tube Furnace, STF1200-450-100 with maximum temperature of 1200°C, maximum operating temperature of 1100°C, and maximum continuous temperature of 1150°C was used to perform a thermal oxidation procedure. This tube furnace is a single zone furnace, meaning that it has only one set of heating elements and controller. Kanthal Coil elements are embedded into the ceramic by surrounding a central chamber for uniformly distributed heaters. It has one (1) unit FUJI programmable temperature control with 64 ramps/soaks that are fitted with type K thermocouple.

This technical report is a guidance on how to do a process of thermal oxidation including cleaning the silicon wafer. Prior to oxidation, cleaning silicon wafer is necessary in order eliminates any particles and contaminants that might affect the finished product.

2 Procedure

Thermal oxidation process for growing oxide layer on silicon wafer involves cleaning wafer procedure and working instruction for thermal oxidation.

Cleaning of silicon wafer

Prior to oxidation, Si wafer has to be cleaned in order to eliminate any inorganic or organic contaminants on the surface. Briefly, 5 mL of H_2O_2 and 15 mL of H_2SO_4 (1:3) were mixed and immersed the wafer into the solution. Then, rinsed the wafer using deionized water (DI) thoroughly. Finally, dried the wafer using nitrogen gas. The wafer needs to be immediately used for oxidation process or else, place it in a desiccator for further used.

Thermal oxidation silicon wafer

Dry thermal oxidation process was carried out in a fused silica tube furnace. Firstly, the valves of nitrogen and oxygen gases need to be opened. Make sure the main opening valves are in a closed position. Then, the furnace needs to be heated up until 800°C. Then, put in the wafer inside the quartz boat and use a quartz push rod to push the boat inside the furnace. Next, flowed the nitrogen gas (20 psi) until it reached at 1000°C. After reached at 1000°C, stop the nitrogen and flowed the oxygen gas for certain time (30, 60, 90 and 120 mins). After that time, stop the oxygen gas and cooling down the furnace. Then, put the oxidized wafer in a desiccator. Finally, turned off the heater.

3 Flow Chart

Refer Figure 1, 2 and 3 on the flowchart of cleaning wafer, opening gas valves before turn on the furnace and furnace operation manual to do a thermal oxidation process.

4 Conclusion

As a conclusion, thermal oxidation is necessary in fabrication of semiconductor in order to form a thin oxide layer on a substrate. This manual will help other researchers or officers to conduct a process using split tube furnace.

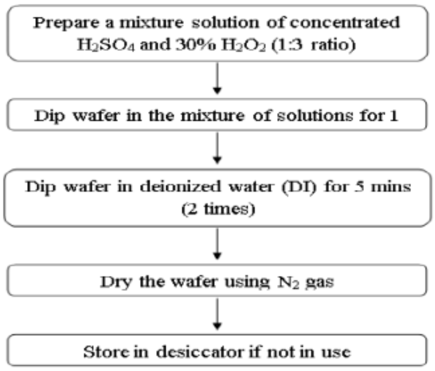

Figure 1: Flow chart for cleaning wafer.

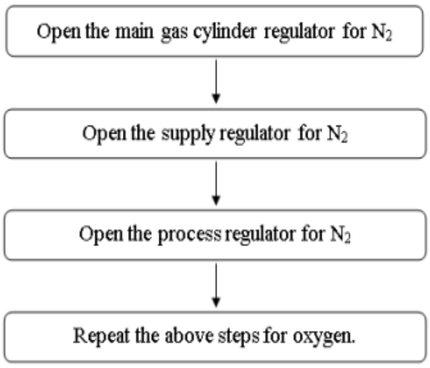

Figure 2: Flow chart for opening gas valves before turn on the furnace

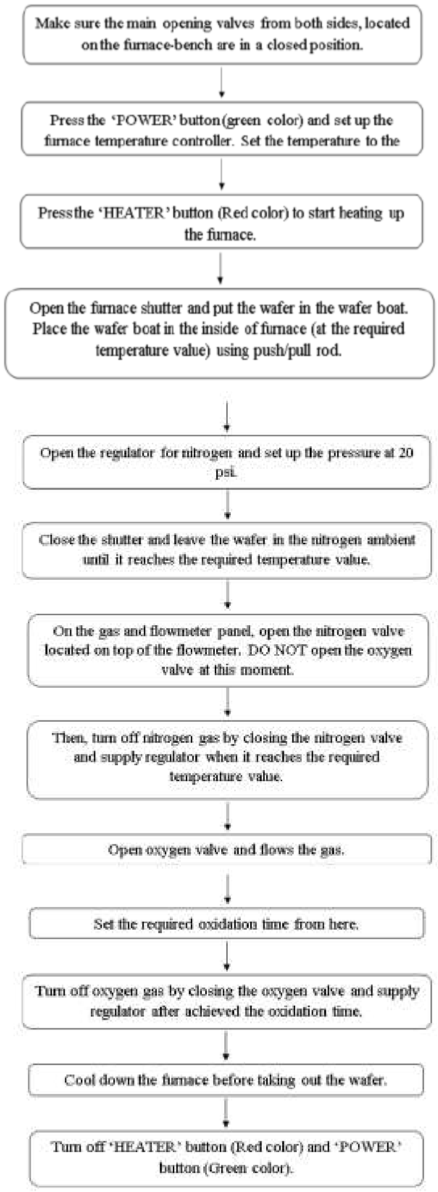

Figure 3: Flow chart of furnace operation manual to do a thermal oxidation process.

References

K. Kayed. 2022. The effect of annealing temperature on the structural and optical properties of Si/SiO_2 composites synthesized by thermal oxidation of silicon wafers. *Silicon*, 14:5157 – 5163.

Worker Practices In Cleanroom (Technical Report)

Umi Zulaikha binti Mohd Azmi
Technical Support Division, Malaysian Nuclear Agency
43000 Kajang, Selangor
umizulaikha@nm.gov.my

Abstract

A cleanroom is a controlled environment which eliminates sub-micron airborne contamination generated from people, processes, facilities and equipment. Some of the most common cleanroom contamination include solid dust, liquid, bacteria, fungus, human skin cells and hair, trace moisture, spills and leaks, cosmetics, perfumes, lint, fibers, and more. The majority of cleanroom contamination comes from those that work within it. Therefore, the best practice for worker in cleanroom is really important so that the cleanroom is protected from contamination. This document describe the practice procedure for worker in cleanroom.

Keywords: Particle monitoring, Cleanroom, Standard Class 100 and 1000

1 Introduction

Semiconductors are found in practically every electronic device such as smartphone, vehicles, defence equipment, and spacecraft. This is because semiconductor wafers are particularly sensitive to environmental contamination. That is why semiconductor fabrication requires the cleanroom facilities. The facilities are designed to minimize the introduction, generation, and retention of particles inside the area.

Standard classes of cleanrooms at Blok 75, Dengkil Complex, Malaysian Nuclear Agency are 100 and 1000. The cleanliness and air quality of the cleanroom need to be controlled (CLIN®, 2022). Therefore, during performing the task in a cleanroom, employees must wear specifically cleanroom attire to prevent contamination from infecting the environment as well as to protect from any hazard might happen in cleanroom. The cleanroom attire is meant to cover the complete body such as hoods, goggles, face masks, gloves, coveralls, boots, and footwear covers. There are several sources of contamination that must be addressed, including environmental and people control.

This document establishes a practice procedure for worker in cleanroom in order to protect cleanroom from contamination and accident.

2 Procedure

i. **Before entering the cleanroom**
The air ventilation was turned on for at least 10 mins. Any outside shoes must be taken out and place on a rack. Worn a complete cleanroom attire (Figure 1) in a changing room. Put on a face mask and hair net appropriately. Worn a cleanroom shoe wear and shoe cover from storage rack. Worn gloves and ensure cover cuff of sleeve with gloves.

Figure 1: Cleanroom attire.

ii. **Entering the cleanroom**
Enter the cleanroom and ensure to walk slowly to minimize the creating air turbulence while in the cleanroom. Turn on the lamp for cleanroom such as photolithography, cleaning, thermal room as well as the air compressor and FFU (photolithography lab). Switch on the fume hood in cleanroom.

iii. **Exiting the cleanroom**
Turn off the cleanroom's lamp such as photolithography, cleaning, thermal room as well as the air compressor and FFU (photolithography lab). Remove and dispose of all the gloves, face mask, hairnet and shoes cover after use in the changing room. Disposable gloves should never be washed or reused. Switch off the cleanroom airflows if it not in use.

3 Flow Chart

Flow for worker practices in the clean room as in Figure 2 to Figure 4 below:

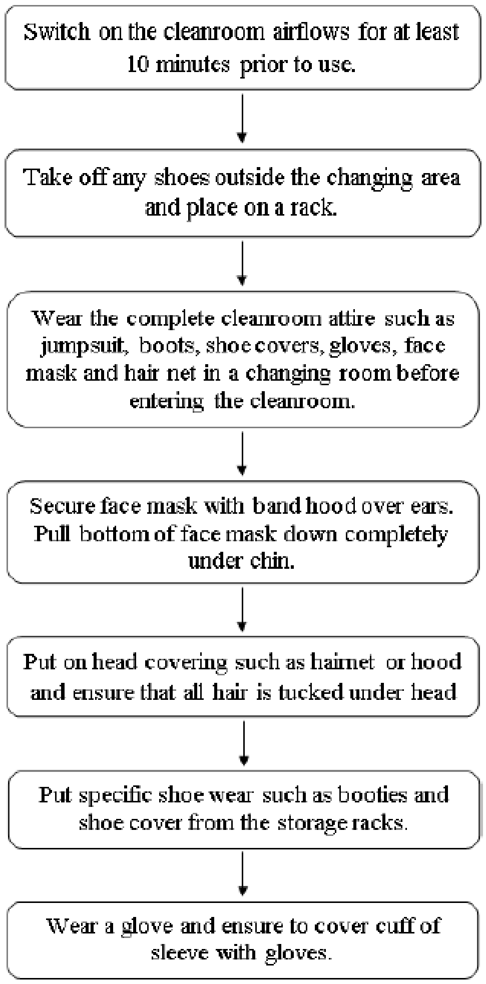

Figure 2: Practice before entering cleanroom.

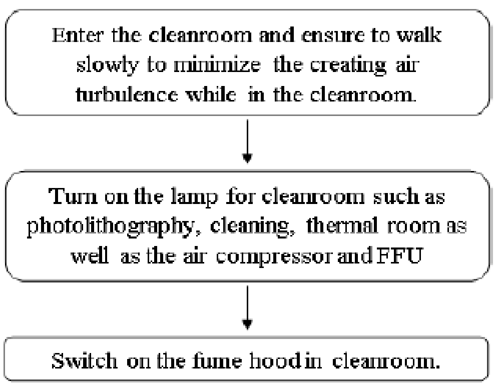

Figure 3: During entering the cleanroom.

4 Conclusion

In conclusion, maintaining a cleanroom is essential. Hence, adhering to best practices for cleanroom workers is crucial to safeguarding the environment from contamination.

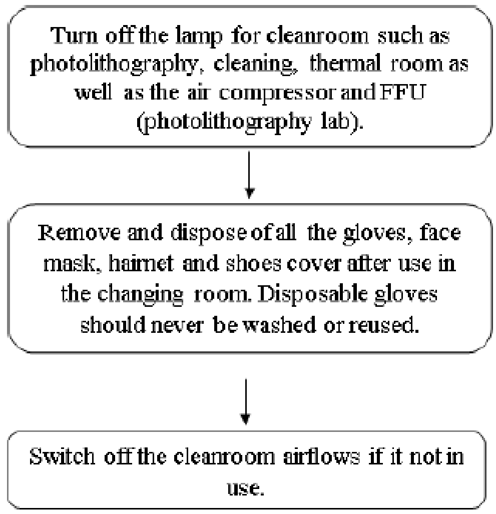

Figure 4: Practice exiting the cleanroom.

References

CLIN®. 2022. Rules for working in a cleanroom. accessed on 21 March 2023,. *https://www.cleanroom-industries. com/en/resources/item/438-rules-forworking-in-a-cleanroom.*

Individual Research Contribution Review, 2023, 1(1): 497–498

Fire Probabilistic Safety Assessment at PUSPATI TRIGA Reactor: Basement

Zaredah Hashim
Technical Support Division, Malaysian Nuclear Agency
43000 Kajang, Selangor
zaredah@nm.gov.my

Abstract

An internal fire analysis Level-I probabilistic safety assessment (PSA) for TRIGA PUSPATI (RTP) nuclear research reactor was initiated. Previous study on half-scope mode Level-I PSA, focusing only on internal initiating event, were developed for both full power and shutdown operational mode. Hence, in ensuring PSA remains relevant, a subsequent study to kept PSA up to date is a compulsory. The aim of this study is to present the step-by-step work done and the insights gained in identifying and screening significant compartments that are potential to had the worst consequences as an ignition sources. This study will only focus on RTP's basement which consist of 3 compartments: switch room, battery room and basement hall. Procedure in data collection were based on IAEA document, Specific Safety Guide No. 3: Development and Application of Level 1 Probabilistic Safety Assessment for Nuclear Power Plants (SSG-3). Microsoft Excel was used as data collection media and internal fire hazard database development. A brief qualitative analysis using failure mode and effect analysis is also presented.

Keywords: IMS, online, TRIGA PUSPATI, ShareFolder, SharePoint

1 Introduction

In Malaysia, at the only nuclear research reactor been built, reactor TRIGA PUSPATI (RTP), an initial work in attempting to incorporate internal fire probabilistic safety assessment (PSA) into Level-I PSA model was implemented in early June 2019. Recently, the Malaysian PSA team developed a level 1 PSA focusing on random failure of systems, components and human error (Brayon et al., 2014; Maskin et al., 2016; Mohamed et al., 2015; Sarif et al., 2017) . As per mention in Maskin et al. (2016), Level-I PSA for RTP is a new adapted project which is develop without any official database.

The main purpose of this paper is to prepare necessary data in assessing internal fire hazard Level-I PSA. This paper aims at introducing a systematic approach in data collection and qualitative assessment throughout the process in preparing the necessary data. It is also intended to serve as a guide in a step-by-step guidelines for the development of fire PSA studies for a nuclear research reactor, as per recommendation by the IAEA (2016), requirement 20, which is:

> 'The level-I PSA for internal fire should be documented in a manner that facilitates review, applications and updating of the Level 1 PSA.'

Finally, a success in this initial work, will be a result to expand the current study from only basement to the entire RTP building.

2 Methods

An illustration of the adapted methodology is illustrated in Figure 1, showing two major processes, which are: (1) Data collection; and (2) Qualitative analysis. The scope of this study covers Level-I internal fire PSA, perform at full power and daily shutdown operational conditions (the shutdown for annual maintenance is not included in this study). Meanwhile, the location considered is focusing only at the reactor basement.

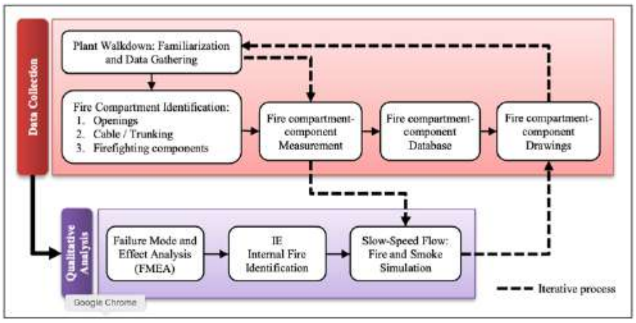

Figure 1: Data collection and qualitative analysis approach for fire PSA

Qualitative analysis using failure mode and effect analysis (FMEA), meanwhile a uniform approach introduced by Šimurka (2014) is perform in qualitative screening to assign appropriate initiating event (IE) as depicted in Figure 2.

3 Results and Discussion

Figure 3a and 3b illustrated 2D drawing for switch room compartment openings and fire suppression systems respectively.

Table 1 presents the lists of components with its failure mode and the consequences or effects to RTP if it fails.

Based on the initial FMEA screening analysis, the 'Yes' value indicated in Table 1 above, only shows one initiating event for both compartments, which is fire spark. However, this result will be reevaluated based on which compartment has the worst fire consequences.

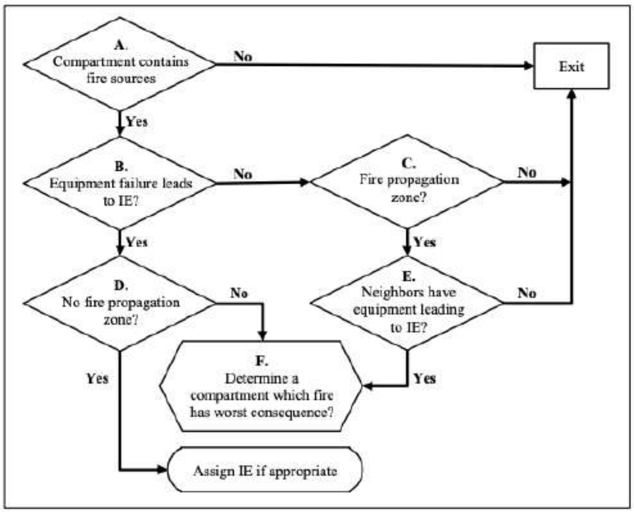

Figure 2: Flowchart for qualitative screening (Šimurka, 2014)

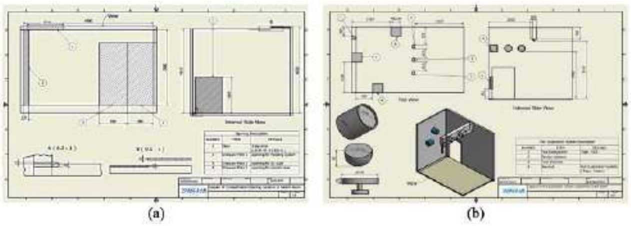

Figure 3: Switch room: (a) Compartment openings layout; and b) Fire suppression systems

Table 1: List of FMEA internal fire for RTP basement for switch and battery room

No.	Compartment	Failure Mode	Consequences or Effects	IE
A.	**Switch room**			
	1. Fire suppression: Heat detector	FS	Operator missing compelling signal/ annunciator after the occurrence of fire	No
	2. Fire suppression: Smoke detector	FS	Operator missing compelling signal/ annunciator after the occurrence of fire	No
	3. DB 'RE'	FiS	Lead to an initiating event (IE)	Yes
	4. DB 'REB'	FiS	Lead to an initiating event (IE)	Yes
	5. Main switchboard (MDB)	FiS	Lead to an initiating event (IE)	Yes
	6. DB 'RNB'	FiS	Lead to an initiating event (IE)	Yes
	7. TNB source	NP	Reactor blackout	
B.	**Battery room**			
	8. Battery	NP	Reactor blackout	No
	9. Uninterruptable power supply (UPS)	NP	Reactor blackout	No
	10. Switchboard	FiS	Lead to an initiating event (IE)	Yes
	11. Fire suppression: Heat detector	FS	Operator missing compelling signal/ annunciator after the occurrence of fire	No

4 Conclusions

To have a typical and comprehensive PSA plant model, a complete list of representative IEs is essentially nonnegligible. Incomplete consideration of IEs adversely affects the quality of a PSA, thus leading to results that underestimate the level of risk. Therefore, this preliminary study on the development of IEs for RTP internal fire is part of the effort towards fulfilling the completeness of a full scope Level-I PSA. This study has addressed both the systematic approach in data collection and qualitative assessment in preparing the necessary data for Fire PSA input. Finally, success in this initial work will be a result to expand the current study from just basement to the entire RTP building.

Data collection is the most crucial part of any study — failure to collect accurate data resulted in an incorrect result. Lesson learnt in a wrongly measured dimension stemmed in measuring the same compartment repeatedly. However, despite the repetitive measurement, all 3D drawings for three compartments were successfully drawn and merged. At the same time, a compartment-component database that records all the plant walk-down sheet which reflects any current modification and component installation was developed as soon as the project starts. Meanwhile, from a qualitative assessment using inductive analysis, for all three compartments, only one IE was identified: fire spark.

Hence, our future works will be focused for the rest of the RTP's building and proceed on the accident sequence modelling, and event tree development for the internal fire.

References

International Atomic Energy Agency. 2016. Safety of research reactors (Specific Safety Requirements). *SSR-3*.

F.C Brayon, Maskin M., Prak Tom P., Mohd Sarif A. H. S., Ramli Z., Zakaria F., Mohamed F., Aslam A., Lyubarskiy A., Kuzmina I., Hughes P., and Ulses A. 2014. Building competence for safety assessment of nuclear installations: Applying IAEA's safety guide for the development of a level 1 probabilistic safety assessment for the TRIGA research reactor in Malaysia. *Probabilistic Safety Assessment and Management Conference 12 (PSAM12)*.

M. M. Maskin, Mohd Sarif A. H. S., Brayon F. C., Phongsakorn P. T., Zakaria M. F., Ramli Z., and Mohamed F. 2018. Quantification of initiating event frequencies and component reliability data in level 1 probabilistic safety assessment at Puspati TRIGA research reactor. *Annals of Nuclear Energy*, 121:22–28.

M. Maskin, Brayon F. C., Mohd Sarif A. H. S., Phongsakorn P. T., Ramli Z., and F. Mohamed. 2016. Selection of important initiating events for level 1 probabilistic safety assessment study at Puspati TRIGA Reactor. *Annals of Nuclear Energy*, 92:198–210.

F. Mohamed, Mohd Sarif A. H. S., Yahaya R., Rahman I., Maskin M., Praktom P., and Charlie F. 2015. Operator reliability study for probabilistic safety analysis of an operating research reactor. *Annals of Nuclear Energy*, 80:409–415.

A. H. S. Mohd Sarif, M. Maskin, P. Prak Tom, F. C. Brayon, P. Hlavac, and F. Mohamed. 2017. Operator response modeling and human error probability in TRIGA Mark II research reactor probabilistic safety assessment. *Annals of Nuclear Energy*, 102:179–189.

P. Šimurka. 2014. Overview of fire PSA and supporting software. *23rd International Conference Nuclear Energy of New Europe*, 503.1-503.8.

Individual Research Contribution Review, 2023, 1(1): 499–500

Fire Probabilistic Safety Assessment at PUSPATI TRIGA Reactor: Control Room

Zaredah Hashim
Technical Support Division, Malaysian Nuclear Agency
43000 Kajang, Selangor
zaredah@nm.gov.my

Abstract

An internal Fire Probabilistic Safety Assessment (FPSA) study was conducted in the control room of the TRIGA PUSPATI (RTP) research reactor. This study aims to determine the likelihood of a fire occurring in the control room of RTP and the probability of fire occurring after an accident loss of instrumentation and control (LOIC) to the core damage frequency (CDF) value. The quantification results of the CDF are compared between LOIC with fire-induced (LOIC-F) and without fire-induced (LOIC). This research will contribute on providing essential information on status of fire in RTP's control room as an insight of identifying any risk of fire scenario that may occur including investigation of current fire protection system sufficiency.

Keywords: fire PSA, control room, nuclear research reactor, TRIGA PUSPATI, Malaysia

1 Introduction

PUSPATI TRIGA reactor (RTP) marked 40 years accidentfree operation since its first criticality on June 28, 1982. Numerous activities were conducted to rejuvenate RTP to accelerate and increase operation and productivity, especially on irradiation services as well as education and training. These activities include refurbishment (Masood et al., 2013), major modifications/upgrading: primary cooling system (Lanyau et al., 2010), instrumentation and control (Izhar and Mohd Idris, 2009), and safety assessment (Ramli et al., 2020) including human actions (Phongsakorn et al., 2016).

However, the effectiveness of RTP in dealing with protection and mitigation of fire and smoke has never been examined. The fire safety and protection assessment of RTP in 2014 (Ab Rahim et al., 2014) merely qualitatively identifying the integrity of the system from the perspective of management and equipment, firefighting procedures and firefighting response teams. No quantitative evaluation was performed such as the probabilistic safety assessment (PSA), which is widely known as an approach to estimate hazardous scenarios that may arise and to evaluate the seriousness of the accidents. Conversely, a study on probable causal of accidental fire ignition at the basement of RTP was conducted in 2020 (Hashim et al., 2020). Yet, this fire probabilistic safety assessment (FPSA) preliminary and pilot study to investigate the possibility of fire ignition as well as fire and smoke pace propagation have not been integrated with failure of any systems or components.

This paper is particularly observing the control room of RTP as another important location that assures main control defense of emergency incidents, consisting of various information, monitoring, and operation of the reactor itself. The control room of the RTP is a reasonable location for fire incidents, specifically electrical component failures Seeing this as a probe to enhance and optimize the current safety system of RTP, fire PSA has been conducted to oversee any potential cause of fire.

The main objective of this study is to quantify the probability of fire occurrence and to assess the adequacy of the current fire protection system at the control room. The scope of this study covers Level-I internal fire PSA, focusing only on the reactor control room. The quantification results of the core damage frequency are compared between with and without fire-induced events.

2 Methods

Methodology adapted in this study replicates as per work done in RTP basement, which are (1) Data collection and system identification and (2) Data analysis.

3 Results and Discussion

3.1 Identification of Initiating Event and Failure Mode and Effect Analysis (FMEA)

Table 1 presents the lists of components with their failure mode and the consequences or effects to RTP if it fails. Based on the initial FMEA screening analysis, the 'Yes' value in Table 1, indicates two initiating events, which are fails to start (FS) and fire spark (FiS). However, these results will be re-evaluated based on the severity of the components in fire consequences over time.

3.2 Development of Event and Fault Tree

The IAEA IRSRR recorded five (5) incidents on the internal fire which then were divided with the total exposure time of all research reactors in hour, resulted with a probability value of 8.0611E-08. This value is used as the IE of fire for this study.

Figure 1 depicted the altered IE for LOIC, with fire induced after the event operator successfully disconnected the instrumentation and control console back panel. LOICF showed four sequences of events with two end state of 1- FDRF and three end state of 3-CDG.

Table 1: Results of FMEA

Components	Failure Mode	Consequences or Effects	IE
Automatic Fire Detection: Smoke detector	FS	Operator missing compelling signal/ annunciator after the occurrence of fire	No
Manual Fire Detection: Detection by operator or reactor personnel	FS	Operator missing compelling signal/ annunciator after the occurrence of fire	No
Automatic fire suppression: pyrogen suppression device	FS	Operator missing compelling signal/ annunciator after the occurrence of fire	No
Manual fire suppression: intervention of personnel	FS	Operator missing compelling signal/ annunciator after the occurrence of fire	Yes
RPS A cabinet	FiS	Lead to an initiating event (IE)	Yes
RPS B cabinet	FiS	Lead to an initiating event (IE)	Yes
DAC C cabinet	FiS	Lead to an initiating event (IE)	Yes

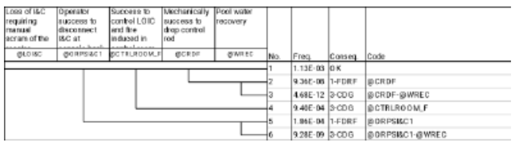

Figure 1: Event tree: Loss of instrumentation induced fire at sequence no. 2 (LOIC-F)

The fault tree analysis for Fire Protection System (FPS) is portrayed in Figure 2, with the most conservative failure rates for both fire detection and suppression in Table 1 are used, 4.0% and 20.0% respectively. For this study, a conservative approach by assuming only one component fails, resulting with failure of FPS, hence OR gate is used.

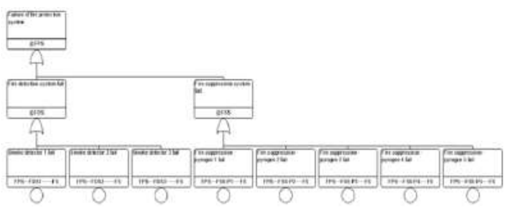

Figure 2: Fault tree: Fire Protection System (FPS)

From Table 2, the CDF value for LOIC and LOIC-F are 2.72E-08 and 9.09E-04 respectively.

Table 2: Core damage end state for both LOIC and LOIC-F

ID	LOIC	LOIC-F
1-FDRF	1.97E-04	1.97E-04
2-FDEA	1.01E-04	1.01E-04
3-CDG	2.72E-08	9.09E-04
4-RPWC	1.01E-04	1.01E-04
OK	8.99E-01	8.99E-01

4 Conclusions

It is concluded that, by inducing fire randomly as a sequence event in IE LOIC, the probability of core damage is 4 order magnitudes higher than the CDF from the original LOIC event tree. Therefore, the needs in making sure both fire detection and suppression works are mandatory. However, a further study by inducing fire in different sequence and other IE needs to be conducted to have an overview of internal fire impact to CDF at different IEs.

In assessing the adequacy of the fire protection system, FPS in the control room is adequate at present. However, as prevention is better than cure, or in this study, better than repair, therefore it is highly recommended that the RTP management should install several heat detectors in the control room to strengthen the existing fire protection system. Supplementary PSA quantification in the addition of heat detectors will be the next follow-up project.

References

A. N. Ab Rahim, A. S. Ligam, N. Ramli, M. F. Zakaria, N. S. Hamzah, P. Prak, M. S. Kassim, and Z Masood. 2014. Evaluation of fire safety and protection at PUSPATI TRIGA reactor (RTP). *Research and Development Seminar 2014*.

Z. Hashim, D. Kumar, M. F. Zakaria, M. H. Hussain, A. H. S. Mohd Sarif, and M. Maskin. 2020. Internal fire probabilistic safety assessment preliminary work at research reactor TRIGA PUSPATI. *IOP Conference Series: Materials Science and Engineering*, 785:012049.

A. H. Izhar and T. Mohd Idris. 2009. The development of a digital instrumentation and control system for PUSPATI TRIGA reactor console-requirement and experience. *Nuclear Malaysia Technical Convention 2009*.

T. Lanyau, M. F. Zakaria, Z. Hashim, and M. S. Abdul Farid, M. F.and Kassim. 2010. Replacement of PUSPATI TRIGA reactor primary cooling system and safety consideration. *Journal of Nuclear and Related Technologies*, 7(2):112–114.

Z. Masood, M. F. Zakaria, and I. A Hussin. 2013. Refurbishment and modernisation of PUSPATI TRIGA reactor: Lessons learnt. *15th Meeting of the International Group on Research Reactors (IGORR15)*.

P. T. Phongsakorn, S. Ahmad Hassan, M. Mazleha, Z. A. Nurul Husna, L. Tonny, and H. Zaredah. 2016. Study on operator actions during the occurrences of undesirable events in PUSPATI TRIGA reactor. *Research and Development Seminar 2016*.

N. Ramli, J. A. Karim, H. Md Razi, M. K. A. Mustafa, N. A. Masenwat, S. Sani, and M. H. Hussain. 2020. Ageing assessment of biological shielding integrity for PUSPATI TRIGA Reactor. *IOP Conference Series: Materials Science and Engineering*, 785:012051.

Individual Research Contribution Review, 2023, 1(1): 501–502

Designing and Installation of Internet of Things (IoT) System for Smart Mushroom House

Mohamad Suhaimi Yahaya
Engineering Division, Malaysian Nuclear Agency
43000 Kajang, Selangor
m.suhaimi@nm.gov.my

Abstract

Agrotechnology & Bioscience Division has received development expenditure (DE) allocation to build Smart Mushroom House in 2022. This smart mushroom house is important to study the potential of mushroom to be commercialized and as a reference centre among the mushroom entrepreneurs. One of the features in smart mushroom house that has been developed was the use of the Internet of Things (IOT) system in parallel with industrial revolution (IR) 4.0. This paper will describe the design process and advantages of IoT system for smart mushroom house. The IoT system was successfully installed and has managed to control the temperature and humidity level in smart mushroom house. As a result, the research on mushroom can be carried out effectively.

Keywords: Smart Mushroom House, Internet of Things (IoT), temperature, humidity

1 Introduction

Agrotechnology & Biosciences Division (BAB) has received development expenditure (DE) allocation to build smart mushroom house in 2022. This smart mushroom house is important to study the potential of mushroom to be commercialized and as a reference centre among the mushroom entrepreneurs. One of the features in smart mushroom house that has been developed was the use of the Internet of Things (IoT) system in parallel with industrial revolution (IR) 4.0. In this facility, the mushrooms that will be studied include the main commercial mushrooms in Malaysia such as Volvariella (Rice Straw), Pleurotus (Grey and White Oyster) and Auricularia (Black Jelly) mushrooms. The important parameters to be controlled in mushroom house are temperature, humidity level, light intensity and carbon dioxide level. This paper will describe the design process and advantages of IoT system for smart mushroom house in order to control temperature and humidity level.

2 Methods

The process flow chart of the study is described in Figure 2. Firstly, the user needs to prepare need statement and their specific requirement. Then, several discussions between user and Engineering Division (BKJ) have been conducted before coming out with a design specification. The next process is procurement process to appoint qualified contractor. After that, the contractor will propose detailed design that meet out requirement before being agreed to proceed with programming work and installation on site.

Figure 1: Mushroom house located near to Block 46 Kompleks Dengkil.

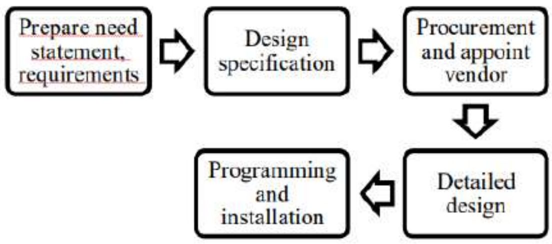

Figure 2: Flowchart of the methodology

3 Result and Discussion

There are two parameters that need to be controlled which are temperature and humidity level. The misting system, circulation fan and ventilation fan will be set to be run in order to ensure the temperature in mushroom house will be between 25 to 30 degC and humidity level is between 65 to 80% RH.

Initially, the IoT control system will utilize external cloud server that allow the user to monitor the mushroom house anywhere outside premise of Nuklear Malaysia. However, Nuklear Malaysia premise is a restricted area, so the use of external servers is not allowed unless approval given by

Malaysia Office of the Chief Government Security Officer (CGSO) and Malaysian Administrative Modernisation and Management Planning Unit (MAMPU) for security reasons based on Kawasan Larangan Dan Tempat Larangan 1959 act. In addition, there is no internet access available at mushroom house and additional budget is needed to provide internet facilities. In order to resolve the issue, IoT system only use local server which is namely as raspberry pi and data been transmitted using modem as shown in Figure 3 below. Unfortunately, data access is only limited to a radius of 2-5m from the mushroom house. For further improvement, users will try to get a budget in the future to provide internet facilities in the mushroom house to improve data accessibility at least accessible in the entire Nuklear Malaysia premises.

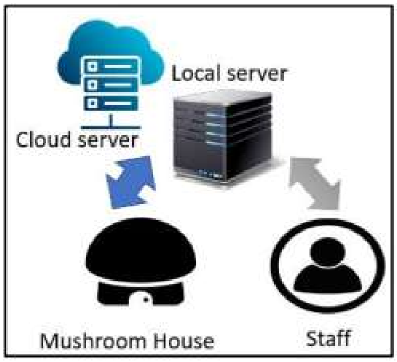

Figure 3: Architecture IoT system.

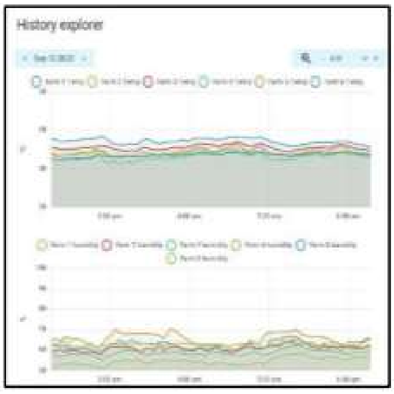

Figure 4: Temperature and humidity data.

The advantages of IoT system for smart mushroom house that has been developed are:

i. Minimize human effort. The staff can monitor the temperature and humidity level via smart phone or computer without need physical monitoring as shown in Figure 4 above.

ii. Real-time monitoring and control. The data can be collected and analysed for further research.

iii. Money and time saving. The owner can save money by not having to hire contract staff to monitor the mushroom house regularly and also time saving.

iv. More efficient and increase productivity of mushroom yield.

However, IoT systems are highly dependent on internet coverage and are somehow exposed to network attacks and data leaks if not properly designed and protected.

4 Conclusion

The IoT system was successfully installed and has managed to control the temperature and humidity level in smart mushroom house. As a result, the research on mushroom can be carried out effectively and produce quality mushroom to be commercialized.

References

Suresh M, Srinivasan M, Gowri Shankar S, Karthikeyan D, Nakhul V, Naveen Kumar A, Sundar S, and Maniraj P. 2021. Monitoring and automatic control ofvarious parameters for mushroom farming. *IOP Conference Series: Materials Science and Engineering*, 1055(1):012011. https://doi.org/10.1088/1757–899x/1055/1/012011.

Azhar Mohamad and Abdul Rahim Harun. 2021. Need statement kerja–kerja menaiktaraf pembinaan Rumah Cendawan Pintar Kajian Agromakanan Agensi Nuklear Malaysia.

Individual Research Contribution Review, 2023, 1(1): 503–504

Determining the Cause of the Growth of Fungus on the Walls in Block 34 and the Measures Taken to Prevent It

Mohamad Suhaimi Yahaya
Engineering Division, Malaysian Nuclear Agency
43000 Kajang, Selangor
m.suhaimi@nm.gov.my

Abstract

Fungus has grown on the walls in block 34 that can cause health problem among the Malaysian Nuclear Agency staff. Fungus growth on the walls is caused by high humidity in addition with a poor ventilation system in the building. A detailed study found that high humidity because of low temperature in rooms, especially rooms that use 24 hours air conditioning. As result, the fungus grows on the wall in adjacent layer. This paper will describe the causes of fungus and also the actions taken to control the growth of fungus in block 34. In order to avoid health problems caused by fungus, the Engineering Division (BKJ) has cleaned the fungus on the wall and repainted it using anti-fungal paint. Furthermore, the ventilation fans have been installed to improve the ventilation system in the building. Meanwhile, the settings on the centralized and split air conditioning systems have been calibrated so that the temperature inside the building reaches a temperature of 22 to 24 degC. Therefore, the efforts taken have successfully removed the fungus on the wall and also prevented the growth of the fungus from happening again.

Keywords: fungus, humidity, temperature, ventilation

1 Introduction

Engineering Division (BKJ) has received report from staff in Block 34 since 2021 about the fungus grown badly on the walls in Block 34 as shown in Figure 1 below. The Block 34 consists of number of offices and laboratories that use centralised air conditioning system packaged type. Some laboratories equipped with scientific equipment that need 24 hours air conditioning. Those laboratories have been installed with air conditioning split unit (ACSU) to meet the requirement. The fungus on wall or known as mold can cause health problem among the Malaysian Nuclear Agency staff. The staff in Block 34 may experience symptoms such as stuffy nose, sneeze, cough, red or itchy eyes or skin. Some people such as those who have asthma may experience more severe reactions include fever and shortness of breath. This paper will describe the causes of fungus growth on Block 34 wall and also the actions taken to control it.

Figure 1: Wall with fungus existence in Block 34.

2 Methods

The process flow chart of the study is described in Figure 2 below. Firstly, the problem has been reported from staff in Block 34. Then, the detail study to identify root cause of fungus growth and identify the solution. The next process is to secure the budget and getting approval from Finance Department. After that, the implementation of improvement works that have been proposed at early stage in order to resolve the health issue due to fungus existence on wall Block 34.

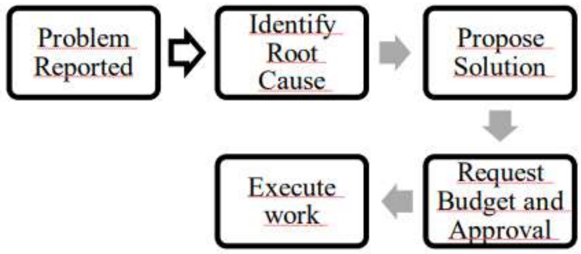

Figure 2: Flowchart of the methodology

3 Result and Discussion

The temperature and humidity level in Block 34 have been measured by using anemometer. The results show that some laboratories having temperature between 20 to 22 degC, meanwhile humidity level were between 60 to 65% RH. A detailed study found that the fungus growth badly on the wall in adjacent layer near to room that use 24 hours air conditioning which has lower temperature as shown in Figure 3 below. In theory, more moisture in air can result high humidity level especially the room that having low temperature with poor ventilation system.

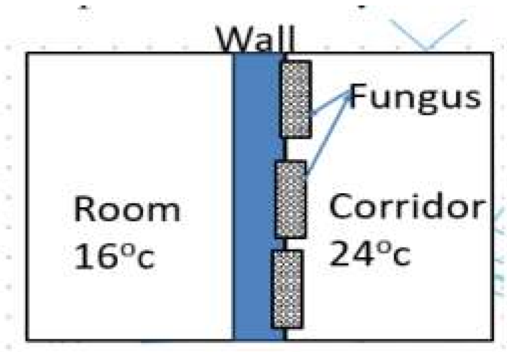

Figure 3: Fungus growth badly near to adjacent wall at 24 hours air conditioned room and low temperature.

In order to avoid health problems caused by fungus, the Engineering Division (BKJ) has appointed the contractor to cleaned up the fungus on the wall and repainted it using anti-fungus paint. In addition, 3 numbers of ventilation fans with size of 16inch and capacity if 1212 cfm each have been installed at suitable location to improve the ventilation system in the building. These ventilation fans will operate 2 times per day for 1 hour at different time to ensure the circulation of air inside the building. The ability of exhaust fans installed have been verified through calculation as shown in Table 1. From the calculation, exhaust fan no. 1 and no. 2 are able to remove air 6.14 rate per hour meanwhile exhaust fan no. 3 is able to remove air at rate of 4.14 per hour.

Table 1: Exhaust fan capacity calculation.

Exhaust Fan	**Fan Capacity, Q**	**Estimated Corridor Volume, V**	**ACH, NN=Qx60/V**	**Remark**
EX 1 and EX2	1212 cfm	11,850 ft^3	6.14/hr	Remove air from north and south corridor
EX3	1212 cfm	17,550 ft^3	4.14/hr	Remove air from main hall/lobby and its corridor

Meanwhile, the settings on the centralised and split air conditioning systems have been changed so that the temperature inside the building reaches a temperature of 23 to 24 degC.

4 Conclusion

Fungus growth on the walls is caused by high humidity in addition with a poor ventilation system in the building. The actions taken have successfully removed the fungus on the wall and also prevented the growth of the fungus from happening again.

Figure 4: Layout of Block 34 with installation of 3 number of exhaust fans at suitable locations.

References

Julie Andrianny Murshidi. 2023. Need statement cadangan kerja-kerja menambahbaik 3 makmal, dinding koridor, tangga dan sebagainya dan naiktaraf sistem ventilasi (masalah kulat) di Blok 34, serta kerja-kerja lain yang berkaitan di Agensi Nuklear Malaysia.

Abdul Rahman Norazumin and Mohamad Suhaimi Yahaya. 2017. Laporan teknikal dinding berkulat di bunker 3 19006 Agensi Nuklear Malaysia. (NUKLEAR-MALAYSIA/L/2017/94).

https://www.cdc.gov/mold/faqs.htm.

Mohamad Suhaimi Yahaya, Mohd Khafidz Shamsuddin, and AsruL Afendi Jaafar. 2022. Laporan teknikal mengenal pasti punca dan cadangan kaedah penyelesaian terhadap aduan dinding berkulat di Blok 34 Agensi Nuklear Malaysia. (NUKLEARMALAYSIA/L/2022/19).

Introduction of Fresh Air Intake in Centralised Air Conditioning System in Block 18 and 19 Agensi Nuklear Malaysia

Mohamad Suhaimi Yahaya
Engineering Division, Malaysian Nuclear Agency
43000 Kajang, Selangor
m.suhaimi@nm.gov.my

Abstract

In centralised air conditioning system, it will either use recirculation indoor air from the building or mixing with fresh air from ambient. During pandemic Covid-19, the Ministry of Health Malaysia had recommended to use fresh air especially in centralised air conditioning system in order to reduce the spread of covid-19 in air-conditioned space. However, by using fresh air intake, the air conditioning system need to re- setting so it will not overload the existing system. To have good ventilation inside the building, Engineering Division (BKJ) has decided to re-introduce fresh air intake in centralised air-conditioning System in Block 18 and 19 of Agensi Nuklear Malaysia. The air damper intake has been installed at AHU room's wall to supply the cooled air into the building. This paper will describe the important of fresh air intake in centralised air conditioning system in order to reduce the spread of covid-19. By introducing the fresh air intake to supply air, it is believed that the spread of the Covid-19 will be effectively controlled.

Keywords: centralised air conditioning system, fresh air, Covid-19, air damper

1 Introduction

In centralised air conditioning system, it will either use recirculation indoor air from the building or mixing with fresh air from ambient. In some cases, such as for radioactive laboratory and medical facilities, 100% fresh air are used for air conditioning and mechanical ventilation (ACMV) system. Air ducts are used to distribute cooled air throughout the building. Centralised air-conditioning also used to provide ventilation inside the building in order to maintain appropriate indoor air quality and eliminating contaminants like coronavirus. During pandemic of Covid-19 in 2020 until 2022, the centralised air conditioning potentially spread the virus throughout the building. Hence, Ministry of Health Malaysia had recommended to use fresh air to control the spread of covid-19. However, by using fresh air intake, the air conditioning system need to re-setting so it will not overload the existing system. Most of the building in Bangi Complex, Agensi Nuklear Malaysia use centralised air conditioning system with recirculating of air from the building. In order to have good ventilation inside the building, Engineering Division (BKJ) has decided to reintroduce fresh air intake in centralised air conditioning system in Block 18 and 19. The reason for only Block 18 and 19 selected to use fresh air intake is because there is an existing primary AHU that can be utilized to cool down the fresh air. Moreover, the initial design of the ACMV system in Block 18 and 19 were to use recirculating air mixed with fresh air for ventilating the radioactive laboratory before some of those laboratories have been converted to general laboratory and office. This paper will describe the important of fresh air intake in centralised air conditioning system in order to reduce the spread of Covid-19.

2 Methods

The process flow chart of the study is described in Figure 1 below. Process 1 is the definition of the problem and objectives of the study. Then process 2 is the detail study of the air conditioning and ventilation system and propose the design. The next process is installation and retrofitting work done by the appointed contractor. After that, the measurement needs to be taken in order to verify the design before concluding the study.

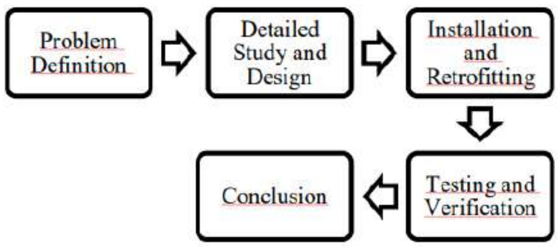

Figure 1: Flowchart of the methodology

3 Result and Discussion

The air damper intake has been installed at air handling unit (AHU) room's wall to supply the fresh air into the building. The location of air intake damper are located at large opening area and far away from any exhaust stack. In Malaysia, average daytime temperature of surrounding is about 32degC. Meanwhile range of 22 to 26degC temperature for working comfort inside the building. Hence, the air conditioning system needs to work out about 6degC the temperature different. In order to reduce the cooling load, the primary AHU is used to primary cool down the fresh air before mixing with return air from the building inside the AHU room that works as a mixing box as shown in Figure 2 and 3. Then those mixing air will pass through secondary AHU and been cooled down before supply to the entire building. The temperatures have been measured in Block 18 and 19 to ensure the usage of fresh air intake does not increase room temperature and does not reduce working comfort. These result can be seen in Table 1 below.

Table 1: Temperature measurement taken in Block 18 and 19.

Parameters	Block 18	Block 19
Ambient Temperature (°C)	30.4	29.0
Temperature Leaving Primary AHU (°C)	17.3	19.8
Temperature return from building (°C)	24.0	25.4
Temperature AHU Room @mixing box (°C)	22.8	21.7
Average Room Temperature (°C)	22.4	22.0

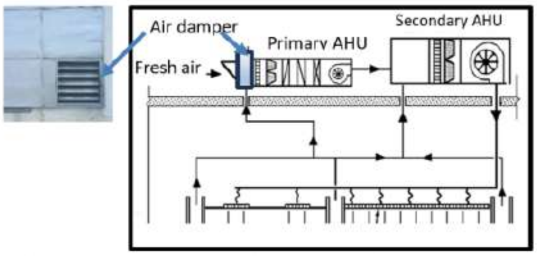

Figure 2: Arrangement of air damper, primary AHU and secondary AHU in AHU room

The used of fresh air in ACMV system can benefit us because more clean air from outside make us fresher and more energetic. Moreover, fresh air will dilute the indoor pollutants and reduce the spread of fume, odour, virus from inside the building. However, ACMV system need to be properly design to ensure air conditioning load and temperature inside the building do not increase and can maintain standard air indoor quality.

4 Conclusion

By introducing the fresh air intake to supply air in centralised air conditioning system in Block 18 and 19 Nuklear Malaysia, it is believed that the spread of the Covid-19 and other virus will be effectively controlled and did not affect working comfort.

Figure 3: Arrangement of air damper, primary AHU and secondary AHU in AHU Room Block 19.

References

Refrigerating American Society of Heating and Air-Conditioning Engineers. 2011. ASHRAE handbook: HVAC applications. Atlanta USA.

https://aristair.com/what-is-the-ideal-office temperature/.

https://www.lung.org/clean-air/at-home/ventilation-buildings breathe.

Malaysian Department Of Occupational Safety and Health. 2021. Guidance Note to Building Owners and Building Managements on Ventilation and Indoor Air Quality (IAQ) for Healthcare Facilities Setting During Covid-19 pandemic. First Edition.

Individual Research Contribution Review, 2023, 1(1): 507–508

Study on Chiller Replacement Works for Centralised Air Conditioning System in Malaysian Nuclear Agency

Mohamad Suhaimi Yahaya
Engineering Division, Malaysian Nuclear Agency
43000 Kajang, Selangor
m.suhaimi@nm.gov.my

Abstract

Chillers for centralised air conditioning system in Malaysian Nuclear Agency (MNA) have been operated for 20 to 35 years. There are 5 chillers where 3 chillers are located in Block 27, and 1 chiller located in Block 42 and 44 respectively. With good practice, operating and maintaining chiller have been going for such a long time than its expected life cycle. However, those chillers need to be replaced with new chiller due to outdated technology and inefficiency for energy consumption. This paper will describe the reason for chiller replacement and also the proposal works to obtain reduction in electricity consumption. As a conclusion, all of chillers in MNA need to be replaced in order to support R&D activities and for reduction of electricity consumption.

Keywords: centralised air conditioning, chiller, energy consumption, thermal energy storage (TES)

1 Introduction

Malaysian Nuclear Agency (MNA) is using district water cooling for centralised air conditioning system. The main components of the system is chiller where the average lifespan is 20 to 25 years depending on the method of use and maintenance. Chillers for centralised air conditioning system in Agensi Nuklear Malaysia have been operated for 20 to 35 years. There are 5 chillers where 3 chillers are located in Block 27, and 1 chiller located in Block 42 and 44 respectively. Chiller CH1 and CH2 in Blok 27 known as brine chiller were different with other chiller because they can use in thermal energy storage (TES). TES district cooling system in MNA uses chiller combine with ice to cater for air conditioning heat load during the daytime or peak cooling periods. During non peak cooling periods, when excess chiller plant capacity is available, storage is recharged by refreezing the ice nodules in STL tank. TES optimize the use of electricity outside of peak hours to reduce the cost of electricity use and increase the system's capacity to accommodate the current demand for air conditioning. With good practice, operating and maintaining chiller have been going for such a long time than its expected life cycle. However, those chillers need to be replaced with new chiller due to outdated technology and inefficiency for energy consumption. Based on the record, the chiller and its anciliary equipment in plant room in Block 27, Block 42 and Block 44 used about 25% to 30% of overall electricity consumption in MNA. Furthermore, chiller replacement activity is in line with Nuklear Malaysia Vision 2030 Strategic thrust 3 for effective and efficient technical support for R&D and service delivery. Thus, Engineering Division (BKJ) has respsonsibility to to enhance the capacity of centralised air conditioning and ventilation system for laboratory and office as part of strategy 12^{th} which is to strengthen the capacity of civil, electrical and mechanical infrastructure to support R&D activities. This paper will describe the reason for chiller replacement and also the proposal works to obtain reduction in electricity consumption.

2 Methods

The process flow chart of the study is described in Figure 1. Process 1 is the definition of the problem and objectives of the study. Then process 2 is the detail study of the latest of chiller and air conditioning system design through product research from internet and from product briefing from several manufacturers. The next process is to estimate the cost for replacement work. After that is to prepare the replacement activities proposal.

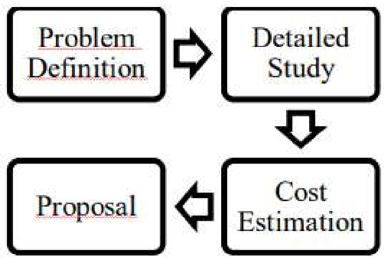

Figure 1: Flowchart of the methodology

3 Result and Discussion

The oldest chiller that is still operating is chiller in Block 42 and Block 44 in Complex Jalan Dengkil which are almost 35 years old. Meanwhile chiller used in Main Complex Bangi are 21 years old for CH1 and CH2 while CH3 is almost 27 years old. Those chillers have exceeded estimated average lifespan suggested by the supplier. Because of that, the chillers need to be replaced before they break down, later can disrupts R&D activities and the comfort of working at MNA. Some of the reasons are those chiller have outdated technology and inefficiency for energy consumption. Besides that, it is very costly to maintain the aging chillers because of its spare part that are expensive and sometime difficult to find its spare part. With more than 40 years, technology has changed progressively and manufacturers have produced more sophisticated chillers that have increased their reliability and efficiency. Meanwhile, the latest chiller technology aims to reduce energy consumption for benefit of the consumers.

For first phase, it is suggested that the chillers in blocks 42 and 44 be replaced because they have been operating for almost 35 years.

3.1 Technology on new chiller

The new chiller is designed to become more efficient by improving compressor design. For example, several of chiller suppliers design a compressor with back-to-back two stage which improves part load efficiency and use economizer to enables better efficiency under different conditions with accurate control. All of the main chiller manufacturers currently provide variable speed chillers, which is deliver better energy performance in most cases especially when operating under part load situations as compared to constant speed chillers. The improved design of tube in heat exchanger located in evaporator and condenser increase heat transfer rate and reduce water pressure drop and ultimately will reduce energy consumption. Besides that, the new chiller is designed for quiet operation by having magnetic bearings, direct drive and optimized flow channel. Furthermore, the latest technology on new chiller is designed for less operational and maintenance cost. For example, oil free magnetic chiller eliminates use of oil lubrication, thus reducing the risk of oil-related failures and reducing maintenance costs. The direct-driven design of compressor uses less parts as compared to outdated chiller, thus eliminates the gears and transmissions experience wear and eventual failure risk and finally improves the overall chiller reliability. Most of the latest chiller is designed to use either chlorine-free R134a or R410A as a refrigerant for environmental sustainability with zero ozone depletion potential as compared use of R22 refrigerant in 1980-1990's year chiller.

3.2 Upgrading work for chiller CH3

For Main Complex Bangi, it is recommended to replace chiller CH3 with a bigger cooling capacity of brine chiller that can be used in TES and an additional STL tank need to be installed in order to increase capacity of TES. So that, the storage is recharged by refreezing the ice nodules during off peak hour and become fully night charging operation. During daytime, only the cold energy stored will be discharged through the water mixed with glycol as heat transfer medium to the air conditioning centralised system. If only cooling demand does not meet, only one chiller will be operating while the other chiller can be rest before operating at non peak hour which is from 10.00pm until 8.00am. The estimated cost for this upgrading works is about RM3.2mil and operational cost saving in electricity bill about RM418,875.36 yearly. The return of investment (ROI) is about 7 years and 8 months.

3.3 Estimation Cost

The estimated cost is based on JKR's schedule rate in 2018 with increment of 30% by taking into account cost changes by suppliers and changes of currency. As overall, at least about RM5.2 million is needed for chillers replacement in MNA.

3.4 Timeline

Proposed timeline for replacement work in line with Nuklear Malaysia Vision 2030 as shown in Figure 2 below.

Chiller	Year						
	2024	2025	2026	2027	2028	2029	2030
B42							
B44							
CH3							
CH1& CH2							

Figure 2: Proposed timeline for chillers replacement.

4 Conclusion

Aging chillers in MNA will experience major or minor breakdown that need a lot of money to troubleshoot and repair. Because of that, it is recommended the chillers replacement need to well planned in order to support R&D activities with estimation cost about RM5.2 million. In addition, with a lot of technology changes in air conditioning chiller, all of chillers in MNA need to be replaced for reduction of electricity consumption and also to reduce operational and maintenance cost.

References

Carrier. 2022. AquaEdge 19MV centrifugal chiller, product catalogue CAT-AQUAEDGE-19MV_202205_01.

Cawangan Kejuruteraan Mekanikal JKR. 2018. Garis panduan anggaran harga sistem mekanikal dalam bangunan tahun 2018, JKR Malaysia.

TRANE. 2020. Trane optimus water-cooled chillers, product catalogue RLC-SL031B-EN.

Individual Research Contribution Review, 2023, 1(1): 509–510

Energy Response Performance and Dose Accuracy at 24 – 1250 keV: Comparison OSLD with TLD-100H and TLD-100

Ahmad Bazlie Bin Abdul Kadir
Radiation Health and Safety Division
Malaysian Nuclear Agency
43000 Kajang, Selangor
bazlie@nm.gov.my

Abstract

OSLD was evaluated in terms of energy response and accuracy of the measured dose in comparison with TLD-100H and TLD-100. The OSLD showed a better energy response performance for Hp(10) whereas for Hp(0.07), TLD-100H is superior than the others. The OSLD dose accuracy is comparable with the other two dosimeters since it fulfilled the requirement of the ICRP trumpet graph analysis.

Keywords: Energy response, Hp(10), Hp(0.07) OSL, TLD-100H, TLD-100

1 Introduction

The Secondary Standard Dosimetry Laboratory of Malaysia Nuclear Agency (SSDL Nuklear Malaysia) currently providing personal dosimetry service using OSLD (optically stimulated luminescence dosimeter) and two type thermoluminescence dosimeters called TLD-100H and TLD-100. In addition, OSLD has been reported been used in more than 80% of healthcare facilities in the United States (Landauer, 2008). The present study reports the results of Hp(10) and Hp(0.07) (Yukihara and McKeever, 2011; Bøtter-Jensen et al., 2003) of the OSL dosimeter, in comparison with the TLD-100H and TLD-100. The aspects that are being studies were the energy response and the dose accuracy.

2 Methods

2.1 OSLD, TLD-100H and TLD-100 Materials

OSL dosimeter also comes in two components, namely the casing and the holder. The front and the back views of the holders are shown respectively as the right and the left photographs of Figure 1(a). The casing (dimensions of 2.4×1.2×0.2 cm^3) is shown as the middle photograph of Figure 1(a) and in Figure 1(b). Figure 1(b) shows the slide coming out from the casing, where the OSLD discs (of material Al_2O_3:C, diameter 0.7 cm, thickness 0.02 cm (Shapiro, 2002) are placed. It can be seen that all together there are four discs, of which each chip has its own filters to provide different radiation attenuation. Only three discs are equipped with filters (of materials of plastic, copper and aluminum) whereas one disc is left empty without any filters (Kobayashi et al., 2012).

Figure 2 shows the Harshaw TLD-100H. The TLD-100H is in the form of circular shaped chip, of material LiF:Mg,Cu,P (Shapiro, 2002) and dimension 3.6 mm diameter and 0.25 mm thick. This chip is fixed in an aluminium card covered by PTFE wrapping. Each card consists of four chips which are labeled as elements 1, 2, 3 and 4. In this study, only the elements 2 and 3 were analyzed as it acts as the Hp(10) and Hp(0.07) detectors respectively. The Hp(10) detector is located beneath a thick dome made by 107 mg/cm^2 ABS + 893 mg/cm^2 PTFE whereas the Hp(0.07) detector is beneath a sheet of 17 mg/cm^2 Mylar (Priharti et al., 2012).

(a) (b)

Figure 1: InLight OSLD: (a) The OSLD casing and the holders, (b) The four OSLD chips coming out from the casing.

Figure 2: Harshaw TLD-100H (from right to left): TLD holder, TLD card, TLD card enclosed in a TLD holder. The only difference between TLD-100H and TLD-100 is the shape of their chip.

The third dosimeter that is being studied is the TLD-100. Not much different can be found in this TLD-100 if compared with TLD-100H, except that the materials and the shape of the discs. LiF:Mg,Ti (Priharti et al., 2012) is the materials for TLD-100 and the chip is in the square form, with side length of 3.2 × 3.2 mm^2 and 0.89 mm thick.

2.2 OSLD, TLD-100H and TLD-100 Irradiation Process

In this study, the delivered doses Hp(10)$_{del}$ and Hp(0.07)$_{del}$ were fixed at 1 mSv. To deliver experimentally this 1 mSv dose to the OSLD, TLD-100H and TLD-100 cards, these cards were irradiated simultaneously to photon energies from the narrow spectrum series (NSS) X-ray machine (ISO 4037-1 quality) and gamma radiation machine (OB85). Eleven photon energies of 24, 32, 47, 65, 84, 102, 121, 171, 218, 662 and 1250 keV were utilized. The experimental set-up has been described elsewhere (Priharti et al., 2012).

The steps to get this 1 mSv dose for Hp(10)$_{del}$ for each energy are as follows: The air kerma rate $\acute{K}_{air}$ (mGy/min) was first determined at 2 m source to detector distance, SSD,

$$\acute{K}_{air}(mGy/min) = R_i \times N_k \times k_{TP} \tag{1}$$

$$Hp(10)(mSv/min) = \acute{K}_{air} \times Hp(10)_{cc} \tag{2}$$

$$t(min) = 1mSv/Hp(10)(mSv/min) \tag{3}$$

OSLD, TLD-100H and TLD-100 Readout Process

Figure 3: (a) OSLD reader, (b) TLD reader

Figure 3(a) and Figure 3(b) respectively shows the Landauer Microstar reader for the OSL dosimeters, and the Harshaw 4500 TLD reader for the TLD-100H and TLD-100. The two readers will yield the measured doses of Hp(10)$_{meas}$ and Hp(0.07)$_{meas}$ of the three dosimeters. The OSLD reader uses optical stimulation whereas TLD reader uses thermal stimulation.

Energy Response comparison

$$R(10)_{std} = \frac{Hp(10)_{meas}}{Hp(10)_{del}} \tag{4}$$

This R(10)$_{std}$ value when normalized to energy of 662 keV (Cs-137) we get R(10)$_{rel}$:

$$R(10)_{rel} = \frac{(Hp(10)_{meas}/Hp(10)_{del})E}{(Hp(10)_{meas}/Hp(10)_{del})Cs} \tag{5}$$

3 Discussion

Figure 4(a) shows the three OSLD, TLD-100H and TLD-100 curves of R(10)rel versus photon energy. Each curve contains eleven points. For (0.07)rel on the other hand, the three curves of OSLD, TLD-100H and TLD-100 are shown in Figure 4(b). These two figures can be used to compare the energy response qualitatively. If the condition of R(10)rel =1 and R(0.07)rel =1 are taken as the ideal case, results showed that (a) for R(10)rel: OSLD is the closest to the ideal case, followed by TLD-100H, then TLD-100, and (b) for R(0.07)rel: TLD-100H is the closest to the ideal case, followed by the OSLD then TLD-100.

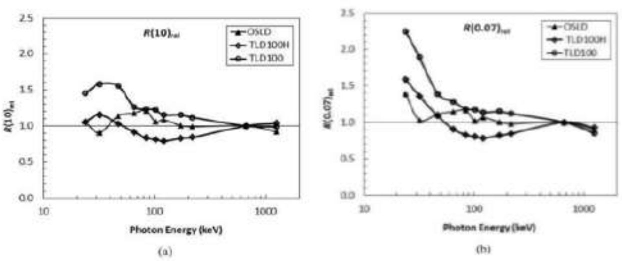

Figure 4: Comparison of (a) Hp(10)rel, (b) Hp(0.07)rel for OSLD, TLD-100H and TLD-100

4 Conclusion

It is concluded that the OSL dosimeter yielded a better energy response performance for the Hp(10) in comparison with the existing TLD-100H and TLD-100 dosimeter. For the Hp(0.07) the energy response of the OSL dosimeter is less superior than the TLD-100H. The accuracy of the measured doses for OSL dosimeter is within the acceptable limit

References

L. Bøtter-Jensen, S.W.S. McKeever, and A.G. Wintler. 2003. Optically stimulated luminescence dosimetry. *Elsevier Science*, Amsterdam.

I. Kobayashi, T. Okazaki, K. Yajima, and H. Yasuda. 2012. *Prog. in Nuclear Sci. & Tech*, 3:79 –81.

Landauer. 2008. InLight System Reader. L. Inc, Editor. Glenwood.

W. Priharti, S.B. Samat, and A.B.A. Kadir. 2012. The study of Hp(10) and Hp(0.07) responses for harshaw TLD-100H at photon energy of 24-1250 keV. *3rd Jogja International Conference on Physics-2012. Yogyakarta, Indonesia*, pages 143–146.

J Shapiro. 2002. Radiation protection: A guide for scientists, regulators, and physicians. Cambridge: Harvard University Press.

E.G. Yukihara and S.W.S. McKeever. 2011. Optically stimulated Luminescence: Fundamentals and applications. New York: John Wiley & Sons.

Individual Research Contribution Review, 2023, 1(1): 511–512

Enhancing Workplace Safety Through Structured Safety Documentation: A Vital Imperative

Andy Kong Shin Shyen
Radiation Health and Safety Division
Malaysian Nuclear Agency
43000 Kajang, Selangor
andy_kong@nm.gov.my

Abstract

This paper explores the critical role of safety documents in mitigating workplace hazards and fostering a culture of safety within the organization. The study emphasizes the systematic development, implementation, and continuous improvement of safety protocols through the utilization of comprehensive safety management documents.

Keywords: Safety Documentation, Workplace Safety, Safety Management

1 Introduction

Workplace safety remains an imperative priority across industries worldwide. Effective safety measures not only protect employees but also contribute significantly to organizational productivity and success. In today's dynamic and multifaceted workplaces, the absence of structured safety documentation poses substantial risks. The lack of a comprehensive and standardized framework for documenting safety procedures not only heightens the potential for accidents but also engenders inefficiencies in responding to and preventing hazards. Recognizing the pivotal role of documentation in shaping safety cultures, this paper delves into the imperative of structured safety documentation systems and their profound impact on mitigating risks, fostering a safety-conscious ethos, and ultimately fortifying the foundation upon which workplaces thrive.

2 Methods

2.1 Literature Review

To comprehend the existing landscape of workplace safety protocols and the significance of safety documents, a comprehensive literature review was conducted. This involved an extensive search of academic databases, governmental guidelines, and relevant publications. The review aimed to gather insights into established safety measures, regulatory frameworks, and best practices for document revision and implementation in workplace safety.

2.2 Analysis of Current Safety Documents

A thorough analysis of the existing safety documents within the organization under study will be carry out. This analysis encompasses safety manuals, procedures and work instructions. The goal is to identify areas for improvement, inconsistencies, outdated information, and potential gaps in the current safety documentation.

2.3 Revision of Safety Documents

Based on the findings from the literature review, and document analysis, a multidisciplinary team shall be collaborated to revise and update the safety documents.

2.4 Implementation Strategy

A strategic plan for implementing the revised safety documents will be developed. This plan includes conducting training sessions and workshops to familiarize employees with the updated safety and documents.

3 Data/Results

A literature review examining established safety measures, regulatory frameworks, and best practices for document revision and implementation in workplace safety reveals a comprehensive array of strategies. It encompasses a diverse range of safety protocols, including but not limited to OSHA guidelines, ISO standards, and industry-specific regulations. The review underscores the significance of regularly updating safety documents to align with evolving regulations and technological advancements. It highlights the pivotal role of clear communication, employee training, and stakeholder engagement in successful implementation. Additionally, it emphasizes the necessity of a systematic approach, robust documentation systems, and periodic audits to ensure compliance and efficacy. The synthesis of these insights provides a multifaceted understanding of the nuanced landscape of workplace safety protocols, serving as a foundational resource for organizations striving to establish and maintain a culture of safety.

On the other hand, the analysis of current safety documents is underway, and the revision of these documents is still in progress; however, at this point, there is no available data or results to present.

4 Discussion/Conclusions

The conclusive findings for this research are pending, as the comprehensive data collection and analysis required for a robust conclusion are still underway.

References

A U Abidin, E M Nurmaya, W Hariyono, and A H Sutomo. 2021. Implementation of occupational safety and health management system (OSHMS) on work-related accident rate in the manufacturing industry, Indonesia. *IOP*

Conference Series: Earth and Environmental Science, 933 012037.

S.L.C. Da Silva and Amaral F.G. 2019. Critical factors of success and barriers to the impl̀ementation of occupational health and safety management systems: A systematic review of literature. *Saf. Sci.*, 117:123 – 132.

Antti Leino. 2002. Intranet-based safety documentation in management of major hazards and occupational health and safety. *International Journal of Occupational Safety and Ergonomics*, pages 331–338, DOI: 10.1080/10803548.2002.11076533.

Helen Lingard. 2013. Occupational health and safety in the construction industry. *Construction Management and Economics*, 31(6):505–514, DOI:10.1080/01446193.2013.816435.

P. Marhavilas, D Koulouriotis, L Nikolaou, and S. Tsotoulidou. 2018. International occupational health and safety management-systems standards as a frame for the sustainability: Mapping the territory. *Sustainability*, 10(3663).

Individual Research Contribution Review, 2023, 1(1): 513–514

Standardization and Maintaining the Standard of Medical Physics Calibration Laboratory

Asmaliza Hashim
Radiation Health and Safety Division
Malaysian Nuclear Agency
43000 Kajang, Selangor
asmaliza@nm.gov.my

Abstract

Medical Physics Calibration Laboratory (MPCL) is a calibration laboratory that provide calibration services for dosimetric detectors and instruments used in diagnostic radiology. Dosimetric detectors and instruments is used to measure the amount of ionising radiation delivered when a technique that relies on ionising radiation for diagnosis of patients is used. Therefore, it is important to ensure that the measurements performed are accurate and traceable to the international system of Units (SI). This paper will explain the standardization and maintenance of standard of MPCL.

Keywords: Calibration, standardization, maintenance

1 Introduction

MPCL was set-up to improve the accuracy in radiation dosimetry in diagnostic radiology. Yearly MPCL received around 300 dosimetric detectors and instruments for calibration. The diagnostic beam qualities of RQR, RQA and RQT was established and followed the IEC 61267 and TRS 457 protocol. This beam qualities also maintained yearly basis. Beam qualities are defined as the added filtration needed to produce the half value layer (HVL) of the beam for species X-ray tube kilovoltage (kV). RQR beam qualities refer to beam on the patient for general radiography, fluoroscopy and dental application. Whereas RQA refer to beam behind the patient. Meanwhile RQT refer to unattenuated beam used in Computed Tomography. The other activities that conducted for maintaining the MPCL was measurement of beam profile and homogeneity. For the quality management system, MPCL also accredited by MS ISO/IEC 17025:2017 with SAMM No 275 under Radiation Metrology Group.

2 Methods

MPCL consists of one bunker and two laboratories as well as three units of X-ray machine. The X-ray machine was Constant Potential Philips Industrial X-Ray Model MG165 (capability kV up to 160 kV), Toshiba Diagnostic Radiography X-Ray System Model KXO-50S (capability kV up to 150 kV) and Bennett Mammographic Machine Model DMF-150 (capability kV up to 35 kV). The reference standard equipment was electrometer PTW UNIDOS Model T10005 and T10002, ion chamber PTW Model TW34060, TN233612, TW4060 and TW30009 and Radcal Dynalyzer IIIU - High Voltage Divider Model M-96311 and Radcal Accu-Dyn+ Digitizer Module Model AGDN+.

The beam qualities in term of HVL were measured using PTW ion chamber with PTW electrometer. Aluminium and copper filter with 99.9% purity was used as additional filter for RQR, RQA and RQT. Whereas aluminium was used as filter for HVL.

The set-up of HVL measurement of beam qualities was shown in Figure 1.

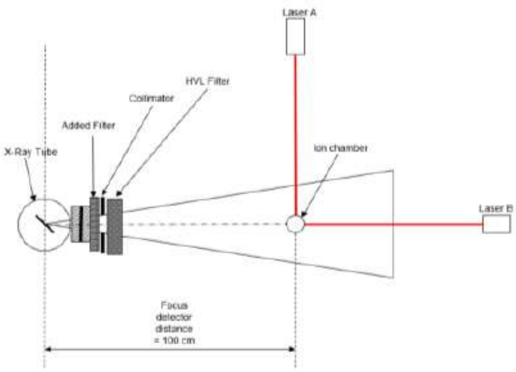

Figure 1: Set-up of HVL measurement of beam qualities

Measurement of beam profile and homogeneity was performed to determine the field size at one meter distance of focal spot to chamber for the various sizes of collimator. The radiographic image was used to determine the field size. To get the accurate field size, the measurement was performed using the ion chamber. The chamber was set-up from the centre of focal spot point and moved left, right, up and down from the centre point of chamber position.

The calibrations are performed by the substitution method where the air kerma of reference standard chamber of MPCL was measured. The air kerma of the dosimeter under calibration was measured. The result of calibration certificate was reported.

3 Results

Table 1, 2 and 3 shown the diagnostic beam qualities for RQR, RQA and RQT that established and used for calibration.

The results of the beam qualities of RQR, RQA and RQT indicate that the MPCL complied the standard beam qualities

Table 1: Beam qualities for RQR

Beam Qualities	kV	1st. HVL	Total Filter RQR (mm Al)
RQR2	40	1.42	2.6
RQR4	60	2.20	2.7
RQR5	70	2.52	2.8
RQR8	100	4.01	3.6
RQR10	150	6.62	4.7

Table 2: Beam qualities for RQA

Beam Qualities	kV	1st. HVL	Total Filter RQA (mm Al)
RQA2	40	2.25	6.7
RQA4	60	5.50	18.8
RQA5	70	6.60	20.9
RQA8	100	10.00	31.7
RQA10	150	13.10	39.8

Table 3: Beam qualities for RQT

Beam Qualities	kV	1st. HVL	Total Filter RQT (mm Al + mm Cu)
RQT8	100	6.91	3.6 mm Al + 0.2 mm Cu
RQT9	120	8.12	4.0 mm Al + 0.2 mm Cu
RQT10	150	10.33	4.7 mm Al + 0.3 mm Cu

at par to international protocol.

Figure 2 shown the results of beam profile for 4 cm collimator. It represents field size of one meter when using 4 cm collimator which is 20 cm diameter.

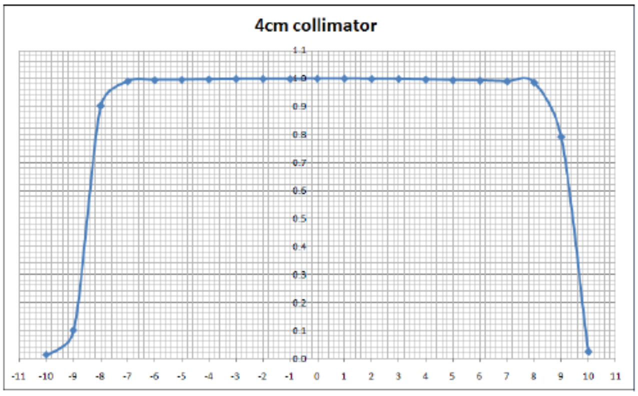

Figure 2: Beam profile for 4 cm collimator.

4 Discussion

The diagnostic beam qualities RQR, RQA and RQT was very important in calibration and need to verified yearly. Hence the experiment was conducting every year to make sure that the result of HVL for beam qualities was between 3%. The beam profiles and homogeneity also conduct yearly basis to make sure the accurate setting during calibration. The check source measurement for the reference and working standard chamber conducted every month to make sure the accuracy of the chambers.

MPCL also participate in IAEA bilateral intercomparison programme for diagnostic radiology level air kerma measurement standards in X-ray radiation qualities. This intercomparison to maintain confidence in the measurement capability of the laboratory.

To maintain the laboratory accreditation for MS ISO/IEC 17025:2017, internal audit was conducted every year and external audit was conducted once in every 18 months.

5 Conclusion

The activities of standardization and maintenance of laboratory is very crucial for calibration services that offer by the MPCL. This is to ensure that the calibration result was accurate and reliable to the hospital and clinics. Hence gave the accurate dos to patients.

References

IEC 61267. 2005. Medical Diagnostic X-Ray Equipment – Radiation conditions for use in the determination of characteristics. pages 1 –14, 17 – 18.

IAEA. 2007. Technical Reports Series (TRS) : Dosimetry in diagnostic radiology: An international code of practice. No 457:7 – 14, 41 – 52, 55 – 75.

SSDL Newsletter. Feb 2021. 73, ISSN 1001 – 2669.

Individual Research Contribution Review, 2023, 1(1): 515–516

Preparedness and Response to Radiological Emergencies at Malaysia Nuclear Agency

Azimawati binti Ahmad
Radiation Health and Safety Division
Malaysian Nuclear Agency
43000 Kajang, Selangor
azima@nm.gov.my

Abstract

Radiological emergencies, cause by various reasons, will be faced by the agency in the future. Therefore, the agency must have an arrangement to response to these emergencies. Planning and preparation in advance for radiological emergencies can help reduce or minimise the potential threat to workers, public and environment when the radiological emergencies occur. At Nuclear Malaysia, the Sub-Committee of Emergency (JKK) under the Committee Environmental Safety and Health (JKSHE) is responsible for managing and implementing emergency management and response to any potential radiological and nuclear emergency.

Keywords: emergency management, preparedness, response

1 Introduction

At Nuclear Malaysia, there are 12 main facilities, and more than 700 radioactive sources are used for research, instrument calibration, sterilization, medicine and other activities. In these past few years, there are several numbers of accident involving using of radioactive material happened at Nuclear Malaysia, and several response and counter measure have been taken to solved the accidents.

At Nuclear Malaysia, the the Sub-Committee of Emergency (JKK) under the Committee Environmental Safety and Health (JKSHE) is responsible for managing and implementing emergency management and response. In order to comply license requirements (LPTA/A/724, LPTA/A/1026 and LPTA/A/3233) for radiological emergency and preparedness, JKK in process and continuous to strengthening the emergency preparedness and response at Nuclear Malaysia.

This paper will discuss about description of the measure to be taken and methods needed in radiological emergencies. Identify the targets for the development of preparedness and response to and recovery from radiological emergencies.

2 Methods

Nuclear Malaysia already has an established document for Emergency Preparedness and Response since 2005. This document consists a proper guideline for Nuclear Malaysia to respond swiftly and in coordinated manner during an emergency through the activation of a set of emergency plans so that the situation can be brought under control and with minimisation of adverse consequence to the employees, properties and environment.

Base on the document and current situation, JKK have re-identified the potential hazard and events that will arise the radiological emergency and reviewing the specific emergency response base on the potential events. A continuous drill and exercise consist table top, functional drill, evacuation drill, hand on training was done continuously to test the effectiveness of the emergency plan. The result of the emergency and practice drill are recorded for the purpose of reviewing and recommendation for improvement to existing procedures.

A new emergency response structure organization was review and establish for more clear understanding response between all squad and technical laboratories.

3 Results and Discussion

In Nuclear Malaysia planning, preparation and response to radiological emergencies involved many parties. From the security department, radiological responder, engineering section, administrative department, technical laboratories and etc. The new emergency response structure organization was review and this organization is more structured for the response to each type of accident and the resources that will be needed.

If the event of radiological emergency involved the emergency level 3, and consider a disaster, in the emergency preparedness document is stated the involvement from the external response authority is needed like National Security Council, Department of Atomic Energy, Fire and Rescue Department, Ministry of Health, Ministry of Defence and other.

Within these five years, there are a few incident cases reported and few drill exercises has been done. The number of cases and report to JKK and number of drills perform shows in Table 1 and Table 2 respectively.

From the drill exercise and incident reported, we identified some the following issues in management of radiological emergencies is:

i) Established emergency response organization with a command structure that is clearly defined and integrated.

ii) Clear information and communication within respond squad.

iii) Clear information and communication within area supervisor and staff.

Table 1: Number of accidents reported at Nuclear Malaysia

Year	Number of accidents
2018	5
2019	3
2020	3
2021	1
2022	2

Table 2: Number of drill exercised at Nuclear Malaysia

Year	Number of functional drill	Number of evacuation drill
2018	1	39
2019	2	39
2020	3	10
2021	1	19
2022	2	5

iv) Use of the compatible methodologies to response for the radiological emergencies.

v) Appropriated training of the related personnel involved.

vi) How to deal with contaminated goods and other items.

vii) Safety equipment and facilities is always at risk for malfunction during the emergency.

viii) Documented logs of all actions, order, and track and update action throughout the emergency.

ix) Financial allocation.

4 Conclusion

An effective emergency preparedness and response program is based on planning basis like an analysis of the risk and hazards involve, a comprehensive description of how a response will be executed with accompanying support equipment. An excellent process to ensure that people, equipment and infrastructure will be ready to execute a response according to the emergency response plan and procedures and excellent management program to assure the effectiveness of emergency preparedness and response at Malaysian Nuclear Agency.

References

Jabatan Tenaga Atom. 2023. Panduan Penyediaan dan Pengujian Pelan Kecemasan Radiologi Jabatan Tenaga Atom. LEM/TEK/66 Sem.3.

IAEA. 2002. IAEA Safety standards series, GS- R-2, Preparedness and response for a nuclear or radiological emergency. Vienna, Austria.

IAEA. 2014. Safety standards: Radiation protection and safety of radiation sources: International basic safety standards. IAEA Safety Standards Series No. GSR Part 3, IAEA, Vienna.

IAEA. 2015. Safety standards: Preparedness and response for a nuclear or radiological emergency. IAEA Safety Standards General Safety Requirement GSR Part 7, IAEA, Vienna.

IAEA. 2018. Safety standards: Occupational radiation protection. IAEA Safety Standards Series No. GSG-7, IAEA, Vienna.

IAEA. August 2000. Safety standards: IAEA-TECDOC-1162, Generic procedures for assessment and response during a radiological emergency. Vienna, Austria.

IAEA. June 1999. Safety standards: IAEA-TECDOC-1092 Generic procedures for monitoring in a nuclear or radiological emergency. Vienna, Austria.

SHE/WP/06 Emergency Preparedness and Response.

Individual Research Contribution Review, 2023, 1(1): 517–518

Utilizing Clay-Based Composites for Effective Shielding in Diagnostic Radiology Environments

Azuhar bin Ripin
Radiation Health and Safety Division
Malaysian Nuclear Agency
43000 Kajang, Selangor
azuhar@nm.gov.my

Abstract

This study explores the application of clay-based composites as a viable and efficient shielding material in diagnostic radiology settings. With the increasing prevalence of medical imaging procedures, ensuring the safety of both patients and healthcare professionals through effective radiation shielding is imperative. Traditional shielding materials present challenges in terms of cost, weight, and environmental impact. The research investigates clay-based composites due to their abundant and sustainable nature, coupled with their potential for tailored radiation attenuation properties.

1 Method

The composites were meticulously designed and synthesized, incorporating clay matrices with additives to optimize their shielding efficiency. Rigorous testing, utilizing X-ray sources representative of diagnostic radiology equipment, was conducted to evaluate the shielding performance of these composites. Measurements of lead equivalence thickness, non-uniformity test and a dose reduction were analyzed to assess the overall effectiveness of the developed clay-based shielding materials.

The fabrication process of clay-based radiation shielding materials is shown in Figure 1.

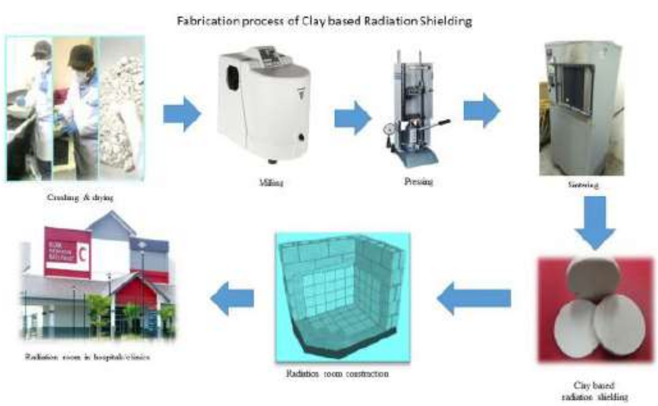

Figure 1: Fabrication process of clay based radiation shielding used dry pressing method.

2 Result

Figure 2 shows the comparison in terms of Lead equivalent thickness of selected clay based shielding materials (M1- M6) and commercial tiles (T1&T2).

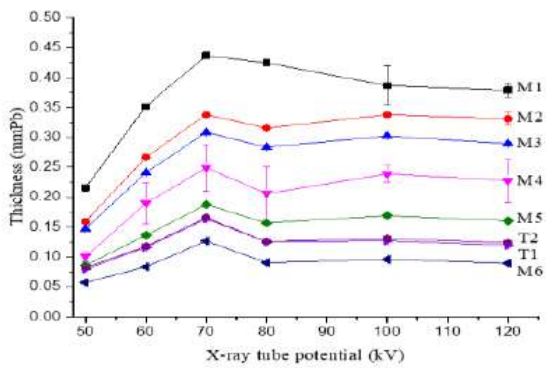

Figure 2: Comparison of clay-based thickness (different compositions) with commercial flooring tiles at different diagnostic energy range (50-120 kV).

The results indicate that clay-based composites exhibit promising characteristics for diagnostic radiology shielding, demonstrating comparable or superior performance to conventional materials. The lightweight and environmentally friendly nature of these composites presents a compelling solution for mitigating the environmental impact associated with traditional shielding materials.

3 Discussion

For the first time we inspected the potential of clay-based materials towards diagnostic X-ray radiation shielding. Clay-based samples are prepared using conventional pressing and sintering method. The presence of dominant monoclinic BAS phase in the mixture is found to enhance the shielding ability against X- ray and gamma rays (ionizing rays). Additionally, the microstructure analysis of the synthesized clay-based materials revealed the existence of single crystalline phase with good compactness and integrity. Lead equivalence and homogeneity test of as-synthesized clay-based authenticated the suitability of the sample as a best candidate for radiation shielding in diagnostic energy range. The optimum shielding ability (highest attenuation of 99.11%) of the samples is discerned at 70 kV. This in turn demonstrated the best shielding competence of the proposed clay-based composition for dental X-ray diagnostic, which is usually performed at the tube potential of 70 kV. It is established that this kind of clay-based materials as a radiation-shielding barrier can protect staff, patients and public from harmful effects of ionizing radiation in the diagnostic energy range. This study may open up new avenues for developing clay-based shielding materials using natural minerals that is abundant in Malaysia for radiation shielding operations in diversified medical and industrial applications such as radiotherapy, non-destructive testing and nuclear reactors.

4 Conclusion

This research contributes to the advancement of shielding materials in diagnostic radiology, offering a potential alternative that aligns with sustainability goals without compromising safety and image quality. The findings encourage further exploration and optimization of clay-based composites for widespread adoption in medical facilities, fostering a balance between effective radiation protection and environmental responsibility.

References

S.S. Amritphale, A. Anshul, N. Chandra, and N. Ramakrishnan. 2007a. Development of celsian ceramics from fly ash useful for x-ray radiation-shielding application. *J. Eur. Ceram. Soc.*, page 4639–4647.

S.S. Amritphale, A. Anshul, N. Chandra, and N. Ramakrishnan. 2007b. A novel process for making radiopaque materials using bauxite –red mud. *J. Eur. Ceram. Soc.*, 27:1945–1951.

F.H. Attix. 1986. Introduction to radiological physics and radiation chemistry. *John Wiley and Sons, Inc, New York*, page 124–157.

T.F. Choo, C.S. Mahmood, and M.A.M. Salleh. 2011. The study of aluminium loss and consequent phase transformation in heat-treated acid-leached kaolin. *J. Mater. Charact.*, 62:373–377.

K.S. Mann. 2017. γ-Ray shielding behaviors of some nuclear engineering materials. *Nucl. Eng. Technol.*, 49(4):792–800.

Z. Yang, J.W. Stevenson, and K.D. Meinhardt. 2003. Chemical interactions of barium-calcium-aluminosilicate-based sealing glasses with oxidation resistant alloys. *J. SolidState Ion.*, 160:213–225.

X.D. Zhang, K.H. Sandhage, and H.L. Fraser. 1998. Synthesis of BaAl2Si2O8 of Solid Ba-Al- Al2O3-SiO2 Precursors: 11, TEM Analyses of Phase Evolution. *J. Am. Ceram. Soc*, 81(11):2983–2997.

Individual Research Contribution Review, 2023, 1(1): 519–520

Assessment of Radon Concentration on Cameron Highlands in Malaysia

Faizal Azrin bin Abdul Razalim
Radiation Health and Safety Division
Malaysian Nuclear Agency
43000 Kajang, Selangor
faizal_azrin@nm.gov.my

Abstract

The indoor and outdoor radon concentrations in Cameron Highlands (Peninsular Malaysia) was measured. The measurements were carried out using passive method based on CR-39 solid state nuclear track detector (SSNTD) for indoor measurements and active method using continuous radon/thoron progeny monitor outdoor measurements in Cameron Highlands. The mean indoor radon concentrations in Cameron Highlands were 50 Bqm^{-3}. The mean indoor radon concentration in Cameron Highlands was slightly higher compare to the world average. The maximum value recorded was 97 Bqm^{-3} which is almost similar to WHO reference level. The mean outdoor radon concentrations in Cameron Highlands were 7.4 Bqm^{-3}. The outdoor concentrations were low and comparable to world outdoor average.

1 Introduction

Naturally occurring radioactive material (NORM) which occurs everywhere pose radiation exposure risks to people throughout the world. The important radionuclides are those from ^{238}U and ^{232}Th decay series. The main components of radiation exposure are inhalation of radon (and thoron) and their progenies and external gamma radiation. Radon (and thoron) and their decay products have been known as a potential health hazard as they can cause a significant inhalation radiation dose to the respiratory tract and other tissue. According to UNSCEAR (2000) report, radon (including thoron) contributed about 52% to the natural radiation dose received by the public. The levels of radon in the open atmosphere and its spatial variation not only depend on the geological conditions but also governed by the balance between the exhalation rate and the atmospheric dilution processes. Radon which emanates from soil grain and exhales from the soil surface into the free atmosphere is rapidly dispersed and diluted by natural convection and turbulence. Radon levels in indoor environment are influenced by building material, building. The objectives of this study were to measure radon concentrations indoor and outdoor on the highland areas. Cameron Highlands in Pahang and to estimate the dose receive by the people in those areas. This project describes the results of radon measurements and their associated risk of exposure.

2 Study Area

The first selected area for the study was Cameron Highlands in Pahang. The geological formation of Cameron Highlands made from igneous rocks (mainly granite). Granite form is one of the most important rock types in Peninsular Malaysia.

The measurements have been conducted involving 30 and 10 houses in Cameron Highlands. In Cameron Highlands, the indoor radon measurements were carried out in brick houses. Most measurements were conducted in the living room. In Cameron Highlands, indoor radon concentrations were measured using passive method based on CR-39 solid state nuclear track detector (SSNTD) that was made and calibrated by Landauer Nordic, Sweden. Principle of detection and measurement procedures has been described by Sulaiman et al. (2017). An exposure period was 3 months. It has been suggested that for nationwide survey of radon concentrations in air, long-term measurement (3 months and above) should be performed. The average radon concentrations were given in Bqm^{-3}.

For outdoor radon concentrations, short-term measurements based on active method were performed using continuous radon progeny monitors model Doseman Pro (Sarad, Germany). The monitors were calibrated by the manufacturer. The monitor is equipped with alpha spectroscopy system which capable of discriminating alpha energy peaks emitted by radon/thoron progenies. The equipment consists of a membrane pump, a USB interface, a semiconductor detector, a filter paper holder and a rechargeable battery. The sampling of radon progenies was performed by pumping the air through the filter paper. The monitor was placed on a tripod stand at a height of 1 m above the ground. As far as possible, the measurement was conducted for a period of about 24 hours in order to obtain a representative average radon concentration for one day. The advantage of using this type of equipment can record radon concentrations variation against time of the day. The radon concentrations are normally high or maximum in the early morning and low or minimum in the afternoon. The radon progenies concentrations in term of Equilibrium Equivalent Concentration (EEC) in Bqm^{-3} were then converted to radon gas concentration using appropriate equilibrium factor (UNSCEAR, 2000).

3 Results and Discussion

The mean indoor and outdoor radon concentration in Cameron Highlands shown in Table 1. The mean indoor radon concentration in Cameron Highlands was 50 Bqm^{-3}. This value was higher than the average world indoor radon concentration of 39 Bqm^{-3} (UNSCEAR, 2000). There were also about 50% of the measured houses have indoor radon concentrations above the world average concentration. The highest indoor radon concentration measured was 97 Bqm^{-3} which is very close to the World Health Organization (WHO) indoor radon reference level of 100 Bqm^{-3} (WHO, 2009). The mean indoor radon concentration in Cameron Highlands was also slightly higher than indoor radon in Ipoh (Kinta Valley - another radon high risk area) of 45 Bqm^{-3} (Sulaiman et al., 2017). Based on the present results and local geology, Cameron Highlands is probably the area which has the highest indoor radon concentration in Malaysia. It is suggested that more houses in Cameron Highlands to be measured their radon concentrations to find out if there are any houses exceed the reference level before any suggestion or action can be taken.

Table 1: Radon concentrations in Cameron Highlands

Location		Indoor (Bqm^{-3})	Outdoor (Bqm^{-3})
Cameron	Mean	50±25	7.4±2.6
Highlands	Minimum	28	5.6
	Maximum	97	9.3
	Mean	1.5±1.1	1.7±1,4

High indoor radon concentration measured in Cameron Highlands was attributable to high radium and uranium concentration in soil, rocks and building materials. The radium concentration of granite in Peninsular Malaysia has been reported by Omar et al. (1999) while radioactivity of soil at two tea plantations in Cameron Highlands has been reported by Hamzah et al. (2011). The mean outdoor radon concentration (also based on progenies measurement) in Cameron Highlands was low i.e. 7.4 Bqm^{-3}. Wind and ventilation play important role in influencing the radon concentrations in air. Furthermore, it also depends on many other factors such as changes in air pressure, temperature, and moisture. There was a significantly huge difference between indoor and outdoor radon concentrations in Cameron Highlands. The changed of occupant's activities by closing doors and windows (especially at night) will reduce ventilation and allowing the accumulation of radon in the houses. While in outdoor air, radon exhaled from the soil and rock surface rapidly dispersed and diluted in the free atmosphere. The ratio of indoor to outdoor radon concentration in Cameron Highlands and was 6.7.

Radioactivity in granite rocks is relatively high compared to sedimentary rocks (Nagaratnam, 1994). Variation of indoor radon levels (from low/normal to high concentrations) in different parts of Himalayan regions in India has been reported (Choubey et al., 2010; Choubey et al., 2000; R.C. et al., 2005). The variation was mainly due to different geological formation of soil and rocks.

3.1 Effective Dose

For the assessment of the annual effective dose received by the public living on those highland areas, it was assumed that peoples were exposed for 24 hours per day and 365 days per year and using the UNSCEAR's established factors such as equilibrium factor of 0.4 (indoor) and 0.6 (outdoor), occupancy factor of 0.8 (indoor) and 0.2 (outdoor) and dose conversion factor of 9 $nSvBq^{-1}h^{-1}m^{-3}$. The estimated annual effective dose was 1.38 mSv and 0.13 mSv in Cameron Highlands. The annual effective dose in Cameron Highlands was higher but slightly higher than world average reported by UNSCEAR (i.e. 1.25mSv).

4 Conclusion

Even though Cameron Highlands are located on highland areas, radon concentrations lower. People in Cameron Highlands was received annual effective dose from radon of 1.38 mSv.

References

V.M. Choubey, S.K. Bartarya, and R.C. Ramola. 2000. Radon in Himalayan springs: A geohydrological control. *Environ. Geol.*, 39:523 – 530.

V.M. Choubey, I. Ahmad, l. Karma, and R.C. Ramola. 2010. Radon variations in soil and groundwater of Bhilagana Valley, Garhwal Himalaya, India. *Jpn. J. Health Phys*, 45(3):278 – 283.

Z. Hamzah, S.D. Riduan, , and A. Saat. 2011. Assessment of radiation health risk in Cameron Highlands tea plantations, Malay. *J. Anal. Sci.*, 15(2):130 – 137.

A. Nagaratnam. 1994. The ubiquitous radon. *Current Sci.*, 66(3):194 – 199.

Ramola R.C., Negi M.S., and V.M. Choubey. 2005. Radon and thoron monitoring in the environment of Kumaun Himalayas: Survey and outcomes. *Journal of Environmental Radioactivity*, 79:85 – 92.

I. Sulaiman, K.M. Kontol, F.A.A. Råzalim, and A. Jaafar. 2017. Indoor radon concentration in Kinta Valley. *J. Sains Nukl. Malaysia*, 29(1):37 – 44.

UNSCEAR. 2000. Sources, effects and risks of ionizing radiation. United Nations Scientific Committee on the Effects of Atomic Radiation, United Nation, New York.

WHO. 2009. WHO Handbook on indoor radon: A public health perspective. World Health Organization, Geneva.

Individual Research Contribution Review, 2023, 1(1): 521–522

Quality Control for Fricke Dosimeter Using Eldorado-8 Theletherapy Machine

Hasan bin Sham
Radiation Health and Safety Division
Malaysian Nuclear Agency
43000 Kajang, Selangor
hasan_sham@nm.gov.my

Abstract

The validation of dosimeter Ferrous Sulfate (Fricke) was done to confirm the quality of the dosimeter before release to use as a reference dosimeter. The comparison test between the dosimeter and ionization chamber was done after a new batch produced. The difference reading allowed was ±5%.

Keywords: Ferrous Sulphate Dosimeter; Fricke; Ionization chamber; Quality Control

1 Introduction

The ferrous sulphate dosimeter (also known as the Fricke dosimeter) has been used as a reference dosimeter for the standardization of the Co-60 gamma source at the radiation processing level at Nuclear Malaysia. The absorbed dose is determined by measuring the Ferric ions resulting from the oxidation of ferrous sulphate solution after irradiation.

This Fricke dosimeter is called a reference dosimeter. It has been tested for its absorbed dose for 2 hours and 43 minutes (~70 Gy) using the Eldorado 8 teletherapy machine and will be compared with the standard dose from the Ionization chamber. The difference allowed is in the range of +5%. If the difference between the Fricke dosimeter and the ionization chamber is within that range, the Fricke dosimeter will be used for the purpose of Ceric-cerous dosimeter calibration. On the other hand, if it exceeds the range, this dosimeter will not be used and a new batch will be prepared. This new 'batch' will then go through the same process as the previous 'batch' where it will be tested first.

2 Method

The Fricke dosimeter contains 0.001 mol/litre ferrous ammonium sulphate and 0.001 mol/litre sodium chloride in 0.4 mol/litre Sulphuric acid. It has been prepared using distilled water from Thermo's water distillation system, Barnstead Smart2Pure. The prepared solution is left overnight before being put into a 5 ml ampoule. The range of use is 40 — 400 Gy.

Quality control on the Fricke dosimeter was carried out using an Eldorado 8 #104 teletherapy machine from Theratronics International Limited, Canada. The source activity was 75.887 TBq (2,051 Ci) on February 14, 2023. It is located in the Teletherapy Bunker, SSDL Block 32.

Irradiation set-up are performed as shown in Figure1. To obtain a standard dose rate, an ionization chamber is used with a distance of 80 cm from the source to the surface of the water phantom (Source Surface Distance - SSD). The ionization chamber was placed at a depth of 5 cm using a perspex cover. The size of the radiation field is 10 cm x 10 cm. After the standard dose measurement is done using the ionization chamber, the Fricke dosimeter will be placed with the same position and distance. A total of 4 units of Fricke dosimeter were tested for each group (batch) produced and were irradiated for 2 hours 43 minutes (Figure 2).

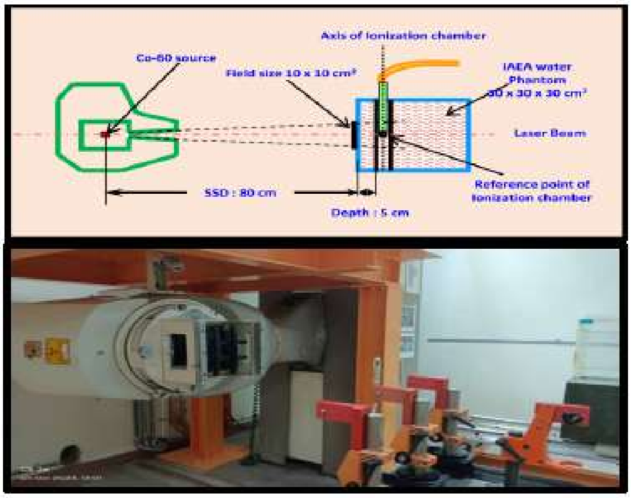

Figure 1: Measurement of absorbed dose in water using an ionization chamber.

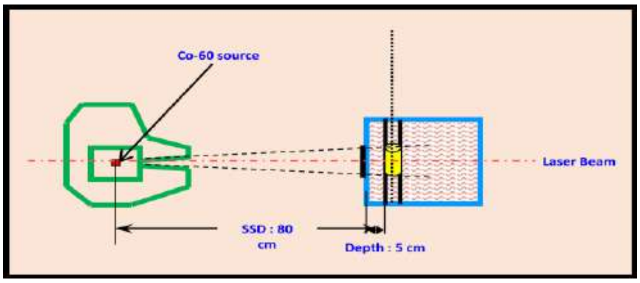

Figure 2: Fricke dosimeter irradiation.

3 Result

The concentration of Ferric ions in the Fricke dosimeter solution after irradiation is determined by the absorption of these ions measured by a spectrophotometer. Dosimeters that have been irradiated will be analyzed using a UV-VIS Spectrophotometer, Shimadzu 1601 at a wavelength of 304 nm.

The absorbed dose for Fricke, D_{fric} is calculated using the formula below:

$$D_{fric}(Gy) = \frac{2.75 \times 10^2 (A - A_0)}{1 + 0.007(T - 25)} \quad (1)$$

where
A: absorption of the solution that has been irradiated at a wavelength of 304 nm
A_0 : absorbance of control solution (unirradiated solution)
T : solution temperature during measurement (°C).

The tolerance value between the Fricke dosimeter, D_{fric} and the ionization chamber, D_{stand} can be calculated using formula below:

$$\text{Tolerance} = \frac{D_{fric} - D_{stand}}{D_{stand}} \times 100 \quad (2)$$

Table 1: Tolerance value for Fricke dosimeters

Dose (Gy)		**Tolerance (%)**
Standard $D_{stand(15.2.2023)}$	**Fricke, D_{fric}**	
69.90	65.40	-3.6

4 Discussion

Table 1 show that the Fricke dosimeters produced by SSDL are within the allowed control range of +5%. The accuracy of the dose measurements from the Fricke dosimeter was monitored using the ionization chamber reference dosimeter that traceable to IAEA.

5 Conclusion

From the results found, the Fricke dosirneters produced by SSDL for use in the standardization of gamma source radiation processing levels are of satisfactory quality.

Using the therapy bunker with the new Co-60 source, a shorter period of time can be implemented for irradiation work that requires a high dose such as Fricke and Ceric-cerous dosimeter irradiation (for the purpose of high-dose dosimeter quality control).

References

J.A. Beck. 1990. Auditing radiation sterilization facilities. *Radiat. Phys. Chem.*, 35:811 – 815.

T.A. Du Plessis and A.H.A. Roediger. 1989. Quality control through dosimetry at a contract radiation processing facility. *Proceedings of a Symposium on High Dose Dosimetry for Radiation Processing*, pages 13 –21.

IAEA. 1977. Manual of food irradiation dosimetry. Technical Reports Series No. 178, IAEA, Vienna.

A. Miller, P. Sharpe, and R. Chu. 2000. Dosimetry for industrial processing. ICRU News June 2000.

J. W. Nam. 1986. International dose assurance services: An IAEA programme for quality control in radiation processing. IAEA Bull. Summer 1986, IAEA, Vienna.

Individual Research Contribution Review, 2023, 1(1): 523–524

Measurement of Radon Concentration in Selected Hotspring in Selangor, Malaysia

Hasbi Husein Bin Sulkifli
Radiation Health and Safety Division
Malaysian Nuclear Agency
43000 Kajang, Selangor
hasbi@nm.gov.my

Abstract

Hot springs are one of the most popular eco-tourism spots, in Selangor several hot springs are identified and serve as ecotourism spots for recreational activity. However; some radioactive gases such as Radon and Thoron is possibly concentrated in these hotsprings which can have significant impact on the visitors and workers health. Total of 10 samples, 1.5 litre each, has been taken from 10 hotspring around Selangor: From each sample, 400 ml is use as representative for measuring radon gas concentrations using SARAD RTM 1688-2. Radon gas contained in the collected samples range from 0.16 Bq/L to 10.58 Bq/L. From the result, it shows that the radon concentration at the selected location is below WHO and USEPA reference level of 100 Bq/L and 11.1 Bq/L respectively.

1 Introduction

Radiation can be divided into two categories, ionising and non-ionising. However, ionising radiation is given more attention because it is more dangerous than the latter. The source of ionising radiation can come from Radon and Thoron gas, produced from the decay of Uranium. These highly mobile and water soluble gases can easily be taken by human through ingestion and respiration thus it is not surprising that they contribute about 52% to the natural radiation dose received by the public (UNSCEAR, 2000).

Hotspring is one of common recreational spots in Selangor, public use them to relax and some even use the water as alternative treatment for their disease. This water, which is heated within the earth's crust (Mohamed Baioumy et al., 2014) may carry with them radioactive material especially Radon gas as they ascend to the surface and accumulated in the hotspring pond (Fonollosa et al., 2016). This study aimed to determine the radon concentrations within selected hotsprings around Selangor.

2 Method

In this study, 10 hot spring location has been chosen based on their accessibility and availability and located within these 3 districts, Hulu Langat (5), Gombak (1) and Hulu Selangor (4). The geological setting for all location is within the main range granite province. To measure the radon concentration in each sample, SARAD RTM 1688-2 has been used. This equipment works by measuring the concentration of Radon ion progenies such as ^{218}Po and ^{214}Po using its semiconductor detector that able to detect Radon and distinguished different energy from its progenies.

For every sample, 400ml out of 1.5 litre will be used for measurement. The equipment is then connected to computer and using Radon Vision software, measurement is done for 3 cycles with each cycle is 5 minutes long. The data is then transferred to Radon in Water software to convert the unit from Bq/m^3 to Bq/L.

3 Result and Discussion

The radon concentration from each sample is shown in Table 1.

Table 1: Radon concentration in each sample. Sample A (Gombak), B (Hulu Selangor) and C (Hulu Langat).

Sample	Radon Concentration (Bq/L)
A1	10.58
B1	1.52
B2	0.26
B3	0.52
B4	1.75
C1	0.72
C2	1.32
C3	0.16
C4	0.73
C5	2.52

The highest concentration of radon is 10.58 Bq/L from sample Al, taken in Selayang Hotspring while the lowest is in sample C3 from Surau Batu 16 hotspring with 0.16 Bq/L. The average concentration for all sample is 2.01 Bq/L. Based on this result, it is found that the selected. hotspring has radon concentration well below the standard set by USEPA and WHO (11.1 Bq/L and Bq/L respectively).

Difference in radon concentration among the samples may be controlled by their lithology (Jobbagy et al., 2017). Hotspring within granite formation have relatively higher radon concentration when compared to other rock formation. This is expected because Uranium content is richer in igneous rock such as granite because they are formed from solidified magmas. Other factors such as water flow rate and device sensitivity could also plays a role in concentration reading.

4 Conclusion

Radon concentration from 10 selected hotspings around Selangor is found to be in the range of 0.16 Bq/L to 10.58 Bq/L. These values is safe since it is lower than the standard set by USEPA (11.1 Bq/L) and WHO (100 Bq/L).

References

E. Fonollosa, A. Penalver, F. Borull, and C. Aguilar. 2016. Radon in springs waters in the South of Catalonia. *Journal of Environmental Radioactivity*, 151:275 – 281.

V. Jobbagy, T. Altzitzoglou, P. Malo, V. Tanner, and M. Hult. 2017. A brief overview on radon measurements in drinking water. *Journal of Environmental Radioactivity*, 173:18 – 24.

H. Mohamed Baioumy, M. Nawawi, K. Wagner, and M. H. Ariffin. 2014. Geological setting and origin of non-volcanic hot springs in West Malaysia. *3rd Annual International Conference on Geological Earth Science (GEOS 2014)*, pages 14–17.

UNSCEAR. 2000. Sources and effects of ionizing radiation. Exposure from Natural Radiation Sources, Annex B. United Nation:1.

USEPA. 1999. Radon in drinking water health risk reduction and cost analysis. 64(38):9560 –9599.

Individual Research Contribution Review, 2023, 1(1): 525–526

Decommissioing Contaminated Building using Resrad-Build Computer Code

Khairuddin Mohamad Kontol
Radiation Health and Safety Division
Malaysian Nuclear Agency
43000 Kajang, Selangor
khairuddin-m@nm.gov.my

Abstract

Decommissioning refers to administrative and technical actions taken to allow removal of some or all of the regulatory controls from a contaminated facility. RESRAD-BUILD, a computer code developed by Argonne National Laboratory, USA was used to calculate estimated doses from building contaminated with radioactive materials. It is one of the available innovative tools to calculate radiological dose so that only the building material/ structure that may pose a risk must be demolished and disposed. Two (2) hypothetical scenarios were modeled in this study where a contaminated room was proposed to be occupied as an office for the new intake of staff members. During previous usage of the room there were some known spillage of Ra-226 radioactive solution to the floor area with the average activity of 2 x 10^7 Bq/m^2. Two (2) scenarios were identified for the proposed activities i.e. worker and office scenarios. The radiological criteria were 20 mSv/y for the decontamination/radiation workers and 0.3 mSv/y for the office workers whom regarded as an individual member of the public. The maximum total dose obtained for worker scenario were 2.05 mSv/y and 0.19 mSv/y for office scenario respectively.

Keywords: Decommissioning, RESRAD-BUILD

1 Introduction

Decommissioning refers to administrative and technical actions taken to allow removal of some or all of the regulatory controls from a contaminated facility. Decommissioning activities involve decontamination, dismantling and removal of radioactive materials, waste, components and structures. The early and proper planning of the decommissioning of facility are essential in order to protect human health, environment and future generations. There are many reasons for decommissioning such as uneconomical operation, technical obsolescence, conclusion of research programme, safety consideration, changes in the government policy and others such as closure due to an accident. Two decommissioning strategies are immediate and deferred dismantling. Besides that, a combination of these two strategies can be considered depends on local conditions and technical considerations. In the decommissioning project, the main players are the regulatory authority and the operator of the facility.

2 Decommissioning Plan

When a facility involving radioactive materials ceased operations, the operator of the contaminated facility has to prepare and submit a decommissioning plan to the regulatory authority before any activities can proceed. One of the keys to successful completion of decommissioning projects is in the preparation of the decommissioning plan documents. The documents should describe how the project would be performed including cost and schedule. It also has to address regulatory compliance issues by identifying goals. It also has to covers waste management, environmental and safety aspect of the project and also supported by other relevant documents.

3 RESRAD-BUILD

RESRAD- BUILD is a computer code designed to evaluate the radiation doses from RESidual RADioactivity in BUILDings. The code was developed by Argonne National Laboratory, United States of America and used a Windows based platform. It is an exposure pathway and analysis code used to determine whether radiologically contaminated buildings the and structures can be free released for a specific use e.g. industrial or residential purposes. The exposure pathways incorporated are external exposure, inhalation and ingestion.

4 Hypothetical Case Study

A hypothetical scenario where a room of 3 m x 3 m and height of 3 m was proposed to be occupied as an office for the newly hired employees. Previously this room was used as a small laboratory for experiment in conducting distribution coefficient (k_d) value where source of radioactive solution was used. During previous usage of the room there were some known spillage of radioactive solution. Before converting the room for the office usage an early screening shows that the floor of the room was contaminated with Ra-226 radionuclide with the average activity of 2 x 10^7 Bq/m^2 . The RESRADBUILD computer code was used to model the hypothetical scenarios for the proposed activities. Two (2) scenarios were identified i.e. worker and office scenarios.

- Worker Scenario
  A radiation worker is decontaminating the floor with the amount of time it takes to decontaminate the floor is 8 hours, and the total time to complete the work is estimated at 5 days.
- Office Scenario
  An office worker will occupy the decontaminated room.

The worker will spend an average of 8 hours per day in the room. A light coat of paint will be applied to the walls, absorbing 50% of the surface contamination. This paint coating is gradually lost from the wall surface until it is gone after 30 years.

4.1 Input Parameters

The site-specific input parameters must be obtained in running the RESRAD-BUILD computer code for the best results of the assessments. The input parameters in this study were based on estimates by using available, reasonable and assumed data. Some of the input parameters used for both scenarios are shown below.

Window	Parameter	Worker Scenario	Office Scenario
Time	Total Time Spent on Site	5	365
	Fraction of Time Spent Inside	0.33	0.23
Receptor	Number of Receptors	1	1
	Location of Receptors	1.5,1.5,1	1.5,1.5,1
	Time Fraction	1	1
	Breathing Rate	$18m^3/d$	$18m^3/d$
	Ingestion Rate	$0.0001m^2/h$	$0.0001m^2/h$
Source	Number of Source	1	1
	Source Location/Direction	1.5,1.5,0/Z	1.5,1.5,0/Z
	Source Type	Area	Area
	Source Area	9 m^2	9 m^2
	Source Activity	2 x 10^7Bq/m^2	2 x 10^7Bq/m^2
Building	Number of Rooms	1	1
	Area	9 m^2	9 m^2
	Height	3 m	3 m
	Exchange Rate	0.81/h	0.81/h
	Deposition Velovity	0.1 m/s	0.1 m/s
	Resuspension Rate	5 x 10^{-7} l/s	5 x 10^{-7} l/s

*Default values for all other parameters

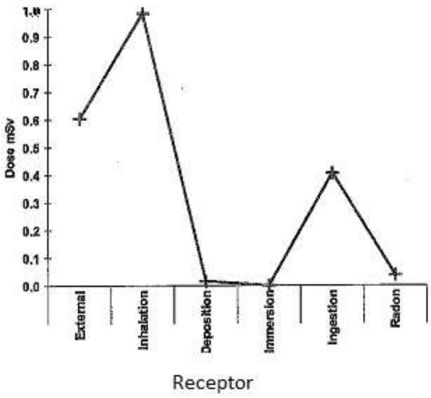

Figure 1: Worker dose scenario

5 Results and Conclusion

The results generated from the assessment for worker and office scenarios were shown in Figure 1 and 2 respectively. The maximum total dose obtained for worker was 2.05 mSv/y. The dose obtained was below the dose limit of 20 mSv/y for the radiation workers. Main contributor for the maximum dose obtained for workers doing the decontamination works is from the inhalation pathway i.e. 0.98 mSv/y. Besides that, significant dose obtained from external (0.60 mSv/y) and ingestion (0.41 mSv/y) pathways respectively. The maximum total

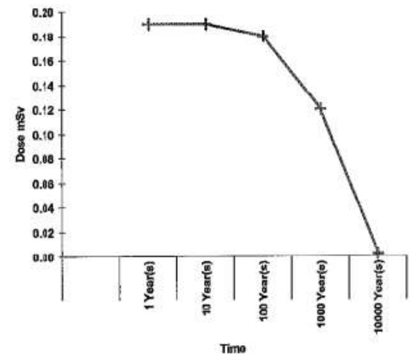

Figure 2: Office dose scenario

dose obtained for office scenario was 0.19 mSv/y. The dose obtained was below the dose constraint limit of 0.3 mSv/y.

References

IAEA. 2014. Safety Standards Series No. GSR Part 6, General Safety Requirements Part 6, Decommissioning of Facilities.

Argonne National Laboratory. 2022. User Manual for RESRAD-BUILD Version 4. ANL/EVS-21/17 vol.2.

Individual Research Contribution Review, 2023, 1(1): 527–528

Management of MS ISO/IEC 17025 in Kumpulan Metrologi Sinaran

Konsoh @ John Konsoh Sangau
Radiation Health and Safety Division
Malaysian Nuclear Agency
43000 Kajang, Selangor
John_Konsoh@nm.gov.my

Abstract

The Kumpulan Metrologi Sinaran (KMS) is one of the service centres at the Malaysian Nuclear Agency (Nuklear Malaysia) under the Radiation Safety and Health Division (BKS). KMS plays an important role as the national metrology centre for ionizing radiation standards and is recognized as a designated institute by the National Metrology Institute of Malaysia (NMIM). The implementation of activities at KMS is done through the implementation of MS ISO/IEC 17025 accreditation. This extended abstract aims to explain the management of MS ISO/IEC 17025 at KMS.

1 Introduction

The Kumpulan Metrologi Sinaran (KMS) was established in 2014 through the merger of the Medical Physics Group (MPL) and the Secondary Standard Dosimetry Laboratory (SSDL). Prior to the merger, SSDL and MPL were awarded MS ISO/IEC 17025 accreditation in 2004 (SAMM No: 275) and 2013 (SAMM No: 583), respectively. In 2021, KMS combined the accreditation scope of SSDL and MPL by using SAMM 275 registration. The scopes of accreditation carried out are calibration of dosimetric detectors used in radiation protection, calibration of dosimetric detectors used in radiation therapy, calibration of dosimetric detectors used in diagnostic radiology, and calibration of Ceric-Cerous dosimeter for high dose dosimetry.

The implementation of MS ISO/IEC 17025, also known as the laboratory management system, is a requirement at KMS to ensure that the calibration service of dosimeters or ionizing radiation monitoring devices is carried out in accordance with the standards set at the international level. Failure to comply with the requirements outlined in this standard will result in KMS being suspended from continuing with the calibration service. In order to ensure continued compliance with the standard, KMS needs to ensure that requirements such as documentation, training and competence, opportunity and risk assessment, data analysis, internal audit, management review and assessment from third parties are carried out consistently with the established procedures.

The success of maintaining the laboratory management system at KMS is vital to the continuity of services that customers very much need in the field of medicine and industry throughout the country. Approximately 2500 private companies and government agencies depend on the services provided at KMS every month. KMS consistently contributes more than RM 2 million annually to the Nuklear Malaysia Trust account through the services. Figure 1 shows the KMS accreditation certificate of MS ISO/IEC 17025:2017.

Figure 1: KMS accreditation certificate of MS ISO/IEC 17025:2017.

2 Methods

The management of MS ISO/IEC 17025 at KMS is done in accordance with the requirements set out in the main reference document, which is General Requirements For The Competence of Testing And Calibration Laboratories ISO/IEC 17025:2017 (Second revision) and the series of documents issued by the Malaysian Laboratory Accreditation Scheme. Through a series of meetings and discussions held, a comprehensive plan was prepared to ensure the successful implementation of MS ISO/IEC 17025 accreditation at KMS. Understanding the requirements stated in the primary reference documents allows KMS to develop a documentation system

Table 1: Implementation of the laboratory management system program at KMS from 2021 to 2023.

Program	**Frequency**			**Remark**
	2021	**2022**	**2023**	
Updating documents	1	20	9	
Training	6	2	6	
Assessment of opportunities and risks	14	1	3	
Resolution of complaints	3	1	8	
Resolution of Nonconforming	-	2	2	No nonconforming recorded in 2021
Customer satisfaction survey	1 (81%)	1 (83%)	1 (*)	* Results have not been obtained
Staff satisfaction survey	1 (80%)	1 (80%)	1 (*)	* Results have not been obtained
Internal audit	1	1	1	
Management Review Meeting	1	1	1	
Assessment from the Department of Standard Malaysia (DSM)	1	1	-	The DSM sets the assessment schedule

consisting of Quality Manuals, Standard Operating Procedures, Work Instructions and forms relevant to the operation of the services provided.

Next, KMS implements programs that are carried out periodically and continuously, such as training and staff competence, opportunity and risk assessment, data analysis, internal audit, management review meetings and third-party evaluations carried out by assessors from the Department of Standard Malaysia. Continuous improvements are also made to the laboratory management system through audit results, customer and staff feedback, and management recommendations, and they are also in line with changes and instructions from the Department of Standard Malaysia.

3 Results

Since 2021, KMS has successfully implemented programs planned to maintain MS ISO/IEC 17025 accreditation. The relevant data is shown in Table 1.

4 Discussion

The management of MS ISO/IEC 17025 at KMS is running smoothly in accordance with the program set in the annual plan. Although there are some constraints, such as insufficient staff and relatively limited allocations, the implementation of the laboratory management system at KMS is still going well and complies with the requirements that have been set. Overall, KMS managed to maintain the accreditation obtained in 2021. However, the input received from sources such as customer complaints, staff feedback, internal discussions, audit findings and recommendations from management must be fully integrated to ensure that existing management can be further improved.

5 Conclusion

The laboratory management system implemented at KMS needs to be maintained to ensure that the services provided can be accepted nationally and internationally. Continuous efforts should be implemented to ensure that the existing system is maintained and even improved in accordance with current needs and changes at a global level.

References

Department of Standards Malaysia. A series of documents published under the Malaysian Laboratory Accreditation Scheme such as SP 1, SP 2, SP 4, SP 5, SP 6, SP 10, SI 1, SAMM Circular 4/2023 and SAMM Circular 3/2023.

Department of Standards Malaysia. 2018. General requirements for the competence of testing and calibration laboratories (Second revision). (ISO/IEC 17025:2017, IDT), ICS: 03.120.20.

Individual Research Contribution Review, 2023, 1(1): 529–530

Quality Controls in Diagnostic Radiology: Computed Radiographic (CR) System

Mohd Khalid Matori
Radiation Health and Safety Division
Malaysian Nuclear Agency
43000 Kajang, Selangor
khalid_matori@nm.gov.my

Abstract

The Medical Physics Laboratory of the Malaysian Nuclear Agency, endorsed by the Ministry of Health (MOH) and in accordance with Malaysian standards and regulations, has been providing Quality Control (QC) services for medical X-ray apparatus since 1997. With the widespread adoption of computerized radiographic (CR) systems in diagnostic radiology, the MOH is committed to complying with quality assurance programs for CR systems. As a Class H licensee, the Nuclear Agency recognizes the need to establish QC procedures for CR systems to ensure that services remain relevant to the latest technological developments. This paper discusses the QC tests specifically developed for CR systems, shedding light on key aspects that contribute to the quality and relevance of the services provided.

Keywords: Quality Control, Computer Radiology (CR)

1 Introduction

The Ministry of Health prioritizes enhancing radiological services for optimal diagnostic information with minimal patient exposure. Adherence to regulations is crucial for maintaining X-ray equipment standards. Since 1997, the Malaysian Nuclear Agency, particularly its Medical Physics Laboratory, actively ensures quality control for diagnostic X-ray apparatus, emphasizing commitment to upholding standards for effective and safe radiological procedures in healthcare.

2 Objective

As conventional medical imaging shifts to computed radiographic (CR) systems, the Ministry of Health Malaysia is dedicated to a robust quality assurance program for CR. This paper explores Malaysian Nuclear Agency-designed quality control tests crucial for ensuring the reliability, accuracy, and safety of CR systems in healthcare, highlighting a commitment to maintaining high imaging standards.

3 Material and Method

In computed radiography (CR), quality control (QC) is as crucial as in conventional systems. Meticulous measurements, following international protocols, were conducted using calibrated equipment as in Figure 2. QC tests, performed on recently validated X-ray units, were documented. Results were analysed by a competent individual, leading to quality assurance reports. Table 1, developed by the Malaysian Nuclear Agency, outlines CR system quality control tests and tolerance limits, ensuring thorough assessment and upholding safety, accuracy, and standards in medical imaging.

Figure 1: Computed Radiography equipment includes an imaging plate, reader, and computer.

Figure 2: Computed Radiography QC Test Tools.

4 Result and Discussion

Nuclear Malaysia has established eighteen tests for computed radiography (CR) systems based on protocols adapted from IPEM and MOH guidelines. Regular checkups are crucial for maintaining high-quality equipment, emphasizing the importance of ongoing quality control. The agency aims to uphold CR system reliability, accuracy, and safety by adhering to established protocols.

Nuclear Malaysia has established eighteen tests for computed radiography (CR) systems based on protocols adapted from IPEM and MOH guidelines. Regular checkups are crucial for maintaining high-quality equipment, emphasizing the importance of ongoing quality control. The agency aims to uphold CR system reliability, accuracy, and safety by adhering

Table 1: Quality control test carried out on Computed Radiography (CR) units with tolerance limit.

No.	Physical Parameter	Tolerance Limit
1	Visual Check of Uniformity & Condition of Cassettes and Image Plates	Cassette is clean and good physical condition
2	Matching of CR Image Plates (if more than one CR Image Plates available)	DAK_{DDI} varies by ≤ ±20% between image plate
3	Dark Noise	Follow to Manufacturer's recommendation (Refer attachment)
4	Detector Dose Indicator (DDI) Accuracy	DDI ≤ ±20%
5	Differences Between CR Readers (applicable if more than 1 reader available)	DAKDDI varies by ≤ ±20% of between readers
6	DDI Repeatability	CoV of DAK_{DDI} ≤ ± 10%
7	DDI Reproducibility	Mean DAK_{DDI} ≤ ± 20% of baseline value
8	Signal Transfer Property (STP)	Simple STP relationship Linear correlation $R^2 \geq 0.98$
9	Variation of Noise with Detector Air Kerma	Linear correlation $R^2 \geq 0.95$
10	Measured Uniformity (if ROI analysis tool available)	No artefacts & mean within ≤ ± 10%
11	Signal to Noise Ratio (SNR)	≤± 15% of baseline value
12	Erasure Cycle Efficiency	No Visible Ghost Image Lag ≤ 1%
13	Threshold Contrast Detail Detectability (TCDD)	As described by the test tool manufacturer
14	Limiting High Contrast Spatial Resolution	Refer to the test object manufacturer's manual
15	Blurring	No obvious blurring
16	Laser Beam Function	Edge continuous across whole image and uniform stair characteristics
17	Scaling Errors: Measurement Calibration & Aspect Ratio	Error ≤ ± 4% Within 1+0.04
18	Moire Patterns and Anti-Scatter Grids (if Bucky system available)	Not Visible

to established protocols. Specific tests, like the Erasure Cycle Efficiency test, address critical aspects, ensuring optimal image quality and patient safety through effective radiation dose management. This comprehensive approach enhances the overall performance of CR systems in healthcare.

5 Conclusion

The Medical Physics Laboratory at the Nuclear Agency, a core in diagnostics quality control (QC), invests significantly to enhance healthcare. The developed CR test procedure sustains the group's relevance in diagnostic radiology.

References

KCARE. 2004. Protocol for the QA of computed radiography system.

Kementerian Kesihatan Malaysia (KKM). 2022. Technical quality control protocol handbook for radiograph system, version 2022.

Institute of Physics and Engineering in Medicine (IPEM). 2010. Recommended standards for the routine performance testing of diagnostic x-ray system (IPEM reports series) Report 91.

Department of Standard Malaysia. 2007. Code of practice for radiation protection – Medical x-ray diagnosis, Malaysian Standards 838 ; 2007.

Individual Research Contribution Review, 2023, 1(1): 531–532

Scattered Radiation Measurement During Intra Oral Radiography

Mohd Khalid Matori
Radiation Health and Safety Division
Malaysian Nuclear Agency
43000 Kajang, Selangor
khalid_matori@nm.gov.my

Abstract

Dental radiography, a common procedure, uses low radiation for imaging teeth and jaw bones. While patient exposure is minimal, operators face scattering radiation risks. This study measures scattered radiation levels from intra-oral dental X-rays at various distances and angles using a 1800 cc ion chamber. Results aim to create a dispersed radiation profile, guiding optimal safety measures for medical personnel during dental X-ray procedures. The study's findings will be detailed in subsequent sections of this paper

Keywords: Intra oral dental X-ray, scattered radiation, radiation protection

1 Introduction

Dental radiography, a common diagnostic practice, employs X-rays to produce images of teeth and jawbones for diagnosing and monitoring conditions. Dentists use these radiographs to assess issues like cavities, jaw conditions, and monitor treatments like root canals and tooth extractions. While modern digital equipment emits low radiation, cumulative effects necessitate understanding. Employers must provide radiation protection for staff and the public. Patient bodies deflect radiation during imaging, requiring precautions for nearby individuals. Excessive X-ray exposure poses risks like cell damage, cancer, and birth defects. Two types of dental X-rays, intraoral and extraoral, serve distinct purposes.

2 Objective

A preliminary study assesses scattered doses during intraoral dental X-rays, aiming to identify safety measures for medical personnel during procedures.

3 Material and Method

This study employed the RXDC intraoral X-ray apparatus in the Medical Physics laboratory, featuring a total filtration equivalent to 2.0 mm aluminium, a 0.4 mm spot focal size, and a minimum focal-to-screen distance of 300 mm. Operating at 60, 65, and 70 kV with current options of 4.0 and 8.0 mA, the study utilized a 70 kV technique, 0.5 s exposure time, and 8 mA current, resulting in a cone tip dose of 498.3 mR. An Alderson Rando phantom, representing adult males, specifically the head, was used for measurements. The

a b

Figure 1: a - The dosimeter Radcal 2026 used in this study b - The measurement set up.

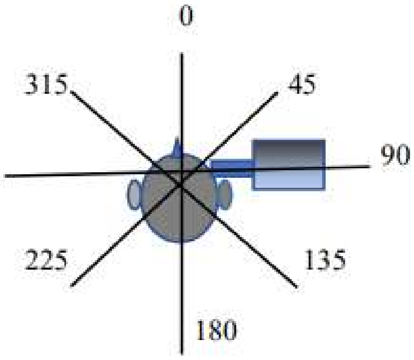

Figure 2: The measurement angles.

Radcal model 2026-1800 ionization chamber, calibrated and maintaining a valid certificate, measured scattered radiation at distances from 50 to 200 cm in 25 cm increments and seven angles at 45-degree intervals. Measurements were taken three times at each position, and the exposure in mR/hr was calculated. The setup and measurement angles are illustrated in Figures 1 and 2, respectively.

4 Result and Discussion

Routine dental X-ray procedures typically pose a small and low-risk exposure for patients, with any associated health risk assumed to be minimal due to the ionizing nature of X-rays. However, increased exposure corresponds to an increased health risk, necessitating efforts to keep radiation exposures as low as reasonably achievable. In intra-oral procedures, operators face potential exposure to unsafe radiation levels, mainly due to scattering radiation. Scatter radiation, a secondary form occurring when X-rays deflect off objects, poses risks for operators and nearby individuals during dental imaging.

To mitigate these risks, the Ministry of Health (MOH) mandates special shielded rooms for dental irradiation, featuring sufficient shielding equivalent to 1 mm Pb. The study's results, presented in Table 1 and Figure 4, demonstrate varying scattered doses during intra-oral procedures based on angles and distances. The highest scattered doses occur at 0 degrees, indicating a dependence on location and the non-uniform distribution of scattering radiation. Figure 5 showcases radiation protection equipment employed in dental clinics, including mobile shields and lead dresses, following the STD principle (shielding, time, distance) to optimize dose reduction for both operators and patients. The inverse square law is evident in the decrease of scattering radiation readings with increasing distance from the radiation source, emphasizing the need for precautions even at considerable distances. Overall, the study underscores the importance of radiation protection measures and ongoing efforts to optimize dose levels in dental X-ray procedures.

Table 1: The results of the scattered dose measurement study received during the dental x-ray procedure for various angles and distances.

Distance (cm)	Dose rate (mR/hr)						
	0°	45°	90°	135°	180°	225°	315°
50	242.63 (± 5.14)	190.07 (± 1.74)	21.27 (± 3.59)	166.13 (± 0.76)	84.23 (± 4.14)	63.30 (± 2.14)	102.73 (± 1.12)
75	109.60 (± 4.69)	87.33 (± 1.47)	10.93 (± 8.88)	86.57 (± 0.59)	34.63 (± 7.81)	36.83 (± 1.22)	56.20 (± 3.91)
100	59.77 (± 5.21)	52.00 (± 2.77)	7.83 (± 9.75)	47.83 (± 3.20)	20.33 (± 7.69)	21.83 (± 0.70)	30.77 (± 5.14)
125	32.97 (± 5.64)	31.00 (± 3.18)	3.00 (± 6.67)	29.97 (± 4.53)	13.53 (± 5.55)	13.20 (± 3.03)	22.00 (± 5.12)
150	24.10 (± 0.72)	15.07 (± 2.76)	2.37 (± 6.45)	23.27 (± 6.83)	9.93 (± 6.07)	9.83 (± 2.56)	10.73 (± 3.88)
175	20.57 (± 5.80)	8.60 (± 2.01)	1.23 (± 4.68)	15.30 (± 3.00)	2.40 (± 8.33)	6.47 (± 6.44)	9.27 (± 8.17)
200	15.10 (± 7.01)	6.43 (± 5.00)	0.83 (± 6.93)	10.57 (± 9.67)	1.17 (± 4.95)	5.47 (± 5.59)	3.13) (± 9.75)

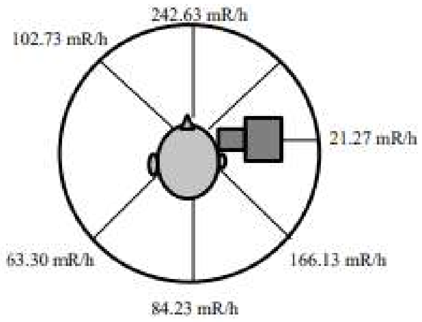

Figure 3: Scattered dose distribution by various angle at 50 cm.

5 Conclusion

The preliminary study aims to discern scatter distribution in intraoral X-ray procedures, informing safe positions for operators and the public. It emphasizes the importance of distance,

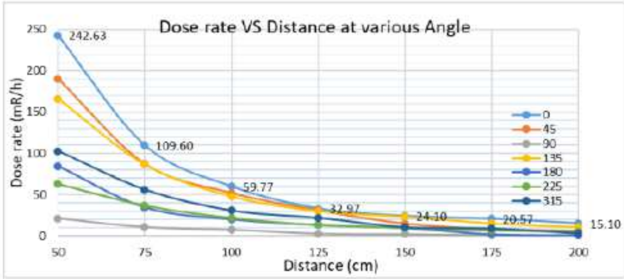

Figure 4: Dose rate vs distance at various angle.

Figure 5: Personnel protective equipment (PPE) normally used during the dental procedure.

shielding, and personnel protective equipment for optimized dose in dental radiography.

References

Tabakov et al. 2000. Instantaneous dose rate of scatter radiation in dental radiographyn. *Phys Med*, 16:27 – 30.

John Holroyd et al. 2018. Measurement of scattered and transmitted x-rays from intra-oral and panoramic dental x-ray equipment. *Journal of Radiological Protection.*

D GCrane and PV Abbo. 2016. Radiation shielding in dentistry: An update. *Australian Dental Journal*, 61:277–281.

K. Kuroyanagi, Y. Hayakawa, H. Fujimofi, and T. Sugiyama. 1998. Distribution of scattered radiation during intraoral radiography with the patient in supine position. *Oral Surg Oral Med Oral Pathol Oral Radiol Endod*, 85:736 – 741.

International Commission on Radiological Protection (ICRP). 2007. The 2007 Recommendations of the International Commission on Radiological Protection. *ICRP publication 103*, Ann ICRP 37:1 – 332.

Individual Research Contribution Review, 2023, 1(1): 533–534

Establishment of ISO 4037-1 X−Ray Narrow Spectrum Series (NSS)

Mohd Taufik Bin Dolah
Radiation Health and Safety Division
Malaysian Nuclear Agency
43000 Kajang, Selangor
taufik@nm.gov.my

Abstract

Establish an X-ray narrow-spectrum series (NSS) recommended by the standard ISO 4037-1 is critical when to calibrate the radiation protection instruments and determine radiation dose using xray. The qualities of filtered X radiation of narrowspectrum series in the range from 60 to 300 kV were established. The homogeneity values for 8 NSS qualities were between 0.89 and 1.02 according to ISO 4037:2019.

Keywords: Half Value Layer, Homogeneity

1 Introduction

Calibrate dosimeters are need to detect the radiation dose. The International Standard ISO 4037-1 specifies the radiation characteristics and production methods. Filtered X radiation of narrow-spectrum series (NSS) in the range from 60 to 300 kV was established based on ISO 4037-1. The quality of a filtered X radiation is characterised by half-value layer (HVL) that can be used to calibrate radiation protection instruments.

The narrow spectrum series of X-rays from 30 kV to 300 kV was established according to the above standards, inherent filtration of the tube, supplementary filtration, first half value layer (1 st HVL), second half value layer (2 nd HVL), quarter value layer (QVL) and homogeneity were measured experimentally.

2 Method

Measurements were performed with an X-ray irradiator model MGC 325, it has a tungsten anode target, a 5.5 mm focal field and inherent 3 mm beryllium filtration.

Without any additional filtration and at 60 kV, the inherent filtration was measured using the M23361 (30 cm^3) ionization chamber placed at 1m from the center of the x-ray tube.

The measurement method consists of 3 charge readings of 60 seconds each. Additional Copper (Cu) filters attached at the HVL wheel were placed in the middle of x-ray tube and ionisation chamber to obtain a reduction of about 50% of the initial charge as shows in Figure 1. The inherent filtration was calculated based on Table 9 of ISO 4037 using interpolation with a second order polynomial. These filters are procured from the RMK12 allocation.

The HVL wheel was adjusted accordingly to increase the thickness of copper until the reading became one-fourth of the initial reading. The temperature, pressure, and humidity readings before and after irradiation were recorded. The steps in exposing the ionisation were repeated with the voltage of 80 kV, 100 kV, 120 kV, 150 kV, 200 kV, 250 kV and 300 kV.

Figure 1: The set-up of the experiment.

3 Result

The collected data was then keyed into Microsoft Excel for calculation and create the graphs as shows in Figure 2. The graph shows the value of the first HVL and quarter value layer (QVL).

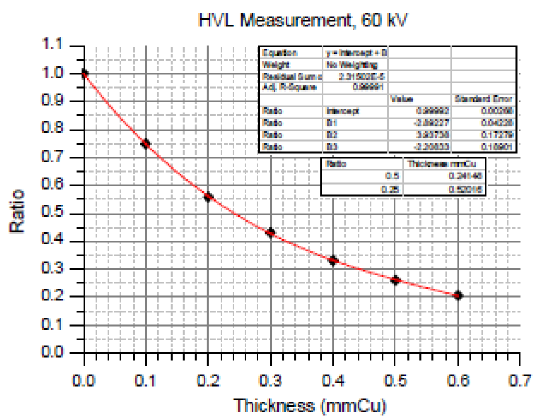

Figure 2: The graphs of the ratio against the thickness of copper for voltage 60 kV.

The values are essential to get the value of the second HVL. The formula in equation 1 is used to calculate the second HVL.

$$2nd\ HVL = QVL - 1st\ HVL \tag{1}$$

The value of the second HVL is used to calculate the homogeneity of the results. Which then can determine whether the HVL is suitable for calibration using the new additional filter. Equation 2 shows the calculation of homogeneity.

$$\text{Homogeneity} = \frac{1st\ HVL}{2nd\ HVL} \tag{2}$$

Table 1: The value of 1st HVL, QVL, 2nd HVL and homogeneity for each voltage.

kV	**1st HVL (mmCu)**	**QVL (mmCu)**	**2nd HVL (mmcu)**	**Homogeneity**
60	0.24	0.51	0.27	0.89
80	0.59	1.18	0.59	1.01
100	1.08	2.25	1.17	0.92
120	1.72	3.47	1.75	0.98
150	2.46	5.00	2.54	0.97
200	4.07	8.10	4.03	1.01
250	5.31	10.50	5.19	1.02
300	6.25	12.38	6.13	1.02

4 Discussion

The homogeneity must be in the range of 0.75 to 1.00 for that HVL value to be accepted. With that, the additional filter can be used for future references. However, from Table 1, the homogeneity value for voltage 80 kV, 200 kV, 250 kV and 300 kV fell from the stated range; hence the value cannot be accepted. The HVL experiment must be repeated for at least that particular tube voltage to determine the cause of deviation. The new additional filter for voltage 60 kV, 100 kV, 120 kV and 150 kV can be used for future calibration and reference dose measurement.

5 Conclusion

The reference qualities of narrow-spectrum series given by ISO 4037-1 were established with the energy from 60 to 300 kV. The results of the measurements shown that only 4 out of 8 qualities are comply with the values given by the standard ISO 4037-1.

References

International Atomic Energy Agency. 2000. Calibration of radiation protection monitoring instruments. IAEA Safety Report Series No.16.

International Organization for Standardization. 1996. X and gamma reference radiation for calibrating dose meters and dose rate meters and for determining their response as a function of photon energy Part1: Radiation characteristics and production methods. ISO4037-1:1996.

Individual Research Contribution Review, 2023, 1(1): 535–536

Radiation Shielding for CWT 3 Mev 30mA Electron Beam Accelerator Bunker

Muhamad Zahidee Taat
Radiation Health and Safety Division
Malaysian Nuclear Agency
43000 Kajang, Selangor
zahidee@nm.gov.my

1 Introduction

This paper addresses the designated of radiation shielding bunker for 3MeV 30mA electron beam accelerator that was installed at Cyprium Wire Technology Sdn. Bhd. (CWT). The bunker was designed by CGN Dasheng Electron Accelerator Technology Company (CGN). The verification focus on the wall thickness at the surrounding bunker at ground floor, the wall thickness at 1st floor of the building and also the rooftop.

The primary design for this facility is for wire and cable crosslinking processing. Malaysian Nuclear Agency has been appointed to monitor, verify and advise CWT in order to ensure the designated shielding bunker is safe and fulfilled all the requirements set up by the regulatory body. This verification will be conducted using a calculation as recommended by NCRP 51.

2 Methods

The electron accelerator emits rays to form a radiation field, which is used to complete the radiation processing process. Radiation source term; electron beam bombardment of targets such as a various structural materials and irradiated products produces bremsstrahlung X-rays is the main source of radiation in the radiation protection design of the accelerator irradiation device. When X-ray passes through the material, it decays with an approximate exponential law. When calculating the shielding, the transmittance of X-ray **Bx** must be determined.

$$Bx = (1.6 \times 10^{-5})\frac{H_m d^2}{D_{10}T}$$

There are two methods for calculating the shield thickness: **the curve diagram method** and the **tenth value layer method**. Here only a tenth value layer method will be used for the calculation.

The shielding design of electron accelerator irradiation equipment must be based on the highest energy and maximum beam intensity of the accelerator.

This report presents the calculation of shielding thickness for Electron Beam Accelerator facilities and the specification as following below:-

i. Maximum electron energy, E : 3.0 MeV

ii. Electron-beam current, I: 30 mA

iii. Maximum power of machine, P: 90 kW

3 Results and Discussion

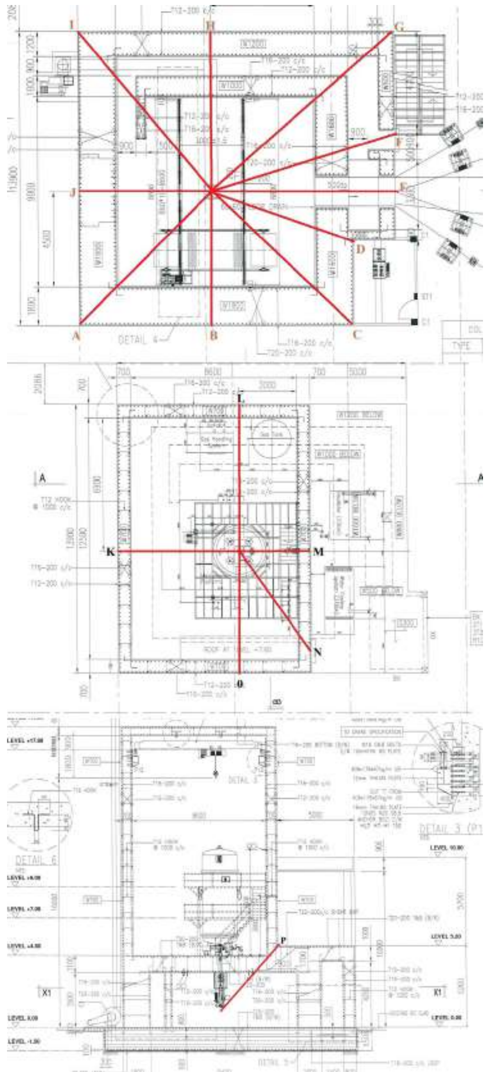

Figure 1: Location reference point

Table 1 show the result of required shielding wall thickness of the bunker. The design thickness of the direct radiation shielding provided by the manufacturer are larger at most of the reference point. Only at the F point, the designed thickness is less than the calculated result, but it has been solved with added 14cm thickness of lead protective door.

Table 1: Result of calculation parameters in each reference point.

Location (Reference Point)	**Distance (m)**	**S in Plan (cm)**	**Dose Rate Hm (μSv/hr)**	**Bx**	**T (Occupancy Factor)**	**D10 (Gy*m^2*h^{-1}**	**Shielding Required (cm)**
A	8.9	**247**	0.5	2.29x10^{-8}	1	1728	**178.7**
B	6.3	**180**	0.5	1.15x10^{-8}	1/4	1728	**171.7**
C	9.2	**260**	0.5	2.45x10^{-8}	1	1728	**178**
D	7.1	**196**	0.5	1.45x10^{-8}	1	1728	**183**
E	8.7	**240**	0.5	2.19x10^{-8}	1	1728	**177.8**
F	9.1	**167**	0.5	2.40x10^{-8}	1	1728	**178.26**
G	11.55	**359**	0.5	3.86x10^{-8}	1	1728	**173.5**
H	7.9	**220**	0.5	1.805x10^{-8}	1	1728	**180**
I	9.86	**365**	0.5	7.55x10^{-8}	1	1728	**176.6**
J	6.3	**180**	0.5	4.59x10^{-8}	1/4	1728	**171.7**
K	6.6	**70**	0.5	4.03x10^{-5}	1/8	4.32	**60.9**
L	7.6	**70**	0.5	5.34x10^{-5}	1/8	4.32	**59.0**
M	4.0	**70**	0.5	1.48x10^{-5}	1/8	4.32	**66.6**
N	6.3	**65**	0.5	3.68x10^{-5}	1/8	4.32	**61.4**
O	6.6	**70**	0.5	4.03x10^{-5}	1/8	4.32	**60.9**
P	5.5	**240**	0.5	8.75x10^{-9}	1/8	1728	**188cm**

4 Conclusions

The design thickness of the shielding walls in the ground and first floor bunker are larger than the calculated results and its meet protection requirement for occupational exposure of radiation worker.

References

NCRP rep. No. 51. March 1, 1977. Radiation Protection Design Guidelines For 0.1 – 100 MeV Particle Accelerator Facilities.

Individual Research Contribution Review, 2023, 1(1): 537–538

Interpersonal Testing for Internal Exposure Assessment using Thyroid Counter System

Noor Ezati Shuib
Radiation Health and Safety Division
Malaysian Nuclear Agency
43000 Kajang, Selangor
noorezati@nm.gov.my

Abstract

The interpersonal testing was carried out to determine the consistency and reliability of results produced by the operators in assessing internal exposure due to intake to Iodine-131 (^{131}I) using thyroid counter system. A total of 4 operators and a reference operator were participated in the testing. Each operator was given the same case scenario in which they have to monitor the internal intake of ^{131}1 via inhalation by the radiation worker and report the final results in form of committed effective dose (CED). The ORTEC Thyroid Counter and ^{133}Ba standard source having traceability to National Physical Laboratory placed in the neck phantom were used to demonstrate the real case scenario. The results show that all three operators given the CED within the percentage deviation of 0.9% to 8.9% , except one operator. The reason of discrepancy was identified due to misleading in selection of dose coefficient for ^{131}I. The E number was calculated based on the results of CED from 4 operators with the percentage deviation within ± 0.03%. The E number for this testing was considered satisfactory with the result less than 1. Through this work, we are able to identify problems in practice and provide corrective and preventive actions to rectify them. Furthermore, the competency of operator during internal exposure assessment to determine CED of ^{131}I could be verified.

1 Introduction

The annual dose limit for occupational doses from external exposures and the committed doses from intakes of radionuclides is 20 millisievert, mSv as stated in the Basic Safety Radiation Protection (BSRP) 2010 (Malaysia, 2010). The ability to provide adequate protection for radiation workers depends on the effectiveness of risk assessment which directly dependent on monitoring and appropriate dosimetry techniques for radiation exposure. Internal exposure assessment for radiation workers with intakes of radionuclides is important to ensure that the doses received not exceeding the annual dose limit.

Exposure to short-lived ^{131}I radioisotope with half-life of 8.04 days, decays radiation by releasing beta particles at 190 keV and gamma radiation at 364 keV. ^{131}I can be rapidly absorbed into the body through inhalation and ingestion which will accumulate in the thyroid and excreted through urine. Because the retention time of ^{131}I is short, measurement of radionuclide activity should be performed immediately after ingestion as suggested by International Commission on Radiological Protection (ICRP) (ICRP, 2017). Doses for ^{131}I uptake may be calculated from monitoring data by using thyroid counter (IAEA, 2004). The study aims to identify problems in practice and provide corrective and preventive actions to rectify the competency of operator during internal exposure assessment to determine CED of ^{131}I.

2 Methods

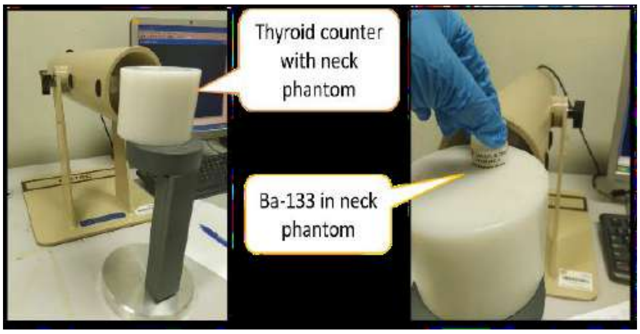

Figure 1: ORTEC Thyroid Counter

The inter-personal testing carried out by 4 technical operators and a reference operator by using ORTEC Thyroid Counter. The detector is equipped with Renaissance software. Each operator requested to perform thyroid monitoring using same scenario with standard sources ^{133}Ba in the neck phantom, counting time for 900 s and same distance (17 cm from collimator).

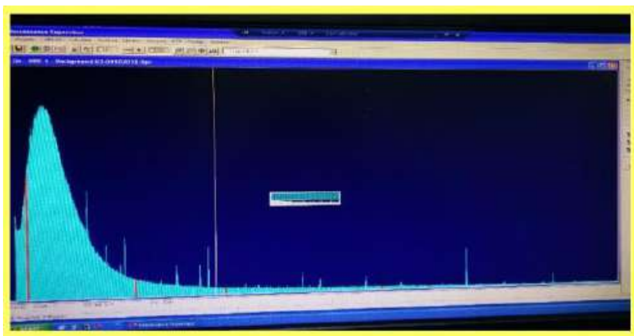

Figure 2: Energy spectrum for thyroid counting by using Renaissance software

The results of committed effective dose for ^{131}I analyzed by using Renaissance software and compared data of all operators with the reference operator. The deviation percentage between each operator should be within ± 10%. The E number then be calculated and result of E that less than 1 considered satisfactory.

3 Results

The results of CED in Table 1 shown that the percentage deviation within ± 10% which ranged from 0.9 to 8.9% as in table above except for operator A5. The overall testing results seem to be satisfactory since the E number less than 1. The unacceptable result was investigated and figured out to be because of wrong selection of peak energy of ^{131}I data analysis and wrong dose coefficient of ^{131}I to determine CED.

Table 1: Result for Interpersonal Testing.

Operator, A_n	**CED (Sv)**	**% deviation of Reference**	**Standard Deviation**	**E Number**
A_1 (Ref)	0.047	-		-
A_2	0.047	0.9		0.001
A_3	0.051	8.9	0.002	0.012
A_4	0.049	3.7		0.005
A_5	0.037	3.1		0.004
Mean	0.048			

4 Discussion

The test shown the consistency and reliable results performed by operators involved in the assessment of internal exposure due to intake of ^{131}I. The performance of all individual operator in evaluating CED due to intake of ^{131}I considered satisfactory. In this study, we are able to identify possible problems that may cause inconsistency and unreliability of results for assessing internal exposure due to intake of radionuclides. The findings and any corrective action documented for future improvement.

5 Conclusion

It was observed that the thyroid counter system used in this study is capable for assessing internal exposure and evaluating committed effective dose due to intake of ^{131}I. Performance of individual operator shown uniformity between all operators involved for the measurement procedures used.

References

IAEA. 2004. Methods for assessing occupational radiation doses due to intakes of radionuclides. Safety Reports Series No.37.

ICRP. 2017. Occupational intakes of radionuclides: Part 3. *ICRP Publication 137*, ICRP 46(3/4).

Malaysia. 2010. Atomic energy licensing regulations (Basic safety radiation protection) 2010.

Individual Research Contribution Review, 2023, 1(1): 539–540

An Overview of Instrumentation for Measuring ^{222}Rn in Environmental Studies

Noor Fadilla Binti Ismail
Radiation Health and Safety Division
Malaysian Nuclear Agency
43000 Kajang, Selangor
fadilla@nm.gov.my

Abstract

Three natural isotopes of radon namely, ^{222}Rn, ^{220}Rn and ^{219}Rn resulting from the radioactive decay of the uranium, thorium and the actinium series. ^{222}Rn is spread as a gas element in the natural radioactive chain of the earth's crust (ICRP, 1993). The presence of ^{222}Rn in the free atmosphere was first noted by Elster and Geitael around 1901 (Althoyaib and El-Taher, 2016). Many studies in Europe and North America confirm that ^{222}Rn gas causes many lung cancers in the general population is ^{222}Rn gas (Althoyaib and El-Taher, 2015). The risk of developing lung cancer increases proportionately to increased exposure to ^{222}Rn gas. Because many people are exposed to low concentrations of ^{222}Rn, most lung cancers with ^{222}Rn are produced at low levels. Thus, it is believed that ^{222}Rn is the second leading cause of lung cancer after smoking (Freyer et al., 2003). In light of the latest scientific data, WHO proposes a reference level of 100 Bqm^{-3} to reduce the health risks of exposure to indoor ^{222}Rn (WHO, 2008).

1 ^{222}Rn Measurements

^{222}Rn measurements are often discussed in terms of either a short-term or long-term test. A short-term test for ^{222}Rn, using a Lucas scintillation cell, activated charcoal detector or another type of detector such as an electret ion chamber, can provide a first indication of the mean long-term ^{222}Rn concentration in a home. However, the daily and seasonal ^{222}Rn changes should be taken into consideration when conducting ^{222}Rn measurements in the short term. Because high ^{222}Rn concentrations usually occur during periods when "houses are closed". Alternatively, a short-term ^{222}Rn measurement conducted during a period when the home has increased ventilation significantly reduces the average annual ^{222}Rn concentration (Eappen, 2010). The most important active methods for ^{222}Rn measurements in air employ the collection of the gas in a scintillation flask/ionization chamber or suction of the gas through a two-filter sampler. On the other hand, progeny levels are measured by collecting them on filter papers and counting for radioactivity at suitable intervals. The major difference in the methods of measurement is that in ^{222}Rn gas estimation using a scintillation cell, the progeny in the sampled air is removed by filtration before the gas is collected in the cell. Active devices used by many countries included electronic fusion devices (EIDs) and continuous ^{222}Rn monitoring devices (CRMs). The passive devices do not require the use of electric power or the pump to operate in the preparation of samples, while the active devices require electricity and include the ability to draw ^{222}Rn concentrations and vibrations during the measurement period.

Table 1: ^{222}Rn gas measurement devices and their characteristics

Detector Type	Passive / Active	Uncertainty[a] [%]	Sampling Period	Cost
Alpha- Track Detector (ATD)	Passive	10-25	1-12 months	Low
Activated Charcoal	Passive	10-30	2-7 days	Low
Electret Ion Chamb	Passive	8-15	5 days - 1 years	Medium
Electronic Integrating Device (EID)	Active	~25	2 days - year(s)	Medium
Continuous Radon Monitor (CRM)	Active	~10	1 hour-year(s)	High

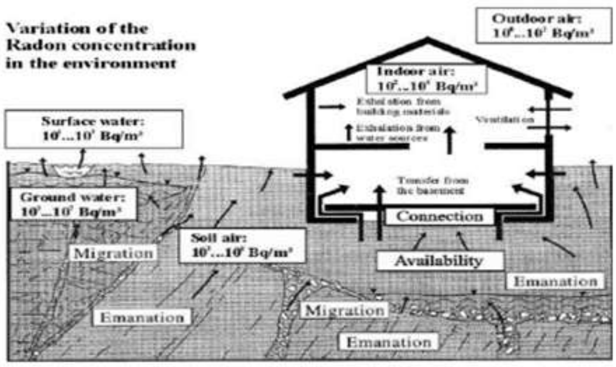

Figure 1: Concentrations of ^{222}Rn in the environment.

2 ^{222}Rn Gas Detectors

The ranges of ^{222}Rn concentrations in environmental samples are given in Figure 1. ^{222}Rn concentrations in surface waters including ocean waters are much lower compared to subsurface groundwater and the methodology of sampling and/or analytical methods often differ. ^{222}Rn concentrations in atmospheric air also are generally low compared to soil air.

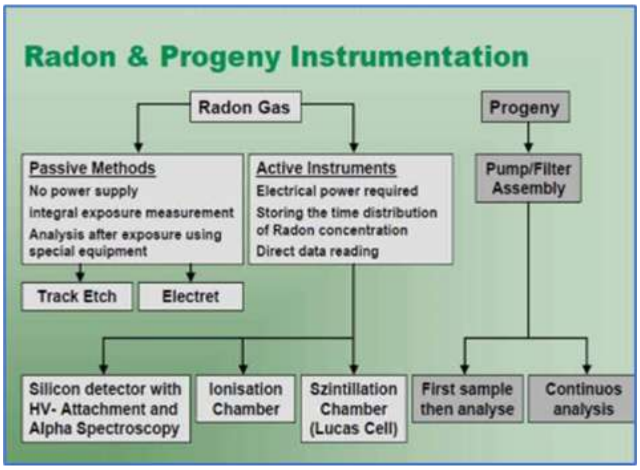

Figure 2: Methods and Instruments to measure ^{222}Rn and its progeny

3 Measurement of ^{222}Rn/^{220}Rn in Water and Air by Durridge RAD7

The RAD7 is a sophisticated quantifying device widely used in laboratories and research work all over the world (Figure 3). The RAD7 is also the simplest computer-driven electronic detector to use, with pre-arranged setups for common practices. It has made to resist day-to-day use in the field. The RAD7 arrives complete, along with a built-in air pump, rechargeable batteries, and a wireless infrared printer.

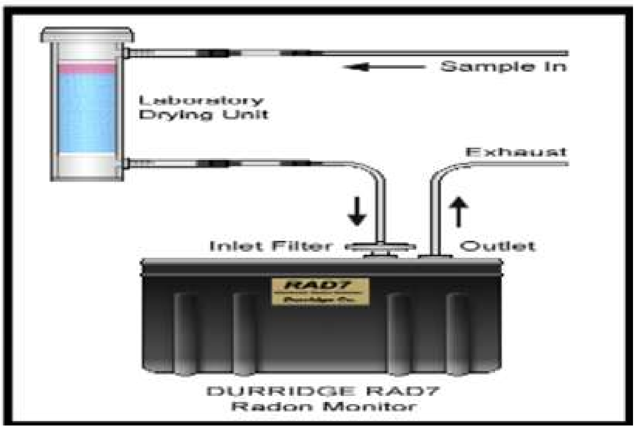

Figure 3: Block diagram of RAD 7

4 Conclusions

A large number of methods have been developed for a measurement of ^{222}Rn. The accuracy of the measurements depends on the applications. The spatial and temporal variation of ^{222}Rn in the middle of the ocean limits the accuracy required. Overall, there is enough.

References

S. S. Althoyaib and A. El-Taher. 2015. The measurement of radon and radium concentrations in well water from Al-Jawa, Saudi Arabia. *J. Radioanal Nucl. Chem.*, 304:547–552.

S. S. Althoyaib and A. El-Taher. 2016. Natural radioactivity levels of radon, radium and the associated health effects in drinking water consumed in Qassim area, Saudi Arabia. *Journal of Environmental Science and Technology*, 9(2):208–213.

K.P. Eappen. 2010. Workshop on 222Rn contamination in groundwater and application of isotopes in groundwater studies. Ministry of Water Resources Government of India, Bengaluru.

K. Freyer, H. C. Treutler, G. Just, and H. v. Philipsborn. 2003. Optimization of time resolution and detection limit for online measurements of 222Rn in water. *Journal of Radioanalytical and Nuclear Chemistry.*, 257:129 – 132.

ICRP. 1993. International Commission on Radiological Protection against Radon-222 at home and at work. ICRP Report 65, Pergamum: Oxford.

WHO. 2008. Guidelines for drinking water quality. 3rd ed. Geneva.

Individual Research Contribution Review, 2023, 1(1): 541–542

Comparison Linearity between Water Phantom and Rod Phantom subjected to X-Ray

Noor Fatin Shuhada Binti Ab Hamid
Radiation Health and Safety Division
Malaysian Nuclear Agency
43000 Kajang, Selangor
fatin@nm.gov.my

Abstract

Safety the most importance part for radiation worker. Dose monitoring not only for human body part. It also extends to fingers and eyes monitoring called extremity dose. The purpose of this study is to compare linearity (absorb dose) for body and fingers using water phantom and rod phantom. This study using dosimeter OSL nanodot. The nanodot are subjected to the X-ray at energy 80 keV. The response plotting the graph dose response against standard dose which are 1, 3, 5, 8 and 10 mSv. It found that both responses show directly proportional to the standard dose.

Keywords: ring dose, extremity dose, rod phantom

1 Introduction

Dose monitoring is one of compulsory to the radiation worker. Usually, all radiation worker used TLD or OSLD batch to measure dose response at body (Hp(10))/ effective dose at 10 mm from the skin surface. However, lately there is radiation worker are handling the radiation directly with the fingers. So, dose at fingers also need to be monitor. This called extremity dose. Extremity dose apply to eyes and fingers called Hp(0.07) means dose at 0.07 mm from the skin surface. The dose limit for extremity is 500 mSv/year. Hence, this study is to compare dose response read by OSL against dose standard and also to compare linearity between water phantom and rod phantom. Water phantom is representing whole body and rod phantom is represent fingers.

2 Methods

a) 33 OSL nanodot dosimeter was annealed to erase previous data. OSL nanodot being annealed using manual annealer for 24 hours.

b) After annealing process, the nanodot was read using its reader; nanodot using MicroStar reader to obtain background reading for the dosimeter.

c) OSL nanodot were placedon water phantom (300 mm x 300 mm x 150 mm) and rod phantom (19 mm x 300 mm) and 1m away from source.

d) Set up apparatus as shown as Figure 1.

e) The exposure time and standard dose as shown as Table 1. The result will be plotting in graph.

Figure 1: Set up apparatus.

Table 1: Exposure time and standard dose

Standard Dose (mSv)	Time (min)
1	3.41
3	6.81
5	17.03
8	25.54
10	34.06

3 Results

Respond dose by nanodot label as measured dose at y -axis and standard dose at x-axis. The data is presenting in graph form. The graph as shown shows the linearity result of nanodot reading for water phantom and rod phantom.

Base on the graph, the orange line representing dose response for rod phantom. While, the orange dot-line representing theoretical linear graph for rod phantom. The blue solid-line representing dose response for water phantom and blue dot-line representing theoretical linear graph for water phantom.

The regression linear as shown in graph in Figure 2.

4 Discussion

The objective of this experiment is to compare the linearity between water phantom or head phantom and ring phantom using OSL nanodot and TLD chip. The experiment starts by annealing 30 OSL nanodots and 30 TLD chips to clear the previous data inside and the background reading of every nanodots and chips obtained using different readers. Next, by labelling each nanodots and chips, they are being exposed

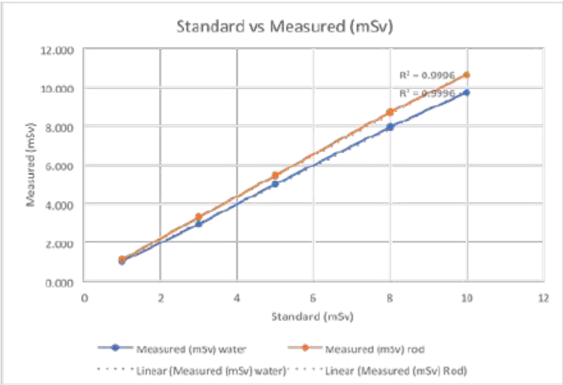

Figure 2: Linearity result of water phantom and rod phantom.

with x-ray for 5 different doses which are 1 mSv, 3 mSv, 5 mSv, 8 mSv and 10 mSv. As the data being read, the linearity graph has been plotted to show the results of this experiment.

As for the result, as for using OSL nanodot, according to the graph (Figure 2), for both water phantom and ring phantom, it clearly shows the linearity, but the ring phantom shows more steeper gradient compared to the water phantom. This could be due to the volume of the phantom itself as the ring phantom having less volume compared to the water phantom. Thus, when checking for surface dose using nanodot, the ring phantom will have higher measured dose compared to when exposed to water phantom. Next, from the graph also it can be seen that the measured dose plotted graph compared to theoretical plotted graph (dotted line in graph (Figure 2)), there is no huge different. This shows that the linearity measured using nanodot is greatly showing the desired results.

5 Conclusion

In conclusion, the result for this project is only can refer to the data from using nanodot and it can be said that the linearity graph of ring phantom having steeper gradient compared to water phantom linearity graph. Both responses show directly proportional to the standard dose.

The measured dose for rod phantom is slightly high compare to water phantom. This is due to volume and shape the phantom. Water phantom represent human body which is the volume and shape is bigger than rod phantom. The measured dose at water phantom low because penetrating energy is low due to high volume or big size.

For further study will be study on TLD and also different type of radiation sources.

References

S. Krim, M. Brodecki, E. Carinou, L. Donadille, J. Jankowski, C. Koukorava, J. Dominiek, D. Nikodemova, N. Ruiz-Lopez, M. Sans-Merce, L. Struelens, and F. Vanhavere. 2011. Extremity doses of medical staff involved in interventional radiology and cardiology: Correlations and annual doses (hands and legs). *Radiation Measurements*, 46(11):1223 – 1227. https://doi.org/10.1016/J.RADMEAS.2011.07.010.

N. Landauer. 2022. OSL dosimeters — Inlight systems. NAGASE LANDAUER, LTD. Nagase-Landauer.co.jp.https://www.nagase-landauer.co.jp/english/inlight/dosimeters.html.

Stanford University. Retrieved September 30, 2021,. Radiation protection guidance for hospital staff – Stanford environmental health safety. (n.d.). https://ehs.stanford.edu/manual/radiationprotectionguidance-hospital-staff/maximum-permissible-occupational-doses.

Individual Research Contribution Review, 2023, 1(1): 543–544

Lead Equivalent Test for locally made Syringe Container Using for Nuclear Medicine

Norriza Mohd Isa
Radiation Health and Safety Division
Malaysian Nuclear Agency
43000 Kajang, Selangor
norriza@nm.gov.my

Abstract

Lead syringe shield is almost used in Nuclear Medicine to protect ionizing radiation worker from secondary radiation. However, it has to undergo integrity testing for guaranty the radiation safety before using for medical facility. The aim of the study is to determine of lead equivalent thickness (LET) for four new samples of syringe container shield from a local manufacturer. Six parts of syringe containers were measured by using a Co-57 radiation, a radiation detector and 14 lead sheets with thickness is 0.1 mm. Based on the calibration graph built up, LET for every part of syringes were determine. All the data were collected and analyzed. The results shown LET for mostly part of the samples container were less than 3.0 mmpb but the corner part almost much less than I mmPb.

Keywords: Syringe Container Shield, Lead Equivalent Thickness, Nuclear Medicine

1 Introduction

Lead syringe shield is almost used in Nuclear Medicine as a carrier used by radiation worker to bring syringe contained of radiopharmaceutical in liquid form from preparation room to injection room for giving radiopharmaceutical to patient via injection and drinking. To protect radiation worker from secondary ionizing radiation, the carrier has to undergo integrity testing for guaranty the radiation safety before using in medical facility. The aim of the study is to determine of lead equivalent thickness (LET) for four new samples of syringe container designed by a local company.

2 Methods

How good the test is conducted is depend on the shielding design and material made from. This will ensure that an appropriate radiation source is selected to perform the tests. Because of the size of the carrier quite small, a smaller size of radiation source than carrier size is required in the test. The concept of measurement is based on the attenuation radiation equation which is given:

$$X_t = X_0 e^{-\mu t}$$

where X_0 is dose rate before shielding, X_t is dose rate after shielding, μ is linear attenuation coefficient and t is the thickness of shielding. t can be determined in the study by plotting a calibration graph using 14 lead (Pb) sheets with 1mm thickness for every sheet, 11 mCi Co-57 (122 keV,γ-ray) and Radiation Alert detector with distance 10 cm from each other.

Four different syringe carriers were exposed to the Co-57. Each of syringe carrier were test on 5 parts of the carriers which are top (T), left side (LS), right side (RS), front (F), back (B) and corner sides. The samples and measurement set-up for the test is shown in Figure 1.

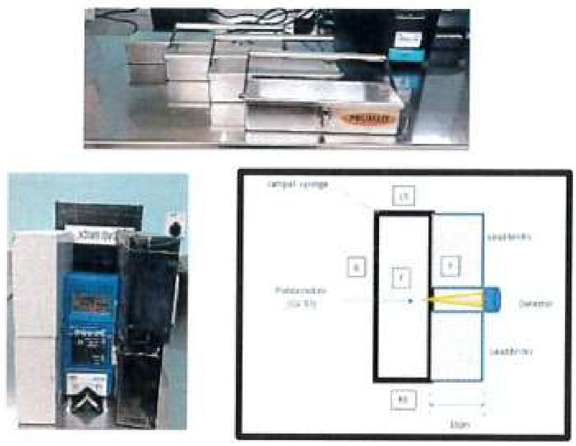

Figure 1: Samples and measurement set-up for the test.

3 Results

The graph of calibration graph using the source and lead sheets is shown in Figure 2.

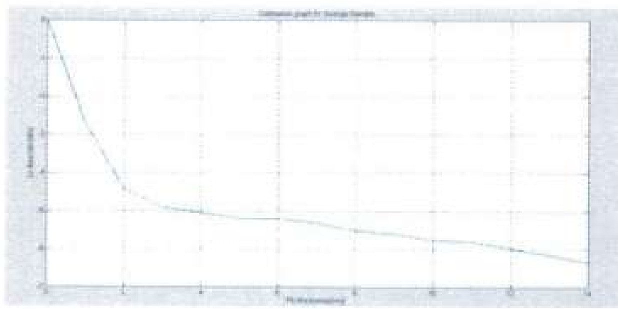

Figure 2: Calibration graph for the Co-57 and Pb sheets.

The lead equivalent thickness (T) for the samples were de-

Table 1: Lead equivalent thickness for the syringe container sample.

Part	Sample (S/N:HKL-RAC-1-1001-22)		Sample(S/N:HKL-RAC-1-1002-22)		Sample (S/N:HKL-RAC-1-1003-22)		Sample (S/N:HKL-RAC-1-1004-22)	
	Xt (uSv/hr)	**T(mmPb)**	**Xt (uSv/hr)**	**T(mmPb)**	**Xt (uSv/hr)**	**T(mmPb)**	**Xt (uSv/hr)**	**T(mmPb)**
F	2.1	**2.95**	1.99	**3.25**	2.17	**2.90**	2.06	**3.02**
B	2.1	**2.94**	2.09	**2.98**	2.36	**2.73**	1.92	**3.49**
LS	3.3	**2.07**	2.96	**2.27**	3.44	**1.99**	2.95	**2.29**
RS	3.3	**2.07**	2.99	**2.25**	3.43	**1.99**	2.95	**2.28**
T	2	**3.16**	1.96	**3.35**	2.04	**3.09**	1.97	**3.32**
C	135	**0.31**	121	**0.42**	129	**0.39**	110	**0.6**

termined by obtaining the exposure net reading after shielding and the calibration graph. The results were represented in Table 1.

4 Discussion

Radioactive source Co -57 with small size was chosen in the test because it will put inside the small sample container carriers. The source was chosen and used in the study because its energy within the range radionuclide energy normally used for diagnosis in Nuclear medicine.

Calibration curve was plotted for the source and a few numbers of lead sheet. The plotted graph decreasing smoothly after additional lead sheets add on with others. These proof that extra x-ray produced from interaction between gamma ray and material of sample which is Compton Scattering were fully block by the lead sheets.

Small portion parts of the samples were penetrated by the radiation. For that, the radiation from the source was collimated by using of lead bricks in order to reduce scattered radiation that can affect the accuracy of result of the study.

Lead equivalent thickness of samples were determined based on the calibration graph when net readings of dose rate from the sample were obtained through calculation.

Based on the data analysis most part of sample carriers is less than 3.0mmPb, but not obviously different each other except corner part. This is because the corner parts were not sealed nicely and completely overlapped with lead equivalent material by the manufacturer.

Only T part of all samples, F part for sample 2 and sample 4 and B part for sample 4 were larger than 3.0mmPb. These parts achieved the goal target of manufacturer for his/her product.

5 Conclusion and attention

Lead equivalent thickness for the samples were not represent obvious different each other's. Generally, only the top layers of the sample carriers were good agreement with manufactory goal which at least more than 3.00mmPb.

Base on the result and physically observation, notice that the products were sealed with lead equivalent material manually. Therefore, it is recommended to fabricate these products using mold technique to ensure all part of carriers lead material is uniform distribution with enough thickness to reduce the radiation to the acceptable level for radiation worker.

References

D. Delacroix, J. P. Guerre, P. Leblanc, and C. Hickman. 2002. Radionuclide and radiation protection data handbook. *Radiation Protection Dosimetry*, 98(1).

IAEA. 2006. Nuclear medicine resources manual. STI/PUB/1198 IAEA, Vienna.

IAEA. 2018a. Radiation protection and safety in medical uses of ionizing radiation. IAEA Specific Safety Specific Safety Guide No. SSG-46, IAEA, Vienna.

IAEA. 2018b. Safety standards: Occupational radiation protection. IAEA Safety Standards Series No. GSG-7, IAEA, Vienna.

Norman B. Levit and Mary Ogiela-Bazner. 1979. Evaluation of shielded syringe carriers for transporting radioactive dosesy. *Journal of Nuclear Medicine Technology*, 7(4).

Ellinor Busemann Sokole, Anna Plachcinska, and Alan Britten. 2010. Acceptance testing for nuclear medicine instrumentation. *Eur J Nucl Med Mol Imaging*, 37:672— 681 DOI 10.1007/500259–009–1348–x.

Individual Research Contribution Review, 2023, 1(1): 545–546

Dose Mapping using Thermoluminescence Dosimeter (TLD) and Geographical Information System (GIS) Tool for Long Term Storage Facility (LTSF), Bukit Kledang, Perak, Malaysia

Nur Khairunisa Zahidi
Radiation Health and Safety Division
Malaysian Nuclear Agency
43000 Kajang, Selangor
khairunisa@nm.gov.my

Abstract

Dose mapping is one of the methods used to identify the dose distribution in any radiation facility. This study aims to visualise dose distribution at Long Term Storage Facility (LTSF), Bukit Kledang using thermoluminescence dosimeter (TLD) by Geographical Information System (GIS). A total of 50 point were identified at LTSF for dose mapping using passive measurement, thermoluminescence dosimeter (TLD). TLD chips undergo anneal process before using, installed at dedicated location, exposed for one month and analysed using TLD reader at Secondary Standard Dosimetry Laboratory (SSDL), Malaysian Nuclear Agency. The obtained results showed, the average cumulative dose per month and annual dose ranged from 0.04 — 0.16 and 0.08 — 0.38 respectively. The results showed that there were no significant increase as compared to previous continuing environmental programme (EMP) in 2017 and the annual dose is also below the stipulated limit for public by Atomic Energy Licensing Board (AELB).

Keywords: Long Term Storage Facility (LTSF), thermoluminescence dosimeter (TLD), Geographical Information System (GIS)

1 Introduction

Environmental surveillance is an important component of the verification system to verify that the controls on the releases of radioactive substances to the environment are functioning under normal working conditions (IAEA, 1982). The previous site license holder of the repository facility is Asian Rare Earth (ARE) Sdn Bhd. ARE is a joint venture between Malaysians and Japanese, which was incorporated in Ipoh on November 23, 1979 and began operating in May 1982, its function being to extract rare earths from monazite sand, a residue of tin mining (Wagner et al., 1989). Monozite sand contains rare earth and the radioactive element thorium. Prior to be collected for further processing, piles of monazite are found throughout the environments of Ipoh in amang factories. Amang is the residue of mixed minerals that remains in sand after the extraction of tin. After extraction rare earth completed, the concentration is twice original content, 12%. The final residue is treated as radioactive waste and stored in controlled area known as LTSF. The surrounding community believes that the study area is hazardous and provides additional external radiation. The main objective of this paper is to establish the dose mapping for LTSF, Bukit Kledang for better understanding of dose distribution in mentioned area.

2 Methods

This study has been carried out at the LTSF, Bukit Kledang, Perak which is located at Mukim Blanja and ~15km driving from Ipoh town. A total 50 points were identified at on-site LTSF and 3 points off-site LTSF and act as a control for this study. Dosimeter box were placed at 1-metre-high at specified location. Each thermoluminescence dosimeter (TLD) undergo annealing process using anneal oven and were placed in dosimeter box for one (1) month. The TLD chips were analyzed using TLD reader at Secondary Standard Dosimetry Laboratory (SSDL), Malaysian Nuclear Agency. The average cumulative dose for each point were visualised by colour using GIS tools. The Inverse Distance Weighted (IDW) technique is used to interpolate dose at LTSF, Bukit Kledang Perak. IDW estimates unknown values with specifying search distance, closet point, power setting and barriers (GISGeography, 2022). The annual dose is calculated using the following equation:

$$\text{Annual effective dose (mSv)} = D \times 12 \times 0.2$$

where,
D: Average cumulative dose in mSv/month,
12: month in a year
0.2: external occupancy factor

3 Results and Discussion

The minimum and maximum average dose per month and per year is 0.04 and 0.16, respectively. The data shown is compared with the previous monitoring using the same passive measurement. In the previous environmental program of continuing EMP for LTSF Bukit Kledang Perak in 2017, the average dose per month ranged between 0.18 - 0.82 at on-site and off-site monitoring station (MB Inc. Perbadanan Menteri Besar Perak, 2019) thus the data shows no remarkable increase of average dose per month at LTSF Bukit Kledang, Perak. Based on Figure 1, the maximum annual dose and the average annual dose is 0.38 and 0.24 ± 0.06 mSv, respectively. The value shown is below the dose limit for public member, 1 mSv/year as stipulated by AELB (IAEA, 2010). There is no similar research related to this study in other country. However, there is one study in German regarding the radiation dose level at fence with additional cask in the repository facility since 1997 until 2011 and the maximum annual dose found to be 0.22 mSv (L. et al., 2013). The results from this study are similar as in Germany repository facility study where the annual dose at fence of LTSF Bukit Kledang is ranged between 0.16 to 0.22 mSv annually.

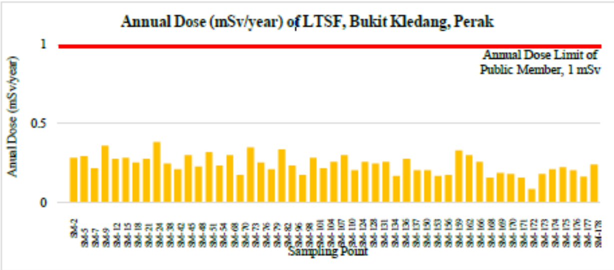

Figure 1: Annual dose (mSv/year) at LTSF Bukit Kledang, Perak and dose limit for public member.

4 Conclusion

The measurement of 50 points at on-site LTSF using TLD were analyzed by monthly basis in each sampling. The maximum annual dose and the average annual dose is 0.38 and 0.24 ± 0.06 mSv, respectively. The value shown is far compared to the dose limit for public member, 1 mSv/year as stipulated by AELB (IAEA, 2010).

References

GISGeography. 2022. Inverse Distance Weighting (IDW) Interpolation. https://gisgeography.com/inverse-distanceweighting-idw-interpolation/.

IAEA. 1982. Nuclear Power, The Environment and Man.

IAEA. 2010. Basic safety radiation protection regulations. Atomic Energy Licensing Act 1984. IAEA, Vienna.

Oelschlager L., M Heck, and Graf W. 2013. GNS Experience on the long-term storage at dry interim storage facilities especially in Ahaus And Gorlebem. Safety of long-term interim storage facilities. Workshop Proceedings Munich. Germany.

Wagner, Henry N, Ketchum, and Linda. E. 1989. Living with radiation. London: The John Hopkns University Press L.

Individual Research Contribution Review, 2023, 1(1): 547–548

Self-Assessments of Safety Culture in Malaysian Nuclear Agency using Safety Culture Perception Questionnaire for License Holder

Raymond Yapp Tze Loong
Radiation Health and Safety Division
Malaysian Nuclear Agency
43000 Kajang, Selangor
raymond@nm.gov.my

Abstract

Safety Culture Perception Questionnaire for License Holder (SCPQ-LH) is one of the data collection methods, developed by IAEA to assess safety culture in a facility. This study is conducted to understand the safety culture in Nuklear Malaysia. 70% of the staff works in Nuklear Malaysia had responded to the SCPQ-LH. The results showed that 74% of the respondents agree that Nuklear Malaysia has a strong safety culture.

Keywords: Safety culture, descriptive analysis

1 Introduction

"Safety culture" is a combination of two concepts, which consist of "safety" and "culture". The International Atomic Energy Agency (IAEA, 2016) define safety culture as the assembly of characteristics and attitudes in organizations and individuals which establishes that, as an overriding priority, protection and safety issues receive the attention warranted by their significance.

Safety culture is recognized as the key component of nuclear safety performance. History has proved that lack of strong safety culture in an organization or individual have contributed to catastrophic nuclear accidents (National Academy of Sciences, 2014, Obu and Fukano, 2011) such as Three Mile Island's accident in 1979, Chernobyl's accident in 1986 and, the recent Fukushima Daiichi nuclear power plant accident in 2011. Thus, safety culture must be improved in order to protect the worker, public and environment.

This article aims to provide the finding of safety culture among the staff working in Nuklear Malaysia.

2 Methods

The questionnaire is fully adapted from IAEA SCPQ-LH working document (IAEA, 2017). The questionnaire was translated to Bahasa Melayu by the Information Management Division.

Both English and Bahasa Melayu questionnaire is circulated via intranet system in Nuklear Malaysia for one (1) month. The identity of the respondent remained anonymous to ensure the freedom of expressing views in terms of safety culture in Nuklear Malaysia and the data collected is analysed using descriptive analysis.

3 Results and Discussion

The Figure 1 shows the overall result of the survey from the staff working in Nuklear Malaysia. The scale is range from 1 – 7 representing from strongly disagree (1) to strongly agree (7).

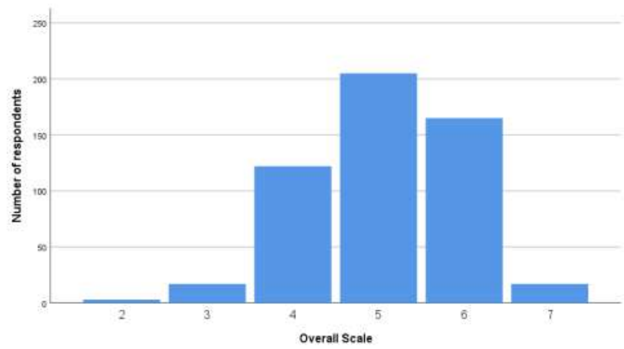

Figure 1: The overall result of the survey from the staff working in Nuklear Malaysia

The result show about 74% of the respondents agree that Nuklear Malaysia has a good safety culture, about 23% of the respondents neither agree or disagree, and about 3% of the respondents do not agree that Nuklear Malaysia has a good safety culture. The overall result is further analyzed with different division. Figure 2 shows the overall result of the survey from different division.

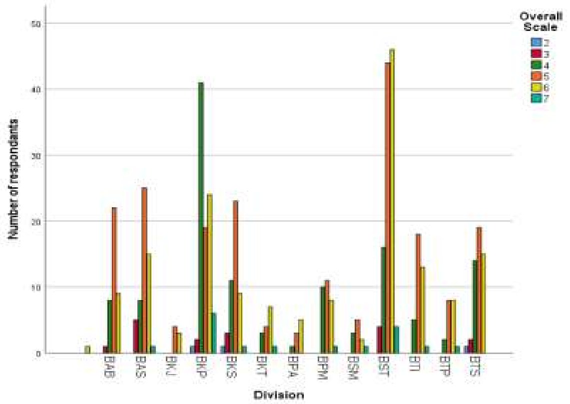

Figure 2: The overall result of the survey from different division

According to Figure 2, the results shows good agreement between divisions in Nuklear Malaysia that strong safety culture is practiced, except for BKP, where majority of the staffs who worked in BKP neither agree or disagree on the safety culture practiced in Nuklear Malaysia. This may be due to the nature of work in BKP, where most staff deal with administrative work and is not involved very much in research, development and technical work.

4 Conclusion

SCPQ-LH was successfully performed in order to understand the degree of safety culture in Nuklear Malaysia. The result shows that strong safety culture is practiced in Nuklear Malaysia. The results can be used as an initial understanding of the safety culture in Nuklear Malaysia and further studies including independent assessment: interviews, observation, focus groups and document reviews should be conducted to support the findings in this study.

References

IAEA. 2009. The management system for nuclear installations. Safety Standards Series No. GS-G-3.5, Vienna, Austria.

IAEA. 2016. Performing safety culture self-assessments. Safety Report Series No. 83, Vienna, Austria.

IAEA. 2017. IAEA Safety culture perception questionnaire for license holders. Working document, Vienna, Austria.

INSAG. 1992. INSAG-7 The Chernobyl accident: Updating of INSAG-1. Safety Series No. 75-INSAG-7, IAEA, Vienna, Austria.

Etsuji Obu, Jun Hamada, and Takuya Fukano. 2011. Considering lessons learned about safety culture and their reflection to activity. After Fukushima Daiichi nuclear power plant accident experience. *Journal of Japan Society for Safety EngineeringI*, 50(6):396 – 401.

National Academy of Sciences. 2014. Lessons learned from the Fukushima accident for improving safety of U.S. Nuclear plants. Washinton D.C., United States of America.

Individual Research Contribution Review, 2023, 1(1): 549–550

Standardization of Dose Rates for Gamma Source (Cobalt-60) in Therapy Bunker

Rozaimah Binti Abdul Rahim
Radiation Health and Safety Division
Malaysian Nuclear Agency
43000 Kajang, Selangor
rozaimah@nm.gov.my

Abstract

Standardization of the Dose Rate for the gamma source (Cobalt-60) in the Therapy Bunker, was carried out before and after the replacement of the gamma source from 80 Curie to 2800 Curie as well as after the modification in the bunker (installation of lead shield).

Keywords: dose rate, ion chamber

1 Introduction

In RMK12, SSDL is given procurement allocation to replace the gamma source (Cobalt-60) which has low activity. In early 2023, the old Cobalt-60 source (80 Ci) was successfully replaced with a Cobalt-60 source, 2800 Ci. This acquisition is important to performance the calibration activity of customer therapy dosimeters used in the medical field.

In order to meet the requirements of ISO 17025, the standardization of gamma source dose rates should be implemented after gamma source changes or modifications in the therapy bunker.

Standardization of the dose rate of the gamma source was implemented after the replacement of the new Co-60 source and the installation of the lead shield. This aims to test the performance of Co-60 for gamma radiation protection by using the existing primary standard ionization chamber. Dose rate standardization is also important for high-dose dosimeter irradiation work (eg: Fricke, Ceric-cerius) and samples from customers/students.

2 Method

This Co-60 performance test was conducted using an NE 2581 ionization chamber attached to a PTW Unidos Webline T10021 electrometer for display readings. The ionization chamber is placed in line with the Cobalt-60 source and at a distance of 80 cm from the radiation source. The electrometer is turned on and in standby mode for 30 minutes beforehand. Next, the gamma source is turned on using the Eldorado 8 control panel.

The electrometer will read the electric charge every 60 seconds for one reading.

The reading will be taken 5 times. This step will be repeated at a distance of the ionization chamber position of 100 cm, 200 cm, 300 cm, 400 cm and 500 cm from the gamma source.

This performance test was also carried out before the replacement of the Co-60 gamma source using the same method as above.

Figure 1: Tool Set-up

Dose rate calculation;

Kerma (mGy/min) = electric charge (nC/min) × Nk × Ktp

3 Result

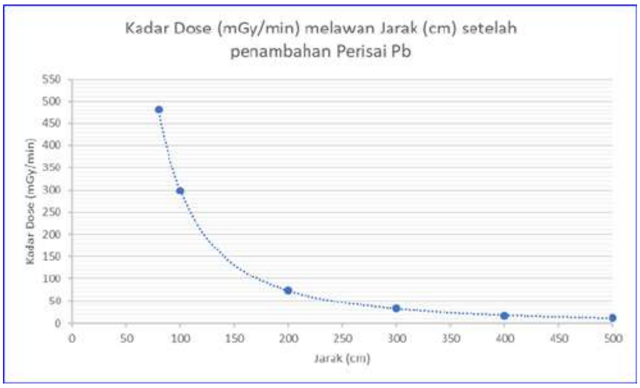

Figure 2: Dose rate (mGray/min) versus Distance (cm) in the therapy bunker (Co-60, 1845.50 Ci)

4 Discussion

Figure 3 shows the results of the dose rate measured before and after the replacement of the Co-60 source and after installation of lead shield. Dose rates tend to decrease as distance increases and gamma source activity decreases.

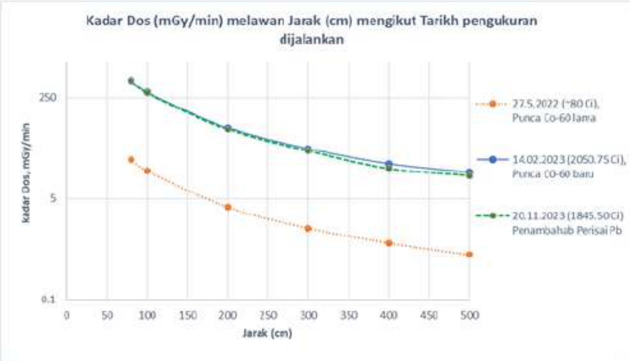

Figure 3: Dose rate (mGray/min) against Distance (cm) in the therapy bunker before and after the replacement of the Co-60 gamma source and after the modification in the therapy bunker (installation of lead shield).

The dose rate graph shows the same pattern for all three conditions, (before and after the replacement of the Co-60 source and after installation of lead shield).

5 Conclusion

Cobalt-60 gamma source irradiation performance is satisfactory and meets the requirements of ISO 17025 for customer therapy dosimeter calibration work.

Automatic calculation of the dose rate according to a certain date has been developed using excel software and restore in shared folder \\nas3\home5\Bunker\Data\\BUNKERTERAPI.

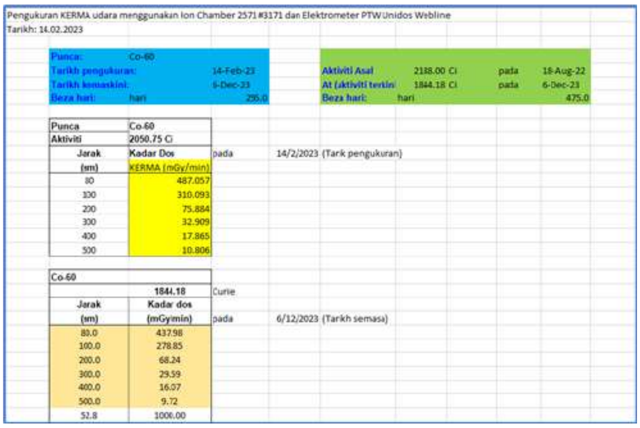
Pengukuran KERMA udara menggunakan Ion Chamber 2571 #3171 dan Elektrometer PTW Unidos Webline
Tarikh: 14.02.2023

Punca:	Co-60	
Tarikh pengukuran:		14-Feb-23
Tarikh kemaskini:		6-Dec-23
Beza hari:	hari	295.0

Aktiviti Asal	2188.00 Ci	pada	18-Aug-22
At (aktiviti terkini	1844.18 Ci	pada	6-Dec-23
Beza hari:	hari		475.0

Punca	Co-60		
Aktiviti	2050.75 Ci		
Jarak (sm)	Kadar Dos KERMA (mGy/min)	pada	14/2/2023 (Tarik pengukuran)
80	487.057		
100	310.093		
200	75.884		
300	32.909		
400	17.865		
500	10.806		

Co-60			
	1844.18	Curie	
Jarak (sm)	Kadar dos (mGy/min)	pada	6/12/2023 (Tarikh semasa)
80.0	437.98		
100.0	278.85		
200.0	68.24		
300.0	29.59		
400.0	16.07		
500.0	9.72		
52.8	1000.00		

Figure 4: Dose rates (according to current date))

Next, the appropriate period of time and distance can also be predicted to obtain the desired radiation dose.

Using the therapy bunker with the new Co-60 source, a shorter period of time can be implemented for irradiation work that requires a high dose such as Fricke and Ceriou-cerius Dosimeter irradiation (for the purpose of high-dose dosimeter quality control).

However, low dose irradiation work is no longer suitable to be carried out in this therapy bunker.

References

IAEA. 2000. Absorbed dose determination in external beam radiotherapy. In Technical Report Series No. 398:pages 1–229, Vienna Austria: IAEA.

Individual Research Contribution Review, 2023, 1(1): 551–552

Environmental Solar Ultraviolet Radiation (UVR): Case study Of several locations in Bangi, Cyberjaya and Putrajaya

Shamesh Raj Parthasarathy
Radiation Health and Safety Division
Malaysian Nuclear Agency
43000 Kajang, Selangor
shamesh@nm.gov.my

Abstract

Everyone is exposed to Ultraviolet Radiation (UVR) from the sun and the irradiance from the sun is by far the strongest source of UVR in our environment. Solar emissions include visible light, infrared (IR) and UVR. The UV radiation spectrum is divided into three regions called UVA, UVB and UVC. The UV region covers the wavelength range from 100nm to 400 nm and is divided into three bands; namely UVA (315-400 nm), UVB (280-315 nm) and UVC (100-280 nm). These three types of UV radiation are classified according to their wavelength and they differ in their biological activity and the extent to which they can penetrate the skin. For this study, the UVR measurement and assessment was conducted at several locations around Bangi, Cyberjaya and Putrajaya utilizing the spectrometer and the UV radiometer. The results from the measurement will be presented in solar irradiance and UV Index (UVI).

1 Introduction

UVR has been a public concern for quite some time. UV has many benefits to human, however over exposure to UVR may cause health risks. This includes our skin and eyes. Safety precautions need to be considered. This research includes analysing irradiance of the sun, hazard analysis and safety assessment. However, this research does not include effects of UVR to human's health. The objectives of the research are to determine the irradiance of the natural UV sources and to analyse the safety level of solar ultraviolet radiation (UVR).

2 Methods

Spectrometer is an instrument used to measure a physical characteristic's variation over a given range. When light enters the optical bench through a sensor which is standard SMA-905 connector and is accumulate by a spherical mirror. A plain grating diffracts the accumulated light after which a second spherical mirror focuses the resulting diffracted light. An image of the spectrum is projected onto a 1-dimensional linear detector array. Apparatus are setup as shown in Figure 1. SMA connectors will be connected to spectrometer. Plastic protection cap should be gently removed from the fibre SMA connectors. The optical fibre needs to be checked whether it transmit light. Light will transmit through the sensor from SMA connector and reflect it to spectrometer. The readings will be converted to the laptop by connecting spectrometer to the laptop using fibre cable. Sensor of SMA connectors should be placed directly to the sun. UV radiometer should be placed as shown in Figure 1. Sensor that is connected with the UV radiometer should be the same model. Sensor of UV radiometer should be placed directly to the sun. Data will be recorded from 8 am until 6 pm for every 30 minutes at selected locations in Bangi, Cyberjaya, and Putrajaya.

Figure 1: Set up of equipment for measuring the solar irradiation and UV Index

3 Results

The recorded solar irradiance was converted to the UV Index (UVI) and the results are shown from Figure 2 to Figure 4.

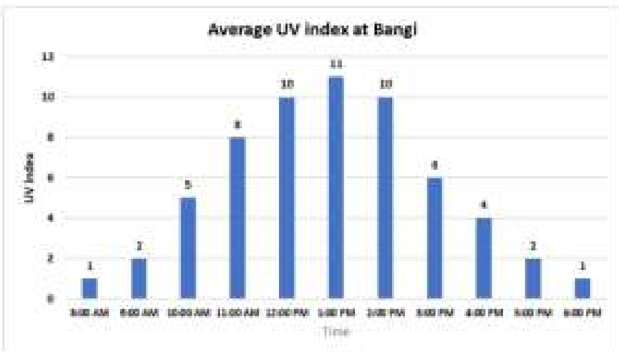

Figure 2: Average UV index at Bangi

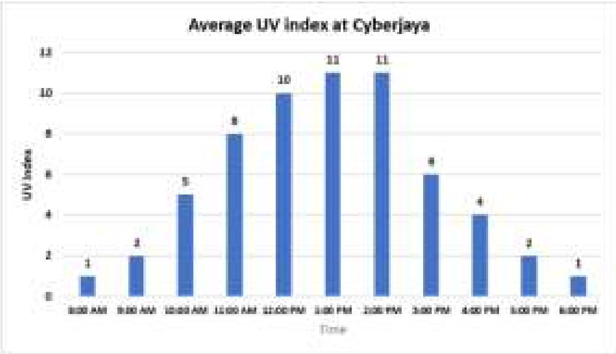

Figure 3: Average UV index at Cyberjaya

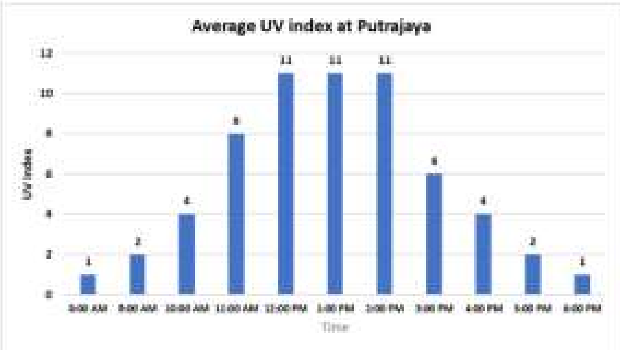

Figure 4: Average UV index at Putrajaya

4 Discussion

The irradiance was observed to drop abruptly on days when there was cloud cover. Generally, the irradiance was observed to be low from 8am till 10am. The irradiance starts to increase from 10am onwards with the highest recorded from 12pm to 2pm. The wavelength recorded from the measurement was from the 280nm to 1100. The intensity of the wavelength from the solar irradiance was at the highest at UVA (315-400nm) and UVB (280-315nm) at mid-day. However, there are some limitations during cloudy and rainy days as they can affect the measurement.

The observations from these results are in conformity with the generally observed trends in UV intensity as the peak values of the measured UV index and intensity were detected about the mid hours of the day. Therefore, people should minimize outdoor activities during this time of the day. Precaution measures need to be taken for people who needs to be outside during high UVI generally from 12pm until 2pm.

5 Conclusion

In conclusion, the measurements of solar UV radiation showed that the intensities of UVR reaching the earth ranged from the wavelength from 280nm to 1100nm as detected from this spectrometer. This research also has pointed out that, a highly exposed solar radiation happens during mid hours of the day which is from 12pm to 2pm. There are also some limitations occurred during measurement due to the cloudy and rainy days which resulted in some measurements could not be performed.

It is essential for the public to be advised on the hazards of solar UV radiation. The effect to the eyes is also seen to be more significant than that to the skin. As such it will be wise to spend as minimal time as possible under the sun or to use protective clothing and sunscreens to minimize hazards to the exposure. Thus, implementation and awareness about global solar radiation needs to be expanded to each country in the world to prevent the public from being affected by various disadvantages and harms due to the overexposure to the solar radiation.

References

D. K. Kaki, N. B. Akaagerger, and V. K Gyaase. 2017. Assessment of solar ultraviolet radiation level in Makurdi, Benue State.

World Health Organization. 20 June 2022. Radiation: The ultraviolet (UV) index. https://www.who.int/news-room/questions-andanswers/item/radiation-the-ultraviolet-(uv)-index.

H. Remus, M. Wittlich, S. Malte, R. Brans, G. Sorin, C. Salavastru, S. Toader, R. Corneliu, E. Fugulyan, G. Horvath, A. Alexa, and A. Irina. 2020. Exposure to solar UV radiation in outdoor construction workers using personal dosimetry.

Individual Research Contribution Review, 2023, 1(1): 553–554

Hand-Held Laser Safety Assessment and Hazard Analysis

Shamesh Raj Parthasarathy
Radiation Health and Safety Division
Malaysian Nuclear Agency
43000 Kajang, Selangor
shamesh@nm.gov.my

Abstract

In this study, the hazard levels of the Hand-held Lasers were determined according to the ANSI Z136.1 and IEC 60825.1 standard. The objective of this study is to first and foremost, determine the wavelength and power of the stated Lasers and compare with the one labelled in the respective label. From the output power measured, the irradiance of each Hand-held Lasers was calculated and compared with the MPE. Finally, a laser hazard evaluation was performed.

1 Introduction

Hand-held Laser consists of variety of colours with different wavelength. The most common ones come in blue with wavelength of 405 nm, green with a wavelength of 532 nm and red with wavelength of 650 nm. Lasers have many benefits in human's lives. However, it can also bring major threat if it was not used wisely. This is because, high-powered lasers may damage our skin and eyes. With just a click of a button, it can either be helpful for human's lives or it can be a threat to human's health. Lasers are not only used by adult, but it can be easily accessed by children which posed more threat because children only see those lasers as toys. Human eye can transmit and focus on light with range wavelengths of 400 to 1400 nm with an optical concentration power of approximately 100,000. In the visible spectrum (400-700nm), the human aversion response to bright visible light can generally be relied upon to protect against potential injury from Class 3R laser with power limit 5mW. However, the aversion response cannot be relied upon for nearinfrared (IR) wavelengths (700-1400nm) where the human eye is less sensitive.

2 Methods

For the purpose of this study, 100 Hand-held Lasers of various types, ranging from presenter, small to medium sized pointers, and USB type were purchased from provision stores, supermarkets and from the online platform within Malaysia. The Hand-held Laser were further divided into 3 range of wavelength Blue (400-420nm), Green (530-550 nm) and Red (650-660nm). The Hand-held Lasers were labeled varying from with output power less than 1 mW up to less than 50,000 mW. The measurement equipment to determine the wavelength and output power of the Hand-held Lasers consists of a Laser Power meter system and a Spectrometer system. The laser power meter system comprises of Ophir Laser Power Meter attached with thermal power sensor. The detector is capable to measure optical power in continuous wave from 100 microWatts up to 10 Watts as shown in Figure 1.

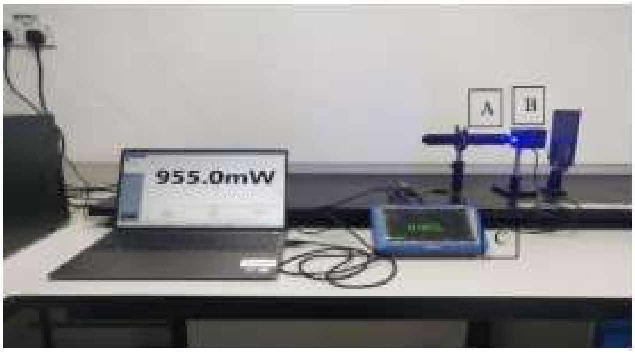

Figure 1: Set up for measuring the output power of Lasers (A) Hand-held Laser (B) Sensor (C) Laser Power Meter

3 Results

The irradiance of each wavelength, Blue, Green and Red is shown respectively in Figure 2, Figure 3 and Figure 4.

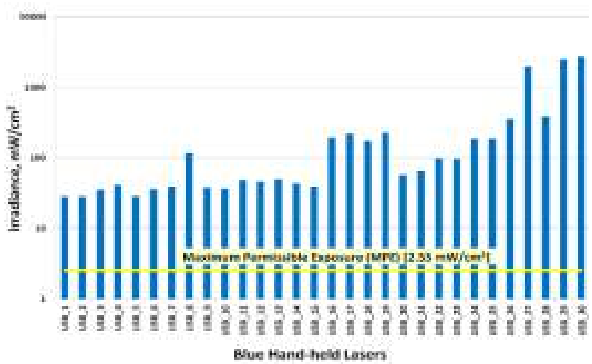

Figure 2: Irradiance of each Blue Hand-held Lasers and comparison with the MPE for the eye.

4 Discussion

4.1 Maximum output power and peak wavelength

The output power and wavelength were compared with the one labeled in the Hand-held Laser, and it was found that 96%

Figure 3: Irradiance of each Green Hand-held Lasers and comparison with the MPE for the eye.

Figure 4: Irradiance of each Red Hand-held Lasers and comparison with the MPE for the eye.

of the stated lasers were emitting higher output power value and 58% of the Lasers were displaying different wavelength compared to the value labeled by the manufacturer.

4.2 Maximum Permissible Exposure (MPE)

Based on the maximum output power recorded from each Hand-held Laser, the irradiance in terms of miliwatt per centimeter squared (mW/cm^2) was calculated and compared with the Maximum Permissible Exposure (MPE) for the eye. The MPE for the eye for the visible wavelength was obtained from the ANSI Z136.1-2022 standard. Based on the computation, it was observed that 97 out of 100 or 97% of the Hand-held were emitting radiation above the MPE of 2.55mW/cm^2 . The highest irradiance was from the USB type Hand-held Blue wavelength emitting at 1059 mW which was producing an irradiance of 2751.36 mW/cm^2.

4.3 Laser Hazard Evaluation

Based on this study it was found that 97% of the Hand-held Lasers are hazardous to the human eye. It should be noted that the wavelength from 400nm to 1400nm is a retinal hazard to humans. Although natural protective mechanisms such as the blink reflex and aversion response limit the duration of laser exposure, the stated mechanisms may fail to protect the eye against a high-powered Lasers, thereby inducing mild to severe retinal damage.

5 Conclusion

From this study on the 100 Hand-held Lasers from the Blue, Green and Red wavelength, 96 were emitting higher output power value and 58% were displaying different wavelength value compared to the value labelled by the manufacturer. On the whole, 97% of the Lasers were emitting above the Maximum Permissible Exposure (MPE). Safety issues regarding Hand-held Lasers and their hazards are the main concern as reflected from this research. From this study, it is recommended that users should purchase low powered Lasers such as the units with less than 1mW of power. It is advisable to expand the knowledge about lasers to the public so they will have awareness about the hazards of laser radiation to the eye and skin. Especially, children should always be supervised by parents to avoid using lasers as they will use the laser as a toy. This may not only bring harm to them but also people around them. In short, everyone should play a crucial part in ensuring safe usage of Hand-held Lasers.

References

Jemellie Galang, Alessandro Restelli, Edward W. Hagley, Joshua Hadler, and Charles W. Clark. 2011. A green hand-held laser hazard. Laser Institute of America. ILSC.

ICNIRP. 2013. ICNIRP Guidelines on limits of exposure to laser radiation of wavelengths between 180nm and 1000μm. 105(3).

David H. Sliney and James A. Hathaway. 2017. Laser radiation. Chapter 14.

ANSI Z136.1. 2022. American national standard for safe use of lasers.

Individual Research Contribution Review, 2023, 1(1): 555–556

Development of Nuclear Forensic in Malaysian Nuclear Agency

Suzilawati Muhd Sarowi
Radiation Health and Safety Division
Malaysian Nuclear Agency
43000 Kajang, Selangor
suzie@nm.gov.my

Abstract

Nuclear forensic is a key element in nuclear security in any country. The result of the nuclear forensic analysis helps law enforcement identified the history and origin of nuclear or radioactive material found outside regulatory control. Thus, it is crucial for the development of nuclear forensic laboratory and personnel to clearly understand the process and procedure when conducting a nuclear forensic investigation. This paper presents the development of nuclear forensic including the process flow in the Malaysian Nuclear Agency (Nuclear Malaysia). The role of Health Physic Group (HPG) will also be discussed when handling the nuclear forensic case at the agency Nuclear Malaysia.

Keywords: Nuclear forensic, Framework, Role

1 Introduction

Nuclear forensic is the comprehensive scientific analysis of nuclear or other radioactive materials or evidence contaminated with radionuclides that are discovered outside regulatory control (Ball et al., 2015). From the nuclear forensic analysis, it can identify what the materials are, how, when, and where the materials were made, and what their intended uses (IAEA, 2015). Therefore, nuclear forensics is an important tool in nuclear security (Kristo, 2016). Nuclear security aims in preventing and detecting of and respond to theft, unauthorized access, illegal transfer, or other malicious acts involving radioactive or nuclear material It was reported that as of 31 December 2022, a total of 4075 incidents involving unauthorized activities and events of nuclear and other radioactive material, including incidents of trafficking and malicious use (IAEA, 2023). Although Malaysia is not involved in producing or processing of nuclear materials, it is crucial for Malaysia preparing the nuclear forensic capabilities.

2 Methods

In 2016, Malaysia carried out an International Atomic Energy Agency (IAEA) expert mission on the assessment of Malaysia's capability in nuclear forensics. During the IAEA expert mission, Nuclear Malaysia learned that the nuclear forensic could be developed in the agency. Nuclear Malaysia already has an infrastructure that capable of being mobilized for nuclear forensic purposes (Smith, 2016).

3 Results

From the expert mission carried out in 2016, Nuclear Malaysia determined the existing nuclear facilities and instruments that could be used and found that nuclear forensic is integration and collaboration among several laboratories. Identified laboratories that could be used in nuclear forensic case together with the task is describe in Table 1.

Table 1: Identified technical laboratories and their task for nuclear forensic analysis.

No.	Laboratory	Task
1.	Health Physic Group (Radiation Safety and Health)	Secretariat
2.	Radiochemistry and Environment Laboratory Analytical Chemistry Application Laboratory (Waste and Environmental Technology Division)	Radio analytical measurement and chemical analysis
3.	Material Technology Laboratory Micro Computed Tomography Laboratory (MicroCT) (Industrial Technology Division)	Material characterization analysiss
4.	Reactor Technology Center (Technical Support Division)	Operating the research reactor for Neutron Activation Analysis (NAA)
5.	Transmission Electron Microscope Laboratory (Radiation Technology Division)	More advanced analysis : nanoscale microscope

4 Discussion

As shown in Table 1, the HPG under the Radiation Safety and Health Division responsible as a secretariat in nuclear forensic case in the agency. Currently, this group is assigned to execute the related national act in the agency and also ensuring all the activities are comply with laws and regulations. Therefore, in handling nuclear forensic case, the group was designed to responsible for receiving evidence from the designated regulator, then conducting physical radiological assessment and physical characterization. This first step is very important to ensure the safety of the analyst. After that, the HPG have to distribute the sample of evidence to specified laboratory for seeking the so called 'nuclear forensic signature'. Those signatures could be carried out through isotopic analysis, radio chronometry and elemental/chemical composition (IAEA, 2015) which will be analyzed in the identified lab shows in Table 1. Finally, the HPG have to produce technical report, communicate and submit the technical report to the designated authority. Above all, maintaining the chain of custody of the evidence is another aspect that have to take into consideration. A break in the chain of custody will decrease transparency, then integrity and reliability of the technical report could be questioned. (CISA, 2013).

The operation of nuclear forensic laboratories must follow the designated and documented structure which is a pillar for the nuclear forensic process. The proposed management framework for handling the nuclear forensic case in Nuclear Malaysia is shown in Figure 1.

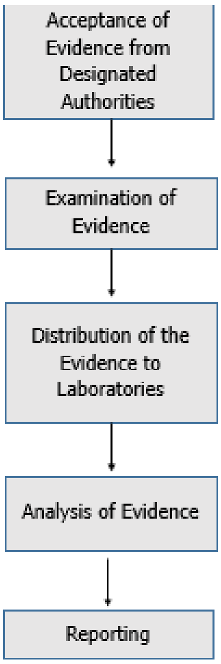

Figure 1: Proposed process flow for handling nuclear forensic case in Malaysian Nuclear Agency

5 Conclusion

Nuclear Malaysia has a capability to serve as a national reference center and conduct nuclear forensic case. To succeed in this field, the agency needs to ensure that the nuclear forensic analysis is smooth and achieves the objectives. As nuclear forensic facilities are the integration of several laboratory in the agency, practices, and familiarization of the process flow is a must. Finally, the documented procedures could serve as a guideline for nuclear forensic analysis not only in Nuclear Malaysia but also could be used in supporting the nuclear security system in Malaysia. In the future, by assistance from the IAEA, Nuclear Malaysia could involve in conducting and examining nuclear material of exercise (MOX) for nuclear forensic that will help all personnel to gain experiences, increase confidence and improve their skills.

References

J. Ball, I. Dimayuga, I Summerell, M. Totland, Jonkmans G. Jonkmans, A El-jaby, and E. Inrig. 2015. Canadian national nuclear forensics capability project. *AECL Nuclear Review*, 4(1):1–7 Implementing Guide: Nuclear Forensics in Support of Investigations. 2015 IAEA Nuclear Security Series No. 2–G (Rev.1); IAEA.

CISA. 2013. Chain of Custody and Critical Infrastructure Systems, CISA Insighthttps://www.cisa.gov/sites/default/files/publications/cisa-insights_chain-of-custody-and-ci-systems_508.pdf. Accessed on 15 August 2023.

IAEA. 2015. Nuclear forensic support. *IAEA Nuclear Security Series No. 2.*, pages 21–34.

IAEA. 2023. Incident and Trafficking Database (ITDB). *Fact Sheet. IAEA.*, https://www.iaea.org/sites/default/files/22/01/itdb factsheet.pdf, Accessed on 17 August 2023.

M.J. Kristo. 2016. Nuclear forensics. In: L'Annunziata, M. (Ed.). *Handbook of Radioactivity Analysis*, 3rd ed. Elsevier Ltd., Oxford:1281–1304.

D.K. Smith. 2016. IAEA Expert Mission Report on Assessment of Malaysia Capability in Nuclear Forensics.

Individual Research Contribution Review, 2023, 1(1): 557–558

Assessment of Activity Concentration of Ilmenite and Its Contribution to Environmental Effective Dose

Syed Asraf Fahlawi Wafa Syed Mohd Ghazi
Radiation Health and Safety Division
Malaysian Nuclear Agency
43000 Kajang, Selangor
asraf@nm.gov.my

Abstract

Ilmenite ($FeTiO_3$), a naturally occurring mineral, contains radioactive elements like radium-226, radon-222 from the uranium decay series and thoron-220 from the thorium series, as well as potassium-40. Elevated levels of these radionuclides can increase radiation exposure risks to people and the environment. In-situ dose rate measurements at the ilmenite processing plant showed the external gamma dose rate was 97.0 ± 23.3 nSv/hr at 1 meter height and 117 ± 26 nSv/hr at 5 cm height from the soil surface. While similar to the Malaysian average, these rates are higher than the global average. Monitoring found that air concentrations of uranium and thorium were below the minimum detection limit of 0.0001 Bq/m^3, indicating negligible environmental dispersion. The activity concentrations in soil for potassium-40, radium-226, thorium-232 and uranium-238 averaged 573 ± 184 Bq/kg, 30.6 ± 10.2 Bq/kg, 18.8 ± 6.4 Bq/kg, and 64.0 ± 34.3 Bq/kg respectively. For ilmenite, the averages were 39.0 ± 10.0 Bq/kg, 28.0 ± 6.7 Bq/kg, 84.0 ± 6.9 Bq/kg and 50.0 ± 7.4 Bq/kg. The estimated 0.17 mSv/yr public effective dose is below the global average background. The radium equivalent values, external hazard indices, and estimated cancer risks were also within recommended safe levels. Although the radiation exposure from current operations is insignificant, safety precautions as per standards and legislation should continue to be followed.

1 Introduction

This study aimed to determine the concentration of natural radionuclides in ilmenite mineral samples and surrounding soil at an ilmenite processing plant. The radionuclides measured were ^{40}K, ^{226}Ra, ^{232}Th, and ^{238}U. External and internal radiation dose rates were calculated to assess the radiological risk to the public living near the plant.

2 Methodology

Twelve soil samples were collected around the plant area and 5 ilmenite samples from different sources were obtained. Gamma spectrometry was used to quantify the radionuclide concentrations. Dose rate meters measured the external gamma dose rate at 1 m and 5 cm from the ground surface. Absorbed dose rates (Ds) were calculated from the soil and ilmenite concentrations and used to determine the annual effective dose rates.

$$D_S = (0.621C_{Th} + 0.462C_U + 0.0417C_K)nGyj^{-1} \quad (1)$$

C_{Th}, C_U, C_K are the average activity concentrations of ^{232}Th, ^{238}U, and ^{40}K in unit Bqkg^{-1} units. The constant values of 0.621, 0.462 and 0.0417 indicate the world average values for the concentrations of ^{232}Th, ^{238}U, dan ^{40}K (Ismail et al., 2009).

$$D_E = (D_S \times 8760hours \times 0.2 \times 0.7SvGy^{-1} \times 10^{-5})mSv/yr \quad (2)$$

where 8760 is the number of hours in a year. The constant 0.2 refers to 20% of time spent outside the home (UNSCEAR 1993). The constant 0.7 SvGy^{-1} is coefficient of conversion of absorbed dose to effective dose.

Radium equivalent activity (Ra_{eq}) and external hazard index (H_{ex}) were calculated. Cancer risk for 50 years of exposure was estimated using ICRP risk factors.

3 Result and Discussion

Table 1: Distribution of Radionuclide Concentration in Soil

Sample code	Concentration, Bqkg^{-1}(Dry) ^{40}K	^{226}Ra	^{232}TH	^{238}U
T1	772.83 ± 206.69	27.76 ± 7.68	16.08 ± 0.97	96.09 ± 8.16
T2	641.36 ± 117.24	32.23 ± 1.22	17.24 ± 2.06	64.31 ± 45.57
T3	817.89 ± 342.42	29.41 ± 0.89	19.8 ± 3.91	60.19 ± 33.82
T4	257.14 ± 3.34	46.93 ± 36.21	21.83 ± 19.2	54.73 ± 35.50
T5	377.2 ± 248.75	16.42 ± 5.06	18.86 ± 6.03	44.5 ± 48.38
Average	573.28 ± 183.69	30.55 ± 10.21	18.76 ± 6.434	63.96 ± 34.29
Malaysia Average	310	67	82	66
World Average	400	35	30	35

The average radionuclide concentrations in soil were comparable to or lower than the Malaysian average, except for higher ^{40}K.

Concentrations in ilmenite were higher, with ^{232}Th being the major contributor. The external gamma dose rate averaged 97-117 nSv/hr, similar to the Malaysian average of 92 nSv/hr. Mean D and annual effective dose rates were 65 nGy/h and 0.08 mSv for soil and 77 nGy/h and 0.09 mSv for ilmenite.

Table 2: Absorbed Dose Rate and Effective Dose

Sample	**Code Sample**	**Absorbed dose rate, D_S ($nGyj^{-1}$)**	**Effective dose rate, D_E (mSv/year)**
Ilmenite	India	42.44 ± 7.10	0.052 ± 0.01
	South Africa	78.66 ± 12.78	0.09 ± 0.02
	Australia	109.54 ± 4.54	0.13 ± 0.01
	Average	76.88 ± 4.21	0.09 ± 0.01
Soil	T1	86.60 ± 11.79	0.11 ± 0.01
	T2	90.23 ± 5.11	0.11 ± 0.01
	T3	51.35 ± 4.85	0.06 ± 0.01
	T4	49.56 ± 28.18	0.06 ± 0.03
	T5	47.99 ± 36.47	0.06 ± 0.04
	Average	65.11 ± 21.25	0.08 ± 0.03

Ra_{eq} and H_{ex} were below recommended limits, indicating negligible radiation hazard.

Table 3: Radium Equivalence Value and External Hazard Index

Sample	**Code Sample**	**Ra_{eq} ($Bqkg^{-1}$)**	**H_{ex}**
Ilmenite	India	93.55 ± 15.52	0.25 ± 0.04
	Australia	247.63 ± 10.14	0.67 ± 0.03
	South Africa	178.16 ± 28.58	0.48 ± 0.07
	Average	173.12 ± 77.16	0.47 ± 0.21
Soil	T1	22.69 ± 0.48	0.48 ± 0.06
	T2	7.81 ± 0.49	0.50 ± 0.02
	T3	10.75 ± 0.28	0.28 ± 0.03
	T4	62.68 ± 0.29	0.26 ± 0.17
	T5	76.16 ± 0.27	0.27 ± 0.21
	Average	42.68 ± 0.36	0.36 ± 0.12

The estimated additional lifetime cancer risk due to plant activities was 4 orders of magnitude lower than natural background risk levels.

4 Conclusions

The radioactivity levels and associated radiological risks from the ilmenite plant operations were very low compared to average background. The public annual dose limit was not exceeded and there was minimal health risk to nearby residents. The industry had no significant radiological environmental impact based on the parameters studied. More long-term and extensive analyses could provide greater insight into temporal or diffuse emissions.

References

P. Akhter, K. Rahman, S.D. Orfi, and Ahmad N. 2007. Radiological impact of dietary intakes of naturally occurring radionuclides on Pakistani adults. *Food and Chemical Toxicology*, 45:272–277.

Aznan Fazli Ismail, Muhamad Samudi Yasir, Amran Ab. Majid, Redzuwan Yahaya, and Ismail Bahari. 2009. Radiological hazard of natural radionuclides in portland cement Peninsular Malaysia. *Malaysian Science*, 38(3):407 – 411.

Ahmad Termizi Ramli. 2007. Radiological study on the effects of amang in the State of Perak, Final report of the research project vot 68876.

Individual Research Contribution Review, 2023, 1(1): 559–560

Determine the Flatness and Symmetry of the Medical X-Ray System used for OSLD Dose Measurement Study

Wan Hazlinda Ismail
Radiation Health and Safety Division
Malaysian Nuclear Agency
43000 Kajang, Selangor
linda@nm.gov.my

Abstract

Al_2O_3:C-based optically stimulated luminescent dosimeters (OSLDs) use in kilovoltage (kV) X-ray beam applications display challenges because OSLDs are energy dependence and variability of energy sensitivity factors (ESFs) at low doses and energies. Clinical or medical x-ray system also produce non-flatness and asymmetry x-ray beam, which affect the dose measurement of the OSLD in the x-ray field. This study aimed to determine the area in the x-ray field that is most flatness and symmetry and therefore reduce the uncertainty of the OSLD dose measurement study due to the x-ray beam uniformity.

Keywords: x-ray beam/field, flatness, symmetry, uniformity, OSLD

1 Introduction

The usage of OSLD for measurement of organ doses in medical application have rapidly employed due to its simplicity technique of usage. However, in diagnostic radiology the dose measurement using OSLD can only be reliable when the performance and characteristics of the OSLD are carefully considered. OSLDs are energy dependence and shows inconsistency of ESFs at low doses and energies. For a reliable result, the OSLDs need to correct with a user-define ESFs and energy depends correction.

Clincal x-ray system produces non-uniform x-ray beam due to the heel effect. The heel effect however does not affect the quality of image production for diagnostic purposes. Nevertheless, the x-ray beam flatness and symmetry are important to minimize the uncertainty of the user-define ESFs and energy depends correction measurement.

In this study, we determine the area in the x-ray field that is most flatness and symmetry for dose measurement of OSLD. In order to minimize the uncertainty budget due to x-ray beam uniformity.

2 Methods

The flatness and symmetry for two x-ray field size of 10 cm x 10 cm standard field size and a larger field size of 30 cm x 30 cm was investigate in this study. For standard field size, 25 points measurement with an interval distance of 2 cm was obtain. Whilst, for the large field size 47 points measurement with interval distance of 2 cm and 4 cm was taken. A solid-state type detector size 2.0 cm x 4.5 cm x 0.74 cm with detector active size is 1 cm x 1 cm was used to measure the dose in mGy at each position. Source to detector distance was fixed at 100cm. X-ray output was set at 80kV, 320mA and 0.2 seconds.

3 Results and discussion

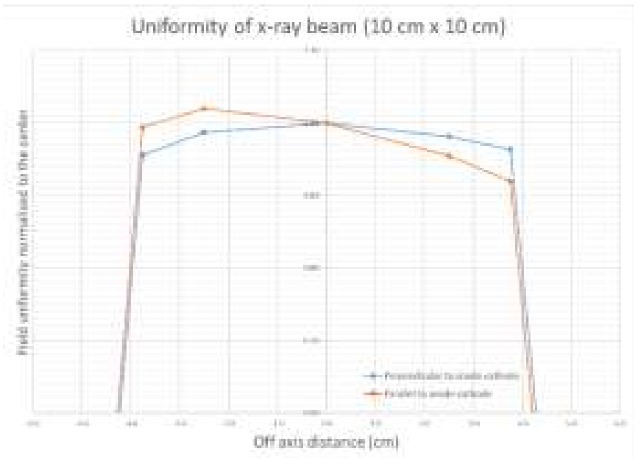

Figure 1: The uniformity for 10 cm x 10 cm x-ray beam field size

From the results in Figure 1, it shows that the uniformity of 10 cm x 10 cm x-ray beam. Within the center of 5 cm x 5 cm x-ray beam perpendicular to anode-cathode, the flatness of the x-ray beam variation is ±1.8% and show slightly symmetry. Whereas the flatness of the x-ray beam parallel to the anode-cathode variation is 3.4% and due to the heel effect of the x-ray beam in this direction, the x-ray field is not symmetry.

Figure 2 shows the uniformity of 30 cm x 30 cm x-ray beam size. The flatness variation of x-ray beam perpendicular to anode-cathode increases up to ±2.3% as the field size increase to 28 cm x 28 cm. However, with in 5 cm x 5 cm the x-ray beam flatness variation is ±1.5% and shows slightly symmetry. Due to the heel effect the flatness of the x-ray beam parallel to the anode-cathode variation increases intensely up to ±12.7% as the field size increase to 28 cm x 28 cm but within 5 cm x 5 cm the x-ray beam flatness variation is ± 3.8% and is not symmetry.

For the user-define ESFs and energy depends correction study, x-ray beam field size of 2 cm x 2 cm within the center of the beam was ideal since the size of one OSLD (nanodot) is only 1 cm x 1 cm. The uniformity of the X-ray field is ±

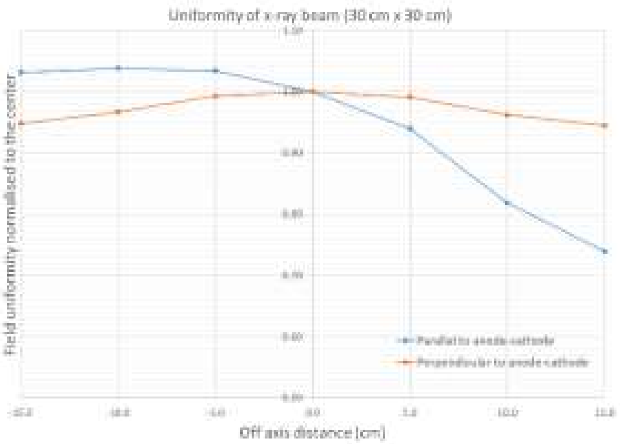

Figure 2: The uniformity for 30 cm x 30 cm x-ray beam field size

1.5% within the central was achieved.

4 Conclusions and attention

To minimize the uncertainty of the user-define ESFs and energy depends correction measurement due to the beam flatness and symmetry of x-ray beam size, OSLD should be position closest to the center of within 2 cm x 2 cm of the x-ray beam. The further the OSLD is position away from the center, the larger the uncertainty measurement is obtain due to the beam uniformity variation.

References

Rani M. Al-Senana and Mustapha R. Hatab. 2011. Characteristics of an OSLD in the diagnostic energy range. *Med. Phys.*, 38(7).

Y Musa, S Hashim, M K A Karim, K A Bakar, W C Ang, and N Salehhon. 2017. Response of optically stimulated luminescence dosimeters subjected to x-rays in diagnostic energy range. *J. Phys.: Conf. Ser.*, 851 012001.

Individual Research Contribution Review, 2023, 1(1): 561–562

Propagation and Titration of Newcastle Disease Virus in Embryonic Chicken Eggs

Abang Abdul Rahim Ossen
Medical Technology Division
Malaysian Nuclear Agency
43000 Kajang, Selangor
aarahim@nm.gov.my

Abstract

Newcastle disease virus (NDV) that mainly affects avian belongs to a virus family of Paramyxoviridae, which is a single-stranded, negative-sense RNA, enveloped in a glycoprotein body that contains hemagglutininneuraminidase proteins. There has been a recent report on an outbreak of this disease in commercial poultry and backyard farms in Sabah, Malaysia. In order to control the disease from further advancement, effective vaccines need to be developed. The most popular vaccine to produce is the liveattenuated or inactivated virus vaccine, which can be made by propagating viral cultures and applying various methods to alter the virulence of the viral particles while preserving the epitopes. The simplest method to propagate the virus culture for research or small-scale production is by using embryonic chicken eggs. The egg is inoculated with seed virus into its allantoic cavity at the age of 9-10 days, incubated for two days for the replication to occur and the allantoic fluid with a high viral titer is then harvested. The titration of the virus is measured using hemagglutination assay, in which serial dilution is performed on the harvested serum and each dilution is mixed with chicken red blood cells (RBC). The titer is measured in HA unit (HAU) based on the hemagglutination activity on every dilution. These quick and easy methods are very reliable and cost-effective for the research and development of NDV vaccines.

Keywords: Newcastle disease virus, virus propagation, virus titration, hemagglutination assay, veterinary virology.

1 Introduction

Newcastle Disease virus (NDV) is a non-segmented, singlestranded, negative-sense RNA virus that belongs to the family paramyxoviridae (Al-Ziaydi et al., 2020). There has been a recent report on an outbreak of this disease in commercial poultry and backyard farms in Sabah, Malaysia (Syamsiah Aini et al., 2022). NDV mainly affects avian can be propagated by using embryonic chicken eggs, which is an old but a reliable method that is still far superior to produce high titre of NDV culture (McGinnes et al., 2006). The titre of the virus can be quantified by using Hemagglutination Assay (HA) test, which is a fast and inexpensive technique that utilized serial dilution and the clumping activity cause by the binding of hemagglutinin neuraminidase protein of the virus with sialic acid residues on the surface of red blood cells (Ryu, 2017). This paper explains the procedure from the viral propagation to titration, which the culture can be utilized in the application of vaccine development not just for avian and veterinary medicine but has the potential to be used on humans as a recombinant vaccine (Kim and Samal, 2016).

2 Methods

2.1 Eggs Sanitation and Storage

The eggs are sanitized by using fumigation method. The eggs are placed inside a container in an open environment or a fume hood. A 5 g of potassium permanganate, $KMnO_4$, is placed inside a glass petri dish. A 17.5 ml of formalin (40% formaldehyde) is poured quickly into the dish. The container is covered immediately and the process is ran for 15 minutes. The eggs are unloaded and aerated for 30 minutes. The eggs are placed with the apex pointing downward inside an incubator at the temperature of 38°C and relative humidity at 85%.

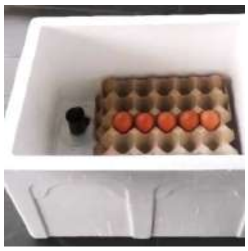

Figure 1: The setup for the fumigation of eggs.

2.2 Candling of the Eggs

Candling is a process to observed and check the viability of the embryo inside the egg. The eggs are candled using a bright LED torchlight in a dark room. The blood vessel and embryo inside the eggs are observed (Figure 2). Candling is performed every day from the day the eggs are acquired until 2 days postinoculation.

2.3 Inoculation of the Virus

The inoculation is performed at Day 9. The blunt end of the eggs is pointed upward and the air sac is located by candling. The inoculation site is marked using a pencil just 2 mm above the level of allantoic fluid at the air sac cavity with the embryo's

Figure 2: Candling of eggs that show healthy blood vessels.

head facing the opposite side of the egg. The marking site is sterilized by using alcohol swab. A sterile thumb tack is pierced into the egg shell. A 0.1 ml of virus (20 HA unit) suspension is inoculated into the allantoic cavity using 26G, 1/2-inch needle. The hole is sealed with a glue. The eggs are incubated for 48 hours and then placed inside a 4°C refrigerator for 12 hours prior to harvest.

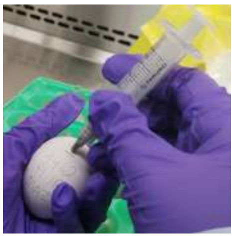

Figure 3: Inoculation of eggs at the marked site.

2.4 Harvesting of the Virus

The blunt end of the eggs is sterilized using 70% ethanol and wiped dry. The shell of the eggs is knocked using a sterile spatula and the fragments are removed with sterile forceps. The allantoic fluid is extracted using a sterile syringe and placed into a sterile tube.

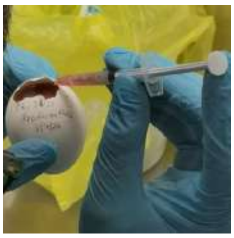

Figure 4: Harvest of the allantoic fluid.

2.5 Preparation of Chicken Red Blood Cell (RBC)

A fresh chicken blood is collected about 25 ml into a sterile Falcon tube containing 1 ml of 0.12 M Na2-EDTA solution. The tube is shaken gently. A 25 ml of 1x PBS buffer (pH 7.5) is added to the tube. The tube is gently mixed. The tube is centrifuged at 15,000 rpm for 5 minutes. The supernatant is discarded. The washing step is repeated for 3 times. A 1x PBS buffer is added to the final volume of the collected RBC to achieve the 10% v/v concentration. The RBC suspension is stored at 4°C.

2.6 Micro Hemagglutination Assay (HA) Test for Viral Titre

A conical 96-well plate is used for the HA test. A 25 μl of 1xPBS buffer (pH 7.5) is pipetted into all the wells. A 25 μl of virus suspension is pipette into one of the well and mixed gently. A 25 μl of virus aliquot is transferred into the next well and the serial dilution is carried out until the eleventh well. A 25 μl of aliquot is discarded from the eleventh well. A 25 μl of PBS is added into all the wells. A 25 μl of 1% RBC suspension is added to all the wells. The sides of the plate are tapped gently to mix the solutions. The plate is placed onto an orbital shaker for 30 minutes. The hemagglutination is observed. HA negative is identified in the form of sharp button at the bottom of the well. HA positive is identified from the formation of hazy film of RBC at the bottom of the well. The last well with a HA positive result of the dilution is the reciprocal of the HA unit.

3 Results and Discussion

A propagated virus suspension in allantoic fluid is shown to have the same colour and opacity of an egg white at room temperature. An unsuccessful propagation will result in the presence of cloudy appearance due to bacterial contamination. The presence of blood or egg yolk in the harvested fluid will also considered as contamination. The titration of the virus culture is determined on the last well of the positive result in the HA test. If the last positive result is shown on the sixth well, which the dilution is $\frac{1}{2^6}$ or $\frac{1}{64}$, the value is reciprocal that is 2^6 or 64. Therefore, the result is 2^6 HA units or 64 HA units per 25 μl of virus suspension.

4 Conclusion

Using embryonic chicken eggs and hemagglutination assay are still the reliable techniques to propagate and titrate NDV or any other influenza viruses.

References

A.G. Al-Ziaydi, A.M. Al-Shammari, and M.I. Hamzah. 2020. Propagation of oncolytic Newcastle disease virus in embryonated chicken eggs and its research applications in cell lines. *Journal of Physics: Conference Series*, 1664(012129).

S.H. Kim and S.K. Samal. 2016. Newcastle disease virus as a vaccine vector for development of human and veterinary vaccines. *Viruses*, 8(7):183.

L.W. McGinnes, H. Pantua, J. Reitter, and T.G. Morrison. 2006. Newcastle disease virus: Propagation, quantification, and storage. *Current Protocols in Microbiology*, 15,15F.2.1¬-15F.2.18.

WS. Ryu. 2017. Molecular virology of human pathogenic viruses. pages 47– 62.Academic Press.

S. Syamsiah Aini, B.L. Leow, M.Y. Faizul Fikri, S. Muhammad Redzwan, and M.S. Faizah Hanim. 2022. Identification of Newcastle disease virus sub-genotype VII 1.1 isolated from chickens in Sabah, Malaysia. *Tropical Biomedicine*, 39(4):579–586.

Individual Research Contribution Review, 2023, 1(1): 563–564

^{68}Ga-DOTA-Octreotate Kit for Diagnosis of Somatostatin Receptor Positive (Neuroendocrine) Tumours

Anee Suryani binti Sued
Medical Technology Division
Malaysian Nuclear Agency
43000 Kajang, Selangor
anee@nm.gov.my

Abstract

The primary objective of this study is to obtain a simple kit formulation for the preparation of ^{68}Ga-DOTA-peptide for clinical use. A thorough optimization of the kit formulation conditions such as the optimal buffer and its concentration, peptide concentration, pH, reaction time and temperature was carried out in order to obtain the DOTA-TATE kit which would enable rapid and reproducible labelling with ^{68}Ga. Prior to the formulation of kit, pre-formulation experiments were carried out to determine the optimum concentration as well as the volume of sodium acetate buffer required to obtain the pH (3.5 to 4.0) desired for optimal ^{68}Ga complexation. After optimising the optimal buffer concentration and volume, the amount of peptide to be used in the formulation was optimised. Towards this aim, wet-labelling experiments were carried out using the peptide DOTA-TATE at concentrations ranging from 5 to 50 μg. Subsequently, the pH, time and temperature required for maximum complexation were also optimised. Radiochemical yield of the ^{68}Ga-DOTA-TATE complexes were estimated using iTLC techniques in 1:1 mixture of 1 M ammonium acetate and methanol as mobile phase immediately after radiolabeling. In this study, sodium acetate buffer of concentration 1.5 M and volume 45 μL was able to maintain the pH 3.9 when liquid DOTA-TATE was labelled with ^{68}Ga eluted in 1 mL of 0.05 N HCl. Peptide concentration of 25 μg was chosen. Radiolabelling parameters were optimised as such; pH 3.9, temperature 90°C and heating time for 10 min. The ^{68}Ga-DOTA-TATE complexes was also stable six hours of labelling (iTLC RCP >97%).

1 Introduction

The dynamic of cancer therapy was reflected by several paradigm changes from small molecule drugs to targeted therapy with small molecule-drug conjugates. Traditional chemotherapeutics not only accumulate in tumors, but affect all tissues, which lead to detrimental side effects. Small molecule ligand-drug conjugate has been used to efficiently to target tumors with specific targets (Figueras et al., 2019).

^{68}Ga-DOTA-Octreotide is a radiolabeled peptide-based ligand that targets somatostatin receptors overexpressed in neuroendocrine tumors (NETs) (Hennrich and Benešovā, 2020). NETs are tumors originating from neuroendocrine cells that are distributed throughout the human body. Approximately two-thirds of NETs derive from the gastrointestinal system and represent the group of gastroenteropancreatic-tumors (GEP-NETs). Other NETs including pituitary adenoma, pheochromocytoma, neuroblastoma, medulloblastoma, medullary thyroid carcinoma and paraganglioma. Most of the NETs demonstrate high expression levels of SSTRs, offering the possibility of molecular imaging and peptide receptor radionuclide therapy using radiolabeled somatostatin analogs.

2 Materials and Methods

2.1 Materials and Reagents

DOTA-(Tyr3)-Octreotate acetate salt (BOC Science, USA), sodium acetate (Supelco, Germany), 30% solution of Suprapur®Hydrochloric acid (Supelco, Germany), water for injection (B/Braun, Malaysia, ammonium acetate (Sigma-Aldrich, Netherland, methanol (Fisher, Korea), iTLC-SG-microfibre chromatography paper impregnated with silica gel (Agilent, USA, iTG 68Ge/68Ga generator (iTG, Germany), pH meter (Mettler Toledo, Switzerland), TLC Radioactive Scanner (Eckert & Ziegler, USA), Radioisotope Dose Calibrator (Capintec, USA).

2.2 Formulation of DOTA-TATE

DOTA-TATE kit comprises of octerotate peptide chelated with DOTA and dissolved in sodium acetate solution. Formulation of DOTA-TATE kit included optimization of sodium acetate buffer concentration and volume; optimisation of concentration of peptide.

The concentration of Sodium acetate was optimised between 0.5 M to 2.0 M. The volume of buffer was determined to achieve pH 3.5 to 4.0 when added with 1 mL of 0.05 N HCl Suprapur®.

Various amount of DOTA-TATE (10, 15, 20, 23, 25, 30, 35, 40, 50 μg) were tested for radiolabeling with ^{68}GaCL3 at pH 3.9 followed by heating at 90°C for 10 min to determine the optimum peptide required for preparation of DOTA-TATE kit.

2.3 Optimisation of radiolabeling conditions

Reaction parameters were optimised by addition of 1 mL from the 6ml of ^{68}GaCl3 eluted in step 2.3. To determine influence of pH radiolabeling was carried out at pH 2, 3, 4 and 5 using standardized amount of DOTA-TATE (25 μg). Temperature variation was performed (25, 50, 75 and 90°C) followed by heating times experiment (5, 8, 10, 15, 20 min) at optimised temperature (90°C).

3 Results and discussion

3.1 Formulation of DOTA-TATE kit

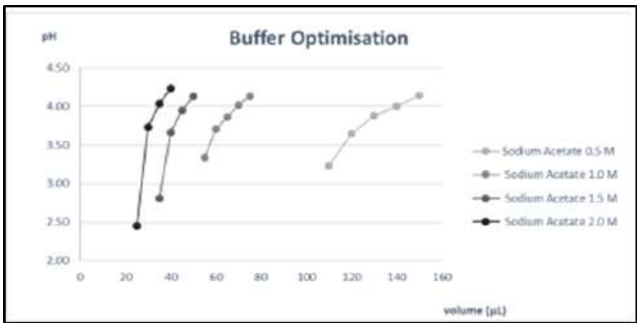

Figure 1: Determination of sodium acetate concentration and volume to serve as buffer and maintaining the pH of liquid kit between pH 3.5 to 4.0 when adding 1 mL of ^{68}GaCl3 eluted in 0.05 N HCl Suprapur ®.

Sodium acetate of concentration 1.5 M and volume of 45 μL was found to be most suitable to maintain pH of 3.9 when the liquid kit preparation was labelled with ^{68}GaCl3/ 1 mL 0.05 N HCl Suprapur®.

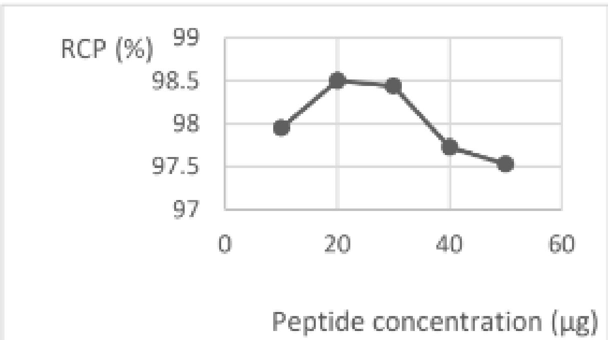

Figure 2: DOTA-TATE concentration with maximum RCP was determined at 20 μg.

For the preparation of DOTA-TATE kit, concentration of 25 μg was chosen to compensate the possible loss of peptide during lyophilisation process

3.2 Optimisation of Radiolabelling Parameters

Optimisation of radiolabeling parameters was based on RCP value from iTLC which yield more than 97%. The parameters were pH, temperature and time of radiolabeling. The radiochemical yield (% RCP) increased drastically from 15% to 98% when pH increased from pH 2 to pH 4 and reduced when pH increased to pH 5(Figure 3 (a)). Incubation temperature and time also had significant influence on the % RCP (Figure 3 (b) and (c)). Incubation temperature of 90°C and time of 10 min was found to be optimum to achieve radiochemical yield of > 98%.

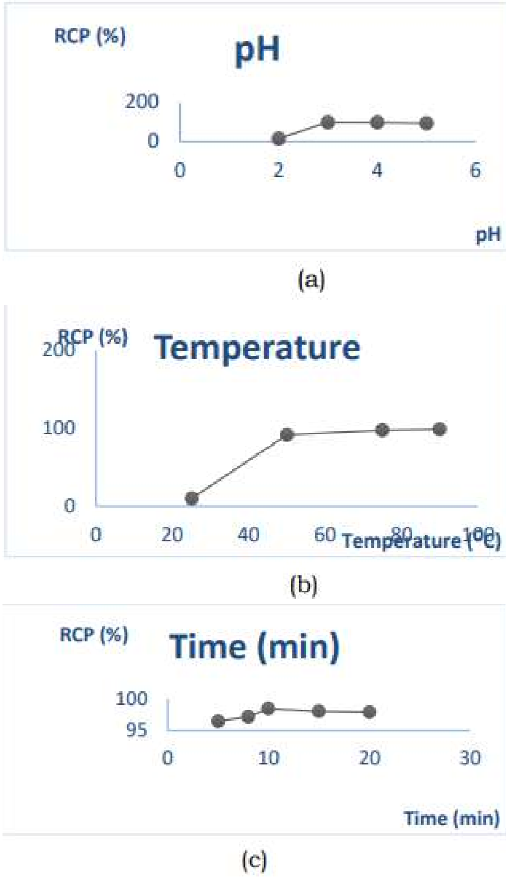

Figure 3: Optimisation of radio-labelling parameters, 24 μg peptide in 45 μL of 1.5 M sodium acetate and 1mL of ^{68}GaCl3 eluted in 0.05 N HCl Suprapur®. (a) different pH, 25 μg DOTA-TATE, incubation at 90°C for 10 min, (b) different incubation temperature, 25 μg DOTA-TATE, pH 3.9 and 10 min heating, (c) different heating time, 25 μg DOTA-TATE, pH 3.9 and incubation temperature 90°C.

4 Conclusion

Formulation of DOTA-TATE was optimised in 1.5M sodium acetate as buffer with 25 μg octerotate. The heating process was set at 90°C for 10 min.

References

E. Figueras, A. Martins, A. Borbély, V. Le Joncour, P. Cordella, R. Perego, D. Modena, P. Pagani, S. Esposito, G. Auciello, M. Frese, P. Gallinari, P. Laakkonen, S. Steinkühler, and N. Sewald. 2019. Octreotide conjugates for tumor targeting and imaging pharmaceutics. 11(220):doi:10.3390.

U. Hennrich and M. Benešovā. 2020. [68Ga]Ga-DOTA-TOC: The first FDA-Approved 68Ga-Radiopharmaceutical for PET Imaging. *Pharmaceuticals*, 13(38):doi:10.3390/ph13030038.

Individual Research Contribution Review, 2023, 1(1): 565–566

Development and Physicochemical Characterization of a Biodegradable Microspheres Formulation Loaded with Samarium-153 and Doxorubicin for Chemoradioembolization of Liver Tumours

Azahari Kasbollah
Medical Technology Division
Malaysian Nuclear Agency
43000 Kajang, Selangor
azahari@nm.gov.my

Abstract

Transarterial chemoembolization (TACE) and transarterial radioembolization (TARE) are promising treatments for unresectable liver tumours. Some recent studies suggested that combining TACE and TARE in one treatment course might improve treatment efficacy through synergistic cytotoxicity effects. Nonetheless, current formulations do not facilitate a combination of chemoand radio-embolic agents in one delivery system. Therefore, this study aimed to synthesise a hybrid biodegradable microsphere loaded with both radioactive agent, samarium-153 (^{153}Sm) and chemotherapeutic drug, doxorubicin (Dox) for potential radio-chemoembolization of advanced liver tumours. ^{153}Sm and Dox-loaded polyhydroxybutyrate-co-3-hydroxyvalerate (PHBV) microspheres were prepared using water-in-oil-in-water solvent evaporation method. The microspheres were then sent for neutron activation in a neutron flux of 2 1012 n/cm^2/s. The physicochemical properties, radioactivity, radionuclide purity, ^{153}Sm retention efficiency, and Dox release profile of the Dox-153SmPHBV microspheres were analysed. In addition, in vitro cytotoxicity of the formulation was tested using MTT assay on HepG2 cell line at 24 and 72 h. The mean diameter of the Dox-153Sm-PHBV microspheres was 30.08 ± 2.79 μm. The specific radioactivity was 8.68 ± 0.17 GBq/g, or 177.69 Bq per microsphere. The ^{153}Sm retention efficiency was more than 99%, tested in phosphate-buffered saline (PBS) and human blood plasma over 26 days. The cumulative release of Dox from the microspheres after 41 days was 65.21 ± 1.96% and 29.96 ± 0.03% in PBS solution of pH 7.4 and pH 5.5, respectively. The Dox-153Sm-PHBV microspheres achieved a greater in vitro cytotoxicity effect on HepG2 cells (85.73 ± 3.63%) than 153Sm-PHBV (70.03 ± 5.61%) and Dox-PHBV (74.06 ± 0.78%) microspheres at 300 μg/mL at 72 h. In conclusion, a novel biodegradable microspheres formulation loaded with chemotherapeutic drug (Dox) and radioactive agent (^{153}Sm) was successfully developed in this study. The formulation fulfilled all the desired physicochemical properties of a chemo-radioembolic agent and achieved better in vitro cytotoxicity on HepG2 cells. Further investigations are needed to evaluate the biosafety, radiation dosimetry, and synergetic anticancer properties of the formulation.

Keywords: biodegradable microspheres, chemo-radioembolization, doxorubicin, liver cancer, Sm-153.

1 Introduction

Liver cancer remains as the sixth most common cancer and the third leading cause of cancer death worldwide.

1. The World Health Organization (WHO) predicted that the incidence rate of liver and intrahepatic bile duct cancers would increase by 58.6% and the number of deaths would increase by 60.9% in 2040. In unresectable liver cancer, transarterial chemoembolization (TACE) and transarterial radioembolization (TARE) are recommended to downstage the disease or improve the patient's quality of life. The treatment involves intra-arterial delivery of an embolic agent that contains either a chemotherapeutic drug or a radionuclide to block the blood supply as well as to kill the tumour(s) by the mean of targeted chemotherapy or radionuclide therapy.

2. In TACE, drug-eluting beads such as polyvinyl alcohol microspheres loaded with doxorubicin (Dox) are commonly used, while in TARE, resin or glass microspheres labelled with radioactive yittrium-90 (90Y) are currently practised. However, there are limitations with the use of 90Y as it is extremely costly to produce using a highenergy cyclotron and a complicated separation and purification process. Furthermore, 90Y is a pure beta emitter with no imaging characteristics for theranostics purposes. Therefore, this study investigated the use of Samarium-153 (^{153}Sm), a radionuclide that emits both beta and gamma radiations, as a potential alternative to Y. The therapeutic and imaging capabilities of ^{153}Sm have been validated in multiple studies.

Therefore, in this study, we expected to develop a hybrid-biodegradable microspheres formulation containing both radioactive agent (^{153}Sm) and chemotherapeutic drug (Dox) for synergistic chemo-radioembolization effects in unresectable liver cancer treatment. The synthesis method, physiochemical properties, ^{153}Sm retention efficiency, Dox release profile, and in vitro cytotoxicity test using HepG2 cells are reported in this article.

2 Methods

The 152SmAcAc-cand Dox-loaded PHBV (Dox-152SmPHBV) microspheres were synthesized using water1-inoil-in-water2 (W1/O/W2) solvent evaporation method as 2 ALREGIB ET AL. described by Mosafer and Teymouri9 with slight modification. To prepare the oil phase, 0.15 g of PHBV and 0.215 g of 152SmAcAc were added to 4.0 mL of chloroform and incubated at 80∘C for 1 min. The 152SmAcAcPHBV mixture was then stirred at 300 rpm overnight at room temperature. The W1 phase was prepared by mixing 10 mg of Dox, 300 μL of TEA, and 100 μL of distilled water under mechanical stirring of 300 rpm for 1 h. Before adding the W1 phase to the oil phase, the oil phase was sonicated using an ultrasonicate for 1 min. The W1/O solution mixture was then homogenized at 23,600 rpm using a homogenizer (T25 digital UltraTurrax, IKA, Germany) for 3 cycles of 30 s with a 30-s stop interval. The W1/O solution mixture was then added to 150 mL of 3.5% (w/v) PVA (W2 phase) and stirred at 850 rpm for 4 h. The microspheres were formed after centrifugation at 8500 rpm for 10 min. The Dox-153Sm-PHBV microspheres were sent for neutron activation using a nuclear research reactor (1-MW thermal TRIGA MARK II, General Atomics, USA) located at the Malaysian Nucelar Agency. The samples were placed in a polyethylene vial and heat sealed. Then, the samples were irradiated in a rotary specimen rack with a thermal neutron flux of 2 1012 n/cm^2/s for 5 h.

3 Results and Discussion

The specific activity of the Dox-153Sm-PHBV microspheres was 8.68 ± 0.17 GBq/g measured at 24 h postneutron activation (to allow for the radioactive decay of short-lived radionuclides). The average activity per microsphere was 177.69 Bq.

One of the factors to be considered in a drug delivery system is the body's reactions towards the carrier. Therefore, the microspheres must be able to dissolve safely in the body after delivering the active drugs without causing toxicity to the host. PHBV is a favourable polymer for biomedical applications due to its null toxicity, absorption capacity, high biocompatibility, low cytotoxicity, and thermoplastic properties. PHBV has been used in several applications, such as drug release, transportation, absorbable surgical sutures, and medical packaging. Therefore, it is an excellent choice of carrier for chemoradioembolization of liver tumours. The current FDA-approved radioembolic agents for liver tumours include SIR-Spheres (90Y resin microspheres) and TheraSphere (90Y glass-beads microspheres). 90Y is a pure beta emitter, with a physical halflife of 64.1 h. However, the absence of diagnostic properties in 90Y makes it a less suitable radionuclide for theragnostic purposes. Therefore, a substitute radionuclide (e.g., 99mTc) is required for pretreatment planning, and a special imaging technique (e.g., Bremsstrahlung X-ray imaging and quantitative positron emission tomography) is performed for postdelivery assessment.

4 Conclusion

A novel biodegradable PHBV microsphere loaded with both radioactive ^{153}Sm and chemotherapeutic Dox was successfully developed. The formulation fulfilled all the desired physicochemical properties of a chemoradioembolic agent potentially useful for intermediate to advanced-stage liver cancer treatment. The microspheres have the combined effects and benefits of biocompatibility, biodegradability, chemotherapeutic release, and emission of therapeutic radiations and diagnostic radiations (i.e., beta and gamma radiation). In addition, the neutron activation method is cheaper, easier, and more readily available than 90Y. However, the therapeutic efficacy of the formulation should be further evaluated and compared with the commercial TACE and TARE treatments. For future development, in-vivo animal studies are planned to study the synergistic effects of chemo-radioembolization using the developed formulation.

References

Bouvry C, Palard X, Edeline J, and et al. 2018. Transarterial radioembolization (TARE) agents beyond 90Y-microspheres. *Biomed Res Int.*, 1435302:doi:10.1155/2018/1435302.

Yeong CH, Abdullah BJJ, Ng KH, and et al. 2012. Production and first use of 153SmCl3-ion exchange resin capsule formulation for assessing gastrointestinal motility. *Appl Radiat Isot.*, 70(3):450–455. doi:10.1016/j.apradiso.2011.11.056.

Tan HY, Wong YH, Kasbollah A, and et al. 2022. Development of neutron-activated samarium-153-loaded polystyrene microspheres as a potential theranostic agent for hepatic radioembolization. *Nucl Med Commun.*, 43(4):410–422. doi:10. 1097/MNM.0000000000001529.

Hashikin NAA, Yeong CH, Abdullah BJJ, and et al. 2015. Neutron activated samarium-153 microparticles for transarterial radioembolization of liver tumour with post-procedure imaging capabilities. *PLoS ONE.*, 10(9):e0138106. doi:10.1371/ journal.pone.0138106.

Siegel RL, Miller KD, Fuchs HE, and Jemal A. 2002. Cancer statistics, 2022. *CA Cancer J Clin.*, 72(1):7–33. doi:10.3322/caac. 21708.

Individual Research Contribution Review, 2023, 1(1): 567–568

Evaluation of Therapeutic Efficacy and Imaging Capabilities of $^{153}Sm_2O_3$-Loaded Polystyrene Microspheres for Intra-Tumoural Radionuclide Therapy of Liver Cancer Using Sprague-Dawley Rat Model

Azahari Kasbollah
Medical Technology Division
Malaysian Nuclear Agency
43000 Kajang, Selangor
azahari@nm.gov.my

Abstract

Neutron-activated samarium-153-oxide-loaded polystyrene ($^{153}Sm_2O_3$-PS) microspheres has been developed in previous study as a potential theranostic agent for hepatic radioembolization. In this study, the therapeutic efficacy and diagnostic imaging capabilities of the formulation was assessed using liver cancer Sprague-Dawley (SD) rat model. Neutron-activated $^{153}Sm_2O_3$-PS microspheres demonstrated excellent therapeutic and diagnostic imaging capabilities for theranostic treatment of liver cancer in a SD rat model. Further studies with different animal and tumour models are planned to validate this finding.

Keywords: samarium-153; polystyrene; microspheres; theranostics; liver tumour; Sprague-Dawley rat

1 Introduction

Primary liver cancer ranks the sixth most frequently diagnosed cancer and the third leading cause of cancer death worldwide, with an estimation of 906,000 new cases and 830,000 deaths in 2020 (Sung et al., 2021). The high mortality rate of liver cancer is primarily due to late diagnosis. Intraarterial radioembolization, also known as selective internal radiation. therapy (SIRT), is a recommended treatment for patients with unresectable liver tumours due to its established evidence in improving patient's survival rate and quality-of-life (Walton et al., 2020). In our previous study, a biocompatible polystyrene (PS) microspheres formulation loaded with non-radioactive samarium-152 oxide ($^{153}Sm_2O_3$) has been developed to overcome these limitations (Tan et al., 2022). The microspheres are non-radioactive during synthesis until they are sent for neutron activation before the treatment. A large quantity of high specific activity samarium-153 (^{153}Sm) can be produced via direct neutron capture process, $^{153}Sm(n,\gamma)^{153}Sm$ due to its high thermal neutron activation cross-section (206 barns) (Van de Voorde et al., 2021). ^{153}Sm has an optimal half-life of 46.3 h, low gamma ray energy of KeV for imaging and high beta radiation of 808 keV for therapy (Tan et al., 2020). It has been used as a therapeutic agent for bone palliation and radiosynovectomy for more than 20 years (IAEA, 1999). Owing to its theranostics properties, ^{153}Sm has a great potential in cancer management (Gomes Marin et al., 2020). Personalized radiation therapy can be achieved with the presence of radiation that allows baseline and restaging imaging using the same radiopharmaceutical with to improve accuracy and safety of the treatment (Jeelani et al., 2014). The purpose of the present study is to evaluate the therapeutic efficacy and diagnostic imaging capabilities of the $^{153}Sm_2O_3$-PS microspheres after intra-tumoural injection in liver tumour-bearing Sprague-Dawley (SD) rats.

2 Methods

Samarium oxide (Sm_2O_3) (99% purity), polyvinyl alcohol (PVA) (99% purity), chloroform, Cyclosporine A, meloxicam sodium salt hydrate (98% purity), formaldehyde (37%), sodium dihydrogen phosphate and disodium hydrogen phosphate were procured from Sigma Aldrich (St. Louis, MO, USA). Isoflurane USP was purchased from Piramal Healthcare Limited (Mumbai, India). The KTX (combination of 2.5 mL ketamine, 125 mg of tiletamine, 125 mg of zolazepam and 12.5 mL of xylazine) anesthesia was purchased from Laboratory Animal Resource Unit, National University of Malaysia (UKM), Kuala Lumpur, Malaysia.

The animal experiments were approved by the National University of Malaysia Animal Ethical Committee (UKMAEC) (FSK/2019/Noorazrul/24-July/1017-Sept.-2019-Aug.-2021).

A total of 18 healthy male SD rats (150–200 g) supplied by a local supplier (Chenur Supplier, Seri Kembangan, Selangor, Malaysia) were used in this study. The rats were bred on standard pelleted rat maintenance diet (PicoLab® Rodent Diet 20 5053 Irradiated, LabDiet®, Richmond, IN, USA) and water ad libitum with 12 h light–dark cycle.

3 Results and Discussion

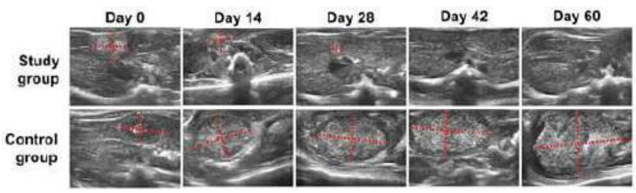

Figure 1: Ultrasound images of the rats in the study and control groups show tumour progression at Day 0, Day 14, Day 28, Day 42, and Day 60 post-injection of $^{153}Sm_2O_3$-PS microspheres and saline solution.

Figure 1 shows the ultrasound images of the rats in study and control groups at Day 0, Day 14, Day 28, Day 42, and Day 60 post-injection. The rats in study group, which had been administered with $^{153}Sm_2O_3$-PS microspheres, showed a more pronounced reduction from Day 0 to Day 14 followed by a gradual reduction from Day 14 to Day 42. At Day 28, 83% of rats showed a significant decrease in tumour size after intra-tumoral injection of $^{153}Sm_2O_3$-PS microspheres while the tumour was not observed in one of the rats. At Day 42, tumours were not observed in 33% of the rats and most of the rats showed a good tumour response. At Day 60, no tumour was observed on the ultrasound images of all rats in the study group. In contrast to the control group, the tumour volume was increased progressively over time.

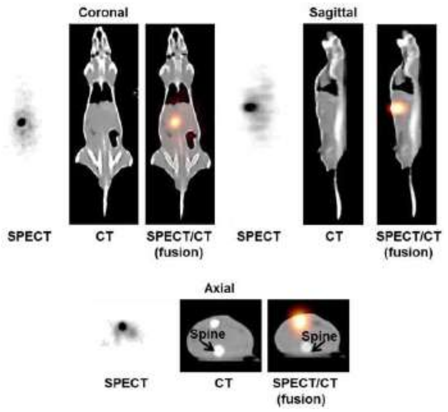

Figure 2: SPECT/CT images of a rat in the study group at Day 5 post-injection. Images displayed the location of ^{153}Sm microspheres in the liver tumour.

The SPECT, CT, and hybrid SPECT/CT images of a rat in the study group are presented in Figure 2. As shown in the figure, the radioactive $^{153}Sm_2O_3$-PS microspheres accumulated at the injection site with no detectable leakage of the microspheres in other organs.

In addition to the gamma imaging capability, the $^{153}Sm_2O_3$-PS microspheres were also visible on the CT images as a radiopaque agent. The location of the microspheres within the tumour can be seen clearly on the CT images acquired at Day 3 and Day 60 post-injection as shown in Figure 3. The CT number of the microspheres was 817.24 ± 49.55 HU which was higher than the CT number of the normal liver (40.41 ± 1.83 HU). The CT number of the microspheres was found comparable to the CT number of the bone at 709.37 ± 36.37 HU.

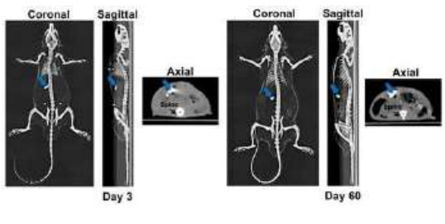

Figure 3: CT images of the rats in the study group at Day 3 and Day 60 post-injection of the $^{153}Sm_2O_3$-PS microspheres. The blue arrow indicates the location of the microspheres.

Despite the promising outcomes, the present study is limited by its small sample size (6 rats for each group) due to the recommendation from the animal ethics committee. Furthermore, the imaging modalities used in this study, including the portable ultrasound, SPECT/CT and CT scanners are clinical systems intended to use for human imaging, and hence the image resolution might be limited for small animals. For future animal studies, it is recommended to apply a larger sample size and to use pre-clinical imaging modalities designated for small animals imaging.

4 Conclusion

This study demonstrated that neutron-activated $^{153}Sm_2O_3$-PS microspheres is an effective therapeutic agent with potential imaging capabilities for liver cancer treatment tested in a SD rat model. A good response rate of 100% was achieved in the study group (n=6) where all the liver tumours disappeared in all rats at 60 days post-treatment, with no hepatoxicity or other abnormalities seen in these rats. The $^{153}Sm_2O_3$-PS microspheres showed its imaging capabilities where the microspheres can be visualized on SPECT/CT and CT images.

References

J.F. Gomes Marin, R.F. Nunes, A.M. Coutinho, E.C. Zaniboni, L.B. Costa, F.G. Barbosa, M.A. Queiroz, G.G. Cerri, and C.A. Buchpiguel. 2020. Theranostics in nuclear medicine: Emerging and re-emerging integrated imaging and therapies in the era of precision oncology. *Radiographics*, 40:1715 – 1740.

IAEA. 1999. Optimization of production and quality control of therapeutic radionuclides and radiopharmaceuticals. *Nucl. Med. Bio.*, International Atomic Energy Agency: Vienna, Austria,.

S. Jeelani, R.J. Reddy, T. Maheswaran, G. Asokan, A. Dany, and B. Anand. 2014. Theranostics: A treasured tailor for tomorrow. *J Pharm. Bioallied. Sci.*, 6:S6 – S8.

H. Sung, J. Ferlay, R.L. Siegel, M. Laversanne, I. Soerjomataram, A. Jemal, and F. Bray. 2021. Global cancer statistics 2020: GLOBOCAN estimates of incidence and mortality worldwide for 36 cancers in 185 countries. *CA Cancer J. Clin.*, 71:209 – 249.

H.Y. Tan, C.H. Yeong, Y.H. Wong, M. McKenzie, A. Kasbollah, M.N.M. Shah, and A.C. Perkins. 2020. Neutron-activated theranostic radionuclides for nuclear medicine. *Nucl. Med. Bio.*, 90 - 91:55 – 68.

H.Y. Tan, Y.H. Wong, A. Kasbollah, M. Shah, B.J.J. Abdullah, A.C. Perkins, and C.H. Yeong. 2022. Development of neutron-activated samarium-153-loaded polystyrene microspheres as a potential theranostic agent for hepatic radioembolization. *Nucl. Med. Commun.*, 43:410 – 422.

M. Van de Voorde, C. Duchemin, R. Heinke, L. Lambert, E. Chevallay, T. Schneider, M. Van Stenis, T.E. Cocolios, T. Cardinaels, B. Ponsard, and et al. 2021. Production of sm-153 with very high specific activity for targeted radionuclide therapy. *Front. Med.*, 8:675221.

M. Walton, R. Wade, L. Claxton, S. Sharif-Hurst, M. Harden, J. Patel, I. Rowe, R. Hodgson, and A. Eastwood. 2020. Selective internal radiation therapies for unresectable early-, intermediate-or advanced-stage hepatocellular carcinoma: Systematic review, network meta-analysis and economic evaluation. *Health Technol. Assess.*, 24:1 – 300.

Individual Research Contribution Review, 2023, 1(1): 569–570

Insights Into Host-Pathogen Interactions : Unveiling *Coxilla Burnetii* Interactions Through Vero Cell Culturing

Daryl Jesus Arapoc
Medical Technology Division
Malaysian Nuclear Agency
43000 Kajang, Selangor
daryl@nm.gov.my

Abstract

Coxilla burnetii, the causative agent of Q fever, exhibits a unique intracellular lifestyle, relying on host cells for survival and replication. This abstract focuses on the culturing of *C. burnetii* in African Green Monkey Kidney (Vero) fibroblasts, shedding light on the interactions between the bacterium and its host. Vero cells have emerged as a valuable in vitro model for studying *C. burnetii* infection. These fibroblastic cells provide an ideal environment for the growth and replication of the bacterium, closely resembling the intracellular conditions found in vivo. The culturing process involves infecting Vero cells with *C. burnetii* and monitoring the growth of the bacterium within the host cells over time. Advanced techniques such as immunofluorescence microscopy and real-time polymerase chain reaction (qPCR) can be employed to visualize and confirm the presence of *C. burnetii* within the infected cells. This culture system enables study on dynamics of bacterial replication, the formation of replicative vacuoles, and the manipulation of host cell processes. Studies using this model have revealed that *C. burnetii* modifies host cell pathways to establish a specialized replicative niche within a modified phagolysosomal compartment. The bacterium's ability to evade lysosomal degradation and modulate host immune responses has been elucidated through Vero cell culture studies. In conclusion, the culturing of *C. burnetii* in African Green Monkey Kidney (Vero) fibroblasts provides a valuable experimental model to investigate the intricate interactions between the bacterium and its host. This system allows for the examination of the intracellular dynamics of *C. burnetii* and provides insights into its survival strategies and manipulation of host cell processes. The use of Vero cell culture contributes significantly to our understanding of Q fever pathogenesis and facilitates the development of targeted therapeutic approaches for combating this infectious disease.

Keywords: Coxiella burnetii, Vero, cell culture, Q fever, zoonotic, infectious disease

1 Introduction

Q fever is a significant zoonotic illness that is regarded as an occupational hazard for persons who deal with animals. Big-scale outbreaks are unusual, but the growing case incidence, along with changing environmental and industrial factors that encourage Q fever transmission, has aroused fears that large and dangerous outbreaks may become more prevalent (Tan et al., 2022). Q fever was initially identified in 1935 in Queensland, Australia, after an outbreak of an unexplained febrile sickness (Query fever) among slaughterhouse employees. Q fever is a bacterial zoonotic disease. Domestic ruminants (cattle, sheep, and goats) are thought to be the pathogen's principal reservoir, since it may infect a wide range of hosts, including mammals (humans, ruminants, small rodents, dogs, and cats), birds, fish, reptiles, and arthropods.

This Q fever is caused by the *Coxiella burnetii (C. burnetti)*, a gram-negative intracellular bacterium. *C. burnetii* is a highly contagious bacterium. This bacterium is regarded a biological terrorist agent due to its extraordinarily high infectivity, resistance to harsh environmental conditions, and capacity to cause serious disease in humans (Mohabbati Mobarez et al., 2017). The Centres for Disease Control and Prevention have classified it as a Category B biological agent which is also considered as a strong bioterrorism (Mohabbati Mobarez et al., 2017). *C. burnetii* is a member of the gamma-subdivision of Proteobaccteria, which also includes *Legionella, Francisella*, and *Rickettsia*. The rickettsia-like bacteria that causes Q fever was initially spotted in the spleen and liver of mice that had been infected with urine from slaughterhouse employees. Macrophages in various organs (such as the lymph nodes, spleen, lungs, and liver) and monocytes in the circulating blood streams are its preferred targets.

In vitro studies of *C. burnetii* infection using African green monkey kidney (Vero) cells have proven to be very efficient. These fibroblastic cells provide an ideal environment for the growth and replication of the bacterium, closely resembling the intracellular condition found in vivo. Culturing *C. burnetii* in Vero cells allow researchers to investigate various aspects of host-pathogen interactions in a controlled and reproducible system. Therefore, the purpose of this study is to provide a comprehensive insight of the significance of culturing *C. burnetii* in Vero cells, covering topics such as the incubation periods of *C. burnetii* in Vero cells, the effect of infection on Vero cell physiology compared to normal cells, and the underlying host-pathogen dynamics.

2 Methods

The Vero cell line (ATCC, CCL-81), kidney epithelial cell line derived from a normal African green monkey were utilised to culture *C. burnetii* in this study. The cell lines were cultured with Dulbecco's Modified Eagle Medium (DMEM), supplemented with 10% fetal bovine serum (FBS; ThermoFisher, A4766801), 1% of GlutaMAX (ThermoFisher, 10566024) and 1% of Penicillin-streptomycin (ThermoFisher, 15140163) in a T75 flask. When cells attained a confluent monolayer, they were passaged (1:3) and maintained in an incubator set to 37°C and 5% carbon dioxide (CO_2). Prior to passage 20, cells were used in enrichment experiments (Anderson et al., 2023). Vero cells were seeded at a sufficient density in a tissue culture flask with a confluence rate of 70-80 percent, then incubate them overnight to facilitate adhesion. Inoculum of *C. burnetii* from a well-characterised strain of bacterium was prepared. These initial inoculam (P0) and supernatants (P1-P3) were placed immediately into ACCM-2 for one week to generate enough C. *burnetii* for LPS extraction and characterisation before being added to Vero cell cultures plated in T75 flasks. At an adequate multiplicity of infection (MOI), *C. burnetii* was introduced to T75 flasks containing a confluent layer of Vero cells. The incubation period of *C. burnetii* in Vero cell lines at 37°C in a humidified atmosphere supplemented with 5% CO_2 for 18- 72 hours. The cellular morphology of Vero cell infected with *C. burnetii* was observed through an inverted light microscope. Following incubation, supernatants were discarded and washed thrice with sterile phosphate saline buffer (PBS). Vero cells were then scraped with a cell scrapper and scrapped cells in ice cooled PBS placed into centrifuge tube filter. The tubes were centrifuged at 10,000xg for 5 minutes. The pellet obtained prior to centrifugation were dissolved in 10 mL PBS. The bacterial density was calculated using decitometer. This procedure was performed repeatedly for a total of three Vero cell-*C. burnetii* passages.

3 Results

Infection of *C. burnetii* in Vero cell demonstrated multiple morphological observation and cytoskeletal rearrangements. Specifically, *C. burnetii* replicated within host cells in compartments known as Coxiella-containing vacuoles (CCVs). Vacuoles exhibited as a distinctive structure within infected Vero cells. Besides, the infected cells observed enlarged compared to the uninfected cells, as they frequently owing to CCV growth. The morphology of infected cells was shown to be more spherical or "balloon-like" than that of uninfected Vero cells, which are flat and elongated. Figure 1 below showed the morphology of Vero cells infected with *C. burnetii*.

4 Discussion

C. burnetii established its internal route by sequentially acquiring the lysosomal enzymes phosphatase and cathepsin D, as well as the early endocytic markers Rab5 and Rab7. At an early stage of infection, newly formed CCVs interact with the autophagy process by recruiting the autophagosomal marker LC3. Even at advanced stages after infection, this connection remains. *C. burnetii*'s intracellular life is prolonged by the delay in reaching lysosomes and the contact with the autophagy process, which supplies membrane, nutrition, and metabolites (Distel et al., 2019; Van Schaik et al., 2013).

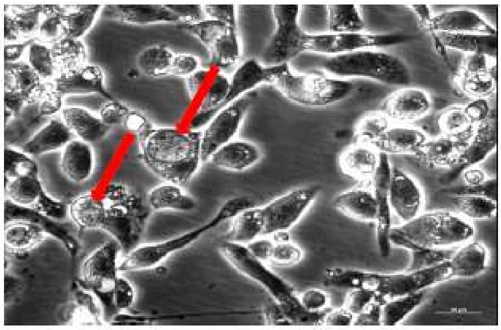

Figure 1: Morphology of Vero cells infected with *C. burnetii*. Arrow indicates the Coxiella-containing vacuoles (CCVs).

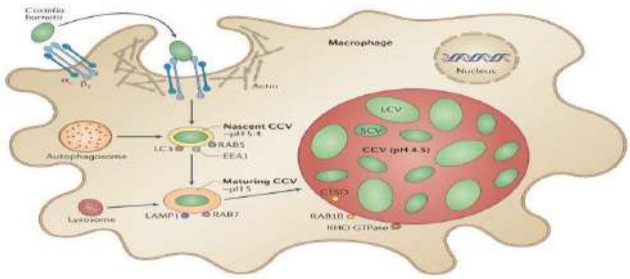

Figure 2: The intracellular trafficking pathway of *C. burnetii* in host cell. Adapted from (Van Schaik et al., 2013).

References

M. W. Anderson, P. Binette, C. Richards, P. A. Beare, R. A. Heinzen, and C. M. Long. 2023. Simple method for enrichment of phase I Coxiella burnetii. *Journal of Microbiological Methods*, 211:106787. https://doi.org/10.1016/J.MIMET.2023.106787.

Beron Distel, J. S., R. Walter, Matias, and O. Flores. 2019. Coxiella burnetii: living inside the host cell. *Biocell*, 43(1):1 – 6.

A. Mohabbati Mobarez, F. Bagheri Amiri, and S. Esmaeili. 2017. Seroprevalence of Q fever among human and animal in Iran; A systematic review and meta-analysis. *PLOS Neglected Tropical Diseases,*, 11(4):e0005521. https://doi.org/10.1371/JOURNAL.PNTD.0005521.

T. S. E. Tan, M. Hernandez-Jover, L. M. Hayes, A. K. Wiethoelter, S. M. Firestone, M. A. Stevenson, and J. Heller. 2022. Identifying scenarios and risk factors for Q fever outbreaks using qualitative analysis of expert opinion. *Zoonoses and Public Health*, 69(4):344–358. https://doi.org/10.1111/ZPH.12923.

E. J. Van Schaik, C. Chen, K. Mertens, M. M. Weber, and J. E. Samuel. 2013. Molecular pathogenesis of the obligate intracellular bacterium Coxiella burnetii. *Nature Reviews. Microbiology*, 11(8):561. https://doi.org/10.1038/NRMICRO304.

Individual Research Contribution Review, 2023, 1(1): 571–572

Isolation and Purification of 4-Phenylcoumarins from *Mesua Assamica* by Fast Centrifugal Partition Chromatography

Hazlina Ahmad Hassali
Medical Technology Division
Malaysian Nuclear Agency
43000 Kajang, Selangor
hazlinaahmad@nm.gov.my

1 Introduction

For centuries, natural products continue to play an essential source for discovery of new drugs throughout the world in treating and preventing human illnesses. Natural products are important sources for drug development. The amounts of bioactive natural products in natural medicines are always fairly low. Today, it is very crucial to develop effective and selective methods for the isolation and purification of those bioactive natural products. Many techniques have been invented and upgraded to make this task easier. Fast Centrifugal Partition Chromatography (FCPC), an efficient and easily scalable approach for the isolation and purification of natural products. This paper will depict a few examples of natural products purification by using FCPC, which demonstrates a fast and effective way of natural products isolation. The *Mesua* (Calophyllaceae) has been known to produce various new chemical compounds of medicinal values. Some *Mesua* species have yielded new potential anticancer agents that are important to the pharmaceutical industry (Hassali et al., 2022). *Mesua assamica* (King & Prain) Kosterm. belongs to the family Calophyllaceae. *Mesua assamica* is commonly known as 'Sia Nahor' in Assam and the tree is found along the foothills of the Himalayas in the North Lakhimpur subdivision of Assam, India (Puppala et al., 2023). Parts of the *M. assamica* have been used traditionally as refrigerant in order to reduce overheat in the body, as well as to cure dizziness and dry skin. The aqueous extract of the stem bark of the *M. assamica* has been valued in traditional medicine for anti-malarial activity and treating fevers. The preliminary screening findings suggest that non-polar extracts of *M. assamica* bark particularly hexane extract exhibited good cytotoxic activity and could be potentially useful for the development of therapeutic agents against cancer (Hassali et al., 2022). *M. assamica* has been identified for its potential anticancerous properties. In vitro cytotoxic evaluation through MTT assay induction against human breast MCF-7 cancer cell lines exhibited that hexane extracts were found to have IC_{50} value below 30μg/ml and conferred effective in inducing cell death MCF-7. The diversity of phytochemicals present suggests that the stem bark and leaves of *Mesua assamica* could serve as a potential source of useful drugs. Exploitation of the pharmacological properties involves further work on isolation, purification and identification of the bioactive compounds from this plant (Hassali et al., 2022). Purification of natural products has frequently been a difficult undertaking for many scientists around the world. FCPC, which demonstrates a quick and efficient method of isolating natural products, will be used in this presentation to illustrate a few examples of natural products purification. Therefore, in this study, the hexane extract of *M. assamica* bark were further explored for its chemical constituents. Various chromatographic methods were used for the fractionation, isolation and purification of the metabolites from hexane extract of *M. assamica* bark, including FCPC.

2 Materials and Methods

2.1 Plant material and reagents

Dried ground bark of *M. assamica* (1.5 kg) was soaked with hexane (3 x 4L, 48 hours) at room temperature. The extract was evaporated to dryness using a rotary evaporator. A yellow gummy residue (110.4 g) was obtained from the hexane extract. A portion of the hexane extract (10.0 g) was subjected to column chromatography fractionation over silica gel (230-400 mesh) and eluted with hexane:EtOAc (9.5:0.5 to 0:10) and EtOAc:MeOH (5:5) to yield fractions H1-H6. Fraction H5 (hexane: EtOAc 95:5) was subjected to FCPC separation as a purified fraction from the hexane extract of *M. assamica*.

2.2 Centrifugal Partition Chromatography (CPC)

Armen Instruments FCPC was used for FCPC separations; FCPC-250 system coupled with Armen Glider Spot Prep II FCPC software and provided by Armen Technologies (France). The FCPC-250 system was equipped with a 250 mL column with injection capacity ranging from 10 mg to 3-6 g. The rotation speed was adjustable from 0 to 3000 rpm. Binary gradient pump with a flow-rate that ranges from 5 to 15 mL/min, built-in automatic injection valve, UV-vis dual wavelength spectrophotometer with high pressure flow cell were also used. The rotor was first filled with the upper phase of the solvent system, as the stationary phase. The separation was performed with the system composed of heptane-ethyl acetate-acetonitrile-water (9:1:9:1, v/v/v/v), containing trifluoroacetic acid 0.1% in the isocratic mode. The apparatus was rotated at 1600 rpm and the lower mobile phase of the solvent mixture was then pumped into the inlet of the column (rotor) at a flow rate of 10 mL/min in the descending mode. Samples were loaded in the 5 mL injection-loop, and injected in the column in a "sandwich" mode, i.e., at the same time with the mobile phase. First elution occurred in the descending mode (reversed-phase mode): the rotor was filled with the upper apolar phase of the solvent mixture, and the pumped mobile phase is the polar lower phase. The first badge was collected in descending mode for 50, 150, 300 and 500mg of samples.

After collecting fractions in the descending mode by peak, another badge was injected to collect as multidual mode, where by the switching valve is turned to the ascending mode and the mobile phase pumped is the upper one this time. The descending-ascending switching went on until all the peaks observed in descending mode came out. Extrusion was performed after the last tube; the lower phase was pumped in the ascending mode to eject the sum of the upper phase out of the rotor. *n*-Heptane (Hept), ethyl acetate (EtOAc), methanol (MeOH), acetonitrile (CH_3CN) were purchased from Carlo Erba Reactifs (Val de Reuil, France) as analytical grade solvents used for CPC analyses. Trifluoroacetic acid (TFA) was purchased from Sigma-Aldrich (Lyon, France). Water was of ultrapure quality. Samples were filtered with 0.45 μm nylon membrane filter prior to injection.

3 Results and Discussion

Various chromatographic methods were used for the fractionation, isolation and purification of the metabolites from hexane extract of *M. assamica* bark, including fast centrifugal partition chromatography (FCPC), thin layer chromatography (TLC), preparative liquid chromatography (Prep-LC) and high-performance liquid chromatography (HPLC). Preparative liquid chromatography of *M. assamica* bark hexane extract yielded a total of 6 fractions namely F1, F2, F3, F4, F5 and F6. All these fractions were screened for MTT assay to determine the cytotoxic activity of the fractions against MCF-7 and MDA-MB 231 cell lines. Fractions from F2 - F6 revealed higher selectivity towards MCF7 cells compared to MDA-MB 231. F1 considered inactive towards both cell lines. F4, F5 and F6 demonstrated as potent fractions. Two 4-phenylcoumarins compounds namely mammea A/BB cyclo F and mammea A/BA cyclo F were isolated by using FCPC and the structures of these two compounds were identified by 1H NMR, 13C NMR and LC-MS/MS.

Figure 1: FCPC-250 system coupled with Armen Glider Spot Prep II

Compound 1 was isolated as white amorphous powder and the LCMS/MS measurement revealed an $[M+H]^+$ ion peak at m/z 423.1819, which corresponded to the molecular formula of $C_{25}H_{26}O_6$. Comparison with the literature values, compound 1 has been identified as mammea A/BA cyclo F, which has previously been purified from Calophyllum dispar for the first time in 2001 (Guilet et al., 2001). Compound 2 was separated as white amorphous solid. The ^{1}H NMR spectra of compound 2 is reminiscent of those of compound 1, which suggested a close structural relationship between these two compounds. The observed data of compound 3 indicated that this compound is mammea A/BB cyclo F, (Guilet et al., 2001).

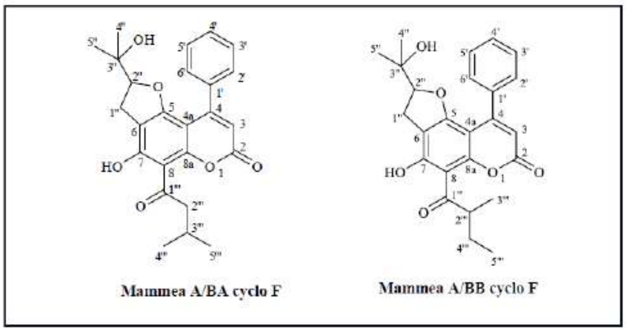

Figure 2: 4-phenylcoumarins from hexane extract of bark of *M. assamica*

4 Conclusions

FCPC attracted great attention in separation science and have been widely used in the separation of natural products. Two 4-phenylcoumarins namely mammea A/BB cyclo F and mammea A/BA cyclo F were isolated by using FCPC and the structures of these two compounds were identified by 1H NMR, 13C NMR and LC-MS/MS.FCPC is cost-effective and dramatically reduces solvent use resulting in a more environmentally-friendly, green technique.

References

D. Guilet, J. J. Hélesbeux, D. Séraphin, T. Sévenet, P. Richomme, and J. Bruneton. 2001. Novel Cytotoxic 4-Phenylfuranocoumarins from Calophyllum d ispar. *Journal of Natural Products*, 64(5):563–568.

H. A. Hassali, C. Gomathi, W. H. W. Bahrin, Z. Adam, and D. JESUS. 2022. Phytochemical evaluation and cytotoxic activities of stem bark and leaf extracts of mesuaassamica. *Sains Malaysiana*, 51(10):3237–3250.

E. R. Puppala, S. S. Yalamarthi, S. L. Aochenlar, N. Prasad, N. P. Syamprasad, M. Singh, S. K. Nanjappan, V. Ravichandiran, D. M. Tripathi, J. K. Gangasani, and V. G. M. Naidu. 2023. Mesua assamica (King&Prain) kosterm. Bark ethanolic extract attenuates chronic restraint stress aggravated DSS-induced ulcerative colitis in mice via inhibition of NF- κB/STAT3 and activation of HO-1/Nrf2/SIRT1 signaling pathways. *Journal of ethnopharmacology*, 301(115765).

Individual Research Contribution Review, 2023, 1(1): 573–574

Pre-Treatment with RNase a in Cytokinesis Block Micronucleus Assay for Analysis using Automated System

Juliana Mahamad Napiah
Medical Technology Division
Malaysian Nuclear Agency
43000 Kajang, Selangor
juliana_m@nm.gov.my

Abstract

Cytokinesis Block Micronucleus (CBMN) Assay is a simple and an alternative way for indicator of chromosome damage. In a large radiation accident, CBMN Assay can be early detect for chromosome damage before we do aberration chromosome assay. RNase as an agent to remove residual stainable cytoplasmic material. Clear background help to easier in analysis of micronuclei (MN). The clear image of background useful for slides assessed with automatic image analysis system.

Keywords: Micronuclei, Rnase A, Remove Residual

1 Introduction

The dicentric chromosome assay is the "gold standard" in biodosimetry for estimating radiation exposure, meanwhile the cytokinesis-block micronucleus (CBMN) assay is a comprehensive technique for measuring DNA damage, including lymphocytes. CBMN assay is a simple and an alternative way for indicator of chromosome damage. It is because researchers only need to measure visible micronuclei (MN) in binucleated cells, micronuclei analysis is much easier than metaphase chromosome aberration analysis. The micronucleus technique was proposed as a reliable method for measuring chromosomal damage caused by cytotoxic agents "in vivo" (Fenech and Morley, 1985) and very useful in a large radiation accident case because of its simplified technique and much easier to analysis. Treatment with RNase A is a pretreatment step in the protocol to remove any residual RNA present. Objective of this study to prove RNase A is a treatment that very useful for analyse binucleated cell using automated analysis system. Automated system is more sensitive to analyse image compared to manual microscope. Digital image analysis tools help automate and quantify findings, reducing or eliminating manual work and providing more objective and quicker input to the final diagnosis compared to traditional microscopy. It helps handle high sample volumes efficiently, improving productivity and reducing turnaround time.

2 Methods

2.1 Cytokinesis Block Micronucleus Assay (CBMN)

Peripheral blood sample were collect using heparinized vacutainer tube. Blood was cultured in 10ml complete media and incubate for 72 h in incubator at 37°C and 5% CO_2. The complete media consisted of 87% of RPMI supplemented with 10% of heat-inactivated fetal bovine serum, 2% of streptomycin-penicillin and 1% of Glutamine. Each 10ml complete media will add with 1 ml blood and 300μl of phytohemagglutinin (PHA). At 44 h, 6 μg/ml of cytochalasin B was added to all the culture flasks. The cell then was centrifuged for 10 minutes at 180 g and the supernatant culture medium is removed. 5 ml of 0.075 M cold (4°C) KCL resuspended and centrifuge for 10 minutes. The cells then were wash with freshly made fixative consisting of methanol: acetic acid (10:1) with three or four further changes of the fixative until the cell pellet is clear.

2.2 RNase A Treatment and Slide Analysis

Cell pellet were dropped onto clean slides, the slides then treated with RNase A. 1250μl RNase A is heated in water bath for 10 minutes at 70°C and then allowed to cool slowly at room temperature. Slides are rinsed in distilled water and place in RNase A solution (stock solution: distilled water 1:39) for 10 minutes at 37°C. The slides then washed in distilled water again and placed in 3:1 (methanol: acetic acid) fixative for 2 minutes, keep the slides overnight to dry it. Next, slides were stained in 2% of Giemsa stain for 10 minutes and dry it overnight. Each slide was scan and capture using Microscope Zeiss with Metafer 4 software.

3 Results and Discussions

Figure 1 show microscopic view of binucleated cells with and without treatment of RNase A. Background for image (a) is darker than image (b). RNase A was reducing the background so that the image much easier to analyse.

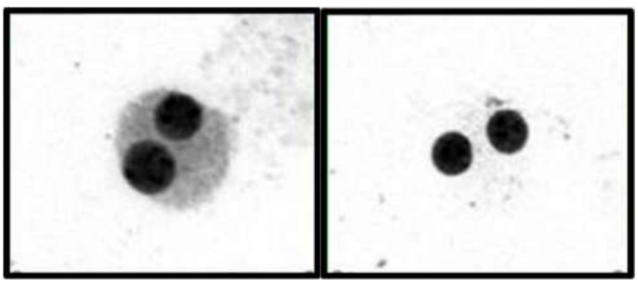

Figure 1: Microscopic view of binucleated cells without RNase A treatment (A) and with treatment RNase A (B).

Binucleated cells with micronuclei shown in Figure 2. Image clearly shows a micronuclei, micronuclei size is small than the binucleated cell and same colour with binucleated cell. Without treatment, the background was darker, and micronuclei look-a-like image will be confusing to analyse.

Figure 2: Microscopic view of binucleated cells with 1 MN (slide treated with RNase A)

4 Conclusion

This study improves the method for analysing Giemsa stained CBMN microscopic images quickly and automatically, with a high detection rate and processing speed. Automated system is more sensitive compared to manual microscope. Clear background of cell is more helpful to analyse the cell.

References

International Atomic Energy Agency. 2011. Cytogenetic Dosimetry: Applications in preparedness for and response to radiation emergencies. International Atomic Energy Agency, Vienna.

M. Fenech and A. A. Morley. 1985. Measurement of micronuclei in lymphocytes. *Mutat. Res.*, 147:29 – 36.

Lidiya Luzhna, Palak Kathiria, and Olga Kovalchuk. 2013. Micronuclei in genotoxicity assessment: From genetics to epigenetics and beyond. *Frontiers in Genetics*, 4:131.

Syaifudin M, Defiyandra VP, Nurhayati S, Purnami S, and Pudjadi E. 2018. Micronucleus assay-based evaluation of radiosensitivity of lymphocytes among inhabitants living in high background radiation area of Mamuju, West Sulawesi, Indonesia. *Genome Integr*, 9:2.

Qing-Zeng Qian, Xiang-Ke Cao, Fu-Hai Shen, and Qian Wang. 2016. Effects of ionising radiation on micronucleus formation and chromosomal aberrations in Chinese radiation workers. *Radiat Prot Dosimetry*, 168(2):197 – 203.

Individual Research Contribution Review, 2023, 1(1): 575–576

Production and Quality Control of Chromium-51 (Cr-51) to Form Cr-51 EDTA for Determination of Glomerular Filtration Rate

Muhammad Hanaffi Bin Mohamad Mokhtar
Medical Technology Division
Malaysian Nuclear Agency
43000 Kajang, Selangor
mhanaffi@nm.gov.my

Abstract

Determination of GFR (glomerular filtration rate) is an important test to determine the kidney health function which carried out in hospitals in Malaysia. Although there are other methods that involve the use of inulin and Tc-99m DTPA, it requires a large quantity of urine sample and is more difficult to control the other reaction factors in the body. The use of Cr-51-EDTA has its own advantages and justifications. The accuracy and response of Cr-51 EDTA which does not affect the internal response of the human body and suitable for patients with excretory problems makes it a better choice than the other options mentioned above.

1 Introduction

The objective of the studies is to produce Cr-51 from the TRIGA Puspati reactor and subsequently to produce radiopharmaceutical namely Cr-51 EDTA. The quality control procedure will also concurrently developed to make sure the Cr-51 EDTA being produce are safe and following safety standard outline by NPRA/ IAEA.

The project output and impacts including:

i. The production of Cr-51 from the reactor can further expand the function of TRIGA PUSPATI.

ii. Cr-51 can be commercialized because there is no producer from Malaysia that produces it yet.

iii. The potential to produce Cr-51 EDTA for the use of hospitals in Malaysia which will benefit the society.

iv. The potential of Cr-51 EDTA to be commercialized at a lower price than the import price.

v. Creating skilled manpower for the production of Cr-51.

2 Methods

2.1 Production of Cr-51 from chromium powder (metal)

In brief the method involved as follow:

i. Study on the target material that is suitable to produce Cr-51 to be irradiated in TRIGA reactor. In what forms (metal, chips or powder), and the suitability of the material to be prepared. The capsulating case such as NAA radiation tube, the quartz ampoule and etc. need to be determined.

ii. Optimization of the amount of weight and energy required to produce stable and reproducible Cr-51 from the TRIGA reactor.

iii. Radionuclide purity studies on Cr-51.

iv. Radiochemical purity studies on Cr-51.

v. Writing the results of the study for further study.

3 Results

3.1 First batch Cr-51 irradiation to find optimization data

0.503g chromium chips in NAA radiation vial were irradiated in Triga Puspati reactor at dry tube position for 6 hours and yield 611 uCi Cr-51 (2.26 Mbq/mL). The yield need to be ramped up because we need at least 7.2-8.8 Mbq of Cr-51 as stated in IAEA Tecdoc-1340. Radionuclide purity study using gamma spectroscopy show that only peak at 320.25 keV appeared.

3.2 Subsequent batch Cr-51 irradiation

Second batch irradiation, using more chromium than previous study (750 mg) giving yield 0.658 mCi/ml (24.346 Mbq/ml). The Cr was irradiated at central thimble (CT) for 5 hours and the sample was contained in NAA radiation vial. This batch giving enough radiaoactivity as outline by IAEA Tecdoc-1340 which need at least 7.2 Mbq/ml. Radionuclide purity study using gamma spectroscopy show that only peak at 320.25 keV appeared.

4 Discussion and conclusion

At the initial stage of irradiation, it was found that the radioactivity of Cr-51 produced did not meet the standards set in the IAEA-TECDOC-1340 (it has low radioactivity, 2.26 Mbq/ml). IAEA-TECDOC-1340 outlines that Cr-51 should have at least 7.2 Mbq/ml of radioactivity. The next irradiation was carried out, this time by increasing the weight of Cr-51 by 750 mg and changing the irradiation location in the reactor. The sample was placed in the Central Thimble (CT) chamber and the sample was also wrapped in a thicker aluminum can to prevent water from the CT entering the sample. As a result, the study found that radioactivity had increased to 24.346 Mbq/ml and this exceeded the minimum value outlined in the IAEA-TECDOC-1340. Unfortunately, there is water that enters the sample even though a thick aluminum can have been used. This issue needs to be controlled because it can cause radiation pollution to the operator. It was found later that this Cr-51 could not be dissolved in the next process to form radiopharmaceutical. Various methods to finely ground Cr-51 chips have been planned but almost all of them are not suitable as the Cr-51 produced needs to be completely pure up to 99%. The fine ground process will accidentally introduce the presence of other impurities which will then be irradiated together with the pure Cr resulting impure Cr-51. The team decided to buy and obtain Cr-51 that is pure and in powder form to overcome this problem.

From the radionuclide study, it was found that the irradiated Cr produced only one peak at 319.48 keV. This is the energy value for Cr-51. The absence of other detected elements shows that the Cr-51 produced is pure without any impurities.

Figure 1: Irradiated chromium-51 chip when dissolved in concentrated HCL

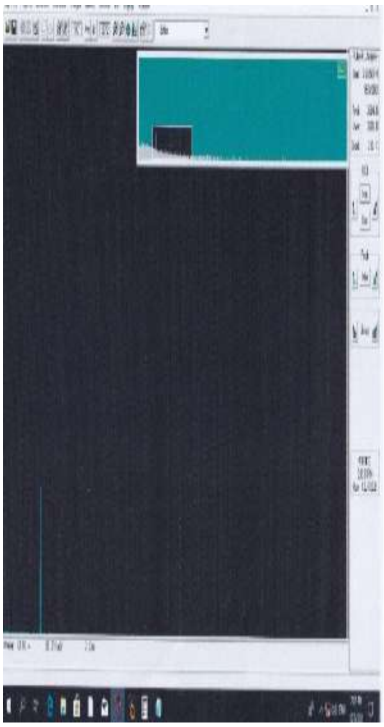

Figure 2: Only peak at 319.48 keV (Cr-51) detected, no inpurities.

References

International Atomic Energy Agency. 2003. Manual for reactor produced radioisotopes. IAEA-TECDOC-1340:IAEA, Vienna (2003).

Individual Research Contribution Review, 2023, 1(1): 577–578

Processing of Samarium-153: Obtaining Optimum Radiotherapeutic Dose while Implementing Sterilization Method

Nadhirah Razanah Shahrol
Medical Technology Division
Malaysian Nuclear Agency
43000 Kajang, Selangor
nrazanah@nm.gov.my

Abstract

Samarium-153 (Sm-153) is a radioisotope used for palliative treatment of painful bone metastases when labelled with ethylenediamine tetra (methylene phosphonic acid) (EDTMP). It is produced by Malaysia's TRIGA MARK II reactor and involves series of processing steps to ensure its safety and effectiveness. Improvisation was being done after few productions of Sm-153, by adding in filtration method using 0.22 μm membrane filter, which may compromise optimum radiotherapeutic dose obtained.

Keywords: Samarium-153 (Sm-153), palliative, processing, filtration

1 Introduction

Production of Sm-153 involves series of processing steps in order to ensure its safety and effectiveness in labelling with EDTMP and injected to patient. Improvisations are made along the way, such as biosafety cabinet was used, aseptic technique was implemented, and filtration technique was added. However, this step would actually reduce radioactivity dose obtained as some would adhere on the filter. Filtration is one of sterilization methods that is used to remove microbes and particulate contaminants from the product and is considered an important aspect in radiopharmaceutical preparation.

2 Methods

Enriched Samarium-152 was sent for irradiation in deposited powder form inside quartz ampoule. It was irradiated in central thimble for a total of 24 hours (with rest time after 12 hours irradiation). Once irradiation was done, Sm-153 was brought to be processed inside biosafety cabinet which has high-efficiency particulate air (HEPA) filter. During processing of Sm-153, the ampoule was broken and 0.1M HCl was added using syringe. It was then resuspended to ensure the whole powder was dissolved before being transferred to an empty vial. At the end of the processing step, filtration was done using membrane filter of size 0.22 μm. Radioactivity reading of Sm-153 inside the ampoule and container were then obtained using dose calibrator. Radioactivity of Sm-153 inside vial, empty ampoule, empty container, used syringe, needle and filter was then measured.

3 Results

Radioactivity readings obtained were as followed:

No.	Subject	Batch 1: No filter Dose (mCi)	Batch 2: Filter added Dose (mCi)
1.	Before processing (Sm-153 in ampoule)	185.0	185.0
2.	After processing (Sm-153 in vial)	172.0	166.0
3.	Loss during processing (%)	7%	10%

No.	Subject (During/ After processing)	Batch 2: Dose (mCi)
1.	Syringe	1.1
2.	Needle	4.2
3.	Filter 0.22	11.5
4.	Ampoule (empty)	5.1

4 Discussion

There are 3% increase in loss of radioactivity while implementing sterile filtration method, however, therapeutic dose can still be obtained as the dose needed is around 100 mCi per patient. Previously, filtration is only done at final stage after radiolabelling with EDTMP. Thus, with this result, it is possible to include filtration during Sm-153 processing before it is radiolabelled so as to remove unwanted contaminants like chips of broken ampoule and also microorganisms. This could ensure sterility and also instil confidence among healthcare practitioners in using Sm-153 produced by Malaysian Nuclear Agency.

5 Conclusion

The result showed that despite lessening of radioactivity, the effective therapeutic dose can still be obtained within optimum range while implementing sterile filtration method. The results however can still be improved with more batches produced with their radioactivity reading monitored during processing.

References

C. Russell, T. Hansen, and M. Paulsson. 2023. Sterilisation methods. *In Practical Pharmaceutics: An International Guideline for the Preparation, Care and Use of Medicinal*

Products, pages 731–748. Cham: Springer International Publishing.

Individual Research Contribution Review, 2023, 1(1): 579–580

Impact of Fetal Bovine Serum (FBS) on Dicentric Chromosome Assay in Increasing the Number of Cells and Improving the Size of Chromosome from the Cells Harvest

Nurul Nazeerah Juarimi
Medical Technology Division
Malaysian Nuclear Agency
43000 Kajang, Selangor
nazeerah@nm.gov.my

Abstract

Chromosome aberration frequency is the most reliable biological marker for detecting acute accidental radiation exposure. In biological dosimetry, dicentric assay using blood lymphocytes is one of the techniques that frequently used. After taking blood sample, several replicate of cultures should be prepared which using Roswell Park Memorial Institute (RPMI) 1640 as the culture media used and supplemented with FBS serum, antibiotics and L-glutamine. Serum is used to act as nutrient source in lymphocyte culture media which support the growth of the lymphocyte cells. This study using 10% and 20% FBS serum in dicentric chromosome aberration assay. After 48 hours of incubation, followed by harvesting, the amount of cells in both serum content are being observed with naked eyes. Then, number of cells will be counted from the auto-capture image using automated Metaphase Finder System. Besides, the size of chromosomes from both serum content will be compared. In general, the amount of cells increases as the percentage of FBS serum used is higher.

1 Introduction

The frequency of chromosome aberrations provides the most reliable biological marker to detect acute accidental radiation exposure (IAEA, 2011). Radiation can cause different types of chromosomal aberrations, which can be divided to stable aberrations like translocations and unstable aberrations like dicentric chromosomes (DC), micronuclei, acentric, and ring-form (Agarwal et al., 2023). Dicentric chromosome assay (DCA) using blood lymphocytes has become the “gold standard” of radiation biological dosimetry due to its reproducibility, relative specificity to radiation and its sensitivity to doses below acute medical significance (Manello and Tonti, 2007). Fetal bovine serum (FBS) and fetal calf serum (FCS) are widely used growth supplements for cell culture, principally due to their high concentrations of growth stimulatory hormones and low concentrations of growth inhibitory factors (IAEA, 2011). FBS act as one of the factors which influence the cell progression rate in cell culture, hence may affect the chromosome aberration frequencies (Kanda, 2000). In this facility, FBS is used as the standard procedure following International Atomic Energy Association (IAEA) technical document and the percentage used as a common practice is 10% FBS for the samples that being received. However, there are only a few journals reported on the effect of different percentage of FBS in the dicentric chromosome aberration assay for higher radiation dose exposure. Hence, the goal of this study is to compare the cells count in chromosome aberration assay using 10% and 20% FBS. In addition, the size of the chromosomes is being observed using automated Metaphase Finder System.

2 Methods

In this study, dicentric chromosome aberration assay using standard method from International Atomic Energy Association (IAEA) technical document is used. A coagulation tube containing lithium heparin is used to hold blood specimens. The blood specimen must be received within 24 hours of the blood sample time and should be transported at a temperature between 18°C and 24°C. Following the receipt of blood samples, the media for the cell culture should be ready, and every process needs to be carried out in a biosafety cabinet using aseptic technique.

The culture medium is using Roswell Park Memorial Institute 1640 (RPMI-1640) which then supplemented with Fetal Bovine Serum (FBS), antibiotics, L-glutamine. In this investigation, two different FBS percentage which are 10% and 20% FBS being employed to compare the number of cells and the effects on the chromosomes size from the cells harvest. For media flask 10% FBS (10A), contains 0.1ml 1% Glutamine, 0.2ml 2% antibiotics, 1.0ml FBS and 8.7ml RPMI-1640 to made up 10.0ml media. In the media flask for 20% FBS (20A), contains 0.1ml 1% Glutamine, 0.2ml 2% antibiotics, 2.0ml FBS and 7.7ml RPMI-1640 to made up 10.0ml media. Then, 2.0ml of blood specimen are being added into each media flask respectively. At final stage of media preparation, add 0.3ml Phytohaemagglutinin (PHA) into each media flasks. After that, incubate the cells at 37°C with 5% CO_2 for 48 hours. At 45 hours of incubation period, add 50μl of colcemide into each flask.

After complete 48 hours incubation period, cells should be harvested by transferring the cell culture into two tubes, labelled with 10A and 20A. Centrifuging the cell cultures with speed of 1000rpm for 10 minutes, then discard the supernatant and replace with hypotonic solution which is 5.0ml of 0.075M Potassium Chloride (KCl). After that, repeat centrifuging with speed of 1000rpm for 10 minutes. Potassium Chloride (KCl) should be removed and replace with 5.0ml freshly prepared fixative (3:1, methanol:acetic acid). During the initial addition, introduce the fixative slowly and steadily at constant rate while stirring it using vortex mixer. Following that, centrifuge the cells with speed of 1000rpm for 5 minutes, resuspended and repeat in four changes fixative. After removing the final wash of fixative, there should left with sufficient volume of suspension for dispensing onto slides. All the process should be done for both tube 10A and 20A.

In slides preparation, use clean and grease free slides. Dispensing the cells from both suspension 10A and 20A onto the slides respectively and pre-treated the slides with RNase. A 10mg/ml RNase solution is heated at 70°C for 10 minutes and then allowed to cool slowly. During pre-treatment of slides with RNase, distilled water, KCl and RNase are used following the sequences. During soaking the slides in the RNase solution, left it in water bath at 70°C for 30 minutes. Next, the slides need to be stained with 2% Giemsa and let to dry. Then, slides are mounted using Dibutylphthalate Polystyrene Xylene (DPX) mountant and a coverslip. Finally, auto-capturing image of chromosome by using Metaphase Finder System.

3 Results and Discussion

In this study, the amount of cells that being harvest, were observed with naked eyes before removing the final wash fixative. The result in Figure 1 shows that the amount of cells in Tube 10A and Tube 20A cannot be differentiated with naked eyes. This may happen when the amount of cells in both tubes are almost the same.

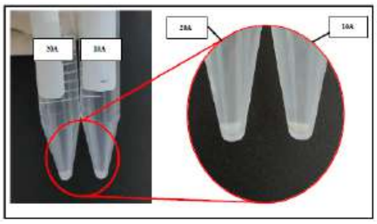

Figure 1: Comparison for amount of cells in Tube 10A (cells with 10% FBS) and Tube 20A (cells with 20% FBS) that were observed with naked eyes.

The slides with cells from both samples were being analysed using automated Metaphase Finder System. The system able to scan through and count the number of cells with chromosome as reported in Table 1. The number of cells when sample added with 20% FBS are slightly higher than sample added with 10% FBS. This may indicate there is effect when increasing the percentage of FBS in the sample. Thus, higher percentage of FBS, 20% can be used when receving sample for higher radiation dose exposure. The samples with high radiation dose exposure received may come in small volume and the cells that will be harvested may be less, hence using percentage of 20% FBS may help in increasing the number of cells during culture and more cells can be seen after harvesting. Kanda R. stated that the measurement of aberration frequencies may be affected by any factor influencing the cell progression rate in culture.

In addition, from the image auto-captured with Metaphase Finder System, it shows that when higher percentage of FBS, 20% used in the sample, it gave bigger size of chromosomes

Table 1: Comparison of number of cells in sample with 10% FBS and sample with 20% FBS.

FBS percentage	Number of cells
10% (Tube 10A)	1188
20% (Tube 20A)	1236

in the cells that harvested (Figure 2). Hence, this demonstrate that using higher percentage of FBS may results in better size of the chromosomes from the cells harvest.

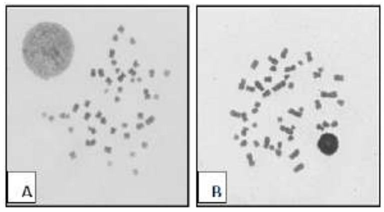

Figure 2: Image of chromosomes in c ell with 10% FBS from Tube 10A A) and cell with 20% FBS from Tube 20A (B) auto captured with Metaphase Finder System.

4 Conclusion

In conclusion, this study shows that the usage of 20% of Fetal Bovine Serum increased the number of cells in the sample of chromosome aberration assay and better size of chromosome captured by the Metaphase Finder System from the cells cultured and harvested. This indicate that this concept can be considered and adapt for higher radiation dose exposure sample. Further study on the usage of percentage 20% of FBS need to be done in higher radiation dose exposure sample, in order to get better view of the results.

References

N. Agarwal, A.K. Rathi, S. Kapoor, K. Singh, S. Arora, A. Jindal, and et al. 2023. Biodosimetric analysis of head and neck cancer patients undergoing radiotherapy by dicentric chromosome aberration assay. *Journal of Cancer Research and Therapeutics*, April 06, 2023.

IAEA. 2011. Cytogenetic dosimetry: Applications in preparedness for and response to radiation emergencies. pages 53–61, International Atomic Energy Agency.

R. Kanda. 2000. Improvement of accuracy of chromosome aberration analysis for biological radiation dosimetry. *Journal of Radiation Research*, 41(1):1–8. http://doi: 10.1269/jrr.41.1.

F. Manello and G.T. Tonti. 2007. Concise review: No breakthroughs for human mesenchymal and embryonic stem cell culture: Conditioned medium, feeder layer, of feeder-free; Medium with fetal calf serum, human serum, or enriched plasma; Serum-free, serum replacement nonconditioned medium, or ad hoc formula? All that glitters is not gold! *Journal of Stem Cells*, 25:1603–1609.

Individual Research Contribution Review, 2023, 1(1): 581–582

Quality Control on Sodium Iodide (I-131) Capsule Produced by Agensi Nuklear Malaysia

Rahimah Abdul Rahim
Medical Technology Division
Malaysian Nuclear Agency
43000 Kajang, Selangor
rahimah@nm.gov.my

Abstract

Radioiodine (Iodine-131) hard gelatin capsules are widely used for the diagnosis and treatment of various thyroid disorders including toxic nodules, thyroid hypofunction, carcinoma of the thyroid gland and hyperthyroidism. Radioiodine with capsule has several advantages compared to radioiodine supplied in the form of a solution. At Bahagian Teknologi Perubatan (BTP), Agensi Nuklear Malaysia, Iodine-131 solution was dispensed into the capsule in the dedicated hot cell using calibrated pipettor. Aim of this study is to test the quality of sodium iodide (I-131) capsule produced by Agensi Nuklear Malaysia.

Keywords: Sodium iodide (I-131) capsule, quality control

1 Introduction

Iodine-131(^{131}I) is an important radioisotope of iodine discovered by Glenn Seaborg and John Livingood in 1938 at the University of California, Berkeley[1]. It is highly radioactive with a half-life of about 8.02 days. ^{131}I is the most used iodine radioisotope, and it decays mostly by beta-emission (606 keV; 90%). It is well-known for causing the death of cells because it can penetrate other cells up to several millimeters away. For this reason, ^{131}I is used for the treatment of thyrotoxicosis (hyperthyroidism) and some types of thyroid cancer that absorb iodine[2]. Quality control and quality assurance are crucial prerequisite for all classes of pharmaceuticals production. A deficient quality of diagnostic radiopharmaceutical, will contribute to the unsafe product, give erroneous information about the patient's condition leading to inappropriate determination of therapy and could lead to excess radiation exposure to non-target tissues and reduced efficacy. Therefore, quality control testing is vital to ensure the radiopharmaceuticals are safe and effective.

2 Methods

The quality control procedures namely the appearance, disintegration, radionuclide identification, radiochemical purity, and microbiology test were carried out at the laboratory as required by standard pharmacopeia. Two batches of capsules were produced with the activity of each capsule was 10 mCi and 100 mCi. The capsule was homogenized with water and methanol and then used for radiochemical purity and radionuclide identification test. Six capsules were placed in each of the tubes of the basket with 800 ml of specified medium maintained at 37± 20°C for the disintegration test. Meanwhile for the microbial test, the decayed capsule was dissolved aseptically in sterile phosphate buffer solution and test for bioburden dan *E.coli*.

3 Results

The ^{131}I solution is dispense and adsorbed on a disodium hydrogen phosphate anhydrous in gelatin bovine capsule. BTP has produced two batches of sodium iodide (I-131) capsule with the activity of each capsule was 10 mCi and 100 mCi. Each batch contains 10 capsules. The quality control procedures were carried out at the laboratory as required by standard pharmacopeia procedure for days 1, 2, 7 and 14. The tests were done until day 14 is indirectly to find out the stability of the product. For the disintegration test procedure, a non-radioactive capsule with filler (disodium hydrogen phosphate anhydrous) was tested. This procedure is acceptable been tested without radioactive material. The specification and the result of sodium iodide (I-131) capsule test as in Table 1 and Table 2.

Table 1: Specification of sodium iodide (I-131) capsule.

	Type of test	Specifications
1.	Physical appearance	White and grey powder in colorless capsule
2.	Disintegration	Dissolve completely within 15 minutes
3.	Radionuclide identification	Gamma ray at energy 0.364MeV
4.	Radiochemical purity	≥95 %
5.	Microbial test ;	
	• Total viable microbial	Not more than 1000 cfu/ml
	• Total fungal count	Not more than 100 cfu/ml
	• *Escherichia coli*	Absent

[1]http://uwlbrachycourse.wikifoundry.com/page/ Iodine-131

[2]Thyroid Hormones, Iodine and Iodides, and Antithyroid DrugsAuthor links open overlay panelVicky V.Mody*AjayN.Singh†RahulDeshmukh‡SamitShah§ https://www.sciencedirect.com/science/journal/ 03786080

Table 2: Quality control test of sodium iodide (I-131) capsule.

Sample/Test	10 mCi				100 mCi			
	1	2	7	14	1	2	7	14
Physical appearance	White and grey powder in colorless capsule				White and grey powder in colorless capsule			
Disintegration (minute)	3.2	3.2	2.6	3.3	2.6	2.1	2.8	2.6
Radionuclide identification	Gamma ray at energy 0.364MeV				Gamma ray at energy 0.364MeV			
Radiochemical purity (%)	96.2	95.6	96.6	95.7	98.3	96.3	97.1	95.4
Microbial test								
Total viable microbial	Nill				Nill			
Total fungal count	Nill				Nill			
Escherichia coli	Absent				Absent			

4 Discussion

Both batches of sodium iodide (I-131) capsule with activity 10 mCi and 100 mCi respectively was tested and results met the specifications accordance in British Pharmacopeia and the United States Pharmacopeia. However, production of sodium iodide (I-131) capsule needs some improvement to achieve more than 99% of radiochemical purity determination.

References

Thyroid Hormones, Iodine and Iodides, and Antithyroid DrugsAuthor links open overlay panelVicky V.Mody*AjayN.Singh†RahulDeshmukh‡SamitShah§ https://www.sciencedirect.com/science/journal/ 03786080.

Production of 131-I iodide capsules in Argentina.

IAEC-Production of ^{131}I Gelatin Capsule.

Refer to Operation Manual for Automated Gamma Counter.

British Pharmacopeia.

United State Pharmacopeia.

http://uwlbrachycourse.wikifoundry.com/page/ iodine-131.

Individual Research Contribution Review, 2023, 1(1): 583–584

Purification of Chalcone Derivative using Preparative Liquid Chromatography

Rosniza binti Razali
Medical Technology Division
Malaysian Nuclear Agency
43000 Kajang, Selangor
rosniza@nm.gov.my

Abstract

Purification means the removal of unwanted impurities present in an organic compound. High-purity target chemicals are separated and refined using preparative liquid chromatography (Prep-LC) from a mixed solution following a synthetic step or from natural extracts. This technique is widely regarded as an excellent purification technique because it can quickly gather high-purity compounds and, in some cases, large quantities of compounds needed for subsequent evaluation, analysis, and processing. In this paper, Prep-LC was used to purify the chalcone derivative, and TLC and LCMS/MS were used to determine its structure. The purification was performed using an Agilent Eclips Plus C18 column (9.4 mm x 250 mm, 3.5 μm) with the mobile phase of 0.1% trifluoroacetic acid in water (mobile phase A) and 0.1% trifluoroacetic acid in acetonitrile (mobile phase B) in a gradient mode as follows: 0 min: 95% A, 4 min: 90% A, 50 min: 40% A, 54 min: 5% A, and 90 min: 95% A, with 2.5 ml/min flow rate at room temperature, and the wavelengths of 254 and 366 nm.

Keywords: Purification, Preparative Liquid Chromatography, chalcone

1 Introduction

The chalcone is a simple chemical scaffold of many naturally occurring compounds and has a widespread distribution in vegetables, fruits, teas, and other plants. Chalcone is a key intermediate in the synthesis of flavonoids, which exhibit a wide range of biological activities including anticancer, anti-inflammatory, antidiabetic, antioxidant, antimicrobial, antileishmanial and antimalarial properties (Elkanzi et al., 2022). Despite its importance, obtaining chalcone with high purity can be challenging due to the presence of impurities during the synthesis process.

Purification is a process of removing impurities, contaminants or unwanted elements from a substance to make it cleaner, safer or more refined. The purity of a compound is crucial because it directly impacts the compound properties and its intended use.

Preparative liquid chromatography (Prep-LC) offers an efficient and scalable solution for the purification of chalcone, allowing for the isolation of the compound from impurities with high selectivity and yield. Prep-LC is a type of chromatography that is used to separate and purify larger amounts of a desired compound from a mixture. It is commonly used in the pharmaceutical, biotechnology, and chemical industries to isolate and purify compounds for further use or analysis. In preparative liquid chromatography, a sample mixture is passed through a column filled with a stationary phase that interacts with the different components of the mixture to varying degrees. The components are separated based on their different affinities for the stationary phase, and the desired component(s) are collected in pure form as they elute from the column.

Prep-LC is different from analytical liquid chromatography, which is used for analyzing small amounts of compounds in a mixture. In analytical liquid chromatography, the goal is to separate and identify different components of a mixture, while in Prep-LC, it aims to isolate and purify a specific compound in larger quantities. Prep-LC is a powerful tool for the production of pure compounds, but it requires appropriate optimization of the chromatography conditions, including the choice of stationary and mobile phases, column dimensions, and flow rate, to achieve the desired separation and purity (Guiochon, 2002).

2 Method

Synthesized chalcone solution was prepared by dissolving 5 mg of synthesized chalcone in 1 mL of 5% acetonitrile to give a final concentration of 5000 μg/mL. Then, the mixture was sonicated for 5 minutes before being filtered with a 0.2μm nylon membrane filter. The Armen Spot Prep II system was used for purification, consisting of interchangeable pump heads, a fraction collector, a quaternary gradient, a UV/VIS detector and a back flush valve. The purification was conducted using an Agilent Eclipse Plus C18 column with a 250 mm length, 9.4 mm width, and particle size of 3.5 μm. The chalcone solution was loaded into the system using a syringe. The gradient method uses a mixture of 0.1% trifluoroacetic acid in water (mobile phase A) and 0.1% trifluoroacetic acid in acetonitrile (mobile phase B). The total runtime of the method was 90 minutes, and the gradient was varied as follows:

a) initially 95%A and 5% B;

b) 4 min 90% A and 10% B;

c) 50 min 40% A and 60% B;

d) 54 min 5% A and 95% B; and

e) 90 min 5% A and 95% B.

A constant flow rate of 2.5 mL/min, and the loaded sample was 1 mL. Prior to loading the sample, the column was equilibrated with the mobile phase. This ensures that the stationary phase is properly hydrated and that any air bubbles in the column are removed. The elution profile was monitored using a UV detector to ensure that chalcone eluted as a single peak. The chalcone peak was collected in a fraction collector, and thin-layer chromatography (TLC) analysis was utilized to verify its purity (Shailendra et al., 2007).

3 Results and Discussion

In order to provide the most chemical information and the best separation in the chromatogram, mobile phases with different compositions were investigated in this study. For this work, we tried different gradient elution conditions with a mixture of 0.1% trifluoroacetic acid in water (mobile phase A) and 0.1% trifluoroacetic acid in acetonitrile (mobile phase B).

Upon oprtimization, the gradient method uses a mixture of mobile phases A and B, varied as follows:

a) initially 95% A and 5% B;

b) 4 min 90% A and 10% B;

c) 50 min 40% A and 60% B;

d) 54 min 5% A and 95% B; and

e) 90 min 5% A and 95% B

was chosen for the separation of the purity of the chalcone sample because it gave a good separation with a high, sharp, and symmetrical peak (Figure 1). To improve the peak shape and prevent the peak tail from the chalcone peak, trifluoroacetic acid was used as a modifier. This is because the presence of acid in the mobile phase can produce good analyte separation.

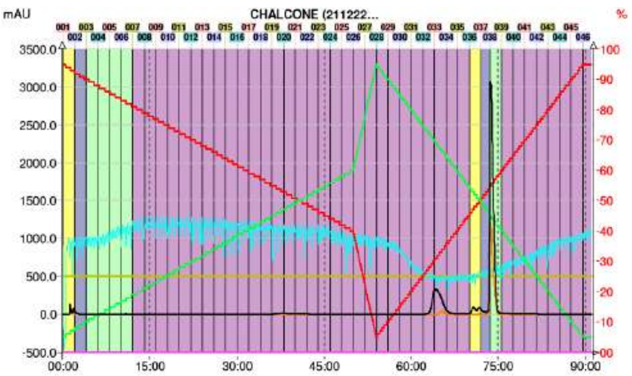

Figure 1: Chromatogram for purification of chalcone derivative using Preparative Liquid Chromatography (Prep-LC)

The results demonstrated an increase in chalcone compound purity rate, upon performing the purification process. This confirmed through the TLC tested, where when the TLC tested was carried out on the chalcone compound before the purification process, it is founded that many bands was produced on the TLC plate, while in the TLC test on the chalcone compound that had undergone the purification process, only one band is produced on the TLC plate (Figure 2). This result signifies that the primary peak presented on the Prep-LC chromatogram corresponds to the peak for the pure chalcone compound. The resulting primary peak was further subjected to analysis used the LCMS/MS method to confirm that the peak's molecular mass was 236 g/mol.

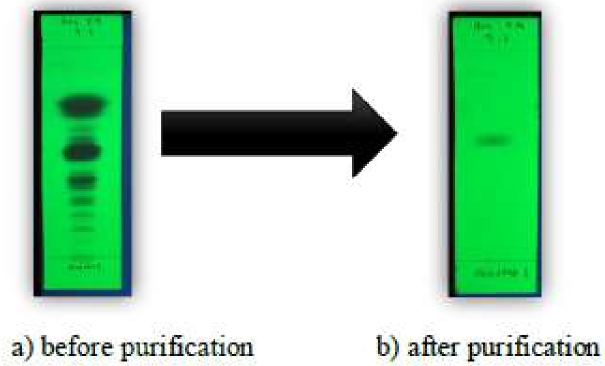

Figure 2: TLC of chalcone a) before purification process and b) after purification process using Hexane- Ethyl Acetate (9:1) as a mobile phase

4 Conclusion

In conclusion, the purification of chalcone using preparative liquid chromatography requires careful optimization of the chromatography conditions to achieve the desired purity and yield. It is crucial to choose a suitable stationary and mobile phase and to monitor the elution profile to ensure that the chalcone is eluted as a single peak.

References

Nadia A. A. Elkanzi, Hajer Hrichi, Ruba A. Alolaya, Wassila Derafa, Fatin M. Zahou, and Rania B. Bakr. 2022. Synthesis of chalcones derivatives and their biological activities: A review. *ACS Omega*, 7(32):27769 – 28684.

Georges Guiochon. 2002. Preparative liquid chromatography. *Journal of Chromatography A*, 965(Issues 1–2, 2 August 2002,):129 – 161.

M. Shailendra, P. S. Hemendra, G. Dutta, and N. S. N. M. 2007. Synthesis and characterization of some chalcone derivatives. *Trends in Applied Science Research*, 2(1):52 – 56.

Individual Research Contribution Review, 2023, 1(1): 585–586

The Stability Study of Sterile and Pyrogen Free DMSA Lyophilized Cold Kit

Saifullizan Mohamad
Medical Technology Division
Malaysian Nuclear Agency
43000 Kajang, Selangor
saifullizan@nm.gov.my

Abstract

Lyophilized dimercaptosuccinic acid (DMSA) cold kit that is labelled with radioisotope Tc^{99m} (Technetium-99m) to form ^{99m} Tc-DMSA complexes which acts as diagnostic agent to study the morphology of kidneys was formulated. However, radiochemical purity (RCP) and quality control testing should be conducted towards each product batches after its production and during the validity period within one year at the recommended storage conditions since it was an important routine practice in nuclear medicine for ensuring the products quality, efficacy and safety. Hence, this study was conducted to evaluate the stability and sterility of DMSA lyophilized cold kit. The lyophilized kit was reconstituted with 1 mL addition of Tc^{99m} solution (20 - 30 mCi) at the optimum pH. By using the Instant Thin Layer Chromatography (iTLC) method, 2-3 uL sample was spotted at the origin of the 1.5 cm pencil marked at the bottom, later the strip was developed with the mobile phase solution of acetone to reach the solvent front which 1.0 cm from the top. The dried duplicate strips were then evaluated by TLC scanner. Sterility and bacterial endotoxin test were also conducted to all three batches of lyophilized cold kit in order to ensure that the kits are sterile and free from pyrogen. The ^{99m}Tc-DMSA complexes showed the RCP values of more than 95% until one year of storage as required by European Pharmacopeia. This study also showed that all three batches of kits passed the sterility and bacterial endotoxin test.

Keywords: DMSA, Technetium-99m, Radiochemical purity (RCP), Instant Thin Layer Chromatography (iTLC)

1 Introduction

Radiopharmaceuticals are generally formulated from kits prepared in authorized manufacturing facilities. A cold kit contains the ligand at which Tc-99m is to be complexed, an adequate quantity of reducing agent (stannous chloride), buffer to adjust the pH to suit the labelling conditions, stabilizing agents and excipients. The radiopharmaceutical kits are prepared in a lyophilized form and have a long shelf life of up to one year. A nuclear medicine renal scan uses radiopharmaceuticals such as ^{99m}Tc-DTPA and ^{99m}Tc-MAG3 injected into a vein, to provide clear images of the kidneys taken with a special camera called a gamma camera or SPECT/CT. A ^{99m}Tc-DMSA is one of the technetium radiopharmaceuticals also used in renal imaging and primarily used to study the morphology of renal cortex. In this study, locally produced lyophilized sterile and pyrogen free DMSA kit (to be reconstituted with Tc-99m) were prepared.

2 Methods

Three batches of lyophilised sterile and pyrogen free DMSA cold kits were formulated at the cleanroom facility in Malaysian Nuclear Agency. Then, the stability study of the ^{99m}Tc-DMSA for a year of storage were carried out by reconstituting lyophilized kit with 1 mL addition of Tc^{99m} solution (20 - 30 mCi) at the optimum pH that is then analysed by the Instant Thin Layer Chromatography (iTLC) method. About 2-3 uL sample was spotted at the origin of the 1.5 cm pencil marked at the bottom, later the strip was developed with the mobile phase solution of acetone to reach the solvent front which 1.0 cm from the top. The dried duplicate strips were then evaluated by TLC scanner in order to obtain radiochemical purity (RCP) values. Sterility and bacterial endotoxin test were also conducted to all three batches of lyophilized cold kit by Quality Control Laboratory of Medical Technology Division, Malaysian Nuclear Agency.

3 Results and discussion

Three batches of lyophilised sterile and pyrogen free DMSA cold kits were formulated at the cleanroom facility in Malaysian Nuclear Agency as shown in Figure 1.

Figure 1: Batch 1(BN01), Batch 2 (BN02) and Batch 3 of DMSA lyophilised cold kit.

Radiochemical purity (RCP) values for all three batches of DMSA lyophilised cold kit were an important parameter to determine the efficacy of radiolabelling DMSA kit with the ^{99m}Tc radionuclide. In this test, ^{99m}Tc-DMSA was subjected to the iTLC in the acetone solvent system to detect the separation between product that is ^{99m}Tc-DMSA and the impurity which is free ^{99m}Tc-pertechnetate. The RCP of radiolabelled complex was determined by subtracting the percentage of impurity from 100%. The higher the RCP, the better the radiolabelling efficiency of the DMSA kit. The equation of RCP was stated in the equation below.

$$\text{RCP values} = 100\% - {}^{99m}\text{ Tc-pertechnetate}$$

Figure 2 and Table 1 show the iTLC of ^{99m}Tc-DMSA in the acetone solvent system. ^{99m}Tc-DMSA complex, which has Rf value of 0.0, was separated from ^{99m}Tc-pertechnetate, which has Rf value of 0.9 to 1.0.

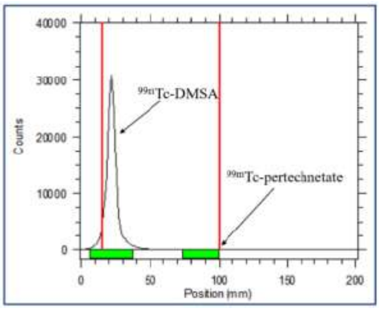

Figure 2: Separation graph of ^{99m}Tc-DMSA and ^{99m}Tc-pertechnetate in acetone solvent system

Table 1: iTLC result in the acetone solvent system.

	Rf	Percentage
^{99m}Tc-DMSA	0.0	99.47%±0.018
^{99m}Tc-pertechnetate	0.9 - 1.0	0.53%±0.018

Figure 3 shows the percentage of RCP for all three batches for month 1, month 2, month 3 and month 12. After 1 month of storage, the RCP values for BN01, BN02 and BN03 were 98.95%±0.021, 99.28±0.015 and 99.41±0.012 respectively. The RCP values for BN01, BN02 and BN03 were 99.48±0.011, 99.10±0.030 and 99.56±0.009 respectively during the second month of storage. During the third month, the RCP values for BN01, BN02 and BN03 were 99.23±0.017, 99.14±0.022, and 99.27±0.012 respectively. The RCP values during month twelve were 99.49±0.021, 99.38±0.018 and 99.62±0.016 for BN01, BN02 and BN03 respectively. ^{99m}Tc-DMSA complexes showed the RCP values of more than 95% up to one year of storage at 2-8°C.

Based on the Figure 4, all three batches which are Batch 1, Batch 2 and Batch 3 passed the sterility and bacterial endotoxin test conducted by Quality Control Laboratory of Medical Technology Division, Malaysian Nuclear Agency.

4 Conclusion

All three batches of DMSA lyophilized cold kit developed in this work is stable up to one year at the recommended storage conditions of 2-8°C. According to European Pharmacopeia (2005), RCP value should pass above 95%. The ^{99m}Tc-DMSA complexes showed the RCP values of more than 95% after a year of storage. All three batches also passed the sterility and bacterial endotoxin test and it is clearly indicated that the cold kits were sterile and pyrogen free.

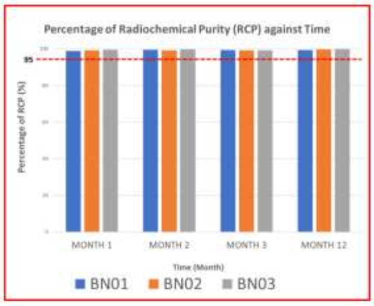

Figure 3: RCP values for all three batches, BN01, BN02 and BN03 of DMSA lyophilised cold kits.

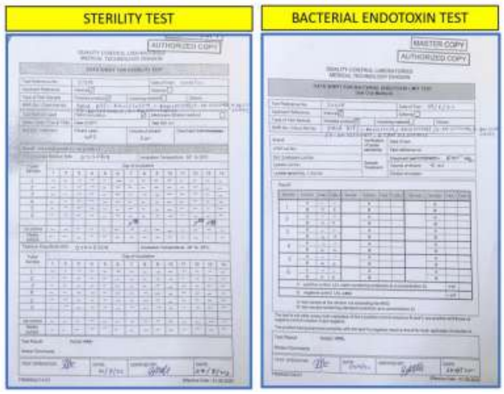

Figure 4: Data sheet of sterility and bacterial endotoxin test conducted by Quality Control Laboratory of Medical Technology Division, Malaysian Nuclear Agency.

References

IAEA TECHNICAL REPORTS SERIES No. 466. 2008. Technetium-99m radiopharmaceuticals: Manufacture of kits. pages 86 – 88. InternationalAtomic Energy Agency, IAEA Vienna, Austria.

EUROPEAN DIRECTORATE FOR THE QUALITY OF MEDICINES. 2005. Technetium (^{99m}Tc) succimer injection. *European Pharmacopoeia*, 5^{th} edition:EDQM, Council of Europe, Strasbourg, 865.

IAEA RADIOISOTOPES and RADIOPHARMACEUTICALS SERIES. No.1. 2009. Technetium-99m radiopharmaceuticals: Status and trend. IAEA Vienna, Austria.

Individual Research Contribution Review, 2023, 1(1): 587–588

Induced and Spontaneous Preclinical Models for Cancer Study

Siti Aminah binti Muhamad
Medical Technology Division
Malaysian Nuclear Agency
43000 Kajang, Selangor
aminah_m@nm.gov.my

Abstract

The models used in cancer treatment discovery are constantly changing and progressing towards advanced preclinical studies. Thus, numerous studies on cancer models have been done in order to gain better understanding of cancer invasion, progression, and early detection. Herein, we discuss on how the generative information of preclinical cancer model potentially improve our understanding on the cancer progression, development of cancer models through genetically engineered and microsurgical induced cancer model.

Keywords: Cancer, genetically engineer, microsurgical induced

1 Introduction

Cancer is an epidemic disease causing approximately 8 million deaths annually worldwide. Nonetheless, cancer cannot be defined as a single characterized tumour, but rather as a heterogeneous and enormously fluctuating system. That is why selecting the most fitting model to best depict the given tumour system is one of the most difficult aspects of cancer assessment (Breitenbach and Hoffmann, 2018). Cancer models, whether naturally or artificially induced will have common characteristics with human tumours. In vitro cancer models' inability to simulate the heterogeneity of human cancer cells, their microenvironment, and the stromal compartment has hampered comprehensive understanding of the tumour development, therapeutic responses, and adverse reactions (Voskoglou-Nomikos et al., 2003). Even all cancer models aim to mimic at least some features of human cancer, but in the end, we do not have a perfect model, yet it should be figured out how to intercept our information within the structure of the limitations of the test used. Hence, the aim of this paper is to show how the development of cancer models can be induced in-vivo.

2 Methods

2.1 Microsurgical Induced Cancer Models

As in Table 1.

Table 1: Selected in-vivo cancer inoculation studies.

Cancer localization	Cancer Type	Animal strain	Xenograph method	Cancer development evaluation
Skin	Melanoma	Balb c	Subcutaneous injection	Western immunoblotting
Blood	Acute myeloid leukemia	NOD-scid-IL2Rg−/− (NSI) mouse	Irradiation followed by retro-orbital vein injection	Flow cytometry for CD45+ cells Bone marrow and spleen staining
	Acute lymphoblastic leukemia	NOD-SCID-γc −/− (NSG) mouse	Tail vein injection	Flow cytometry Bioluminescent imaging
Head and neck	Head and neck squamous cell carcinoma	Athymic nude NCI-Frederick	Mouth floor injection	Intravital imaging Immunohistochemistry
Thorax	Breast cancer	Balb/c and NSG	Subcutaneous, Intracranial and Lateral tail vein injection	Immunohistochemistry
	Lewis lung carcinoma	C57BL/6 and BALB/c	Inferior vena cava, and subcutaneous injection	Immunohistochemistry
Abdomen	Gastric cancer	Bl6/Rag2/GammaC double knockout	Orthotopic injection	Bioluminescence imaging Immunohistochemistry
Pelvis	Pancreatic cancer Prostate cancer	BALB/c CB.17. SCID	Orthotopic injection Orthotopic and subcutaneous injection	Immunohistochemistry Bioluminiscence Intravital microscopy Immunohistochemistry
	Epithelial ovarian cancer	BALB/c nude	Subrenal capsule implantation	Immunohistochemistry Western blot

2.2 Genetically Induced Cancer Models

The most commonly used models for oncology research are immunocompetent or immunocompromised mice transplanted subcutaneously or orthotopically with syngeneic and xenografted tumours; their usage is primarily justified by their low cost and ease of creation. However, in a clinical practice, the malignant environment within an oncological patient is far more complex. Transgenic mice are another type of cancer research model used in preclinical settings, in which tumour suppressor genes are downregulated or oncogenes are expressed preferentially via three main methods: DNA construct microinjection, retroviral infection, and "gene-targeted transgene" method.

2.2.1 Methods for Generation of Genetically Induced Model

(a) Spontaneous mutations; these changes occur spontaneously in mouse colonies after multiple breeding events and are usually recognized when they are linked with a phenotypic change. The genetic background of spontaneously altered mice can be linked to events in human disorders and used to develop models of specific diseases.

(b) Mutations caused by chemicals or radiation; these genetic changes are based on the exposure of mice to mutagens such as ethylnitrosourea (ENU), which can be utilized for large-scale mutagenesis programs and the identification of specific genetic alteration patterns responsible for human disease.

Table 2: Advantages and disadvantages of the widely used methods for genetically induced model

Method of Induction	**Advantages**	**Disadvantages**
Spontaneous Mutation	• Disvovery of novel mutations associated with specific traits/pathologies • No cost in induction of mutations	• Low mutation frequency • Hard to detect if not associated with phenotypic changes
Chemical/ Radiation Induced Mutation	• High mutational rate • Minimal cost for induction of mutation	• Random integrative mutations • Hard to associate specific mutations with pathologies
Retroviral Infection	• Insertion of specific gene • Low controlled events	• Vector capacity in carrying large genes • Random integration in the genome
Micro-injection of DNA construct	• Direct insertion of specific gene • Medium controlled events	• DNA silencing mechanisms • Insertion of multiple copies in tandem

(c) Retroviral infection; this method is one of the first partially controlled protocols for generation of transgenic mice and is based on the transfection of preimplantation embryos with a retrovirus that contains the gene to be replaced/modified. The modified embryos are implanted into recipient females and analysed for the presence or absence of the genetic modifications in concordance with the developed phenotype.

(d) Microinjection of DNA constructs; it comprises the direct injection of DNA constructs into one-cell fertilized embryos followed by transfer in recipient females and analysis of the presence or absence of the genetic modifications in concordance with the developed phenotype.

3 Conclusion

Nowadays, cancer research is already drawing significant funding for research projects focusing on novel early diagnostic tools and treatment formulations. However, the availability of experimental animal models suitable for testing new hypotheses prior to prospective clinical adoption is critical for all of these funding opportunities. The resemblance of human characteristics of cancer models is directly proportional to the relevance and safety of clinical trials. As important as the benefits are, establishing comprehensive and relevant animal models is also tough. The ability to mimic the evolution of a human tumour, a malignant microenvironment, a reaction of the organism to a testing strategy, drug metabolism, toxicity and pharmacokinetics, and other potential side effects, in concordance with a functional immune system, they are difficult, time consuming, and expensive to mimic at once in an animal model.

References

M. Breitenbach and J. Hoffmann. 2018. Cancer models. *Frontiers in oncology*, 8:401. https://doi.org/10.3389/fonc.2018.00401.

Data sharing [Infographic]. www.mdpi.com/journal/diagnostics.

T. Voskoglou-Nomikos, J. L. Pater, and L. Seymour. 2003. Clinical predictive value of the in vitro cell line, human xenograft, and mouse allograft preclinical cancer model. *Clinical cancer research*, 9(11):4227 – 4239.

C. Wang, Z. Tang, Y. Zhao, R. Yao, L. Li, and W. Sun. 2014. Three-dimensional in vitro cancer models: A short review. *Biofabrication*, 6(2):022001. https://doi 10.1088/1758–5082/6/2/022001.

P. Workman, E. O. Aboagye, F. Balkwill, A. Balmain, G. Bruder, D. J. Chaplin, and S. A. Eccles. 2010. Guidelines for the welfare and use of animals in cancer research. *British journal of cancer*, 102(11):1555–1577. http://doi:10.1038/sj.bjc.6605642.

Individual Research Contribution Review, 2023, 1(1): 589–590

IRCR

Tetrofosmin Radiolabelled with Technetium-99m (^{99m}Tc) for Myocardial Perfusion Imaging

Siti Selina Abdul Hamid
Medical Technology Division
Malaysian Nuclear Agency
43000 Kajang, Selangor
selina@nm.gov.my

Abstract

Heart disease is the second most common cause of death in humans after cancer. However, the mortality rate could be reduced through early detection. The aim of this study is therefore to produce a radiopharmaceutical tetrofosmin kit and to evaluate its quality, stability and sterility. The ^{99m}Tc-tetrofosmin complexes show good radiochemical purity at room temperature for up to 6 hours. The sterility and pyrogenicity of these lyophilized tetrofosmin kits were also verified. These results brought us one step closer to locally produced radiopharmaceuticals.

Keywords: Tetrofosmin, Technetium-99m (^{99m}Tc), Heart disease

1 Introduction

Nuclear medicine is a discipline of medicine that uses radiation to obtain image-based information about human anatomy and organ function. Radioactive materials can be used alone as radioisotopes or in combination with certain pharmaceutical substances as radiopharmaceuticals. The distribution of the radiopharmaceuticals in the body is detected and the information obtained helps to plan the patient's future therapy.

The radionuclide technetium-99m (^{99m}Tc) is particularly attractive to the nuclear physician due to its optimal gamma energy for SPECT, its availability, low cost and can be easily labelled with a radiopharmaceutical kit. Another advantage is that its short half-life minimises radiation exposure to patients.

Tetrofosmin is a diagnostic agent used to assess areas of reversible myocardial ischemia in the presence or absence of myocardial infarction and to evaluate ventricular function (Kelly et al., 1993). It is also used to identify perfusion changes caused by pharmacologic stress in individuals with coronary artery disease.

The aim of this study is to produce a radiopharmaceutical tetrofosmin kit and evaluate its quality, stability and sterility.

2 Materials and Methods

Each vial of the tetrofosmin kit consists of a lyophilized mixture of 1.38 mg tetrofosmin, 0.09 mg stannous chloride dehydrate, 1.92 mg disodium sulfosalicylate, 3 mg sodium D-gluconate, and 11 mg sodium hydrogen carbonate (Healthcare, 2018; IAEA, 2008A). The lyophilized powder is sealed with a rubber stopper under a nitrogen atmosphere (S.Pervez and A.Mushtaq., 2009). The sterility study of the tetrofosmin kit was evaluated by the growth of microorganism in tryptone soy broth (TSB) and thioglycollate media. The presence of endotoxin was investigated using the gel-clot technique. The tetrofosmin kits were radiolabeled with Tc-99m and incubated for 15 minutes at room temperature. The radiolabelling efficiency and radiochemical purity (RCP) were then determined using the ITLC technique at different time points: 0, 15, 30, 60, 120, 240 and 360 minutes (Hammes et al., 2004). The percentage of labelling efficiency of radiolabeled tetrofosmin was measured for free ^{99m}Tc and reduced-hydrolysed technetium as well as for radiocolloids. Free ^{99m}Tc-pertechnetate migrates to the top of the strip (Rf = 0.8-1), ^{99m}Tc-tetrofosmin migrates to the centre of the strip (Rf = 0.3-0.7) and colloidal impurities remain at the origin.together with two reduced impurities (Rf = 0.0-0.1),

3 Result and discussion

Three batches of the pyrogen-free lyophilized tetrofosmin kit were prepared and stored at 2 - 8°C in the refrigerator.

The lyophilized tetrofosmin kits were successfully labelled with Tc-99m. The average RCP of radiolabeled tetrofosmin, ^{99m}Tc-tetrofosmin is greater than 90% at all times point at room temperature. Therefore, radiopharmaceuticals used for diagnostic or therapeutic purposes must have an RCP greater than 90%. The length of time a radiopharmaceutical remains at this RCP value indicates the shelf life of the product. The results of the Rf value and RCP analysis of the three manufactured batches of tetrofosmin kits are shown in Table 1. Figure 1 shows a radiochromatogram of ^{99m}Tc-tetrofosmin by ITLC.

Table 1: The average of the Rf values of ^{99m}Tc-tetrofosmin using the solvent acetone: dichloromethane (35:65, vol./vol.)

Batch No	**Reduced ^{99m}Tc (0.0–0.1)**	**^{99m}Tc-tetrofosmin (0.3-0.7)**	**^{99m}TcO$_4$- (0.8-1.0)**	**RCP (%) (% RCP ± 0.05)**
1	0.064	0.562	0.856	94
2	0.086	0.581	0.905	95
3	0.099	0.634	0.914	95

The stability of the tetrofosmin kit was also determined monthly by the radiochemical purity test. The results show that the RCP is greater than 90% up to the second month. In the third month, however, the RCP falls below 90%. The decrease in RCP indicates that the tetrofosmin produced is unstable. Therefore parameters such as storage conditions, especially temperature and relative humidity, need to be examined to ensure that such a radiopharmaceutical product continues to meet the stated specifications.

Reg	(mm) Start	(mm) Stop	(mm) Centroid	RF	Region Counts	Region CPM	% of Total	% of ROI
Rgn 1	13.6	40.6	25.5	0.124	13702.0	13702.0	3.20	3.22
Rgn 2	39.7	95.4	76.4	0.722	410700.0	410700.0	96.02	96.52
Rgn 3	95.4	100.8	97.1	0.966	1114.0	1114.0	0.26	0.26
3 Peaks					425516.0	425516.0	99.49	100.00

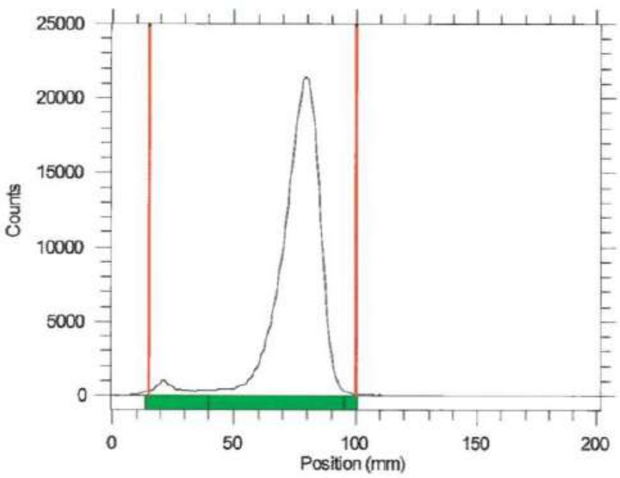

Figure 1: A double peak at the base of the ITLC-SG strip. The first peak corresponds to $^{99m}TcO_4^-$, while the second peak represents ^{99m}Tc-tetrofosmin. The labeling efficiency of 97% was determined by calculating the area under the curve.

The lyophilized tetrofosmin kit remained sterile and pyrogen-free during the storage period (3 months) although no antimicrobial preservatives were added. The addition of antimicrobial preservatives is not mandatory in the production of radiopharmaceuticals.

4 Conclusion

In conclusion, ^{99m}Tc-tetrofosmin has been successfully developed locally as a potential for nuclear medicine imaging. The lyophilized tetrofosmin kits produced meet the pharmacopoeia requirements because its radiochemical purity is on average above 90%. However, the lyophilized tetrofosmin kits are only stable for 2 months. Therefore, further studies need to be conducted before the product is approved and released for use in patients.

References

Richard Hammes, Lori A Joas, Thomas E Kirschling, Jamie R Ledford, Tara L Knox, Mark R Nybo, and John J Sterzinger. 2004. Better method of quality control of 99mTc-Tetrofosmin. *J. Nucl Med Technol*, 32(2):72 – 78.

Ge Healthcare. 2018. Product Monograpgh MYOVIEWTM (Kit for the preparation of Technetium Tc-99m Tetrofosmin Injection).

IAEA. 2008A. Technetium-99m Radiopharmaceuticals: Manufacture of Kits. Technical Report Series No. 466.

J. Duncan Kelly, Alan M. Forster, Brian Higley, Cohn M. Archer, Fong S. Booker, Lewis R. Canning, K. Wai Chiu, Barbara Edwards, Harjit K. Gill, Mary McPartlin, Katharine R. Nagle, Ian A. Latham, Roger D. Pickett, Anthony E. Storey, and Peter M. Webbon. 1993. Technetium-99m-Tetrofosmin as a New Radiopharmaceutical for Myocardial Perfusion Imaging. *The Journal of Nuclear Medicine*, 34(2):222–227.

S.Pervez and A.Mushtaq. 2009. Formulation of a freeze-dried kit for the preparation of 99mTc-tetrofosmin. *Journal of Radioanalytical and Nuclear Chemistry*, 281:371 – 377.

Individual Research Contribution Review, 2023, 1(1): 591–592

Development of Single Vial Cold Kit for Preparation of ^{68}Ga-DOTA-PSMA I&T for PET Imaging of Prostate Cancer

Wan Hamirul Bahrin Wan Kamal
Medical Technology Division
Malaysian Nuclear Agency
43000 Kajang, Selangor
mirul@nm.gov.my

Abstract

The production of ^{68}Ga-radiopharmaceuticals through kit methodology has allowed smooth accommodation of ^{68}Ga-PET in radiopharmacy. The formulation of ^{68}Ga-radiopharmaceuticals from a lyophilized, cold kits of sterile and pyrogen free is an impending breakthrough in clinical setting. In this study, an attempt was made to produce DOTA- PSMA I&T cold kits to be reconstituted with [68Ga]$GaCl_3$ in one step. The study also focussed at the optimization and evaluation of the ^{68}Ga-DOTA-PSMA I&T preparation prior to the kit formulation.

Keywords: diopharmaceutical cold kit, ^{68}Ga-DOTA-PSMA, lyophilization

1 Introduction

The current radiopharmaceutical of DOTA-PSMA-I&T cold kit is imported; therefore, an attempt to produce local pharmaceutical DOTA-PSMA-I&T cold kit is to reduce the cost of importing. A government sector such as Kuala Lumpur General Hospital under Ministry of Health (MOH) mentions their concern on the high cost of imported radiopharmaceutical kits. Nuklear Malaysia has been asked to produce DOTA-PSMA-I&T cold kits. Therefore, locally produced radiopharmaceuticals are necessary to reduce the cost of importation.

2 Methods

The optimization steps were carried out to obtain the parameters of peptide concentration, pH, incubation time and incubation temperature. The radiolabeling optimum condition was found to be 40μg of peptide per vial, an addition of 1.5M sodium acetate (40μL, to give pH 3.0 to 4.0 at final mixing with Ga-68 elution) and 15 minutes incubation at 90°C. Single vial kit of 1,4,7,10-tetraazacyclododecane-1,4,7,10-tetraacetic acid (DOTA)-PSMA I&T was formulated (Figure 1), followed by dispensing 1.0 mL each into a clean vial and was lyophilized (aseptic technique in a clean room facility). The lyophilized cold kit was sent to microbiology laboratory for sterility and pyrogen testing. The kit was reconstituted with 1.0 mL [68Ga]$GaCl_3$ solution to obtain the ^{68}Ga-labeled DOTA- PSMA I&T.

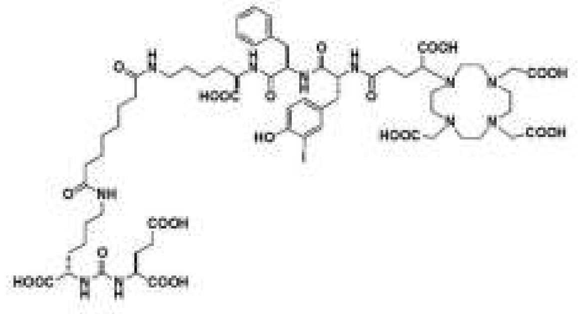

Figure 1: DOTA-PSMA I&T chemical structure.

3 Results

A batch of lyophilized cold kit prepared was sterile and pyrogen free (Figure 2). The radiochemical purity (RCP) of the ^{68}Ga-DOTA-PSMA I&T preparation and stability study (hourly at room temperature) incubated in human serum albumin (HSA) at 37°C were analyzed by using the radio-iTLC method. In average, the RCP of prepared ^{68}Ga-DOTA-PSMA I&T was stable of up to 7 hours at room temparature with RCP between 95.34%-98.02%. Whereas for the serum challenge, the prepared ^{68}Ga-DOTA-PSMA I&T was stable of up to 5 hours with RCP between 96.82%-97.86% incubated at 37°C (Figure 3). The passing RCP values from the quality control specification is more than 95%.

Figure 2: Sterile and pyrogen free DOTA-PSMA I&T lyophilized cold kits

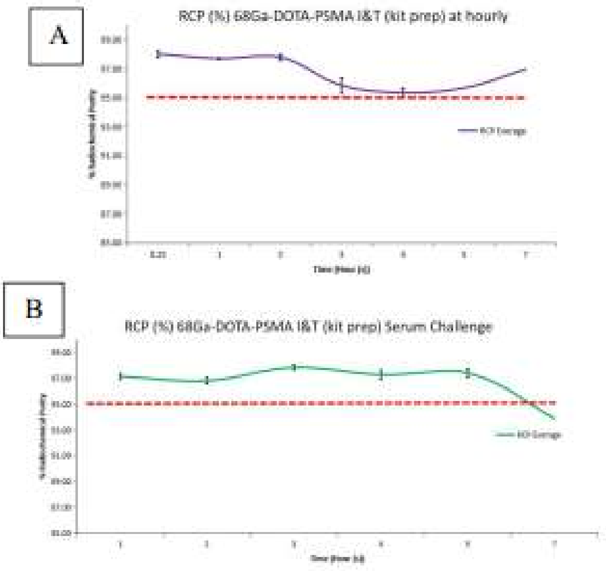

Figure 3: A; Stability of ^{68}Ga-DOTA-PSMA I&T at room temperature (%RCP), B; Stability of ^{68}Ga-DOTA-PSMA I&T at serum challenge (%RCP)

4 Discussion

This study aimed to formularize and evaluate a ^{68}Ga-labeled PSMA for specific targeting to GRPR overexpressed on prostate cancer cells. The optimum radiolabeling condition was found to be at pH 3.0 to 4.0, 10-15 minutes heating at 95°C. Herein, we reported the formulation of lyophilized cold kit of DOTA-PSMA-I&T as a single vial kits using sodium acetate, optimization of radiolabelling with generator-eluted ^{68}Ga, characterization of the ^{68}Ga-labelled peptides, stability studies in serum and long term evaluation of stability of the formulated kits.

5 Conclusion

The sterile and pyrogen free lyophilized DOTA-PSMA I&T cold kits, suitable for the preparation of patient dose of ^{68}Ga-DOTA-PSMA I&T for prostate cancer PET imaging.

References

Eric W. Price and Chris Orvig. 2013. Matching chelators to radiometals for radiopharmaceuticals. *The Royal Society of Chemistry*, Review Article.

Drishty Satpa. 2021. Recent breakthrough in ^{68}Ga-radiopharmaceuticals cold kits for convenient PET radiopharmacy. *Bioconjugate Chemistry*, 32:430 – 447.

M.I. Tsionou, C.E. Knapp, C.A. Foley, C.R. Munteanu, A. Cakebread, C. Imberti, T.R. Eykyn, J.D. Young, B.M. Paterson, P.J. Blower, and et al. 2017. Comparison of macrocyclic and acyclic chelators for gallium-68 radiolabelling. *RSC Adv*, 7:49586 – 49599.

Breeman WAP, de Blois E, Chan H, Konijnenberg M, Kwekkeboom DJ, and Krenning P. 2011. ^{68}Ga-labeled DOTA-peptides and ^{68}Ga-labeled radiopharmaceuticals for positron mission tomography: current status of research, clinical applications, and future perspectives. *Semin Nucl Med*, 41:314 – 321.

Individual Research Contribution Review, 2023, 1(1): 593–594

Gamma Irradiation of Virus towards Development of Inactivated Vaccine

Zainah Adam
Medical Technology Division
Malaysian Nuclear Agency
43000 Kajang, Selangor
zainah@nm.gov.my

Abstract

Gamma radiation has the potential to be applied in production of inactivated vaccine. Inactivation of pathogen using gamma radiation is known to be safer and clean, as it will avoids generation of chemical residues that could lead to adverse reactions. Ionizing radiation has the ability to permeate pathogen and destroy nucleic acid without compromising the antigenic protein, hence ensure preservation of immunogenic properties of the pathogen. As of now, Malaysia has not yet produced any vaccines using gamma radiation. In response to this gap, Malaysian Nuclear Agency has taken proactive actions to initiate research and development of vaccine by employing gamma radiation and other nuclear technology.

Keywords: inactivated vaccine, nuclear technology

1 Introduction

Vaccine is a biological preparation that provides active acquired immunity against the particular disease. Vaccines contain active components (antigen) that generate immune response to the disease (Saxena and Rawat, 2013). There are several different types of vaccines such as inactivated, live-attenuated, messenger RNA, subunit, recombinant, conjugated vaccine and etc. In the case of inactivated vaccines, a common method of inactivation involves the use of chemicals like formaldehyde and β-propiolactone. However, chemical inactivation is associated with safety concerns, such as allergic reactions and potential disease outbreaks. Furthermore, the use of chemicals can modify the antigenic protein of the pathogen, leading to a loss of immunogenic properties (Delrue et al., 2012). Hence, the search for an inactivation method that ensures both safety and efficacy remains ongoing. An alternative approach to chemical inactivation is the use of gamma radiation for inactivation process. Gamma rays possess the advantage of penetrating the virus and destroying its nucleic acid (DNA) without compromising the antigenic structure of the pathogen. This will ensures effective protection against the disease. Various types of vaccines have been produced using nuclear technology such as malaria, influenza and salmonellosis (Seo, 2015). In this study, we used the Newcastle disease virus as the pathogen model to prove that gamma radiation is capable of inactivating the pathogen, and can subsequently be used as the vaccine candidate.

2 Methods

Seed of Newcastle disease virus (NDV) was obtained from University Putra Malaysia. NDV samples were exposed to gamma radiation at dose of 0, 10, 20 and 50 kGy from a Cobalt-60 source at SINAGAMA facility. Virus was kept in ice pack during radiation process. The irradiated NDV was inoculated in 9-days embryonated chicken egg (three eggs per gamma dose) and incubated at 37°C for 48 hours. The eggs were then cooled at 4°C prior to harvesting. The allantoic fluid that contain irradiated NDV was harvested in sterile tubes and kept at -40°C. This propagated irradiated NDV was then subjected to hemagglutination assay (HA) to confirm the virus titer and morphology analysis using FESEM method to confirm the virus structure.

3 Results and discussion

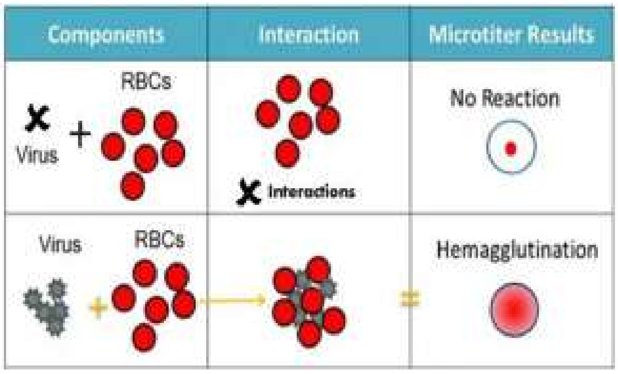

Figure 1: Brief explanation of hemagglutination.

Figure 1 explains in brief of the hemagglutination process. In the absence of viruses, the red blood cells precipitate by gravity to the bottom of the well, giving rise to a distinct red-colored dot in a conical shaped well. Vice versa, in the presence of viruses, the red blood cells clump together as a result of interaction between hemaglutinin protein of the viruses and red blood cells, leading to a lattice formation (Wang-Shick, 2017). Figure 2 showed the HA analysis of the irradiated and non-irradiated Newcastle disease virus. For the non-irradiated (0 kGy) virus, a clear lattice formation occurs, indicates the presence of virus. In the all irradiated viruses (10, 20 and 50 kGy), a clear red-colored dot appear at the bottom of the well, indicates the absence of virus. The clear dot is seen from the well of the first end of the plate. This indicates that the virus has been completely inactivated, in other words the virus titer is zero. Through these results, we suggest that the above dose of gamma radiation were able to inactivate the Newcastle disease.

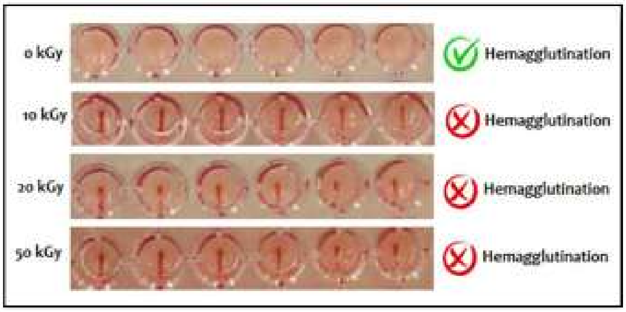

Figure 2: HA analyses of irradiated NDV

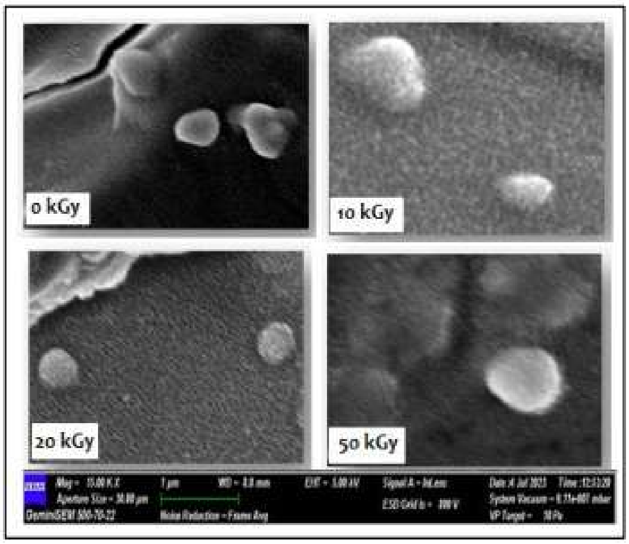

Figure 3: FESEM analyses of irradiated NDV

A scanning electron microscopy (SEM) is an imaging method to assess visualizes the morphology and shape of the virus (Richert-Pöggeler et al., 2019). In this study, field emission scanning electron microscopy was used to elucidate the morphology and size of the irradiated NDV. Analysis of FESEM image of gamma-irradiated NDV shows the existence of almost spherical shape images with a size of 200-300 nm (Figure 3). This size is the specific characteristic of NDV (Ganar et al., 2014). It can also be seen that the irradiated NDV morphology remains intact and does not fragmented after exposure to gamma radiation. This shows that gamma radiation up to 50 kGy preserves the structural and morphological integrity of the virus. These are the desired characteristics in the virus inactivation process for vaccine production.

4 Conclusion

The results showed that gamma irradiation at dose of 10, 20 and 50 kGy were able to in-activate the NDV and preserve the morphological and structure of the NDV. This preliminary study shows that gamma radiation is capable of inactivating NDV and can be applied for the production of inactivated NDV vaccine. This promising result can be used as a starting point in the research and development of gamma irradiated inactivated vaccine in Malaysia.

References

Delrue, Dieter Verzele, Annemieke Madder, and Hans J Nauwynck. 2012. Inactivated virus vaccines from chemistry to prophylaxis: merits, risks and challenges. *Expert Review of Vaccines*, 11(6):695–719, DOI: 10.1586/erv.12.38.

K Ganar, Das M, Sinha S, and Kumar S. 2014. Newcastle disease virus: Current status and our understanding. *Virus Res.*, 184:71–81. doi: 10.1016/j.virusres.2014.02.016. Epub 2014 Mar 1. PMID: 24589707; PMCID: PMC7127793.

KR Richert-Pöggeler, Franzke K, Hipp K, and Kleespies RG. 2019. Electron microscopy methods for virus diagnosis and high resolution analysis of viruses. *Front. Microbiol.*, 9:3255. doi: 10.3389/fmicb.2018.03255.

J. Saxena and S. Rawat. 2013. Edible vaccines. *Advances in Biotechnology*, pages 207–216. doi: 10.1007/978–81–322–1554–712. PMCID: PMC7120417.

HS. Seo. 2015. Application of radiation technology in vaccines development. *Clin Exp Vaccine Res.*, 4(2):145–148.

Ryu Wang-Shick. 2017. in Molecular virology of human pathogenic viruses. ISBN978-0-12-800838-6.